Doppler Ultrasound in Obstetrics and Gynecology

Dev Maulik
Christoph C. Lees
Editors

MOREMEDIA
Springer

Doppler Ultrasound in Obstetrics and Gynecology

Dev Maulik • Christoph C. Lees
Editors

Doppler Ultrasound in Obstetrics and Gynecology

Third Edition

Springer

Editors
Dev Maulik
Department of Obstetrics and Gynecology
University of Missouri–Kansas City
Kansas City, MO, USA

Christoph C. Lees
Department of Metabolism, Digestion and Reproduction
Imperial College Healthcare NHS Trust
London, UK

ISBN 978-3-031-06188-2 ISBN 978-3-031-06189-9 (eBook)
https://doi.org/10.1007/978-3-031-06189-9

This Springer imprint is published by the registered company Springer Nature Switzerland AG
The registered company address is: Gewerbestrasse 11, 6330 Cham, Switzerland

To my wife Shibani for sustaining me with her love, and giving me strength and inspiration for this long but worthy endeavor, and to our incredible grandchildren, Kiran, Sarit and Tara, for bringing sunshine into our lives.

Dev Maulik

To my wife Paula and sons Daniel and Rafael, for their love, enthusiasm and encouragement throughout the years that it has taken this book to grow, develop and finally be born.

Christoph Lees

Preface

Almost two decades have passed since the publication of the second edition of the book. This relatively long interval has witnessed major innovations in the diagnostic Doppler sonography, a greater depth of knowledge on fetal and maternal cardiovascular physiology and pathology, and the emergence of new evidence for guiding clinical practice. In many areas of practice, the use of Doppler has become an essential pre-requisite to appropriate investigation and diagnosis. These advances have provided a powerful rationale for bringing the book up to date so that it may continue to serve our readers in the future. We have critically examined the information contained in the second edition, and comprehensively revised and expanded the contents as deemed appropriate. The process has been successfully concluded and we are very pleased to offer the third edition of "Doppler Ultrasound in Obstetrics and Gynecology" to our readers.

This book has, accordingly, undergone a significant renewal. We take this opportunity to welcome the 35 new authors and co-authors who have substantially contributed to enriching this edition by providing new chapters or rewriting and updating preexisting ones. We removed one chapter due to lack of any significant development and have added 17 new chapters. Some of these are combinations of several previous chapters and four present new areas of current research and clinical application.

In this complex and extensive endeavor, we were greatly assisted by a dedicated team of internationally recognized experts who have generously and enthusiastically participated in this venture despite their enormous responsibilities and hectic schedules. But the overwhelming challenge we had to face and survive was the once in a century pandemic that overshadowed almost everything that we had to do personally or professionally. Our deadlines had to shift several times. We are very grateful to Linda Franta, our highly skilled and dedicated editorial assistant, who organized the work schedule, continuously acted as the liaison between the editors, the authors and the publishing house of Springer.

We remain appreciative of the success of the first two editions and hope that the third edition will be worthy of continuing enthusiastic reception.

Contents

1 Doppler Sonography: A Brief History

Dev Maulik

1.1 Introduction

The origins of modern medical technology may be traced to nineteenth century Europe, when the industrial revolution ushered in sweeping changes in every aspect of life. Of all the momentous discoveries and inventions of this period, there was one relatively obscure scientific event that laid the foundation for the subsequent development of Doppler technologies in the twelfth century—the discovery of a natural phenomenon that came to be known as the Doppler effect. Another critical event was the discovery of the piezoelectric phenomenon by Pierre Curie and Jacques Curie, which enabled the development of ultrasonic transducers many decades later. This chapter briefly describes the origin of the Doppler theory during the nineteenth century, traces the development of diagnostic Doppler ultrasound technology, and its pioneering applications in obstetrics and gynecology.

1.2 Christian Andreas Doppler and the Doppler Theory

1.2.1 Early Life

The phenomenon bears the name of its discoverer, Christian Andreas Doppler, an Austrian mathematician and physicist (Fig. 1.1), born to

Fig. 1.1 Christian Andreas Doppler. The oil painting was done by an unidentified artist probably at the time of Doppler's marriage in 1836. The original is in the Austrian Academy of Sciences to which it was donated by Mathilda von Flugl, the great granddaughter of Christian Doppler. (Reprinted from [1], with permission)

D. Maulik (✉)
Department of Obstetrics and Gynecology, UMKC School of Medicine/Truman Medical Center, UMKC School of Medicine, Kansas City, MO, USA
e-mail: dmaulik2014@gmail.com

D. Maulik, C. C. Lees (eds.), *Doppler Ultrasound in Obstetrics and Gynecology*,
https://doi.org/10.1007/978-3-031-06189-9_1

Johann Evangialist and Therese Doppler on November 29, 1803 in Salzburg, Austria. The house in which he was born and raised still stands across the square from the family home of Wolfgang Amadeus Mozart in the Markart Platz. For nearly a century, Doppler's Christian's name has been consistently misquoted in the literature as Johann Christian. Doppler was baptized on the day of his birth at the Church of St. Andra, which was originally in close proximity of the Doppler home. Eden [1] conducted a thorough search for Doppler's birth and baptismal records and found them still preserved in the Church of St. Andra, which had moved to a new location in Salzburg in 1898. These documents conclusively established that Doppler had been christened Christian Andreas. It appears, however, that Doppler never used his second name.

Doppler's father, a master stone mason, was a man of wealth and fame. Because of frail health, Doppler was sent to school instead of joining the family trade. In 1822, Johann Doppler requested that Simon Stampfer, a professor at the local Lyceum, evaluate his son's aptitude. Stampfer was impressed with young Christian's scholastic abilities in mathematics and science, and at his recommendation, Doppler was sent to the Polytechnic Institute of Vienna for further education.

Doppler studied mathematics and physics in Vienna for 3 years and then returned to Salzburg where he concluded his education and eventually graduated in 1829. For 4 years, he held the position of assistant in higher mathematics at the Vienna Polytechnic Institute. Following this assistantship, he experienced difficulty finding an appropriate position, and in 1835, he seriously considered emigrating to the United States. At this point, however, he was offered and accepted the position of Professor of Elementary Mathematics and Commercial Accounting at the State Secondary School in Prague. The following year, he was also appointed Supplementary Professor of Higher Mathematics at the Technical Institute in Prague. In 1841, Christian Doppler became a full Professor of Mathematics and Practical Geometry at the latter institution.

1.2.2 The Doppler Theory

The Doppler effect is defined as the observed shifts in the frequency of transmitted waves when relative motion exists between the source of the wave and an observer. The frequency increases when the source and the observer move closer and decreases when they move apart. On May 25, 1842, Doppler presented his landmark paper on the Doppler effect at a meeting of the Natural Sciences Section of the Royal Bohemian Society of Sciences in Prague. Ironically, there were only five people and a transcriber in the audience. The paper was entitled "On the Colored Light of the Double Stars and Certain Other Stars of the Heavens" (Fig. 1.2) and was published in 1843 in the Proceedings of the society [2]. Of 51 papers Doppler published, this one was destined to bring him lasting recognition.

Doppler's work was based on the theory of the aberration of light developed by Edmund Bradley, the eighteenth century British Astronomer Royal. Doppler established the principle of frequency shift and developed the formula for calculating the velocity from the shift. For elucidating the theoretic background of the principle, Doppler used various analogies and examples primarily based on transmission of light and sound. Although his examples of sound transmission were correct, those involving light transmission were erroneous, as he presumed that all stars emitted only pure white light. He postulated that the color of a star was caused by the relative motions of the star and the earth causing apparent spectral shifts of the emitted white light. The spectrum would shift toward blue if the star approached the earth; conversely, the spectrum would shift to red if the star receded away from the earth. When describing these phenomena, Doppler did not take into account preexisting research on light transmission and spectrum. Herschel [3] had already discovered infrared radiation, and Ritter [4] had described ultraviolet radiation; but it appears that Doppler was unaware of these important developments.

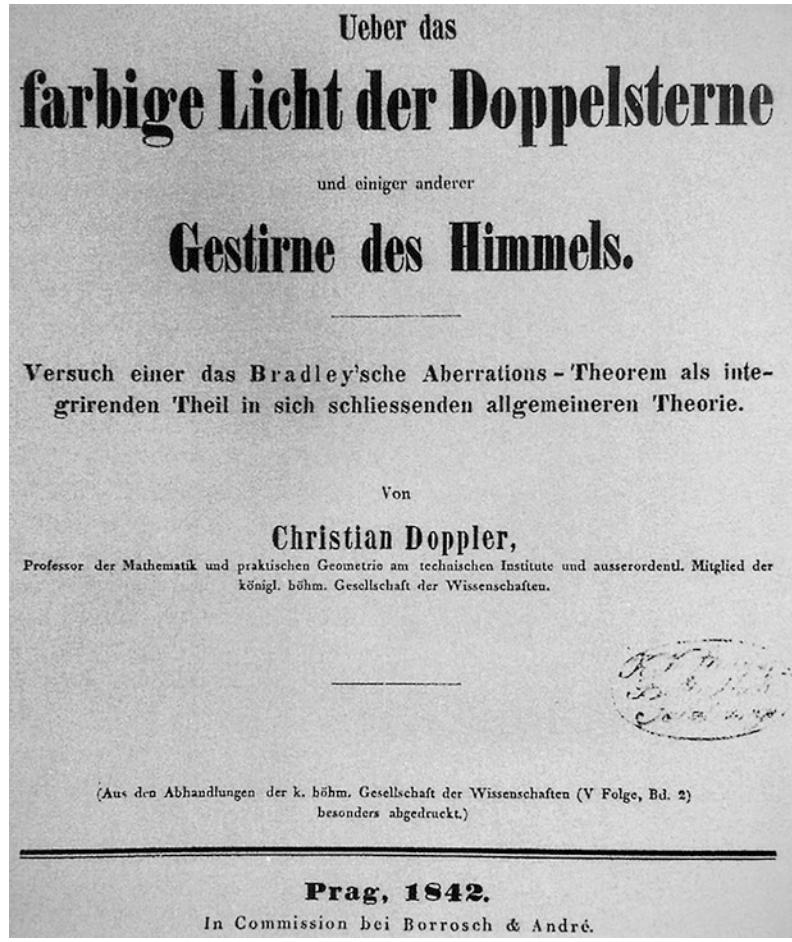

Ueber das

farbige Licht der Doppelsterne

und einiger anderer

Gestirne des Himmels.

Versuch einer das Bradley'sche Aberrations-Theorem als integrirenden Theil in sich schliessenden allgemeineren Theorie.

Von

Christian Doppler,

Professor der Mathematik und praktischen Geometrie am technischen Institute und ausserordentl. Mitglied der königl. böhm. Gesellschaft der Wissenschaften.

(Aus den Abhandlungen der k. böhm. Gesellschaft der Wissenschaften (V Folge, Bd. 2) besonders abgedruckt.)

Prag, 1842.

In Commission bei Borrosch & André.

Fig. 1.2 Title page of Christian Doppler's paper titled "On the Coloured Light of the Double Stars and Certain Other Stars of the Heavens." (Reprinted from [1], with permission)

1.2.3 Verification of Doppler's Theory

As was to be expected, the paper generated critical responses. The most significant challenge came from a young Dutch scientist working at the University of Utrecht in Holland, Christoph Hendrik Diederik Buys Ballot (Fig. 1.3). In 1844, Buys Ballot proposed to refute the Doppler theory by designing an experiment involving sound transmission as his doctoral research project. Conveniently for him, a new railroad had just been established between Amsterdam and Utrecht, and the Dutch government gave him permission to use this railway system to verify the Doppler effect on sound transmission (Fig. 1.4). The first experiment was designed in February 1845. Two horn players who apparently had perfect pitch were chosen to participate in the experiment. The calibration was accomplished by one musician blowing a note and the other identifying the pitch of the tone. After this calibration was performed, one player was positioned on the train, and the other stood along the track. As the train passed, the stationary musician on the trackside perceived that the note blown by the musician on the train was half a note higher when the train approached him and half a note lower when it moved away. Unfortunately, a raging blizzard forced Buys Ballot to abandon his experiment and to reschedule it in a more temperate season. The results from the first experiment were published within less than a month in a music journal [5].

Fig. 1.3 C. H. D. Buys Ballot (1817–1890). (From [40], with permission)

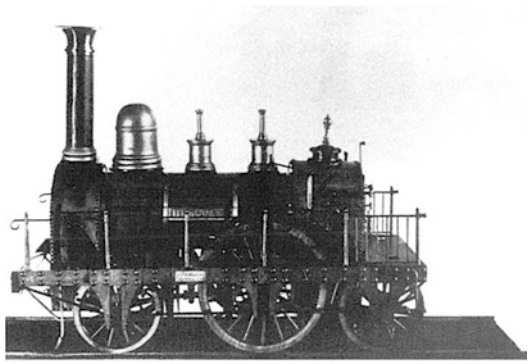

Fig. 1.4 Model of the locomotive (named Hercules) used in the first experiments. (From [40], with permission)

Buys Ballot conducted the experiment again in early June of the same year [6]. Three teams were stationed along the track. Each team was composed of a horn player, an observer, and a manager. A fourth team was on a flat car behind the locomotive. Buys Ballot positioned himself on the foot plate next to the engineer. This experiment was more sophisticated, but it also encountered environmental complications as the summer heat seriously interfered with the correct tuning of the musical instruments. The musicians originally tried to use one-sixteenth of a single note but failed, and the final experiment was done in eights. The results were remarkable despite all the trials and tribulations. The study that set out to refute the Doppler theory ultimately confirmed it. Buys Ballot proved not only the existence of the Doppler effect in relation to sound transmission, but its angle dependency as well. Incredibly, Buys Ballot still refused to accept the validity of the theory for the propagation of light and most of the scientific community of the nineteenth century did not acknowledge the validity of Doppler's theory because of his erroneous interpretation of astronomical phenomena.

As translated by Eden [1], Doppler's response was impressive in its foresight: "I still hold the trust—indeed, stronger than ever before—that in the course of time, this theory will serve astronomers as a welcome help to probe the happenings of the universe, at times when they feel deserted by all other methods" [7]. This statement was prophetic. Since the beginning of the twentieth century, the Doppler principle has been used extensively not only in astronomy, but also in the immensely diverse fields of science and technology.

1.2.4 Later Life

Doppler lived only 10 years after publishing his paper on the frequency shift; however, these few years brought him well-deserved recognition and honor. He was elected to the membership of the Royal Bohemian Society of Sciences in 1843 and of the highly prestigious Imperial Academy of Sciences in Vienna in 1847. In 1850, he was appointed by Emperor Franz Josef of the Austro-Hungarian Empire to the coveted position of the Chair of Experimental Physics at the University of Vienna. Sadly, however, he was in poor health at this point because of the chronic respiratory disease which was presumed to be "consumption" or pulmonary tuberculosis and which he apparently had contracted in Prague years earlier. With the hope of recuperation, he went to the warmer climate of Venice in the winter of 1852, where he died on March 17, 1853 at the age of only 49 in the arms of his wife Mathilde. He was

given a grand funeral at the Parish Church of San Giovanni in Bragora and many academic and civil dignitaries were in attendance. A more comprehensive account of Doppler's life is beyond the scope of this review. For those who are interested, I strongly recommend the excellent monograph written by Professor Alec Eden titled The Search for Christian Doppler [1].

1.3 Early Application of Doppler Theory

Initial applications of the Doppler principle were mostly for astronomic studies. Over the years, the Doppler effect for light and radio waves has yielded information on a cosmic scale, from orbital velocity of planets and stars to galactic rotation and an ever-expanding universe. The principle still serves as a major tool for cosmologic research. With the beginning of the twentieth century, other applications gradually emerged. The first sonar equipment for detecting submarines was developed by Paul Langevin of France, who also pioneered the use of piezoelectric crystals for transmitting and receiving ultrasound waves. This technology was used to detect submarines, initially during World War I and more extensively during World War II. The ensuing decades witnessed widespread application of the principle of the Doppler effect, from roadside radar speed detectors used by the police to the highly sophisticated military defense and weather forecasting Doppler radar systems. Doppler radio signals are used for navigation, surveying, monitoring animal migration, and estimating crop yields. The development of diagnostic Doppler ultrasound technology offers yet another example of the extensive use of the Doppler principle.

1.4 Development of Spectral Doppler Ultrasonography

The first medical applications of Doppler sonography were initiated during the late 1950s, and impressive technologic innovations have been continuing ever since. Shigeo Satomura from the Institute of Scientific and Industrial Research of Osaka University in Japan developed the first Doppler ultrasound device for medical diagnostic purposes and reported the recording of various cardiac valvular movements [8]. Based on their experience, Satomura suggested the potential use of Doppler ultrasonography for percutaneous measurement of blood flow. In 1960, he and Kaneko were the first to report construction of an ultrasonic flowmeter [9]. A significant amount of the pioneering work occurred at the University of Washington in Seattle in the United States. Major driving forces of this group included Robert Rushmer, a physician, and Dean Franklin, an engineer. They initiated the development of a prototype continuous-wave Doppler device in 1959 and reported blood flow assessment using the ultrasound Doppler frequency shift [10]. The Seattle team refined this instrument into a small portable device, and the earliest clinical trials were undertaken during the mid-1960s by Eugene Strandness, who at the time was undergoing training as a vascular surgeon [11].

The first pulsed-wave Doppler equipment was developed by the Seattle research team. Donald Baker, Dennis Watkins, and John Reid began working on this project in 1966 and produced one of the first pulsed Doppler devices [12]. Other pioneers of pulsed Doppler include Wells of the United Kingdom [13] and Peronneau of France [14]. The Seattle team also pioneered the construction of duplex Doppler instrumentation based on a mechanical sector scanning head in which a single transducer crystal performed both imaging and Doppler functions on a time-sharing basis. The duplex Doppler technique allowed the ultrasound operator to determine for the first time the target of Doppler insonation. This development is of critical importance in obstetric and gynecologic applications, as such range discrimination allows reliable Doppler interrogation of a deep-lying circulation, such as that of the fetus and of the maternal pelvic organs. It must be recognized that many others also have made immense pioneering contributions in the development and utilization of diagnostic Doppler sonography, a detailed discussion of which is beyond the scope of this chapter.

1.5 Development of Color Doppler Ultrasonography

Spectral Doppler ultrasound interrogates along the single line of ultrasound beam transmission. The hemodynamic information thus generated is limited to unidimensional flow velocity characterization from the target area. This limitation provided the impetus to develop a method for depiction of flow in a two-dimensional plane in real time. Potential clinical utility of such an approach was obvious, particularly for cardiovascular applications characterizing complex hemodynamic abnormalities associated with acquired and congenital cardiac diseases. However, the unidimensional spectral pulsed Doppler method was inadequate to cope with the processing needs of real-time two-dimensional Doppler ultrasonography, which involves analysis of an enormous number of signals derived from multiple sampling sites along multiple scan lines. The initial attempts involved various invasive and noninvasive modifications of the existing echocardiographic approach, including the use of a sonocontrast agent to obtain information on blood flow patterns during two-dimensional echocardiographic imaging [15] and the development of multichannel duplex Doppler systems [16]. However, the spectral pulsed Doppler ultrasound used in these techniques could produce velocity information only along a single beam line.

The development of real-time two-dimensional color Doppler ultrasonography, therefore, represents a major technologic breakthrough, which became possible because of the introduction of two critical pieces of technology for processing the Doppler ultrasound signal. First was the Doppler sonographic application by Angelsen and Kristofferson [17] of the sophisticated filtering technique of "the moving target indicator" used in radar systems. This filter allows removal of the high-amplitude/low-velocity clutter signals generated by the movement of tissue structures and vessel walls. The second was development of the autocorrelation technique by Namekawa et al. [18]. The autocorrelator is capable of processing mean Doppler phase shift data from the two-dimensional scan area in real time, so two-dimensional Doppler flow mapping is possible (see Chap. 5). In 1983, the Japanese group, which included Omoto, Namekawa, Kasai, and others, reported the use of a prototype device incorporating the new technology for visualizing intracardiac flow [19]. Extensive clinical development of this new approach was accomplished by Nanda and associates in the United States [20].

1.6 Development of Doppler Sonography in Obstetrics

Continuing collaboration between clinical scientists, engineers, and the industry led to advances in this field, which took place in several countries. A brief narration of the pioneering contributions is presented in this section. A more comprehensive historical review of all the seminal innovations and investigations is beyond the scope of this single chapter; however, additional information is available in other chapters in this book.

1.6.1 Early Work

The first known obstetrical application of Doppler ultrasound was published by Callagan and colleagues. Working at the United States Naval Research Institute in Bethesda, they used Doppler ultrasound for detecting fetal heart movements [21]. Subsequently, in collaboration with Rushmer and his team at the University of Washington in Seattle, Johnson reported the use of Doppler fetal heart signals in early pregnancy [22]. Employing a Doppler flowmeter, they detected audible placental flow signals, which were described as "a rushing wind or whirlwind sound" [23]. These early investigations led to an era of research productivity that extended the utilization of Doppler ultrasound for evaluating various fetal and the maternal circulations, which are summarized below.

1.6.2 Doppler Ultrasound of the Umbilical Artery

According to Nimura's historical review, Ashitaka, Takemura, and others were probably

the first to describe distinct Doppler waveforms from the umbilical artery and vein [24]. Further advances in the use of Doppler velocimetry for fetal flow assessment occurred in several centers. In 1977, FitzGerald and Drumm at the Coombe Lying-in Hospital in Dublin [25] performed pulse echo two-dimensional image directed continuous-wave Doppler sonogram of the umbilical arterial and venous flows, although the accuracy of identification of the umbilical arterial and venous Doppler flow waveforms was questionable, given the technological limitations at the time. Contemporaneously, MacCallum, in collaboration with Baker and his team in Seattle, used range-gated pulse wave Doppler to describe the distinct umbilical arterial and venous waveforms [26]. Subsequently, others also reported on Doppler velocimetry of the umbilical artery [27–31].

1.6.3 Doppler Ultrasound of the Fetal Venous Circulation

Doppler of inferior vena cava was first described by Chiba and associates at the National Cardiovascular Center in Osaka [32]. In Sydney, Australia, Gill and others in Kossoff's team pioneered umbilical venous flow measurement [33]. Kiserud and colleagues at Trondheim University in Norway were the first to report on the Doppler characterization of the ductus venosus flow [34]. Kiserud continued in-depth investigations of the ductus venosus hemodynamics and has updated these topics in his chapters in this book (Chaps. 5 and 28).

1.6.4 Doppler Ultrasound of the Fetal Cerebral Circulation

Doppler assessment of fetal cerebral circulation was pioneered by Wladimiroff and colleagues at the University of Rotterdam in Holland [35], and Arbeille and his colleagues at the University of Tours in France [36]. The former interrogated fetal internal carotid artery, aorta, and umbilical artery and suggested flow redistribution in fetal growth restriction. At the University of Tours in France, Arbeille and others were the first to report middle cerebral artery Doppler and innovated the cerebro-placental ratio as a measure of fetal flow redistribution. This ratio has emerged currently as a major tool for the assessment of fetal decompensation.

1.6.5 Doppler Ultrasound of the Miscellaneous Fetal Arterial Circulation

At the University of Lund in Sweden, Eik Nes working with Marsal's group innovated a duplex Doppler system by attaching a pulse Doppler transducer to a real-time B-Mode imaging transducer at a fixed angle and measured fetal aortic flow [37]. Fetal renal artery assessment was reported by Vyas et al. [38] and Veille [39].

1.6.6 Doppler Ultrasound of the Uteroplacental Circulation

In 1983, Campbell and his team at the King's College, London, pioneered Doppler investigation of the uteroplacental circulation. Using a range-gated pulse Doppler device, they interrogated uterine arcuate artery and observed increased uteroplacental flow resistance in pregnancy complication including preeclampsia and fetal growth restriction [40]. Campbell and his associates continued to advance the use of uterine Doppler in obstetrics. Schulman and his group at Winthrop University Hospital in New York used a continuous-wave Doppler device and recorded evolution of the uterine artery flow through the advancing gestation [41].

1.6.7 Fetal Doppler Echocardiography

In 1980, at the University of Rochester, New York, Maulik initiated fetal Doppler research in collaboration with Nanda, who

headed the Noninvasive Cardiovascular Laboratory at the University, and Saini, a faculty in the School of Engineering. The Rochester group was the first to develop the method for fetal Doppler echocardiography and characterized fetal cardiac circulation in normal and abnormal pregnancies [42]. The same group also pioneered fetal color Doppler echocardiography [43] and real-time 3D color echocardiography using a two-dimensional matrix probe [44]. In 1986, Reed et al. published their investigation of fetal cardiac flow velocities [45]. Huhta and associates utilized Doppler echocardiography to demonstrate the feasibility of detection and measurement of fetal ductal constriction [46]. Devore also explored the application of color Doppler echocardiography for assessing congenital heart disease [47]. The history of the development of fetal echocardiography has recently been reviewed [48].

1.6.8 Promotion of Fetal Doppler

Perinatal Doppler research and application received a significant boost from the National Institute of Child Health and Development in 1987, when McNellis and Maulik organized a Doppler meeting cochaired by Hobbins and Maulik in Bethesda [49]. This was preceded in 1986 by an international perinatal Doppler workshop organized by Maulik on behalf of European Placenta Group; during this time, it was proposed to form a scientific forum for perinatal Doppler. In 1988, the International Perinatal Doppler Society was created in Kansas City during its first congress, hosted by Maulik, and supported by an international leadership of pioneering investigators including Marsal, Campbell, Platt, Hobbins, Arbeille, and others (Fig. 1.5). In the early days of the perinatal use of Doppler, the Society played a crucial role in providing an open scientific forum for advancing perinatal Doppler sonography. In 2002, after the 15th Congress in Prague, the Society merged with the International Society of Ultrasound in Obstetrics and Gynecology.

Fig. 1.5 Some participants in the International Perinatal Doppler Society, First Congress, 1988, Kansas City, Missouri, USA. From left: Prof John Hobbins, Prof. Stuart Campbell, Prof. Harold Schulman, Prof. Dev Maulik (the Host)

1.7 Doppler Application in Gynecology

In contrast to the prolific publications on the obstetric uses of Doppler sonography, reports on gynecologic applications of the technique did not begin to appear until the mid-1980s. Initial reports included feasibility studies, investigation of pelvic masses, screening for ovarian malignancy, optimizing in vitro fertilization, and assisting in detecting ectopic pregnancy. Taylor and colleagues at the Yale University demonstrated the feasibility of Doppler characterization of the ovarian and uterine arterial circulations utilizing pulsed duplex Doppler [50]. The technique was validated by direct Doppler interrogation during laparotomy. Kurjak, Zalud, and others at University of Zagreb used transvaginal color Doppler to investigate pelvic circulation in normal women and those with known pelvic masses [51]. The role of transvaginal color Doppler was investigated as a screening tool for ovarian malignancy by Bourne and others in the Campbell group in London [52]. In Israel at the Rambam Medical Center, Thaler, Manor, and others suggested the use of transvaginal duplex pulsed Doppler of pelvic vessels in reproductive medicine [53]. Steer and colleagues from

Kings College in London actually showed the potential utility of pulsatility index of the uterine arteries to improve the implantation rate in embryo transfer [54]. Utility of duplex and color Doppler as diagnostic tool for ectopic pregnancy was explored by Taylor et al. [55] and by Kurjak and others [56]. Since these early reports, Doppler sonographic research and application in gynecology has steadily expanded.

References

1. Eden A. The search for Christian Doppler. Vienna: Springer; 1992.
2. Doppler C. Uber das farbige Licht der Doppler-sterne und einiger anderer Gestirne des Himmels. Abhandl Konigl Bohm Ges Ser. 1843;2:465–82.
3. Herschel JFW. Experiments on the refrangibility of the invisible rays of the sun. Philos Trans R Soc Lond. 1800;90:284–92.
4. Ritter JW. Ausfindung nicht lichtbarer Sonnenstrahlen ausserhalb des Farbenspectrums, an der Seite des Violetts. Widerhohlung der Rouppachen Versuche. Wien, Mathemat-Naturw Klasse Sitzungsbericht. 1801;79:365–80.
5. Buys Ballot CHD. Bedrog van het gehoororgaan in het bepalen van de hoogte van een waargenomen toon. Caecilia. Algemeen Muzikaal Tijdschrift van Ne-derlandl Tweede Jaargang No. 1845;7:78–81.
6. Buys Ballot CHD. Akustische Versuche auf der Niederlandischen Eisenbahn nebst gelegentlichen Bemerkungen zur Theorie des Herrn Prof Doppler. Pogg Ann. 1845;66:321–51.
7. Doppler C. Bemerkungen zu meiner Theorie des Farbigen Lichtes der Doppelsterne etc, mit vorzuglicher Rucksicht auf die von Herrn Dr Buys Ballot zu Utrecht dagegen erhobenen Bedenken. Pogg Ann. 1846;68:1–35.
8. Satomura S. Ultrasonic Doppler method for the inspection of cardiac functions. J Acoust Soc Am. 1957;29:1181–3.
9. Satomura S, Kaneko Z. Ultrasonic blood rheograph. In: Proceedings of the 3rd International Conference on Medical Elect, London, IEEE; 1960, p 254.
10. Franklin DL, Schlegel W, Rushmer RF. Blood flow measured by Doppler frequency shift of back scattered ultrasound. Science. 1961;134:564–5.
11. Strandness DE, Schultz RD, Sumner DS, Rushmer RF. Ultrasonic flow detection—a useful technic in the evaluation of peripheral vascular disease. Am J Surg. 1967;113:311–4.
12. Baker DW. Pulsed ultrasonic Doppler blood flow sensing. IEEE Trans Sonic Ultrasonics. 1970;SU-17(3):170–85.
13. Wells PNT. A range gated ultrasonic Doppler system. Med Biol Eng. 1969;7:641–52.
14. Peronneau PA, Leger F. Doppler ultrasonic pulsed blood flowmeter. In: Proceedings of the 8th conference on medical and biological engineering; 1969, pp. 10–11.
15. Gramiak R, Shah PM, Kramer DH. Ultrasound cardiography: contrast studies in anatomy and function. Radiology. 1969;92:939–48.
16. Fish PJ. Multichannel direction resolving Doppler angiography (abstract). Presented at the 2nd European congress of ultrasonics in medicine; 1975, p 72.
17. Angelsen BAJ, Kristofferson K. On ultrasonic MTI measurement of velocity profiled in blood flow. IEEE Trans Biomed Eng. 1979;BME-26:665–771.
18. Namekawa K, Kasai C, Tsukamoto M, Koyano A. Imaging of blood flow using autocorrelation (abstract). Ultrasound Med Biol. 1982;8:138–41.
19. Omoto R, Yokote Y, Takamoto S, et al. Clinical significance of newly developed real time intracardiac two dimensional blood flow imaging system (2-D-Doppler) (abstract). Jpn Circ J. 1983;47:191.
20. Omoto R. History of color flow mapping technologies. In: Nanda NC, editor. Textbook of color Doppler echocardiography. Philadelphia: Lea & Febiger; 1989. p. 1–5.
21. Callaghan DA, Rowland TC, Goldman DE. Ultrasonic Doppler observation of the fetal heart. Obstet Gynecol. 1964;23:637–41.
22. Johnson WL, Stegall HF, Lein JN, Rushmer RF. Detection of fetal life in early pregnancy with an ultrasonic Doppler flowmeter. Obstet Gynecol. 1965;26(3):305–6.
23. Johnson WL, Smith MR, Brewer LL. Observations of placental blood flow with a Doppler flowmeter. Am J Obstet Gynecol. 1968;100(8):1125–7.
24. Nimura Y. Introduction of the ultrasonic Doppler technique in medicine: a historical perspective. J Med Ultrasound. 1988;6:5–13.
25. FitzGerald DE, Drumm JE. Noninvasive measurement of the fetal circulation using ultrasound: a new method. BMJ. 1977;2:1450–1.
26. McCallum WD, Olson RF, Daigle RE, Baker DW. Real time analysis of Doppler signals obtained from the fetoplacental circulation. Ultrasound Med. 1977;3B:1361–4.
27. Maulik D, Saini VD, Nanda NC, Rosenzweig MS. Doppler evaluation of fetal hemodynamics. Ultrasound Med Biol. 1982;8(6):705–10.
28. Arbeille P, Asquier E, Moxhon E, Magnin M, Pourcelot L, Berger C, Lansac J. Study of fetal and placental circulation by ultrasound. New technic in the surveillance of pregnancy. J Gynecol Obstet Biol Reprod (Paris). 1983;12(8):851–9.
29. Reuwer PJ, Bruinse HW, Stoutenbeek P, Haspels AA. Doppler assessment of the fetoplacental circulation in normal and growth-retarded fetuses. Eur J Obstet Gynecol Reprod Biol. 1984;18(4):199–205.
30. Schulman H, Fleischer A, Stern W, Farmakides G, Jagani N, Blattner P. Umbilical velocity wave

ratios in human pregnancy. Am J Obstet Gynecol. 1984;148(7):985–90.
31. Trudinger BJ, Giles WB, Cook CM. Uteroplacental blood flow velocity-time waveforms in normal and complicated pregnancy. BJOG Int J Obstet Gynaecol. 1985;92(1):39–45.
32. Chiba Y, Utsu M, Kanzaki T, Hasegawa T. Changes in venous flow and intratracheal flow in fetal breathing movements. Ultrasound Med Biol. 1985;11(1):43–9.
33. Gill RW, Kossoff G. Pulsed Doppler combined with B-mode imaging for blood flow measurement. Contrib Gynecol Obstet. 1979;6:139–41.
34. Kiserud T, Eik-Nes SH, Blaas HK, Hellevik LR. Ultrasonographic velocimetry of the fetal ductus venosus. Lancet. 1991;338(8780):1412–4.
35. Wladimiroff JW, Tonge HN, Stewart PA. Doppler ultrasound assessment of cerebral blood flow in the human fetus. Br J Obstet Gynaecol. 1986;93:471–5.
36. Arbeille P, Patat F, Tranquart F, Body G, Berson M, Roncin A, Saliba E, Magnin G, Berger C, Pourcelot L. Doppler examination of the umbilical and cerebral arterial circulation of the fetus. J Gynecol Obstet Biol Reprod (Paris). 1987;16(1):45–51.
37. Eik-Nes SH, Bruback AO, Ulstein MK. Measurement of human fetal blood flow. BMJ. 1980;28:283–7.
38. Vyas S, Nicolaides KH, Campbell S. Renal artery flow-velocity waveforms in normal and hypoxemic fetuses. Am J Obstet Gynecol. 1989;161:168–72.
39. Veille JC, Kanaan C. Duplex Doppler ultrasonographic evaluation of the fetal renal artery in normal and abnormal fetuses. Am J Obstet Gynecol. 1989;161:1502–7.
40. Campbell S, Diaz-Recasens J, Griffin DR, et al. New Doppler technique for assessing uteroplacental blood flow. Lancet. 1983;1:675–7.
41. Schulman H, Fleischer A, Farmakides G, Bracero L, Rochelson B, Grunfeld L. Development of uterine artery compliance in pregnancy as detected by Doppler ultrasound. Am J Obstet Gynecol. 1986;155(5):1031–6.
42. Maulik D, Nanda NC, Saini VD. Fetal Doppler echocardiography: methods and characterization of normal and abnormal hemodynamics. Am J Cardiol. 1984;53:572–8.
43. Maulik D, Nanda NC, Hsiung MC, Youngblood J. Doppler color flow mapping of the fetal heart. Angiology. 1986;37:628–32.
44. Maulik D, Nanda NC, Singh V, Dod H, Vengala S, Sinha A, Sidhu MS, Khanna D, Lysikiewicz A, Sicuranza G, Modh N. Live three-dimensional echocardiography of the human fetus. Echocardiography. 2003;20(8):715–21.
45. Reed KL, Meijboom EJ, Sahn DJ, Scagnelli SA, Valdes-Cruz LM, Shenker LE. Cardiac Doppler flow velocities in human fetuses. Circulation. 1986;73(1).:41–6.45.
46. Huhta JC, Moise KJ, Fisher DJ, Sharif DS, Wassersturm N, Martin C. Detection and quantitation of constriction of the fetal ductus arteriosus by Doppler echocardiography. Circulation. 1987;75:406–12.
47. DeVore GR, Horenstein J, Siassi B, Platt LD. Fetal echocardiography. VII. Doppler color flow mapping: a new technique for the diagnosis of congenital heart disease. Am J Obstet Gynecol. 1987;156(5):1054–64.
48. Maulik D, Nanda NC, Maulik D, Vilchez G. A brief history of fetal echocardiography and its impact on the management of congenital heart disease. Echocardiography. 2017;34(12):1760–7.
49. Maulik D, McNellis D, editors. Doppler ultrasound measurement of maternal-fetal hemodynamics: proceedings from the National Institute of child health and development workshop. Ithaca, NY: Perinatology Press; 1987.
50. Taylor KJW, Burns PN, Wells PNT, Conway DI, Hull MGR. Ultrasound Doppler flow studies of the ovarian and uterine arteries. Br J Obstet Gynaecol. 1985;92:240–6.
51. Kurjak A, Zalud I, Jurkovic D, Alfrevic Z, Miljan M. Transvaginal color Doppler for the assessment of pelvic circulation. Acta Obstet Gynecol Scand. 1989;68:131–5.
52. Bourne T, Campbell S, Steer C, Whitehead MI, Collins WP. Transvaginal colour flow imaging: a possible new screening technique for ovarian cancer. BMJ. 1989;299(6712):1367–70.
53. Thaler I, Manor D, Brandes J, Rottem S, Itskowvitz J. Basic principles and clinical applications of the transvaginal Doppler duplex system in reproductive medicine. J In Vitro Fertil Embryol Transfer. 1990;7:74–5.
54. Steer CV, Campbell S, Tan SL, Crayford T, Mills C, Mason BA, Collins WP. The use of transvaginal color flow imaging after in vitro fertilization to identify optimum uterine conditions before embryo transfer. Fertil Steril. 1992;57(2):372–6.
55. Taylor KJ, Ramos IM, Feyock AL, Snower DP, Carter D, Shapiro BS, Meyer WR, De Cherney AH. Ectopic pregnancy: duplex Doppler evaluation. Radiology. 1989;173(1):93–7.
56. Kurjak A, Zalud I, Schulman H. Ectopic pregnancy: transvaginal color Doppler of trophoblastic flow in questionable adnexa. J Ultrasound Med. 1991;10(12):685–9.

2 Physical Principles of Doppler Ultrasonography

Dev Maulik

2.1 Propagation of Sound

Sound is a form of mechanical energy that travels through solid or liquid media as pressure waves (Fig. 2.1). Sound waves are generated when an object vibrates in a medium. For example, percussion causes a drum membrane to vibrate and to generate sound waves in the air. During vibration, the forward movement of the sound source causes a pressure rise in the adjacent medium, so the molecules of the medium become crowded. As the source moves backward, there is a pressure drop in the medium, so the molecules now move apart. This phenomenon of alternating molecular compression and rarefaction accompanies the waves of sound energy as they propagate along the medium (Fig. 2.2). Although the molecules vibrate, they remain in their original location and are not displaced. Sound travels faster in solids than in liquids and faster in liquids than in gases.

Although usually considered in a unidimensional plane, in reality sound is transmitted in a three-dimensional space. Sound waves from a vibratory source or from a reflector are moving surfaces of high and low pressures. These surfaces are called *waveforms*. The shape of a waveform depends on the shape of the source or the interface. Thus, a plane waveform emanates from a flat source and a spherical waveform from a spherical source. With Doppler ultrasonics, the scattered waveform is spherical, as red blood cells (RBCs) behave as spherical sources during the scattering of an incident beam.

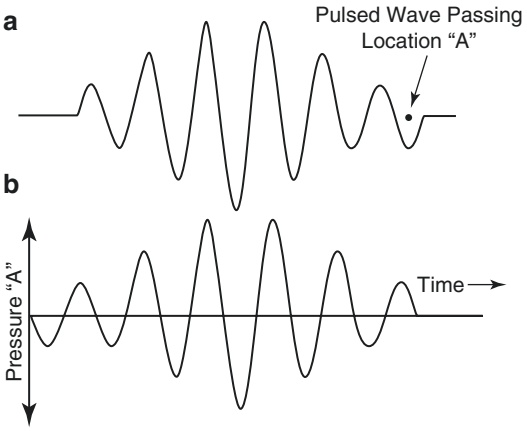

Fig. 2.1 (**a**, **b**) Propagation of sound. (**a**) Passage of a sound pulse through point "A" in the medium. (**b**) Consequent changes in the pressure at that point

D. Maulik (✉)
Department of Obstetrics and Gynecology, UMKC School of Medicine/Truman Medical Center, UMKC School of Medicine, Kansas City, MO, USA
e-mail: dmaulik2014@gmail.com

D. Maulik, C. C. Lees (eds.), *Doppler Ultrasound in Obstetrics and Gynecology*,
https://doi.org/10.1007/978-3-031-06189-9_2

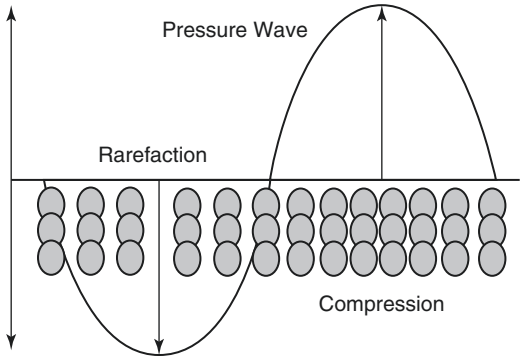

Fig. 2.2 Propagation of sound. Compression and rarefaction of the molecules in a medium associated with the propagation of a pressure wave related to sound or ultrasound transmission. Horizontal axis represents the distance; vertical axis represents the magnitude of pressure wave deflections around the baseline. Upward deflection represents the positive pressure changes and downward deflection the negative pressure changes

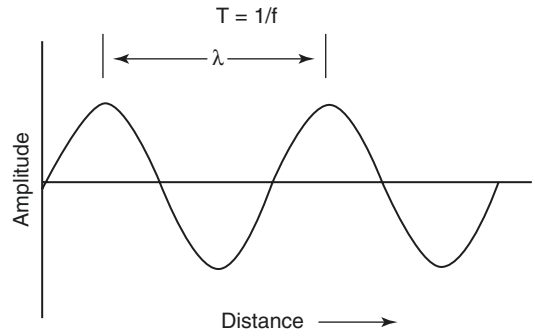

Fig. 2.3 Wavelength of sound. Horizontal axis represents the distance and the vertical axis the magnitude of pressure wave deflections around the baseline. The peak-to-peak distance (λ) between the consecutive pressure waves is one wavelength

Table 2.1 Frequency and corresponding wavelength of commonly used Doppler transducers in obstetrics

Frequency (MHz)	Wavelength (μm)
2.0	770
2.5	616
3.0	513
3.5	440
4.0	385
4.5	342
5.0	308
5.5	280
6.0	257
6.5	236
7.0	220
7.5	205

2.2 Propagation Speed of Sound

The *propagation speed* of sound in a medium is the rate of change of position of the sound wave in unit time in that medium. It is called *velocity* when the direction of motion is also specified. The speed of ultrasound propagation in a medium is directly related to the bulk modulus of elasticity and density of the medium. A change in transmitting frequency within the range of clinical usage does not alter the speed. Although speed of sound is affected by temperature, no appreciable effects are known in clinical applications. With diagnostic ultrasonography, the propagation speed information is used to compute the depth distance from the echo return time. It is also a component of the Doppler equation that allows determination of speed of the scatterer from the Doppler frequency shift. The average propagation speed of ultrasound in soft tissues is approximately 1540 meters per second (m/s).

2.3 Wavelength, Frequency, Pulse

The *wavelength* of sound is comprised of one cycle of compression and rarefaction. Therefore, it is the distance between a pair of consecutive peaks or troughs of adjacent pressure waves (Fig. 2.3). The *frequency* of sound is the number of such cycles occurring in 1 second. One *cycle* is called a hertz (Hz). Wavelength and frequency are inversely related:

$$\lambda = c / f$$

where λ represents the wavelength, c the speed of sound, and f the frequency. As the propagation speed of sound in tissue is known and is relatively constant, one can determine the frequency from the wavelength and vice versa (Table 2.1). The duration of one cycle, or wavelength, of sound is called its *period* (Fig. 2.4). Period is measured in seconds and microseconds. It is inversely related to the frequency:

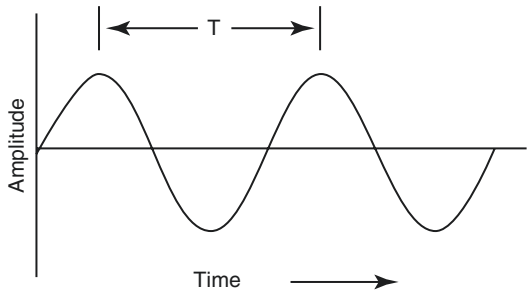

Fig. 2.4 Period of sound. The duration of one wavelength of sound is its period. Horizontal axis represents the time and the vertical axis the magnitude of pressure wave deflections around the baseline

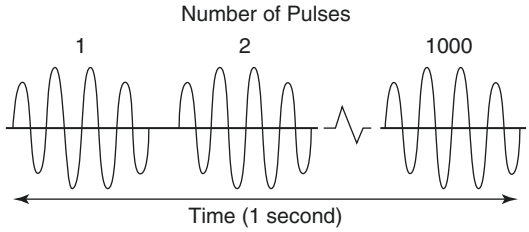

Fig. 2.5 Concept of pulse repetition frequency (PRF). The illustration shows a PRF of 1 kHz (1000 pulses per second)

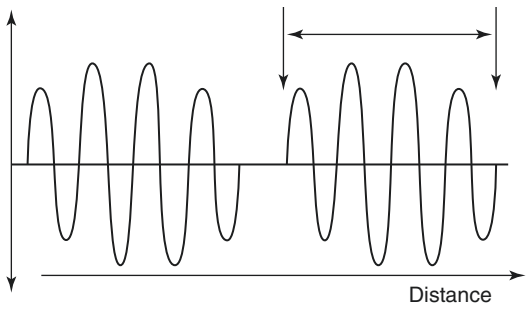

Fig. 2.6 Pulse length, which is the distance in space occupied by one ultrasound pulse. Horizontal axis represents the distance and the vertical axis the pressure amplitude

$$T = 1/f$$

where T is the period, and f is the frequency of sound.

Pulsed Doppler (both spectral and color flow mapping) and pulse echo imaging systems transmit ultrasound waves in pulses. The number of such pulses transmitted per second is known as the *pulse repetition frequency* (PRF) (Fig. 2.5). The length of one ultrasound pulse is known as the *spatial pulse length* (Fig. 2.6). Pulse length varies according to the mode of ultrasound. With pulsed Doppler ultrasound, the pulse length ranges from 5 to 30 cycles. In contrast, the length is much shorter for pulsed echo imaging system, as they generate two to three cycles per pulse.

For pulsed Doppler applications, the PFR limits the highest velocity that can be measured without creating the artifact known as aliasing. This subject is further discussed in Chap. 3.

2.4 Amplitude, Power, Intensity

The maximum variation in pressure generated in a medium by a propagating sound wave is called *pressure amplitude* (Fig. 2.7). Pressure amplitude is directly related to the amount of sound energy emanating from a vibratory source. It is therefore a measure of the strength of sound radiation. The rate of flow of ultrasonic energy through the cross-sectional area of the beam is expressed as its *power.* The *intensity* of a sound wave at a location is the rate of flow of energy per unit of cross-sectional area of the beam at that location. It is therefore power divided by beam cross-sectional area. Pressure amplitude is measured using a device called a hydrophone. Intensity (I) is derived from the pressure amplitude (p) as they are directly related:

$$I = p^2 / c$$

Intensity is expressed by several descriptor parameters based on its peak and average values.

For continuous-wave Doppler ultrasound, intensity is measured as the spatial peak value (I_{sp}) and the spatial average value (I_{sa}). The former is measured usually at the focal point of the beam, the latter at the cross-sectional location of the beam. For pulsed Doppler ultrasound, it is necessary to consider both the spatial and the temporal intensity values. Both peak and average values are measured in various combinations, as follows: spatial peak temporal peak (I_{sptp}), spatial peak temporal average (I_{spta}), spatial average temporal peak (I_{satp}), and spatial average temporal average (I_{sata}). Additional descriptors of pulsed ultrasound intensity include the spatial peak

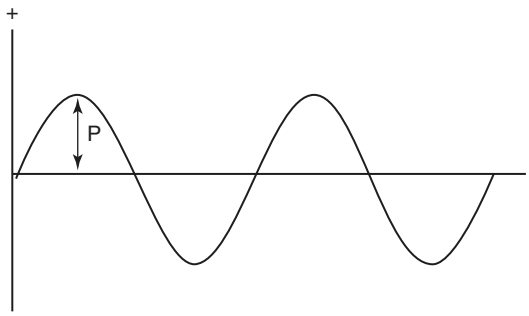

Fig. 2.7 Pressure amplitude of a sound wave. Horizontal axis depicts distance or time. Vertical axis represents variations in the acoustic pressure. The plus and minus signs indicate the positive and negative fluctuations of the pressure, respectively. *P*, the amplitude that is the maximum change in the pressure above or below the baseline value represented by the horizontal line

pulse average intensity (I_{sppa}), which is the intensity at the spatial peak averaged over the pulse length. These measures of sound energy of a transmitted Doppler ultrasound beam are important for biosafety considerations and are discussed in Chap. 6.

2.5 Ultrasound and Piezoelectric Effect

Audible sound frequency ranges from approximately 10 Hz to 20 kHz. Sound with a frequency of more than 20 kHz is inaudible to the human ear and is known as *ultrasound*. With Doppler ultrasound used for medical diagnostics, the commonly employed frequency range is 2–10 MHz. The frequency range for obstetric transducers is 2–5 MHz. To produce vibrations or oscillations at the rate of millions of cycles per second, special materials with piezoelectric properties are used. These piezoelectric elements are solid, nonconducting substances that demonstrate physical properties whose measurements are different along different axes (anisotropic). When compressed in certain directions, these elements undergo electrical polarization, and a corresponding voltage is generated that is proportional to the pressure. Conversely, when such an element is subjected to an electric field, it exhibits mechanical distortion by an amount proportional to the applied field. This phenomenon is known as the *piezoelectric effect* (Fig. 2.8). The piezoelectric effect allows interconversion between sound and electricity and forms the basis for the construction of Doppler and other types of ultrasound transducer. The naturally occurring piezoelectric elements include crystals such as quartz, tourmaline, and rochelle salt. Synthetic ceramic elements employed in the construction of Doppler and other ultrasound transducers are polycrystalline substances consisting of tetravalent metal ions such as zirconium or titanium embedded in a lattice of bigger divalent metal ions such as lead or barium, and oxygen. The most common piezoelectric ceramics include barium titanium trioxide and lead zirconium trioxide. More recently, synthetic single crystals are being developed which include lead zirconate niobate/lead titanate, barium titanate trioxide, and lithium niobate trioxide. These newer single elements demonstrate much greater strain, which is directly related to their performance.

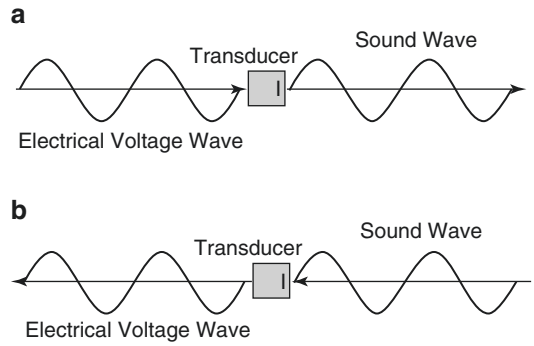

Fig. 2.8 (**a**, **b**) Piezoelectric effect. (**a**) Conversion of the electrical energy to sound energy. (**b**) Conversion of sound to electrical energy

2.6 Characteristics of Sound Transmission in a Medium

The resistance offered by a medium to sound transmission is known as its *acoustic impedance.* The acoustic impedance of a medium is the product of its density and the velocity of sound, and it is measured in rayl units. Most soft tissues demonstrate only minor variations in their acoustic

impedance [1]. For example, the impedance rayl values for blood, brain, kidney, and muscle are 1.61×10^5, 1.58×10^5, 1.62×10^5, and 1.70×10^5, respectively. In contrast, bones possess a significantly higher acoustic impedance (7.8×10^5). The significance of acoustic impedance lies in the fact that it is the impedance inhomogeneities in tissues that give rise to echoes, which form the basis for ultrasonic imaging and Doppler velocimetry. The boundary between adjacent media with differing acoustic impedance values is called an *acoustic interface.* The characteristics of sound transmission change at the interface. Such changes include reflection and refraction. The amplitude of reflection is directly proportional to the magnitude of impedance difference at the interface. However, even minor differences in acoustic impedance generate echoes. When impedance inhomogeneity exists across an acoustic interface, a variable portion of an ultrasound beam is reflected. At most soft tissue interfaces, it involves only a small portion of the ultrasound energy, with the rest being transmitted and reaching the medium beyond the interface (Fig. 2.9). In contrast, thick bone offers a large acoustic mismatch in relation to the surrounding soft tissue medium, so a major portion of the ultrasound energy is reflected. This situation inevitably results in markedly diminished transmission of the beam, and the resultant "acoustic shadow" affects optimal imaging of structures lying posterior to the bone. At most tissue interfaces, an incident beam is echoed in different directions, a process known as *diffuse reflection.* In relation to Doppler ultrasonic reflections, however, an entirely different phenomenon occurs, known as *scattering*. This phenomenon is discussed below.

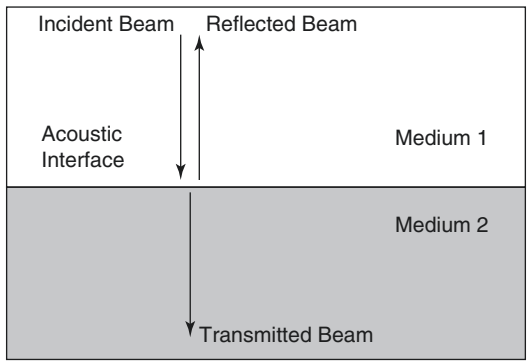

Fig. 2.9 Reflection and transmission of sound at the interface acoustically mismatched in medium 1 and medium 2. In this example, the beam strikes the interface perpendicularly

When an ultrasound beam travels with an oblique angle of incidence across an interface, the beam path deviates and the angle of transmission differs from the angle of incidence (Fig. 2.10). The phenomenon is similar to refraction of light. Refractive deviation in the beam path may compromise image quality. For pulsed Doppler duplex applications, where two-dimensional gray-scale imaging is used for placing the Doppler sample volume in deep vascular locations, refraction may lead to error. However, the propagation speed of sound does not vary appreciably in most soft tissues; therefore only minimal refraction occurs at most tissue interfaces. For example, an ultrasound beam passing through a muscle-blood interface at an incident angle of 30° undergoes only a 0° 47′ refractive deviation [2].

Progressive decline in the pressure amplitude and intensity of a propagating ultrasonic wave is known as *attenuation.* Attenuation is caused by many factors, including absorption, scattering, reflection, and wave-front divergence. *Absorption*

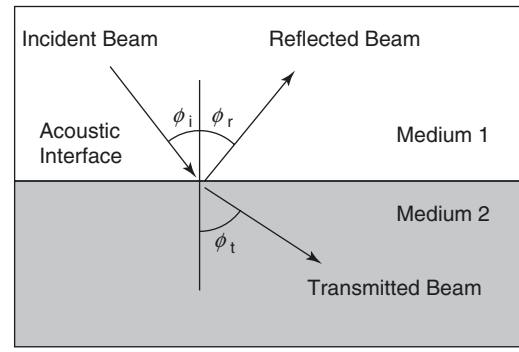

Fig. 2.10 Reflection, refraction, and transmission of sound. The beam, in this example, is encountering the acoustic interface obliquely. A portion of the incident sound is reflected back, and the rest is transmitted. The angle of reflection (Φ_r) equals the angle of incidence (Φ_i). The transmitted sound is refracted. The angle of refraction (Φ_t) depends on the angle of incidence and the propagation speeds of sound in medium 1 and medium 2

is the phenomenon whereby sound energy is converted to heat and is therefore responsible for thermal bioeffects. Attenuation is also affected by the transmitting frequency of a transducer: the higher the frequency, the greater the attenuation. It limits the use of high-frequency transducers for Doppler interrogation of deep vascular structures. These considerations influence the choice of a transducer for a specific use. Thus, for Doppler examinations of fetal circulation, a 5-MHz transducer may be less efficient for obtaining adequate signals than a 2-MHz transducer.

2.7 Doppler Effect

The Doppler effect is the phenomenon of observed changes in the frequency of energy wave transmission when relative motion occurs between the source of wave transmission and the observer. The change in the frequency is known as the Doppler frequency shift, or simply the Doppler shift:

$$f_d = f_t - f_r$$

where f_d is the Doppler shift frequency, f_t is the transmitted frequency, and f_r is the received frequency. When the source and the observer move closer, the wavelength decreases and the frequency increases. Conversely, when the source and the observer move apart, the wavelength increases and the frequency decreases. The Doppler effect is observed irrespective of whether the source or the observer moves (Fig. 2.11). The principle is applicable to all forms of wave propagation. The utility of the Doppler effect originates from the fact that the shift in frequency is proportional to the speed of movement between the source and the receiver and therefore can be used to assess this speed. The Doppler effect is observed irrespective of whether the source or the observer moves.

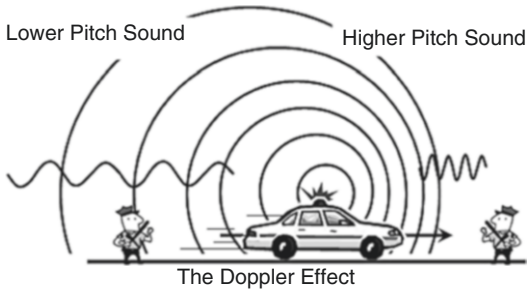

Fig. 2.11 Graphic depiction of the Doppler shift when a source of sound transmission moves away or toward a stationary observer

2.8 Doppler Ultrasound

For sound transmission, the Doppler shift sound is of a higher frequency when the source and the receiver move closer and of a lower frequency when they recede. The phenomenon of the Doppler effect is also observed when an ultrasound beam encounters blood flow (Fig. 2.12). With blood circulation, millions of red blood cells (RBCs) act as moving scatterers of the incident ultrasound. In this circumstance, the eryth-

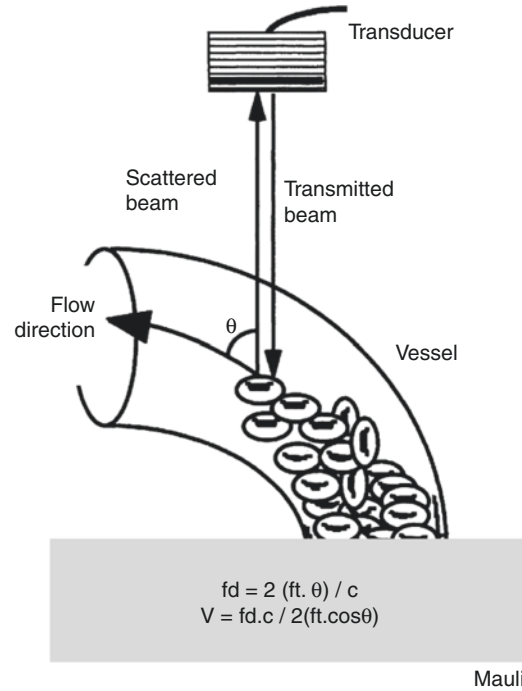

Fig. 2.12 Doppler effect when an ultrasound beam interrogates circulating blood. f_d Doppler shift, f_t transmitted beam, V velocity of blood flow, c speed sound propagation in tissue, θ angle of incidence between the ultrasound beam and the direction of blood flow

rocytes act first as moving receivers and then as moving sources [3], forming the basis for the Doppler equation:

$$f_d = 2f_t \cdot v / c$$

where f_d represents the Doppler frequency shift, f_t the frequency of the incident beam (transducer frequency), v the velocity of the scatterer in a given direction, and c the propagation speed of sound in the medium. Note that the transmitted ultrasound undergoes double Doppler shift before returning to the receiving transducer, the scatterer acting first as a receiver and then as a transmitter. This phenomenon accounts for the factor of 2 in the above equation.

If the direction of the incident beam is at an angle (θ) to the direction of blood flow, the v in the Doppler equation is replaced by the component of the velocity in the direction of the flow (obtained by the cosine of the angle, cosθ):

$$f_d = 2f_t \cdot \cos\theta \cdot v / c$$

To determine the velocity of the scatterer, the equation can be rewritten as follows:

$$v = f_d \cdot c / 2f_t \cdot \cos\theta$$

Thus, if the angle of beam incidence and the Doppler shift are known, the velocity of blood flow is also known, assuming that the transducer frequency and the velocity of sound in tissue remain relatively constant (Fig. 2.12). The above equation forms the basis for clinical application of the Doppler principle.

2.9 Backscattering

We briefly alluded to a special category of sound reflection called scattering. The process of ultrasonic scattering is analogous to scattering of light by gas molecules and is known as *Rayleigh scattering* [4, 5]. Light so reflected is called Tyndall light and is responsible for the blue sky. Interestingly, it was inquiry into the cause of blue sky at the turn of the century by a group of scientists, including Lord Rayleigh and Tyndall, which led to our understanding of this phenomenon [6]. Rayleigh scattering occurs when energy waves traveling through a medium encounter reflectors whose size is much smaller than the wavelength of the propagating energy; a portion of the energy is then reflected in all directions. The scattered energy wave is spherical in shape irrespective of the shape of the scatterer.

One characteristic of Rayleigh scattering is that the power, or intensity, of the scattered energy (I) is proportional to the fourth power of the frequency (f).

$$I \sim f_4$$

The frequency dependence of scattering power has important consequences for selecting the appropriate transducer frequency for Doppler applications. Increasing the incident ultrasonic frequency immensely amplifies the power of the reflected echoes. Thus, raising the transducer frequency from 3 to 4 MHz leads to fivefold augmentation of the scattered echo intensity. Ironically, this increase also limits the ability of the transducer to sample deep-lying circulations, as a higher frequency leads to greater attenuation. Obviously, one must balance these contrary effects when selecting the optimal frequency for a specific application. For example, for most fetal Doppler insonations via the maternal abdomen, transducers with a frequency range of 2–4 MHz are commonly used to reach the deep-lying vascular targets in the fetus. In contrast, with a transvaginal approach, where the transducer lies in close proximity to pelvic structures, such as the uterine or ovarian arteries, the use of a higher frequency (e.g., 5 MHz) increases the Doppler sensitivity without significant attenuation of the beam.

When a propagating ultrasonic wave encounters an acoustic interface, reflection occurs. Scattering takes place when the size of the interface is smaller than the incident sound wavelength. Such an interface is known as a *point target*. In regard to Doppler shift, the scatterer is significantly smaller than the wavelength and is in motion. The Doppler-shifted ultrasound reflecting from such a moving scatter propagates in all directions (Fig. 2.13). Obviously, it also reaches any receiving transducer at the source of transmission. The process of scattered ultrasound

returning to the source-receiver is called *backscattering*.

It is well-accepted that the primary sources of scattering in blood are the circulating RBCs [7]. These cells are so numerous that the contribution of the other formed elements of blood, such as white blood cells and platelets, to scattering ultrasound is inconsequential. An RBC has a biconcave discoid shape with a mean diameter of 7.2 μm and a mean thickness of 2.2 μm. In comparison, the wavelength of Doppler ultrasound for diagnostic applications varies from 1540 μm to 154 μm, corresponding to 1–10 MHz transducer frequency. As is apparent, the RBCs are several magnitudes smaller than the wavelengths, so they can be regarded as point targets. In reality, however, circulating erythrocytes do not act as discrete scatterers but as volumes of randomly distributed point targets. The number of RBCs in such a scattering volume fluctuates around a mean value and causes fluctuations in the scattering power. Turbulent blood flow increases fluctuations in the RBC concentration and is therefore associated with increases in the scattering power and consequently the power of the Doppler shift signal [7]. In regard to whole blood, it has been experimentally demonstrated that the scattering power becomes maximum at a hematocrit range of 25%–30% [7]. At higher hematocrit values, the scattering behavior of blood becomes more complex as the RBCs become too crowded and can no longer be treated as randomly distributed scatterers.

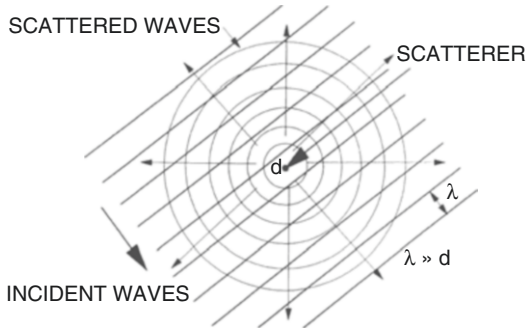

Fig. 2.13 Phenomenon of scattering. *d* Scatter, *λ* wavelength of the incident beam. The large arrow shows the direction of propagation of the incident ultrasound. The smaller arrows radiating from d indicate the directions of scattering. Note that scattering occurs when the wavelength is much greater than the size of the reflector ($\lambda \gg d$)

In addition to hematocrit, scattering is also affected by the state of red cell aggregation. Spatial variations in the flow field can result in changes in the variance of red cell packing and backscattering cross section which will influence the Doppler power at a given frequency [8]. In this circumstance, the mean Doppler frequency will not necessarily be proportional to the mean flow through the sample volume and may affect volumetric flow quantification and the power mode display of color Doppler. Scattering is also dependent on certain characteristics of the transmitted ultrasound including the frequency and the angle of insonation [9]. The phenomenon is a complex subject and a comprehensive review is beyond the scope of this chapter.

2.10 Magnitude of Doppler Shift

Relative velocities of the sound and the scatterers are important determinants of the magnitude of the Doppler frequency shift. In regard to blood flow, the speed of RBCs is significantly less than the speed of sound in a biologic medium. Consequently, the Doppler shift is much smaller than the incident ultrasonic frequency. Assuming a sound propagation speed of 1540 m/s in soft tissues, the Doppler shift for a given blood flow speed and the transducer frequency can be calculated from the Doppler equation. This exercise is illustrated in Table 2.2, which lists the Doppler frequency shifts for most obstetric transducer fre-

Table 2.2 Doppler frequency shifts for various transducer frequencies at three blood flow velocities and an insonation angle of 0°

	Doppler shift at three flow velocities (kHz)		
Transducer frequency (MHz)	At 25 cm/s	At 50 cm/s	At 75 cm/s
2	1.3	0.7	1.9
3	1.9	1.0	2.9
4	2.6	1.3	3.9
5	3.2	1.6	4.9
6	3.9	1.9	5.8
7	4.6	2.3	6.8

quencies (2–7 MHz) at blood flow speeds of 25, 50, and 75 cm/s. As is evident, the frequency shifts are approximately 1/1000 of their corresponding transducer frequencies. Furthermore, the Doppler-shifted sound is well within the limits of human hearing as its frequency is in the kilohertz range.

2.11 Angle Dependence of Doppler Shift

It is evident from the Doppler equation that the greatest frequency shift occurs when the transmitted ultrasound beam is parallel to the flow axis. When the beam intersects the vessel, it is the component or the vector of the RBC velocity along the beam path that contributes to the Doppler effect. This vector is determined from the cosine of the beam-vessel angle and is incorporated into the Doppler equation (see above). As the angle increases, the frequency shift proportionately decreases. When the angle exceeds 60°, the fall in the Doppler-shifted frequency exceeds 50%. When the angle reaches 90°, the Doppler shift is virtually nonexistent. However, minimal Doppler signals may still be generated because of beam divergence and nonuniform flow in the vessel.

As the angle of insonation decreases, the frequency shift increases; and maximum Doppler shift is obtained, at least in theory, when the angle becomes zero with the ultrasound beam being parallel to the flow axis. In reality, however, as the angle drops below 30°, significant reflection of the incident beam occurs at the interface between blood and the vessel wall, and the Doppler sensitivity becomes seriously compromised. In contrast to general vascular applications, the phenomenon of loss of sensitivity with a low angle is not observed in cardiac Doppler insonations. With fetal and postnatal Doppler echocardiography, optimal Doppler waveforms are obtained when the incident beam is aligned with the vessel axis in pulmonic or aortic outflow tracts (Fig. 2.14). Apparently, complex cardiac anatomy does not reflect the incident beam the same way as do peripheral vessel walls.

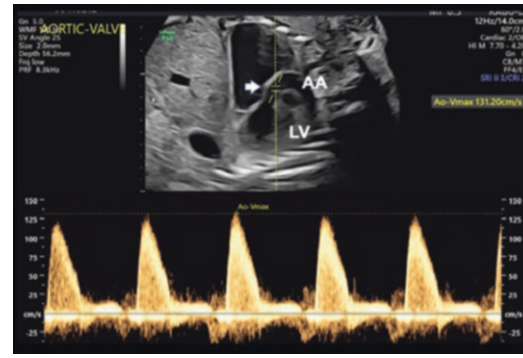

Fig. 2.14 Duplex Doppler interrogation. Top: Spectral Doppler flow image of the fetal ascending aorta (AA). LV = left ventricle. The vertical line is the cursor representing the beam path. The Doppler sample volume (two short horizontal lines, white arrow) is placed in AA just distal to the aortic valve. Bottom: Doppler shifts from AA. The left and right margins of the Doppler panel show the blood flow velocity scale in centimeters per second. The peak systolic velocity (131.20 cm/s) is shown in the upper panel

As is apparent from the Doppler equation, the estimation of blood flow speed from the Doppler shift requires a reliable measurement of the angle of insonation. Although the Doppler shift is angle-dependent, flow speed calculated from the Doppler shift is not affected, in theory, by the magnitude of the angle. This situation, however, assumes ideal circumstances—such as insonation of a uniform flow in a straight vessel of uniform diameter—which one does not encounter often in reality. Therefore, the desirable angle range for flow speed estimation remains, as indicated above, 30°–60°. Measurement of the angle in a duplex Doppler device is usually accomplished with apparent ease. The operator uses the two-dimensional image to align an angle indicator cursor with the vessel axis (the presumed flow axis) and determines the angle it incurs with the beam path indicator cursor. The device computes this angle and produces the velocity information in real time. The procedure is subjective, and the precision of the measurement obviously depends on operator skill.

Determination of the flow velocity may be clinically useful during fetal echocardiographic examination, as abnormal flow velocities in the pulmonary artery, aorta, or ductus arteriosus may assist in identifying structural or functional abnormalities. A reliable measurement of the Doppler angle is also a requirement for measuring volumetric blood flow and inaccuracies in measuring the angle and can introduce significant errors in this measurement. Finally, an optimal angle is important for an appropriate interpretation of Doppler waveforms from the arteries that demonstrate continuing forward flow during the end-diastolic phase, as a large angle may artificially reduce the magnitude of the end-diastolic frequency shift. This point is of critical importance when assessing an umbilical arterial circulation in which a reduced or absent end-diastolic frequency shift may indicate fetal jeopardy. The challenge of the angle of insonation in Doppler sonography has prompted the development of angle-independent approaches for circulatory investigations; this is further discussed in Chap. 4.

References

1. Goss SA, Johnston RL, Dunn F. Comprehensive compilation of empirical ultrasonic properties of mammalian tissues. J Acoust Soc Am. 1978;64:423–57.
2. McDicken WN. Diagnostic ultrasonics: ultrasonic in tissue. In: Principles and use of instruments. 2nd ed. New York: Wiley; 1981. p. 54–70.
3. Atkinson P, Woodcock JP. Doppler ultrasound. London: Academic Press; 1982.
4. Rayleigh L. Scientific papers 8 and 9. Philos Mag. 1871;41:107, 274, 447.
5. Van de Hulst HC. Light scattering by small particles. New York: Dover; 1982.
6. Van de Hulst HC. Scattering in the atmospheres of the earth and planets. In: Kuiper GP, editor. The atmospheres of the earth and planets. Chicago: University of Chicago Press; 1952.
7. Shung KK, Sigelman RA, Reid JM. Scattering of ultrasound by blood. IEEE Trans Biomed Eng. 1976;BME-23:460–7.
8. Bascom PA, Cobbold RS. Origin of the Doppler ultrasound spectrum from blood. IEEE Trans Biomed Eng. 1996;43:562–71.
9. Fontaine I, Cloutier G. Modeling the frequency dependence (5–120 MHz) of ultrasound backscattering by red cell aggregates in shear flow at a normal hematocrit. J Acoust Soc Am. 2003;113:2893–900.

3 Spectral Doppler: Basic Principles and Instrumentation

Dev Maulik

Spectral Doppler ultrasound velocimetry involves systematic analysis of the spectrum of frequencies that constitute the Doppler signal. This chapter presents a general perspective on Doppler signal analyses and describes the spectral Doppler ultrasound devices commercially available for clinical use. They include continuous-wave (CW) Doppler, pulsed-wave (PW) Doppler, and duplex Doppler devices. Within the realm of obstetric practice, the spectral Doppler is used widely for hemodynamic assessment ranging from the relative simplicity of umbilical flow to the complexity of fetal cardiac circulation. This chapter offers a basic understanding of the implementation of spectral Doppler ultrasound technology.

3.1 Doppler Signal Processing

As discussed in Chap. 2, the Doppler frequency shift signal represents the summation of multiple Doppler frequency shifts backscattered by millions of red blood cells (RBCs). The RBCs travel at different speeds, and the number of cells traveling at these speeds varies as well. As the speed of the scatterers determines the magnitude of the frequency shift and the quantity of the amplitude, the Doppler signal is composed of a range of frequencies with varying amplitude content. Moreover, the total received Doppler signal contains low-frequency and high-amplitude signals generated by tissue movements and high-frequency noise generated by the instrumentation. Obviously, systematic processing is necessary before the Doppler-shifted frequencies can be used clinically. The Doppler signal is processed in sequential steps (Fig. 3.1), consisting of reception and amplification, demodulation and

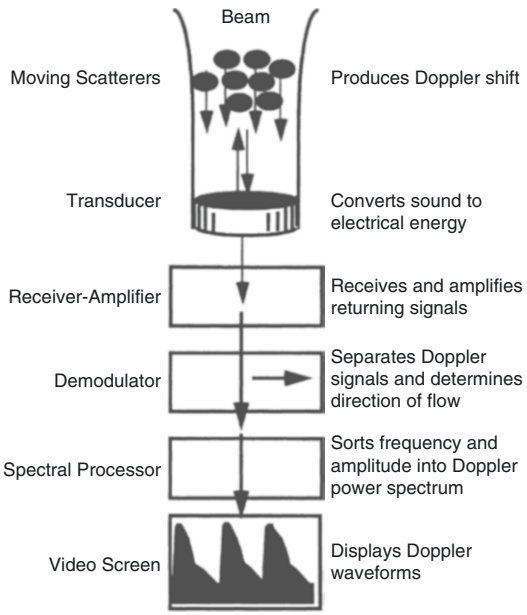

Fig. 3.1 Sequential steps of Doppler signal processing

D. Maulik (✉)
Department of Obstetrics and Gynecology, UMKC School of Medicine/Truman Medical Center, UMKC School of Medicine, Kansas City, MO, USA
e-mail: dmaulik2014@gmail.com

D. Maulik, C. C. Lees (eds.), *Doppler Ultrasound in Obstetrics and Gynecology*,
https://doi.org/10.1007/978-3-031-06189-9_3

determination of directionality of flow, and spectral processing.

3.2 Reception-Amplification

The returning signals are first received and amplified by a radiofrequency (RF) receiving device. Amplification is necessary, as the Doppler frequency shift generates weak electrical voltage at the receiving transducer.

3.3 Demodulation

The total received and amplified echoes contain not only the Doppler-shifted frequencies, but also the carrier frequency, which is the frequency of the incident beam. During the next step, the Doppler-shifted frequencies are extracted from the carrier frequency. This process is known as *demodulation*. There are various methods of demodulation [1], among which the coherent phase quadrature procedure is commonly employed. Phase quadrature implies that one signal is one fourth of a cycle out of phase or delayed compared to the other. With this technique, the incoming signals are mixed with the direct and the one fourth of a cycle (90°) phase-shifted reference electrical signals. With coherent demodulation, the reference signal is supplied by the master oscillator, which is a voltage generator whose primary function is to produce the driving frequency for the source transducer. Demodulation results in generation of a direct and a quadrature output. When the flow is toward the transducer, the direct signal lags the quadrature signal by one fourth of a cycle. When the flow is away from the transducer, the direct signal leads the quadrature signal by one fourth of a cycle.

3.4 Direction Discrimination

The resulting directional separation of the flow, however, is not complete and requires additional processing. The latter is achieved by frequency domain processing in which the demodulator outputs are mixed with the direct and quadrature (phase-shifted by one fourth of a cycle) outputs of a voltage generator. The resultant single-channel output separates the forward and reverse flow signals. With the pilot frequency of the quadrature oscillator providing the baseline, or zero frequency, the flow toward the transducer is presented as the positive Doppler shift and the flow away as the negative Doppler shift. The next step is comprised of removing the undesirable frequency components from the demodulated Doppler signal by digital filtration.

3.5 High-Pass and Low-Pass Filters

The total signal input of a Doppler system is comprised of not only Doppler frequency shift signals from the target vessel, but also low-frequency/high-amplitude signals originating from moving adjacent structures such as vessel walls and cardiac valves. It also contains high-frequency noise contributions from within the instrumentation. Obviously, the frequencies from the extraneous sources represent error components of the total signal, and their reduction or elimination improves the signal quality. Electronic digital filters are used to accomplish this objective. By and large, two types of filter are used: a high-pass filter and a low-pass filter.

The purpose of a high-pass filtering system is to eliminate the extrinsic low-frequency components of Doppler signals, which arise predominantly from the vessel walls or other adjacent slow-moving structures (Fig. 3.2). For peripheral vascular applications, this type of processing often improves the signal quality. Such low-frequency signals may also originate from the slow-moving boundary layer of blood flow adjoining the vascular wall. Moreover, with low-impedance circulations where forward flow continues through the end of the diastolic phase, the important end-diastolic velocity information is lost, which may lead to the erroneous inference of compromised or absent end-diastolic velocity. The importance of this situation can be appreciated from the fact that absent or reverse end-diastolic flow is associated with high perina-

tal mortality and morbidity. Obviously, for most fetal applications, the high-pass filter should be either turned off or kept at the lowest setting, preferably at 50 Hz and not exceeding 100 Hz. With most Doppler instruments, the high-pass filter is adjustable.

A low-pass filter allows frequencies only below a certain threshold to pass, thereby removing any frequencies higher than that level (Fig. 3.2). This threshold is set higher than the maximum frequency shifts expected in a circulation. Such low-pass filters, in general, improve the signal-to-noise ratio. However, if the low-pass filter is set at an inappropriately low level, it may eliminate valuable high-frequency information from a high-velocity circulation, which in turn leads to underestimation of the maximum and mean frequency shifts.

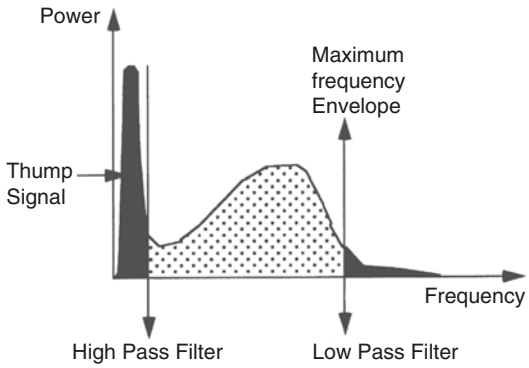

Fig. 3.2 Doppler amplitude-frequency (power) spectrum illustrating the concept of high- and low-pass filtering. *Vertical axis* represents the amplitude or the power of the spectrum. *Horizontal axis* represents the frequency scale. The *left dark area* of the spectrum indicates signals arising from slow-moving tissue structures such as the vessel wall (thump signal). The *right dark area* shows high-frequency noise in the spectrum. The *vertical downward arrows* indicate the frequency cutoff levels of the high- and low-pass filters

3.6 Doppler Spectral Analysis

The steps described above generate demodulated and filtered Doppler frequency shift signals displayed as a complex, uninterpretable waveform consisting of variations of amplitude over time (Fig. 3.3). Spectral analysis converts this waveform to an orderly array of constituent frequencies and corresponding amplitudes of the signal. The amplitude approximately represents the number of scatterers traveling at a given speed and is known as the *power of the spectrum*. A full spectral processing that provides comprehensive information on both the frequency and its average power content is called the *power spectrum analysis.* As circulation is a pulsatile phenomenon, the speed of flow varies with time, as does the Doppler frequency shift generated by the flow. Spectral processing must therefore estimate temporal changes in the Doppler power spectrum.

Of the various approaches for spectral processing, Fourier analysis and autoregression techniques are commonly used at present. The Fourier-based approaches are usually used for Doppler spectral analysis, whereas autoregression techniques are usually employed for two-dimensional (2D) Doppler flow mapping.

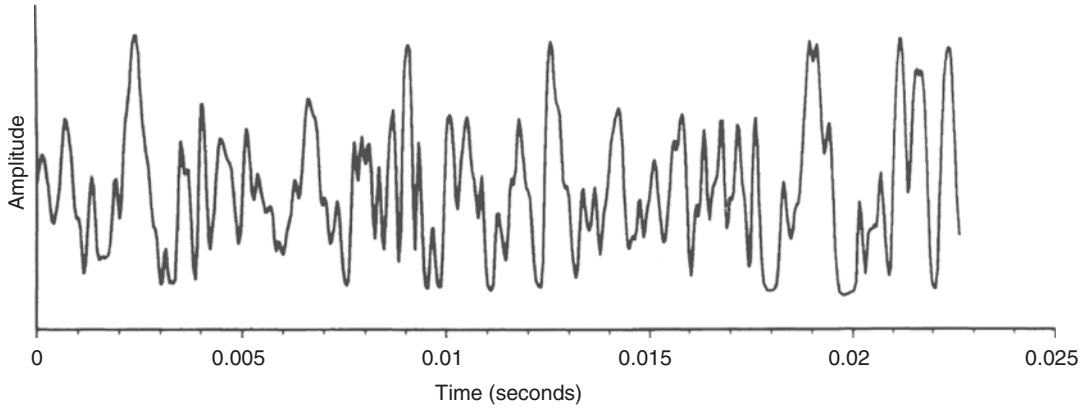

Fig. 3.3 Demodulated Doppler signal prior to spectral processing. The signal was derived from the umbilical arteries

3.7 Fourier Transform Spectral Analysis

Fourier transform is a powerful mathematical technique for spectral analysis of constantly repeating cyclic phenomena, such as alternating electrical current, sound waves, or electromagnetic waves. Baron Jean Baptiste Joseph Fourier, a French mathematician of the Napoleonic era, first described this approach in 1807. The process breaks down a complex periodic signal or waveform into its constituent frequencies of specific amplitudes and phases (Fig. 3.4). The spectrum of a periodic signal, such as that obtained from Doppler insonation, consists not of discrete values but of a continuous function distributed over the range of the constituent frequencies. For practical implementation, however, samples are drawn, so a finite, or discrete, series of frequency points are chosen for analysis. It is called the *discrete* Fourier transform. The *fast* Fourier transform (FFT) is a computer programming sequence for rapid digital implementation of the discrete Fourier transform [2]. FFT processing significantly reduces computational need and is a highly effective tool for power spectral analysis of the Doppler signal [3, 4]. FFT-based Doppler analysis has been used extensively for assessing various circulatory systems, including the carotid [5] and umbilical arterial [6] hemodynamics; and it is the current industry standard for Doppler ultrasound devices used for medical diagnostic applications. The number of discrete frequency components usually analyzed varies between 64 and 512. Maulik et al. described a 256-point FFT analysis for umbilical arterial velocimetry yielding a frequency resolution of 31.25 Hz (1.23 cm/s) [7]. The initial step involves sampling the demodulated signal at given intervals and then digitizing the sampled signals, converting them to numeric values. It is achieved by an analog-to-digital converter. For the next step, the digitized data are processed by the FFT processor, which determines the power spectrum of the sample. Each spectrum is computed over a time window, and a number of consecutive overlapping time windows are averaged to prevent spectral loss. This procedure, regrettably, also compromises the spectral resolution. FFT-derived power spectrum is an approximation of the true spectrum, is relatively noisy, and demonstrates a considerable amount of variance. The latter can be reduced to some extent by various windowing and averaging techniques. Figure 3.5 shows a three-dimensional (3D) display of the Doppler power spectrum from the umbilical artery generated by FFT processing.

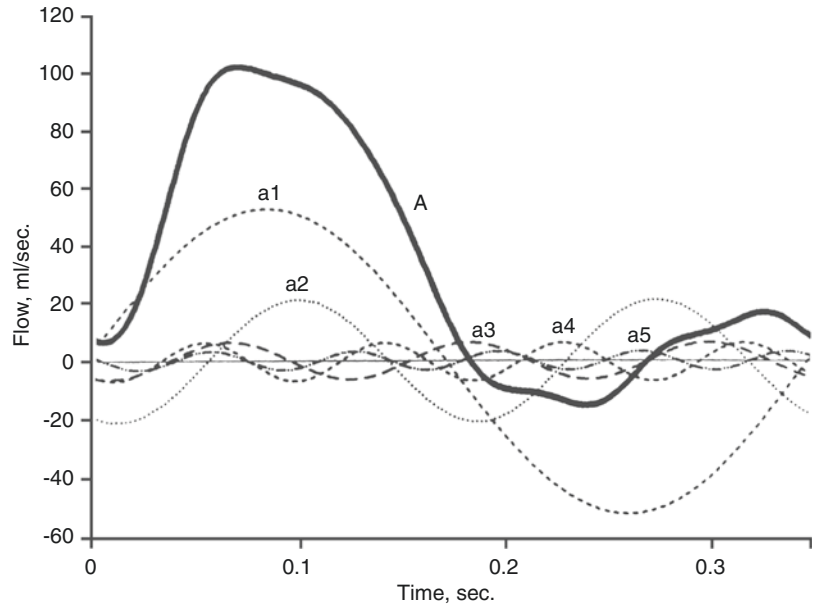

Fig. 3.4 Principle of Fourier transform analysis. The complex flow waveform (*A*) is transformed into its constituent since waves of different frequencies and phases (*a1*, *a2*, *a3*, *a4*, *a5*). *Vertical axis* shows the flow magnitude, and *horizontal axis* shows time. The process converts a time domain phenomenon into a frequency domain phenomenon

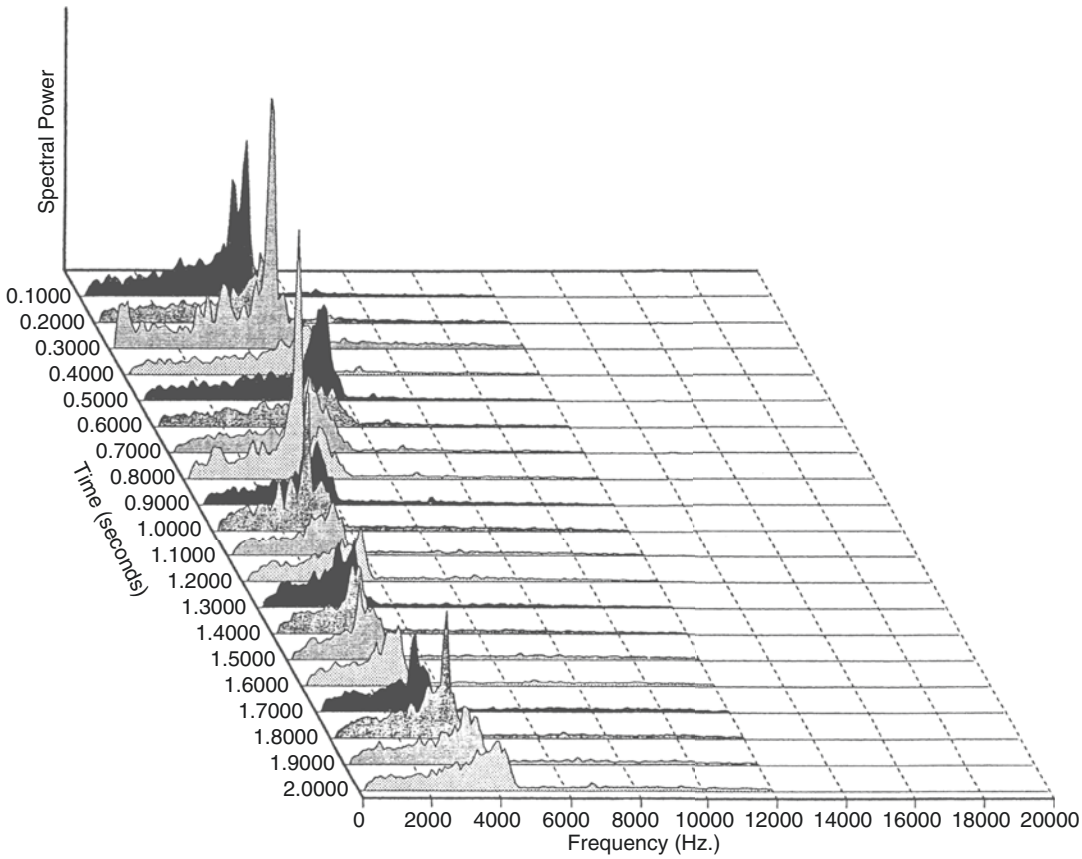

Fig. 3.5 Three-dimensional plot of Doppler power spectrum generated by fast Fourier transform analysis. The spectrum was obtained from the umbilical circulation

3.8 Limitations of FFT Spectral Analysis

There are basic limitations of the FFT approach for spectral processing of the Doppler signal. They include spectral variance and intrinsic spectral broadening.

3.8.1 Spectral Variance

The Doppler frequency spectrum from an arterial circulation varies with the changing hemodynamics of the cardiac cycle. Therefore, the duration of the Doppler signal sample for FFT analysis during which the flow condition, and therefore the power spectrum, can be considered unchanging is limited. For an arterial circulation, it is usually 10–20 ms. In the fetus, the assumption of the spectral nonvariance may be valid for only 5 ms because the faster fetal heart rate produces faster temporal changes in the blood flow speed and in the power spectral density. A shorter temporal length of the sample ensures spectral nonvariance. However, the shorter the duration of the Doppler data segment, the worse is the frequency resolution. A signal segment of 5 ms gives a resolution of only 200 Hz, whereas increasing the duration to 20 ms improves the resolution to 50 Hz. Prolonging the duration, however, introduces uncertainty regarding the constancy of the power spectrum density. Under this circumstance, FFT processing does not function reliably, as it is based implicitly on the assumption of spectral constancy for the duration of the sample.

3.8.2 Intrinsic Spectral Broadening

When a single scatterer moves at a constant speed across an ultrasound beam of limited width, the resultant Doppler spectrum has a range of frequencies instead of a single frequency. Because the phenomenon of broadening the Doppler spectrum is caused by the inherent properties of the measurement system, it is known as *intrinsic spectral broadening* (also *transit time broadening*). Spectral broadening mostly encompasses the following phenomena: (1) transit time broadening caused by the inhomogeneity of the ultrasound field causing amplitude fluctuations of the returning echo; this produces a range of frequencies distributed around the centroid Doppler shift frequency; (2) geometric broadening which results from the changing angles of insonation incurred by the scatterer as it moves across the beam; (3) nonstationary broadening caused by the changes in velocity during the sampling time; and (4) velocity gradient broadening originating from the changes in velocity within the sampling volume [8]. The problem of spectral broadening is compounded by the contribution from multiple moving RBCs traversing the ultrasound beam. The RBCs do not act as discrete scatterers but as volumes of randomly distributed scatterers. The number of RBCs in such a scattering volume in an ultrasonic field varies continually and randomly around a mean value, which causes swings in the scattering power. The consequences are similar to the spectral broadening of the Doppler signal observed with a single moving scatterer.

Spectral broadening is affected by the beam width, pulse length, and angle of insonation. Wider and more homogeneous beams, longer pulses, and smaller angles of insonation narrow the spectral spread. Obviously, the situation is worse with the short-gate pulsed Doppler ultrasound applications, where a scatterer can traverse only a part of the beam of a transmitted short pulse. The consequent transit time broadening effect generates a significant degree of ambiguity regarding the true distribution of velocity in the sample volume. The main clinical significance of spectral broadening is that it potentially compromises the precision of the maximum frequency shift envelope (Fig. 3.6). The mean frequency definition, however, is not affected, as the distribution of the frequencies around the mean shift is symmetric.

3.9 Analog Fourier Spectral Analysis

Analog Fourier spectral analysis allows fast spectral processing of the Doppler signals utilizing analog techniques as opposed to the digital approach of FFT. One such implementation, known as Chirp Z analysis, is also a discrete Fourier transform-based method and requires less computing power and offers a wide dynamic signal processing range.

3.10 Autoregression Analysis

Although Fourier-based methods dominate, alternative approaches for Doppler spectral processing are available. These methods are theoretically capable of eliminating many of the inherent disadvantages of the FFT method. Kay and Marple comprehensively described the autoregressive approach for spectral analysis [9]. Such procedures have been widely used for spectral analysis of speech and other periodic phenomena. The autoregression method acts as a digital filter and assumes the signal at a given time to be the sum of the previous samples. In contrast to power quantification of the discrete frequencies in the FFT analysis, autoregression allows power quantification of all the frequencies of the spectrum. Moreover, it produces cleaner spectra and better frequency resolution than those generated by FFT processing.

We have evaluated autoregressive (AR), moving average (MA), and autoregressive moving average (ARMA)-based spectral processing approaches as possible alternatives to the FFT analysis [10]. Compared to the FFT processing, these parametric techniques produce cleaner spectra. The AR model estimates maximum frequency well, and the MA model indicates velocities at which most scatterers (erythrocytes) travel.

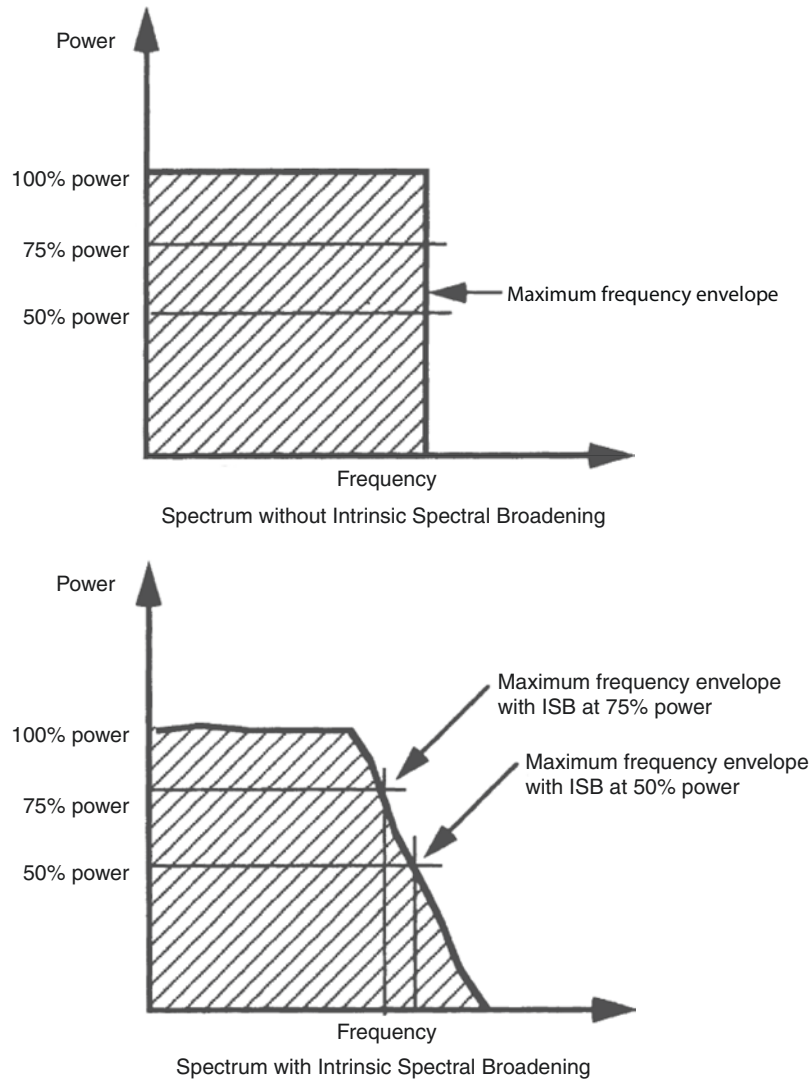

Fig. 3.6 Amplitude-frequency spectrum from a circulation with a parabolic flow velocity profile. *Top*: Ideal spectrum with an even distribution of amplitudes (scattering power) at various frequencies, indicating erythrocytes traveling at various speeds. *Bottom*: Effect of spectral broadening on the maximum frequency definition of the same spectrum. *ISB* intrinsic spectral broadening

The ARMA shows the potential of producing superior spectral analysis by combining the advantages of the AR and MA models. These parametric methods depend on appropriate system identification of the data.

3.11 Continuous-Wave Doppler Ultrasonography

A continuous-wave (CW) Doppler transducer continuously transmits and receives ultrasonic signals. A CW Doppler system essentially consists of a double element transducer for both emitting and receiving signals, a radiofrequency receiver amplifier for the acquisition and amplification of the electrical voltage signals from the receiving transducer, a voltage generator that provides the driving frequency of the emitting transducer and the reference frequency for the demodulator, a demodulator that extracts the Doppler-shifted frequencies from the total echo signals, and a direction detector that completely separates the signals of the forward flow from those of the backward flow. Details of these components of Doppler signal analyses and subsequent spectral processing are described at the outset of this chapter. The transducer assembly

encases two piezoelectric elements; one continuously emits ultrasound and the other continuously receives the backscattered echoes (Fig. 3.7). For most transducers, the emitting and receiving elements are either rectangular or half-circle in shape. There may also be a concentric arrangement with a central circular element surrounded by a ring element. The elements are positioned in such a manner that their faces sustain a suitable angle to each other, and consequently there is an overlap between the transmitted ultrasound field generated by the emitting element and the sensitive zone for the receiving element.

A CW Doppler setup does not have range discrimination, and any movement within the sensitive region causes backscattering and consequently Doppler shift of the incident beam. If the beam interrogates more than one vessel, the Doppler signals from all the vessels merge to form a composite display. The only discrimination that exists is that the signals from a deep location are more attenuated because of the longer transmission path through tissues. A CW system is sensitive also to the movements of nonhemodynamic objects in its path, such as pulsating vascular walls or moving cardiac structures. These sources of Doppler shift produce high-amplitude/low-frequency signals, which may overwhelm a receiver–amplifier of limited dynamic range. This situation leads to loss of important hemodynamic signals. The problem can be resolved by ensuring an extended dynamic range of the receiver and by use of an appropriate high-pass filter, as described above.

Continuous-wave Doppler ultrasound instruments are used extensively in obstetrics for nonvelocimetric applications, such as fetal heart rate detection and external electronic fetal heart rate monitoring. For velocimetric applications, CW devices with a spectral analyzer have been used for insonation of the umbilical arteries and often the uterine arteries. Despite the inherent absence of range discrimination, Doppler signals from the umbilical or uterine arteries can be obtained with relative ease. However, CW Doppler instruments are infrequently used at present for velocimetric assessment in obstetrical practice.

3.12 Pulsed-Wave Doppler Ultrasonography

With the PW Doppler setup, a single transducer crystal emits pulses of short bursts of ultrasound energy (Fig. 3.8). Between the pulses, the same crystal acts as the receiving transducer. As the velocity of sound in soft tissues is virtually constant, the time interval between transmission and reception of the ultrasound beam determines the distance, or range, of the target area from the transducer. Thus, the location of the target area can be selected by varying this time delay. This process is known as *range gating*.

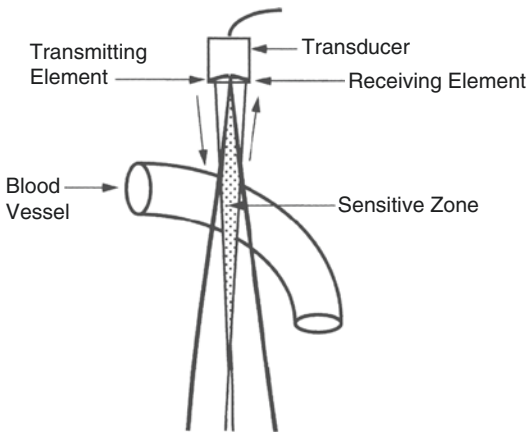

Fig. 3.7 Principle of continuous-wave Doppler transducer

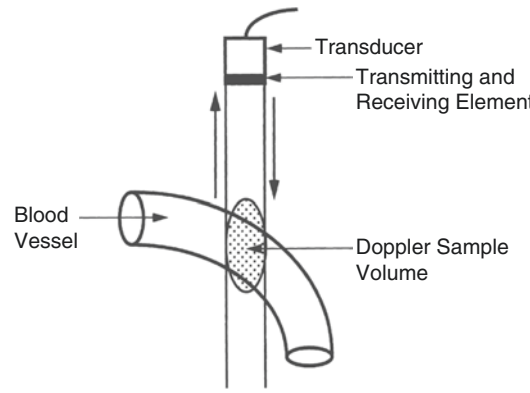

Fig. 3.8 Principle of Pulsed-wave Doppler transducer

A simplified description of the pulsed Doppler ultrasound system is presented: As mentioned above, the same transducer crystal acts as both the transmitter and the receiver of ultrasound signals. A master oscillator generates a reference signal at the resonant frequency of the transducer. An electronic gate controls the transmission of the signal to the transducer, so a pulse of only a few cycles reaches it. The rate at which the pulses are generated (pulse repetition frequency) is determined by an electronic device called the pulse repetition frequency generator. The generator also controls the delay gate, which in turn controls the range gate and therefore the time interval between the ultrasonic transmission and reception. As described above, a demodulating system extracts the Doppler frequency shifts from the carrier frequency. The Doppler signals thus produced are stored, integrated, and updated with the signals from the next pulse. After appropriate filtering, the signals are now ready for audio output and spectral analysis. A more complete review of the pulsed Doppler system has been presented by Evans and associates [1].

3.13 Doppler Sample Volume

The 3D region in the path of the transmitted ultrasound beam from which the frequency shift signals are obtained is called the Doppler *sample volume* (DSV). For the CW Doppler system, the totality of the superimposed region represents the DSV and is therefore of no relevance. For the PW Doppler system, the range-gated zone from which the backscattered echoes are received constitutes the sample volume. The DSV is an important consideration for PW Doppler applications because its location and axial dimension can be controlled by the examiner. The examiner therefore has the ability to interrogate a target area of appropriate location and size and to obtain more precise spatial velocity information. This subject is discussed further below.

The length of the DSV along the ultrasonic beam axis is known as its axial dimension. The lateral measurable limits of the beam, perpendicular to the beam axis, define its transverse dimension, or width. The shape resembles a pear or a teardrop (Fig. 3.9). The axial dimension is determined by the pulse length or duration as sensed by the receiving transducer and is therefore dependent on the duration of the transmitted ultrasonic pulse and the time window during which the receiver gate is open. As the last two factors are amenable to controlled variations, the axial dimension of the DSV can be altered by the operator. Many current duplex systems allow sample length variations, from 1.5 to 25.0 mm.

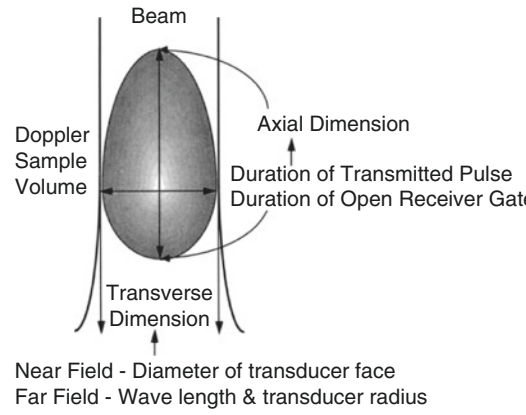

Fig. 3.9 Graphic representation of the Doppler sample volume and the factors controlling its dimensions

The transverse dimension of the DSV is determined by the ultrasonic beam width, which approximates the diameter of the transducer face in the near field. In the far field, the beam progressively diverges. In this circumstance, the angle of beam divergence, which depends on the wavelength and the transducer radius, dictates the transverse dimension of the DSV. Obviously, the width of the DSV is better defined in the near field than in the far field. Consequently, operating in the near field ensures greater certainty of velocity assessment. In contrast to the sample length, the sample width is not amenable to ready manipulation. However, owing to progress in transducer technology, including acoustic focusing, a few instruments allow controlled variations of the beam width in the far field and therefore of the transverse dimension of the DSV.

The dimensions of the sample volume can significantly affect the accuracy of velocity assess-

ment. A sample volume that is large in relation to the dimensions of the target vessel can significantly compromise the range resolution of the measured velocities and lower the signal-to-noise ratio [11]. Conversely, a sample size smaller than the vascular dimension can diminish the sensitivity of the system. Moreover, depending on its relative size and location in the lumen of a large vessel, the assessed velocity profile can be significantly distorted. This subject is further discussed in Chap. 4.

3.14 Artifacts of Spectral Doppler Sonography

Limitations of Fourier-based spectral analysis have been described in a previous section of this chapter. There are additional device-dependent false representations of the Doppler information that may compromise interpretive clarity. These artifacts are discussed herein.

3.15 Nyquist Limit

A major problem of the PW Doppler system is its inherent limitation in accurately representing Doppler shifts from circulations with high-speed flow. A PW Doppler is essentially a sampling tool for a cyclic phenomenon. The sampling rate is the pulse repetition frequency of the Doppler system; the cyclic phenomenon is the Doppler shift frequencies generated by blood flow. The relation between the pulse repetition frequency and appropriate measurement of the maximum frequency shift is dictated by Shannon's theorem on sampling, which states that for unambiguous measurement of a periodic phenomenon the maximum frequency must not exceed half the sampling rate [12], which amounts to a minimum of two samples per cycle of the highest frequency. This maximum frequency threshold is known as the *Nyquist frequency* or *Nyquist limit*. The relation is expressed in the following equation:

$$f_{\max} = f_{\mathrm{pr}} / 2$$

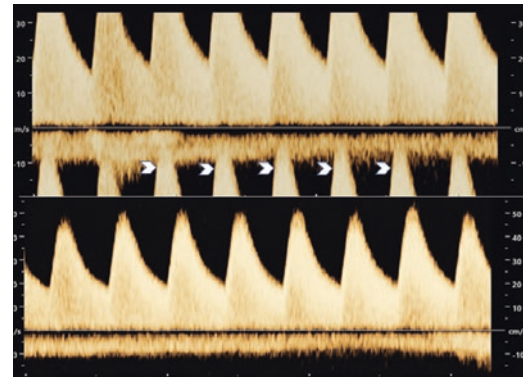

Fig. 3.10 Example of aliasing and its correction. *Top* Aliased waveforms. Note the abrupt termination of the peak portion of the waveforms and the display of these peaks in the *lower part* of the panel below the baseline (*horizontal arrowheads*). *Bottom*: Correction of aliasing of the waveforms by increased pulse repetition frequency

where $f_{\max}$ is the maximum frequency measurable without ambiguity (Nyquist limit), and f_{pr} is the sampling rate or the pulse repetition frequency.

Ambiguity in frequency resolution occurs when the PW Doppler beam interrogates a vessel with such a high blood flow velocity that the maximum frequency content of the Doppler signal exceeds the Nyquist limit. In this circumstance, the frequency cannot be estimated precisely. The frequency component in excess of the limit is subtracted from the Nyquist frequency and is negatively expressed (Fig. 3.10). This phenomenon is known as the *Nyquist effect*. It is also known as *aliasing*, as it produces a representation of the frequency shift that is false in terms of magnitude and direction.

Aliasing does not pose a problem with most fetal PW Doppler measurements, particularly those involving the umbilical and cerebral circulations. However, the phenomenon may be observed when a high-velocity flow is encountered in fetal intracardiac and aortic circulations.

3.16 Implications of Aliasing

Aliasing distorts the spectral display with an abrupt discontinuity at the Nyquist limit. The aliased part of the signal is displaced into the

opposite frequency range of the display (Fig. 3.10). Such distortion also affects the audio output of the Doppler signal. The problem can be corrected in a number of ways.

1. The Nyquist limit can be raised by increasing the pulse repetition frequency, thereby resolving aliasing. However, this measure may introduce range ambiguity, as the Doppler signals from varying depths may be received at the same time.
2. Shifting the baseline resolves the problem by increasing the positive frequency range and decreasing the negative frequency range in the display. It effectively extends the maximum velocity limit, and the spectra are displayed in the same direction without ambiguity.
3. As the operating frequency of the transducer is directly proportional to the magnitude of the Doppler shift, reducing the former may lower the maximum frequency enough for the elimination of aliasing without changing the sampling rate.
4. Increasing the angle of insonation between the Doppler beam and the flow axis reduces the maximum Doppler shift, which may eliminate aliasing.

If these measures are inadequate for resolving aliasing, one may use a CW Doppler setup, which is not limited by the Nyquist frequency and does not produce aliasing, although rane resolution is lost with this approach.

3.17 Range-Velocity Resolution

The maximum range, or depth, at which the velocity of blood flow can be measured accurately by a PW Doppler system is limited. As the distance on the target from the transducer increases, more total time is required for a transmitted ultrasound pulse to travel to the target and the backscattered echo to return to the source. The device must wait this period of time before transmitting the next pulse. If more than one pulse propagates in the target at the same time, the PW Doppler system is incapable of determining the spatial origins of the different returning echoes, resulting in range ambiguity. To avoid this problem, the interpulse interval must be increased with the greater depth of the target vessels. Obviously, the maximum depth at which PW Doppler measurement can be performed without range confusion is limited by the interpulse interval. This relation is shown in the following equation:

$$D_{\max} = c \cdot T_{\mathrm{p}} / 2$$

where $D_{\max}$ indicates the maximum depth of the target vessel, c is the velocity of sound in soft tissue, and T_{p} is the interpulse interval. As the pulse repetition frequency (f_{pr}) is the reciprocal of the interpulse interval, the equation can be expressed as:

$$D_{\max} = c / 2 f_{\mathrm{pr}}$$

The pulse repetition frequency also determines the maximum allowable Doppler frequency shift and therefore the blood flow velocity that can be measured without producing aliasing. It follows therefore that the deeper the PW Doppler sampling location, the lower the maximum measurable velocity.

For the above consideration, it has been assumed that the frequency of the transmitted ultrasound is fixed. However, another variable comes into play when the ultrasound frequency can be changed. The lower the ultrasonic frequency, the lower the attenuation and the greater the maximum depth at which the Doppler measurement can be made. Given a maximum sampling depth, an upper limit is established for the pulse repetition frequency and correspondingly for the Nyquist frequency. It follows therefore that for a given sampling depth and pulse repetition frequency, higher flow velocities can be measured using lower transmitted frequencies. For most obstetric applications, a transducer frequency of 3–4 MHz provides the best Doppler output.

It is interesting to consider the CW Doppler operation as a special case of the pulsed mode, where the pulses are transmitted at an exceedingly high speed, theoretically, at an infinite pulse repetition frequency. Obviously, no range information is available for the received pulses, as it

becomes impossible to relate a given reflection to any particular pulse. However, because of the theoretically infinite pulse repetition frequency, the Nyquist limit for the Doppler frequency shift is also infinite. With the CW Doppler system, then, there are no limits on the maximum measurable velocity.

3.18 Mirror Imaging

With the artifact of mirror imaging, a Doppler device falsely represents unidirectional flow as bidirectional flow. The artifactual flow is depicted as a mirror image of the true flow on the opposite side of the baseline (Fig. 3.11). The problem afflicts both CW and PW Doppler systems and is caused by leakage of the Doppler signal from one directional quadrature channel to the other (quadrature channel cross-talk), so the signals are duplicated. Although there is directional ambiguity, there is no subtraction and relocation of Doppler spectral information as encountered with the Nyquist effect. Quadrature cross-talk can occur with high-velocity flows, excessive gain setting, preponderance of high-amplitude Doppler signals, and paradoxically also with low-velocity flows.

The mirror imaging artifact may be eliminated by decreasing the gain, which reduces the quadrature cross-talk. Increasing the high-pass filter may also improve the problem by removing the high-amplitude/low-frequency signals and decreasing the signal leakage in the quadrature channels. Increasing the angle of insonation may also effectively prevent quadrature leakage while interrogating high-speed circulations. Finally, prior knowledge of the target circulation should prevent erroneous interpretation of the Doppler tracing.

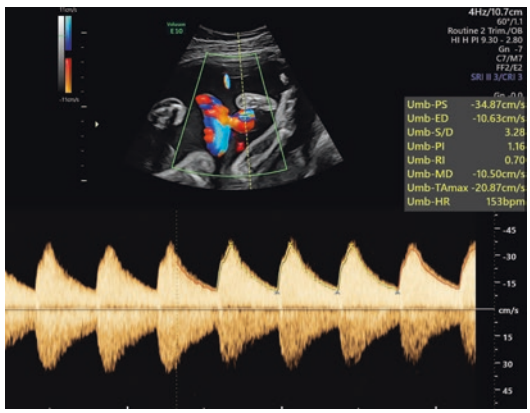

Fig. 3.11 An example of mirror imaging of the Doppler waveform. Doppler waveforms from the umbilical artery are displayed above the baseline. The vertical line is the cursor representing the beam path. The Doppler sample volume (two short horizontal lines) is placed in the umbilical artery. The mirror image is seen on the reverse side of the baseline

False depiction of a unidirectional flow as bidirectional due to system limitation should be distinguished from the situation where the Doppler beam insonates a true bidirectional flow system and consequently the Doppler waveforms appear on both sides of the baseline. For example, a Doppler beam with a sufficiently long sample volume interrogating the umbilical cord may encounter flows in the adjacent loops of the umbilical arteries in opposite directions relative to the transducer, and the Doppler waveform is correctly depicted on either side of the baseline. Similar nonartifactual mirror imaging may also occur when a focused pulsed Doppler beam intersects the flow axis at a right angle, and the same unidirectional flow is toward the transducer in one part of the beam and away from the transducer in the other part. The Doppler tracing in this situation is correctly bidirectional in relation to the transducer and is depicted as such.

3.19 Duplex System

3.19.1 Principles of the Duplex Doppler System

A duplex ultrasound system combines the modalities of a real-time 2D B-mode imaging with Doppler ultrasound modalities. Although the inherent range resolution feature of a PW Doppler system potentially allows collection of Doppler signals from a specific vascular target, this capability is hardly useful unless a method exists for placing the Doppler sample volume at the desired vascular location. A duplex system resolves this problem. The real-time B-mode imaging offers guidance, so the Doppler sample volume can be placed at the vascular target from which the

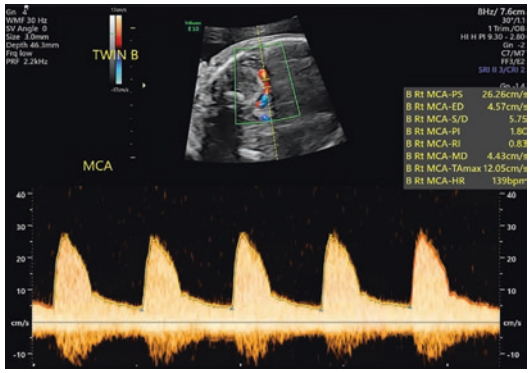

Fig. 3.12 Typical example of a duplex Doppler display. *Top*: Two-dimensional gray-scale and color Doppler image of the fetal middle cerebral artery. The spectral Doppler beam path is indicated by the *dotted cursor line*. The Doppler sample volume is indicated by *two horizontal lines*. *Bottom*: Spectral Doppler frequency shift waveforms from the sampled middle cerebral artery location

Doppler signals can be obtained. An electronically produced cursor line is directed across any targeted component of the 2D real-time cross-sectional image (Fig. 3.12). The cursor line indicates the Doppler beam path. The location of the Doppler sample volume is indicated on the cursor line by a marker. This location can be moved along the cursor line. Moreover, the axial dimension of the sample volume can be varied in most duplex instruments.

Experience with fetal Doppler echocardiography illustrates the significant advantages of duplex Doppler for fetal circulatory assessment [13]. A 2D echocardiographic B-mode and color Doppler imaging allow pulsed Doppler interrogation of complex intracardiac flow channels and outflow tracts. Similarly, it would be impossible to perform reliable spectral Doppler assessment of fetal middle cerebral or maternal uterine arteries without the guidance of B-mode and color Doppler imaging.

3.19.2 Optimal Configuration of a Duplex System: Imaging Versus Doppler System

One of the challenges of configuring a duplex ultrasound system lies in reconciling the conflicting needs of B-mode anatomical imaging and Doppler scanning. For the former, spatial resolution is of importance. System features (e.g., short pulses, well-damped transducers, and wide-band receivers) contribute significantly to improving the image resolution. These factors are therefore important considerations for B-mode imaging. However, because of the low amplitude of the backscattered Doppler signals, the optimal performance of a Doppler system is mostly dependent on its sensitivity, not on spatial resolution. In contrast to the imaging needs, the sensitivity of a Doppler system is enhanced by longer pulses, which by interrogating larger clusters of RBCs increase the amplitude of returning signals and improve the sensitivity. The sensitivity is increased by reducing the transducer damping and using narrow-band receivers.

It is obvious that the optimal configuration of a transducer system for duplex application is a trade-off between the conflicting needs of imaging and Doppler sonography. For the latter, lower frequencies are preferred as they ensure adequate depth penetration and minimize the changes of producing range-velocity ambiguity. Higher frequencies, on the other hand, compromise Doppler sensitivity. In contrast, low frequencies reduce spatial resolution, which is of central importance for imaging. These factors are important considerations when choosing appropriate transducers for fetal Doppler applications where deep-lying small vascular structures demand both sufficient spatial resolution and adequate Doppler sensitivity. Obviously, depending on the specific use of a duplex system, varying degrees of compromise are needed between these competing needs.

3.19.3 Duplex Implementation

Efficient integration of imaging and Doppler functions in a duplex transducer assembly offers a significant challenge for engineering innovation. Any comprehensive description of the current state of duplex Doppler transducer technology is beyond the scope of this chapter. Therefore, only a brief account of the Doppler implementation of the duplex probes is presented

in this section. These transducers can be classified into two broad categories according to the mechanism of scanning and focusing: (1) mechanical sector scanners, and (2) electronic array scanners, in which electronic means are employed for scanning and focusing.

Mechanical sector scanners use electric motors to rotate or oscillate the active transducer elements for sweeping the ultrasound beam to scan the tissue plane. Alternatively, a mirror may be used to sweep the beam, while the transducer element remains stationary. The inherent disadvantage of a mechanical system where the same elements are used for both imaging and Doppler scanning is the discontinuity between these two functions. Mechanical sector transducers are no longer used in obstetrical duplex Doppler applications, which now invariably involve electronic array transducers.

3.19.4 Electronic Array Scanner

In contrast to the mechanical scanners, electronic array transducers contain multiple piezoelectric elements (128 or more), and the ultrasonic scanning beam is formed by electronically controlled firing of these elements [4–17]. Over the years, these transducers have evolved in terms of the complexity of their construction and the sophistication of their operation. The beam formation, steering, focusing, and aperture control are electronically implemented. Currently, several varieties of electronic array transducers are available. They are classified according to the arrangement of the piezoelectric elements in the transducer assembly and the electronic mechanism of beam formation.

The elements may be arranged in the transducer assembly: (1) in a straight line, which constitutes a linear array transducer: (2) in a convex arc, in which case the assembly is labeled as a convex array transducer, (3) in concentric rings, called the annular array; and (4) in a 2D rectangular space for 3D sonography, usually termed a 2D array or matrix array. According to the electronic mechanism of producing the scanning beam, there are two types of array transducer: (1) the sequential array, which operates by sequentially triggering batches of piezoelectric elements for scanning the beam; and (2) the phased array, which electronically triggers all or most of the piezoelectric elements as a group during a given pulse. Time delays (known as *phasing*) are used in consecutive pulses to form the scanning beam. For both of these arrays, the beam is focused by appropriate phasing, or time delay, of the piezoelectric elements. A specific transducer may have mixed features; for example, a linear sequential array has phasic operation for focusing, or an annular array focuses electronically but scans mechanically. Currently, the following electronic array transducers are most frequently used in obstetric applications.

1. *Convex sequential array*. The piezoelectric elements are arranged in a convex arc and are fired sequentially in small groups as with the previous two categories. They are also known as curvilinear, curved, or radial array transducers. The field of image is sector-shaped. This design allows a small transducer footprint with a wide field of imaging at depth—a combination of features particularly useful for obstetric scanning. Furthermore, the wide field of view is achieved without the grating lobe problem of the linear phased array. With the phased convex sequential array, the focusing is achieved by phasing of the firing sequence. Doppler insonation is performed by a batch of phased elements that can be steered in the sector field of exposure.
2. *Linear phased array*. This configuration is also known as the phased or electronic sector array. As the name implies, the piezoelectric elements are arranged in a straight line, and the beam is formed by the simultaneous phased firing of all the elements. Focusing and steering is accomplished electronically by the phased triggering of the elements. The field of image created by a linear phased array is sector-shaped. Although these transducers do not often provide optimal imaging for general obstetric applications, they are useful for fetal cardiac imaging. The Doppler ultrasonic beam is produced by a batch of elements that

are phased and can be steered within the scanned image area to interrogate the target vessel.

3.20 Integration of the Doppler and Imaging Functions in Array Transducer

We referred earlier in the chapter to the conflicting needs of optimal transducer frequency for imaging and Doppler sonography. In many current duplex systems, the problem has been addressed by providing dual-frequency transducers, a higher operating frequency for imaging and a lower frequency for Doppler ultrasound. The latter improves the Doppler sensitivity and sets a higher Nyquist limit, whereas the former improves spatial resolution for imaging. For example, the transducer has 3.5 MHz for imaging function and 2.5 MHz for Doppler insonation. Such an arrangement has been possible only since the advent of broad bandwidth electronic array transducers and advanced processing capability.

In contrast to mechanical scanners, electronic transducer array scanners are capable of seemingly simultaneous execution of imaging and Doppler functions. The simultaneous operation, which is only apparent and not real, can be achieved by several methods. With one such technique, alternate pulses are shared between the 2D imaging mode and Doppler sonography. This technique is similar to that used when performing simultaneous imaging and M-mode scanning. However, it reduces the Doppler pulse repetition frequency and therefore the Nyquist limit, which results in significant restriction in the maximum velocity that can be measured without aliasing. The 2D imaging, frame rate is also slowed. To address the aliasing problem, a modified time-sharing approach limits the time for imaging in favor of the time for Doppler scanning. However, this method produces slow, sweeping images, which restrict the utility of the imaging guidance and are visually disconcerting for the operator [18].

A more efficient solution, used with the current generation of devices, consists in devoting more scanning time to imaging than to Doppler sonography, so a single but full image frame can be formed. The Doppler data lost during this interval are simulated from the preceding recorded spectrum by an interpolation algorithm, known as the missing signal estimator. Although it still reduces the imaging frame rate, the results are superior to those of other alternatives for approximating simultaneity. In a typical scenario, the Doppler scan is performed for 10 ms, followed by pulse echo imaging for 20 ms. During the 20-ms interruption, the missing Doppler spectrum is interpolated from the immediate prior recording and is displayed without discontinuity. The system performs this routine with great swiftness many times a second, which allows Doppler shift assessment along with the imaging guidance to continuously verify the source of Doppler signals [19]. Obviously, this level of system performance is possible only in an electronic array with powerful processors and efficient algorithms.

3.21 Doppler Display

During operation, the Doppler information is displayed on a monitor screen. The details of the display vary according to the type of instrumentation and manufacturer. The CW Doppler instruments obviously have simpler displays (Fig. 3.13) in comparison with duplex Doppler systems (Fig. 3.12). During real-time Doppler interrogation, the spectral display scrolls from the right of the screen to the left with time, as progressively newer spectral information is added to the display. In addition to the spectral waveform, a CW Doppler display also includes the zero line, the frequency (or velocity) scale in the vertical axis, and the time scale in the horizontal axis. The spectral display area also includes the cursor lines for measuring the peak systolic or end-diastolic frequency shifts. Additional information is shown outside the spectral display window but within the screen area. It may include measures of the frequency shift including the peak systolic

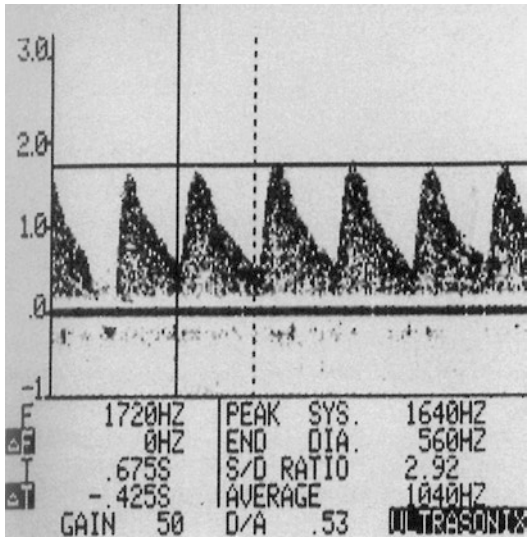

Fig. 3.13 Continuous-wave Doppler sonogram derived from the umbilical arteries. It was obtained with a free-standing Doppler device without duplex imaging guidance. *Vertical axis* represents the magnitude of the Doppler shift in kilohertz and the *horizontal axis* the time. *Bottom*: Peak systolic (*S*), end-diastolic (*D*), and average frequency shift (*A*) values. The indices (*S/D*, *D/A*) are also shown

and end-diastolic components, Doppler indices, and various indicators of the system function.

A duplex Doppler system display is complex because of its extended function, encompassing both imaging and Doppler modes (Fig. 3.12). To maintain user-friendliness, the devices employ a software menu approach to their system control, which is usually reflected in the control panel display and the monitor display, so the operator is guided through the multiplicity of functions with relative ease. In the Doppler mode the monitor screen should display not only the spectra, the data of examination, and the patient's identity, but comprehensive Doppler information as well, including transducer frequency, mode of Doppler, depth and size of the sample volume, angle of insonation, frequency or velocity mode, pulse repetition frequency, and Nyquist limit. It is imperative to indicate the filter and gain settings and to offer some meaningful information on the power output of the transducer to ensure that the fetus is not exposed to a high level of ultrasonic energy when a lower output is sufficient to yield the desired information. All current instruments include real-time energy output displays, the thermal index, and the mechanical index. A number of options are available for archival storage of the Doppler information, including digital storage and hard-copy prints.

References

1. Evans DH, McDicken WN, Skidmore R, Woodcock JP. Doppler ultrasound: physics, instrumentation and clinical applications. Chichester: Wiley; 1989.
2. Cooley JW, Tukey JW. An algorithm for the machine calculation of complex Fourier series. Math Comput. 1985;19:297–301.
3. Brigham EO. The fast Fourier transform. Englewood Cliffs, NJ: Prentice Hall; 1974.
4. Macpherson PC, Meldrum SJ, Tunstall-Pedoe DS. Angioscan: a spectrum analyzer for use with ultrasonic Doppler velocimeters. J Med Eng Technol. 1981;5:84–9.
5. Johnston KW, Brown PM, Kassam M. Problems of carotid Doppler scanning which can be overcome by using frequency analysis. Stroke. 1982;13:660–6.
6. Maulik D, Saini VD, Nanda NC, Rosenzweig MS. Doppler evaluation of fetal hemodynamics. Ultrasound Med Biol. 1982;8:705–10.
7. Welch PD. The use of fast Fourier transform for the estimation of power spectra: a method based on time averaging over short, modified periodogram. IEEE Trans Audio Electroacoust. 1967;AU-15:70–3.
8. Hoskins PR. Ultrasound techniques for measurement of blood flow and tissue motion. Biorheology. 2002;39:451–9.
9. Kay SM, Marple SL. Spectrum analysis—a modern perspective. Proc IEEE. 1981;69:1380–419.
10. Kadado T, Maulik D, Chakrabarti S. Comparison of parametric and nonparametric spectral estimation of continuous Doppler ultrasound shift waveforms. IEEE Proc Digit Sig Process WS. 1994;6:145–8.
11. Gill RW. Measurement of blood flow by ultrasound: accuracy and sources of error. Ultrasound Med Biol. 1985;11:625–31.
12. Jenkins GM, Watt DG. Spectral analysis. London: Holden Day; 1969.
13. Maulik D, Nanda NC, Saini VD. Fetal Doppler echocardiography: methods and characterization: methods and characterization of normal and abnormal hemodynamics. Am J Cardiol. 1984;53:572–8.
14. Bom N, Lancee CT, Honkoop J, Hugenholtz PC. Ultrasonic viewer for cross-sectional analysis of moving cardiac structures. Biomed Eng. 1971;6:500–7.

15. Eggleton RC, Johnston KW. Real time mechanical scanning system compared with array techniques. IEEE Proc Sonics (Ultrasonics Cat No 74-CH 0896-1; 16); 1974.
16. VonRamm RC, Thurston FL. Cardiac imaging using a phased array ultrasound system. Circulation. 1976;53:258–62.
17. Kremkau FW. Transducers. In: Diagnostic ultrasound. Philadelphia: Saunders; 1989. p. 65–104.
18. Hatle L, Angelsen B. Blood velocity measurement. In: Doppler ultrasound in cardiology. Philadelphia: Lea & Febiger; 1985. p. 32–73.
19. Angelsen BAJ, Kristoffersen K. Combination of ultrasound pulse echo amplitude imaging and Doppler blood velocity measurement. In: Proceeding of cardiac Doppler Symposium. Martinus Nijhoff, The Hague. Clearwater, FL; 1983.

4 Spectral Doppler Sonography: Waveform Analysis and Hemodynamic Interpretation

Dev Maulik

The spectral Doppler power waveform contains an immense amount of hemodynamic information from the sampled circulation. As we saw in Chap. 3, the spectral information consists of three fundamental variables: frequency, amplitude, and time. Spectral frequency reflects the speed of blood flow. The amplitude approximately represents the number of scatterers traveling at a given speed and is also known as the power of the spectrum. Amplitude depends on the quantity of moving red blood cells (RBCs) in the sample and therefore reflects the volume of blood flow. The time over which the frequency and amplitude vary is the third variable. A comprehensive depiction of the Doppler spectrum is therefore three-dimensional (see Chap. 3). Such a display is complex, however, and not particularly useful for clinical application. Fortunately, there are alternative approaches for effectively characterizing the spectral waveform, including two-dimensional sonograms and various frequency envelope waveforms. These approaches can be utilized to evaluate various aspects of hemodynamics of flow, ranging from the presence and directionality of flow to downstream impedance. This chapter discusses these subjects and other related issues.

D. Maulik (✉)
Department of Obstetrics and Gynecology, UMKC School of Medicine/Truman Medical Center, UMKC School of Medicine, Kansas City, MO, USA
e-mail: dmaulik2014@gmail.com

4.1 Spectral Doppler Sonogram

A typical two-dimensional sonographic display of Doppler frequency shift waveforms from the umbilical circulation is shown in Fig. 4.1. Each spectrum of the Doppler shift is depicted in a vertical line whose vertical dimension represents the magnitude of the frequency; the image intensity or brightness represents the amplitude. Each successive spectrum is added to the right of the previous spectrum as the display is scrolled from right to left. Thus, the horizontal axis indicates the temporal dimension of the Doppler recording. When sampled from an arterial circulation, a Doppler waveform depicts one cardiac cycle. The left limit of the wave corresponds with the onset of systole, the zenith of the wave with peak systole, and the right limit with the end of diastole. In a two-dimensional Doppler sonogram, only the frequency and time are quantitatively depicted, whereas the amplitude, or power of the spectrum, is expressed only qualitatively. The directionality is depicted in terms of whether the flow is toward or away from the transducer. The flow toward the transducer is shown as an upward deflection from the baseline and flow away as a downward deflection; this configuration may be reversed in the display. The hemodynamic interpretation and utilization of the various characteristics of the Doppler wave sonogram are discussed later in this chapter.

D. Maulik, C. C. Lees (eds.), *Doppler Ultrasound in Obstetrics and Gynecology*,
https://doi.org/10.1007/978-3-031-06189-9_4

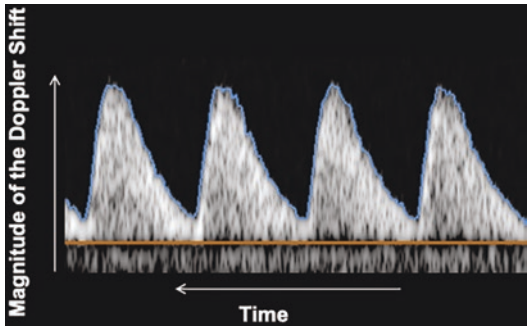

Fig. 4.1 Spectral Doppler waveform from the umbilical arteries. Vertical axis represents the magnitude of the Doppler frequency shift. Horizontal axis represents time. Brightness of the tracing indicates the amplitude of the Doppler spectrum. Note that the recording is scrolled from right to left as new information is continuously added to the right end of the spectral display

4.2 Doppler Frequency Shift Envelopes

Although the full power spectral display of the Doppler signal as described above provides a comprehensive account of the dynamics of flow velocity, often more limited and focused spectral information based on the various envelope definitions of the Doppler frequency shift waveform is used (Fig. 4.2). Of the various envelopes, the maximum and mean frequency shift waveforms are most commonly used for clinical applications. These envelopes and an additional one, the first moment, are discussed here.

4.2.1 Maximum Frequency Shift Envelope

The maximum frequency shift envelope may be derived manually by outlining the spectral waveform or electronically by analog or digital techniques. Many devices allow superimposition of the maximum frequency envelope over the spectral display waveform. It should be noted that most Doppler descriptor indices are based on the maximum frequency shift values (see below), although most indices are usually determined without defining the total envelope. This envelope is not significantly affected by uneven

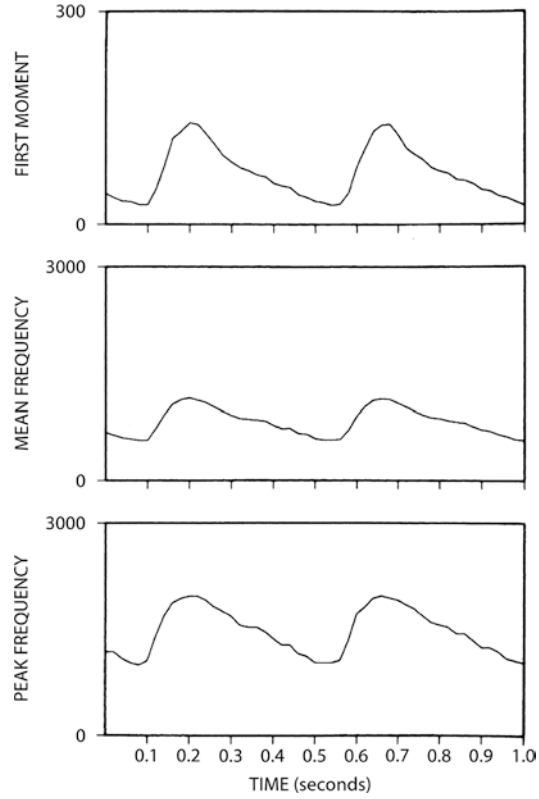

Fig. 4.2 Descriptor envelopes of the Doppler frequency shift waveform. (Reprinted from [2] with permission)

insonation so long as the ultrasound beam includes the fastest flow within the lumen. It is also resistant to the flow velocity profile of the circulation, the attenuation variation between blood and soft tissue, the signal-to-noise ratio, and the high-pass filter. The maximum frequency envelope is susceptible to spectral broadening as the definition of maximum frequency in relation to the spectral power becomes imprecise, and the maximum frequency values form a gradual slope at the various cutoff levels of peak power (see Fig. 3.6).

4.2.2 Mean Frequency Shift Envelope

Under the ideal circumstances of complete and uniform insonation of the target vessel, the mean frequency provides an indirect estimate of mean

flow velocity; corrected for angle of insonation, it yields actual velocity values. The accuracy of the mean frequency depends on the velocity profile and is compromised when a vessel is incompletely insonated. The envelope is affected by the differential attenuation of sound between blood and tissue, which favors transmission of Doppler signals from the center of the vascular lumen; it results in false elevation of the mean frequency. It is also susceptible to high-pass filtering, which increases the mean frequency estimate by eliminating low-frequency signals along with the tissue-derived clutter signals. The mean frequency has the advantage of being unaffected by spectral broadening because of the symmetric nature of the spectral spread.

4.2.3 First Moment Envelope

Of the additional definitions of the Doppler envelope, the first moment of the Doppler power spectrum is of particular interest. The Doppler-shifted frequency is proportional to the speed of the backscattering erythrocytes, and the power of a Doppler spectrum is proportional to the density of erythrocytes moving at a corresponding speed. On this theoretic basis, Saini and associates [1] proposed that being a summation of the power-frequency product the first moment represents the integrated cell count-velocity product within the sample volume and is therefore indicative of instantaneous volumetric flow. Maulik and colleagues [2] investigated the potential of the first moment-derived Doppler waveform from the umbilical artery and observed that the first moment-based pulsatility index was twice that derived by the maximum frequency shift envelope. This phenomenon may be explained by the relative flattening of the velocity profile during early systole and by changes in the arterial diameter.

The utility of first moment remains uncertain. Although this approach contains more hemodynamic information, its practical application is limited by the impracticality of ensuring uniform insonation. Moreover, as pointed out by Evans and coinvestigators [3], the total power of the Doppler spectrum may be affected by many factors other than the vascular cross-sectional dimension.

4.3 Hemodynamic Information from Doppler Sonography

The Doppler frequency shift estimates, but does not directly measure, blood velocity. Doppler ultrasound can generate a wide range of hemodynamic information, including the presence of flow, directionality of flow, flow velocity profile, quantity of flow, and the state of downstream flow impedance.

4.3.1 Flow Detection

Doppler ultrasound allows identification of blood flow. Pulsed duplex Doppler insonation, especially with the two-dimensional color flow mapping mode, has multiple utilities in clinical practice. For example, color Doppler insonation is used to identify the fetal middle cerebral artery for precise spectral Doppler interrogation (Fig. 4.3). In the human fetus, detection of anomalous flow using pulsed Doppler

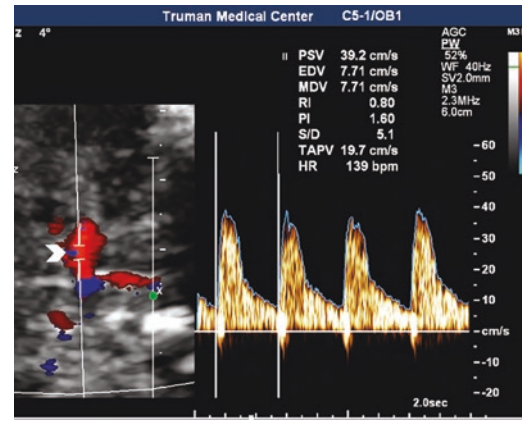

Fig. 4.3 Hemodynamic assessment of the fetal middle cerebral artery. Left: Color Doppler imaging shows middle cerebral artery flow and spectral Doppler interrogation. Right: Spectral Doppler flow waveforms from the artery. White arrow shows the location of the Doppler interrogation

echocardiography may significantly supplement the two-dimensional echocardiographic technique for diagnosing cardiac abnormalities. For example, Doppler ultrasound detection of flow in an echo-deficient area adjacent to the main pulmonary artery of the fetus was noted to assist the diagnosis of congenital aneurysm [4].

A major application of duplex Doppler flow identification is the diagnosis of proximal vein thrombosis. An absent or anomalous flow in a proximal vein suggests complete or partial occlusion. The technique has been used to assess peripheral vascular competence with varying degrees of success. However, caution should be exercised when interpreting failure to detect Doppler shift because in this circumstance the flow may be present but not within the sensitivity of the Doppler device. The maternal and fetal placental circulation offer prime examples of this problem. Although these circulations carry an immense amount of blood flow, Doppler interrogation fails to produce any recognizable Doppler shifts from most of the placental mass. Power mode of color Doppler ultrasound significantly improves the capability of recognizing slow- and low-flow states. This subject is further discussed in Chap. 6.

4.3.2 Flow Direction

The demodulation technique allows determination of the directionality of flow; forward and reverse flows are displayed on the opposite sides of the baseline. Flow directionality provides basic hemodynamic information that can be of significant clinical utility. For perinatal applications, flow directionality allows assessment of the status of continuing forward flow during end-diastole in umbilical and uteroplacental circulations. Absence or reversal of this end-diastolic forward flow is of ominous prognostic significance and is further discussed in Chap. 25. Depiction of flow directionality during echocardiographic assessment may assist in recognizing pathology. For example, atrioventricular valvular incompetence may be diagnosed from the demonstration of reverse flow during systole at the tricuspid or mitral orifice.

4.3.3 Flow Velocity Profile

Doppler shift spectral range may reflect the velocity profile of blood flow in the insonated vessel. When the spectral range is wide it is called *spectral broadening*, and when it is slim it is known as *spectral narrowing*.

Spectral narrowing usually indicates a flat or plug flow velocity profile in which most RBCs are moving at a similar speed; it is usually seen in large vessels. For obstetric applications, this flow profile is encountered in fetal ventricular outflows (Fig. 4.4). Spectral narrowing is seen during the early systolic phase (from the outset to peak systole) in a great vessel as the ventricular ejection force at its prime imparts similar speeds of flow to the RBCs; however, such an appearance may be artifactual because of the steepness of the trace [5]. Spectral narrowing is also observed when the sample volume size is smaller than the lumen, and it is placed in the center of the lumen where the flow speed is fastest.

Spectral broadening is seen with a parabolic flow where the RBCs travel at a wide range of speeds and produce a wide range of Doppler-shifted frequencies. In a parabolic velocity profile, the RBCs travel at varying speeds, with the cells at the center of the vessel traveling at the highest velocity and those near the vascular

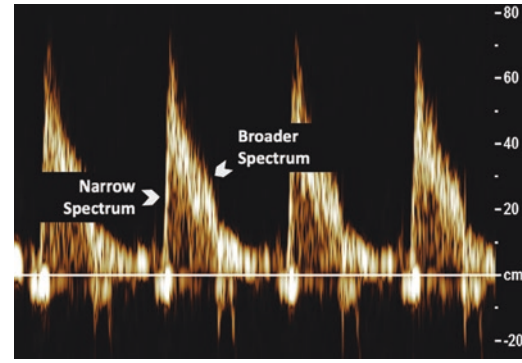

Fig. 4.4 Spectral narrowing. Doppler waveforms from the pulmonary artery demonstrating very narrow spectrum during the early systolic phase with blood flowing in relatively uniform velocity, which becomes broader in the diastolic phase

wall at the lowest velocity because of the viscous drag. Such a wide distribution of RBC velocities provides uniform broadening of the Doppler spectral display, which is usually encountered in small vessels, such as the uterine and ovarian arteries. Figure 4.5 shows an example of spectral broadening of the Doppler waveform. In obstetrics, blunted parabolic flow is seen in the umbilical arteries. It is also encountered in a turbulent flow characterized by a wide distribution of RBC speed across the vascular lumen. Finally, as noted with spectral narrowing, partial insonation of an artery may also lead to spectral broadening. If a small sample volume is placed near the wall of a large vessel, spectral broadening occurs as the flow layers toward the vessel wall show wider speed distribution.

4.3.4 Doppler Flow Quantification

Measurement of volumetric blood flow remains a parameter of fundamental hemodynamic importance. There are various noninvasive sonographic methods for quantifying flow. Of these, Doppler ultrasound velocimetry still remains the standard modality. There are also non-Doppler-based ultrasound technologies for measuring volumetric blood flow without some of the limitations of the Doppler technique. These approaches are discussed below.

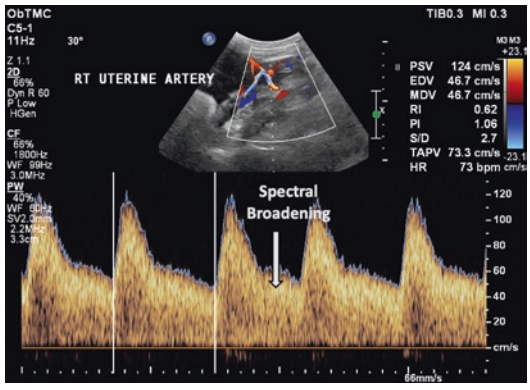

Fig. 4.5 Spectral broadening. Top: Flow-guided placement of the Doppler sample volume in the uterine artery. Note the spectral broadening of the waveform

4.4 Principle of Doppler Flowmetry

The Doppler flowmetric technique has been used to measure umbilical venous flow [6], descending aortic flow [7], and fetal right and left ventricular outputs [8]. The theoretical basis of Doppler flow quantification is as follows (Fig. 4.6). The volumetric flow in a given instant (Q) is the product of the spatial mean velocity across the vascular lumen at that instant ($v(t)$) multiplied by the vascular cross-sectional area at that instant ($A(t)$):

$$Q(t) = \bar{v}(t)\,A(t) \tag{4.1}$$

The mean velocity is estimated from the mean Doppler frequency shift $\left(\bar{f}_d\right)$ by Doppler velocimetry provided the angle of insonation (θ) is also known:

$$\bar{v}(t) = \bar{f}_d(t)\,c / 2 f_t \cos\theta \tag{4.2}$$

where f_t is the transducer frequency and c is the speed of sound in blood. The Eq. (4.1) can now be rewritten as follows:

$$Q(t) = \left(\bar{f}_d(t)\,c / 2 f_t \cos\theta\right) A(t) \tag{4.3}$$

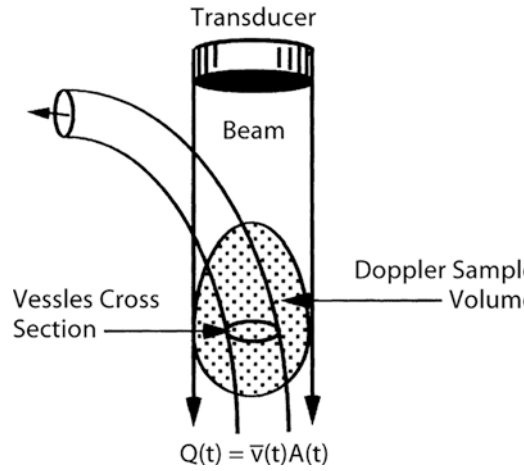

Fig. 4.6 Doppler sonographic volumetric quantification. Graphic depiction of the principle of even insonation technique. Q volumetric flow in a given instant, $\bar{v}(t)$ spatial mean velocity across the vascular lumen at that instant, A(t) vascular cross-sectional area at that instant

Arterial circulation is pulsatile. Therefore, the volumetric flow passing through the arterial tree fluctuates through the cardiac cycle. The temporal average flow over the cardiac cycle is obtained from the temporal average product of the instantaneous mean velocity (mean frequency shift) and the vascular cross-sectional area.

4.5 Doppler Velocity Measurement

There are several sonographic approaches to Doppler measurement of blood flow velocity. These include the uniform insonation method and the assumed velocity profile method.

4.5.1 Uniform Insonation Method

In this approach, a duplex Doppler ultrasound device is used to insonate uniformly and completely the lumen of the target vessel, and to determine the instantaneous mean frequency shift, the cross-sectional area of the vessel, and the angle of insonation. The Doppler sample volume needs to be large enough to encompass the entire vascular cross-sectional area, but not to include the surrounding structures. It is also assumed that the angle of insonation is constant over the entire sample volume.

Error in estimating mean frequency shift can be due to uneven insonation, intrinsic spectral broadening, blood-tissue attenuation difference, high-pass filter, and poor signal-to-noise ratio. Of these, uneven insonation is potentially the most significant contributor. For example, partial insonation of a vessel in the periphery of the lumen will underestimate the mean frequency, whereas similar insonation in the center of the lumen will overestimate it. Most duplex Doppler devices available at present utilize a narrow beam for Doppler insonation and therefore may not be able to uniformly insonate the whole vessel even in the fetus.

4.5.2 Assumed Velocity Profile Method

A modification of the uniform insonation, the assumed velocity profile technique, attempts to address the problem related to the mean frequency measurement by estimating the mean velocity from the time-averaged maximum frequency shift value. In this approach, the velocity profile across the flow cross-sectional area is assumed rather than measured, and maximum frequency shift data from a point target are translated into mean frequency shift values. The mean velocity is estimated by multiplying the angle-corrected instantaneous maximum frequency shift with an arbitrary calibration factor and is based on the assumption that the flow velocity profile is either flat or parabolic. In case of a flat profile, the calibration factor has a value of 1 as the mean and maximum velocities are theoretically the same. However, when the profile is parabolic, the mean velocity is half of the maximum velocity and the calibration factor has a value of only 0.5. Although this technique obviates to some extent the problem of mean velocity determination, the underlying assumptions regarding the flow velocity profile often do not exist in reality and the technique still suffers from the other limitations of the uniform insonation method. An example of the use of this technique which describes the measurement of fetal cardiac output is given in Chap. 30. This approach may introduce inaccuracies in quantifying flow. These errors are related to measuring of the mean frequency shifts, the vascular luminal cross-sectional area, and the angle of insonation.

4.6 Determination of Vascular Luminal Area

The cross-sectional area of the vessel lumen may be measured from the two-dimensional image or from the M-mode tracing of the vessel. The radius, which is half the diameter of the luminal cross section, is measured first and the area is estimated according to the equation:

$$A = \pi r^2 \tag{4.4}$$

where A is the cross-sectional area and r is the radius. This equation assumes that the vascular cross section is circular in shape. This assumption, however, is erroneous as the shape of the vascular lumen is more ellipsoidal than circular, and the shape and the dimensions of the arterial cross section are known to vary during the cardiac cycle. The problem is confounded by the fact that any error in measuring the vessel diameter is significantly amplified in the volumetric flow value. Because of these limitations, measurement of the vascular cross-sectional area is the most significant source of error for Doppler sonographic estimation of volume flow. This is especially relevant for deep-lying smaller fetal vessels. However, the error may be minimized by averaging several measurements of the diameter. Temporal averaging of the diameter during the cardiac cycle is especially important for arterial circulations. Magnification of the digital image of the vessel off line in a computer may also improve the accuracy and has been reported [9]. Simultaneous measurement of the vascular cross section and the mean velocity remains technically challenging. The best sonographic approach for imaging and measuring vascular dimension may not often be optimal for Doppler insonation.

4.7 Determination of the Angle of Insonation

Finally, the angle of insonation is an important source of inaccuracy for volumetric flow quantification as the cosine value of the angle ascertains the component of blood flow velocity reflected in the Doppler shift. The higher the angle of insonation, the greater the error of measurement. This is discussed in greater depth in Chap. 2.

4.8 Alternative Methods of Doppler Flowmetry

As discussed above and in Chap. 2, the standard Doppler velocimetry is limited in providing comprehensive hemodynamic information because of its angle dependency. The current technology utilizes a single beam Doppler, which measures the velocity only along the beam axis, whereas blood flow has velocity vectors in three-dimensional space. Angle correction cannot mitigate against this limitation because vessel orientation may not permit an optimal angle of insonation or the actual flow vector may change in a complex hemodynamic environment. This has led to the development of vector velocity imaging (VVI) which allows estimation of flow velocity vector components in more than one direction [10–14]. Several approaches have been described, which include:

(a) Multiple beam Doppler that employs Doppler beams from different angles and derives flow vectors angle independently [15]; (b) Speckle tracking velocimetry which is a non-Doppler-based approach that tracks speckles to estimate velocity vectors [16]; (c) Transverse oscillation method which uses transverse oscillations to derive the lateral velocity vectors [17]; and (d) Color Doppler vector flow imaging based on postprocessing for the estimation of velocity vectors perpendicular to the ultrasound beam direction [18].

These innovations have been validated in clinical settings involving mostly adult patients. For example, Brandt and associates compared the accuracies of VVI and spectral Doppler for assessing common carotid artery peak velocities against the gold standard magnetic resonance phase contrast angiography. VVI was found to be more accurate than spectral Doppler in evaluating peak systolic velocities compared with magnetic resonance angiography [19]. In a study involving 11 healthy volunteers, Hansen and colleagues validated directional beamforming, synthetic aperture flow imaging, and transverse oscillation methods against magnetic resonance phase contrast angiography in assessing blood flow velocity in the right common carotid artery (Fig. 4.7) [14]. In 60 healthy subjects, Goddi et al. compared a plane wave-based vector flow imaging system to color Doppler imaging in assessing complex hemodynamics of the carotid bifurcation and observed that VVI was more effective than the color Doppler [20]. Most of these technological advances, however, have not yet been validated or utilized in perinatal clinical practice.

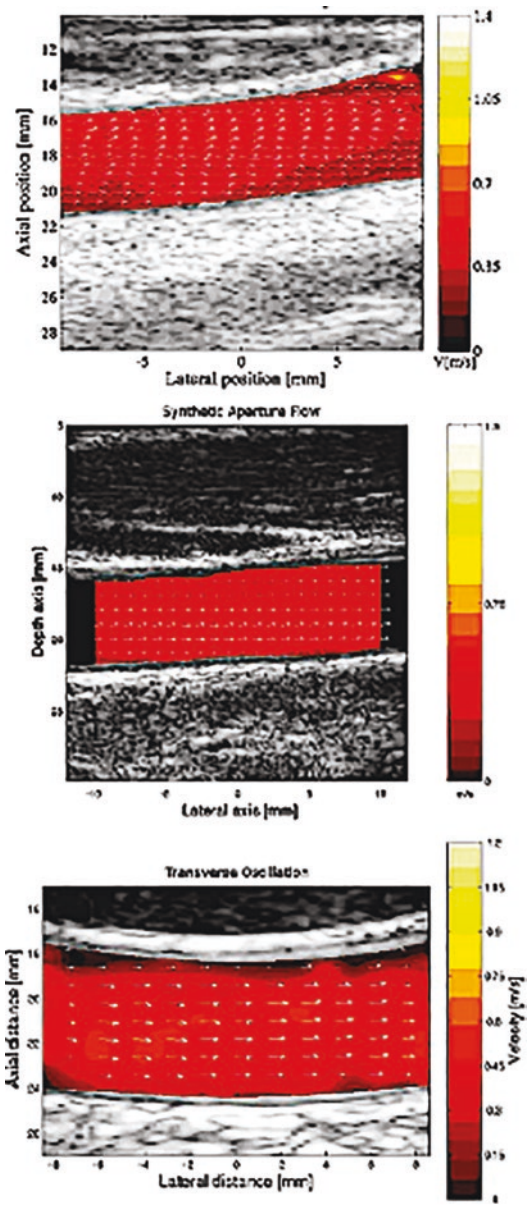

Fig. 4.7 The frames obtained with the three methods are recorded on different volunteers and to different time. The vector arrows, superimposed onto color flow maps, delineate magnitude and direction of the moving blood scatterers. (Reprinted from [14] with permission)

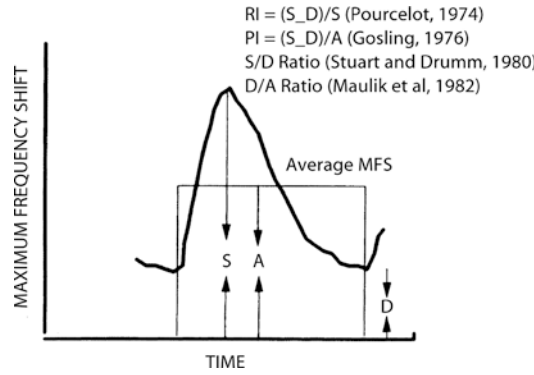

Fig. 4.8 Doppler indices derived from the maximum frequency shift envelope. *S* peak systolic frequency shift, *D* end-diastolic frequency shift, *A* temporal average frequency shift over one cardiac cycle. (Reprinted from [30] with permission)

4.9 Doppler Waveform Analysis and Doppler Indices

Because of the problems related to volumetric flow assessment, there has been a need to seek alternative ways to investigate vascular flow dynamics using the Doppler method. The maximum Doppler frequency shift waveform represents the temporal changes in the peak velocity of RBC movement during the cardiac cycle. It is therefore under the influence of both upstream and downstream circulatory factors [21]. The objective has been to obtain information specifically on distal circulatory hemodynamics. Techniques have been developed for analyzing this waveform in an angle-independent manner. Most of these analytic techniques involve deriving Doppler indices or ratios from the various combinations of the peak systolic, end-diastolic, and temporal mean values of the maximum frequency shift envelope (Fig. 4.8). Because these parameters are obtained from the same cardiac cycle, the ratios are virtually independent of the angle of insonation.

A unique feature of the uteroplacental, umbilical, and fetal cerebral circulations is the continuing forward flow during diastole, so the perfusion of vital organs is uninterrupted throughout the cardiac cycle. This feature develops progressively in the fetoplacental circulation. The essential effects of this phenomenon include not only a progressive increase in the end-diastolic component of the flow velocity, but also a concomitant decrease in the pulsatility, which is the difference between the maximum systolic and end-diastolic components (Fig. 4.9). The pulsatility of the flow

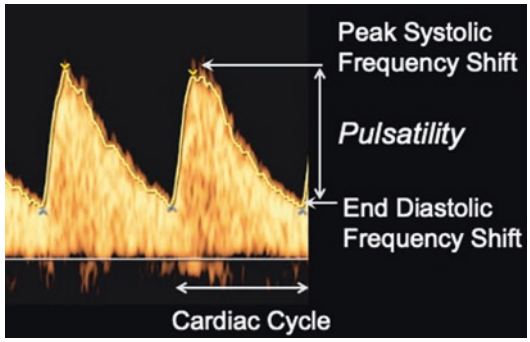

Fig. 4.9 Pulsatility of an arterial velocity waveform. The example shows Doppler waveforms from the umbilical arteries. Vertical axis represents the velocity magnitude. Horizontal axis represents the time

velocity was originally investigated using Doppler ultrasonography in the peripheral vascular system.

Gosling and King were the first to develop the pulsatility index (PI) as a measure of the systolic-diastolic differential of the velocity pulse [22]. The PI was first derived from Fourier transform data and is known as the Fourier PI. Subsequently, a simpler version, the peak-to-peak PI (Fig. 4.8), was introduced based on the peak systolic frequency shift (S), the end-diastolic frequency shift (D), and the temporal mean of the maximum frequency shift over one cardiac cycle (A):

$$\mathrm{PI} = \frac{S - D}{A} \tag{4.5}$$

Almost at the same time, Pourcelot reported a similar index, called the resistance index (RI) [23]. It also gave an angle-independent measure of pulsatility:

$$\mathrm{RI} = \frac{S - D}{S} \tag{4.6}$$

where S represents the peak systolic and D the end-diastolic frequency shift. Stuart and associates [24] described a simpler index for pulsatility in which the numerator is the peak systolic frequency and the denominator is the end-diastolic frequency shift:

$$S / D \tag{4.7}$$

where S represents the peak systolic, and D represents the end-diastolic maximum frequency shift. (Originally, it was called the A/B ratio). Because the variations in the end-diastolic frequency shift appear to be the most relevant component of the waveform. Maulik and associates [8] suggested the direct use of this parameter normalized by the mean value of the maximum frequency shift envelope over the cardiac cycle:

$$D / A \tag{4.8}$$

There has been a proliferation of indices over the years. Most of them refer to the pulsatility of the maximum frequency shift envelope of the Doppler waveform, but some reflect various hemodynamic parameters, such as transit time broadening. For obstetric applications, assessment of the pulsatility and the end-diastolic frequency shift is of clinical importance.

4.10 Comprehensive Waveform Analysis

Attempts have also been made to analyze the Doppler waveform in a more comprehensive manner. Maulik and colleagues [2] described a comprehensive feature characterization of a coherently averaged Doppler waveform from the umbilical artery (Fig. 4.10). The measured parameters included the PI and the normalized systolic slope and end-diastolic velocity. In 1983, Campbell and colleagues [25] reported a technique for normalization of the whole waveform, called the frequency index profile. Thompson and associates [26] described yet another technique of comprehensive waveform analysis that involved a four-parameter curve-fitting analysis of an averaged waveform. More recently, Maršál reported use of a classification system based on the PI value and end-diastolic flow characteristics [27]. This classification system was superior to other measures of the waveform for predicting fetal distress and operative delivery due to fetal distress. Most of these techniques have not been thoroughly evaluated, and currently there is no evidence that they offer any advantages over the simpler Doppler indices.

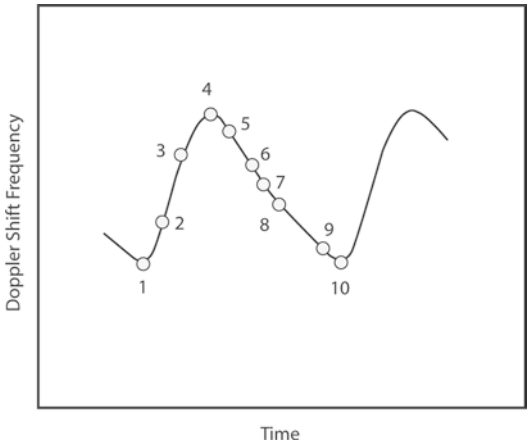

Fig. 4.10 Reference points in a typical velocity envelope waveform obtained from the umbilical arteries. 1 trough, 2–3 ascending slope, 4 peak, 5–6 initial descending slope, 8–9 final descending slope, 10 trough. (Reprinted from [2] with permission)

4.11 Choice of Indices

Of the various indices, the systolic/diastolic (S/D) ratio, RI, and PI have been used most extensively in obstetric practice. Of these, the S/D ratio and RI, being based on the same set of Doppler parameters (peak systolic and end-diastolic frequency shifts), are related to each other as shown in Eq. (4.8) and Fig. 4.11:

$$\mathrm{RI} = 1 - \frac{\mathrm{S}}{\mathrm{D}} \tag{4.9}$$

As the end-diastolic frequency shift declines, the *S*/*D* ratio rises exponentially; and when the end-diastolic flow disappears, the value of the index becomes infinity. Hence, the *S*/*D* ratio value becomes meaningless beyond a certain point as the fetoplacental flow impedance continues to rise. This behavior of the *S*/*D* ratio is inherent in its formulation and is reflected in its distribution characteristics [28] (Fig. 4.12) and its total variance (Fig. 4.13). Despite these limitations, this index is used extensively in obstetrics, particularly in the United States. The RI values, on the other hand, have defined limits with a minimum value of 0 and a maximum value of 1.0. Unlike the *S*/*D*, the RI shows gaussian distribu-

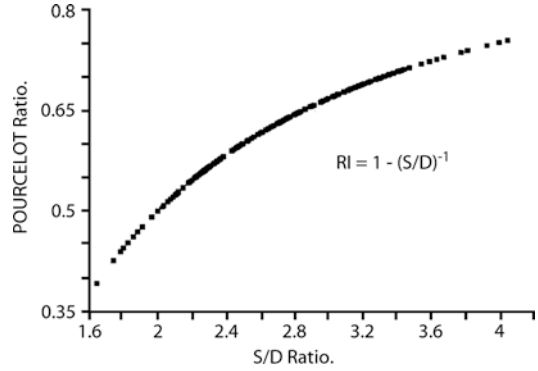

Fig. 4.11 Correlation between the resistance index (RI) and the systolic/diastolic (*S*/*D*) ratio

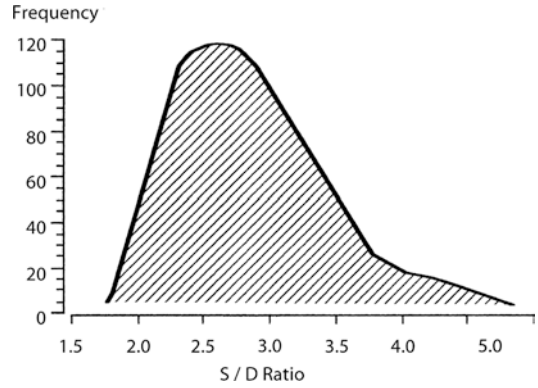

Fig. 4.12 Distribution of the umbilical arterial systolic/diastolic ratio in the study population. Note its non-Gaussian distribution. (Based on data from [28])

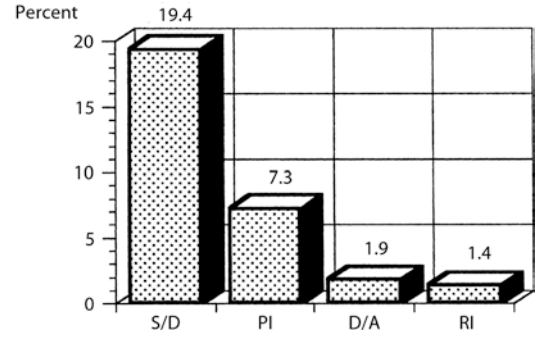

Fig. 4.13 Total variance values (percentage) of the various Doppler indices. *S*/*D* systolic/diastolic ratio, PI pulsatility index, *D*/*A* diastolic/average ratio, RI resistance index. Note that the *S*/*D* ratio varies the most and the RI the least under the same hemodynamic conditions

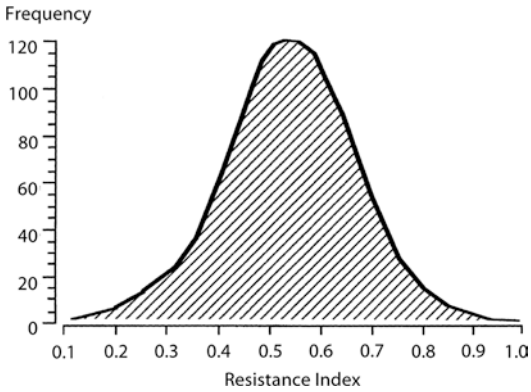

Fig. 4.14 Gaussian distribution of the umbilical arterial resistance index. (Based on data from [29])

tion and is therefore amenable to parametric statistical analyses (Fig. 4.14). The limitation of RI is due to its inability to reflect impedance increases with the reversal of end-diastolic flow. Theoretically, the PI provides more hemodynamic information than the RI and *S*/*D* ratio, as it includes data on the whole cardiac cycle in the form of its denominator, which is the time-averaged value of the maximum frequency shift envelope over one cardiac cycle. Furthermore, it expresses hemodynamic alterations associated with absent or reversed end-diastolic flow. In practice, however, computation of the time-averaged value is not as precise as determination of the peak systolic or end-diastolic frequency shifts. In a prospective blinded study, Maulik and associates [29] showed that the RI had the best and PI the worst discriminatory performance. This subject is further discussed in Chap. 14.

4.12 Sources of Variance of the Doppler Indices

The configuration of an arterial Doppler waveform is modulated by hemodynamic and nonhemodynamic factors [30]. The hemodynamic modulators may be short-term or long-term in nature. Examples of short-term factors include any acute changes in the impedance or heart rate; examples of long-term changes in the impedance include those encountered in the umbilical or uterine circulation with the progression of pregnancy. The nonhemodynamic modulators are those related to the examiners and devices, and they constitute the error component of the variance in the Doppler indices. Interobserver and intraobserver variations are the main examples of such errors. The error component of the variance may be systematic or random. The former remains relatively constant from examination to examination. This relative constancy permits it to be considered as predictable when interpreting results. In contrast, random errors are unpredictable and significantly compromise the clinical utility of a test. As an example of the hemodynamic modulation of Doppler waveforms from a circulation, we may briefly consider the sources of variance of the umbilical arterial Doppler indices. Of the various vascular systems of the fetus, the umbilical circulation has been most widely investigated in this regard. The sources of variance that influence the indices through direct or indirect hemodynamic mechanisms include gestational age-related changes in fetoplacental vascular impedance, the site of examination in the cord, fetal breathing, and fetal heart rate. The sources of variance that are not related to any hemodynamic phenomenon and constitute error consist of inter- and intraobserver variations, and interdevice variations. The latter constitute a systematic error. A detailed discussion of the sources of variance of umbilical arterial circulation may be found in Chap. 14.

4.13 Hemodynamic Basis of Doppler Waveform Analysis

Studies on the hemodynamic basis of Doppler waveform analysis have, in general, looked for any correlation between the commonly used Doppler indices and independently measured parameters of central and peripheral hemodynamics. The latter included the heart rate, peripheral resistance, and components of arterial input impedance. In addition, the association between placental angiomorphological changes and the

Doppler indices has been investigated by several workers. This section summarizes these findings and presents a brief description of basic hemodynamic concepts relevant for Doppler validation studies. This topic has also been reviewed in the literature [31].

4.14 Experimental Approaches to Hemodynamic Validation of Doppler Indices

Experimental procedures to validate Doppler indices hemodynamically often require not only the direct measurement of relevant hemodynamic parameters, such as pressure and flow, but also controlled alterations of the circulatory state. Such interventions are too invasive to be performed in relation to human pregnancy because of risks to the mother and fetus. This limitation has led to the utilization of physical and animal models. In vitro circulatory simulation exemplifies the physical model and has been used widely to investigate complex hemodynamic phenomena. Nonbiologic materials are used for prototyping circulatory systems for this type of simulation. In an intact organism, it may be difficult to perform comprehensive hemodynamic measurements without profoundly altering the physiologic state of the preparation. Indeed, it may be impossible to conduct certain hemodynamic experiments in vivo because of the inherent complexities of modeling. It is also well-recognized that the fundamental hydrodynamics principles are equally applicable to explaining circulatory phenomena in a physical simulation and in a biologic system. The principles of in vitro simulation for hemodynamic studies have been comprehensively reviewed by Hwang [32]. More specifically, hemodynamic parameters for designing an in vitro circulatory system for validating the Doppler indices have been reviewed by Maulik and Yarlagadda [33]. Regarding animal models, lamb fetuses and newborns have been used in both acute and chronic preparations. These models have been utilized traditionally to elucidate the circulatory phenomenon in human fetuses.

4.15 Arterial Input Impedance: Basic Concepts and Relevance to Doppler Waveform Analysis

The relevant aspects of peripheral circulatory dynamics are briefly reviewed here. Specifically, the basic principle of arterial input impedance and its relevance to Doppler waveform analysis are discussed. Traditionally, opposition to flow has been expressed in terms of peripheral resistance (Z_{pr}), which is the ratio of mean pressure (P_m) to mean flow (Q_m):

$$Z_{pr} = P_m / Q_m \tag{4.10}$$

Although peripheral resistance has been the prevalent concept for describing the opposition to flow, it is applicable only to steady, nonpulsatile flow conditions. Flow of blood in the arterial system, however, is a pulsatile phenomenon driven by myocardiac contractions with periodic rise and fall of pressure and flow associated with systole and diastole of the ventricles. The pressure and flow pulses, thus generated, are profoundly affected by the downstream circulatory conditions, specifically the opposition to flow offered by the rest of the arterial tree distal to the measurement point in the peripheral vascular bed. The idea of vascular impedance provides the foundation for understanding this complex phenomenon in a pulsatile circulation. Vascular impedance is analogous to electrical impedance in an alternating current system. Womersley [34] showed that the equations dealing with electrical impedance are applicable to solving the problems of vascular impedance. It should be noted in this context that the idea of vascular resistance is analogous to the principle of electrical resistance in direct-current electrical transmissions.

Closely related to impedance is the phenomenon of wave reflection in a vascular tree. The shape of pressure and flow waves at a specific vascular location results from the interaction of the forward propagating (orthograde) waves with the reflected backward propagating (retrograde) waves [35, 36].

$$P_m = P_o + P_r \tag{4.11}$$

$$Q_m = Q_o + Q_r \quad (4.12)$$

where P is pressure, Q is flow, m is the measured wave, o is the orthograde wave, and r is the retrograde wave. The presence of reflected pressure and flow waves in the arterial circulation has long been recognized by hemodynamics experts. Comprehensive analysis and understanding of the phenomenon was facilitated by using the analogy of the theory of electrical current transmission.

The existence of wave reflections in the circulatory system is evident from the observation that as one samples along the arterial tree from the heart to the periphery, the pulsatility of pressure waves progressively increases and that of the flow or flow velocity waves declines. Consequently, pressure and slow waves acquire distinctly differing configurations as they propagate down the arterial tree. The phenomenon has been analyzed mathematically by separating the observed pressure and flow waves into their constituent orthograde and retrograde components [36]. It should be noted that the forward propagating waves of pressure and flow demonstrate the same configuration. When wave reflection occurs, the retrograde flow waves are inverted, but not the retrograde pressure waves. Consequently, the observed pressure waves, which are produced by the summation of orthograde and retrograde waves, show an "additive" effect; in contrast, the observed flow (or flow velocity) waves demonstrate a "subtractive" effect. In the absence of wave reflection, the two waves would have the same shape. Wave reflections arise whenever there is a significant alteration of vascular impedance in a circulation.

Although there have been considerable theoretical and experimental basis for the role of wave reflection shaping the umbilical arterial Doppler waveforms, the phenomenon was not verifiable in the umbilical arterial circulation because of the technological challenges. Recently, utilizing an innovative computational approach, Sled et al. demonstrated the phenomenon of wave reflections in the umbilical arterial circulation in pregnant women between 26 and 37 weeks of pregnancy, thus providing clinical experimental verification of the role of wave reflection in modulating the umbilical arterial Doppler waveforms [37]. The study showed reflections ranging from 3 to 52% of the forward wave amplitude and demonstrated that marked reflections were associated with significant variances in the pulsatility between the fetal and placental ends of the umbilical cord. This is illustrated in Fig. 4.15.

Current evidence suggests that the arterial-arteriolar junctions serve as the main source of wave reflections in an arterial system. Vasodilation decreases impedance and wave reflection. In contrast, vasoconstriction increases impedance and wave reflection. As the Doppler wave represents the flow velocity wave, it is apparent that downstream impedance and wave reflection play a central part in modulating the configuration of this waveform and therefore the descriptor indices. An in-depth discussion of arterial impedance and wave reflection is beyond the scope of this review, although relevant impedance parameters are briefly described below.

The input impedance of an arterial system [33] at a specific vascular site is the ratio of the pulsatile pressure and the pulsatile flow at that location. As the pressure and flow waves are complex in shape, they are first converted by Fourier analysis to their constituent sinusoidal harmonic components. Two parameters are generated: the modulus and the phase (Fig. 4.16). The modulus is the magnitude of the pressure/flow harmonic ratios as a function of frequency; the units of measurement for the modulus are dynes·s·cm^{-3} for velocity and dynes·s·cm^{-5} for volumetric flow. The *impedance* phase expresses the phase relation between the pressure and the flow waves as a function of frequency. The phase is measured in negative or positive radians. The descriptors of vascular impedance include the following:

1. *Input impedance* is the opposition to pulsatile flow in an arterial system. Impedance at zero frequency is the peripheral resistance, which represents the steady, nonpulsatile component of vascular impedance.

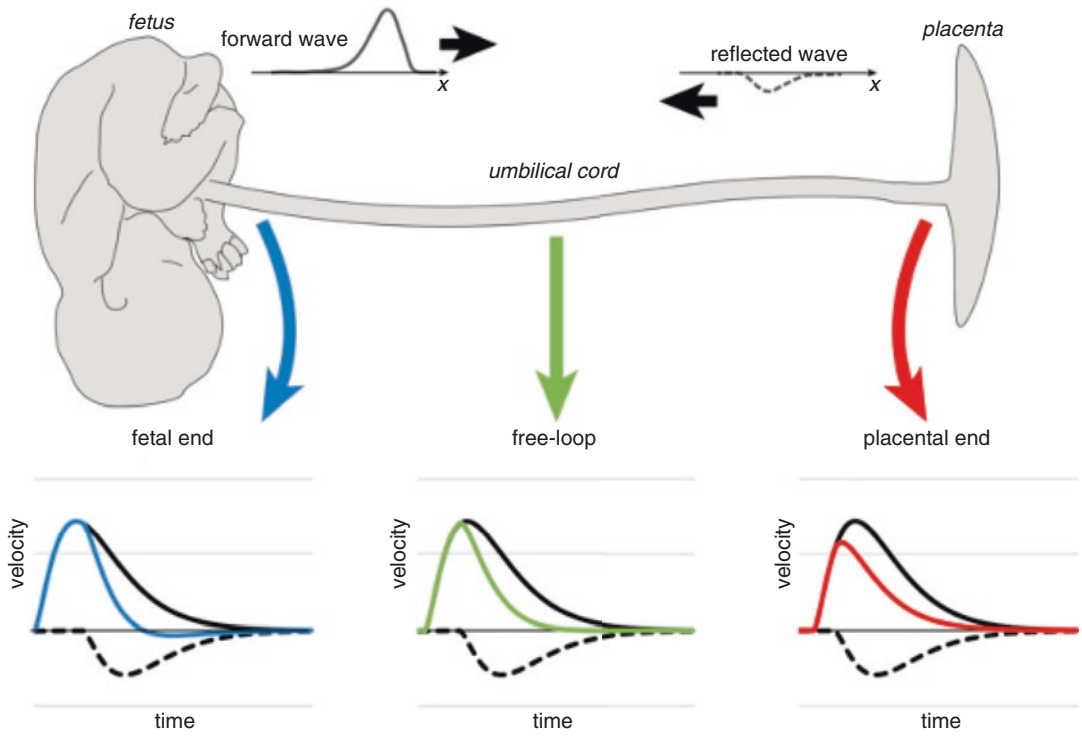

Fig. 4.15 Illustration of velocity waveforms at 3 locations along the umbilical artery. The wave reflection model predicts that the observed waveform (blue, green, or red) is the superposition of a forward traveling wave (solid black line) and a backward traveling reflected wave (dashed black line). Note that the relative arrival time of the 2 waves at each location leads to a different shape of the observed waveform (Reprinted from [37] with permission)

2. *Characteristic impedance* reflects the properties or characteristics of the arterial system, such as the cross-sectional area, wall thickness, and vascular elasticity. Any discontinuity or change in these properties gives rise to reflections of pressure and flow waves.
3. *Reflection coefficient* expresses the magnitude of the phenomenon of wave reflection in an arterial tree.

These well-established hemodynamic concepts provide the bases for hemodynamic interpretation of fetal Doppler waveforms in various physiologic and pathologic states. As the arterial Doppler wave represents the arterial flow velocity wave, it is apparent that downstream impedance and wave reflection are among the principal modulators of the waveform and therefore of the descriptor indices. As gestation progresses, umbilical arterial Doppler waveforms demonstrate a continuing increase in the end-diastolic frequency shifts (see Chap. 14), which is attributable to a progressive decline in fetoplacental vascular impedance. The latter is necessarily associated with diminished wave reflections, although it has not been feasible to study the phenomenon directly.

4.16 Doppler Indices and Peripheral Resistance

Investigations in this field were aimed at establishing a hemodynamic foundation for the Doppler indices in terms of peripheral vascular resistance. In vitro and in vivo models were used. The experimental approach essentially consisted of increasing the circulatory resistance and analyzing the changes in the indices.

Spencer and coinvestigators [38] used an in vitro flow model to validate the Doppler indices in terms of peripheral resistance (mean pres-

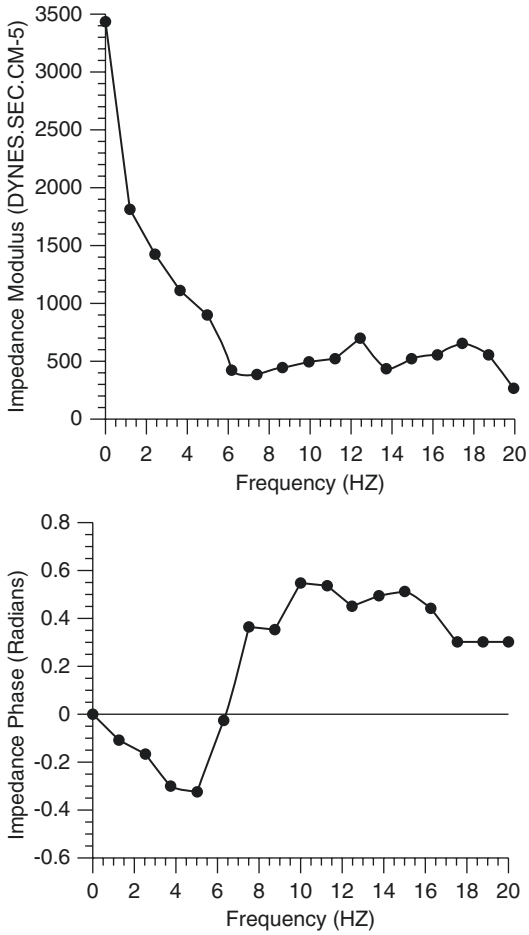

Fig. 4.16 Input impedance modulus (top) and phase (bottom) as functions of frequency

sure/mean flow). The flow was reduced in a stepwise fashion using a clamp. The decline in flow led to increases in RI, PI, and *S*/*D* ratio. The pressure and pressure waveform remained unchanged. The authors noted that rises in the Doppler indices reflected an increasing peripheral resistance; the RI and PI had a mostly linear increase, whereas the *S*/*D* ratio demonstrated an exponential increase. Maulik and colleagues [39] investigated the relation between the various umbilical arterial Doppler indices and umbilical arterial resistance in fetal lambs. The hemodynamic perturbation was induced by mechanical constriction of the umbilical artery, which resulted in declines in flow by 74%–89% and increases in pressure by 8%–23%. The correlation between the Doppler indices and the hemodynamic parameters is shown in Table 4.1, which indicates that with a well-defined obstruction to the downstream flow the indices correlate highly with the downstream hemodynamic parameters, including the peripheral resistance ($p < 0.005$).

Table 4.1 Correlation coefficients, Doppler indices versus hemodynamic parameters: constriction experiments (from [37] with permission)

Parameter	*S*/*D*	PI	RI
Peripheral resistance	0.95	0.89	0.88
Volumetric flow	−0.91	−0.96	−0.97
Pressure	0.81	0.84	0.82

S/*D* Systolic/diastolic ratio; PI Pulsatility index, *RI* Resistance index. All significant at $p < 0.005$

Trudinger and associates [40] studied the effects of chronic embolization of the umbilical circulation on the umbilical arterial *S*/*D* ratio and umbilical circulatory resistance in fetal lambs. Chronic embolization resulted in: (1) increased fetoplacental vascular resistance (0.25–0.35 mmHg mL^{-1} min^{-1}); (2) increased umbilical arterial *S*/*D* ratios; (3) significant ($p < 0.05$) declines in the umbilical total flow and the umbilical/ splanchnic flow ratio (from 3.36 to 1.53). The authors concluded that the umbilical artery flow velocity waveform *S*/*D* ratio measures the reflection coefficient at the peripheral vascular bed of the placenta. It should be noted, however, that the reflection coefficient, which has a precise hemodynamic definition (see above), was not measured in these experiments; and no correlations were performed between the hemodynamic parameters and the indices. Nevertheless, the study established a relation between chronic circulatory alteration and the umbilical arterial Doppler waveform. The above findings were corroborated by Morrow and colleagues [41], who observed progressive increases in the umbilical arterial pulsatility consequent to fetoplacental arterial embolization. In this study involving chronically catheterized sheep fetuses, the umbilical arterial *S*/*D* ratio correlated significantly ($r = 0.76$, $p = 0.001$) with placental resistance derived from the aortic-inferior vena caval pressure gradient and mean peak velocity.

One of the limitations of these studies was that resistance, rather than impedance, was used to assess the peripheral circulatory state in a pulsatile flow system. Vascular input impedance, however, is the hemodynamic parameter of choice when assessing the opposition to flow in a pulsatile circulation. In contrast, peripheral resistance is applicable only to the nonpulsatile component of a circulation and as such constitutes one of the parameters of arterial impedance.

4.17 Doppler Indices and Input Impedance

There have been a few studies investigating the relation between the Doppler indices and vascular impedance using an in vitro model and a neonatal lamb model [42–45].

Maulik and Yarlagadda [42] used an in vitro circulatory simulation system for hydrodynamic validation of the Doppler indices. The in vitro system consisted of a ventricular pump, an "arterial" line, a proximal "arterial" compliance unit, a "fetal placental vascular" branching model, a systemic bypass circuit, and a "venous" line for return of the perfusate into an "atrial" reservoir, which was connected to the pump. The impedance to flow was increased progressively by sequentially occluding the vessels of the branching model. All the indices correlated significantly ($p < 0.01$) with the peripheral resistance and reflection coefficient, indicating that changes in the peripheral resistance and the wave reflections from the downstream circulation are expressed by changes in the Doppler waveform as described by the indices. This study indicated that, within the general confines of a hydrodynamic model characterized by an increasing downstream opposition to a pulsatile flow and by a constant pump function, the descriptor indices of the Doppler waveform are capable of reflecting the state of the downstream flow impedance.

The correlation between vascular impedance and Doppler indices was also investigated in in vivo models. Downing and associates [43] developed a pharmacologic model of hemodynamic alteration using chronic term neonatal lamb preparations (Fig. 4.17). General anesthesia was used for the initial surgical preparation, which allowed in situ placement of a 4-MHz continuous-wave Doppler transducer and a transit time flow transducer on the infrarenal descending aorta. A pressure transducer was introduced retrogradely up to the level of the flow probe by the left femoral artery. Each animal was allowed to recover for 4 days, following which experimental intervention was initiated. After baseline recording of the blood pressure, heart rate, aortic flow rate, and Doppler waveforms, either vasodilation or vasoconstriction was produced with the administration of hydralazine or norepinephrine, respectively. The following parameters were measured: peripheral vascular resistance, characteristic impedance, reflection coefficient, and PI. The basic hemodynamic changes are shown in Table 4.2. Evidently, vasodilation led to tachycardia, hyperperfusion, and hypotension. Opposite changes were noted with vasoconstriction. Significant increases in the PI, peripheral vascular resistance, characteristic impedance, and reflection coefficient were seen in response to the administration of norepinephrine, and decreases in PI were noted with the administration of hydralazine. Figure 4.18 depicts the changes in the PI and reflection coefficient and Fig. 4.19 the changes in the input impedance moduli and phase. As is evident, the impedance modulus curve showed distinct changes with vasoconstriction and vasodilation. Further analysis of the data showed a statistically significant correlation between the PI and peripheral resistance. However, changes in the PI did not significantly correlate with the changes in characteristic impedance and reflection coefficient.

The next study investigated this issue [45]. The experimental model was the same as in the previous study. The experimental protocol, however, ensured that the heart rate changes due to vasoactive interventions were pharmacologically suppressed by trimethophan during vasodilation or atropine methyl-bromide during vasoconstriction. The results are presented in Table 4.3. In response to both vasodilation and vasoconstriction without controlling the reflex heart rate responses, the aortic PI was highly and positively correlated with peripheral resistance ($r = 0.78$, $p < 0.001$) but not with characteristic impedance. However, when

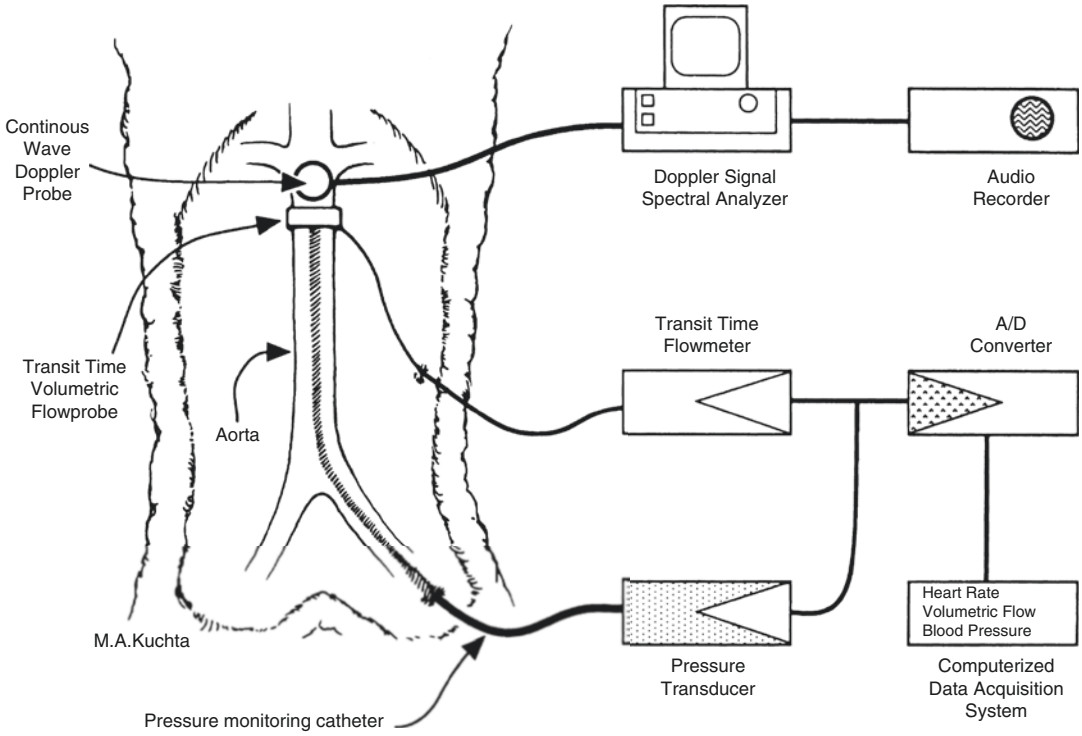

Fig. 4.17 Experimental model. Newborn lambs were instrumented with indwelling pressure transducers, volumetric flow probes, and continuous-wave Doppler flow probes around the infrarenal descending aorta. Probe wires were externalized to a flank pouch. During monitoring periods, data were collected via the use of a computerized data acquisition system, which permitted conversion of online recording of Doppler frequency shift signals, continuous aortic blood pressure, and volumetric blood flow. (Reprinted from [45] with permission)

Table 4.2 Alterations of circulatory parameters in response to vasodilation and vasoconstriction (from [41] with permission)

Parameter	Baseline	Hydralazine	Norepinephrine
Heart rate (bpm)	132 ± 15	164 ± 14	82 ± 10*
Mean arterial blood pressure (mmHg)	78 ± 5	55 ± 5*	122 ± 8*
Mean volumetric flow, descending aorta (ml/min)	319 ± 21	405 ± 28*	138 ± 22*

Data are means ± SEM
*Significant difference from baseline parameter ($p < 0.005$)

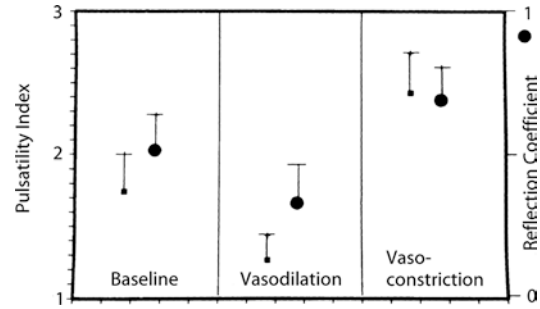

Fig. 4.18 Responses of the pulsatility index (PI) and the reflection coefficient (Rc) to vasodilation with hydralazine and vasoconstriction with norepinephrine. PI and Rc increased significantly from baseline in response to hydralazine, but Rc was not significantly affected. (From [43] with permission)

the reflex heart rate responses were inhibited, the changes in PI correlated well with peripheral resistance and characteristic impedance ($r = 0.92$, 0.95; $p < 0.001$). It is reasonable to conclude from these findings that the Doppler indices of pulsatility reflect the state of downstream circulation independent of the changes in the heart rate. However, the heart rate does influence the pulsatility and should therefore be taken into consideration. This subject is further discussed below.

4.18 Doppler Indices and Central Circulation

Central circulation potentially influences the Doppler waveform and should be an important consideration when interpreting the changes in Doppler indices. The clinical significance of fetal heart rate effect on the indices has been somewhat controversial. Although earlier studies found no significant effect of the heart rate on the Doppler indices [26], several subsequent reports refuted these findings [46, 47]. There is no evidence at present to indicate that correcting the indices for fetal heart rate improves their diagnostic efficacy when the baseline heart rate remains within the normal range. The mechanism of the heart rate effect on the Doppler indices has been well-studied in animal and in vitro models. It is well-recognized in clinical practice that when the heart rate drops the diastolic phase of the cardiac cycle is prolonged, which results in a decrease in the end-diastolic frequency shift (Fig. 4.20). This condition obviously increases the pulsatility of the waveform, which is reflected in the descriptor indices, such as the PI or the *S*/*D* ratio.

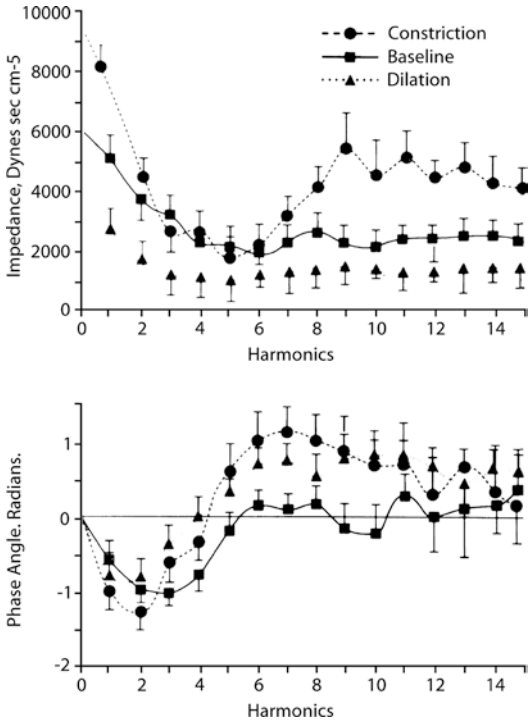

Fig. 4.19 Impedance moduli and phase angle during baseline, vasodilation, and vasoconstriction with hydralazine and norepinephrine, respectively. Each curve represents the mean ± SEM impedance moduli for all study animals. (From [43] with permission)

This phenomenon was clearly demonstrated in fetal ovine models in which fetal bradycardia was experimentally induced by either acute uteroplacental flow occlusion [48] or maternal hypoxia [49]. The Doppler indices measured were the RI, *S*/*D* ratio, and PI. The duration of the cardiac cycle and its systolic and diastolic times were approximated from the Doppler waveform. In the uteroplacental flow insufficiency model, transient occlusion of the maternal common uterine artery produced statistically significant ($p < 0.005$) increases in the Doppler indices and cardiac cycle time. The increases in the Doppler indices disappeared ($p > 0.05$) when the latter were corrected for changes in the cardiac cycle time (Fig. 4.21). As expected, the diastolic time was noted to be the principal contributor to the changes in heart rate (Fig. 4.22). The effect of heart rate was also investigated in a chronic ovine model in which changes in the umbilical arterial Doppler waveform in response to acute maternal hypoxemia were assessed. During the periods of

Table 4.3 Hemodynamic parameters and Doppler indices in drug-induced vasodilation and vasoconstriction with and without heart rate changes (from [43], with permission)

Parameters	Control	Hydralazine	Hydralazine, trimethophan	Phenylephrine	Phenylephrine, atropine MB
HR	128 ± 10	186 ± 12	130 ± 8	65 ± 7	126 ± 8
PI	1.91 ± 13	1.50 ± 21	1.71 ± 13	2.54 ± 19	2.28 ± 0.21
Z_{pr}	39,960 ± 8728	12,350 ± 1210	10,460 ± 961	65,380 ± 8130	60,840 ± 7590
Z_o	4010 ± 340	1683 ± 350	1333 ± 410	8960 ± 760	7683 ± 630

HR Heart rate (bpm), PI Pulsatility index, Z_{pr} peripheral resistance, Z_o characteristic impedance

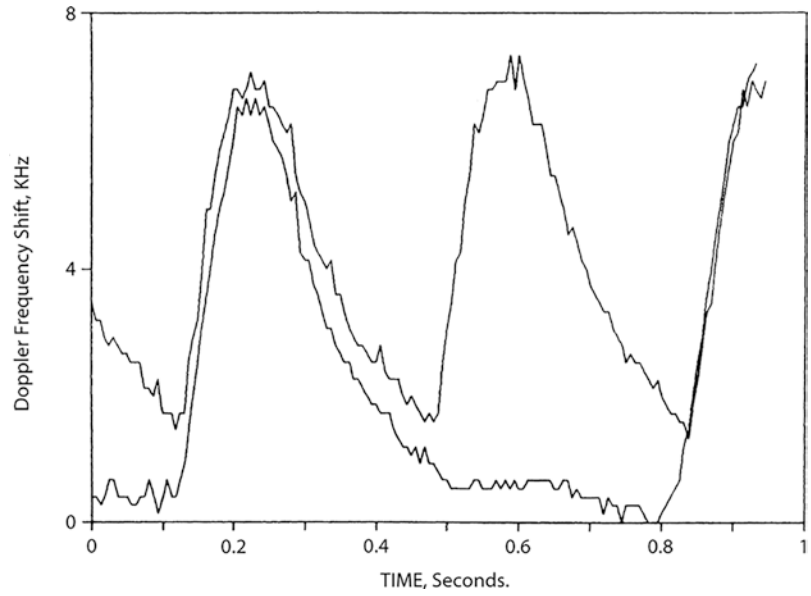

Fig. 4.20 Comparison of the umbilical arterial Doppler waveforms with normal heart rate (125 bpm) and bradycardia (77 bpm). Vertical axis represents the magnitude of Doppler frequency shift. Horizontal axis represents the time

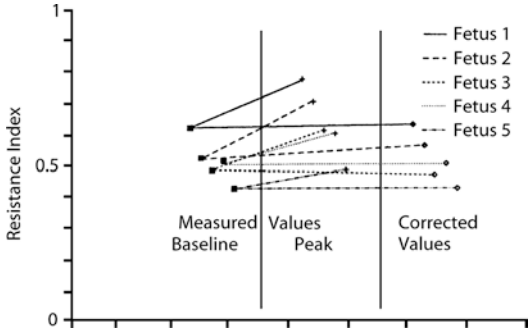

Fig. 4.21 Effect of variations in the cardiac cycle time correction on the resistance index (RI). The three divisions in this figure correspond to baseline, measured peak, and corrected values, respectively. Please note that the differences between the baseline and the measured peak values (all significant at $p < 0.005$) disappeared when corrected for fetal heart rate (none significant at $p < 0.005$). (From [48] with permission)

maternal hypoxemia, the fetal heart rate decreased (to <80 bpm) and umbilical arterial Doppler indices increased ($p < 0.001$). Furthermore, the Doppler indices were highly but negatively correlated with alterations in the fetal heart rate ($p < 0.001$). Analysis of the Doppler waveform phase intervals revealed nearly constant systolic intervals, whereas diastolic intervals varied inversely with the heart rate alterations. Moreover, the umbilical arterial Doppler indices, when corrected for the fetal heart rate changes, were relatively unchanged from baseline measurements. Both studies confirmed that the fetal cardiac cycle, and therefore the fetal heart rate, plays an important role in shaping the umbilical arterial Doppler waveform. Furthermore, this effect is mediated predominantly via changes in the diastolic phase of the cardiac cycle. There is also evidence that the fetal heart rate may affect the ability of the Doppler waveform analysis to reflect completely the changes in downstream impedance. It should be noted that there is a paucity of information on the central circulatory factors, other than heart rate, that influence the Doppler waveform.

Legarth and Thorup [50, 51] utilized an in vitro model of circulation in which they studied the influence of central and peripheral circulations on the Doppler waveform. The in vitro model allowed independent control over pulse rate, volumetric flow, stroke volume, pressure, and peripheral resistance. The authors observed that the velocity indices changed with the pulse rate, although flow and peripheral resistance were constant. They also noted that the rising slope of the Doppler waveform did not correlate with cardiac contractility as measured by the changes in pressure (the first maximum derivative of the intraventricular pressure: *dP*/*dt*).

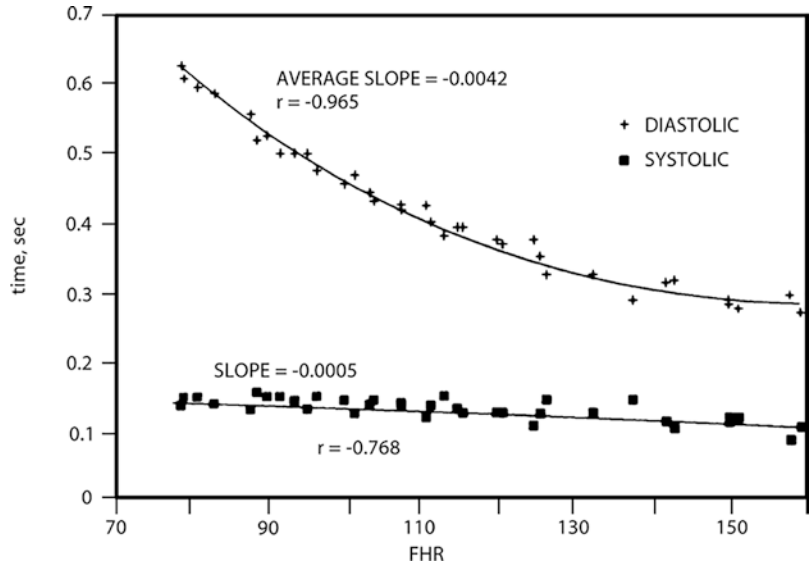

Fig. 4.22 Correlation between systolic and diastolic components of the Doppler waveform and the fetal heart rate (FHR), which is the reciprocal of the cardiac cycle time. Note that the slope of the diastolic time versus FHR is approximately 9 times greater than the slope of the systolic time versus FHR. (Based on data from [48])

This finding is intriguing and deserves further investigation. Regarding the effect of resistance on the rising slope, the two parameters did not correlate when the flow was kept constant, but when the pressure was kept constant the rising slope increased significantly with resistance.

These studies emphasize the relative importance of the central circulatory changes to alterations in the Doppler waveform.

4.19 Placental Vascular Changes and Abnormal Doppler Waveforms

The dependence of arterial Doppler waveform on downstream circulatory impedance is also reflected in the pathology of the distal vascular bed. Various investigators reported fetoplacental morphological changes in relation to umbilical arterial velocimetry and pregnancy complications including fetal growth compromise. Giles and coinvestigators [52] correlated fetoplacental histopathological changes with umbilical arterial *S*/*D* ratio in women with normal and complicated pregnancies. A statistically significant decrease ($p < 0.01$) in the modal small arterial count (arteries in the tertiary stem villi measuring less than 90 μm in diameter) was observed in abnormal pregnancies with an abnormal Doppler index. The authors suggested fetoplacental vaso-obliterative pathologic processes as the underlying cause of an abnormal Doppler waveform. Subsequently, Krebs and coinvestigators [53] demonstrated that in preterm intrauterine growth restriction pregnancies with umbilical arterial absent end-diastolic flow velocity, the capillary loops were sparse in number and significantly longer, and had significantly less branching and coiling than in the control cases. These findings are more reflective of villous maldevelopment rather than a vaso-obliterative process. This was further corroborated by Todros and associates [54] who demonstrated that, compared with those with positive end-diastolic flow in the umbilical artery, the placentas from growth-restricted fetuses with absent or reverse end-diastolic flow showed a normal pattern of stem artery development, accompanied by significantly decreased capillary angiogenesis and terminal villous development. The authors speculated that these findings suggested fetoplacental adaptive response in the presence of uteroplacental ischemia.

Maulik and associates recently provided insights into the underlying angiogenic molecular mechanisms [55]. In a prospective study involving pregnancies complicated with fetal growth restriction and umbilical artery absent or reversed end-diastolic flow, they demonstrated a significant downregulation of placental neuropilin1 (NRP-1)

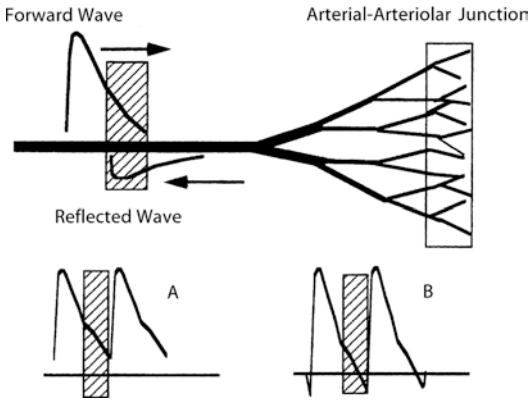

Fig. 4.23 Effect of wave reflection on umbilical arterial Doppler waveforms. Note that as the pulse wave propagation velocity in the fetus is slower than in the adults, retrograde waves affect forward propagating waves during late diastole (cross-hatched box). (**A**) Normal waveforms with minimal wave reflection because of low impedance in the fetoplacental arterial circulation. (**B**) Effect of significant wave reflection when fetoplacental impedance becomes high, resulting in the absence or reversal of end-diastolic frequency shift

gene and protein expression utilizing quantitative real-time polymerase chain reaction and Western blot, respectively. Placental immunohistochemistry provided further corroboration. These findings are significant as NRP-1 is known to promote sprouting angiogenesis and suggests its downregulation may be involved in the deficient vascular branching observed in FGR placentas and further supports the presence of an antiangiogenic state.

Based on these observations, the following vascular and hemodynamic mechanism may be suggested for abnormal umbilical arterial Doppler waveforms in pregnancies complicated with fetal growth restriction and highly abnormal umbilical arterial Doppler indices. Abnormal uteroplacental angiogenesis and consequent ischemia lead to fetoplacental villous maldevelopment and deficient angiogenesis. These changes result in an increase in the arterial impedance, which is necessarily associated with enhanced pressure and flow velocity wave reflections. The reflected flow velocity waves propagating backward will change the shape of arterial flow velocity waves. A graphic depiction of this concept in relation to umbilical arterial Doppler waveforms is presented in Fig. 4.23.

References

1. Saini VD, Maulik D, Nanda NC, Rosenzweig MS. Computerized evaluation of blood flow measurement indices using Doppler ultrasound. Ultrasound Med Biol. 1983;9:657–60.
2. Maulik D, Saini VD, Nanda NC, Rosenzweig MS. Doppler evaluation of fetal hemodynamics. Ultrasound Med Biol. 1982;8:705–10.
3. Evans DH, McDicken WN, Skidmore R, Woodcock JP. Doppler signal processors: theoretical considerations. In: Doppler ultrasound: physics, instrumentation and clinical applications. Chichester: Wiley; 1989. p. 144.
4. Maulik D, Nanda NC, Moodley S, Saini VD, Thiede HA. Application of Doppler echocardiography in the assessment of fetal cardiac disease. Am J Obstet Gynecol. 1985;151:951–7.
5. Kremkau F. Doppler ultrasound: principles and instrumentation. Philadelphia: Saunders; 1990.
6. Gill RW. Pulsed Doppler with B-mode imaging for quantitative blood flow measurements. Ultrasound Med Biol. 1979;5:223–35.
7. Eik Nes SH, Brubakk AO, Ulstein MK. Measurement of human fetal blood flow. BMJ. 1980;280:283–4.
8. Maulik D, Nanda NC, Saini VD. Fetal Doppler echocardiography: methods and characterization of normal and abnormal hemodynamics. Am J Cardiol. 1984;53:572–8.
9. Boito S, Struijk PC, Ursem NT, Stijnen T, Wladimiroff JW. Umbilical venous volume flow in the normal developing and growth restricted human fetus. Ultrasound Obstet Gynecol. 2002;19:344–9.
10. Hoskins PR, Kenwright DA. Recent developments in vascular ultrasound technology. Ultrasound. 2015;23(3):158–65.
11. Jensen JA, Nikolov SI, Alfred CH, Garcia D. Ultrasound vector flow imaging—part I: sequential systems. IEEE Trans Ultrasonics Ferroelectrics Frequency Control. 2016;63(11):1704–21.
12. Jensen JA, Nikolov SI, Yu AC, Garcia D. Ultrasound vector flow imaging—part II: parallel systems. IEEE Trans Ultrasonics Ferroelectrics Frequency Control. 2016;63(11):1722–32.
13. Yiu BY, Lai SS, Yu AC. Vector projectile imaging: time-resolved dynamic visualization of complex flow patterns. Ultrasound Med Biol. 2014;40:2295–309.
14. Hansen KL, Nielsen MB, Jensen JA. Vector velocity estimation of blood flow - a new application in medical ultrasound. Ultrasound. 2017;25:189–99.
15. Dunmire KW, Beach KW, Labs KH, et al. Cross-beam vector Doppler ultrasound for angle independent velocity measurements. Ultrasound Med Biol. 2000;26:1213–35.
16. Trahey GE, Allison JW, Ramm OT. Angle independent ultrasonic detection of blood flow. IEEE Trans Biomed Eng. 1987;34:965–7.
17. Pihl MJ, Jensen JA. A transverse oscillation approach for estimation of three-dimensional velocity vec-

tors, part I: concept and simulation study. IEEE Trans Ultrasonics Ferroelectrics Frequency Control. 2014;61:1599–607.
18. Asami R, Tanaka T, Shimizu M, Seki Y, Nishiyama T, Sakashita H, Okada T. Ultrasonic vascular vector flow mapping for 2-D flow estimation. Ultrasound Med Biol. 2019;45(7):1663–74.
19. Brandt AH, Hansen KL, Ewertsen C, Holbek S, Olesen JB, Moshavegh R, Thomsen C, Jensen JA, Nielsen MB. A comparison study of vector velocity, spectral Doppler and magnetic resonance of blood flow in the common carotid artery. Ultrasound Med Biol. 2018;44:1751–61.
20. Goddi A, Bortolotto C, Raciti MV, Fiorina I, Aiani L, Magistretti G, Sacchi A, Tinelli C, Calliada F. High-frame rate vector flow imaging of the carotid bifurcation in healthy adults: comparison with color Doppler imaging. J Ultrasound Med. 2018;37:2263–75.
21. McDonald D. Blood flow in arteries. Baltimore: Williams & Wilkins; 1974.
22. Gosling RG, King DH. Ultrasound angiology. In: Macus AW, Adamson J, editors. Arteries and Veins. Edinburgh: Churchill-Livingstone; 1975. p. 61–98.
23. Pourcelot L. Applications clinique de l'examen Doppler transcutance. In: Pourcelot L, editor. Velocimetric ultrasonore Doppler. Paris: INSERM; 1974. p. 213.
24. Stuart B, Drumm J, FitzGerald DE, Diugnan NM. Fetal blood velocity waveforms in normal pregnancy. Br J Obstet Gynaecol. 1980;87:780–5.
25. Campbell S, Diaz-Recasens J, Griffin DR, et al. New Doppler technique for assessing uteroplacetal blood flow. Lancet. 1983;1:675–7.
26. Thompson RS, Trudinger BJ, Cook CM. Doppler ultrasound waveforms in the fetal umbilical artery: quantitative analysis technique. Ultrasound Med Biol. 1985;11:707–18.
27. Maršál K. Ultrasound assessment of fetal circulation as a diagnostic test: a review. In: Lipshitz J, Maloney J, Nimrod C, Carson G, editors. Perinatal development of the heart and lung. Ithaca, NY: Perinatology Press; 1987. p. 127–42.
28. Maulik D, Yarlagadda P, Youngblood JP, Ciston P. The diagnostic efficacy of umbilical arterial systolic/diastolic ratio as a screening tool: a prospective blinded study. Am J Obstet Gynecol. 1990;162:1518–23.
29. Maulik D, Yarlagadda P, Youngblood JP, Ciston P. Comparative efficacy of umbilical arterial Doppler indices for predicting adverse perinatal outcome. Am J Obstet Gynecol. 1991;164:1434–9.
30. Maulik D, Yarlagadda P, Youngblood JP, Willoughby L. Components of variability of umbilical arterial Doppler velocimetry: a prospective analysis. Am J Obstet Gynecol. 1989;160:1406–9.
31. Maulik D. Hemodynamic interpretation of the arterial Doppler waveform. Ultrasound Obstet Gynecol. 1993;3(3):219–27.
32. Hwang NHC, Norman A. An engineering survey of problems in cardiovascular flow dynamics and measurements. Baltimore: University Park Press; 1977.
33. Maulik D, Yarlagadda P. In vitro validation of Doppler waveform indices. In: Maulik D, McNellis D, editors. Doppler ultrasound measurement of maternal-fetal hemodynamics. Ithaca, NY: Perinatology Press; 1987. p. 257.
34. Womersley JR. The mathematical analysis of the arterial circulation in a state of oscillatory motion. Technical report WADC-TR56-614. Wright Air Development Center, Maryland; 1957.
35. Westerhof N, Sipkema P, Van den Bos GC, Elzinga G. Forward and backward waves in the arterial system. Cardiovasc Res. 1972;6:648–56.
36. Murgo JP, Westerhof N, Giolma JP, Altobelli SA. Manipulation of ascending aortic pressure and flow ave reflections with Valsalva maneuver: relationship to input impedance. Circulation. 1981;63:122–32.
37. Sled JG, Stortz G, Cahill LS, Milligan N, Ayyathurai V, Serghides L, Morgen E, Seravalli V, Delp C, McShane C, Baschat A. Reflected hemodynamic waves influence the pattern of Doppler ultrasound waveforms along the umbilical arteries. Am J Phys Heart Circ Phys. 2019;316(5):H1105–12.
38. Spencer JAD, Giussani DA, Moore PJ, Hanson MA. In viro validation of Doppler indices using blood and water. J Ultrasound Med. 1991;10:305–8.
39. Maulik D, Yarlagadda P, Nathaniels PW, Figueroa JP. Hemodynamic validation of Doppler assessment of fetoplacental circulation in a sheep model system. J Ultrasound Med. 1989;8:177–81.
40. Trudinger BJ, Stevens D, Connelly A, et al. Umbilical artery velocity waveform and placental resistance: the effects of embolization of the umbilical circulation. Am J Obstet Gynecol. 1987;157:1443–8.
41. Morrow RJ, Adamson SL, Bull SB, Knox Ritchie JW. Effect of placental embolization on the umbilical arterial velocity waveform in fetal sheep. Am J Obstet Gynecol. 1989;161:1055–60.
42. Maulik D, Yarlagadda P. Hemodynamic validation of the Doppler indices: an in vitro study (abstract). Presented at the International Perinatal Doppler Society: 3rd Congress, Malibu, CA; 1990.
43. Downing GJ, Yarlagadda AP, Maulik D. Comparison of the pulsatility index and input impedance parameters in a model of altered hemodynamics. J Ultrasound Med. 1991;10:317–21.
44. Downing GJ, Maulik D. Correlation of the pulsatility index (PI) with input impedance parameters during altered hemodynamics (abstract). J Matern Fetal Invest. 1991;1:114.
45. Downing GJ, Maulik D, Phillips C, Kadado T. In vivo correlation of Doppler waveform analysis with arterial input impedance parameters. Ultrasound Med Biol. 1993;19:549–59.
46. Mires G, Dempster J, Patel NM, et al. The effect of fetal heart rate on umbilical artery flow velocity waveform. Br J Obstet Gynaecol. 1987;94:665–9.
47. Yarlagadda P, Willoughby L, Maulik D. Effect of fetal heart rate on umbilical artery Doppler indices. J Ultrasound Med. 1989;8(215–218):47.

48. Maulik D, Downing GJ, Yarlagadda P. Umbilical arterial Doppler indices in acute uteroplacental flow occlusion. Echocardiography. 1990;7:619.
49. Downing GJ, Yarlagadda P, Maulik D. Effects of acute hypoxemia on umbilical arterial Doppler indices in a fetal ovine model. Early Hum Dev. 1991;25:1–10.
50. Legarth J, Thorup E. Characteristics of Doppler blood velocity waveforms in a cardiovascular in vitro model. II. The influence of peripheral resistance, perfusion pressures and blood flow. Scan J Clin Lab Invest. 1989;49:459–64.
51. Legarth J, Thorup E. Characteristics of Doppler blood velocity waveforms in a cardiovascular in vitro model. I. the model and the influence of pulse rate. Scand J Clin Lab Invest. 1989;49:451–7.
52. Giles WB, Trudinger JB, Baird PJ. Fetal umbilical artery flow velocity waveforms and placental resistance: pathologic correlation. Br J Obstet Gynaecol. 1985;92:31–8.
53. Krebs C, Macara LM, Leiser R, Bowman AW, Greer IA, Kingdom JC. Intrauterine growth restriction with absent end-diastolic flow velocity in the umbilical artery is associated with maldevelopment of the placental terminal villous tree. Am J Obstet Gynecol. 1996;175:1534–42.
54. Todros T, Sciarrone A, Piccoli E, Guiot C, Kaufmann P, Kingdom J. Umbilical Doppler waveforms and placental villous angiogenesis in pregnancies complicated by fetal growth restriction. Obstet Gynecol. 1999;93:499–503.
55. Maulik D, De A, Ragolia L, Evans J, Grigoryev D, Lankachandra K, et al. Down-regulation of placental neuropilin-1 in fetal growth restriction. Am J Obstet Gynecol. 2016;214(2):279–e1.

Venous Hemodynamics

5

Torvid Kiserud and Jörg Kessler

Evaluation of the venous system is an integrated part of the hemodynamic assessment of the fetus. Understanding the underlying fluid-dynamic mechanisms of our Doppler recordings is essential when assessing the various components of hemodynamics; e.g., blood velocity, volume flow, pressure, resistance, and wave formations and propagation. The present chapter is not intended to cover all details, but addresses these issues from a clinical point of view to help clinicians appreciate the significance and limitations of venous Doppler recordings. For the interested reader, more extensive discussions of blood flow dynamics are available in the literature [1–5].

5.1 Blood Velocity in Veins

Conventionally, venous flow is expected to have a steady low velocity until approaching the pumping fetal heart when the velocity turns pulsatile. However, high velocities also occur in the fetus, e.g., in the umbilical vein entrance into the abdomen [6, 7], the ductus venosus [8], inferior vena cava (IVC) during augmented respiratory activity [9, 10], or in pathological conditions with altered pressures and dimensions. And, pulsations may occur in peripheral sections of the vein caused by transmitted energy of cardiac activity or other sources.

5.1.1 Laminar Flow, Turbulent Flow, or Whirls

In the fetal venous system, blood flows are essentially laminar, which means that the velocity is organized with the highest velocity in the center of the tubular vein with concentric layers of decreasing velocities. The lowest velocity is at the vessel wall where sheer force, and resistance, is highest. When the flow is steady, it has a parabolic velocity profile across the cross section (Fig. 5.1). This flow pattern is energy-efficient and linearly related to the pressure gradient. However, if transformed into turbulent flow, the energy expenditure rises. In turbulent flow, the laminar pattern has dissolved into unpredictable velocity directions, the result being a blunted, or flat, spatial velocity profile (Fig. 5.1). In general, the wider the vein is, the higher the velocity is, and the longer the velocity stays high, the higher is the probability of breaking into turbulence. *Reynold's number* (R_e) gives a rough estimate of the risk for turbulence, and the risk increases with the number. R_e can be calculated using the diameter D in cm and velocity V in cm/s, while dynamic viscosity is represented by the constant 0.041 [1]:

T. Kiserud (✉) · J. Kessler
Department of Obstetrics and Gynecology, Haukeland University Hospital, Bergen, Norway

Department of Clinical Science, Faculty of Medicine, University of Bergen, Bergen, Norway
e-mail: torvid.kiserud@uib.no

D. Maulik, C. C. Lees (eds.), *Doppler Ultrasound in Obstetrics and Gynecology*,
https://doi.org/10.1007/978-3-031-06189-9_5

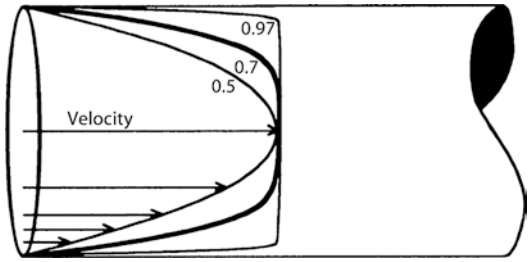

Fig. 5.1 The velocity profile represents the velocity distribution across the vessel (spatial velocity profile) and is characterized by the ratio $h = V_{wmean}/V_{tamax}$. The V_{wmean} is the weighted mean velocity across the entire vessel cross section, and V_{tamax} the time-averaged maximum velocity (confer Fig. 5.9). The steady blood flow in the umbilical vein has a parabolic velocity profile corresponding to $h = 0.5$. The accelerated blood velocity at the ductus venosus inlet has a partially blunted velocity profile of $h = 0.7$, while at the cardiac outlets the profile is even more blunted (e.g., $h = 0.97$). (Modified from [11])

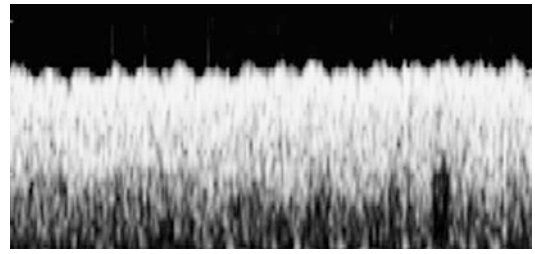

Fig. 5.2 Vortex formation (whirls) recorded as velocity variation, which mimics pulsation, in the umbilical vein. Such whirls tend to occur in large bore vessels with a steady flow, particularly if there is a diameter variation, curvature, or bifurcation. The velocity variation is not synchronized with the heart rate. (Modified from [12])

$$R_e = D \cdot V / 0.041$$

In blood, $R_e \geq 2300$ is associated with risk of turbulence. In general, venous flow in the fetus is laminar with R_e far below this limit. E.g., in the sizeable intra-abdominal umbilical vein during late gestation, R_e hardly exceeds 500. And, in the extremes of physiological conditions, i.e., forceful fetal breathing, velocities of 250 cm/s can be recorded in the ductus venosus, but without turbulence since the diameter at the isthmus hardly exceeds 0.2 cm, the R_e being 1200 and way below the critical 2300. Similar velocities can be recorded in the abdominal IVC when squeezed during fetal respiratory activity and the pressure gradient between abdomen and chest increases [9, 10]. When this high-velocity is projected into the confluence of the IVC below the diaphragm, the expanded diameter here (e.g., ≥0.6 cm) results in $R_e \geq 3700$ with high risk of turbulence. However, since this blood velocity is not steady but pulsating, the velocity variation counteracts the transition to turbulence.

Whirls, or vortices, on the other hand, such as those observed in a river, may also occur in the fetal venous system, but are not regarded as turbulence in the present fluid-dynamic sense. Such vortices can be observed during Doppler recording where the vessel is wide, e.g., the intra-abdominal umbilical vein distension near the abdominal wall, a curvature, or bifurcation (Fig. 5.2).

5.1.2 Parabolic Flow and Other Velocity Profiles

In a straight venous section, e.g., the umbilical vein with a steady velocity, the distribution of the velocity across the cross-sectional area of the vessel is expected to be parabolic with the highest velocity (V_{tamax}) in the center of the cross section (Fig. 5.1). The ratio of the average velocity across the vessel (V_{wmean}) and V_{tamax} characterizes the velocity profile (*h*). For a parabolic flow, it is $h = V_{wmean}/V_{tamax} = 0.5$.

However, changes in the geometrical properties of the vein impact the velocity profile (Fig. 5.3). For example, when the umbilical blood leaves the venous confluence at the placenta to enter the narrower vein of the cord, the blood accelerates and the velocity profile is more blunted [13]. It takes a few cm into the cord to restore the parabolic profile. Similarly, in the narrow isthmus of the ductus venosus, blood accelerates and the velocity profile increases to $h = 0.7$ (Fig. 5.1) [11, 14, 15]. Beyond this isthmus, the ductus venosus tends to have a widening shape where the peripheral velocities decrease, while the central maximum velocity is kept high for some distance. This has been verified in mathematical modeling and animal experiments for the second half of pregnancy [15–18], but for the first trimes-

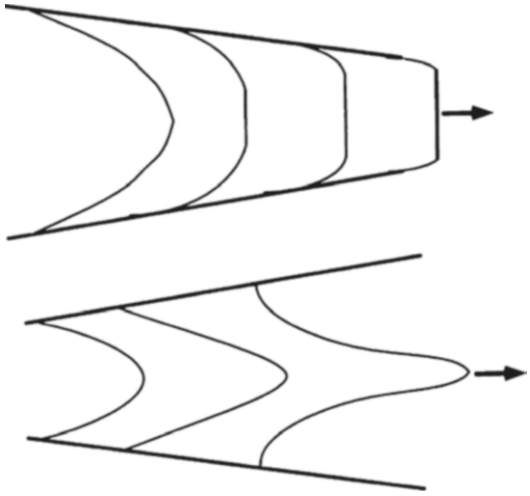

Fig. 5.3 The impact of geometry on the velocity profile *h*. The profile changes from a parabolic shape to a more blunted (flat) shape at converging vessel lumen (*upper panel*). A funnel-shaped geometry with increasing diameter is associated with reduced velocities at the periphery and a more or less maintained axial velocity resulting in a pointed velocity profile (*lower panel*). (Modified from [5])

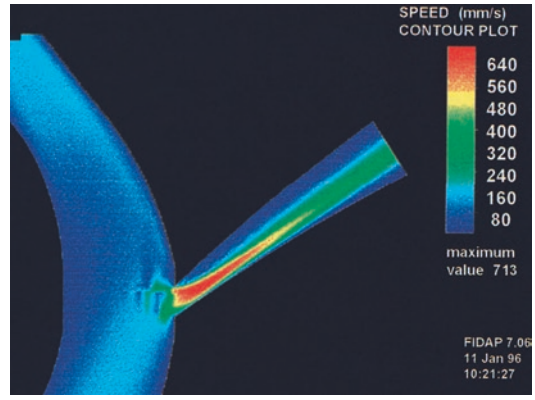

Fig. 5.4 Two-dimensional velocity profile in the ductus venosus predicted by computer modeling. Note the increased velocity in front of the inlet to the ductus venosus, and the skewed velocity distribution in the body of the ductus. (Modified from [15])

ter where velocities are generally low and diameters smaller, the profile is calculated to be $h = 0.53$ [19]. It is also worth noting that the velocity and its profile start to change before the blood has reached the narrow section of a constriction, and gradually return to parabolic or more pointed velocity profile on the other side of the constriction, again depending on geometrical details (Figs. 5.4 and 5.5).

Curvature, bifurcation, or other changes in blood flow direction cause changes in the velocity profile. The blood starts spiraling along the wall of the curvature and the velocity maximum is commonly dislodged toward the periphery of the vessel cross section and even a negative (reversed) velocity may occur (Fig. 5.5).

An example would be the physiological constriction of the umbilical vein at the abdominal inlet. The abrupt expansion of the umbilical vein diameter after the constriction at the abdominal wall makes the blood slow down and regain parabolic flow within a short distance. In some cases, this expansion is extensive and permits vortex formation (whirls) and may be regarded as a post-stenotic dilatation, or aneurysm. In contrast,

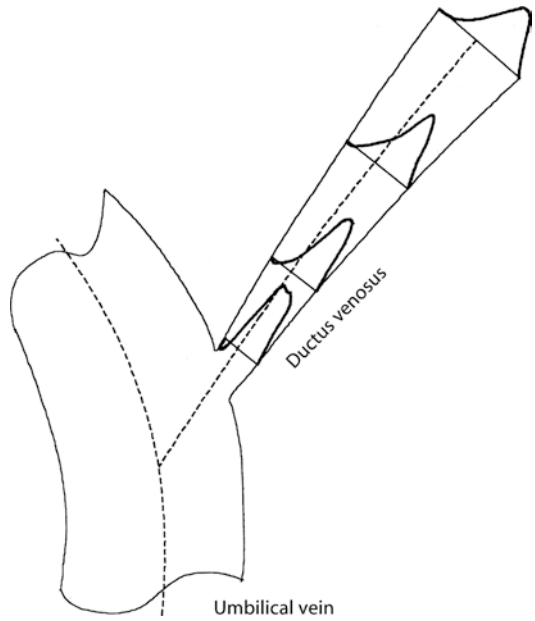

Fig. 5.5 Estimated spatial velocity distribution at the umbilical vein–ductus venosus junction based on a computer model. The accelerated blood velocity has a blunted profile that gradually reduces to a parabolic profile but modified by vessel geometry. The high axial velocity is maintained for a longer distance compared with the peripheral velocities. Note the small proportion of reversed (negative) velocity that may occur depending on geometrical details (see also Figs. 5.3 and 5.4). (Modified from [16])

the modest gradual widening geometry of the ductus venosus central to the isthmus maintains the high axial velocity for a longer distance (Fig. 5.5).

5.2 Viscosity Effect on Venous Flow

At high velocity, blood behaves like water, Newtonian, i.e., the viscosity is constant with increasing shear rate. However, when velocities are low, that is no longer the case as viscosity has an increasing effect on the resistance to flow, and energy dissipation, i.e., non-Newtonian.

A clinically important example is the umbilical perfusion of the fetal liver (Fig. 5.6). As much as 70–80% of the umbilical venous return perfuses the liver which has a huge capillary cross section compared with the umbilical vein. Thus, the blood velocity reduces correspondingly when entering the liver parenchyma. With the low velocity, flow is now non-Newtonian and viscous resistance is high. If the perfusion pressure is too low, the blood stops (closing pressure or opening pressure). The viscosity changes with hematocrit, and in particular, the fetal liver perfusion is sensitive to such changes since the driving pressure (umbilicocaval or portocaval pressure gradient) normally operates at a very low level, ≈3 mmHg [9, 20].

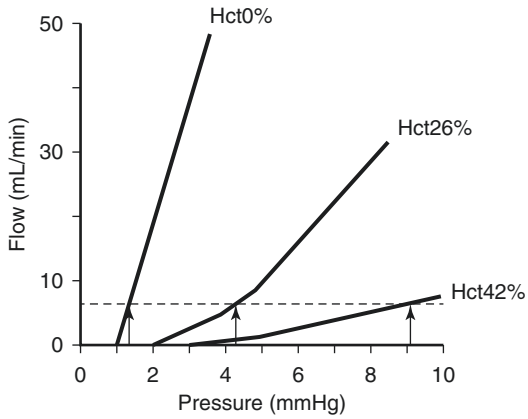

Fig. 5.6 Effect of blood viscosity on umbilical perfusion of the fetal liver tested in a fetal lamb experiment near term using saline and blood of hematocrit (Hct) 26 or 42% to represent increasing levels of viscosity. Note that the opening pressure (closing pressure) for perfusion is 1, 2, and ≥3.5 mmHg for Hct 0, 26, or 42%. To maintain a flow of 7 mL/min, a pressure of >1, >4, and >9 mmHg was needed correspondingly (Modified from [21])

This is an important part of the passive regulation of blood distribution between the liver and ductus venosus [21]. Since the ductus venosus has a high blood velocity, it is less affected, and an increase in hematocrit will cause a shift of umbilical blood flow from the liver to the ductus venosus. On top of this comes the active endocrine regulation. Similar effects can be expected in other sections of the circulation where the vascular cross section is large compared with the feeding vessel (e.g., placenta), but the liver portal circuit is special since the feeding vessels are veins with low pressure and velocity compared with circuits fed by arteries.

5.3 Pressure Gradient and Resistance in Venous Flow

In any section of the venous system, there is a pressure gradient Δp involved in maintaining a steady flow and overcome resistance (R):

$$R = \frac{128\eta L}{\pi D^4}$$

which is dependent on viscosity η, diameter D, and length L. There is a long historic discussion whether the ductus venosus has a dedicated muscular sphincter at its inlet to regulate flow (confer Chap. 29). The focus on this short venous section is understandable since the ductus venosus is remarkably narrow, 0.5–2 mm, during the second half of pregnancy [9, 22], and any change in D, in the power of four, will have a profound effect on R. However, the isthmus is but a short and ill-defined section of the otherwise long and slender ductus venosus (Fig. 5.7), and experiments have shown that the entire length of the vessel dilates as a response to a hypoxic challenge [23] with a major reduction in R, which is proportional to L in the equation. The pressure gradient (Δp) along the vein, on the other hand, can be calculated as $\Delta p = R\dot{V}$, where $\dot{V}$ signifies blood flow volume, provided the flow is steady without variation in diameter or velocity.

A well-established method of assessing pressure gradients using Doppler ultrasound in

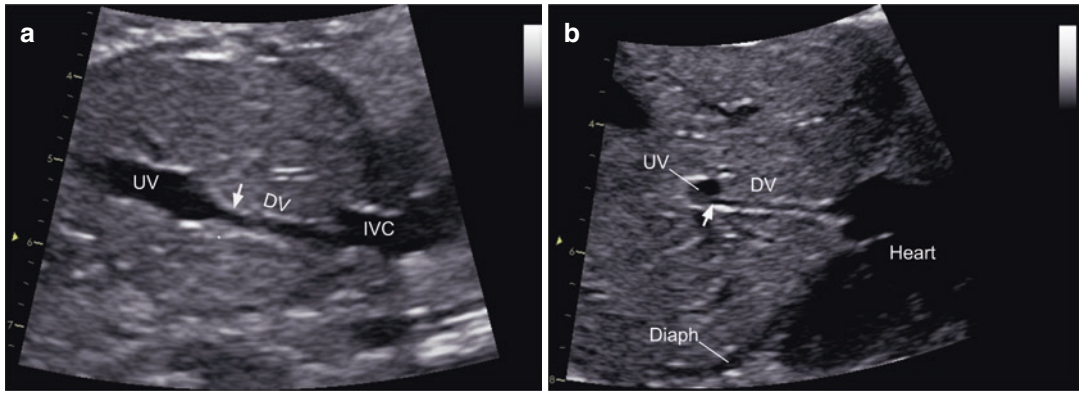

Fig. 5.7 The shunt ductus venosus (DV) connects the intra-abdominal umbilical vein (UV) to the inferior vena cava (IVC). Typically, it is a slender slightly trumpet-shaped vessel with a narrow isthmus at its entrance (arrow) in panel (**a**). However, variation in the details is common such as in panel (**b**) where almost the entire length of the ductus maintains a similarly small diameter and thus contributes considerably to resistance and flow regulation. *Diaph* Diaphragm

cardiology [24, 25] has also been tested and proven to be valid in the fetal venous system [9, 26]. Since the ductus venosus and the portal circuit in the fetus both connect the intra-abdominal umbilical vein with the IVC, it is possible to exploit the high velocity at the ductus venosus inlet to determine the umbilicocaval (i.e., portocaval) Δp, which is the driving pressure for the venous liver perfusion [9]. Since there is a substantial velocity acceleration as the umbilical blood enters the narrow ductus venosus, the *Bernoulli equation* can be used to calculate Δp:

$$\Delta p = \frac{1}{2}\rho\left(V_{DV}^2 - V_{UV}^2\right) + \rho\int_{UV}^{DV}\frac{\delta V}{\delta t}dx + R(V)$$

For practical purposes, this equation can be simplified [9]. The blood density ρ is $1.06{\cdot}10^3$, and in the first term, the umbilical blood velocity V_{UV} is low compared with the velocity in the ductus venosus V_{DV}, has little impact on the overall calculation, and is therefore neglected. The second term can be disregarded as it expresses inertia shift and does not impact the magnitude of the Δp. The last term $R(V)$ represents the viscous resistance and is dependent on the vessel geometry and velocity profile. In the present venous section where blood velocities have some degree of parabolic profile and blood flow has Newtonian properties, the viscous pressure loss is estimated to be in the order of 0.1 mmHg [26], which is small and therefore also omitted when the simplified version of *Bernoulli equation* is used to determine the pressure gradient:

$$\Delta p = 4V_{\max}^2$$

Here $V_{\max}$ is maximum blood velocity in m/s at the ductus venosus isthmus and Δp comes directly in mmHg. Further discussion on these issues is available in the literature [9, 24, 25, 27].

Using the simplified *Bernoulli equation*, the umbilicocaval Δp is found to be fairly constant during the second half of pregnancy varying between 0.5 and 3.5 mmHg according to stage of the cardiac cycle if flow is pulsatile (Fig. 5.8). During maximal fetal respiratory activity, pressures up to 25 mmHg can be recorded [9], and the same magnitude is found in the abdominal portion of the IVC [10], both quantifying the capacity of fetal respiratory force.

5.4 Measuring Blood Flow in Veins

The volume of blood flow is a fundamental measure in circulation physiology, also in the fetus. Although other noninvasive methods have been used and new are being introduced,

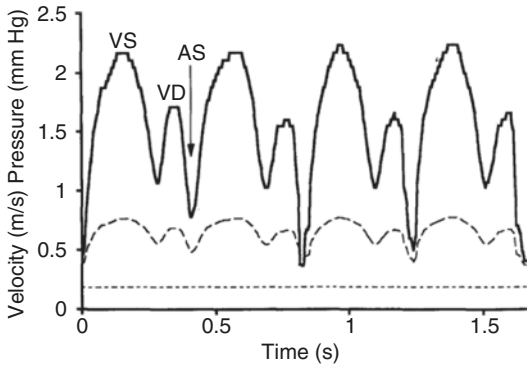

Fig. 5.8 The umbilicocaval (portocaval) pressure gradient (solid line) in a fetus at 19 weeks' gestation, estimated based on *Bernoulli equation* using Doppler measurements of the ductus venosus blood velocity (broken line) and umbilical venous velocity (dotted line). *VS* Ventricular systole, *VD* Ventricular diastole, *AS* Atrial systole (Modified from [9])

it is the Doppler ultrasound technique combined with biometry of the vessel cross section that provides most of the data available to us today. The technique has been known and used for research purposes for 40 years until it now is increasingly regarded as a possible clinical tool. Two sites have been chosen for the measurement, either the straight portion of the intra-abdominal umbilical vein (preferably distal to the first branching), or a section of the vein in a free-floating loop of the cord [28–35]. Both seem applicable, although the intra-abdominal approach is the more commonly used. Personal skills, optimized equipment and settings, well-founded measurement protocols, and consistency matters when the measurement is made reproducible. Thus, the following paragraphs focus on the key components of blood flow ($\dot{V}$) calculation (usually in mL/min):

$$\dot{V} = \pi\left(\frac{D}{2}\right)^2 hV_{\max} \text{ or } \dot{V} = \pi\left(\frac{D}{2}\right)^2 V_{\text{wmean}}$$

i.e., diameter D, blood velocity $V_{\max}$ (maximum velocity in the cross section) and V_{wmean} (intensity-weighted mean velocity), and the spatial velocity profile h (confer Fig. 5.2).

5.4.1 Determining Blood Velocity

In obstetric and fetal medicine environments, too commonly, the quality of the 2D-imaging modalities is prioritized and determines which scanner to be purchased, while assuming that the Doppler functions hold a satisfactory level. However, that is by far not the case. If Doppler recording is priority, it is commendable to have a dedicated machine to crack the toughest Doppler challenges. For most, a sector scanner, rather than a curved or linear transducer, facilitates a perfect alignment of the Doppler beam avoiding the disadvantage of angle correction. As in 2D-imaging, it is an advantage for the Doppler recording to have the option of increasing the ultrasound frequency (MHz), thus refining the resolution of the signal, while reducing the frequency improves the penetration and access to distant vessels.

V_{wmean} represents the average of all velocities in the sample volume at one point on the timeline of the Doppler recording (Fig. 5.9). The averaged V_{wmean} over time is an option for calculating flow. However, this V_{wmean} derived from the Doppler shift is easily influenced by signal quality, particularly low-velocity signals such as clutter artifacts along the zero-line, vessel wall movements (Fig. 5.9), loss of low-velocity signals due to filters or inaccurate sample volume placement, interference of neighboring vessels, or loss of weakest signals (i.e., lowest velocities) when recording deep-sited veins. We also have to bear in mind that the Doppler gate (sample volume) is droplet-shaped and hardly ever represents a concise composition of velocities of a vessel cross section. In short, the representation of low velocities from the perifery of the vessel is more likely to be affected and over- or underrepresented in the V_{wmean}.

$V_{\max}$, on the other hand, is merely representing the highest velocity in the vessel cross section (Fig. 5.9). With accurately aligned Doppler insonation and sample volume, this is easily

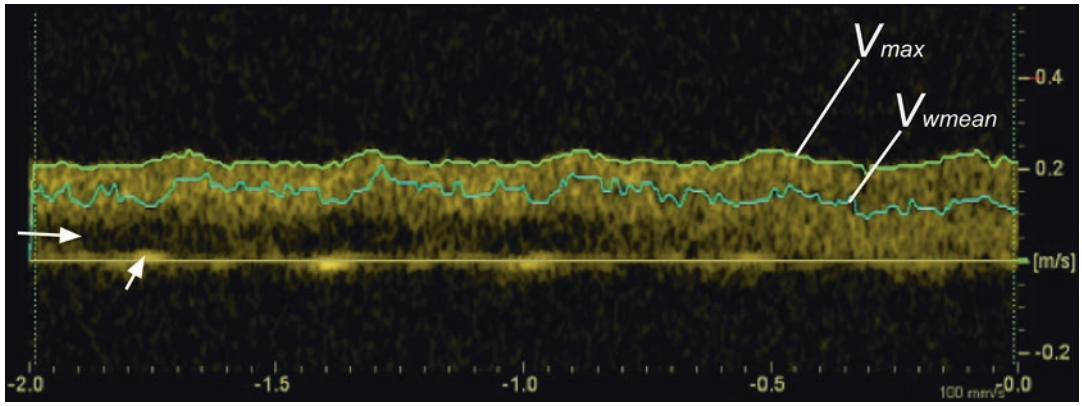

Fig. 5.9 Doppler recording of the intra-abdominal umbilical vein with automatic tracing of the maximum velocity (V_{max}), and, correspondingly, the intensity-weighted mean velocity (V_{wmean}). Since V_{wmean} includes all the velocities recorded, it is susceptible to missing velocity recordings (horizontal arrow), in this case, caused by temporarily dislodged sample volume, leading to an artificially high V_{wmean} value. V_{wmean} is also sensitive to wall motion signals along the zero-line (short arrow) correspondingly reducing the V_{wmean}. Such factors tend to make the V_{wmean} less reliable than V_{max}, which, on its side, needs just a sufficiently large sample volume to ensure that the highest velocity is included

recorded, and it constitutes a more robust measurement than V_{wmean}. However, V_{max} alone cannot be used in the flow calculation without including the constant h for the spatial velocity profile. In the sections of intra-abdominal umbilical vein where the flow is steady, it should be parabolic and correspondingly $h = 0.5$, which is supported by studies [34, 36]. However, for the umbilical venous flow at the placental cord insertion with accelerating velocities, h will be higher, and even more so at the physiological vein constriction at the abdominal wall. Similarly, in the ductus venosus entrance, the blunted profile of $h = 0.7$ is well-documented [11, 14].

Which method should be preferred for venous flow calculation? The literature has examples of both alternative flow calculations [22, 28, 29, 31, 32, 37–39]. For sections that have been more thoroughly explored (e.g., ductus venosus and intra-abdominal umbilical vein), it is probably safer to use the experimentally validated method of maximum tracing of the Doppler velocity recording combined with the corresponding velocity profile $h = 0.7$ and 0.5. However, in first trimester when velocities are generally lower, the ductus venosus flow has $h = 0.53$, i.e., practically parabolic [40]. Such standardization makes the volume flow assessment less prone to technical errors and artifacts due to interference from neighboring vessels, wall motion, and low-velocity artifacts.

5.4.2 Determining Vessel Diameter

When calculating blood flow, diameter measurement stands out as a contributor to random error because it is magnified by the power of two in the equation, and the smaller the diameter, the higher the relative risk of error will be [41, 42]. So, there is good reason to search all possibilities to control such errors.

First, choice of equipment makes a difference: high frequency transducer rather than lower frequency, a linear scanner focuses better than others, single frequency is commonly an advantage to harmonics, and a standardized set up reduces random error.

The site of measurement should be where the Doppler was recorded, but perpendicular to the vessel wall as that gives the best definition of the interface between vessel wall and blood. Measurements in a lateral direction to the ultrasound beam should preferably be avoided as the interfaces are less well-defined, the resolution inferior, and prone to overestimation.

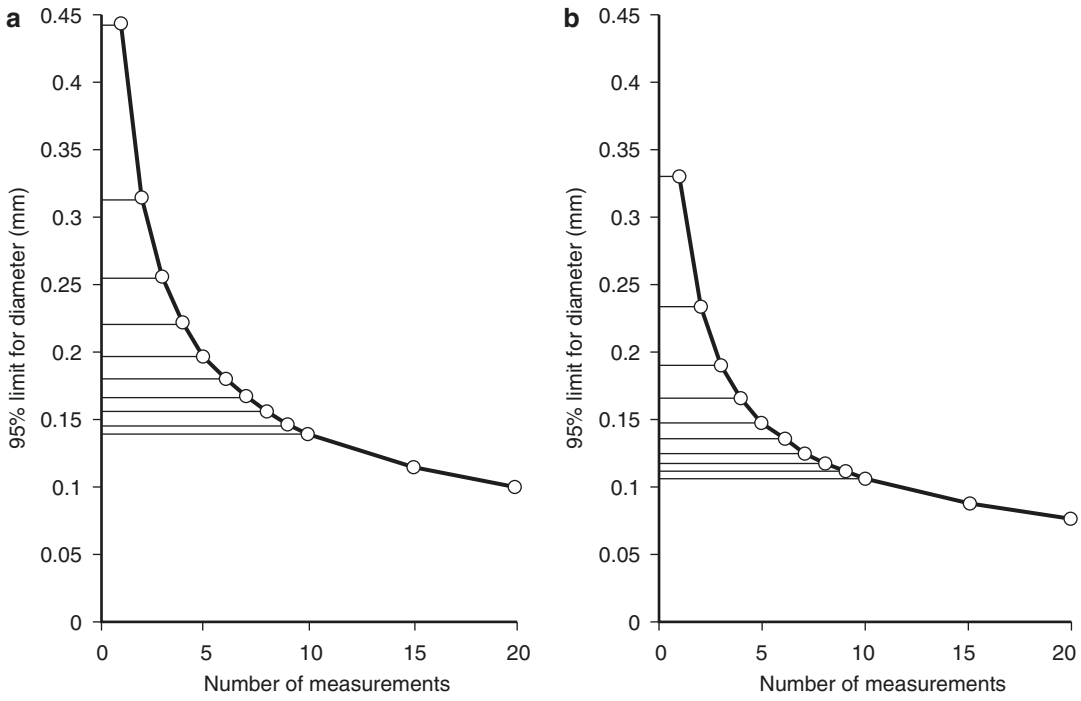

Fig. 5.10 Repeat measurement of diameter is a powerful method of reducing random error of the vessel cross section, here exemplified by the intra-abdominal umbilical vein (**a**) and ductus venosus (**b**) and presented with the upper 95% CI limit for variation. (Modified from [41])

Early works commonly used the leading-edge principle, that is outer-inner measurement since that ensured consistency with the technology of the day [43]. That explains some of the variance compared with modern studies using the inner-inner measurement technique, the presently preferred method [41].

Repeat measurement is a commendable and powerful method of reducing random error (Fig. 5.10), which is important particularly in small bore vessels such as the ductus venosus [41, 42]. E.g., with an umbilical vein diameter of 4 mm, the 95% IC for blood flow estimation reduces from ±23% to ±13 or ±9% if the diameter is based on 3 or 6 measurements, respectively. On the other hand, for the slim ductus venosus with a diameter of, e.g., 1.5 mm, the flow error reduces from ±49% to ±27 or ±18% when the diameter measurement is repeated 3 or 6 times, respectively. And, further improvement is achieved when repeating 10 or 20 times, yielding ±13 or ±10% error (for the ductus). Yet, as both numbers and graphs indicate (Fig. 5.10.), the benefit tapers off with increasing number of measurements and time consumed.

Semiautomated diameter measurement has been suggested and used (Fig. 5.11.) [44, 45]. The method is originally designed for standardized measurement of fetal nuchal translucency. When applied in measuring umbilical vein diameter, it was shown to reduce intra- and interobserver variation, thus being relevant candidate for vessel measurement protocols.

5.5 Pulsation in Veins

The blood velocity pulse recorded with our Doppler equipment is just one part of the entire pulse, the other components being a pressure wave and a diameter wave, together following the principle of energy preservation for motion of

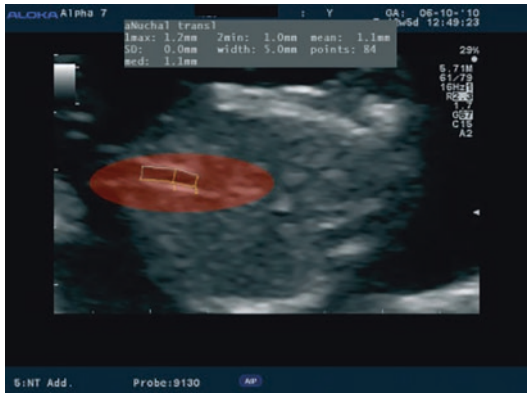

Fig. 5.11 Semiautomated diameter measurement of the umbilical vein (here at 12 weeks' gestation) is a suggested method of reducing intra- and interobserver variation. (Modified from [44])

incompressible fluids as described in Navier-Stokes' equations [1]. Here, we highlight some consequences that may help us interpret our recordings.

5.5.1 Transmission Lines

The pulse generated in the heart is not transmitted equally well in all tissues. It travels better along transmission lines, and arteries and veins connected to the heart constitute such transmission lines. While blood flow velocity in the venous system rarely exceeds 1 m/s, the pulse wave travels faster, typically 1–2.5 m/s in the umbilical vein [46]. The stiffer the vessel wall is, the faster it runs. An important transmission line is formed by the IVC, ductus venosus, and umbilical vein (Fig. 5.12) [47, 48]. Agenesis of the ductus venosus has been shown to interrupt the transmission of the cardiac wave to the umbilical vein [12]. The wave propagating along this line reflects the changes in both the left and the right atrium since the IVC is connected to the left atrium through the foramen ovale in addition to the connection to the right atrium. Conversely, the pulmonary veins reflect predominantly the left atrium, and to some extent the right atrium, depending on the size of the foramen ovale [49].

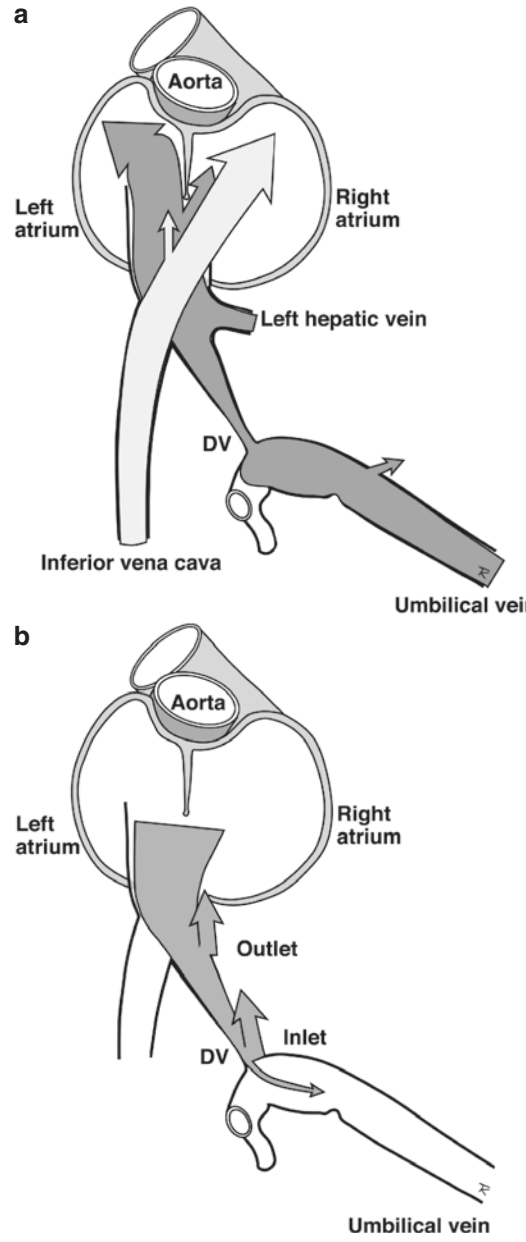

Fig. 5.12 The same veins that direct blood toward the heart (**a**) act as transmission lines in the opposite direction for pulse waves generated in the heart. The most studied transmission line is formed by the proximal portion of the inferior vena cava, ductus venosus (*DV*), and the umbilical vein (**b**). The wave is partially reflected at the junctions according to the difference in impedance above and below the junction (broad arrows). Due to the large difference in impedance between the ductus venosus inlet and the intra-abdominal umbilical vein, most of the wave is reflected at this junction. The small wave energy (slim arrow) transmitted into the umbilical vein is usually not enough to cause visible velocity pulsation at this site. (Modified from [48, 50]

5.5.2 Wave Reflections

The pulse wave traveling along the transmission line is modified according to the local physical conditions [1, 13, 14, 16, 26, 47, 49, 51]. Pulsation at the ductus venosus outlet is more pronounced than at the inlet [52]. The stiffness of the vessel wall is different at the ductus venosus outlet, ductus venosus inlet, and intra-abdominal umbilical vein, and so are cross section and compliance [46]. The single most important mechanism for changing the propagating pulse in the veins is reflections. In much the same fashion as light is reflected or transmitted when the beam encounters a medium with a different density, the pulse wave in the veins is reflected and transmitted when it hits a change in impedance (Fig. 5.12b) [47, 48, 53]. Vascular junctions often represent a significant change in cross section (and thus impedance). The junction between the ductus venosus inlet and the umbilical vein is of great diagnostic interest and has been particularly well-examined. During the second half of pregnancy, pulsation is regularly observed at the ductus venosus inlet, but on the other side of the junction, millimeters away, there is no pulsation in the umbilical vein velocity. The reason is reflections [53]. The Reflex coefficient (R_c) determines the degree of reflection and depends on the impedance of the two sections of veins (e.g., Z_{DV}, ductus venosus, and Z_{UV}, umbilical vein):

$$R_c = \frac{\text{Reflected wave}}{\text{Incident wave}} = \frac{Z_{UV} - Z_{DV}}{Z_{UV} + Z_{DV}}$$

In this case, Z_{UV} represents the terminal (distal) impedance in fluid-dynamic terms, whereas Z_{DV} represents the characteristic impedance. From a practical point of view, the single most important determinant for impedance is the cross section of the vessel (A):

$$Z = \rho c / \mathrm{A}$$

(ρ = density, and c = wave velocity). In the case of the ductus venosus–umbilical vein junction, there is an extraordinary difference in cross section, and thus impedance; the ratio of the diameter of the umbilical vein and the ductus venosus being 4 (95% CI 2; 6) [47]. Correspondingly, most of the wave will be reflected and little energy transmitted further down. The small proportion of the energy transmitted to the umbilical vein, commonly, is not sufficient to cause visible pulsation. In extreme conditions, such as during hypoxia, the ductus venosus distends [23, 54], and the difference in vessel area between the two sections is reduced, and less wave is reflected and more transmitted (Fig. 5.13a); thus, a larger proportion of the wave arrives in the umbilical vein and may induce pulsation, particularly if the a-wave was augmented in the first place.

In 3% of all recordings, there is no pulsation in the ductus venosus (Fig. 5.14a), which is a normal phenomenon [55]. The pattern is in many cases caused by the position of the fetus bending forward and thus squeezing the IVC and ductus venosus outlet (Figs. 5.13b) [47]. The extensively reduced cross section causes a total reflection of wave at the level of the IVC–ductus venosus junction and hardly any pulse is transmitted further down until the squeeze has been released (Fig. 5.14b). A similar effect can probably be obtained by the spontaneous variation in cross section sometimes seen in the proximal portion of the IVC.

5.5.3 Direction of Pulse and Blood Velocity

We are well-acquainted with blood pressure wave traveling down our brachial artery associated with corresponding transient rise in blood velocity, the velocity pulse. On the venous side, however, this is inversely related; the pressure pulse from the heart travels down the venous system but causes a velocity deflection, the reason being that the pressure this time is imposed on flow in the opposite direction, toward the heart (Fig. 5.15 upper panel). The phenomenon is addressed in the concept of "wave intensity" introduced to explain the wave in arteries [56], but the concept is equally valid for veins [49, 57].

A particularly instructive example is found in the left portal branch (Fig. 5.15 lower panel), where the negative velocity wave of the umbilical

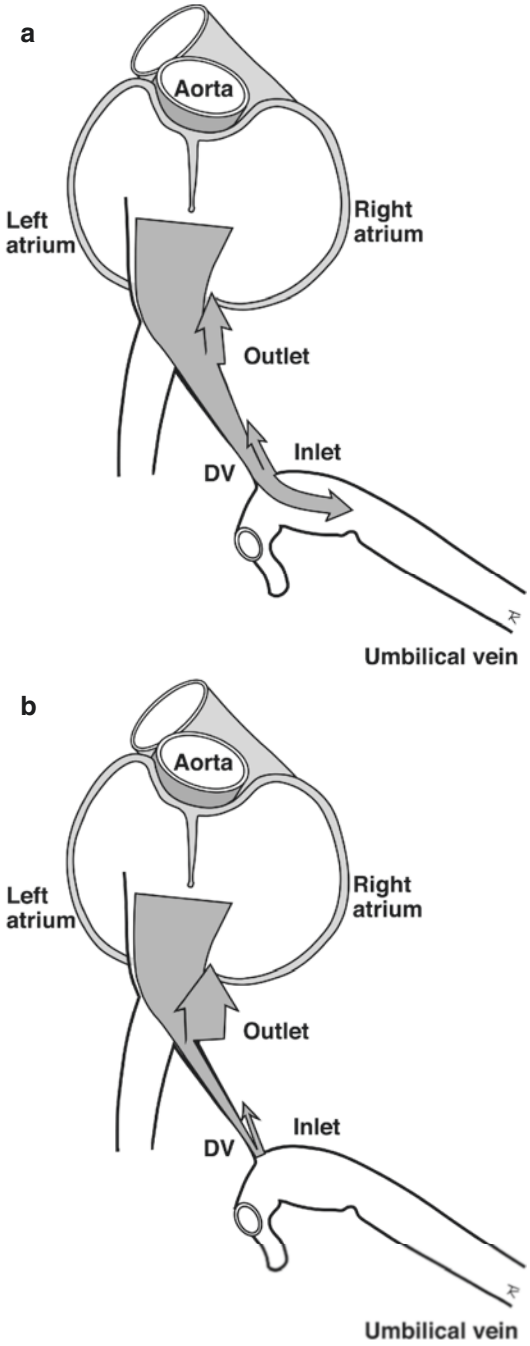

Fig. 5.13 A distension of the ductus venosus (*DV*) inlet and increased tone in the umbilical vein with reduced diameter reduce the difference of impedance between the two sections. Correspondingly, less reflection and more transmission increase the likelihood that velocity pulsations are observed in the umbilical vein (**a**). When the DV is squeezed right up to the outlet, a larger proportion of the wave is reflected at the level of outlet (**b**), leaving little wave energy to be transmitted further down the transmission line. No pulsation may then be observed at the DV inlet. (Modified from [48])

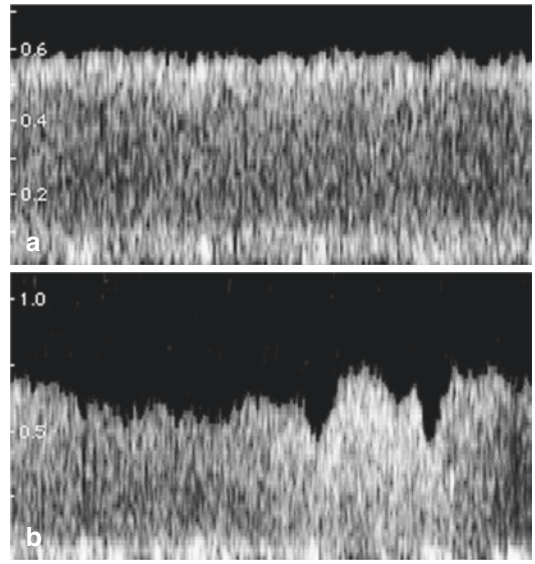

Fig. 5.14 Doppler recording of the ductus venosus blood velocity without pulsation (**upper panel**) due to the fetal position bending forward and squeezing the ductus venosus outlet. The wave has been completely reflected at the junction with the inferior vena cava (see Fig. 5.13b). Seconds later, a change in fetal position restores the dimension of the vessel (corresponds to Fig. 5.13a) and the pulsatile flow pattern (**lower panel**). (Modified from [48])

vein (Fig. 5.15 upper panel) has turned positive [57]. The explanation is as follows. Blood flows up the umbilical vein toward the ductus venosus and heart, but is also directed into the left portal branch (the transverse sinus (Fig. 5.16)). The pressure wave from the heart is traveling in opposite direction and imposes a negative atrial contraction wave in the ductus venosus and umbilical vein. This pressure wave, however, also propagates into the left portal branch now running in the same direction as the blood flow there and, accordingly, the atrial contraction wave turns positive (Fig. 5.15 lower panel).

In the compromised fetal circulation, the left portal vein also acts as a watershed area between the left and right part of the liver [57–59]; thus, blood velocity in this section may be low, pendulate, or reversed. Depending on the direction of flow in this section, the waveform will turn the same way or be inverted when compared with the umbilical vein pulse.

This effect of mirroring waves is particularly observed when the wave is augmented as in placental compromise causing cardiac decompensation.

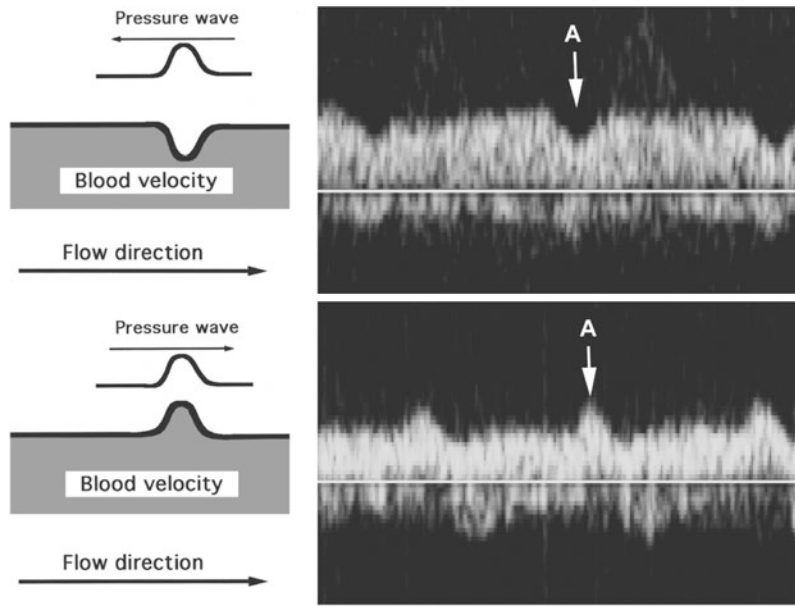

Fig. 5.15 *Upper panel:* When the pressure pulse and blood velocity travel in *opposite* directions, the resulting velocity change during the pulse will be a deflection. A common example is the atrial contraction wave recorded in the umbilical vein (*A*). *Lower panel:* When the pressure pulse and blood flow travel in the *same* direction, the resulting blood velocity change during the pulse will be an increase. Accordingly, the atrial contraction wave recorded in the left portal vein is recognized as a peak (*A*). For further explanation see Fig. 5.16. (Modified from [57])

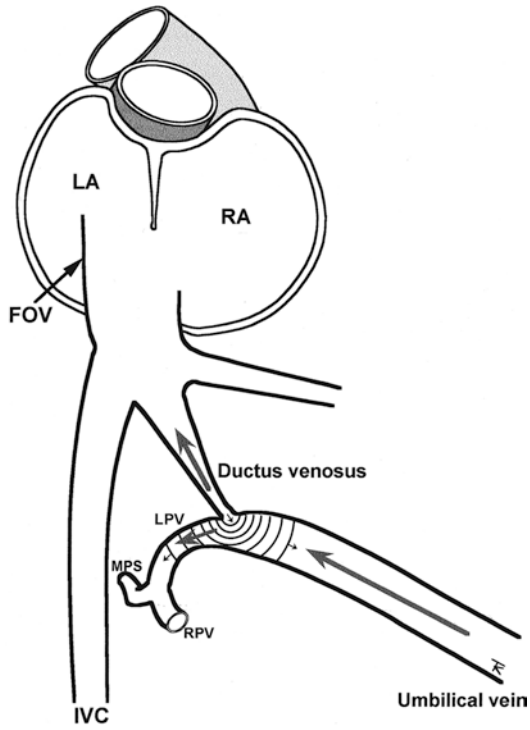

Fig. 5.16 The pressure pulse emitted from the heart travels along the veins acting as transmission lines. When the pulse reaches the junction between the ductus venosus inlet and the umbilical vein, the pulse wave (concentric rings and minute arrows) continues in two directions: (1) along the umbilical vein *against* the flow direction (large arrows), or (2) follows the left portal branch (*LPV*) into the liver *with* the flow direction. *FOV* Foramen ovale valve, *IVC* Inferior vena cava, *LA* Left atrium, *MPS* Main portal stem, *RA* Right atrium, *RPV* Right portal branch. (Modified from [57])

The same wave with an augmented amplitude found at the ductus venosus isthmus is imposed on the left portal vein, but inverted (Fig. 5.17). Although essentially being the same pressure wave imposed on the two different venous sections, the calculated pulsatility in the left portal vein comes out substantially higher than for the ductus venosus. The reason is that the time-averaged velocity (included as denominator in the index) is much lower in the left portal vein than in the ductus venosus.

5.5.4 Compliance and Reservoir Function of the Umbilical Vein

Another determinant affecting pulsation is the reservoir effect [51]. Whether a pulse that arrives in the umbilical vein induces velocity pulsation depends on the amount of energy it carries and the local compliance. The umbilical vein is a sizeable vessel and acts as a reservoir. The larger and more compliant the reservoir is, the higher wave energy is required to induce a visible pulsation of the blood velocity (Fig. 5.18). Accordingly, pulsation should be a rare event in late pregnancy, whereas the small vascular dimensions in early pregnancy predispose for pulsation. Correspondingly, pulsation in the umbilical vein is reported as a normal phenomenon, particularly before 13 weeks of gestation [60]. It follows that an increased tone of the

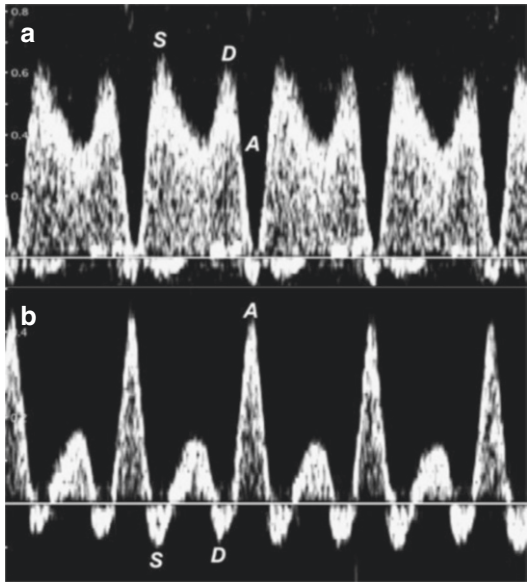

Fig. 5.17 Doppler recording of the ductus venosus (**a**), and the left portal branch (**b**), in a fetus of 25 weeks' gestation with placental compromise. For anatomical references, see Fig. 5.16. The ductus venosus recording shows an augmented velocity deflection during atrial contraction (*A*) reaching the zero-line and beyond. The same wave recorded in the left portal branch is now a peak (*A* in **b**) and the entire wave mirrors the ductus venosus recording. The reason is that in the left portal branch, pressure wave and blood flow have same direction, while in the ductus venosus, pressure wave and blood flow are opposite. *D* Diastolic peak, *S* Systolic peak. (Modified from [57])

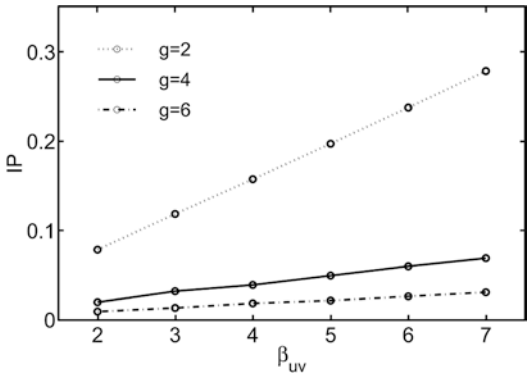

Fig. 5.18 Mathematical model showing how umbilical venous pulsation changes with wall stiffness (β_{UV}), a determinant for compliance. Index of pulsation for the pressure wave (IP = pulse amplitude/time-averaged pressure) increases with stiffness. The model also demonstrates the effect of increased diameter ratio between the umbilical vein and ductus venosus ($D_{UV}/D_{DV} = g$) on pressure transmission to the umbilical vein. Increased ratio is associated with less pulsation in the umbilical vein blood velocity due to increased umbilical vein compliance, but also due to increased degree of reflection at the junction. (Modified from [51])

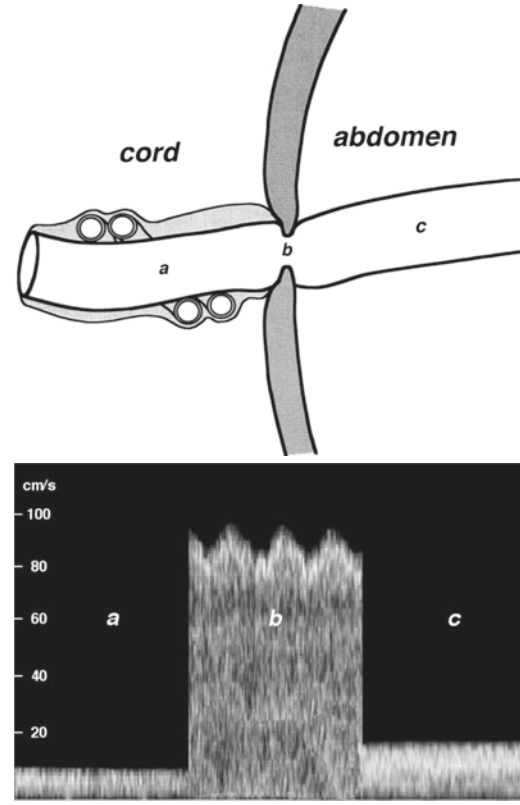

Fig. 5.19 *Upper panel:* The physiological constriction of the umbilical vein at the abdominal inlet (*b*) represents a reduction in compliance compared with the section in the cord (*a*) or intra-abdominal portion (*c*; from [6]). *Lower panel:* High velocity is recorded at the constriction (*b*) compared with outside (*a*) or inside (*c*) the abdominal wall. The pulsation from the neighboring umbilical artery induces velocity pulsation in the vein at the constriction area, but not in the neighboring sections where the compliance is higher (*a* and *c*). (Modified from [62])

vessel wall (e.g., adrenergic drive, venous congestion) and small diameter, such as in fetal growth restriction, may be accompanied by pulsation in the umbilical vein.

The effect of compliance is particularly well-illustrated by the physiological stricture of the umbilical vein at the entrance through the abdominal wall. Once the period of physiological umbilical herniation has completed at 12 weeks of gestation, there is an increasing tightening of the umbilical ring causing a constricting impact on the vein in quite a few fetuses during the following weeks and months [6, 7, 61]. The stricture causes a high velocity, which, interestingly, often pulsates (Fig. 5.19)

[62]. Although the pulsation may be a velocity inflection caused by the a-wave transmitted from the heart, probably a more common waveform would be a smooth increment of velocity caused by the neighboring umbilical arteries. The same phenomenon can be traced in the umbilical cord with increased turgor, angulation, or extreme twisting [63]. Another example is the left portal vein, i.e., the transvers sinus between the ductus venosus inlet and the junction with the main portal stem (Fig. 5.16). Here the diameter is smaller than in the umbilical vein, compliance correspondingly lower, and pulsation common [64, 65], roughly 70% of all normal pregnancies during the second half of pregnancy [59].

5.5.5 Source of Pulse

Whenever a pulse is generated, it will be transmitted into the neighboring structures modified by the local physical conditions. Although the pulse wave commonly carries the "fingerprint" of its source (e.g., cardiac cycle) [20, 66, 67], at some distance such characteristics may have disappeared making the identification of the source less certain. Pulsation in the umbilical vein is of clinical interest if it signifies an augmented atrial contraction that has reached that far out [63, 68–71]; however, the velocity pulse could have been transmitted locally from the umbilical artery, or could have been caused by rapid fetal respiratory movements or any other rhythmic fetal activity. The vibration of the heart is also transmitted into the liver tissue and beyond and may impact the venous flow. Vortices, like whirls in a river, may occur in large veins and cause velocity variation recorded in the Doppler shift. They may constitute a pitfall and should not be interpreted as cardiac dysrhythmia as these changes are not synchronized with cardiac activity (Fig. 5.2). In some cases, information on pulse-wave direction, time of the pulse, and details of its form do permit the discrimination between sources.

5.5.6 Cardiac Function and Waveform

The waveform of the pulse emitted from the fetal heart into the precordial veins reflects functional details both of the ventricles and the atria during the entire cardiac cycle. Usually, there is a systolic peak (during ventricular systole), a diastolic peak (during passive filling of the ventricles), and a diastolic nadir (reflecting the atrial contraction; Fig. 5.20). The more energy put into the pulse, the higher is the amplitude and the further out in the system it will reach. That is particularly obvious during atrial contraction. The Frank-Starling mechanism causes an augmented contraction in a distended atrium during congestive heart failure or in fetal bradycardia, and the wave propagating along the veins reflects the augmented atrial systole. A particularly strong atrial wave is seen in cases of arrhythmia when atria and ventricles happen to beat simultaneously. An augmented atrial wave is also seen in cases with increased afterload and adrenergic drive during hypoxemia [66–68, 72, 73]. Although the atrial contraction wave is the most commonly used sign for cardiac function, there is additional information hidden in the waveform [74, 75].

The smooth systolic peak of the wave of a precordial vein also reflects a normal compliance of the heart. External constricting conditions (e.g., high-pressure pleural effusion; Fig. 5.20) and a stiffer and less compliant myocardium (e.g., hypoxia, acidosis, cardiomyopathy) give a quick rise in pressure during systolic filling of the atrium, and a corresponding early and steep downstroke of velocity resulting in the more pointed systolic peak velocity (Fig. 5.20) [49, 76]. A quick rise in atrial pressure is sometimes caused by a significant tricuspid regurgitation, leading to a similar but less acute downstroke during systole.

In addition to an early and steep systolic downstroke, an increasing dissociation between systolic and diastolic peak signals aggravation of cardiac function (Fig. 5.20) and is regarded as an ominous sign [49, 77].

It follows from what is presented in this section that pulsatile venous flow, both in precordial

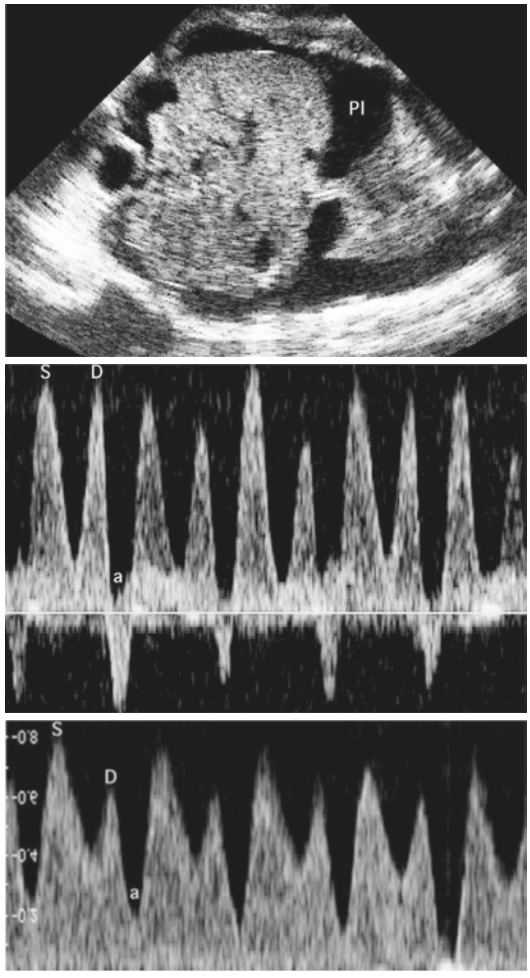

Fig. 5.20 Effect of cardiac compliance on the venous waveform in the ductus venosus. Although a stiff myocardium due to acidosis or hypoxia is the most common cause, in this case it was the fetal pleural effusion (*Pl*) at 30 weeks of gestation (*upper panel*) that had a constrictive effect on the heart. The reduced compliance was reflected in the rapid downstroke of the peak velocity during ventricular systole (*S*) causing the dissociation between S and the diastolic peak (*D*; *middle panel*). Doppler recording 2 min after the pleural effusion had been drained off (*lower panel*) showed an instantaneous improvement in myocardial compliance (less pointed *S* and reduced dissociation between *S* and *D*), and the end-diastolic pressure was less, signified by the less pronounced atrial contraction wave (*a*)

veins and in peripheral veins, such as the umbilical vein and intracranial veins, is determined by cardiac function *and* the local physical properties of the vasculature. All determinants vary with gestational age. Unless these facts are taken into account, we shall not be able to use the diagnostic techniques of venous Doppler recordings to their full potential, but face a commonly occurring risk of misinterpretation.

References

1. Nichols WW, O'Rourke MF. McDonald's blood flow in arteries. Theoretical, experimental and clinical principles. 4th ed. London: Arnold; 1998, 564 p.
2. Fung YC. Biomechanics. New York, Springer-Verlag New York; 1993.
3. Fung YC. Biomechanics. New York, Berlin: Springer-Verlag; 1984.
4. Fung YC. Biodynamics. New York, Berlin, Heidelberg, Tokyo: Springer-Verlag New York; 1984.
5. Taylor KJW, Burns PN, Wells PNT, editors. Clinical applications of Doppler ultrasound. 2nd ed. New York: Raven Press; 1995.
6. Skulstad SM, Rasmussen S, Iversen OE, Kiserud T. The development of high venous velocity at the fetal umbilical ring during gestational weeks 11-19. Br J Obstet Gynaecol. 2001;108(3):248–53.
7. Kilavuz O, Vetter K. The umbilical ring—the first rapid in the fetoplacental venous system. J Perinat Med. 1998;26(2):120–2.
8. Kiserud T, Eik-Nes SH, Blaas HG, Hellevik LR. Ultrasonographic velocimetry of the fetal ductus venosus. Lancet. 1991;338(8780):1412–4.
9. Kiserud T, Hellevik LR, Eik-Nes SH, Angelsen BA, Blaas HG. Estimation of the pressure gradient across the fetal ductus venosus based on Doppler velocimetry. Ultrasound Med Biol. 1994;20(3):225–32.
10. Nyberg MK, Johnsen SL, Rasmussen S, Kiserud T. Hemodynamics of fetal breathing movements: the inferior vena cava. Ultrasound Obstet Gynecol. 2011;38(6):658–64.
11. Kiserud T, Hellevik LR, Hanson MA. Blood velocity profile in the ductus venosus inlet expressed by the mean/maximum velocity ratio. Ultrasound Med Biol. 1998;24(9):1301–6.
12. Kiserud T, Crowe C, Hanson M. Ductus venosus agenesis prevents transmission of central venous pulsations to the umbilical vein in fetal sheep. Ultrasound Obstet Gynecol. 1998;11(3):190–4.
13. Pennati G, Bellotti M, De Gasperi C, Rognoni G. Spatial velocity profile changes along the cord in normal human fetuses: can these affect Doppler measurements of venous umbilical blood flow? Ultrasound Obstet Gynecol. 2004;23(2):131–7.
14. Pennati G, Redaelli A, Bellotti M, Ferrazzi E. Computational analysis of the ductus venosus fluid dynamics based on Doppler measurements. Ultrasound Med Biol. 1996;22(6):1017–29.

15. Pennati G, Bellotti M, Ferrazzi E, Bozzo M, Pardi G, Fumero R. Blood flow through the ductus venosus in human fetuses: calculation using Doppler velocimetry and computational findings. Ultrasound Med Biol. 1998;24:477–87.
16. Pennati G, Bellotti M, Ferrazzi E, Rigano S, Garberi A. Hemodynamic changes across the human ductus venosus: a comparison between clinical findings and mathematical calculations. Ultrasound Obstet Gynecol. 1997;9(6):383–91.
17. Acharya G, Kiserud T. Ductus venosus blood velocity and diameter pulsations are more prominent at the outlet than at the inlet. Eur J Obstet Gynecol Reprod Biol. 1999;84:149–54.
18. Leinan PR, Degroote J, Kiserud T, Skallerud B, Vierendeels J, Hellevik LR. Velocity profiles in the human ductus venosus: a numerical fluid structure interaction study. Biomech Model Mechanobiol. 2013;12(5):1019–35.
19. Leinan PR, Kiserud T, Hellevik LR. Human ductus venosus velocity profiles in the first trimester. Cardiovasc Eng Technol. 2013;4(3):257–66.
20. Schröder HJ, Tchirikov M, Rybakowski C. Pressure pulses and flow velocities in central veins of the anesthetized sheep fetus. Am J Physiol Heart Circ Physiol. 2003;284(4):H1205–11.
21. Kiserud T, Stratford L, Hanson MA. Umbilical flow distribution to the liver and the ductus venosus: an in vitro investigation of the fluid dynamic mechanisms in the fetal sheep. Am J Obstet Gynecol. 1997;177(1):86–90.
22. Kiserud T, Rasmussen S, Skulstad SM. Blood flow and degree of shunting through the ductus venosus in the human fetus. Am J Obstet Gynecol. 2000;182:147–53.
23. Kiserud T, Ozaki T, Nishina H, Rodeck C, Hanson MA. Effect of NO, phenylephrine, and hypoxemia on ductus venosus diameter in fetal sheep. Am J Physiol Heart Circ Physiol. 2000;279(3):H1166–71.
24. Hatle L, Brubakk A, Tromsdal A, Angelsen B. Noninvasive assessment of pressure drop in mitral stenosis by Doppler ultrasound. Br Heart J. 1978;40:131–40.
25. Holen J, Aaslid R, Landmark K, Simonsen S. Determination of pressure gradient in mitral stenosis with a non-invasive ultrasound Doppler technique. Acta Med Scand. 1976;199:455–60.
26. Hellevik LR, Kiserud T, Irgens F, Ytrehus T, Eik-Nes SH. Simulation of pressure drop and energy dissipation for blood flow in a human fetal bifurcation. ASME J Biomech Eng. 1998;120:455–62.
27. Hatle L, Angelsen B. Doppler ultrasound in cardiology. 1st ed. Philadelphia: Lea & Febiger; 1982. p. 238.
28. Gill RW, Kossoff G. Pulsed doppler combined with B-mode imaging for blood flow measurement. Contrib Gynecol Obstet. 1979;6:139–41.
29. Eik-Nes SH, Marsál K, Brubakk AO, Ulstein M. Ultrasonic measurements of human fetal blood flow in aorta and umbilical vein: Influence of fetal breathing movements. In: Kurjak A, editor. Recent advances in ultrasound diagnosis: Proceedings of the International Symposium on Recent Advances in Ultrasound Diagnosis. 2: Exerpta Medica; 1980. p. 233–40.
30. Gill RW, Kossoff G, Warren PS, Garrett WJ. Umbilical venous flow in normal and complicated pregnancies. Ultrasound Med Biol. 1984;10:349–63.
31. Kiserud T, Eik-Nes SH, Blaas H-G, Hellevik LR, Simensen B. Ductus venosus blood velocity and the umbilical circulation in the seriously growth retarded fetus. Ultrasound Obstet Gynecol. 1994;4:109–14.
32. Barbera A, Galan HL, Ferrazzi E, Rigano S, Jozwik M, Battaglia FC, et al. Relationship of umbilical vein blood flow to growth parameters in the human fetus. Am J Obstet Gynecol. 1999;181(1):174–9.
33. Boito S, Struijk PC, Ursem NT, Stijnen T, Wladimiroff JW. Umbilical venous volume flow in the normally developing and growth-restricted human fetus. Ultrasound Obstet Gynecol. 2002;19(4):344–9.
34. Acharya G, Wilsgaard T, Rosvold Berntsen GK, Maltau JM, Kiserud T. Reference ranges for umbilical vein blood flow in the second half of pregnancy based on longitudinal data. Prenat Diagn. 2005;25(2):99–111.
35. Ferrazzi E, Rigano S, Bozzo M, Bellotti M, Giovannini N, Galan H, et al. Umbilical vein blood flow in growth-restricted fetuses. Ultrasound Obstet Gynecol. 2000;16(5):432–8.
36. Galan HL, Jozwik M, Rigano S, Regnault TR, Hobbins JC, Battaglia FC, et al. Umbilical vein blood flow determination in the ovine fetus: comparison of Doppler ultrasonographic and steady-state diffusion techniques. Am J Obstet Gynecol. 1999;181(5 Pt 1):1149–53.
37. Jouppila P, Kirkinen P, Puukka R. Correlation between umbilical vein blood flow and umbilical blood viscosity in normal and complicated pregnancies. Arch Gynecol. 1986;237(4):191–7.
38. Tchirikov M, Rybakowski C, Hünecke B, Schröder HJ. Blood flow through the ductus venosus in singleton and multifetal pregnancies and in fetuses with intrauterine growth retardation. Am J Obstet Gynecol. 1998;178:943–9.
39. Bellotti M, Pennati G, De Gasperi C, Battaglia FC, Ferrazzi E. Role of ductus venosus in distribution of umbilical blood flow in human fetuses during second half of pregnancy. Am J Physiol Heart Circ Physiol. 2000;279(3):H1256–63.
40. Leinan PR, Kiserud T, Hellevik LR. Human ductus venosus velocity profile in the first trimester. Cardiovasc Eng Technol. 2013;4(3):257–66.
41. Kiserud T, Rasmussen S. How repeat measurements affect the mean diameter of the umbilical vein and the ductus venosus. Ultrasound Obstet Gynecol. 1998;11(6):419–25.
42. Kiserud T, Saito T, Ozaki T, Rasmussen S, Hanson MA. Validation of diameter measurements by ultrasound: intraobserver and interobserver variations assessed in vitro and in fetal sheep. Ultrasound Obstet Gynecol. 1999;13(1):52–7.

43. Eik-Nes SH, Marsal K, Kristoffersen K. Methodology and basic problems related to blood flow studies in the human fetus. Ultrasound Med Biol. 1984;10(3):329–37.
44. Rizzo G, Capponi A, Aiello E, Arduini D. First-trimester assessment of umbilical vein diameter using the semiautomated system for nuchal translucency measurement. Ultrasound Obstet Gynecol. 2011;37(6):741.
45. Rizzo G, Mappa I, Bitsadze V, Khizroeva J, Makatsarya A, D'Antonio F. The added value of umbilical vein flow in predicting fetal macrosomia at 36 weeks of gestation: a prospective cohort study. Acta Obstet Gynecol Scand. 2021;100:900–7.
46. Hellevik LR, Kiserud T, Irgens F, Stergiopulos N, Hanson M. Mechanical properties of the fetal ductus venosus and umbilical vein. Heart Vessel. 1998;13:175–80.
47. Kiserud T. Hemodynamics of the ductus venosus. Eur J Obstet Gynecol Reprod Biol. 1999;84(2):139–47.
48. Kiserud T. Fetal venous circulation—an update on hemodynamics. J Perinat Med. 2000;28:90–6.
49. Kiserud T. The fetal venous circulation. Fetal Matern Med Rev. 2003;14(1):57–95.
50. Kiserud T, Rasmussen S. Ultrasound assessment of the fetal foramen ovale. Ultrasound Obstet Gynecol. 2001;17(2):119–24.
51. Hellevik LR, Stergiopulos N, Kiserud T, Rabben SI, Eik-Nes SH, Irgens F. A mathematical model of umbilical venous pulsation. J Biomech. 2000;33:1123–30.
52. Acharya G, Kiserud T. Pulsations of the ductus venosus blood velocity and diameter are more pronounced at the outlet than at the inlet. Eur J Obstet Gynecol Reprod Biol. 1999;84(2):149–54.
53. Hellevik LR, Vierendeels J, Kiserud T, Stergiopulos N, Irgens F, Dick E, et al. An assessment of ductus venosus tapering and wave transmission from the fetal heart. Biomech Model Mechanobiol. 2009;8(6):509–17.
54. Bellotti M, Pennati G, Pardi G, Fumero R. Dilatation of the ductus venosus in human fetuses: ultrasonographic evidence and mathematical modeling. Am J Physiol. 1998;275(Heart Circ Physiol 44):H1759–67.
55. Kiserud T, Eik-Nes SH, Hellevik LR, Blaas H-G. Ductus venosus—a longitudinal doppler velocimetric study of the human fetus. J Matern Fetal Invest. 1992;2:5–11.
56. Parker KH, Jones CJH. Forward and backward running waves in the arteries: analysis using the method of characteristics. ASME J Biomech Eng. 1990;112:322–6.
57. Kiserud T, Kilavuz Ö, Hellevik LR. Venous pulsation in the left portal branch—the effect of pulse and flow direction. Ultrasound Obstet Gynecol. 2003;21:359–64.
58. Kilavuz O, Vetter K, Kiserud T, Vetter P. The left portal vein is the watershed of the fetal venous system. J Perinat Med. 2003;31(2):184–7.
59. Kessler J, Rasmussen S, Kiserud T. The left portal vein as an indicator of watershed in the fetal circulation: development during the second half of pregnancy and a suggested method of evaluation. Ultrasound Obstet Gynecol. 2007;30(5):757–64.
60. Rizzo G, Arduini D, Romanini C. Umbilical vein pulsations: a physiologic finding in early gestation. Am J Obstet Gynecol. 1992;167(3):675–7.
61. Skulstad SM, Kiserud T, Rasmussen S. Degree of fetal umbilical venous constriction at the abdominal wall in a low risk population at 20–40 weeks of gestation. Prenatal Diagnosis. 2002;22:1022–7.
62. Skulstad SM, Kiserud T, Rasmussen S. The effect of vascular constriction on umbilical venous pulsation. Ultrasound Obstet Gynecol. 2004;23(2):126–30.
63. Nakai Y, Imanaka M, Nishio J, Ogita S. Umbilical venous pulsation associated with hypercoiled cord in growth-retarded fetuses. Gynecol Obstet Investig. 1997;43(1):6–7.
64. Mari G, Uerpairojkit B, Copel JA. Abdominal venous system in the normal fetus. Obstet Gynecol. 1995;86(5):729–33.
65. van Splunder IP, Huisman TWA, Stijnen T, Wladimiroff JW. Presence of pulsations and reproducibility of waveform recording in the umbilical and left portal vein in normal pregnancies. Ultrasound Obstet Gynecol. 1994;4:49–53.
66. Reed KL, Appleton CP, Anderson CF, Shenker L, Sahn DJ. Doppler studies of vena cava flows in human fetuses; insights into normal and abnormal cardiac physiology. Circulation. 1990;81:498–505.
67. Kanzaki T, Chiba Y. Evaluation of the preload condition of the fetus by inferior vena caval blood flow pattern. Fetal Diagn Ther. 1990;5:168–74.
68. Gudmundsson S, Gunnarsson G, Hökegård K-H, Ingmarsson J, Kjellmer I. Venous Doppler velocimetry in relationship to central venous pressure and heart rate during hypoxia in ovine fetus. J Perinat Med. 1999;27:81–90.
69. Lingman G, Laurin J, Marsal K. Circulatory changes in fetuses with imminent asphyxia. Biol Neonate. 1986;49(2):66–73.
70. Gudmundsson S, Huhta JC, Wood DC, Tulzer G, Cohen AW, Weiner S. Venous Doppler ultrasonography in the fetus with nonimmune hydrops. Am J Obstet Gynecol. 1991;164:33–7.
71. Nakai Y, Miyazaki Y, Matsuoka Y, Matsumoto M, Imanaka M, Ogita S. Pulsatile umbilical venous flow and its clinical significance. Br J Obstet Gynaecol. 1992;99:977–80.
72. Reuss ML, Rudolph AM, Dae MW. Phasic blood flow patterns in the superior and inferior venae cavae and umbilical vein of fetal sheep. Am J Obstet Gynecol. 1983;145:70–6.
73. Hasaart TH, de Haan J. Phasic blood flow patterns in the common umbilical vein of fetal sheep during umbilical cord occlusion and the influence of autonomic nervous system blockade. J Perinat Med. 1986;14:19–26.
74. Huhta JC. Deciphering the hieroglyphics of venous Doppler velocities. Ultrasond Obstet Gynecol. 1997;9:300–1.

75. Kiserud T. In a different vein: the ductus venosus could yield much valuable information. Ultrasound Obstet Gynecol. 1997;9:369–72.
76. Kiserud T. The ductus venosus. Seminars Perinat. 2001;25(1):11–20.
77. Kiserud T. Venous flow dynamics: intrauterine growth restriction and cardiac decompensation. In: Yagel S, Gembruch U, Silverman N, editors. Fetal cardiology—embryology, genetics, physiology, echocardiographic evaluation, diagnosis, and perinatal management of cardiac diseases, Series in Maternal-Fetal Medicine. 1. 3rd ed. Boca Raton, FL: CRP Press, Taylor & Francis Group; 2019. p. 842.

6 Doppler Color Flow: Basic Principles

Dev Maulik

6.1 Introduction

Color flow mapping consists of real-time depiction of two-dimensional flow patterns superimposed on cross-sectional pulse echo images of anatomic structures [1–5]. The flow patterns are color-coded to present a variety of hemodynamic information. Doppler color flow mapping is based on the estimation of mean Doppler-shifted frequency and does not provide information on peak frequency shift or actual flow. Furthermore, the hemodynamic information provided is qualitative rather than quantitative. Nevertheless, color flow mapping has proved highly useful for elucidating structural and functional abnormalities of the circulatory system. The technique was first introduced in cardiology practice and has revolutionized noninvasive diagnosis of cardiac pathology. The use of this method has since been extended to other medical disciplines. In obstetrics and gynecology, color flow mapping has been used to investigate fetal and maternal hemodynamics during pregnancy and pelvic vessels in nonpregnant women. Color flow has been found to be useful for elucidating complex cardiac malformations of the fetus, directing spectral Doppler interrogation of fetal cerebral, renal, and other circulations, diagnosing ectopic pregnancy, and assessing pelvic tumor vascularity. However, the information generated by Doppler color flow mapping is significantly influenced by the instrumental features and setting, and the operator skill.

In this chapter, we describe the basic principles, instrumentation, and limitations of Doppler color flow mapping and present practical guidelines for its use. We also briefly address select technological advances.

6.2 Principles of Doppler Color Flow Mapping

6.2.1 Multigated Doppler Interrogation

Doppler color flow mapping is based on multigated sampling of multiple scan lines using bursts of short pulses of ultrasound (Fig. 6.1). Many range-gated samples are obtained for each emitted pulse of ultrasound along a single scan line by opening the receiving gate sequentially to the echo signals arriving from various depths along the scan line. The time needed for the return journey of the echo is used to determine the spatial origin of the returning echoes. Assuming a sound propagation speed of 1540 m/s in tissue, the echo return time for an emitted sound pulse is 13 ms per cm of tissue depth. Thus, a signal from a

D. Maulik (✉)
Department of Obstetrics and Gynecology, UMKC School of Medicine/Truman Medical Center, UMKC School of Medicine, Kansas City, MO, USA
e-mail: dmaulik2014@gmail.com

D. Maulik, C. C. Lees (eds.), *Doppler Ultrasound in Obstetrics and Gynecology*,
https://doi.org/10.1007/978-3-031-06189-9_6

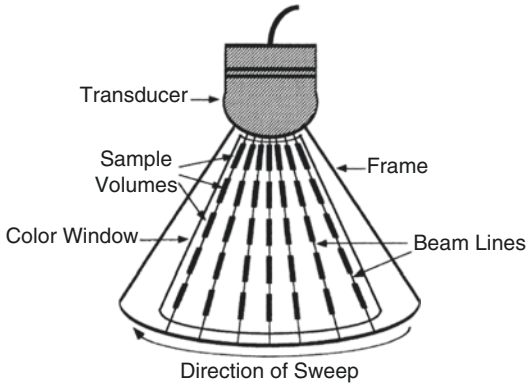

Fig. 6.1 Doppler color flow mapping. Graphic representation of the concept of multigated sampling of multiple scan lines sweeping across the field of color Doppler interrogation

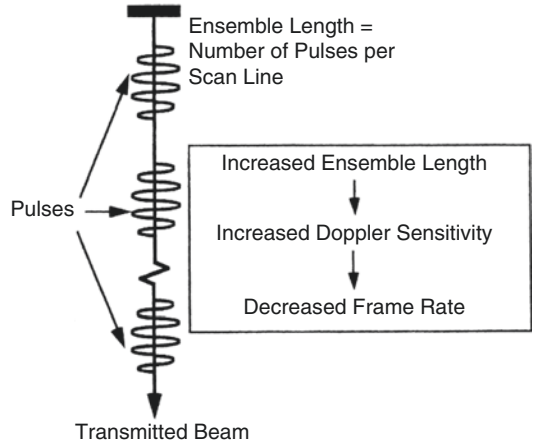

Fig. 6.2 Concept of ensemble length

depth of 5 cm takes 65 ms from the moment of transmission to its return to the transducer. If the second sample is to be obtained from a depth of 10 cm, the range gate is opened at 65 ms after reception of the first sample (130 ms after transmission of the pulse). In reality, many samples are collected, and the consecutive sampling of the signals along the scan line is timed according to the depth of the sampling location.

Each scan line is repeatedly sampled using multiple pulses. The signals from the identical range gates are collected and compared to obtain mean Doppler shifts, which are averaged for each gate. The number of pulses per scan line is called the *ensemble length* (Fig. 6.2). There are several reasons for this repeated sampling of a single scan line: (a) Blood flow is a continuously changing phenomenon, and the duration of each pulse in Doppler color flow mapping is too short (<2 ms) to provide an acceptable mean value. As the number of pulses per scan line is increased, the quality of flow information improves in terms of reliability and completeness. (b) Increasing the samples enhances Doppler sensitivity to detect low-velocity circulations. (c) Moreover, as the samples are repeated and averaged against a constant background of noise, the signal-to-noise ratio improves. (d) Multiple sampling also contributes to stabilization of the high-pass filter.

Once sampling of a scan line is completed, the next scan line is interrogated in the same manner as described above. The color flow map is completed by multiple scan lines sweeping across the imaging field (Fig. 6.1).

6.2.2 Color Doppler Signal Analysis

Multigated sampling of multiple scan lines of the color flow imaging field generates an enormous amount of data. Color flow mapping utilizes autocorrelation techniques for real-time processing and display of these data [4, 5] (Fig. 6.3). Autocorrelation generates mean Doppler shift information, rather than the comprehensive power spectral data generated by full spectral processing.

The mean Doppler shift is based on phase differences between the echoes generated from consecutive sound pulses transmitted in the same direction and sampled from the same location. *Phase* is defined in physics as a specific degree of progression of a cyclic phenomenon. When two waves are in step, they are in phase. The movement of the scatterer during the elapsed time between the two consecutive pulses causes the resulting echoes to be out of step or phase. The autocorrelator measures this phase difference by multiplying the successive signals. The mean Doppler shift is related to the phase difference, as shown in the following equation:

$$\varphi = 360^\circ \times MF_d / PRF$$

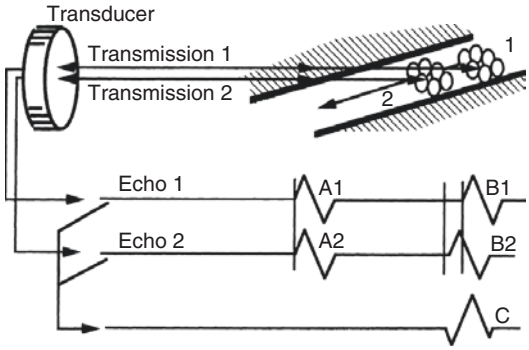

Fig. 6.3 Principle of two-dimensional Color Doppler signal analysis. During the first ultrasound transmission, the stationary tissue objects and the moving erythrocytes generated echoes (*A1* and *B1*, respectively). During the second transmission, echoes are produced again (*A2* and *B2*, respectively). Note that the echoes from the stationary objects remain the same (*A1* and *A2*), whereas those originating from the moving objects (*B1* and *B2*) differ. Correlating the first echo with the next echo cancels the signals from the stationary targets and identifies the signals from the moving scatterers (*C*). This process is repeated with the successive echoes from moving targets to estimate the mean Doppler frequency shift in real time

where φ is the phase angle, MF_d is the mean Doppler frequency shift, and PRF is the pulse repetition frequency. The autocorrelation is achieved by electronically delaying an echo signal, which is then processed with the subsequent echo signal (see above).

6.2.3 Instrumentation

The instrumentation for Doppler color mapping consists of two-dimensional and three-dimensional multiplex systems that combine multiple ultrasound modalities, providing a comprehensive array of sophisticated diagnostic tools. Commercially available devices demonstrate a fair degree of diversity in the engineering implementation of the Doppler technology; they also differ in the organization and the choice of system controls they offer to the operator. Although a comprehensive discussion is beyond the scope of this chapter, we present here the basic principles of Doppler color flow instrumentation.

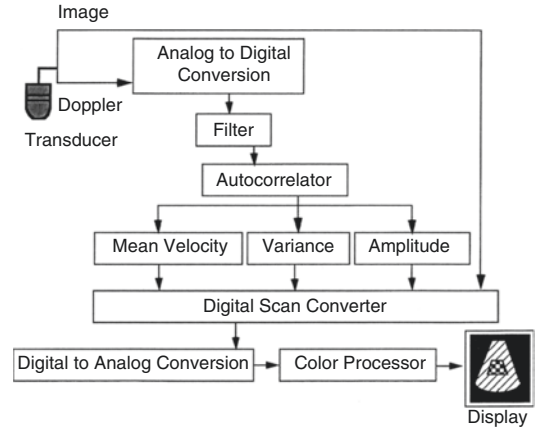

Fig. 6.4 A simplified schematic of Doppler color flow signal processing system

6.2.4 Color Flow Processor

The basic components of a color flow signal processing system consist of the following (Fig. 6.4):

1. Transducer for transmitting the ultrasound beam and receiving the echoes for both imaging and Doppler analysis.
2. Receiver, which receives and amplifies the incoming signals from the transducer for further processing for gray-scale tissue imaging and for Doppler color flow mapping.
3. Echo information for tissue imaging is processed and converted to digital format. It is stored in the digital scan converter for subsequent integration with color flow mapping.
4. Backscattered echoes for Doppler processing are first converted from analog (electrical voltage variations) data to numeric or digital data.
5. Digitized signals are then subjected to filtering to remove noise generated by stationary and slow-moving tissue structures. The filter is known as the moving target indicator.
6. Filtered data are then analyzed by the autocorrelator to determine the Doppler phase shift. The autocorrelator output consists of three types of information: Doppler mean frequency shift, variance, and Doppler amplitude (power or energy). These data are fed to the digital scan converter, where they are integrated with the tissue image information.

7. Doppler-related data are color-coded by the color processor and the combined gray-scale tissue image, and the Doppler color map is sent to the video display via digital-to-analog conversion.

The above description is only a general outline. The implementation of color Doppler sonography involves highly complex technology and proprietary engineering innovations—information not accessible in the public domain.

6.2.5 Transducers for Two-Dimensional Doppler Color Flow Mapping

Electronic array systems are used for color flow mapping which allows electronic beam steering and include linear sequential, convex sequential, linear phased, and annular phased array transducers. For obstetrical scanning, the convex sequential array offers distinct advantages over the linear sequential array because of its smaller footprint, a wider field of imaging at depth, and the absence of the grating lobe problem associated with the linear phased array. Moreover, the angle of Doppler is better achieved in the convex than in the linear array.

The linear phased array offers a sector-shaped field of image and is useful for echocardiographic applications. These transducers, however, are not optimal for fetal imaging as they do not provide a wide angle of view at depth and may produce side lobe problems, resulting in spurious flow depiction. Annular array transducers are seldom used for color flow obstetric applications.

6.2.6 Color Mapping

Color flow mapping is based on color-encoding each pixel representing the averaged mean Doppler shift. The color is used to represent the direction, magnitude, and flow characteristics of the sampled circulation. These parameters are qualitative rather than quantitative. The color scheme is based on color classification, which is derived from the fundamental properties of light perception composed of hue, luminance, and saturation.

6.2.7 Color Classification

Hue is the property of light by which the color of an object is classified as the primary colors of red, blue, green, or yellow in reference to the light spectrum. The basic classification is based on the presence or absence of hue. Those colors with hue are termed chromatic colors and include red, orange, yellow, green, blue, and so on. Those without hue are called achromatic colors and include black, gray, and white. The chromatic colors are further classified into groups according to their hue. All hues of red are grouped together, all blues are together, and so on, resulting in a continuous circle of overlapping hues. The human eye is incapable of differentiating between two superimposed primary hues, which led to the discovery that it was possible to produce any given color using a combination of three primary colors. The selection of the three primary hues is arbitrary. Red, blue, and green colors are used in color video displays, including color flow mapping, whereas artists use red, blue, and yellow pigments as their three primary colors.

The next characteristic of light for color classification is *luminance*, which is the brightness: Some of the chromatic colors of a single hue are darker or lighter than others, analogous to the degrees of gray of the achromatic colors. This classification is known as luminance or brightness.

The third property for color grouping is *saturation*, which indicates the combination of a hue of particular brilliance with an achromatic color of the same brightness. The consequent light stimulus depends on the relative amount of the chromatic and achromatic components in which the latter has 0 saturation and the former has a saturation value between 0 and 1.0.

6.2.8 Color Perception

Color is the perception generated by the stimulus of light falling on the retina of the human eye.

The eye can distinguish a wide range of gradations of hue and saturation. In contrast, the ability to differentiate various grades of luminance is relatively limited. Therefore, refined appreciation of color maps is achieved better with hue and saturation than with luminance. Hues with higher luminance are better perceived by older observers.

In regard to the impact of color blindness on a diagnostician's ability to assess color flow mapping, about 8.0% of men and fewer than 0.5% of women suffer from varying degrees of deficiency of color perception. Total absence of color vision is rare. Anomalopia is partial color blindness, in which both red and green are poorly recognized. Most color-blind persons find it easier to recognize saturation characteristics of a color flow map because saturation involves mixing of achromatic colors with chromatic hues.

6.2.9 Color Encoding of Doppler Flow Signals

Hemodynamic attributes of the interrogated blood flow are expressed by color encoding of the mean Doppler shift signals. These attributes are the direction of flow in relation to the transducer, the magnitude of velocity, variance of the measured mean parameter (mean Doppler shift), and the amount of scattering power (the amplitude or energy or power of the Doppler shift).

6.2.10 Color Mapping of Direction of Flow

The directionality of flow in relation to the transducer is depicted in the primary colors of red and blue. With most Doppler color flow systems, the default mode depicts the flow toward the transducer as red and the flow away as blue. The magnitude of the flow velocity is qualitatively expressed by assigning levels of luminance to the primary hue. The highest velocity flow is depicted by the most luminance and the lowest velocity by the least luminance or black. The highest measurable velocity toward the transducer is shown in the most brilliant red, and the highest measurable velocity away from the transducer in the most brilliant blue. The highest limit of the velocity unambiguously measurable by a Doppler color flow mapping system, based on the pulse Doppler interrogation, is the *Nyquist limit*. As noted before (see Chap. 3), this limit depends on pulse repetition frequency and the depth of Doppler interrogation. The lowest measurable velocity in a color flow mapping device depends on multiple factors and varies from device to device.

The calibration of the velocity magnitude as a function of luminance gradation is displayed graphically on the screen as a color bar (Fig. 6.5). It is customary to display the magnitude of the Doppler shift on the vertical axis and the variance (see below) on the horizontal axis. The Doppler shift may be displayed as either frequency or velocity. The velocity information is merely an approximation, as the Doppler angle of insonation is not measurable in color flow mapping. For color flow mapping, it is usually assumed that this angle is zero. The scales are not quantitative, and a particular level of luminance does not reflect a specific single value of Doppler shift but, rather, a range of values. In addition, the color bars of the devices do not have any uniformity of scale for depicting the magnitude of Doppler shift, as the corresponding levels of brightness are assigned arbitrarily and on a nonlinear scale. The baseline, which indicates zero frequency shift, divides the color bar into positive and negative frequency shifts. The baseline is indicated as a black band on the color bar, and its location can be adjusted to vary the proportion of positive or negative shifts. The vertical measure of the baseline is variable and reflects the magnitude of the wall filter.

6.2.11 Clinical Utility of Color Flow Mapping

Despite its qualitative nature, the velocity information provided by color flow mapping is of significant clinical utility as evident throughout this book. Identification of different vessels traversing in close proximity may be facilitated by the luminance and hue of the color display, with the former indicating velocity magnitude and the lat-

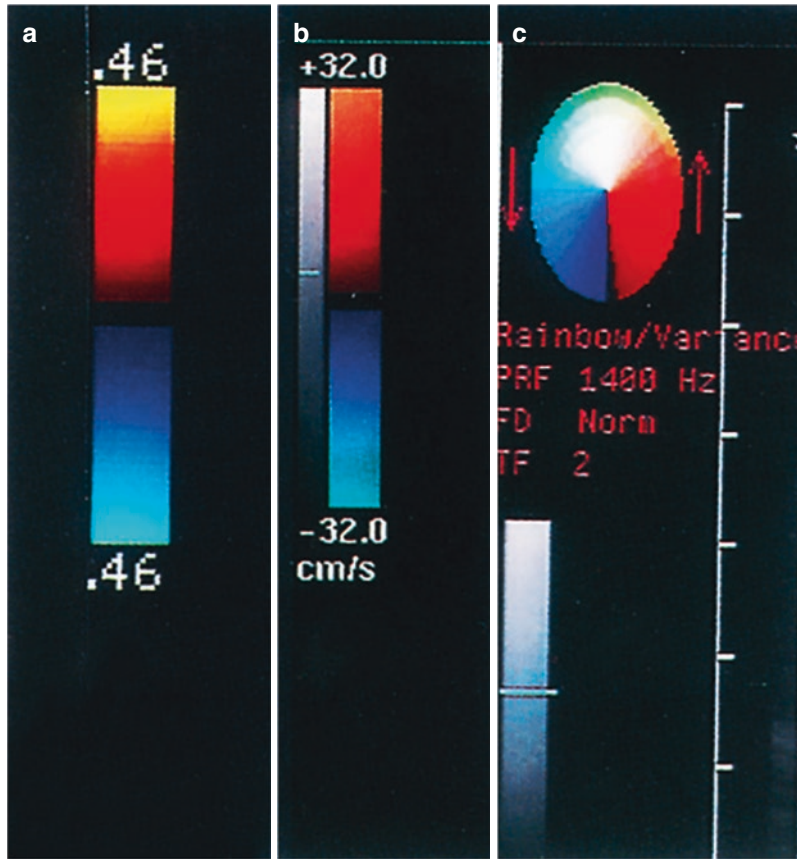

Fig. 6.5 Examples of color indicators from three ultrasound devices (*A, B, C*). The *first two panels* show the color velocity information in the form of a color bar. The flow toward the transducer is encoded in *red*, and flow away from the transducer is encoded in *blue*. The baseline is the *black band* between the two colors. Its vertical dimension varies with the magnitude of the wall filter. The magnitude of velocity is indicated by the brightness of colors, which progressively increases toward the upper and lower ends of the color bar. The magnitude of the velocity is indicated either as Doppler frequency shift (kilohertz) or as velocity (centimeters per second). The *third panel* (*C*) represents the Doppler information as a *color circle*, with the color flow directionality indicated by *arrows*. The color coding in this example is the same as that in the previous examples. The variance information is indicated by the additional mixing of color in the horizontal axis. Examples B and C also include indicators for gray-scale imaging priority

ter providing directional information. For example, with fetal echocardiography, ascending aortic and pulmonary trunk systems can be distinguished and their "cross-over" spatial relationship confidently established with the assistance of color flow mapping (see Chap. 30). This information helps to exclude various outflow tract malformations, such as the transposition of great vessels or the common outflow tract. Although this diagnostic information may be obtained through two-dimensional gray-scale imaging alone, addition of color flow mapping significantly augments the diagnostic efficacy. Similarly, the technique eases identification of the ductus arteriosus, noting the directionality of flow in conjunction with brightness of color because of a high ductal flow velocity. Often the ductal flow velocity exceeds the Nyquist limit, so aliasing can be observed, which also assists the process of identification.

6.2.12 Color Mapping of Variance

Variance is statistically defined as a measure of dispersion of the values around the mean. As dis-

cussed above, color flow mapping is based on the estimation of mean Doppler shift calculated by autocorrelation from the phase difference between consecutive echo signals. Variance in color flow mapping is the spread of the mean Doppler shift value and is determined statistically by the autocorrelator. Variance information is displayed only when the value exceeds a certain threshold and is achieved by changing the hue. With most devices, this change consists in adding green to the primary color. If the flow is toward the transducer, mixing of green with red results in yellow. If the flow is away, addition of green to blue results in cyan color. In either situation, the brightness of the mixed color is determined by the luminance of the primary hue.

The presence of variance above the threshold value may indicate spectral broadening caused by flow turbulence. However, the variance display may also be activated in a nonturbulent flow by variations in the flow velocity. In addition, if the flow velocity exceeds the Nyquist threshold, consequent aliasing may produce mosaic patterns in the color display that may be misinterpreted as turbulent flow.

6.2.13 Formation of a Color Frame

A color frame is a single complete cross-sectional display of a two-dimensional color flow map superimposed on a gray-scale image of the tissue structures produced by one complete sweep of the ultrasound beam. Obviously, there are two primary components of such a frame: the color flow map and the gray-scale image. The color flow map is generated by the multigated interrogation of multiple scan lines sweeping across the target field as discussed above. A two-dimensional B-scan tissue image is formed by pulse echo interrogation of the same scan lines. There are various procedures for achieving this image:

1. Imaging and flow information are sampled from each scan line synchronously and collated in the digital scan converter. When both imaging and flow mapping fields are completely scanned, the completed frame is displayed with the flow image superimposed on the tissue image.
2. Imaging and flow data are synchronously sampled for each line similar to the previous approach, but are displayed sequentially as each line is interrogated rather than when a complete frame is formed.
3. Scanning for tissue imaging is performed first followed by scanning for flow. Flow information is then superimposed on the tissue image.

While only one pulse per scan line is sufficient for tissue imaging, 3–32 pulses are needed for color Doppler imaging, which is therefore a more time-consuming process. One way to minimize the demand on time is to restrict Doppler flow sampling to an area smaller than the total available field. This color window or color box is superimposed on the gray-scale tissue image, and its size can be manipulated by the operator. A small color window improves Doppler sensitivity and temporal resolution. Therefore, it is advisable to restrict the size of this window to the area of interest for Doppler interrogation.

6.2.14 Persistence

Interpolation algorithms may be used to produce temporal averaging of color Doppler information. The process of averaging is known as *persistence*, as it allows more prolonged display or lingering of the color image. It produces a smoother color Doppler image at the cost of losing some detail. Most devices allow selection of different degrees of averaging or persistence. As the color Doppler image remains displayed longer with a higher persistence setting, areas of circulation with a lower flow velocity become more visible in the color map. The application of persistence control may therefore be useful when color mapping such as slow-flow conditions are encountered in the ovarian, placental, and fetal splanchnic circulations. Similarly, as the blood flow velocity declines near the vessel wall because of viscous drag, persistence may produce a more complete outline of a vascular image.

6.2.15 Frame Rate

Frame rate is the number of image frames produced per second. For Doppler color flow mapping, the rate varies from 10 to 60 frames per second. As discussed above, Doppler color flow interrogation places great demand on time. The frame rate (FR) is directly affected by the pulse repetition frequency (PRF); it is inversely influenced by the scan line density (SLD) in the color field and the number of pulses per scan line or the ensemble length (EL):

$$\mathrm{FR} = \mathrm{PRF} / (\mathrm{SLD} \cdot \mathrm{EL})$$

Therefore, the frame rate of color imaging can be changed by manipulating these factors, which, however, alter other imaging parameters due to their interdependence. For example, a higher frame rate can be achieved by increasing the PRF, which also limits the depth of interrogation. Similarly, a reduction in the line density not only increases the frame rate, it also compromises the spatial resolution; a decline in the number of samples per line also reduces the Doppler sensitivity. These trade-offs should be taken into consideration when ensuring optimal color imaging for a given situation. Thus, a low frame rate improves image quality by producing better sensitivity and spatial resolution. Slow flows are better detected with a low frame rate. The latter also allows more effective high-pass filtering, which results in more effective elimination of motion artifacts, such as ghosting. A low frame rate decreases temporal resolution, however, so asynchronous events may be displayed in the same frame. As expected, the problem becomes worse with a high heart rate, as observed in the fetus. A high frame rate improves the temporal resolution, provided the line density and number of pulses per scan line remain adequate to maintain an acceptable spatial resolution and Doppler sensitivity, respectively.

6.2.16 M-Mode Color Frame Formation

In Doppler color M-mode, multigated Doppler sampling is performed on a single scan line sampled 1000 times per second. The unidimensional tissue and color flow images are scrolled (usually from right to left on the display screen) and therefore are displayed as a function of time (Fig. 6.6). In the time-motion format, the vertical axis represents tissue depth, and the horizontal axis represents time. As with gray-scale M-mode insonation, the spatial location of the beam path is ascertained using two-dimensional color flow imaging. Because of the high sampling rate from a single line, color M-mode insonation provides high Doppler sensitivity and temporal resolution, and it allows reliable timing of the flow with the events of the cardiac cycle. For this reason, color M-mode sonography is a useful tool for fetal echocardiographic examination.

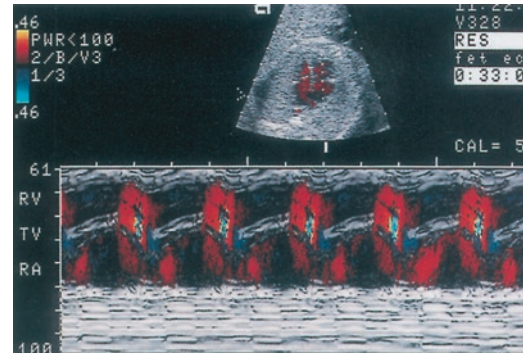

Fig. 6.6 Color M-mode sonogram. *Top*: Two-dimensional color Doppler echocardiogram of the fetal heart (four-chamber view). M-mode cursor is indicated by the *dotted line*. *Bottom*: Color M-mode tracing of flow from the right atrium (*RA*) to the right ventricle (*RV*) across the tricuspid orifice. The movement of the tricuspid valve (*TV*) is visible in the *middle* of the panel. As the flow is toward the transducer, it is coded *red*. Note the aliasing at the tricuspid orifice level (*blue* and *yellow*)

6.3 Operational Considerations

6.3.1 Transducer Frequency

The operating frequency of the transducer is an important contributor to the functional efficacy of the system. A high carrier frequency results in better spatial resolution of the image, but reduces the depth of penetration. The Doppler mode is more vulnerable to depth limitation than gray-scale tissue imaging. For most obstetric applica-

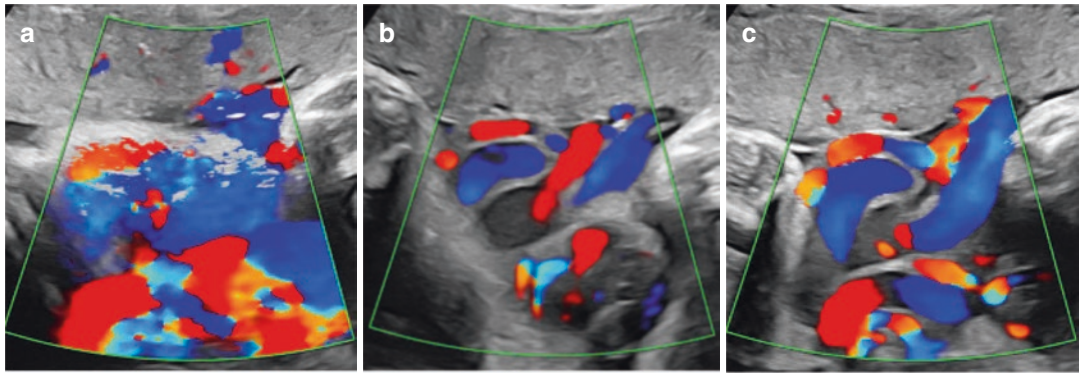

Fig. 6.7 (**a**–**c**) Doppler color gain. The examples illustrate the effect of variations in color gain on color flow imaging. Color flow in the umbilical cord is being depicted. (**a**) Image at high color gain. Note color is seen extending beyond the umbilical vessels; (**b**) image at low color gain. Color flow is not seen in many areas of the vessels; (**c**) image at medium color gain more accurately depicting color flow in the vessels

tions, a frequency of 2–4 MHz provides adequate penetration and resolution and is usually preferred. For transvaginal applications, a higher frequency (5–12 MHz) is used, as penetration is not a problem. Currently, piezoelectric elements capable of resonating at more than one frequency are available, so a single transducer can operate at multiple frequencies. This capability offers a unique advantage for color flow mapping, as a low frequency may be used for the combined tissue imaging and color Doppler mode, and one may then default to a high frequency for tissue imaging to ensure a higher gray-scale resolution.

6.3.2 Pulse Repetition Frequency

Doppler color flow mapping is based on pulsed Doppler insonation. The magnitude of the frequency shift in color flow Doppler sonography therefore depends on the PRF of the transmitted ultrasound. The PRF is adjustable and should be optimized for specific applications. As the PRF is changed, the range of Doppler shifts for a given PRF is shown in the color bar. The displayed range is a qualitative approximation and cannot be used as quantitative information. The PRF setting should be manipulated to accommodate a changing velocity pattern. A low PRF in the presence of a high-velocity flow results in aliasing of the displayed frequencies. A high PRF, on the other hand, reduces the sensitivity so that a low-velocity flow may not be identified. The location of the baseline can be changed to depict optimally the entire range of frequencies encountered in a target vessel in the appropriate direction. As indicated in the previous section, the PRF is related to the frame rate and affects the depth of imaging. These factors should be taken into consideration for increasing the efficiency of color flow imaging.

6.3.3 Doppler Color Flow Gain

The gain control deals with signal amplification. Most color flow devices offer separate gain controls for pulse echo imaging, spectral Doppler, and Doppler color mapping functions. The greater the gain, the more sensitive the Doppler procedure. Appropriate color gain adjustment is essential for generating reliable hemodynamic information. A higher gain setting improves the sensitivity of color Doppler sonography for identifying low-velocity flow states. However, increased gain also amplifies the noise component of the signal (Fig. 6.7), which causes display of misleading information, including the appearance of random color speckles in the color window, overflow of color outside vascular areas, and semblance of mosaic patterns. The latter falsely suggests the presence of turbulence when the flow is nonturbulent. The optimal gain setting should therefore be tailored to the specific exami-

nation. As a practical guideline, the gain should be initially increased until random color speckles start to appear; the gain is then reduced until the speckles disappear. Further manipulation should take into account other attributes of the color image and the characteristics of the flow.

6.3.4 High-Pass Filter (Wall Filter, Clutter Filter)

A high-pass filter eliminates high-amplitude/low-frequency Doppler signals generated by the movements of vessel wall and surrounding tissues. Such signals, because of their high-power content, obfuscate Doppler signals from low-velocity blood flow. This filter is called *high pass* because it allows high frequencies to pass through for further processing. As discussed in Chap. 4, high-pass filters are an essential part of signal processing in spectral Doppler ultrasonography. They are also an integral part of Doppler color flow mapping. The technique, however, is relatively more complex in this application, as an immense amount of Doppler data must be processed in real time. A filter that simply eliminates low-frequency signals also removes low-velocity blood flow signals with consequent loss of important hemodynamic information. For obstetric and gynecologic applications, low-speed flow is encountered in ovarian and tumor vessels, placental circulation, and fetal splanchnic vessels. The filters can be implemented at various levels of high-pass threshold. The thresholds are defined in terms of either frequency values or predesignated levels optimized for specific applications. The threshold may change automatically as the PRF is increased. With many devices, a minimum level of filtering operates at all times. Most current systems have default settings for various applications.

Although the exact algorithm of filtering is proprietary and varies according to the vendor, the current generation of high-pass filters uses multivariate techniques capable of discriminating between low-velocity blood flow and wall motion. Introduction of such filtering techniques has led to the recent resurgence of interest in Doppler amplitude mode (also known as power Doppler or energy Doppler) for color flow mapping, which may be helpful for microvascular flow imaging (see below).

6.4 Limitations of Color Doppler

Despite the impressive technologic innovations of Doppler color flow ultrasonography that have revolutionized noninvasive cardiovascular diagnosis, there are important limitations of the method that are inherent in the physical principles and the engineering implementation of the method. They are also responsible for various artifacts. An understanding of these limitations and artifacts is essential for the appropriate use and interpretation of Doppler color flow mapping. The following section discusses these factors, which include aliasing, range ambiguity, temporal ambiguity, problems related to the angle of insonation, tissue ghost signals, and mirror imaging.

6.4.1 Aliasing

As color flow mapping is based on pulsed Doppler insonation, its ability to measure the maximum frequency shift without ambiguity is limited by the PRF rate of the system. The threshold level of Doppler shift beyond which the measurement becomes ambiguous is called the Nyquist limit, and the phenomenon of Doppler shift ambiguity beyond the Nyquist limit is called the Nyquist effect, or *aliasing*. This phenomenon is known as aliasing because it falsely depicts the frequency shift in terms of both magnitude and direction. Aliasing in spectral pulsed Doppler sonography is discussed in detail in Chap. 3.

Aliasing in a color flow system is shown in a spatial two-dimensional plane in which the aliased flow is depicted in reversed color surrounded by the nonaliased flow (Fig. 6.8). This pattern mimics the color flow appearance of separate streams in differing directions. In an aliased flow, the higher velocity generates a higher Doppler-shifted frequency, which is depicted

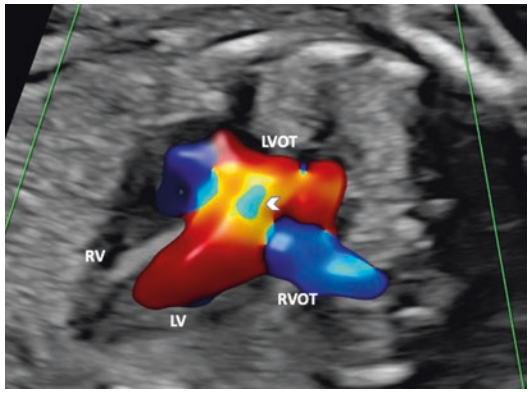

Fig. 6.8 Color Doppler Nyquist effect. The image shows Radiant color flow mapping of the left ventricular outflow. Note the change of color from *red* to *yellow* with increasing velocity and then aliases to *blue* demonstrating the Nyquist effect. *LV* Left ventricle, *LVOT* Left ventricular outflow tract, *RV* Right ventricle, *RVOT* Right ventricular outflow tract

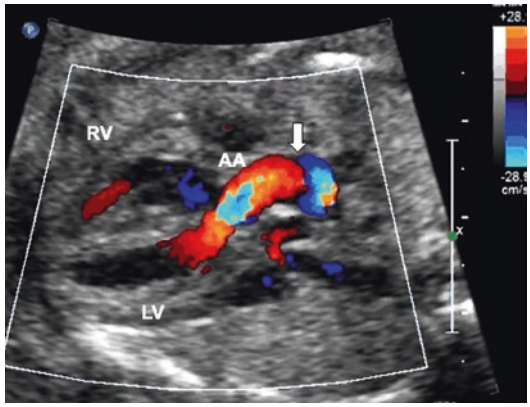

Fig. 6.9 Doppler color flow depiction of change in the direction of flow. The image shows Doppler color mapping of flow through the ascending aorta (*AA*) and the arch of the aorta. In the ascending aorta, the flow is toward the transducer and is therefore depicted as *red* according to the color bar setting. As the direction of flow changes, the color becomes *blue* with a dark line separating the two hues (vertical arrow). *LV* Left ventricle, *RV* Right ventricle

with greater brightness: the higher the frequency shift, the brighter the color. In the example (Fig. 6.8), the flow toward the transducer with an increasing velocity is depicted with an increasingly bright red color changing to yellow. As the Nyquist limit is exceeded, flow is shown in the bright blue. Thus, in an aliased flow, the bright or pale color of one direction is juxtaposed against the bright color of the opposite direction. In contrast, with genuine flow separation, the distinct flow streams are depicted in the directionally appropriate colors separated by a dark margin (Fig. 6.9). Note that the hue that demarcates an aliased flow depends on the choice of the color mapping scheme.

When demonstrating aliasing, an apparent contradiction may be seen between the spectral Doppler and the Doppler color flow interrogations. Doppler color flow mapping may show a nonaliased flow pattern when aliasing is observed with the spectral Doppler waveform. This phenomenon is explained by the fact that the mean frequency is less than the peak frequency, and Doppler color flow depiction is based on the use of mean frequency, so the Nyquist limit is not reached as readily as with the peak frequency depiction by the spectral Doppler method.

Color Doppler aliasing can be eliminated by elevating the Nyquist limit, which can be achieved by either increasing the PRF or decreasing the transducer frequency. However, an increasing PRF may eventually result in such shortening of the interpulse interval as to cause range ambiguity of the returning echoes – unless the depth of interrogation is reduced so that all the echoes from one pulse are received at the transducer before the next pulse is transmitted. As Doppler color flow mapping technology critically depends on identifying the spatial origin of an echo, color Doppler devices are preset to prevent range ambiguity by automatically reducing the color imaging depth.

6.4.2 Range Ambiguity

The occurrence of range ambiguity in regard to pulsed spectral Doppler sonography is discussed in Chap. 3. Range ambiguity arises when the interpulse interval is short in relation to the depth of the field of insonation, so echoes from deeper sampling locations do not reach the transducer before transmission of the next pulse. These Doppler signals are then treated as the early returning echoes of the second pulse being

reflected from a superficial location and are displayed as such. Consequently, spurious color flow is shown in areas devoid of any vascularity. In practice, however, most Doppler color flow devices prevent this problem by automatically reducing the depth when the PRF is increased to the threshold of range ambiguity.

Table 6.1 Relation between frame rate, completed frames per cardiac cycle, and fetal heart rate

Frames per second	Duration of a frame (ms)	Complete frames per cardiac cycle	
		FHR 120 bpm	FHR 160 bpm
10	100	5	3
15	66	7	5
30	33	15	11

FHR Fetal heart rate

6.4.3 Temporal Ambiguity

Temporal ambiguity occurs when Doppler color flow mapping fails to depict hemodynamic events with temporal accuracy. Specifically, such a situation arises when the frame rate for color flow is slow relative to the circulatory dynamics. As discussed earlier, the basic unit of color flow depiction is a single frame that, when completed, shows the average mean frequency shifts color-coded and superimposed on the gray-scale tissue image. The flow dynamics are therefore summarized for the duration of one frame. As we noted above, the frame rate is inversely proportional to the number of scan lines and the number of samples per scan line. The slower the frame rate, the better the color image quality in terms of both spatial resolution and Doppler sensitivity. Herein lies the paradox, as a slower rate means longer duration of a frame. As the frame duration increases, there is progressive loss of the ability to recognize discrete hemodynamic events.

This decline in the temporal relevance of the flow map is accentuated by hyperdynamic circulatory states. One may encounter such a situation in the fetal circulation, which is driven by a fast heart rate, normally 120–160 bpm. A faster rate means a shorter cardiac cycle. The shorter the cardiac cycle, the lower the number of complete frames available for depicting each cardiac cycle (Table 6.1) and the greater the risk of temporal ambiguity. This artifact may be apparent in the simultaneous depiction of temporally sequential circulatory phenomena. For example, with fetal echocardiography, one may see in the same frame atrioventricular flow across the mitral orifice and left ventricular outflow into the aortic root. The former is related to ventricular diastole and the latter to ventricular systole. One may also experience temporal ambiguity in color flow devices that form gray-scale and color flow images separately in a frame that may depict discordance between the gray-scale depiction and the color flow mapping of the cardiac events.

6.4.4 Angle of Insonation

Angle dependence of the Doppler-shifted frequencies, discussed in Chap. 2 in relation to spectral Doppler sonography, is a critical factor in color flow mapping. With sector scanning, multiple scan lines spread out from the transducer in a fan-like manner. When the sector scanner is used to interrogate a circulatory system in which the direction of flow is across these scan lines in a color window, the angle of insonation between the flow axis and the ultrasound beam changes. The angle is smallest when the flow stream enters in the sector field and progressively rises to 90° as the flow approaches the center of the field. Concurrently, the Doppler-shifted frequencies progressively decline and may become undetectable at the center of the color field (Fig. 6.10).

A sector scanner also creates apparently contradictory directional information in a vessel traversing the color field. As the flow approaches the midline of the field, the flow is depicted in color encoding for flow toward the transducer, which usually is red; as the flow moves away, it is encoded blue. Thus, the same vessel shows bidirectional flow (Fig. 6.11). This paradox highlights the basic concept of representation of flow directionality by any Doppler system. The latter does not depict the actual flow direction, merely the vector of flow toward the transducer.

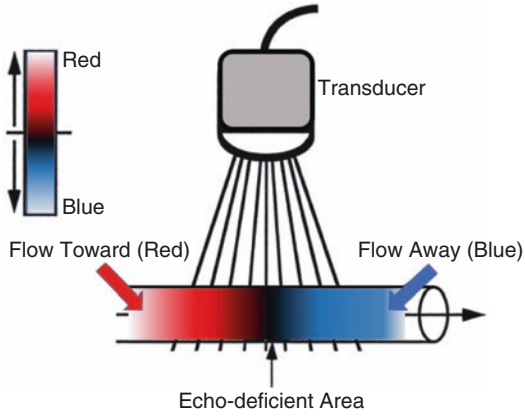

Fig. 6.10 Graphic representation of the effect of progressive increases in the angle of insonation and changes in color coding of flow as a vessel traverses a sector field

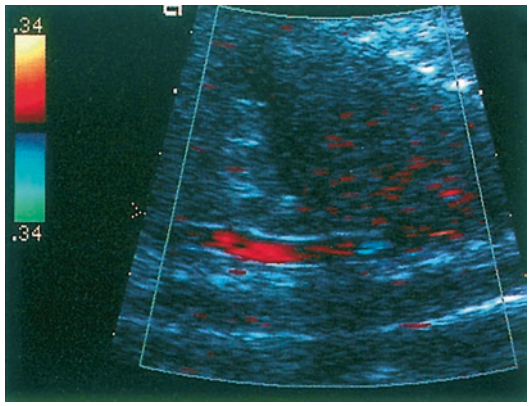

Fig. 6.11 Color Doppler sonogram of the fetal thoracoabdominal aorta demonstrating the effect of varying angles of insonation in a sector field. Although the flow in reality is unidirectional, the color coding of flow changes as the vessel traverses across the sector field giving a false impression of bidirectional flow. Note also the absence of color flow at the center of the color field as the beam intersects the vessel at a right angle

6.4.5 Wall Motion Ghost Signals

Spurious color flow signals may be generated by movements of the cardiac structures or vascular walls. These signals may be easily distinguished from the blood flow-related color map, as they are of lower frequency, are usually displayed outside the intracardiac or intravascular space, and may be asynchronous with the cardiac or vascular hemodynamic events (Fig. 6.12). These signals are seen more frequently with hyperdynamic circulations with high-speed wall movements. They may also be noted with deep cardiovascular structures whose motion generates Doppler signals; these signals reverberate at various structures and become more visible as the real blood flow signals are attenuated because of the depth. With obstetric applications, this artifact is of relevance mostly in relation to fetal echocardiography. Ghost signals may be reduced by elevating the high-pass filtering threshold, by increasing the PRF (which raises the minimum detectable velocity), or by the reject function (which cuts off low frequencies).

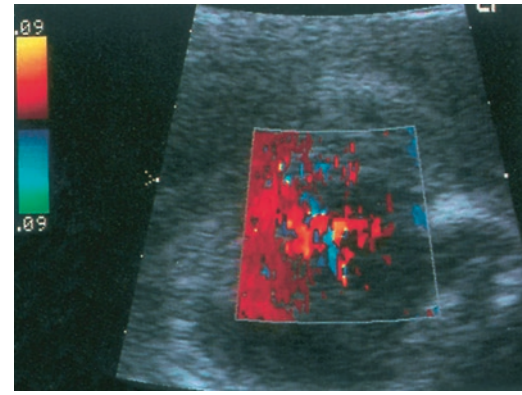

Fig. 6.12 Example of tissue motion-generated color signals unrelated to flow (*horizontal arrow*). The echogram depicts a fetal thoracic cross section at the level of the heart

6.4.6 Mirroring

Mirror images of color flow are produced by reflection of the Doppler signal at a vessel wall or other structures, so it takes longer to return to the transducer. The system recognizes and depicts the signal as originating from a deeper location than its real source.

6.5 Color Flow Visualization

One of the recent innovations in color flow imaging is the introduction of photorealistic visualization methods by the various ultrasound

manufacturers. One such innovation provides simulated 3D appearance to 2D color images with much improved definition of the vessel contours by shadowing and adding reflective highlighting. Examples include "Luniflow™" by Samsung and "Radiantflow™" by GE Healthcare. This is visualization postprocessing of the already acquired and processed 2D color flow signals and as such does not add any additional hemodynamic information. However, photorealistic visualization techniques significantly enhance the clarity of a vascular image and therefore perception and interpretation of the flow images as shown in Figs. 6.13 and 6.14.

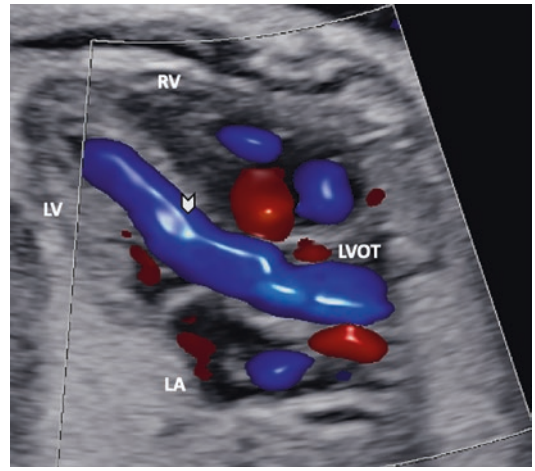

Fig. 6.13 Three-dimensional visualization of two-dimensional color Doppler depiction of left ventricular outflow tract (Lumiflow™). Note the three-dimensional appearance of the vessel with shadowing of the vessel margins and reflective highlighting (vertical arrow), achieved by Phong filtering technique. *LV* Left ventricle, *LVOT* Left ventricular outflow tract, *RV* Right ventricle

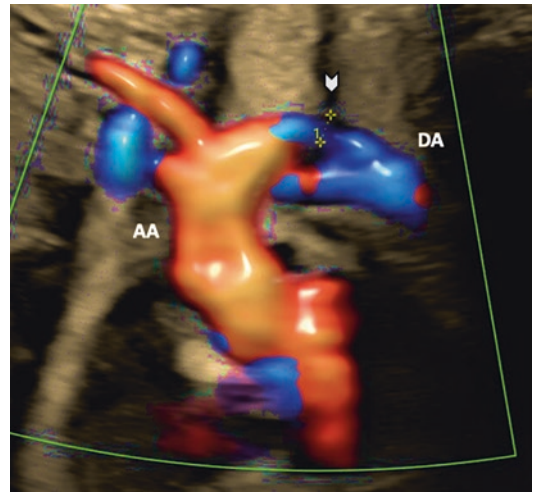

Fig. 6.14 Three-dimensional visualization of two-dimensional color Doppler depiction of aortic coarctation (white arrow). Note the clarity of the image achieved by the three-dimensional appearance of the vessel with shadowing of the vessel margins and reflective highlighting by Phong filtering technique. *AA* Aortic arch, *DA* Descending thoracic aorta

6.6 Power Doppler

The Doppler signal amplitude implies the intensity of the signal and is also referred to as Doppler power or energy. Power Doppler flow mapping is based on the amplitude of the Doppler signals. As discussed in Chaps. 3 and 4, Doppler flow signals have three dimensions: (1) frequency, which is proportional to the speed of red blood cell (RBC) movement; (2) amplitude, or intensity, of the signal, which is proportional to the number of RBCs scattering the transmitted ultrasound beam; and (3) time, during which the above two parameters change. While the frequency information and its temporal changes form the basis for clinical application of the Doppler technique, the amplitude data remain largely unutilized. However, amplitude reflects the scattering power of Doppler signals from blood flow and therefore provide useful hemodynamic information for clinical applications. During Doppler color flow processing, the autocorrelator measures the amplitude from the phase analysis of the returning echoes and generates two-dimensional Doppler color flow mapping based on the intensity of the Doppler signal.

With color flow processing, which is based on phase-difference analysis, the amplitude of the Doppler signal is estimated by the autocorrelator. The output is color-coded and is displayed along with the gray-scale tissue images. The Doppler power display, however, does not indicate directionality of flow in relation to the transducer. In contrast to the frequency mode, which as is apparent from the Doppler equation is angle-dependent, the amplitude mode is virtually unaffected by the angle of insonation (Fig. 6.15).

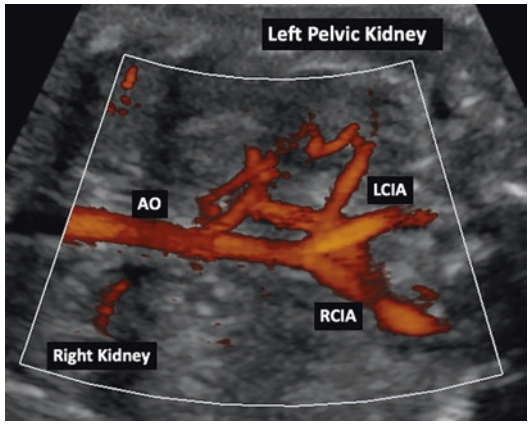

Fig. 6.15 Power Doppler image of renal vascular supply of a fetal pelvic kidney. The Doppler image is confirmatory of B-mode finding. Note monochromatic color flow with no demonstrable angle effect. *AO* Aorta, *RCIA* Right common iliac artery, *LCIA* Left common iliac artery

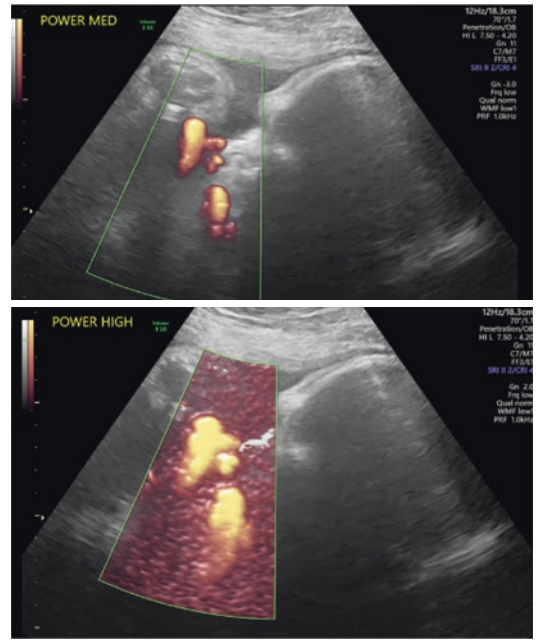

Fig. 6.16 Power Doppler images of umbilical artery demonstrating the effect of increasing the gain from medium (upper panel) to high (lower panel)

The amplitude output is affected by the wall (high-pass) filter as it removes high-amplitude/low-frequency Doppler signals generated by tissue movements. If the filter setting were identical to the frequency-based color flow mapping, the amplitude map would offer no more flow information than the former. Current filter algorithms, particularly those utilizing the multivariate approach, have substantially minimized this problem. An appropriate filter setting is essential for optimal color Doppler amplitude imaging. A low threshold of wall filter is needed for identifying low-flow states. Doppler power, or energy, imaging is also affected by the gain (Fig. 6.16). A high gain results in increased sensitivity for detecting slow-velocity circulations, but also in blooming artifacts where color flow areas extend beyond the vascular margin overwriting B-mode tissue signals. Other factors that interdependently or independently affect the power or energy mode display include the transmitted acoustic power, depth, color sensitivity, preponderance of gray scale (write priority), and persistence. The implementation of these controls and the resultant changes in the amplitude color maps vary from device to device. Most devices offer application specific default settings.

Over the recent years, significant technological advances have substantially expanded the capabilities of the power Doppler imaging and enhanced its clinical utility. These include directional power Doppler and power Doppler microvascular imaging and are presented below.

6.6.1 Directional Power Doppler

One of the advances in power Doppler imaging is the incorporation of directional information from the Doppler frequency shift signals into the Doppler power or amplitude signals, thus expanding its hemodynamic information content. In high definition power Doppler, short pulses with smaller Doppler sample volumes are used to obtain the flow direction. The advantages include improved axial resolution, lessening of blooming artifacts, better adaptive filtering of clutter signals, and higher temporal resolution. Preliminary reports demonstrated the potential of this modality in assessing fetal heart, prenatal diagnosis of cleft lip, and adult hepatic circulation [6–8]. The superior flow imaging capability of directional power Doppler compared to color Doppler and

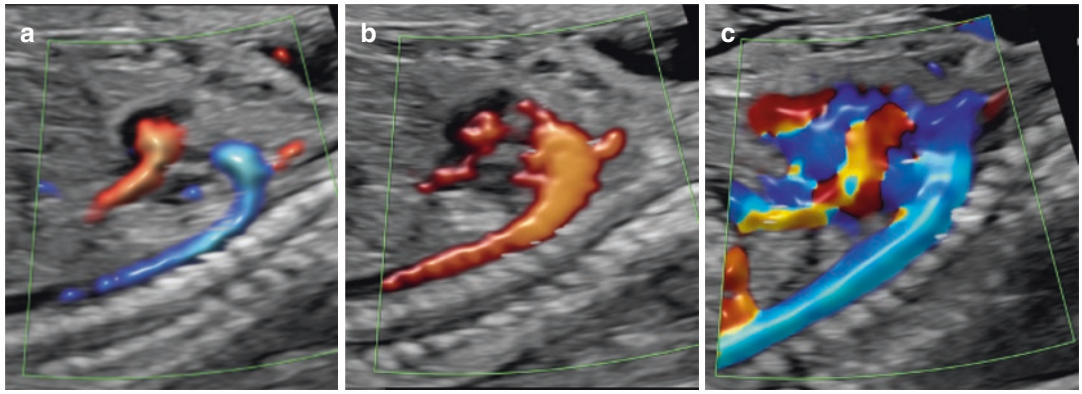

Fig. 6.17 Comparison of color Doppler (A), power Doppler (B), and directional power Doppler (C) images of fetal aortic flow

nondirectional power is illustrated in Fig. 6.17. The directional power Doppler image showed clearly defined flow through the whole length of the aorta within the color window without any loss of signal from the angle effect. Photorealistic visualization technique as described above was used in all three Doppler images, providing a simulated 3D appearance with clearly defined vascular margins (Radiantflow™, GE).

6.6.2 Power Doppler Microvascular Flow Imaging

In microvascular flow imaging (MVFI), advanced adaptive filtering techniques have been developed to eliminate high-amplitude low-frequency clutter signals from the low flow low-amplitude signals from small vessels. This approach results in exceptional sensitivity and spatial resolution in microvascular imaging. Preliminary experience has demonstrated its superiority over color Doppler and power Doppler imaging for assessing thyroid microvascular circulation in normal thyroid tissue and thyroid nodules [9]. More recently, MVFI has shown a significantly greater sensitivity and accuracy in detecting intratumor vascularity in hepatocellular tumor compared to color or power Doppler [10]. Our own initial imaging experience shows its potential for investigating fetal microcirculation in organs such as the fetal liver (Fig. 6.18). Noteworthy is the spatial resolution of the small vasculature (MV-Flow™, Samsung), further enhanced by 3D visualization as discussed earlier ((Lumiflow™, Samsung).

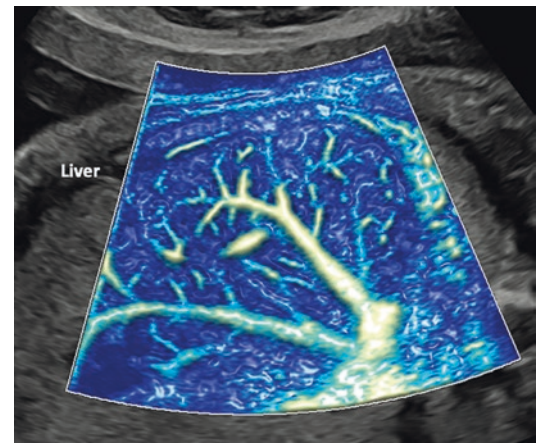

Fig. 6.18 Microvascular power Doppler imaging of fetal hepatic circulation

6.7 Four-Dimensional Doppler Color Flow Mapping

Color Doppler has also been implemented in four-dimensional (4D) imaging and has been applied in fetal hemodynamic assessment.

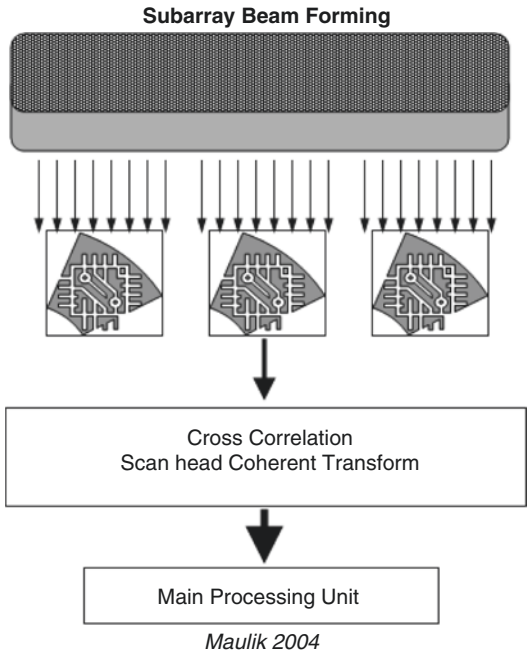

Fig. 6.19 Graphic depiction of the concept of sub-array beam forming

Initially, this was implemented with a motor driven mechanical probe, which generates a reconstructed 3D image volume. Significant advances have occurred in this field with the innovation of matrix array technology which allows electronic 3D volume generation in real time. The two-dimensional matrix array transducers utilize thousands of piezoelectric elements, all of which transmit and receive ultrasound. The enormous volume of data thus generated are processed in real time by sub-array beamforming involving several custom integrated circuits located in the handle of the transducer, and then transmitted to the main computer system of the device for further processing and generation of 3D images in real time (Fig. 6.19). The inherent limitations of Doppler sonography such as angle dependence are valid in these modalities.

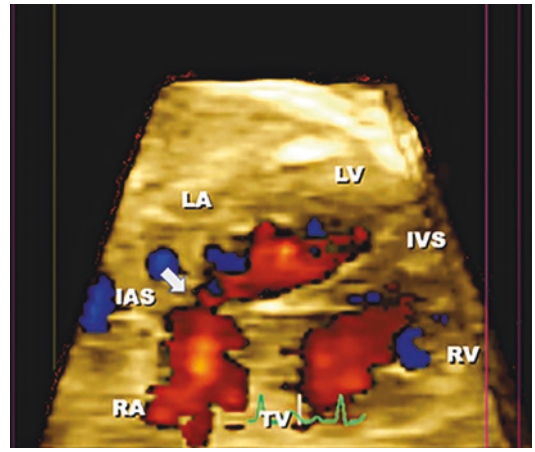

Fig. 6.20 Four-dimensional echocardiography using a two-dimensional matrix phased array in a fetus depicting interatrial flow. Arrow points to the foramen ovale. *RA* Right atrium, *LA* Left atrium, *RV* Right ventricle, *LV* Left ventricle, *TV* Tricuspid valve, *IVS* Interventricular septum, *IAS* Interatrial septum

It was initially introduced as a phased array system and shown to be effective in demonstrating normal and abnormal fetal cardiac anatomy and flow dynamics (Figs. 6.20 and 6.21) [11]. More recently, curved array matrix technology has been introduced and applied for fetal echocardiography [12].

The unit of three-dimensional spatial graphic information is known as a voxel, which can be digitally quantified to represent objective properties such as opacity, density, color, velocity, or even time. The ability to modify the opacity of a voxel is critical for three-dimensional imaging. This is known as opacity transformation which allows visualization of internal morphology of an image which would otherwise be obscured by more opaque surface voxels. An example of transparency mode (glass body) depiction of aortic and pulmonary cross-over view is given in Fig. 6.22. A review of the 4D Doppler echocardiography is presented in Chap. 33.

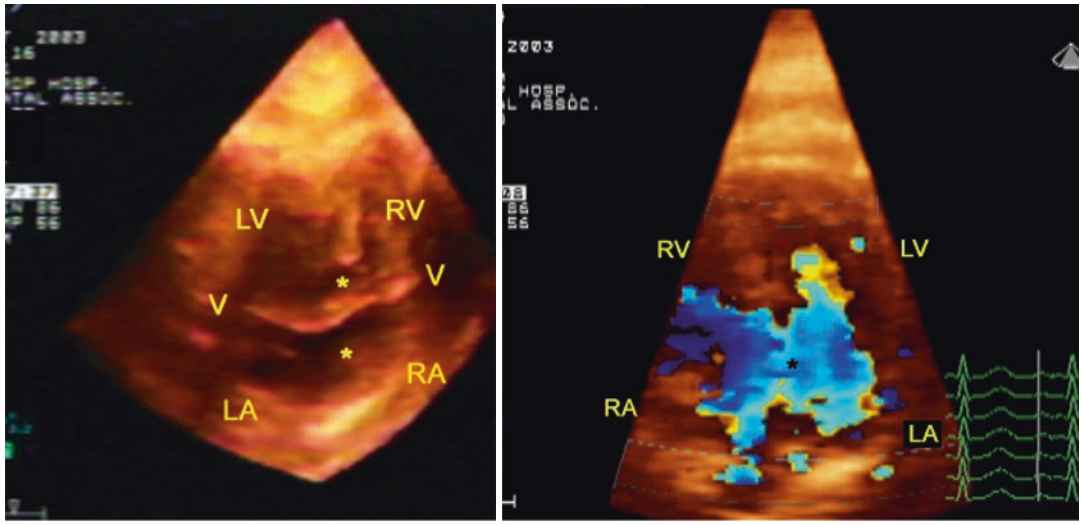

Fig. 6.21 Four-dimensional echocardiography using a two-dimensional matrix phased array in a fetus with complete atrioventricular septal defect. Four-chamber view cropped to show the atrial and ventricular septal defect with common atrioventricular valve (left panel) and color Doppler depiction of shunt across the septal defect (right panel). *RA* Right atrium, *LA* Left atrium, *RV* Right ventricle, *LV* Left ventricle, *V* Common atrioventricular valve. (With permission from reference [12])

Fig. 6.22 Four-dimensional echocardiography of the aortic and pulmonary cross-over relationship using a two-dimensional matrix curved array transducer, and Radiantflow™ with transparency or glass body mode. *AO* Aorta, *PA* Pulmonary artery, *LV* Left ventricle, *RV* Right ventricle

References

1. Omoto R, Kasai C. Physics and instrumentation of Doppler color flow mapping. Echocardiography. 1987;4:467–83.
2. Lee R. Physical principles of flow mapping in cardiology. In: Nanda NC, editor. Textbook of color Doppler echocardiography. Philadelphia: Lea & Febiger; 1989. p. 18.
3. Kremkau FK. Principles of color flow imaging. J Vasc Tech. 1991;15:104–9.
4. Namekawa K, Kasai C, Tsukamoto M, Koyano A. Real time bloodflow imaging system utilizing autocorrelation techniques. In: Lerski R, Morley P, editors. Ultrasound "82". London: Pergamon; 1983. p. 203–8.
5. Angelsen BAJ, Kristoffersen K. On ultrasonic MTI measurement of velocity profiles in blood flow. IEEE Trans Biomed Eng. 1979;26:665–71.
6. Hata T. Modern 3D/4D sonographic studies on fetal heart. Ultrasound Rev Obstet Gynecol. 2006;6:115–22.
7. Kennelly MM, Moran P. Directional power Doppler in the midsagittal plane as an aid to the prenatal diagnosis of cleft lip and palate. Prenat Diagn. 2008;28(1):56–8.
8. Kim SH, Lee JM, Kim YJ, Lee JY, Han JK, Choi BI. High-definition flow Doppler ultrasonographic technique to assess hepatic vasculature compared with color or power Doppler ultrasonography: preliminary experience. J Ultrasound Med. 2008;27:1491–501.
9. Machado P, Segal S, Lyshchik A, Forsberg F. A novel microvascular flow technique: initial results in thyroids. Ultrasound Q. 2016;32:67–74.
10. Kang HJ, Lee JM, Jeon SK, Ryu H, Yoo J, Lee JK, Han JK. Microvascular flow imaging of residual or recurrent hepatocellular carcinoma after transarterial chemoembolization: comparison with color/power doppler imaging. Korean J Radiol. 2019;20:1114–23.
11. Maulik D, Nanda NC, Singh V, Dod H, Vengala S, Sinha A, Sidhu MS, Khanna D, Lysikiewicz A, Sicuranza G, Modh N. Live three-dimensional echocardiography of the human fetus. Echocardiography. 2003;20:715–21.
12. DeVore GR, Satou G, Sklansky M. 4D fetal echocardiography—an update. Echocardiography. 2017;34:1788–98.

Biosafety of Diagnostic Doppler Ultrasound

7

Kjell Å. Salvesen and Ragnar K. Sande

7.1 Introduction

Ultrasound has an enviable safety record. Despite its use for almost 50 years, there are no proven harmful effects in humans. It would be wrong, however, to suppose that this risk does not exist. Ultrasound is used for tissue ablation and surgery, to lyse cells and create emulsions, to melt metal, and has been investigated for use as a weapon.

There are two major concerns; the vast number of babies exposed during fetal life, and gaps in knowledge about ultrasound safety. Most developed countries offer from one to four routine ultrasound examinations to all pregnant women. Many of these are carried out using new generations of ultrasound scanners, which have the potential to produce higher acoustic outputs than older devices. Furthermore, there are many gaps in our knowledge about ultrasound safety. Many of the studies on which we base our recommendations have been carried out in animal models whose relevance to the human is poorly understood, ultrasound exposure conditions which have little relevance to diagnostic ultrasound pulses, or on scanners that are no longer in common clinical use.

When reading this chapter, it must be remembered that absence of evidence of harm is not the same as absence of harm. It is never possible to prove a negative ("there is no such thing as zero risk"). It should also be remembered that Doppler ultrasound always has the highest risk of producing adverse effects, and that there are hardly any human data regarding safety of Doppler ultrasound.

7.2 Acoustic Output from Diagnostic Scanners

The lack of a consistent method of describing "dose" has made interpreting studies of ultrasound bioeffects difficult. Ultrasound fields are described in terms of pressure or intensity, neither of which give a measure of energy deposition. Nevertheless, acoustic power and intensity are of central importance when considering their safe use.

Acoustic power is a measurement of the rate at which the energy is emitted by the transducer measured in watts (joules per second). Acoustic powers in diagnostic beams vary from less than 1 mW to several hundred milliwatts. All this power is absorbed by the tissue, and the temperature can be raised.

K. Å. Salvesen (✉)
National Center for Fetal Medicine, Department of Obstetrics and Gynecology, St. Olavs Hospital, Trondheim University Hospital, Trondheim, Norway

Institute of Clinical and Molecular Medicine, Norwegian University of Science and Technology (NTNU), Trondheim, Norway
e-mail: pepes@ntnu.no

R. K. Sande
Department of Obstetrics and Gynecology, Stavanger University Hospital, Stavanger, Norway

D. Maulik, C. C. Lees (eds.), *Doppler Ultrasound in Obstetrics and Gynecology*,
https://doi.org/10.1007/978-3-031-06189-9_7

It is also relevant to describe how the power is distributed throughout the beam and across the scanning plane. This variation is measured as acoustic intensity, which is obtained by averaging the power over an area. The practical unit of measurement is milliwatt per square centimeter (mW/cm^2). A commonly quoted intensity is the spatial-peak temporal-average (SPTA), which is the greatest intensity in the beam (where the beam is "brightest"). For pulsed Doppler, this will be in the focal zone.

Modern ultrasound scanners have become so complex and have so many different output combinations that it is impossible for anyone other than the manufacturer or a specialized laboratory to measure the output. The most comprehensive surveys of acoustic output values for ultrasound systems were published in the 1990s [1–3], and one survey was published in 2010 [4] (Fig. 7.1).

This figure demonstrates that the most recent survey (2010) found an increase for B-mode (green bars), but a reduction for pulsed Doppler mode (red bars) compared to 1998 values, resulting in increased overlap in values between modes. But the figure also shows that maximum values are more than 1000 times greater than those reported for the first real-time B-mode scanners, and that the highest values are for pulsed Doppler ultrasound.

7.3 Safety Standards and Regulation

Pressure, intensity, and power parameters describe the acoustic field and are related to the field the patient is exposed to during diagnosis. However, they are not good indicators of the risk of adverse effects. Current standards and regulations refer to parameters intended to relate more directly to cavitation (bubble formation) and tissue heating (temperature rise). The mechanical index (MI) indicates the probability of cavitation, and the thermal index (TI) is an indicator of the likely maximum temperature rise in tissues exposed to ultrasound.

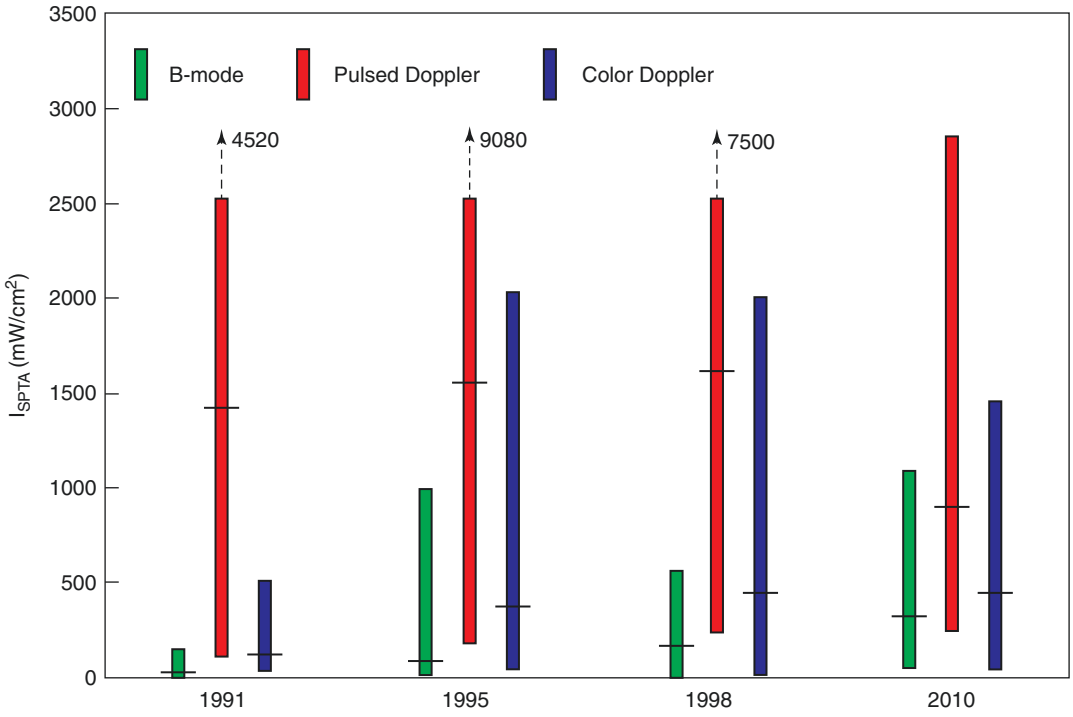

Fig. 7.1 Manufacturer declared values of spatial-peak temporal-average (SPTA) intensity from surveys in 1998–2010 in B-mode, pulsed Doppler, and color Doppler mode (Modified from Martin 2010 [4])

In 1991, the maximally permitted intensity during obstetric scanning was increased from 94 mW/cm^2 to 720 mW/cm^2 [5]. In order to maintain the safety of obstetric scanning, all scanners able to produce intensities above 94 mW/cm^2 were required to display TI and MI on-screen during the examination. The examiner is responsible for the safety of the examination; the TI and MI are meant to be an aid to the examiner in making sure that the ultrasound exposure is limited to what is needed to obtain the necessary clinical information [6].

7.4 Thermal Index

The formula for the TI is as follows:

$$\mathrm{TI} = W_0 / W_{1\mathrm{C}}$$

W_0 is the power currently being used, and $W_{1\mathrm{C}}$ is the power needed to raise the tissue temperature by one degree Celcius, in a reasonable worst-case scenario steady state. It thus follows that a TI of 1.0 corresponds to a maximal theoretical increase in tissue temperature of 1.0 degrees Celcius; a TI of 2.0 corresponds to a maximal theoretical increase in tissue temperature of 2.0 degrees Celcius, etc.

Different tissues have different ultrasound absorption properties, therefore three different versions of the TI have been developed; the TI for soft tissue (TIS), to be used when there is only soft tissue in the scanning field, TI for bone (TIB) to be used when there is bone present in the field, and TI for cranial bone (TIC) for direct cranial insonation. The British medical ultrasound society (BMUS) recommends the use of TIB from week 10 of pregnancy [7].

The TI is a rough estimate for exposure, based on power, modality, and scanning depth, as such it can never be 100% accurate. It has been criticized for being too inaccurate to be of clinical use, due to an unclear definition and calculation difficulties [8]. Considerable inconsistency has been found between TIB and the corresponding measured intensities in vitro [9].

7.5 Mechanical Index

The formula for the MI is as follows:

$$\mathrm{MI} = \mathrm{PNP} / \sqrt{F_{\mathrm{c}}}$$

PNP is the peak negative pressure and F_c is the center frequency of the ultrasound wave. The MI is designed to assess the risk for cavitation phenomena, a process where ultrasound causes gas bubbles to form and expand in tissue. These bubbles implode when they reach a threshold size, with sufficient force to perforate cell membranes.

It has been argued that fetal tissue contains insufficient gas in solution for cavitation phenomena to occur. The MI has not been evaluated as a marker for non-cavitational mechanical effects, such as streaming.

Despite their limits, the MI and TI are valuable tools in monitoring fetal exposure to ultrasound and the risk for bioeffects. We recommend that one employs the lowest power setting that is compatible with obtaining the necessary clinical information. The guidelines of BMUS indicate no upper time limit for ultrasound examinations where the TIB is kept below 0.7 and the MI is kept below 0.3. TI above 3.0 and/or MI above 1.7 is not compatible with safe obstetric ultrasound. Doppler is not recommended as a routine modality in the first trimester, but can be used with caution for precision diagnostics where pathology is suspected [10].

7.6 What Can the Operator Do?

We recommend that ultrasound exposure be kept to the lowest level compatible with obtaining good-quality clinically relevant information. Studies indicate that such information can be obtained using intensities well below that which we have reason to believe is currently applied in most clinical settings [11, 12]. It seems that ultrasound scanners in clinical use are commonly used with the power set to 100%, and rarely reduced. There is also evidence pointing to insufficient knowledge of how to adjust output power

even among experienced operators of obstetric ultrasound [13].

We have compared Doppler examinations at different intensities of five clinically relevant vessels; the umbilical artery, fetal middle cerebral artery, ductus venosus, and both maternal uterine arteries. The examinations were done at TIB 1.0, 0.5, and 0.1, respectively. Relevant information was obtained in all cases; statistical analysis revealed no significant differences between measurements obtained at low and high intensities [11, 12] (Fig. 7.2).

Based on this, we recommend that the default power setting is set to 85% of the maximal value; normally, this would result in TIB below 0.7 and MI below 0.3. From this level, the examiner may increase the power when particularly difficult conditions necessitate this.

7.7 Evidence from Human Studies

For interpretation of data derived from epidemiological studies, there is a hierarchy of studies based on study design and the quality of the research methods. Highest value should be given to systematic reviews of randomized controlled trials, and less value to cohort studies, case-control studies, and other observational studies (in that order).

One randomized controlled trial has assessed the effect of regular Doppler ultrasound in low-risk pregnancies, reporting data on 1415 women who had frequent Doppler ultrasound throughout pregnancy and 1419 who did not. The aims of the trial were not to study safety aspects of Doppler ultrasound, but the results indicated increased risk for birth weight below the third centile (odds

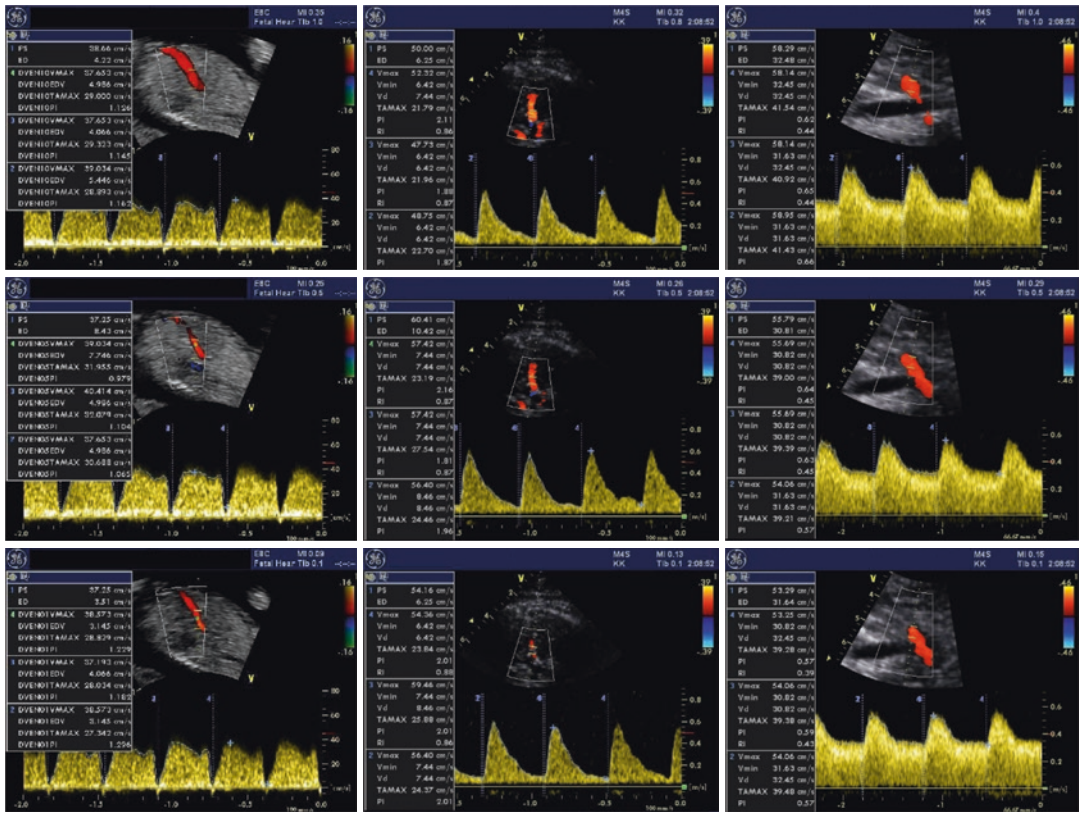

Fig. 7.2 From left to right: Ductus venosus at 12 weeks, the middle cerebral artery at 18 weeks, and the right uterine artery at 24 weeks. Top row obtained at TIB 1.0, middle row at TIB 0.5, and bottom row at TIB 0.1

ratio 1.84) and below the tenth centile (odds ratio 1.46) [14].

A follow-up study was published 19 years after the initial trial. This study assessed development of autism spectrum disorders (ASD) [15]. There was no difference in the occurrence of ASD between the exposed group (7 cases of ASD among 1167 children) and the control group (9 cases of ASD among 1125 children) [15]. A subgroup of 586 cases and 595 controls was subject to assessment by a ASD quotient scale, and this analysis did not reveal any difference between the groups.

There are very few other epidemiological studies concerned with safety aspects of Doppler ultrasound. However, pulsed Doppler has the highest risk of producing adverse effects, and acoustic outputs from modern devices have increased 10–15-fold during the last decades. In addition, the number of scans per pregnancy and exposure times have increased over time. If there is evidence of adverse effects using lower acoustic outputs and exposure times, the users of the new generations of ultrasound scanners must acknowledge that there is a potential risk. Thus, there is a need to explore other available epidemiological evidence.

Two systematic reviews of epidemiological studies of the safety of ultrasound in pregnancy have been published [16, 17]. A Cochrane review [16] included all registered published and ongoing randomized controlled trials and quasi-randomized trials, but no other studies. An ISUOG-WHO review [17] included 16 controlled randomized controlled trials, 13 cohort, and 12 case-control studies published between January 1950 and October 2007 that assessed any type of short- and long-term effects of at least one exposure to ultrasound during pregnancy. The outcomes assessed included maternal outcomes, perinatal outcomes, childhood growth, neurological development and school performance, non-right-handedness, childhood malignancies, intellectual performance, and mental diseases after childhood [17].

The conclusions from the systematic reviews are that epidemiological studies have demonstrated no confirmed associations between prenatal ultrasound and adverse perinatal outcomes, childhood malignancies, neurological development, dyslexia, speech development, school performance, intellectual performance, and adult mental disease. However, there is a weak statistically significant association between prenatal ultrasound and being non-right-handed.

According to the data presented in the Cochrane review [17], there was no statistically significant association between prenatal ultrasound and non-right-handedness. However, in a more recent meta-analysis including three randomized controlled trials, there was a statistically significant association [18] (Fig. 7.3).

If results from cohort studies are included [22, 23], as was done in the ISUOG-WHO review, the strength of the association was similar for randomized trials and cohort studies [17]. Thus, the conclusion must be that five epidemiological studies report a 15% increase in the likelihood of sinistrality (in particular among males), and no other epidemiological evidence contradicts this association.

The discussion of prenatal ultrasound and handedness is complex and will not be extended here. An editorial explores this issue in detail [24]. A statistical association between ultrasound and left-handedness should not lead to the con-

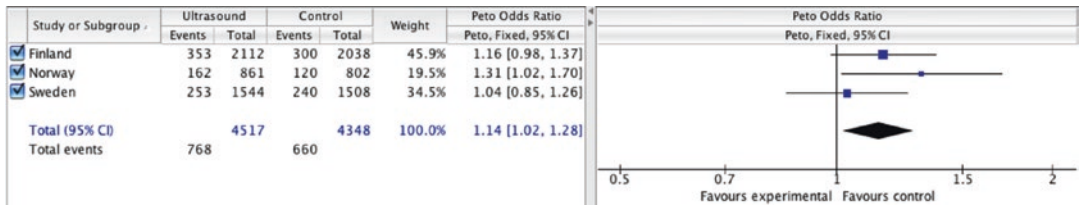

Fig. 7.3 Forest plot of odds ratios of non-right-handedness according to randomized groups in a Finnish study [19], Norwegian study [20], Swedish study [21], and overall

clusion that ultrasound causes harm to the developing brain. The current biological understanding of handedness is limited and partly contradictory to the epidemiological evidence.

Autism spectrum disorder (ASD) is a neurodevelopmental disorder with mainly genetic origin, but there is evidence that environmental factors may play a role, and that the initiating process leading to ASD originates during fetal life. Reported registered prevalence rates are increasing, but it seems that much of the increase reflects better awareness of the disorder rather than a true rise in prevalence. Nevertheless, a recent study has created some concern.

Webb reported a case series of 1749 children with ASD aged 4–18 years. ASD severity was characterized using measures of cognitive ability, social ability, and repetitive behaviors [25]. Genetic predisposition was characterized by the presence of ASD-associated copy-number variations (CNV). The authors compared 84 exposed and 41 nonexposed children with ASD and CNV, and a subsample of 73 exposed and 38 nonexposed boys with ASD and CNV. They concluded that the combination of first trimester ultrasound and presence of CNV in male children with ASD correlated with poorer cognitive outcomes and increased repetitive behaviors. This study has a high risk of bias: it was a case-series with no control group, exposure information was collected by recall 4–18 years after the pregnancy, multiple testing without correction of statistical significance level was undertaken, and possible confounding factors were not addressed.

Three other studies of a possible association between ultrasound exposure and ASD have been published; one case-control study [26] and two long-term follow-up of a large number of children from randomized controlled trials [15, 27]. None of these studies found any association between prenatal ultrasound and ASD. Based on the available data, we must conclude that there is no scientifically proven association between ultrasound exposure in first or second trimester and ASD, or its severity.

7.8 Guidelines and Recommendations

Sonograms can be safely performed during pregnancy by trained and accredited sonologists, when medically indicated and when the "as low as reasonably achievable" (ALARA) principle on the use of ultrasound intensities is employed. Since, in Doppler mode, relatively high intensities are usually transmitted, ISUOG (and other ultrasound organizations) recommend that pulsed Doppler (spectral, power, and color flow imaging) ultrasound should not be used routinely in early pregnancy [10]. When performing Doppler ultrasound in the first trimester on clinical grounds, the displayed thermal index (TI) should be $\leq$1.0 and exposure time should be kept as short as possible.

References

1. Duck FA, Martin K. Trends in diagnostic ultrasound exposure. Phys Med Biol. 1991;36:1423–32.
2. Henderson J, Wilson K, Jago J, Whittingham TA. A survey of the acoustic outputs of diagnostic ultrasound equipment in current clinical use in the Northern region. Ultrasound Med Biol. 1995;21:699–705.
3. Wittingham TA. The acoustic output of diagnostic machines. In: ter Haar G, Duck FA, editors. The safe use of ultrasound in medical diagnosis. 2nd ed. London: BMUS/BIR; 2000.
4. Martin K. The acoustic safety of new ultrasound technologies. Ultrasound. 2010;18:110–8. https://doi.org/10.1258/ult.2010.010024.
5. Nyborg WLCP, Carstensen EL, Dunn F, Miller D, Miller MW, Thompson HE, Ziskin MC. Exposure criteria for medical diagnostic ultrasound: II. Criteria based on all known mechanisms. National Council on Radiation Protection and Measurements 2002; Report NO 140.
6. Abramowicz JS, Kossoff G, Marsal K, Ter Haar G. Safety Statement, 2000 (reconfirmed 2003). International Society of Ultrasound in Obstetrics and Gynecology (ISUOG). Ultrasound Obstet Gynecol. 2003;21:100.
7. BMUS. Guidelines for the safe use of diagnostic ultrasound equipment. In: The Safety Group of the British Medical Ultrasound Society, editor. Guidelines for the safe use of diagnostic ultrasound equipment; 2009.
8. Bigelow TA, Church CC, Sandstrom K, Abbott JG, Ziskin MC, Edmonds PD, Herman B, Thomenius KE, Teo TJ. The thermal index: its strengths, weaknesses, and proposed improvements. J Ultrasound Med. 2011;30:714–34.

9. Retz K, Kotopoulis S, Kiserud T, Matre K, Eide GE, Sande R. Measured acoustic intensities for clinical diagnostic ultrasound transducers and correlation with thermal index. Ultrasound Obstet Gynecol. 2017;50:236–41.
10. Salvesen K, Lees C, Abramowicz J, Brezinka C, Ter Haar G, Marsal K. ISUOG statement on the safe use of Doppler in the 11 to 13 +6-week fetal ultrasound examination. Ultrasound Obstet Gynecol. 2011;37:628.
11. Sande RK, Matre K, Eide GE, Kiserud T. Ultrasound safety in early pregnancy: reduced energy setting does not compromise obstetric Doppler measurements. Ultrasound Obstet Gynecol. 2012;39:438–43.
12. Sande RK, Matre K, Eide GE, Kiserud T. The effects of reducing the thermal index for bone from 1.0 to 0.5 and 0.1 on common obstetric pulsed wave Doppler measurements in the second half of pregnancy. Acta Obstet Gynecol Scand. 2013;92:790–6.
13. Marsal K. The output display standard: has it missed its target? Ultrasound Obstet Gynecol. 2005;25:211–4.
14. Newnham JP, Evans SF, Michael CA, Stanley FJ, Landau LI. Effects of frequent ultrasound during pregnancy: a randomised controlled trial. Lancet. 1993;342:887–91.
15. Stoch YK, Williams CJ, Granich J, Hunt AM, Landau LI, Newnham JP, Whitehouse AJ. Are prenatal ultrasound scans associated with the autism phenotype? Follow-up of a randomised controlled trial. J Autism Dev Disord. 2012;42:2693–701.
16. Whitworth M, Bricker L, Neilson JP, Dowswell T. Ultrasound for fetal assessment in early pregnancy. Cochrane Database Syst Rev. 2010;(4):CD007058. https://doi.org/10.1002/14651858.CD007058.pub2.
17. Torloni MR, Vedmedovska N, Merialdi M, Betran AP, Allen T, Gonzalez R, Platt LD. Safety of ultrasonography in pregnancy: WHO systematic review of the literature and meta-analysis. Ultrasound Obstet Gynecol. 2009;33:599–608.
18. Salvesen KÅ. Ultrasound in pregnancy and non-right handedness—meta-analysis of randomized trials. Ultrasound Obstet Gynecol. 2011;38(3):267–71. https://doi.org/10.1002/uog.9055. Epub Jul 15.
19. Heikkilä K, Vuoksimaa E, Oksava K, Saari-Kemppainen A, Iivanainen M. Handedness in the Helsinki ultrasound trial. Ultrasound Obstet Gynecol. 2011; https://doi.org/10.1002/uog.8962.
20. Salvesen KÅ, Vatten LJ, Eik-Nes SH, Hugdahl K, Bakketeig LS. Routine ultrasonography in utero and subsequent handedness and neurological development. BMJ. 1993;307:159–64.
21. Kieler H, Axelsson O, Haglund B, Nilsson S, Salvesen KÅ. Routine ultrasound screening in pregnancy and the children's subsequent handedness. Early Hum Dev. 1998;50:233–45.
22. Kieler H, Cnattingius S, Haglund B, Palmgren J, Axelsson O. Sinistrality - a side-effect of prenatal sonography: a comparative study of young men. Epidemiology. 2001;12:618–23.
23. Kieler H, Cnattingius S, Palmgren J, Haglund B, Axelsson O. First trimester ultrasound scans and left-handedness. Epidemiology. 2002;13:370.
24. Salvesen KÅ. Ultrasound and left-handedness: a sinister association? Ultrasound Obstet Gynecol. 2002;19:217–21.
25. Webb SJ, Garrison MM, Bernier R, McClinic AM, King BH, Mourad PD. Severity of ASD symptoms and their correlation with the presence of copy number variations and exposure to first trimester ultrasound. Autism Res. 2017;10:472–84.
26. Grether JK, Li SX, Yoshida CK, Croen LA. Antenatal ultrasound and risk of autism spectrum disorders. J Autism Dev Disord. 2009; https://doi.org/10.1007/s10803-009-0859-4.
27. Carlsson LH, Saltvedt S, Anderlid BM, Westerlund J, Gillberg C, Westgren M, Fernell E. Prenatal ultrasound and childhood autism: long-term follow-up after a randomized controlled trial of first- vs second-trimester ultrasound. Ultrasound Obstet Gynecol. 2016;48:285–8.

Fetal Cardiovascular Physiology

8

Dino A. Giussani, Kimberley J. Botting, Youguo Niu, Caroline J. Shaw, Sage G. Ford, and Avnesh S. Thakor

8.1 Fetal Oxygenation

The survival of cells depends upon the delivery of oxygen and nutrients. The rates of supply of oxygen and nutrients and the removal of waste products must be adequate to support cellular metabolism, the growth of tissues, and the function of organs. In multicellular organisms, size creates a problem because diffusional time is related to the square of the diffusional distance, meaning that these demands cannot be met by direct diffusive exchange with the environment. Therefore, multicellular organisms have evolved a cardiovascular system to bypass the limitations of diffusional distance and time and deliver oxygen closer to the target organs where then diffusion can take over [1]. The transport function of blood is highly dependent on the architecture of the circulatory system which, in turn, determines blood flow dynamics and rates of diffusive exchange with local tissues [2].As there is no long-term storage of oxygen in the mammalian fetus, the supply of oxygenated blood to fetal tissues is dependent on a specialized cardiovascular network, in which oxygen is able to pass from the maternal uterine circulation to the fetal umbilical circulation across the placenta, which serves as the exchange interface. Hence, the fetal circulation is anatomically arranged to take oxygenated blood from the placenta via the umbilical vein to the most important organs in fetal life, largely bypassing the fetal liver and lungs [3]. In addition,

D. A. Giussani (✉)
Department of Physiology Development & Neuroscience, University of Cambridge, Cambridge, UK

BHF Centre for Research Excellence, Cambridge, UK

Cambridge Strategic Research Initiative in Reproduction, Cambridge, UK
e-mail: dag26@cam.ac.uk

K. J. Botting
Department of Physiology Development & Neuroscience, University of Cambridge, Cambridge, UK

Cambridge Cardiovascular Strategic Research Initiative, Cambridge, UK

Y. Niu
Department of Physiology Development & Neuroscience, University of Cambridge, Cambridge, UK

Cambridge Cardiovascular Strategic Research Initiative, Cambridge, UK

Cambridge Strategic Research Initiative in Reproduction, Cambridge, UK

C. J. Shaw
Institute of Reproductive and Developmental Biology, Imperial College London, London, UK

S. G. Ford
Department of Physiology Development & Neuroscience, University of Cambridge, Cambridge, UK

A. S. Thakor
Interventional Regenerative Medicine and Imaging Laboratory, Department of Radiology, Stanford University School of Medicine, Stanford, CA, USA

D. Maulik, C. C. Lees (eds.), *Doppler Ultrasound in Obstetrics and Gynecology*,
https://doi.org/10.1007/978-3-031-06189-9_8

there are a number of adaptations, unique to life in the womb, which allow the supply of oxygen to the fetus to exceed its metabolic needs. For example, relative to the adult, these adaptations allow the fetus to bind greater concentrations of oxygen in its hemoglobin [4–6], to have an increased basal blood flow to hypoxia-sensitive tissues, such as the brain [7], and to relinquish bound oxygen to the fetal tissues at lower oxygen tensions [8, 9]. Furthermore, shunts in the fetal circulation and enhanced preferential streaming ensure an adequate supply of oxygenated blood to tissues most at risk of damage during reductions in oxygenation [10, 11]. Finally, the fetus also has a greater capacity than the adult to hinder oxygen-consuming processes [12, 13]. Combined, these cardiovascular adaptations equip the unborn child with a considerable margin of safety for alterations in oxygenation during fetal development.

8.2 Development of Fetal Basal Cardiovascular Function

Toward term, there are maturational changes in a number of physiological systems in the fetus, which ensure survival in utero as the fetus grows and the successful transition to independent cardiovascular function at birth. In several species, fetal arterial blood pressure increases and fetal heart rate decreases with advancing gestational age (see [14] for review). The rise in arterial blood pressure can, in simple terms, be attributed to either an increase in cardiac output and/or in total peripheral vascular resistance. However, although there is an increase in cardiac output in the fetus with advancing gestation, this is unlikely to contribute to the increase in arterial blood pressure, since Rudolph and Heyman [15] showed that the relative fetal cardiac output, expressed per kg of body weight, does not increase toward term. By contrast, in several species, there is an ontogenic increase in fetal peripheral vascular resistance [16–23]. Basal circulating concentration of constrictor hormones as well as the reactivity of the peripheral vasculature to constrictor agonists increase with advancing gestational age [18, 23–26]. Toward term, the fetal cardiac baroreflex also matures, showing a rightward shift in the baroreflex set point, which allows a greater resting fetal arterial blood pressure with advancing gestational age [21, 27]. Combined, these developmental changes in cardiovascular function ensure that the delivery of oxygen and nutrients to the fetal tissues is appropriate for their mass and nutrient requirements with advancing gestational age and fetal development.

8.3 Fetal Cardiovascular Function During Stress

The fetal sheep preparation surgically instrumented with catheters and flow probes under general anesthesia has been the experimental model of choice to study the fetal cardiovascular responses to stress. In this way, following several days of post-surgical recovery, the fetal responses to acute or prolonged stress can be investigated in the unanesthetized animal in a highly physiological preparation. A wide variety of acute (minutes-to-hours) and prolonged (days-to-months) experimental stressors have been used to elicit fetal homeostatic responses. Acute short-term challenges include fetal hypotension [28], hemorrhage [29], hypoxaemia [30, 31], hypercapnia [16], acidaemia [32], anemia [33], reduction in uterine blood flow [34], umbilical cord compression [35], and obstruction of the vena cava [36]. Prolonged challenges include maternal dietary nutrient restriction [37], reductions in placental capacity via carunclectomy [38], exposure to hypobaric [39] or isobaric [40–42] chronic hypoxia, and pregnancy at high altitude [43].

8.4 Fetal Hypoxia

One of the most common challenges in fetal life is acute fetal hypoxia (see [44] for review). If the rate of oxygen exchange between the maternal and fetal circulation becomes inadequate to meet the fetal demands for oxygen, there will be a fall in the partial pressure of oxygen within the fetal arterial blood (P_aO_2; hypoxaemia), with accompanying reductions in regional partial pressures of oxygen in tissue (PO_2; hypoxia). Fetal hypoxaemia may occur by insufficiency of either uterine blood flow [34] or umbilical blood flow [12],

or by a decrease in maternal arterial oxygen content [31]. Other mechanisms such as fetal anemia or increased fetal oxygen consumption (e.g., in pyrexia) are relatively rare in clinical practice [45]. Risk factors which predispose to fetal hypoxaemia can be broadly classified into maternal (e.g., diabetes [46], pregnancy-induced or chronic hypertension [47], Rh sensitization [48], maternal infection [49], sickle cell anemia [50], chronic substance abuse [51], asthma [52], seizure disorders [53], maternal obesity [54], or smoking [55, 56]), intrapartum (e.g., multiple pregnancy [57], pre- or post-term birth [58, 59], prolonged labor [60], placental abruption [58], placenta praevia [61], prolapsed umbilical cord [62], or abnormal presentation of the fetus [63]), and iatrogenic (e.g., epidural anesthesia [64]).

Several experimental techniques to induce fetal hypoxaemia in animal models like the pregnant sheep have arisen over the years. By far the most common approach is by maternal inhalational hypoxia, which reduces her inspired fraction of oxygen (F_iO_2; [44]). The challenge usually involves the ewe breathing a gas mixture of 6–10% O_2 in N_2 with 3–4% CO_2, which in turn lowers the fetal P_aO_2 in the descending aorta from baseline values of ca. 20–25 mmHg to around 10–12 mmHg while maintaining fetal P_aCO_2. The main advantage of this technique is that the level of reduction in fetal P_aO_2 can be controlled with remarkable precision while maintaining isocapnic conditions. A disadvantage is that it also induces hypoxia in the mother and the placenta, which may produce hormones and metabolites that may enter the fetal circulation. However, in studies using extracorporeal membrane oxygenation (ECMO), which allows maternal and fetal P_aO_2 to be independently controlled, it was found that in maternal hypoxaemia during fetal normoxaemia, the impact of the materno-placental responses in affecting the fetal cardiovascular physiology was negligible [65].

8.5 Fetal Cardiovascular Responses to Acute Hypoxia

The exact pattern and magnitude of the fetal cardiovascular defence responses to acute hypoxaemia vary not only with gestational age, but also with the degree of the challenge. Hence, in fetal sheep, prior to 110 days of gestation (term is ca. 150 days), acute isocapnic hypoxaemia produces no change in arterial blood pressure or blood flow in peripheral circulations, but heart rate and blood flow in the cerebral, myocardial, and adrenal circulations are increased [16, 66]. By contrast, at gestational ages greater than 110 days, a similar degree of hypoxaemia is associated with a transient bradycardia, an increase in arterial blood pressure, and a redistribution of the fetal cardiac output in favor of the adrenal, myocardial, and cerebral circulations at the expense of perfusion of peripheral vascular beds - the so-called fetal brain sparing effect [30, 31, 44]. Furthermore, while umbilical blood flow falls during acute hypoxaemia at 0.6–0.7 of gestation [66], umbilical blood flow increases in hypoxic conditions in fetuses of greater gestational ages, thereby increasing the proportion of the fetal cardiac output received by the placenta [30, 67]. In experiments where varying grades of fetal hypoxaemia were imposed, the onset, degree, and duration of the bradycardic response [68] as well as the change in organ blood flow [69] were correlated with the magnitude of the reduction in fetal arterial oxygen content.

8.6 Functional Importance of the Fetal Cardiovascular Responses to Acute Hypoxaemia

In the late gestation fetus, the bradycardia during acute hypoxaemia has several functional advantages. Fisher and colleagues [70] suggested that the product of the heart rate and blood pressure (the rate-pressure product) is a useful correlate of myocardial oxygen consumption as it reflects myocardial workload. In late gestation fetal sheep, the rate-pressure product decreases during acute hypoxaemia, thereby decreasing myocardial workload and cardiac oxygen consumption. If the fetal heart continued to beat at the same rate during the hypoxaemic episode, the oxygen demand of the myocardial cells would exceed their supply, thereby rendering them vulnerable

to ischaemic injury, which may result in irreversible damage. Fetal bradycardia also retards the speed of cardiac blood flow, which has at least two advantages. First, it slows the passage of coronary flow, which enhances myocardial oxygen extraction [70, 71]. Second, it prolongs end-diastolic filling time, which increases ventricular end-diastolic volume, promoting a greater stretch and thereby force of ventricular contraction through the Frank-Starling mechanism, thus maintaining stroke volume [72]. Combined, this allows fetal cardiac output to be maintained during acute hypoxaemia, despite a pronounced fall in heart rate. The increase in fetal perfusion pressure [31] during acute hypoxaemia has important functional implications for oxygen delivery to the fetal tissues. Since oxygen delivery is a product of blood oxygen content and blood flow [73], the increases in adrenal, myocardial, and cerebral blood flow during acute hypoxaemia will offset the reductions in fetal arterial blood oxygen content. This will maintain oxygen delivery to these essential circulations, usually without a need for increased oxygen extraction from the blood [69]. In addition, the increases in fetal adrenal cortical and medullary blood flows during acute isocapnic hypoxaemia may play an important role, not only in maintaining oxygen delivery to the gland, but also in facilitating release of catecholamines and glucocorticoids into the fetal circulation [74]. In more hypoxia-tolerant organs such as the liver, kidneys, gastrointestinal tract, and carcass, blood flow is either unaltered or reduced during acute hypoxaemia, thereby decreasing oxygen delivery to these organs [30, 44]. Consequently, oxygen extraction from the fetal blood increases in these peripheral circulations, thereby allowing oxygen consumption to be maintained [73, 75]. However, when oxygen delivery falls beyond the point of maximal oxygen extraction, fetal oxygen consumption will decline. This principle has been demonstrated in the fetal intestines [75] and hind limbs [73], where abrupt falls in oxygen consumption occur when oxygen delivery falls below critical threshold values, and anaerobic metabolism and lactate production ensue [73]. Hence, it has been shown in the sheep fetus that, as a result of compensatory increases in overall oxygen extraction, blood oxygen content can be reduced by up to 50% before global fetal oxygen consumption declines [76].

Therefore, the fetal bradycardia and the redistribution of blood flow during acute hypoxaemia exemplify some of the strategies of the fetal cardiovascular system to withstand episodes of oxygen deprivation by decreasing oxygen consumption and making best use of the available oxygen supply.

8.7 Physiology Underlying the Fetal Cardiovascular Responses to Acute Hypoxaemia

Study of the mechanisms mediating the fetal cardiovascular responses to acute hypoxaemia has been a vibrant field of investigation over the last 30 years. Pathways are now very well-delineated and include neural, endocrine, and local components (Fig. 8.1).

8.7.1 Afferent Neural Pathways

Fetal bradycardia and the fetal peripheral vasoconstriction are now known to be triggered exclusively by a carotid chemoreflex [31, 44]. The carotid chemoreceptors are located bilaterally at the bifurcation of the common carotid and occipital arteries [77]. Afferent nerve fibers from the carotid body run in the carotid sinus nerve before joining the glossopharyngeal (IX) nerve and passing to the nucleus tractus solitarius (NTS) in the medulla [78]. The importance of the carotid sinus nerves in initiating the fetal cardiovascular defence responses to acute hypoxaemia was demonstrated by Giussani and colleagues [31] who found in late gestation fetal sheep that bilateral section of the carotid sinus nerves abolished the fetal bradycardia and the initial elevation in femoral vascular resistance during acute hypoxaemia (Fig. 8.1). There is some evidence for the presence of central chemoreceptors in the fetus [79]. Although little is known about their location and physiology, Edelman and colleagues [80] have

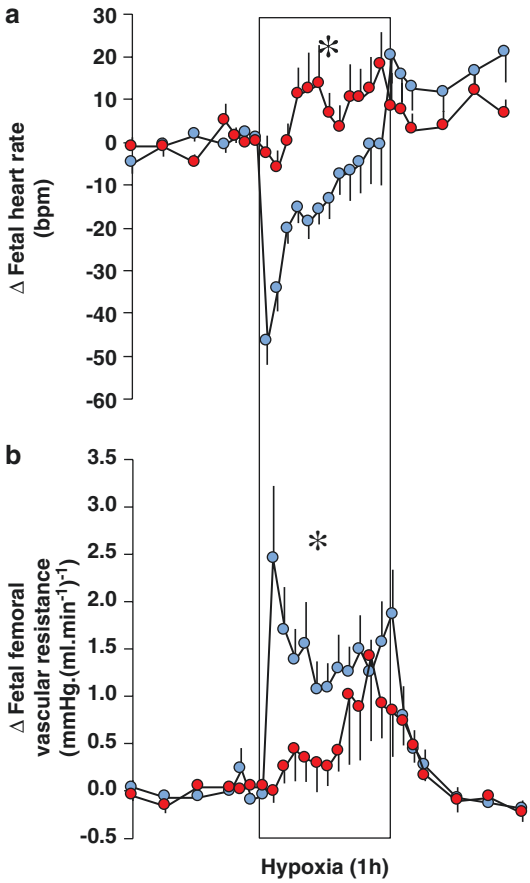

Fig. 8.1 *Effect of carotid body denervation on fetal cardiovascular responses to acute hypoxaemia.* The data show the mean ± SEM for the change in fetal heart rate (**a**) and in fetal femoral vascular resistance (**b**) in intact (blue, $n = 14$) and carotid body denervated (red, $n = 12$) chronically instrumented sheep fetuses at 0.8 of gestation during a 1 h episode of acute hypoxaemia (PaO_2 reduced from ca. 23–12 mmHg, box). Fetal heart rate is triggered from the arterial blood pressure pulsatility. Femoral blood flow is measured via an implanted Transonic flow probe around one of the main femoral arteries. Femoral vascular resistance is calculated by extending Ohm's law to the circulation and by dividing fetal arterial blood pressure by fetal femoral blood flow. Bilateral section of the carotid sinus nerves prevents the fetal bradycardia and abolishes the initial increase in fetal femoral vascular resistance during acute hypoxaemia, showing that these responses are triggered by a carotid chemoreflex. *$P < 0.05$, intact vs. denervated. Redrawn from Giussani et al. 1993, with permission (Ref. [31])

suggested that central nervous system hypoxia can have an important modulatory influence on peripheral chemoreceptor input. Compared to the abundant knowledge of the physiology of oxygen sensing by the carotid body in the adult period [81], research on mechanisms mediating carotid body sensitivity in fetal life is almost absent. Koos [82] proposed that adenosine A_{2A} receptors mediate fetal chemoreflex responses, linked to activation of 5′nucleotidase. Work by independent investigators supports this idea, since treatment with the adenosine receptor antagonist 8-(p-sulfophenyl)-theophylline of the late gestation sheep fetus prevented fetal bradycardia and fetal femoral vasoconstriction during acute hypoxaemia, mimicking the effect of bilateral section of the carotid sinus nerves [83].

8.7.2 Efferent Neural Pathways

Once acute hypoxaemia triggers a carotid chemoreflex, the fetal brainstem activates the autonomic nervous system. During late gestation, acute hypoxaemia will increase both vagal and sympathetic outflow to the pacemaker cells of the fetal heart. However, there is vagal dominance leading to a fall in fetal heart rate [31, 44]. Accordingly, the initial fetal bradycardia is not only abolished by carotid sinus nerve section [31, 44], but also by vagotomy [16] or muscarinic acetylcholine receptor blockade using atropine [30, 31, 44]. In fact, treatment with atropine switches the fetal heart rate response to tachycardia rather than bradycardia, unveiling the unopposed increased sympathetic drive to the fetal heart during acute hypoxaemia [31]. Carotid chemoreflexes are also important in activating sympathetic pathways innervating the peripheral circulation in the fetus, contributing to an increase in peripheral vascular tone [31, 44]. This includes femoral vasoconstriction, which is mediated by α-adrenergic efferent fibers [31, 44, 84]. The importance of the sympathetic nervous system in mediating fetal peripheral vasoconstrictor responses to acute hypoxaemia was demonstrated by Iwamoto and colleagues [85] and by Giussani and colleagues [31] who reported that the hypertensive and peripheral vasopressor responses to acute hypoxaemia could be blocked with the sympathetic neurotoxin, 6-hydroxydopamine, or with the α-adrenergic antagonist, phentolamine.

8.7.3 Endocrine Mechanisms

Once triggered by a carotid chemoreflex, the fetal heart and vascular responses are modified during hypoxaemia by the release of chemicals into the fetal circulation. These include catecholamines, neuropeptide Y, arginine vasopressin, and angiotensin II. During the last third of gestation, concentrations of adrenaline and noradrenaline have been shown to increase in ovine fetal plasma in response to acute hypoxaemia [86], which are strongly correlated with the degree of the challenge [87]. Under basal conditions in the fetus, all the circulating concentrations of adrenaline originate from the adrenal gland, while the majority of plasma noradrenaline has been attributed to transmitter overspill from sympathetic nerve terminals of extra chromaffin tissue [88]. In contrast, the fetal adrenal has been shown to be the major source of origin of the increase in both adrenaline and noradrenaline in fetal plasma during acute hypoxaemia since adrenal demedullation completely abolished the rise in plasma adrenaline concentration and reduced the noradrenaline response to 10% of normal [89]. This rise may be stimulated both by the direct effects of hypoxia on the gland and by neuronal activation of the sympathetic splanchnic nerves [89], with the relative contribution of the splanchnic nerves increasing with advancing gestation [90]. Increased plasma concentrations of catecholamines during acute hypoxaemia in the fetal circulation is responsible for restoring the fetal heart rate back to baseline, opposing the increased vagal tone [30, 31]. Therefore, fetal treatment with β_1-adrenergic receptor blockers during acute hypoxaemia prolongs the fetal bradycardia [91]. Increased plasma concentrations of catecholamines during acute hypoxaemia also helps maintain the fetal peripheral vasoconstriction triggered by α-adrenoreceptor stimulation since fetal treatment with the α-adrenoreceptor antagonists, such as phentolamine, abolished the response [31, 44, 84]. In addition, catecholamines may also act on β-adrenoreceptors to promote vasodilatation in the myocardial and umbilical circulations [30, 91].

The role of neuropeptide Y in the maintenance of the peripheral vasoconstrictor response to acute hypoxaemia in the ovine fetus has been highlighted by Fletcher and colleagues [92]. This peptide is co-localized and co-released with noradrenaline at sympathetic nerve terminals [93]. However, in contrast to noradrenaline, the hypoxaemia-induced increase in fetal plasma neuropeptide Y concentration is more likely to represent increased overspill from perivascular sympathetic nerve terminals. Despite the relatively high adrenal medullary neuropeptide Y content, evidence suggests a negligible role for the gland in contributing to circulating plasma neuropeptide Y levels during acute stress [94]. Since neuropeptide Y lacks synaptic reuptake mechanisms, elevations in plasma neuropeptide Y concentrations may provide a more robust measure than noradrenaline of increased sympathetic nervous activity [95]. A few studies have implicated calcitonin gene-related peptide (cGRP) in the activation of the sympathetic neuroendocrine responses during acute hypoxaemia in the late gestation ovine fetus. Thakor et al. [96] reported that treatment of fetal sheep with cGRP antagonists markedly diminished neural and endocrine responses triggered by sympathetic outflow, namely the fetal peripheral vasoconstrictor and the plasma neuropeptide Y and catecholamine responses to acute hypoxaemia.

In the sheep fetus, plasma concentrations of arginine vasopressin (AVP) have been shown to increase during periods of acute hypoxaemia, independent of aortic or carotid chemoreceptor stimulation [97]. Infusions of AVP in the sheep fetus, to produce circulating levels similar to those measured during acute hypoxaemia, elicit vasoconstriction in the gastrointestinal tract and fetal carcass and increase blood flow to the cerebral, myocardial, adrenal, and umbilico-placental vasculature. Indeed, the functional role of AVP in the redistribution of the fetal cardiac output during acute hypoxaemia can be further demonstrated following V_1-receptor antagonism, which reverses the rise in fetal arterial blood pressure and attenuates both the vasoconstriction in the gastrointestinal, hepatic, and placental vascular

beds and the vasodilatation in cerebral and myocardial vascular beds [98].

Although plasma concentrations of both renin and angiotensin II have also been shown to increase in response to acute hypoxaemia in the late gestation sheep fetus [99, 100], administration of the angiotensin-converting enzyme inhibitor, captopril, had no effect on the femoral vasoconstrictor response to acute hypoxaemia [101]. However, captopril was shown to attenuate the fetal femoral vasoconstriction to acute hypoxaemia in carotid sinus nerve sectioned fetuses [101], thereby suggesting a compensatory role for angiotensin II in fetuses lacking carotid chemoreflexes.

8.7.4 Local Mechanisms

In addition to endocrine mechanisms, agents released locally from tissues also play an important role in the modulation of the fetal cardiovascular defence responses to acute hypoxaemia. For instance, the fetal cerebrovascular bed dilates during acute hypoxaemia as a result of local increases in adenosine, nitric oxide (NO), and prostanoids [102–104]. There is also evidence that NO concentrations can increase during acute hypoxaemia in the late gestation fetus and that this increased nitrergic tone opposes fetal chemoreflex and neuroendocrine constrictor influences in the fetal peripheral circulation. Therefore, fetal treatment with the NO clamp, a technique that permits blockade of de novo synthesis of NO during acute hypoxaemia without affecting fetal basal cardiovascular function [67, 105–107], revealed a significantly greater peripheral vasoconstrictor response to acute hypoxia in the late gestation fetus [108]. Accumulating evidence in the last few years has now revealed that increases in NO during acute hypoxaemia in the fetus are themselves limited by the increased rate of generation of reactive oxygen species during acute hypoxaemia. Reactive oxygen species, like the superoxide anion, react with NO to produce peroxynitrite, and in so doing, the reaction decreases NO bioavailability in the late gestation sheep fetus during acute hypoxaemia. Strong evidence to support this comes from sheep studies in which fetal treatment with antioxidants, such as with vitamin C, allopurinol, or melatonin, all markedly blunt the fetal peripheral vasoconstrictor response to acute hypoxaemia [109–111]. Further, treatment of the sheep fetus with antioxidants during NO blockade with the NO clamp abolishes the depressive effect of these agents on the fetal peripheral vascular response to acute hypoxaemia [109–111]. Therefore, these data show that antioxidant treatment in the fetus quenches free radicals, like the superoxide anion, enhancing NO bioavailability, which acts to oppose chemoreflex and endocrine vasoconstrictor pathways. A similar depressive effect on fetal peripheral vasoconstrictor responses to acute hypoxaemia occurs following fetal treatment with statins [112]. Statins increase NO bioavailability via separate pathways [112] and their depressive actions on the fetal peripheral constrictor response to hypoxaemia can also be blocked with the NO clamp [112]. The interaction between NO with the superoxide anion during acute hypoxaemia therefore creates an oxidant tone that supplements chemoreflex and endocrine mechanisms, contributing to the overall constrictor response in the peripheral circulations during acute hypoxaemia (Fig. 8.2).

8.8 Maturation of the Fetal Cardiovascular Responses to Acute Hypoxaemia

Toward term, the exponential increase in fetal plasma cortisol is responsible for maturing a number of fetal organs and systems in preparation for the successful transition to life after birth [14, 113]. By far, the most studied system affected by fetal plasma cortisol has been the fetal pulmonary system, with investigations revealing that the prepartum increase in fetal glucocorticoid levels matures surfactant production [14, 113]. This effect of endogenous fetal cortisol on the fetal lung has been exploited clinically by antenatal glucocorticoid therapy of pregnancies threatened with preterm birth to accelerate fetal lung maturation [14, 114]. Maternal treatment with

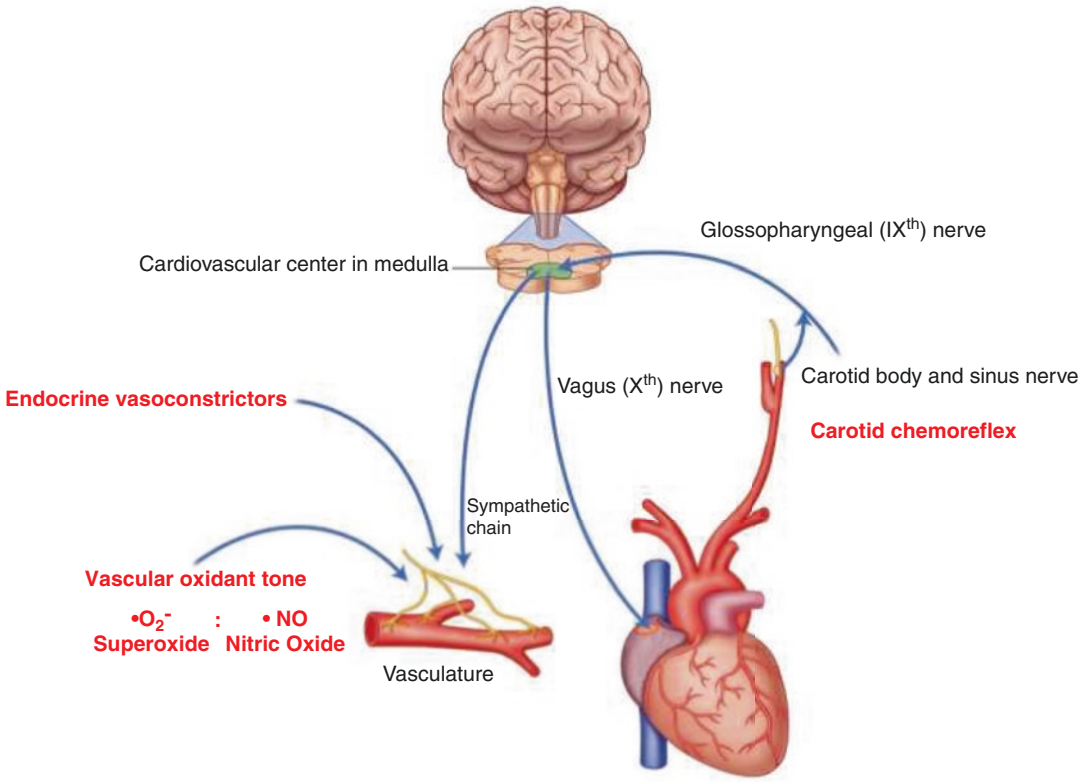

Fig. 8.2 *Physiology of fetal brain sparing during hypoxia.* The fetal brain sparing response to acute hypoxia is triggered by a carotid chemoreflex which leads to bradycardia and an increase in peripheral vasoconstriction. The bradycardia is mediated by a dominant vagal influence on the fetal heart. The neurally triggered peripheral vasoconstriction is maintained by the release of constrictor hormones into the fetal circulation as well as a local vascular oxidant tone, determined by the interaction between nitric oxide (•NO) and ROS, such as the superoxide anion ($•O_2^-$). Redrawn from Giussani et al. 2016, with permission (Ref. [44])

synthetic glucocorticoids, such as with beta- and dexa-methasone, thereby mimics the maturational effects on the fetal lung of the endogenous increase in fetal plasma cortisol, markedly improving survival of the preterm infant [113, 115]. More recently, it has now become appreciated that the prepartum surge in fetal cortisol also plays a role in maturing basal and stimulated fetal cardiovascular function [14].

Evidence supports that the ontogenic increase in fetal arterial blood pressure and the fall in fetal heart rate with advancing gestation are both dependent on the endogenous increase in fetal plasma cortisol toward term, as both can be abolished by fetal bilateral adrenalectomy and restored in adrenalectomized fetuses by cortisol replacement [22, 113]. Similarly, fetal treatment with exogenous glucocorticoids can promote a rightward shift in the fetal cardiac baroreflex setpoint, mimicking the actions of advancing gestational age to allow a greater resting arterial blood pressure [116]. Additional studies have also reported that the pattern and magnitude of the fetal cardiovascular responses to acute stress can change as the fetus approaches term and in close temporal association with the prepartum surge in fetal plasma cortisol concentrations. Prior to the exponential increase in fetal plasma cortisol toward term, in fetal sheep less than 120 days of gestation, the fetal bradycardic response to acute hypoxaemia is transient and the magnitude of the fetal femoral vasoconstrictor response is modest. In contrast, following the onset of the exponential increase in fetal plasma cortisol, the pattern of

the fetal bradycardia progressively switches from being transient to sustained, and the magnitude of the fetal peripheral vasoconstrictor response to acute hypoxaemia becomes markedly enhanced [117]. These altered cardiovascular responses to acute hypoxaemia by advancing gestational age reflect a more mature cardiovascular defence phenotype. For instance, the sustained fetal bradycardic response to acute hypoxaemia may better limit oxygen consumption by the fetal heart during episodes of oxygen deprivation [14, 117]. Similarly, the more intense peripheral vasoconstriction during acute hypoxaemia may represent a more efficient redistribution of the fetal cardiac output away from peripheral circulations, improving the fetal brain sparing effect [14, 117]. Advancing gestational age and the endogenous increase in fetal plasma cortisol toward term mature carotid chemoreflex responses and they increase the magnitude of the fetal plasma vasoconstrictor hormone responses to acute hypoxaemia [14, 117]. Advancing gestational age also causes reciprocal changes in the responsiveness of the fetal heart to autonomic agonists; while there is a fall in β_1 adrenergic receptor sensitivity, there is an increase in muscarinic receptor responsiveness of the fetal heart with advancing gestation [14, 118]. Combined, these altered mechanisms by advancing gestational age may explain the switch in the pattern and magnitude of the fetal cardiovascular response to acute hypoxaemia from the immature to the mature phenotype [14, 117, 118].

In similar fashion to the effects of antenatal glucocorticoid therapy accelerating fetal lung maturation, studies have also now reported that synthetic glucocorticoids can also accelerate the maturation of fetal basal and stimulated cardiovascular function. Treatment of immature fetal sheep with dexa- or beta-methasone in human clinically relevant doses increases fetal arterial blood pressure and femoral vascular resistance and the reactivity of the peripheral vasculature to constrictor agonists [116, 119–121]. Similarly, treatment of immature fetal sheep with dexamethasone in human clinically relevant doses also accelerates the switch in the pattern and magnitude of the fetal cardiovascular defence to hypoxia from the immature to the mature fetal phenotype ([14]; Fig. 8.3). Because of this body of work, obstetric practice worldwide should now appreciate that antenatal glucocorticoid therapy is not only beneficial to the fetal lungs, but that it also accelerates the maturation of fetal cardiovascular function.

8.9 Modulation of Fetal Cardiovascular Function by Adverse Intrauterine Conditions

It is generally accepted that growth-restricted infants from complicated pregnancies are at greater risk of cardiovascular compromise, fetal demise, or fetal brain injury during intrapartum asphyxia. However, surprisingly, there is little evidence in the literature to support or refute this belief [122, 123]. Since one of the most common outcomes of complicated pregnancy is chronic fetal hypoxia, the implication is that exposure of the fetus to chronic hypoxia earlier in gestation may somehow weaken the fetal brain sparing response, rendering the fetal brain susceptible to ischaemic damage. However, progress in this field to address these particular questions has been slow due to the technical difficulties in creating appropriate experimental designs in which adverse intrauterine conditions can be induced in a controlled manner, ideally while also being able to record from the fetal cardiovascular system at the same time. A few available studies support that pregnancy complicated by chronic fetal hypoxia weakens the fetal cardiovascular defence responses to subsequent acute hypoxia, as may occur in intrapartum [105, 124]. Recently, we have created isobaric hypoxic chambers able to maintain pregnant sheep for long period of gestation under highly controlled chronic hypoxic conditions [40–42]. This system has now been combined with the design of a wireless data acquisition system able to record maternal and fetal cardiovascular data longitudinally beat-to-beat in free-moving ewes as the hypoxic pregnancy is actually occurring. Using this system for the first time, we have shown that chronic hypoxic

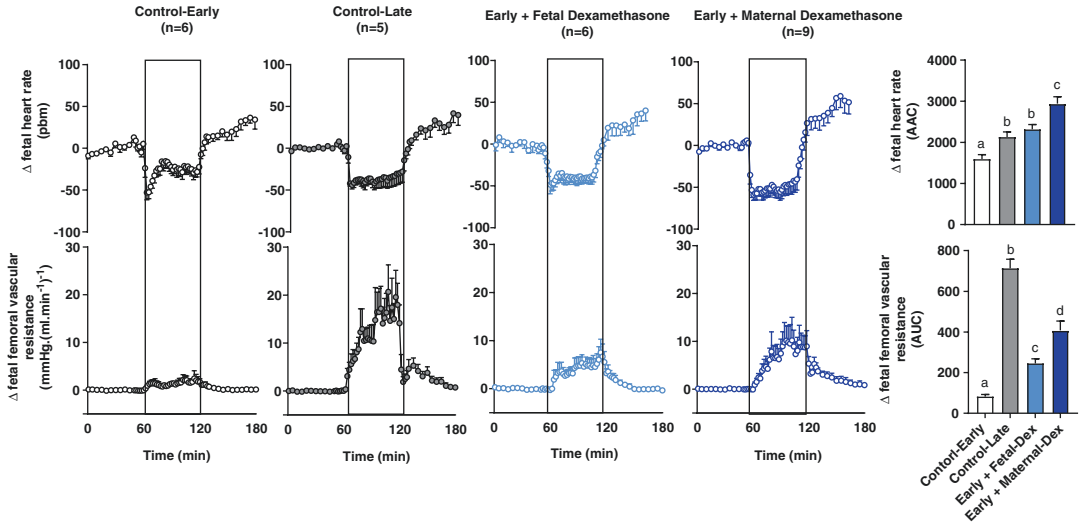

Fig. 8.3 *Effect of advancing gestation or synthetic glucocorticoids on the fetal cardiovascular defence to acute hypoxia.* Advancing gestation toward term matures the fetal cardiovascular defence responses to acute hypoxia. Preterm fetal sheep at 0.8 of gestation, prior to the fetal plasma cortisol surge (Control-Early), have a transient bradycardia and a modest increase in femoral vascular resistance in response to acute hypoxia. In fetal sheep at term, 2–3 days before labor, when the prepartum fetal plasma cortisol surge has occurred (Control-Late), the bradycardia switches from transient to sustained, and the femoral vasoconstrictor response to acute hypoxia becomes markedly enhanced. Exposure of preterm fetal sheep (0.8 of gestation) to human clinically relevant doses of dexamethasone administered either by fetal intravenous infusion (Early+Fetal Dexamethasone) or by maternal intramuscular injection (Early+Maternal Dexamethasone) has a maturational effect on the fetal heart and circulatory defence responses to acute hypoxia. Maternal compared with fetal treatment with dexamethasone has a greater maturational effect on the fetal cardiovascular defence to acute hypoxia. Sustained rather than transient bradycardia during acute hypoxia better limits myocardial oxygen consumption. A greater increase in femoral vascular resistance during acute hypoxia reflects greater peripheral vasoconstriction and thereby more efficient redistribution of blood flow to maintain oxygen delivery toward the developing central nervous system. Combined, therefore, the pattern and magnitude of the mature cardiac and vasomotor responses in the preterm fetus treated with dexamethasone enhance mechanisms that limit oxygen consumption and improve oxygen delivery to maximize fetal brain sparing and protection during episodes of acute oxygen deprivation. Values are mean ± S.E.M. for each minute during the experimental protocol for the change from baseline in fetal heart rate (ΔFHR) or in femoral vascular resistance (ΔFVR). The boxed area represents the period of fetal hypoxia. The histogram represents the area above the curve (AAC) and the area below the curve (AUC) for the fetal heart and femoral vascular responses to acute hypoxia, respectively. Different letters are significantly different ($P < 0.05$) by One way ANOVA+ Tukey test. Data derived from references 117, 119, 120. Redrawn from Jellyman et al. 2020, with permission (Ref. [14])

pregnancy markedly alters the ontogenic development of fetal cardiovascular function toward term [41, 42]. Chronically hypoxic fetuses showed an impaired ontogenic increase in arterial blood pressure and a delayed ontogenic fall in fetal heart rate with advancing gestation [41]. Further, we show that fetal heart rate variability in sheep is reduced by chronic hypoxia, predominantly due to dysregulation of the sympathetic control of the fetal heart rate [42]. This presents a potential mechanism by which a reduction in indices of fetal heart rate variability predicts fetuses at increased risk of neonatal morbidity and mortality in humans. Reduction in overall fetal heart rate variability may therefore provide a biomarker that autonomic dysregulation of fetal heart rate control has taken place in a fetus where uteroplacental dysfunction is suspected [42]. Whether exposure to chronic hypoxia using this model in sheep affects the fetal cardiovascular defence response to acute stress, such as acute hypoxia, acute asphyxia, or acute hypotension, awaits investigation. The most recent data now show that exposure of sheep to chronic hypoxia

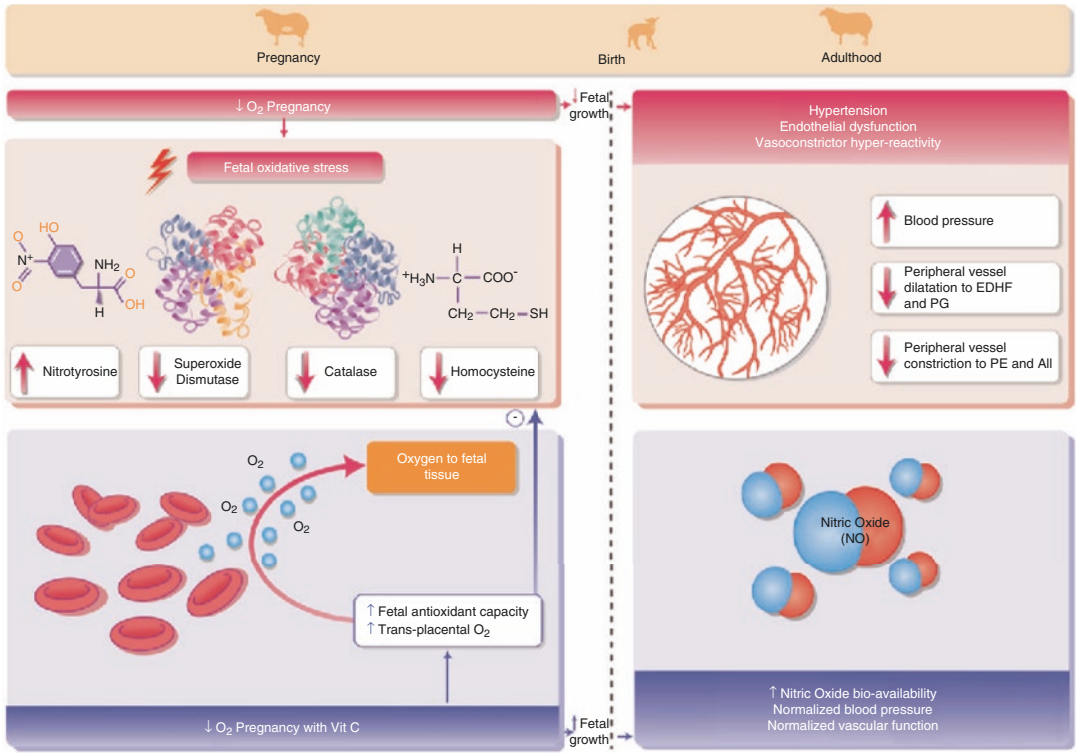

Fig. 8.4 *Programmed cardiovascular risk in adult offspring by hypoxic pregnancy.* Hypoxic pregnancy in sheep increases fetal oxidative stress, reduces fetal growth, and programs NO-independent endothelial dysfunction in the peripheral vasculature, femoral vasoconstrictor hyper-reactivity, and hypertension in the adult offspring. Maternal treatment with vitamin C in hypoxic pregnancy increases trans-placental oxygenation and fetal antioxidant capacity. This protects fetal growth and restores NO bioavailability, normalizing peripheral vascular function and arterial blood pressure in the adult offspring. Redrawn from Brain et al. 2018, with permission (Ref. [125])

for the last third of gestation can in fact program an increased risk of cardiovascular disease in the adult offspring via alterations in oxidative stress and in NO biology (Fig. 8.4; [125]). This highlights that pregnancy affected by chronic hypoxia, such as in placental insufficiency, preeclampsia, gestational diabetes, or maternal obesity (see [44]), not only poses a threat to the well-being of the infant during or immediately after birth, but can also have longer-term implications for the overall cardiovascular health of the adult offspring. Future research efforts will therefore focus on isolating mechanisms underlying the adverse effects of hypoxic pregnancy on fetal cardiovascular physiology in order to identify plausible candidates for intervention, to improve the cardiovascular health of the offspring not only in the perinatal period, but also in the longer term.

Acknowledgments Professor Dino Giussani's current programs of research are funded by the British Heart Foundation and the Medical Research Council, UK.

References

1. Intaglietta M, Johnson PC, Winslow RM. Microvascular and tissue oxygen distribution. Cardiovasc Res. 1996;32:632–43.
2. Pries AR, Secomb TW, Gaehtgens P. Biophysical aspects of blood flow in the microvasculature. Cardiovasc Res. 1996;32:654–67.
3. Rudolph AM. Distribution and regulation of blood flow in the fetal and neonatal lamb. Circ Res. 1985;57:811–21.
4. Petschow R, Petschow D, Bartels R, Baumann R, Bartels H. Regulation of oxygen affinity in blood of fetal, newborn and adult mouse. Respir Physiol. 1978;35:271–82.
5. Bard H, Shapiro M. Perinatal changes of 2,3-diphosphoglycerate and oxygen affinity in mam-

mals not having fetal type hemoglobins. Pediatr Res. 1979;13:167–9.
6. Bard H, Teasdale F. Red cell oxygen affinity, hemoglobin type, 2,3-diphosphoglycerate, and pH as a function of fetal development. Pediatrics. 1979;64:483–7.
7. Robinson R, Iida H, O'Brien TP, Pane MA, Traystman RJ, Gleason CA. Comparison of cerebrovascular effects of intravenous cocaine injection in fetal, newborn, and adult sheep. Am J Physiol Heart Circ Physiol. 2000;279:H1–6.
8. Merlet-Benichou C. Oxygen transport by the fetal blood. Poumon Coeur. 1975;31:197–203.
9. Oski FA. Clinical implications of the oxyhemoglobin dissociation curve in the neonatal period. Crit Care Med. 1979;7:412–8.
10. Coceani F, Olley PM. The control of cardiovascular shunts in the fetal and perinatal period. Can J Physiol Pharmacol. 1988;66:1129–34.
11. Kiserud T. Fetal circulation--from passive knowledge to current hemodynamics. Tidsskr Nor Laegeforen. 2001;121:313–7.
12. Itskovitz J, LaGamma EF, Rudolph AM. The effect of reducing umbilical blood flow on fetal oxygenation. Am J Obstet Gynecol. 1983b;145:813–8.
13. Asakura H, Ball KT, Power GG. Interdependence of arterial PO2 and O2 consumption in the fetal sheep. J Dev Physiol. 1990;13:205–13.
14. Jellyman JK, Fletcher AJW, Fowden AL, Giussani DA. Glucocorticoid maturation of fetal cardiovascular function. Trends Mol Med. 2020;26(2):170–84.
15. Rudolph AM, Heymann MA. Circulatory changes during growth in the fetal lamb. Circ Res. 1970;26:289–99.
16. Boddy K, et al. Foetal respiratory movements, electrocortical and cardiovascular responses to hypoxaemia and hypercapnia in sheep. J Physiol. 1974;243(3):599–618.
17. Dawes GS, Johnston BM, Walker DW. Relationship of arterial pressure and heart rate in fetal, new-born and adult sheep. J Physiol. 1980;309:405–17.
18. Giussani DA, Forhead AJ, Fowden AL. Development of cardiovascular function in the horse fetus. J Physiol. 2005;565(Pt 3):1019–30.
19. Kitanaka T, et al. Fetal responses to long-term hypoxemia in sheep. Am J Phys. 1989;256(6 Pt 2):R1348–54.
20. Macdonald AA, Colenbrander B, Wensing CJ. The effects of gestational age and chronic fetal decapitation on arterial blood pressure in the pig fetus. Eur J Obstet Gynecol Reprod Biol. 1983;16(1):63–70.
21. Segar JL. Ontogeny of the arterial and cardiopulmonary baroreflex during fetal and postnatal life. Am J Phys. 1997;273(2 Pt 2):R457–71.
22. Unno N, et al. Blood pressure and heart rate in the ovine fetus: ontogenic changes and effects of fetal adrenalectomy. Am J Phys. 1999;276(1):H248–56.
23. Forhead AJ, et al. Developmental changes in blood pressure and the renin-angiotensin system in pony fetuses during the second half of gestation. J Reprod Fertil Suppl. 2000;56:693–703.
24. Tangalakis K, Lumbers ER, Moritz KM, Towstoless MK, Wintour EM. Effect of cortisol on blood pressure and vascular reactivity in the ovine fetus. Exp Physiol. 1992;77:709–17.
25. Docherty CC, Kalmar-Nagy J, Engelen M, Nathanielsz PW. Development of fetal vascular responses to endothelin-1 and acetylcholine in the sheep. Am J Physiol Regul Integr Comp Physiol. 2001;280:R554–62.
26. Anwar MA, Ju K, Docherty CC, Poston L, Nathanielsz PW. Developmental changes in reactivity of small femoral arteries in the fetal and postnatal baboon. Am J Obstet Gynecol. 2001a;184:707–12.
27. Blanco CE, Dawes GS, Hanson MA, McCooke HB. Carotid baroreceptors in fetal and newborn sheep. Pediatr Res. 1988;24:342–6.
28. Rose JC, Meis PJ, Morris M. Ontogeny of endocrine (ACTH, vasopressin, cortisol) responses to hypotension in lamb fetuses. Am J Phys. 1981;240:E656–61.
29. Toubas PL, Silverman NH, Heymann MA, Rudolph AM. Cardiovascular effects of acute hemorrhage in fetal lambs. Am J Phys. 1981;240:H45–8.
30. Cohn HE, Sacks EJ, Heymann MA, Rudolph AM. Cardiovascular responses to hypoxemia and acidemia in fetal lambs. Am J Obstet Gynecol. 1974;120:817–24.
31. Giussani DA, Spencer JA, Moore PJ, Bennet L, Hanson MA. Afferent and efferent components of the cardiovascular reflex responses to acute hypoxia in term fetal sheep. J Physiol. 1993;461:431–49.
32. Faucher DJ, Lowe TW, Magness RR, Laptook AR, Porter JC, Rosenfeld CR. Vasopressin and catecholamine secretion during metabolic acidemia in the ovine fetus. Pediatr Res. 1987;21:38–43.
33. Fumia FD, Edelstone DI, Holzman IR. Blood flow and oxygen delivery to fetal organs as functions of fetal hematocrit. Am J Obstet Gynecol. 1984;150:274–82.
34. Yaffe H, Parer JT, Block BS, Llanos AJ. Cardiorespiratory responses to graded reductions of uterine blood flow in the sheep fetus. J Dev Physiol. 1987;9:325–36.
35. Giussani DA, Unno N, Jenkins SL, Wentworth RA, Derks JB, Collins JH, Nathanielsz PW. Dynamics of cardiovascular responses to repeated partial umbilical cord compression in late-gestation sheep fetus. Am J Phys. 1997;273:H2351–60.
36. Wood CE, Keil LC, Rudolph AM. Hormonal and hemodynamic responses to vena caval obstruction in fetal sheep. Am J Phys. 1982;243:E278–86.
37. Hawkins P, Steyn C, McGarrigle HH, Calder NA, Saito T, Stratford LL, Noakes DE, Hanson MA. Cardiovascular and hypothalamic-pituitary-

adrenal axis development in late gestation fetal sheep and young lambs following modest maternal nutrient restriction in early gestation. Reprod Fertil Dev. 2000;12:443–56.
38. Owens JA, Falconer J, Robinson JS. Effect of restriction of placental growth on oxygen delivery to and consumption by the pregnant uterus and fetus. J Dev Physiol. 1987;9:137–50.
39. Jacobs R, Robinson JS, Owens JA, Falconer J, Webster ME. The effect of prolonged hypobaric hypoxia on growth of fetal sheep. J Dev Physiol. 1988;10:97–112.
40. Brain KL, Allison BJ, Niu Y, Cross CM, Itani N, Kane AD, Herrera EA, Giussani DA. Induction of controlled hypoxic pregnancy in large mammalian species. Physiol Rep. 2015;3(12):pii: e12614. https://doi.org/10.14814/phy2.12614.
41. Allison BJ, Brain KL, Niu Y, Kane AD, Herrera EA, Thakor AS, Botting KJ, Cross CM, Itani N, Skeffington KL, Beck C, Giussani DA. Fetal in vivo continuous cardiovascular function during chronic hypoxia. J Physiol. 2016;594(5):1247–64. https://doi.org/10.1113/JP271091.
42. Shaw CJ, Allison BJ, Itani N, Botting KJ, Niu Y, Lees CC, Giussani DA. Altered autonomic control of heart rate variability in the chronically hypoxic fetus. J Physiol. 2018;596(23):6105–19. https://doi.org/10.1113/JP275659. Epub 2018 Apr 29
43. Llanos AJ, Riquelme RA, Sanhueza EM, Hanson MA, Blanco CE, Parer JT, Herrera EA, Pulgar VM, Reyes RV, Cabello G, Giussani DA. The fetal llama versus the fetal sheep: different strategies to withstand hypoxia. High Alt Med Biol. 2003;4:193–202.
44. Giussani DA. The fetal brain sparing response to hypoxia: physiological mechanisms. J Physiol. 2016;594(5):1215–30. https://doi.org/10.1113/JP271099. Epub 2016 Jan 6. Review
45. Parer JT, Livingston EG. What is fetal distress? Am J Obstet Gynecol. 1990;162:1421–5.
46. Macfarlane CM, Tsakalakos N. Evidence of hyperinsulinaemia and hypoxaemia in the cord blood of neonates born to mothers with gestational diabetes. S Afr Med J. 1985;67:81–4.
47. Galanti B, Kaihura CT, Ricci L, Bedocchi L, Rossi T, Benassi G, Benassi L. Perinatal morbidity and mortality in children born to mothers with gestational hypertension. Acta Biomed Ateneo Parmense. 2000;71(Suppl 1):361–5.
48. Thilaganathan B, Salvesen DR, Abbas A, Ireland RM, Nicolaides KH. Fetal plasma erythropoietin concentration in red blood cell-isoimmunized pregnancies. Am J Obstet Gynecol. 1992;167:1292–7.
49. Kendall G, Peebles D. Acute fetal hypoxia: the modulating effect of infection. Early Hum Dev. 2005;81:27–34.
50. Manzar S. Maternal sickle cell trait and fetal hypoxia. Am J Perinatol. 2000;17:367–70.
51. Mukherjee AB, Hodgen GD. Maternal ethanol exposure induces transient impairment of umbilical circulation and fetal hypoxia in monkeys. Science. 1982;218:700–2.
52. Witlin AG. Asthma in pregnancy. Semin Perinatol. 1997;21:284–97.
53. Tomson T, Danielsson BR, Winbladh B. Epilepsy and pregnancy. Balancing between risks to the mother and child. Lakartidningen. 1997;94:2827–32, 2835.
54. Fernandez-Twinn DS, Gascoin G, Musial B, Carr S, Duque-Guimaraes D, Blackmore HL, Alfaradhi MZ, Loche E, Sferruzzi-Perri AN, Fowden AL, Ozanne SE. Exercise rescues obese mothers' insulin sensitivity, placental hypoxia and male offspring insulin sensitivity. Sci Rep. 2017;14(7):44,650. https://doi.org/10.1038/srep44650.
55. Longo LD. Carbon monoxide: effects on oxygenation of the fetus in utero. Science. 1976;194(4264):523–5.
56. Socol ML, Manning FA, Murata Y, Druzin ML. Maternal smoking causes fetal hypoxia: experimental evidence. Am J Obstet Gynecol. 1982;142:214–8.
57. Maier RF, Bialobrzeski B, Gross A, Vogel M, Dudenhausen JW, Obladen M. Acute and chronic fetal hypoxia in monochorionic and dichorionic twins. Obstet Gynecol. 1995;86:973–7.
58. Salafia CM, Minior VK, Lopez-Zeno JA, Whittington SS, Pezzullo JC, Vintzileos AM. Relationship between placental histologic features and umbilical cord blood gases in preterm gestations. Am J Obstet Gynecol. 1995;173:1058–64.
59. Stubblefield PG, Berek JS. Perinatal mortality in term and post-term births. Obstet Gynecol. 1980;56:676–82.
60. Leszczynska-Gorzelak B, Poniedzialek-Czajkowska E, Oleszczuk J. Fetal blood saturation during the 1st and 2nd stage of labor and its relation to the neonatal outcome. Gynecol Obstet Investig. 2002a;54:159–63.
61. Kovalovszki L, Villanyi E, Benko G. Placental villous edema: a possible cause of antenatal hypoxia. Acta Paediatr Hung. 1990;30:209–15.
62. Faiz SA, Habib FA, Sporrong BG, Khalil NA. Results of delivery in umbilical cord prolapse. Saudi Med J. 2003;24:754–7.
63. Mukhopadhyay S, Arulkumaran S. Breech delivery. Best Pract Res Clin Obstet Gynaecol. 2002;16:31–42.
64. Preston R, Crosby ET, Kotarba D, Dudas H, Elliott RD. Maternal positioning affects fetal heart rate changes after epidural analgesia for labour. Can J Anaesth. 1993;40:1136–41.
65. Kuipers IM, Maertzdorf WJ, Keunen H, De Jong DS, Hanson MA, Blanco CE. Effect of maternal hypoxemia on behavior in unanesthetized normoxic

or mildly hyperoxic fetal lambs. J Appl Physiol (1985). 1994;76(6):2535–40.
66. Iwamoto HS, Kaufman T, Keil LC, Rudolph AM. Responses to acute hypoxemia in fetal sheep at 0.6-0.7 gestation. Am J Phys. 1989;256:H613–20.
67. Gardner DS, Powlson AS, Giussani DA. An in vivo nitric oxide clamp to investigate the influence of nitric oxide on continuous umbilical blood flow during acute hypoxaemia in the sheep fetus. J Physiol. 2001;537(Pt 2):587–96.
68. Itskovitz J, Goetzman BW, Rudolph AM. The mechanism of late deceleration of the heart rate and its relationship to oxygenation in normoxemic and chronically hypoxemic fetal lambs. Am J Obstet Gynecol. 1982;142:66–73.
69. Peeters LL, Sheldon RE, Jones MD Jr, Makowski EL, Meschia G. Blood flow to fetal organs as a function of arterial oxygen content. Am J Obstet Gynecol. 1979;135:637–46.
70. Fisher DJ, Heymann MA, Rudolph AM. Fetal myocardial oxygen and carbohydrate consumption during acutely induced hypoxemia. Am J Phys. 1982;242:H657–61.
71. Thornburg KL, Reller MD. Coronary flow regulation in the fetal sheep. Am J Phys. 1999;277:R1249–60. 351.
72. Anderson PA, Glick KL, Killam AP, Mainwaring RD. The effect of heart rate on in utero left ventricular output in the fetal sheep. J Physiol. 1986;372:557–73.
73. Boyle DW, Hirst K, Zerbe GO, Meschia G, Wilkening RB. Fetal hind limb oxygen consumption and blood flow during acute graded hypoxia. Pediatr Res. 1990;28:94–100.
74. Cohen WR, Piasecki GJ, Cohn HE, Young JB, Jackson BT. Adrenal secretion of catecholamines during hypoxemia in fetal lambs. Endocrinology. 1984;114:383–90.
75. Edelstone DI, Holzman IR. Fetal intestinal oxygen consumption at various levels of oxygenation. Am J Phys. 1982;242:H50–4.
76. Wilkening RB, Meschia G. Fetal oxygen uptake, oxygenation, and acid-base balance as a function of uterine blood flow. Am J Phys. 1983;244:H749–55.
77. Blanco CE, Dawes GS, Hanson MA, McCooke HB. The response to hypoxia of arterial chemoreceptors in fetal sheep and new-born lambs. J Physiol. 1984;351:25–37.
78. Dampney RA. Functional organization of central pathways regulating the cardiovascular system. Physiol Rev. 1994;74(323–364):13452.
79. Hohimer AR, Bissonnette JM, Richardson BS, Machida CM. Central chemical regulation of breathing movements in fetal lambs. Respir Physiol. 1983;52:99–111.
80. Edelman NH, Melton JE, Neubauer JA. The modulation of peripheral chemoreceptor input by central nervous system hypoxia. Adv Exp Med Biol. 1993;337:345–52.
81. López-Barneo J, López-López JR, Ureña J, González C. Chemotransduction in the carotid body: K+ current modulated by PO2 in type I chemoreceptor cells. Science. 1988;241(4865):580–2.
82. Koos BJ. Adenosine A2a receptors and O2 sensing in development. Am J Physiol Regul Integr Comp Physiol. 2011;301(3):R601–22.
83. Giussani DA, Gardner DS, Cox DT, Fletcher AJ. Purinergic contribution to circulatory, metabolic, and adrenergic responses to acute hypoxemia in fetal sheep. Am J Physiol Regul Integr Comp Physiol. 2001;280(3):R678–85.
84. Reuss ML, Parer JT, Harris JL, Krueger TR. Hemodynamic effects of alpha-adrenergic blockade during hypoxia in fetal sheep. Am J Obstet Gynecol 142, 410-415. Physiol. 1982;1:283–93.
85. Iwamoto HS, Rudolph AM, Mirkin BL, Keil LC. Circulatory and humoral responses of sympathectomized fetal sheep to hypoxemia. Am J Phys. 1983;245:H767–72.
86. Jones CT, Robinson RO. Plasma catecholamines in foetal and adult sheep. J Physiol. 1975;248:15–33.
87. Cohen WR, Piasecki GJ, Jackson BT. Plasma catecholamines during hypoxemia in fetal lamb. Am J Phys. 1982;243:R520–5.
88. Jones CT, Roebuck MM, Walker DW, Lagercrantz H, Johnston BM. Cardiovascular, metabolic and endocrine effects of chemical sympathectomy and of adrenal demedullation in fetal sheep. J Dev Physiol. 1987;9:347–67.
89. Jones CT, Roebuck MM, Walker DW, Johnston BM. The role of the adrenal medulla and peripheral sympathetic nerves in the physiological responses of the fetal sheep to hypoxia. J Dev Physiol. 1988;10:17–36.
90. Cheung CY. Fetal adrenal medulla catecholamine response to hypoxia-direct and neural components. Am J Phys. 1990;258:R1340–6.
91. Court DJ, Parer JT, Block BS, Llanos AJ. Effects of beta-adrenergic blockade on blood flow distribution during hypoxaemia in fetal sheep. J Dev Physiol. 1984;6:349–58.
92. Fletcher AJ, Edwards CM, Gardner DS, Fowden AL, Giussani DA. Neuropeptide Y in the sheep fetus: effects of acute hypoxemia and dexamethasone during late gestation. Endocrinology. 2000;141:3976–82.
93. Ekblad E, Edvinsson L, Wahlestedt C, Uddman R, Hakanson R, Sundler F. Neuropeptide Y co-exists and co-operates with noradrenaline in perivascular nerve fibers. Regul Pept. 1984;8:225–35.
94. Mormede P, Castagne V, Rivet JM, Gaillard R, Corder R. Involvement of neuropeptide Y in neuroendocrine stress responses. Central and peripheral studies. J Neural Transm Suppl. 1990;29:65–75.
95. Lundberg JM, Fried G, Pernow J, Theodorsson-Norheim E. Co-release of neuropeptide Y and cat-

echolamines upon adrenal activation in the cat. Acta Physiol Scand. 1986;126:231–8.
96. Thakor AS, Bloomfield MR, Patterson M, Giussani DA. Calcitonin gene related peptide antagonism attenuates the haemodynamic and glycaemic responses to acute hypoxaemia in the late gestation sheep fetus. J Physiol. 2005;566(2):587–97.
97. Giussani DA, McGarrigle HH, Spencer JA, Moore PJ, Bennet L, Hanson MA. Effect of carotid denervation on plasma vasopressin levels during acute hypoxia in the late-gestation sheep fetus. J Physiol. 1994;477(Pt 1):81–7.
98. Perez R, Espinoza M, Riquelme R, Parer JT, Llanos AJ. Arginine vasopressin mediates cardiovascular responses to hypoxemia in fetal sheep. Am J Phys. 1989;256:R1011–8.
99. Broughton PF, Lumbers ER, Mott JC. Factors influencing plasma renin and angiotensin II in the conscious pregnant ewe and its foetus. J Physiol. 1974;243:619–36.
100. Robillard JE, Weitzman RE, Burmeister L, Smith FG Jr. Developmental aspects of the renal response to hypoxemia in the lamb fetus. Circ Res. 1981;48:128–38.
101. Green LR, McGarrigle HH, Bennet L, Hanson MA. Angiotensin II and cardiovascular chemoreflex responses to acute hypoxia in late gestation fetal sheep. J Physiol. 1998a;507(Pt 3):857–67.
102. Kjellmer I, Andiné P, Hagberg H, Thiringer K. Extracellular increase of hypoxanthine and xanthine in the cortex and basal ganglia of fetal lambs during hypoxia-ischemia. Brain Res. 1989;478(2):241–7.
103. van Bel F, Sola A, Roman C, Rudolph AM. Role of nitric oxide in the regulation of the cerebral circulation in the lamb fetus during normoxemia and hypoxemia. Biol Neonate. 1995;68:200–10.
104. Pearce WJ. Mechanisms of hypoxic cerebral vasodilatation. Pharmacol Ther. 1995;65(1):75–91.
105. Gardner DS, Fowden AL, Giussani DA. Adverse intrauterine conditions diminish the fetal defense against acute hypoxia by increasing nitric oxide activity. Circulation. 2002b;106:2278–83.
106. Gardner DS, Giussani DA. Enhanced umbilical blood flow during acute hypoxemia after chronic umbilical cord compression: a role for nitric oxide. Circulation. 2003;108:331–5.
107. Thakor AS, Giussani DA. The role of nitric oxide in mediating in vivo vascular responses to calcitonin gene related peptide in essential and peripheral circulations in the fetus. Circulation. 2005;112(16):2510–6.
108. Morrison S, Gardner DS, Fletcher AJ, Bloomfield MR, Giussani DA. Enhanced nitric oxide activity offsets peripheral vasoconstriction during acute hypoxaemia via chemoreflex and adrenomedullary actions in the sheep fetus. J Physiol. 2003;547:283–91.
109. Thakor AS, Richter HG, Kane AD, Dunster C, Kelly FJ, Poston L, Giussani DA. Redox modulation of the fetal cardiovascular defence to hypoxaemia. J Physiol. 2010b;588(Pt 21):4235–47.
110. Thakor AS, Allison BJ, Niu Y, Botting KJ, Serón-Ferré M, Herrera EA, Giussani DA. Melatonin modulates the fetal cardiovascular defense response to acute hypoxia. J Pineal Res. 2015; https://doi.org/10.1111/jpi.12242. [Epub ahead of print].
111. Kane AD, Hansell JA, Herrera EA, Allison BJ, Niu Y, Brain KL, Kaandorp JJ, Derks JB, Giussani DA. Xanthine oxidase and the fetal cardiovascular defence to hypoxia in late gestation ovine pregnancy. J Physiol. 2014;592(Pt 3):475–89.
112. Kane AD, Herrera EA, Hansell JA, Giussani DA. Statin treatment depresses the fetal defence to acute hypoxia via increasing nitric oxide bioavailability. J Physiol. 2012;590(Pt 2):323–34.
113. Fowden AL, Li J, Forhead AJ. Glucocorticoids and the preparation for life after birth: are there long-term consequences of the life insurance? Proc Nutr Soc. 1998;57(1):113–22.
114. Ballard PL, Ballard RA. Scientific basis and therapeutic regimens for use of antenatal glucocorticoids. Am J Obstet Gynecol. 1995;173(1):254–62.
115. Liggins GC, Howie RN. A controlled trial of antepartum glucocorticoid treatment for prevention of the respiratory distress syndrome in premature infants. Pediatrics. 1972;50(4):515–25.
116. Fletcher AJ, et al. Effects of low dose dexamethasone treatment on basal cardiovascular and endocrine function in fetal sheep during late gestation. J Physiol. 2002;545(2):649–60.
117. Fletcher AJ, et al. Development of the ovine fetal cardiovascular defense to hypoxemia towards full term. Am J Physiol Heart Circ Physiol. 2006;291(6):H3023–34.
118. Fletcher AJ, et al. Effects of gestational age and cortisol treatment on ovine fetal heart function in a novel biventricular Langendorff preparation. J Physiol. 2005;562(Pt 2):493–505.
119. Fletcher AJ, et al. Cardiovascular and endocrine responses to acute hypoxaemia during and following dexamethasone infusion in the ovine fetus. J Physiol. 2003;549(Pt 1):271–87.
120. Jellyman JK, et al. Fetal cardiovascular, metabolic and endocrine responses to acute hypoxaemia during and following maternal treatment with dexamethasone in sheep. J Physiol. 2005;567(Pt 2):673–88.
121. Jellyman JK, et al. Antenatal glucocorticoid therapy increases glucose delivery to cerebral circulations during acute hypoxemia in fetal sheep during late gestation. Am J Obstet Gynecol. 2009;201(1):82.e1–8.
122. Block BS, Schlafer DH, Wentworth RA, Kreitzer LA, Nathanielsz PW. Intrauterine asphyxia and the breakdown of physiologic circulatory com-

pensation in fetal sheep. Am J Obstet Gynecol. 1990;162(5):1325–31.
123. Prior T, Mullins E, Bennett P, Kumar S. Prediction of fetal compromise in labor. Obstet Gynecol Clin N Am. 2014;123:1263–71.
124. Herrera EA, Rojas RT, Krause BJ, Ebensperger G, Reyes RV, Giussani DA, Parer JT, Llanos AJ. Cardiovascular function in term fetal sheep conceived, gestated and studied in the hypobaric hypoxia of the Andean altiplano. J Physiol. 2016;594(5):1231–45. https://doi.org/10.1113/JP271110. Epub 2015 Oct 1.
125. Brain KL, Allison BJ, Niu Y, Cross CM, Itani N, Kane AD, Herrera EA, Skeffington KL, Botting KJ, Giussani DA. Intervention against hypertension in the next generation programmed by developmental hypoxia. PLoS Biol. 2019;17(1):e2006552. https://doi.org/10.1371/journal.pbio.2006552. eCollection 2019 Jan.

9 Maternal Cardiovascular Physiology and Assessment

Marc E. A. Spaanderman

9.1 Introduction

Pregnancy is accompanied by substantial compensatory changes in central hemodynamic and vascular function triggered by a profound drop in total peripheral vascular resistance compared to the nonpregnant situation. On the one hand, in healthy individuals, the gestational decrease in vascular resistance provides a sustained signal to make long-term compensatory adjustments to maintain healthy blood pressure, perfusion, and vascular strain also at substantial increased basal demands as in the third gestational trimester. As such, it may be viewed upon as an aerobic training protocol in preparation of an endurance performance. On the other hand, this circulatory stress may be such that it induces adjustments that only compensate the short-term imminent decrease in blood pressure, without making proper cardiovascular modifications that will also preserve perfusion and vascular stress at low blood pressure. Obviously, this maladaptive response will translate to larger fluctuations in blood pressure, perfusion, and endothelial shear stress, ultimately preluding hypertensive complications of pregnancy and compromised placental perfusion and with it fetal growth. To make a comparison, in analogy to endurance exercise, these adjustments seem to be more in line with power resistance response.

M. E. A. Spaanderman (✉)
Maastricht University Medical Center,
Maastricht, The Netherlands
e-mail: marc.spaanderman@mumc.nl

9.2 Blood Pressure Regulation

Blood pressure is kept within narrow boundaries by beat-to-beat monitoring of arterial pressure. Spontaneous fluctuations in blood pressure are followed by direct baroreceptor-mediated adjustments in heart rate and with it stroke volume. In addition, rapid changes in autonomic system-regulated vascular compliance, both venous as cardiac and arterial, affect returning venous filling pressure, cardiac contractility, heart rate as well as arterial outflow total peripheral vascular resistance. When the blood pressure lowering signal sustains, humoral volume regulating responses (Renin-Angiotensin-Aldosterone System (RAAS)) will increase volume retention, but also Angiotensin-induced arterial tone. As healthy gestation is accompanied by reduced vascular responsiveness to Angiotensin II (AII), plasma volume expansion will predominantly represent the RAAS-induced effect. Moreover, the concomitant reduced blood viscosity will lower vascular shear and resistance, whereas the increased flow will induce increased endothelial-dependent production of NO, that, in turn, increases arterial vascular diameter, compliance, and with it reduction of resistance. If the gestational drop in total peripheral vascular resistance is antagonized by fortified sympathetic

D. Maulik, C. C. Lees (eds.), *Doppler Ultrasound in Obstetrics and Gynecology*,
https://doi.org/10.1007/978-3-031-06189-9_9

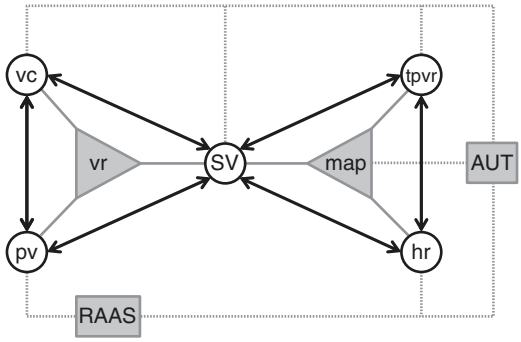

Fig. 9.1 Simplified diagram of the interrelation of the major players and its resultants venous return and mean arterial blood pressure in hemodynamic regulation of blood pressure by adjustments in venous, arterial, and its controlling central and humoral autonomous function throughout gestation
PV Plasma volume, *VC* Venous compliance, *SV* Stroke volume, *TPVR* Total peripheral vascular resistance, *HR* Heart rate, *VR* Venous return, *MAP* Mean arterial pressure, *RAAS* Renin Angiotensin Aldosterone System, and *AUT* Central autonomous regulatory system

responses, functionally, the increased arterial demand is likely to be counterbalanced by increased venous and arterial tone, blunting the subtle decrease in blood pressure seen in healthy pregnancy. As a result, cardiac strain increases by not only a rise in venous tone and return-induced atrial stretch, but also ventricular pressure load, and with it the healthy gestational plasma volume expansion. Therefore, generally, volume load, that is venous filling and compliance, and pressure load, total peripheral vascular resistance, and heart rate all affect stroke volume, the central player in adequate perfusion. Autonomic responses all regulate these major parameters (Fig. 9.1). In monitoring gestation, assuming healthy cardiac functioning, following cardiac output (CO = stroke volume x heart rate) and blood pressure throughout pregnancy most likely provides the essentials of circulatory guidance in detecting adaptive from maladaptive responses.

9.3 Clinical Consequences of Circulatory Maladaptation to Pregnancy

Hypertensive complications during pregnancy and fetal growth restriction are mostly preceded by deviant hemodynamic adaptation [1]. Women who ultimately develop gestational hypertension or late-onset preeclampsia usually have higher CO along with low total peripheral vascular resistance early in pregnancy, while in early-onset preeclampsia, low first trimester CO along with elevated peripheral vascular resistance is commonly seen [2–5]. Impaired fetal growth is often preceded by restricted rise in maternal CO paralleled by attenuated fall in total peripheral vascular resistance [6, 7]. Alterations in arterial circulatory characteristics can be caused by cardiac or arterial features, but may also originate from aberrant venous return primarily affecting stroke volume. During uncomplicated pregnancy, blood volume increases because of an increase in plasma volume and to a lesser extent a rise in red cell volume. In pregnancy complicated by hypertension, preeclampsia, or fetal growth restriction, the increase in circulatory volume is thought to be less, but much of these data come from cross-sectional studies. The lower plasma volume, seen in complicated pregnancy, may therefore originate from prepregnancy shallow volume, defective gestational rise, or loss of volume around the clinical phase of vascular complicated pregnancy.

From a clinical point of view, follow-up of cardiac output and blood pressure early in pregnancy may be helpful in timely identifying women at risk for later complications [8, 9]. It could improve our prevention and intervention opportunities to decrease the short- and long-term maternal and fetal morbidity and mortality that comes with maternal gestational hypertensive disorders and impaired fetal growth [10]. Moreover, categorizing maternal hemodynamic constituents determining cardiac output and total peripheral vascular resistance when gestational hypertensive complications are imminent or present may guide personalized counteractive measures to normalize stroke volume, heart rate, or vascular resistance [11, 12].

9.4 Magnitude of Healthy Circulatory Changes

One of the central hallmarks of healthy pregnancy is the drop in total peripheral vascular resistance. On the one hand, in order to maintain

basal cardiac output while preserving enough circulatory reserves to compensate for changes in arterial demand (as walking and running), venous compliance and plasma volume increase at such extent that resting volume load toward the heart increases. On the other hand, the imminent drop in blood pressure is counterbalanced by an increase in heart rate and stroke volume, preferably not at substantially increased autonomous sympathetic activity that may attenuate the decrease in vascular resistance and with it the volume retaining response necessary to build up sufficient circulatory responsive reserves. The magnitude of these changes as compared to the nonpregnant condition is likely to be of utmost importance for healthy pregnancy. But what is the magnitude of these changes?

In order to answer this question, we must rely on pooled serial collected data from different populations, which must include a nonpregnant reference (prepregnancy, post pregnancy, or separate nonpregnant control group). Moreover, as assessment method may affect the found value, preferably, serial assessments are done by employing one measurement technique, making the interpretation of relative changes reliable. As data are combined, the effect of the chosen control group, population, and assessment method should be weighted, since these findings may affect the clinical translation. If available, systematic appraisal of the current facts with meta-analysis and regression on studies with these characteristics may represent the best estimate of physiological gestational changes (Fig. 9.2).

First, the venous compartment. Although respiration depth and rate affect venous return, let's first focus on the most dominant drivers of venous return, plasma volume, and venous compliance. Under resting healthy conditions, two thirds of plasma volume are located in the venous circulation and are hemodynamically inactive, whereas the remainder located in the arterial compartment. The venous compartment serves as a readily available resource to supply blood if arterial needs demand so. The venous compartment is able to compensate for lessened total peripheral vascular resistance by increasing venous tone that increases cardiac preload at the expense of venous reserves by exchanging hemodynamically unstressed to actively participating stressed blood. Activation of the renin-angiotensin-aldosterone system (RAAS) eventually counterbalances the loss in venous reserve by a renin, angiotensin, and aldosterone-driven rise in plasma volume and thereby restoring the venous fullness. Plasma volume starts to rise in the very early phase of the first trimester and continues to increase progressively in the second trimester of pregnancy, thereafter flattening until it reaches its maximum late third-trimester value 45.6 (95%CI 43.0–48.1)% above nonpregnant corresponding +1.13 (95%CI 1.07–1.19)L. [13]

Much less attention has been given to venous vascular changes throughout gestation. Venous compliance is the amount of fluid that can be contained per mmHg intravascular rise in pressure. Both forearm and calf venous compliance are assessable by strain gauge plethysmography, but data on serial assessments throughout gestation are hardly available, not always comparable in measurement method and sometimes not unambiguously. But from the data available, we can construct the gestational adjustments in venous compliance changes throughout gestation. Serial measurements during the menstrual cycle and very early healthy pregnancy show that the very early profound sudden drop in total peripheral vascular resistance is initially, as compared to prepregnancy forearm venous compliance, at 5 weeks gestational age counterbalanced by unaltered venous compliance but increase in plasma volume, but shortly thereafter, at 7 weeks, followed by an increase in venous compliance [14]. Throughout gestation, as compared to postpartum function, calf and forearm venous compliance seems to be consistently increased (approximately 25%) [15–17].

Venous return itself is not easy to estimate. But, as under healthy conditions both venous compliance and volume together determine venous return and with it, ultimately, cardiac output, venous return equals cardiac output. In healthy nonpregnant females, at average, resting cardiac output and thus venous return is 4.97 L/min (95% CI 4.78–5.16)L/min. It progressively rises in pregnancy from the early first trimester onwards and levels out out at mid-gestation, about 25% above nonpregnant conditions, but

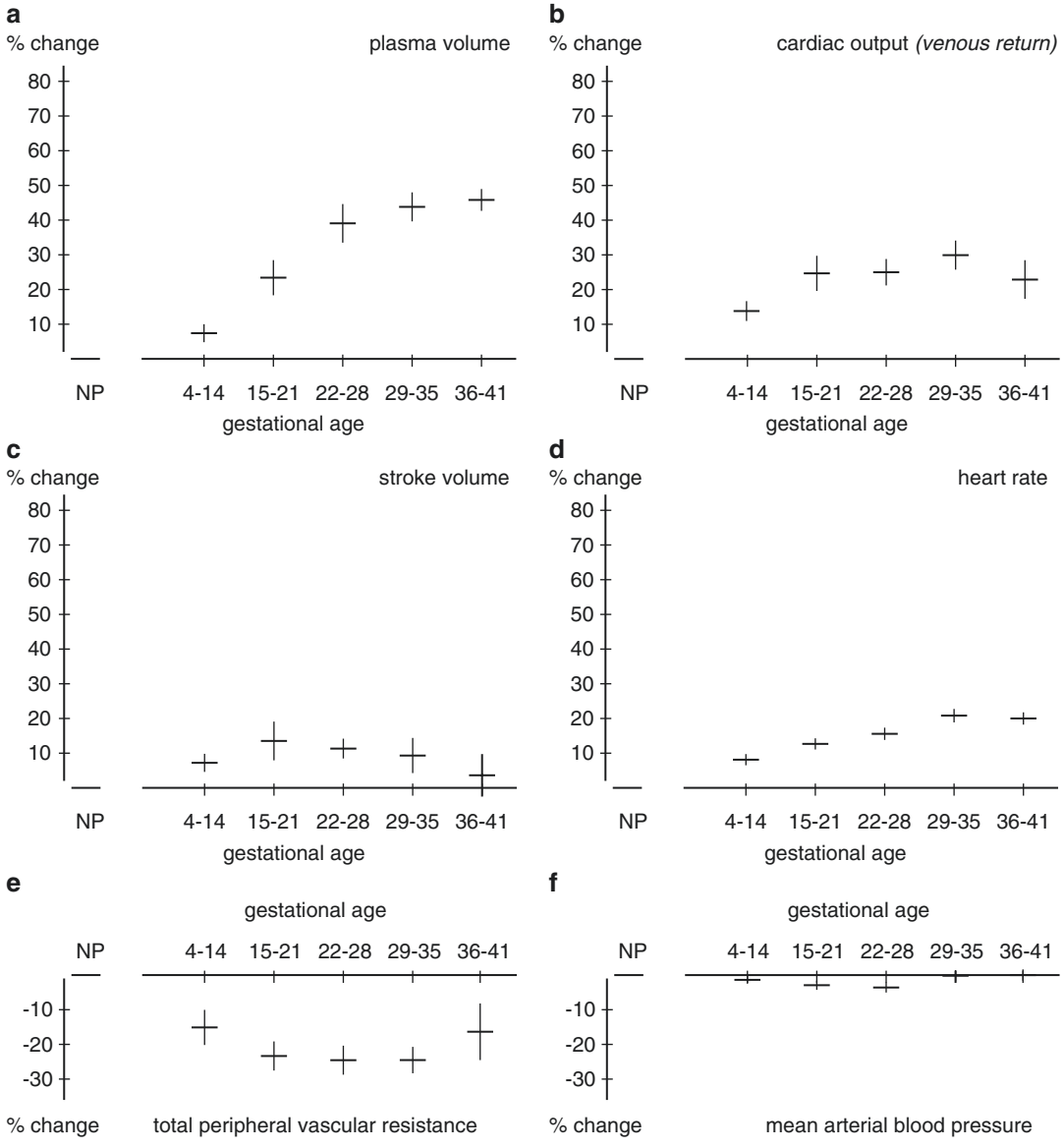

Fig. 9.2 Magnitude of pooled healthy hemodynamic changes (systematic review and meta-analysis) in (**a**) plasma volume, (**b**) cardiac output (*venous return*), (**c**) stroke volume, (**d**) heart rate, (**e**) total peripheral vascular resistance, and (**f**) mean arterial blood pressure throughout pregnancy as % change compared to nonpregnant. [13, 16]

reaches its maximum increase between 29 and 35 weeks gestational age of 1.47 L/min (95%CI 1.24–1.70 L/min), corresponding a 30.2% (95%CI 25.5–34.9%) rise above nonpregnant [18].

What gestational changes can be anticipated in the arterial compartment? In resting nonpregnant condition, total peripheral vascular resistance is at average 1315 (95%CI 1264–1366) Dyne s^{-1} cm^{-5}. It progressively decreases in pregnancy from the very early first trimester onwards and levels out out at mid-gestation, 20–25% below nonpregnant conditions, but reaches its lowest level between 29 and 35 weeks gestational age, 976 (95%CI 934–1019) Dyne s^{-1} cm^{-5}, corresponding −24.5 (95%CI −28.4 to −20.5)% decrease below nonpregnant [18]. Concomitantly, in young healthy women, average resting non-

pregnant heart rate is approximately 70 (95%CI 69–71) beats per minute. It increases in pregnancy from the first trimester onwards, reaching its maximum rate in the early third trimester, 85 (83–87) beats per minute, corresponding 15 (95%CI 14–16)% increase above nonpregnant [18]. In lying nonpregnant women, cardiac stroke volume is about 72 (95%CI 69–74)mL. It reaches its maximum increase before the second half of pregnancy 79 (95%CI 74–85)mL, corresponding 13 (95%CI 8–17)% after which it slowly decreases in the last part of the third trimester 74 (95%CI 70–79)mL [18].

Blood pressure is kept within narrow boundaries. All above-mentioned changes, increase in plasma volume, venous compliance increasing venous return, and decrease in total peripheral vascular resistance along with a rise in stroke volume and heart rate should result in an almost stable resting blood pressure throughout gestation. As compared to nonpregnant, mean arterial pressure lowers in the first trimester at average −3.0 (95%CI −4.1 to −2.0)mmHg and reaches its nadir at 22–28 weeks gestational age −4.6 (95%CI −5.4 to −3.7)mmHg, corresponding −5.6 (95%CI −6.7 to −4.5)% after which it slowly rises again toward nonpregnant values by the end of the third trimester −0.2 (95%CI −1.7 to 1.4)mmHg [19]. It is highly questionable if this marginal change in resting blood pressure is detectable in clinical care. Given the magnitude of changes in those variables affecting the resultant blood pressure, serial assessment of these parameters, especially those easily measurable, may be better in timely detecting imminent gestational hypertensive disease rather than blood pressure itself. In these, as compound variable, cardiac output may be most suitable. But the clinical value still has to be proven in large population studies.

9.5 Assessment of Cardiac Output

Many consider the pulmonary artery catheter method the golden standard for CO measurement. The invasiveness of the procedure and associated risks of injury and infection make longitudinal and outpatient use impossible [20]. Alternative techniques that allow serial assessments without the necessity of invasiveness are inert gas rebreathing (pulmonary flow), thoracal bio-impedance, continuous wave Doppler ultrasound, and transthoracic echocardiography (TTE) with Doppler ultrasound. The first three methods are easy to operate, but both inert gas rebreathing and bio-impedance method require disposables. The continuous wave Doppler ultrasound technique, a portable device, estimates stroke volume by multiplying the aortic valve area by the flow integral during systole at the ascending aorta just above the aortic valve. In contrast to the TTE, aortic valve area is modeled as function of height, and not measured. TTE requires training and expertise, results must be computed off-line, but the aortic valve is measured and possible stroke volume affecting valve conditions, such as bicuspid aortic valves, stenosis, or insufficiency affecting accuracy, can be detected. But at any rate, Doppler ultrasound techniques can be employed to noninvasively assess stroke volume and heart rate and with it cardiac output, but for serial assessment, one should use only one technique, as different measurement methods result in different outcomes [21–23].

9.6 Practical Assessment of Stroke Volume

From a theoretical point of view, stroke volume is calculated by subtracting end-systolic volume from end-diastolic volume. A more precise technique makes use of the assessment of the left ventricular outflow tract (LVOT) area and aortic valve velocity-time integral (AVA VTI). To determine the cross-sectional area ((CSA, cm^2), the diameter(d) of the LVOT is taken from the zoomed parasternal long axis view (PLAX) at mid systole, parallel to the aortic valve taken from the inner-to-inner lining. The CSA = $¼ \cdot \pi \cdot d^2$ The AVA VTI is determined by pulsed wave Doppler ultrasound from the apical 5 view, in which the sample volume, parallel to flow, is taken proximal to the aortic valve and the sample volume is adjusted until a laminar flow curve is obtained. From 3 to 5 consecutive beats, LVOT VTI is averaged. (Fig. 9.3).

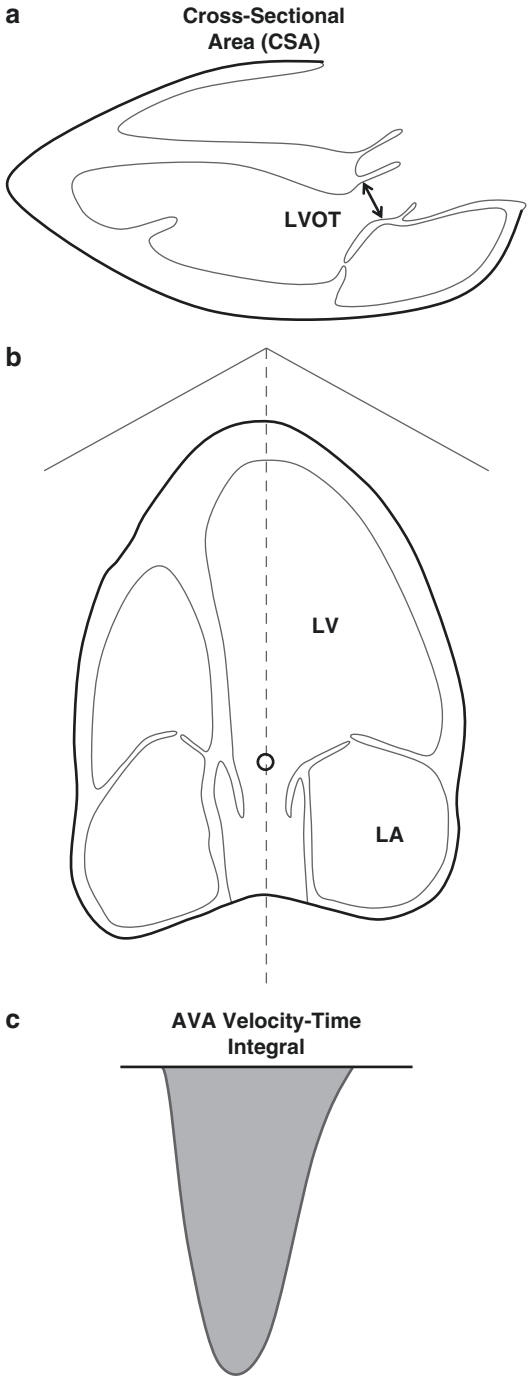

Fig. 9.3 Ultrasonographical assessment of stroke volume using the determination of the left ventricular outflow tract (LVOT) area (**a**) and aortic valve velocity-time integral (AVA VTI) (**b** and **c**)

9.7 Summary

In conclusion, during pregnancy, tremendous hemodynamic changes are seen in response to a drop in total peripheral vascular resistance, to balance an imminent loss of blood pressure. Compensatorily, plasma volume and venous compliance rise and increase the resulting venous return, whereas concomitantly stroke volume and heart rate increase, thereby stabilizing mean arterial blood pressure. Consequently, blood pressure hardly changes clinically significantly. Therefore, to detect upcoming hypertensive complications, serial assessment of stroke volume, heart rate, and cardiac output may be much better variables to assess for early detection of imminent problems rather than monitoring blood pressure itself. Stroke volume and heart rate can be easily measured by Doppler ultrasound techniques. Although theoretically powerful, the additive clinical value of this alternative approach still must be proven in large population studies.

References

1. Easterling TR, Benedetti TJ, Schmucker BC, et al. Maternal hemodynamics in normal and preeclamptic pregnancies: a longitudinal study. Obstet Gynecol. 1990;76:1061–9.
2. Bosio PM, McKenna PJ, Conroy R, et al. Maternal central hemodynamics in hypertensive disorders of pregnancy. Obstet Gynecol. 1999;94:978–84.
3. Valensise H, Vasapollo B, Gagliardi G, et al. Early and late preeclampsia: two different maternal hemodynamic states in the latent phase of the disease. Hypertension. 2008;52:873–80.
4. Giannubilo SR, Pasculli A, Tidu E, et al. Relationship between maternal hemodynamics and plasma natriuretic peptide concentrations during pregnancy complicated by preeclampsia and fetal growth restriction. J Perinatol: official journal of the California Perinatal Association. 2017;37:484–7.
5. Melchiorre K, Sutherland G, Sharma R, et al. Mid-gestational maternal cardiovascular profile in preterm and term pre-eclampsia: a prospective study. BJOG. 2013;120:496–504.
6. Khaw A, Kametas NA, Turan OM, et al. Maternal cardiac function and uterine artery Doppler at 11-14 weeks in the prediction of pre-eclampsia in nulliparous women. BJOG. 2008;115:369–76.

7. Tiralongo GM, Lo Presti D, Pisani I, et al. Assessment of total vascular resistance and total body water in normotensive women during the first trimester of pregnancy. A key for the prevention of preeclampsia. Pregnancy Hypertension. 2015;5:193–7.
8. Easterling TR, Brateng D, Schmucker B, et al. Prevention of preeclampsia: a randomized trial of atenolol in hyperdynamic patients before onset of hypertension. Obstet Gynecol. 1999;93:725–33.
9. Ferrazzi E, Stampalija T, Monasta L, et al. Maternal hemodynamics: a method to classify hypertensive disorders of pregnancy. Am J Obstet Gynecol. 2018;218:124 e121–11. https://doi.org/10.1016/j.ajog.2017.10.226.
10. Abalos E, Cuesta C, Grosso AL, et al. Global and regional estimates of preeclampsia and eclampsia: a systematic review. Eur J Obstet Gynecol Reprod Biol. 2013;170:1–7.
11. Valensise H, Vasapollo B, Novelli GP, et al. Maternal total vascular resistance and concentric geometry: a key to identify uncomplicated gestational hypertension. BJOG. 2006;113:1044–52.
12. Lees C, Ferrazzi E. Relevance of Haemodynamics in treating pre-eclampsia. Curr Hypertens Rep. 2017;19:76.
13. de Haas S, Ghossein-Doha C, van Kuijk SM, van Drongelen J, Spaanderman ME. Physiological adaptation of maternal plasma volume during pregnancy: a systematic review and meta-analysis. Ultrasound Obstet Gynecol. 2017;49(2):177–87.
14. Spaanderman ME, Willekes C, Hoeks APG, Ekhart THA, Peeters LLH. The effect of pregnancy on the compliance of large arteries and veins in normal parous controls and formerly preeclamptic women. Am J Obstet Gynecol. 2000;183:1278–86.
15. Parker R, Yoo J, Jarvis S, Okada Y, Best S, Stickford A, Levine B, Fu Q. Time course of changes in calf venous compliance during pregnancy and postpartum in humans. FASEB J. 2017;31(1_supplement):851.11.
16. Sakai K, Imaizumi T, Maeda H, Nagata H, Tsukimori K, Takeshita A, Nakano H. Venous distensibility during pregnancy. Comparisons between normal pregnancy and preeclampsia. Hypertension. 1994 Oct;24(4):461–6.
17. Martin A, Brown MA, Bucci J, Whitworth JA. Measuring venous capacitance and blood flow in pregnancy. Aust N Z J Obstet Gynaecol. 1997;37(3):335–9.
18. Mulder E, De Haas S, Ghossein-Doha C, Schartmann N, Mohseni Z, Abo Hasson F, Alsadah F, van Kuijk S, van Drongelen J, Spaanderman M. Cardiac output and peripheral vascular resistance during physiologic and non-physiologic pregnancy—a systematic review and meta-analysis. BJOG. 2022;129:696–707.
19. de Haas S, Mulder E, Schartmann N, Mohseni Z, Abo Hasson F, Alsadah F, van Kuijk S, van Drongelen J, Ghossein-Doha C, Spaanderman M. Blood pressure adjustments throughout healthy and hypertensive pregnancy: A systematic review and meta-analysis. Pregnancy Hypertens. 2022;27:51–8.
20. Cornette J, Laker S, Jeffery B, et al. Validation of maternal cardiac output assessed by transthoracic echocardiography against pulmonary artery catheterization in severely ill pregnant women: prospective comparative study and systematic review. Ultrasound Obstet Gynecol. 2017;49:25–31.
21. Nguyen HB, Banta DP, Stewart G, et al. Cardiac index measurements by transcutaneous Doppler ultrasound and transthoracic echocardiography in adult and pediatric emergency patients. J Clin Monit Comput. 2010;24:237–47.
22. Mulder E, Basit S, Oben J, van Kuijk S, Ghossein-Doha C, Spaanderman M. Accuracy and precision of USCOM versus transthoracic echocardiography before and during pregnancy. Pregnancy Hypertens. 2019;17:138–43.
23. Vinayagam D, Patey O, Thilaganathan B, Khalil A. Cardiac output assessment in pregnancy: comparison of two automated monitors with echocardiography. Ultrasound Obstet Gynecol. 2017;49(1):32–8.

Venous Doppler Sonography in Pregnancy

10

Wilfried Gyselaers

10.1 Aspects of Venous Physiology

In normal physiologic conditions, the venous compartment serves three important functions [1]. It is the single organ actively involved in drainage of blood from the microcirculation and venous return to the heart, as such preventing the organs from volume overload and congestion. It is also actively involved in control of cardiac output via modulation of venous return, and for this, it cooperates with the heart as one functional unit [2]. Finally, it serves as a reservoir for noncirculating blood, mainly located in liver and splanchnic system, that is not actively participating in interorgan gas and metabolite transport, but is constantly available for immediate redirection into the circulation when a sudden increase of cardiac output is needed [1, 2]. Compared to nonpregnant conditions, these functions are strongly upgraded during uncomplicated pregnancy, as this is a condition associated with increased blood volume and cardiac output, and nearly always with disseminated edema near term [3, 4]. The importance of the contributive role of venous physiology to gestational outcome is illustrated by the reported association between maternal cardiac output, maternal hepatic vein Doppler parameters, and neonatal birth weight percentile [5].

While arterial blood distribution is controlled via power regulating mechanisms, venous drainage mainly operates via volume shifts at low pressures and flow velocities. Although changes of venous pressure or flow velocity can be very small, the subsequent volume changes may be huge with important impact on cardiac and arterial function [4]. Next to this, the venous system efficiently uses the support by external physiologic properties, such as negative suction forces from cardiac diastole or inspiration, or compression by extravenous pressure from the abdominal or peripheral muscle pump [1, 4]. This mode of functional activity very much troubles simple and straight forward Doppler assessment of the venous vascular tree as compared to the arterial side. With systematic application of a standard protocol, as explained further in this chapter, venous Doppler sonography not only has been shown feasible, but is also proven to be useful for maternal hemodynamics assessment in normal and pathologic pregnancies [6].

10.2 The Venous Doppler Waveform Explained

The venous Doppler waveform is well-described at the level of the internal jugular vein [7, 8]. The typical waveform deflections relate to the cyclic

W. Gyselaers (✉)
Department of Obstetrics & Gynaecology, Ziekenhuis Oost-Limburg, Genk, Belgium

Department Physiology, Hasselt University, Diepenbeek, Belgium
e-mail: wilfried.gyselaers@zol.be

D. Maulik, C. C. Lees (eds.), *Doppler Ultrasound in Obstetrics and Gynecology*,
https://doi.org/10.1007/978-3-031-06189-9_10

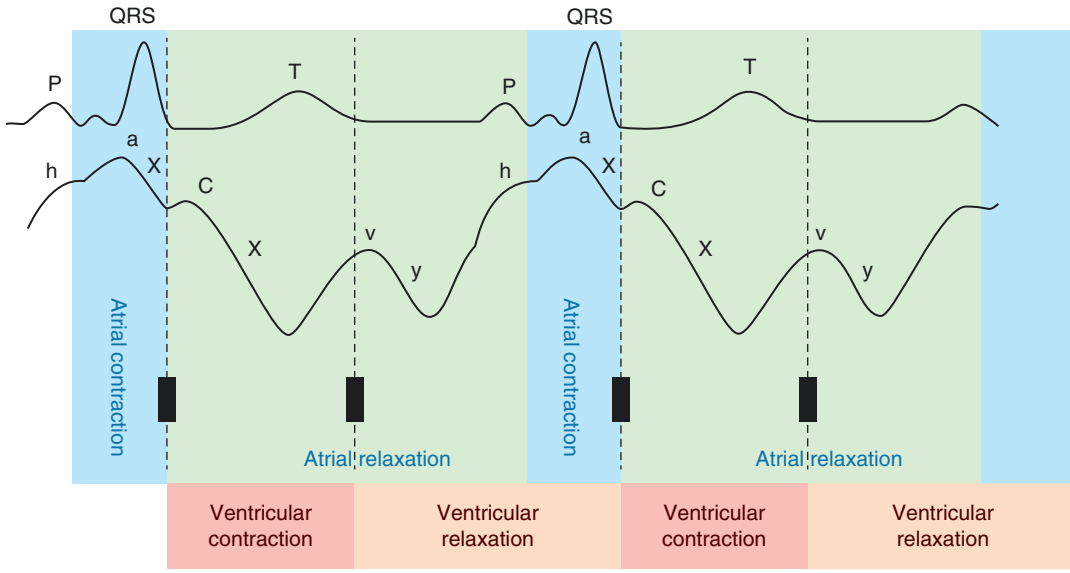

Fig. 10.1 Illustration of the simultaneous deflections of the electrocardiogram (upper) and venous flow velocities (lower), in relation to different stages of atrial and ventricular function during the cardiac cycle
ECG P Electrophysiologic induction of atrial contraction, *QRS* Electrophyciologic induction of ventricular contraction, *T* Electrophysiologic induction of ventricular relaxation
Venous Doppler X: fast forward venous flow velocity as a result of atrial relaxation; V: deceleration of forward venous flow velocity at atrial filling until the opening of the tricuspid valve; Y: fast forward venous flow velocity as a result of ventricular relaxation with open tricuspid valve; A: reversed blood flow, backwards into the venous circulation, as a result of atrial contraction in the absence of a valve system between atrium and vena cava; C: reverberation wave resulting from closure of the tricuspid valve; H: backward venous flow wave resulting from rebouncing of the blood at full passive filling of the cardiac chambers
Black boxes with dotted lines: closure and opening of the atrioventricular valves with associated cardiosonographic sounds

changes of right atrial pressure (Fig. 10.1) [7]. The A-wave represents transient venous deceleration or even reversal of forward flow, caused by retrograde pressure from the contraction of the right atrium by lack of a valve mechanism between the right atrium and the vena cava. The X-descent is a temporary acceleration of forward flow, which relates to the fast filling of the right atrium during atrial relaxation. The V-deflection is the deceleration of forward venous flow, at the moment of full passive filling of the right atrium when the tricuspid valve is still closed. Opening of the tricuspid valve in early ventricular diastole allows rapid emptying of the right atrium into the right ventricle and a strong suction force induces fast forward venous flow velocity, reflected in the Y-descent. Sometimes, a small upward deflection (C-wave) presents between A and X, resulting from closure of the tricuspid valve closure (Fig. 10.1). Another infrequent deflection is the H-wave, occuring milliseconds before the A-wave, representing retrograde rebound of venous blood from a passively filled atrium before atrial systole (Fig. 10.1).

The typical venous waveform changes under physiological conditions, such as respiration, position, the intravascular volume (i.e., the filling status), the venous distensibility (i.e., venous tone), the pressure in the surrounding tissues (the intra-abdominal pressure at the level of splanchnic organs or the muscle activity in the lower extremities), and pregnancy. The shape of the waveform also differs depending on the distance from the heart: central veins show a pattern similar to that of the internal jugular veins, whereas peripheral veins exhibit a flat pattern, representing more or less constant forward flow velocity. The different shapes of hepatic and renal interlobar venous wave forms are illustrated in Fig. 10.2. The gestation-induced changes in the venous

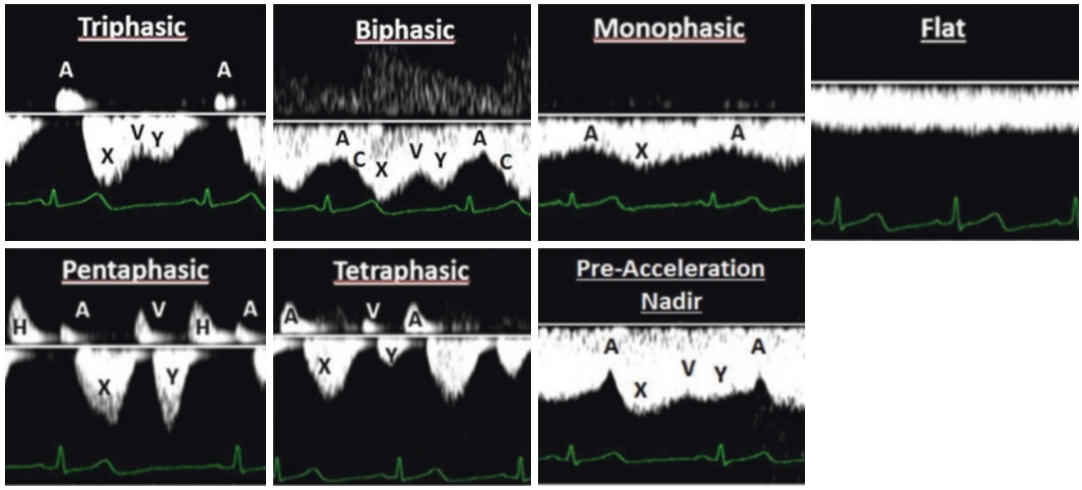

Fig. 10.2 Illustration of different venous Doppler wave forms in hepatic and renal interlobar veins in uncomplicated pregnancy (upper panels) and in specific physiologic or pathophysiologic conditions
In healthy, nonpregnant individuals, the venous Doppler waveform is triphasic at hepatic veins and biphasic at renal interlobar veins. During the course of pregnancy, hepatic venous waveforms change from triphasic to biphasic, monophasic, and flat whereas this shift is less dramatic at renal interlobar veins where biphasic patterns become monophasic. Pentaphasic and tetraphasic patterns can be seen in athletes with a muscular heart and slow heart rate, and a pre-acceleration nadir in the left kidney of persons with the so-called nutcracker phenomenon (compression of the left renal vein between aorta and upper mesenteric artery). During severe preeclampsia, hepatic veins may show penta- and tetraphasic patterns and a pre-acceleration nadir may be present in both kidneys. Deflections H, A, C, X, V, Y are explained in Fig. 10.1

Doppler waveform can be used to study venous hemodynamics in pregnant women [9–11].

Similar to the calculation of the arterial resistivity index RI, which is defined as (maximum velocity − minimum velocity)/maximum velocity, the maximum and minimum venous Doppler flow velocities can be used to calculate the venous impedance index VI [12]. VI is defined as (X − A)/X and offers some indirect information on the compliance of the vein with which there is an inverse relation [12, 13].

The venous Doppler A-wave, resulting from atrial contraction, is the hemodynamic equivalent of the ECG P-wave, the electrophysiological inductor of atrial contraction. The time-interval between the corresponding signals A and P can be measured (Fig. 10.3) and, when corrected for the duration of the cardiac cycle or heart rate (R-R interval), represents the venous pulse transit time ratio (VPTT) [14]. VPTT is considered an estimate of venous vascular wall tone with which there is an inverse relation.

10.3 Technique of Intrahepatic and Intrarenal Venous Doppler Sonography

Similar to obstetric scanning, pregnant women can be examined in supine position randomly throughout the day [11], irrespective of food intake [15] using a conventional obstetric 3.5–7 MHz probe. Functional aspects of venous hemodynamics can be assessed, as well as the impact of external venous compression by the growing uterus and increased intra-abdominal pressure [16, 17]. The safety of the non-semi-recumbent supine position has been questioned [18]; however, in our experience, despite demonstrable reduction of cardiac output in this position [19], risks for supine hypotension syndrome and/or fetal distress are very low.

Both kidneys and liver are scanned in the transverse plane at the craniocaudal midportion of the organs (Fig. 10.4). The impact of breathing movements on the ultrasound image is demonstrated to every patient and the relevance of hold-

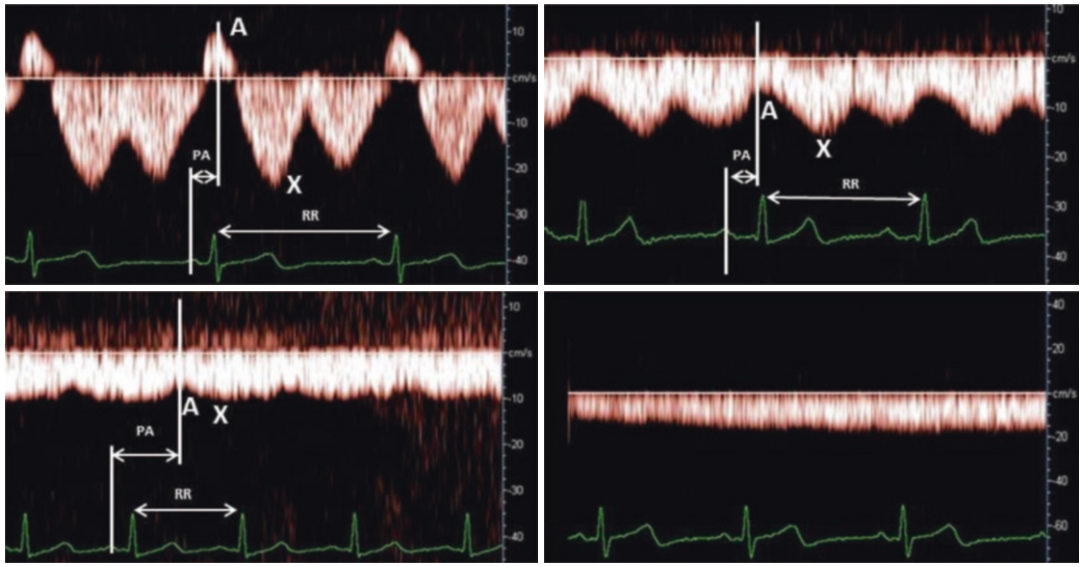

Fig. 10.3 Identification of the different venous Doppler wave landmarks for measurement of venous Doppler flow impedance index and pulse transit time ratio
Venous impedance index is defined as (X − A)/X and pulse transit time ratio as (PA/RR). As is illustrated, landmark identification is straightforward in triphasic, biphasic, and monophasic waveforms (upper left & right, lower left), but can be very difficult or even impossible in flat waves (lower right)

ing breath during Doppler measurements is explained and demonstrated. Once the patient is familiar with the instructions given by the sonographer, the examination starts according to a standardized protocol. (a) The direction of blood flow, as indicated by color Doppler, is used to discriminate the right, left, and middle branch of the hepatovenous tree from the portal branches and hepatic arteries and to distinguish renal interlobar veins from arteries. (b) The real-time ultrasound image in combined B-D mode is frozen after visualization of at least three similar venous Doppler flow patterns during interrupted breathing, and the middle waveform is selected for off-line analysis. (c) As the direction of the Doppler beam is mostly parallel and always within a maximum of ±30° of the examined vessel, Doppler angle correction is rarely needed. (d) For every woman, three consecutive images are taken at the midportion of each of three hepatic veins and for each kidney at random locations in the middle region between pyelon and cortex (Fig. 10.4). (e) Three images per organ are stored at the hard disc of the scanner for later off-line analysis. (f) After the scan, velocities of distinct hepatic vein deflections as well as renal interlobar vein maximum (MxV) and minimum velocity (MnV) are measured off-line and results printed. From these, hepatic and renal interlobar vein impedance index are calculated as explained above (Fig. 10.2). (g) Time intervals between the physiologically corresponding ECG P-wave and venous Doppler A-wave are measured and expressed as a fraction of the ECG R-R interval to correct for heart rate variation. (f) The mean of three measurements per organ is considered the organ-specific value, which is registered in the database.

10.4 Methodologic Improvement of Venous Doppler Flow Imaging

Compared to the arterial site, obtaining venous Doppler flow measurements is much more difficult, due to interindividual anatomic variations, large anastomic networks, and multiple interfering variables: intra- and interobserver correlations of single measurements of VI vary around 30–40% [20]. Averaging of three consecutive measurements per organ using maximum likeli-

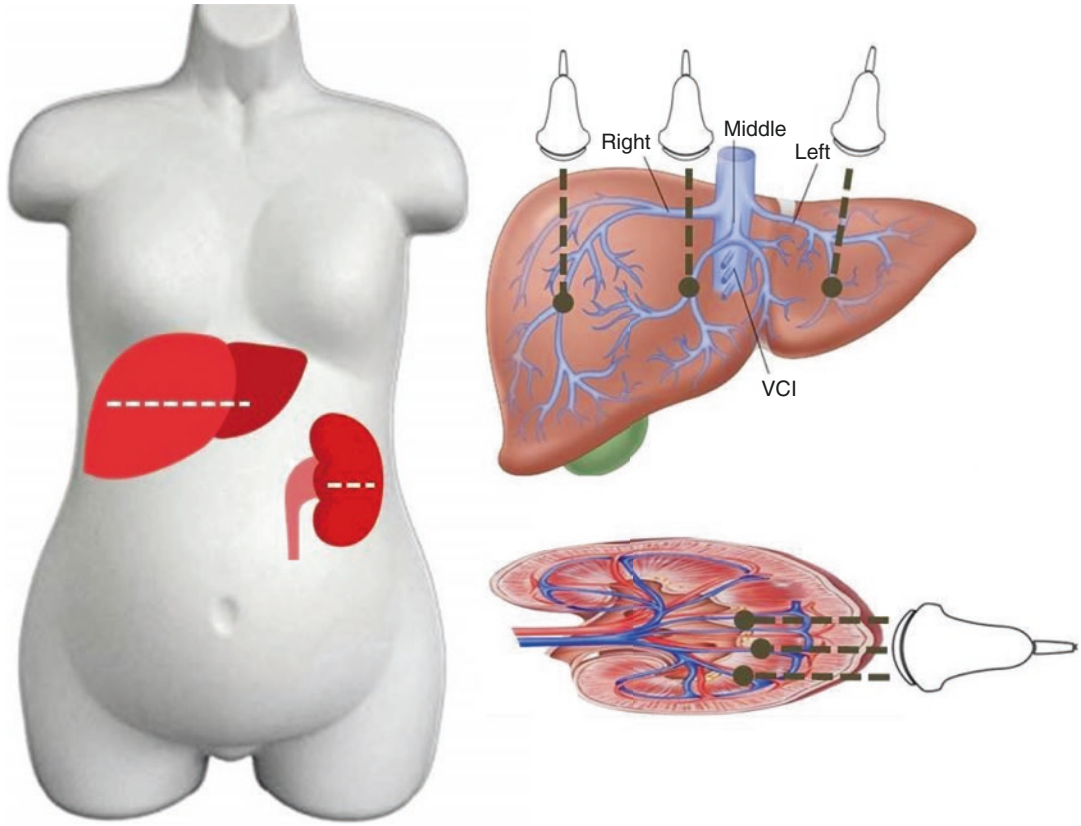

Fig. 10.4 Illustration of probe positioning and focus points of maternal venous Doppler flow imaging, as reported in this chapter
While the woman is in supine position (left panel), a horizontal scanning plane is searched at the midportion of liver (via intercostal probe positioning) and kidneys (probe positioning in the loins). For each organ, three consecutive focus points are chosen, preferrably one at left, middle, and right hepatic vein (upper right panel) and randomly in the kidneys at the middle distance between pyelum and cortex (lower right panel). The average of three measurements per organ is considered the assessment-specific value

hood estimation for the linear mixed model [21, 22] allows obtaining intra- and inter class correlation coefficients ≥0.66 [20], which improves further to ≥0.8 with assistance of a maternal ECG signal [23]. Finally, both theoretical and practical training allowed obtaining intra- and interrater correlation coefficients ≥0.9 [23].

10.5 Venous Doppler Flow Characteristics in Normal and Pathologic Pregnancies

In healthy nonpregnant individuals, the typical waveforms at the level of the liver show a triphasic pattern, and those at the renal interlobar veins a bi- or monophasic pattern (Fig. 10.2) [9]. With increased intravascular filling, the hepatic waveform deflections become more prominent, whereas during valsalva manoever, the triphasic pattern becomes totally flat [16].

10.5.1 Normal Pregnancy

– Renal Interlobar venous flow changes during the course of normal pregnancy [12, 24, 25]. This change is slightly different between left and right kidney [24] due to interkidney anatomic differences of renal veins [25] and relates inversely to diameter of the intrarenal pyelon [12, 24]. Venous impedance index decreases with advancing gestation (Fig. 10.5a), which is in line with the reported

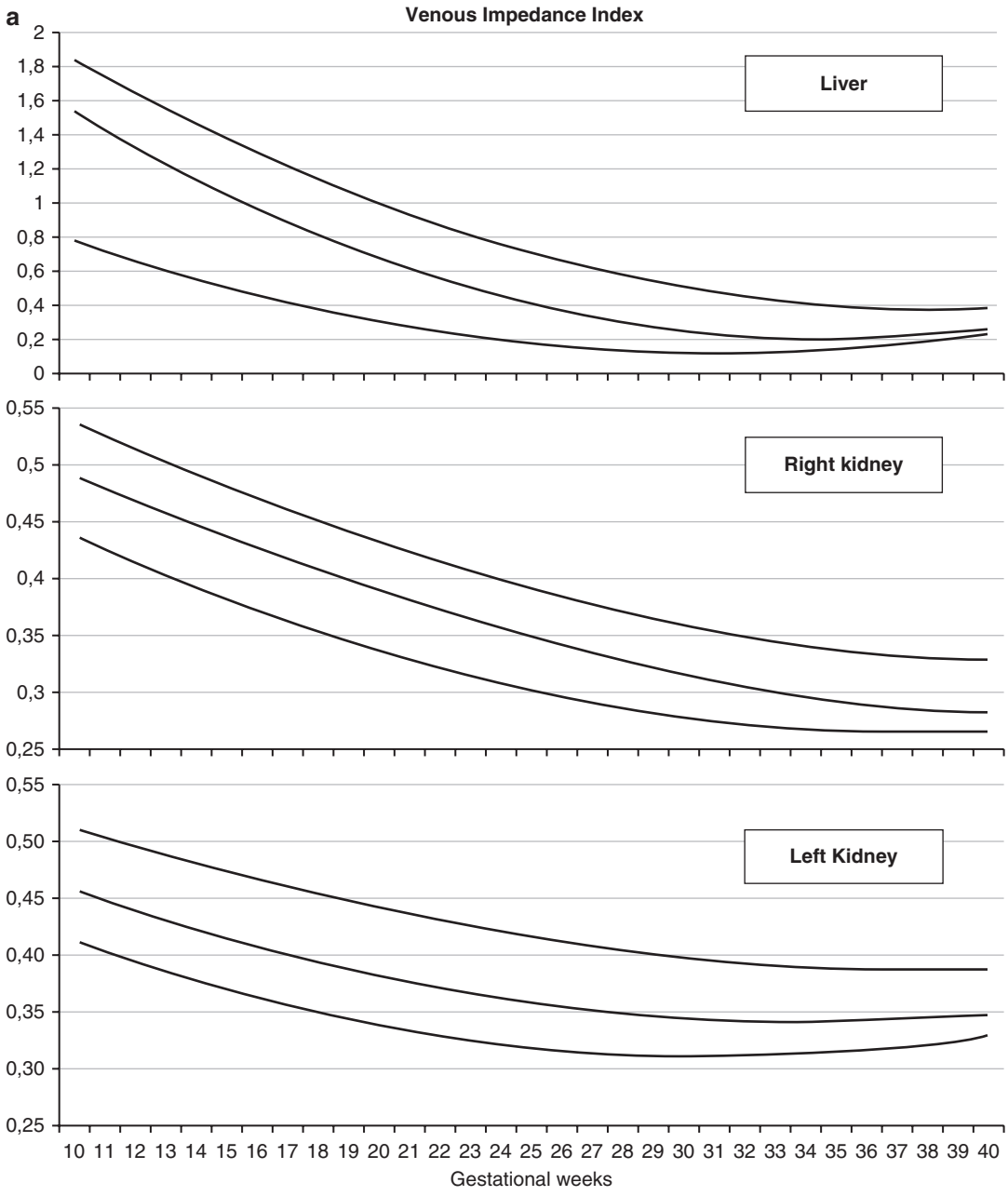

Fig. 10.5 (**a**) Reference Interquartile Range (P75-P50-P25) of venous impedance index at the level of hepatic and renal interlobar veins [26–29]. (**b**) Reference Interquartile Range (P75-P50-P25) of venous pulse transit time ratio at the level of hepatic and renal interlobar veins [26–29]

gestation-induced increase of venous distensibility [30].

– Hepatic venous flow changes from a pulsatile to a flat pattern during the course of pregnancy [31], with the most dramatic shift occuring at 22–24 weeks of gestation [32]. During the third trimester of uncomplicated pregnancies, there is a constant cyclical change between undulating and flat patterns until term [32]. This is in line with the

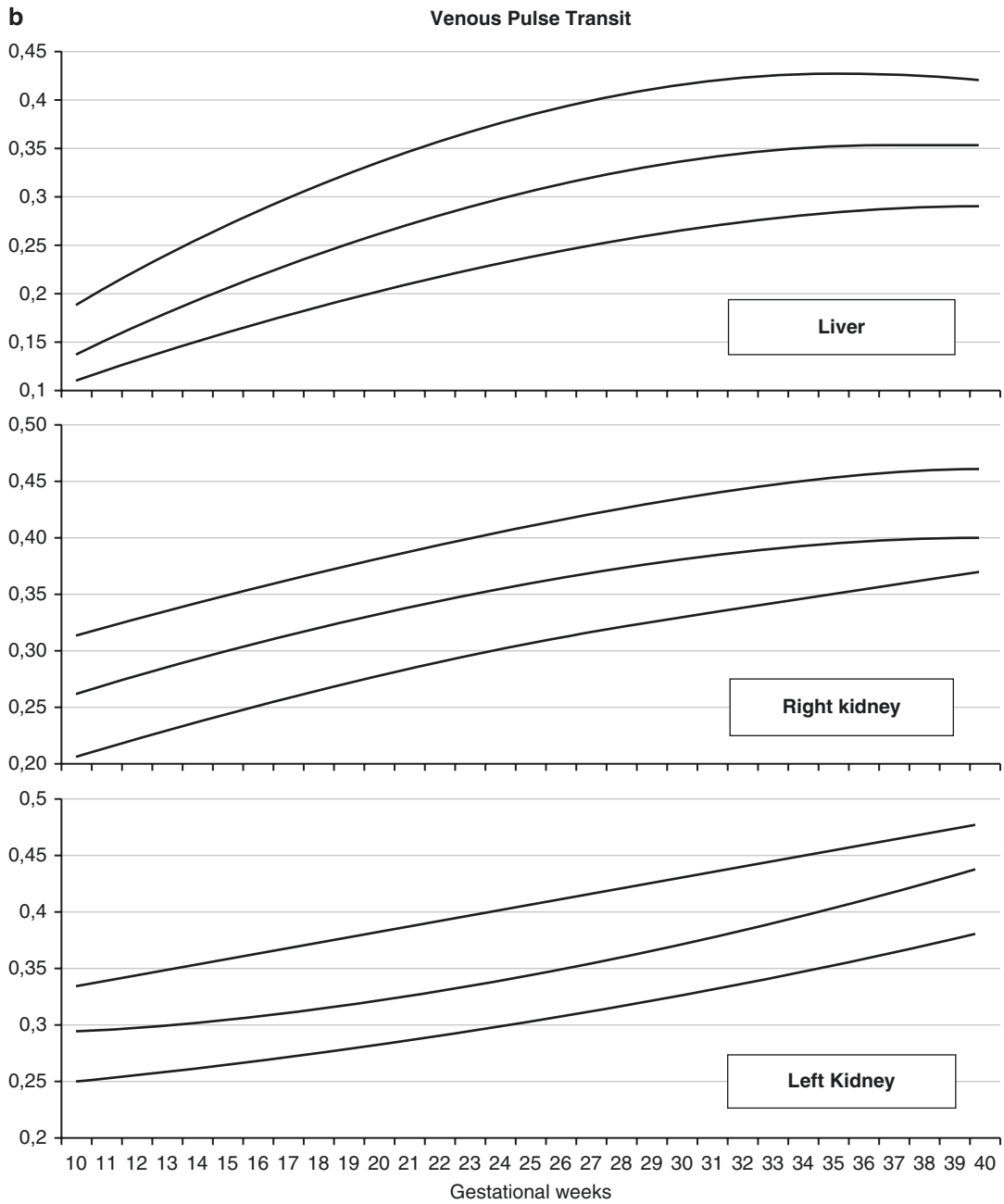

Fig. 10.5 (continued)

reported role of the liver in supporting maternal cardiac output under all physiologic circumstances [1–5].

– Heart rate-corrected venous pulse transit time in right renal interlobar veins is longer than in hepatic veins, but shorter than in left renal interlobar veins [14]. During normal pregnancy, venous pulse transit time ratio increases at each point of measurement (Fig. 10.5b) [14]. This is in line with the reported gestation-induced reduction of intra-abdominal venous tone [33, 34].

10.5.2 Preeclampsia

- In preeclampsia, renal interlobar vein impedance index is higher than in normal pregnancy [13, 25], and this difference is more pronounced in early- than in late-onset preeclampsia [35]. In late- but not early-onset PE, there is a weak but significant correlation between renal interlobar vein impedance index and degree of proteinuria [36]. In both kidneys, impedance index shows a slow oscillitory pattern which alternates between left and right, a pattern becoming more prominent in preeclampsia [11]. In early-onset preeclampsia, a typical venous pre-acceleration nadir can be observed, representing retrograde backflow of venous blood following atrial contraction up to the level of the kidneys [9, 37]. In early onset preeclampsia, bilateral abnormal renal interlobar vein impedance index presents weeks before onset of disease, whereas in late-onset preeclampsia, this may present unilaterally and simultaneously with onset of proteinuria [38].
- In early onset preeclampsia, hepatic venous flow may show a triphasic pattern, similar to that observed during the first trimester, and hepatic venous impedance index is higher than in uncomplicated pregnancies [9, 32]. Abnormal hepatic Doppler measurements are observed already from the second trimester onward in early-onset preeclampsia, whereas for late-onset preeclampsia this is only present in the third trimester [26].
- Heart rate-corrected venous pulse transit, measured at each location, is shorter in preeclampsia than in normal pregnancies [14, 39], and this effect is more pronounced in early- than in late-onset preeclampsia [35]. For early-onset preeclampsia, hepatic vein pulse transit time ratio is shortened from the second trimester onward, and this becomes associated with short renal interlobar vein pulse transit time ratio in the third trimester. For third trimester late-onset preeclampsia, hepatic but not intrarenal venous pulse transit time ratio is short [26].

10.5.3 Gestational and Essential Hypertension

- None of the above mentioned venous Doppler flow abnormalities are observed in non-proteinuric gestational hypertension [26, 37, 40] or in chronic hypertension without superimposed preeclampsia. When the latter is complicated with superimposed preeclampsia, similar venous flow changes are observed as in preeclampsia.

10.5.4 Normotensive Pregnancies with Newborns Small for Gestational Age

- In normotensive women giving birth to neonates small for gestational age (<P10), abnormal venous Doppler characteristics are present already from the first trimester onward [27]. Short venous pulse transit time ratios at the level of liver and both kidneys are associated with increased hepatic vein impedance index. Renal interlobar vein impedance index is abnormal only in the third trimester. These findings suggest early gestational venous hemodynamic activation as a physiologic response to enhance chronic low cardiac output in these women [27].

10.6 Relevance of Maternal Venous Hemodynamics Assessment

From the evidence outlined above, it is becoming clear that the assesment of maternal cardiovascular function in complicated pregnancies is incomplete without considering aspects of filling and/or venous return [3]. Even more, including venous function analysis into maternal hemodynamics assessment allows for better understanding the pathophysiologic background mechanisms of circulatory dysfunctions, and this knowledge is helpful in screening for and management of gestional hypertension disorders, with or without fetal growth restriction [6, 26, 28].

10.6.1 Pathophysiology of Preeclampsia and Gestational Hypertension

A key observation in venous hemodynamics assessments is that abnormal venous Doppler measurements are observed in preeclampsia—less pronounced in late than in early onset PE—but not in gestational hypertension or chronic hypertension without superimposition of preeclampsia [37, 40]. The latter two primarily present with arterial hemodynamic dysfunctions with or without cardiac involvement [26, 29]. It has been shown that the overall cardiovascular (dys-)function in the third trimester of pregnancies complicated with gestational hypertension very much resembles the first trimester condition of women who eventually develop late onset preeclampsia [26]. Given the observation that all pregnancies, irrespective of their outcome, present with increase of body water volume and cardiac output, although not to the same degree [29], it seems that the clinical presentation of gestation-induced hypertension with or without organ dysfunction and/or proteinuria is the cardiovascular response to intravascular volume load [41, 42]. The early gestational cardiovascular condition, which may originate from a subclinical CV dysfunction already present before conception [43], determines the eventual presentation of the type of gestational hypertensive disorder [26]. When abnormal venous hemodynamics becomes part of this overall circulatory dysfunction, a process similar to cardiorenal syndrome can be triggered with development of organ congestion and subsequent dysfunction [42, 44]. From this perspective, the relation between gestational hypertensive disorders might be theoretically described as "preeclampsia = gestational hypertension + venous dysfunction." This interesting hypothesis invites for more research with different technologies to study in depth venous hemodynamics during pregnancy.

10.6.2 Screening for Preeclampsia

The observation of venous Doppler abnormalities presenting weeks before clinical presentation of early-onset preeclampsia opens opportunities to implement venous hemodynamics assesment in screening for PE [38]. However, the lack of abnormal venous Doppler parameters in the first trimester and the different time onset of venous dysfunction in early- and late-onset PE imply that longitudinal assessments are required for each individual screenend, which is impractical and not universally applicable [45]. It has been reported that venous Doppler assesment can succesfully be added to a screening algorithm, using biophysical markers only, with high sensitivity and specificity for all types of gestational hypertensive disorders [6, 26, 28]. Today, the performance of this algorithm requires confirmation from a large prospective trial in a low-risk population before its universal application can be recommended.

10.6.3 Management

Documentation of abnormal functioning of the venous compartement in preeclampsia opens perspectives to evaluate the application of venoactive drugs, such as nitroglycerin and/or magnesium sulfate.

Nitroglycerin and other nitrates are well-known endothelium-dependent vasodilating agents targeting coronary, but also venous, vasculature, [46], which have been successfully applied in the management of preeclampsia, with or without pulmonary edema [47, 48]. Recently, nitric oxide donors have caught the attention of obstetric researchers, because of the combination of beneficial cardiovascular effects with maternal and fetal safety [49]. Nitric oxide donors associated with plasma volume expansion have been reported to improve diastolic blood flow velocity in the umbilical artery in parallel with a reduction of maternal peripheral arterial resistance [50, 51].

Magnesium sulfate is widely used for the prevention and treatment of maternal eclamptic seizures and for neonatal neuroprotection during preterm birth [52]. Despite its widespread application, the mechanisms of action are poorly

understood [53]. A role for magnesium has been reported in the physiologic control of blood pressure and the pathophysiology of hypertension [54]. Reversal of vasospasms offers potential to magnesium supplementation as a pharmacologic treatment for cerebral or coronary vasoconstriction [55, 56]. Experimental evidence from laboratory models and animal studies supports magnesium-induced vasorelaxation activity in both the arterial and venous compartment, with maximal dilation of the venous capacitance vessels even at relatively low concentrations [57].

Before the introduction of these drugs in other settings or indications than generally used today, more experimental, clinical, and epidemiological research is required.

10.7 Pitfalls and Limitations of Maternal Venous Hemodynamics Assessment

As explained above, the venous compartment is a very dynamic system with activity variation over time and location, and this troubles the interpretation of venous Doppler assessments. Next to this, the system is very vulnerable to interfering factors, such as respiration, movement, and sympathetic tone. Specifically in cases where women get stressed from the breath-hold instructions of the sonographer and start performing unvoluntary valsalva, obtaining valuable data is difficult. Renal diseases, such as polycystic dysplasia or hydronephrosis, are responsible for flattening of the intrarenal venous waveform and as such interfere with Doppler measurements [58]. Finally, several diseases can strongly effect the venous vascular function, but this does not necessarily influence the outcome of pregnancy, as is illustrated by a case report of systemic lupus erythematodes [58]. These limitations are important to consider when interpreting venous Doppler measurements in isolated settings, without obtaining additional information on the functioning of other parts of the circulation.

10.8 Conclusion

Although venous Doppler sonography is troubled with much more biological variation and practical difficulties than at the arterial side, the evidence outlined in this chapter shows that obtaining repeatable and reproducible venous Doppler measurements is feasible when the assessment is performed under standardized conditions. Doing this, important information can be added to the current knowledge of maternal hemodynamics in both normal pregnancies and those complicated with gestational hypertension disorders. Venous Doppler sonography in combination with other technologies enables the assessment of global maternal circulatory function; data obtained as such suggest that the role of venous hemodynamics in the pathophysiology of preeclampsia and fetal growth restriction may be much more important than currently considered. This is an open invitation to physiologists, scientists, and clinicians all over the world to explore more into depth with different kinds of technologies the currently "forgotten" organ of the maternal circulation: the venous compartment.

References

1. Pang CC. Autonomic control of the venous system in health and disease: effects of drugs. Pharmacol Ther. 2001;90(2–3):179–230. Review.
2. Sunagawa K. Guyton's venous return curves should be taught at medical schools (complete English translation of Japanese version). J Physiol Sci. 2017;67(4):447–58. https://doi.org/10.1007/s12576-017-0533-0. Epub 2017 Mar 27. Review.
3. Gyselaers W, Spaanderman M. International working group on maternal hemodynamics. Assessment of venous hemodynamics and volume homeostasis during pregnancy: recommendations of the international working group on maternal hemodynamics. Ultrasound Obstet Gynecol. 2018;52(2):174–85. https://doi.org/10.1002/uog.18952. Epub 2018 Jun 6.
4. Gelman S. Venous function and central venous pressure: a physiologic story. Anesthesiology. 2008;108(4):735–48. https://doi.org/10.1097/ALN.0b013e3181672607. Review.
5. Vonck S, Staelens AS, Mesens T, Tomsin K, Gyselaers W. Hepatic hemodynamics and fetal growth: a relationship of interest for further research. PLoS One. 2014;9(12):e115594. https://doi.org/10.1371/journal.pone.0115594. eCollection 2014.

6. Oben J, Tomsin K, Mesens T, Staelens A, Molenberghs G, Gyselaers W. Maternal cardiovascular profiling in the first trimester of pregnancies complicated with gestation-induced hypertension or fetal growth retardation: a pilot study. J Matern Fetal Neonatal Med. 2014;27(16):1646–51. https://doi.org/10.3109/14767058.2013.871700. Epub 2014 Jan 13.
7. Devine PJ, Sullenberger LE, Bellin DA, Atwood JE. Jugular venous pulse: window into the right heart. South Med J. 2007;100(10):1022–7. quiz 1004. Review.
8. Dierickx I, Van Hooland S, Tomsin K, Vanhercke D, Cools W, Fransen H, Gyselaers W. Feasibility of combined Doppler-ECG assessment of internal jugular veins. Ultrasound Med Biol. 2017;43(9):1853–60. https://doi.org/10.1016/j.ultrasmedbio.2017.04.001. Epub 2017 Jul 11.
9. Gyselaers W. Hemodynamics of the maternal venous compartment: a new area to explore in obstetric ultrasound imaging. Ultrasound Obstet Gynecol. 2008;32(5):716–7. https://doi.org/10.1002/uog.6113.
10. Gyselaers W, Mesens T, Tomsin K, Peeters L. Doppler assessment of maternal central venous hemodynamics in uncomplicated pregnancy: a comprehensive review. Facts Views Vis Obgyn. 2009;1(3):171–81. Review.
11. Gyselaers W, Mullens W, Tomsin K, Mesens T, Peeters L. Role of dysfunctional maternal venous hemodynamics in the pathophysiology of pre-eclampsia: a review. Ultrasound Obstet Gynecol. 2011;38(2):123–9. https://doi.org/10.1002/uog.9061. Review.
12. Karabulut N, Baki Yağci A, Karabulut A. Renal vein Doppler ultrasound of maternal kidneys in normal second and third trimester pregnancy. Br J Radiol. 2003;76(907):444–7.
13. Bateman GA, Giles W, England SL. Renal venous Doppler sonography in preeclampsia. J Ultrasound Med. 2004;23(12):1607–11.
14. Tomsin K, Mesens T, Molenberghs G, Gyselaers W. Venous pulse transit time in normal pregnancy and preeclampsia. Reprod Sci. 2012;19(4):431–6. https://doi.org/10.1177/1933719111424440. Epub 2012 Feb 28.
15. Teichgräber UK, Gebel M, Benter T, Manns MP. Effect of respiration, exercise, and food intake on hepatic vein circulation. J Ultrasound Med. 1997;16(8):549–54.
16. Tomsin K, Vriens A, Mesens T, Gyselaers W. Non-invasive cardiovascular profiling using combined electrocardiogram-Doppler ultrasonography and impedance cardiography: an experimental approach. Clin Exp Pharmacol Physiol. 2013;40(7):438–42.
17. Staelens AS, Van Cauwelaert S, Tomsin K, Mesens T, Malbrain ML, Gyselaers W. Intra-abdominal pressure measurements in term pregnancy and postpartum: an observational study. PLoS One. 2014;9(8):e104782. https://doi.org/10.1371/journal.pone.0104782. eCollection 2014.
18. Archer TL, Suresh P, Ballas J. Don't forget aortocaval compression when imaging abdominal veins in pregnant patients. Ultrasound Obstet Gynecol. 2011;38(4):479–80.; author reply 480-1. https://doi.org/10.1002/uog.10065.
19. Staelens AS, Vonck S, Mesens T, Tomsin K, Molenberghs G, Gyselaers W. Type-specific orthostatic hemodynamic response of hypertensive diseases in pregnancy. Clin Exp Pharmacol Physiol. 2015;42(10):1036–44. https://doi.org/10.1111/1440-168112463.
20. Mesens T, Tomsin K, Molenberghs G, Gyselaers W. Reproducibility and repeatability of maternal venous Doppler flow measurements in renal interlobar and hepatic veins. Ultrasound Obstet Gynecol. 2010;36(1):120–1.
21. Verbeke G, Fieuws S, Molenberghs G, Davidian M. The analysis of multivariate longitudinal data: a review. Stat Methods Med Res. 2014;23(1):42–59. https://doi.org/10.1177/0962280212445834. Epub 2012 Apr 20. Review.
22. Laenen A, Vangeneugden T, Geys H, Molenberghs G. Generalized reliability estimation using repeated measurements. Br J Math Stat Psychol. 2006;59(Pt1):113–31.
23. Staelens AS, Tomsin K, Oben J, Mesens T, Grieten L, Gyselaers W. Improving the reliability of venous Doppler flow measurements: relevance of combined ECG, training and repeated measures. Ultrasound Med Biol. 2014;40(7):1722–8. https://doi.org/10.1016/j.ultrasmedbio.2014.01.014. Epub 2014 Mar 14.
24. Gyselaers W, Verswijvel G, Molenberghs G, Ombelet W. Interlobar venous flow is different between left and right kidney in uncomplicated third trimester pregnancy. Gynecol Obstet Investig. 2008;65(1):6–11. Epub 2007 Jul 31.
25. Gyselaers W, Molenberghs G, Van Mieghem W, Ombelet W. Doppler measurement of renal interlobar vein impedance index in uncomplicated and preeclamptic pregnancies. Hypertens Pregnancy. 2009;28(1):23–33. https://doi.org/10.1080/10641950802233056.
26. Gyselaers W, Vonck S, Staelens AS, Lanssens D, Tomsin K, Oben J, Dreesen P, Bruckers L. Gestational hypertensive disorders show unique patterns of circulatory deterioration with ongoing pregnancy. Am J Physiol Regul Integr Comp Physiol. 2019;316(3):R210–21. https://doi.org/10.1152/ajpregu.00075.2018. Epub 2019 Jan 23.
27. Vonck S, Staelens AS, Lanssens D, Tomsin K, Oben J, Dreesen P, Bruckers L, Gyselaers W. Low volume circulation in normotensive women pregnant with neonates small for gestational age. Fetal Diagn Ther. 2019;6:1–8. https://doi.org/10.1159/000495507. [Epub ahead of print].
28. Vonck S, Staelens AS, Lanssens D, Tomsin K, Oben J, Bruckers L, Gyselaers W. Development of a biophysical screening model for gestational hypertensive diseases. J Biomed Sci. 2019;26(1):38. https://doi.org/10.1186/s12929-019-0530-0.
29. Gyselaers W, Vonck S, Staelens AS, Lanssens D, Tomsin K, Oben J, Dreesen P, Bruckers L. Body fluid volume homeostasis is abnormal in pregnancies com-

plicated with hypertension and/or poor fetal growth. PLoS One. 2018;13(11):e0206257. https://doi.org/10.1371/journal.pone.0206257. eCollection 2018.
30. Sakai K, Imaizumi T, Maeda H, Nagata H, Tsukimori K, Takeshita A, Nakano H. Venous distensibility during pregnancy. Comparisons between normal pregnancy and preeclampsia. Hypertension. 1994;24(4):461–6.
31. Roobottom CA, Hunter JD, Weston MJ, Dubbins PA. Hepatic venous Doppler waveforms: changes in pregnancy. J Clin Ultrasound. 1995;23(8):477–82.
32. Gyselaers W, Molenberghs G, Mesens T, Peeters L. Maternal hepatic vein Doppler velocimetry during uncomplicated pregnancy and pre-eclampsia. Ultrasound Med Biol. 2009;35(8):1278–83. https://doi.org/10.1016/j.ultrasmedbio.2009.03.014. Epub 2009 Jun 21.
33. Stainer K, Morrison R, Pickles C, Cowley AJ. Abnormalities of peripheral venous tone in women with pregnancy-induced hypertension. Clin Sci (Lond). 1986;70(2):155–7.
34. Pang CC. Measurement of body venous tone. J Pharmacol Toxicol Methods. 2000;44(2):341–60. Review.
35. Gyselaers W, Mesens T, Tomsin K, Molenberghs G, Peeters L. Maternal renal interlobar vein impedance index is higher in early- than in late-onset pre-eclampsia. Ultrasound Obstet Gynecol. 2010;36(1):69–75.
36. Mesens T, Tomsin K, Staelens AS, Oben J, Molenberghs G, Gyselaers W. Is there a correlation between maternal venous hemodynamic dysfunction and proteinuria of preeclampsia? Eur J Obstet Gynecol Reprod Biol. 2014;181:246–50. https://doi.org/10.1016/j.ejogrb.2014.08.008. Epub 2014 Aug 17.
37. Gyselaers W, Tomsin K, Staelens A, Mesens T, Oben J, Molenberghs G. Maternal venous hemodynamics in gestational hypertension and preeclampsia. BMC Pregnancy Childbirth. 2014;23(14):212. https://doi.org/10.1186/1471-2393-14-212.
38. Gyselaers W, Mesens T. Renal interlobar vein impedance index: a potential new Doppler parameter in the prediction of preeclampsia? J Matern Fetal Neonatal Med. 2009;22(12):1219–21. https://doi.org/10.3109/14767050903019635.
39. Tomsin K, Mesens T, Molenberghs G, Peeters L, Gyselaers W. Time interval between maternal electrocardiogram and venous Doppler waves in normal pregnancy and preeclampsia: a pilot study. Ultraschall Med. 2012;33(7):E119–25. https://doi.org/10.1055/s--0029-1245698. Epub 2010 Oct 11.
40. Gyselaers W, Staelens A, Mesens T, Tomsin K, Oben J, Vonck S, Verresen L, Molenberghs G. Maternal venous Doppler characteristics are abnormal in pre-eclampsia but not in gestational hypertension. Ultrasound Obstet Gynecol. 2015;45(4):421–6. https://doi.org/10.1002/uog.13427. Epub 2015 Mar 9.
41. Melchiorre K, Sharma R, Khalil A, Thilaganathan B. Maternal cardiovascular function in Normal pregnancy: evidence of Maladaion to chronic volume overload. Hypertension. 2016;67(4):754–62. https://doi.org/10.1161/HYPERTENSIONAHA.115.06667. Epub 2016 Jan 25.
42. Gyselaers W, Thilaganathan B. Preeclampsia: a gestational cardiorenal syndrome. J Physiol. 2019; https://doi.org/10.1113/JP274893. [Epub ahead of print].
43. Foo FL, Mahendru AA, Masini G, Fraser A, Cacciatore S, MacIntyre DA, McEniery CM, Wilkinson IB, Bennett PR, Lees CC. Association between Prepregnancy cardiovascular function and subsequent preeclampsia or fetal growth restriction. Hypertension. 2018;72(2):442–50. https://doi.org/10.1161/HYPERTENSIONAHA.118.11092. Epub 2018 Jul 2.
44. Gyselaers W. Maternal venous hemodynamic dysfunction in proteinuric gestational hypertension: evidence and implications. J Clin Med. 2019;8(3):pii: E335. https://doi.org/10.3390/jcm8030335. Review.
45. Mesens T, Tomsin K, Oben J, Staelens A, Gyselaers W. Maternal venous hemodynamics assessment for prediction of preeclampsia should be longitudinal. J Matern Fetal Neonatal Med. 2015;28(3):311–5. https://doi.org/10.3109/14767058.2014.916673. Epub 2014 May 20.
46. Silber S. Nitrates: why and how should they be used today? Current status of the clinical usefulness of nitroglycerin, isosorbide dinitrate and isosorbide-5-mononitrate. Eur J Clin Pharmacol. 1990;38(Suppl 1):S35–51. Review.
47. Cetin A, Yurtcu N, Guvenal T, Imir AG, Duran B, Cetin M. The effect of glyceryl trinitrate on hypertension in women with severe preeclampsia, HELLP syndrome, and eclampsia. Hypertens Pregnancy. 2004;23(1):37–46.
48. Cotton DB, Jones MM, Longmire S, Dorman KF, Tessem J, Joyce TH 3rd. Role of ntravenous nitroglycerin in the treatment of severe pregnancy-induced hypertension complicated by pulmonary edema. Am J Obstet Gynecol. 1986;154(1):91–3.
49. Johal T, Lees CC, Everett TR, Wilkinson IB. The nitric oxide pathway and possible therapeutic options in pre-eclampsia. Br J Clin Pharmacol. 2014;78(2):244–57. https://doi.org/10.1111/bcp.12301. Review.
50. Valensise H, Vasapollo B, Novelli GP, Giorgi G, Verallo P, Galante A, Arduini D. Maternal and fetal hemodynamic effects induced by nitric oxide donors and plasma volume expansion in pregnancies with gestational hypertension complicated by intrauterine growth restriction with absent end-diastolic flow in the umbilical artery. Ultrasound Obstet Gynecol. 2008;31(1):55–64.
51. Vasapollo B, Novelli GP, Gagliardi G, Tiralongo GM, Pisani I, Manfellotto D, Giannini L, Valensise H. Medical treatment of early-onset mild gestational hypertension reduces total peripheral vascular resistance and influences maternal and fetal complications. Ultrasound Obstet Gynecol. 2012;40(3):325–31. https://doi.org/10.1002/uog.11103.

52. Pryde PG, Mittendorf R. Contemporary usage of obstetric magnesium sulfate: indication, contraindication, and relevance of dose. Obstet Gynecol. 2009;114(3):669–73. https://doi.org/10.1097/AOG.0b013e3181b43b0e. Review.
53. Euser AG, Cipolla MJ. Magnesium sulfate for the treatment of eclampsia: a brief review. Stroke. 2009;40(4):1169–75. https://doi.org/10.1161/STROKEAHA.108.527788. Epub 2009 Feb 10. Review.
54. Touyz RM. Role of magnesium in the pathogenesis of hypertension. Mol Asp Med. 2003;24(1–3):107–36. Review.
55. Keyrouz SG, Diringer MN. Clinical review: prevention and therapy of vasospasm in subarachnoid hemorrhage. Crit Care. 2007;11(4):220. Review.
56. Teragawa H, Kato M, Yamagata T, Matsuura H, Kajiyama G. The preventive effect of magnesium on coronary spasm in patients with vasospastic angina. Chest. 2000;118(6):1690–5.
57. Upton RN, Ludbrook GL. Pharmacokinetic-pharmacodynamic modelling of the cardiovascular effects of drugs—method development and application to magnesium in sheep. BMC Pharmacol. 2005;5:5.
58. Staelens AS, Vonck S, Tomsin K, Gyselaers W. Clinical inference of maternal renal venous Doppler ultrasonography. Ultrasound Obstet Gynecol. 2017;49(1):155–6. https://doi.org/10.1002/uog.17328.

11 Relationship Between Maternal and Fetal Cardiovascular Function

Christoph C. Lees and Giulia Masini

11.1 Overview of Maternal Cardiovascular Function in Health and Disease

Maternal cardiovascular function experiences major changes during pregnancy, which are identifiable from the early stages of trophoblast invasion and vary with gestational age, with a specific pattern for each stage of pregnancy and parameter [1, 2]. To give an overview of cardiovascular changes in healthy pregnancies, it is useful to separate central changes in hemodynamics (cardiac output and vascular resistance) from arterial vascular function (stiffness and compliance).

It is well-known that there is an increase in maternal cardiac output in the first trimester [3–6], due to an increase in stroke volume. Beyond the second trimester, an increase in heart rate is the major driver in increasing cardiac output, which reaches its peak in the early third trimester [2]. Peripheral vascular resistance decreases early in gestation due to the vasodilatory effects of progesterone and vasoactive mediators and following the changes in cardiac output, then rising again in the third trimester [2]. The greater decrease of peripheral vascular resistance compared to the increase in cardiac output triggers a fall in mean arterial pressure, with a nadir at 16–20 weeks gestation gradually increasing to prepregnancy levels near term [1]. Left ventricular mass rises progressively through gestation reaching a maximum increase in the early third trimester [2].

With regard to large artery function, which is a predictor of cardiovascular disease in nonpregnant subjects, this also changes during pregnancy. The elastic properties of the aorta are responsible for mitigation of the blood pressure pumped by the heart at every contraction; an increase of arterial stiffness, typically occurring with aging, results in an increment in blood pressure [7]. Arterial stiffness can be assessed through the aortic pulse wave velocity, a measurement of the blood flow velocity into our largest systemic artery, although an earlier marker of arterial compliance is the assessment of the wave propagation properties by measuring the augmentation index. This is a measure of pressure wave reflection within the systemic circulation, considered to be more dependent on endothelial dysfunction and arterial resistance [8]. A fall in these parameters, and in particular in augmentation index (Fig. 11.1), can be observed early in the first trimester, with a nadir in the second trimester and a subsequent rise in the third trimester [3, 9–11].

C. C. Lees (✉)
Centre for Fetal Care, Queen Charlotte's and Chelsea Hospital, Imperial College Healthcare NHS Trust, London, UK

Department of Metabolism, Digestion and Reproduction, Imperial College Healthcare NHS Trust, London, UK
e-mail: christoph.lees@nhs.net

G. Masini
Centre for Fetal Medicine, Azienda Ospedaliero-Universitaria Careggi, Florence, Italy

D. Maulik, C. C. Lees (eds.), *Doppler Ultrasound in Obstetrics and Gynecology*,
https://doi.org/10.1007/978-3-031-06189-9_11

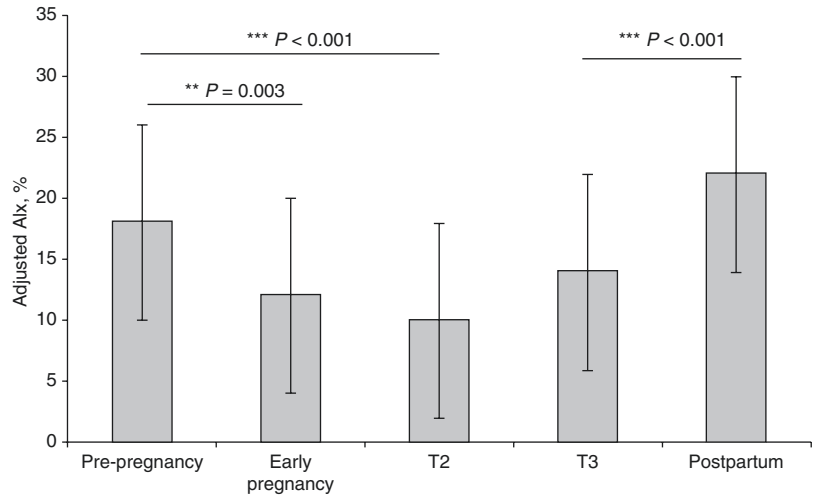

Fig. 11.1 Modifications in augmentation index (AI) from prior to pregnancy to postpartum [3]

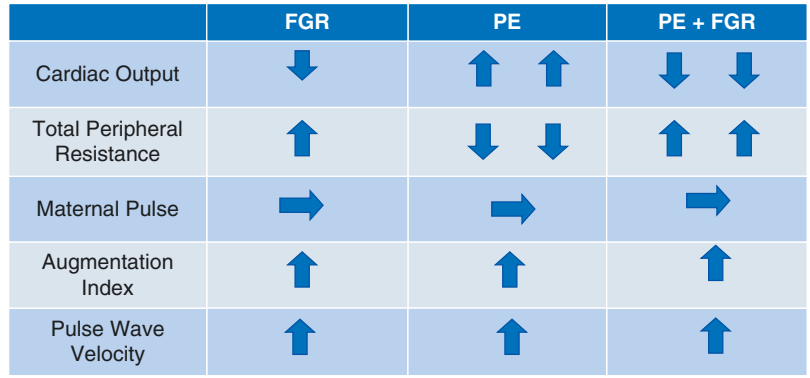

Fig. 11.2 Schematic representation of maternal cardiovascular changes in pathological pregnancy conditions [12]

With the rapid hormonal changes and reduced cardiovascular demand after delivery, maternal hemodynamic parameters return to nonpregnant values in the early postpartum (first 12 weeks after delivery) or later depending on breastfeeding and physical activity. Some studies, however, suggest that cardiovascular changes persist for longer as multiparous pregnant women show a slightly different hemodynamic profile compared to nulliparous, with more rapid and greater modifications of cardiac output, peripheral vascular resistance, and cardiac mass in subsequent pregnancies [1, 2].

It is increasingly evident that deviations from normal physiology of these hemodynamic changes not only accompany pregnancy complications, particularly preeclampsia and fetal growth restriction, but can be their early predictors. Based on maternal hemodynamic status, different patterns can be recognized and associated to preeclampsia alone, fetal growth restriction alone, or the combination of both (Fig. 11.2).

Preeclampsia that occurs without fetal growth restriction is generally a "late" complication in pregnancy and is characterized by a hyperdynamic overfilling state with high cardiac output, low peripheral vascular resistance, and larger left ventricular diameters when compared to normal pregnancies [12–14]. In contrast, when fetal growth restriction occurs, a hypovolemic underfilling state is commonly observed, with low cardiac output, elevated peripheral vascular resistance, smaller left ventricular diameters, and altered diastolic function [13, 15–17]. These characteristics are even more marked when fetal growth restriction is associated with preeclampsia [12, 14, 18].

In pregnancies complicated by preeclampsia, particularly with fetal growth restriction, arterial function is abnormal, with increase of augmentation index and, to a lesser extent, pulse wave velocity above normal values [14, 19, 20]. Studies of arterial function in fetal growth restriction alone are less numerous, but seem to confirm the same findings obtained in preeclamptic subjects [14]. This supports the well-known observation that both preeclampsia and fetal growth restriction are risk factors for cardiovascular disease for women who have experienced these complications during gestation [21].

Deviations from normal maternal hemodynamic adaptation can be observed in the very early stages of pregnancy, as early as 5 weeks gestation [10, 22]. Furthermore, the importance of prepregnancy cardiovascular status has recently been investigated in a preconception study which demonstrated that healthy normotensive women who experience preeclampsia and/or fetal growth restriction had altered hemodynamics before gestation compared with those women who had normal pregnancy outcomes [23]. Indeed, these findings give the opportunity to identify women at higher risk of pregnancy complication, and potentially prevent them, in the very early phases of gestation or even prior to pregnancy.

11.2 Uterine Artery Doppler, Trophoblast Invasion, and Maternal Cardiovascular Function

Doppler assessment of the uterine artery blood flow in pregnant women is a ubiquitous test, commonly used to obtain indirect information about placental vascular function: adequate uterine artery impedance through gestation is considered reflective of a healthy placenta and carries a lower risk of pregnancy complications. Abnormally high uterine artery Doppler impedance is thought to reflect suboptimal uteroplacental perfusion and is strongly linked to compromised fetal growth and hypertensive disorders in pregnancy [24–26]. Screening based on measurement of uterine artery pulsatility indices has widely been adopted as predictor of preeclampsia and fetal growth restriction. Once used in mid second trimester to assess individualized risk of adverse outcome, this test has more recently been combined with maternal history, mean arterial pressure, and serum biomarkers and applied in the first trimester of pregnancy giving the chance for a preventive therapy with acetylsalicylic acid from the first weeks of pregnancy [27–31].

The process of placentation starts with the trophoblast invasion of the endothelium and muscular wall of the spiral arteries. This is an early process in pregnancy, which leads to the development of high-flow-low-resistance vessels able to adequately perfuse the uterus and support the development of a fetomaternal unit which guarantees enough nutrients to the product of conception. Defects in this vascular invasion have long been considered the primary cause for the development of preeclampsia and fetal growth restriction, supported by the observation that placentas of pregnancies with such complications share typical anatomopathological characteristics (i.e., vascular and villous abnormalities, fibrinoid deposition, intervillositis, thrombotic vasculopathy) [32, 33]. However, impaired placental invasion documented with hystopathological studies neither is a unique characteristic of pregnancies with hypertensive disorders or restricted fetal growth, nor is present in all pregnancies with the previously mentioned abnormal outcome [34–36].

As previously discussed in this chapter, the most substantial adaptations of maternal cardiovascular system to pregnancy occur early in the first trimester and most importantly there is evidence that they can be predicted prior to pregnancy. The timing of these changes is crucial as they occur before the development of a functional placental unit, suggesting that maternal hemodynamics may play a key role in uterine artery blood flow changes [36].

This view is supported by studies that have investigated the association between maternal cardiovascular changes and those of the uteroplacental circulation from 24 weeks gestation in

Table 11.1 Extrauterine factors affecting uterine artery Doppler impedance [38]

Extrauterine factor		Effect
Hormonal	Estrogen	⇩
	Progesterone	⇩
	Polycystic ovarian syndrome	⇧
Pharmacological	Labetalol	⇔
	Nifedipine	⇔[a]
	Verapamil	⇔
	Hydralazine	⇔
	α-Methyldopa	⇩
	Nitric oxide donors	⇩[b]
Infective	Malaria	⇧
Extrauterine pregnancy		⇩

[a]Decrease in high dose regimen
[b]Some studies show no change

healthy pregnancies and those affected by preeclampsia, fetal growth restriction, or both. They have shown that a relationship with uterine Doppler impedance exists, namely, a decrease in maternal cardiac output and rise in peripheral vascular resistance are associated with increased maternal uterine arteries pulsatility index, irrespective of pregnancy outcome [37].

In addition to this, drugs, hormones, and even infections are known to exert vasoactive effects documented to change uterine artery Doppler indices (Table 11.1) [38]; therefore, considering spiral arteries invasion as the sole determinant of changes in uterine vessels impedance is at any rate reductive.

11.3 Maternal Cardiovascular Function and Fetal Doppler Indices: Umbilical Artery, Middle Cerebral Artery, and Ductus Venosus

Maternal cardiovascular function is able to influence fetal circulation. This happens physiologically during maternal physical activity: several studies have reported the association between maternal exercise and its effect on fetal heart rate and umbilical artery impedance: overall, the influence of acute maternal exercise is more marked on fetal heart rate which appears to increase during and after exercise, whereas chronic exercise seems to play a role in reducing both umbilical artery pulsatility index and fetal heart rate at rest, with no adverse effect in terms of episodes of fetal bradycardia [39]. By contrast, strenuous exercise (at intensity above 90% of maximal maternal heart rate) may compromise fetal the fetal circulation, by causing episodes of fetal bradycardia, increasing umbilical artery pulsatility index, and decreasing by 50% the uterine artery blood flow [40].

The effects of maternal exercise in pregnancies with uteroplacental insufficiency have also been investigated. In this situation, umbilical artery Doppler may conversely deteriorate; some studies report an increase in pulsatility index and transient episodes of absent end-diastolic flow [41]; therefore, fetal growth restriction with abnormal Dopplers could be considered a relative contraindication to aerobic exercise during pregnancy [42]. The examples mentioned above report what happens when maternal hemodynamic state changes due to exercise, a physiological activity. But what happens when maternal cardiovascular phenotype is chronically altered such as in preeclampsia or early-onset fetal growth restriction?

When fetal growth is impaired, fetal Doppler indices deteriorate progressively, as a result of progressive fetal hypoxia and acidemia that lead to compensatory changes in the fetal circulation; this defensive response has the aim to ensure the delivery of oxygen and substrates to fetal essential organs [43–45] and follow a well-defined temporal sequence with early Doppler abnormalities (increase in umbilical artery pulsatility index and middle cerebral artery changes) preceding late Doppler changes (reverse flow in the umbilical artery, abnormal ductus venosus with exaggerated "a" wave) [46–50].

Recent studies have assessed whether there is an association between maternal cardiac output/peripheral vascular resistance and fetal

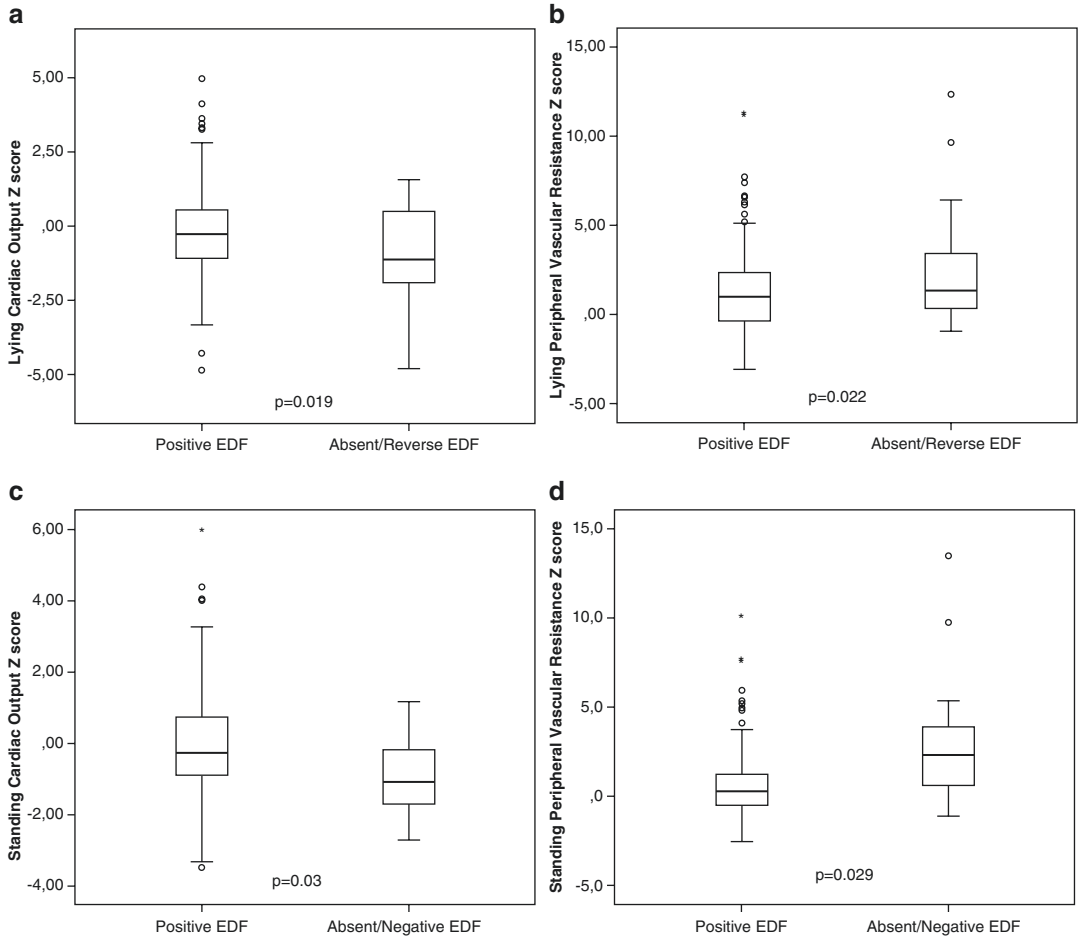

Fig. 11.3 Positive end-diastolic flow (EDF) vs. absent or reversed EDF in the Umbilical artery: (**a**) Lying cardiac output *z* score, (**b**) Lying peripheral vascular resistance *z* score, (**c**) Standing cardiac output *z* score, (**d**) Standing peripheral vascular resistance *z* score [51]

Doppler changes from 24 weeks gestation to term showing that lower maternal cardiac output and high maternal peripheral vascular resistance are associated with raised impedance in the fetal umbilical arteries. This is true not only in pathological (i.e., affected by preeclampsia and/or fetal growth restriction), but also in healthy pregnancies [37]. Further strengthening the link between maternal cardiovascular function and fetal Doppler findings, absent or reversed end-diastolic flow in the umbilical artery is associated with lower maternal cardiac output and higher vascular resistance [51] (Fig. 11.3):

11.4 Maternal Cardiovascular Function, Fetal Growth, and Birthweight

The association between maternal cardiovascular changes and fetal growth has classically been studied in athletes or more generally in women who exercised regularly during pregnancy. Only minimal differences in birthweight have been found in women who practised physical activity compared with controls, although neonates born from women who practiced vigorous physical activity in the last trimester of pregnancy were 200–400 g less than in controls [52–54].

Independent from maternal exercise status, recent studies have shown that maternal cardiovascular adaptation to pregnancy in healthy women is associated with fetal size and growth, observing that the increase in cardiac output from prepregnancy to the second trimester is significantly positively associated with both birthweight and second-to-third-trimester fetal growth velocity; reduction in peripheral vascular resistance is also associated with a greater birthweight [55]. This is also supported by the relationship between maternal hemodynamics and uterine artery impedance: a good placental perfusion is related to its function and therefore to fetal growth [37].

These findings raise the prospect of early therapy. In "proof of principle" studies on oral volume loading and administration of vasodilators have been observed to improve material hemodynamic indices in early-onset preeclampsia and fetal growth restriction [56, 57]. Whether these potential therapies could have a meaningful therapeutical impact in pathological pregnancy or at/prior to conception in women found to have abnormal cardiovascular function remains unknown.

References

1. Clapp JF, Capeless E. Cardiovascular function before, during, and after the first and subsequent pregnancies. Am J Cardiol. 1997;80(11):1469–73.
2. Meah VL, Cockcroft JR, Backx K, Shave R, Stöhr EJ. Cardiac output and related haemodynamics during pregnancy: a series of meta-analyses. Heart. 2016;102(7):518–26.
3. Mahendru AA, Everett TR, Wilkinson IB, Lees CC, McEniery CM. A longitudinal study of maternal cardiovascular function from preconception to the postpartum period. J Hypertens. 2014 Apr;32(4):849–56. https://doi.org/10.1097/HJH.0000000000000090.
4. Easterling T, Benedetti T, Schmucker B, Millard S. Maternal hemodynamics in normal and preeclamptic pregnancies: a longitudinal study. Obstet Gynecol. 1990;76(6):1061-106932(4):849-856.
5. Robson SC, Hunter S, Boys RJ, Dunlop W. Serial study of factors influencing changes in cardiac output during human pregnancy. Am J Physiol. 1989;256(4):H1060–5.
6. Masini G, Foo LF, Cornette J, et al. Cardiac output changes from prior to pregnancy to post partum using two non-invasive techniques. Heart. 2019;105(9):715–20.
7. Foo FL, McEniery CM, Lees C, Khalil A. International working group on maternal hemodynamics. Assessment of arterial function in pregnancy: recommendations of the international working group on maternal hemodynamics. Ultrasound Obstet Gynecol. 2017;50(3):324–31.
8. Iacobaeus C, Andolf E, Thorsell M, et al. Longitudinal study of vascular structure and function during normal pregnancy. Ultrasound Obstet Gynecol. 2017;49(1):46–53.
9. Khalil A, Jauniaux E, Cooper D, Harrington K. Pulse wave analysis in normal pregnancy: a prospective longitudinal study. PLoS One. 2009;4(7):–e6134.
10. Mahendru A, Everett T, Wilkinson I, Lees C, McEniery C. Maternal cardiovascular changes from pre-pregnancy to very early pregnancy. J Hypertens. 2012;30(11):2168–72.
11. Poppas A, Shroff SG, Korcarz CE, Hibbard JU, Berger DS, Lindheimer MD, Lang RM. Serial assessment of the cardiovascular system in normal pregnancy. Role of arterial compliance and pulsatile arterial load. Circulation. 1997;95(10):2407–15.
12. Masini G, Foo LF, Tay J, Wilkinson IB, Valensise H, Gyselaers W, Lees CC. Preeclampsia has two phenotypes which require different treatment strategies. Am J Obstet Gynecol. 2022;226(2S):S1006–18. https://doi.org/10.1016/j.ajog.2020.10.052. Epub 2021 Jun 10.
13. Valensise H, Vasapollo B, Gagliardi G, Novelli GP. Early and late preeclampsia: two different maternal hemodynamic states in the latent phase of the disease. Hypertension. 2008;52(5):873–80.
14. Tay J, Foo L, Masini G, et al. Early and late preeclampsia are characterized by high cardiac output, but in the presence of fetal growth restriction, cardiac output is low: insights from a prospective study. Am J Obstet Gynecol. 2018;218(517):e1–12.
15. Melchiorre K, Sutherland GR, Liberati M, Thilaganathan B. Maternal cardiovascular impairment in pregnancies complicated by severe fetal growth restriction. Hypertension. 2012;60(2):437–43.
16. Vasapollo B, Valensise H, Novelli GP, et al. Abnormal maternal cardiac function and morphology in pregnancies complicated by intrauterine fetal growth restriction. Ultrasound Obstet Gynecol. 2002;20:452–7.
17. Gyselaers W, Spaanderman M, International Working Group on Maternal Hemodynamics. Assessment of venous hemodynamics and volume homeostasis during pregnancy: recommendations of the International Working Group on Maternal Hemodynamics. Ultrasound Obstet Gynecol. 2018;52(2):174–85.
18. Melchiorre K, Thilaganathan B. Maternal cardiac function in preeclampsia. Curr Opin Obstet Gynecol. 2011;23:440–7.
19. Perry H, Gutierrez J, Binder J, Thilaganathan B, Khalil A. Maternal arterial stiffness in hypertensive pregnancies with and without a small-for-gestational-age neonate [published online ahead of print, 2019

Oct 15]. Ultrasound Obstet Gynecol. 2019; https://doi.org/10.1002/uog.21893.
20. Franz MB, Burgmann M, Neubauer A, et al. Augmentation index and pulse wave velocity in normotensive and pre-eclamptic pregnancies. Acta Obstet Gynecol Scand. 2013;92(8):960–6.
21. Smith GC, Pell JP, Walsh D. Pregnancy complications and maternal risk of ischaemic heart disease: a retrospective cohort study of 129,290 births. Lancet. 2001;357(9273):2002–6.
22. Duvekot JJ, Cheriex EC, Pieters FA, Peeters LL. Severely impaired fetal growth is preceded by maternal hemodynamic maladaptation in very early pregnancy. Acta Obstet Gynecol Scand. 1995;74:693–7.
23. Foo FL, Mahendru AA, Masini G, Fraser A, Cacciatore S, MacIntyre DA, McEniery CM, Wilkinson IB, Bennett PR, Lees CC. Association between Prepregnancy cardiovascular function and subsequent preeclampsia or fetal growth restriction. Hypertension. 2018;72(2):442–50.
24. Campbell S, Diaz-Recasens J, Griffin DR, et al. New doppler technique for assessing uteroplacental blood flow. Lancet. 1983;1:675–7.
25. Harrington K, Cooper D, Lees C, Hecher K, Campbell S. Doppler ultrasound of the uterine arteries: the importance of bilateral notching in the prediction of pre-eclampsia, placental abruption or delivery of a small-for-gestationalage baby. Ultrasound Obstet Gynecol. 1996;7:182–8.
26. Kuzmina IY, Hubina-Vakulik GI, Burton GJ. Placental morphometry and Doppler flow velocimetry in cases of chronic human fetal hypoxia. Eur J Obstet Gynecol Reprod Biol. 2005;120:139–45.
27. Gallo DM, Wright D, Casanova C, Campanero M, Nicolaides KH. Competing risks model in screening for preeclampsia by maternal factors and biomarkers at 19-24 weeks' gestation. Am J Obstet Gynecol. 2016;214(619):e1–17.
28. Lees C, Parra M, Missfelder-Lobos H, Morgans A, Fletcher O, Nicolaides KH. Individualized risk assessment for adverse pregnancy outcome by uterine artery Doppler at 23 weeks. Obstet Gynecol. 2001;98:369–73.
29. Papageorghiou AT, Yu CK, Bindra R, Pandis G, Nicolaides KH. Multicenter screening for preeclampsia and fetal growth restriction by transvaginal uterine artery Doppler at 23 weeks of gestation. Ultrasound Obstet Gynecol. 2001;18:441–9.
30. Stampalija T, Monasta L, Di Martino DD, et al. The association of first trimester uterine arteries Doppler velocimetry with different clinical phenotypes of hypertensive disorders of pregnancy: a longitudinal study. J Matern Fetal Neonatal Med. 2017:1–9.
31. Rolnik DL, Wright D, Poon LC, et al. Aspirin versus placebo in pregnancies at high risk for preterm preeclampsia. N Engl J Med. 2017;377(7):613–22.
32. Khong TY, De Wolf F, Robertson WB, Brosens I. Inadequate maternal vascular response to placentation in pregnancies complicated by pre-eclampsia and by small-for gestational age infants. BJOG. 1986;93:1049–59.
33. Kingdom JC, Audette MC, Hobson SR, Windrim RC, Morgen E. A placenta clinic approach to the diagnosis and management of fetal growth restriction. Am J Obstet Gynecol. 2018;218(suppl2):S803–17.
34. Fisher SJ. Why is placentation abnormal in preeclampsia? Am J Obstet Gynecol. 2015;213(suppl4):S115–22.
35. Labarrere CA, DiCarlo HL, Bammerlin E, et al. Failure of physiologic transformation of spiral arteries, endothelial and trophoblast cell activation, and acute arthrosis in the basal plate of the placenta. Am J Obstet Gynecol. 2017;216(287):e1–16.
36. Ridder A, Giorgione V, Khalil A, Thilaganathan B. Preeclampsia: the relationship between uterine artery blood flow and trophoblast function. Int J Mol Sci. 2019;20(13):3263.
37. Tay J, Masini G, McEniery CM, Giussani DA, Shaw CJ, Wilkinson IB, Bennett PR, Lees CC. Uterine and fetal placental Doppler indices are associated with maternal cardiovascular function. Am J Obstet Gynecol. 2019;220(1):96.e1–8. https://doi.org/10.1016/j.ajog.2018.09.017. Epub 2018 Sep 19.
38. Everett TR, Lees CC. Beyond the placental bed: placental and systemic determinants of the uterine artery Doppler waveform. Placenta. 2012;33(11):893–901.
39. Skow RJ, Davenport MH, Mottola MF, Davies GA, Poitras VJ, Gray CE, Jaramillo Garcia A, Barrowman N, Meah VL, Slater LG, Adamo KB, Barakat R, Ruchat SM. Effects of prenatal exercise on fetal heart rate, umbilical and uterine blood flow: a systematic review and meta-analysis. Br J Sports Med. 2019;53(2):124–33.
40. Salvesen KÅ, Hem E, Sundgot-Borgen J. Fetal well-being may be compromised during strenuous exercising among pregnant elite athletes. Br J Sports Med. 2012;46(4):279–83.
41. Chaddha V, Simchen MJ, Hornberger LK, Allen VM, Fallah S, Coates AL, Roberts A, Wilkes DL, Schneiderman-Walker J, Jaeggi E, Kingdom JC. Fetal response to maternal exercise in pregnancies with uteroplacental insufficiency. Am J Obstet Gynecol. 2005;193(3 Pt 2):995–9.
42. ACOG Committee Opinion No. 650: physical activity and exercise during pregnancy and the postpartum period. Obstet Gynecol 2015;126(6):e135–42.
43. Allison BJ, Brain KL, Niu Y, et al. Fetal in vivo continuous cardiovascular function during chronic hypoxia. J Physiol. 2016;594:1247–64.
44. Bodelsson G, Marsal K, Stjernquist M. Reduced contractile effect of endothelin-1 and noradrenalin in human umbilical artery from pregnancies with abnormal umbilical artery flow velocity waveforms. Early Hum Dev. 1995;42:15–28.
45. Campbell S, Vyas S, Nicolaides KH. Doppler investigation of the fetal circulation. J Perinat Med. 1991;19:21–6.

46. Hecher K, Bilardo CM, Stigter RH, et al. Monitoring of fetuses with intrauterine growth restriction: a longitudinal study. Ultrasound Obstet Gynecol. 2001;18(6):564–70.
47. Baschat AA, Cosmi E, Bilardo CM, et al. Predictors of neonatal outcome in early-onset placental dysfunction. Obstet Gynecol. 2007;109(2 Pt 1):253–61.
48. Ferrazzi E, Bozzo M, Rigano S, et al. Temporal sequence of abnormal Doppler changes in the peripheral and central circulatory systems of the severely growth-restricted fetus. Ultrasound Obstet Gynecol. 2002;19:140–6.
49. Frusca T, Todros T, Lees C, Bilardo CM, TRUFFLE investigators. Outcome in early-onset fetal growth restriction is best combining computerized fetal heart rate analysis with ductus venosus Doppler: insights from the trial of umbilical and fetal flow in Europe. Am J Obstet Gynecol. 2018;218(suppl 2):S783–9.
50. Karsdorp VH, van Vugt JM, van Geijn HP, et al. Clinical significance of absent or reversed end diastolic velocity waveforms in umbilical artery. Lancet. 1994;344:1664–8.
51. Masini G, Tay J, McEniery CM, Wilkinson IB, Valensise H, Tiralongo GM, Farsetti D, Gyselaers W, Vonck S, Lees CC. Maternal cardiovascular dysfunction is associated with hypoxic cerebral and umbilical Doppler changes. J Clin Med. 2020;9(9):2891. https://doi.org/10.3390/jcm9092891.
52. Kramer MS, McDonald SW. Aerobic exercise for women during pregnancy. Cochrane Database Syst Rev. 2006;(3):CD000180. https://doi.org/10.1002/14651858.CD000180.pub2.
53. Leet T, Flick L. Effect of exercise on birthweight. Clin Obstet Gynecol. 2003;46:423–31.
54. Lokey EA, Tran ZV, Wells CL, Myers BC, Tran AC. Effects of physical exercise on pregnancy utcomes: a metaanalytic review. Med Sci Sports Exerc. 1991;23:1234–9.
55. Mahendru AA, Foo FL, McEniery CM, Everett TR, Wilkinson IB, Lees CC. Change in maternal cardiac output from preconception to mid-pregnancy is associated with birth weight in healthy pregnancies. Ultrasound Obstet Gynecol. 2017;49:78–84.
56. Tiralongo GM, Pisani I, Vasapollo B, Khalil A, Thilaganathan B, Valensise H. Effect of a nitric oxide donor on maternal hemodynamics in fetal growth restriction. Ultrasound Obstet Gynecol. 2018;51(4):514–8. https://doi.org/10.1002/uog.17454.
57. Valensise H, Vasapollo B, Novelli GP, et al. Maternal and fetal hemodynamic effects induced by nitric oxide donors and plasma volume expansion in pregnancies with gestational hypertension complicated by intrauterine growth restriction with absent end-diastolic flow in the umbilical artery. Ultrasound Obstet Gynecol. 2008;31:55–64.

12 Intrauterine Blood Flow and Postnatal Development

David Ley and Karel Maršál

Fetal experience forms the basis for postnatal life. This relationship may be obvious in the newborn infant, although it is sometimes not apparent until later in development. One fetal condition with known implications for later life is fetal growth restriction (FGR), which ranges from being an important factor in perinatal mortality to affecting morbidity in adulthood.

The process of growth, usually measurable as change in anatomical size, is intimately related to that of development, the latter referring to a gradual acquisition of physiological function. Dobbing defined the *brain growth spurt* as that transient period of growth when the brain is growing most rapidly and the period of time when the brain is most susceptible to adverse influence [1]. Fetal malnutrition during the brain growth spurt may reduce the number of synapses per neuron by 40% [2]. Other authors have demonstrated a lower myelin lipid content in the brain of a small-for-gestational age (SGA) newborn as compared to that of an appropriate-for-gestational age (AGA) newborn [3, 4]. In the human, a large part of the brain growth spurt takes place in the years after birth. Therefore, the nutritional as well as the psychosocial environment during the first postnatal years may add to, but equally compensate for, previous adverse influence during fetal development.

D. Ley
Department of Pediatrics, Clinical Sciences Lund, Lund University, Lund, Sweden

K. Maršál (✉)
Department of Obstetrics and Gynecology, Clinical Sciences Lund, Lund University, Lund, Sweden
e-mail: karel.marsal@med.lu.se

12.1 Background

12.1.1 Neurodevelopmental Outcome in FGR

In follow-up studies of FGR, growth restriction has been mainly defined on the basis of gestational age-related birthweight (birthweight SGA). A study group selected on the basis of such a definition will not only include truly growth-restricted infants of various etiologies, but also genetically small but healthy infants. This is probably the main reason why the numerous follow-up studies of SGA infants published in the past did not give a clear answer to the question concerning the effect of FGR on neurodevelopmental outcome. Other major reasons for inconsistent results concerning outcome are the confounding variables associated with impaired fetal growth, perhaps the two most important variables being prematurity at birth and social class. The lower the socioeconomic status of the parents, the higher the chance of delivering an SGA infant, and independent of this, the greater the risk of poor cognitive outcome [5].

D. Maulik, C. C. Lees (eds.), *Doppler Ultrasound in Obstetrics and Gynecology*,
https://doi.org/10.1007/978-3-031-06189-9_12

In prospective studies, SGA infants rarely developed major neurological impairment such as cerebral palsy (CP) and seizures, although Fitzhardinge & Stevens [6] reported an incidence of 7% major neurological sequelae at 4–6 years of age in children born SGA. On the other hand, retrospective studies of children with CP have shown FGR to be an important etiological factor [7].

Several studies have shown an increased frequency of minor neurological dysfunction at early school age [8, 9] and of attention deficit disorder [10] in children born SGA. Ounsted et al. [11] found significantly lower neurobehavioral scores in SGA infants from 2 months up to the age of 1 year. Berg [12] found an increased risk of neurological abnormality at 7 years of age in children born SGA only in the presence of hypoxia-related factors, especially in those children with symmetrical body proportions at birth. A part of the cohort previously studied by Fitzhardinge and Stevens [6] has been examined at a later age; only minor differences were found between those born SGA and those born AGA after the exclusion of subjects with complications related to asphyxia at birth [13].

In the review by Lou [14], an intriguing hypothesis was offered, supported by substantial evidence concerning the perinatal anatomical and biochemical correlates of minor neurological dysfunction and behavioral problems observed in numerous follow-up studies of children in perinatal risk groups. Studies using single photon emission tomography (SPECT) in children with minor neurological abnormalities have shown evidence of hypoperfusion in the striatum (globus pallidus and putamen). The striatum samples information from the entire cortex through spiny neurons, enormously rich in glutaminergic synapses. Repeated asphyxia in fetal sheep causing hypotension and acidosis resulted in neuronal loss primarily in the striatum [15]. The reason for preferential neuron loss in the striatum may partly be due to its localization in an arterial border zone, making it vulnerable in a state of circulatory compromise. Of note, the striatum has also been indicated as a preferential region for altered dopamine metabolism following induced FGR which may relate to the observed dose-dependent relationship between decreased partial oxygen pressure and accelerated dopamin synthesis [16]. FGR is, as previously mentioned, associated with fetal hypoxia and circulatory changes. One may speculate that the increased frequency of minor neurological dysfunction observed in children with FGR may be due to metabolic alterations induced by hypoxic damage in the striatal area.

12.1.2 FGR and Cardiovascular Morbidity

An increasing body of studies have appeared on the relationship between suboptimal fetal growth and morbidity in adulthood. An early study on Swedish male army conscripts suggested that being born SGA may be a predictor of raised blood pressure in early adult life [17]. Epidemiological surveys of men born in Britain during the first three decades of the nineteenth century have shown an inverse relationship between weight at birth and blood pressure in adult age [18]. Morbidity in cardiovascular disease and incidence of non-insulin-dependent diabetes have further been demonstrated to relate to low birthweight [19, 20]. Barker and coworkers have speculated that changes in fetal blood flow and in activities of substances engaged in the regulation of fetal growth such as insulin and insulin-like growth factor I (IGF-I) may permanently affect vessel wall structure and have persisting effects on metabolism [21]. An increased vulnerability to maternal glucocorticoid levels in the growth-restricted fetus has also been suggested as a mechanism that may alter vasoregulatory mechanisms during fetal life and lead to subsequent hypertension [22].

Results from prospective postnatal studies have not been as convincing as those derived from large populations studied retrospectively. No inverse correlation was found between size at birth and blood pressure at 8 years of age in a cohort of 616 prematurely delivered children; on the contrary, blood pressure decreased with decreasing birthweight for gestational age [23]. Williams et al. [24] observed a weak inverse association between blood pressure and birthweight for gestational age in children at 7 years of age, but when the same cohort was analyzed

at 18 years of age the relationship had disappeared. In a Dutch study, a U-shaped relationship was shown between birthweight for gestational age and blood pressure at 4 years of age, implying an increase in blood pressure in children with both low and high birthweight for gestational age [25].

12.2 Postnatal Implications of Abnormal Fetal Blood Flow

In the recent years, it was realized that pregnancies with the early-onset and late-onset of FGR can have different clinical course and outcome and that they might have different phenotypes [26]. The cutoff gestational age between the two has been estimated at 32 gestational weeks [26, 27]. In early-onset FGR, the main challenge for the clinician is the proper timing of delivery when balancing the risks of intrauterine death against postnatal problems of prematurity. Later in pregnancy, when the majority of FGR occurs, the clinical challenge is mainly the detection of FGR rather than the management of those pregnancies. In the postnatal development of fetuses with early-onset FGR, the effects of growth restriction and prematurity often coincide and increase the burden for the infant.

Abnormal flow velocity waveform in the umbilical artery and/or fetal descending aorta has been shown in a large number of studies to be associated with adverse outcome of pregnancy and high perinatal mortality rate [28–30]. A multicenter European study [31] differentiated the outcome according to the presence, absence, or reversal of the end-diastolic flow in the umbilical artery. The odds ratio for perinatal mortality was 4.0 with absent end-diastolic flow and 10.6 with reversed end-diastolic flow when compared to high-risk pregnancies with positive end-diastolic flow in the umbilical artery. The experience from descriptive studies has been used to design randomized controlled trials, which showed that the use of Doppler velocimetry as a method of fetal surveillance in high-risk pregnancies leads to a significant decrease of perinatal mortality [32]. The Doppler method became a method of choice for monitoring fetal health in pregnancies with complications caused by placental dysfunction. The changes of blood velocities recorded from the fetal descending aorta using Doppler ultrasound have been shown to parallel those found in the umbilical artery [33].

With modern ultrasound technique, it is relatively easy to examine fetal vessels such as the middle cerebral artery, ductus venosus, and the intra-abdominal part of umbilical vein. The fetal venous changes occur quite late in the process of intrauterine hypoxia and are recommended to be used in management of very preterm FGR [34]. In hypoxic fetuses, changes in diastolic velocities of the fetal middle cerebral artery reflect the redistribution of fetal blood flow with preferential supply to the brain. It was suggested that the middle cerebral artery pulsatility index (PI) or the ratio between the umbilical artery PI and middle cerebral artery PI might be of clinical use in late-onset FGR, when the umbilical artery Doppler velocimetry is not as informative as earlier in pregnancy [35]. The place of the above Doppler examinations in clinical management of FGR has not yet been finally demonstrated. Similarly, the long-term effects of a proactive perinatal management, in order to prevent superposition of severe hypoxia on the FGR, await evaluation in proper longitudinal studies.

12.2.1 Neonatal Outcome

Several studies have been published on the association between abnormal fetal blood flow and short-term perinatal outcome. Absent or reverse end-diastolic flow (AREDF) in the umbilical artery or fetal descending aorta has been associated with an increased neonatal mortality and increased morbidity in terms of cerebral intraventricular hemorrhage and necrotizing enterocolitis (NEC) [31, 36, 37]. The relationship between abnormal fetal aortic velocities and necrotizing enterocolitis in the neonate is supported by the study by Kempley et al. [38], who found decreased velocities in the superior mesenteric artery in SGA infants who had absent end-diastolic velocities in the aorta during fetal life.

McDonnell et al. [39] performed a case-control study of AREDF, matching for gestational age and pregnancy complications in 61 pairs of infants. They found that AREDF was associated with a higher degree of growth restriction, thrombocytopenia, and NEC. A more recent case-control study of umbilical AREDF, including 36 pairs of infants, matching for the same variables as in the study of Mc Donnell et al. [39] but also for degree of deviation in birthweight, found no differences in outcome except a lower prevalence of ventilator requirement for respiratory distress syndrome in infants with AREDF [40]. In a prospective study of mothers with pregnancy-induced hypertension, Eronen et al. [41] found AREDF in the umbilical artery to be associated with a higher incidence of gastrointestinal complications, bronchopulmonary dysplasia, intraventricular hemorrhage, and vascular hypotension in the newborns. Although the infants with AREDF were delivered at an earlier gestational age, AREDF remained as a predictor of poor perinatal outcome after correction for prematurity. The increased morbidity of infants who showed AREDF in utero was confirmed by other authors with regard to the occurrence of cerebral hemorrhage, anemia, and hypoglycemia [31], as well as chronic lung disease, retinopathy of prematurity, and impaired intestinal motility [42].

Weiss et al. [43] found an increased frequency of abnormal neurological signs in newborn infants with AREDF as compared to a control group, matched for gestational age, with normal umbilical velocity waveforms in the umbilical artery. They found also in fetuses with preceding AREDF a significant increase in the cord blood levels of brain type isoenzyme of creatine kinase (CK-BB) as a possible indication of intrauterine brain cell damage [44]. Rizzo et al. [45] described a decreased fetal cerebrovascular resistance as determined by a decreased PI in the internal carotid artery to be associated with post-asphyxial encephalopathy, as determined by neurological signs, in a cohort of high-risk pregnancies. On the other hand, in a study of 117 infants delivered between 25 and 33 gestational weeks in high-risk pregnancies, no relationship was observed between the ratio of PI in the fetal umbilical and cerebral circulation, and neither cerebral hemorrhage nor neurological abnormality in the neonatal period [46]. However, both Ley and Maršál [47] and Scherjon et al. [48] found a sustained abnormal cerebral blood flow in growth-restricted neonates and preterm neonates who showed signs of brain sparing in utero. It was speculated that this might be due to a different setting of cerebral autoregulation as a consequence of intrauterine redistribution of blood flow.

12.3 Long-Term Neurodevelopmental Implications

An increasing number of long-term follow-up studies of growth-restricted infants has been published during the recent years, thus reflecting the importance of the information on postnatal development when evaluating various perinatal management policies. Still, because of the inherent problems in the execution of longitudinal long-term follow-up studies, current information remains limited due to relatively small numbers of included children/young adults and very few studies providing outcome data beyond 6–8 years of age. (Table 12.1).

12.3.1 Umbilical Artery Blood Flow

Weiss et al. [49] found that the combination of AREDF in the umbilical artery, severe respiratory distress syndrome, and delivery before 28 gestational weeks was predictive of neurological abnormality at 6 months of age. A similar finding of a greater risk of permanent neurologic sequelae at the age of 18 months was reported by Valcamonico et al. [50] for growth-restricted fetuses with AREDF. Abnormal fetal heart rate patterns were shown to be more predictive of poor cognitive outcome at 2 years of age than abnormal waveforms in the umbilical artery in fetuses of high-risk pregnancies delivered before 34 gestational weeks [51]. In a descriptive follow-up study, Wilson et al. [52] found no

Table 12.1 Intrauterine blood flow and postnatal neurodevelopment

Study	Study group			Control group			Follow-up study		
Name, year, [reference]	*N*	Doppler finding	GA at birth (weeks)	*n*	Doppler finding	GA at birth (weeks)	Age	Test	Finding in the study group
Umbilical artery									
Weiss et al. (1992) [49]	37	AREDF	26–40	37	Normal RI	32.4 (3.3)	Up to 6 months	Neurology at discharge	More infants with abnormal neurological evaluation
Todd et al. (1992) [51]	25	Abnormal S/D, c.s.	<34	17 40 67	Normal S/D,c.s. Vaginal delivery	<34 <34 >37	2 years	Denver[a] Bayley-II[b]	Poor cognitive progress, delayed motor development
Wilson et al. (1992) [52]	7 10	Abnormal PI AREDF	32.1	23	Normal	36.6	4–6 years	Neurological exam Denver[a]	No significant differences
Valcamonico et al. (1994) [50]	20	AREDF	~31	26	Positive EDF	~33	1–2 years	Uzgiris & Hunt[c] Militerni[d] Bottos[e]	Greater risk of permanent neurologic sequelae
Kirsten et al. (2000) [53]	31	AEDF	<34 (?)	95	Positive EDF	<34 (?)	Every 6 months up to 4 years	Amiel-Tisson[f] Griffith[g] Snijders-Oomen[h]	No differences in the developmental quotients or motor outcomes; at 2 years lower performance subscale test
Voβbeck et al. (2001) [42]	16	AREDF	27	16	Matched controls (AGA)	27	13–91 months	Lietz[i] Kaufman[j] Bayley-II[b]	Increased risk for mental retardation and severe motor impairment
Wienerroither et al. (2001) [54]	23	AREDF	28–40	23	Matched controls	28–40	6 years (3–8.5 years)	Kaufman[j] Man-drawing test[k] Zürich Neuromotor test[l]	Long-term impairment of intellectual development and partial neurodevelopmental delay
Schreuder et al. (2002) [55]	27 9	AEDF REDF	27–37 27–32	40	Positive EDF	26–38	5–12 years	BAS-II[m] QNST-II[n] SDQ[o] visual function, hearing	AEDF—not associated with adverse neurodevelopmental outcome; REDF—associated with a wide range of problems
Valcamonico et al. (2004) [57]	14	AREDF	31	11	No AREDF (SGA)	33	9 years	WISC-R[p]	Increase in major and minor neurological sequelae; no difference in IQ
Padilla et al. (2010) [59]	45	Increased PI (SGA)	30	46	No Doppler (AGA)	30	1 year	HINE[q] Bayley-II[b]	No difference in neurology or neurodevelopmental performance

(continued)

Table 12.1 (continued)

Study	Study group			Control group			Follow-up study		
Name, year, [reference]	*N*	Doppler finding	GA at birth (weeks)	*n*	Doppler finding	GA at birth (weeks)	Age	Test	Finding in the study group
Morsing et al. (2011) [64]	34	AREDF (SGA, VPT)	27	34 34	Matched controls (AGA, VPT) Matched controls (AGA, term)	27 40	5–8 years	WPPSI-III[r] WISC-III[p] SDQ[o] Brown's ADD[s]	Decreased verbal IQ and full-scale IQ compared with both control groups. No difference between VPT SGA nad VPT AGA in behavior and ADD scales.
Eger et al. (2013) [60]	38	AREDF	24–32	33	No AREDF (SGA)	23–31	5 years	WPPSI-R[r]	AREDF not associated with CP or reduced IQ
Chen et al. (2013) [61]	15	AREDF (SGA, VPT)	31	28 38	Doppler unknown (SGA, VPT) Doppler unknown (AGA, VPT)	31 27	2 years	Bayley-II[b]	No overall differences. At ≤29 weeks, decreased MDI, but not PDI
Llurba et al. (2013) [62]	87	Increased PI or increased ICA PI (SGA)	36	122	Normal (SGA)	37	3 years and 9 years	SBIS[t]	No association with lower developmental scores
Mone et al. (2016) [58]	40	Elevated PI (AGA)	40	110	Normal PI	40	12 years	BAS-II[m], CBCL[u]	Lower scores of declarative memory
Delorme et al. (2020) [56]	179	AREDF	29	305	No AREDF	30	2 years	ASQ[v] Clinical examination	Severe or moderate neuromotor and/or sensory disability. No association with low ASQ score
Morsing et al. (2020) [63]	139	AREDF (SGA, VPT)	26	946	Doppler unknown (VPT)	26	≥2 years	Bayley-II[b] or Bayley-III[b] Clinical examination	Lower survival without neurodevelopmental impairment
Fetal middle cerebral artery and cerebroplacental ratio									
Scherjon et al. (1996) [67]	34	Raised U/C PI ratio	26–33 (med 31 + 5)	56	Normal U/C PI ratio	26-33 (med 29+5)	6 and 12 months	visual evoked potentials	Accelerated neurophysiologic maturaion (beneficial adaptive process)
Scherjon et al. (1998) [69]	34	Raised U/C PI ratio	26–33 (31 + 4)	62	Normal U/C PI ratio	26-33 29+6	3 years	Hempel test[w]	No association with Hempel outcome
Scherjon et al. (2000) [70]	28	Raised U/C PI ratio	26–33 (30 + 6)	45	Normal U/C PI ratio	26-33 29+4	5 years	RAKIT[x]	Fetal brain sparing associated with a poorer cognitive outcome

Kutschera et al. (2002) [72]	16 15	AREDF Abnormal CPR	28–36 27–39	31	Matched AGA	27-39	4.5 years	Denver[a] Kaufman[j] Snijders-Oomen[h]	Impaired cognitive development
Eixarch et al. (2008) [76]	25	Decreased PI UA normal (SGA)	40	100	Normal PI UA normal (SGA)	40	2 years	ASQ[v]	Higher incidence of suboptimal neurodevelopmental outcome
Oros et al. (2010) [75]	70/98 81/98	Decreased PI Decreased ACA, PI UA normal	38	101	No Doppler (AGA)	38	40 weeks PMA	NBAS[y]	Decreased MCA PI associated with increased risk of abnormal neurobehaviour. Decreased ACA PI associated with increased risk of abnormal state organization only.
von Beckerath et al. (2013) [117]	146	Decreased PI or CPR <1 or increased UA PI or AREDF	35	215	Normal Doppler (SGA)	38	2 years	Bayley-III[b] Neurological dysfunction. acc. Touwen[z] Disability acc. Marlow[aa]	Increased risk for neurodevelopmental impairment
Bellido-Gonzáles et al. (2016) [118]	32	Abnormal CPR (SGA)	37	27 61	Normal CPR (SGA) No Doppler (AGA)	37	6–8 years	WISC-IV[p] Woodcock-Munoz test[ab] HOME[ac]	Abnormal CPR associated with deficits in all areas related to cognitive functioning
Fetal aortic isthmus									
Fouron et al. (2001) [77]	5	UA PI >95th centile; Retrograde net isthmic flow	≥29	39	UA PI >95th centile; Antegrade net isthmic flow	2–4 years	Amiel-Tisson[f] Griffith[g]		RR of 2.05 (95% CI 1.49–2.83) for neurodevelopmental deficit
Fetal descending aorta									
Ley et al. (1996) [81]	42	Abnormal BFC (36 AREDF)	29–41	105	Normal BFC (normal aortic PI)	7 years	Touwen[z]		Abnormal BFC was significant predictor of minor neurological dysfunction
Ley et al. (1996) [82]	41	Abnormal BFC (35 AREDF)	29–41	105	Normal BFC (normal aortic PI)	6.5 years	WPPSI[r]		Abnormal BFC was significant predictor of impaired intellectual outcome
Ley et al. (2004) [86]	19	FGR (19 AREDF)	35–41	23	AGA Normal BFC	18 years	Quantitative analysis of ocular fundus photography		Decreased neuroretinal rim area of the optic nerve disc
Martin et al. (2004) [87]	26	FGR (17 AREDF)	34–41	20	AGA Normal BFC	18 years	Rarebit microdot perimetry		Decreased central field vision (lower rarebit hit rate)
Tideman et al. (2007) [84]	19	AREDF	38	23	Normal BFC	18 years	WAIS-III[ad] Wender Utah[ae] School results		Impaired executive cognitive function

(continued)

Table 12.1 (continued)

AEDF Absent end-diastolic flow, *AGA* Appropriate-for-gestational age, *AREDF* Absent or reverse end-diastolic flow, *BFC* Blood flow class, *CI* Confidence interval, *CPR* Cerebroplacental ratio = ratio between the middle cerebral artery and umbilical artery PI, *c.s.* Cesarean section, *EDF* End-diastolic flow, *FGR* Intrauterine growth restriction, *GA* Gestational age, *MDI* Mental developmental index, *PDI* Psychomotor developmental index, *PI*: Pulsatility index, *PMA* Postmenstrual age, *REDF* Reverse end-diastolic flow, *RI* Resistance index, *RR* Risk ratio, *S/D* Systolic-to-diastolic ratio, *SGA* Small-for-gestational age, *UA* Umbilical artery, *U/C PI ratio* Ratio between the umbilical artery and middle cerebral artery PI, *VPT* Very preterm

[a]Denver Developmental Screening Test

[b]Bayley Scales of Infant or Toddler Development; 2nd or 3rd edition

[c]Uzgiris and Hunt's criteria of postural function

[d]Militerni's criteria of sensorial function

[e]Bottos' criteria of cognitive function

[f]motor developmental assessment acc. Amiel-Tisson

[g]Griffith's Mental Developmental Scales

[h]Snijders-Oomen Nonverbal Intelligence Scale for Young Children

[i]standardized neurological examination acc. Lietz

[j]Kaufman Assessment Battery for Children

[k]Man Drawing Test acc. Ziler

[l]Zürich Neuromotor Test acc. Largo and Caflisch

[m]British Ability Scales

[n]Quick Neurological Screening Test

[o]Strength and Difficulties Questionnaire

[p]Wechsler Intelligence Scale for Children, R:Revised, III: 3rd edition

[q]Hammersmith Infant Neurological Examination

[r]Wechsler Preschool and Primary Scale of Intelligence, R:Revised, III: 3rd edition

[s]Brown's Attention-Deficit Disorder scales

[t]Stanford-Binet Intelligence Scale

[u]Achenbach Child Behavioral Checklist

[v]Ages and Stages Questionnaire

[w]Hempel examination of neurological development

[x]Revision of the Amsterdam Children's Intelligence Test

[y]Neonatal Behavioral Assessment Scale

[z]Touwen's examination of the child with minor neurological dysfunction

[aa]Marlow's classification of disability according to the EPICure study

[ab]Bateria III Woodcock-Munoz Test of Achievement

[ac]Home Observation for Measurement of the Environment

[ad]Wechsler Adult Intelligence Scale, 3rd edition

[ae]Wender Utah Rating Scale

association between abnormal umbilical velocity waveforms and major neurological abnormality at 5 years of age. Similarly, in a group of 193 infants born to women with severe preeclampsia, there were no differences between those with and without AREDF in utero, when their neurodevelopmental outcome was evaluated at the age of 2 and 4 years [53]. The only exception was the lower performance subscale test at 24 months in the infants with previous AREDF.

The study by Voβbeck et al. [42] demonstrated that infants with AREDF born before 30 gestational weeks and followed up for between one and 8 years were more often mentally retarded (44% vs. 25%) and had more often severe motor impairment (38% vs. 19%) than the matched controls. Another 5-year prospective follow-up of fetuses with AREDF showed 6 out of 42 infants to be mentally handicapped [29]. A long-term impairment of intellectual capacity and partial neurodevelopmental delay were also observed at school age in 23 infants who have had severely compromised blood flow in utero [54].

In the study by Schreuder et al. [55], the neurodevelopmental outcome at 5–12 years of age was related to the presence (n = 40), absence (n = 27), or reversal (n = 9) of the end-diastolic flow velocity in the umbilical artery. The absence of diastolic flow was not associated with adverse outcome. However, the reversal of end-diastolic flow was associated with a wide range of problems at school age, decreased mental ability, and impaired neuromotor function.

Similarly, in a recent large study by Delorme et al. [56] on very preterm infants delivered because of FGR or maternal preeclampsia (EPIPAGE-2 study), 179 infants with AREDF were compared with 305 infants with positive end-diastolic flow in the umbilical artery. AREDF was associated with severe or moderate neuromotor and/or sensory disability at the age of 2 years. Valcamonico et al. [57] also found an increase in major and minor neurological sequelae at 9 years of age in children who were SGA at birth and had AREDF in utero as compared with children who were SGA without AREDF. There were no differences in the mean intelligence quotient (IQ) between the two groups.

Interestingly, Mone et al. [58] reported in 2016 lower scores of declarative memory at 12 years of age in a group of 40 AGA fetuses with elevated umbilical artery PI when compared with 110 controls with normal PI. No differences were found in overall academic ability, mental processing, and reasoning or overall behavioral function. The authors speculated that a certain degree of placental dysfunction, not influencing the growth of the fetus, might have selectively affected the development of fetal hippocampus and some brain functions.

During the past decade, several case-control follow-up studies did not report neurocognitive impairment in FGR fetuses with AREDF or increased PI in the umbilical artery [59–62]. In these studies, children born both at very preterm and term gestational age were represented, and the age at follow-up examination ranged 1–9 years (Table 12.1). Those results might be explained, at least partly, by the fact that, in modern studies, the clinicians were aware of the results of umbilical artery Doppler examinations, which could have influenced the perinatal management.

12.3.1.1 The Lund-Malmö Study

In longitudinal follow-up studies, we have investigated two cohorts of FGR subjects previously examined during antenatal life with ultrasound measurements of intrauterine blood flow and fetal growth—one cohort comprising fetuses with late-onset FGR (followed up to 25 years of age) and one on very preterm fetuses with early-onset FGR (followed up to 8 years of age). The studies have focused on evaluation of possible effects of FGR with abnormal fetal blood flow on subsequent neurological and cardiovascular development including neural and vascular morphology and function.

Early-Onset FGR Cohort—Background Material

Outcomes of 139 fetuses with early-onset FGR (26% of them twins) delivered before 30 weeks of gestation were retrospectively analyzed [63]. All fetuses had AREDF in the umbilical artery and SGA birthweight. The antenatal data were

prospectively collected over 17 years. A proactive clinical perinatal management protocol based on the Doppler information on intrauterine blood flow was used during the whole time period. There were 7 intrauterine deaths (all before 26 weeks); all liveborn infants were delivered with cesarean section. The outcome of the study group was compared with the clinical data of all AGA infants (n = 946; 28% twins), delivered before 30 gestational weeks and hospitalized at the same period of time at the Perinatal Centre level III and Neonatal Intensive Care Unit in Lund, Sweden [63]. The antenatal Doppler examinations were not performed in the control group. Subsequently, a number of functional and morphological examinations were performed in a subcohort of 34 very preterm SGA infants with AREDF at the age of 6–8 years. The results were compared with those of two matched control groups comprising 34 very preterm AGA infants and 34 AGA infants born at term, respectively [64–67].

Neurological and Cognitive Development

In the overall study on very preterm infants, severe cerebral intraventricular hemorrhage was less frequent in the FGR group with AREDF than in the AGA controls [63]. The survival of liveborn infants at 2 years was similar (83% and 82%, respectively) as was the rate of CP (7% and 8%, respectively). The infants in the AGA group had a higher rate of survival without neurodevelopmental impairment (defined as any of following: CP, severe cognitive impairment, severe hearing impairment, blindness) than those of the FGR group (83% and 62%, respectively). The risk of impairment was highest in the FGR fetuses with AREDF born before 25 gestational weeks. No differences in outcome were found between the singleton and twin fetuses of the FGR group.

In the study on cognitive function at 5–8 years of age, the FGR fetuses with AREDF born at 24–29 gestational weeks had significantly lower mean verbal IQ and full-scale IQ compared with the matched very preterm AGA fetuses [64]. Both preterm groups had lower mean performance IQ and full-scale IQ than the matched term control group. Interestingly, the differences in cognition between the two very preterm groups were restricted to the subgroup of boys with AREDF, suggesting that male fetuses may be especially vulnerable to early-onset FGR.

12.3.2 Fetal Cerebral Blood Flow

In the previously referred to study by Scherjon et al. [46], subsequent assessment of neurological signs at 6 and 12 months of age showed no relationship between the ratio of PI in the fetal umbilical and cerebral circulation and neurological abnormality. A parallel study showed that infants at 6 months of age with a raised umbilical artery/middle cerebral artery PI ratio had shorter visual-evoked potential latencies as compared to infants with a normal ratio [68]. This was interpreted as a sign of accelerated neurophysiological maturation, being of benefit to the fetus. At the age of 3 years, adverse neurodevelopment, as evaluated by Hempel examination in a subgroup of 96 infants from the original cohort, was mainly related to neonatal cranial ultrasound abnormality rather than to signs of brain sparing in utero [69]. Seventy-three of the children were subsequently examined at the age of 5 years; the mean IQ score was significantly lower in children born with signs of brain sparing, i.e., with a raised umbilical artery/middle cerebral artery PI ratio, than in those with normal intrauterine blood flow [70]. This led the authors to revise their previous interpretation of fetal brain sparing acting as a beneficial adaptive mechanism.

Chan et al. [71] used the ratio of resistance indices in the umbilical and cerebral circulation of high-risk fetuses and did not find any association with major neurological handicap at 2 years of age. Ratio of middle cerebral artery PI and umbilical artery PI (cerebroplacental ratio; CPR) was used by Kutschera et al. [72] to characterize the intrauterine blood flow. At the age of 3–6 years, they did not find any difference in the cognitive, neurological, and somatic development between the group with abnormal CPR and the group with AREDF in the umbilical artery. However, both groups showed impaired cognitive development as compared to controls.

The Barcelona research group systematically studied term SGA fetuses with normal umbilical artery PI and decreased middle cerebral artery PI. The studies followed on two reports by their group on term SGA fetuses with normal umbilical artery PI and cerebral blood flow unknown; at 40 weeks' corrected age, the infants had poorer neurobehavioral competencies [73] and, at 2 years of age, they exhibited lower performance results in problem solving and personal-social areas [74]. Oros et al. [75] evaluated the neonatal neurobehavior at 40 weeks of corrected age in SGA fetuses with normal umbilical artery PI and signs of cerebral blood flow redistribution in comparison with term AGA control infants. The SGA infants with decreased middle cerebral artery PI had increased risk for abnormal neurobehavioral performance in motor and state organization areas. The SGA infants with decreased PI in the anterior cerebral artery had abnormal performance in state organization only. Eixarch et al. [76] examined a corresponding group of SGA infants at 2 years of age and found a higher incidence of suboptimal neurodevelopmental outcome (24-month Age & Stage Questionnaire results below mean-1SD) when there was a combination of normal umbilical artery PI and decreased middle cerebral artery PI as compared to SGA controls with normal Doppler findings in both vessels.

The collected evidence this far, from relatively few follow-up studies, suggests the redistribution of blood flow in FGR to be associated with suboptimal postnatal neurodevelopment. Thus, the increased cerebral blood flow, potentially beneficial during fetal life, is not necessarily beneficial for the developing brain when it exceeds certain level.

Changes in the diastolic flow recorded from the aortic isthmus of FGR fetuses were described to reflect an early redistribution of fetal blood flow with increased flow to the fetal head. Fouron et al. [77] followed up a group of 44 fetuses with abnormal umbilical artery Doppler velocimetry and related their neurodevelopmental condition at 2–4 years of age to the flow patterns in the fetal aortic isthmus. All five fetuses with a net retrograde isthmic flow had nonoptimal neurodevelopment. This finding seems to support the previous conclusion by the authors that the Doppler examination of the aortic isthmus flow pattern in utero might identify fetuses with impending cerebral hypoxia [78].

12.3.3 Fetal Aortic Blood Flow

12.3.3.1 The Lund-Malmö Study

Late-Onset FGR Cohort—Background Material

In a longitudinal prospective study, serial fetal blood flow velocity examinations and measurements of fetal growth using ultrasound and Doppler velocimetry were performed in 178 pregnancies during a three-year period, 1982–1985, at the Department of Obstetrics and Gynecology in Malmö [79, 80]. The blood flow velocity waveform in the fetal descending aorta was transformed into a semiquantitative variable, blood flow class (BFC), four BFCs being defined to describe the appearance of the waveform, with emphasis on its diastolic part. These classes were as follows: BFC 0 (normal), positive flow throughout the heart cycle and a normal PI; BFC I, positive flow throughout the cycle and a PI ≥mean + 2 SD and <mean + 3 SD of normal; BFC II, PI ≥mean + 3 SD of normal; and BFC III, absence of positive flow throughout the major part of the diastole and/or reverse flow in diastole, i.e., AREDF. Fetal aortic BFC was defined according to the result of the last measurement performed before delivery. Seventy-four infants had birthweight ≥2 SD below the mean of the normal population, i.e., they were SGA. In three cases, the fetus died in utero. The clinicians managing the pregnancies were not informed of the results of Doppler examination.

Neurological and Cognitive Development at 7 Years of Age

At the age of 6.5–7 years, 149 children underwent an intellectual evaluation and neurological examination [81, 82]. Special emphasis was put on minor neurological dysfunction (MND) according to Touwen [83]. According to the num-

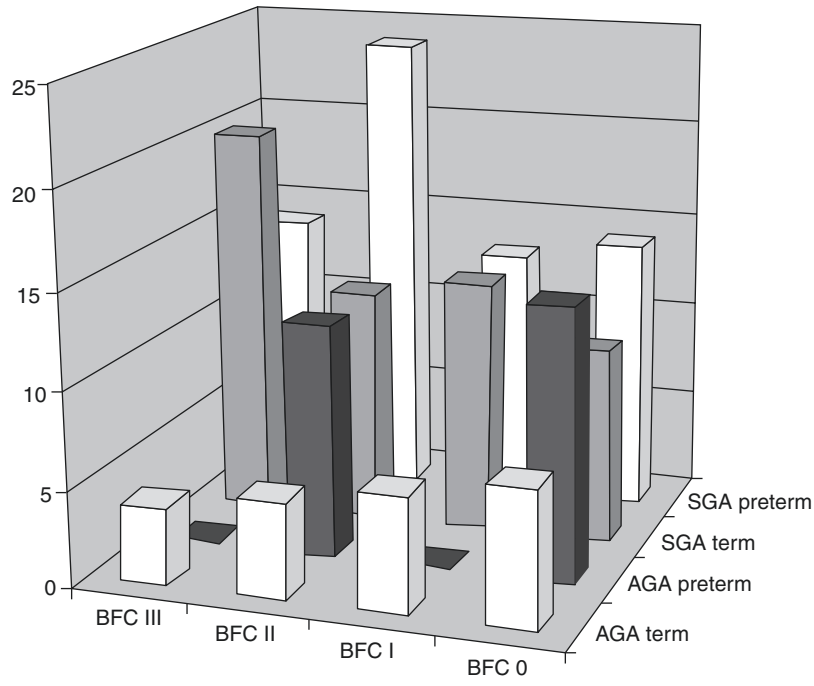

Fig. 12.1 Neurological score at 6 years of age in relation to fetal aortic blood flow class (BFC), gestational age at birth, and birthweight for gestational age. Higher score indicates increasing deviation from optimality. (From Marsal K and Ley D [119])

ber of deviant subsystems of the total of 6, the result of the neurological examination was classified as normal, MND-1 (1–2 deviant subsystems), or MND-2 (>2 deviant subsystems). The intellectual development was evaluated using a standardized intelligence test, WPPSI (Wechsler Preschool and Primary Scale of Intelligence).

The frequency of the more severe form of MND, MND-2, was significantly higher in the BFC III group than in the group with BFC 0 (normal) (Fig. 12.1) [81]. The frequency of MND-1 was higher in the BFC II group than in the group with BFC 0. When compared with the BFC 0 group, the group of children with BFC III deviated more frequently in three neurological subsystems—coordination and balance, dyskinesia, and fine motor ability.

The group with abnormal fetal BFC had lower mean verbal IQ and global IQ as compared to the group with normal fetal BFC [82]. The groups did not differ significantly in performance IQ. The largest discrepancies between groups were found in the subtests information, comprehension, and arithmetic. In multivariate analysis that included independent ante- and postnatal variables, interval complications occurring during postnatal life, and a social-economic variable, MND-1 was best predicted by the combination of increasing birthweight deviation and male sex, whereas the best combination of variables contributing significantly to MND-2 was abnormal BFC and male sex. Global IQ ≤85 was best predicted by abnormal BFC, fetal gestational age at measurement, and social group. Fetal gestational age at measurement was present as an additional risk factor, due to interaction with BFC. When the last BFC measurement was normal and performed after 37 gestational weeks of pregnancy, only one child out of forty had a global IQ ≤85. The dichotomous variable SGA/AGA showed no association with any of the intellectual outcome variables.

The association found between an abnormal fetal aortic waveform and unfavorable neurodevelopmental outcome, which remained after adjustment for other confounding variables, may be attributed to fetal hypoxia. The fetal aortic velocity waveform reflects conditions both in the peripheral fetal circulation and in the placental circulation. The hemodynamic mechanism responsible for the abnormal waveform may therefore be reduced peripheral blood supply due to hypoxia or increased impedance of the placental circulation, or both.

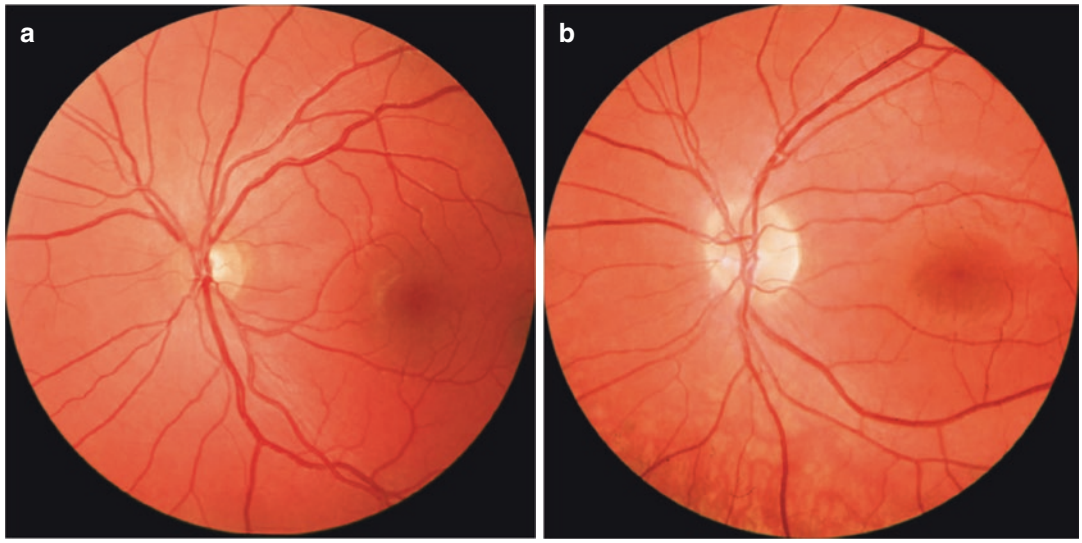

Fig. 12.2 (**a**) Ocular fundus photography showing a reduced neuroretinal rim area of the optic nerve in an 18-year old male subject with a SGA birthweight and reverse diastolic flow in fetal descending aorta (BFC III). (**b**) Neuroretinal rim area of the optic nerve in a 18-year old male subject with normal fetal growth and normal fetal aortic blood flow. (From Ley et al. [86])

Cognitive Outcome at 18 Years of Age

We continued the prospective follow-up study on a subgroup of the previously described cohort. A total of fifty-one subjects were examined at a median age of 18 years [84]. Twenty-eight of the subjects were SGA at birth with a median deviation of weight at birth of −31% (range −42 to −22%) from the gestational age-related mean. Nine subjects had BFC III, ten subjects had BFC II, two subjects had BFC I, and seven subjects had a normal BFC. The remaining 23 subjects had normal aortic BFC and an AGA weight at birth. Both groups were delivered at or close to term; their median gestational age at birth was 39 and 40 weeks, respectively.

At 18 years of age, a psychologist evaluated the cognitive capacity using the Wechsler Adult Intelligence Scale (WAIS). The SGA subjects had a lower performance IQ as compared to those with birthweight AGA, but did not differ significantly in verbal IQ [84]. Fetal aortic blood flow class was not related to global IQ. However, the subjects with BFC II and III had a lower Processing Speed Index as compared to those with BFC 0 and I. The Processing Speed Index measures fine motor ability, visual and working memory, and psychomotor speed. We found a high correlation between cognitive test results at 6 years and those at 18 years of age [85]. Interestingly, the correlation between test results at the respective ages was higher for the SGA group. The results suggest that cognitive level at 6 years of age as determined by a standardized IQ test is more predictive of cognitive level at 18 years of age in subjects with FGR than in those with normal fetal growth and birthweight. A retrospective assessment of attention-deficit hyperactivity disorder (ADHD) showed that the rate of ADHD was increased in the SGA group. These subjects had low IQ scores at both 6 and 18 years of age and also reported more psychiatric symptoms at 18 years. Although the majority of subjects with FGR had IQ score within the normal range at 18 years of age, we found an increased rate of individuals with multiple impairments, i.e., ADHD, decreased cognitive capacity, and emotional disturbance [84].

Retinal Neural Morphology and Function

At 18 years of age, visual function was evaluated in all subjects including fundus photography [86]. Quantitative analysis of fundus photographs, utilizing a computer-assisted digital mapping system, evaluated two outcome measures: (1) The neuroretinal rim area as a measure of the optic nerve central nervous tissue (Fig. 12.2); (2)

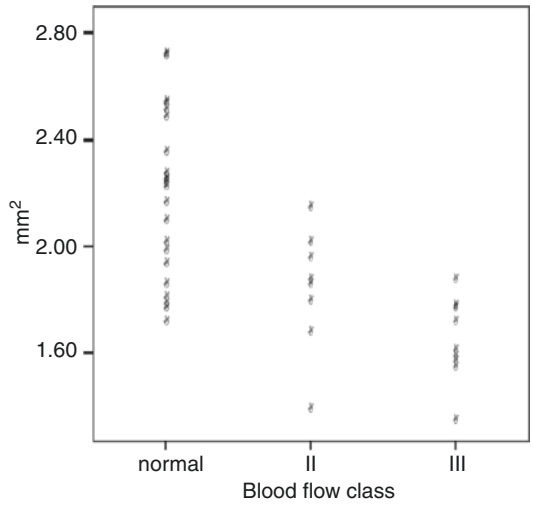

Fig. 12.3 Relationship between neuroretinal rim area of the optic nerve examined at 18 years of age and fetal aortic blood flow class (BFC). BFC III corresponds to absent or reverse flow in diastole. (From Ley et al. [86])

The number of branching points of retinal arterioles and venules as a measure of vascularization. The mean of the measurements from the two eyes in one subject represented the value of each ocular fundus variable. Visual function was assessed by using Rarebit perimetry measuring central field vision [87].

We found that a more pronounced negative birthweight deviation was associated with a decrease in neuroretinal rim area [86]. The subjects with fetal aortic BFC III had a significantly reduced neuroretinal rim area (median 1.59 mm^2) as compared to those with fetal aortic BFC II (1.85 mm^2) and to those with normal fetal aortic BFC (2.22 mm^2) (Fig. 12.3). These findings indicate that FGR is associated with a reduced axonal area in the optic nerve at young adult age. Degree of deviation in weight at birth and extent of fetal blood flow velocity abnormality were both associated with an increased reduction of the axonal area of the optic nerve. The observed reduction in axonal area may reflect either reduced axonal growth with a reduction of axonal volume or a decrease in the number of axons, i.e., in the number of neurons.

It can be speculated whether the observed reduction in axonal area is restricted to the optic nerve tract or represents a more global affection of neuronal growth within the brain. We found a strong association between MND at 6 years of age and a reduced axonal area suggesting that other regions of the central nervous system might be affected. The subjects with severe MND at 6 years of age had among other deviations consistent abnormalities in test items measuring coordination and balance suggestive of changes in the cerebellum or basal ganglia [81]. Experimental studies on induced fetal growth restriction during late pregnancy in guinea pigs and fetal sheep have shown a reduction in volume of cerebellar layers and in the number of Purkinje neurons in the cerebellum [88, 89].

Fetal hypoxia as well as fetal malnutrition may be considered as plausible cause for the observed reduction in axonal area of the optic nerve. Fetal malnutrition during FGR may be an important factor in disturbing cellular growth and differentiation in the central nervous system. Trophic factors such as insulin-like growth factor 1 (IGF-I) are essential for cellular growth and differentiation as well as for tissue repair after a damaging insult. Undernutrition in humans and in experimental animals decreases IGF-I expression in many tissues and in the circulation [90–92]. Circulatory levels of IGF-I have been shown to be decreased in SGA fetuses and in fetuses with abnormal blood flow velocity [93, 94].

In our study at 18 years of age, the central field vision, as represented by the Rarebit mean hit rate [87], ranged from 93% to100% in AGA subjects and from 48% to 100% in those with birthweight SGA with the median hit rate being significantly lower in the SGA group as compared to that in the AGA group. Eight of the SGA subjects and none of the controls had a hit rate below the normal range. The deviant hit rates may reflect defects in the matrix of detectors, i.e., the neural channels, and may be caused by disturbed axonal growth or development. This finding of abnormal function lends support to the previously mentioned morphological finding of reduced neuroretinal rim area in subjects with FGR.

12.4 Postnatal Brain Morphology

The advent of improved technologies in magnetic resonance imaging (MRI) increased both the clinical and research interest in brain examinations in neonates and children. During the past decade, several reports were published on relationships between brain morphology evaluated with MRI and FGR with intrauterine blood flow changes (Table 12.2). Esteban et al. [95] performed MRI volumetry of the total brain, gray matter (GM), and white matter (WM) at 1 year of age in a group of moderately preterm SGA infants with abnormal umbilical artery blood flow. They did not find any differences in the brain volumes in comparison with two control groups, preterm AGA infants and term AGA infants, respectively. However, when the authors applied 3D fractal dimension measuring topical complexity, they found

Table 12.2 Intrauterine blood flow and postnatal brain morphology examined with magnetic resonance imaging

Study	Study group			Control group			Follow-up MRI study		
Name, year, [reference]	*n*	Doppler finding	GA at birth (weeks)	*n*	Doppler finding	GA at birth (weeks)	Age	MRI method/ variable	Finding in the study group
Esteban et al. (2010) [95]	18	AREDF or increased UA PI (preterm SGA)	32	15 15	No Doppler (preterm AGA) No Doppler (term AGA)	31 40	1 year	3D fractal dimension (FD)	Decreased FD of the GM and WM. Significant regression of the language and motor Bayley scales with the FD of the GM.
Padilla et al. (2011) [96]	18	Increased UA PI (preterm SGA)	32	15 15	No Doppler (preterm AGA) No Doppler (term AGA)	31 40	1 year	Lobar volumetry Voxel-based morphometry	Reduced volumes of the insular and temporal lobes. Decreased GM in several regions. Increased WM in temporal regions; decreased WM in cerebellum. Decreased Bayley scores correlated with GM.
Padilla et al. (2014) [97]	20	Increased UA PI (preterm SGA)	31	20 20	No Doppler, matched (preterm AGA) Matched (term AGA)	30 40	1 year	GM volumetry WM—tract-based spatial statistics	Differential effect on WM (increased fractional anisotropy and axial diffusivity) and GM (specific set of structural decrements)
Morsing et al. (2018) [67]	23	AREDF (VPT SGA)	26	24 27	No Doppler (VPT AGA) No Doppler (term AGA)	27 40	5–8 years	Volumetry	No differences in volumes between VPT FGR and VPT AGA. Cognitive impairment not related to brain volumes.

3D Three dimensional; *AGA* Appropriate-for-gestational age, *AREDF* Absent or reverse end-diastolic flow, *FD* Fractal dimension, *GA* Gestational age, *GM* Gray matter, *MRI* Magnetic rtesonance imaging, *PI* Pulsatility index, *SGA* Small-for-gestational age, *UA* Umbilical artery, *VPT* Very preterm, *WM* White matter

decreased fractal dimension of the brain GM and WM in the preterm FGR group as compared with the two control groups. There was a significant association between the GM fractal dimension and the language and motor Bayley scales.

In a subsequent report on lobar MRI volumetry and voxel-based morphometry in the same cohort of children, the Barcelona group observed reduced relative volumes of the insular and temporal lobes in the preterm FGR group [96]. Both preterm groups had bilaterally decreased GM in several brain regions and increased WM in temporal region. In comparison with the term AGA controls, the preterm FGR group had increased WM in several brain regions and decreased WM in the cerebellum. The decreased Bayley scores correlated well with GM volumes. The authors concluded that FGR induces specific structural brain changes that persist at 1 year of age. This was supported by another study in a different cohort of preterm FGR fetuses and two corresponding control groups [97]. GM volumes were estimated using voxel-based morphometry and the WM was examined with track-based spatial statistics. Decrease in GM volume correlated exclusively with birthweight, i.e., with the degree of FGR. The WM showed a different and unusual pattern; the authors concluded that the development of WM was affected by the FGR and prematurity in combination.

A subcohort of the Lund-Malmö early-onset FGR children described above underwent MRI volumetry at the age of 5–8 years (Fig. 12.4) [67]. In contrast to other studies performed at toddler age, WM and GM volumes of very preterm FGR children actively delivered because of AREDF did not differ from those of very preterm AGA children matched for degree of prematurity and gender. The degree of growth restriction at birth correlated with reduction of hippocampal volume. Degree of cognitive impairment, which was more pronounced in the preterm FGR group than in the preterm AGA group, was not associated with brain volumes as determined by MRI. In summary, degree of prematurity at birth had a pronounced effect on regional brain volumes at preschool age which potentially obscured the ability to detect consequences of early FGR on brain growth. Inclusion of extremely preterm infants with severe postnatal growth restriction in conjunction with other major postnatal morbidities limits the possibility of detecting additional effects caused by FGR. Therefore, studies aiming to discriminate effects of early FGR from those of postnatal morbidities following extremely preterm birth will require sufficient sample sizes and MRI-determined outcomes with a high spatial and functional resolution. Application of recently developed diffusion techniques and assessment of functional connectivity may enable a discrimination of effects caused by early FGR from those of extremely preterm birth on brain development.

12.5 Cardiovascular Morphology and Function

The circulatory changes in FGR are to be seen as an adaptive response of the fetus helping it to survive the hostile intrauterine environment with undernutrition and hypoxia. This adaptation is positive, at least initially, for the FGR fetus; however, it can lead to permanent changes in the cardiovascular system like altered vascular growth and endothelial function. If the phenotype of the FGR fetus is mismatched to the postnatal environment, long-lasting effects on future health can occur. Epigenetic mechanisms play important roles in such a process, frequently referred to as the developmental origin of health and disease. Some of the fetal cardiovascular changes in FGR can be identified already in utero, e.g., Doppler signs of flow redistribution, abnormal ventriculovascular interaction [98], cardiac morphologic changes [99], or changes in the vascular function [100]. So far, only few long-term follow-up studies examined the possible associations between the intrauterine hemodynamics characterizing FGR and postnatal cardiovascular development (Table 12.3).

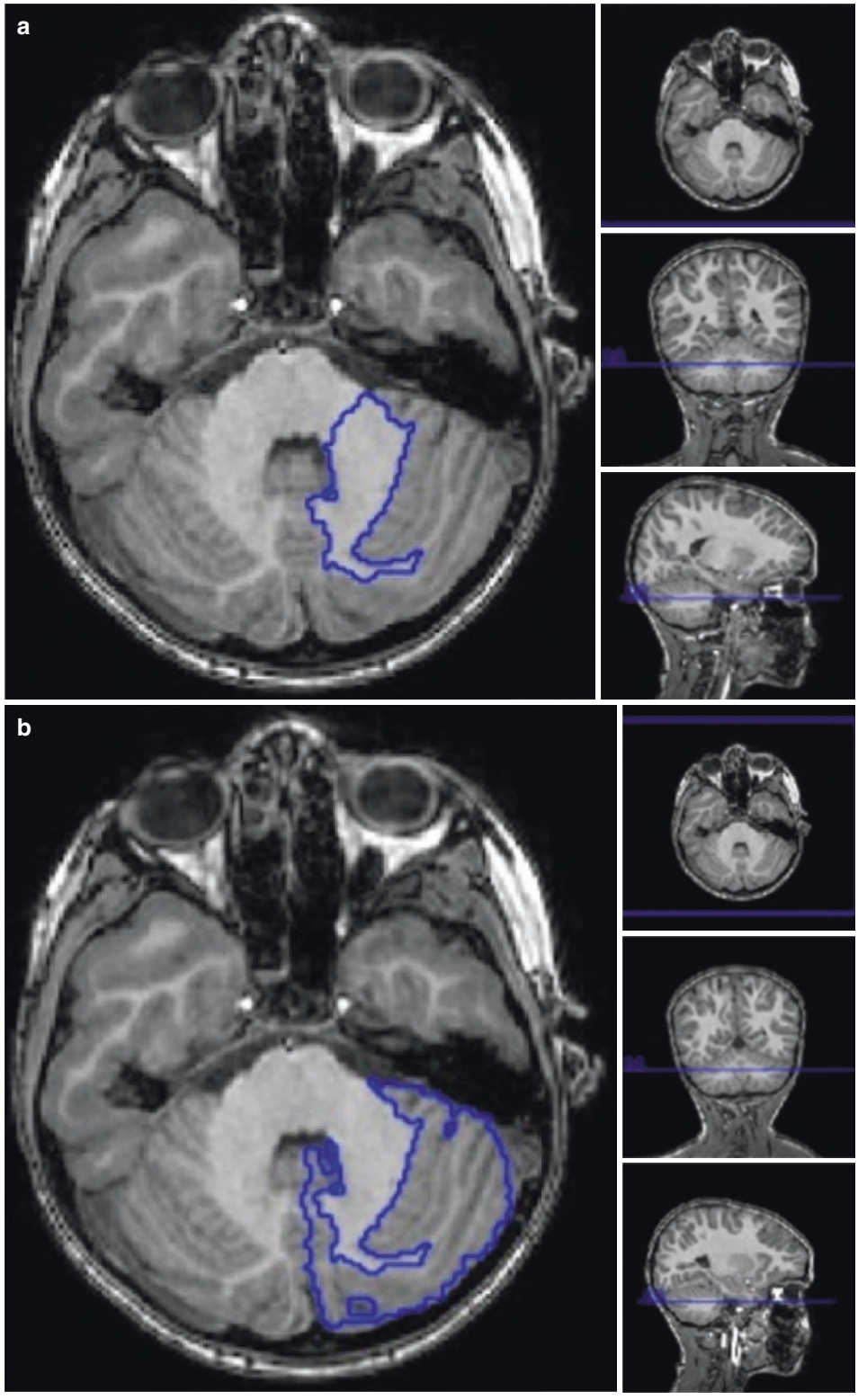

Fig. 12.4 Magnetic resonance imaging brain volumetry. The two screen shots illustrate the segmentation and delineation of cerebellar white (**a**) and gray (**b**) matter in an axial slice through the cerebellum of a 7-year old child

Table 12.3 Intrauterine blood flow and postnatal cardiovascular development

Study	Study group			Control group			Follow-up study		
Name, year, [reference]	*n*	Doppler finding	GA at birth (weeks)	*n*	Doppler finding	GA at birth (weeks)	Age	Test	Finding in the study group
Umbilical artery									
Morsing et al. (2014) [66]	32	AREDF (SGA, VPT)	27	32 32	Matched controls (AGA, VPT) Matched controls (AGA, term)	27 40	7 years	Echocardiography; echo-tracking sonography; carotid art. intima-media thickness; laser Doppler; blood pressure	Decreased aortic stiffness and carotid intima-media thickness. Increased systolic blood pressure. No difference in cardiac function and size.
Fetal descending aorta									
Hellström et al. (2004) [109]	25	AREDF	39	23	Normal	40	18 years	Digital image analysis of retinal vessels	Abnormal retinal vessel morphology.
Brodszki et al. (2005) [108]	21	AREDF	39	23	Normal	40	18 years	Echo-tracking sonography Vasodilation brachial art.	Decreased diameters of abdominal aorta and a. poplitea. Increased rest heart rate. No difference in endothelial function.
Bjarnegård et al. (2013) [112]	19	AREDF	39	18	Normal	40	22–25 years	Echocardiography; carotid art. intima-media thickness; laser Doppler flowmetry; aplanation tonometry; blood pressure	Decreased diameter of ascending aorta. Increased aortic pressure augmentation index. No differences in blood pressure, intima-media thickness, and endothelial function
Fetal middle cerebral artery and cerebroplacental ratio									
Crispi et al. (2010) [113]	80	Raised UA PI; decreased MCA PI	30–40	120	Normal	38	5 years	Echocardiography Carotid art. intima-media thickness Blood pressure	Heart: more globular shape and increased transversal diameters. Subclinical systolic and diastolic dysfunction. Increased carotid intima-media thickness. Increased blood pressure.

Crispi et al. (2012) [114]	25	Decreased CPR (SGA)	39	25 100	Normal CPR (SGA) Normal CPR (AGA)	39 39	3–6 years	Echocardiography Carotid art. intima-media thickness Blood pressure	More globular hearts and reduced longitudinal motion. Increased carotid intima-media thickness. Increased blood pressure.
Cruz-Lemini et al. (2014) [116]	100	Decreased CPR; increased aortic isthmus PI (SGA)	37	100	Normal (AGA)	40	6.5 months	Aortic intima-media thickness; Echocardiography; Tissue Doppler; Blood pressure	Increased aortic intima-media thickness. Increased blood pressure.
Stergiotou et al. (2014) [115]	32	Decreased CPR and/or increased a.uterina PI (SGA)	39	35 134	Normal Doppler (SGA) No Doppler (AGA)	39 40	Neonatal within 1 week	Abdominal aortic and carotid art. intima-media thickness Blood pressure	Increased intima-media thickness in SGA disregarding the Doppler findings.

AGA Appropriate-for-gestational age, *AREDF* Absent or reverse end-diastolic flow, *CPR* Cerebroplacental ratio = ratio between the middle cerebral artery and umbilical artery PI, *GA* Gestational age, *MCA* Middle cerebral artery, *PI* Pulsatility index, *SGA* Small-for-gestational age, *UA* Umbilical artery, *VPT* Very preterm

12.5.1 Umbilical Artery Blood Flow

12.5.1.1 The Lund-Malmö Study

Early-Onset FGR Cohort

The cardiovascular function of 32 children from the cohort of very preterm early-onset FGR cohort described above was examined at the age of 7 years and the results were compared with those of matched control groups of very preterm and term born AGA children [66]. The preterm FGR children with AREDF in utero had lower microvascular response to acetylcholine, lower aortic stiffness, and higher aortic distensibility than the preterm AGA children. The carotid intima-media thickness was decreased compared to the term AGA children. Echocardiography did not reveal any differences in cardiac function and size between the three groups. Systolic blood pressure was higher in both FGR and AGA preterm children than in AGA children born at term. The latter finding suggests that prematurity rather than FGR is associated with increased blood pressure. In the literature, also in very large registry studies, no clear answer is given whether the fetal smallness [101] or prematurity [102] is the most important factor for development of hypertension in adult life.

12.5.2 Fetal Aortic Blood Flow

12.5.2.1 The Lund-Malmö Study

Late-Onset FGR Cohort

With an electronic phase-locked echo-tracking system [103], we examined the diameter changes in descending aorta of a subgroup of 68 children from the original Malmö cohort described above [104]. Neither abnormal fetal aortic blood flow nor birthweight deviation was reflected in any significant changes in elastic modulus or stiffness of the abdominal aorta at 9 years of age. Within the examined group, the subjects with the highest body weight at the time of examination had the highest levels of systolic blood pressure. There was no evidence of an increase in diastolic blood pressure related to restricted fetal growth; on the contrary, FGR was associated with lower diastolic blood pressure. As the influence of the increased resistance to fetal blood flow caused by the abnormal placenta in FGR will cease to exist after birth, it would seem plausible that the postulated compensatory increase in blood pressure during the fetal period would no longer be present in childhood. The present results support the hypothesis that the possible link between fetal growth failure and high blood pressure in adult life may mainly be expressed among those with obesity.

Children born SGA had significantly lower vessel diameters than those born AGA and these differences remained significant after adjustment for body surface area [104]. Pulse pressure was significantly higher within the group of children born SGA than in those born AGA. An increase in pulse pressure has previously been described in SGA infants at 6 weeks of age [105] and has been associated with signs of low arterial compliance and hypertensive disease in adults [106]. However, we were unable to detect any corresponding changes in aortic compliance in association with either abnormal fetal aortic blood flow or SGA birthweight. A previous study of human aortic compliance and its normal variation with age found a profound increase in compliance between 4 and 11 years of age [107]. Aortic compliance thereafter exhibited a gradual decrease with values beyond sixteen years being similar to those of healthy adults. This may imply that changes in aortic vessel compliance due to fetal causes may be detectable at a later age when aortic compliance decreases due to the normal aging process. The increase in pulse pressure observed in the SGA group [104] might suggest, in the absence of changes in elastic modulus and stiffness of the abdominal aorta, the possibility of corresponding changes in more peripheral segments of the arterial tree.

At 18 years of age, vascular mechanical properties of the common carotid artery, abdominal aorta, and popliteal artery were assessed by echo-tracking sonography in 21 adolescents with FGR and abnormal fetal aortic blood flow and in 23 adolescents with normal fetal growth and normal fetal aortic blood flow [108]. Endothelium-

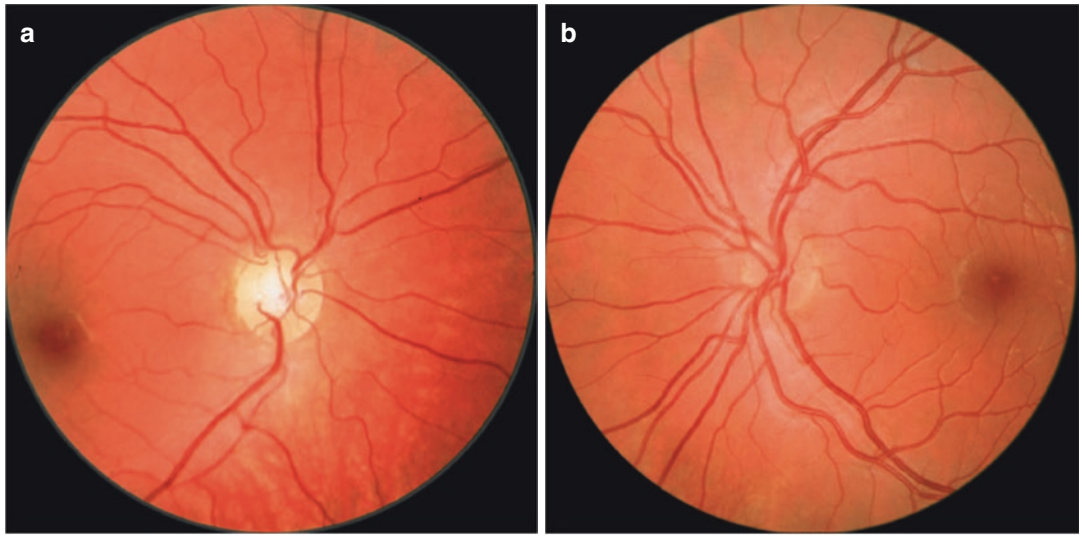

Fig. 12.5 (**a**) Ocular fundus photography demonstrating a reduced number of retinal vessel branching points in an 18-year old female with a SGA birthweight and abnormal fetal aortic blood flow (BFC III). (**b**) Ocular fundus photography with a normal number of retinal vessel branching points in an 18-year old female with normal fetal growth and normal fetal aortic blood flow. (From Hellström et al. [109])

dependent and -independent vasodilatation of the brachial artery was measured by high-resolution ultrasound. Compared to controls, the FGR group had significantly smaller mean vessel diameters in the aorta and popliteal artery in proportion to the body size. Stiffness in all three vascular regions was comparable between the two groups. Resting heart rate was increased in the FGR group. Smaller aortic dimensions and minor functional deviations seen in adolescents with previous FGR may influence the future cardiovascular health of these individuals. Sustained flow-mediated vasodilatation may indicate an increased synthesis of nitric oxide in response to forearm occlusion.

In the same cohort, we examined the retinal vascular morphology at 18 years of age and found that increasing negative birthweight deviation was associated with a decrease in the number of retinal vascular branching points ($p = 0.02$) (Fig. 12.5) [109]. Neither age at examination, gender, nor the degree of abnormal fetal blood flow was associated with the number of retinal vessel branching points. It is unclear whether the finding of reduced vessel branching points in FGR subjects is restricted to the retina or whether it reflects a more general affection of vascular growth within the body. A previous study in FGR rats induced by protein restriction has shown reduced vasculature in the cerebral cortex [110]. Our findings of a reduced size of large arteries in subjects with FGR detected at 9 and 19 years of age and that of a reduced number of branches in the retinal vasculature support a general affection of angiogenesis. Others have shown signs of impaired endothelial function in small and large arteries in school children born SGA [111]. These findings of functional and morphological deficits may contribute to a better understanding of the link between restricted fetal growth and cardiovascular disease.

After another 4–7 years, additional cardiovascular examinations were performed in the young adults belonging to the Lund-Malmö late-onset FGR cohort [112]. Blood pressure did not differ between the FGR group and control group; however, the FGR individuals had increased aortic systolic pressure augmentation index. The diameter of the ascending aorta was smaller in the FGR group. In the common carotid artery, the vessel diameter, distensibility, and the intima-media thickness did not differ between the two groups. The left ventricular mass and function did not differ either. The results suggest that the

changes in aortic blood flow of FGR fetuses might have induced minor, however, irreversible vascular changes that might lead to negative consequences for future cardiovascular health.

12.5.3 Fetal Cerebral Blood Flow

Several postnatal cardiovascular studies were performed by the Barcelona research group on FGR fetuses with signs of redistribution of flow. In two studies, Crispi and coworkers found the heart of children who were growth-restricted in utero with signs of increased cerebral blood flow (decreased middle cerebral artery PI or decreased CPR) to have a more globular shape at preschool age, at 5 years and 3–6 years, respectively [113, 114]. Similar remodeling with globular shape of the heart in FGR fetuses could be identified already in utero [99]. In the follow-up studies, the authors also found increased transversal heart diameters, reduced longitudinal motion, and signs of subclinical systolic and diastolic dysfunction. In both studies, the growth-restricted children had increased blood pressure and carotid intima-media thickness [113, 114].

Intima-media thickness of the proximal abdominal aorta and carotid artery was measured within 1 week after birth in term SGA fetuses with signs of severe FGR (fetal weight <3rd percentile or increased mean uterine artery PI or decreased CPR) [115]. The control groups comprised SGA infants with normal intrauterine hemodynamics and term AGA infants, respectively. Blood pressure was not significantly different between the three groups. Vascular intima-media thickness was increased in SGA infants irrespective of their intrauterine Doppler findings. These results might be interpreted as questioning the generally accepted concept that SGA fetuses with normal hemodynamics should be considered as uncompromised genetically small subjects and therefore call for more studies.

In the study by Cruz-Lemini et al. [116], signs of hypertension and arterial remodeling (mean blood pressure >95th percentile and intima-media thickness in the proximal abdominal aorta >75th percentile) at 6.5 months of age were looked for in a group of 100 SGA fetuses with decreased CPR and increased aortic isthmus PI. The results were compared with those in 100 control AGA infants with normal intrauterine hemodynamics. All infants were born at or close to term. Variables describing the morphology and function of fetal heart (right sphericity index, tricuspid annular-plane systolic excursion, and isovolumic relaxation time) and CPR strongly predicted the postnatal vascular remodeling. These findings may be valuable for the identification of fetuses that might benefit from postnatal monitoring and possibly interventions aiming to promote cardiovascular health.

12.6 Conclusion

In conclusion, several studies have shown abnormal fetal hemodynamics in the growth-restricted fetus, especially umbilical AREDF, to be associated with a clear increase in perinatal mortality and neonatal morbidity. The long-term follow-up studies performed until now did not show clear evidence of major neurological handicap being associated with abnormal fetal hemodynamics. This is not surprising as the much larger body of prospective follow-up studies on FGR in terms of birthweight SGA seldom showed an increase in major neurologic impairment associated with fetal growth impairment. Minor neurological dysfunction, behavioral abnormality, and learning problems at school age, all frequently reported as overrepresented in perinatal risk groups, would probably be more adequate as outcome variables when assessing the effects of fetal hemodynamics on postnatal neurodevelopment.

Hemodynamic evaluation of the fetus has increased our understanding of the physiological mechanisms involved in fetal growth restriction and is of proven clinical value in the management of high-risk pregnancies. Knowledge of changes in umbilical and fetal blood flow has also been of great value in the definition of true FGR in subjects with deviation in weight during fetal life or at birth. Thus, follow-up studies in subjects with

abnormal fetal blood flow with varying degrees of deviation in weight have supplied valuable information on effects of FGR on different aspects of postnatal development. Abnormal fetal blood flow reflects changes in the feto-placental unit associated with a reduced fetal supply of oxygen and nutrients. Others and we have shown that such fetal deprivation may lead to longstanding disturbances in morphology and subsequent function of the nervous and cardiovascular system. This information coupled with insights derived from experimental and clinical studies allowing for interaction with genetic differences will increase understanding of mechanisms, leading to postnatal morbidity due to restricted fetal growth. Furthermore, this knowledge will make it possible to design clinical trials evaluating management protocols aiming not only to prevent perinatal mortality, but also to improve the postnatal development and health later in life of individuals with abnormal intrauterine blood flow.

References

1. Dobbing J. The later development of the brain and its vulnerability. In: Davis JA, Dobbing J, editors. Scientific foundation of pediatrics. 2nd ed. London: William Heinemann Medical Books Ltd; 1981. p. 744–59.
2. Dobbing J. Nutrition and brain development. In: Thalhammer O, Baumgarten K, Pollak A, editors. Perinatal medicine. 6th European Congress, Vienna. Stuttgart: Thieme; 1979.
3. Chase HP, Welch NN, Dabiere CS, Vasan NS, Butterfield LJ. Alterations in human brain biochemistry following intrauterine growth retardation. Pediatrics. 1972;50:403–11.
4. Sarma MKJ, Rao KS. Biochemical compositions of different regions in brains of small-for-date infants. J Neurochem. 1974;22:671–7.
5. Breart G. Available evidence relating intrauterine growth retardation to neuromotor dysfunction and mental handicap. In: Kubli F, Patel N, Schmidt W, editors. Perinatal events and brain damage in surviving infants. Berlin, Heidelberg: Springer Verlag; 1988. p. 92–8.
6. Fitzhardinge PM, Stevens EM. The small for date infant. II. Neurological and intellectual sequelae. Pediatrics. 1972;50:50–7.
7. Hagberg G, Hagberg B, Olow I. The changing panorama of cerebral palsy in Sweden 1954-1970. III. The importance of fetal deprivation of supply. Acta Paediatr Scand. 1976;65:403–8.
8. Hadders-Algra M, Huisjes HJ, Touwen BCL. Preterm or small-for-gestational age infants. Neurological and behavioural development at the age of 6 years. Eur J Pediatr. 1988;147:460–7.
9. Walther FJ, Raemakers LHJ. Developmental aspects of subacute fetal distress: behaviour problems and neurological dysfunction. Early Hum Dev. 1990;6:1–10.
10. Hawdon JM, Hey E, Kolvin I, Fundudis T. Born too small. Is outcome still affected ? Dev Med Child Neurol. 1990;32:943–53.
11. Ounsted M, Moar VA, Scott WA. Neurological development of small-for-gestational age babies during the first year of life. Early Hum Dev. 1988;16:163–72.
12. Berg AT. Indices of fetal growth retardation, perinatal hypoxia-related factors and childhood neurological morbidity. Early Hum Dev. 1989;19:271–83.
13. Westwood M, Kramer MS, Muntz D, Locett JM, Watters GV. Growth and development of full-term nonasphyxiated small for gestational age newborns: follow up through adolescence. Pediatrics. 1983;71:367–82.
14. Lou HC. Etiology and pathogenesis of attention-deficit hyperactivity disorder (ADHD): significance of prematurity and perinatal hypoxic-haemodynamic encephalopathy. Acta Paedatr. 1996;85:1266–71.
15. Mallard EC, Williams CE, Johnston BM, Gunning MI, Davis S, Gluckman PD. Repeated asphyxia causes loss of striatal projection neurons in the fetal sheep brain. Neuroscience. 1995;65:827–36.
16. Bauer R, Walter B, Vorwieger G, Bergmann R, Füchtner F, Brust P. Intrauterine growth restriction induces up-regulation of cerebral aromatic amino acid decarboxylase activity in newborn piglets: [^{18}F] fluorodopa positron emission tomographic study. Pediatr Res. 2001;49(4):474–80.
17. Gennser G, Rymark P, Isberg PE. Low birth weight and risk of high blood pressure in adulthood. Br Med J. 1988;296:1498–500.
18. Barker DJP, Bull AR, Osmond O, Simmons SJ. Fetal and placental size and risk of hypertension in adult life. BMJ. 1990;301:259–62.
19. Barker DJP, Osmond C, Golding J, Kuh D, Wadsworth MEJ. Growth in utero, blood pressure in childhood and adult life, and mortality from cardiovascular disease. BMJ. 1989;298:564–7.
20. Hales CN, Barker DJP, Clark PMS. Fetal and infant growth and impaired glucose tolerance at age 64. BMJ. 1991;303:259–62.
21. Barker DJP, Hales CN, Fall CHD, Osmond C, Phipps K, Clark PMS. Type 2 (non-insulin dependent) diabetes mellitus, hypertension and hyperlipidaemia (syndrome X): relation to reduced fetal growth. Diabetologia. 1993;36:62–7.
22. Edwards C, Benediktsson R, Lindsay R, Seckl J. Dysfunction of placental glucocorticoid barrier:

link between fetal environment and adult hypertension? Lancet. 1993;341:355–7.
23. Morley R, Lister G, Leeson-Payne C, Lucas A. Size at birth and later blood pressure. Arch Dis Child. 1994;70:536–7.
24. Williams S, St George IM, Silva PA. Intrauterine growth retardation and blood pressure at age seven and eighteen. J Clin Epidemiol. 1992;45:1257–63.
25. Launer LJ, Hofman A, Grobbee DE. Relation between birth weight and blood pressure: longitudinal study of infants and children. BMJ. 1993;307:1451–4.
26. Savchev S, Figueras F, Sanz-Cortes M, Cruz-Lemini M, Triunfo S, Botet F, Gratacos E. Evaluation of an optimal gestational age cut-off for the definition of early- and late-onset fetal growth restriction. Fetal Diagn Ther. 2014;36(2):99–105.
27. Gordijn SJ, Beune IM, Thilaganathan B, Papageorghiou A, Baschat AA, Baker PN, Silver RM, Wynia K, Ganzevoort W. Consensus definition of fetal growth restriction: a Delphi procedure. Ultrasound Obstet Gynecol. 2016;48(3):333–9.
28. Illyés M, Gáti I. Reverse flow in the human fetal descending aorta as a sign of severe fetal asphyxia preceding intrauterine death. J Clin Ultrasound. 1988;16(6):403–7.
29. Montenegro N, Santos F, Tavares E, Matias A, Barros H, Leite LP. Outcome of 88 pregnancies with absent or reversed end-diastolic blood flow (ARED flow) in the umbilical arteries. Eur J Obstet Gynecol Reprod Biol. 1998;79:43–6.
30. Brar HS, Platt LD. Reverse end-diastolic flow velocity and on umbilical artery velocimetry in high-risk pregnancies; an ominous finding with adverse pregnancy outcome. Am J Obstet Gynecol. 1988;159:559–61.
31. Karsdorp VHM, van Vugt JMG, van Geijn HP, Kostense PJ, Arduini D, Montenegro N, Todros T. Clinical significance of absent or reversed end diastolic velocity waveforms in umbilical artery. Lancet. 1994;344:1664–8.
32. Westergaard HB, Langhoff-Roos J, et al. A critical appraisal of the use of umbilical artery Doppler ultrasound in high risk pregnancies: use of meta-analyses in evidence-based obstetrics. Ultrasound Obstet Gynecol. 2001;17:466–76.
33. Gudmundsson S, Marsal K. Blood velocity waveforms in the fetal aorta and umbilical artery as predictors of fetal outcome—a comparison. Am J Perinatol. 1991;8:1–6.
34. Lees CC, Stampalija T, Baschat AA, da Silva CF, Ferrazzi E, Figueras F, Hecher K, Kingdom J, Poon LC, Salomon LJ, Unterscheider J. ISUOG practice guidelines: diagnosis and management of small-for-gestational-age fetus and fetal growth restriction. Ultrasound Obstet Gynecol. 2020;56:298–312.
35. DeVore GR. The importance of the cerebroplacental ratio in the evaluation of fetal well-being in SGA and AGA fetuses. Am J Obstet Gynecol. 2015;213:5–15.
36. Hackett GA, Campbell S, Gamsu H, Cohen-Overbeek T, Pearce JMF. Doppler studies in the growth retarded fetus and prediction of neonatal necrotising enterocolitis, haemorrhage and neonatal morbidity. BMJ. 1987;294:13–5.
37. Malcolm G, Ellwood D, Devonald K, Beilby R, Henderson-Smart D. Absent or reversed end diastolic flow velocity in the umbilical artery and necrotising enterocolitis. Arch Dis Child. 1991;66:805–7.
38. Kempley ST, Gamsu HR, Vyas S, Nicolaides K. Effects of intrauterine growth retardation on postnatal visceral and cerebral blood flow velocity. Arch Dis Child. 1991;66:1115–58.
39. McDonnell M, Serra-Serra V, Gaffney G, Redman CW, Hope PL. Neonatal outcome after pregnancy complicated by abnormal velocity waveforms in the umbilical artery. Arch Dis Child. 1994;70:F84–9.
40. Adiotomre P, Johnstone FD, Laing IA. Effect of absent end diastolic flow velocity in the fetal umbilical artery on subsequent outcome. Arch Dis Child. 1997;76:35–8.
41. Eronen M, Kari A, Pesonen E, Kaaja R, Wallgren EI, Hallman M. Value of absent or retrograde end-diastolic flow in fetal aorta and umbilical artery as a predictor of perinatal outcome in pregnancy-induced hypertension. Acta Paediatr. 1993;82:919–24.
42. Voβbeck S, Kraus de Camargo O, Grab D, Bode H, Pohlandt F. Neonatal and neurodevelopmental outcome in infants born before 30 weeks of gestation with absent or reversed end-diastolic flow velocities in the umbilical artery. Eur J Pediatr. 2001;160:128–34.
43. Weiss E, Ulrich S, Berle P. Condition at birth of infants with previously absent or reverse umbilical artery end-diastolic flow velocities. Arch Gynecol Obstet. 1992;252:37–43.
44. Weiss E, Ulrich S, Berle P, Picard-Maureau A. CK-BB as indicator of prenatal brain-cell injury in fetuses with absent or reverse end-diastolic flow velocities of the umbilical arteries. J Perinat Med. 1994;22:219–26.
45. Rizzo G, Arduini D, Luciano R, Rizzo C, Tortorolo G, Romanini C, Mancuso S. Prenatal cerebral doppler ultrasonography and neonatal neurologic outcome. J Ultrasound Med. 1989;8:237–40.
46. Scherjon SA, Smolders-DeHaas H, Kok JH, Zondervan HA. The "brain-sparing" effect: antenatal cerebral doppler findings in relation to neurologic outcome in very preterm infants. Am J Obstet Gynecol. 1993;169:169–75.
47. Ley D, Marsal K. Doppler velocimetry in cerebral vessels of small for gestational age infants. Early Hum Dev. 1992;31:171–80.
48. Scherjon SA, Smolders-DeHaas H, Oosting H, Kok JH, Zondervan HA. Neonatal cerebral circulation in relation to neurosonography and neurological outcome: a pulsed Doppler study. Neuropediatrics. 1994;25:208–13.
49. Weiss E, Ulrich S, Berle P. Blood flow velocity waveforms of the middle cerebral artery and abnor-

mal neurological evaluations in live-born fetuses with absent or reverse end-diastolic flow velocities of the umbilical arteries. Eur J Obstet Gynecol Reprod Biol. 1992;45:93–100.
50. Valcamonico A, Danti L, Frusca T, Soregaroli M, Zucca S, Abrami F, Tiberti A. Absent end-diastolic velocity in umbilical artery: risk of neonatal morbidity and brain damage. Am J Obstet Gynecol. 1994;170:796–801.
51. Todd AL, Trudinger BJ, Cole MJ, Cooney GH. Antenatal tests of fetal welfare and development at age 2 years. Am J Obstet Gynecol. 1992;167:66–71.
52. Wilson DC, Harper A, McClure G, Halliday H, Reid M. Long term predictive value of doppler studies in high risk fetuses. Br J Obstet Gynecol. 1992;99:575–8.
53. Kirsten GF, Van Zyl JI, Van Zijl F, Maritz JS, Odendaal HJ. Infants of women with severe early pre-eclampsia: the effect of absent end-diastolic umbilical artery doppler flow velocities on neurodevelopmental outcome. Acta Paediatr. 2000;89(5):566–70.
54. Wienerroither H, Steiner H, Tomaselli J, Lobendanz M, Thun-Hohenstein L. Intrauterine blood flow and long-term intellectual, neurologic and social development. Obstet Gynecol. 2001;97:449–53.
55. Schreuder AM, McDonnell M, Gaffney G, Johnson A, Hope PL. Outcome at school age following antenatal detection of absent or reversed end diastolic flow velocity in the umbilical artery. Arch Dis Child Fetal Neonatal Ed. 2002;86:F108–14.
56. Delorme P, Kayem G, Lorthe E, Sentilhes L, Zeitlin J, Subtil D, Rozé JC, Vayssière C, Durox M, Ancel PY, Pierrat V, Goffinet F, EPIPAGE-2 Obstetric Writing Group. Neurodevelopment at 2 years and umbilical artery Doppler in cases of very preterm birth after prenatal hypertensive disorder or suspected fetal growth restriction: EPIPAGE-2 prospective population-based cohort study. Ultrasound Obstet Gynecol. 2020;56(4):557–65.
57. Valcamonico A, Accorsi P, Battaglia S, Soregaroli M, Beretta D, Frusca T. Absent or reverse end-diastolic flow in the umbilical artery: intellectual development at school age. Eur J Obstet Gynecol Reprod Biol. 2004;114(1):23–8.
58. Mone F, McConnell B, Thompson A, Segurado R, Hepper P, Stewart MC, Dornan JC, Ong S, McAuliffe FM, Shields MD. Fetal umbilical artery Doppler pulsatility index and childhood neurocognitive outcome at 12 years. BMJ Open. 2016;6(6):e008916.
59. Padilla N, Perapoch J, Carrascosa A, Acosta-Rojas R, Botet F, Gratacós E. Twelve-month neurodevelopmental outcome in preterm infants with and without intrauterine growth restriction. Acta Paediatr. 2010;99(10):1498–503.
60. Eger SH, Sommerfelt K, Kiserud T, Markestad T. Foetal umbilical artery Doppler in small preterms: (IQ) neurocognitive outcome at 5 years of age. Acta Paediatr. 2013;102(4):403–9.
61. Chen CY, Wang KG, Wang SM, Chen CP. Two-year neurological outcome of very-low-birth-weight children with prenatal absent or reversed end-diastolic flow velocity in the umbilical artery. Taiwan J Obstet Gynecol. 2013;52(3):323–8.
62. Llurba E, Baschat AA, Turan OM, Harding J, McCowan LM. Childhood cognitive development after fetal growth restriction. Ultrasound Obstet Gynecol. 2013;41(4):383–9.
63. Morsing E, Brodszki J, Thuring A, Maršál K. Infant outcome after active management of early-onset fetal growth restriction with absent or reverse umbilical artery blood flow. Ultrasound Obstet Gynecol. 2021;57(6):931–41.
64. Morsing E, Åsard M, Ley D, Stjernqvist K, Marsal K. Cognitive function after intrauterine growth restriction and very preterm birth. Pediatrics. 2011;127(4):e874–82.
65. Morsing E, Gustafsson P, Brodszki J. Lung function in children born after foetal growth restriction and very preterm birth. Acta Paediatr. 2012;101(1):48–54.
66. Morsing E, Liuba P, Fellman V, Marsal K, Brodszki J. Cardiovascular function in children born very preterm after intrauterine growth restriction with severely abnormal umbilical artery blood flow. Eur J Prev Cardiol. 2014;21(10):1257–66.
67. Morsing E, Malova M, Kahn A, Lätt J, Björkman-Burtscher IM, Maršál K, Ley D. Brain volumes and developmental outcome in childhood following fetal growth restriction leading to very preterm birth. Front Physiol. 2018;9:a1583.
68. Scherjon S, Oosting H, Ongerboer de Visser BW, de Wilde T, Zondervan HA, Kok JH. Fetal brain sparing is associated with accelerated shortening of visual evoked potential latencies during early infancy. Am J Obstet Gynecol. 1996;175:1569–75.
69. Scherjon SA, Oosting H, Smolders-DeHaas H, Zondervan HA, Kok JH. Neurodevelopmental outcome at three years of age after fetal "brain-sparing". Early Hum Dev. 1998;52:67–79.
70. Scherjon S, Briet J, Oosting H, Kok J. The discrepancy between maturation of visual-evoked potentials and cognitive outcome at five years in very preterm infants with and without hemodynamic signs of fetal brain-sparing. Pediatrics. 2000;105(2):385–91.
71. Chan FY, Pun TC, Lam P, Lam C, Lee CP, Lam YH. Fetal cerebral doppler studies as a predictor of perinatal outcome and subsequent neurological handicap. Obstet Gynecol. 1996;87:981–8.
72. Kutschera J, Tomaselli J, Urlesberger B, Maurer U, Hausler M, Gradnitzer E, Burmucic K, Müller W. Absent or reversed end-diastolic blood flow in the umbilical artery and abnormal Doppler cerebroplacental ratio—cognitive, neurological and somatic development at 3 to 6 years. Early Hum Dev. 2002;69:47–56.
73. Figueras F, Oros D, Cruz-Martinez R, Padilla N, Hernandez-Andrade E, Botet F, Costas-Moragas C, Gratacos E. Neurobehavior in term, small-for-

gestational age infants with normal placental function. Pediatrics. 2009;124(5):e934–41.
74. Figueras F, Eixarch E, Meler E, Iraola A, Figueras J, Puerto B, Gratacos E. Small-for-gestational-age fetuses with normal umbilical artery Doppler have suboptimal perinatal and neurodevelopmental outcome. Eur J Obstet Gynecol Reprod Biol. 2008;136(1):34–8.
75. Oros D, Figueras F, Cruz-Martinez R, Padilla N, Meler E, Hernandez-Andrade E, Gratacos E. Middle versus anterior cerebral artery Doppler for the prediction of perinatal outcome and neonatal neurobehavior in term small-for-gestational-age fetuses with normal umbilical artery Doppler. Ultrasound Obstet Gynecol. 2010;35(4):456–61.
76. Eixarch E, Meler E, Iraola A, Illa M, Crispi F, Hernandez-Andrade E, Gratacos E, Figueras F. Neurodevelopmental outcome in 2-year-old infants who were small-for-gestational age term fetuses with cerebral blood flow redistribution. Ultrasound Obstet Gynecol. 2008;32(7):894–9.
77. Fouron JC, Gosselin J, Amiel-Tison C, Infante-Rivard C, Fouron C, Skoll A, Veilleux A. Correlation between prenatal velocity waveforms in the aortic isthmus and neurodevelopmental outcome between the ages of 2 and 4 years. Am J Obstet Gynecol. 2001;184:630–6.
78. Sonesson SE, Fouron JC. Doppler velocimetry of the aortic isthmus in human fetuses with abnormal velocity profiles in the umbilical artery. Ultrasound Obstet Gynecol. 1997;10:107–11.
79. Laurin J, Lingman G, Marsal K, Persson P-H. Fetal blood flow in pregnancies complicated by intrauterine growth retardation. Obstet Gynecol. 1987;69:895–902.
80. Lingman G, Marsal K. Fetal central blood circulation in the third trimester of normal pregnancy: longitudinal study. II. Aortic blood velocity waveform. Early Hum Dev. 1986;13:151–9.
81. Ley D, Laurin J, Bjerre I, Marsal K. Abnormal fetal aortic velocity waveform and minor neurological dysfunction at 7 years of age. Ultrasound Obstet Gynecol. 1996;8:160–5.
82. Ley D, Tideman E, Laurin J, Bjerre I, Marsal K. Abnormal fetal aortic velocity waveform and intellectual function at 7 years of age. Ultrasound Obstet Gynecol. 1996;8:160–5.
83. Touwen BCL. Examination of the child with minor neurological dysfunction. Clinics in developmental medicine, Nr 71. 2nd ed. London: SIMP/Heinemann Medical Books; 1979.
84. Tideman E, Marsal K, Ley D. Cognitive function in young adults following intrauterine growth restriction with abnormal fetal aortic blood flow. Ultrasound Obtet Gynecol. 2009;29(6):614–8.
85. Ley D, Tideman E, Brodszki J, Liuba C, Marsal K, Hellström A. Decrease in cognitive ability and neuroretinal rim area in 18 year olds with intrauterine growth restriction and abnormal fetal blood flow. Czech Gynecology. 2002;67:222.
86. Ley D, Marsal K, Dahlgren J, Hellström A. Abnormal retinal optic nerve morphology in young adults following intrauterine growth restriction. Pediatr Res. 2004;56:139–43.
87. Martin L, Ley D, Maršál K, Hellström A. Visual function in young adults following intrauterine growth restriction. J Pediatr Ophthalmol Strabismus. 2004;48:212–8.
88. Mallard EC, Rees S, Stringer M, Cock ML, Harding R. Effects of chronic placental insufficiency on brain development in fetal sheep. Pediatr Res. 1998;43:262–70.
89. Mallard C, Loeliger M, Copolov D, Rees S. Reduced number of neurons in the hippocampus and the cerebellum in the postnatal guinea-pig following intrauterine growth restriction. Neuroscience. 2000;100:327–33.
90. Thissen J-P, Ketelslegers J-M, Underwood LE. Nutritional regulation of the insulin-like growth factors. Endocr Rev. 1994;15:80–101.
91. Lowe JRWL, Adamo M, Werner H, Roberts CT Jr, LeRoith D. Regulation by fasting of rat insulin-like growth factor 1 and its receptor: effects on gene expression and binding. J Clin Invest. 1989;84:619–26.
92. Sveinsdóttir K, Länsberg JK, Sveinsdóttir S, Garwicz M, Ohlsson L, Hellström A, Smith L, Gram M, Ley D. Impaired cerebellar maturation, growth restriction, and circulating insulin-like growth factor 1 in preterm rabbit pups. Dev Neurosci. 2017;39(6):487–97.
93. Larsen T, Main K, Andersson AM, Juul A, Greisen G, Skakkebaek NE. Growth hormone, insulin-like growth factor I and its binding proteins 1 and 3 in last trimester intrauterine growth retardation with increased pulsatility index in the umbilical artery. Clin Endocrinol. 1996;45:315–9.
94. Spencer JA, Chang TC, Jones J, Robson SC, Preece MA. Third trimester fetal growth and umbilical venous blood concentrations of IGF-1, IGFBP-1 and growth hormone at term. Arch Dis Child Fetal Neonatal Ed. 1995;73:87–90.
95. Esteban FJ, Padilla N, Sanz-Cortés M, de Miras JR, Bargalló N, Villoslada P, Gratacós E. Fractal-dimension analysis detects cerebral changes in preterm infants with and without intrauterine growth restriction. NeuroImage. 2010;53(4):1225–32.
96. Padilla N, Falcón C, Sanz-Cortés M, Figueras F, Bargallo N, Crispi F, Eixarch E, Arranz A, Botet F, Gratacós E. Differential effects of intrauterine growth restriction on brain structure and development in preterm infants: a magnetic resonance imaging study. Brain Res. 2011;1382:98–108.
97. Padilla N, Junqué C, Figueras F, Sanz-Cortes M, Bargalló N, Arranz A, Donaire A, Figueras J, Gratacos E. Differential vulnerability of gray matter and white matter to intrauterine growth restriction in preterm infants at 12 months corrected age. Brain Res. 2014;1545:1–11.

98. Gardiner HM. Intrauterine programming of the cardiovascular system. Ultrasound Obstet Gynecol. 2008;32(4):481–4.
99. Rodríguez-López M, Cruz-Lemini M, Valenzuela-Alcaraz B, Garcia-Otero L, Sitges M, Bijnens B, Gratacós E, Crispi F. Descriptive analysis of different phenotypes of cardiac remodeling in fetal growth restriction. Ultrasound Obstet Gynecol. 2017;50(2):207–14.
100. Stale H, Marsal K, Gennser G, Benthin M, Dahl P, Lindström K. Aortic diameter pulse waves and blood flow velocity in the small for gestational age fetus. Ultrasound Med Biol. 1991;17:471–8.
101. Bonamy AK, Norman M, Kaijser M. Being born too small, too early, or both: does it matter for risk of hypertension in the elderly? Am J Hypertens. 2008;21(10):1107–10.
102. Johansson S, Iliadou A, Bergvall N, Tuvemo T, Norman M, Cnattingius S. Risk of high blood pressure among young men increases with the degree of immaturity at birth. Circulation. 2005;112:3430–6.
103. Benthin M, Dahl P, Ruzicka R, Lindström K. Calculation of pulse-wave velocity using cross correlation - effects of reflexes in the arterial tree. Ultrasound Med Biol. 1991;17:471–8.
104. Ley D, Stale H, Marsal K. Aortic vessel wall characteristics and blood pressure in children with intrauterine growth retardation and abnormal foetal aortic blood flow. Acta Paediatr. 1997;86:299–305.
105. Gardiner HM, O'Brien C, Greenwald SE, Bull C, Hunter AS, Robson SC. Postnatal adaptation: vascular compliance and reactivity in growth retarded and normal infants. In Proceedings of the 22nd Annual Meeting of the Society for the Study of Fetal Physiology. Malmö, Sweden; 1995.
106. Safar ME, St. Laurent S, Safavian AL, Pannier BM, London GM. Pulse pressure in sustained essential hypertension: a haemodynamic study. J Hypertens. 1987;5:213–8.
107. Newman DL, Lallemand RC. The effect of age on the distensibility of the abdominal aorta of man. Surg Gynecol Obstet. 1978;147:211–4.
108. Brodszki J, Länne T, Marsal K, Ley D. Impaired vascular growth in late adolescence after intrauterine growth restriction. Circulation. 2005;111:2623–8.
109. Hellström A, Dahlgren J, Marsal K, Ley D. Abnormal retinal vascular morphology in young adults following intrauterine growth restriction. Pediatrics. 2004;113:e77–80.
110. Bennis-Taleb N, Remacle C, Hoet J, Reusens B. A low-protein isocaloric diet during gestation affects brain development and alters permanently cerebral cortex blood vessels in rat offspring. J Nutr. 1999;129(8):1613–9.
111. Martin H, Hu J, Gennser G, Norman M. Impaired endothelial function and increased carotid stiffness in 9-year-old children with low birthweight. Circulation. 2000;102:2739–44.
112. Bjarnegård N, Morsing E, Cinthio M, Länne T, Brodszki J. Cardiovascular function in adulthood following intrauterine growth restriction with abnormal fetal blood flow. Ultrasound Obstet Gynecol. 2013;41(2):177–84.
113. Crispi F, Bijnens B, Figueras F, Bartrons J, Eixarch E, Le Noble F, Ahmed A, Gratacós E. Fetal growth restriction results in remodeled and less efficient hearts in children. Circulation. 2010;121(22):2427–36.
114. Crispi F, Figueras F, Cruz-Lemini M, Bartrons J, Bijnens B, Gratacos E. Cardiovascular programming in children born small for gestational age and relationship with prenatal signs of severity. Am J Obstet Gynecol. 2012;207(2):121.e1–9.
115. Stergiotou I, Crispi F, Valenzuela-Alcaraz B, Cruz-Lemini M, Bijnens B, Gratacos E. Aortic and carotid intima-media thickness in term small-for-gestational-age newborns and relationship with prenatal signs of severity. Ultrasound Obstet Gynecol. 2014;43(6):625–31.
116. Cruz-Lemini M, Crispi F, Valenzuela-Alcaraz B, Figueras F, Gómez O, Sitges M, Bijnens B, Gratacós E. A fetal cardiovascular score to predict infant hypertension and arterial remodeling in intrauterine growth restriction. Am J Obstet Gynecol. 2014;210(6):552.e1–552.e22.
117. von Beckerath AK, Kollmann M, Rotky-Fast C, Karpf E, Lang U, Klaritsch P. Perinatal complications and long-term neurodevelopmental outcome of infants with intrauterine growth restriction. Am J Obstet Gynecol. 2013;208(2):130.e1–6.
118. Bellido-González M, Díaz-López MÁ, López-Criado S, Maldonado-Lozano J. Cognitive functioning and academic achievement in children aged 6-8 years, born at term after intrauterine growth restriction and fetal cerebral redistribution. J Pediatr Psychol. 2017;42(3):345–54.
119. Marsál K, Ley D. Intrauterine blood flow and postnatal neurological development in growth-retarded fetuses. Biol Neonate. 1992;62(4):258–64.

Fetal Renal Artery

13

Stephen Contag

13.1 Embryology

The kidneys have multiple functions including filtering blood, excreting waste, reabsorbing water and other compounds, and endocrine functions. Each adult kidney contains approximately 750,000 nephrons which can vary from 250,000 to as many as 2,000,000 [1]. Each nephron is composed of an afferent artery, a glomerulus, an efferent artery, Bowman's capsule that surrounds the glomerulus and collects the filtrate, a proximal tubule, the Loop of Henle, and a distal tubule, which connects to the collecting duct. The most reknown endocrine products of the kidney include renin, prostaglandins, erythropoietin, 1, 25 dihydroxycholecalciferol (vitamin D), and prekallikreins, which participate in vascular permeability.

Its functional unit, the nephron, contains over 10,000 cells and at least 12 different cell types, with each cell type located in a particular place in relation to the others along the length of the nephron [2]. The mammalian kidney develops in three major stages. The first two stages are transient, while the last persists as a functional kidney [2]. The first signs of renal development begin on day 22 in the human as the pronephric duct, which arises in the intermediate mesoderm ventral to the anterior somites. The pronephric cells migrate caudally, while the anterior region of the duct induces the formation of tubules from the surrounding mesenchyme, leading to the formation of the pronephros [2]. The pronephric tubules and the pronephric duct degenerate in mammals, but the most caudal portion persists as the nephric or Wolffian duct [3, 4]. As the pronephric tubules degenerate, the middle portion of the nephric duct induces a new set of tubules from the adjacent mesenchyme at around day 25. This is known as the mesonephros and it does not produce urine [5]. Its main function appears to be related to formation of hematopoietic stem cells [6]. In males, it contributes to the formation of the vas deferens and sperm carrying ducts of the testes [2]. The permanent kidney develops from the metanephros, which develops from the same components as the transient kidneys [2]. It appears to originate through interactions between epithelial and mesenchymal components of the intermediate mesoderm. Initially, the metanephrogenic mesenchyme forms in the posterior regions of the intermediate mesoderm. This mesenchyme induces the formation of a branch from each of the nephric ducts called the ureteric buds. The ureteric buds induce formation of nephrons from the surrounding metanephric mesenchyme, which in turn induce branching of the ureteric bud. The ureteric bud eventually separates from

S. Contag (✉)
Division of Maternal-Fetal Medicine, University of Minnesota Medical School, Minneapolis, MN, USA
e-mail: scontag@umn.edu

D. Maulik, C. C. Lees (eds.), *Doppler Ultrasound in Obstetrics and Gynecology*,
https://doi.org/10.1007/978-3-031-06189-9_13

the nephric duct and will become the ureters that will take urine to the bladder [2]. The kidney develops because of the mutual induction of the two types of mesoderm on each other with ongoing branching of the ureteric bud and development of the nephrons from the metanephrogenic mesenchyme [2, 7]. The epithelial buds develop into the components of the nephron and break down the adjacent ureteric bud forming a connection between the tubules and the ureteric bud [7, 8]. Several transcription factors including WT1, glial-derived neurotrophic factor (GDNF), hepatocyte growth factor (HGF), Wnt11, Wnt4, fibroblast growth factor 2 (FGF2), and bone morphogenetic protein 7 (BMP7) participate in this mutual induction [9–12]. If any of these factors are not available, kidney development will not occur and there will be apoptosis of the metanephrogenic mesenchyme [2]. Nephrogenesis continues well into the third trimester (34–36 weeks). Fetal urine production is limited compared with postnatal production after glomerular filtration increases because of a drop in renal artery and arteriolar vascular resistance.

The kidneys are initially in the pelvic cavity, but with growth and straightening of the fetus, they displace cephalad and laterally into the retroperitoneal space at the level of the lower thoracic and upper lumbar spine. The renal arteries arise from the aorta. As the kidneys ascend into the retroperitoneal space to the level of the lower thoracic spine, successive arteries arise from the aorta and with regression of the transitory branches as the kidneys ascend [13]. The definitive renal arteries are at the level of the second lumbar vertebra. Approximately 25% of the population can have more than one renal artery. The three key branches of the renal artery include the inferior adrenal artery, the capsular artery, and the ureteric artery. Just after the renal artery reaches the hilum, it gives off the ventral and dorsal rami, which further divide into many smaller segmental arteries before they enter the renal parenchyma. These segmental arteries further divide into lobar branches. The afferent arterioles, which come off the interlobular arteries, supply the glomeruli [14].

13.2 Anatomy

The right renal artery has a long downward course due to the inferior position of the right kidney and it usually lies behind the inferior vena cava (IVC). Classically, each kidney has a single renal vein that usually lies anterior to the renal artery at the renal hilum [15].

The kidneys are surrounded by the renal neural plexus, whose fibers course along with the renal artery on each side. There is also input from the sympathetic nervous system, which can cause vasoconstriction and reduce blood flow in the renal vessels. The kidneys receive parasympathetic nerve innervation via the vagus nerve. The sensory output from the kidneys is transmitted to the spinal cord at T10-T11. When the kidney is inflamed, referred pain is usually felt along the flank [14].

13.3 Urine Production

Fetal urine production actually begins in the mesonephros by about 5 weeks of gestation in the mesonephros. The metanephros or subsequent adult kidney begin to produce urine at 9 to 11 weeks of gestation when it is excreted into the amniotic sac [16]. During the second and third trimesters, it contributes to a significant proportion of the total amniotic fluid volume [17]. Fetal urine production increases from 110 mL/kg/24 h at 25 weeks to almost 200 mL/kg/24 h at term, which is almost 25% of body weight per day or approximately 1000 mL/day at term [17, 18]. After 40 weeks, it appears that fetal urine production gradually decreases [19]. The fetus can regulate diuresis in response to intravascular volume by endocrine regulation of blood blow and tubular resorption [16]. Acute hypoxia produces fetal polyuria with relatively small changes in amniotic fluid volume [20].

13.4 Blood Flow in the Aorta and Through the Fetal Kidneys by Gestational Age

The combined cardiac output (CCO) in the human fetus has been calculated as the sumtotal of the right (RVO) and left (LVO) ventricular output.

Flow is calculated as the product of the cross-sectional area of the vessel or valve being measured (radius^2 * 3.14), the velocity time integral (VTI) at the site being measured, and the heart rate (HR). Using direct dilution techniques, the calculated combined ventricular output in the fetal lamb is 450 mL/kg/min. In the healthy fetus, aortic blood flow is characterized by the presence of both systolic and diastolic flow, with increasing diastolic flow as the measurements are obtained lower in the abdominal compared to the thoracic aorta [21]. The first accelerated half of the waveform reflects the cardiac systolic ventricular performance [22]. The basal velocity measured prior to the subsequent upswing of the velocity waveform reflects diastolic flow and is indicative of the low resistance within the placental vascular system. Because of this, the aortic resistance indices are lower in the abdominal compared with the thoracic aorta [23, 24]. Time-averaged velocities in the abdominal aorta during the third trimester are 30–40 cm/s and do not change substantially throughout pregnancy [25]. This suggests that the changes and increasing flow rates observed with advancing gestational age are related to increasing aortic diameter with concurrent decrease of the resistance indices up to 36 weeks of gestation [25]. When flow volume is corrected for fetal weight, the lower abdominal aorta has flows that range from 140 to 180 mL/kg*min^{-1} [26, 27]. If conditions that lead to increasing resistance of the placental blood flow develop, the diastolic flow within the lower abdominal aorta will decrease. Through measurement of the blood flow in the abdominal aorta and in the intra-abdominal umbilical vein, the proportion of aortic flow directed to the placenta can be calculated [27]. This varies from approximately 60% of aortic flow at 28 weeks to 33% at term [27]. This may be partially due to the increasing ratio of fetal to placental weight that occurs with advancing gestational age [28].

13.5 The Renal Artery Blood Flow and Resistance

The documented aortic, placental, and renal blood flow in the human fetus demonstrate that the flow to the kidney is a significant and relatively stable proportion of abdominal aortic flow and represents 14–40% of the flow volume reaching the abdominal aorta.

In the fetal lamb, the kidneys receive approximately 150 mL/100 g organ weight per minute of blood flow. This corresponds to 2–3% of the combined ventricular output [29, 30]. In the human fetus, renal blood flow calculated using Doppler techniques corresponds to approximately 5–8%, and this proportion remains constant throughout pregnancy [31, 32]. These levels can rise to as high as 16% of the cardiac output in the newborn period [30]. Combined ventricular output in the human fetus is calculated to be 400–475 mL/kg*min^{-1} between 18 and 41 weeks of gestation [33, 34]. This means that renal blood flow in the human fetus is approximately 20–40 to as high as 75 mL/kg body weight*min^{-1} or 1–2 mL/g kidney weight*min min^{-1} [35]. The low flow rates increase substantially in newborn animal models and reflect an elevated renal vascular resistance and low filtration fraction [36].

Angiotensin 1 receptor (AT1) is present in the fetal kidney afferent and efferent arteries, mesangial cells, and tubules [37, 38]. Within these structures, AT1 receptors respond to angiotensin II and cause efferent arteriolar vasoconstriction that leads to increased glomerular filtration (GFR), in the mesangial cells, AT1 activation causes constriction and decreases the GFR, and in the ascending tubules of Henle's loop, it increases sodium reabsorption with a concurrent decrease in urinary output. Treatment of the fetus with ACE enzyme inhibitors decreases renal vascular resistance and GFR by decreasing efferent arteriolar tone [39]. In the newborn lamb, there is a significant and sudden increase in renal blood flow with redistribution of flow from the inner cortex to the outer cortex compared with the fetal lamb [35, 36]. This redistribution of flow continues during the subsequent week secondary to increasing newborn blood pressure and decreasing renal vascular resistance [40]. Multiple factors can modify renal artery resistance and the fetal kidney has been shown to exhibit moderate degrees of autoregulation despite low fetal perfusion pressure [41–43]. The sympathetic nervous system appears to play a significant role in the autoregulatory process [44]. A significant role is

also been attributed to the renin angiotensinogen system, which not only helps autoregulate renal blood flow, but is also very important in nephrogenesis [45, 46].

13.6 Ultrasound Assessment of the Fetal Kidney

The technique for obtaining renal artery Doppler flow waveforms is most commonly performed with the patient in a semi-recumbent position. The ultrasound probe is used to visualize a sagittal section of the fetal body, and the beam is then directed lateral to the spine to obtain a coronal section of the fetal kidneys and descending aorta. Color flow is then activated with a high pass filter between 50–70 Hz. The pulsed Doppler gate (1.5–2.0 mm) is then placed within the renal artery lumen, and a pulsed Doppler waveform is obtained. The angle of insonation is kept as close to 0 degrees as possible and always less than 30 degrees (Fig. 13.1) [47]. Waveforms should be recorded within 30–45 s to minimize exposure and adhere to ALARA principles. Recordings should be obtained during periods of fetal apnea and absence of movement with a fetal heart rate of 120–160 beats per minute [48].

Earlier reports of fetal renal artery Doppler used a more distal site of sampling along the course of the renal artery, given concern for increased turbulence close to the abdominal aorta [49, 50]. However, recent studies have used a more proximal sampling site to avoid unpredictable branching of the vessel [51, 52]. Haugen and colleagues demonstrated that there was no difference in mean pulsatility index (PI) or mean resistance index (RI) when compared between proximal and distal sites [48]. Mean peak systolic velocity (PSV) and end diastolic velocity (EDV) were significantly higher when measured at the proximal site compared to the distal site. These differences are postulated to represent anatomic variation in the vessels [48]. When the renal artery branches from the aorta, the flow is equal whether in the middle of the vessel or adjacent to the vessel walls. As the renal artery advances into the renal parenchyma, the vessel narrows and flow becomes laminar with a parabolic distribution of the velocities. The blood flow in the center of the vessel is faster than the velocities adjacent to the vessel wall [53]. This range of velocities is observed in laminar flow and is corrected through use of the wall filter [54].

Haugen and colleagues also compared sampling the left versus right renal artery and found higher absolute velocities on the right side compared to the left. Based on these findings, the authors suggest standardization of renal artery Doppler waveform measurement by sampling in the renal artery trunk before any distal branches and favoring the left renal artery over the right [50].

13.7 Methods to Quantify Fetal Renal Artery Flow and Resistance

Renal blood flow measured by use of pulsed Doppler uses the flow velocity waveform to obtain measures of maximum systolic velocity, end diastolic velocity, and time-averaged mean velocity. These assessments are angle-dependent and require insonation in the same vector of flow, whether in the same or in the opposite direction. The precision of the measurements decreases the greater the angle of insonation from the flow vector. Angles greater than 30 degrees are unreliable. With increasing angle of insonation greater than 30°, there is increasing reflection of the incident ultrasound beam at the interface of the vessel wall and the blood flowing beneath it, decreasing the sensitivity of the signal [55]. The most commonly used measures of impedance or resistance to flow rely on the relationships between systolic and diastolic flow velocities. These are most often expressed as ratios or indices and are not angle-dependent, as the angle of insonation affects both systolic and diastolic flow velocities equally [56]. The three most commonly used measures of impedance to flow are the systolic diastolic ratio, the pulsatility index, and the resistance index. All three have the same relationship with impedance, the higher the value, the higher the impedance and they have no unit of measurement [57–59].

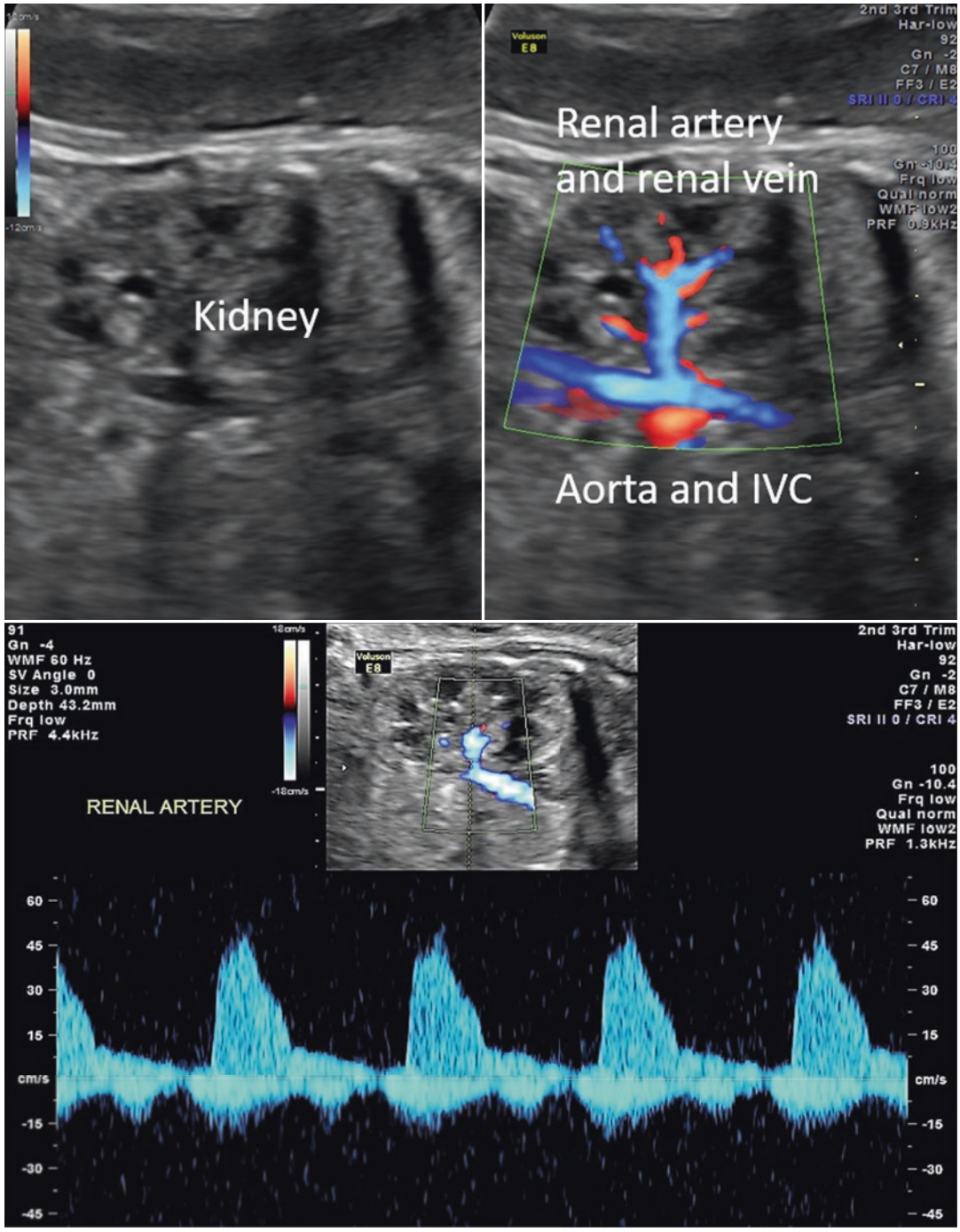

Fig. 13.1 Grayscale (top left panel) and application of color Doppler (top right panel) on a coronal view of the fetal kidney and vascular pedicle. The lower panel demonstrates the high resistance waveform of the renal artery

Actual blood flow, as determined in the sheep or human models, regardless of the vessel or structure being measured, is calculated from Poiseuille's law: $Q = dP/R$. In this formula, blood flow rate in volume per unit time (Q) is directly proportional to the differ-

ence in pressure (mmHg) between two points (dP) and inversely proportional to the resistance to flow (R). Resistance is dependent on viscosity of the fluid, vessel length, and vessel radius. In this relationship, small changes in the radius of the vessel have an exponentially greater effect on the flow rate than that of vessel length, pressure difference, or viscosity of the fluid (as in anemia). As an example, if the estimated flow rate is 100 mL/s, doubling the length of the vessel or doubling the viscosity would decrease the rate to 50 mL/s, doubling the pressure would increase the flow to 200 mL/s, and doubling the vessel diameter would increase the flow to 1600 mL/s. However, if the estimated flow rate is 100 mL/s, halving the length of the vessel or halving the viscosity would increase the rate to 200 mL/s, halving the pressure would decrease the flow to 50 mL/s, and halving the vessel diameter would decrease the flow to 0.625 mL/s.

Pulsed spectral Doppler does not measure volume of flow, actual resistance, or pressure difference, what it measures is flow velocity, which is a rate of distance per unit time (cm/s), which is not the same as flow, and which is volume per unit time (mL/s). As previously observed, in the clinical setting, flow is calculated as the product of the cross-sectional area of the vessel or valve being measured, the velocity time integral (VTI) at the site being measured, and the heart rate. Vascular physiology has demonstrated that the same principles that govern hydrodynamics also apply to the circulatory system. As such, the rate, or velocity of blood flow varies inversely with the total cross-sectional area of the blood vessels. As the total cross-sectional area of the vessels increases, the velocity of flow decreases. The renal artery is usually a single artery, and as noted above, can occasionally be duplicated. At the level of the main stem renal arteries, the cross section of that artery will determine the velocity of flow, where small changes in the vessel radius will have a significant impact in the measured velocities, with smaller vessels showing significant increases in the velocities, especially when pressure difference is highest such as during systole [60, 61].

13.8 Normal Values over Gestational Age

As multivessel fetal Doppler gained popularity in the 1980s–1990s, investigators began evaluating the fetal renal artery as representative of the peripheral fetal circulation. Initial small longitudinal cohort studies demonstrated that renal size and blood flow rise, while pulsatility index (PI) decreases linearly with advancing gestational age [32, 52, 62]. Renal artery resistance index (RI) did not demonstrate a distinct pattern across gestation [63]. These changes are thought to be secondary to the progressive maturation of fetal renal blood vessels in the third trimester, leading to decreased vascular resistance and increased perfusion at unchanged pressures. This leads to increasing fetal urine output in the third trimester [64].

In contrast, Figueras and colleagues demonstrated that PI values showed little variation across gestation; whereas, systolic velocity values increased until 36–37 weeks, decreasing thereafter [65]. Most recently, in a large cohort of 1915 patients, Contag and colleagues generated reference values for renal artery peak systolic velocity (Fig. 13.2) and Doppler resistances indices (Fig. 13.3). They also observed a stable PI value across gestation and an increasing peak systolic velocity value up until 36 weeks [47]. Understanding normal reference ranges is critical for interpreting changes in these Doppler indices in the setting of pathologic fetal conditions.

13.9 Changes with FGR

Despite using a sensitive method to detect low velocity flow, Doppler, B-mode ultrasound, and a low wall filter setting, absent end diastolic flow is not consistently seen in fetuses with intrauterine fetal growth restriction (FGR) [49]. What was observed was an increase in the measures of impedance to flow. The pulsatility index (PI) was significantly increased, and although the systolic to diastolic ratio (SDR) was also increased, this difference was not significant. These changes were attributed to decreased fetal growth rather

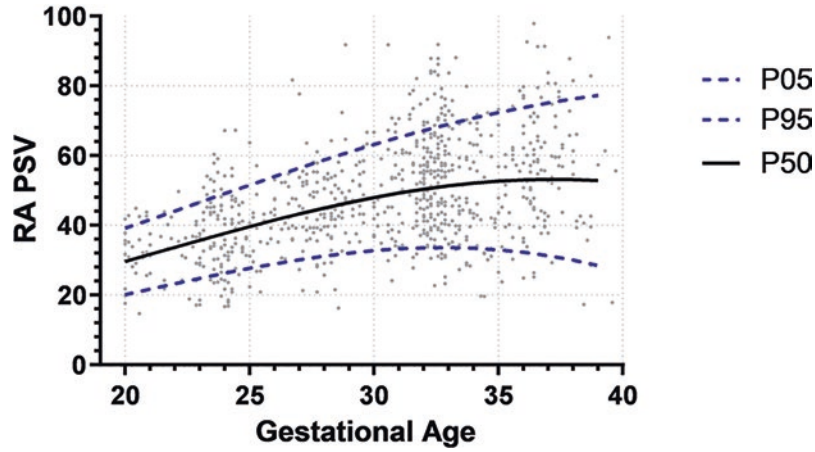

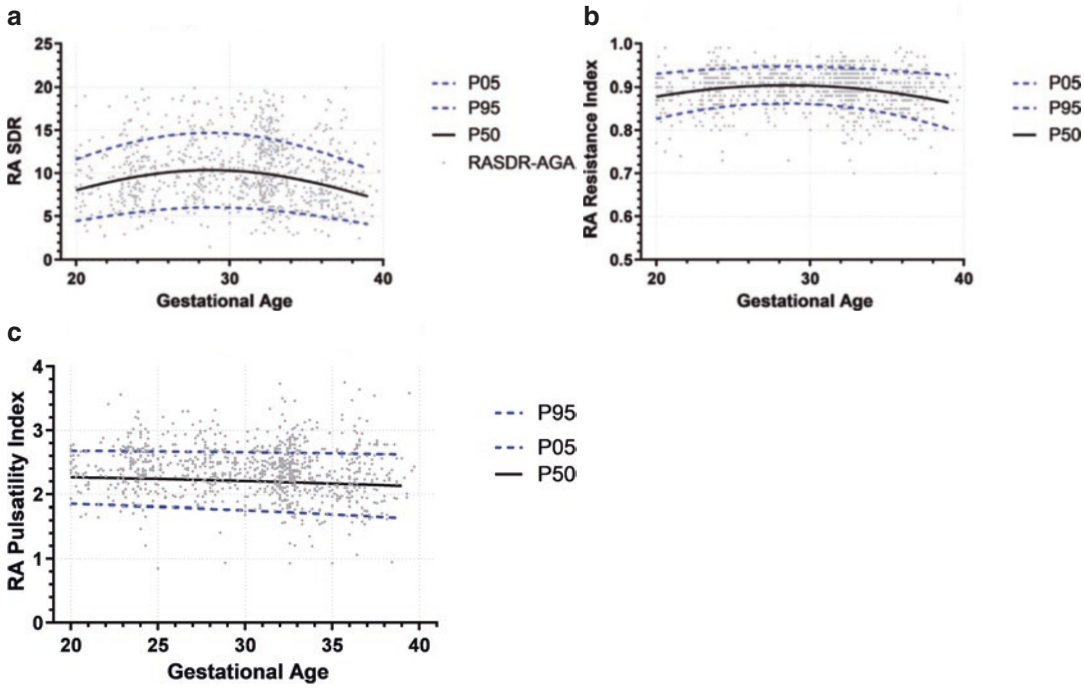

Fig. 13.2 Renal artery peak systolic velocity

Fig. 13.3 (**a**) Renal artery systolic diastolic ratio. (**b**) Renal artery resistance index. (**c**) Renal artery pulsatility index

than hypoxia and presumably mediated through local neurogenic and humoral mechanisms [49]. Acute hypoxia accentuated these changes with additional reductions in renal blood flow and vasoconstriction evident when fetal lamb arterial pO2 fell to less than 20 mmHg [49, 66]. Among fetuses with estimated fetal weight less than the 10the percentile, 64% of fetuses had an elevated renal artery PI greater than the 90th percentile [62, 67].

Current understanding of blood flow in animal studies exposed to hypoxia supports the idea that there is preferential perfusion of the fetal brain, heart, and adrenals at the expense of the carcass (bone, muscle, and skin), gut, and kidneys [68]. In the sheep model of extended hypoxia for 3–10 days, blood flow had a tendency to remain constant or increase gradually in the transition from high to moderately low levels of arterial O2 content and then to decrease abruptly with severe

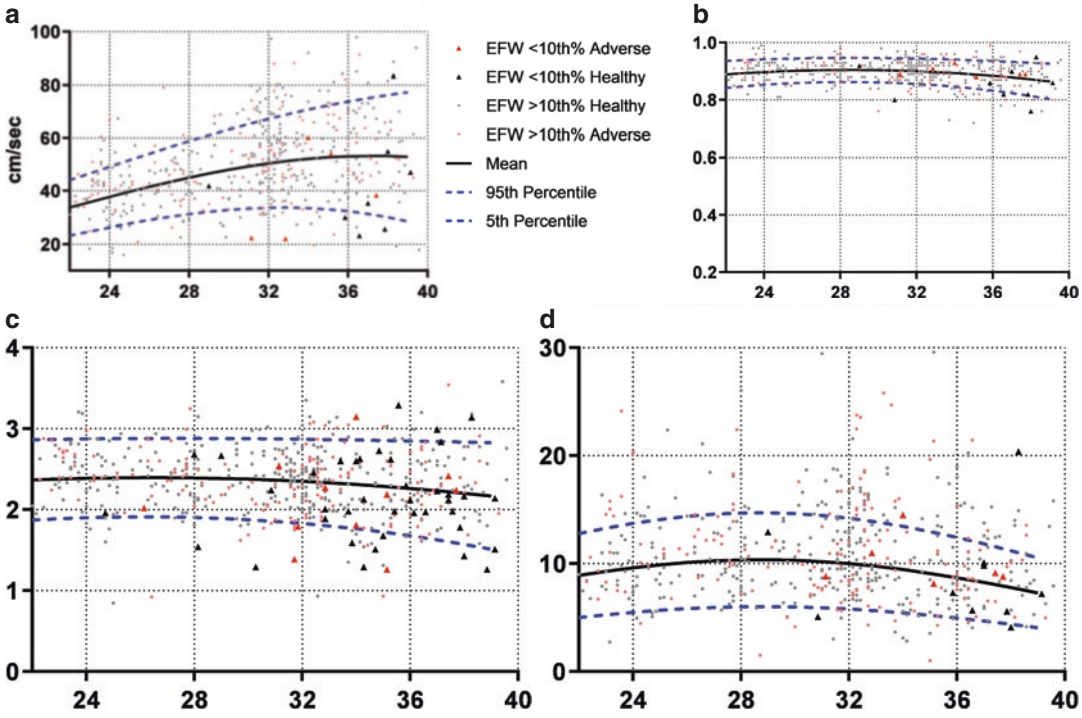

Fig. 13.4 (**a**) Renal artery peak systolic velocity. (**b**) Renal artery resistance index. (**c**) Renal artery pulsatility index. (**d**) Renal artery systolic diastolic ratio

hypoxia. Umbilical blood flow did not change systematically in relation to arterial O2 content, but vascular impedance indices decreased progressively from 18 to 40 weeks because of placental maturation and increasing vascularity of the tertiary stem villi [68, 69]. Early studies performed among fetuses diagnosed with growth restriction that underwent cordocentesis with arterial blood gas assessments found that alterations in the fetal circulation apparently occur before the development of fetal hypoxia [70]. These alterations in the fetal circulation are measured using quantitative assessments of vascular impedance or qualitatively by observation of absent of reversed end diastolic flow velocities. Qualitative assessments are consistent with severe increases in vascular impedance where systole reflects cardiac systole and the corresponding compression wave, while diastole corresponds to reflected waves from the distal arteriolar bed [67].

Two concerns arising from these early interpretations are that fetal arterial vascular tone normally decreases with advancing gestational age [71], and second, vascular impedance to flow also decreases with advancing gestational age, most likely as a function of greater vessel diameter, a significant contributor to impedance to flow. As noted previously, fluid flow through any given segment of a vessel is related to a number of factors: the viscosity of the fluid, the pressure gradient across the vessel being interrogated, and the length and diameter of the vessel. This relationship can have a substantial effect on measured flow velocities as halving the diameter of a vessel can decrease the flow rate by 16-fold. The larger the vessel, the greater the flow. For these reasons, many of the assessments of Doppler flow in the renal artery have reported contradictory results among fetuses diagnosed with fetal growth restriction at any given gestational age, when differences in estimated fetal weight can influence the diameter of the renal vessels. This effect can be observed when normalizing Doppler measurements by estimated fetal weight (Figs. 13.4 and 13.5). Additional changes can occur because of the wall filter used. When evaluating the renal artery, it is important to

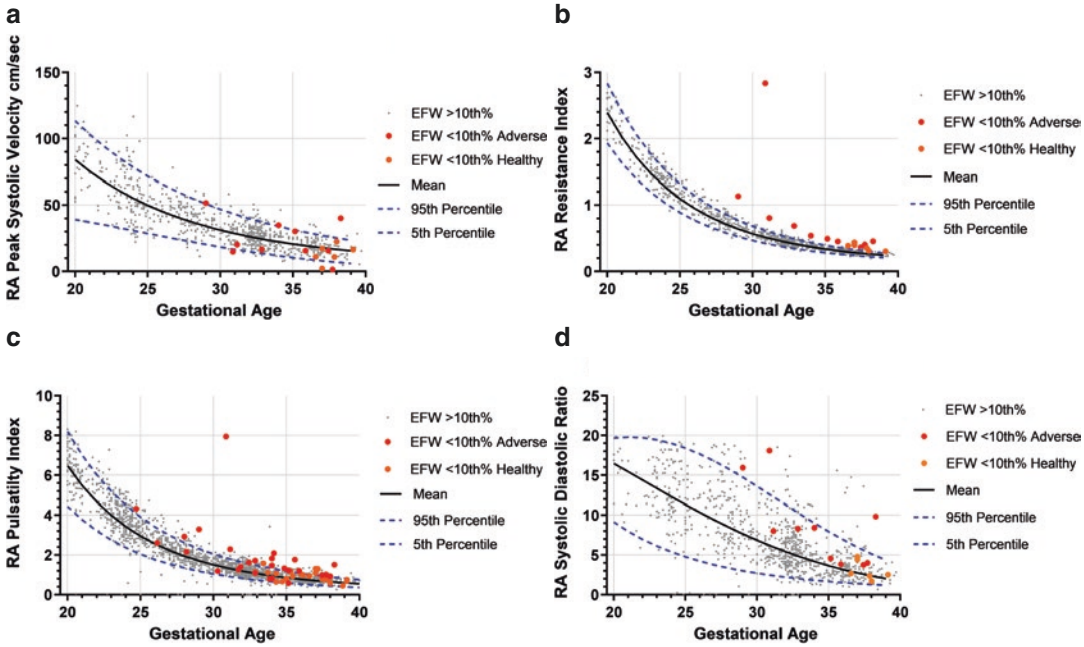

Fig. 13.5 (**a**) Renal artery peak systolic velocity. (**b**) Renal artery resistance index. (**c**) Renal artery pulsatility index. (**d**) Renal artery systolic diastolic ratio

limit the wall filter to low frequencies, as the high frequency filters will remove those signals corresponding to the renal vascular flow, especially those observed during end diastolic flow [49].

Studies of fetal renal artery PI assessment report a gradual decrease in the PI with advancing gestational age among normally grown fetuses [48, 50, 52, 62, 63, 65, 72]. Among growth-restricted fetuses, the PI is reportedly greater than among normally grown fetuses [49]. The increase in the impedance is even greater when associated with fetal hypoxia [49].

Although it is possible that at greater degrees of hypoxia, qualitative changes in blood velocity waveforms will develop, the quantitative differences in renal artery PI may not necessarily correlate with clinically relevant changes in the fetal umbilical pO2 or pH [25, 62]. This is different from what is observed for the middle cerebral artery, where peak velocity and vascular impedance can change according to pO2 and pCO2. This autoregulatory process in the cerebral circulation develops with advancing gestational age [73]. These findings may be due to the conditions in which flow velocity waveforms are measured in the renal artery. When acute changes in fetal oxygenation occur, these eventually lead to the development of fetal heart rate decelerations secondary to the peripheral chemoreceptor response. The efferent arm of this acute response includes a vagally mediated fetal heart rate deceleration and a sympathetically mediated peripheral vasoconstriction, including the renal arteries [74, 75]. Sheep models have demonstrated that when the hypoxia is prolonged and not severe, the sympathetic response is blunted such that fetal heart rate decelerations may develop without peripheral vasoconstriction, but with sustained cerebral vasodilation or centralization of flow [76–78]. If the peripheral vasoconstrictive response is blunted, hypoxia may no longer trigger a change in the renal artery pulsatility index after controlling for gestational age and estimated fetal weight.

13.10 Changes with Fetal Anemia

In addition to gestational age-associated decrease in renal artery impedance, it appears that an acute decrease in intravascular fetal volume can also

lead to an increase in renal vascular impedance [79, 80]. Hypovolemia would be an unusual event in a singleton pregnancy, but is more commonly seen in the donor twin in the setting of twin-to-twin transfusion syndrome [81, 82]. The increase in arterial impedance to flow associated with hypovolemia is also seen in other vascular systems including the middle cerebral and the umbilical artery [83, 84]. In the fetal sheep, the renal artery is more sensitive to alpha-1 adrenergic stimulation than the newborn or the adult sheep [85]. The increased resistance is also evident among fetuses undergoing intravascular transfusions where an increase in renal blood flow occurs within the first hour after volume expansion [79]. The decrease in renal artery resistance allows the cardiovascular system to accommodate the increased volume, and most likely occurs as a result of decreasing tissue hypoxia and inhibition of the sympathetic peripheral chemoreceptor response, renin angiotensin system, and other renal regulatory systems [86].

13.11 Changes Associated with Oligohydramnios or Polyhydramnios

Isolated oligohydramnios refer to the presence of oligohydramnios without fetal structural and chromosomal abnormalities, without fetal growth restriction, without intrauterine infection, and in the absence of known maternal disease [87]. It is proposed that oligohydramnios are caused by decreased renal perfusion due to redistribution of fetal blood among growth-restricted fetuses. In a study of 45 fetuses with isolated oligohydramnios, renal artery Doppler velocimetry and cerebral placental ratio (CPR) were not significantly different in the women with isolated oligohydramnios, compared to 65 women with normal amniotic fluid [87].

Recent analysis of women with isolated oligohydramnios or polyhydramnios found that adjusting the renal artery PI by the calculated renal volume increased the predictive value of the renal artery PI for oligohydramnios better than the unadjusted values or gestational age-adjusted values [88]. The adjusted values were not helpful in the prediction of isolated polyhydramnios, without fetal structural or chromosomal abnormalities, or without the presence of maternal comorbidities [88].

In a study comparing perinatal outcomes among fetuses with low normal amniotic fluid indices (AFI) compared with normal AFI, the renal artery PI was lower among those fetuses with low normal fluid. These fetuses were also delivered earlier which could explain the quantitative difference in renal artery PI between the two groups. It is not clear what the Doppler assessment to delivery interval was, but the lack of qualitative differences would also explain the absence of differences in perinatal outcomes [89].

Longitudinal assessments of the renal artery pulsatility indices confirm the decrease in values with advancing gestational age. A recent study that compared the pulsatility indices between women with normal fluid and those with oligohydramnios at 22, 28 and 34 weeks found higher values among the fetuses with oligohydramnios at 28 weeks, but not at 22 or 34 weeks. In this study, there was a significant difference in birthweight between the groups, affecting fetal outcomes. Those that were diagnosed with oligohydramnios had a lower birthweight, which as noted could be associated with higher values of the PI [90]. These findings replicate reports from earlier studies showing that fetuses with oligohydramnios have higher renal artery PI compared with those with normal amniotic fluid (AF). However, they also report significantly lower birthweights among those with oligohydramnios, which also confounds the association between quantitative increases in the renal artery PI and oligohydramnios in preterm, term, and post term pregnancies [52, 91–94]. The variations in amniotic fluid status associated with maternal hydration or dehydration do not affect the renal artery PI, supporting the notion that the differences are secondary to systemic fetal or local fetal renal cardiovascular regulatory mechanisms [95].

One study looking at the relationship between oligohydramnios and increased renal artery PI among post-term pregnancies did not find a sig-

nificant relationship between the degree of oligohydramnios and quantitative changes in the renal or umbilical artery PI. The differences in the PI values were attributed to birthweight; supporting the confounding effect that birthweight may have on this relationship [96]. The majority of studies are consistent with the earliest reports related to fetal growth restriction and oligohydramnios [51] in that fetal growth restriction are associated with higher renal artery PI, which directly affects renal artery diameter and confounds the relationship between oligohydramnios and renal artery PI. Future studies in this area need to be performed controlling for the effect of fetal weight or fetal kidney weight and vessel size on renal artery PI.

The studies evaluating changes in renal artery PI associated with polyhydramnios have been few and nonconclusive, most finding no association [52, 90]. The most relevant association was the lower renal artery PI associated with increasing fetal birthweight [90, 91].

13.12 Changes with Renal Anomalies

In addition to the presence, size, shape, and position of the kidneys in the diagnosis of renal anomalies, power Doppler assessment of the renal vasculature is very helpful in defining the origin, number, and presence of renal arteries. This is very helpful, particularly in cases of oligohydramnios, women with elevated body mass index, or prior to 20–24 weeks, when identification of the renal contours can be complicated and confused with an enlarged adrenal gland occupying the renal fossa [97]. The origin of the renal arteries assessed with 2D ultrasound has been described in detail [98]. The right renal artery usually arises slightly from the aorta above the left renal artery. Although it usually arises at a right angle from the aorta, in about one third of cases it arises at an angle. Duplications of the renal artery or division after arising from the aorta occur in 1–2% of cases with normal kidneys, but in as many as two thirds of the cases with known renal anomalies. The renal artery can arise from the iliac arteries in cases of horseshoe or pelvic kidney [98, 99]. In cases of diaphragmatic hernia, identification of the renal artery coursing toward the thorax can help identify a herniated kidney [100, 101]. There are formulas to predict the origin of the renal arteries in cases of suspected renal agenesis [102], although recent assessment in normal fetuses suggests that over 95% of the time the renal arteries arise at the level of T12 to L1 [98]. Crossed ectopic kidney should be suspected in cases presenting with an empty renal fossa and a normal positioned kidney. Thorough anatomical scan should be performed as well as periodic follow-up throughout pregnancy given the reported association with other abnormalities including single umbilical artery, ventricular septal defects, and persistent left superior vena cava [103].

Blood flow in the fetal vasculature and specifically in the renal artery has been evaluated among fetuses with polycystic kidneys or hydronephrosis. Prior case series have reported normal renal artery PI indices in cases of hydronephrosis with elevated values in the most severe cases of hydronephrosis or polycystic kidneys [104]. The authors from one study report that the systolic velocity of the renal artery and ductus arteriosus in fetuses with renal disease correlates with fetal renal function. Specifically, a maximum velocity of the renal artery of 1.5 standard deviations below the mean should be the lower normal limit [105]. Cases with urinary tract malformations resulting in severe renal impairment have been shown to be associated with biventricular myocardial hypertrophy and elevated concentrations of circulating pro-brain natriuretic peptide during fetal life. The cardiovascular findings do not always correlate with kidney function or morphology. In the presence of advanced renal disease, assessment of cardiovascular function is warranted [106].

13.13 Changes with Exposure to Medications

The most commonly used medication in obstetrics that could potentially modify renal function is indomethacin. Concerns for use of indometha-

cin in pregnancy are related to its association with development of ductal constriction and oligohydramnios. One early study evaluating its effect among 17 fetuses with polyhydramnios, preterm labor, and growth restriction reported that 7 fetuses manifested ductal constriction. Three fetuses also manifested tricuspid regurgitation. All ductal constrictions and the tricuspid regurgitations resolved in utero after discontinuation of indomethacin. There were no significant differences in the renal artery PI before and during indomethacin therapy. These results suggested that there is no change in fetal renal artery PI during the first 24 h of maternal indomethacin therapy [107]. Recent evidence reporting on the safety of indomethacin use among women with a short cervix or in preterm labor suggests that the risk for oligohydramnios and ductal constriction is much lower than initially assumed, especially when this medication is used in the second trimester and prior to 32 weeks [108–110]. This is in contrast to earlier assessments among pregnancies in preterm labor exposed to indomethacin. The increased risk for adverse outcomes is confounded by gestational age and reported neonatal survival at the time of those reports [111–115].

References

1. Nyengaard JR, Bendtsen TF. Glomerular number and size in relation to age, kidney weight, and body surface in normal man. Anat Rec. 1992;232(2):194–201.
2. Gilbert SF. Developmental biology. Intermediate mesoderm. Sunderland (MA): Sinauer Associates; 2000; 2000 [cited 2019. 6th edition.:[Embryology of the Kidney]. https://www.ncbi.nlm.nih.gov/books/NBK10089/#A3501
3. Saxen L, Sariola H. Early organogenesis of the kidney. Pediatr Nephrol (Berlin, Germany). 1987;1(3):385–92.
4. Toivonen S. Uber die Entwicklung der Vor- und Uriniere beim Kaninchen. Ann Acad Sci Fenn Ser A. 1945;1945(8):1–27.
5. Sainio K, Raatikainen-Ahokas A. Mesonephric kidney—a stem cell factory? Int J Dev Biol. 1999;43(5):435–9.
6. Wintour EM, Butkus A, Earnest L, Pompolo S. The erythropoietin gene is expressed strongly in the mammalian mesonephric kidney. Blood. 1996;88(9):3349–53.
7. Grobstein C. Mechanisms of organogenetic tissue interaction. Natl Cancer Inst Monogr. 1967;26:279–99.
8. Bard JB, Gordon A, Sharp L, Sellers WI. Early nephron formation in the developing mouse kidney. J Anat. 2001;199(Pt 4):385–92.
9. Bard JB, Ross AS. LIF, the ES-cell inhibition factor, reversibly blocks nephrogenesis in cultured mouse kidney rudiments. Development. 1991;113(1):193–8.
10. Dudley AT, Lyons KM, Robertson EJ. A requirement for bone morphogenetic protein-7 during development of the mammalian kidney and eye. Genes Dev. 1995;9(22):2795–807.
11. Perantoni AO, Dove LF, Karavanova I. Basic fibroblast growth factor can mediate the early inductive events in renal development. Proc Natl Acad Sci U S A. 1995;92(10):4696–700.
12. Kispert A, Vainio S, McMahon AP. Wnt-4 is a mesenchymal signal for epithelial transformation of metanephric mesenchyme in the developing kidney. Development. 1998;125(21):4225–34.
13. Fukuoka K, Wilting J, Rodriguez-Vazquez JF, Murakami G, Ishizawa A, Matsubara A. The embryonic ascent of the kidney revisited. Anatomical Record (Hoboken, NJ : 2007). 2019;302(2):278–87.
14. Lescay HA, Tuma F. Anatomy, abdomen and pelvis, ureter. StatPearls. Treasure Island (FL): StatPearls Publishing LLC.; 2019.
15. Kumar S, Neyaz Z, Gupta A. The utility of 64 channel multidetector CT angiography for evaluating the renal vascular anatomy and possible variations: a pictorial essay. Korean J Radiol. 2010;11(3):346–54.
16. Ross MG, Beall MH. Creasy and Resnik's maternal-fetal medicine: amniotic fluid dynamics. 8th ed. Philadelphia, PA: Elsevier, Inc.; 2019. 1388 p
17. Takeuchi H, Koyanagi T, Yoshizato T, Takashima T, Satoh S, Nakano H. Fetal urine production at different gestational ages: correlation to various compromised fetuses in utero. Early Hum Dev. 1994;40(1):1–11.
18. Lee SM, Park SK, Shim SS, Jun JK, Park JS, Syn HC. Measurement of fetal urine production by three-dimensional ultrasonography in normal pregnancy. Ultrasound Obstet Gynecol. 2007;30(3):281–6.
19. Trimmer KJ, Leveno KJ, Peters MT, Kelly MA. Observations on the cause of oligohydramnios in prolonged pregnancy. Am J Obstet Gynecol. 1990;163(6 Pt 1):1900–3.
20. Thurlow RW, Brace RA. Swallowing, urine flow, and amniotic fluid volume responses to prolonged hypoxia in the ovine fetus. Am J Obstet Gynecol. 2003;189(2):601–8.
21. Veille JC, McNeil S, Hanson R, Smith N. Renal hemodynamics: longitudinal study from the late fetal life to one year of age. J Maternal-Fetal Investig. 1998;8(1):6–10.

22. Silverman NH, Schmidt KG. The current role of Doppler echocardiography in the diagnosis of heart disease in children. Cardiol Clin. 1989;7(2):265–97.
23. Andriani G, Persico A, Tursini S, Ballone E, Cirotti D, Lelli CP. The renal-resistive index from the last 3 months of pregnancy to 6 months old. BJU Int. 2001;87(6):562–4.
24. Yasuhi I, Hirai M, Oka S, Nakajima H, Ishimaru T. Effect of maternal meal ingestion on fetal renal artery resistance. Obstet Gynecol. 1997;90(3):340–3.
25. Stigter RH, Mulder EJ, Bruinse HW, Visser GH. Doppler studies on the fetal renal artery in the severely growth-restricted fetus. Ultrasound Obstet Gynecol. 2001;18(2):141–5.
26. Eldridge MW, Berman W Jr, Greene ER. Serial echo-Doppler measurements of human fetal abdominal aortic blood flow. J Ultrasound Med. 1985;4(9):453–8.
27. Lingman G, Marsal K. Fetal central blood circulation in the third trimester of normal pregnancy—a longitudinal study. I. Aortic and umbilical blood flow. Early Hum Dev. 1986;13(2):137–50.
28. Lurie S, Feinstein M, Mamet Y. Human fetal-placental weight ratio in normal singleton near-term pregnancies. Gynecol Obstet Investig. 1999;48(3):155–7.
29. Fineman JR, Maltepe E. Creasy and Resnik's maternal-fetal medicine: fetal cardiovascular physiology. 8th ed. Philadelphia, PA: Elsevier, Inc.; 2019. p. 1388.
30. Paton JB, Fisher DE, Peterson EN, DeLannoy CW, Behrman RE. Cardiac output and organ blood flows in the baboon fetus. Biol Neonate. 1973;22(1):50–7.
31. Rudolph AM, Heyman MA. Fetal and neonatal circulation and respiration. Annu Rev Physiol. 1974;36:187–207.
32. Veille JC, Hanson RA, Tatum K, Kelley K. Quantitative assessment of human fetal renal blood flow. Am J Obstet Gynecol. 1993;169(6):1399–402.
33. Kiserud T, Ebbing C, Kessler J, Rasmussen S. Fetal cardiac output, distribution to the placenta and impact of placental compromise. Ultrasound Obstet Gynecol. 2006;28(2):126–36.
34. Vimpeli T, Huhtala H, Wilsgaard T, Acharya G. Fetal cardiac output and its distribution to the placenta at 11-20 weeks of gestation. Ultrasound Obstet Gynecol. 2009;33(3):265–71.
35. Aperia A, Broberger O, Herin P, Joelsson I. Renal hemodynamics in the perinatal period. A study in lambs. Acta Physiol Scand. 1977;99(3):261–9.
36. Robillard JE, Weismann DN, Herin P. Ontogeny of single glomerular perfusion rate in fetal and newborn lambs. Pediatr Res. 1981;15(9):1248–55.
37. Ausiello DA, Kreisberg JI, Roy C, Karnovsky MJ. Contraction of cultured rat glomerular cells of apparent mesangial origin after stimulation with angiotensin II and arginine vasopressin. J Clin Invest. 1980;65(3):754–60.
38. Contag SA, Bi J, Chappell MC, Rose JC. Developmental effect of antenatal exposure to betamethasone on renal angiotensin II activity in the young adult sheep. Am J Physiol Renal Physiol. 2010;298(4):F847–56.
39. Lumbers ER, Burrell JH, Menzies RI, Stevens AD. The effects of a converting enzyme inhibitor (captopril) and angiotensin II on fetal renal function. Br J Pharmacol. 1993;110(2):821–7.
40. Jose PA, Slotkoff LM, Montgomery S, Calcagno PL, Eisner G. Autoregulation of renal blood flow in the puppy. Am J Phys. 1975;229(4):983–8.
41. Robillard JE, Kulvinskas C, Sessions C, Burmeister L, Smith FG Jr. Maturational changes in the fetal glomerular filtration rate. Am J Obstet Gynecol. 1975;122(5):601–6.
42. Robillard JE, Smith FG, Nakamura KT, Sato T, Segar J, Jose PA. Neural control of renal hemodynamics and function during development. Pediatr Nephrol (Berlin, Germany). 1990;4(4):436–41.
43. Smith FG, Lumbers ER. Comparison of renal function in term fetal sheep and newborn lambs. Biol Neonate. 1989;55(4–5):309–16.
44. Segar JL, Hajduczok G, Smith BA, Merrill DC, Robillard JE. Ontogeny of baroreflex control of renal sympathetic nerve activity and heart rate. Am J Phys. 1992;263(6 Pt 2):H1819–26.
45. Ingelfinger JR, Woods LL. Perinatal programming, renal development, and adult renal function. Am J Hypertens. 2002;15(2 Pt 2):46s–9s.
46. Robillard JE, Gomez RA, VanOrden D, Smith FG Jr. Comparison of the adrenal and renal responses to angiotensin II fetal lambs and adult sheep. Circ Res. 1982;50(1):140–7.
47. Contag S, Patel P, Payton S, Crimmins S, Goetzinger KR. Renal artery Doppler compared with the cerebral placental ratio to identify fetuses at risk for adverse neonatal outcome. J Maternal-Fetal Neonatal Med. 2019:1–9.
48. Haugen G, Godfrey K, Crozier S, Hanson M. Doppler blood flow velocity waveforms in the fetal renal arteries: variability at proximal and distal sites in the right and left arteries. Ultrasound Obstet Gynecol. 2004;23(6):590–3.
49. Veille JC, Kanaan C. Duplex Doppler ultrasonographic evaluation of the fetal renal artery in normal and abnormal fetuses. Am J Obstet Gynecol. 1989;161(6 Pt 1):1502–7.
50. Hecher K, Spernol R, Szalay S. Doppler blood flow velocity waveforms in the fetal renal artery. Arch Gynecol Obstet. 1989;246(3):133–7.
51. Arduini D, Rizzo G. Fetal renal artery velocity waveforms and amniotic fluid volume in growth-retarded and post-term fetuses. Obstet Gynecol. 1991;77(3):370–3.
52. Mari G, Kirshon B, Abuhamad A. Fetal renal artery flow velocity waveforms in normal pregnancies and pregnancies complicated by polyhydramnios and oligohydramnios. Obstet Gynecol. 1993;81(4):560–4.
53. Deane CR, Markus HS. Colour velocity flow measurement: in vitro validation and application to

human carotid arteries. Ultrasound Med Biol. 1997;23(3):447–52.
54. Picot PA, Fruitman M, Rankin RN, Fenster A. Rapid volume flow rate estimation using transverse colour Doppler imaging. Ultrasound Med Biol. 1995;21(9):1199–209.
55. Eicke BM, Kremkau FW, Hinson H, Tegeler CH. Peak velocity overestimation and linear-array spectral Doppler. J Neuroimaging. 1995;5(2):115–21.
56. Thompson RS, Trudinger BJ, Cook CM. Doppler ultrasound waveforms in the fetal umbilical artery: quantitative analysis technique. Ultrasound Med Biol. 1985;11(5):707–18.
57. Trudinger BJ, Giles WB, Cook CM, Bombardieri J, Collins L. Fetal umbilical artery flow velocity waveforms and placental resistance: clinical significance. Br J Obstet Gynaecol. 1985;92(1):23–30.
58. Wladimiroff JW, vd Wijngaard JA, Degani S, Noordam MJ, van Eyck J, Tonge HM. Cerebral and umbilical arterial blood flow velocity waveforms in normal and growth-retarded pregnancies. Obstet Gynecol. 1987;69(5):705–9.
59. Rifkin MD, Needleman L, Pasto ME, Kurtz AB, Foy PM, McGlynn E, et al. Evaluation of renal transplant rejection by duplex Doppler examination: value of the resistive index. AJR Am J Roentgenol. 1987;148(4):759–62.
60. Reneman RS, Hoeks A, Spencer MP. Doppler ultrasound in the evaluation of the peripheral arterial circulation. Angiology. 1979;30(8):526–38.
61. Iaizzo PA. Atlas of human cardiac anatomy. Blood Flow University of Minnesota; 2019.
62. Vyas S, Nicolaides KH, Campbell S. Renal artery flow-velocity waveforms in normal and hypoxemic fetuses. Am J Obstet Gynecol. 1989;161(1):168–72.
63. Konje JC, Abrams KR, Taylor DJ. Normative values of Doppler velocimetry of five major fetal arteries as determined by color power angiography. Acta Obstet Gynecol Scand. 2005;84(3):230–7.
64. Mitra SC, Ganesh V, Apuzzio JJ. Fetal renal artery and umbilical artery Doppler flow and fetal urine output. Am J Perinatol. 1995;12(1):11–3.
65. Figueira CO, Surita FG, Dertkigil MS, Pereira SL, Bennini JR Jr, Morais SS, et al. Longitudinal reference intervals for Doppler velocimetric parameters of the fetal renal artery correlated with amniotic fluid index among low-risk pregnancies. Int J Gynaecol Obstet. 2015;131(1):45–8.
66. Cohn HE, Sacks EJ, Heymann MA, Rudolph AM. Cardiovascular responses to hypoxemia and acidemia in fetal lambs. Am J Obstet Gynecol. 1974;120(6):817–24.
67. Campbell S, Vyas S, Nicolaides KH. Doppler investigation of the fetal circulation. J Perinat Med. 1991;19(1–2):21–6.
68. Peeters LL, Sheldon RE, Jones MD Jr, Makowski EL, Meschia G. Blood flow to fetal organs as a function of arterial oxygen content. Am J Obstet Gynecol. 1979;135(5):637–46.
69. Kaufmann P, Sen DK, Schweikhart G. Classification of human placental villi. I Histology. Cell Tissue Res. 1979;200(3):409–23.
70. Bilardo CM, Nicolaides KH, Campbell S. Doppler measurements of fetal and uteroplacental circulations: relationship with umbilical venous blood gases measured at cordocentesis. Am J Obstet Gynecol. 1990;162(1):115–20.
71. Gregg AR, Weiner CP. "Normal" umbilical arterial and venous acid-base and blood gas values. Clin Obstet Gynecol. 1993;36(1):24–32.
72. Azpurua H, Dulay AT, Buhimschi IA, Bahtiyar MO, Funai E, Abdel-Razeq SS, et al. Fetal renal artery impedance as assessed by Doppler ultrasound in pregnancies complicated by intraamniotic inflammation and preterm birth. Am J Obstet Gynecol. 2009;200(2):203.e1–11.
73. Kooi EMW, Verhagen EA, Elting JWJ, Czosnyka M, Austin T, Wong FY, et al. Measuring cerebrovascular autoregulation in preterm infants using near-infrared spectroscopy: an overview of the literature. Expert Rev Neurother. 2017;17(8):801–18.
74. Lear CA, Galinsky R, Wassink G, Yamaguchi K, Davidson JO, Westgate JA, et al. The myths and physiology surrounding intrapartum decelerations: the critical role of the peripheral chemoreflex. J Physiol. 2016;594(17):4711–25.
75. Giussani DA, Gardner DS, Cox DT, Fletcher AJ. Purinergic contribution to circulatory, metabolic, and adrenergic responses to acute hypoxemia in fetal sheep. Am J Physiol Regul Integr Comp Physiol. 2001;280(3):R678–85.
76. Allison BJ, Brain KL, Niu Y, Kane AD, Herrera EA, Thakor AS, et al. Fetal in vivo continuous cardiovascular function during chronic hypoxia. J Physiol. 2016;594(5):1247–64.
77. Gardner DS, Fowden AL, Giussani DA. Adverse intrauterine conditions diminish the fetal defense against acute hypoxia by increasing nitric oxide activity. Circulation. 2002;106(17):2278–83.
78. Giussani DA. The fetal brain sparing response to hypoxia: physiological mechanisms. J Physiol. 2016;594(5):1215–30.
79. Mari G, Moise KJ Jr, Deter RL, Carpenter RJ Jr. Doppler assessment of renal blood flow velocity waveforms in the anemic fetus before and after intravascular transfusion for severe red cell alloimmunization. J Clin Ultrasound. 1991;19(1):15–9.
80. Schroder H, Gilbert RD, Power GG. Urinary and hemodynamic responses to blood volume changes in fetal sheep. J Dev Physiol. 1984;6(2):131–41.
81. Simpson LL. Twin-twin transfusion syndrome. Am J Obstet Gynecol. 2013;208(1):3–18.
82. Mahieu-Caputo D, Muller F, Joly D, Gubler MC, Lebidois J, Fermont L, et al. Pathogenesis of twin-twin transfusion syndrome: the renin-angiotensin system hypothesis. Fetal Diagn Ther. 2001;16(4):241–4.
83. van Huisseling H, Muijsers GJ, de Haan J, Hasaart TH. The acute response of the umbilical artery

pulsatility index to changes in blood volume in fetal sheep. Eur J Obstet Gynecol Reprod Biol. 1992;43(2):149–55.
84. Baschat AA, Harman CR, Alger LS, Weiner CP. Fetal coronary and cerebral blood flow in acute fetomaternal hemorrhage. Ultrasound Obstet Gynecol. 1998;12(2):128–31.
85. Matherne GP, Nakamura KT, Robillard JE. Ontogeny of alpha-adrenoceptor responses in renal vascular bed of sheep. Am J Phys. 1988;254(2 Pt 2):R277–83.
86. Stevens AD, Lumbers ER. The relationship between plasma renin activity and renal electrolyte excretion in the fetal sheep. J Dev Physiol. 1981;3(2):101–10.
87. Budunoglu MD, Yapca OE, Yldildiz GA, Atakan AR. Fetal renal blood flow velocimetry and cerebroplacental ratio in patients with isolated oligohydramnios. J Gynecol Obstet Human Reprod. 2019;48:495–9.
88. Seravalli V, Miller JL, Block-Abraham D, McShane C, Millard S, Baschat A. The relationship between the fetal volume-corrected renal artery pulsatility index and amniotic fluid volume. Fetal Diagn Ther. 2019;46:97–102.
89. Sahin E, Madendag Y, Tayyar AT, Sahin ME, Col Madendag I, Acmaz G, et al. Perinatal outcomes in uncomplicated late preterm pregnancies with borderline oligohydramnios. J Maternal-Fetal Neonatal Med. 2018;31(23):3085–8.
90. Benzer N, Pekin AT, Yilmaz SA, Kerimoglu OS, Dogan NU, Celik C. Predictive value of second and third trimester fetal renal artery Doppler indices in idiopathic oligohydramnios and polyhydramnios in low-risk pregnancies: a longitudinal study. J Obstet Gynaecol Res. 2015;41(4):523–8.
91. Akin I, Uysal A, Uysal F, Oztekin O, Sanci M, Gungor AC, et al. Applicability of fetal renal artery Doppler values in determining pregnancy outcome and type of delivery in idiopathic oligohydramnios and polyhydramnios pregnancies. Ginekol Pol. 2013;84(11):950–4.
92. Oz AU, Holub B, Mendilcioglu I, Mari G, Bahado-Singh RO. Renal artery Doppler investigation of the etiology of oligohydramnios in postterm pregnancy. Obstet Gynecol. 2002;100(4):715–8.
93. Selam B, Koksal R, Ozcan T. Fetal arterial and venous Doppler parameters in the interpretation of oligohydramnios in postterm pregnancies. Ultrasound Obstet Gynecol. 2000;15(5):403–6.
94. Veille JC, Penry M, Mueller-Heubach E. Fetal renal pulsed Doppler waveform in prolonged pregnancies. Am J Obstet Gynecol. 1993;169(4):882–4.
95. Flack NJ, Sepulveda W, Bower S, Fisk NM. Acute maternal hydration in third-trimester oligohydramnios: effects on amniotic fluid volume, uteroplacental perfusion, and fetal blood flow and urine output. Am J Obstet Gynecol. 1995;173(4):1186–91.
96. Bar-Hava I, Divon MY, Sardo M, Barnhard Y. Is oligohydramnios in postterm pregnancy associated with redistribution of fetal blood flow? Am J Obstet Gynecol. 1995;173(2):519–22.
97. Sepulveda W, Stagiannis KD, Flack NJ, Fisk NM. Accuracy of prenatal diagnosis of renal agenesis with color flow imaging in severe second-trimester oligohydramnios. Am J Obstet Gynecol. 1995;173(6):1788–92.
98. Degani S, Leibovitz Z, Shapiro I, Ohel G. Variations of the origin of renal arteries in the fetus identified on power Doppler and 3D sonography. J Clin Ultrasound. 2010;38(2):59–65.
99. Hsu CY, Chen CP, Lin CJ. An aberrant renal artery arising from the iliac artery imaged by three-dimensional power Doppler ultrasonography: a sign of fetal horseshoe kidney. Ultrasound Obstet Gynecol. 2007;29(3):358–9.
100. Masturzo B, Kalache KD, Cockell A, Pierro A, Rodeck CH. Prenatal diagnosis of an ectopic intrathoracic kidney in right-sided congenital diaphragmatic hernia using color Doppler ultrasonography. Ultrasound Obstet Gynecol. 2001;18(2):173–4.
101. Panda B, Rosenberg V, Cornfeld D, Stiller R. Prenatal diagnosis of ectopic intrathoracic kidney in a fetus with a left diaphragmatic hernia. J Clin Ultrasound. 2009;37(1):47–9.
102. DeVore GR. The value of color Doppler sonography in the diagnosis of renal agenesis. J Ultrasound Med. 1995;14(6):443–9.
103. Zajicek M, Perlman S, Dekel B, Lahav E, Lotan D, Lotan D, et al. Crossed ectopic kidney: prenatal diagnosis and postnatal follow-up. Prenat Diagn. 2017;37(7):712–5.
104. Wladimiroff JW, Heydanus R, Stewart PA, Cohen-Overbeek TE, Brezinka C. Fetal renal artery flow velocity waveforms in the presence of congenital renal tract anomalies. Prenat Diagn. 1993;13(7):545–9.
105. Iura T, Makinoda S, Tomizawa H, Watanabe Y, Waseda T, Inoue H, et al. Hemodynamics of the renal artery and descending aorta in fetuses with renal disease using color Doppler ultrasound—longitudinal comparison to normal fetuses. J Perinat Med. 2005;33(3):226–31.
106. Merz WM, Kubler K, Fimmers R, Willruth A, Stoffel-Wagner B, Gembruch U. Cardiorenal syndrome is present in human fetuses with severe, isolated urinary tract malformations. PLoS One. 2013;8(5):e63664.
107. Mari G, Moise KJ Jr, Deter RL, Kirshon B, Carpenter RJ. Doppler assessment of the renal blood flow velocity waveform during indomethacin therapy for preterm labor and polyhydramnios. Obstet Gynecol. 1990;75(2):199–201.
108. Turan OM, Driscoll C, Cetinkaya-Demir B, Gabbay-Benziv R, Turan S, Kopelman JN, et al. Prolonged early antenatal indomethacin exposure is safe for fetus and neonate. J Maternal-Fetal Neonatal Med. 2019:1–10.
109. Doni D, Paterlini G, Locatelli A, Arnoldi S, Magri MC, Bernasconi D, et al. Effects of antenatal indomethacin on ductus arteriosus early closure and on

adverse outcomes in preterm neonates. J Maternal-Fetal Neonatal Med. 2018:1–6.
110. Dathe K, Hultzsch S, Pritchard LW, Schaefer C. Risk estimation of fetal adverse effects after short-term second trimester exposure to non-steroidal anti-inflammatory drugs: a literature review. Eur J Clin Pharmacol. 2019;75:1347–53.
111. Amin SB, Sinkin RA, Glantz JC. Metaanalysis of the effect of antenatal indomethacin on neonatal outcomes. Am J Obstet Gynecol. 2007;197(5):486.e1–10.
112. Bivins HA Jr, Newman RB, Fyfe DA, Campbell BA, Stramm SL. Randomized trial of oral indomethacin and terbutaline sulfate for the long-term suppression of preterm labor. Am J Obstet Gynecol. 1993;169(4):1065–70.
113. Dudley DK, Hardie MJ. Fetal and neonatal effects of indomethacin used as a tocolytic agent. Am J Obstet Gynecol. 1985;151(2):181–4.
114. Loe SM, Sanchez-Ramos L, Kaunitz AM. Assessing the neonatal safety of indomethacin tocolysis: a systematic review with meta-analysis. Obstet Gynecol. 2005;106(1):173–9.
115. Macones GA, Marder SJ, Clothier B, Stamilio DM. The controversy surrounding indomethacin for tocolysis. Am J Obstet Gynecol. 2001;184(3):264–72.

14 Umbilical Doppler Velocimetry: Normative Data and Diagnostic Efficacy

Dev Maulik, Tabitha Schrufer-Poland, and Emily M. Williams

14.1 Introduction

The umbilical artery was the first fetal vessel to be evaluated by Doppler velocimetry in the fetus and has since become the most widely investigated component of the fetal circulation. The attention paid to this vessel may be explained partly by its ready accessibility to Doppler interrogation and because it is a vital component of the fetal circulation, acting as the lifeline between the fetus and the placenta. Numerous studies have reported the methodology of Doppler interrogation of the umbilical artery and have elucidated the factors that modulate the umbilical artery Doppler indices under normal conditions. This chapter describes the procedure of Doppler sonography of the umbilical circulation and reviews the normative data on the umbilical artery Doppler indices.

14.2 Doppler Interrogation of the Umbilical Artery

Doppler interrogation of the umbilical artery circulation is a relatively simple procedure of short duration. Consistent with the general approach for conducting fetal surveillance tests, the mother should be counseled regarding the reason for the test, the nature of the information generated, its reliability and safety, and other relevant issues. Similar to the practice for fetal heart rate monitoring, the mother lies in a semi-recumbent position with a slight lateral tilt, which minimizes the risk of developing supine hypotension syndrome due to caval compression. The examination should be conducted only during fetal quiescence and apnea. Umbilical artery circulation is amenable to interrogation by either a pulsed-wave Doppler duplex system or a continuous-wave Doppler device. The former is currently the standard approach. The procedure of Doppler insonation varies with the choice of Doppler mode.

14.3 Pulsed-Wave Doppler Interrogation

Pulsed Doppler sonography has become the most frequently used mode for umbilical artery interrogation. The principle for the safe use of ultrasound should be observed with the thermal and mechanical indices set below 1. The wall filter settings for pulsed Doppler are kept at the lowest level (approximately 50 to 60 Hz) to prevent loss of low flow velocity signals. The spectral Doppler panel should be about 50% of the B-mode image window and the pulse repetition frequency scale

D. Maulik (✉) · T. Schrufer-Poland · E. M. Williams
Department of Obstetrics and Gynecology, UMKC School of Medicine/Truman Medical Center, UMKC School of Medicine, Kansas City, MO, USA
e-mail: dmaulik2014@gmail.com

D. Maulik, C. C. Lees (eds.), *Doppler Ultrasound in Obstetrics and Gynecology*,
https://doi.org/10.1007/978-3-031-06189-9_14

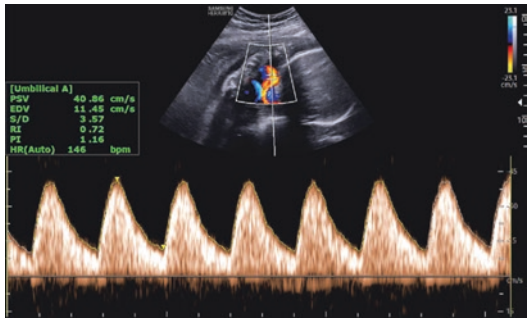

Fig. 14.1 Pulsed Doppler interrogation of umbilical arteries. *Upper Panel*: Two-dimensional sonogram depicting the flow mapping of the umbilical vessels and placement of the Doppler sample volume at the umbilical arterial location. *Lower Panel*: Umbilical arterial Doppler waveforms

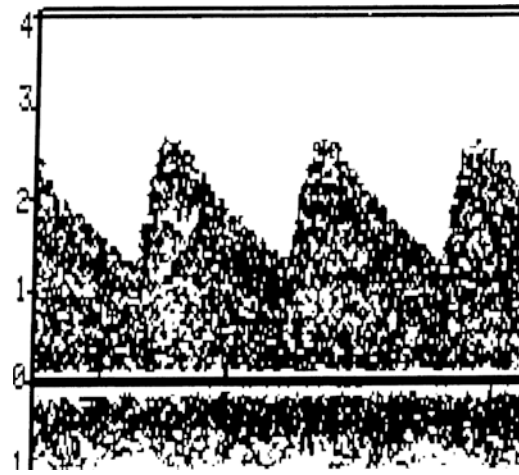

Fig. 14.2 Continuous-wave Doppler interrogation of umbilical vessels. Doppler frequency shift recordings *above* the baseline are derived from the umbilical arteries, and those *below* the baseline are from the umbilical vein

should be adjusted so that the waveform occupies approximately 75% of the Doppler panel. With a pulsed-wave duplex Doppler system, loops of the umbilical cord are identified by B-mode and color Doppler imaging. Unlike the continuous-wave mode, pulsed-wave Doppler insonation permits selection of the location in the cord for interrogation. As discussed below, the site of interrogation in the cord affects the Doppler waveform. Usually a free-floating portion of the cord is insonated. The cursor line representing the beam path is aligned to intersect the selected portion of the cord with an angle of insonation less than 30^0, and the Doppler sample volume is placed in that location. The Doppler mode is then activated, and the umbilical arterial Doppler waveforms are obtained (Fig. 14.1). At least 3–4 consistent waveforms are recorded. Most current devices will automatically generate the indices.

14.4 Continuous-Wave Doppler Interrogation

Continuous-wave Doppler interrogation of the umbilical artery is one of the simplest procedures available for fetal surveillance. However, it is now seldom used in clinical practice. The procedure is conducted using a freestanding Doppler instrument with an integrated fast Fourier transform (FFT)-based spectrum analyzer. The transducer is usually a pencil-shaped probe with an operating frequency of 2–4 MHz. The transducer is placed on the mother's abdomen overlying the fetus with an acoustic coupling jelly intervening between the transducer face and the maternal abdominal skin. The transducer position is adjusted to obtain the characteristic Doppler frequency shift waveforms from the umbilical artery, which is seen on the device display. The process of identification is facilitated by listening to the typical audible sound of the Doppler shift. Complete Doppler interrogation of the cord can be ensured by obtaining the umbilical venous Doppler signals simultaneously with the arterial signals (Fig. 14.2).

14.5 Doppler Display and Archiving

The Doppler waveforms are exhibited on the ultrasound monitor and scrolled from right to left on the screen. The screen is frozen when appropriate signals are displayed, and the desired measurements are performed on these waveforms. Usually, three to five uniform waveforms are measured, and the individual results are averaged and shown on the screen. Most modern devices offer autotrace functions for Doppler assessment, in addition to manual. The image and the results

are digitally saved in an image archiving system and can also be printed.

14.6 Descriptor Indices of the Umbilical Arterial Doppler Waveform

The Doppler frequency shift information from the umbilical artery is predominantly utilized to assess downstream impedance in the fetoplacental vascular bed. As discussed in Chap. 4, it is accomplished by calculating indices that analyze the pulsatility of the waveform in an angle-independent manner. Of the numerous indices described in the literature, the systolic/diastolic (S/D) ratio, resistance index (RI), and pulsatility index (PI) are most commonly used in clinical practice. The relative merits of the commonly used indices are discussed in Chap. 4.

The comparative diagnostic efficacy of the above Doppler indices and the diastolic/average (D/A) ratio for predicting adverse perinatal outcome were investigated by Maulik and associates [1] in a prospective blinded study in a high-risk pregnancy population. A continuous-wave Doppler device with a 4-MHz transducer was used. The analytic technique consisted of the receiver operating characteristic (ROC) method, which evaluates a test's ability to discriminate the diseased from the nondiseased population. The ROC curves showed that the RI had the best discriminatory ability when compared with other Doppler indices, and the PI fared the worst (Fig. 14.3). The area under the ROC curve of these indices showed that these differences were statistically significant (Table 14.1). In the United States, the S/D ratio remains the most widely used Doppler index for evaluating umbilical arterial hemodynamics. In Europe, PI is preferred. In practice, the choice of an index may not significantly affect its clinical efficacy.

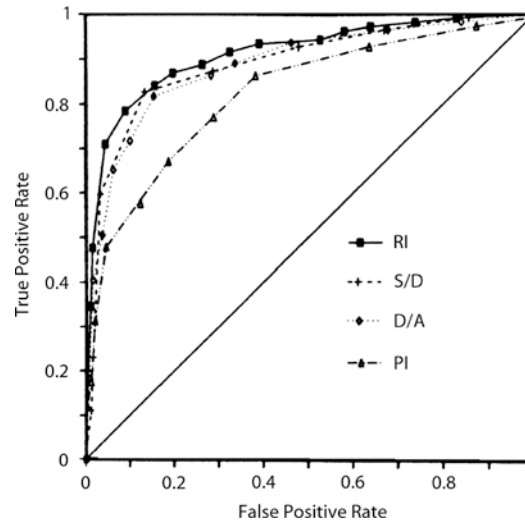

Fig. 14.3 Receiver operating characteristics curve of umbilical arterial Doppler indices. *RI* Resistance index, *S/D* Systolic/diastolic ratio, *D/A* Diastolic/average ratio, *PI* Pulsatile index. Data points are measured values of indices. (From [1] with permission)

Table 14.1 Receiver operating characteristic curve areas of Doppler indices (modified from Maulik et al. [1])

Indices	Area ± SE	Significance (p) of the difference in the ROC areas		
		vs S/D	vs D/A	vs PI
RI	0.921 ± 0.021	<0.05	<0.05	<0.001
S/D	0.905 ± 0.019		>0.05	<0.001
D/A	0.887 ± 0.029			<0.006
PI	0.803 ± 0.023			

SE Standard error, *ROC* Receiver operating characteristic, *RI* Resistance index, *S/D* Systolic/diastolic ratio, *D/A* Diastolic/average ratio, *PI* Pulsatility index

14.7 Reproducibility of Umbilical Arterial Doppler Indices

A critical factor to the utility of a test is its precision, which is defined as the degree to which a measured variable is reproducible. The reproducibility of a Doppler index is determined by all factors that contribute to the variance of that index (see Chap. 4). The variance is affected by hemodynamic and nonhemodynamic factors [2]. The hemodynamic factors may be physiologic, such as gestational age-dependent changes and those associated with fetal breathing, or pathologic, such as maternal preeclampsia or fetal growth restriction. The nonhemodynamic factors constitute the error component, which includes intra- and interobserver variations. Although the latter factors are important when considering the precision of the technique, hemodynamic variations are the principal determinants of the variance of the umbilical Doppler indices [2].

Table 14.2 Reproducibility of the umbilical arterial Doppler indices

Study	Doppler index	Interobserver		Intraobserver	
		Reliability	Variation (%)	Reliability	Variation (%)
Schulman et al. [3]	S/D				6
Nienhuis et al. [4]	PI	0.74		0.62	
Maulik et al. [2]	RI	0.89	11	0.95	5
	S/D	0.91	10	0.96	4
	PI	0.86	14	0.92	8
Gudmundsson et al. [5]	PI		8		
Davies et al. [6]	RI				7
	PI				12
	S/D				11, 15
Scherjon et al. [7]	PI	0.39		0.91	

S/D Systolic/diastolic ratio, *PI* Pulsatility index, *RI* Resistance index

Maulik and colleagues [2] prospectively investigated the reproducibility of the umbilical arterial Doppler indices (S/D ratio, RI, PI, D/A) in terms of the proportion of variance attributable to intra- and interobserver errors. A continuous-wave Doppler instrument with a 4-MHz transducer was used. Analysis of variance was utilized to determine the intraclass correlation. The proportion of total variance attributable to intra-and interobserver variances was comparable to those of other investigators as shown in Table 14.2 [3–7]. As evident, umbilical arterial Doppler indices demonstrate satisfactory precision for clinical applications.

14.8 Continuous-Wave Versus Pulsed-Wave Doppler Indices

Although one may not expect any discrepancy between the Doppler indices obtained by continuous-wave or pulsed-wave Doppler interrogation, in practice there are enough differences between these techniques to warrant an objective inquiry into the issue. Brar and associates [8] compared the S/D ratios obtained by continuous-wave and pulsed-wave Doppler ultrasonography from the umbilical artery in high-risk pregnancies during the third trimester and found no significant difference in the mean S/D ratios obtained by either method for the entire population (continuous-wave S/D 2.81 ± 1.79, pulsed-wave S/D 2.71 ± 1.83; $r = 0.98$), the normal group (continuous-wave S/D 1.96 ± 0.41, pulsed-wave S/D 1.95 ± 0.40, $r = 0.91$), or the abnormal group (continuous-wave S/D 6.23 ± 1.58, pulsed-wave S/D 6.35 ± 1.52, $r = 0.94$). Mehalek and coinvestigators [9] also observed no significant differences ($p > 0.05$) between the continuous-wave and pulsed-wave Doppler devices when measuring the peak S/D ratios in the umbilical arteries. The S/D ratios of the umbilical artery measured by each device showed a strong correlation, whether measured by one observer ($r = 0.93$) or two observers ($r = 0.89$). Most other investigations corroborated this finding [5, 10].

Although van Vugt and coinvestigators [11] found that the A/B ratio (which is the same as the S/D ratio), RI, and PI were slightly higher for the continuous-wave Doppler system compared to the pulsed-wave Doppler system, these differences were not significant ($p = 0.18$, $p = 0.21$, and $p = 0.44$, respectively). The authors speculated that the difference in the signal-to-noise ratio (S/N ratio) between the pulsed-wave and continuous-wave Doppler systems may account for the discrepancy in values. Jorn and associates [12] observed differences between duplex pulsed Doppler and nonduplex continuous-wave and pulsed-wave Doppler systems in terms of their clinical efficacy. The sensitivity was higher with the simple nonduplex Doppler technique (74.3% versus 52.9%), whereas the specificity was higher with the duplex Doppler technique (77.9% versus 52.6%). The authors thought that this finding was attributable to the inability to localize the vessel

precisely using the simpler stand-alone Doppler devices. Gaziano and colleagues [13] reported the use of a threshold value of 4.5 for the umbilical arterial S/D ratio derived with pulsed duplex Doppler. This value is considerably higher than the common S/D ratio cutoff value of 3.0 obtained by continuous-wave Doppler and not consistent with the current data. Importantly, this issue may not be relevant anymore as pulsed duplex Doppler is universally used in the current clinical practice.

14.9 Factors Influencing the Umbilical Artery Doppler Indices

14.9.1 Doppler Sampling Site

Introduction of duplex pulsed Doppler ultrasound for interrogation of umbilical arteries allowed for discrimination of the sampling site in the umbilical cord. Utilization of this approach led to the realization that the site of Doppler sampling in the umbilical cord may contribute significantly to variations in the Doppler indices. Several studies addressed this issue. Most observed that the location of the Doppler sampling site in the umbilical cord affects the Doppler waveform and is reflected in the Doppler indices, which are higher at the fetal abdominal end of the cord than at this placental end [14, 15]. Abramowicz and coinvestigators [14] studied the effect of the examination site in 30 normal pregnancies and noted statistically significant differences (p <0.01–<0.0007) in the umbilical arterial S/D ratio between the two measurement sites. The values (mean ± standard deviation) at the placental insertion ranged from 4.2 ± 0.4 at 17–20 weeks to 2.1 ± 0.5 at 37–40 weeks. The corresponding values at the fetal abdominal end were 6.1 ± 0.8 and 3.3 ± 0.5, respectively. In comparison, the continuous-wave Doppler interrogation, which was blind to the site of sampling in the cord, generated values of 4.8 ± 1.3 and 2.3 ± 0.3, respectively.

Maulik and associates [2] prospectively investigated the components of variance and error contributions of umbilical arterial Doppler indices in a normal pregnant population (308 mothers) with gestational ages ranging from 27 to 40 weeks. In 46 women, duplex pulsed Doppler ultrasound was used to interrogate the placental and fetal ends of the cord. The study demonstrated that the site of measurement was a significant source of variance; the PI was affected the most and the D/A ratio the least (Table 14.3). The effect of the measurement site on the umbilical arterial indices was confirmed by Mehalek and colleagues [15] who performed pulsed duplex Doppler on 58 patients and noted that the Doppler indices were significantly higher at the fetal end of the cord than at the placental end. Because of the dependence of the indices on the site of interrogation, most investigators emphasize the importance of indicating which sampling location was utilized when duplex pulsed Doppler ultrasound is used. Obviously, this point is not an issue with continuous-wave Doppler insonation.

Table 14.3 Location of measurement and reliability of Doppler indices (modified from Maulik et al. [1] with permission)

Doppler index	Reliability coefficient (%)	Error variance (%)
D/A	71	29
S/D	62	38
PI	54	46
RI	68	32

D/A Diastolic/average ratio, *S/D* Systolic/diastolic ratio, *PI* Pulsatility index, *RI* Resistance index

The mechanism of this phenomenon was investigated by Vieyres and coinvestigators [16] in a computer model, which showed that placental resistance is the primary factor for the observed differences between the Doppler waveforms from the placental end and from the fetal end of the cord, whereas viscosity and cord length have secondary influences. The phenomenon may be explained more adequately by the concept of impedance and wave reflection (see Chap. 4). The fetoplacental vascular bed is a low-impedance system associated with minimal wave reflection, which explains the presence of continuing forward flow in the umbilical artery during diastole. The closer the measurement site is to the placenta, the less the wave reflection and the greater the end-diastolic flow. Consequently, the Doppler waveform that represents arterial

flow velocity demonstrates progressively declining pulsatility and, therefore, the Doppler indices.

In a large, prospective longitudinal study, Acharya and [17] established reference ranges for umbilical artery PI based on both site of interrogation and gestational age. Their findings corroborated those of previous cross-sectional previous studies, confirming that site of interrogation had a significant effect on the various indices, with higher velocity and pulsatility noted at the intra-abdominal and fetal portions of the umbilical artery, than the placental end.

Not all studies, however, agree with the above findings. Ruissen and associates [18] observed that although the PI values differed among the various locations in the umbilical artery (within the fetal abdomen, 0–5 cm from the origin of the umbilical cord, in the free-floating segment, 0–5 cm from its insertion in the placenta), no unequivocal tendency or statistically significant difference in the PI could be demonstrated. The authors concluded that possible variations in the Doppler waveform along the course of the umbilical artery have no clinical relevance in uncomplicated pregnancies.

This has been further supported recently by Bhide and colleagues who prospectively investigated the importance of the umbilical artery Doppler sampling site in 158 singleton pregnancies after 24 weeks of gestation [19]. Umbilical artery PI was measured from the free loop of the umbilical cord and from the paravesical site. Although the PI was significantly lower in the free loop, the contribution of the measurement site to the total variability of the PI was insignificant ($p = 0.254$).

14.9.2 Short-Term Temporal Variations: The Circadian Rhythm

Short-term temporal variations in the umbilical arterial Doppler indices may affect their reproducibility and efficacy and should be considered when interpreting changes in the indices. FitzGerald and associates [20] failed to observe any appreciable diurnal changes in the umbilical arterial Doppler waveform. This point was further investigated by Hastie and colleagues [21] and observed no significant day-to-day variations ($p > 0.05$) in the S/D ratio or the PI. A more recent report by Avitan and colleagues, however, contradicts these findings. These investigators observed significant diurnal changes in middle cerebral and umbilical flow velocities in a prospective study which included 68 uncomplicated singleton pregnancies in the third trimester [22]. This observation requires further investigation.

14.9.3 Long-Term Temporal Variations: Gestational Age Effect

As gestation advances, umbilical arterial Doppler waveforms demonstrate a progressive rise in the end-diastolic velocity (Fig. 14.4). This phenomenon was first described by Stuart and associates [23]. The gestational age at which end-diastolic velocity may be first noticed in the umbilical arterial circulation depends on the examination technique. It is imperative to ensure that the high-pass filter is either turned off or set at the lowest value irrespective of the sonographic approach. In addition, the use of transvaginal Doppler sonography with color flow-assisted pulsed-wave Doppler interrogation significantly improves our ability to identify the end-diastolic velocity during early pregnancy.

Early investigators, utilizing the transabdominal approach, noted the universal presence of the end-diastolic velocity by about 22 weeks' pregnancy [24] However, the high-pass filter was set at 200 Hz, which is unacceptably high for this application. Arduini and Rizzo [25] utilized color Doppler-guided transvaginal spectral Doppler sonography and demonstrated that the end-diastolic forward flow may be present in the umbilical artery as early as 10 weeks' gestation. After week 10, the pro-

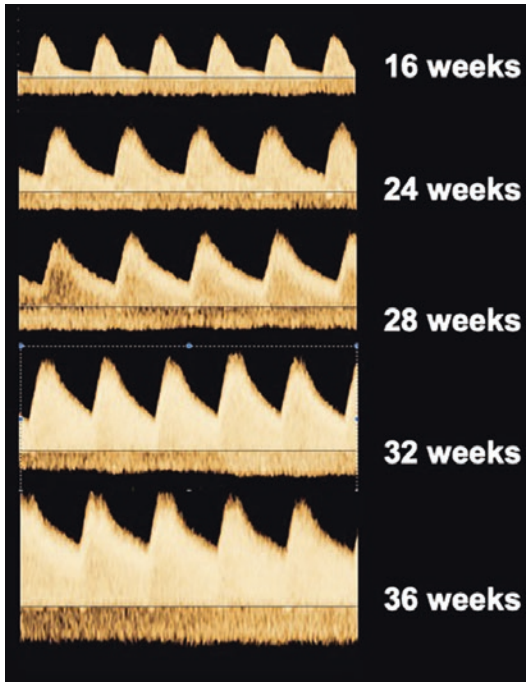

Fig. 14.4 Gestational age effect on the umbilical arterial Doppler waveforms. Panels are organized from top to the bottom according to the advancing gestation. Note the progressive increase in end-diastolic velocity and the concomitant fall in pulsatility as the gestation advances

portion of cases with end-diastolic forward flow progressively increased with the advancing gestation and it was present in almost all cases by about 15 weeks. At this early stage, the phenomenon was not noted during every cardiac cycle, although the percentage of cardiac cycles in which end-diastolic velocities were present increased with the progression of pregnancy. Other investigators also noted the presence of end-diastolic velocity in the umbilical artery by 15 weeks [26]. Our own experience with transabdominal duplex pulsed-wave Doppler insonation indicates that end-diastolic velocity is detectable at the placental end of the cord in most cases by about 16 weeks' gestation.

The end-diastolic velocity in the umbilical artery continues to increase throughout the pregnancy, which is reflected in the Doppler indices. The indices that reflect the wave pulsatility, such as the RI, S/D ratio, and PI, continue to decrease, whereas the D/A ratio, which is the normalized end-diastolic frequency shift, continues to increase [27]. In a prospective study involving 308 normal pregnant mothers, Maulik and associates [2] quantified the contribution of the duration of pregnancy to the total variance of the umbilical arterial Doppler indices. It was observed that the gestational age was the single major contributor to the total variance of the indices, ranging from 33% for the PI to 46% for the S/D ratio.

These trends in the Doppler waveform are consistent with the crucial physiological changes that occur in the fetoplacental circulation characterized by the gestational age-dependent decline in the fetoplacental flow impedance [28]. Anderson and Faber [29] estimated that the fetoplacental circulatory resistance in the ovine fetus decreased by 2.8% per day, and during the last third of pregnancy, the decrease in resistance was calculated to be tenfold. As discussed above, Acharya and associates published normative data on the effects of both the site of interrogation and gestational age [17].

The mechanism for this phenomenon relates to progressive changes in the placental circulation. It has been shown in human placental studies that there is continuing expansion of the fetoplacental vascular system throughout the pregnancy [30]. Furthermore, the villous vascular system undergoes a transformation, resulting in the appearance of sinusoidal dilation in the terminal villous capillaries as pregnancy approaches term, and more than 50% of the stromal volume may be vascularized. The progressive decrease in fetoplacental flow impedance is associated with a concomitant decline in the flow wave reflection from the downstream vascular bed, which results in an increase in the end-diastolic velocity. The latter ensures continuing forward flow and perfusion of the fetal placenta during the entire cardiac cycle.

14.9.4 Fetal Heart Rate

Heart rate influences the configuration of the arterial Doppler waveform (see Chap. 4). Thompson and colleagues [31] did not observe any significant effect of fetal heart rate on the umbilical arterial S/D ratio. The correlation between the fetal cardiac cycle, which is the reciprocal of the heart rate, and the S/D ratio was poor ($r = 0.1$). Other Doppler indices (PI and RI) demonstrated a similar relation with the heart rate. This finding was contradicted, however, by Mires and associates [32], who specifically investigated the relation between fetal heart rate and the umbilical arterial Doppler indices in 85 normal pregnancies: 25 of the women were antepartum and 60 were in labor. Among the antepartum patients, both the S/D ratio and RI had a significant correlation with heart rate ($r = -0.49$; $p < 0.02$). The intrapartum mothers demonstrated a similar significant negative correlation between the heart rate and the indices ($r = -0.65$; $p < 0.001$). A heart rate variation of 117 and 162 bpm resulted in corresponding S/D ratio values of 2.0 and 2.8, respectively. The effect was more pronounced with a wider range of heart rate. For example, when the latter varied between 90 and 175, the S/D ratio changed from 3.4 to 1.7. Thus, significant changes in the indices may occur due to changes in the fetal heart rate, especially when bradycardia is present. Mires et al. concluded that it is important to correct the indices by changing the fetal heart rate.

To address this contradiction, a prospective study was undertaken by Yarlagadda and colleagues [33]. The population consisted of 194 mothers with uncomplicated pregnancies and gestational ages ranging from 27 to 39 weeks. Linear regression of the data grouped in 2-week intervals demonstrated a moderate but statistically significant ($p < 0.05$) correlation between the fetal heart rate and the umbilical Doppler indices. The influence of the heart rate on the indices was then further analyzed by a multiple regression technique, which demonstrated that 15%–18% of the total variance of the indices was attributable to fetal heart rate effect. Moreover, when the Doppler indices were standardized for a heart rate of 140 bpm and a gestation of 34 weeks, using a multiple regression-based equation the 95% limits of the umbilical artery Doppler indices were reduced by 32%, 34%, 26%, and 32% for D/A, S/D, PI, and RI, respectively. This study corroborated the findings of Mires and coinvestigators [32] that the fetal heart rate significantly influences umbilical arterial Doppler indices.

The mechanism of the heart rate effect on the Doppler indices is discussed in Chap. 4. To recapitulate, it is well-recognized that when the heart rate drops, the diastolic phase of the cardiac cycle is prolonged and the end-diastolic frequency shift declines. These changes are reflected in the Doppler indices that depict the pulsatility of the Doppler waveform. It has been reconfirmed [34, 35] that the diastolic time is the main component of the changes in the duration of a cardiac cycle (see Chap. 4) and that the effect of the heart rate changes on the Doppler indices is mediated predominantly through the diastolic phase of the cardiac cycle. There is also evidence that the fetal heart rate may affect the ability of the Doppler waveform analysis to reflect completely the changes in the downstream impedance [36].

It remains controversial, however, whether correcting the indices for fetal heart rate improves their diagnostic efficacy when the baseline heart rate remains within the normal range. The general consensus is that although the Doppler indices are affected by the fetal heart rate, it may not be a significant factor when the rate is within the normal range. For example, Mansouri and colleagues [37] observed in uncomplicated pregnancies that an upper limit of 3.0 for a normal umbilical artery peak S/D ratio was acceptable only if the instantaneous fetal heart rate was 130 bpm or higher. Similar observation was reported by Ruhle and coinvestigators [38] who found negligible variations in the umbilical arterial S/D ratio within the normal range of fetal heart rate (120–160 bpm). Most investigators therefore do not recommend correction of the indices for the heart rate.

14.9.5 Fetal Breathing

Substantial changes in the intrathoracic pressure and central hemodynamics occur during fetal breathing, leading to dynamic variations in the umbilical arterial Doppler waveform and Doppler indices (Fig. 14.5). The effect of fetal breathing on umbilical arterial indices has been recognized from the early days of Doppler velocimetry and led to the recommendation that the indices should be measured only during fetal apnea [39]. Fetal breathing movement-induced changes in cardiovascular function were originally reported in the fetal lamb by Dawes and associates [40]. The initiation of rapid, irregular respiratory movement in the fetal lamb was often associated with tachycardia and hypertension. Vigorous breathing led to increases in the arterial pressure of as much as 20%. However, transient falls in arterial pressure were also seen coinciding with decreases in the intrathoracic pressure. In addition, there were significant variations in the aortic flow, which declined to 400 mL/min and rose to 900 mL/min from a mean of 650 mL/min.

Chiba and coworkers [41] were the first to report changes in the human fetal venous circulation during fetal breathing movements. Using pulsed-wave Doppler ultrasound combined with real-time B-mode imaging, these investigators demonstrated that the umbilical venous blood flow increased with fetal inspiration (during which the fetal abdominal wall moved inward) and decreased with expiration (during which the wall moved outward). Koppelaar and Wladimiroff [42] compared the effect of breathing on the umbilical venous and arterial Doppler waveforms and noted that, in contrast to venous flow velocity, the magnitude of breathing-related modulation of arterial pulsatility was small and independent of breathing amplitude. This finding was corroborated in a subsequent study by Nyberg, and associates, in 2010 [43]. Furthermore, Spencer and associates [44] demonstrated that even during the breathing episodes, deriving the indices from a minimum of six waveforms ensured coefficients of variation of 10% or less. Despite these findings, it is generally recommended that UA Doppler should be performed during fetal apnea.

The issue of the need to use duplex imaging to ensure fetal apnea was addressed by Hoskins and coinvestigators [45], who showed that when stand-alone continuous-wave Doppler units are used to acquire umbilical artery Doppler waveforms during fetal apnea, the presence of apnea can be ascertained using the variability of the arterial and venous trace without using imaging equipment. Our own experience corroborates this finding.

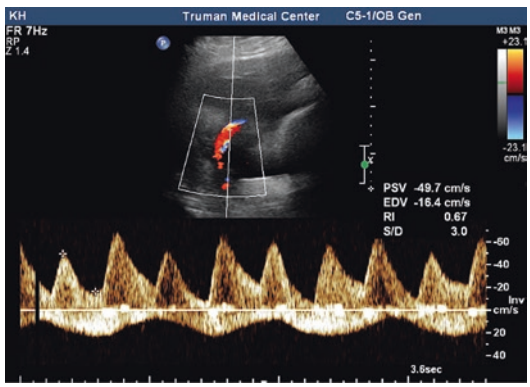

Fig. 14.5 Fetal breathing and umbilical arterial Doppler waveforms. Observe the dynamic variations in the arterial and venous Doppler tracings

14.9.6 Behavioral States

Behavioral states may be defined as the neurobiological functional conditions, exemplified by sleep or wakefulness. These states are characterized by multiple parameters, including open or closed eyes, eye movement, body movement, breathing, and heart rate activity. Prechtl and Bientema [46] were the first to describe the various behavioral states in neonates. For the human fetus, four behavioral states were described by Nijhuis and coworkers [47] based on fetal eye and body movements and the heart rate. Of these states, the quiet sleep state (1F) and the active sleep state (2F) are important considerations for fetal cardiovascular function.

Mulders and associates [39] investigated the effect of fetal behavioral states on 19 normal pregnancies between 37 and 39 weeks' gestation. The fetal heart rate pattern was used to determine states 1F and 2F. The umbilical arterial PI was noted to be higher during the 1F periods than during 2F. This difference disappeared when the effect of the heart rate was taken into account by normalizing all PI values to the standard heart rate value of 140 bpm. This question was further investigated by van Eyck and coinvestigators [48], who utilized simultaneous measurements of fetal heart rate and eye and body movements. The PI values for states 1F and 2F demonstrated no significant differences and considerable overlaps. This insensitivity of the umbilical arterial circulation to behavioral state implies that behavioral states should not be considered when measuring the umbilical arterial Doppler indices.

14.9.7 Blood Viscosity

Viscosity is an attribute of a fluid that reflects its intrinsic resistance to flow. The contribution of viscosity to impedance to flow is defined by Poiseuille's law. Blood viscosity is dependent on hematocrit and plasma viscosity. With certain pregnancy disorders (e.g., preeclampsia), fetal blood viscosity has been shown to be increased [49]. The influence of fetal blood viscosity on the umbilical arterial Doppler indices was studied by Giles and Trudinger [50], who observed significantly ($p < 0.01$) higher blood viscosity at high shear in the high-risk group with abnormal Doppler indices. The investigators, regrettably, did not consider the possible effect of gestational age in this analysis. Steel and coinvestigators [51] investigated the contribution of viscosity to the impedance of blood flow in the umbilical artery as determined by the RI for 31 pregnancies complicated by preeclampsia, intrauterine growth restriction, or both and 20 normal pregnancies. The authors found a significant correlation between the RI and both plasma viscosity and gestational age. Furthermore, 55% of the variance seen in the RI could be explained by plasma viscosity. The major determinants of fetoplacental flow impedance, however, were peripheral vascular factors, not whole-blood viscosity. Therefore, the viscosity of fetal blood may not be considered when interpreting the umbilical arterial Doppler indices.

14.9.8 Maternal Posture and Umbilical Arterial Doppler Indices

Most biophysical fetal surveillance tests, including electronic fetal heart rate monitoring, the biophysical profile examination, and Doppler interrogation of the fetal circulation, are performed with the mother in the semirecumbent position with left lateral tilt so that the risk of supine hypotension is minimized. Kinsella and coinvestigators [52] assessed maternal and fetal cardiovascular effects of position change in 20 women in late pregnancy. Upon changing from the left lateral to the supine position, there was a 45% reduction in leg blood flow, although there were no changes in femoral, brachial, or uterine arterial resistance as measured with Doppler ultrasonography. The leg blood pressure was not affected, indicating the absence of significant aortic compression. However, the maternal heart rate increased in the supine position, suggesting the presence of inferior vena caval compression. Notably, the fetal heart rate and umbilical Doppler indices did not vary with maternal postural change. The effect of posture was investigated more extensively by Sorensen and associates [53], who studied the effects of orthostatic stress and maternal hemodynamics on the umbilical arterial S/D ratios in normal and hypertensive pregnancies. Although all mothers demonstrated a decline in cardiac output and increased total peripheral resistance on standing, there was no change in the

S/D ratio in normotensive patients when they were moved to the upright position. In contrast, the ratio significantly increased with a postural change in hypertensive patients.

14.9.9 Maternal Exercise and Yoga

The fetal circulatory response to maternal exercise may be an important consideration when timing a fetal Doppler investigation. Several investigators have addressed this issue [54–56]. All of these studies, which employed bicycle ergometry, demonstrated an exercise-induced response in the maternal cardiovascular system. The fetal cardiac chronotropic response was variable. Often the response was tachycardia, although a lack of variation was also noted. Most studies failed to show changes in the umbilical arterial Doppler indices. When such changes were noted, they were associated with fetal heart rate alterations. Subsequent studies have been performed with treadmill and walking protocols, demonstrating similar findings [57–59] In a study by Babbar and associates on prenatal yoga, there were no changes in placental hemodynamics following after 1 h of activity [60]. From these investigations, it appears that mild to moderate exercise does not affect flow impedance in the umbilical artery independent of changes in the fetal heart rate.

Strenuous activity, however, may have significant, although transient, changes in umbilical artery Doppler parameters. Intense exercise reaching patient's anaerobic threshold resulted in significantly increased uterine artery PI and decreased umbilical artery PI in several studies, returning to baseline shortly after the cessation of activity [61, 62]. In a study of pregnant elite athletes, Salvesen et al. observed that exercise at >90% maternal oxygen consumption resulted in fetal bradycardia and elevated umbilical artery PI. These changes returned to baseline shortly after cessation of exercise [58].

Several authors evaluated exercise in pregnancies complicated by FGR. In one study of 10 pregnancies complicated by FGR and 33 control pregnancies, exercise did not alter uterine or umbilical Doppler parameters; however, submaximal exercise was associated with abnormalities in fetal middle cerebral artery and increased resistance in the fetal aorta suggestive of cerebral vasodilation [62]. These changes persisted following cessation of exercise. In contrast, in another study, although mean umbilical S/D was higher in FGR pregnancies, it was not statistically different than control pregnancies following exercise [57]. Based on these studies, we encourage physical activity in moderation in uncomplicated pregnancies under medical guidance, but caution against intense exertion. There is still a dearth of studies on the effects of physical activity on the fetal health as highlighted in a recent nonsystematic review on this issue [63].

14.10 Reference Ranges for Umbilical Artery Doppler Indices

It is apparent from the above review that short and long-term factors affect the umbilical artery Doppler indices in normal pregnancies. These factors, particularly the long-term temporal effect of gestational age, must be considered in percentile-based quantitative interpretation of the umbilical artery Doppler indices. Many nomograms of umbilical artery Doppler indices have been reported over the years and a full review is beyond the scope of this chapter. However, we review here a few recent studies and a recent systematic review. Acharya and colleagues [17] conducted a prospective longitudinal study of umbilical artery PI measured at the intra-abdominal, fetal end, and placental end location at 4-weekly intervals at 19–42 weeks of gestation in 130 low-risk singleton pregnancies. As expected, UA Doppler parameters vary significantly at different locations. Ciobanu et al.

Table 14.4 Umbilical artery systolic/diastolic ratio (S/D Ratio) centile values according to gestational age. International gestational age-specific centiles for umbilical artery Doppler systolic/diastolic ratio: a longitudinal prospective cohort study of the INTERGROWTH-21st Project. (From [67], with permission)

Gestational age	Centile						
(Weeks + days)	3rd	5th	10th	50th	90th	95th	97th
24 + 0	2.38	2.46	2.61	3.23	4.12	4.46	4.72
25 + 0	2.30	2.39	2.53	3.15	4.03	4.38	4.63
26 + 0	2.23	2.32	2.46	3.07	3.95	4.29	4.54
27 + 0	2.18	2.26	2.40	3.00	3.86	4.19	4.44
28 + 0	2.13	2.22	2.35	2.93	3.77	4.09	4.33
29 + 0	2.09	2.17	2.31	2.87	3.68	3.99	4.22
30 + 0	2.06	2.14	2.26	2.81	3.58	3.89	4.11
31 + 0	2.03	2.10	2.22	2.74	3.49	3.78	4.00
32 + 0	2.00	2.07	2.19	2.68	3.40	3.67	3.88
33 + 0	1.97	2.04	2.15	2.62	3.30	3.57	3.76
34 + 0	1.94	2.01	2.11	2.56	3.21	3.46	3.65
35 + 0	1.91	1.97	2.08	2.50	3.12	3.35	3.53
36 + 0	1.88	1.94	2.04	2.44	3.02	3.24	3.41
37 + 0	1.85	1.91	2.00	2.38	2.93	3.14	3.30
38 + 0	1.82	1.87	1.96	2.32	2.83	3.03	3.18
39 + 0	1.79	1.84	1.92	2.25	2.73	2.92	3.06
40 + 0	1.75	1.80	1.87	2.19	2.64	2.81	2.94

recently published reference ranges for the umbilical artery PI, middle cerebral artery PI, and CPR developed from a cross-sectional study that comprised of over 70,000 singleton pregnancies, normal and complicated, undergoing routine ultrasound examinations between three periods in the second and third trimesters [64]. Analysis included the effects of maternal age, body mass index, race, method of conception, and parity. More recently, Flateley and associates reported another reference range for umbilical artery, PI, middle cerebral artery PI, and CPR from a prospective cross-sectional study involving over 6000 low-risk cohort of pregnancies [65].

Oros et al. reported a systematic review of observational studies with the primary aim of developing reference ranges [66]. The authors followed the MOOSE [67] and PRISMA [68] guidelines. From over 2900 publications, 38 studies met the inclusion criteria. There was significant heterogeneity in the studies and only a few studies were of high methodological quality, highlighting the need for rigorously conducted future studies in creating reference ranges for these Doppler indices.

More recently, Drukker et al. published prospectively collected longitudinal gestational age-specific reference values for umbilical artery Doppler indices measured in carefully selected 431 low-risk pregnancies from three centers in three continents [69]. Standardized protocols were strictly implemented including early confirmation of pregnancy. Low-risk nature of pregnancy was confirmed by an uneventful obstetrical course, assuring perinatal and long-term postnatal outcomes followed up to 2 years. Tables 14.4 and 14.5 present their data on S/D and PI, respectively. The project was a continuation of the INTERGROWTH21 project [70] and represents a significant addition to the clinically useful normative data.

These reports represent significant advances in reliably identifying elevations of Doppler indices that could impact clinical management.

Table 14.5 Umbilical artery pulsatility index (PI) centile values according to gestational age. International gestational age-specific centiles for umbilical artery Doppler pulsatility index: a longitudinal prospective cohort study of the INTERGROWTH-21st Project. (From [67], with permission)

Gestational age	Centile						
(Weeks + days)	3rd	5th	10th	50th	90th	95th	97th
24 + 0	0.83	0.86	0.91	1.10	1.31	1.38	1.42
25 + 0	0.80	0.84	0.89	1.08	1.30	1.37	1.41
26 + 0	0.78	0.81	0.87	1.07	1.29	1.35	1.40
27 + 0	0.76	0.79	0.85	1.05	1.27	1.34	1.38
28 + 0	0.74	0.78	0.83	1.03	1.25	1.32	1.36
29 + 0	0.73	0.76	0.81	1.01	1.23	1.30	1.34
30 + 0	0.71	0.75	0.80	1.00	1.21	1.28	1.32
31 + 0	0.70	0.73	0.78	0.98	1.19	1.26	1.30
32 + 0	0.68	0.72	0.77	0.96	1.17	1.24	1.28
33 + 0	0.67	0.70	0.75	0.94	1.15	1.21	1.25
34 + 0	0.66	0.69	0.74	0.92	1.13	1.19	1.23
35 + 0	0.64	0.67	0.72	0.90	1.10	1.16	1.20
36 + 0	0.63	0.66	0.70	0.88	1.08	1.14	1.18
37 + 0	0.61	0.64	0.69	0.86	1.05	1.11	1.15
38 + 0	0.59	0.62	0.67	0.84	1.03	1.08	1.12
39 + 0	0.58	0.60	0.65	0.82	1.00	1.06	1.09
40 + 0	0.56	0.59	0.63	0.79	0.97	1.03	1.06

References

1. Maulik D, Yarlagadda P, Youngblood JP, Ciston P. Comparative efficacy of umbilical arterial Doppler indices for predicting adverse perinatal outcome. Am J Obstet Gynecol. 1991;164:1434–40.
2. Maulik D, Yarlagadda AP, Youngblood JP, Willoughby L. Components of variability of umbilical arterial Doppler velocimetry: a prospective analysis. Am J Obstet Gynecol. 1989;160:1406–12.
3. Schulman H, Fleischer A, Stern W, et al. Umbilical velocity wave ratios in human pregnancy. Am J Obstet Gynecol. 1984;148:985–90.
4. Nienhuis SJ, van Vugt JM, Hoogland HJ, Ruissen CJ, de Haan J. Interexaminer variability of fetal Doppler velocity waveforms. Gynecol Obstet Investig. 1988;25:152–7.
5. Gudmundsson S, Fairlie F, Lingman G, Marsal K. Recording of blood flow velocity waveforms in the uteroplacental and umbilical circulation: reproducibility study and comparison of pulsed and continuous wave Doppler ultrasonography. J Clin Ultrasound. 1990;18:97–101.
6. Davies JA, Lee A, Spencer JA. Variability of continuous-wave Doppler flow velocity waveform indices from the umbilical artery. Obstet Gynecol. 1990;76:366–99.
7. Scherjon SA, Kok JH, Oosting H, Zondervan HA. Intra-observer and inter-observer reliability of the pulsatility index calculated from pulsed Doppler flow velocity waveforms in three fetal vessels. Br J Obstet Gynaecol. 1993;100:134–8.
8. Brar HS, Medearis AL, De Vore GR, Platt LD. Fetal umbilical velocimetry using continuous-wave and pulsed-wave Doppler ultrasound in high-risk pregnancies: a comparison of systolic to diastolic ratios. Obstet Gynecol. 1988;72:607–12.
9. Mehalek KE, Berkowitz GS, Chitkara U, Rosenberg J, Berkowitz RL. Comparison of continuous-wave and pulsed Doppler S/D ratios of umbilical and uterine arteries. Obstet Gynecol. 1988;72:603–6.
10. Chan FY, Pun TC, Lee CP, et al. A comparative study of continuous- and pulsed-wave Doppler velocimetry in fetal and uteroplacental circulation. J Ultrasound Med. 1991;10:277–80.
11. Van Vugt JM, Ruissen CJ, Nienhuis SJ, Hoogland HJ, de Hann J. Comparison of blood velocity waveform indices recorded by pulsed Doppler and continuous wave Doppler in the umbilical artery. J Clin Ultrasound. 1988;16:573–6.
12. Jorn H, Fendel H, Christ B. Ein Vergleich zwischen einfachen Dopplermethoden (kontinuierlicher oder gepulster Doppler) und dem Duplex-System (Kombination von B-Bild und gepulstem Doppler). Z Geburtshilfe Perinatol. 1991;195:107.
13. Gaziano EP, Knox GF, Wager GP, Bendel RP, Olson JD. Pulsed Doppler umbilical artery waveforms: significance of elevated umbilical artery systolic/diastolic ratios in the normally grown fetus. Obstet Gynecol. 1990;75:189–95.

14. Abramowicz JS, Warsof SL, Arrington J, Levy DL. Doppler analysis of the umbilical artery: the importance of choosing the placental end of the cord. J Ultrasound Med. 1989;8:219–21.
15. Mehalek KE, Rosenberg J, Berkowitz GS, Chitkara U, Berkowitz RL. Umbilical and uterine artery flow velocity waveforms: effect of the sampling site on Doppler ratios. J Ultrasound Med. 1989;8:171–6.
16. Vieyres P, Durand A, Patat F, et al. Influence of the measurement location on the resistance index in the umbilical arteries: a hemodynamic approach. J Ultrasound Med. 1991;10:671–5.
17. Acharya G, Wilsgaard T, Berntsen GK, Maltau JM, Kiserud T. Reference ranges for serial measurements of blood velocity and pulsatility index at the intra-abdominal portion, and fetal and placental ends of the umbilical artery. Ultrasound Obstet Gynecol. 2005;26(2):162–9.
18. Ruissen CJ, von Drongelen MM, Hoogland HJ, Jager W, Hoeks AP. Characteristics of the umbilical artery velocity waveform as function of measurement site. Gynecol Obstet Investig. 1990;30:212–6.
19. Bhide A, Badade A, Khatal K. The effect of sampling site on the variability of umbilical artery PI. Eur J Obstet Gynecol Reprod Biol. 2019;235:102–5.
20. FitzGerald DE, Stuart B, Drumm JE, Duignan NM. The assessment of fetoplacental circulation with continuous wave Doppler ultrasound. Ultrasound Med Biol. 1984;10:371–6.
21. Hastie SJ, Howie CA, Whittle MJ, Rubin PC. Daily variability of umbilical and lateral uterine wall artery blood velocity waveform measurements. Br J Obstet Gynaecol. 1988;95:571–4.
22. Avitan T, Sanders A, Brain U, Rurak D, Oberlander TF, Lim K. Variations from morning to afternoon of middle cerebral and umbilical artery blood flow, and fetal heart rate variability, and fetal characteristics in the normally developing fetus. J Clin Ultrasound. 2018;46:235–40.
23. Stuart B, Drumm JE, FitzGerald DE, Duignan NM. Fetal blood flow velocity waveforms in normal pregnancy. Br J Obstet Gynaecol. 1980;87:780–6.
24. Reuwer PJHM, Bruinse HW, Stoutenbeek P, Haspels AA. Doppler assessment of the fetoplacental circulation in normal and growth retarded fetuses. Eur J Obstet Gynecol Reprod Biol. 1984;18:199–205.
25. Arduini D, Rizzo G. Umbilical artery velocity waveforms in early pregnancy: a transvaginal color Doppler study. J Clin Ultrasound. 1991;19:335–9.
26. Wladimiroff JW, Huisman TW, Stewart PA. Fetal and umbilical flow velocity waveforms between 10–16 weeks' gestation: a preliminary study. Obstet Gynecol. 1991;78:812–4.
27. Maulik D. Basic principles of Doppler ultrasound as applied in obstetrics. Clin Obstet Gynecol. 1989;32:628.
28. Dawes GS. Fetal and neonatal physiology. Chicago: Year Book; 1968.
29. Anderson DF, Faber JJ. Regulation of the fetoplacental blood flow in the lamb. Am J Phys. 1984;247:R567–74.
30. Kaufmann P, Luckhardt M, Leiser R. Three dimensional representation of the fetal vessel system in the human placenta. Trophoblast Res. 1984;3:113–38.
31. Thompson RS, Trudinger BJ, Cook CM. Doppler ultrasound waveforms in the fetal umbilical artery: quantitative analysis technique. Ultrasound Med Biol. 1985;11:707–14.
32. Mires G, Dempster J, Patel NB, et al. The effect of fetal heart rate on umbilical artery flow velocity waveform. Br J Obstet Gynaecol. 1987;94:665–9.
33. Yarlagadda P, Willoughby L, Maulik D. Effect of fetal heart rate on umbilical arterial Doppler indices. J Ultrasound Med. 1989;8:215–8.
34. Maulik D, Downing GJ, Yarlagadda P. Umbilical arterial Doppler indices in acute uteroplacental flow occlusion. Echocardiography. 1990;7:619–27.
35. Downing GJ, Yarlagadda P, Maulik D. Effects of acute hypoxemia on umbilical arterial Doppler indices in a fetal ovine model. Early Hum Dev. 1991;25:1–10.
36. Downing GJ, Maulik D, Phillips C, Kadado T. In vivo correlation of Doppler waveform analysis with arterial input impedance parameters. J Ultrasound Med Biol. 1993;19:549–59.
37. Mansouri H, Gagnon R, Hunse C. Relationship between fetal heart rate and umbilical blood flow velocity in term human fetuses during labor. Am J Obstet Gynecol. 1989;160:1007–12.
38. Ruhle W, Gnirs J, Schmidt W. Fetal heart rate and Doppler flow parameters in fetal blood vessels—evaluation of 2517 individual signals. Z Geburtshilfe Perinatol. 1993;197:90–4.
39. Mulders LG, Muijers GJ, Jongsma HW, Nijhuis JG, Hein PR. The umbilical artery blood flow velocity waveform in relation to fetal breathing movements, fetal heart rate and fetal behavioural states in normal pregnancy at 37 to 39 weeks. Early Hum Dev. 1986;14:283–93.
40. Dawes GS, Fox HE, Leduc BM, Liggins GC, Richards RT. Respiratory movements and rapid eye movement sleep in the fetal lamb. J Physiol Lond. 1972;220:119–43.
41. Chiba Y, Utsu M, Kanzaki T, Hasegawa T. Changes in venous flow and intratracheal flow in fetal breathing movements. Ultrasound Med Biol. 1985;11:43–9.
42. Koppelaar I, Wladimiroff JW. Quantitation of breathing-related modulation of umbilical arterial and venous flow velocity waveforms in the normal term fetus. Eur J Obstet Gynecol Reprod. 1992;45:177–80.
43. Nyberg MK, Johnsen SL, Rasmussen S, Kiserud T. Fetal breathing is associated with increased umbilical blood flow. Ultrasound Obstet Gynecol. 2010;36(6):718–23.
44. Spencer JA, Price J, Lee A. Influence of fetal breathing and movements on variability of umbilical Doppler indices using different numbers of waveforms. J Ultrasound Med. 1991;10:37–41.
45. Hoskins PR, McDicken WN, Johnstone FD, et al. Determination of the presence of fetal apnoea using umbilical artery and umbilical vein Doppler waveforms. Ultrasound Med Biol. 1988;14:589–92.

46. Prechtl HFR, Beintema DJ. The neurological examination of the full term newborn infant. Clinics in developmental medicine no 12. London: Heinmann Medical Books Ltd; 1964.
47. Nijhuis JG, Prechtl HFR, Martin CB Jr, Bots RSGM. Are there behavioral states in the human fetus? Early Hum Dev. 1982;6:177–95.
48. Van Eyck J, Wladimiroff JW, van der Wijngaard JA, Noordam MJ, Prechtl HFR. The blood flow velocity waveform in the fetal internal carotid and umbilical artery; its relationship to fetal behavioral states in normal pregnancy at 37–38 weeks of gestation. Br J Obstet Gynaecol. 1987;94:736–41.
49. Buchan PC. Pre-eclampsia—a hyperviscosity syndrome. Am J Obstet Gynecol. 1982;142:111–5.
50. Giles WB, Trudinger BJ. Umbilical cord whole blood viscosity and the umbilical artery flow velocity time waveforms: a correlation. Br J Obstet Gynaecol. 1986;93:466–70.
51. Steel SA, Pearce JM, Nash G, et al. Correlation between Doppler flow velocity waveforms and cord blood viscosity. Br J Obstet Gynaecol. 1989;96:1168–72.
52. Kinsella SM, Lee A, Spencer JA. Maternal and fetal effects of the supine and pelvic tilt positions in late pregnancy. Eur J Obstet Gynecol Reprod Biol. 1990;36:11–7.
53. Sorensen TK, Hendricks S, Easterling TR, Carlson KL, Benedetti TJ. Effect of orthostatic stress on umbilical Doppler waveforms in normal and hypertensive pregnancies. Am J Obstet Gynecol. 1992;167:643–7.
54. Drack G, Kirkinen P, Baumann H, Muller R, Huch R. Doppler ultrasound studies before and following short-term maternal stress in late pregnancy. Z Geburtshilfe Perinatol. 1988;192:173–7.
55. Veille JC, Bacevice AE, Wilson B, Janos J, Hellerstein HK. Umbilical artery waveform during bicycle exercise in normal pregnancy. Obstet Gynecol. 1989;73:957–60.
56. Erkkola RU, Pirhonen JP, Kivijarvi AK. Flow velocity waveforms in uterine and umbilical arteries during submaximal bicycle exercise in normal pregnancy. Obstet Gynecol. 1992;79:611–5.
57. Nabeshima Y, Sasaki J, Mesaki N, Sohda S, Kubo T. Effect of maternal exercise on fetal umbilical artery waveforms: the comparison of IUGR and AFD fetuses. J Obstet Gynaecol Res. 1997;23(3):255–9.
58. Salvesen KÅ, Hem E, Sundgot-Borgen J. Fetal well-being may be compromised during strenuous exercise among pregnant elite athletes. Br J Sports Med. 2012;46(4):279–83.
59. de Oliveria Melo AS, Silva JL, Tavares JS, Barros VO, Leite DF, Amorim MM. Effect of a physical exercise program during pregnancy on uteroplacental and fetal blood flow and fetal growth: a randomized controlled trial. Obstet Gynecol. 2012;120(2 Part 1):302–10.
60. Babbar S, Hill JB, Williams KB, Pinon M, Chauhan SP, Maulik D. Acute feTal behavioral response to prenatal yoga: a single, blinded, randomized controlled trial (TRY yoga). Am J Obstet Gynecol. 2016;214(3):399–e1.
61. Morrow RJ, Ritchie JK, Bull SB. Fetal and maternal hemodynamic responses to exercise in pregnancy assessed by Doppler ultrasonography. Am J Obstet Gynecol. 1989;160(1):138–40.
62. Kennelly MM, Geary M, McCaffrey N, McLoughlin P, Staines A, McKenna P. Exercise-related changes in umbilical and uterine artery waveforms as assessed by Doppler ultrasound scans. AJOG. 2002;187(3):661–6.
63. Preissl H. Spotlight on the fetus: how physical activity during pregnancy influences fetal health: a narrative review. BMJ Open Sport Exerc Med. 2020;6(1):e000658.
64. Ciobanu A, Wright A, Syngelaki A, Wright D, Akolekar R, Nicolaides KH. Fetal Medicine Foundation reference ranges for umbilical artery and middle cerebral artery pulsatility index and cerebroplacental ratio. Ultrasound Obstet Gynecol. 2019;53:465–72.
65. Flatley C, Kumar S, Greer RM. Reference centiles for the middle cerebral artery and umbilical artery pulsatility index and cerebro-placental ratio from a low-risk population–a generalised additive model for location, shape and scale (GAMLSS) approach. J Matern Fetal Neonatal Med. 2019;32(14):2338–45.
66. Oros D, Ruiz-Martinez S, Staines-Urias E, Conde-Agudelo A, Villar J, Fabre E, Papageorghiou AT. Reference ranges for Doppler indices of umbilical and fetal middle cerebral arteries and cerebroplacental ratio: systematic review. Ultrasound Obstet Gynecol. 2019;53(4):454–64.
67. Stroup DF, Berlin JA, Morton SC, Olkin I, Williamson GD, Rennie D, Moher D, Becker BJ, Sipe TA, Thacker SB. Meta-analysis of observational studies in epidemiology: a proposal for reporting. Meta-analysis of observational studies in epidemiology (MOOSE) group. J Am Med Assoc. 2000;283:2008–12.
68. Liberati A, Altman DG, Tetzlaff J, Mulrow C, Gøtzsche PC, Ioannidis JP, Clarke M, Devereaux PJ, Kleijnen J, Moher D. The PRISMA statement for reporting systematic reviews and meta-analyses of studies that evaluate healthcare interventions: explanation and elaboration. BMJ. 2009;339:b2700.
69. Drukker L, Staines-Urias E, Villar J, Barros FC, Carvalho M, Munim S, McGready R, Nosten F, Berkley JA, Norris SA, Uauy R. International gestational age-specific centiles for umbilical artery Doppler indices: a longitudinal prospective cohort study of the INTERGROWTH-21st Project. Am J Obstet Gynecol. 2020;222:602.e1–15.
70. Papageorghiou AT, Ohuma EO, Altman DG, Todros T, Ismail LC, Lambert A, Jaffer YA, Bertino E, Gravett MG, Purwar M, Noble JA. International standards for fetal growth based on serial ultrasound measurements: the fetal growth longitudinal study of the INTERGROWTH-21st project. Lancet. 2014;384(9946):869–79.

Fetal Aortic Isthmus and Descending Aorta

15

Karel Maršál and Edgar Hernandez-Andrade

15.1 Fetal Aortic Isthmus

15.1.1 Importance

The aortic isthmus is the first anatomical segment of the descending aorta and is located between the left subclavian artery and the junction with the ductus arteriosus (Fig. 15.1). The aortic isthmus has a major importance as it is an open channel from where blood from the right ventricle and the ductus arteriosus can be forwarded to the aortic branches to perfuse the upper part of the fetal body and the fetal brain when needed. In fetuses with congenital cardiac anomalies or placental insufficiency (chronic hypoxia), the aortic isthmus acts as a "shunt" forwarding blood from the right ventricle and the ductus arteriosus to the aortic arch [1]. Some authors consider the aortic isthmus as a "watershed" and a link between the fetal cerebral and placental circulations [2, 3].

In congenital cardiac anomalies, where blood cannot be ejected by the left ventricle either due to stenotic mitral or aortic valves, or to severe narrowing of the aorta (coarctation) leading to hypoplastic left heart, blood from the right fetal heart will be deviated to the aortic arch and coronary circulation through the aortic isthmus. The function of the aortic isthmus is critical in the survival of such neonates as the ductus arteriosus must be kept open after birth to maintain the circulation to the brain and upper body of the newborn. In these babies, the systemic circulation is almost entirely handled by the right ventricle ejecting the systemic blood through the pulmonary artery and ductus arteriosus. In fetuses with a right hypoplastic ventricle, the entire fetal circulation is handled by the left ventricle, increasing the amount of blood flow passing through the ascending aorta, the aortic arch, and the aortic isthmus. Consequently, due to the higher amount of blood ejected by the left ventricle, the proportion of blood passing through the aortic isthmus is higher, thus increasing its diameter since early stages of pregnancy as compared to normal fetuses [1].

The absence of aortic isthmus is a rare variant of an interrupted aortic arch. These fetuses still have a normal blood perfusion to the brain and a normal subdiaphragmatic circulation as each ventricle ejects blood through each great artery, aorta or pulmonary. However, after birth, an interrupted aortic arch is not compatible with life as, at the time of ductus arteriosus closure, there is no more blood flow to subdiaphragmatic

K. Maršál (✉)
Department of Obstetrics and Gynecology, Clinical Sciences Lund, Lund University, Lund, Sweden
e-mail: karel.marsal@med.lu.se

E. Hernandez-Andrade
Department of Obstetrics, Gynecology & Reproductive Sciences, University of Texas McGovern Medical School, University of Texas, Health Science Center at Houston (UTA Health), Houston, TX, USA

D. Maulik, C. C. Lees (eds.), *Doppler Ultrasound in Obstetrics and Gynecology*,
https://doi.org/10.1007/978-3-031-06189-9_15

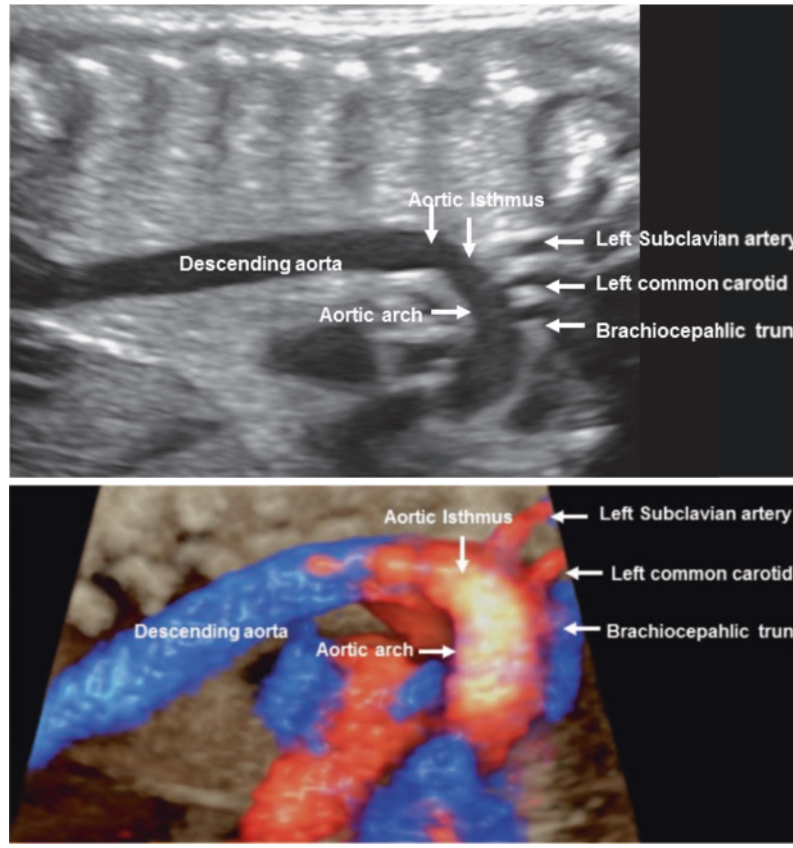

Fig. 15.1 Sagittal plane of the fetal thorax showing the aortic arch, its branches, and the aortic isthmus

organs. The congenital absence of aortic isthmus does not justify an aggressive approach during intrauterine life; nevertheless, an accurate diagnosis is needed to improve the clinical management and survival after birth. In normal newborns, after the closure of the ductus arteriosus, the aortic isthmus is no longer a shunt and becomes an integral part of the descending aorta [1].

Other fetal vascular anomalies such as an arterial-venous fistula in the fetal brain can greatly increase the net flow to the brain. This additional blood is obtained from the ductus arteriosus and can be manifested as retrograde flow in the aortic isthmus. In fetuses exposed to chronic hypoxia/asphyxia (placental insufficiency with increased resistance to fetoplacental flow), the aortic isthmus allows delivery of a higher amount of blood to the fetal upper body and head. Severe fetal brain vasodilation is a manifestation of an increased need of oxygenated blood by the fetal brain which is compensated by deviating blood from the ductus arteriosus through the aortic isthmus. These anatomical and physiological functions of the aortic isthmus highlight the importance of its evaluation in fetuses with cardiac anomalies and in fetuses exposed to hypoxia/asphyxia of placental origin.

15.1.2 Anatomical Features

The first aortic segments can be divided into: (1) aortic root, (2) ascending aorta (before the first aortic branch, the brachiocephalic trunk), (3) transverse aorta (starts before the origin of the brachiocephalic trunk and ends after the left subclavian artery), (4) aortic isthmus (between the left subclavian artery and the ductus arteriosus), and (5) descending aorta (after the junction of the ductus arteriosus). The diameter of each aortic segment increases linearly during pregnancy [4]. The aortic isthmus is the narrowest section of the aorta, with a diameter 28% smaller than the aortic root and 15% smaller than the descending aorta after

the junction with the ductus arteriosus. Hornberger et al. [4] evaluated five cases with clinical suspicion of coarctation confirmed at birth and reported that the diameters of the aortic root, ascending and descending aorta, as well as the left common carotid artery diameters were within "normal" range in all five cases. However, the transverse aorta and aortic isthmus diameters were below the third percentile for gestational age in all five cases. The authors explained the differences in size to be related to the amount of blood received by each segment. In normal pregnancies, the aortic isthmus receives approximately 10–15% of the total cardiac output, whereas the descending aorta after the joint with the ductus arteriosus receives approximately 67% of the total cardiac output [5].

Differences in size of the five aortic segments were also reported by Angelini et al. [6] The authors evaluated the histological characteristics of the aortic segments in 20 stillbirths and showed that the aortic isthmus diameter was about 37% shorter than that of the ascending aorta. Using ultrasound in fetal life, the same authors reported that the aortic isthmus diameter was approximately 27% shorter than that of the descending aorta, and that the aortic isthmus and the arterial duct were usually of similar size. After birth, due to the closure of the ductus arteriosus and the establishment of two separate circulations, the size of the aortic isthmus increased until reaching the size of the descending aorta.

In pregnancies before 20 weeks of gestation, Vimpeli et al. [7] reported that approximately 75% of blood ejected from the left ventricle passes through the aortic isthmus. The authors also observed an increment in aortic isthmus blood velocities, i.e., peak systolic, end-diastolic, and time velocity integral, whereas the pulsatility index (PI) remained similar during that period of pregnancy, with a success rate of acquiring the aortic isthmus Doppler waveform of 33% at 11–13 weeks, 62% at 14–16 weeks, and 83% at 17–20 weeks of gestation. The diameter of the aortic isthmus in late gestation was evaluated in 110 low risk pregnancies between 30 and 40 weeks of gestation by Nomiyama et al. [8]. The authors reported a linear increment in the aortic isthmus diameter from 3.8 mm at 30 weeks of gestation to 4.6 mm at 40 weeks of gestation and no significant differences in aortic isthmus diameters measured in the middle segment or before the junction with the ductus arteriosus.

15.1.3 Doppler Recordings of the Aortic Isthmus Flow Velocity

The acquisition of the aortic isthmus Doppler waveform was originally proposed in a sagittal plane of the thorax with a clear view of the aortic arch and the descending aorta (Fig. 15.1). This anatomical plane, either with the fetal spine located anteriorly or posteriorly, allows a reliable identification of the aortic isthmus as the subclavian artery is clearly visualized, thus reducing the variation between operators [9]. The Doppler sample gate is located in the aorta after the origin of the left subclavian artery and before the ductus arteriosus. In some cases, a proper visualization of the sagittal plane of the aortic arch cannot be obtained; therefore, a cross-sectional image of the thorax at the level of the three vessels and trachea view (Fig. 15.2) has been proposed as an alternative plane for obtaining the aortic isthmus signals. The Doppler sample gate is placed in the aortic segment just before the junction with the ductal arch, in the "V" formed by the two great

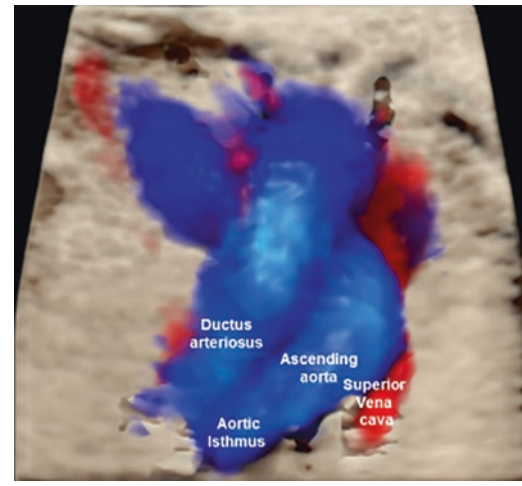

Fig. 15.2 Cross-sectional image of fetal thorax at the level of the three vessel view and the aortic isthmus

vessels. In this plane, Pasquini et al. [10] reported a mean difference in the measurement of the aortic isthmus diameter between operators of −0.04 mm (95% limits of agreement [LOA] −0.8 to 0.71 mm) and in the sagittal plane of 0.02 mm (LOA −0.39 to 0.43 mm], suggesting that the sagittal view might be a more reproducible plane for identification of the aortic isthmus.

The aortic isthmus Doppler waveform has four components (Fig. 15.3): (1) a systolic peak, (2) an end-systolic notch, (3) an end-systolic reversed peak velocity also called systolic "nadir" [3, 11], and (4) a diastolic component with positive velocities.

The presence of an end-systolic notch is related to a delayed and longer ejection interval in the right ventricle [12]. The "nadir" (end-systolic reversed peak velocity) steadily increases as gestation progresses. The presence of "nadir" has been related to reflux caused by the delayed onset and higher and prolonged acceleration of the ductus arteriosus flow velocity [13]. The Doppler waveform of ductus arteriosus is different from that of aortic isthmus; the ductus arteriosus has a higher peak systolic velocity, no notch and no nadir. In some cases, the two waveforms can overlap in the same Doppler recording (Fig. 15.4).

The systolic and diastolic components of the aortic isthmus Doppler waveform can change the direction of the blood flow (Fig. 15.5). In normal pregnancies, most of the systolic and diastolic flow in the aortic isthmus has a positive direction, i.e., antegrade flow. The diastolic velocities are normally reduced at the end of pregnancy due to the physiological dilation of the fetal cerebral vessels; however, the net aortic isthmus flow is still antegrade. In growth restricted fetuses, the diastolic flow is reduced due to cerebral vasodilation. As the resistance to flow in the fetoplacental circulation and the need of oxygen from the fetal brain increase, a part of blood from the ductus arteriosus is sent upwards from the ductus arteriosus, thus changing the net aortic isthmus flow from antegrade to retrograde.

Changes in the systolic and diastolic flows in the aortic isthmus might represent the individual contributions of the two fetal circulations. The ratio between the time velocity integrals (VTI) in systole and diastole (systolic VTI + diastolic

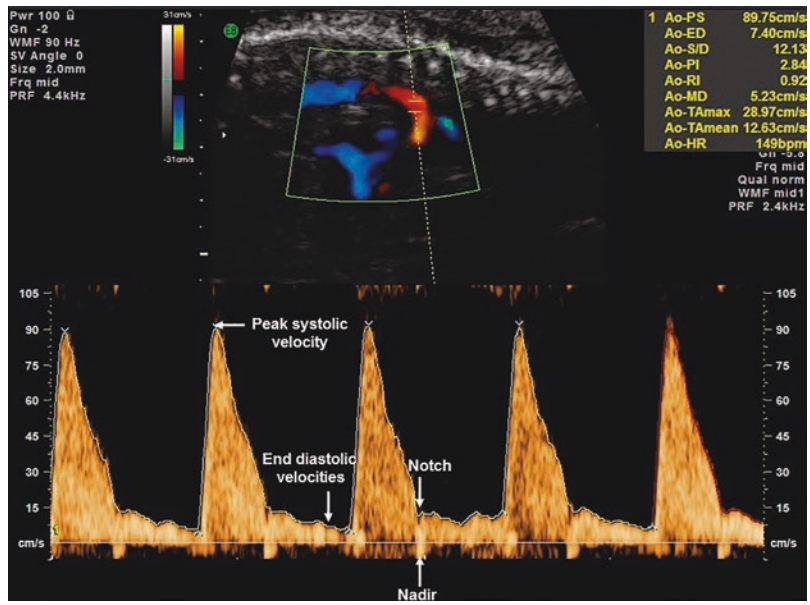

Fig. 15.3 Components of the aortic isthmus Doppler waveform

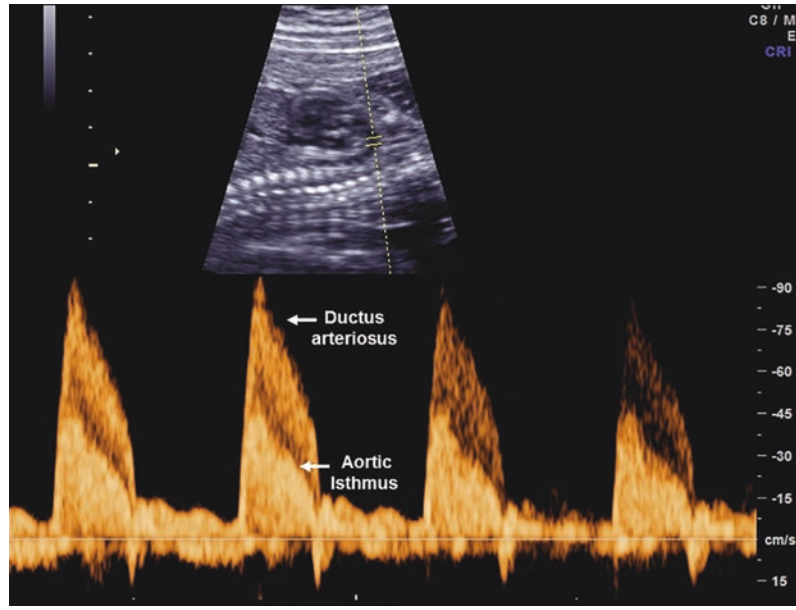

Fig. 15.4 Overlapping of the Doppler signals from the ductus arteriosus and the aortic isthmus. The Doppler sample volume is located in the lower part of the aortic isthmus partly covering the outflow of the arterial duct

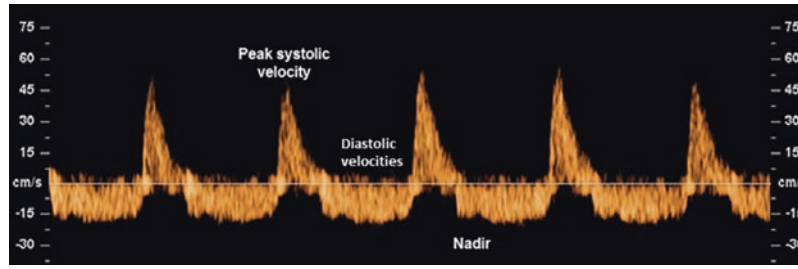

Fig. 15.5 Abnormal aortic isthmus Doppler waveform with reversed velocities during diastole

VTI)/systolic VTI) is called the isthmic flow index (IFI) and can be used to estimate changes in the two circulations (Fig. 15.6) [14].

Five types of IFI have been described:

Type 1, IFI > 1, antegrade diastolic flow is present.
Type 2, IFI = 1, the diastolic flow is absent.
Type 3, IFI > 0 but <1.0, diastolic retrograde flow, but still dominant antegrade flow in the complete Doppler waveform.
Type 4, IFI = 0, antegrade and retrograde blood flows are equal.
Type 5, IFI < 0, predominant retrograde diastolic flow in the complete Doppler waveform.

Other semiquantitative evaluations of the aortic isthmus Doppler waveform have been also proposed such as the pulsatility (PI) and resistance (RI) indices. Del Rio et al. [15] compared the aortic isthmus Doppler recordings obtained in the sagittal plane and in the three vessel and trachea view in 40 normal fetuses between 24 and 36 weeks of gestation. The authors reported similar values of the PI, RI, peak systolic velocity (PSV), and end-diastolic velocity (EDV) between the two anatomical planes, and an interobserver correlation coefficient for the PI of 0.78 with 95% LOA showing a mean difference of 0.04 (SD = 0.41). The authors suggested the three vessel and tracheal view to be a valid alternative for recording the aortic isthmus Doppler waveform when the sagittal plane is difficult to visualize.

Del Rio et al. [16] also reported the Doppler reference values of the aortic isthmus between 19 and 37 weeks of gestation obtained from 458 fetuses in uncomplicated pregnancies either in the sagittal or in the three vessels and trachea

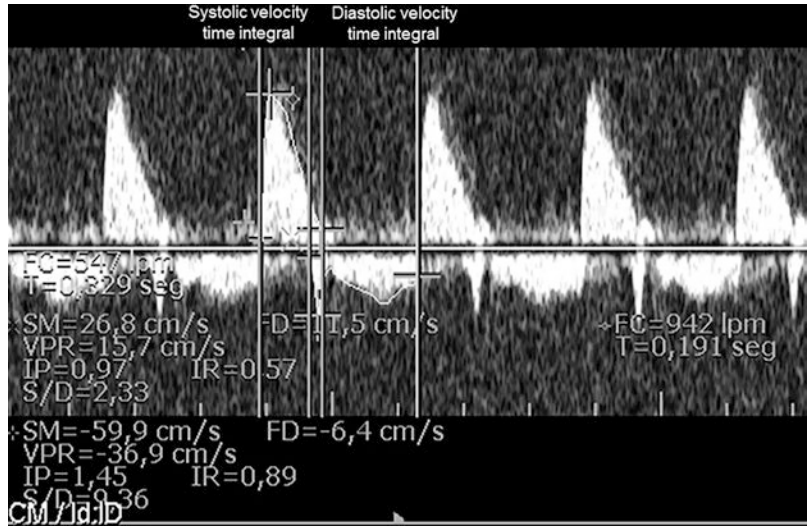

Fig. 15.6 Individual estimation of the Doppler velocities during systole and diastole for evaluation of the aortic isthmus flow index (IFI)

Table 15.1 Reference values of the aortic isthmus pulsatility index (PI) from 19 to 37 weeks of gestation and of the aortic isthmus flow index (IFI) from 17 to 39 weeks of gestation according to Del Rio et al. [16] and Ruskamp et al. [14], respectively

Aortic isthmus pulsatility index (aortic isthmus PI) [16]				Aortic isthmus flow index (IFI) [14]			
Weeks	5th percentile	Mean	95th percentile	5th percentile	Mean	SD	95th percentile
17				1.273	1.327	0.033	1.381
18				1.259	1.323	0.039	1.387
19	2.16	2.55	2.94	1.244	1.318	0.045	1.392
20	2.16	2.56	2.94	1.239	1.313	0.045	1.387
21	2.15	2.58	3.00	1.215	1.309	0.057	1.403
22	2.15	2.60	3.04	1.200	1.304	0.063	1.408
23	2.15	2.61	3.07	1.185	1.299	0.069	1.413
24	2.14	2.63	3.11	1.171	1.295	0.075	1.419
25	2.14	2.64	3.14	1.156	1.290	0.081	1.424
26	2.14	2.66	3.18	1.141	1.285	0.087	1.429
27	2.13	2.67	3.21	1.125	1.280	0.094	1.435
28	2.13	2.69	3.25	1.111	1.276	0.100	1.441
29	2.12	2.70	3.28	1.096	1.271	0.106	1.446
30	2.12	2.72	3.32	1.081	1.266	0.112	1.451
31	2.12	2.73	3.35	1.067	1.262	0.118	1.457
32	2.11	2.75	3.38	1.052	1.257	0.124	1.462
33	2.11	2.76	3.42	1.038	1.252	0.130	1.467
34	2.11	2.78	3.45	1.023	1.247	0.136	1.471
35	2.10	2.80	3.49	1.009	1.243	0.142	1.477
36	2.10	2.81	3.52	0.994	1.238	0.148	1.482
37	2.09	2.83	3.56	0.979	1.233	0.154	1.487
38				0.965	1.229	0.160	1.493

planes. The authors showed a linear increase in PSV and time-averaged maximum velocities (TAMV) throughout gestation with no changes in EDV. The aortic isthmus PI and RI showed a linear increment during pregnancy. Table 15.1 shows the normal aortic isthmus PI by Del Rio et al. [16] and aortic IFI values reported by Ruskamp et al. [14].

The authors reported for aortic isthmus PI an intraobserver correlation coefficient of 0.76 and

an interobserver correlation coefficient of 0.46 with a mean difference between paired measurements of −0.05 (LOA −045 to 0.35).

The isthmic systolic index (ISI) is the ratio between the "nadir" velocity and aortic isthmus PSV [3, 17]. ISI seems to be a technically feasible and reliable estimation of the systolic components of the aortic isthmus; however, more studies are needed to evaluate the clinical value of this index as many components of the cardiac cycle and peripheral resistance can affect the flow through the aortic isthmus [18].

15.1.4 Fetal Growth Restriction

Several research groups have studied the hemodynamic characteristics of the aortic isthmus in pregnancies complicated with "placental insufficiency." Whereas this term is still not well-defined, such complications usually include fetal growth restriction (FGR) and preeclampsia with or without fetal growth restriction.

15.1.4.1 Intrauterine Hypoxia and Changes in the Aortic Isthmus Blood Flow

The effect of hypoxia/asphyxia on the aortic isthmus blood flow was investigated in an experimental sheep model. Term lamb fetuses were exposed to acute reduction in cord blood flow by clamp compression; Doppler recordings of the umbilical artery and aortic isthmus were performed and related to blood gases analyzed during each cord compression [19]. The placental blood flow decreased from 253 mL kg^{-1} min^{-1} (baseline) to 197 mL kg^{-1} min^{-1}, 178 mL kg^{-1} min^{-1}, 115 mL kg^{-1} min^{-1}, and 63 mL kg^{-1} min^{-1} during the first, second, third, and four compressions, respectively. A significant correlation between reduced placental blood flow and reduced aortic isthmus blood flow ($r = 0.89$) was found. The Doppler waveform in the aortic isthmus changed significantly when a 75% reduction in placental blood was reached, with reversed aortic isthmus diastolic volume blood flow similar to systolic volume blood flow. The fetal heart rate showed a reduction after the first compression but no changes in subsequent compressions, whereas mean arterial blood pressure and pO_2 did not change throughout the entire experiment. On the contrary, a higher pCO_2 concentration and low pH value were observed when the placental blood flow was reduced by 75%. The authors suggested that the evaluation of changes in the aortic isthmus systolic and diastolic blood flow might be clinically applicable.

Despite the retrograde flow in the aortic isthmus aiming to increase the oxygen supply to the fetal brain, experimental studies have shown that when retrograde flow in the aortic isthmus is observed, the delivery of oxygen to the fetal brain is already decreased. In the human, a higher prevalence of nonoptimal neurodevelopment at 2 and 4 years of age was shown in growth restricted fetuses with aortic isthmus retrograde flow as compared to growth restricted fetuses with aortic isthmus antegrade flow [20, 21].

The shape and characteristics of the aortic isthmus Doppler waveform vary according to the degree of changes in the umbilical arteries. Lecarpentier et al. [22] showed that when both umbilical arteries had absent or reversed end-diastolic (ARED) velocities, the IFI was −6.28 (SD 4.3) as compared to the group with unilateral ARED in the umbilical artery (IFI −1.72 [SD 3.2], $p < 0.05$) and to the group with positive diastolic velocities in the two umbilical arteries (IFI −0.83 [SD 2.4]; $p < 0.05$) [22].The positive correlation between umbilical artery Doppler PI and aortic isthmus PI was also reported by Sonesson et al. [23] in 100 fetuses referred for hemodynamic evaluation due to various pregnancy complications.

15.1.4.2 Early-Onset Fetal Growth Restriction

In early-onset FGR, there is a strong correlation between the Doppler velocimetry of aortic isthmus and other fetal vascular territories. Changes in the aortic isthmus are associated with changes in the fetal venous system and with right ventricle hemodynamics. Mäkikallio et al. [24] studied two groups of fetuses with placental insufficiency—group 1 with antegrade aortic isthmus blood flow and group 2 with retrograde aortic

isthmus blood flow. Fetuses of group 2 had a higher prevalence of coronary artery dilation, tricuspid regurgitation, increased right ventricle systolic diameter, and higher ductus venosus (DV) PI, despite no differences in the umbilical artery (UA) PI as compared to fetuses of group 1. The same group of researchers reported an increased mitral valve E/A time velocity integral in fetuses with aortic isthmus retrograde flow as compared with fetuses with antegrade flow [25]. However, no differences in combined cardiac output were observed between the groups.

The contribution of the aortic isthmus Doppler velocimetry (IFI) to the prediction of perinatal mortality in early-onset FGR was evaluated in 97 fetuses with an estimated fetal weight <10th percentile and UA-PI >95th percentile delivered between 24 and 34 weeks of gestation [26]. Several fetal vascular territories were examined and the associations with perinatal mortality analyzed. The authors reported a total of 22 perinatal deaths (22.7%). DV-PI as an independent predictor for perinatal mortality had the highest association (odds ratio [OR] 3.69; $p = 0.008$) of all variables. In the multivariate analysis, aortic isthmus IFI did not add any value to the DV-PI in the prediction of mortality which seems to be explained by an intrinsic association between aortic isthmus IFI and DV-PI. The data suggested that the aortic isthmus IFI became abnormal before the DV-PI. Nevertheless, the aortic isthmus seemed to be a better predictor for abnormal neurological outcome rather than for perinatal mortality.

Del Rio et al. [27] examined a cohort of 51 fetuses between 24 and 36 weeks of gestation with severe FGR characterized by an estimated fetal weight (EFW) <10th percentile, increased UA-PI (>95th percentile), and/or a cerebroplacental ratio (CPR) <5th percentile. The authors grouped the fetuses according to antegrade ($n = 41$) or retrograde flow ($n = 10$) in the aortic isthmus. The results showed perinatal mortality of 70% (7/10) in fetuses with aortic isthmus retrograde flow as compared to 4.8% (2/41) in fetuses with antegrade flow (OR 19; 95% confidence interval [CI] 3.4–106.8) and a prevalence of composite adverse perinatal outcome of 90% (9/10) in fetuses with aortic isthmus retrograde flow vs. 24.3% (10/41) in fetuses with aortic isthmus antegrade flow ($p < 0.001$). The authors reported a significant association between the aortic isthmus and the DV Doppler waveforms, as all cases with absent or reversed DV a-wave (corresponding to the end-diastolic atrial contraction) showed retrograde blood flow in the aortic isthmus, and 8/10 (80%) cases with aortic isthmus retrograde flow had absent or reversed DV a-wave velocities. In 4/5 (80%) fetuses, the reversal of flow in the aortic isthmus preceded an abnormal DV Doppler waveform by 24–48 h. The prediction performance of each individual Doppler parameter is presented in Table 15.2.

The study concluded that: (1) there is indeed a high association between retrograde flow in the aortic isthmus and adverse perinatal outcome, (2) a bimodal classification in antegrade and retrograde flow seems to be more clinically useful than using other types of aortic isthmus classifications, and (3) there is a high correlation between the aortic isthmus and the DV Doppler parameters, aortic isthmus changes preceding those in the DV. Therefore, aortic isthmus retrograde blood flow might be considered a strong indication for delivery even when positive DV a-wave velocities still are present.

The sequence of hemodynamic deterioration, including changes in the aortic isthmus, in early-onset FGR was reported by Figueras et al. [28]. The authors followed 46 fetuses with an EFW <10th percentile requiring delivery before 34 weeks of gestation. The UA-PI, middle cerebral artery PI (MCA-PI), DV-PI, and aortic isthmus PI were evaluated every 2 weeks until delivery. The authors reported an impairment of all Doppler parameters in all cases between the first and the last Doppler examinations as follows: UA-PI >95th percentile from 60.9% to 78.3%, MCA-PI <5th percentile from 54.3% to 78.3%, aortic isthmus PI >95th percentile from 28.3% to 50%, and DV-PI >95th percentile from 23.9% to 43.5%. In the sequence of impairment, the UA-PI and MCA-PI became abnormal approximately 24–20 days before delivery, whereas the aortic isthmus PI was affected approximately 13 days, and the DV-PI approxi-

Table 15.2 Predictive performance of fetal Doppler parameters, including aortic isthmus diastolic retrograde flow, for adverse perinatal outcome and perinatal mortality

	Sens (%)	Spec (%)	PPV (%)	NPV (%)	LR +
Adverse perinatal outcome					
Absent or reverse diastolic velocities in the umbilical artery	73.7	65.6	56	80.8	2.1
Middle cerebral artery vasodilation	84.2	28.1	41	75	1.2
Absent/reverse atrial velocities in the ductus venosus	36.8	96.9	87.5	72.1	11.5
Aortic isthmus retrograde diastolic flow	**47.4**	**96.9**	**90**	**75.6**	**15.2**
Umbilical vein pulsations	36.8	84.3	70	69.2	2.3
Perinatal mortality					
Absent or reverse diastolic velocities in the umbilical artery	88.9	59.5	32	96.1	2.2
Middle cerebral artery vasodilation	88.9	26.2	20.5	91.7	1.2
Absent/reverse atrial velocities in the ductus venosus	77.8	97.6	87.5	95.3	32.3
Aortic isthmus retrograde diastolic flow	**77.8**	**92.9**	**70**	**95.1**	**10.8**
Umbilical vein pulsations	66.7	90.5	60	92.7	6.9

Sens Sensitivity, *Spec* Specificity, *PPV* Positive predictive value, *NPV* Negative predictive value, *LR+* Positive likelihood ratio. Adverse perinatal outcome included any of the following: small for gestational age at birth, low cord blood pH, low Apgar score at 5 min, bronchopulmonary dysplasia, respiratory distress syndrome, grade III/IV periventricular hemorrhage, necrotizing enterocolitis, sepsis, admission to neonatal intensive care unit (NICU) >14 days. Modified from: Del Río M et al. [27]

mately 7 days before delivery. These results are consistent with previous reports showing that deterioration of the aortic isthmus Doppler parameters precedes that of the DV.

Similar results were reported by Cruz Martinez et al. [29] who longitudinally evaluated three Doppler parameters related to cardiac dysfunction: aortic isthmus PI, DV-PI, and myocardial performance index (MPI) in 115 growth restricted fetuses with UA-PI >95th percentile who were delivered before 34 weeks of gestation. Doppler evaluations were performed at 1–7 days intervals according to the severity of FGR. The results showed that the prevalence of abnormal cardiac parameters increased from the first to the last ultrasound examination: DV-PI >95th percentile from 33% to 48%, aortic isthmus PI >95th percentile from 32% to 55%, and MPI >95th percentile from 58% to 72%. The authors also reported that the DV-PI became abnormal approximately 7 days before delivery, whereas the corresponding time interval for the aortic isthmus PI was approximately 14 days. The MPI became abnormal approximately 26 days before delivery, being the first sign of cardiac dysfunction in growth restricted fetuses. In agreement with previous reports, the aortic isthmus PI became abnormal 1 week before the DV-PI in fetuses with early-onset growth restriction.

The contribution of the aortic isthmus in the identification of growth restricted fetuses at risk of neurological lesions was reported by Cruz-Martinez et al. [30] The authors evaluated 90 growth restricted fetuses with UA-PI >95th percentile delivered between 28 and 34 gestational weeks and 90 control fetuses with normal EFW and normal birthweight matched by gestational age at delivery (±1 week), and without clinical signs of chorioamnionitis. The

authors registered the Doppler signals of the UA, MCA, DV, and aortic isthmus and calculated the MPI. Neurological lesions were defined as the presence of intraventricular hemorrhage, periventricular leukomalacia, and basal ganglia hyperechogenicities observed at 40 weeks of corrected postnatal age. The results showed that among fetuses with MCA-PI <5th percentile, those with aortic isthmus retrograde flow had a higher prevalence of neurological lesions (16/24; 66.7%) as compared to those with antegrade flow (17/44; 38.6%; $p = 0.03$). The authors concluded that among growth restricted fetuses with an UA-PI >95th percentile and MCA-PI <5th percentile, those with aortic isthmus retrograde flow had a 67% prevalence of neurological lesions as compared to 14% in growth restricted fetuses with an UA-PI >95th and an MCA-PI <5th but with aortic isthmus antegrade flow.

15.1.4.3 Late-Onset Fetal Growth Restriction

Doppler examinations after 38 gestational weeks were performed in 178 small for gestational age (SGA) fetuses with birthweight <10th percentile and in 178 fetuses with normal size and normal birthweight [29]. The fetuses of both groups had a normal umbilical artery PI (<95th percentile). The authors reported a higher prevalence of perinatal complications in SGA fetuses, including cesarean section for non-reassuring fetal heart rate (FHR), and earlier gestational age at delivery than in normally grown fetuses. Significantly higher MPI (0.56 vs. 0.49; $p < 0.01$) and aortic isthmus PI (3.84 vs. 2.87; $p < 0.01$) values were observed in SGA fetuses as compared to normally grown fetuses, whereas no differences in DV-PI were registered. The prevalence of aortic isthmus PI >95th percentile in SGA fetuses was almost three times higher (14%) than in normally grown fetuses (5%). The study concluded trhat increased aortic isthmus PI and MPI are manifestations of an altered cardiac function in fetuses with late-onset growth restriction. Conversely, Kennelly et al. [31] reported no differences in aortic isthmus PI or in the prevalence of aortic isthmus retrograde flow in late-onset SGA fetuses with normal UA-PI (<95th percentile) as compared to normally grown fetuses of the same gestational age. The authors also examined 10 SGA fetuses with an UA-PI >95th percentile, but could not document differences in the aortic isthmus Doppler waveform as compared with normally grown fetuses. Similar results were more recently reported by Villalain et al. [32] in 142 growth restricted fetuses diagnosed after 32 weeks of gestation with moderately abnormal Doppler parameters (UA-PI >95th percentile and/or MCA <5th percentile but no ARED flow in the umbilical artery). The authors found aortic isthmus antegrade flow in 79 cases and retrograde flow in 69 cases. No differences in adverse outcomes such as cesarean section for non-reassuring FHR, or perinatal mortality were observed between the two groups. The study concluded that presence of aortic isthmus retrograde flow does not increase the risk of perinatal complications above the baseline risk already stablished by growth restriction and abnormal UA-PI.

15.1.5 Aortic Isthmus and Coarctation of the Aorta

Coarctation of the aorta is one of the most frequent cardiac anomalies and one of the most difficult to diagnose antenatally. It accounts for 6–20% of all congenital cardiac anomalies seen at birth [33, 34]. Narrowing and lack of growth of the aortic isthmus is one of the most consistent ultrasound findings in newborns with coarctation of the aorta. Hornberger et al. [35] found in a multicenter study including 20 fetuses with suspicion of coarctation of the aorta that narrowing of the distal part of the aortic arch and of the aortic isthmus had a very high predictive value for coarctation. They also suggested that the ratio between the aortic isthmus and the descending aorta diameters is a good parameter to identify fetuses with coarctation.

15.1.6 Aortic Isthmus in Twin Pregnancies

Assessment of the aortic isthmus Doppler waveform in twin pregnancies has been mainly done

in monochorionic twins. In a study including 48 monochorionic twin pregnancies (24 with twin-to-twin transfusion syndrome [TTTS], 4 selective FGR [sFGR], 12 TTTS + sFGR, and 8 uncomplicated), the authors reported a lower aortic IFI in the small twin with sFGR with or without TTTS, as compared with uncomplicated monochorionic twin pregnancies [36]. No differences in IFI were observed between donors and recipients in cases with TTTS. The aortic IFI was significantly correlated with left ventricular cardiac output and stroke volume. Similarly, no significant differences in aortic ISI between donors and recipients before and after laser therapy were reported in 55 women with monochorionic twin pregnancies complicated with TTTS. The authors reported that a lower ISI in the recipient twin before laser therapy was associated with a higher risk of mortality within 24 h after laser treatment.

Kim et al. [37] evaluated 30 women with dichorionic twin pregnancies and 19 women with monochorionic twin pregnancies. The authors showed a significantly higher aortic isthmus PI and RI in the small twin (≥20% differences in EFW between the twins) disregarding chorionicity and a significant negative correlation between the birthweight and the aortic isthmus PI and aortic isthmus PSV, respectively.

15.1.7 Maternal Hyperoxygenation and Aortic Isthmus

Changes in the UA-PI, MCA-PI, and aortic IFI in relation to maternal hyperoxygenation were reported by Almström et al. [38] in 16 pregnant women examined twice during gestation, at 20–23 weeks and at 30–33 weeks. Women were exposed to 100% oxygen at a rate of 8–10 L/min. There was a reduction in the IFI and an increment in the MCA-PI with no changes in the UA-PI during maternal hyperoxygenation. Similar results were reported by Brantberg et al. [39] who exposed 25 pregnant women, 24 with FGR and one with tetralogy of Fallot, to 100% oxygen administrated by face mask for 15 min at a rate of 8–10 L/min. The authors showed a significant improvement in the Doppler waveform of the aortic isthmus, and a significant increase in the MCA-PI with no changes in the UA-PI after maternal oxygen administration.

In fetuses with coarctation or severe FGR, Edwards et al. [40] showed a significant increase in the aortic isthmus diameter after maternal exposure to oxygen. The authors suggested that hyperoxygenation might improve the perinatal outcome of fetuses with coarctation of the aorta.

15.2 Fetal Descending Aorta

The first reports on Doppler recordings of blood velocity signals from the umbilical artery stimulated attempts to record blood flow in fetal vessels [41, 42]. In 1979, Gill presented a method combining a quasi-real-time imaging and pulsed-wave Doppler technique for estimating the volume flow in the intraabdominal part of the umbilical vein [43]. The ultrasound system used (Octoson, Ultrasonic Institute, Millers Point, Australia) did not allow the recording of high blood velocities owing to the low repetition frequency of the Doppler ultrasound pulses (2 kHz) necessitated by the long distance between the ultrasound transducers emerged in a water bath and the target vessel. Eik-Nes et al. [44] applied the principle of intermittently using two-dimensional and pulsed-wave Doppler ultrasound by combining a linear array scanner and a 2-MHz Doppler velocimeter. The two transducers were mounted firmly to a unit with an inclination of the Doppler transducer of 45° to the linear array transducer. By placing the linear array transducer on the maternal abdomen so that it was parallel with a sufficiently long portion of the vessel of interest, insonation by Doppler ultrasound under a known angle (45°) was achieved and thus the possibility of correcting the recorded mean blood velocity for the insonation angle (Fig. 15.7).

With the above arrangement, the Doppler transducer could be located relatively close to the fetal body, and so a high repetition rate (9.75 kHz) of Doppler pulses could be used. This technique allowed velocities up to 1.7 m/s to be detected

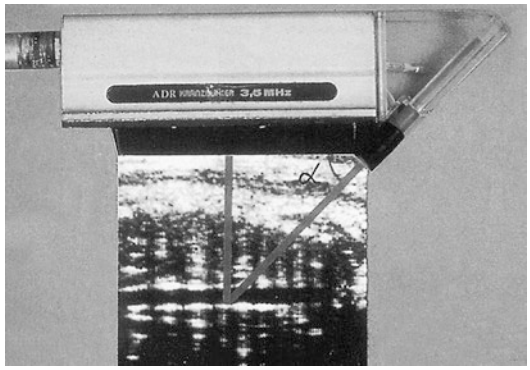

Fig. 15.7 Doppler velocimetry of fetal descending aorta: original method combining a linear array real-time scanner and a 2-MHz pulsed Doppler instrument according to Eik-Nes S et al. [44]. The Doppler transducer is firmly attached to the linear array transducer at an angle of 45°(α)

down to a depth of 6.5 cm [45], and the first recordings of blood velocity signals from the fetal descending aorta were obtained. Unfortunately, during these first recordings a high-pass filter with a cutoff frequency of 600 Hz was employed, in agreement with the experience from Doppler recordings in the adult aorta, where it is necessary to eliminate disturbing low-frequency Doppler shift signals from the vessel walls. This technique caused an erroneous appearance of the fetal aortic velocity waveforms noted in the two first reports [44, 45] with only systolic velocities present. Today, such waveforms would be recognized as highly abnormal [46]. The estimated time-averaged mean velocity was also influenced by erroneous high-pass filtering of Doppler signals; consequently, the calculated values of the volume flow in the first reports cannot be considered reliable.

The Malmö research group evaluated and further developed the Doppler method for estimating fetal aortic blood flow. In an experimental study comparing the electromagnetic and Doppler measurements of aortic flow in pigs, the erroneous filtering of the aortic signals was recognized [47]. This discovery enabled correction of the original reports on fetal aortic flow and the recommendation of not using a high-pass filter with a cutoff frequency higher than 100 Hz.

For recording Doppler shift signals from the fetal descending aorta, a duplex system combining pulsed Doppler ultrasound and real-time imaging is necessary to localize the vessel and to precisely position the sample volume. Nowadays, duplex ultrasound systems employing a sector scanner are most often used for Doppler examinations of the fetal circulation. They are less suitable for fetal aorta examination owing to the difficulty of ensuring an acceptable (i.e., <55°, preferably <30°) insonation angle. Figures 15.8 and 15.9 demonstrate the problems of obtaining a good image of a sufficiently long portion of the fetal descending aorta, and at the same time, an acceptable angle of insonation by Doppler ultrasonography. Also, with the duplex system employing linear array transducer, achieving acceptable insonation angle is difficult (Fig. 15.10).

15.2.1 Fetal Aortic Doppler Velocimetry

15.2.1.1 Aortic Flow Estimation

The combination of the linear array real-time scanner and pulsed Doppler was originally designed to estimate volume flow in the fetal aorta from the values of time-averaged mean velocity and the aortic diameter [44]. For correct estimation of the mean velocity, proper location of a sufficiently large sample volume is necessary; hence the whole lumen of the vessel is insonated during both systole and diastole. Furthermore, the insonation angle must be reliably controlled to enable correction of the recorded mean Doppler shift frequency. The use of a high-pass filter causes overestimation of the mean velocity. Unfortunately, because of the pulsatile character of the aortic flow and the changing velocity profile during the cardiac cycle, it is impossible to use a standard correction factor.

The errors in the velocity measurement can be kept to a minimum by meticulous performance of the examination by experienced operators who are aware of the problems noted above. Much greater risk of error is involved when measuring

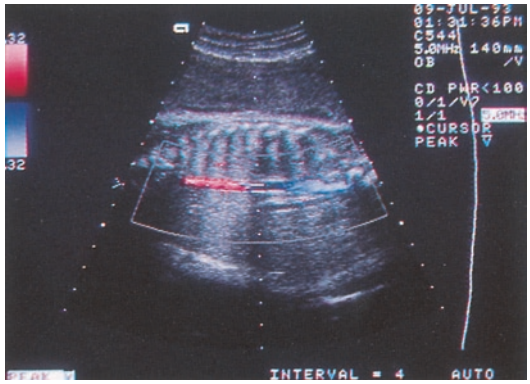

Fig. 15.8 Recording of fetal aortic velocities with a duplex ultrasound system including a sector scanner and a pulsed and color Doppler mode. A good image of the fetal descending aorta is obtained. The insonation angle for Doppler ultrasound is close to 90°, however, which gives no or low amplitude shift signals in the spectral Doppler mode and no color in the color Doppler mode

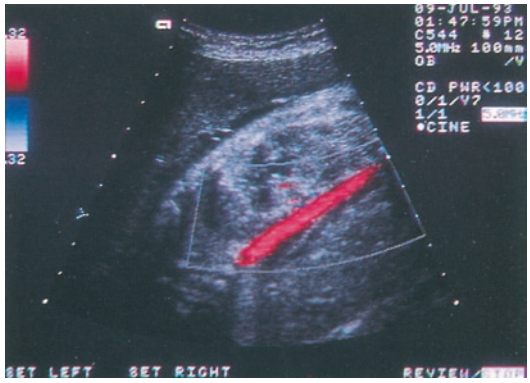

Fig. 15.9 Fetal descending aorta in an oblique projection illustrates the difficulty of obtaining a suitable angle of insonation for Doppler recording of aortic velocities with a duplex sector scanner

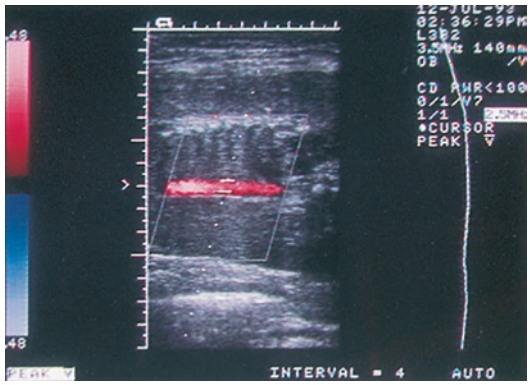

Fig. 15.10 Examination of the fetal descending aorta with a linear array duplex system. The color Doppler box and the pulsed Doppler beam are inclined; the insonation angle is still high

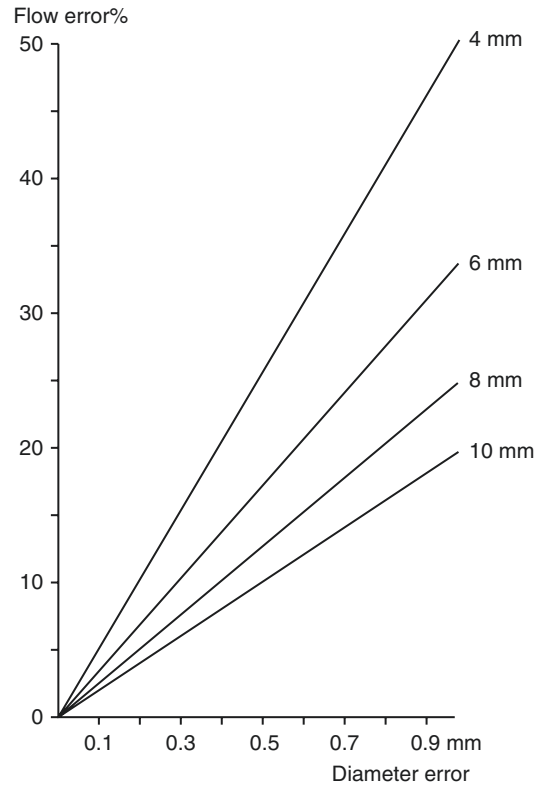

Fig. 15.11 Error in flow measurements due to errors when measuring diameter of four vessels of different caliber. (Re-printed from Eik-Nes et al. [45] with permission)

the aortic diameter because of the relatively low spatial resolution of the ultrasound scanners and dynamic diameter changes during aortic pulsations. Each error is squared in the calculation of the cross-sectional area of the vessel and thus has a significant impact on the resulting value of the calculated volume flow. The smaller the caliber of the vessel, the more significant the impact (Fig. 15.11).

Various methods for measuring the diameter of the fetal aorta have been used: averaging of measurements using calipers in 10 subsequently frozen images of the aorta, M-mode recording, and time-distance recording (a phase-locked loop echo-tracking system) [48, 49]. It has been shown that recording changes in the fetal aortic diameter can provide an estimate of the changes in intrauterine blood pressure [50].

The problems involved when estimating volume blood flow in the fetal descending aorta were elaborated in the paper by Eik-Nes et al. [51] In a comparative study mentioned above,

good agreement was found between simultaneous flow measurements in pig aorta with an electromagnetic and Doppler ultrasound method: correlation coefficient (r) = 0.91 [47]. Similar good correlation was found for the descending aorta of the fetal lamb when comparing the Doppler ultrasonographic estimation of flow with electromagnetic flowmeters (r = 0.93) [52] or radionuclide-labeled microspheres (r = 0.94) [53]. These results were obtained under experimental conditions. Similar accuracy might be achieved in the hands of experienced operators in carefully performed examinations of human fetuses near term. There is little doubt, however, that the method of estimating volume flow in the fetal aorta is open to overwhelming errors when applied in a clinical situation. Therefore, the interest of clinicians and researchers has focused on waveform analysis of fetal aortic velocities.

Various subsequently developed ultrasound systems that allow estimation of the fetal aortic volume flow have been tested by our group in vitro and in vivo—one utilizing the time-domain principle (CVI-Q, Philips Ultrasound, Santa Ana, CA) [54, 55] and the other combining online the time-distance recording of aortic diameter using a phase-locked loop echo-tracking system with the 2-MHz pulsed Doppler estimation of mean blood velocity [56] (Fig. 15.12). Power Doppler images of the fetal descending aorta were also used for measurement of the vessel diameter to be used together with the mean velocity for calculation of volume flow [58]. Recently, phase-contrast cardiovascular imaging has been employed for estimation of volume blood flow in the fetal descending aorta [59]. All these methods necessitate further development before possible clinical application.

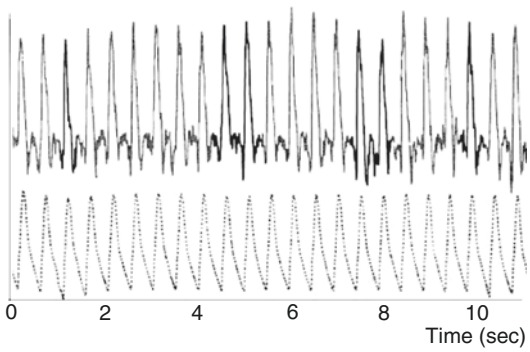

Fig. 15.12 Simultaneous recording of blood velocity (*upper tracing*) and vessel diameter (*lower tracing*) from descending aorta of a healthy 30-week fetus. (Reprinted from Gardiner H et al. [57, 58] with permission)

15.2.1.2 Aortic Velocity Waveform Analysis

Several of the errors inherent in volume flow estimation are eliminated when waveform analysis of the maximum blood velocity is used. Uniform insonation of the vessel is not as critical as it is when performing the mean velocity estimation, there is no influence of high-pass filters and the insonation angle (so long as the diastolic velocities exceed the cutoff frequency of the filter), and values for the aorta diameter and fetal weight are not needed. On the other hand, waveform indices do not directly represent the blood flow.

The waveform of the fetal maximum aortic velocity is usually characterized by some of the waveform indices described elsewhere in this book. In hypoxic fetuses, similar to the umbilical artery waveform, diastolic velocities in the descending aorta decrease and eventually disappear or even become reversed, a condition called ARED flow. In 1984, Jouppila and Kirkinen [46] described the absence of diastolic velocity in the fetal descending aorta and called it a total end-diastolic block; and in 1986, Lingman et al. [60] reported the first four cases of reversal of diastolic velocities in the fetal aorta. A semiquantitative method of assessing the waveform has been evolved for clinical use, four blood flow classes (BFCs) being defined to describe the waveform with emphasis on its diastolic part [61] (Fig. 15.13): BFC 0 (normal), positive flow throughout the heart cycle and a normal PI; BFC I, positive flow throughout the cycle and an elevated PI (≥mean + 2 SD of the normal); BFC II, non-detectable end-diastolic velocity; BFC III, absence of positive flow throughout the major part of the diastole or reverse flow during diastole. Subsequently, the BFCs have been applied for waveform analysis of umbilical artery Doppler signals and found to be a simple and powerful tool for clinical use [62].

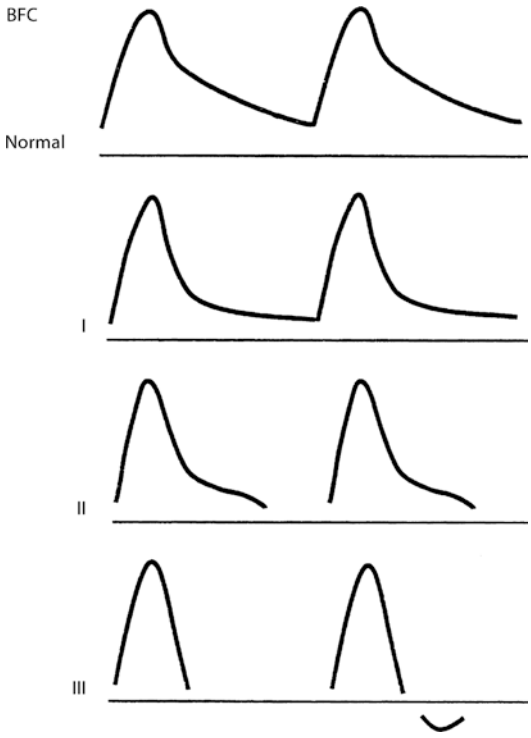

Fig. 15.13 Blood flow classes (*BFC*) of fetal aortic waveforms. *BFC normal* positive flow throughout the heart cycle and a normal pulsatility index, *BFC I* positive flow throughout the cycle and a pulsatility index ≥mean + 2 SD of the normals, *BFC II* non-detectable end-diastolic velocity, *BFC III* absence of positive flow throughout the major part of diastole or reverse flow during diastole

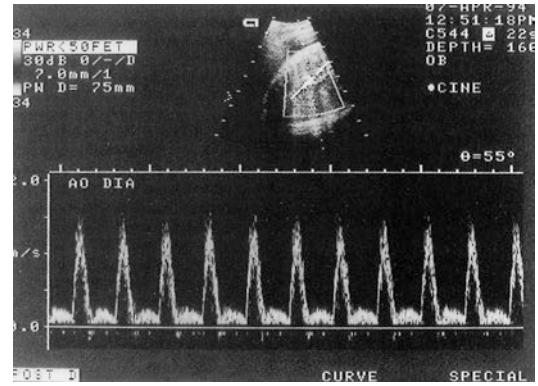

Fig. 15.14 Doppler shift spectrum recorded from the thoracic descending aorta of a healthy fetus at 28 weeks' gestation

When evaluating the end-diastolic portion of the aortic velocity waveform, it is important for the operator to be aware of the risk of reporting a falsely absent flow. The combination of a high insonation angle and a high cutoff level of the high-pass filter included in the Doppler instrument eliminates Doppler shift signals of considerably high amplitude. Obviously, the recommendation not to use an insonation angle of more than 55° and a high-pass filter higher than 100 Hz [63] is valid not only for estimating mean velocity, but also for waveform analysis.

The appearance of the fetal aortic maximum velocity waveform and the values of waveform indices are independent of the direction of insonation (i.e., upstream or downstream). The position of the sample volume is important, as the waveform of aortic blood velocity changes with increasing distance from the heart. Recorded in the fetal thorax, the velocity waveform of the descending aorta shows high pulsatility with a low proportion of diastolic flow (Fig. 15.14); recorded in the fetal abdominal aorta, the proportion of diastolic flow increases [64]. It is therefore crucial to standardize the site of recording; typically, in the thoracic aorta the sample volume is located just above the diaphragm.

15.2.2 Fetal Aortic Flow in Uncomplicated Pregnancies

Blood flow in the fetal descending aorta is characterized by high blood velocity, higher than that found in adult descending aorta [65], and the waveform of the aortic velocity is influenced by the low vascular resistance in the placenta. Consequently, the PI is typically lower in the abdominal than in the thoracic fetal aorta [64]. In the uncompromised fetus during the second half of pregnancy, aortic diastolic velocity is present throughout the cardiac cycle. The narrow spectrum of Doppler shift signals recorded from the thoracic aorta during systole indicates a fairly flat flow profile. In the abdominal aorta, lower and more dispersed frequencies can be seen owing to the change of flow profile toward a more parabolic pattern [64].

The time-averaged mean velocity in the fetal thoracic descending aorta does not change significantly during the third trimester (35.0 ± 5.5 cm/s, mean ± SD) [66], the increase in the volume flow being related to the growing aortic diameter. The volume flow corrected for fetal weight was found to be stable during late pregnancy; the reports in the literature range from 206 to 280 mL min^{-1} kg^{-1} (Table 15.3). The mean aortic PI was reported to range from 1.83 to 2.80 and to be rather stable until 36 weeks (Tables 15.4 and 15.5). Thereafter, a slight increase was observed toward term [58, 64]. Concomitantly, a slight decrease in the volume flow was reported [66].

Estimation of flow at two levels of the fetal descending aorta, and in the abdominal part of the umbilical vein, enabled calculation of the

Table 15.3 Volume blood flow in the fetal descending aorta reported in the literature

Study	Gestational age (weeks)	Number of pregnancies	Volume flow (mL min^{-1} kg^{-1})	Comment
Thoracic descending aorta				
Eik-Nes et al. [44]	32–41	26	191 ± 12	Erroneous signal filtering
Griffin et al. [67]	28–40	75	246 ± 30	
Van Lierde et al. [68]	37–40	20	216 ± 24	
Maršál et al. [69]	27–40	64	238 ± 40	
Erskine and Ritchie [70]	28–40	71	206 ± 72	
Lingman and Maršál [66]	27–36	21	238 ± 46	Longitudinal study
	37–38	21	221 ± 41	
	39–40	21	213 ± 37	
Rasmussen [71]	29–40	58	234 (184–289)	
Räsänen et al. [72]	40 ± 2.3	51	290 ± 67	
Cameron et al. [73]	28	9	143 ± 34	Low values for unclear reaswon
	36	13	149 ± 45	
Brodszki et al. [56]	28–31	20	213 ± 77	Longitudinal study; simultaneous automatic measurement of the velocity and diameter
	32–35	20	239 ± 66	
Abdominal aorta				
Eldridge et al. [74]	18–40	18	184 ± 20	Longitudinal study
Lingman and Maršál [66]	27–36 37–38 39–40	21 21 21	167 ± 43 133 ± 38 136 ± 30	Longitudinal study
Konje et al. [58]	24 28 32 36 38	81 81 81 81 81	110 ± 54 153 ± 72 216 ± 124 307 ± 195 391 ± 245	Longitudinal study; volume flow (mL min^{-1}); not corrected for fetal weight

Mean values ± SD or median (range) are given

Table 15.4 Fetal aortic pulsatility index reported in the literature

Study	Gestational age (weeks)	Number of pregnancies	Pulsatility Index (PI)	Comment
Griffin et al. [75]	24–42	98	1.83 ± 0.29	
Van Eyck et al. [76]	37–38	13	2.7 ± 0.3	Mean velocity, PI; state 1F[a]
Jouppila and Kirkinen [77]	30–42	43	2.49 (1.94–3.10)	
Lingman and Maršál [64]	28–40	21	1.96 ± 0.31	Longitudinal study
Tonge et al. [78]	26–29	10	2.0 ± 0.2	
	32–33	15	2.2 ± 0.3	
	38–41	13	2.3 ± 0.2	
Arabin et al. [79]	20–40	137	2.56 ± 0.47	
Rasmussen [71]	29–40	58	1.83 (1.32–2.20)	
Räsänen et al. [72]	40 ± 2.3	51	2.07 ± 0.44	
Årström et al. [80]	25	22	1.81 ± 0.19	Longitudinal study
	40	22	1.95 ± 0.30	
Hecher et al. [81]	29–42	209	1.86 (1.49–2.24)	
Ferrazi et al. [82]	26		1.86	Regression line based on 120 measurements
	38		2.30	
De Koekkoek-Doll et al. [83]	36–40	23	1.92 ± 0.18	State 1F[a]
Bahlmann et al. [84]	18–21	926	1.79–1.79	Cross-sectional study; numbers per week not given
	22–25		1.80–1.81	
	26–29		1.82–1.83	
	30–33		1.82–1.84	
	34–37		1.80–1.92	
	38–41		1.93–1.95	

Mean values ± SD or median (range) are given
[a]State 1F, fetal quiescence: absent eye movements, stable fetal heart rate

percentual distribution of the aortic flow (Fig. 15.15). The placental proportion of blood flow in the descending thoracic aorta related to the fetal weight diminished with increasing pregnancy length: at 28 weeks, it was 59% and at term 33% [66]. This finding is in good agreement with the reports of other authors, who have described the umbilical venous blood flow to be 64% [67], 55% [85], or 54% [68] of the fetal aortic blood flow from 26 weeks onward. In fetal lambs, 65% of the blood flow in the descending aorta was found to be directed to the placenta [86]. The decrease in the placental proportion of the flow with the progression of pregnancy might be due to the changing ratio of fetal to placental weight [87].

The velocity waveform in the fetal aorta is subject to several influences, one of them being fetal heart function. In a study on exteriorized lamb fetuses, a strong correlation was found between the rising slope of the velocity waveform and myocardial contractility (measured as *dP*/*dt*) in the left heart ventricle [88]. Interestingly, the next best correlation was found for the aortic PI.

Räsänen et al. [72] found in human fetuses a good correlation between the growth of the fetal heart, the lumen of the descending aorta, and aortic volume flow. The aortic velocity indices were independent of cardiac size and fractional shortening. The authors interpreted this finding as myocardial contractility that remained stable despite the changing peripheral vascular resistance as long as the changes of resistance remained within the normal range.

Table 15.5 Reference values of the mean fetal aortic pulsatility index (PI) measured at the level of diaphragm from 18 to 41 weeks of gestation according to Bahlmann et al. [84]

Gestational age (weeks)	PI	90% confidence interval
18	1.788	1.496–2.149
19	1.788	1.493–2.155
20	1.790	1.492–2.161
21	1.793	1.491–2.168
22	1.796	1.491–2.176
23	1.801	1.492–2.184
24	1.806	1.493–2.194
25	1.812	1.496–2.205
26	1.819	1.499–2.216
27	1.826	1.503–2.228
28	1.835	1.508–2.241
29	1.826	1.513–2.254
30	1.819	1.519–2.268
31	1.812	1.525–2.282
32	1.806	1.532–2.296
33	1.801	1.538–2.311
34	1.796	2.545–2.325
35	1.793	1.552–2.340
36	1.790	1.558–2.354
37	1.923	1.564–2.369
38	1.932	1.570–2.382
39	1.941	1.575–2.395
40	1.948	1.579–2.407
41	1.954	1.581–2.417

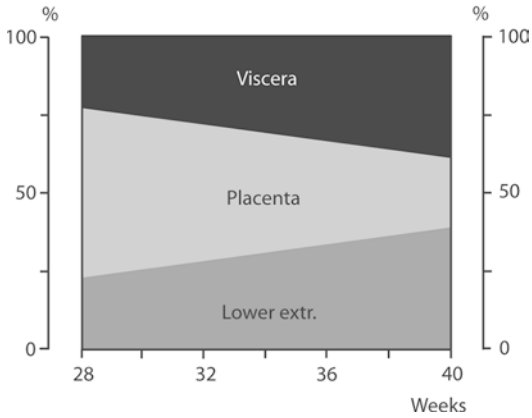

Fig. 15.15 Distribution of the fetal aortic blood flow during the third trimester of normal pregnancy. Blood flow in the thoracic descending aorta corresponds to 100%. (Reprinted from Lingman & Maršál [66] with permission)

The nonsimultaneous measurements of pulsatile mean flow velocity and vessel diameter in the fetal descending aorta can be synchronized by transabdominal fetal electrocardiography (ECG) [89–91]. A more accurate estimation of the aortic flow is then possible, and the aortic stroke volume can be calculated. In the above studies, the stroke volume has been reported to range from 2.8 to 5.6 mL/min in the thoracic aorta and from 2.4 to 4.3 mL/min in the abdominal aorta of healthy third trimester fetuses. The relative stroke volume was found to be stable during the last trimester of gestation (1.7–2.1 mL min^{-1} kg^{-1}) [89–91]. The method used for these examinations is laborious, mainly because of the difficulty obtaining transabdominal fetal ECG signals of acceptable quality. To circumvent this problem, Tonge et al. [90] applied their experience from animal experiments and recommended that the first derivative of the mean velocity and diameter waveforms is used to synchronize heart cycles.

15.2.3 Intrinsic Influences on Fetal Aortic Flow and Flow Indices

Similar to other fetal vessels (e.g., the carotid artery [92]), a negative correlation has been found between the aortic PI and fetal heart rate, with correlation coefficients in the range −0.43 to −0.73 [64, 76, 83, 93]. This inverse relation was pronounced mainly during periods of behavioral state 2F (active sleep) in term fetuses [76].

In a series of studies, the Rotterdam research group reported a clear dependence of fetal aortic velocity waveform indices on fetal behavioral states in term pregnancies [76, 83] and on the fetal activity state during the early third trimester [93]. The values for the fetal aortic PI were higher during fetal quiet sleep than during active sleep, with decreased impedance and increased flow in fetal musculature.

All non-compromised fetuses perform periodic breathing movements, with contraction of the diaphragm, expansion of the abdominal wall, and retraction of the thorax during "inspiration" and a return to the rest position during "expiration" [94]. Fetal breathing movements have a pronounced effect on blood circulation in the umbilical cord and the intrafetal vessels [69]. The aortic blood flow velocity waveforms exhibit modulation of their shape, with rhythmic oscillations in the amplitude of their peak velocities and diastolic velocities. The end-diastolic velocities sometimes eventually disappear during fetal "inspiration." The time-averaged mean velocity usually increases—up to 40%—during periods of fetal breathing movements [69]. Probably, the cardiac output also increases as a consequence of increased venous blood return to the fetal heart [95].

As also true for all fetal and umbilical vessels, the above observation is important to consider when recording fetal aortic blood velocities: To obtain reproducible results, only Doppler traces recorded during periods without fetal breathing should be accepted for analysis. Fetal breathing movements can usually be recognized in the two-dimensional real-time image of the fetus, the aortic Doppler shift signals, or the Doppler traces of umbilical venous velocities.

15.2.4 Fetal Aortic Blood Flow during Labor

The fetal aortic volume blood flow has been shown to increase with progression of labor in a study in which the measurements were performed between contractions [96]. The increased fetal flow might be a phenomenon similar to the reactive hyperemia found in the uteroplacental circulation of experimental animals between contractions [97]. In the study by Lindblad et al. [96] there was no change in the aortic PI with advancing labor, and there was no difference between patients with and those without ruptured membranes. Fendel et al. [98] measured the mean fetal aortic velocity during labor and found a decrease in the velocity during contractions; the aortic PI remained unchanged.

15.2.5 Pathophysiologic Changes of Fetal Aortic Flow during Intrauterine Hypoxia

Blood flow in the fetal descending aorta supplies the placenta and lower body of the fetus, including kidneys, splanchnic and pelvic organs, and lower extremities. Considerable portion of blood in fetal descending aorta is directed to the placenta. Thus, an increase in the resistance to flow in the placental vascular bed can profoundly influence the flow not only in the umbilical artery, but also in the descending aorta. It would be reflected by typical changes of the velocity waveform (i.e., decreased or absent diastolic velocity) (Fig. 15.16). Possibly, vasoconstriction in the lower fetal body, which is known to be one of the mechanisms involved in the centralization of flow during hypoxia, potentiates the effect on aortic velocity waveforms.

Doppler indication of increased resistance to flow in the fetoplacental circulation was found to be related to the increased neonatal nucleated red blood cell counts that are considered a sign of intrauterine hypoxia [99]. Doppler results from the fetal descending aorta, umbilical artery, and maternal uterine arteries were independent determinants of neonatal nucleated red blood cell count.

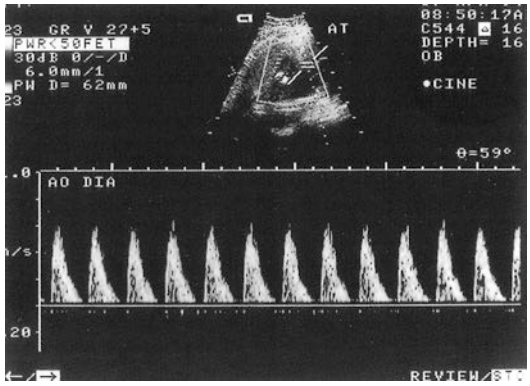

Fig. 15.16 Absent end-diastolic velocity in the descending aorta of a growth restricted fetus at 27 weeks' gestation

In an experimental fetal lamb model, increasing the placental and hind limb resistance by embolization with microspheres caused a progressive increase in the aortic PI [100]. In another study in pigs, the aortic PI, recorded by Doppler ultrasonography, was shown to correlate with the total peripheral resistance calculated from the invasively measured blood flow and pressure ($r = 0.64–0.87$) [101]. In the study by Adamson and Langille [100], the aortic PI reflected not only the vascular resistance, but also the pulsatile flow and pressure pulsatility. Thus, an increasing fetal aortic PI should not be interpreted solely as an expression of increasing placental vascular resistance.

When studying the aortic blood velocity waveforms of lamb fetuses during experimental asphyxia, Malcus et al. [102] found a loss of aortic end-diastolic flow velocities, a significant increase in the PI, and a decrease in mean velocity. Concomitantly, increases in the diameter and mean velocity were recorded in the fetal common carotid artery [103], and there was a slight decrease in the carotid artery PI. These changes indicate a redistribution of flow, although the changes occurred as relatively late phenomena in the development of acute asphyxia.

15.2.6 Clinical Studies

15.2.6.1 Fetal Cardiac Arrhythmias

Doppler recording of fetal aortic velocities provides important information on the hemodynamic consequences of fetal cardiac arrhythmias. Simultaneous detection of Doppler signals from the fetal abdominal aorta, reflecting ventricular contractions, and from the inferior vena cava, reflecting atrial contractions, can facilitate the classification of arrhythmias [104–106]. In most cases of fetal arrhythmia, the estimated aortic volume flow remains within normal limits, indicating the ability of the fetal heart to maintain cardiac output [105, 107]. Abnormal low values of aortic flow were found in fetuses with severe arrhythmias that caused heart failure [105]. In cases of bradyarrhythmias and tachyarrhythmias, a decrease in the aortic flow was observed when the fetal heart rate was found lower than 50 bpm or higher than 230 bpm, respectively [107].

In fetuses with premature heartbeats (ventricular contractions), an increase in peak aortic velocities was observed with the first postextrasystolic beats [108]. Similarly, the peak systolic velocities are higher in fetuses with complete atrioventricular block than in those with regular sinus rhythm [109]. These findings, together with the above-described compensation for negative effects of cardiac arrhythmias on fetal cardiac output, indicate that the Frank-Starling mechanism is valid for fetal myocardium.

Fetuses with congestive heart failure caused by cardiac arrhythmia sometimes require transplacental treatment with digoxin or antiarrhythmic drugs. In addition to the effect of treatment on heart rhythm, the improved performance of the fetal heart can be followed by serial measurements of fetal aortic volume blood flow [109].

15.2.6.2 Fetal Anemia

One of the early reports on alloimmunized pregnancies suggested that there was an inverse correlation between the cord hemoglobin at birth and the time-averaged mean velocity and volume blood flow recorded antenatally in the intraabdominal portion of the umbilical vein using Doppler ultrasonography [110]. In the descending aorta of previously untransfused alloimmunized fetuses, Rightmire et al. [111] reported an increased mean blood velocity and a negative correlation with the hematocrit of umbilical cord blood obtained by cord puncture under fetoscopic control. Their finding was confirmed by

Nicolaides et al. [112], who related the values of mean aortic velocity to the hemoglobin deficit in blood samples obtained by cordocentesis. The findings of increased fetal aortic velocities in anemic fetuses (Fig. 15.17) are in accordance with an increase in their cardiac output as a consequence of lowered blood viscosity, increased venous return, and cardiac preload. Doppler cardiac studies of anemic fetuses showed indications of increased cardiac output [114, 115]. Copel et al. [114] found the peak systolic velocity from the fetal descending aorta to correlate well with the hematocrit in blood samples obtained before intrauterine blood transfusion. After intrauterine transfusion, a decrease or even normalization of the mean velocity in the fetal aorta has been observed [116]. In contrast to the changes in aortic time-averaged mean velocity seen with fetal anemia, there were no significant changes in the waveform indices.

Subsequently, Mari et al. [117] showed that Doppler examination of the fetal middle cerebral artery can be used for clinical management of pregnancies with red-cell alloimmunization. The sensitivity of the PSV in the middle cerebral artery Doppler velocimetry for detection of fetal anemia proved to be superior to that of the Doppler velocimetry of fetal descending aorta (see Chap. 18).

Recently, a relatively small study suggested that in cases of alloimmunization needing repeated intrauterine transfusions, the descending aorta PSV might be a useful adjunct diagnostic tool to middle cerebral artery PSV after two transfusions in judging on fetal hematocrit [118].

15.2.6.3 Diabetes Mellitus

Serial Doppler examinations were performed in a group of 40 pregnant women with diabetes mellitus [119]. A high volume blood flow in the fetal descending aorta was found during the early third trimester; near term, blood flow approached normal values. The PI in the umbilical artery and fetal aorta was within the normal range, so long as there were no signs of fetal growth restriction or hypoxia. Otherwise, no flow variations specific for diabetic pregnancies were seen. Similar findings were also reported for pregnant women with gestational diabetes [120].

15.2.6.4 Fetal Growth Restriction

FGR can have various etiologies, restricted flow through the placental vasculature being the most common cause of this relatively frequent compli-

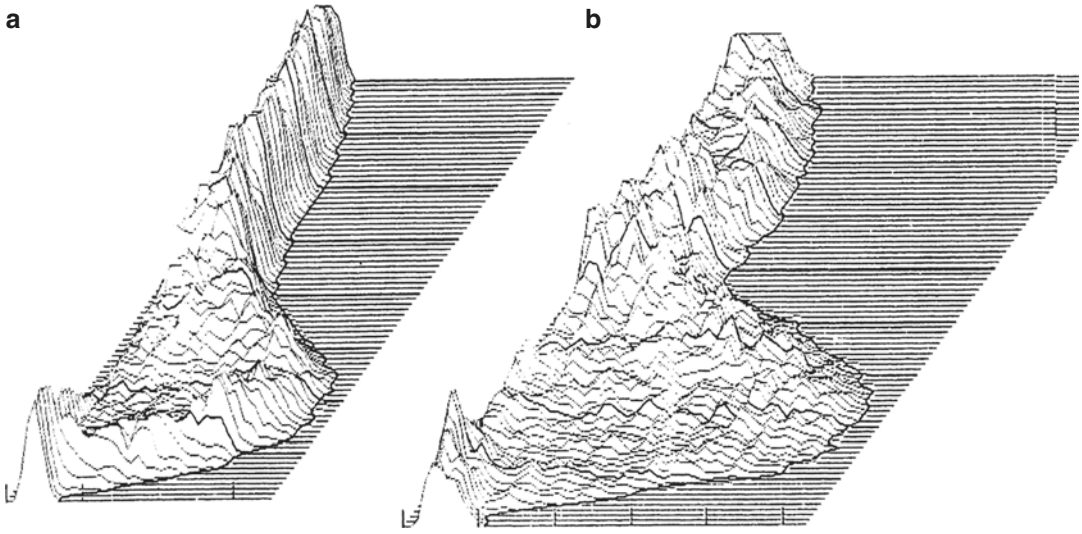

Fig. 15.17 Three-dimensional presentation of Doppler signals recorded from the descending aorta of a normal fetus (**a**) and an anemic fetus (**b**). Note the increase of velocity amplitudes and the right shift of the velocity power in the anemic fetus. (Reprinted from Vetter [113] with permission)

cation of pregnancy. As described above, the increased vascular impedance in the placenta is reflected in a changed blood velocity waveform in the descending fetal aorta, with a reduction of diastolic velocities and a corresponding increase in PI [46, 61, 75]. These findings are similar to those reported for the umbilical artery of growth restricted fetuses [62, 121].

In a study that evaluated placental morphology in relation to intrauterine flow in FGR, only the presence of placental infarction was significantly associated with abnormal flow velocity findings in the fetal descending aorta (high PI, BFC I–III, low mean velocity) [122].

In the descending aorta of growth restricted fetuses, low values were obtained for the time-averaged mean velocity and volume flow, though they did not differ significantly from those of controls [61]. This similarity was probably due to the already mentioned methodologic difficulty of precisely estimating volume flow. Using an improved technique combining an ultrasonic phase-locked echo-tracking system for diameter measurement synchronized with a pulsed Doppler velocimeter [56], Gardiner et al. [123] found the relative pulse amplitude, mean blood velocity, and volume flow to be significantly lower in the descending aorta of growth restricted fetuses than in the controls. Also, the aortic pulse waves of growth restricted fetuses showed values significantly different from those in controls, reflecting the chronic ventriculovascular responses to increased placental impedance [57]. A recent case-control study examined intima media thickness (aIMT) in fetal abdominal aorta and found that growth restricted fetuses (EFW <10th percentile and UA-PI >mean + 2SD) had significantly increased aIMT, PI, PSV, and differences between systolic and diastolic diameters when compared to controls [124]. Within the FGR group, aIMT significantly correlated to aortic PSV and diameter pulsations, which was not the case for controls. The authors concluded that the findings in the FGR group reflected aortic wall adaptation to blood flow changes [124].

In severely growth restricted fetuses developing signs of intrauterine distress, the aortic end-diastolic velocity disappears or even becomes reversed (BFC II and III; Fig. 15.16) [60]. An association has been found to exist between the degree of fetal hypoxia, hypercapnia, acidosis, and hyperlactemia, as diagnosed in blood samples obtained by cordocentesis from growth restricted fetuses and changes in the mean fetal aortic velocity [125] and the velocity waveform [126]. The aortic velocity waveform changes have been observed to precede the cardiotocographic changes, the median time lag being 2–3 days [61, 127], though the interval between the first blood velocity changes and the first changes in cardiotocographic tracings may be as much as several weeks [61, 128].

The finding of ARED flow in the fetal aorta is associated with an adverse outcome of the pregnancy [61, 62] and increased neonatal morbidity [129, 130]. Reverse flow during diastole identifies fetuses in danger of intrauterine death. Perinatal mortality in cases with reverse flow is reported to be high—in some series as high as 100% [131]. The combination of ARED flow in the fetal descending aorta and pulsations in the umbilical vein seems to indicate a fetus with severe hypoxia and imminent heart failure [60].

15.2.7 Aortic Doppler Velocimetry as a Diagnostic Test of FGR and Fetal Hypoxia

Several prospective studies on FGR pregnancies have been performed to evaluate the predictive capacity of fetal aortic velocity waveforms with regard to birth weight, occurrence of fetal distress, and perinatal outcome. Tables 15.6 and 15.7 summarize results of some of the studies in terms of sensitivity, specificity, and positive and negative predictive values. For the ratios between the common carotid artery resistance index (RI) and descending thoracic aorta RI of SGA fetuses redistributing their flow, a sensitivity of 94% was reported for prediction of cesarean section for fetal distress [58]. It is obvious that in growth restricted fetuses, the aortic velocimetry is a better predictor of fetal health than fetal size, which is not surprising in view of the multiplicity of determinants of fetal growth.

Table 15.6 Diagnostic capacity of fetal aortic Doppler velocimetry with regard to the prediction of fetal growth restriction

Study	Number of pregnancies	Prevalence (%)	Sensitivity(%)	Specificity (%)	PPV (%)	NPV (%)	Kappa value
Aortic PI							
Gudmundsson and Maršál [62]	139	52	40	87	76	57	0.26
ARED flow							
Laurin et al. [133]	159	47	50	97	67	93	0.48
Chaoui et al. [128]	954	?	87	82	67	94	–
Gudmundsson and Maršál [62]	139	52	87	61	46	93	0.38

PI Pulsatility index, *ARED* Absent or reversed end-diastolic flow, *PPV* Positive predictive value, *NPV* Negative predictive value

Table 15.7 Diagnostic capacity of fetal aortic Doppler velocimetry with regard to the prediction of operative delivery for fetal distress

Study	Number of pregnancies	Prevalence (%)	Sensitivity (%)	Specificity (%)	PPV (%)	NPV (%)	Kappa value
Aortic PI							
Arabin et al. [132]	171	?	68	88	58	93	–
Gudmundsson and Maršál [62]	139	34	62	87	71	81	0.50
ARED flow							
Laurin et al. [133]	159	19	83	90	66	96	0.66
Chaoui et al. [128]	954	?	88	82	85	95	–
Gudmundsson and Maršál [62]	139	34	91	88	74	96	0.74

PI Pulsatility index, *ARED* Absent or reversed end-diastolic flow, *PPV* Positive predictive value, *NPV* Negative predictive value

The accumulated evidence suggests that, as is also the case for umbilical artery velocimetry, Doppler fetal aortic examination is better suited for use as a secondary diagnostic test in preselected high-risk pregnancies than as a primary screening test in a whole pregnant population [134]. In a prospective study of growth restricted fetuses, Gudmundsson and Maršál [62] compared the predictive value of aortic versus umbilical artery velocity waveforms. The PI in the umbilical artery was found to be a slightly better predictor of fetal outcome than the aortic PI, though the BFC was similarly predictive in the two vessels. Two longitudinal studies confirmed that the changes in the umbilical artery PI preceded changes in the thoracic aorta of growth restricted fetuses [135, 136]. Doppler examination of the umbilical artery is technically easier and can be done with less sophisticated and less expensive instruments. Therefore, for monitoring of fetal health in suspected cases of FGR, umbilical artery Doppler velocimetry is preferable. In clinical studies, the investigation of fetal aortic arterial waveforms might provide more detailed information on the circulatory adaptation and pathophysiologic mechanisms in the process of FGR.

Similar to the umbilical artery, changes in the intrauterine aortic waveforms in growth restricted fetuses have been shown to be significantly correlated to the perinatal outcome and to the long-term postnatal neurologic and psychological development (Chap. 12).

15.3 Summary

Key Points

Fetal Aortic Isthmus

- Doppler examination of the fetal aortic isthmus might improve the early identification of growth restricted fetuses at risk of abnormal neurological outcome.
- The sagittal and the three vessel and trachea planes can be used to obtain reliable Doppler recordings of the aortic isthmus.
- The most used estimations of abnormal blood flow through the aortic isthmus are the retrograde flow defined by aortic isthmus flow index (IFI) of types 3–5 or the aortic isthmus pulsatility index >95th percentile.
- Impairment of the aortic isthmus Doppler waveform precedes changes in the ductus venosus by 1 week.
- Narrowing of the aortic isthmus is highly correlated with coarctation of the aorta.
- There is consistent data on the clinical value of the aortic isthmus Doppler velocimetry in the evaluation of early-onset fetal growth restriction.
- No consistent data have been reported on the clinical benefit of Doppler evaluation of the aortic isthmus in late-onset fetal growth restriction.
- In twin pregnancies, either monochorionic or dichorionic, deterioration of the aortic isthmus

Doppler waveform is mainly observed in the small twin with selective growth restriction.
- No changes in the aortic isthmus blood flow have been related to twin to twin transfusion syndrome.

Fetal Descending Aorta
- A combined linear array real-time and pulsed Doppler velocimetry makes it possible to estimate fetal aortic volume flow. However, the volume flow method is open to error and is therefore less suitable for application to the clinical situation.
- The waveform of the maximum velocities recorded from the fetal descending aorta reflects the impedance to flow in the placenta and the lower fetal body. The waveform is also influenced by other factors (e.g., fetal heart function).
- The aortic waveform can be characterized by various indices (preferably the PI). In a situation of increased peripheral vascular resistance, the aortic diastolic velocities decrease and eventually disappear or reverse (ARED flow).
- The finding of ARED aortic flow is associated with an adverse outcome of pregnancy.
- For practical application, a semiquantitative method (blood flow classes) has been designed to evaluate fetal aortic velocity waveforms. The BFC method emphasizes especially the appearance of the diastolic part of the waveform.
- In uncomplicated pregnancies, the velocity waveform of the fetal descending aorta shows positive flow throughout the cardiac cycle, the proportion of diastolic flow being higher in the abdominal aorta than in the thoracic aorta.
- The aorta PI values are stable during the last trimester of gestation, with a slight increase at term.
- The aortic mean velocity and the relative flow do not change significantly with gestational age during late pregnancy. About 50%–60% of the blood flow in the thoracic descending aorta supplies the placenta.
- Fetal aortic Doppler velocimetry can facilitate the diagnosis of arrhythmias, and the estimation of aortic flow can provide an early indication of imminent heart failure.
- In anemic alloimmunized fetuses, the mean aortic and peak systolic velocities are increased; however, for clinical use, they are inferior to the middle cerebral artery PSV.
- The predictive capacity of fetal aortic velocimetry for fetal growth restriction and development of fetal distress is comparable to that of umbilical artery velocimetry.
- Doppler examination of the fetal descending aorta is suited for application as a secondary diagnostic test in high-risk pregnancies similarly to umbilical artery velocimetry.
- Analysis of the fetal aortic flow velocity pattern can be applied, together with examination of other vessel areas, for a more detailed study of redistribution of flow in the presence of fetal hypoxia.

References

1. Fouron JC. The unrecognized physiological and clinical significance of the fetal aortic isthmus. Ultrasound Obstet Gynecol. 2003;22:441–7.
2. Acharya G, Tronnes A, Rasanen J. Aortic isthmus and cardiac monitoring of the growth-restricted fetus. Clin Perinatol. 2011;38:113–25.
3. Tynan D, Alphonse J, Henry A, Welsh AW. The aortic isthmus: a significant yet underexplored watershed of the fetal circulation. Fetal Diagn Ther. 2016;40:81–93.
4. Hornberger LK, Weintraub RG, Pesonen E, et al. Echocardiographic study of the morphology and growth of the aortic arch in the human fetus. Observations related to the prenatal diagnosis of coarctation. Circulation. 1992;86:741–7.
5. Rudolph AM, Heyman MA, Spitznas U. Hemodynamic considerations in the development of narrowing of the aorta. Am J Cardiol. 1972;30:514–25.
6. Angelini A, Allan LD, Anderson RH, Crawford DC, Chita SK, Ho SY. Measurements of the dimensions of the aortic and pulmonary pathways in the human fetus: a correlative echocardiographic and morphometric study. Br Heart J. 1988;60:221–6.
7. Vimpeli T, Huhtala H, Wilsgaard T, Acharya G. Fetal aortic isthmus blood flow and the fraction of car-

diac output distributed to the upper body and brain at 11–20 weeks of gestation. Ultrasound Obstet Gynecol. 2009;33:538–44.
8. Nomiyama M, Ueda Y, Toyota Y, Kawano H. Fetal aortic isthmus growth and morphology in late gestation. Ultrasound Obstet Gynecol. 2002;19:153–7.
9. Fouron JC, Siles A, Montanari L, et al. Feasibility and reliability of Doppler flow recordings in the fetal aortic isthmus: a multicenter evaluation. Ultrasound Obstet Gynecol. 2009;33:690–3.
10. Pasquini L, Mellander M, Seale A, et al. Z-scores of the fetal aortic isthmus and duct: an aid to assessing arch hypoplasia. Ultrasound Obstet Gynecol. 2007;29:628–33.
11. Acharya G. Technical aspects of aortic isthmus Doppler velocimetry in human fetuses. Ultrasound Obstet Gynecol. 2009;33:628–33.
12. Garcia-Canadilla P, Crispi F, Cruz-Lemini M, et al. Understanding the aortic isthmus Doppler profile and its changes with gestational age using a lumped model of the fetal circulation. Fetal Diagn Ther. 2017;41:41–50.
13. Schmidt KG, Silverman NH, Rudolph AM. Phasic flow events at the aortic isthmus -ductus arteriosus junction and branch pulmonary artery evaluated by multimodal ultrasonography in fetal lambs. Am J Obstet Gynecol. 1998;179:1338–47.
14. Ruskamp J, Fouron JC, Gosselin J, Raboisson MJ, Infante-Rivard C, Proulx F. Reference values for an index of fetal aortic isthmus blood flow during the second half of pregnancy. Ultrasound Obstet Gynecol. 2003;21:441–4.
15. Del Río M, Martínez JM, Figueras F, et al. Doppler assessment of fetal aortic isthmus blood flow in two different sonographic planes during the second half of gestation. Ultrasound Obstet Gynecol. 2005;26:170–4.
16. Del Río M, Martínez JM, Figueras F, et al. Reference ranges for Doppler parameters of the fetal aortic isthmus during the second half of pregnancy. Ultrasound Obstet Gynecol. 2006;28:71–6.
17. Chabaneix J, Fouron JC. Profiling left and right ventricular proportional output during fetal life with a novel systolic index in the aortic isthmus. Ultrasound Obstet Gynecol. 2014;44:176–81.
18. Rychik J. Comments on: profiling left and right ventricular proportional output during fetal life with a novel systolic index in the aortic isthmus. Ultrasound Obstet Gynecol. 2014;44:136.
19. Bonnin P, Fouron J, Teyssier G, Sonesson S, Skoll A. Quantitative assessment of circulatory changes in the fetal aortic isthmus during progressive increase of resistance to umbilical blood flow. Circulation. 1993;88:216–22.
20. Fouron JC, Gosselin J, Raboisson MJ, et al. The relationship between an aortic isthmus blood flow velocity index and the postnatal neurodevelopmental status of fetuses with placental circulatory insufficiency. Am J Obstet Gynecol. 2005;192:497–503.
21. Fouron JC, Skoll A, Sonesson SE, Pfizenmaier M, Jaeggi E, Lessard M. Relationship between flow through the fetal aortic isthmus and cerebral oxygenation during acute placental circulatory insufficiency in ovine fetuses. Am J Obstet Gynecol. 1999;181:1102–7.
22. Lecarpentier E, Cordier AG, Proulx F, et al. Hemodynamic impact of absent or reverse end-diastolic flow in the two umbilical arteries in growth-restricted fetuses. PLoS One. 2013;8:e81160.
23. Sonesson SE, Fouron JC. Doppler velocimetry of the aortic isthmus in human fetuses with abnormal velocity waveforms in the umbilical artery. Ultrasound Obstet Gynecol. 1997;10:107–11.
24. Mäkikallio K, Jouppila P, Räsänen J. Retrograde net blood flow in the aortic isthmus in relation to human fetal arterial and venous circulations. Ultrasound Obstet Gynecol. 2002;19:147–52.
25. Mäkikallio K, Jouppila P, Räsänen J. Retrograde aortic isthmus net blood flow and human fetal cardiac function in placental insufficiency. Ultrasound Obstet Gynecol. 2003;22:351–7.
26. Hernández-Andrade E, Crispi F, Benavides-Serralde JA, et al. Contribution of the myocardial performance index and aortic isthmus blood flow index to predicting mortality in preterm growth-restricted fetuses. Ultrasound Obstet Gynecol. 2009;34:430–6.
27. Del Río M, Martínez JM, Figueras F, et al. Doppler assessment of the aortic isthmus and perinatal outcome in preterm fetuses with severe intrauterine growth restriction. Ultrasound Obstet Gynecol. 2008;31:41–7.
28. Figueras F, Benavides A, Del Río M, et al. Monitoring of fetuses with intrauterine growth restriction: longitudinal changes in ductus venosus and aortic isthmus flow. Ultrasound Obstet Gynecol. 2009;33:39–43.
29. Cruz-Martinez R, Figueras F, Benavides-Serralde A, Crispi F, Hernández-Andrade E, Gratacós E. Sequence of changes in myocardial performance index in relation to aortic isthmus and ductus venosus Doppler in fetuses with early-onset intrauterine growth restriction. Ultrasound Obstet Gynecol. 2011;38:179–84.
30. Cruz-Martinez R, Tenorio V, Padilla N, Crispi F, Figueras F, Gratacos E. Risk of ultrasound-detected neonatal brain abnormalities in intrauterine growth-restricted fetuses born between 28 and 34 weeks' gestation: relationship with gestational age at birth and fetal Doppler parameters. Ultrasound Obstet Gynecol. 2015;46:452–9.
31. Kennelly MM, Farah N, Hogan J, Reilly A, Turner MJ, Stuart B. Longitudinal study of aortic isthmus Doppler in appropriately grown and small-for-gestational-age fetuses with normal and abnormal umbilical artery Doppler. Ultrasound Obstet Gynecol. 2012;39:414–20.
32. Villalaín C, Herraiz I, Quezada MS, et al. Prognostic value of the aortic isthmus Doppler assessment on late onset fetal growth restriction. J Perinat Med. 2019;47:212–7.

33. Hoffman J, Kaplan. The incidence of congenital heart disease. J Am Coll Cardiol. 2002;39:1890–900.
34. Kenny D, Hijazi ZM. Coarctation of the aorta: from fetal life to adulthood. Cardiol J. 2011;18:487–95.
35. Hornberger LK, Sahn DJ, Kleinman CS, Copel J, Silverman NH. Antenatal diagnosis of coarctation of the aorta: a multicenter experience. J Am Coll Cardiol. 1994;23:417–23.
36. Leduc F, Delabaere A, Gendron R, et al. Aortic isthmus flow recording predicts the outcome of the recipient twin after laser coagulation in twin-twin transfusion syndrome. Fetal Diagn Ther. 2018;44:135–41.
37. Kim SY, Lee SP, Lee CM, Jung SY, Park HN. Doppler assessment of fetal aortic isthmus flow in twin. Obstet Gynecol Sci. 2015;58:17–23.
38. Almström H, Sonesson SE. Doppler echocardiographic assessment of fetal blood flow redistribution during maternal hyperoxygenation. Ultrasound Obstet Gynecol. 1996;8:256–61.
39. Brantberg A, Sonesson SE. Central arterial hemodynamics in small-for-gestational-age fetuses before and during maternal hyperoxygenation: a Doppler velocimetric study with particular attention to the aortic isthmus. Ultrasound Obstet Gynecol. 1999;14:237–43.
40. Edwards LA, Lara DA, Sanz Cortes M, et al. Chronic maternal hyperoxygenation and effect on cerebral and placental vasoregulation and neurodevelopment in fetuses with left heart hypoplasia. Fetal Diagn Ther. 2019;46:45–57.
41. FitzGerald DE, Drumm J. Non-invasive measurement of human fetal circulation using ultrasound: a new method. BMJ. 1977;2:1450–1.
42. McCallum WD, Williams CB, Napel S, Diagle RE. Fetal blood velocity waveforms. Am J Obstet Gynecol. 1978;132:425–9.
43. Gill RW. Pulsed Doppler with B-mode imaging for quantitative blood flow measurement. Ultrasound Med Biol. 1979;5:223–35.
44. Eik-Nes SH, Brubakk AO, Ulstein MK. Measurement of human fetal blood flow. BMJ. 1980;2:283–4.
45. Eik-Nes SH, Maršál K, Brubbakk AO, Kristoffersen K, Ulstein M. Ultrasonic measurements of human fetal blood flow. J Biomed Eng. 1982;4:28–36.
46. Jouppila P, Kirkinen P. Increased vascular resistance in the descending aorta of the human fetus in hypoxia. Br J Obstet Gynaecol. 1984;91:853–6.
47. Eik-Nes SH, Maršál K, Kristoffersen K, Vernersson E. Noninvasive Messung des fetalen Blutstromes mittels Ultraschall. Ultraschall Med. 1981;2:226–31.
48. Sindberg Eriksen P, Gennser G, Lindström K, Benthin M, Dahl P. Pulse wave recording – development of a method for investigating foetal circulation in utero. J Med Eng Technol. 1985;9:18–27.
49. Saburi Y, Mori A, Yasui I, Makino T, Iwabuchi M. Fetal aortic blood flow assessment from the relationship between fetal aortic diameter pulse and flow velocity waveforms during fetal development. Early Hum Dev. 2001;65:57–70.
50. Stale H, Maršál K, Gennser G, et al. Aortic diameter pulse waves and blood flow velocity in the small for gestational age fetus. Ultrasound Med Biol. 1991;17:471–8.
51. Eik-Nes SH, Maršál K, Kristoffersen K. Methodology and basic problems related to blood flow studies in the human fetus. Ultrasound Med Biol. 1984;10:329–37.
52. Veille JC, Tavill M, Sivakoff M, et al. Evaluation of pulsed Doppler echocardiography for measurement of aortic blood flow in the fetal lamb. Am J Obstet Gynecol. 1989;161:1610–4.
53. Schmidt KG, Di Tommaso M, Silverman NH, Rudolph AM. Doppler echocardiographic assessment of fetal descending aortic and umbilical blood flows: validation studies in fetal lambs. Circulation. 1991;83:1731–7.
54. Bonnefous O, Pesque P. Time domain formulation of pulsed ultrasound and blood velocity estimation by cross correlation. Ultrason Imaging. 1986;8:73.
55. Länne T, Solvig J, Eriksson A, Olofsson PÅ, Maršál K, Hansen F. Time domain ultrasonography—a reliable method of percutaneous volume flow measurement in large arteries. Clin Physiol. 1997;17:371–82.
56. Brodszki J, Gardiner HM, Eriksson A, Stale H, Maršál K. Reproducibility of ultrasonic fetal volume blood flow measurements. Clin Physiol. 1998;18:479–85.
57. Gardiner H, Brodszki J, Maršál K. Ventriculovascular physiology of the growth-restricted fetus. Ultrasound Obstet Gynecol. 2001;18:47–53.
58. Konje JC, Abrams K, Bell SC, de Chazal RC, Taylor DJ. The application of color power angiography to the longitudinal quantification of blood flow volume in the fetal middle cerebral arteries, ascending aorta, descending aorta, and renal arteries during gestation. Am J Obstet Gynecol. 2000;182:393–400.
59. Salehi D, Sun L, Steding-Ehrenborg K, et al. Quantification of blood flow in the fetus with cardiovascular magnetic resonance imaging using Doppler ultrasound gating: validation against metric optimized gating. J Cardiovasc Magnetic Resonance. 2019;21:74. https://doi.org/10.1186/s12968-019-0586-8.
60. Lingman G, Laurin J, Maršál K. Circulatory changes in fetuses with imminent asphyxia. Biol Neonate. 1986;49:66–73.
61. Laurin J, Lingman G, Maršál K, Persson PH. Fetal blood flow in pregnancies complicated by intrauterine growth retardation. Obstet Gynecol. 1978;69:895–902.
62. Gudmundsson S, Maršál K. Blood velocity waveforms in the fetal aorta and umbilical artery as predictors of fetal outcome: a comparison. Am J Perinatol. 1991;8:1–6.
63. European Association of Perinatal Medicine. Regulation for the use of Doppler technology in perinatal medicine. Consensus of Barcelona. Barcelona: Instituto Dexeus; 1989. p. 20, 26.

64. Lingman G, Maršál K. Fetal central blood circulation in the third trimester of normal pregnancy: longitudinal study. II. Aortic blood velocity waveform. Early Hum Dev. 1986;13:151–9.
65. Mills CJ, Gabe IT, Gault JH, et al. Pressure-flow relationships and vascular impedance in man. Cardiovasc Res. 1970;4:405–17.
66. Lingman G, Maršál K. Fetal central blood circulation in the third trimester of normal pregnancy: longitudinal study. I. Aortic and umbilical blood flow. Early Hum Dev. 1986;13:137–50.
67. Griffin D, Cohen-Overbeek T, Campbell S. Fetal and utero-placental blood flow. Clin Obstet Gynecol. 1983;10:565–602.
68. Van Lierde M, Oberweis D, Thomas K. Ultrasonic measurement of aortic and umbilical blood flow in the human fetus. Obstet Gynecol. 1984;63:801–5.
69. Maršál K, Lindblad A, Lingman G, Eik-Nes SH. Blood flow in the fetal descending aorta: intrinsic factors affecting fetal blood flow, i.e. fetal breathing movements and fetal cardiac arrhythmia. Ultrasound Med Biol. 1984;10:339–48.
70. Erskine RLA, Ritchie JWK. Quantitative measurement of fetal blood flow using Doppler ultrasound. Br J Obstet Gynaecol. 1985;92:600–4.
71. Rasmussen K. Quantitative blood flow in the fetal descending aorta in the umbilical vein in normal pregnancies. Scand J Clin Lab Invest. 1987;47:319–24.
72. Räsänen J, Kirkinen P, Jouppila P. Fetal aortic blood flow and echocardiographic findings in human pregnancy. Eur J Obstet Gynecol Reprod Biol. 1988;27:115–24.
73. Cameron A, Nicholson S, Nimrod C, et al. Duplex ultrasonography of the fetal aorta, umbilical artery, and placental arcuate artery throughout normal human pregnancy. J Can Assoc Radiol. 1989;40:145–9.
74. Eldridge ME, Berman W Jr, Greene ER. Serial echo-Doppler measurements of human fetal abdominal aortic blood flow. J Ultrasound Med. 1985;4:453–8.
75. Griffin D, Bilardo K, Masini L, et al. Doppler blood flow waveforms in the descending thoracic aorta of the human fetus. Br J Obstet Gynaecol. 1984;91:997–1006.
76. Van Eyck J, Wladimiroff JW, Noordam MJ, Tonge HM, Prechtl HFR. The blood velocity waveform in the fetal descending aorta: its relationship to fetal behavioural states in normal pregnancy at 37–38 weeks. Early Hum Dev. 1985;12:137–43.
77. Jouppila P, Kirkinen P. Blood velocity waveforms of the fetal aorta in normal and hypertensive pregnancies. Obstet Gynecol. 1986;67:856–60.
78. Tonge HM, Wladimiroff JW, Noordam MJ, van Kooten C. Blood flow velocity waveforms in the descending fetal aorta: comparison between normal and growth-retarded pregnancies. Obstet Gynecol. 1986;67:851–5.
79. Arabin B, Bergmann PL, Saling E. Qualitative Analyse von Blutflußspektren uteroplazentarer Gefäße, der Nabelarterie, der fetalen Aorta and der fetalen Arteria carotis communis in normaler Schwangerschaft. Ultraschall Klin Prax. 1987;2:114–9.
80. Årström K, Eliasson A, Hareide JH, Maršál K. Fetal blood velocity waveforms in normal pregnancies: a longitudinal study. Acta Obstet Gynecol Scand. 1989;68:171–8.
81. Hecher K, Spernol R, Szalay S, Stettner H, Ertl U. Referenzwerte für den Pulsatilitätsindex und den Resistance-Index von Blutflußkurven der Arteria umbilicalis und der fetalen Aorta im dritten Trimenon. Ultraschall. 1989;10:226–9.
82. Ferrazi E, Gementi P, Bellotti M, et al. Doppler velocimetry; critical analysis of umbilical, cerebral and aortic reference values. Eur J Obstet Gynecol Reprod Biol. 1990;38:189–1.
83. De Koekkoek-Doll PK, Stijnen T, Wladimiroff JW. Behavioural state dependency of renal artery and descending aorta velocimetry and micturation in the normal term fetus. Br J Obstet Gynaecol. 1994;101:975–8.
84. Bahlmann F, Wellek S, Reinhardt I, Krummenauer F, Merz E, Welter C. Reference values of fetal aortic flow velocity waveforms and associated intra-observer reliability in normal pregnancies. Ultrasound Obstet Gynecol. 2001;17:42–9.
85. Chen HY, Chang FM, Huang HC, Hsieh FJ, Lu CC. Antenatal fetal blood flow in the descending aorta and the umbilical vein and their ratio in normal pregnancy. Ultrasound Med Biol. 1988;14:263–8.
86. Longo LD, Wyat JF, Hewitt CW, Gilbert RD. A comparison of circulatory responses to hypoxic and carbon monoxide hypoxia in fetal blood flow and oxygenation. In: Longo LD, Rewean DD, editors. Fetal and newborn cardiovascular physiology. New York: Garland STPM Press; 1978. p. 259.
87. Gruenwald P. Pathology of the deprived fetus and its supply line. In: Size at birth. Ciba Foundation Symposium 27. Amsterdam: Elsevier, Excerpta Medica; 1974. p. 1–26.
88. Maršál K, Lingman G, Rosén KG, Kjellmer I. Myocardial contractility and ultrasonically measured blood velocity in fetal lamb. In: Gill RW, Dadd MJ, editors. WFUMB ‘85. Sydney: Pergamon; 1985. p. 256.
89. Lingman G, Gennser G, Maršál K. Ultrasonic measurements of the blood velocity and pulsatile diameter changes in the fetal descending aorta. In: Rolfe P, editor. Fetal physiological measurements. London: Butterworth; 1986. p. 206–10.
90. Tonge HM, Struijk PC, van Kooten C, Wladimiroff JW, Bom N. The first derivative as a means of synchronizing pulsatile flow velocity and vessel diameter waveforms in the fetal descending aorta. J Perinat Med. 1988;16:299–304.
91. Stale H, Gennser G, Maršál K. Blood flow velocity and pulsatile diameter changes in the fetal descend-

ing aorta: a longitudinal study. Am J Obstet Gynecol. 1990;163:26–9.
92. Van Eyck J, Wladimiroff JW, van den Wijngaard JAGW, Noordam MJ, Prechtl HFR. The blood flow velocity waveform in the fetal internal carotid and umbilical artery; its relation to fetal behavioural states in normal pregnancy at 37–38 weeks. Br J Obstet Gynaecol. 1987;94:736–41.
93. Van Eyck J, Wladimiroff JW, Noordam MJ, Cheung KL, van den Wijngaard JAGW, Prechtl HFR. The blood flow velocity waveform in the fetal descending aorta; its relationship to fetal heart rate pattern, eye and body movements in normal pregnancy at 27–28 weeks of gestation. Early Hum Dev. 1988;17:187–94.
94. Maršál K. Fetal breathing movements in man: characteristics and clinical significance. Obstet Gynecol. 1978;52:394–401.
95. Walz W. Über die Bedeutung der intrauterinen Atembewegungen. Monatsschr Geburtshilfe Gynaekol. 1922;60:715–6.
96. Lindblad A, Bernow J, Maršál K. Obstetric analgesia and fetal blood flow during labour. Br J Obstet Gynaecol. 1987;94:306–11.
97. Lees MH, Hill JD, Ochsner AJ III, Thomas CL, Novy MJ. Maternal placental and myometrial blood flow of the rhesus monkey during uterine contractions. Am J Obstet Gynecol. 1971;110:68–81.
98. Fendel H, Fettweis P, Billet P, et al. Doppleruntersuchungen des arteriellen utero-feto-plazentaren Blut-flusses vor und während der Geburt. Z Geburtshilfe Perinatol. 1987;191:121–9.
99. Axt-Fliedner R, Ertan K, Hendrik HJ, Schmidt W. Neonatal nucleated red blood cell counts: relationship to abnormal fetoplacental circulation detected by Doppler studies. J Ultrasound Med. 2001;20:183–90.
100. Adamson SL, Langille BL. Factors determining aortic and umbilical blood flow pulsatility in fetal sheep. Ultrasound Med Biol. 1992;18:255–66.
101. Gudmundsson S, Eik-Nes SH, Lingman G, et al. Evaluation of blood flow velocity indices in an animal model. Echocardiography. 1990;7:647–56.
102. Malcus P, Hökegård K-H, Kjellmer I, et al. The relationship between arterial blood velocity waveforms and acid-base status in the fetal lamb during experimental asphyxia. J Matern Fetal Invest. 1991;1:29–34.
103. Malcus P, Kjellmer I, Lingman G, et al. Diameters of the common carotid artery and aorta change in different directions during acute asphyxia in the fetal lamb. J Perinat Med. 1991;19:259–67.
104. Lingman G, Dahlström JA, Eik-Nes SH, et al. Hemodynamic evaluation of fetal heart arrhythmias. Br J Obstet Gynaecol. 1984;91:647–52.
105. Lingman G, Maršál K. Circulatory effects of fetal heart arrhythmias. J Pediatr Cardiol. 1986;7:67–74.
106. Chan FY, Woo SK, Ghosh A, Tang M, Lam C. Prenatal diagnosis of congenital fetal arrhythmias by simultaneous pulsed Doppler velocimetry of the fetal abdominal aorta and inferior vena cava. Obstet Gynecol. 1990;76:200–4.
107. Tonge HM, Wladimiroff JW, Noordam MJ, Stewart PA. Fetal cardiac arrhythmias and their effect on volume blood flow in descending aorta of human fetus. J Clin Ultrasound. 1986;14:607–12.
108. Maršál K, Eik-Nes SH, Persson P-H, Ulstein M. Blood flow in human fetal aorta in normal pregnancy and in fetal cardiac arrhythmia. Acta Obstet Gynecol Scand Suppl. 1980;93:39.
109. Lingman G, Lundström N-R, Maršál K. Clinical outcome and circulatory effects of fetal cardiac arrhythmia. Acta Paediatr Scand Suppl. 1986;329:120–6.
110. Kirkinen P, Jouppila P. Umbilical venous flow as indicator of fetal anaemia. Lancet. 1981;1:1004–5.
111. Rightmire DA, Nicolaides KH, Rodeck CH, Campbell S. Fetal blood velocities in Rh isoimmunization: relationship to gestational age and to fetal hematocrit. Obstet Gynecol. 1986;68:233–6.
112. Nicolaides KH, Bilardo CM, Campbell S. Prediction of fetal anemia by measurement of the mean blood velocity in the fetal aorta. Am J Obstet Gynecol. 1990;162:209–12.
113. Vetter K. Dopplersonographie in der Schwangerschaft. Weinheim: VCH Verlagsgesellschaft; 1991. p. 142.
114. Copel JA, Grannum PA, Green JJ, et al. Fetal cardiac output in the isoimmunized pregnancy: a pulsed Doppler-echocardiographic study of patients undergoing intravascular intrauterine transfusion. Am J Obstet Gynecol. 1989;161:361–5.
115. Rizzo G, Nicolaides KH, Arduini D, Campbell S. Effects of intravascular fetal blood transfusion on fetal intracardiac Doppler velocity waveforms. Am J Obstet Gynecol. 1990;163:1231–8.
116. Bilardo CM, Nicolaides KH, Campbell S. Doppler studies in red cell isoimmunization. Clin Obstet Gynecol. 1989;32:719–27.
117. Mari G, Deter RL, Carpenter RL, et al. Noninvasive diagnosis by Doppler ultrasonography of fetal anemia due to maternal red-cell alloimmunization. Collaborative Group for Doppler Assessment of the blood velocity in anemic fetuses. N Engl J Med. 2000;342:9–14.
118. Kumari S, Deka D, Dadhwal V, Perumal V. Correlation of fetal blood vessel Doppler measurements with fetal anemia among rhesus isoimmunized pregnancies after two intrauterine transfusions. Int J Gynaecol Obstet. 2019;146:218–22.
119. Olofsson P, Lingman G, Sjöberg N-O, Maršál K. Ultrasonic measurement of fetal blood flow in diabetic pregnancy. J Perinat Med. 1987;15:545–53.
120. Fadda GM, D'Antona D, Ambrosini G, et al. Placenta and fetal pulsatility indices in gestational diabetes mellitus. J Reprod Med. 2001;46:365–70.
121. Erskine RLA, Ritchie JWK. Umbilical artery blood flow characteristics in normal and growth-retarded fetuses. Br J Obstet Gynaecol. 1985;92:605–10.
122. Laurini R, Laurin J, Maršál K. Placental histology and fetal blood flow in intrauterine growth retardation. Acta Obstet Gynecol Scand. 1994;73:529–34.

123. Gardiner H, Brodszki J, Eriksson A, Maršál K. Volume blood flow estimation in the normal and growth-restricted fetus. Ultrasound Med Biol. 2002;28:1107–13.
124. Visentin S, Londero AP, Calanducci M, et al. Fetal abdominal aorta: Doppler and structural evaluation of endothelial function in intrauterine growth restriction and controls. Ultraschall Med. 2019;40:55–63.
125. Soothill PW, Nicolaides KH, Bilardo CM, Campbell S. Relation of fetal hypoxia in growth retardation to mean blood velocity in the fetal aorta. Lancet. 1986;2:1118–20.
126. Bilardo CM, Nicolaides KH, Campbell S. The relationship of fetal blood gases and pH to Doppler investigations of the fetal circulation. In: Maršál K, editor. Abstracts, third international conference on fetal and neonatal physiologic measurements. Malmö/Ronnby: Malmö General Hospital, Malmö; 1988. p. 106.
127. Arabin B, Siebert M, Jimenez E, Saling E. Obstetrical characteristics of a loss of end-diastolic velocities in the fetal aorta and/or umbilical artery using Doppler ultrasound. Gynecol Obstet Investig. 1988;25:173–80.
128. Chaoui R, Hoffmann H, Zienert A, et al. Klinische Bedeutung und fetal outcome beim enddiastolischen Flowverlust in der A. umbilicalis und/oder fetalen Aorta: Analyse von 51 Fällen. Geburtshilfe Frauenheilkd. 1991;51:532–9.
129. Hackett GA, Campbell S, Gamsu H, Cohen-Overbeek T, Pierce JMF. Doppler studies in the growth retarded fetus and prediction of neonatal necrotising enterocolitis, haemorrhage, and neonatal morbidity. BMJ. 1987;294:13–6.
130. Eronen M, Kari A, Pesonen E, et al. Value of absent or retrograde end-diastolic flow in fetal aorta and umbilical artery as a predictor of perinatal outcome in pregnancy-induced hypertension. Acta Paediatr. 1993;82:919–24.
131. Illyes M, Gati I. Reverse flow in the human fetal descending aorta as a sign of severe fetal asphyxia preceding intrauterine death. J Clin Ultrasound. 1988;16:403–10.
132. Arabin B. Doppler blood flow measurement in uteroplacental and fetal vessels: pathophysiological and clinical significance. Berlin Heidelberg New York: Springer; 1990. p. 85.
133. Laurin J, Maršál K, Persson P-H, Lingman G. Ultrasound measurement of fetal blood flow in predicting fetal outcome. Br J Obstet Gynaecol. 1987;94:940–8.
134. Maršál K, Persson P-H. Ultrasonic measurement of fetal blood velocity waveform as a secondary diagnostic test in screening for intrauterine growth retardation. J Clin Ultrasound. 1988;16:239–44.
135. Harrington K, Thompson MO, Carpenter RG, Nguyen M, Campbell S. Doppler fetal circulation in pregnancies complicated by pre-eclampsia or delivery of a small for gestational age baby: 2. Longitudinal analysis. Br J Obstet Gynaecol. 1999;106:453–66.
136. Hecher K, Bilardo CM, Stigter RH, et al. Monitoring of fetuses with intrauterine growth restriction: a longitudinal study. Ultrasound Obstet Gynecol. 2001;18:564–70.

16 The Cerebroplacental Ratio and Hypoxic Index in the Prediction of Fetal Outcome

Philippe Arbeille, Gabriel Carles, Gustavo Vilchez, and Dev Maulik

16.1 Fetal Cerebral Flow Adaptation to Hypoxia

Hypoxia is present in most of the chronic or acute fetal patency stages. In severely growth-restricted fetuses, the pO_2 is about 15 mmHg, whereas in normal fetuses it is about 23 mmHg. Fetal adaptation to hypoxia consists mainly of a humoral process and a cardiovascular process. Severe hypoxia is generally associated with a pCO_2 increase and pH decrease. Erythropoiesis is stimulated, leading to polycythemia and polycythemia. The fetus protects against hypoxia by using the glucose reserves and the acid-base buffers. The initial cardiovascular response includes a redistribution of the main fetal flows and later blood pressure increase, bradycardia, and modification of the cardiac (left and right) hemodynamics. It is generally accepted that there is significant vasoconstriction of most of the fetal territories (pulmonary, splanchnic, skeletal, and muscular areas) and increased perfusion of the brain, the heart, and the adrenal glands [1–4]. This phenomenon called the "brain-sparing effect" attempts to compensate for fetal hypoxia by providing more oxygen to the brain via cerebral vasodilation. Nevertheless, in the case of hypoxia blood oxygen saturation may not be normal [5, 6], and the increased brain perfusion may be responsible for brain edema with tissue deterioration. Finally, although the adapted response to hypoxia (brain vasodilation) is observed, it is difficult to evaluate if the brain tissue is protected against the deleterious effects of hypoxia and to what extent.

It was demonstrated that in cases of transient or chronic placental insufficiency (malaria, hypertension, drug abuse), abnormal fetal heart rate patterns occur after some days and brain damage can develop after some weeks despite flow redistribution [7–10]. These observations suggest that the occurrence of functional (abnormal fetal heart rate) or organic fetal damage may depend on the amplitude of the pO_2 decrease as already suggested and on the duration of the exposure to hypoxia [8]. Severe maternal anemia, which induces acute but reversible hypoxia without placental insufficiency, is frequently associated with prematurity, reduced neonatal weight, and infant iron deficiency [11–14]. In this condition, oxygen supply to the fetus might be reduced

P. Arbeille (✉)
Universite de Tours, Universite INSERM 316, Med. Nucleaire and Ultrasons, C.H.U. Trousseau, Tours, France
e-mail: arbeille@med.univ-tours.fr

G. Carles
Department of Gynecology/Obstetrics, Hospital de St. Laurent du Maroni, St. Laurent du Maroni, French, Guyana

G. Vilchez · D. Maulik
Department of Obstetrics and Gynecology, UMKC School of Medicine/Truman Medical Center, UMKC School of Medicine, Kansas City, MO, USA

D. Maulik, C. C. Lees (eds.), *Doppler Ultrasound in Obstetrics and Gynecology*,
https://doi.org/10.1007/978-3-031-06189-9_16

and result in blood flow redistribution with similar consequences (abnormal fetal heart rate) as previously described, despite no evidence of placental insufficiency. On the other hand, several studies have suggested that decelerations in the fetal heart rate are a late sign of fetal deterioration before which the fetus might be delivered [15–18]; thus, anticipation of fetal heart rate abnormality by Doppler monitoring of the fetal flow redistribution occurring before worsening hypoxia could provide opportunity for early intervention [19–21].

Animal studies have demonstrated that fetal cerebral circulation is also affected by vasoconstrictive drugs administered during pregnancy. For example, nicotine induces in fetal lambs a reduction of the flow toward the brain affects the cerebral flow response to the CO_2 test. Even drugs considered necessary to treat a mother's pathology (hypertension) may have, after long-term treatment, unsuitable effects on the fetus by blocking or reducing the fetal adaptation to hypoxia.

16.2 Examination Technique

16.2.1 Human Investigations (Duplex B, Pulsed Wave Doppler, and Color Doppler)

The first studies were based on the exploration of the anterior and middle cerebral arteries [22–24] or of the intracranial portion of the internal carotid artery [25]. Due to the generally poor resolution of the ultrasound images, it was necessary to visualize well-known cerebral structures (cerebral peduncles, middle cerebral line) and use them as anatomical references to identify the intracerebral vessels. By locating a pulsed-Doppler sample volume anterior to the middle cerebral line, a Doppler signal with moderate diastolic amplitude was detected in approximately 80% of the cases. At that time, the Doppler signal was only considered to be the anterior cerebral artery velocity signal. The subsequent significant improvements in ultrasound technology have facilitated this examination. It is now easy to detect the arterial pulsation of the cerebral vessels and to localize correctly the Doppler sample volume (Figs. 16.1 and 16.2). On the biparietal image plane, the middle cerebral arteries are found on a transverse line passing anterior to the cerebral peduncles, and the anterior arteries are found on a line perpendicular to the previous line approximately 2 cm in front of the peduncles' anterior limit.

With color Doppler technology, it became possible to visualize and investigate the main cerebral arteries and to evaluate vascular resistance in various vascular areas of the brain supplied by these arteries [26]. In Fig. 16.1d, the two anterior, middle, and posterior cerebral arteries and the posterior communicating arteries can be easily identified. The incidence displaying these vessels is similar to the "biparietal incidence" used for measuring the fetal head diameter. The vessels most easily investigated by this incidence are the middle cerebral arteries because they are oriented toward the Doppler transducer. In this case, the angle between the vessel axis and the Doppler beam is close to zero and the Doppler frequency is maximum.

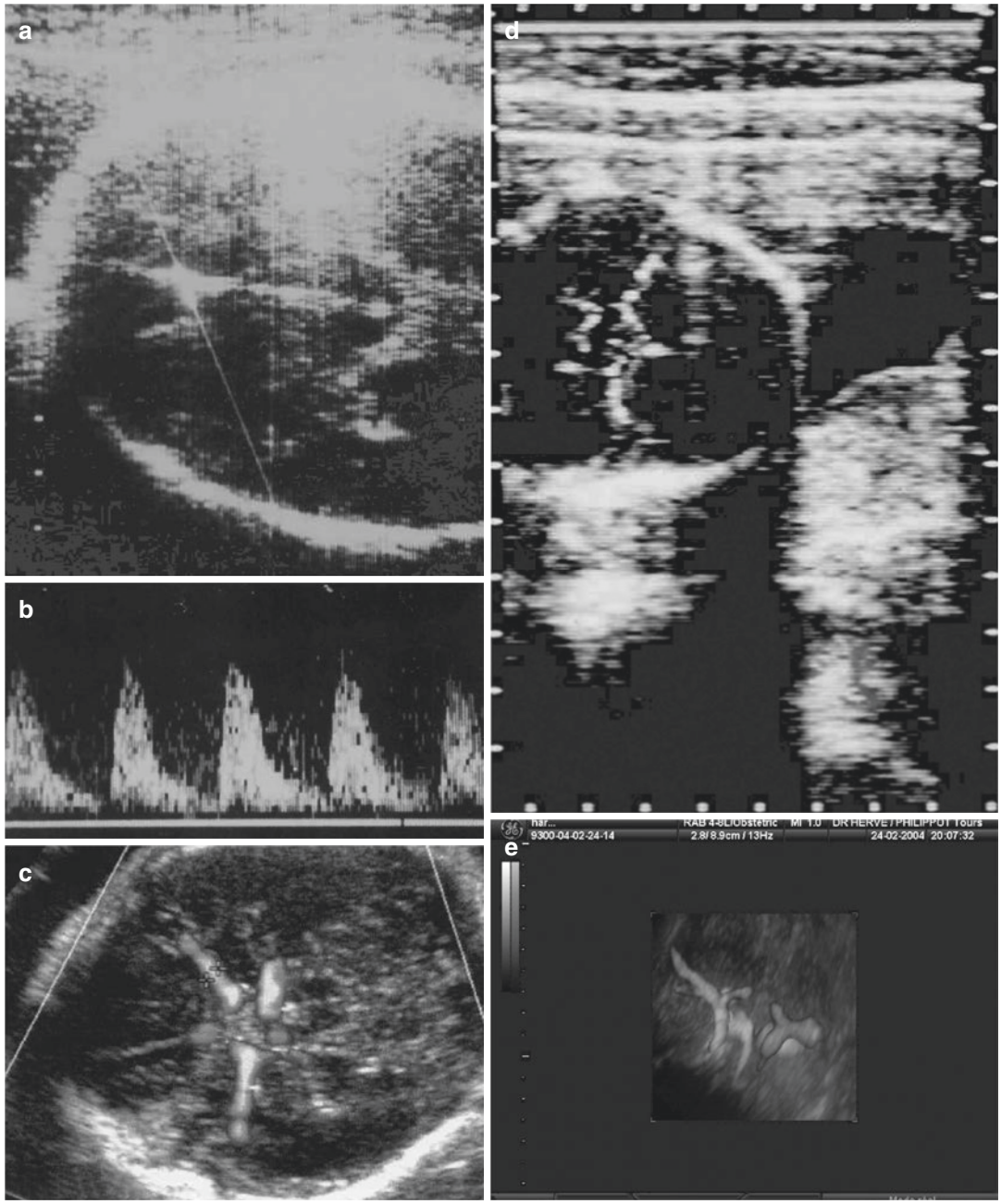

Fig. 16.1 Investigation of the fetal cerebral arteries. (**a**, **b**) Fetal cranial cross section with the cerebral peduncle and the Doppler sample volume on the anterior cerebral arteries and the corresponding Doppler spectrum (1986). (**c**, **d**) Color Doppler of the circle of Willis (1988). (**e**) Three-dimensional color Doppler (2004) [22]

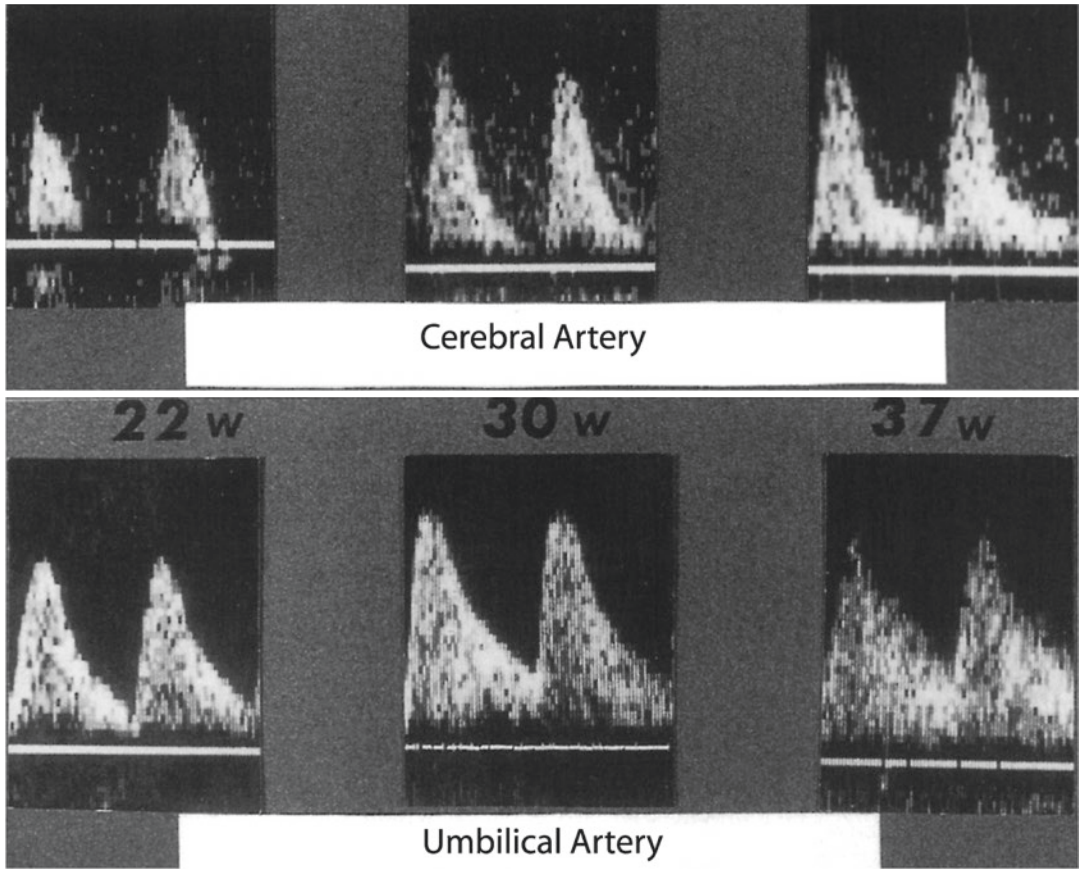

Fig. 16.2 Umbilical and cerebral velocity waveform in normal pregnancies at 22, 30, and 37 weeks of gestation. Note that the cerebral end-diastolic flow velocity is always lower than the umbilical flow velocity; thus, the cerebral to umbilical index is always higher than the umbilical to cerebral index (1986) [22]

16.2.2 Animal Investigations (Implanted Doppler Sensors)

Although fetal Doppler examinations in the human pregnancy provide useful information to the obstetrician, it is not possible to collect all the biological and hemodynamic data required to understand the physiopathological mechanisms involved in the development of the intrauterine growth restriction (IUGR) and the hypoxia.

With the animal model, it is possible to measure blood pressure, blood velocity, and blood volume, to collect blood samples, to perform pharmacological tests, and to simulate some human pathologies.

Several studies have been carried out on lamb fetuses using electromagnetic flowmeters placed around the umbilical cord and catheters with pressure sensors inserted into the fetal aorta. Mostly, only the umbilical flow was assessed on the fetal side. Flat Doppler probes were developed to be implanted in the fetus and the mother, making it possible to assess atraumatically the fetal (cerebral/umbilical) and maternal flows in real time over a period of approximately 20 days' gestation. The 4-MHz continuous wave (CW) or pulsed wave (PW) Doppler probe consists of two rectangular piezoelectric transducers pre-oriented at 45° from the surface of the probe and placed in a plastic case (6 mm high, 2 cm^2 area) with small holes on the edges to sew the probe to the fetal skin. The sensors are affixed to the fetal skin, facing the umbilical cord, the fetal cerebral arteries, and in front of the uterine arteries. The output wires and

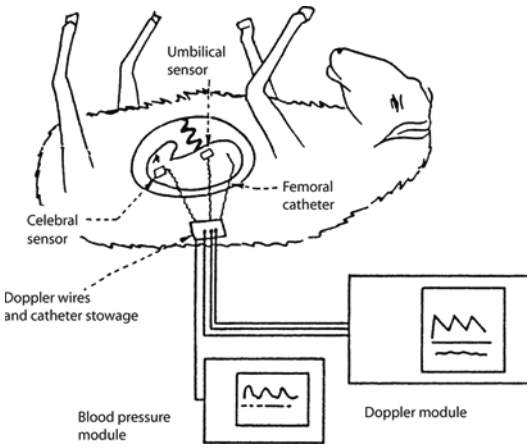

Fig. 16.3 Instrumentation of the fetus. Flat Doppler sensors are sewn on the fetal skin in front of the artery to be investigated (on the abdomen for the umbilical arteries, on the neck for the internal carotid artery, on the maternal abdomen for the uterine artery). A catheter is inserted into the fetal femoral artery, for blood pressure measurements and blood sampling (blood gases)

the fetal catheter connectors are stowed in a pocket affixed to the back of the ewe, and at each measurement session, the fetus is simply connected for 1 or 2 h (without any anesthesia) to the Doppler and pressure system (Fig. 16.3) [27, 28].

On the Doppler waveforms, the blood flow volume and the vascular resistance changes in the area supplied by the vessel (placenta, brain, uterus) and the fetal heart rate are calculated. This system has been tested on normal gestations, during simulated fetal hypoxia, and during pharmacological treatments (Fig. 16.3) [7, 27, 28].

16.3 Cerebral Hemodynamics and Doppler Indices

16.3.1 Cerebral Resistance to Flow

Accessibility to the main fetal cerebral arteries by Doppler has led to the development of various hemodynamic indices. The amplitude of the end-diastolic flow in the fetal vessels is directly related to the vascular resistances in the area

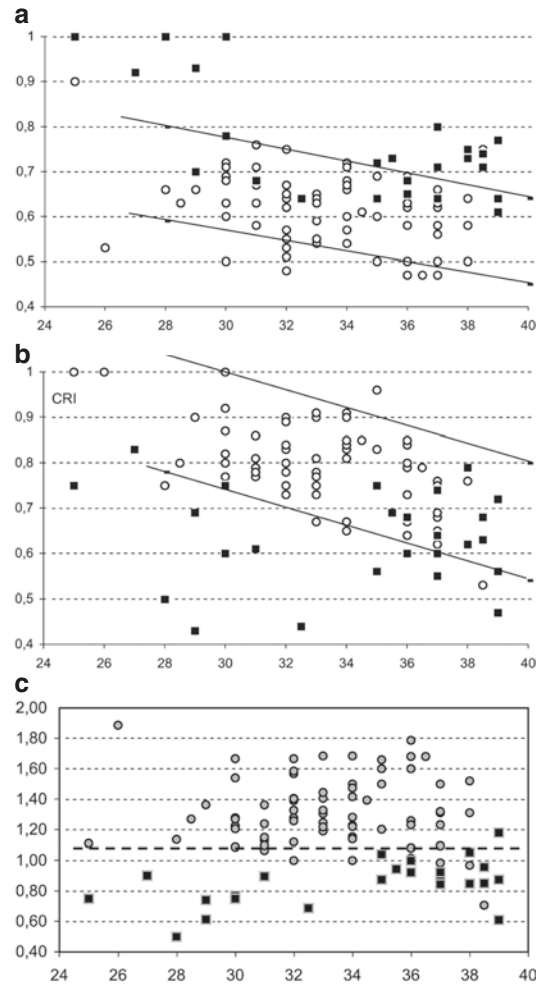

Fig. 16.4 Resistance index [R = (S − D/S)] and cerebral-umbilical ratio (CPR = CRI/URI) in a population of 90 hypertensive pregnancies, with 17 (19%) having moderate IUGR (S = systolic peak, D = end-diastolic velocity). Normal range delimited from a population of 100 normal pregnancies. (**a**) Evolution of the umbilical vascular resistance index (URI) in normal (open symbols), and in growth-restricted (closed symbols) fetuses. The URI is abnormal when higher than the upper limit of the normal range. The sensitivity of these indices for the detection of IUGR is about 60%. (**b**) Evolution of the cerebral (CRI) vascular resistance in normal (open symbols), and in growth-restricted (closed symbols) fetuses. The CRI is abnormal when it is lower than the lower limit of the normal range. (**c**) Cerebral-umbilical ratio in normal (open symbols) and growth-restricted (closed symbols) fetuses. The sensitivity of this index for the detection of IUGR is about 85%

supplied by these vessels [29–31]. In order to quantify the vascular resistances, various indices, which measure the proportion of systolic flow within the total forward flow (M) during one cardiac cycle, or the relative amplitude of systolic (S) to diastolic (D) flow, have been proposed: PI = (S−D)/M [32]; R = D/S [30]; RI = (S−D)/S [33]; and R = S/D [34]. Most of these parameters change according to the resistance to flow into the vascular territory under investigation; therefore, any increase of these indices above the upper limit of the normal range corresponds to an increase of the vascular resistances (Fig. 16.4). In contrast, the D/S index decreases as the resistance to flow increases. The vascular resistance increase may be due to vascular disease (placental infarction or fibrosis) or to distal arteriolar vasoconstriction (brain response to increased pO_2 or to vasoactive drugs). Conversely, abnormally decreased resistance to flow values are displayed below the lower limit of the normal range of the index for S-D/M, S-D/S, and S/D (Fig. 16.4) and above the upper limit for the D/S index. The decreased resistance to flow may be due to the existence of arterio-venous shunts, or to an arteriolar vasodilation (brain adaptation to hypoxia or to drugs).

16.3.2 The Cerebroplacental (Cerebral-Umbilical) Ratio: The History

In the 1980s, researchers started publishing findings from systematic recordings of the anterior cerebral and umbilical artery Dopplers on normal pregnancies at different gestational ages [22]. In 1986, Abeille reported that the diastolic Doppler component of the anterior cerebral artery was lower than that of the umbilical artery. Also, both cerebral and umbilical artery diastolic components were noted to increase in parallel with gestational age (Fig. 16.2). After gathering information from 50 uncomplicated pregnancies, the normal limits of both the cerebral and umbilical resistance indices were able to be displayed in the same graph [23].

In the same decade, Wladimiroff et al. published their results of normal values of the fetal internal carotid artery resistance index [25]. However, the normal ranges of this index at each gestational age were significantly larger compared to the cerebral artery ranges, likely because the fetal internal carotid artery resistance index is fetal heart rate-dependent. Therefore, the measurement of this vessel was not considered to be as useful for fetal surveillance as the cerebral vessels.

One of the first unexpected abnormal observations was made on a severely growth-restricted fetus at 25 weeks of gestation [22]. In this fetus, the anterior cerebral artery Doppler spectrum was noted to have a considerably large diastolic component (approximately 40% of the systolic peak); and the umbilical artery diastolic component was absent. The hypothesis made from these findings was that increased cerebral artery diastolic component was secondary to increased cerebral blood flow due to fetal hypoxia. This hypoxic status was thought to be triggered by the reduced umbilical artery blood flow secondary to placental insufficiency.

After these observations, Arbeille et al. published the first paper on the cerebroplacental ratio (CPR) in April 1986 [22]. The CPR (formerly known as the cerebral-umbilical ratio or C/U) was defined as the ratio between the cerebral artery resistance index (CRI) and the umbilical artery resistance index (URI). In pregnancies with normal estimated fetal weight, the CPR was consistently noted to be above 1; while in pregnancies complicated by fetal growth restriction the CPR was consistently noted to be less than 1 [22, 23] (Fig. 16.5). At that time, the findings suggested that fetal hypoxia could be present in cases of fetal growth. Hypoxia would induce fetal cerebral vasodilation to increase cerebral blood flow and to compensate for the lack of oxygenated blood from the placenta. The CPR was then proposed as a parameter to quantify fetal blood flow redistribution to the brain in response to hypoxia. The normal ranges of the cerebral artery resistance index (CRI) were subsequently reported, and the CPR cutoff for normal limits was established to be above 1 [23].

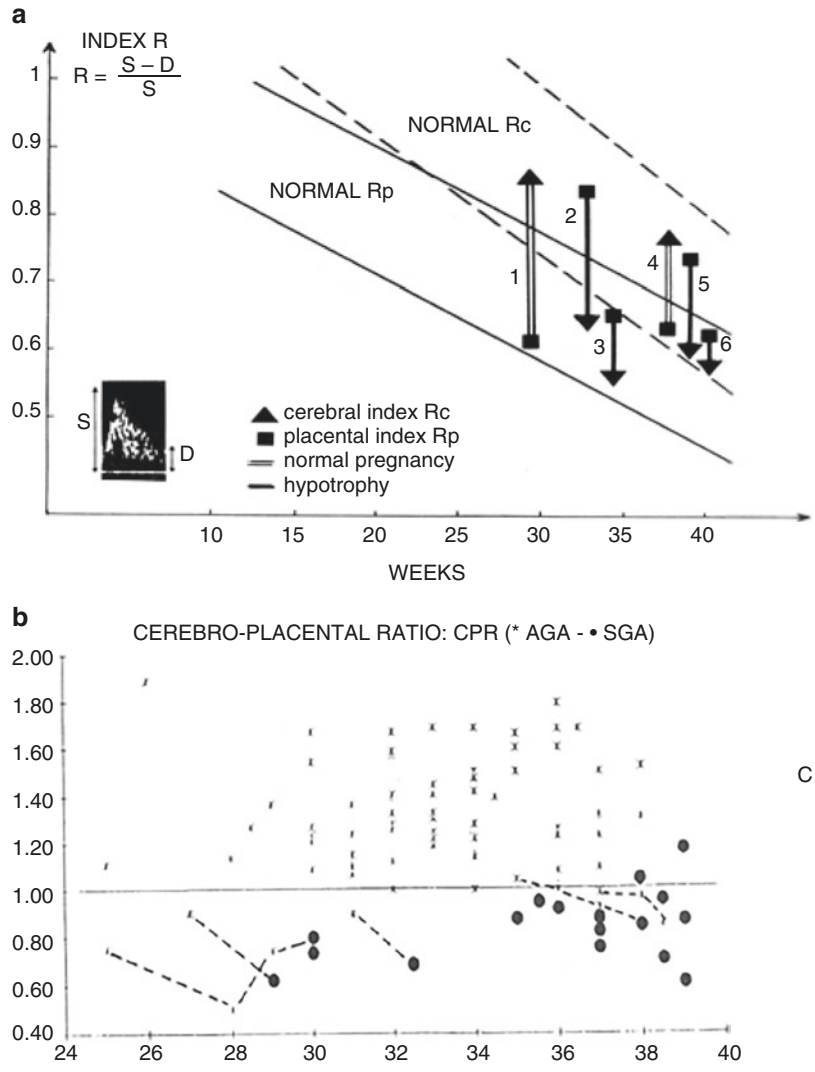

Fig. 16.5 (**a**) Diagram of umbilical RI (URI), cerebral RI (CRI), and CPR < 1. It can be noted that the CPR becomes abnormal while only one of either the URI or CRI is abnormal. Case 1 & 4: Normal CPR (CRI > URI). Case 2: CPR < 1, both CRI and URI were abnormal (CRI < URI). Case 3: CPR < 1, only CRI was abnormal (CRI < URI). Case 5: CPR < 1, only URI was abnormal (CRI < URI). Case 6: CPR < 1, both CRI and URI were normal but CRI < URI [22]. (**b**) Diagram of the CPR between 24 and 40 weeks of gestation, normal range (CPR > 1), black circle corresponds to growth-restricted fetuses

The CPR normal ranges according to gestational age were noted to be more consistent compared to the CRI and URI normal ranges, probably because the CPR is not fetal heart rate-dependent. The CPR cutoff value (>1) was also noted to remain stable throughout pregnancy.

Initially, these hypotheses were only considered reasonable speculations. Some researchers questioned the existence of cerebral vasodilation since the fetal sympathetic nervous system is not mature earlier in pregnancy. The hypothesis that CPR was a marker of flow redistribution and fetal hypoxia was subsequently confirmed in animal models and several other studies targeting pregnancies complicated by hypertension, malaria, and drug abuse, among other comorbidities.

In 1988, using a color-Doppler echograph, Arbeille presented the first color display of the fetal circle of Willis in real time (Fig. 16.6) confirming former assumptions that previous recordings were indeed cerebral artery Doppler signals. The middle cerebral artery was more easily recorded since it was in the direction of the Doppler beam, while the anterior cerebral artery formed an angle of 60°with the Doppler beam. Given this, the middle cerebral artery was subsequently used for PCR estimation. The cerebral resistance normal ranges and the CPR cutoff val-

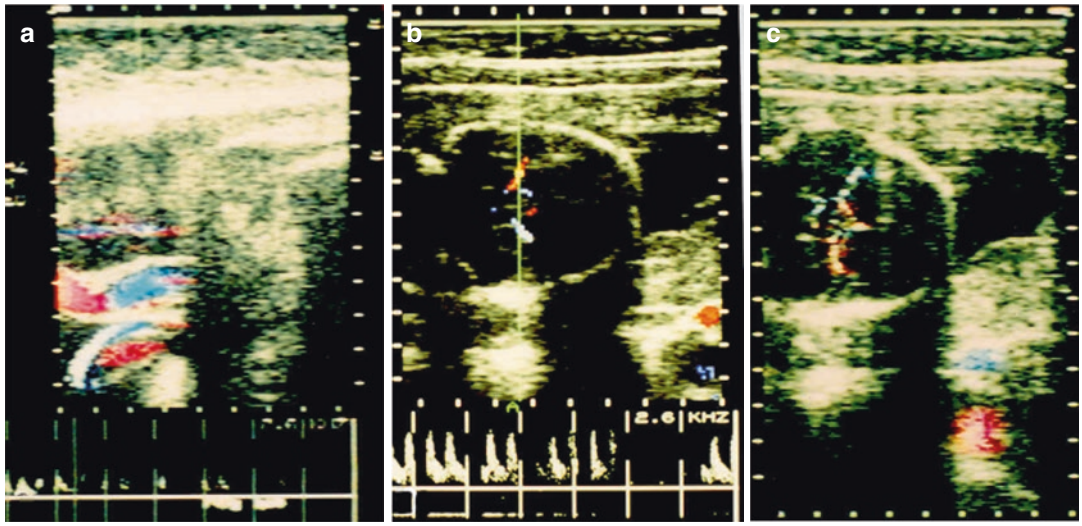

Fig. 16.6 (**a**) Umbilical artery and vein flow by color and pulsed Doppler. (**b**) Fetal middle cerebral arteries with corresponding Doppler. (**c**) Fetal Willis circle by color Doppler [35] (Echograph HP Quantum 1988)

ues remained the same. As the quality of the echography improved, the middle cerebral artery became easier to detect. The cerebral Doppler recording then became obtainable with any commercial echograph [35].

16.3.3 Cerebroplacental Ratio for Evaluating pO_2 Changes

The CPR changes are indicators of peripheral fetal flow distribution. These parameters, based on the comparison of the brain CRI and URI, are expressed as either CRI/URI [22, 23] or URI/CRI [2]. The cerebral vascular resistance is measured from one of the intracerebral arteries (anterior or middle) or from the intracranial part of the carotid artery. By measuring the flow redistribution between the placenta and brain, these CPR (in cases of pathologic pregnancies) take into account the placental disturbances due to vascular disease at this level and the cerebral response (vasodilation) to the hypoxia induced by placental dysfunction.

In normal pregnancies, the diastolic component in the cerebral arteries is lower than that in the umbilical arteries at any gestational age (Fig. 16.2); therefore, the cerebral vascular resistances remain higher than the placental resistances and the CPR (CPR = CRI/URI) is >1.1 (Figs. 16.4 and 16.7). The CPR (CRI/URI) becomes <1.1 if any flow redistribution in favor of the brain occurs (Figs. 16.8, 16.9, and 16.10). In such a case, the cerebral diastolic flow amplitude is higher than normal, and the umbilical flow amplitude is lower. Animal and human studies have demonstrated that the CPR changes in proportion to fetal pO_2 [36, 37]. The URI/CRI ratio used by other authors to detect fetal flow redistribution varies in the opposite direction.

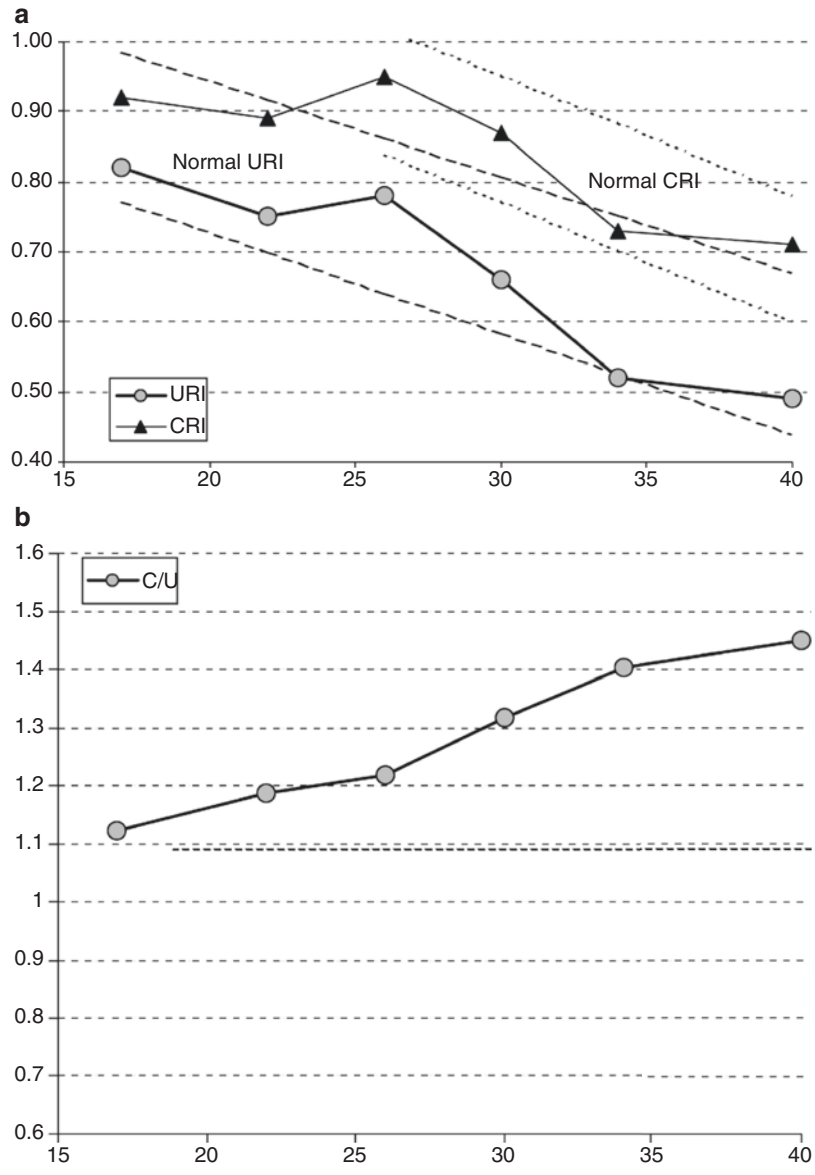

Fig. 16.7 (**a**) Evolution of the cerebral (CRI) and umbilical (URI) vascular resistances in the same fetus during a normal gestation. The fluctuations in parallel on the two indices are related to the variations of the fetal heart rate. Note that the cerebral resistances remain superior to the placental resistances at any gestational age. (**b**) Evolution of the CPR during the same normal gestation (CRI > URI → normal CRI/URI always >1.1)

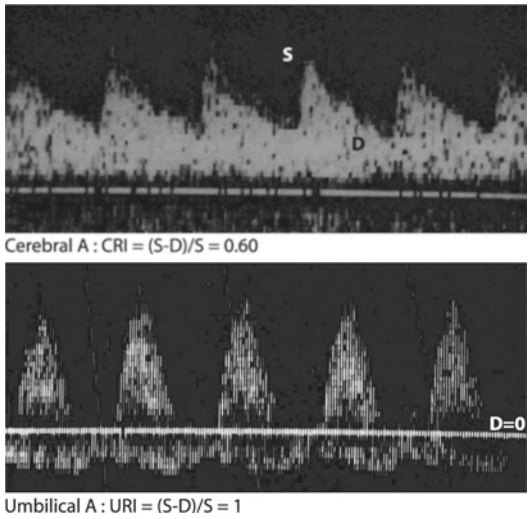

Fig. 16.8 Brain-sparing effect. Note the absent diastolic flow on the umbilical velocity waveform and increased diastolic flow on the cerebral velocity waveform in relation to a decrease in the cerebral vascular resistance by vasodilation (growth-retarded and hypoxic fetus delivered at 35 weeks). S systolic peak, D end-diastolic velocity

16.3.4 Effect of Fetal Heart Rate on Doppler Vascular Resistance Indices

It is well-known that an elevation of the fetal heart rate increases the end-diastolic velocity and therefore decreases the resistance index (Fig. 16.11). On the other hand, the diminution of the heart rate increases the index value. This effect of the heart rate is eliminated by the use of the CPRs because both indices, CRI and URI, are measured on the same fetus with the same heart rate. The two CPRs mentioned above are not heart rate-dependent, because the cerebral and the umbilical index are equally affected by the heart rate changes. Figure 16.7 shows the fluctuations of both the placental and the umbilical indices (due to the heart rate variations) and the stability of the CPR in a normal fetus. Finally, it was demonstrated that the normal range of the CPR is limited by a single lower cutoff value of 1 to 1.1 at least for the second half of the pregnancy and is unaffected by the fetal heart rate value (Fig. 16.7) [22, 23, 38–40].

16.3.5 The Cumulative Reduction in the CPR and the Hypoxic Index

In a study of the effect of malaria on the fetal circulation and behavior, the CPR was used to quantify the flow redistribution (i.e., reduction in pO_2) throughout the period of observation (malaria crisis) until delivery. By adding the successive CPR decreases (in percentage of the cutoff value) measured every 2 days, we measured the presumed cumulative relative deficit in pO_2 to which the fetus was submitted during this period. The hypoxic index (HI) proposed by Arbeille (1992) is calculated by adding the percentage decrease of CPR (when CPR becomes lower than 1.1), each measurement from admission to delivery. This number corresponds to the area between the percentage CPR curve and the time axis (days) (Fig. 16.12) [8]. In the case of the malaria study, the HI > 150 predicted abnormal fetal heart rate at delivery several weeks ahead.

In normal pregnancies, the HI remains equal to zero as only CPR values lower than 1.1 which indicate a flow redistribution are taken into account. A flow redistribution characterized by a CPR equal to 0.77 (−20% below 1.1) means that it could correspond to a 20% pO_2 reduction. If the situation remains stable for 10 days, the HI will be equal to 20% × 10 = 200%. The CPR and HI again predicted abnormal fetal heart rate patterns in cases of pregnancies complicated by hypertension.

A subsequent study conducted by Salihagic et al. analyzed the value of the hypoxic index in predicting functional and/or structural brain lesions caused by fetal hypoxia and examined the relationship between CPR and neonatal neurosonography in growth-restricted and hypoxic fetuses [41, 42]. A CPR < 1 and HI > 150 were found to be associated with poor perinatal outcome, showing the value of both parameters for early detection of fetal hypoxia, but the HI had greater sensitivity and specificity.

These three studies demonstrated that: (a) CPR monitors the fetal pO2 changes during an acute and reversible placenta dysfunction process

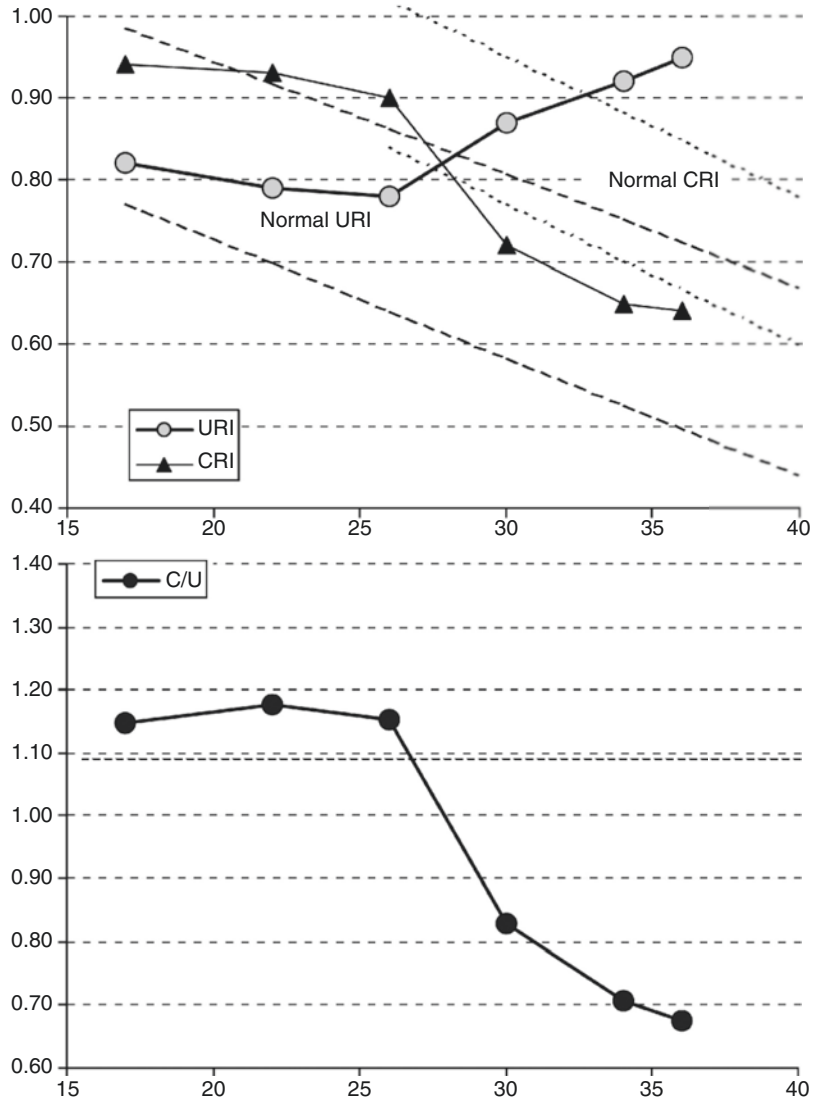

Fig. 16.9 Evolution of URI and CRI in a pregnancy complicated by hypertension. The umbilical resistance increases progressively, whereas the cerebral resistance decreases to adapt to the reduction in fetal pO_2. When the URI reached 1 (absent end-diastolic flow), the CPR had already entered the pathological area several weeks previously. It is noteworthy that the CRI is not far from its normal zone, but the CRI/URI ratio is very far from the normal limit

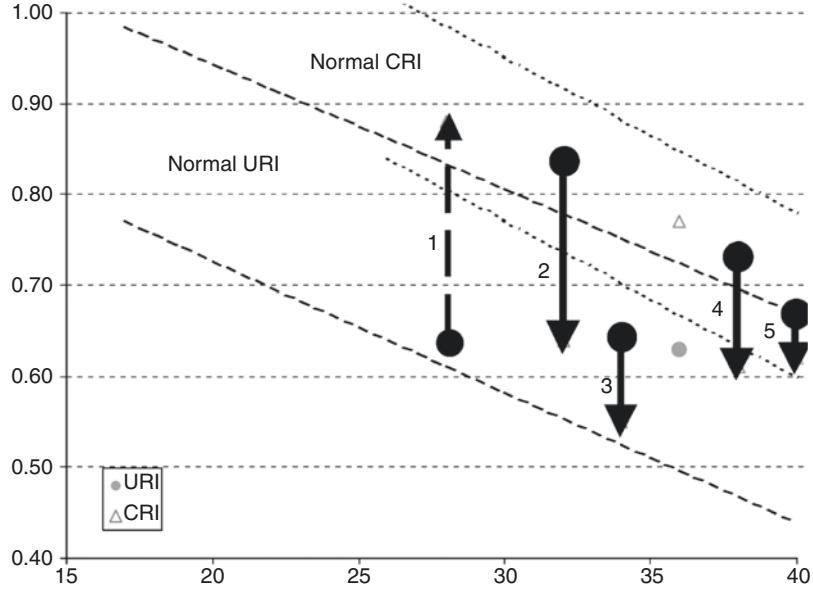

Fig. 16.10 Different (CRI) and (URI) values associated either with a normal fetus (CPR = CRI/URI >1) or with an IUGR (CPR <1). Normal fetal hemodynamics → 1 normal CRI and URI (CPR >1.1). Abnormal flow distribution: 2 abnormal CRI and URI (CPR <1.1); 3 abnormal CRI, normal URI (CPR <1.1); 4 normal CRI; abnormal URI (CPR <1.1); 5 normal CRI, normal URI (CPR <1.1)

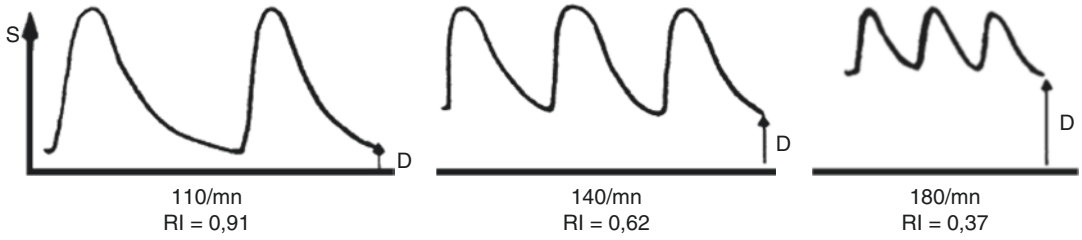

Fig. 16.11 Effect of the heart rate (beats per minute, bpm) on the end-diastolic flow and on the resistance index (RI). At 110 bpm the diastolic flow decreases during a longer period than at 140 bpm; therefore, the end-diastolic flow amplitude is lower than at 140 bpm and the RI = [(S − D)/S] at 110 bpm becomes higher (0.91) than at 140 bpm (0.62). A high fetal heart rate (180 bpm) increases the diastolic flow and decreases the RI (at 180 bpm, R = 0.37)

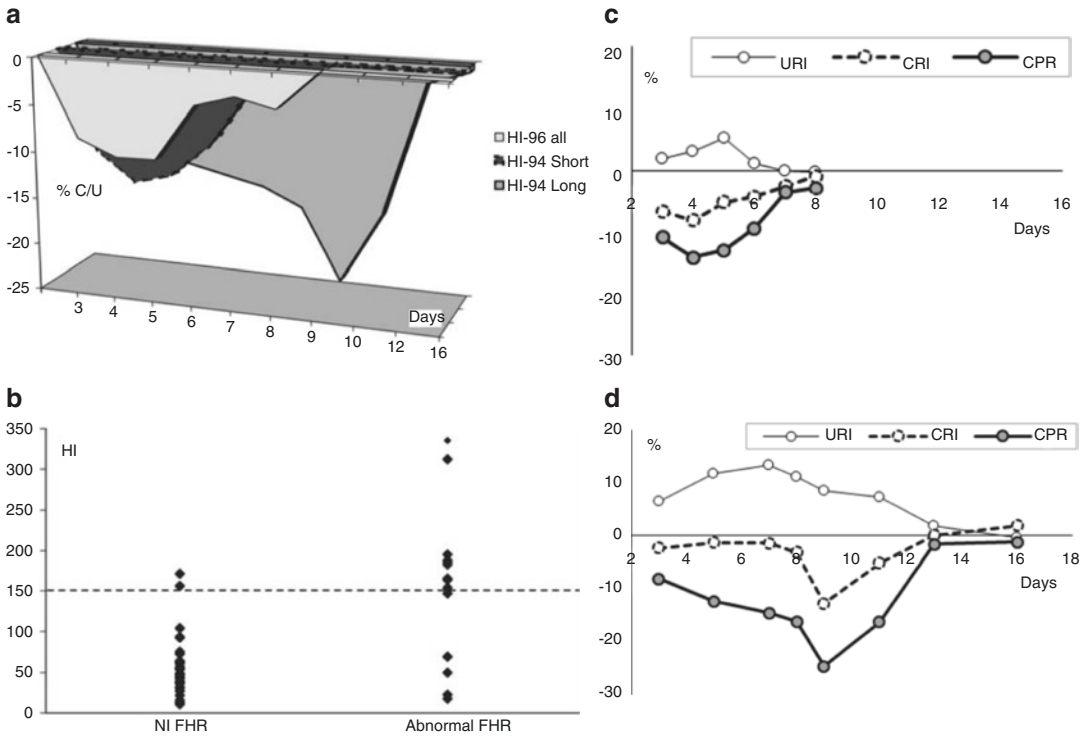

Fig. 16.12 (**a**) Mean variations of the ratio (CPR = cerebral resistance/umbilical resistance) during the malaria crises in group 1 (1994 short and long crisis) and in group 2 (1996 crisis). The CPR change is expressed in percentage from cutoff limit 1.1. In group 1 CPR decreased significantly more during long crisis than during short ones ($p < 0.05$). The area (in gray) between the CPR curve and the time axis is the hypoxic index (HI). As the CPR changes proportionately to the fetal pO_2, this gray area represents the cumulated deficit in pO_2 over the crisis. (**b**) Correlation between occurrence of abnormal fetal heart rate vs HI. The HI is abnormal when >150% → PPV = 80%, NPV = 85%. (**c** and **d**) show umbilical (URI), cerebral (CRI) resistances, and CPR during short crisis (<7d) in 1994, and long crisis (>7d) in 1994. Amplitude of variation of CPR is higher than URI and CRI change

(i.e., Malaria), or during a chronic and nonreversible placenta dysfunction process (i.e., hypertension in pregnancy); and (b) HI predicts the occurrence of fetal heart rate abnormalities at delivery.

16.4 Cerebral Circulation in Normal Pregnancy

16.4.1 Cerebral Flow Changes with Gestational Age

The diastolic flow in the cerebral vessels is reduced at the beginning of the second half of pregnancy (20–25 weeks), but continues developing progressively. The increase in the diastolic component with the gestational age is interpreted as a decrease in the cerebral resistance due to brain development. The cerebral vascular resistance changes are measured using the same Doppler indices as for the placenta (Figs. 16.2, 16.4, and 16.7).

The increase in the diastolic component begins later in the cerebral arteries (at approximately 25 weeks) than in the umbilical arteries (at approximately 15 weeks). The amplitude of the diastolic flow in the cerebral arteries is always lower than in the umbilical arteries, meaning that in normal pregnancy the cerebral vascular resistances are higher than the umbilical resistances. In other words, the umbilical flow volume is higher than the cerebral flow volume. This led to the definition of the CPR (cerebral resistance/

umbilical resistances), which is inversely proportional to cardiac output distribution between brain and placenta and which is higher than 1.1 in normal pregnancies.

16.4.2 Variations According to the Site of Examination

In normal fetuses, the resistance index is significantly higher in the middle cerebral artery ($p < 0.01$) [31] than in the anterior and posterior cerebral arteries. In pathological pregnancies with cerebral vasodilation (decreased cerebral index), the sensitivity of cerebral Doppler examination is not dependent on the choice of the cerebral artery explored. Since the Doppler indices measured on two different vessels will not differ by more than 5–10%, the conclusions of the Doppler investigation will not be changed. Nevertheless, during assessment of the fetal circulation over several days or weeks, successive examinations must be performed on the same vessel.

16.4.3 Cerebral Flow Changes with Behavioral States

Fetal behavioral states are defined according to the fetal heart rate pattern, as well as in the body and eye movements [43, 44]. In normal pregnancies at 37–38 weeks' gestation, blood flow velocity waveforms in the descending aorta and the internal carotid artery are affected by fetal behavioral states. In both vessels, a significant reduction in the pulsatility index was established during behavioral state 2F (active sleep), compared with behavioral state 1F (quiet sleep) [44–46]. The decreased peripheral vascular resistance induces increased perfusion to the musculature and brain required by the increased energy demand during active sleep. In addition, peak flow velocity decrease in the fetal ductus arteriosus during active sleep has been demonstrated [46]. This observation confirms the existence of a redistribution of flow between the two ventricles with increased left cardiac output, which may contribute to the increased brain perfusion.

16.5 Clinical Significance of Cerebral and Cerebral/Umbilical Indices

16.5.1 Cerebral Flow in Growth-Restricted and Hypoxic Human Fetuses

The Doppler indices measured in the main fetal cerebral arteries are sensitive to any vasoconstriction or vasodilatation of the brain vessels. An increase in the diastolic cerebral flow is interpreted as a vasomotor response (vasodilation) to hypoxia [25, 26, 47]. Comparisons between the cerebral Doppler index and the measurement of pO_2, pCO_2, pH, and O_2 content by cordocentesis have demonstrated a good correlation between pO_2 and the cerebral Doppler index in cases of severe hypoxia (the cerebral index decreases with the pO_2). Nevertheless, when acidosis appears, there is sometimes an increase in the cerebral vascular resistance index due to a decrease in the diastolic flow [37, 48].

At first, it appears difficult to quantify hypoxia using the CRI, but if it is measured every day in fetuses with abnormally decreased CRI, the evolution of the hypoxia can be followed through the brain's vascular resistance changes as illustrated in the following scenarios:

- Scenario 1: The cerebral vascular index is abnormal (lower than normal), but decreases progressively, as in normal fetuses. This can be related to high HR values, or to a hypoxic stable stage, but no reliable answer can be provided.
- Scenario 2: The abnormal cerebral index continues to decrease significantly and becomes more and more pathological. Hypoxia develops, but the fetus is probably not acidemic.
- Scenario 3: A cerebral RI below the normal range but not changing over 2–3 days means that the small vessels beyond the measuring

point can no longer change their diameters. Such a pattern was observed in premortem fetuses in which brain edema and neuronal deterioration were observed at postmortem anatomical examination [10].

- Scenario 4: Lastly, the cerebral index, already much lower than the normal limit, increases and enters the normal range again. In this case, the capability of the brain vessels to vasodilate has been overwhelmed. Hypoxia is decompensated and the fetus becomes acidemic.

In all these circumstances, it is hazardous to use only one absolute value of the cerebral Doppler index for the assessment of hypoxia and for deciding about delivery. Only the evolution of the cerebral index or the CPR over several days may provide information on the development of fetal hypoxia. Nevertheless, a good correlation has been found between the existence of significantly decreased (<2 SD) cerebral resistance and the development of post-asphyxial encephalopathy in the neonate [49]. In this study, the specificity and the sensitivity of fetal cerebral Doppler as a predictor of neonatal outcome were about 75% and 87%, respectively. However, it is emphasized that the vasodilation compensates only partially for the hypoxia, and its persistence over a long period of time does not guarantee the absence of brain tissue damage.

16.5.2 Cerebroplacental Ratio Change in Cases of Hypoxia and IUGR

The comparison between the cerebral and the placental vascular resistance for the assessment of IUGR was proposed in 1986 [22] and the results were confirmed in 1987 [2, 23]. In pathological pregnancies (hypertensive pregnancies, for example) with IUGR, we frequently observe a reduction in placental perfusion and an increase in flow toward the brain. This phenomenon, called "brain-sparing effect," is supposed to compensate fetal hypoxia. The main advantage of comparing placental and cerebral vascular resistance is that we take into account, first, the existence of placental vascular disease which can be responsible for an alteration of the maternal to fetal exchanges, and second, the cerebral hemodynamic consequences of these abnormalities (vasodilation).

Nevertheless, the CPR may become pathological by various situations:

- There is an increase in the placental resistances, but no hypoxia and a normal cerebral perfusion (malaria beginning of crisis).
- The placental resistances are normal, but hypoxia exists and therefore the cerebral resistance is abnormally decreased (moderate anemia).
- Both placental and cerebral resistances are abnormal (pregnancy-induced hypertension, malaria).
- Both indices are within their normal range, but the cerebral index is lower than the placental one (Fig. 16.10; early stage of pathological process).

All these combinations describe a fetal flow redistribution and are associated in most cases with IUGR and/or hypoxia. Several similar studies using either the ratio between the anterior cerebral artery index and the umbilical index (CPR = CRI/URI, which is pathologic when <1.1; Fig. 16.4) [23, 38, 39, 50], or the ratio between the umbilical index and the internal carotid index (I = URI/ICRI, which is pathological when >1) [2], demonstrated a sensitivity of approximately 86% and a specificity of about 98%.

The CPR has been tested on hypertensive pregnancies with severe IUGR, moderate IUGR, or twin gestations [23, 51, 52] and showed the same accuracy. This high sensitivity and specificity of the CPR as a predictor of IUGR, including cases of moderate IUGR without fetal distress, confirms that the fetal flow redistribution in favor of the brain always exists, even at the early stage of development of IUGR, and is detectable by Doppler.

Figure 16.9 shows the evolution of both URI and CRI in a pregnancy complicated by hyper-

tension. The umbilical resistance increases progressively, whereas the cerebral resistance decreases to adapt to the reduction in fetal pO_2. When the URI reaches 1 (absent end-diastolic flow), the CPR had reached the pathological stage several weeks previously. It may be noted that the CRI is not far from its normal zone, but the CRI/URI ratio is very far from normal.

16.5.3 Cerebroplacental Ratio and Perinatal Outcome

Kjellmer et al. [6] demonstrated in animals that IUGR is generally associated with cerebral metabolism disturbances and delayed development of the brain. Moreover, Fouron et al. [5] showed that in the case of fetal flow redistribution, there is a reverse diastolic flow into the aortic arch, confirming that hypoxic blood coming from the right ventricle flows into the brain. This phenomenon probably limits the beneficial effect of the brain-sparing reflex; therefore, the CPR was tested as an indicator of adverse perinatal outcome. Gramellini et al. [39] studied 45 growth-retarded fetuses and found a 90% sensitivity for the CPR when used as a predictor of poor perinatal outcome, compared with 78% for the middle cerebral artery index and 83% for the umbilical artery index. In their study, the parameters used to evaluate fetal well-being were: fetal heart rate; gestational age; birth weight; Cesarean rate; umbilical vein pH; 5-min Apgar score; the incidence of admission to the neonatal intensive care unit; and neonatal complications.

16.5.4 Hypoxic Index for Predicting Effect of Hypoxia

The hypoxic index (HI) was found to predict abnormal fetal heart rate with a sensitivity and specificity close to 80%. The cutoff limit for HI was found retrospectively in a previous study on pregnancies complicated by malaria to be 150% and was 160% in a pregnancy-induced hypertension study [8, 52]. For example, an HI of 150% may correspond either to 3 days under a reduction of 50% in pO_2 ($3 \times 50\% = 150\%$), or 15 days under a reduction of 10% of fetal pO_2 ($15 \times 10\% = 150\%$; Fig. 16.12).

The HI takes into account the amount of reduction in fetal pO_2 as well as the duration of exposure to hypoxia. Moreover, the product of the pO_2 value at delivery (umbilical vein pO_2) by the number of days with fetal flow redistribution (CPR <1.1) correlated well with the HI value (regression). The HI increases progressively in the case of a nonreversible placental insufficiency, whereas it can return to normal (equal zero) in the case of reversible placental insufficiency (malaria) [8] or reversible reduced pO_2 supply (anemia) [53].

16.5.5 Cerebrovascular Reactivity Tests (O_2, CO_2)

When the cerebral Doppler index is lower than the normal range or when the CPR indicates a fetal flow redistribution, the fetus is considered hypoxic. It is difficult to evaluate the consequences of such hypoxia on the brain structures and on cerebral functions [47, 49].

The oxygen test (maternal oxygenation administration) was used to test fetal brain reactivity [49, 54–56]. During maternal oxygen treatment, the cerebral index was measured at the level of the internal carotid artery. In fetuses with brain-sparing effect (cerebral resistance below normal) but who did not develop fetal distress, the oxygen treatment induced an increase in cerebral resistance. In contrast, those fetuses with cerebral vasodilatation who did not respond to the oxygen test (no increase in cerebral resistance) developed fetal distress. The sensitivity of the oxygen test when used as a predictor of imminent fetal distress is about 70% [49]. The positive cerebral response proves that placental transfer is maintained and may justify intrauterine treatment of fetuses with long-term maternal oxygen therapy. Conversely, the absence of vascular response to the oxygen test indicates that either the placental transfer and/or the cerebral reactivity are impaired.

The cerebral vascular resistance of the fetus is also sensitive to the variation of CO_2 content in the air inspired by the mother. It was demonstrated that a mixture with 2% CO_2 induces a decrease in fetal cerebral resistance, but does not affect either the fetal heart rate or the umbilical flow [57].

16.6 Cerebral Flow Response to Induced Hypoxia and Drugs in Animal Models

Validation of CPR as a marker of fetal pO_2 in the animal model [27, 36].

The ewe research model allowed for fetal extraction, placement of Doppler sensors and catheters for blood sampling and pO_2 measurement, and fetal reinsertion into the uterus for the subsequent induction of fetal hypovolemia and hypoxia. Doppler sensors were fixed to the fetal abdomen with the Doppler beam targeting the umbilical arteries. Sensor fixation to the umbilical cord was not performed due to vasoconstriction after sensor placement. For Doppler interrogation of the cerebral arteries, sensors were fixed to the fetal skull with the Doppler beam facing one of the cerebral arteries. Fetal hypoxia was induced by compressing the maternal aorta for 1 min. Fetal hypovolemia and hypoxia were induced by compressing the umbilical cord for 10 min. Before cord compression, umbilical and cerebral arteries' resistance indices were 0.5 and 0.8, respectively (CPR > 1). During umbilical cord compression, the URI increased from 0.5 to 1.0, and the CRI dropped from 0.8 to 0.4. The CPR became abnormal as low as 0.5 (50% reduction). The pO_2 was also reduced by 50%. After several experiments with different levels of compression, a significant correlation was found between CPR and pO_2 (Fig. 16.13). Aorta compression also showed similar findings. These findings suggested that cord compression trapped fetal blood into the placenta, which triggered fetal hypovolemia and hypoxia, with subsequent vasodilation response. Conversely, the aorta compression did not cause fetal hypovolemia, but reduced the pO_2 at the placenta level. Thus, researchers demonstrated that the CPR was a marker of the pO_2 in the animal model.

These concepts were used to design subsequent studies in human pregnancies with different complications such as malaria, hypertension, illicit drug use, and induced anemia (such as in the ingestion of hemoglobin chelators in the Amazonian population). These conditions could present reversible fetal pO_2 reduction (malaria, anemia) or nonreversible pO_2 reduction (hypertension, illicit drug use). Additionally, the placental function could be normal (anemia) or impaired (malaria, hypertension, drug abuse).

16.6.1 Cerebroplacental Ratio and Mechanically Induced Hypoxia

Induced hypoxia (Fig. 16.13) in lamb fetuses has demonstrated a sensitive and rapid brain vasodilation. The fetal cerebral and umbilical flows were assessed by Doppler sensors implanted on the fetus during fetal hypoxia induced by umbilical cord compression, aortic compression, and drug injection [27, 36].

Umbilical cord compression ($n = 8$) decreases the venous return and the umbilical arterial flow, which induces hypoxia instantaneously and simulates fetal central hypovolemia. During a 10-min compression, the cerebral vascular resistance decreased and the cerebral flow was maintained or only slightly decreased. Simultaneous recordings of the cerebral and umbilical Doppler waveforms together with the pO_2 showed that the CPR decreased proportionately with the pO_2. The umbilical flow (Q_p) decreased together with the CPR (Fig. 16.13a, c). The pH and the heart rate remained normal. In the case of progressive cord compression (progressive changes of the umbilical resistance), the CPR closely followed the changes in fetal pO_2.

Aortic compression ($n = 8$) reduced the uterine flow and induced fetal hypoxia after about 30 s. After 1 min of compression, the heart rate dropped and the compression was interrupted. The heart rate recovered 30 s after the end of the compression. The pH did not change during the

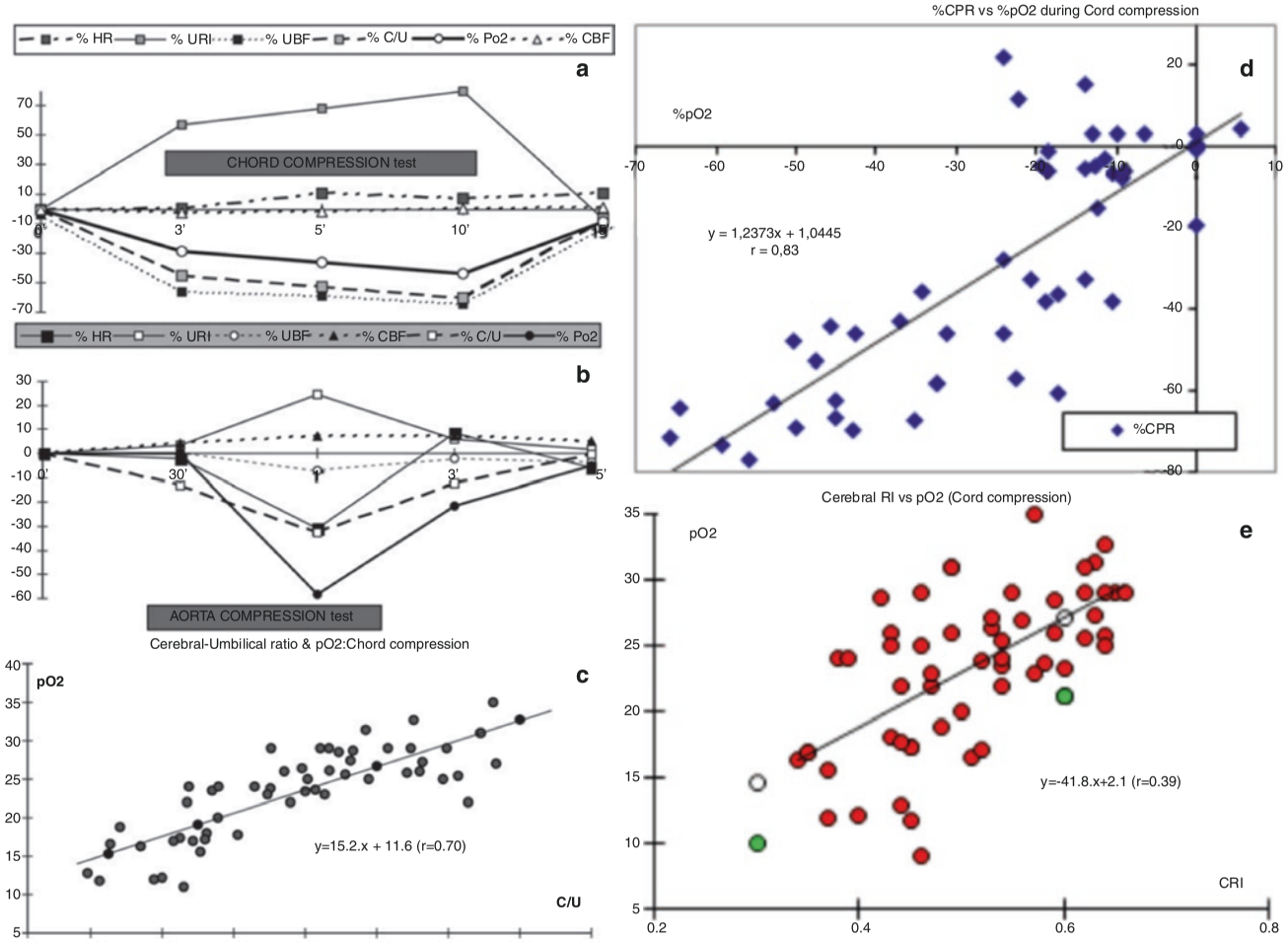

Fig. 16.13 (**a**) Umbilical cord compression. Variations in percentage from the pretest value of the: Heart rate (HR), umbilical vascular resistances (URI), umbilical flow (UBF), cerebral-umbilical ratio (CPR), fetal pO_2, and cerebral flow (CBF) during a period of *chord compression*. The CPR decreases in proportion with the fetal pO_2 and the UBF, whereas CBF remains unchanged. (**b**) *Aortic compression*. Variations in percentage from the pretest value of the HR, URI, UBF, CPR, fetal pO_2, and CBF during a period of aortic compression. The CPR decreases also in proportion with the fetal pO_2, whereas the UBF and CBF remain unchanged. (**c**) Relationship between absolute values of the CPR and the pO_2 during induced hypoxia by chord compression. (**d**) Relationship between %CPR and %pO_2 during chord compression. (**e**) Relationship between CRI and fetal pO_2 during chord compression

test and the umbilical flow remained stable; however, the umbilical resistance increased and the cerebral resistance decreased. As with umbilical cord compression, the CPR follows the variations of the fetal pO_2 (Fig. 16.13b).

Simultaneous measurements of the fetal pO_2 and the CPR during these compression tests showed a good correlation between the two parameters (Fig. 16.13c). Nevertheless, the amplitude of the CPR variations was higher during umbilical cord compression than during the aortic compression. In fact, cord compression induces a central hypovolemia, which does not exist with aortic compression; therefore, one can speculate that during cord compression the CPR drop may be related to the hypoxia and the hypovolemia, which may stimulate the baroreflex.

16.6.2 Cerebral Flow and Long-Term Nicotine Treatment (Animal Model)

The effect of nicotine on fetal cerebral flow and reactivity has been studied in pregnant ewes ($n = 6$) given a daily dose of nicotine intramuscularly equivalent to 20 cigarettes [28]. In the nicotine group there was no decrease in vascular resistance (RI) at the end of gestation, as in the control group (Fig. 16.14). This phenomenon, more evident on the cerebral arteries ($p < 0.01$) than in the umbilical arteries ($p < 0.05$), could be interpreted as cerebral vasoconstriction, or as a delayed brain development. Moreover, the increased CPR in the nicotine group ($p < 0.01$) confirmed reduced brain perfusion. In addition to these hemodynamic findings, there was a higher percentage of stillborns in the nicotine group (63%) than in the control group (13%). The newborns in the nicotine group showed an abnormal cerebrovascular response when submitted to a CO_2 inhalation test (no cerebral vasodilation). It was concluded that repeated administration of nicotine was responsible for abnormal brain vascular development, with loss of cerebral reactivity and poor fetal outcome. These results led to the hypothesis that if fetal hypoxia develops in "nicotine fetuses," the capability of the brain vessels to adapt by vasodilation is reduced because of the "vasoconstrictive" effect of nicotine and the deleterious effects of the drug on the growth and the maturation of the brain structures.

16.6.3 Cerebral Flow and Long-Term Cocaine Treatment (Animal Model)

Uteroplacental flow and fetal cerebral flow were assessed by Doppler ultrasonography in pregnant ewes treated daily with cocaine beginning on gestational day 60 (Fig. 16.15). Fetal weight and fetal pO_2 were measured at delivery. The study groups received 70 mg ($n = 7$) or 140 mg ($n = 7$) of cocaine intramuscularly and the control group ($n = 7$) was given an intramuscular placebo. The maternal heart rate and the uterine RI (vascular resistance index) were always significantly higher ($p < 0.01$) in the cocaine groups. The fetal heart rate and the URI were also significantly higher ($p < 0.01$) in the two cocaine groups than in the control group.

Prior to delivery, the fetal cerebral RI and the CPR were significantly lower ($p < 0.01$ for CRI; $p < 0.001$ for CPR) in the cocaine groups than in the control group. At delivery, the pO_2 was also significantly lower in the cocaine groups ($p < 0.05$ for the 70 mg/kg group; $p < 0.01$ for the 140 mg/kg group) than in the control group (Fig. 16.15). The mean birth weight was significantly lower in the two cocaine groups in comparison with the control group; therefore, repeated injections of cocaine to pregnant ewes induce uteroplacental disorders with fetal growth restriction and a redistribution of the fetal flows in response to moderate hypoxia. This study confirmed the value of measuring the CPR for follow-up of the abnormal fetal pO_2 during chronic hypoxia [7]. Magnetic resonance imaging (MRI) and histology investigation were subsequently performed on the fetal brains [9, 58] (Fig. 16.16). Fetal brain structure was studied by optical and electron microscopy (Fig. 16.16). The authors found significantly more abnormalities in the cocaine group. Computerized analysis showed that 88% areas of the brain exceeded a reference level in

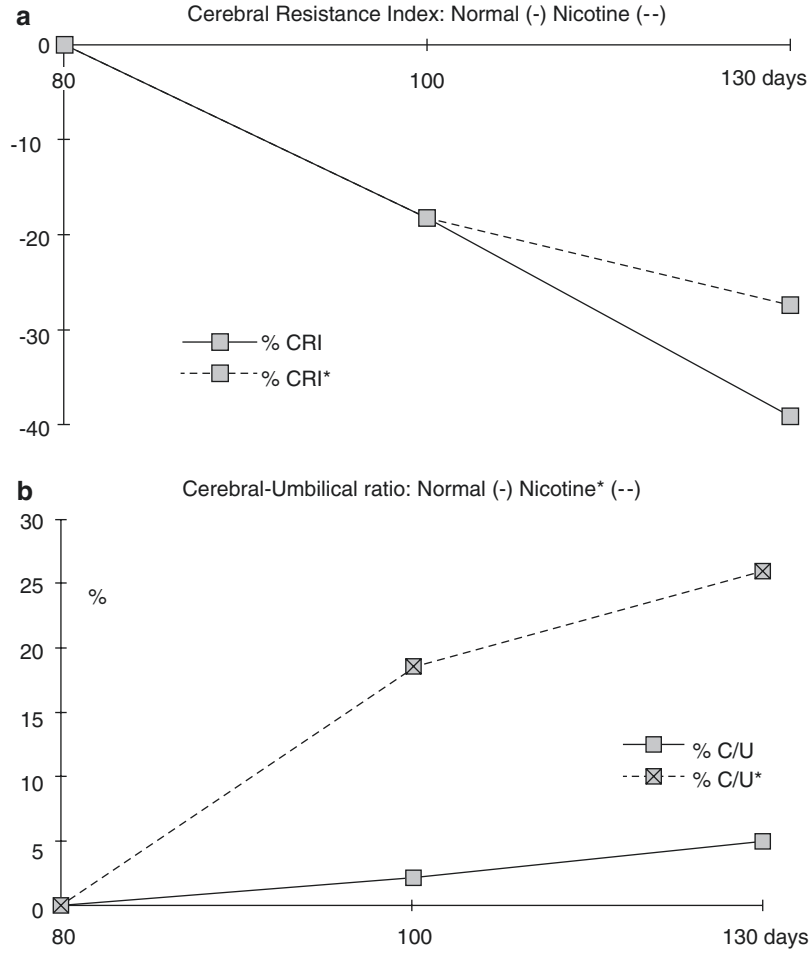

Fig. 16.14 (**a**) Chronic nicotine administration. Variations of the fetal cerebral resistance index (CRI), on lamb fetuses, during gestation (140 days). On the "control-placebo" group, the CRI decreases progressively from gestation day 80 until the end of the gestation, but not on the nicotine group submitted to repeated daily maternal injections of nicotine since gestation day 30. (**b**) During the same period, the CPR remains constant in the control group; however, it increases by 25% in the nicotine group (reduction of cerebral perfusion in the nicotine group)

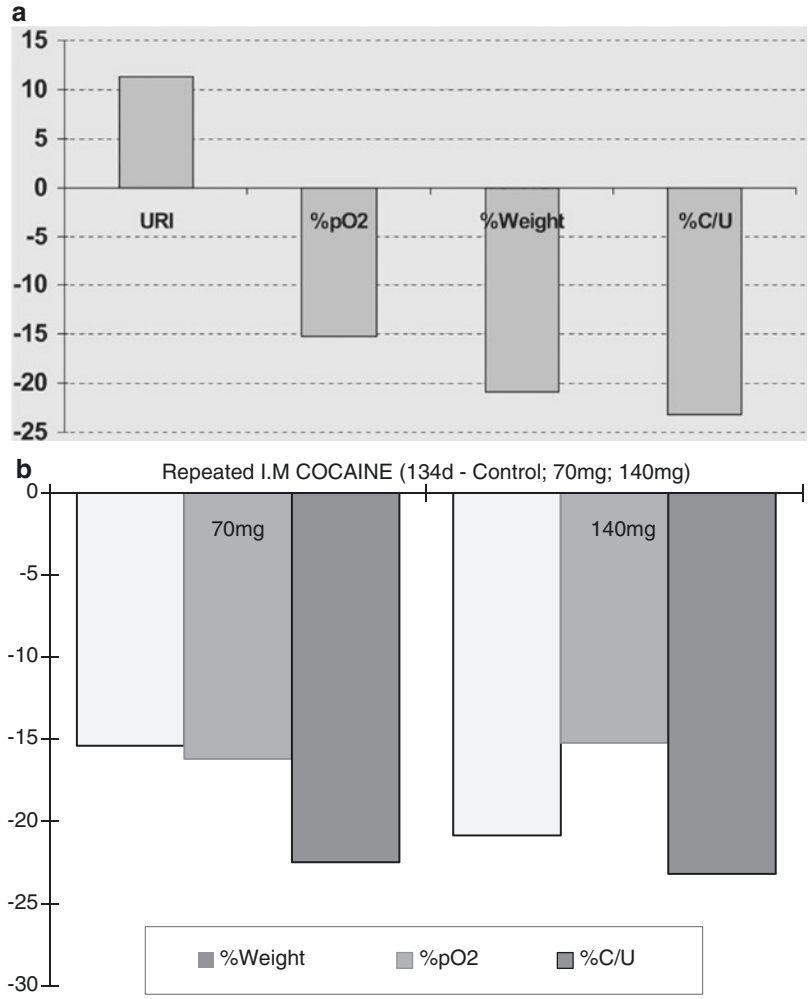

Fig. 16.15 Chronic cocaine administration. Fetal umbilical resistance (URI), cerebral resistance (CRI), cerebral-umbilical (CPR) ratio, fetal weight, and pO_2 (in the "70 mg/kg day^{-1}," and "140 mg/kg day^{-1}" cocaine groups (64 to 134 gestational day)), expressed in percentage of the control group value. a Data collected at the end of the gestation (134 days). The CPR and pO_2 are significantly decreased (in parallel) in the cocaine groups (20–25% for CPR and 10–15% for pO_2). The CPR is decreased in response to the development of a chronic fetal hypoxia. b Percent Loss, in lamb fetal weight, in fetal pO_2 and in CPR (CRI/URI) in the 2 cocaine gr (70 mg and 140 mg daily 60–134) compared to control gr at delivery. Variations between the cocaine groups and control group are expressed in percentage of the control group values

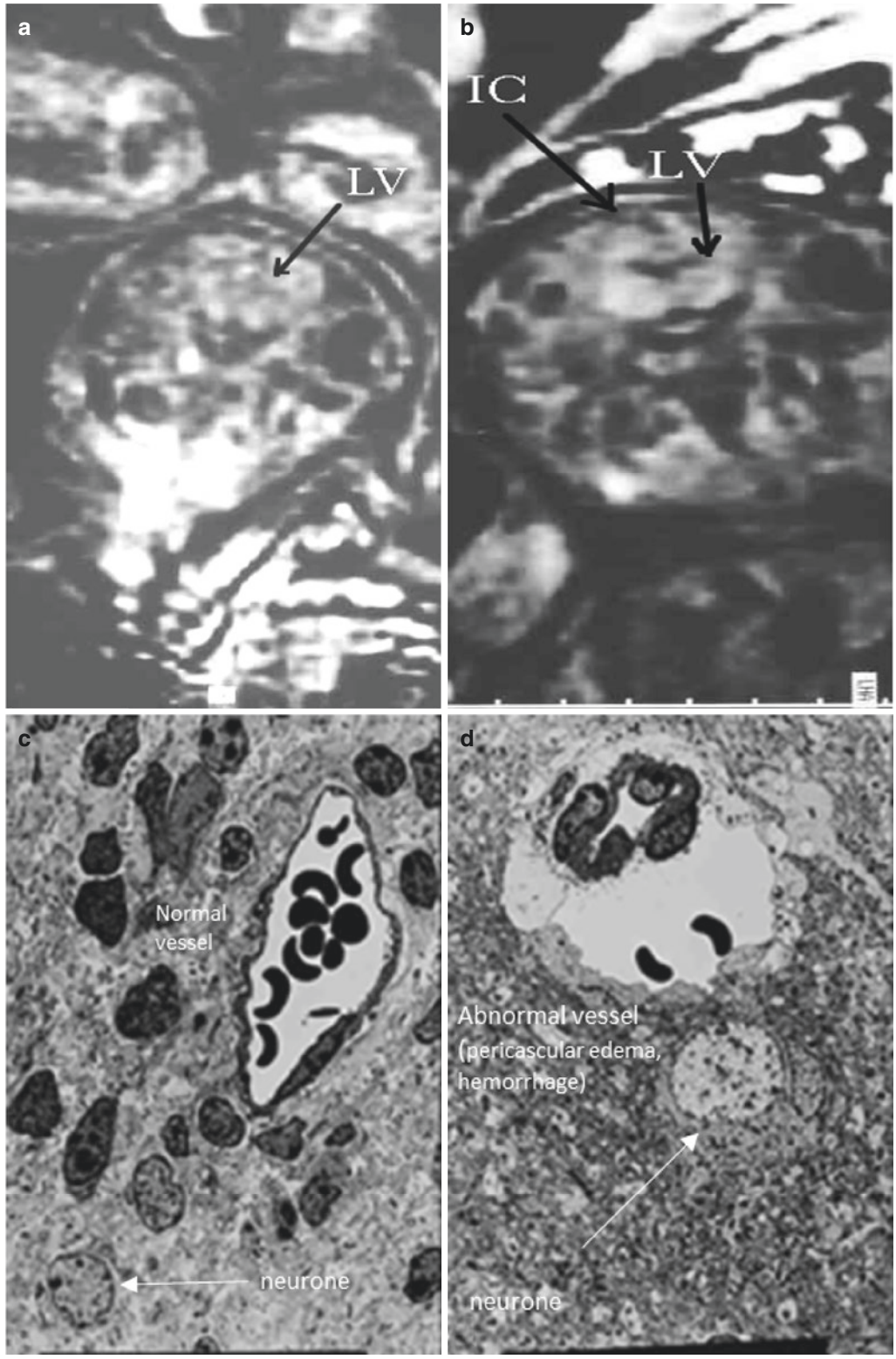

Fig. 16.16 (**a**, **b**) Magnetic resonance imaging of the fetal brain in a control fetus (**a**) and study fetus (**b**). (**c**, **d**) Brain tissue analysis by electron microscopy on control (**c**) and cocaine (**d**) fetuses (LV = Lateral ventricle)

the cocaine group, whereas only 14% in the control group. These findings confirmed significant brain abnormalities due to fetal hypoxia in the cocaine group. The hypoxic index was 500, significantly higher than the cutoff (>160). This correlates with brain damage observed by MRI and histology.

16.6.4 Cerebroplacental Ratio and Acute Drug Effect

Propranolol (4 μg/kg) was injected intravenously into pregnant ewes (n = 3), which were instrumented 24 h before (Fig. 16.3). The umbilical resistance increased and the cerebral resistance decreased beginning 1 min after injection, leading to a significantly decreased CPR [27]. In this study, pO_2 was not measured, but the fetal flow redistribution detected by CPR after each injection leads us to suspect that repeated injections of this drug may induce repeated hypoxic stresses for the fetus; hence, the beneficial effects of any drug (for the mother) and its deleterious effects (i.e., hypoxia) on the fetus must be evaluated before its use.

16.7 Cerebral Resistance Index, Flow Redistribution Ratio (CPR), and Hypoxic Index in Specific Human Pathologies

16.7.1 Cerebral Resistance Index and CPR in Acute Reversible Hypoxia: Prediction of Abnormal Fetal Heart Rate at Delivery

16.7.1.1 Without Placental Insufficiency: Maternal Anemia

Moderate (Hb >6 g/100 mL) or severe (Hb <6 g/100 mL) maternal anemia (Fig. 16.17) may develop during pregnancy and relates mainly to non-adapted food intake (ingestion of iron-chelating agent such as clay in South America or African tropical forest). Severe maternal anemia induces significant cerebral vasodilation as confirmed by a cerebral resistance lower than normal with an increase in cerebral blood flow which likely increases the fetal oxygen supply and a reduction in amniotic fluid. Umbilical flow is not affected, which is in agreement with the fact that there was no placental alteration. The flow redistribution is probably related to a reduction in maternal blood oxygen carrier induced by the iron-chelating agents and its subsequent reduction in fetal pO_2. The increase in cerebral resistance and CPR after red cell injection without a significant change in umbilical resistance confirms that maternal anemia does not create placental dysfunction, and that the condition can be relatively quickly corrected by a single red blood cell unit transfusion to the patient [53]. The cerebral adaptation is similar to the one observed in anemic fetuses during pregnancies complicated by red cell alloimmunization [59–61]. These authors showed that the fetal cerebral pulsatility index decreased in anemic fetuses, but reached abnormal values only in cases of severe fetal anemia. A hemoglobin content lower than 5 g/100 mL was closely associated with fetal flow redistribution and abnormal fetal heart rate. On the other hand, the occurrence of abnormal fetal heart rate was associated with CPR <1.1, which indicates that fetal flow redistribution plays a role in the development of cardiac dysfunction. Sixty-seven percent of the fetuses with abnormal fetal heart rate had a CPR <1.1. Nevertheless, the modest values of the sensitivity (73%), specificity (33%), positive predictive value (PPV; 50%), and negative predictive value (NPV; 57%) confirm that the amplitude of the flow redistribution (CPR) is not sufficient to predict the effects of this hemodynamic adaptation over time.

Other studies demonstrated that fetal cerebral vasodilation during a period of several weeks does not protect against cerebral organic damages [7, 9, 10]; thus, as the severe maternal anemia triggers a marked fetal cerebral vasodilation, the hemoglobin content has to be recovered as soon as possible in order to suppress the cerebral vasodilation. Moderate maternal anemia (Hb

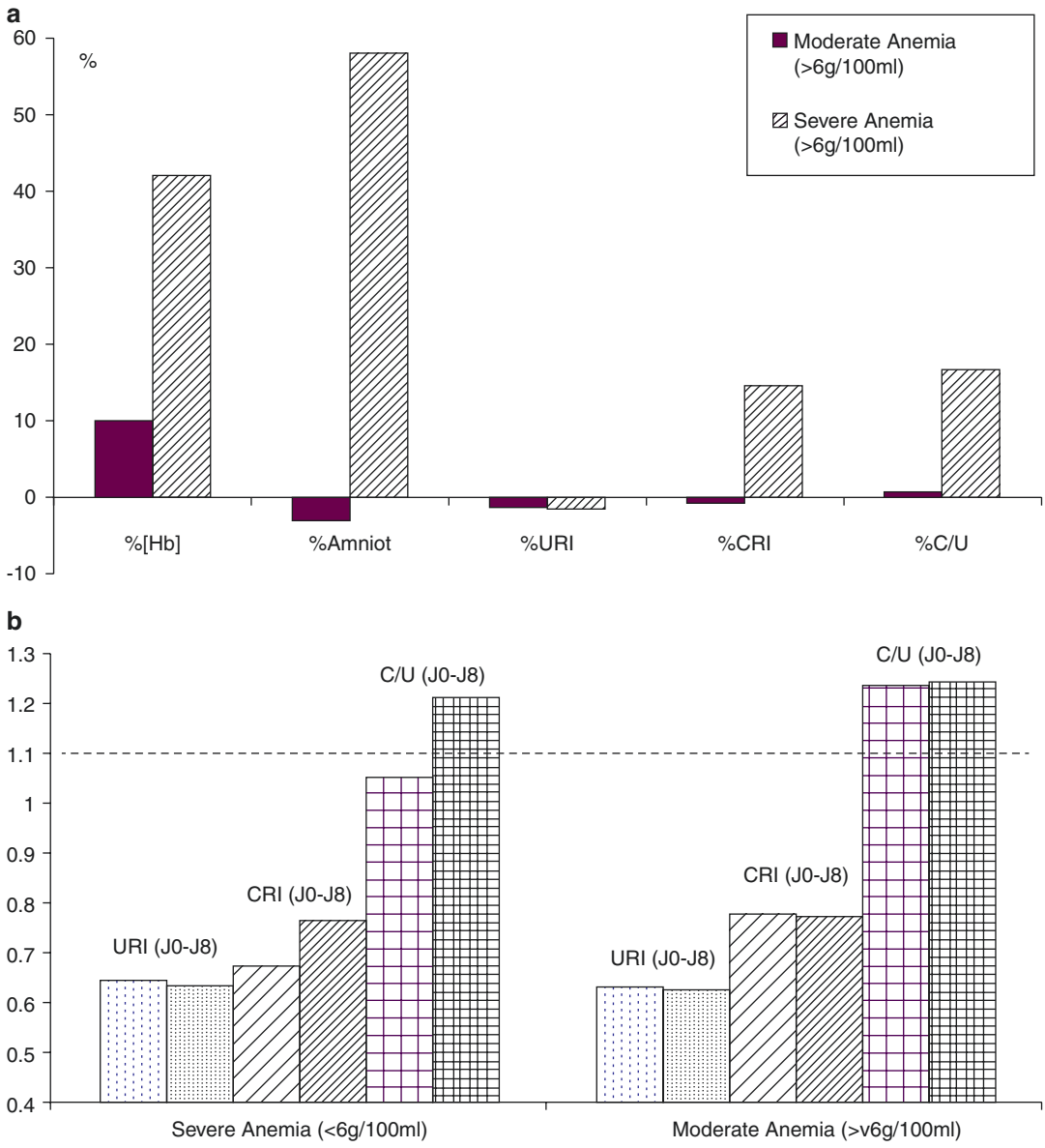

Fig. 16.17 (**a**) Changes from admission to 8 days after maternal treatment for the parameters listed below. Group 1: moderate anemia [Hb] >6 g/100 mL; group 2: severe anemia: [Hb] <6 g/100 mL. [Hb] maternal hemoglobin content, Amniot amniotic index, URI umbilical resistance index, CRI cerebral resistance index, CPR cerebral to umbilical resistance ratio. Note that the parameters change significantly only in the group with severe anemia. (**b**) Changes from admission (J0, gray bar) to 8 days after maternal treatment (J8, black bar) in the 2 groups of severe and moderate maternal anemia: Umbilical resistance index (URI), Cerebral resistance index (CRI), Cerebral to Umbilical resistance ratio (CPR). CRI and CPR increase from J0 to J8, in the severe anemia gr only, which means that such level of anemia had induced a flow redistribution (sign of hypoxia) that normalized with the maternal treatment

>6 g/100 mL) did not trigger fetal flow redistribution or abnormal fetal heart rate which suggests that fetal oxygenation was still satisfactory.

16.7.1.2 With Placenta Insufficiency (Malaria)

During a malaria crisis, destruction of red blood cells and inflammatory processes probably affect the placental microcirculation and thus the fetal-maternal exchanges. The fetus triggers a flow redistribution in favor of the brain, most likely in response to hypoxia, but this redistribution disappears at the end of the crisis. Thus, malaria deteriorates the placental function for the duration of the crisis, causing a reduction of nutrients and oxygen to the fetus and consequently abnormal fetal heart rate tracing.

A 1994 study of fetal hemodynamic changes investigated cerebral and umbilical responses to short- and long-term malaria crises [8, 62]. Umbilical artery and middle cerebral artery fetal Doppler were performed daily until the end of the crisis. In the short crisis group (<7 days), 61% of the fetuses were premature, 23% had abnormal fetal heart rate at delivery (several weeks later), CPR decreased by −8 ± 6%, and the mean HI was equal to −62 ± 54. In the long crisis group (>7 days), 70% of the fetuses were premature, 70% had abnormal fetal heart rate at delivery (several weeks later), CPR decreased by −14 ± 6%, and the mean HI was equal to −187 ± 54 (Fig. 16.12). Further, HI >150 predicted the occurrence of abnormal fetal heart rate with high sensitivity and specificity (100% and 91%, respectively). Additionally, the highest fetal flow disturbance (max %CPR) and the duration of the period with flow disturbance (>7 days) predicted abnormal fetal heart rate at delivery with a sensitivity of 10% and 40% and a specificity of 77% and 78%, respectively. It was concluded that the HI was more predictive of abnormal fetal heart rate at delivery than the amplitude or the duration of the fetal flow redistribution alone.

A second similar study performed in 1996 [8] in the same area and using the same protocol showed only a short crisis (<7 days). In this group, 35% of the fetuses were premature, 17.5% had abnormal fetal heart rate at delivery (several weeks later), CPR decreased by −7 ± 4%, and the mean HI was equal to −49 ± 26. In both studies, a HI > 150% was predictive of abnormal fetal heart rate at delivery with a sensitivity of 80% and specificity of 85%.

The HI allowed prediction of abnormal fetal heart rate at delivery several weeks in advance. Moreover, the lower amplitude of the hemodynamic response (lower HI) in the second group associated with a lower rate of abnormal fetal heart rate was likely related to an improvement in pregnancy recruitment and management or with the acquisition of an adapted immunity by the mother.

16.7.2 CPR in Nonreversible Hypoxia (Hypertension in Pregnancy) Prediction of Abnormal Fetal Heart Rate at Delivery

In a study of fetal cerebral and umbilical flow adaptation in pregnancies complicated by hypertension, which included 82% with IUGR, the fetal hemodynamics were monitored every 2 days by Doppler over several days from admission until delivery [63].

As flow redistribution was identified at its early stage, both the intensity and the duration of the flow redistribution period (hypoxic period) were considered for predicting the occurrence of abnormal fetal heart rate. By the end of the study, the limit for the HI was 160%. Figure 16.18 shows a graphic representation of HI (area between the CPR curve and the CPR = 1.1 cutoff line). This area represents the total oxygen deficit during the period of observation.

A HI higher than 160% was much more powerful (PPV: 87%; NPV: 88%) than the final URI, CRI, or CPR value measured for predicting abnormal fetal heart rate at delivery [URI (PPV: 63%; NPV: 74%) – CRI (PPV: 59%; NPV: 70%) – CPR (PPV: 57%; NPV: 92%)]. Moreover, as shown in Fig. 16.18, the CPR may change from one day to another; thus, a single Doppler measurement is not sufficient to identify the real hemodynamic stage induced by hypoxia. On the other hand, the HI increase is

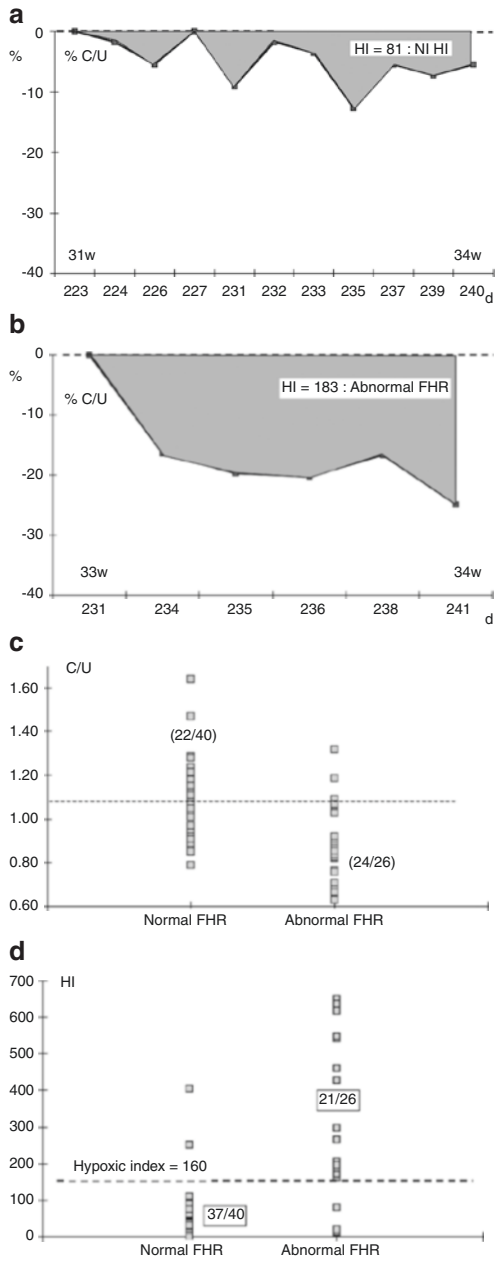

Fig. 16.18 Evolution of CPR reduction (in percentage from 1.1 cutoff value). The HI is represented as the area between % CPR (bold curve) and the 0% (horizontal dotted line corresponding to CPR = 1.1). (**a**) IUGR fetus delivered at 34 weeks, normal fetal heart rate, HI = 81% (mean CPR decrease of −5% × 17 days). (**b**) IUGR fetus delivered at 34 weeks, abnormal fetal heart rate, HI =183% (mean CPR decrease of −18% × 10 days). (**c**) Correlation between occurrence of abnormal fetal heart rate vs CPR (CPR abnormal when >1.1 → PPV =57%, NPV = 92%). (**d**) Correlation between occurrence of abnormal FHR vs hypoxic index. The HI is abnormal when >160% → PPV = 87%, NPV = 88%

associated with an increase in the degree of fetal growth restriction as expressed in percentile. This suggests that the HI, by measuring the cumulated oxygen deficit during the observation period, also likely expresses the deficit in the nutrition supply responsible for the fetal growth restriction.

Finally, it should be noted that this study addressed high-risk pregnancy but not very poor fetal outcomes: 22% of all fetuses required intensive care assistance (but <2 days and two thirds of them <33 weeks) and all survived in good health; only one fetus died at delivery. Thus, HI is a very early predictor of poor fetal outcome. In contrast, absent end-diastolic flow in the umbilical arteries was found in 9 cases (13% of the whole population), but all delivered before 33 weeks; all presented abnormal fetal heart rate; all were severely growth-restricted (centile: 6 + 2); 8 (88%) delivered by Cesarean section; and 5 (56%) required intensive care assistance. These fetuses presented the lowest CPR (0.7 ± 0.1) and umbilical cord pO_2 value at delivery (16 ± 6) and the highest HI values (387 ± 173%) in the population.

These results confirm that absent end-diastolic flow close to delivery means that the fetus has already been submitted to severe and long-term hypoxia and has entered the danger zone in which the risk of brain lesion is high [64, 65]. A retrospective study [10] showed that fetuses that developed brain lesions had an HI much higher than those in our study and frequently showed absent or reverse diastolic flow at admission. In these situations, HI is underestimated as we do not know how many days diastolic flow was absent and how long the CPR was below the cutoff limit; thus, it is recommended to use other later hemodynamic markers of fetal deterioration, such as the loss of fluctuation of the cerebral RI over 3 days [10], or the presence of abnormal ductus venosus or umbilical vein flow patterns if these signs appear before reaching a HI =160% [19–21, 66, 67].

16.7.3 Cerebral Flow During Maternal Anesthesia

The fetal cerebral and umbilical flows (Fig. 16.19) were monitored during maternal anesthesia of 7 h duration, the objective being to detect any fetal hemodynamic change (response to hypoxia) in relation to the different drugs used during this period: phenoperidine 7.5 mg, thiopental 500 mg, gamma hydroxy-butyrate 6 g, and isoflurane (Forane) 0.3–0.5% at 90 min after the beginning of the anesthesia. The patient was surgically treated at 21 weeks' gestation for angioma of the posterior cranial fossa. Doppler recordings of the umbilical arteries and the fetal anterior cerebral arteries were performed before anesthesia, during the anesthesia (at 10, 45, 60, and 90 min, and 3 and 7 h), and after anesthesia (2 h, 7 days, and 5 months). The fetal heart rate decreased progressively beginning 2 h after the start of anesthesia (from 150/min to 110/min at 3 h) and had recovered partially at 2 h after anesthesia was discontinued. At 7 days and at 5 months, the fetal heart rate was normal for the gestational age (145/min). At the same time, the cerebral (CRI) and the placental (URI) resistance indices decreased moderately, although the CPR is stable around its basal value. These three parameters stayed within the normal range for the gestational age throughout the anesthesia. After the anesthesia, the cerebral and placental indices decreased normally from 22 to 40 weeks, and the CPR remained stable. The evolution of the fetal vascular parameters demonstrates the effects of drugs on the fetal heart rate (significant decrease) and the stability of the fetal flow distribution (cerebral and placental), despite the marked hemodynamic changes in the mother.

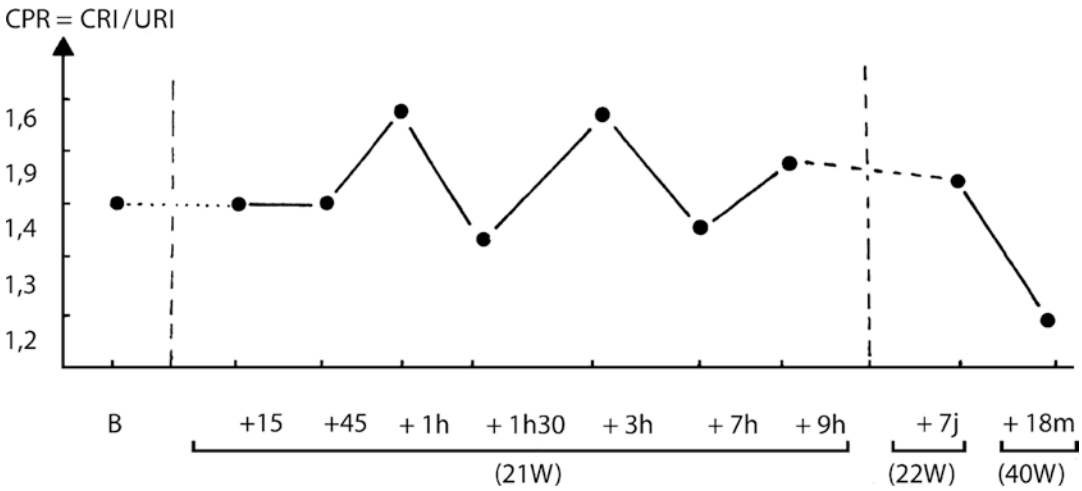

Fig. 16.19 Evolution of the CPR resistance ratio during maternal anesthesia (3 h). The CPR remains stable even when the fetal heart rate changes significantly (no fetal flow redistribution). After the anesthesia, the CPR decreases slightly with the gestational age and stays within the normal range until delivery (normal delivery at 40 weeks, normal fetus)

16.8 CPR Change During Febrile Episodes

Previous studies have demonstrated that malaria complicating pregnancy is associated with complications such as abortion, placental insufficiency, oligohydramnios, stillbirth, abnormal fetal heart rate tracing, and preterm delivery. In these cases, the umbilical and cerebral arteries' blood flow was found to be reduced and increased, respectively. This indicates that the fetus is hypoxic during febrile episodes. It was unclear whether fever itself could also cause fetal hemodynamic changes as a response to fetal hypoxia. Thus, researchers studied changes in fetal blood flow, amniotic fluid, and fetal heart rate tracing during fever episodes in 30 normal pregnancies complicated by febrile morbidity [68]. The authors found normal uterine artery resistance index, URI, CRI, CPR, amniotic fluid volume, and fetal heart rate tracing. The authors concluded that episodes of limited maternal fever did not alter the CPR (Fig. 16.20).

16.9 Clinical Effectiveness and Guidelines

The clinical utility and importance of CPR are supported by at least three recent systematic reviews and meta-analyses. In 2016, Nassr et al. published a meta-analysis that included seven studies analyzing the predictive ability of CPR in the prediction of adverse perinatal outcomes in growth-restricted fetuses. In this population, the authors found that abnormal CPR was significantly associated with higher risk of cesarean delivery due to fetal distress, low APGAR scores, neonatal intensive care unit admission, and other neonatal complications. This effect was higher in studies that included fetuses diagnosed with fetal growth restriction compared to fetuses that were considered at risk of fetal growth restriction [69].

More recently in 2018, Vollgraff et al. published their meta-analysis of 128 studies that analyzed the prognostic accuracy of CPR and middle cerebral artery Doppler compared to the umbilical artery in predicting adverse perinatal out-

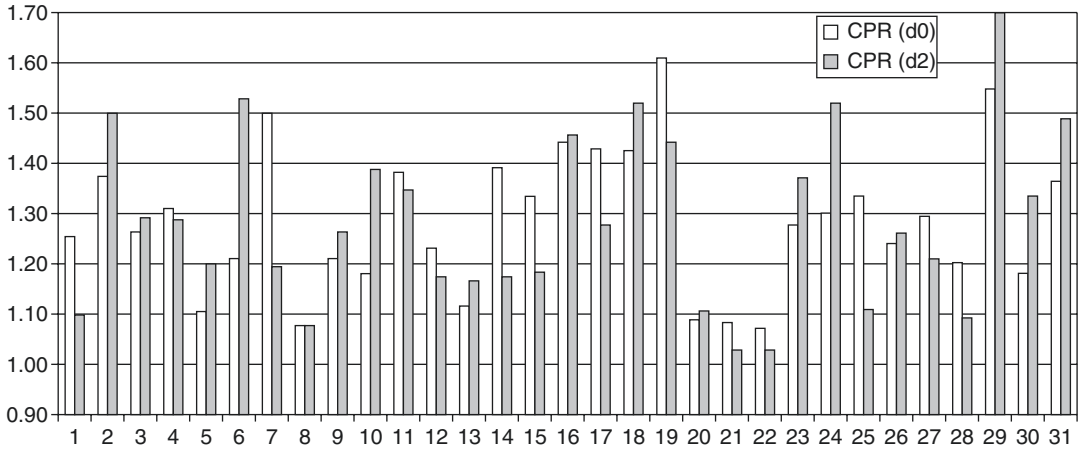

Fig. 16.20 CPR variations during episodes of ordinary fever during human pregnancy. White bars correspond to the day of admission (with fever), gray bars after 2 days of treatment and fever release. Note that CPR was never lower than 1 (no significant hypoxia)

comes in a low-risk population (including pregnancies without fetal growth restriction). The objective was to identify whether CPR and middle cerebral artery Doppler evaluation are of added value to umbilical artery Doppler [70]. The authors found that CPR outperformed umbilical artery Doppler in the prediction of composite adverse outcome and emergency delivery for fetal distress. The authors concluded that CPR with middle cerebral artery Doppler could add value to umbilical artery Doppler assessment in the prediction of adverse perinatal outcomes (Fig. 16.21).

In the same year, Conde-Agudelo et al. published their meta-analysis of 22 cohort and cross-sectional studies analyzing the accuracy of CPR for predicting adverse perinatal and neurodevelopmental outcomes in suspected fetal growth restriction [71]. The authors found that the predictive accuracy of CPR was moderate to high for perinatal death, and low for the composite of adverse perinatal outcomes, cesarean section for non-reassuring fetal status, Apgar score < 7, admission to the neonatal intensive care unit, neonatal acidosis, and neonatal morbidity. An abnormal CPR result was found to have moderate accuracy for predicting small-for-gestational age at birth. CPR was also found to have higher predictive accuracy in pregnancies with suspected early-onset fetal growth restriction. The authors concluded that CPR appeared to be useful in predicting perinatal death in pregnancies with suspected fetal growth restriction (Fig. 16.21).

The three meta-analyses described above noted the lack of randomized clinical trials on the topic and recommended assessing the value of CPR in a clinical trial setting before its incorporation into clinical practice.

In the clinical institutions of the authors, the URI, CRI, and CPR are considered important tools for monitoring fetal growth and behavior of complicated pregnancies. CPR is also evaluated systematically in all pregnancies. In high-risk pregnancies, the umbilical artery, cerebral artery, and the CPR indices are monitored on a weekly basis. The frequency of monitoring is increased if the CPR becomes abnormal. It is the experience of some of the authors that a fetus with an abnormal CPR will likely not tolerate labor, even with a normal fetal heart rate tracing, which would lead to counseling the patient about the potential need for cesarean delivery.

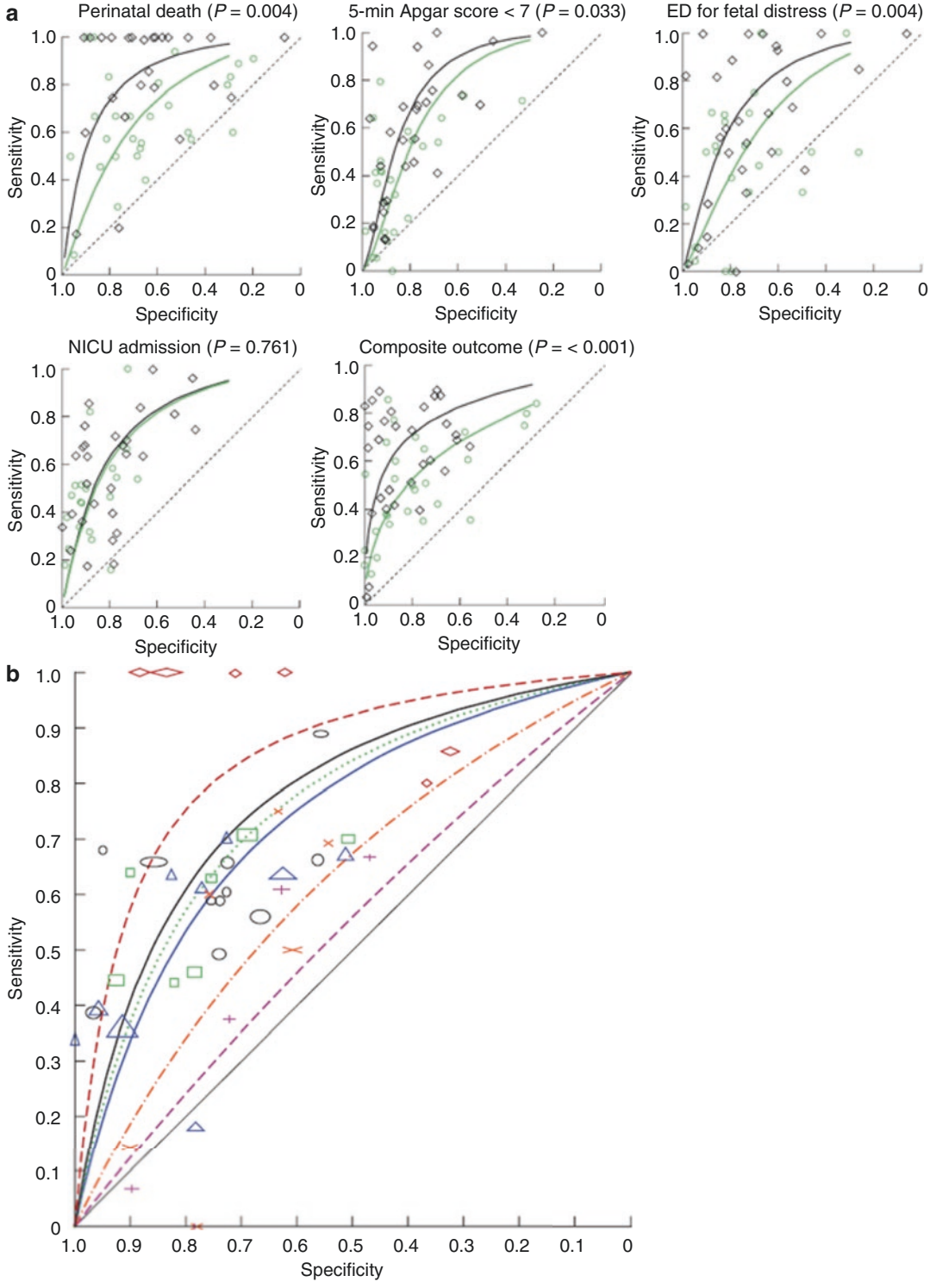
a
Perinatal death (P = 0.004)
5-min Apgar score < 7 (P = 0.033)
ED for fetal distress (P = 0.004)
NICU admission (P = 0.761)
Composite outcome (P = < 0.001)
Sensitivity
Specificity
1.0
0.8
0.6
0.4
0.2
0
b
Sensitivity
Specificity
1.0
0.9
0.8
0.7
0.6
0.5
0.4
0.3
0.2
0.1
0

16.10 Summary of the Design, Validation, and Significance of the Cerebroplacental Ratio and the Hypoxic Index

The CPR was defined as the ratio between the CRI and the URI. It was initially described by Arbeille et al. in 1986 [22]. Researchers started investigating specific hemodynamic processes that could be measured by using the CPR, and which specific situations could trigger variations on it. It was later found that the CPR changed with fetal hypoxia and hypovolemia. The drop in the CPR was found to be proportional to the drop in the fetal pO_2.

Subsequently, researchers investigated whether the CPR could measure the fetal response to fetal hypoxia to protect brain tissue from hypoxic aggression. Thereafter, it was found that the fetal flow redistribution by brain vessel vasodilation (CPR < 1.1) compensated for the lack of pO_2 after days/weeks. However, this response did not prevent the occurrence of hypoxic effects such as abnormal fetal heart rate tracing or brain tissue damage. This hypoxic index was then defined as the sum of the percentage decrease in the CPR (below its cutoff value of 1.1) over several days. The hypothesis was that if the CPR drop approximates the pO_2 drop, the sum of the CPR deficit should approximate the cumulative deficit in oxygen; and it should correlate with the hypoxic effects on fetal tissue. If the CPR was 10% below the cut value for 5 days or 25% below the cut off for 7 days, the HI was 50 (10% × 5 days) or 175 (25% × 7 days), respectively. It was later established that a HI > 150 was associated with an abnormal fetal heart rate tracing and/or fetal brain damage.

16.11 Conclusion

The objective of fetal Doppler is to detect at an early stage any hemodynamic changes that allow us to identify and quantify a placental dysfunction (with associated fetal malnutrition and low oxygenation). Fetal Doppler studies also allow us to determine the consequences of this abnormality on fetal growth and well-being.

The URI has been used to confirm the existence of placental hemodynamic disorders in the case of IUGR, but the sensitivity of this parameter for the follow-up of fetal growth remains at only 60%. Nevertheless, the absence of end-diastolic flow in the umbilical or aortic Doppler waveform is an indicator of severe fetal distress and neonatal cerebral complications [64, 72–78].

Cerebral flow changes in relation to hypoxia and fetal distress continue to be one of the most interesting areas of investigation. Even though many studies have already demonstrated positive correlations between cerebral Doppler data and fetal hypoxia or fetal well-being, it is too early to draw a conclusion as to how to use cerebral Doppler studies in routine practice for the management of fetal distress and for making the decision to interrupt a gestation.

The CPR, which measures the proportion of flow supplying the brain and the placenta, is now the most widely used parameter for the assessment of IUGR and hypoxia. First, it takes into account the causes and consequences of the placental insufficiency responsible for IUGR and hypoxia. Second, it is not heart rate-dependent. Third, it has a single cutoff value (CPR is normal if >1.1), at least during the second half of the pregnancy. On the other hand, because IUGR is

Fig. 16.21 (**a**) Hierarchal summary receiver–operating characteristics curves and p-values for indirect comparisons of prognostic accuracy of CPR (◊, black line) and middle cerebral artery Doppler (○, green line) for outcomes perinatal death, 5-min Apgar score < 7, emergency delivery for fetal distress, admission to neonatal intensive care unit and composite adverse perinatal outcome (as defined in included studies) [70]. (**b**) Summary receiver–operating characteristics curves of CPR for predicting composite of adverse perinatal outcomes (○, black line), perinatal death (◊, red line), cesarean delivery for non-reassuring fetal status (□, green line), admission to neonatal intensive care unit (▲, blue line), 5-min Apgar score < 7 (×, orange line), and neonatal acidosis (+, purple line) in singleton pregnancies with fetal growth restriction suspected antenatally [71]

frequently associated with hypoxia, brain metabolism disturbances, and delayed brain development, the CPR, already an indicator of IUGR, is also an accurate parameter for the prediction of poor perinatal outcome.

It is also clear that since the resistance indices are heart rate-dependent, it is hazardous to draw any conclusion from a single value of any of these parameters. Only several successive daily measures of the Doppler indices can lead to a more realistic evaluation of cerebral hemodynamic changes. Moreover, any significant increase in the umbilical index or decrease in the cerebral or CPR index, even within the normal range, must be considered pathological; however, in such cases the CPR may approach the lowest normal limit (CPR of 1, 1) or pass into the abnormal range (CPR <1, 1).

On the other hand, the amplitude of CPR change was in the same range at any of the gestational ages investigated in cases of maternal anemia and hypertension. Such observations suggest that the capacity of the cerebral vessels to vasodilate does not change during the gestation and thus is not mediated by the nervous system. It may be a biochemical reaction originating from the cerebral vessels. Similar observations were made in animal (fetal lamb: gestation 145 days) studies, the flow redistribution amplitude in response to a calibrated reduction in pO_2 being the same at 80 days or at 134 days (personal data).

In all the acute or chronic fetal hypoxic conditions in relation to placental insufficiency (i.e., anemia, malaria, hypertension), the CPR was the most appropriate parameter to detect and quantify the fetal flow redistribution [3, 8, 70]. The assessment of the flow redistribution amplitude (CPR change) and the duration of the flow redistribution period allowed prediction of the consequences of the exposure to hypoxia (HI).

Finally, even though Doppler measurements increasingly help the obstetrician, and current evidence supports the contribution of CPR to clinical practice, the objectives for the near future must be (a) to test the true possibilities of Doppler indices in large randomized clinical studies, and (b) to point out the physiopathological phenomena responsible for fetal flow disturbances. For the latter aims, animal experimentation will be of great interest. Figure 16.22 shows the evolution of URI and CRI in a pregnancy without evident complication, but in which the fetal weight at term was at the tenth centile; however, the CPR was at the limit of its normal range, demonstrating that even in the absence of any fetal or maternal clinical signs, the fetal circulation can change with consequent alterations in the oxygen and nutrient supply.

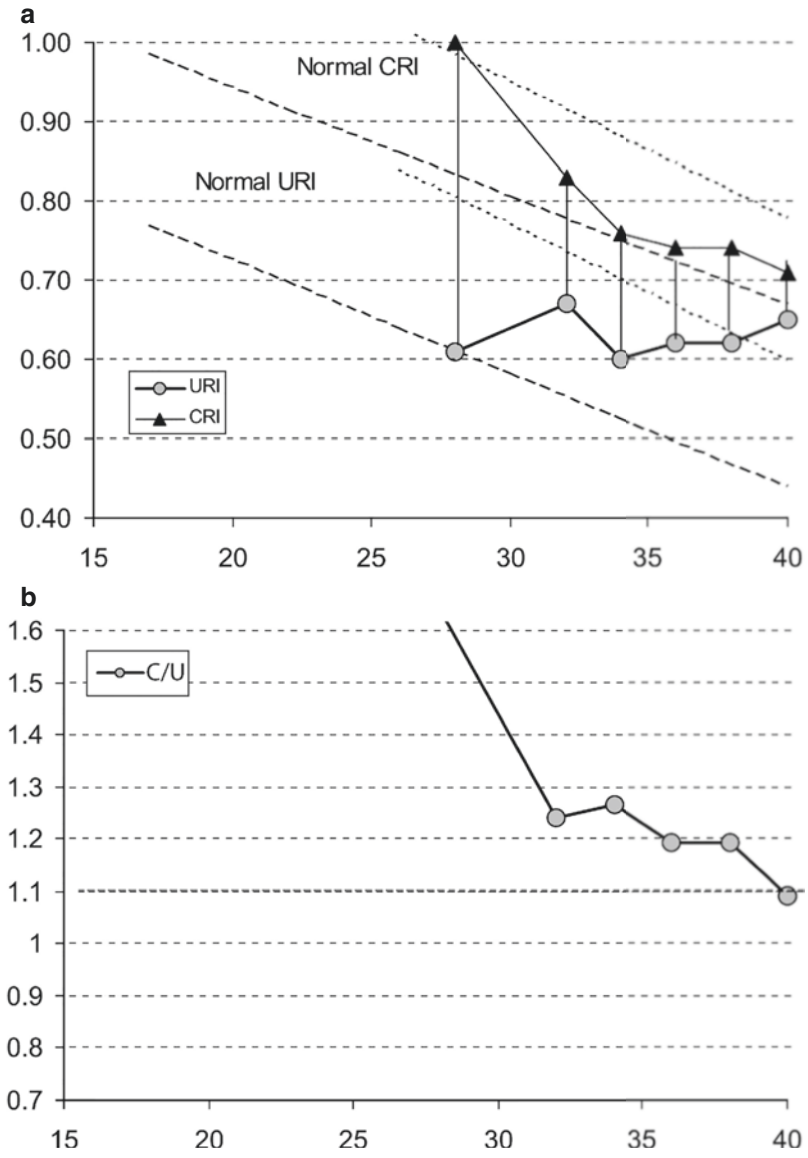

Fig. 16.22 (**a**) Evolution of the umbilical and the cerebral resistance indices during the early phase of development of moderate IUGR (normal delivery, fetal weight 10 centile). (**b**) Evolution of the CPR. Note that the two resistance indices show large fluctuations even within or at the limit of their normal range; however, the CPR decreases regularly toward its cutoff line of normality (1.1)

References

1. Cohn HE, Sacks EJ, Heymann MA, Rudolph AM. Cardiovascular responses to hypoxemia and acidemia in fetal lambs. Am J Obstet Gynecol. 1974;120(6):817–24.
2. Wladimiroff JW, vd Wijngaard JA, Degani S, Noordam MJ, van Eyck J, Tonge HM. Cerebral and umbilical arterial blood flow velocity waveforms in normal and growth-retarded pregnancies. Obstet Gynecol. 1987;69(5):705–9.
3. Arbeille PMD, Laurini R. Fetal hypoxia. London: The Parthenon Publishing Group; 1999.
4. Itskovitz J, LaGamma EF, Bristow J, Rudolph AM. Cardiovascular responses to hypoxemia in sinoaortic-denervated fetal sheep. Pediatr Res. 1991;30(4):381–5.
5. Fouron JC, Teyssier G, Maroto E, Lessard M, Marquette G. Diastolic circulatory dynamics in the presence of elevated placental resistance and retrograde diastolic flow in the umbilical artery: a Doppler echographic study in lambs. Am J Obstet Gynecol. 1991;164(1 Pt 1):195–203.
6. Kjellmer I, Thordstein M, Wennergren M. Cerebral function in the growth-retarded fetus and neonate. Biol Neonate. 1992;62(4):265–70.
7. Arbeille P, Maulik D, Salihagic A, Locatelli A, Lansac J, Platt LD. Effect of long-term cocaine

administration to pregnant ewes on fetal hemodynamics, oxygenation, and growth. Obstet Gynecol. 1997;90(5):795–802.
8. Arbeille P, Caries G, Tobal N, Herault S, Georgescus M, Bousquet F, et al. Fetal flow redistribution to the brain in response to malaria infection: does protection of the fetus against malaria develop over time? J Ultrasound Med. 2002;21(7):739–46.
9. Laurini RN, Arbeille B, Gemberg C, Akoka S, Locatelli A, Lansac J, et al. Brain damage and hypoxia in an ovine fetal chronic cocaine model. Eur J Obstet Gynecol Reprod Biol. 1999;86(1):15–22.
10. Salihagic A, Georgescus M, Perrotin F, Laurini R, Arbeille B, Fignon A, et al. Daily Doppler assessment of the fetal hemodynamic response to chronic hypoxia: a five-case report. Prenat Neonatal Med. 2000;5:35–41.
11. Allen LH. Pregnancy and iron deficiency: unresolved issues. Nutr Rev. 1997;55(4):91–101.
12. Steer P, Alam MA, Wadsworth J, Welch A. Relation between maternal haemoglobin concentration and birth weight in different ethnic groups. BMJ. 1995;310(6978):489–91.
13. Allen LH. Anemia and iron deficiency: effects on pregnancy outcome. Am J Clin Nutr. 2000;71(5 Suppl):1280S–4S.
14. Colomer J, Colomer C, Gutierrez D, Jubert A, Nolasco A, Donat J, et al. Anaemia during pregnancy as a risk factor for infant iron deficiency: report from the Valencia Infant Anaemia Cohort (VIAC) study. Paediatr Perinat Epidemiol. 1990;4(2):196–204.
15. Ribbert LS, Snijders RJ, Nicolaides KH, Visser GH. Relation of fetal blood gases and data from computer-assisted analysis of fetal heart rate patterns in small for gestation fetuses. Br J Obstet Gynaecol. 1991;98(8):820–3.
16. Dawes GS, Moulden M, Redman CW. Improvements in computerized fetal heart rate analysis antepartum. J Perinat Med. 1996;24(1):25–36.
17. Lenstrup C, Haase N. Predictive value of antepartum fetal heart rate non-stress test in high-risk pregnancy. Acta Obstet Gynecol Scand. 1985;64(2):133–8.
18. Weiner Z, Farmakides G, Schulman H, Lopresti S, Schneider E. Surveillance of growth-retarded fetuses with computerized fetal heart rate monitoring combined with Doppler velocimetry of the umbilical and uterine arteries. J Reprod Med. 1996;41(2):112–8.
19. Hecher K, Bilardo CM, Stigter RH, Ville Y, Hackeloer BJ, Kok HJ, et al. Monitoring of fetuses with intrauterine growth restriction: a longitudinal study. Ultrasound Obstet Gynecol. 2001;18(6):564–70.
20. Baschat AA, Gembruch U, Harman CR. The sequence of changes in Doppler and biophysical parameters as severe fetal growth restriction worsens. Ultrasound Obstet Gynecol. 2001;18(6):571–7.
21. Ferrazzi E, Bozzo M, Rigano S, Bellotti M, Morabito A, Pardi G, et al. Temporal sequence of abnormal Doppler changes in the peripheral and central circulatory systems of the severely growth-restricted fetus. Ultrasound Obstet Gynecol. 2002;19(2):140–6.
22. Arbeille PTF, Body G, et al. Evolution de la circulation artérielle ombilicale et cérébrale du foetus au cours de la grossesse. In: Relier JP, editor. Progrés en néonatologie, vol. 6. Basel: Karger; 1986. p. 30–7.
23. Arbeille P, Roncin A, Berson M, Patat F, Pourcelot L. Exploration of the fetal cerebral blood flow by duplex Doppler—linear array system in normal and pathological pregnancies. Ultrasound Med Biol 1987;13(6):329–337.
24. Woo JS, Liang ST, Lo RL, Chan FY. Middle cerebral artery Doppler flow velocity waveforms. Obstet Gynecol. 1987;70(4):613–6.
25. Wladimiroff JW, Tonge HM, Stewart PA. Doppler ultrasound assessment of cerebral blood flow in the human fetus. Br J Obstet Gynaecol. 1986;93(5):471–5.
26. Arbeille P, Montenegro N, Tranquart F, Berson M, Roncin A, Pourcelot L. Assessment of the Main fetal cerebrovascular areas by ultrasound color-coded Doppler. Echocardiography. 1990;7(5):629–34.
27. Arbeille P, Berson M, Maulik D, Locatelli A, Bodard S. New implanted Doppler sensors for the assessment of the main fetal hemodynamics. Ultrasound Med Biol. 1992;18(1):97–103.
28. Arbeille P, Bosc M, Vaillant MC, Tranquart F. Nicotine-induced changes in the cerebral circulation in ovine fetuses. Am J Perinatol. 1992;9(4):270–4.
29. Adamson SL, Morrow RJ, Langille BL, Bull SB, Ritchie JW. Site-dependent effects of increases in placental vascular resistance on the umbilical arterial velocity waveform in fetal sheep. Ultrasound Med Biol. 1990;16(1):19–27.
30. Maulik D, Yarlagadda P, Nathanielsz PW, Figueroa JP. Hemodynamic validation of Doppler assessment of fetoplacental circulation in a sheep model system. J Ultrasound Med. 1989;8(4):177–81.
31. Maulik D, Arbeille P, Kadado T. Hemodynamic foundation of umbilical arterial Doppler waveform analysis. Biol Neonate. 1992;62(4):280–9.
32. Gosling R. Extraction of physiological information from spectrum-analysed Doppler-shifted continuous-wave ultrasound signals obtained non-invasively from the arterial system. IEE Med Elect Monographs. 1976;13(22):73–125.
33. Pourcelot L. Applications cliniques de l'examen Doppler transkutane. Velocimetrie ultrasonore Doppler. 1974:213–40.
34. Stuart B, Drumm J, FitzGerald DE, Duignan NM. Fetal blood velocity waveforms in normal pregnancy. Br J Obstet Gynaecol. 1980;87(9):780–5.
35. Arbeille PH, Tranquart F, Berson M, Roncin A, Saliba E, Pourcelot L. Visualization of the fetal circle of Willis and intra-cerebral arteries by color-coded Doppler. Eur J Obstet Gynecol Reprod Biol. 1989;32(3):195–8.
36. Arbeille P, Maulik D, Fignon A, Stale H, Berson M, Bodard S, et al. Assessment of the fetal PO2 changes by cerebral and umbilical Doppler on lamb fetuses during acute hypoxia. Ultrasound Med Biol. 1995;21(7):861–70.

37. Bonnin P, Guyot B, Bailliart O, Benard C, Blot P, Martineaud JP. Relationship between umbilical and fetal cerebral blood flow velocity waveforms and umbilical venous blood gases. Ultrasound Obstet Gynecol. 1992;2(1):18–22.
38. Brar HS, Horenstein J, Medearis AL, Platt LD, Phelan JP, Paul RH. Cerebral, umbilical, and uterine resistance using Doppler velocimetry in postterm pregnancy. J Ultrasound Med. 1989;8(4):187–91.
39. Gramellini D, Folli MC, Raboni S, Vadora E, Merialdi A. Cerebral-umbilical Doppler ratio as a predictor of adverse perinatal outcome. Obstet Gynecol. 1992;79(3):416–20.
40. Bahado-Singh RO, Kovanci E, Jeffres A, Oz U, Deren O, Copel J, et al. The Doppler cerebroplacental ratio and perinatal outcome in intrauterine growth restriction. Am J Obstet Gynecol. 1999;180(3 Pt 1):750–6.
41. Jugovic D, Tumbri J, Medic M, Jukic MK, Kurjak A, Arbeille P, et al. New Doppler index for prediction of perinatal brain damage in growth-restricted and hypoxic fetuses. Ultrasound Obstet Gynecol. 2007;30(3):303–11.
42. Salihagic-Kadic A, Medic M, Jugovic D, Kos M, Latin V, Kusan Jukic M, et al. Fetal cerebrovascular response to chronic hypoxia—implications for the prevention of brain damage. J Matern Fetal Neonatal Med. 2006;19(7):387–96.
43. Groome L, Watson J. Assessment of inutero neurobehavioral development. 1. Fetal behavioral states. J Matern Fetal Invest. 1992;2(3):183–94.
44. van Eyck J, Wladimiroff JW, van den Wijngaard JA, Noordam MJ, Prechtl HF. The blood flow velocity waveform in the fetal internal carotid and umbilical artery; its relation to fetal behavioural states in normal pregnancy at 37-38 weeks. Br J Obstet Gynaecol. 1987;94(8):736–41.
45. Maršál K, Lindblad A, Lingman G, Eik-Nes S. Blood flow in the fetal descending aorta; intrinsic factors affecting fetal blood flow, ie fetal breathing movements and cardiac arrhythmia. Ultrasound Med Biol. 1984;10(3):339–48.
46. van der Mooren K, van Eyck J, Wladimiroff JW. Human fetal ductal flow velocity waveforms relative to behavioral states in normal term pregnancy. Am J Obstet Gynecol. 1989;160(2):371–4.
47. Archer LN, Levene MI, Evans DH. Cerebral artery Doppler ultrasonography for prediction of outcome after perinatal asphyxia. Lancet. 1986;2(8516):1116–8.
48. Bilardo CM, Nicolaides KH, Campbell S. Doppler measurements of fetal and uteroplacental circulations: relationship with umbilical venous blood gases measured at cordocentesis. Am J Obstet Gynecol. 1990;162(1):115–20.
49. Arduini D, Rizzo G, Romanini C, Mancuso S. Hemodynamic changes in growth retarded fetuses during maternal oxygen administration as predictors of fetal outcome. J Ultrasound Med. 1989;8(4):193–6.
50. Gaziano E, Gaziano C, Brandt D. Doppler velocimetry determined redistribution of fetal blood flow: correlation with growth restriction in diamniotic monochorionic and dizygotic twins. Am J Obstet Gynecol. 1998;178(6):1359–67.
51. Arbeille P, Henrion C, Paillet C. Hemodynamique cerebrale et placentaire dans les grossesses gemellaires. Progrès Néonatol (Karger edition). 1988;7:223–9.
52. Arbeille P, Maulik D, Stree JL, Fignon A, Amyel C, Deufel M. Fetal cerebral and renal Doppler in small for gestational age fetuses in hypertensive pregnancies. Eur J Obstet Gynecol Reprod Biol. 1994;56(2):111–6.
53. Carles G, Tobal N, Raynal P, Herault S, Beucher G, Marret H, et al. Doppler assessment of the fetal cerebral hemodynamic response to moderate or severe maternal anemia. Am J Obstet Gynecol. 2003;188(3):794–9.
54. Edelstone DI, Peticca BB, Goldblum LJ. Effects of maternal oxygen administration on fetal oxygenation during reductions in umbilical blood flow in fetal lambs. Am J Obstet Gynecol. 1985;152(3):351–8.
55. Mori A. Effect of maternal oxygen inhalation on fetal hemodynamics in chronic hypoxia with IUGR. J Matern Fetal Invest. 1992;2:93–9.
56. Nicolaides KH, Campbell S, Bradley RJ, Bilardo CM, Soothill PW, Gibb D. Maternal oxygen therapy for intrauterine growth retardation. Lancet. 1987;1(8539):942–5.
57. Veille JC, Penry M. Effects of maternal administration of 3% carbon dioxide on umbilical artery and fetal renal and middle cerebral artery Doppler waveforms. Am J Obstet Gynecol. 1992;167(6):1668–71.
58. Akoka S, Descamps P, Genberg C, Franconi F, Arbeille B, Laurini R, et al. Cerebral MRI on fetuses submitted to repeated cocaine administration during the gestation: an ovine model. Eur J Obstet Gynecol Reprod Biol. 1999;85(2):185–90.
59. Mari G, Moise KJ Jr, Deter RL, Kirshon B, Stefos T, Carpenter RJ Jr. Flow velocity waveforms of the vascular system in the anemic fetus before and after intravascular transfusion for severe red blood cell alloimmunization. Am J Obstet Gynecol. 1990;162(4):1060–4.
60. Teixeira J, Duncan K, Letsky E, Fisk N. Middle cerebral artery peak systolic velocity in the prediction of fetal anemia. Ultrasound Obstet Gynecol. 2000;15(3):205–8.
61. Vyas S, Nicolaides KH, Campbell S. Doppler examination of the middle cerebral artery in anemic fetuses. Am J Obstet Gynecol. 1990;162(4):1066–8.
62. Arbeille P, Carles G, Bousquet F, Body G, Lansac J. Fetal cerebral and umbilical artery blood flow changes during pregnancy complicated by malaria. J Ultrasound Med. 1998;17(4):223–9.
63. Arbeille P, Perrotin F, Salihagic A, Sthale H, Lansac J, Platt LD. Fetal Doppler hypoxic index for the prediction of abnormal fetal heart rate at delivery in chronic fetal distress. Eur J Obstet Gynecol Reprod Biol. 2005;121(2):171–7.

64. Brar HS, Platt LD. Reverse end-diastolic flow velocity on umbilical artery velocimetry in high-risk pregnancies: an ominous finding with adverse pregnancy outcome. Am J Obstet Gynecol. 1988;159(3):559–61.
65. Fleischer A, Schulman H, Farmakides G, Bracero L, Blattner P, Randolph G. Umbilical artery velocity waveforms and intrauterine growth retardation. Am J Obstet Gynecol. 1985;151(4):502–5.
66. Hofstaetter C, Gudmundsson S, Dubiel M, Marsal K. Ductus venosus velocimetry in high-risk pregnancies. Eur J Obstet Gynecol Reprod Biol. 1996;70(2):135–40.
67. Kiserud T. Fetal venous circulation-an update on hemodynamics. J Perinat Med. 2000;28(2):90–6.
68. Carles G, Dallah F, Helou G, Alassas N, El Guindi W, Arbeille P. Redistribution of fetal blood flow in response to an acute fever episode during pregnancy in comparison with malaria. J Infect Dis Immun. 2011;3:68–72.
69. Nassr AA, Abdelmagied AM, Shazly SA. Fetal cerebro-placental ratio and adverse perinatal outcome: systematic review and meta-analysis of the association and diagnostic performance. J Perinat Med. 2016;44(2):249–56.
70. Vollgraff Heidweiller-Schreurs CA, De Boer MA, Heymans MW, Schoonmade LJ, Bossuyt PMM, Mol BWJ, et al. Prognostic accuracy of cerebroplacental ratio and middle cerebral artery Doppler for adverse perinatal outcome: systematic review and meta-analysis. Ultrasound Obstet Gynecol. 2018;51(3):313–22.
71. Conde-Agudelo A, Villar J, Kennedy SH, Papageorghiou AT. Predictive accuracy of cerebroplacental ratio for adverse perinatal and neurodevelopmental outcomes in suspected fetal growth restriction: systematic review and meta-analysis. Ultrasound Obstet Gynecol. 2018;52(4):430–41.
72. Arbeille P, Asquier E, Moxhon E, Magnin G, Pourcelot L, Berger C, et al. Nouvelle technique dans la surveillance de la grossesse: l'étude de la circulation foetale et placentaire par les ultrasons. J Gynecol Obstet Biol Reprod (Paris). 1983;12:851–9.
73. Arbeille P, Leguyader P, Fignon A, Locatelli A, Maulik D. Fetal hemodynamics and flow velocity indices. In: Doppler ultrasound in obstetrics and gynecology, vol. 2. New York: Raven Press Ltd; 1994.
74. Divon MY, Girz BA, Lieblich R, Langer O. Clinical management of the fetus with markedly diminished umbilical artery end-diastolic flow. Am J Obstet Gynecol. 1989;161(6 Pt 1):1523–7.
75. Nicolaides K, Bilardo C, Soothill P, Campbell S. Absence of end diastolic frequencies in umbilical artery: a sign of fetal hypoxia and acidosis. Br Med J. 1988;297(6655):1026.
76. Rochelson B, Schulman H, Farmakides G, Bracero L, Ducey J, Fleischer A, et al. The significance of absent end-diastolic velocity in umbilical artery velocity waveforms. Am J Obstet Gynecol. 1987;156(5):1213–8.
77. Schulman H, Fleischer A, Stern W, Farmakides G, Jagani N, Blattner P. Umbilical velocity wave ratios in human pregnancy. Am J Obstet Gynecol. 1984;148(7):985–90.
78. Trudinger BJ, Giles WB, Cook CM, Bombardieri J, Collins L. Fetal umbilical artery flow velocity waveforms and placental resistance: clinical significance. BJOG Int J Obstet Gynaecol. 1985;92(1):23–30.

The Cerebroplacental Ratio

17

Edgar Hernandez Andrade and Eleazar Soto

17.1 Fetal Brain Circulation and Hypoxia

Evidence of fetal and neonatal hemodynamic changes related to hypoxia/asphyxia was first described in experimental animal models. Variations in blood flow perfusion to different fetal/newborn organs were estimated using radiolabeled microspheres injected during hypoxic periods [1]. There was an increment in blood flow to the fetal heart, brain, and adrenals, and a reduction in blood flow to the skin, bones, bowel, and bladder [2]. This hemodynamic distribution was termed "sparing" and a specific term for each organ was coined, i.e., "brain-sparing," "heart-sparing," or "adrenal-sparing," and considered as a protective mechanism for key organs from the hypoxic insult. The fetal brain-sparing mechanism was confirmed in primates at advanced stages of pregnancy, showing that the fraction of the combined cardiac output forwarded to the fetal brain was about 16% in normal conditions, which increased to 31% during a hypoxic insult [3, 4].

E. H. Andrade (✉) · E. Soto
Department of Obstetrics and Gynecology and Reproductive Sciences, University of Texas McGovern Medical School, University of Texas, Health Science Center at Houston (UTA Health), Houston, TX, USA
e-mail: Edgar.A.HernandezAndrade@uth.tmc.edu

17.2 Fetal Brain Circulation

The first Doppler studies on human fetal blood flow were done in the descending aorta [5–7], carotid [8, 9], and umbilical arteries [10]. A great advance was achieved when directional color Doppler was used for identification of fetal vascular territories, thus allowing visualization of the circle of Willis and of all major fetal cerebral arteries and a more reproducible location of the Doppler sample gate [11–15].

While most of the studies on fetal brain circulation have been performed in the middle cerebral artery (MCA) [16], other fetal brain arteries, i.e., the anterior [17, 18], and posterior cerebral arteries [19], the pericallosal [20], carotid [21, 22], and vertebral arteries [23, 24], have been also evaluated. Figueroa Diesel et al. [20] reported Doppler parameters from the middle, anterior, pericallosal, and posterior cerebral arteries in 55 normally grown and in 14 growth-restricted fetuses. There was a significant reduction in the pulsatility index of all major cerebral arteries in growth-restricted fetuses, suggesting a similar response in all cerebral arteries as part of the brain-sparing process. The fetal brain veins also showed changes in growth-restricted fetuses characterized by an increased prevalence of pulsations in the Vein of Galen and in the straight, transverse, and sagittal venous sinuses [25]. This increment in fetal brain veins pulsations was associated with a higher preva-

D. Maulik, C. C. Lees (eds.), *Doppler Ultrasound in Obstetrics and Gynecology*,
https://doi.org/10.1007/978-3-031-06189-9_17

lence of adverse perinatal outcomes [25–27]. Other researchers applied 2D and 3D power Doppler ultrasound showing dynamic changes in fetal brain blood flow perfusion according to the severity of growth restriction [28–32]. Yet, the standard for fetal brain vascular evaluation is the middle cerebral artery. Doppler assessment of the MCA significantly changed the clinical management of fetuses at risk of anemia due to red cell isoimmunization [33–35], fetal placental hemorrhage [36], or twin to twin transfusion syndrome [37] and in fetuses with growth restriction [38].

17.3 Fetal Size/Growth and Brain Circulation

Fetal growth implies change in size over time [39–43]. Abnormal fetal growth is the most frequent complication during pregnancy and is associated with increased prevalence of perinatal complications and perinatal mortality [44–49]. The standard criterion to define a small fetus is a biometry below a defined cutoff either <10th, <5th, or <3rd percentile for gestational age [50–54]. Recently, a consensus to define fetal growth restriction, including Doppler and biometry, has been proposed to differentiate between constitutionally small but normal fetuses and pathologic small fetuses with a higher risk of adverse outcomes [55]. Nevertheless, a clear differentiation is still not easy to achieve [54, 55]. The estimated fetal weight cutoff value to define a small or a normal size fetus might vary depending on the standard used for comparison. Several studies have been performed proposing biometric standards either combining data from a large number of pregnant women from different ethnicities [56–59], or by customized fetal growth standards taking into account maternal and fetal factors affecting the fetal size [60, 61]. The use of the appropriate standard might improve the definition of a normal or a small fetus; however, performing only one fetal biometric estimation during the second or third trimesters of pregnancy is not enough to clearly define normal/abnormal fetal growth. There is a need for alternative markers to identify small fetuses with growth restriction and with an increased risk for complications [41, 62–64]. The cerebroplacental ratio (CPR) might contribute to solve this clinical problem as it represents early hemodynamic changes in the placental and fetal cerebral circulations that may be considered as a manifestation of increased placental vascular resistance [65, 66].

Doppler velocimetry of the umbilical artery (UA) is a complimentary test in SGA fetuses to identify those at a higher risk of perinatal complications. An increased UA pulsatility index (PI), or absent/reverse UA end diastolic velocities have a significant association with adverse perinatal outcomes and perinatal mortality and can be used to define the optimal time for delivery. Brain vasodilation expressed as a reduced MCA-PI has been associated with low umbilical blood oxygen saturation in growth-restricted fetuses. Akalin-Sel et al. [67] performed umbilical cord blood sampling and Doppler velocimetry in 32 growth-restricted fetuses at 21–37 weeks of gestation. There was a significant association between reduced MCA-PI or reduced MCA-RI with low O_2 and increased CO_2 saturations in the umbilical blood. While severe brain vasodilation is a known manifestation of fetal hypoxia/asphyxia, several authors have also reported that a "back to" or "reversal to" normal values of the MCA-PI (vasoconstriction) also reflect advanced stages of hypoxia and a higher risk of mortality probably related to intracranial edema [68]. The available evidence supports the use of UA and MCA Doppler velocimetry in small for gestational age fetuses [53, 54]. Presence of abnormal Doppler findings, i.e., absent or reversed end diastolic UA blood velocities, severely reduced MCA-PI, or absence of diastolic velocities in the MCA, should be considered as strong manifestations of fetal deterioration. As a complementary test, the ratio between MCA-PI and UA-PI (CPR) might contribute to identify SGA fetuses who eventually will develop growth restriction and perinatal complications. As the MCA-PI is usually higher than the UA-PI, a normal CPR will always be above 1 at any gestational age (Fig. 17.1a). When the MCA-PI and the UA-PI

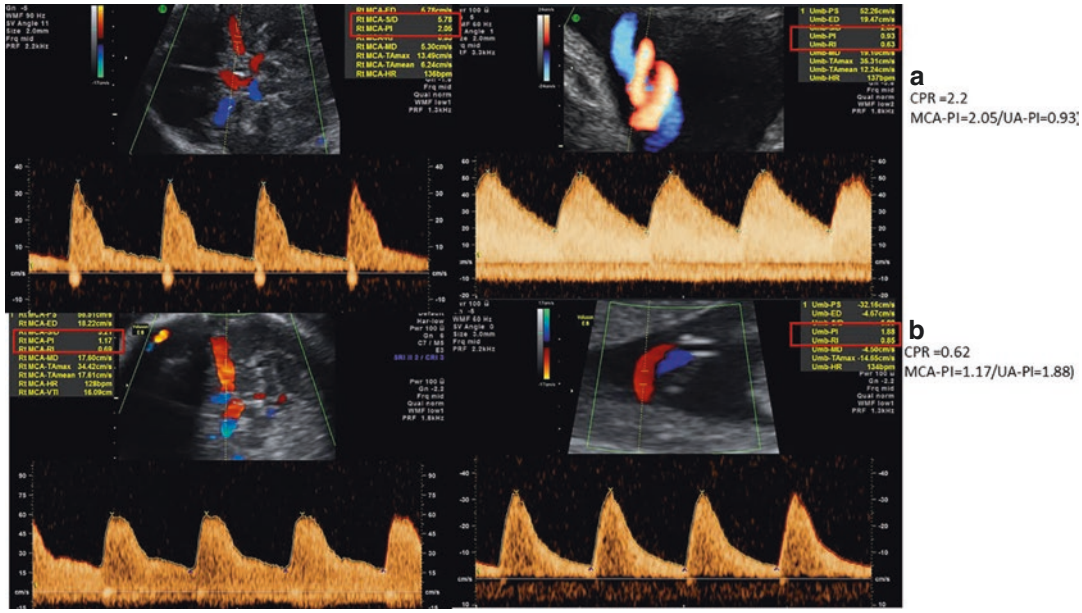

Fig. 17.1 Individual components of the cerebroplacental ratio (CPR): middle cerebral artery (MCA; left panels) and umbilical artery (UA; right panels). (**a**) Normal CPR, the MCA pulsatility index (PI) is higher than the UA-PI; (**b**) reduced CPR, the MCA-PI is lower than the UA-PI

are the same, the CPR is 1.0, and when the MCA-PI is lower than the UA-PI, the ratio is below 1.0 (Fig. 17.1b). A reduced CPR can be due to a low MCA-PI (reduced cerebral vascular resistance), or to an increased UA-PI (increased placental resistance), or both, and should be considered as a manifestation of fetal blood flow redistribution. Figueras et al. [69] reported that the CPR performs better than its two individual components (MCA-PI and UA-PI) for the prediction of low birthweight and perinatal complications in SGA fetuses. The authors concluded that SGA fetuses with a reduced CPR during the third trimester of pregnancy should be considered as late growth restriction.

17.4 Fetal Brain-Sparing and Brain Vasodilation

Initial stages of fetal hemodynamic blood flow redistribution can be identified by a reduced CPR, despite still having normal UA-PI and MCA-PI values. Brain vasodilation refers to a clearly reduced MCA-PI either <10, <5th percentiles, or <2 standard deviations from the normal mean for gestational age. Both, blood redistribution and brain vasodilation, are sequential steps of the same physiological response aiming to protect key fetal organs. Nevertheless, the general concept that fetal hemodynamic redistribution/brain vasodilation is a protective mechanism has been challenged by several authors. Roza et al. [70] reported that fetuses with brain-sparing are more likely to present neurobehavioral problems, suggesting that "brain-sparing" does not protect the brain but indicates an underlying pathology. Eixarch et al. [71] evaluated the neurodevelopment at 2 years of age of 125 children born small-for-gestational age with normal umbilical artery Doppler, either with or without brain vasodilation (MCA-PI <5th percentile). The results showed significant reduced abilities in communication and in solving problems in SGA newborns with brain vasodilation. On contrary, SGA neonates with no brain vasodilation did not show significant differences in neurodevelopment as compared to newborns with normal birthweight. In a systematic review by Meher et al., [72] including nine original studies, showed

that early SGA with brain vasodilation was associated with abnormal psychomotor development at 1 year of age, and that late-onset SGA fetuses with brain vasodilation had a higher prevalence of motor and state organizational problems and lower performance in communication and problem solving at 2 years of age. Monthieth et al. [73] reported a poorer neurological outcome in growth-restricted fetuses than in SGA newborns, and that growth-restricted fetuses with a reduced CPR (<1.0) had the poorest neurological outcome at 3 years of age. The abnormal neurodevelopment seems to persist at later scholar ages. In a study evaluating 77 children at 8–10 years of age who were growth-restricted and had Doppler velocimetry performed before birth, the results showed a significant association between increased UA-PI (>2 SD) (Odds ratios from 3.5 to 19.1) or a reduced CPR (Odds ratios from 4.2 to 28.1) with poor literacy and communications skills, and with the need for speech and language therapies [74].

17.5 Pioneering Studies on the Cerebroplacental Ratio

The cerebroplacental ratio (CPR) was originally reported by Arbeille et al. [75] by computing the ratio between the anterior cerebral artery PI (ACA-PI; ACA was technically easier to obtain than MCA due to the type of combined linear and Doppler ultrasound probes available at that time) and the UA-PI. The authors evaluated two groups of fetuses: (1) normally grown ($n = 40$), and small for gestational age ($n = 21$), six of them with gestational hypertension. Doppler evaluations started at 25 weeks of gestation and continued until the end of pregnancy. The results showed that in normally grown fetuses, the CPR was always >1.0 throughout pregnancy. Among SGA fetuses, 15/21 (71%) had normal birthweight and all have a CPR >1.0. In contrast, six fetuses (6/21; 29%) had low birthweight and all had a CPR ≤ 1.0. The same research group reported the CPR values in a larger group of patients comprised by 40 normal pregnancies and 29 women with gestational hypertension (12 of them with fetal growth restriction), and in 11 women with isolated fetal growth restriction [76]. Serial Doppler examinations were obtained from 15 to 40 weeks of gestation showing a CPR >1.0 throughout pregnancy in all normal fetuses. Among women with gestational hypertension ($n = 29$), 52% (15/29) had newborns with normal birthweights and all had a CPR >1.0; 14/29 (48%) patients had newborns with low birthweights, from them 12/14 (86%) had a CPR ≤1.0. Among fetuses with idiopathic fetal growth restriction, 8/11 (73%) had a CPR ≤1.0. The authors concluded that the CPR significantly contributed in the assessment of fetal hemodynamic changes and in the detection of fetal growth restriction. The same research group conducted an experimental study in lambs exploring hemodynamic changes in response to blood flow reductions in the fetal aorta and in the umbilical arteries [77]. The results showed: (1) significant changes in the CPR when a 70% reduction of the aortic blood flow was reached; (2) changes in the CPR were mainly associated to a reduction in the umbilical artery blood flow.

A different cutoff value to define a reduced CPR was proposed by Grammelini et al. [78] who evaluated the CPR in 90 fetuses, 45 normally grown, and 45 small for gestational age. Eighteen fetuses had a CPR ≤1.08, all were SGA (18/45; 40%) and 11 (11/18; 61%) had a cesarean section for a non-reassuring fetal heart rate. Fetuses with a CPR ≤1.08 had significantly lower pH values in the umbilical cord blood, lower Apgar scores, and higher prevalence of NICU admission than fetuses with a CPR >1.08. The authors concluded that a fixed value ≤1.08 is a practical approach to define a reduced CPR in the assessment of fetuses at risk of perinatal complications.

17.6 Normal Values of the Cerebroplacental Ratio

The normal distribution of UA-PI and MCA-PI values follows different patterns throughout gstation. While the UA-PI shows a linear reduction

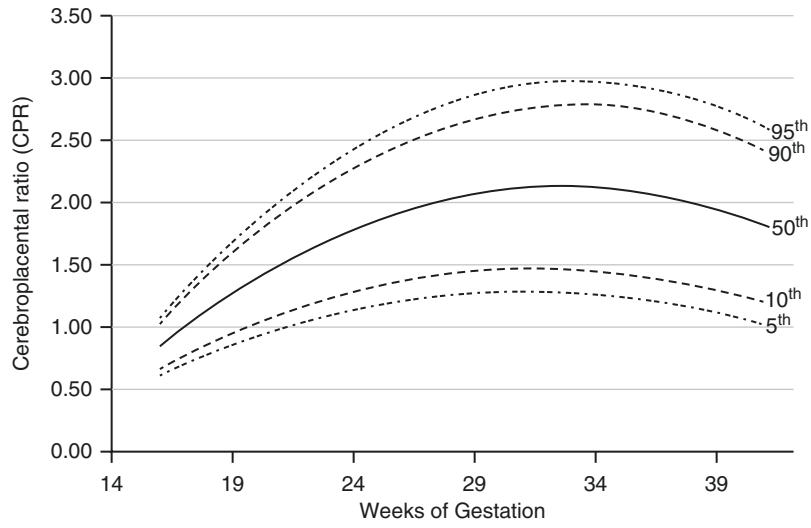

Fig. 17.2 Distribution of cerebroplacental ratio (CPR) values throughout pregnancy. (Modified from: Medina Castro N, Hernández Andrade E. et al. Normal reference values of the pulsatility index from the uterine middle cerebral and umbilical arteries during pregnancy. Ginecol Obstet Mex. 2006; 74: 509–15, and Ginecol Obstet Mex. 2006; 74: 376–82 [82, 83])

toward the end of pregnancy, the MCA shows a quadratic behavior, with increased PI values in the early third trimester as compared to those in the second and in late third trimesters [79–83]. The distribution of CPR values reflects those of the MCA-PI, with an increment toward the end of the second trimester and a further reduction in the early third trimesters of pregnancy (Fig. 17.2). CPR values for the 5th, 10th, 50th, 90th, and 95th percentiles throughout gestation are shown in Table 17.1.

Several authors reported a similar trend of CPR values throughout pregnancy; however, still a considerable variation among different charts can be observed. This variation is mainly caused by a poor methodology and quality in recording Doppler signals from the UA and MCA [80]. Fetal factors, such as fetal sex, can also affect the CPR values. Acharya et al. reported that female fetuses had significantly lower CPR z-scores than male fetuses in early pregnancy, and that after 33 weeks of gestation no differences were longer observed [81].

For practical purposes, the following CPR thresholds have been proposed to define a reduced CPR: ≤1.0, or ≤1.08. A fixed CPR value <1.0 is below the 5th percentile after 23 weeks of gestation, and a fixed CPR value <1.08 is below the 5th percentile from 25 weeks of gestation, both until the end of pregnancy. Nevertheless, using either fixed cutoff value, many fetuses with a

Table 17.1 Reference values of the cerebroplacental ratio (CPR) throughout pregnancy

GA	5th	10th	50th	90th	95th
16	0.77	0.84	1.10	1.36	1.43
17	0.79	0.86	1.12	1.38	1.45
18	0.79	0.87	1.18	1.49	1.57
19	0.82	0.91	1.20	1.49	1.58
20	0.89	0.98	1.27	1.56	1.65
21	0.83	0.95	1.36	1.77	1.89
22	0.95	1.05	1.41	1.77	1.87
23	1.02	1.14	1.56	1.98	2.10
24	1.04	1.18	1.68	2.18	2.32
25	1.15	1.29	1.79	2.29	2.43
26	1.19	1.33	1.86	2.39	2.53
27	1.25	1.41	1.97	2.53	2.69
28	1.27	1.46	2.11	2.76	2.95
29	1.32	1.50	2.14	2.78	2.96
30	1.32	1.51	2.19	2.87	3.06
31	1.37	1.55	2.19	2.83	3.01
32	1.40	1.59	2.27	2.95	3.14
33	1.34	1.54	2.23	2.92	3.12
34	1.28	1.49	2.23	2.97	3.18
35	1.26	1.46	2.15	2.84	3.04
36	1.28	1.47	2.14	2.81	3.00
37	1.12	1.33	2.06	2.79	3.00
38	1.23	1.39	1.95	2.51	2.67
39	1.09	1.26	1.86	2.46	2.63
40	1.00	1.18	1.81	2.44	2.62
41	0.92	1.09	1.69	2.29	2.46

Modified from: Medina Castro N, Hernández Andrade E. et al. Normal reference values of the pulsatility index from the uterine middle cerebral and umbilical arteries during pregnancy. Ginecol Obstet Mex. 2006; 74: 509–15 and Ginecol Obstet Mex. 2006; 74: 376–82 [82, 83]

CPR < 5th percentile between 25 and 38 weeks will be missed (Table 17.1). The use of multiples of median (MoM′ 0.6765) or percentiles (<10th or <5th) has been also proposed as they can be reliably used at any gestational age [84, 85]. Conditional percentiles (change over time) have been also suggested as reliable standards to define a normal/abnormal CPR [86].

17.7 Longitudinal Changes of the Cerebroplacental Ratio

Flatley et al. [87] analyzed whether changes in the CPR over time can predict a composite adverse perinatal outcome defined by: perinatal death, cesarean section for non-reassuring fetal heart rate, admission to the intensive care unit (ICU), severe respiratory distress, Apgar score <7 at 5 min, hypoglycemia, and acidosis at birth. They evaluated 1860 women having at least two CPR evaluations between 30 and 37 weeks of gestation. Univariate logistic regression showed a significant association between a reduced CPR, identified at any Doppler evaluation, and adverse outcomes, but not for changes over time in the CPR. The best prediction was obtained when the CPR was evaluated between 35 and 37 weeks of gestation.

17.8 Should the Cerebroplacental Ratio Be Evaluated in all Pregnant Women?

In a study evaluating 9772 women with singleton pregnancies having a Doppler evaluation within 2 weeks of delivery, the authors reported a reduced risk of operative delivery for fetal distress (CPR MoM: adjusted odds ratios [aOR], 0.67; 95% CI 0.52–0.87; $p = 0.003$) and of NICU admissions (aOR, 0.55; 95% CI, 0.33–0.92; $P = 0.02$) in presence of a normal CPR MoM [84]. Khalil et al. [88] studied 7944 fetuses with serial biometry and Doppler and reported a significant association between a low CPR and a further reduction in fetal abdominal growth velocity and with low birthweight. When low birthweight newborns were excluded from the analysis, the CPR also showed a significant association with reduced abdominal growth velocity and with a higher frequency of operative delivery for fetal distress. The authors concluded that a low CPR should be considered as a surrogate marker for fetal growth restriction and as a useful clinical tool to identify fetuses at a higher risk of perinatal complications.

Morales Rosello et al. [89] studied a large group of pregnant women having the CPR, MCA-PI, and UA-PI evaluated during the third trimester. Newborns were classified according to birthweight percentile and the Doppler parameters obtained before birth compared among birthweight groups. The results showed a continuous reduction in CPR values in relation to low birthweight groups ($p \leq 0.0001$). This association was also observed in fetuses considered as normally grown for gestational age, but had a low birthweight. Further, the same research group evaluated 2927 women with singleton pregnancies having a Doppler evaluation within 14 days of delivery [90]. Fetuses were classified in relation to birthweight as: small for gestational age (birthweight ≤10th percentile), adequate for gestational age (birthweight 10–90 percentiles), and large for gestational age (>90th percentile). The authors defined a low CPR as a MoM <0.6765. Among adequate for gestational age fetuses, a reduced CPR increased the prevalence of low pH values in the umbilical cord as compared to those with a normal CPR. According to the authors, these observations challenge the conventional concept that only SGA fetuses are at risk of placental insufficiency, fetal hypoxemia, and growth restriction and suggested that a reduced CPR might be considered a sign of placental insufficiency, even though the estimated fetal weight is still within normal range.

The association between fetal Doppler and NICU admissions in the general obstetric population was evaluated in 2518 patients with singleton pregnancies at 34 + 0 to 35 + 6 weeks of gestation [91]. The results showed that gesta-

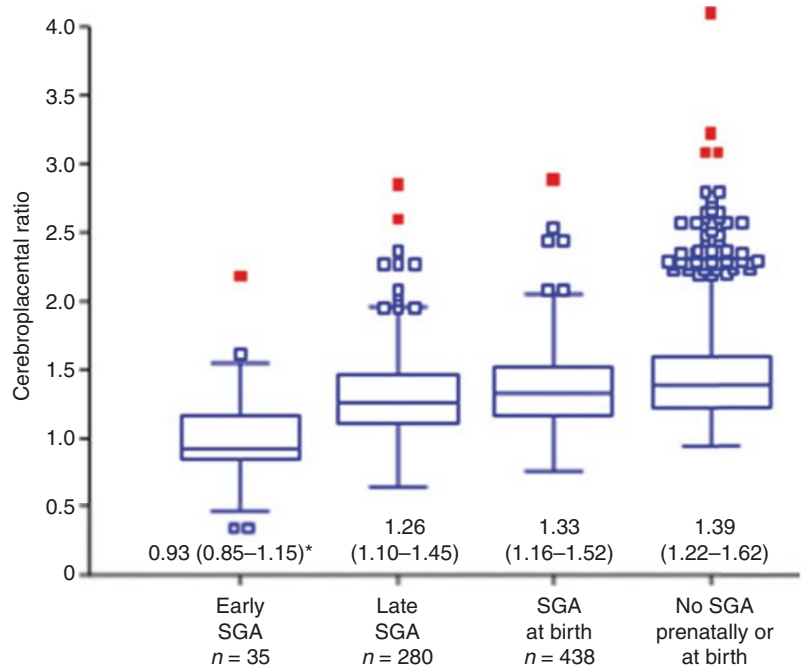

Fig. 17.3 Cerebroplacental ratio at 20–24 weeks in fetuses who later developed early small for gestational age (SGA; ≤32 weeks), late SGA (>32 weeks), SGA at birth (birthweight <10th per percentile), and in those with normal fetal growth and normal birthweight. Median and interquartile ranges are provided. (From Hernandez-Andrade E, et al. A Low Cerebroplacental Ratio at 20–24 Weeks of Gestation Can Predict Reduced Fetal Size Later in Pregnancy or at Birth. Fetal Diagn Ther. 2018; 44: 112–123 [94])

tional age at delivery and a reduced CPR before birth were significantly associated to NICU admission due to respiratory complications. The CPR was a better predictor for NICU admission than birthweight or EFW percentile, ($P < 0.001$). The rate of NICU admissions was almost three times higher in SGA neonates with a low CPR than in SGA neonates with a normal CPR (23% vs. 8%, respectively; $p < 0.05$).

Flatley et al. [92] compared EFW and CPR for prediction of adverse perinatal outcomes (umbilical cord pH <7.0, cord lactate ≥6 mmol/L, or base excess ≤−12 mmol/L, Apgar score ≤ 3 at 5 min NICU admission, and perinatal death) in 2425 low-risk pregnant women. The sensitivity for any of these outcomes for a reduced CPR was 23.3% which increased to 36.7% when combined with an EFW <10th percentile. The authors concluded that the prediction of adverse outcomes by a low CPR was improved when the EFW was <10th percentile. Similar findings have been reported by other authors [93].

In midterm pregnancies between 20 and 24 weeks of gestation, Hernandez-Andrade et al. [94] performed fetal biometry and Doppler examinations in 2986 pregnant women as part of the routine second trimester scan. The follow-up of these patients showed a prevalence of 1.2% (n = 35) of early fetal growth restriction, 9.6% (n = 288) of late fetal growth restriction, and 14.7% (n = 439) of small for gestational age at birth. The results showed that a CPR ≤5th percentile significantly predicted early and late fetal growth restriction and small for gestational age at birth (Fig. 17.3). The predictive performance of a reduced CPR was significantly higher among fetuses with an EFW <10th percentile (Table 17.2). The authors suggested that the CPR should be evaluated in all fetuses with fetal biometry <10th percentile at 20–24 weeks of gestation regardless the early gestational age.

A low predictive performance of a reduced CPR was reported by Akolekar et al. [95] when evaluated in all pregnant women. The authors studied 6178 pregnant women at 35 + 0 to 37 + 6 weeks of gestation and reported a 6–15% detection rate for adverse perinatal outcomes, i.e., cesarean section for fetal distress, arterial cord blood pH ≤7.0, venous cord blood pH ≤7.1, 5-min Apgar score < 7, and admission to the neo-

Table 17.2 Prediction performance of a reduced cerebroplacental ratio (CPR <5th percentile) at 20–24 weeks of gestation for fetal growth restriction and small for gestational age at birth

All fetuses at 20–24 weeks of gestation (*n* = 2986)								
	Sens	*Spec*	*PPV*	*NPV*	*LR+*	*LR−*	*Adj OR*	*RR*
Early FGR ≤32 weeks	54.0	93.0	9.1	99.4	8.2 (5.7–12.0)	0.5 (0.3–0.7)	13.9 (6.5–24.5)	15.4 (7.7–30.7)
Late FGR >32 weeks	10.8	93.1	14.1	90.9	1.6 (1.1–2.3)	0.9 (0.9–1.0)	1.6 (1.0–2.6)	1.5 (1.1–2.2)
SGA at birth	12.1	93.5	23.8	86.3	1.9 (1.4–2.6)	0.9 (0.9–1.0)	1.8 (1.2–2.6)	1.7 (1.3–2.3)
Fetuses with estimated fetal weight <10th percentile at 20–24 weeks (*n* = 186)								
	Sens	*Spec*	*PPV*	*NPV*	*LR+*	*LR−*	*Adj OR*	*RR*
Early FGR ≤32 weeks	69.2	93.2	47.4	97.2	10 (5.1–24)	0.3 (0.2–0.8)	41.6 (8.2–327.7)	16.8 (5.7–49.3)
Late FGR >32 weeks	7.0	86.4	15.8	71.8	0.5 (0.2–1.7)	1.1 (0.9–1.2)	0.4 (0.1–1.5)	06 (0.2–1.6)
SGA at birth	20.6	93.9	68.4	64.7	3.4 (1.4–8.4)	0.8 (0.7–1.0)	3.0 (1.0–10.1)	1.9 (1.0–3.5)

FGR (estimated fetal weight <10th percentile) SGA, small for gestational age at birth (birthweight <10th percentile). Adjusted for maternal age, race, nulliparity, smoking, alcohol use, drug use, prepregnancy body mass index, and mean arterial blood pressure

Sens sensitivity, *Spec* specificity, *PPV* positive predictive value, *NPV* negative predictive value, *LR* likelihood ratio, *Adj* adjusted, *OR* odds ratio, *RR* relative risk

From Hernandez-Andrade E, et al. A Low Cerebroplacental Ratio at 20–24 Weeks of Gestation Can Predict Reduced Fetal Size Later in Pregnancy or at Birth. Fetal Diagn Ther. 2018; 44: 112–123 [94]

natal intensive care unit (NICU), for a reduced CPR. The prediction improved to 14–50% when the CPR was obtained within 2 weeks of delivery. Nevertheless, the authors concluded that the CPR might contribute in the identification of small for gestational age fetuses at a higher risk of complications. Similar results were obtained by Bakalis et al. [96] in 30,780 singleton pregnancies at 30–34 weeks of gestation. The authors reported that despite the low prediction for adverse perinatal outcomes, the CPR significantly contributed in the identification of newborns with low birthweight. The association between a reduced CPR and low birthweight was improved when the CPR was obtained within 2 weeks of delivery. A reduced CPR also showed a significant contribution in the identification of fetuses at risk of low umbilical cord pH values and NICU admissions, but not for perinatal mortality, cesarean section for fetal distress, or low Apgar scores (<7). The conclusion of this study was that, a reduced CPR has a poor prediction for adverse outcomes in the general obstetric population, and it is unlikely to change the clinical management.

17.9 Can a Reduced Cerebroplacental Ratio Predict an Abnormal Fetal Heart Rate During Labor?

Liu et al. [97] studied 476 low-risk pregnant women with singleton pregnancies between 37 and 42 weeks of gestation who had a Doppler evaluation within 1 week of delivery. The association between CPR values and abnormal fetal heart rate (FHR) during labor was analyzed. Fetuses with Category III FHR traces had a significantly lower CPR and higher prevalence of perinatal complications than fetuses with Category II and Category I FHR traces. The association between a reduced CPR and Category III FHR was: (OR) 2.16 (95% CI, 0.76–3.01), and with FHR Categories II and I were: OR, 1.98

(95% CI, 0.67–3.11), and OR, 1.13 (95% CI, 0.61–2.85), respectively. The CPR showed an ROC AUC of 0.87 for prediction of FHR category III tracings. The optimal discriminatory CPR value was 1.23, with 63.4% sensitivity and 9.9% false-positive rate. In a multicenter observational study including 562 low-risk pregnant women at early stages of labor**,** a reduced CPR MoM (corresponding to the 10th percentile) increased by threefold the rate of cesarean section for non-reassuring fetal heart rate [98]. Nevertheless, the authors concluded that the CPR is a poor predictor for adverse outcomes in low-risk pregnant women. A recent prospective observational study including 1902 women with singleton pregnancies ≥37 weeks of gestation with fetal Doppler assessment obtained within 24 h of induction of labor reported that a CPR <10th percentile was associated with increased risk of cesarean section for fetal distress and with a higher prevalence of adverse neonatal outcomes. However, the screening performance of the CPR for such adverse outcomes was poor. The study concludes that an abnormal CPR prior to induction may not be able to clearly identify pregnant women at high risk of developing fetal distress during labor [99]. Contrary to these studies, Dehaene et al. in normal term fetuses reported no association between a reduced CPR and abnormal perinatal outcomes and with abnormal fetal heart tracings during labor [100].

The association between a reduced CPR and abnormal fetal heart during labor has been mainly observed in SGA fetuses. Cruz-Martinez et al. [101] studied 210 SGA and 210 normally grown fetuses to evaluate if the CPR obtained before induction of labor could predict cesarean delivery for fetal distress. The rates of cesarean section were: 4.8% (9/210) among normally grown fetuses, and 29% (60/210; $p < 0.001$) among SGA fetuses. In normally grown fetuses, no significant prediction for cesarean section was observed for a low CPR (<5th percentile). In SGA fetuses, despite not having signs of brain vasodilation (normal CPR, normal MCA, and normal perfusion), there was a significant association with cesarean section for fetal distress (OR 5.1; 95% CI, 3.27–12.7), but no for neonatal acidosis, as compared to normally grow fetuses. However, among SGA fetuses with a reduced CPR, the OR for cesarean section for fetal distress increased to 10.3 (95% CI, 3.22–52.8), and for neonatal acidosis OR 5.0 (95% CI, 1.06–46.9) as compared to normally grown fetuses. Among SGA fetuses, those with a reduced MCA-PI had a 67.7% prevalence of cesarean section due to fetal distress; no further improvement by a reduced CPR was observed. However, among SGA fetuses with normal MCA-PI, those with a reduced CPR had a 51.4% rate of cesarean section for fetal distress as compared to 27.5% among SGA fetuses with normal MCA and normal CPR. The authors concluded that the CPR can contribute in the identification of SGA fetuses at a higher risk of cesarean delivery for fetal distress during labor. Similar results were reported by Figueras et al. [102] in a cohort of 509 SGA fetuses undergoing trial of labor. A CPR <5th percentile and an EFW <3rd percentile had 82% sensitivity, 47.7% specificity, 36.2% and 88.6% positive and negative predictive values, and 1.58 positive, and 0.36 negative likelihood ratios for cesarean delivery due to fetal distress during labor.

Based on current evidence, it can be concluded that despite a significant association with cesarean section for fetal distress during labor and for adverse neonatal outcomes, the predictive value of a reduced CPR in the general obstetric population is poor. There is not enough evidence to suggest that all normally grown fetuses should have a CPR evaluation during the third trimester of pregnancy, or that clinical decisions should be taken in presence of an isolated low CPR [103].

17.10 The Cerebroplacental Ratio in Fetal Growth Restriction

Bahado Singh et al. [104] evaluated the CPR in 203 fetuses referred for the suspicion of intrauterine growth restriction and in 83 normally grown fetuses. Abnormal outcomes were consid-

Table 17.3 Prediction of performance of a CPR <0.5 MoMs for adverse perinatal outcomes

Outcome	Sensitivity	Specificity	PPV	NPV
Birthweight <10th percentile	47.0	90	95	43
Birthweight <5th percentile	42.0	90	83	62
Birthweight <10th percentile and complications	63.0	90	81	77
Birthweight <5th percentile and complications	51.5	90	60	84
Complications irrespective of birthweight	43.5	90	91	45

Complications Apgar score <7 at 5′, Cesarean section for non-reassuring fetal heart rate admission to the NICU, hypoglycemia, and polycythemia

Modified from: Bahado-Singh RO, et al. The Doppler cerebroplacental ratio and perinatal outcome in intrauterine growth restriction. Am J Obstet Gynecol. 1999; 180: 750–6 [104]

ered as: birth weight <10th percentile, perinatal death, cesarean section for fetal distress, meconium staining of the amniotic fluid, 5-min Apgar score <7, hypoglycemia, polycythemia, and NICU admission. The results showed that SGA fetuses, particularly before 34 weeks of gestation, had significantly lower CPR values than normally grown fetuses, and among SGA fetuses presenting adverse outcomes, the CPR was significantly lower than SGA newborns with no perinatal complications (Table 17.3). The study concluded that among SGA fetuses, the CPR predicted better perinatal complications than umbilical artery Doppler, particularly when the CPR was obtained <34 weeks of gestation and within 3 weeks from delivery.

Flood et al. [105], as part of the PORTO (Prospective Observational Trial to Optimize Pediatric Health in IUGR fetuses) study, reported a 16.5% (146/881) prevalence of a reduced CPR (≤1.0) among 881 small for gestational age fetuses evaluated at a median gestational age 33 weeks. In SGA fetuses, a reduced CPR increased by 11 fold the risk of adverse perinatal outcomes, i.e., intraventricular hemorrhage, periventricular leukomalacia, hypoxic ischemic encephalopathy, necrotizing enterocolitis, sepsis, and death, as compared to SGA fetuses with a normal CPR. The authors reported a similar predictive performance of different cutoff values to define a low CPR: CPR <1.0, 66% sensitivity and 85% specificity; CPR <1.08, 73% sensitivity and 80% specificity; CPR <5th percentile, 80% sensitivity and 60% for adverse perinatal outcomes.

Conde Agudelo et al. [106] performed a systematic review and meta-analysis on the predictive performance of a reduced CPR for abnormal perinatal outcomes in growth-restricted fetuses. The authors included 22 studies and 4301 women with singleton pregnancies. The definition of a low CPR was ≤1.08 or <5th percentile. The results showed that a reduced CPR had a moderate to high prediction for perinatal mortality with a pooled sensitivity of 93%, and pooled specificity of 76%; and a low predictive performance for cesarean delivery for non-reassuring fetal heart rate, Apgar score <7 at 5 min, NICU admission, neonatal acidosis, and the need of mechanical ventilation (Table 17.4). The authors mentioned that despite the significant prediction of perinatal mortality by a reduced CPR, caution should be taken as most of the studies included in this review did not blind the CPR results to the clinicians, thus increasing the risk of bias.

The progression of Doppler anomalies in late SGA fetuses was described by Oros et al. [107] in 171 SGA fetuses at 30–36 weeks of gestation. Serial Doppler examinations were performed, with the last obtained within 7 days of delivery. The authors reported a significant increment in the frequency of reduced CPR (<5th percentile) from 7% in the first Doppler evaluation to 22.8% in the last ultrasound scan. A higher frequency of abnormal CPR values over time were observed as compared to the MCA, UA, or uterine arteries. Normalization of the CPR values were reported by Monteith et al. [108] in 87 SGA fetuses with a reduced CPR. Forty five fetuses (45/87; 52%) remained with an abnormal CPR until the last Doppler evaluation, and ten (10/45 (22%) had an adverse perinatal outcome. Forty two fetuses

Table 17.4 Prediction of adverse outcomes and perinatal outcome by a CPR <1.0 in growth-restricted fetuses

	Pooled sensitivity	Pooled specificity	LR+ (95% CI)	LR− (95% CI)
Perinatal death	93	76	3.9 (3.4–4.5)	0.09 (0.0–0.3)
Any adverse outcome	57	77	2.5 (2.3–2.8)	0.6 (05–0.6)
Cesarean section for non-reassuring FHR	59	74	2.3 (2.0–2.6)	0.6 (0.5-0.6)
Apgar score <7 at 5 in	54	72	1.9 (1.5–2.4)	0.6 (0.5–0.8)
NICU admission	45	79	2.2 (1.9–2.5)	0.7 (0.6–0.8)
Neonatal acidosis	48	70	1.6 (1.3–2.0)	0.7 (0.6–0.9)
Neonatal morbidity other than brain lesion	78	33	1.2 (1.0–1.3)	0.7 (0.4–1.1)
Mechanical ventilation	90	39	1.5 (1.2–1.7)	0.3 (0.1–0.7)
SGA at birth	43	94	7.4 (2.5–22.4)	0.6 (0.5–0.7)

SGA small for gestational age, *NICU* neonatal intensive care unit, *LR* likelihood ratio

From: Conde-Agudelo A et al. Predictive accuracy of cerebroplacental ratio for adverse perinatal and neurodevelopmental outcomes in suspected fetal growth restriction: systematic review and meta-analysis. Ultrasound Obstet Gynecol. 2018; 52: 430–441 [106]

(42/87; 48%) showed a normalized CPR on serial examinations and two (2/42; 5%) had an adverse perinatal outcome (χ^2 5.58 $p = 0.01$). Fetuses with a normalized CPR delivered at later weeks of gestation than those with a constantly reduced CPR (36.5 vs. 33.4 weeks, respectively; $p = 0.001$). Contrary to the "back to normal" values in the MCA usually associated to a higher risk of complications, the reported "back to normal" values of the CPR seemed to improve the perinatal outcome.

17.11 The Cerebroplacental Ratio in Other High Risk Conditions

Khalil et al. [109] evaluated 2812 pregnant women undergoing ultrasound and Doppler examination during the third trimester of pregnancy for various indications including: suspected fetal growth restriction, reduced fetal movements, history of a SGA or a large-for-gestational-age newborn, high mid-trimester uterine artery Doppler, and gestational diabetes. Stillbirth ($n = 10$) was defined as fetal death after 24 weeks of gestation, and perinatal mortality as that occurring from 24 weeks of gestation until 28 days after delivery ($n = 18$). A reduced CPR was defined as ≤0.6765 MoM's corresponding to the 5th percentile for gestational age. The results showed that a CPR >0.6765 MoM's reduced the risk of stillbirth (unadjusted OR 0.004, 95% CI, 0.00–0.035; $p < 0.001$; adjusted for EFW, OR 0.003, 95% CI, 0.00–0.11; $p < 0.003$) and perinatal mortality (OR, 0.003, 95% CI, 0.00–0.14; $p < 0.001$, adjusted for EFW OR, 0.001 95% CI, 0.00–0.03; <0.001) as compared to fetuses with a CPR ≤0.6765 MoM's. The combination of reduced EFW, reduced CPR, and increased uterine arteries PI showed an ROC AUC of 0.86, 77.8% sensitivity, 14.3% false-positive rate, likelihood ratio positive 5.42, and a likelihood ratio negative 0.26, for perinatal mortality. Nevertheless, due to the low prevalence of perinatal mortality, the positive predictive value of a reduced CPR was still low.

In pregnancies at ≥41 weeks of gestation, no differences in the prevalence of a CPR <5th percentile have been observed between fetuses presenting adverse outcomes and those with normal perinatal results [110]. The CPR does not contribute in the identification of fetuses who might benefit from induction of labor ≥41 weeks of gestation.

A recent systematic review and meta-analysis compared the prognostic accuracies of a reduced CPR and/or a reduced MCA-PI, against UA-PI in predicting adverse perinatal outcome in high risk pregnant women. Over 100 studies were included for this analysis. The authors concluded that the

CPR outperformed UA Doppler in the prediction of composite adverse outcome ($P < 0.001$) and emergency delivery for fetal distress ($p = 0.003$). This lead to the conclusion that the CPR and MCA-PI can improve the accuracy of UA Doppler assessment in the prediction of adverse perinatal outcomes [111].

A reduced CPR has been reported as a predictor of cesarean delivery for fetal distress and NICU admission in pregnancies complicated with preeclampsia [112, 113]; other researchers suggested that a low CPR (<1.08) may be a predictor of preeclampsia in pregnancies complicated with fetal growth restriction. In fact, mothers of fetuses with a reduced CPR were four times more likely to develop severe preeclampsia and to deliver at earlier gestational age than mothers having fetuses with a normal CPR [114]. Other authors reported that the CPR may be abnormal between 28 and 32 weeks in patients with chronic hypertension who subsequently developed preeclampsia [115].

The association between reduced fetal movements and reduced CPR was reported by Binder et al. [116] in 4500 pregnant women admitted due to reduced fetal movements and in 1527 pregnant women referring normal fetal movements. Women with reduced fetal movements had a significantly lower CPR MoM and lower MCA-PI MoM values than women with normal fetal movements. The authors suggested that reduced movements in fetuses with a low CPR might be a clinical manifestation of fetal hypoxemia.

17.12 The Cerebroplacental Ratio and Maternal Serum Biomarkers

The combination of Doppler parameters with maternal serum biomarkers can improve the identification of pregnant women at risk of adverse outcomes [117]. Miranda et al. [118] proposed a prediction model for adverse outcomes (stillbirth, emergency operative delivery due to non-reassuring fetal status, low APGAR scores, or neonatal metabolic acidosis), including a priori risk (chronic hypertension and socioeconomic status), EFW percentile, UA-PI, CPR, and maternal serum concentrations of estriol and placental growth factor (PlGF) with a ROC AUC of 0.86 (95% CI, 0.80–0.92), 62% sensitivity, and 10% false-positive rate for adverse outcomes. Further studies are needed to evaluate the clinical value of maternal serum biomarkers and the CPR for predictions of adverse perinatal outcomes.

17.13 Conclusion

The available evidence shows that small for gestational age fetuses with a reduced CPR have an increased risk of perinatal mortality, abnormal perinatal outcomes, cesarean section for fetal distress, and abnormal neurodevelopment, despite still having a normal MCA-PI and/or a normal UA-PI. These fetuses should be considered as growth-restricted and followed closely with serial ultrasound and Doppler evaluations for identification of signs of fetal deterioration.

Several studies have shown that normal size fetuses with a reduced CPR have a higher risk to develop growth restriction, low birthweight, and abnormal outcomes, i.e., low pH values in the umbilical artery, low Apgar scores, and cesarean section for fetal distress. However, there is no robust evidence supporting that the CPR must be evaluated in all low-risk pregnant women, or that the clinical management should be modified in presence of an isolated reduced CPR [119].

Key Points

- A reduced cerebroplacental ratio (CPR) can be defined as that ≤1.0 or ≤1.08, or ≤5th percentile per gestational age, all having a similar predictive performance for adverse perinatal outcomes.
- Alternative definitions of a reduced CPR are a ≤0.6976 MoMs, and reduced conditional percentiles.
- In SGA fetuses, a reduced CPR should be considered as an initial manifestation of blood flow redistribution and a significant risk factor for perinatal mortality, adverse perinatal

outcomes, cesarean section for fetal distress, and abnormal neurodevelopment.
- The prediction performance of the CPR for adverse outcome in SGA fetuses is higher <34 weeks of gestation and when it is obtained within 2 weeks from delivery.
- In low-risk pregnancies, a reduced CPR increases the risk for cesarean section due to fetal distress during labor and for adverse perinatal outcomes; however, there is no robust evidence showing a clear benefit in evaluating the CPR in all pregnant women in the third trimester of pregnancy.
- SGA fetuses with a normalized CPR have a better perinatal outcome and a later gestational age at delivery.

References

1. Iwamoto HS, Teitel D, Rudolph AM. Effects of birth-related events on blood flow distribution. Pediatr Res. 1987;22:634–40.
2. Sidi D, Kuipers JR, Teitel D, Heymann MA, Rudolph AM. Developmental changes in oxygenation and circulatory responses to hypoxemia in lambs. Am J Physiol. 1983;245:H674–82.
3. Behrman RE, Lees MH. Organ blood flows of the fetal, newborn and adult rhesus monkey: a comparative study. Biol Neonate. 1971;18:330–40.
4. Behrman RE, Lees MH, Peterson EN, De Lannoy CW, Seeds AE. Distribution of the circulation in the normal and asphyxiated fetal primate. Am J Obstet Gynecol. 1970;108(6):956–69.
5. Eik-Nes SH, Marsal K, Brubakk AO, Kristofferson K, Ulstein M. Ultrasonic measurement of human fetal blood flow. J Biomed Eng. 1982;4(1):28–36.
6. Eik-Nes SH, Marsál K, Kristoffersen K. Methodology and basic problems related to blood flow studies in the human fetus. Ultrasound Med Biol. 1984;10:329–37.
7. Marsál K, Lindblad A, Lingman G, Eik-Nes SH. Blood flow in the fetal descending aorta; intrinsic factors affecting fetal blood flow, i.e. fetal breathing movements and cardiac arrhythmia. Ultrasound Med Biol. 1984;10:339–48.
8. Arabin B, Bergmann PL, Saling E. Pathophysiologic and clinical aspects of measuring blood flow in uteroplacental vessels, the umbilical artery, the fetal aorta and the fetal common carotid artery. Geburtshilfe Frauenheilkd. 1987;47:587–93.
9. Bilardo CM, Campbell S, Nicolaides KH. Mean blood velocities and flow impedance in the fetal descending thoracic aortic and common carotid artery in normal pregnancy. Early Hum Dev. 1988;18:213–21.
10. FitzGerald DE, Drumm JE. Non-invasive measurement of human fetal circulation using ultrasound: a new method. Br Med J. 1977;2:1450–1.
11. Wladimiroff JW, Tonge HM, Stewart PA. Doppler ultrasound assessment of cerebral blood flow in the human fetus. Br J Obstet Gynaecol. 1986;93:471–5.
12. Wladimiroff JW, van Bel F. Fetal and neonatal cerebral blood flow. Semin Perinatol. 1987;11:335–46.
13. van den Wijngaard JA, Groenenberg IA, Wladimiroff JW, Hop WC. Cerebral Doppler ultrasound of the human fetus. Br J Obstet Gynaecol. 1989;96:845–9.
14. Wladimiroff JW, Heydanus R, Stewart PA. Doppler colour flow mapping of fetal intracerebral arteries in the presence of central nervous system anomalies. Ultrasound Med Biol. 1993;19:355–7.
15. Noordam MJ, Heydanus R, Hop WC, Hoekstra FM, Wladimiroff JW. Doppler colour flow imaging of fetal intracerebral arteries and umbilical artery in the small for gestational age fetus. Br J Obstet Gynaecol. 1994;101:504–8.
16. Romero R, Hernandez-Andrade E. Doppler of the middle cerebral artery for the assessment of fetal well-being. Am J Obstet Gynecol. 2015;213:1.
17. Benavides-Serralde JA, Hernández-Andrade E, Figueroa-Diesel H, Oros D, Feria LA, Scheier M, Figueras F, Gratacós E. Reference values for Doppler parameters of the fetal anterior cerebral artery throughout gestation. Gynecol Obstet Invest. 2010;69:33–9.
18. Dubiel M, Gunnarsson GO, Gudmundsson S. Blood redistribution in the fetal brain during chronic hypoxia. Ultrasound Obstet Gynecol. 2002;20:117–21.
19. Benavides-Serralde JA, Hernandez-Andrade E, Cruz-Martinez R, Cruz-Lemini M, Scheier M, Figueras F, Mancilla J, Gratacos E. Doppler evaluation of the posterior cerebral artery in normally grown and growth restricted fetuses. Prenat Diagn. 2014;34:115–20.
20. Figueroa-Diesel H, Hernandez-Andrade E, Acosta-Rojas R, Cabero L, Gratacos E. Doppler changes in the main fetal brain arteries at different stages of hemodynamic adaptation in severe intrauterine growth restriction. Ultrasound Obstet Gynecol. 2007;30:297–302.
21. Wladimiroff JW, vd Wijngaard JA, Degani S, Noordam MJ, van Eyck J, Tonge HM. Cerebral and umbilical arterial blood flow velocity waveforms in normal and growth-retarded pregnancies. Obstet Gynecol. 1987;69:705–9.
22. van den Wijngaard JA, van Eyck J, Noordam MJ, Wladimiroff JW, van Strik R. The Doppler flow velocity waveform in the fetal internal carotid artery with respect to fetal behavioural states. A longitudinal study. Biol Neonate. 1988;53:274–8.

23. Morales-Roselló J. Doppler sonography of normal fetal vertebral and internal carotid arteries during pregnancy. J Clin Ultrasound. 2002;30:257–63.
24. Roselló JM, Llorens NP. Fetal vertebral artery Doppler reference values at 19-41 weeks of gestation. Fetal Diagn Ther. 2012;32:209–15.
25. Figueroa-Diesel H, Hernandez-Andrade E, Benavides-Serralde A, Crispi F, Acosta-Rojas R, Cabero L, Gratacos E. Cerebral venous blood flow in growth restricted fetuses with an abnormal blood flow in the umbilical artery before 32 weeks of gestation. Eur J Obstet Gynecol Reprod Biol. 2008;140:201–5.
26. Dubiel M, Breborowicz GH, Laurini R, Gudmundsson S. Blood velocity in the fetal vein of Galen and the outcome of high-risk pregnancy. Eur J Obstet Gynecol Reprod Biol. 2001;99:14–8.
27. Cheema R, Dubiel M, Breborowicz G, Gudmundsson S. Fetal cerebral venous Doppler velocimetry in normal and high-risk pregnancy. Ultrasound Obstet Gynecol. 2004;24:147–53.
28. Hernandez-Andrade E, Jansson T, Figueroa-Diesel H, Rangel-Nava H, Acosta-Rojas R, Gratacós E. Evaluation of fetal regional cerebral blood perfusion using power Doppler ultrasound and the estimation of fractional moving blood volume. Ultrasound Obstet Gynecol. 2007;29:556–61.
29. Hernandez-Andrade E, Figueroa-Diesel H, Jansson T, Rangel-Nava H, Gratacos E. Changes in regional fetal cerebral blood flow perfusion in relation to hemodynamic deterioration in severely growth-restricted fetuses. Ultrasound Obstet Gynecol. 2008;32:71–6.
30. Yadav BK, Hernandez-Andrade E, Krishnamurthy U, Buch S, Jella P, Trifan A, Yeo L, Hassan SS, Haacke EM, Romero R, Neelavalli J. Dual-imaging modality approach to evaluate cerebral hemodynamics in growth-restricted fetuses: oxygenation and perfusion. Fetal Diagn Ther. 2020;47:145–55. https://doi.org/10.1159/000500954.
31. Cruz-Martinez R, Figueras F, Hernandez-Andrade E, Benavides-Serralde A, Gratacos E. Normal reference ranges of fetal regional cerebral blood perfusion as measured by fractional moving blood volume. Ultrasound Obstet Gynecol. 2011;37:196–201.
32. Heck S, Schindler T, Smyth J, Lui K, Meriki N, Welsh A. Evaluation of neonatal regional cerebral perfusion using power Doppler and the index fractional moving blood volume. Neonatology. 2012;101:254–9.
33. Mari G, Deter RL, Carpenter RL, Rahman F, Zimmerman R, Moise KJ Jr, Dorman KF, Ludomirsky A, Gonzalez R, Gomez R, Oz U, Detti L, Copel JA, Bahado-Singh R, Berry S, Martinez-Poyer J, Blackwell SC. Noninvasive diagnosis by Doppler ultrasonography of fetal anemia due to maternal red-cell alloimmunization. Collaborative Group for Doppler Assessment of the Blood Velocity in anemic fetuses. N Engl J Med. 2000;342(1):9–14.
34. Scheier M, Hernandez-Andrade E, Carmo A, Dezerega V, Nicolaides KH. Prediction of fetal anemia in rhesus disease by measurement of fetal middle cerebral artery peak systolic velocity. Ultrasound Obstet Gynecol. 2004;23:432–6.
35. Scheier M, Hernandez-Andrade E, Fonseca EB, Nicolaides KH. Prediction of severe fetal anemia in red blood cell alloimmunization after previous intrauterine transfusions. Am J Obstet Gynecol. 2006;195:1550–6.
36. Cosmi E, Rampon M, Saccardi C, Zanardo V, Litta P. Middle cerebral artery peak systolic velocity in the diagnosis of fetomaternal hemorrhage. Int J Gynaecol Obstet. 2012;117:128–30.
37. Robyr R, Lewi L, Salomon LJ, Yamamoto M, Bernard JP, Deprest J, Ville Y. Prevalence and management of late fetal complications following successful selective laser coagulation of chorionic plate anastomoses in twin-to-twin transfusion syndrome. Am J Obstet Gynecol. 2006;194:796–803.
38. Mari G, Hanif F, Kruger M, Cosmi E, Santolaya-Forgas J, Treadwell MC. Middle cerebral artery peak systolic velocity: a new Doppler parameter in the assessment of growth-restricted fetuses. Ultrasound Obstet Gynecol. 2007;29:310–6.
39. Grantz KL, Kim S, Grobman WA, Newman R, Owen J, Skupski D, Grewal J, Chien EK, Wing DA, Wapner RJ, Ranzini AC, Nageotte MP, Hinkle SN, Pugh S, Li H, Fuchs K, Hediger M, Buck Louis GM, Albert PS. Fetal growth velocity: the NICHD fetal growth studies. Am J Obstet Gynecol. 2018;219(285.e1):–285.e36.
40. Hiersch L, Melamed N. Fetal growth velocity and body proportion in the assessment of growth. Am J Obstet Gynecol. 2018;218:S700–S711.e1.
41. Romero R, Deter R. Should serial fetal biometry be used in all pregnancies? Lancet. 2015;386(10008):2038–40.
42. Sovio U, White IR, Dacey A, Pasupathy D, Smith GCS. Screening for fetal growth restriction with universal third trimester ultrasonography in nulliparous women in the Pregnancy Outcome Prediction (POP) study: a prospective cohort study. Lancet. 2015;386:2089–97.
43. Deter RL, Lee W, Kingdom J, Romero R. Second trimester growth velocities: assessment of fetal growth potential in SGA singletons. J Matern Fetal Neonatal Med. 2019;32:939–46.
44. Maršál K. Fetal growth surveillance - current guidelines, practices and challenges. J Perinat Med. 2017;45:775–7.
45. Demicheva E, Crispi F. Long-term follow-up of intrauterine growth restriction: cardiovascular disorders. Fetal Diagn Ther. 2014;36:143–53.
46. Tarca AL, Hernandez-Andrade E, Ahn H, Garcia M, Xu Z, Korzeniewski SJ, Saker H, Chaiworapongsa T, Hassan SS, Yeo L, Romero R. Single and serial fetal biometry to detect preterm and term small- and large-for-gestational-age neonates: a longitudinal cohort study. PLoS One. 2016;11:e0164161.

47. Kabiri D, Romero R, Gudicha DW, Hernandez-Andrade E, Pacora P, Benshalom-Tirosh N, Tirosh D, Yeo L, Erez O, Hassan SS, Tarca AL. Prediction of adverse perinatal outcomes by fetal biometry: a comparison of customized and population-based standards. Ultrasound Obstet Gynecol. 2020;55(2):177–88. https://doi.org/10.1002/uog.20299. [Epub ahead of print].
48. Unterscheider J, O'Donoghue K, Daly S, Geary MP, Kennelly MM, McAuliffe FM, Hunter A, Morrison JJ, Burke G, Dicker P, Tully EC, Malone FD. Fetal growth restriction and the risk of perinatal mortality-case studies from the multicentre PORTO study. BMC Pregnancy Childbirth. 2014;14:63.
49. Vollmer B, Edmonds CJ. School age neurological and cognitive outcomes of fetal growth retardation or small for gestational age birth weight. Front Endocrinol (Lausanne). 2019;10:186.
50. Gordijn SJ, Beune IM, Ganzevoort W. Building consensus and standards in fetal growth restriction studies. Best Pract Res Clin Obstet Gynaecol. 2018;49:117–26.
51. ACOG Practice Bulletin No. 204: fetal growth restriction. Obstet Gynecol. 2019;133:e97–e109.
52. Figueras F, Caradeux J, Crispi F, Eixarch E, Peguero A, Gratacos E. Diagnosis and surveillance of late-onset fetal growth restriction. Am J Obstet Gynecol. 2018;218:S790–S802.e1.
53. Figueras F, Gratacos E. An integrated approach to fetal growth restriction. Best Pract Res Clin Obstet Gynaecol. 2017;38:48–58.
54. Salomon LJ, Alfirevic Z, Da Silva Costa F, Deter RL, Figueras F, Ghi T, Glanc P, Khalil A, Lee W, Napolitano R, Papageorghiou A, Sotiriadis A, Stirnemann J, Toi A, Yeo G. ISUOG practice guidelines: ultrasound assessment of fetal biometry and growth. Ultrasound Obstet Gynecol. 2019;53:715–23.
55. Gordijn SJ, Beune IM, Thilaganathan B, Papageorghiou A, Baschat AA, Baker PN, Silver RM, Wynia K, Ganzevoort W. Consensus definition of fetal growth restriction: a Delphi procedure. Ultrasound Obstet Gynecol. 2016;48:333–9.
56. Papageorghiou AT, Ohuma EO, Altman DG, Todros T, Cheikh Ismail L, Lambert A, Jaffer YA, Bertino E, Gravett MG, Purwar M, Noble JA, Pang R, Victora CG, Barros FC, Carvalho M, Salomon LJ, Bhutta ZA, Kennedy SH, Villar J. International Fetal and Newborn Growth Consortium for the 21st century (INTERGROWTH-21st). International standards for fetal growth based on serial ultrasound measurements: the fetal growth longitudinal study of the INTERGROWTH-21st project. Lancet. 2014;384:869–79.
57. Buck Louis GM, Grewal J, Albert PS, Sciscione A, Wing DA, Grobman WA, Newman RB, Wapner R, D'Alton ME, Skupski D, Nageotte MP, Ranzini AC, Owen J, Chien EK, Craigo S, Hediger ML, Kim S, Zhang C, Grantz KL. Racial/ethnic standards for fetal growth: the NICHD fetal growth studies. Am J Obstet Gynecol. 2015;213(449.e1):–449.e41.
58. Kiserud T, Piaggio G, Carroli G, Widmer M, Carvalho J, Neerup Jensen L, Giordano D, Cecatti JG, Abdel Aleem H, Talegawkar SA, Benachi A, Diemert A, Tshefu Kitoto A, Thinkhamrop J, Lumbiganon P, Tabor A, Kriplani A, Gonzalez Perez R, Hecher K, Hanson MA, Gülmezoglu AM, Platt LD. The World Health Organization fetal growth charts: a multinational longitudinal study of ultrasound biometric measurements and estimated fetal weight. PLoS Med. 2017;14:e1002220.
59. Nicolaides KH, Wright D, Syngelaki A, Wright A, Akolekar R. Fetal Medicine Foundation fetal and neonatal population weight charts. Ultrasound Obstet Gynecol. 2018;52:44–51.
60. Tarca AL, Romero R, Gudicha DW, Erez O, Hernandez-Andrade E, Yeo L, Bhatti G, Pacora P, Maymon E, Hassan SS. A new customized fetal growth standard for African American women: the PRB/NICHD Detroit study. Am J Obstet Gynecol. 2018;218:S679–S691.e4.
61. Gardosi J, Francis A. A customized standard to assess fetal growth in a US population. Am J Obstet Gynecol. 2009;201:25.e1–7.
62. Seravalli V, Di Tommaso M, Petraglia F. Managing fetal growth restriction: surveillance tests and their interpretation. Minerva Ginecol. 2019;71:81–90.
63. Audette MC, Kingdom JC. Screening for fetal growth restriction and placental insufficiency. Semin Fetal Neonatal Med. 2018;23:119–25.
64. Leite DFB, Cecatti JG. Fetal growth restriction prediction: how to move beyond. ScientificWorld Journal. 2019;2019:1519048. https://doi.org/10.1155/2019/1519048.
65. Kalafat E, Khalil A. Clinical significance of cerebroplacental ratio. Curr Opin Obstet Gynecol. 2018;30:344–54.
66. DeVore GR. The importance of the cerebroplacental ratio in the evaluation of fetal well-being in SGA and AGA fetuses. Am J Obstet Gynecol. 2015;213:5–15.
67. Akalin-Sel T, Nicolaides KH, Peacock J, Campbell S. Doppler dynamics and their complex interrelation with fetal oxygen pressure, carbon dioxide pressure, and pH in growth-retarded fetuses. Obstet Gynecol. 1994;84:439–44.
68. Konje JC, Bell SC, Taylor DJ. Abnormal Doppler velocimetry and blood flow volume in the middle cerebral artery in very severe intrauterine growth restriction: is the occurrence of reversal of compensatory flow too late? BJOG. 2001;108:973–9.
69. Figueras F, Gratacós E. Update on the diagnosis and classification of fetal growth restriction and proposal of a stage-based management protocol. Fetal Diagn Ther. 2014;36:86–98.
70. Roza SJ, Steegers EA, Verburg BO, Jaddoe VW, Moll HA, Hofman A, Verhulst FC, Tiemeier H. What is spared by fetal brain-sparing? Fetal circulatory redistribution and behavioral problems in the general population. Am J Epidemiol. 2008;168:1145–52.

71. Eixarch E, Meler E, Iraola A, Illa M, Crispi F, Hernandez-Andrade E, Gratacos E, Figueras F. Neurodevelopmental outcome in 2-year-old infants who were small-for-gestational age term fetuses with cerebral blood flow redistribution. Ultrasound Obstet Gynecol. 2008;32:894–9.
72. Meher S, Hernandez-Andrade E, Basheer SN, Lees C. Impact of cerebral redistribution on neurodevelopmental outcome in small-for-gestational-age or growth-restricted babies: a systematic review. Ultrasound Obstet Gynecol. 2015;46:398–404.
73. Monteith C, Flood K, Pinnamaneni R, Levine TA, Alderdice FA, Unterscheider J, McAuliffe FM, Dicker P, Tully EC, Malone FD, Foran A. An abnormal cerebroplacental ratio (CPR) is predictive of early childhood delayed neurodevelopment in the setting of fetal growth restriction. Am J Obstet Gynecol. 2019;221:273.e1–9.
74. Korkalainen N, Partanen L, Räsänen J, Yliherva A, Mäkikallio K. Fetal hemodynamics and language skills in primary school-aged children with fetal growth restriction: a longitudinal study. Early Hum Dev. 2019;134:34–40.
75. Arbeille P, Roncin A, Berson M, Patat F, Pourcelot L. Exploration of the fetal cerebral blood flow by duplex Doppler—linear array system in normal and pathological pregnancies. Ultrasound Med Biol. 1987;13:329–37.
76. Arbeille P, Body G, Saliba E, Tranquart F, Berson M, Roncin A, Pourcelot L. Fetal cerebral circulation assessment by Doppler ultrasound in normal and pathological pregnancies. Eur J Obstet Gynecol Reprod Biol. 1988;29:261–73.
77. Arbeille P, Maulik D, Fignon A, Stale H, Berson M, Bodard S, Locatelli A. Assessment of the fetal PO2 changes by cerebral and umbilical Doppler on lamb fetuses during acute hypoxia. Ultrasound Med Biol. 1995;21:861–70.
78. Gramellini D, Folli MC, Raboni S, Vadora E, Merialdi A. Cerebral-umbilical Doppler ratio as a predictor of adverse perinatal outcome. Obstet Gynecol. 1992;79:416–20.
79. Ciobanu A, Wright A, Syngelaki A, Wright D, Akolekar R, Nicolaides KH. Fetal Medicine Foundation reference ranges for umbilical artery and middle cerebral artery pulsatility index and cerebroplacental ratio. Ultrasound Obstet Gynecol. 2019;53:465–72.
80. Oros D, Ruiz-Martinez S, Staines-Urias E, Conde-Agudelo A, Villar J, Fabre E, Papageorghiou AT. Reference ranges for Doppler indices of umbilical and fetal middle cerebral arteries and cerebroplacental ratio: systematic review. Ultrasound Obstet Gynecol. 2019;53:454–64.
81. Acharya G, Ebbing C, Karlsen HO, Kiserud T, Rasmussen S. Sex-specific reference ranges of cerebroplacental and umbilicocerebral ratios: a longitudinal study. Ultrasound Obstet Gynecol. 2020;56(2):187–95. https://doi.org/10.1002/uog.21870.
82. Medina Castro N, Figueroa Diesel H, Guzmán Huerta M, Hernández Andrade E. Normal reference values of the pulsatility index from the uterine and umbilical arteries during pregnancy. Ginecol Obstet Mex. 2006;74:509–15.
83. Medina Castro N, Figueroa Diesel H, Hernández Andrade E. Normal reference values of the pulsatility index and peak systolic velocity in the fetal middle cerebral artery during normal pregnancy. Ginecol Obstet Mex. 2006;74:376–82.
84. Khalil AA, Morales-Rosello J, Morlando M, Hannan H, Bhide A, Papageorghiou A, Thilaganathan B. Is fetal cerebroplacental ratio an independent predictor of intrapartum fetal compromise and neonatal unit admission? Am J Obstet Gynecol. 2015;213:54.e1–54.e10.
85. Ebbing C, Rasmussen S, Kiserud T. Middle cerebral artery blood flow velocities and pulsatility index and the cerebroplacental pulsatility ratio: longitudinal reference ranges and terms for serial measurements. Ultrasound Obstet Gynecol. 2007;30:287–96.
86. Karlsen HO, Ebbing C, Rasmussen S, Kiserud T, Johnsen SL. Use of conditional percentiles of middle cerebral artery pulsatility index and cerebroplacental ratio in the prediction of adverse perinatal outcomes. Acta Obstet Gynecol Scand. 2016;95:690–6.
87. Flatley C, Greer RM, Kumar S. Magnitude of change in fetal cerebroplacental ratio in third trimester and risk of adverse pregnancy outcome. Ultrasound Obstet Gynecol. 2017;50:514–9.
88. Khalil A, Morales-Rosello J, Khan N, Nath M, Agarwal P, Bhide A, Papageorghiou A, Thilaganathan B. Is cerebroplacental ratio a marker of impaired fetal growth velocity and adverse pregnancy outcomes. Am J Obstet Gynecol. 2017;216:606.e1–606.e10.
89. Morales-Roselló J, Khalil A, Morlando M, Papageorghiou A, Bhide A, Thilaganathan B. Changes in fetal Doppler indices as a marker of failure to reach growth potential at term. Ultrasound Obstet Gynecol. 2014;43:303–10.
90. Morales-Roselló J, Khalil A, Morlando M, Bhide A, Papageorghiou A, Thilaganathan B. Poor neonatal acid-base status in term fetuses with low cerebroplacental ratio. Ultrasound Obstet Gynecol. 2015;45:156–61.
91. Khalil AA, Morales-Rosello J, Elsaddig M, Khan N, Papageorghiou A, Bhide A, Thilaganathan B. The association between fetal Doppler and admission to neonatal unit at term. Am J Obstet Gynecol. 2015;213:57.e1–7.
92. Flatley C, Kumar S. Is the fetal cerebroplacental ratio better that the estimated fetal weight in predicting adverse perinatal outcomes in a low risk cohort? J Matern Fetal Neonatal Med. 2019;32:2380–6.
93. Bligh LN, Al Solai A, Greer RM, Kumar S. Diagnostic performance of Cerebroplacental ratio thresholds at term for prediction of low birthweight and adverse intrapartum and neonatal outcomes in a term, low-risk population. Fetal Diagn Ther. 2018;43:191–8.

94. Hernandez-Andrade E, Maymon E, Erez O, Saker H, Luewan S, Garcia M, Ahn H, Tarca AL, Done B, Korzeniewski SJ, Hassan SS, Romero R. A low cerebroplacental ratio at 20-24 weeks of gestation can predict reduced fetal size later in pregnancy or at birth. Fetal Diagn Ther. 2018;44:112–23.
95. Akolekar R, Syngelaki A, Gallo DM, Poon LC, Nicolaides KH. Umbilical and fetal middle cerebral artery Doppler at 35-37 weeks' gestation in the prediction of adverse perinatal outcome. Ultrasound Obstet Gynecol. 2015;46:82–92.
96. Bakalis S, Akolekar R, Gallo DM, Poon LC, Nicolaides KH. Umbilical and fetal middle cerebral artery Doppler at 30-34 weeks' gestation in the prediction of adverse perinatal outcome. Ultrasound Obstet Gynecol. 2015;45:409–20.
97. Liu J, Song G, Zhao G, Meng T. The value of the cerebroplacental ratio for the prediction of intrapartum fetal monitoring in low-risk term pregnancies. Gynecol Obstet Invest. 2017;82:475–80.
98. Dall'Asta A, Ghi T, Rizzo G, Cancemi A, Aloisio F, Arduini D, Pedrazzi G, Figueras F, Frusca T. Cerebroplacental ratio assessment in early labor in uncomplicated term pregnancy and prediction of adverse perinatal outcome: prospective multicenter study. Ultrasound Obstet Gynecol. 2019;53:481–7.
99. Fiolna M, Kostiv V, Anthoulakis C, Akolekar R, Nicolaides KH. Prediction of adverse perinatal outcome by cerebroplacental ratio in women undergoing induction of labor. Ultrasound Obstet Gynecol. 2019;53:473–80.
100. Dehaene I, Page AS, Page G. The value of the cerebroplacental ratio in appropriate-for-gestational-age fetuses. Am J Obstet Gynecol. 2017;217:622–3.
101. Cruz-Martínez R, Figueras F, Hernandez-Andrade E, Oros D, Gratacos E. Fetal brain Doppler to predict cesarean delivery for nonreassuring fetal status in term small-for-gestational-age fetuses. Obstet Gynecol. 2011;117:618–26.
102. Figueras F, Savchev S, Triunfo S, Crovetto F, Gratacos E. An integrated model with classification criteria to predict small-for-gestational-age fetuses at risk of adverse perinatal outcome. Ultrasound Obstet Gynecol. 2015;45:279–85.
103. Dunn L, Sherrell H, Kumar S. Review: systematic review of the utility of the fetal cerebroplacental ratio measured at term for the prediction of adverse perinatal outcome. Placenta. 2017;54:68–75.
104. Bahado-Singh RO, Kovanci E, Jeffres A, Oz U, Deren O, Copel J, Mari G. The Doppler cerebroplacental ratio and perinatal outcome in intrauterine growth restriction. Am J Obstet Gynecol. 1999;180:750–6.
105. Flood K, Unterscheider J, Daly S, Geary MP, Kennelly MM, McAuliffe FM, O'Donoghue K, Hunter A, Morrison JJ, Burke G, Dicker P, Tully EC, Malone FD. The role of brain sparing in the prediction of adverse outcomes in intrauterine growth restriction: results of the multicenter PORTO study. Am J Obstet Gynecol. 2014;211:288.e1–5.
106. Conde-Agudelo A, Villar J, Kennedy SH, Papageorghiou AT. Predictive accuracy of cerebroplacental ratio for adverse perinatal and neurodevelopmental outcomes in suspected fetal growth restriction: systematic review and meta-analysis. Ultrasound Obstet Gynecol. 2018;52:430–41.
107. Oros D, Figueras F, Cruz-Martinez R, Meler E, Munmany M, Gratacos E. Longitudinal changes in uterine, umbilical and fetal cerebral Doppler indices in late-onset small-for-gestational age fetuses. Ultrasound Obstet Gynecol. 2011;37:191–5.
108. Monteith C, Flood K, Mullers S, Unterscheider J, Breathnach F, Daly S, Geary MP, Kennelly MM, McAuliffe FM, O'Donoghue K, Hunter A, Morrison JJ, Burke G, Dicker P, Tully EC, Malone FD. Evaluation of normalization of cerebro-placental ratio as a potential predictor for adverse outcome in SGA fetuses. Am J Obstet Gynecol. 2017;216:285.e1–6.
109. Khalil A, Morales-Roselló J, Townsend R, Morlando M, Papageorghiou A, Bhide A, Thilaganathan B. Value of third-trimester cerebroplacental ratio and uterine artery Doppler indices as predictors of stillbirth and perinatal loss. Ultrasound Obstet Gynecol. 2016;47(1):74–80.
110. D'Antonio F, Patel D, Chandrasekharan N, Thilaganathan B, Bhide A. Role of cerebroplacental ratio for fetal assessment in prolonged pregnancy. Ultrasound Obstet Gynecol. 2013;42:196–200.
111. Vollgraff Heidweiller-Schreurs CA, De Boer MA, Heymans MW, Schoonmade LJ, Bossuyt PMM, Mol BWJ, De Groot CJM, Bax CJ. Prognostic accuracy of cerebroplacental ratio and middle cerebral artery Doppler for adverse perinatal outcome: systematic review and meta-analysis. Ultrasound Obstet Gynecol. 2018;51:313–22.
112. Alanwar A, El Nour AA, El Mandooh M, Abdelazim IA, Abbas L, Abbas AM, Abdallah A, Nossair WS, Svetlana S. Prognostic accuracy of cerebroplacental ratio for adverse perinatal outcomes in pregnancies complicated with severe pre-eclampsia; a prospective cohort study. Pregnancy Hypertens. 2018;14:86–9.
113. Shahinaj R, Manoku N, Kroi E, Tasha I. The value of the middle cerebral to umbilical artery Doppler ratio in the prediction of neonatal outcome in patient with preeclampsia and gestational hypertension. J Prenat Med. 2010;4:17–21.
114. Regan J, Masters H, Warshak CR. Association between an abnormal cerebroplacental ratio and the development of severe pre-eclampsia. J Perinatol. 2015;35:322–7.
115. Zeeman GG, McIntire DD, Twickler DM. Maternal and fetal artery Doppler findings in women with chronic hypertension who subsequently develop superimposed pre-eclampsia. J Matern Fetal Neonatal Med. 2003;14:318–23.
116. Binder J, Monaghan C, Thilaganathan B, Morales-Roselló J, Khalil A. Reduced fetal movements and cerebroplacental ratio: evidence for worsening

fetal hypoxemia. Ultrasound Obstet Gynecol. 2018;51:375–80.
117. Irvine KM, Bligh LN, Kumar S. Association between the fetal cerebroplacental ratio and biomarkers of hypoxia and angiogenesis in the maternal circulation at term. Eur J Obstet Gynecol Reprod Biol. 2020;245:198–204. https://doi.org/10.1016/j.ejogrb.2019.11.018. pii: S0301-2115(19)30533-0. [Epub ahead of print].
118. Miranda J, Triunfo S, Rodriguez-Lopez M, Sairanen M, Kouru H, Parra-Saavedra M, Crovetto F, Figueras F, Crispi F, Gratacós E. Performance of third-trimester combined screening model for prediction of adverse perinatal outcome. Ultrasound Obstet Gynecol. 2017;50:353–60.
119. Kumar S, Figueras F, Ganzevoort W, Turner J, McCowan L. Using cerebroplacental ratio in non-SGA fetuses to predict adverse perinatal outcome: caution is required. Ultrasound Obstet Gynecol. 2018;52:427–9.

18 Cerebral Blood Flow Velocity Waveforms and Fetal Anemia

Jennifer J. Barr and Giancarlo Mari

This chapter reviews the clinical application of Doppler ultrasound velocimetry to the diagnosis and management of fetal anemia. The application of Doppler technology has revolutionized the management of these pregnancies.

18.1 Causes of Fetal Anemia

Fetal hemoglobin increases with advancing gestation (Table 18.1) [1]. Fetal anemia is categorized as mild, moderate, or severe, based on the degree of deviation from the median for gestational age. Severe anemia may cause hydrops and fetal demise.

There are many causes of fetal anemia (Table 18.2). The most common cause of fetal anemia in the United States is red cell alloimmunization. The primary cause of red cell alloimmunization is maternal sensitization to D antigen of the rhesus blood group system. However, many other antigens, the so-called irregular antigens, may be responsible for maternal sensitization. While prophylaxis with rhesus immunoglobulins has decreased the incidence of Rh-hemolytic disease, this phenomenon is still present.

Table 18.1 Increase of fetal hemoglobin with advancing gestation (Modified with permission from Mari et al. [1])

Weeks	Mean	95	5	0.55 MoM	0.65 MoM
18	10.6	11.8	9.4	5.8	6.9
19	10.9	12.2	9.6	6.0	7.1
20	11.1	12.5	9.8	6.1	7.2
21	11.4	12.8	9.9	6.2	7.4
22	11.6	13.0	10.1	6.4	7.5
23	11.8	13.3	10.2	6.5	7.6
24	12.0	13.6	10.3	6.6	7.8
25	12.1	13.8	10.4	6.7	7.9
26	12.3	14.0	10.5	6.8	8.0
27	12.4	14.3	10.6	6.8	8.1
28	12.6	14.5	10.7	6.9	8.2
29	12.7	14.7	10.7	7.0	8.3
30	12.8	14.9	10.8	7.1	8.3
31	13.0	15.1	10.8	7.1	8.4
32	13.1	15.3	10.9	7.2	8.5
33	13.2	15.5	10.9	7.2	8.6
34	13.3	15.7	10.9	7.3	8.6
35	13.4	15.8	10.9	7.4	8.7
36	13.5	16.0	10.9	7.4	8.7
37	13.5	16.2	10.9	7.5	8.8
38	13.6	16.4	10.9	7.5	8.9
39	13.7	16.5	10.9	7.5	8.9
40	13.8	16.7	10.9	7.6	9.0

Several other conditions can lead to fetal anemia. Hematological disorders can lead to fetal anemia and are implicated in approximately 10–27% of cases of nonimmune hydrops [2–4]. Fetal anemia may also result from excessive

J. J. Barr
Department of Obstetrics and Gynecology, UTHSC, Memphis, TN, USA

G. Mari (✉)
Department of Obstetrics and Gynecology, Cleveland Clinic Foundation, Cleveland, OH, USA
e-mail: giancarlomari@hotmail.com

D. Maulik, C. C. Lees (eds.), *Doppler Ultrasound in Obstetrics and Gynecology*,
https://doi.org/10.1007/978-3-031-06189-9_18

Table 18.2 Causes of fetal anemia

Red cell alloimmunization
Alpha-thalassemia
Enzyme disorder
Pyruvate kinase deficiency
Glucose phosphate isomerase deficiency
G6PD deficiency
Kasabach-Merritt sequence
Fetomaternal hemorrhage
Intracranial hemorrhage
Parvovirus B19 infection
Twin-to-twin transfusion
Blackfan-Diamond syndrome
Transient myeloproliferative disorder
Congenital leukemia

erythrocyte loss by hemolysis or hemorrhage, or erythrocyte underproduction [3].

In Southeast Asia homozygous, alpha-thalassemia-1 (hemoglobin Bart's) is the most common cause of fetal hydrops, accounting for 60–90% of cases [5]. This condition has become more frequent in Canada and in North America due to an increased number of immigrants from Southeast Asia [6, 7].

Massive fetomaternal hemorrhage, defined as loss of more than 150 mL, is a rare condition that may result in severe fetal anemia with or without hydrops, and fetal death [8–10]. Red blood cell enzymopathies, such as autosomal-recessive inherited deficiencies of pyruvate kinase and glucose phosphate isomerase, and G6PD deficiency, are rare conditions that may cause fetal anemia and hydrops [3, 11–13].

Parvovirus infection can lead to severe fetal anemia and consequently hydrops because of virus tropism for immature erythrocytes in the bone marrow or fetal liver [14]. Conditions such as large placental chorioangioma, twin-twin transfusion syndrome, transient myeloproliferative disorder, congenital leukemia, intracranial hemorrhage, and Blackfan-Diamond syndrome, may also cause fetal anemia [15–17].

There is evidence that cerebral Doppler velocimetry is useful for identifying fetal anemia across this spectrum of potential etiologies. These include red cell alloimmunization [1], parvovirus [18, 19], fetomaternal hemorrhage [10, 20], twin-twin transfusion syndrome following laser coagulation of the placental vessels [21], and following maternal chemotherapy [22]. Current evidence shows that MCA-PSV is reliable for detecting moderate to severe fetal anemia and need for fetal transfusion regardless of the cause of the anemia.

18.2 Which Cerebral Vessel to Assess

The circle of Willis is composed anteriorly of the anterior cerebral arteries (branches of the internal carotid artery that are interconnected by the anterior communicating artery) and posteriorly of the two posterior cerebral arteries (which are branches of the basilar artery and are interconnected on either side with the internal carotid artery by the posterior communicating artery). These two trunks and the middle cerebral artery (MCA), another branch of the internal carotid artery, supply the cerebral hemispheres on each side. These arteries have different flow velocity waveforms (FVWs) [23, 24]. Therefore, it is important to know which artery is being studied (Fig. 18.1). The MCA is the vessel of choice to assess the fetal cerebral circulation because it is easy to identify and has a high reproducibility [25, 26]. Additionally, it can be studied easily with an angle of zero degrees between the ultrasound beam and the direction of blood flow

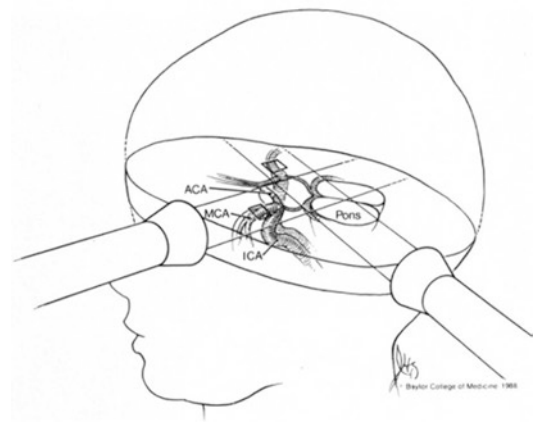

Fig. 18.1 Planes used for obtaining measurements of middle cerebral artery. (Reproduced with permission from Mari G [23])

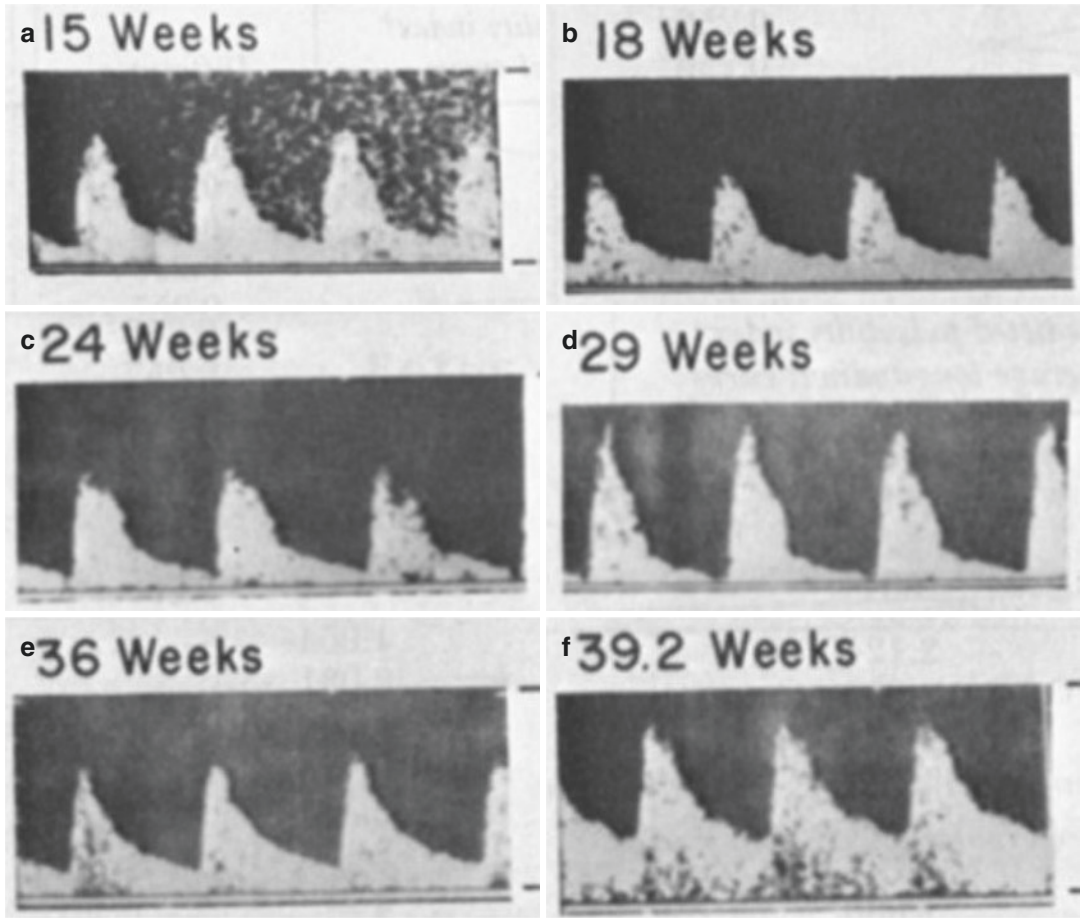

Fig. 18.2 Flow velocity waveforms of the middle cerebral artery in appropriate-for-gestational-age (AGA) fetuses at different gestational ages. (Reproduced with permission from Mari and Deter [26])

allowing the sonographer to obtain information on the true velocity of the blood flow [27]. Flow velocity waveforms of the middle cerebral artery change with advancing gestation (Fig. 18.2). Middle cerebral artery peak systolic velocity (MCA-PSV) increases exponentially with advancing gestation (Fig. 18.3) [27].

18.3 Technique for Measurement of Middle Cerebral Artery Doppler

It is important to emphasize that training sonographers and sonologists is the "conditio sine qua non" for the correct sampling of MCA-PSV.

As demonstrated in Fig. 18.4, the following steps are necessary for the correct assessment of the MCA.

1. The fetus needs to be in a period of rest (no breathing or movements).
2. The circle of Willis is imaged with color Doppler.
3. The sonographer zooms the area of the MCA so that it occupies more than 50% of the screen. The MCA should be visualized for its entire length.
4. The sample volume (1 mm) is placed soon after the origin of the MCA from the internal carotid artery (1–2 mm).
5. The angle between the direction of blood flow and the ultrasound beam is as close as possi-

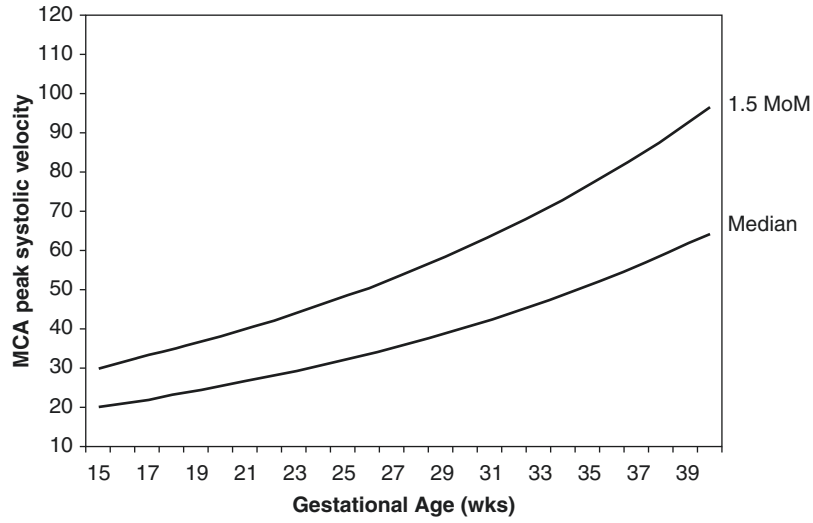

Fig. 18.3 Reference range of the fetal middle cerebral artery (*MCA*) peak systolic velocity during gestation. (Adapted with permission from Mari et al. [27])

ble to zero degrees. The angle corrector should not be used.

6. The waveforms (between 15 and 30) should be similar to each other. The highest PSV is measured.
7. Repeat the above steps at least three times.

The MCA distal to the transducer can be an alternative to the MCA proximal to the transducer [29]; however, the proximal vessel is preferable because it has lower intra- and interobserver variability [30] (Fig. 18.5).

18.4 Historical Development of Middle Cerebral Artery Technique

Early attempts to use the middle cerebral artery as a tool to predict fetal anemia focused on use of the pulsatility index. However, the pulsatility index of fetal cerebral vessels does not have as good of parameters to diagnose fetal anemia as does the MCA-PSV [32]. The PI of the cerebral arteries, however, can become abnormal when the hematocrit is close to 10%. In such a condition, the PI of the middle cerebral artery decreases, suggesting hypoxemia in the severely anemic fetus. The MCA PI in 101 cases of fetal anemia was below 2 SD in 7 anemic fetuses (unpublished data). In these fetuses, the hematocrit was less than 15%. When the anemia is severe, there is an increase of blood flow to the brain, which is reflected by a low MCA PI; however, this phenomenon is not always present and allows recognition only of a small number of anemic fetuses.

In 1995, a retrospective study showed that the MCA-PSV was a good parameter to identify fetal anemia [27]. The authors plotted the PSV of 135 healthy fetuses and 23 fetuses at risk of anemia. This was used to establish gestational age-based nomograms for MCA-PSV. These nomograms were then applied to a third group of 16 fetuses at risk for anemia who were undergoing cordocentesis. All the fetuses with anemia had MCA-PSV above the mean.

A larger, multicentered study was published in 2000 that evaluated the ability of MCA Doppler screening to detect moderate to severe fetal anemia, i.e., that anemia which would necessitate fetal transfusion [1]. Of the 35 fetuses studied with moderate to severe anemia, all of them had a PSV more than 1.5 MoM. Therefore, the sensitivity of the MCA-PSV for detecting moderate to severe fetal anemia was 100% with a false-positive rate of 12% and a PPV of 65%. For fetuses with anemia, the MCA-PSV correlates with the degree of anemia and can be used to specifically predict the fetal hemoglobin [33]. Even in Kell-alloimmunized pregnancies, MCA-

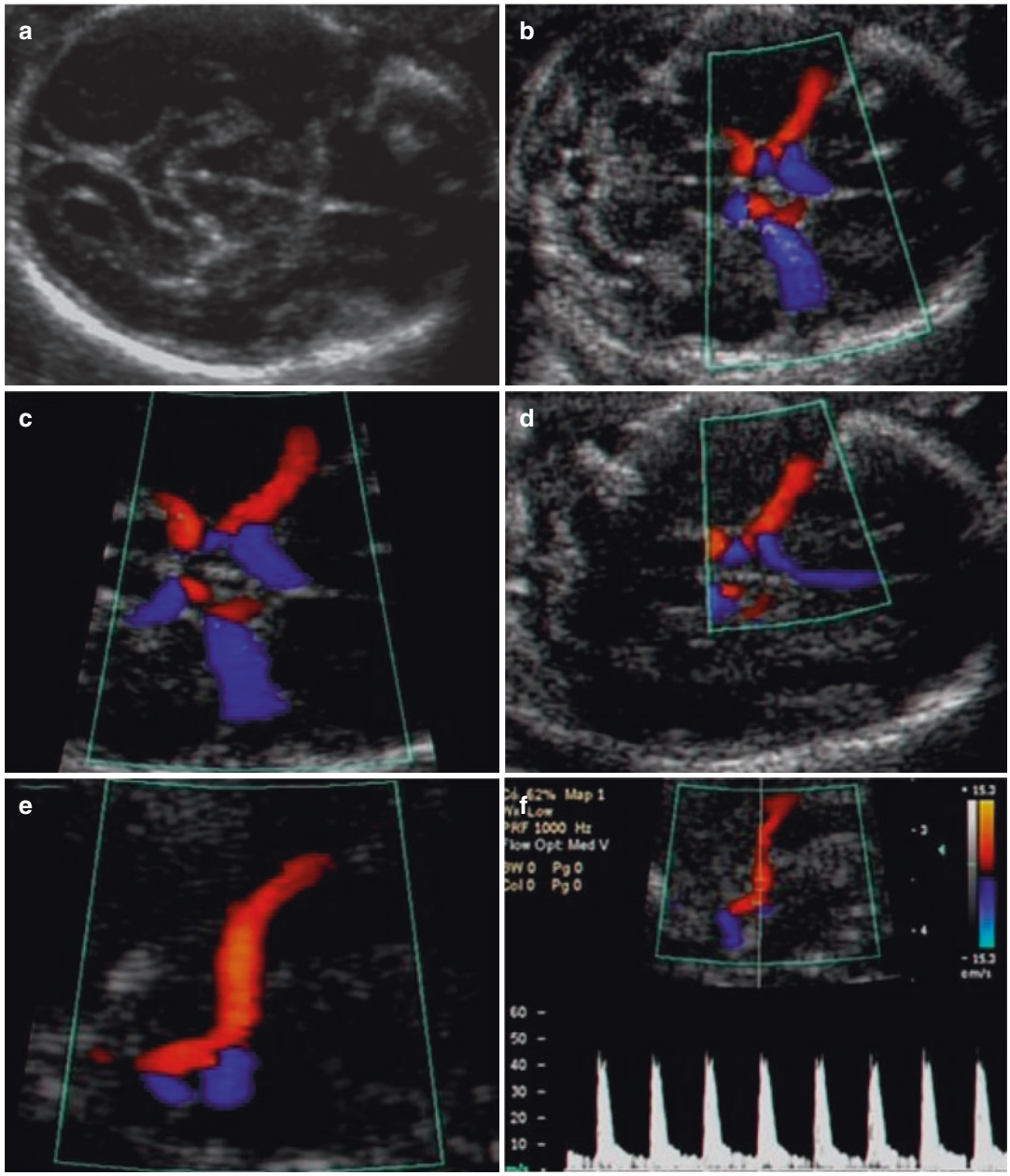

Fig. 18.4 Steps for correct MCA sampling. Top left, Axial section of the head at the level of the sphenoid bones; top right, color Doppler evidence of the circle of Willis; center left, the circle of Willis is enlarged; center right, the color box is placed around the MCA; bottom left, the MCA is zoomed and an angle off insonation as close to zero as possible is attained; bottom right, the sample volume is positioned soon after the origin of the MCA from the internal carotid artery. The MCA flow velocity waveforms are displayed, and the highest point of the waveform (PSV) is measured. (Reproduced with permission from Mari [28])

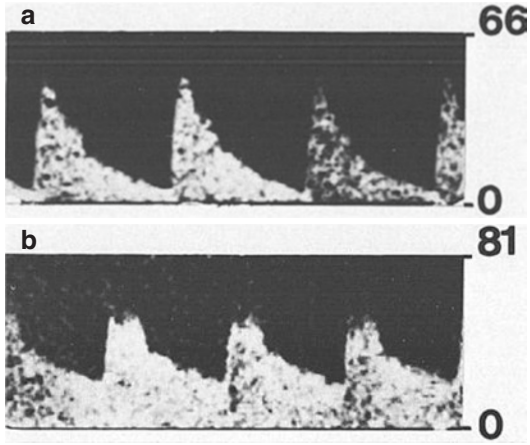

Fig. 18.5 Flow velocity waveforms of the MCA in a fetus (**a**) before and (**b**) after transfusion for fetal anemia. (Reproduced with permission from Mari et al. [31])

PSV is useful to detect fetal anemia [34]. Others have continued to replicate the diagnostic utility of MCA-PSV [35].

In a comparison of MCA-PSV to other noninvasive parameters, MCA-PSV was the best predictor of fetal anemia [36]. In a multicenter study, the sensitivity of MCA-PSV for prediction of moderate and severe anemia prior to the first cordocentesis was 100%, with false-positive rates of 12% at 1.50 multiples of the median [1].

Other robust data for the use of MCA-PSV have been reported in a multicenter trial with intention to treat. In this study, the authors monitored pregnancies complicated by red cell alloimmunization by studying MCA-PSV longitudinally. The MCA-PSV was used for timing cordocentesis [37]. This prospective study confirmed that MCA-PSV is an accurate method of monitoring pregnancies complicated by red cell antibodies. In this study, two anemic fetuses were missed in a group of 125 fetuses at risk of anemia. The interval between the last assessment of MCA-PSV and the delivery in those two fetuses was 3.5 and 2.5 weeks. This suggested that a closer assessment of MCA-PSV is necessary. This study also demonstrated that the number of false positives increased following 35 weeks' gestation.

In 1997, it was reported that the MCA-PSV is at least as good as the Delta OD 450 in predicting fetal anemia, but has the advantage of being noninvasive [38]. A recent prospective study compared MCA-PSV with Delta OD 450 in the prediction of moderately and severely anemic fetuses [39]. The authors concluded that both procedures are useful in the prediction of fetal anemia, but Doppler ultrasound assessment remains a method that has the advantage of being less expensive and less invasive than amniocentesis. A more recent prospective study confirmed the ability of MCA-PSV to replace invasive screening for fetal anemia [40]. The MCA-PSV represents a more suitable tool in the diagnosis and management of pregnancy complicated by alloimmunizations than Delta OD 450 [41].

18.5 Practical Application of MCA Peak Systolic Velocity to Red Cell Alloimmunization

Amniocentesis and cordocentesis are invasive tools for diagnosis and management of fetal anemia due to red cell alloimmunization. They are associated with significant complications. Both invasive procedures could worsen maternal alloimmunization due to secondary fetal hemorrhage. It has been reported that more than 70% of fetuses that underwent invasive procedures because they were defined as severely anemic based on traditional criteria were found to be either non-anemic or mildly anemic [1]. The use of MCA-PSV could have detected all the cases of significant fetal anemia requiring transfusion and would have avoided approximately 70% of the unnecessary invasive procedures [1] (Fig. 18.6).

The MCA-PSV performed prior to the first transfusion has been used to estimate the real value of fetal hemoglobin (Fig. 18.7) [33]. The difference between the observed and calculated hemoglobin was lower in fetuses that exhibited moderate to severe anemia compared with cases when the fetus was mildly anemic; therefore, MCA-PSV performs better in cases of clinically significant anemia. The explanation is that initial small decreases in fetal hemoglobin only slightly change cardiac output and blood viscosity. When the anemia becomes more severe, these compen-

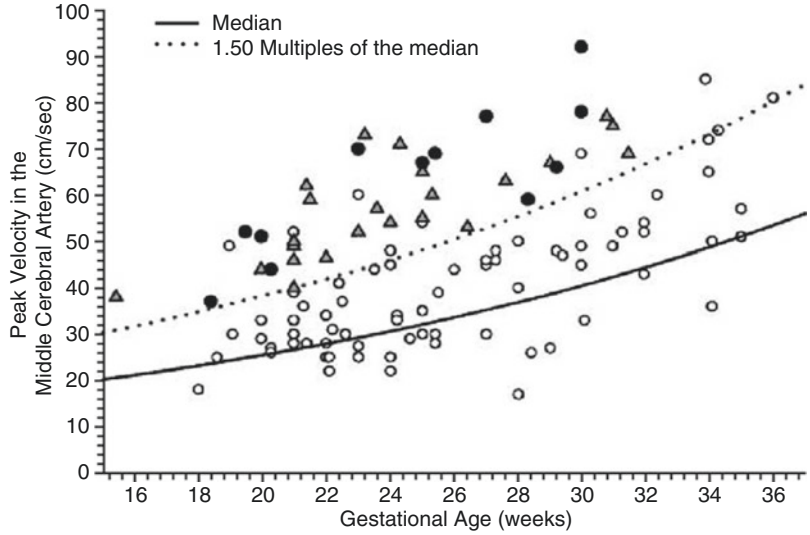

Fig. 18.6 Middle cerebral artery peak systolic velocity values used for detection of anemia. Open circles indicate fetuses with either no anemia or mild anemia. Triangles indicate fetuses with moderate or severe anemia. The solid circles indicate fetuses with hydrops. The solid curve indicates the median peak systolic velocity. Fetuses with MCA-PSV value above 1.5 multiples of the median are likely to be anemic. (Reproduced with permission from Mari et al. [1])

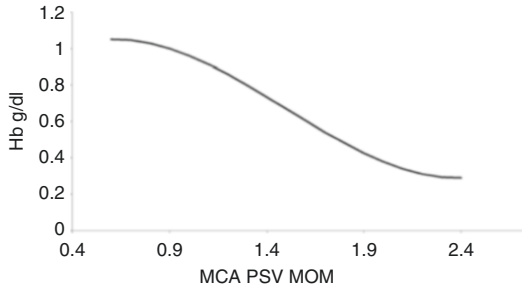

Fig. 18.7 Cubic function describing the relationship between middle cerebral artery peak systolic velocity (MCA-PSV) and fetal hemoglobin. The values are expressed as multiples of the median (MoM). $Y = 0.6835 + \text{MCA-PSV MoM} \times 1.2794 - 1.2885\ \text{MCA-PSV}^2 + 0.2861 \times \text{MCA-PSV}^3$. (Reproduced with permission from Mari G [42])

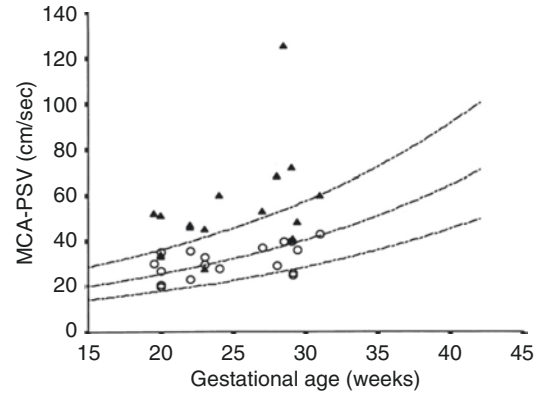

Fig. 18.8 Middle cerebral artery peak systolic velocity before (▲) and after (○) transfusion in a group of fetuses never previously transfused. The values are compared to the reference range for gestational age. (Reproduced with permission from Stefos et al. [43])

satory mechanisms operate more to maintain the oxygen and metabolic equilibrium in the various organs.

Intrauterine transfusion decreases fetal anemia significantly and normalizes the value of fetal MCA-PSV (Figs. 18.8 and 18.9) due to an increased blood viscosity and an increased oxygen concentration in fetal blood [43]. The MCA-PSV may also be used for timing the second fetal transfusion. However, in patients who have already received fetal transfusion, a higher cutoff point of 1.69 MoM to detect severe anemia is used [44]. This is probably the consequence of the different blood viscosity of the adult blood when compared with the fetal blood.

Most studies have used only one value of MCA-PSV to indicate whether the fetus is anemic or not at the time of the evaluation. However, a single value does not predict whether the fetus will become anemic. In a longitudinal study, it has been shown that the MCA slope is an excellent tool for identifying those fetuses that will become severely anemic and, therefore, need to be followed up more closely during the pregnancy (Fig. 18.10) [45]. The same author suggested the following protocol for monitoring pregnancies at risk for fetal anemia due to red cell alloimmunization [46]:

1. MCA-PSV should be performed in fetuses at risk of fetal anemia on a weekly basis for three consecutive weeks.
2. Cordocentesis is indicated when the MCA-PSV value is over 1.5 MoM.
3. If the MCA-PSV remains below 1.5 MoM, a regression line is obtained from the following three values.

If the plotted regression line is to the right of the dotted line shown in Fig. 18.10, the examination is repeated every 2 or 4 weeks based on the initial risk of the patient - with a lower initial risk (e.g., a Coombs titer between 1:16 and 1:32), the examination can be repeated every 4 weeks, but with a higher initial risk it should be repeated every 2 weeks. If the plotted regression line is between the dotted and the thin line (Fig. 18.10), the examination is repeated every 1–2 weeks based on the initial risk to the patient. If the plotted regression line is to the left of the thin line and the MCA-PSV value is below 1.50 MoM, the examination is repeated in 1 week. Figure 18.11 illustrates the importance of serial MCA-PSV measurements.

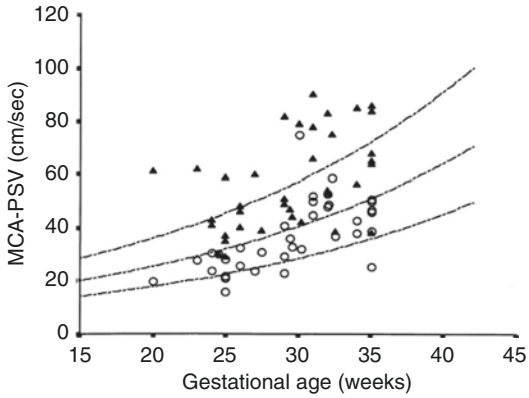

Fig. 18.9 Middle cerebral artery peak systolic velocity before (▲) and after (○) transfusion in a group of fetuses previously transfused. (Reproduced with permission from Stefos et al. [43])

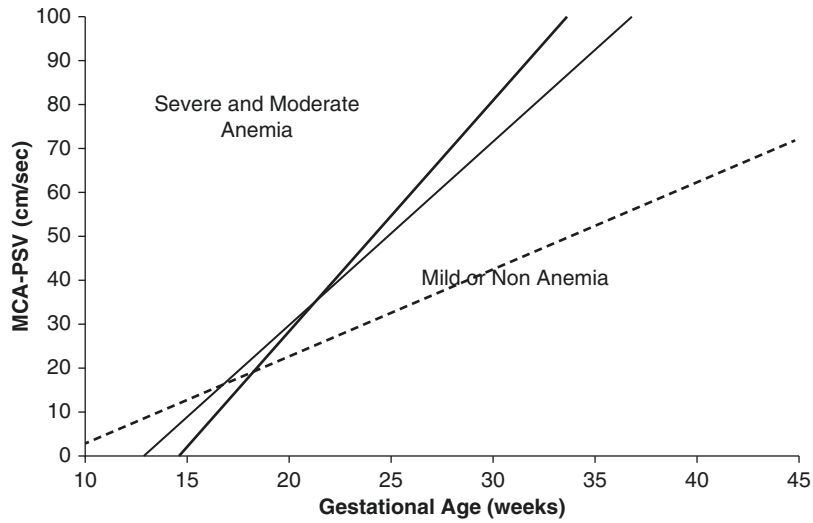

Fig. 18.10 Slopes for normal fetuses (*dotted line*), mildly anemic fetuses (*thin line*), and severely anemic fetuses (*thick line*). (Reproduced with permission from Detti et al. [45])

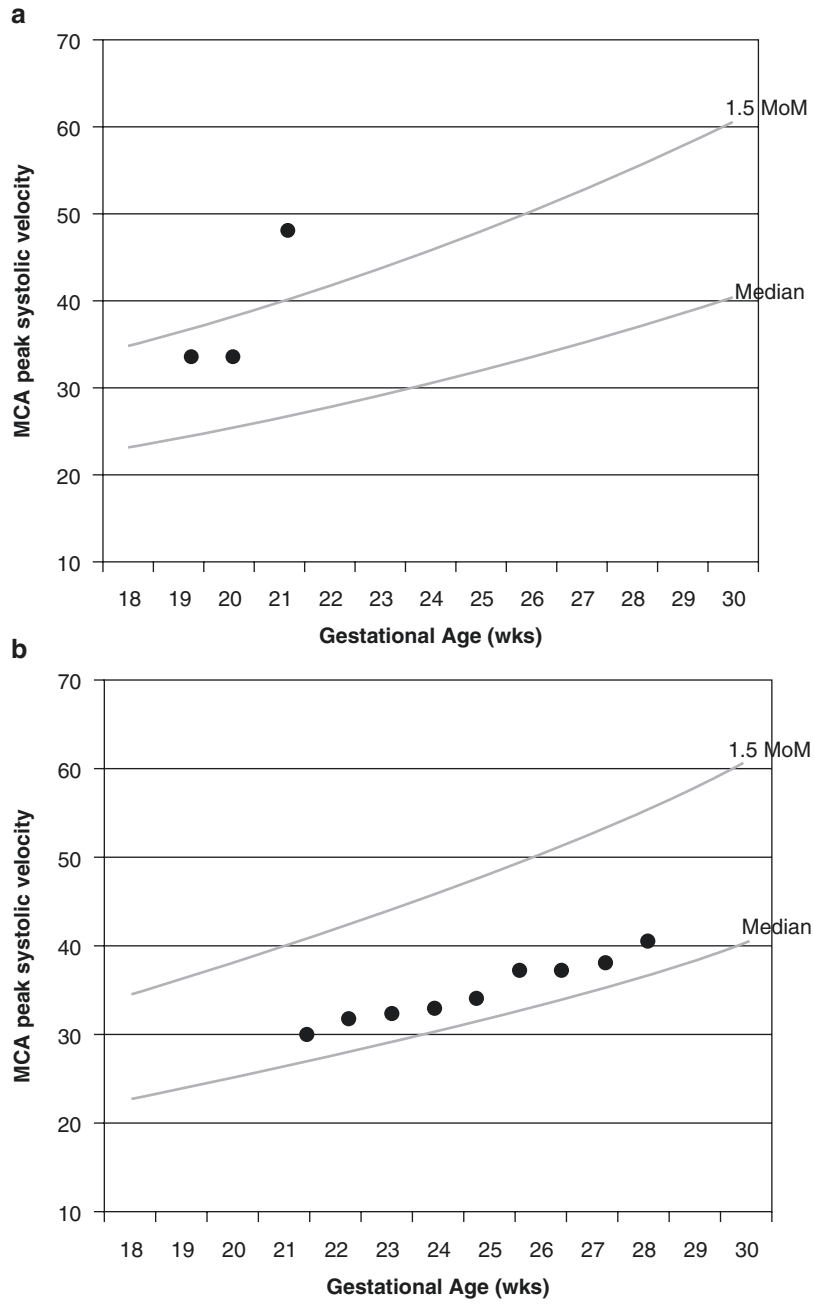

Fig. 18.11 Clinical examples of importance of serial MCA-PSV measurement. (**a**) Pregnancy complicated by Kell isoimmunization. The initial MCA-PSV measurements were normal. When a third measurement was performed and showed a steep increase, cordocentesis was performed. Fetal hematocrit was 17%. (**b**) Pregnancy complicated by Duffy isoimmunization. MCA-PSV showed minimal rise throughout pregnancy. Fetus was delivered at term with a hematocrit of 41%

18.6 False Positives with Middle Cerebral Doppler

Certain conditions may present with elevated MCA-PSV even in the absence of fetal anemia. The first of these is intrauterine growth restriction. In growth-restricted fetuses, increased MCA-PSV is driven more by hypoxemia and hypercapnia than fetal hemoglobin. This relationship was demonstrated by Hanif et al. [47]. They demonstrated that in fetuses with growth restriction, the PCO2 and the PO2 correlated well with the MCA-PSV, but no relationship was found between the MCA-PSV and the hemoglobin

concentration. The hypoxemia and hypercapnia trigger a complex group of regulatory mechanisms that affect circulatory redistribution in fetuses with growth restriction [48]. Mari et al. found that once developed, this elevated MCA-PSV persists in fetuses with growth restriction and increases the risk of perinatal morality [49]. However, this increase in mortality does not appear to be driven by fetal anemia.

False positives in the MCA-PSV may also occur during certain fetal infections such as cytomegalovirus. While fetuses infected with cytomegalovirus are at risk for anemia, changes in their MCA-PSV may occur in the absence of fetal anemia. Our group reported two fetuses with cytomegalovirus infection with extremely elevated MCA-PSV (3.4 and 2.8 MoM), but no fetal anemia [50]. Cerebrovascular involvement of the infection may be responsible for these grossly elevated Dopplers. We suggest that MCA-PSV trend may be more beneficial than a single value in determining which of these patients require cordocentesis (see Fig. 18.11). By using the trend of the MCA-PSV in patients at risk of fetal anemia, the false-positive rate decreases to less than 5% [37].

18.7 The Middle Cerebral Doppler in Alloimmunization

The MCA-PSV appears to be the best test for the noninvasive monitoring of fetuses at risk for hemolytic disease of the fetus; the Society for Maternal-Fetal Medicine (SMFM) now lists the MCA-PSV as the primary technique for detection of fetal anemia [51]. However, due to the risk of false positives, the use of the MCA-PSV should be reserved for those at risk for fetal anemia [51]. The SMFM guidelines specify if the MCA-PSV is greater than 1.5 MoM; a cordocentesis to determine fetal hemoglobin is recommended. The timing of a second transfusion may be based on either MCA-PSV or on the expected decline in the hemoglobin (Fig. 18.12).

18.8 The Middle Cerebral Doppler in Infection

It is well-documented that the MCA PSV is a good parameter to identify anemia in cases of fetal infection. Delle Chiaie et al. first reported the utility of MCA-PSV in detecting parvovirus-related fetal anemia [18]. Further, Cosmi et al. reported in a multicenter study of fetuses exposed to maternal parvovirus infection that a MCA-PSV >1.5 MoM had a positive predictive value of 94.1% and a negative predictive value of 93.3% for fetal anemia [19]. They concluded that MCA-PSV is a reliable noninvasive method to assess fetal anemia in pregnancies exposed to parvovirus. They emphasized the importance of assessing MCA-PSV trend and not single measurement values (see Fig. 18.13).

18.9 The Middle Cerebral Doppler in Fetal Hydrops

Another clinical condition where the MCA PSV may be useful is in hydrops.

An important differential for fetal hydrops is fetal anemia. The SMFM has incorporated MCA-PSV in their evaluation for fetal hydrops (Fig. 18.14) [52]. The MCA-PSV in this condition identifies those fetuses that are anemic and would benefit from a fetal transfusion.

18.10 The Middle Cerebral Doppler in Twin Anemia-Polycythemia Syndrome

In the last 15 years, a new condition in twin gestation has been described. It is called Twin Anemia-Polycythemia Syndrome (TAPS). TAPS occurs in monochorionic twin gestations when small anastomoses allow shunting of red blood cells, but not total blood volume from one fetus to the other. As the name suggests, this results in one fetus developing polycythemia and the other developing anemia.

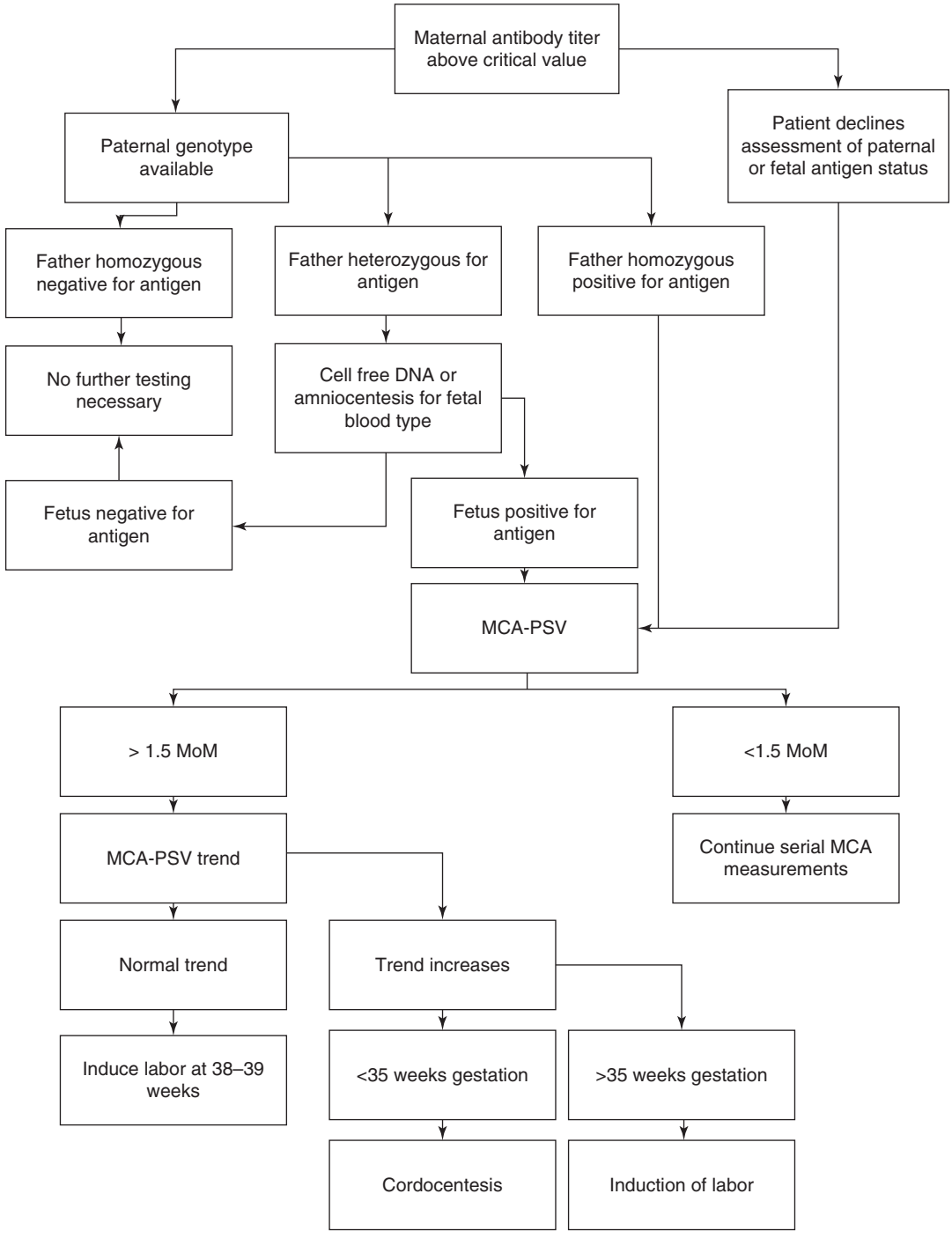

Fig. 18.12 Management algorithm in pregnancies at risk of having an anemic fetus because of red cell alloimmunization. (Adapted with permission from Mari G [42])

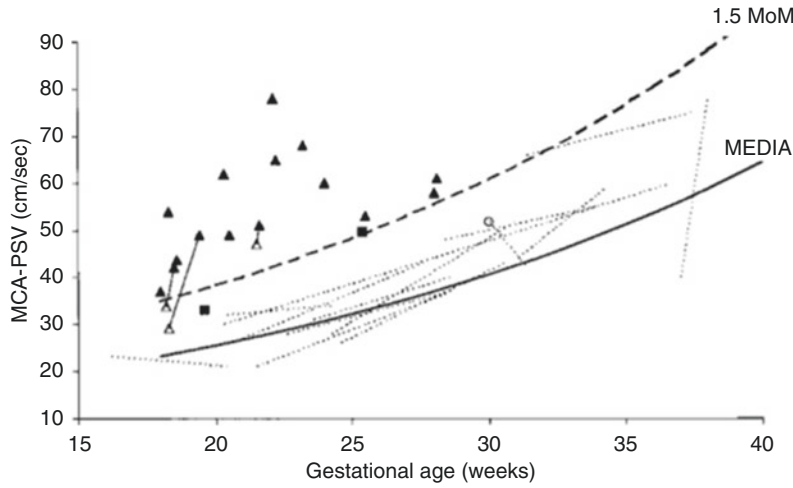

Fig. 18.13 Serial MCA-PSV in 32 fetuses who were at risk for anemia caused by parvovirus infection. The triangles indicate fetuses with severe anemia; the squares indicate fetuses with mild anemia; the circle indicates the MCA-PSV in a fetus who was not anemic at cordocentesis; and the lines indicate the trend of the MCA-PSV in fetuses who had no signs of anemia. (Reproduced with permission from Cosmi et al. [19])

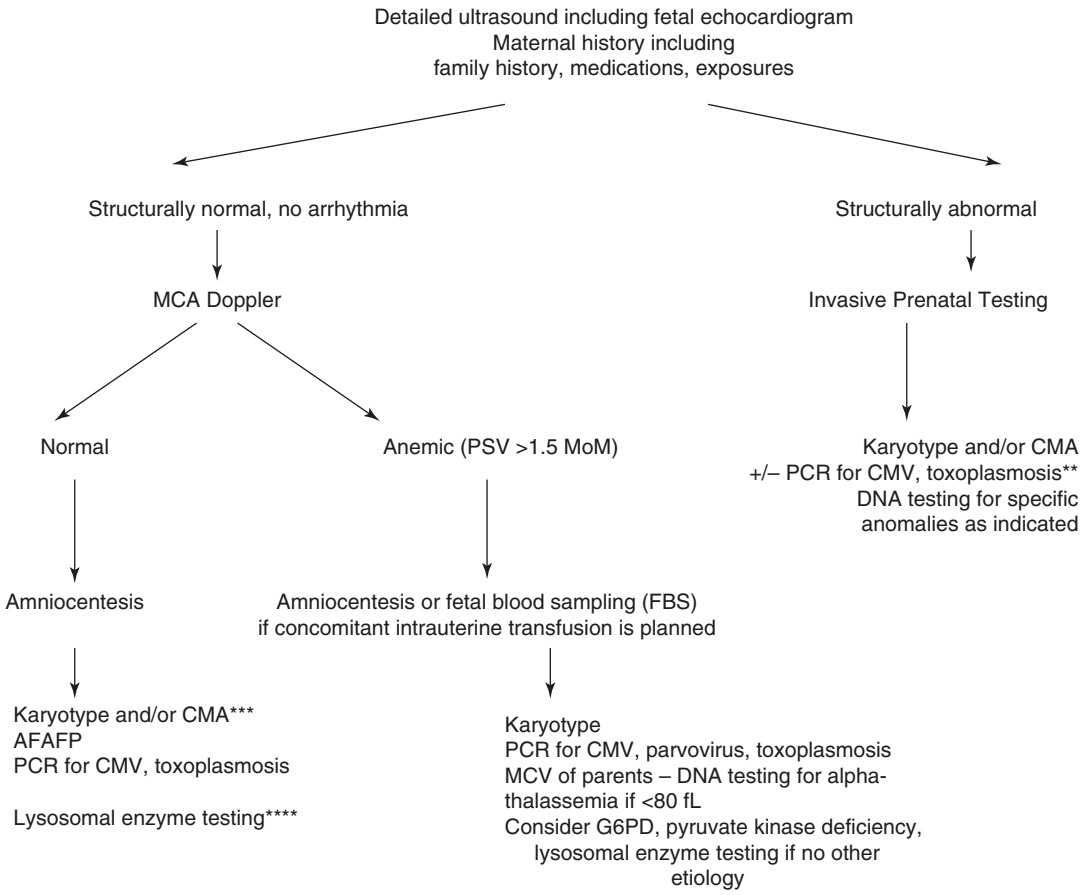

Fig. 18.14 Algorithm for evaluation of fetal hydrops. (Reproduced with permission from Society for Maternal Fetal Medicine [52])

Table 18.3 Antenatal classification for twin anemia-polycythemia sequence (TAPS). Fetal cardiac compromise is indicated by absent or reversed end-diastolic flow in the umbilical artery, pulsatile flow in the umbilical vein, and/or increased pulsatility index or reversed flow in the ductus venosus. (Adapted with permission from Tollenaar [53])

Antenatal stage	Classic criteria	Tollenaar criteria
Stage 1	MCA-PSV donor >1.5 MoM, recipient <1.0 MoM; no fetal compromise	Delta MCA-PSV >0.5 MOM; no fetal compromise
Stage 2	MCA-PSV donor >1.5 MoM, recipient <1.0 MoM; no fetal compromise	Delta MCA-PSV >0.7 MoM; no fetal compromise
Stage 3	Stage 1 or 2 with cardiac compromise of donor	Stage 1 or 2 with cardiac compromise of donor
Stage 4	Hydrops of donor	Hydrops of donor
Stage 5	Demise of one or both fetuses	Demise of one or both fetuses

The MCA-PSV plays a paramount role in the diagnosis of this condition. Historically, fixed cutoff values of MCA-PSV <1.0 MoM in the recipient and >1.5 MoM in the donor have been used to indicate TAPS (Table 18.3) [54]. More recently, a retrospective study has suggested that any difference (delta) of the MCA-PSV of more than 0.5 MoM between the two fetuses [53]. Tollenaar and colleagues have therefore proposed a new classification system, as detailed in Table 18.3. The use of the MCA-PSV in either of these classification schemes can identify fetuses that will benefit from intrauterine transfusion or fetoscopic laser surgery.

18.11 The Middle Cerebral Doppler in Fetomaternal Hemorrhage

The MCA-PSV is also useful in the diagnosis of fetomaternal hemorrhage. The majority of signs and symptoms of fetomaternal hemorrhage are nonspecific. These include abnormal fetal heart rate tracings and maternal perception of decreased fetal movement. A systematic review of 35 cases of laboratory confirmed fetomaternal hemorrhage, all but 1 had an abnormal MCA-PSV (Fig. 18.15) [55]. MCA-PSV is the best-known indicator of fetomaternal hemorrhage.

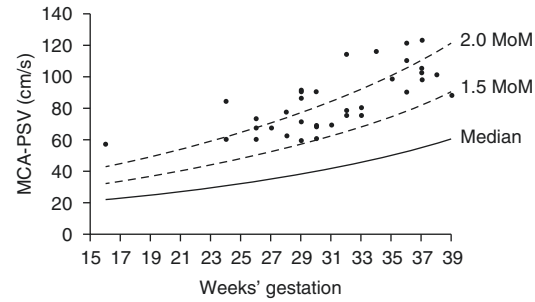

Fig. 18.15 MCA-PSV in women with laboratory confirmed fetomaternal hemorrhage. (Adapted with permission from Bellussi et al. [55])

References

1. Mari G, Deter RL, Carpenter RL, et al. Non-invasive diagnosis by Doppler ultrasonography of fetal anemia due to maternal red-cell alloimmunization. Collaborative group for Doppler assessment of the blood velocity in anemic fetuses. N Engl J Med. 2000;342:9–14.
2. Jauniaux E, Van Maldergem L, De Munter C, et al. Nonimmune hydrops fetalis associated with genetic abnormalities. Obstet Gynecol. 1990;75:568–72.
3. Murat OA, Gallagher PG. Hematologic disorders and nonimmune hydrops fetalis. Semin Perinatol. 1995;19:502–15.
4. Norton ME. Nonimmune hydrops fetalis. Semin Perinatol. 1994;18:321–32.
5. Chui DH, Waye JS. Hydrops fetalis caused by alpha-thalassemia: an emerging health care problem. Blood. 1998;91:2213–22.
6. Old J. Haemoglobinopathies. Prenat Diagn. 1996;16:1181–6.
7. Leung WC, Oepkes D, Seaward G, Ryan G. Serial sonographic findings of four fetuses with homozygous alpha-thalassemia-1 from 21 weeks onwards. Ultrasound Obstet Gynecol. 2002;19:56–9.
8. Owen J, Stedman CM, Tucker TL. Comparison of predelivery versus postdelivery Kleihauer-Betke stains in cases of fetal death. Am J Obstet Gynecol. 1989;161:663–6.
9. Giacoia GP. Severe fetomaternal hemorrhage: a review. Obstet Gynecol Surv. 1997;52:372–80.
10. Sueters M, Arabin B, Oepkes D. Doppler sonography for predicting fetal anemia caused by massive fetomaternal hemorrhage. Ultrasound Obstet Gynecol. 2003;22:186–9.

11. Tercanli S, Gembruch U, Holzgreve W. Nonimmune hydrops fetalis in diagnosis and management. In: Callen PW, editor. Ultrasonography in obstetrics and gynecology. 4th ed. Philadelphia: Saunders; 2000. p. 563–6.
12. Mentzer WC, Collier E. Hydrops fetalis associated with erythrocyte G-6-PD deficiency and maternal ingestion of fava beans and ascorbic acid. J Pediatr. 1975;86:565–7.
13. Perkins RP. Hydrops fetalis and stillbirth in a male glucose-6-phosphate dehydrogenase-deficient fetus possibly due to maternal ingestion of sulfisoxazole: a case report. Am J Obstet Gynecol. 1971;111:379–81.
14. Brown KE, Anderson SM, Young NS. Erythrocyte P antigen: cellular receptor for B19 parvovirus. Science. 1993;262:114–7.
15. Haak MC, Oosterhof H, Mouw RJ, et al. Pathophysiology and treatment of fetal anemia due to placental chorioangioma. Ultrasound Obstet Gynecol. 1999;14:68–70.
16. Rogers BB, Bloom SL, Buchanan GR. Autosomal dominantly inherited Diamond-Blackfan anemia resulting in nonimmune hydrops. Obstet Gynecol. 1997;89:805–7.
17. McLennan AC, Chitty LS, Rissik J, Maxwell DJ. Prenatal diagnosis of Blackfan-Diamond syndrome: case report and review of the literature. Prenat Diagn. 1996;16:349–53.
18. Delle Chiaie LD, Buck G, Grab D, Terinde R. Prediction of fetal anemia with Doppler measurement of the middle cerebral artery peak systolic velocity in pregnancies complicated by maternal blood group alloimmunization or parvovirus B19 infection. Ultrasound Obstet Gynecol. 2001;18:232–6.
19. Cosmi E, Mari G, Delle Chiaie L, et al. Noninvasive diagnosis by Doppler ultrasonography of fetal anemia resulting from parvovirus infection. Am J Obstet Gynecol. 2002;187:1290–3.
20. Mari G, Detti L. Doppler ultrasound: application to fetal medicine. In: Fleischer AC, Manning AF, Jeanty P, Romero R, editors. Sonography in obstetrics and gynecology: principles and practice. 6th ed. New York: McGraw-Hill; 2001. p. 274–6.
21. Senat MV, Loizeau S, Couderc S, Bernard JP, Ville Y. The value of middle cerebral artery peak systolic velocity in the diagnosis of fetal anemia after intrauterine death of one monochorionic twin. Am J Obstet Gynecol. 2003;189:1320–4.
22. Halaska MJ, et al. A pilot study on peak systolic velocity monitoring of fetal anemia after administration of chemotherapy during pregnancy. Eur J Obstet Gynecol Reprod Biol. 2014;174:76–9.
23. Mari G, Moise KJ Jr, Deter RL, et al. Doppler assessment of the pulsatility index in the cerebral circulation of the human fetus. Am J Obstet Gynecol. 1989;160:698–703.
24. Mari G. Regional cerebral flow velocity waveforms in the human fetus. J Ultrasound Med. 1994;13:343–6.
25. Woo JK, Liang ST, Lo RS, Chan FY. Middle cerebral artery Doppler flow velocity waveforms. Obstet Gynecol. 1987;70:613–6.
26. Mari G, Deter RL. Middle cerebral artery flow velocity waveforms in normal and small-for-gestational-age fetuses. Am J Obstet Gynecol. 1992;166:1262–70.
27. Mari G, Adrignolo A, Abuhamad AZ, Pirhonen J, Jones DC, Ludomirsky A, Copel JA. Diagnosis of fetal anemia with Doppler ultrasound in the pregnancy complicated by maternal blood group immunization. Ultrasound Obstet Gynecol. 1995;5:400–5.
28. Mari G, Abuhamad A, Cosmi E, Segata M, Altaye M, Akiyama M. Middle cerebral artery peak systolic velocity technique and variability. J Ultrasound Med. 2005;24:425–30.
29. Abel DE, Grambow SC, Brancazio LR, Hertzberg BS. Ultrasound assessment of the fetal middle cerebral artery peak systolic velocity: a comparison of the near-field versus the far-field vessel. Am J Obstet Gynecol. 2003;189:986–9.
30. Akiyama M, Detti L, Abuhamad A, Bahado-Singh R, Mari G. Is the middle cerebral artery peak systolic velocity measurement affected by the site of vessel sampling? Am J Obstet Gynecol. 2002;187:S164.
31. Mari G, Moise KJ, Deter RL, Carpenter RJ. Flow velocity waveforms of the umbilical and cerebral arteries before and after intravascular transfusion. Obstet Gynecol. 1990;75:584–9.
32. Mari G, Deter RL, Carpenter R, et al. The peak systolic velocity of the middle cerebral artery is a better indicator of fetal anemia than the pulsatility index. Proc Soc Gynecologic Investigation, St. Louis; 1990.
33. Mari G, Detti L, Oz U, et al. Accurate prediction of fetal hemoglobin by Doppler ultrasonography: a preliminary study. Obstet Gynecol. 2002;99:589–93.
34. van Dongen H, Klumper FJ, Sikkel E, et al. Noninvasive tests to predict fetal anemia in Kell-alloimmunized pregnancies. Ultrasound Obstet Gynecol. 2005;25(4):341–5.
35. Scheier M, Hernandez-Andrade E, Carmo A, et al. Prediction of fetal anemia in rhesus disease by measurement of fetal middle cerebral artery peak systolic velocity. Ultrasound Obstet Gynecol. 2004;23(5):432–6.
36. Dukler D, Oepkes D, Seaward G, et al. Noninvasive tests to predict fetal anemia: a study comparing Doppler and ultrasound parameters. Am J Obstet Gynecol. 2003;188(5):1310–4.
37. Zimmerman R, Durig P, Carpenter RJ Jr, Mari G. Longitudinal measurement of peak systolic velocity in the fetal middle cerebral artery for monitoring pregnancies complicated by red cell alloimmunisation: a prospective multicenter trial with intention-to-treat. Br J Obstet Gynaecol. 2002;109:746–52.
38. Mari G, Penso C, Sbracia M, et al. Delta OD 450 and Doppler velocimetry of the middle cerebral artery peak velocity in the evaluation for fetal alloimmune hemolytic disease. Which is best? Am J Obstet Gynecol. 1997;176:S18.
39. Nishie EN, Brizot ML, Liao AW, et al. A comparison between middle cerebral artery peak systolic velocity and amniotic fluid optical density at 450 nm in the prediction of fetal anemia. Am J Obstet Gynecol. 2003;188:214–9.

40. Oepkes D, Seaward PG, Vandenbussche FP, et al. Doppler ultrasonography versus amniocentesis to predict fetal anemia. N Engl J Med. 2006;355(2):156–64.
41. Pereira L, Jenkins TM, Berghella V. Conventional management of maternal red cell alloimmunization compared with management by Doppler assessment of middle cerebral artery peak systolic velocity. Am J Obstet Gynecol. 2003;189:1002–6.
42. Mari G. Middle cerebral artery peak systolic velocity for the diagnosis of fetal anemia: the untold story. Ultrasound Obstet Gynecol. 2005;25(4):323–30.
43. Stefos T, Cosmi E, Detti L, Mari G. Correction of fetal anemia and the middle cerebral artery peak systolic velocity. Obstet Gynecol. 2002;99:211–5.
44. Detti L, Oz U, Guney I, et al. Doppler ultrasound velocimetry for timing the second intrauterine transfusion in fetuses with anemia from red cell alloimmunization. Am J Obstet Gynecol. 2001;185:1048–51.
45. Detti L, Mari G, Akiyama M, et al. Longitudinal assessment of the middle cerebral artery peak systolic velocity in healthy fetuses and in fetuses at risk for anemia. Am J Obstet Gynecol. 2002;187:937–9.
46. Detti L, Mari G. Noninvasive diagnosis of fetal anemia. Clin Obstet Gynecol. 2003;46:923–30.
47. Hanif F, Drennan K, Mari G. Variables that affect the middle cerebral artery peak systolic velocity in fetuses with anemia and intrauterine growth restriction. Am J Perinatol. 2007;24(8):501–5.
48. Akalin-Sel T, Nicolaides KH, Peacock J, Campbell S. Doppler dynamics and their complex interrelation with fetal oxygen pressure, carbon dioxide pressure, and pH in growth-retarded fetuses. Obstet Gynecol. 1994;84(3):439–44.
49. Mari G, Hanif F, Cosmi E, Santolaya-Forgas J, Treadwell MC. Middle cerebral artery peak systolic velocity: a new Doppler parameter in the assessment of growth-restricted fetuses. Ultrasound Obstet Gynecol. 2007;29(3):310–6.
50. Duncan JR, Schenone MH, Argoti PS, Mari G. Middle cerebral artery peak systolic velocity in perinatal cytomegalovirus infection. J Clin Ultrasound. 2019;47(6):372–5.
51. Society for Maternal-Fetal Medicine. Society for Maternal-Fetal Medicine (SMFM) clinical guideline #8: the fetus at risk for anemia—diagnosis and management. Am J Obstet Gynecol. 2015;212(6):697–710.
52. Society for Maternal-Fetal Medicine. Society for Maternal-Fetal Medicine (SMFM) clinical guideline #7: nonimmune hydrops fetalis. Am J Obstet Gynecol. 2015;212(2):127–39.
53. Tollenaar LSA, Lopriore E, Middeldorp JM, Haak MC, et al. Improved prediction of twin anemia-polycythemia sequence by delta middle cerebral artery peak systolic velocity: new antenatal classification system. Ultrasound Obstet Gynecol. 2019;53:788–93.
54. Slaghekke F, Kist WJ, Oepkes D, Pasman SA, et al. Twin anemia–polycythemia sequence: diagnostic criteria, classification, perinatal management and outcome. Fetal Diagn Ther. 2010;27:181–90.
55. Bellussi F, Perolo A, Ghi T, Youssef A, et al. Diagnosis of severe fetomaternal hemorrhage with fetal cerebral Doppler: case series and systematic review. Fetal Diagn Ther. 2017;41:1–7.

19 First- and Second-Trimester Doppler Velocimetry of the Uteroplacental Circulation

Victoria Mumford and Asma Khalil

19.1 Physiological Changes in the Uteroplacental Circulation During Pregnancy

The uteroplacental circulation is primarily supplied by the uterine arteries, with just a small supply from the ovarian arteries. These arteries anastomose to become arcuate arteries, which flow into the radial arteries that enter the outer third of the myometrium. These arteries finally flow into the spiral arteries, which supply the intervillous space during pregnancy. This space is where there is an exchange of nutrients and waste from the fetus via the placenta [1].

Adequate placental function relies on trophoblastic invasion of the spiral arteries. In the first trimester, trophoblastic invasion produces thick muscular vessels with high vascular resistance, but trophoblastic invasion in the second trimester leads to thin walled vessels with low resistance [2]. As gestational age increases, the impedance flow in the uterine arteries decreases. A fall in the impedance flow from beyond 26 weeks is believed to be due to a hormonal effect on the arterial wall's elasticity [1].

V. Mumford · A. Khalil (✉)
Fetal Medicine Unit, St. George's Hospital, and St. George's University of London, London, UK

Vascular Biology Research Centre, Molecular and Clinical Sciences Research Institute, St George's University of London, London, UK
e-mail: asmakhalil79@googlemail.com

19.1.1 Abnormal Changes in the Uteroplacental Circulation

An impairment in the physiological process of trophoblastic invasion of the maternal spiral arteries manifests as an increased uterine artery pulsatility index (UtA-PI). This can consequently result in placental ischaemia and placental insufficiency. The cause may be due to the immunological differences between maternal and fetal cells. There is research to suggest that this may play a role in the pathogenesis of intrauterine growth restriction (IUGR), pre-eclampsia, placental abruption and stillbirth [1, 3]. The assessment of impedance to flow in the uterine artery may therefore identify pregnancies at risk of these complications and is thus suggested as a screening tool during pregnancy [1].

Trophoblastic invasion is not the only pathophysiological process of pre-eclampsia; there is also a relative deficiency of prostacyclin, which is a vasodilator, plus an increase in thromboxane A2, which is a vasoconstrictor [2]. The exact reason why pre-eclampsia occurs is unknown, but it has been suggested that the maternal inflammatory response and end-organ damage could be associated with widespread endothelial vascular dysfunction [2].

Placental volume can be variable; in early-onset pre-eclampsia, it can be hypoplastic, and, in term-onset pre-eclampsia, it can be hyper-

D. Maulik, C. C. Lees (eds.), *Doppler Ultrasound in Obstetrics and Gynecology*,
https://doi.org/10.1007/978-3-031-06189-9_19

plastic. This supports the theory that pre-eclampsia is a heterogeneous disease with different pathophysiologies depending on the gestational age of disease onset [4, 5].

Pre-eclampsia is divided into early, preterm and term, depending on the gestational age of disease onset. Term is from 37 weeks' gestation onwards, preterm is before 37 weeks' gestation and early is before 34 weeks' gestation [6, 7]. The differences between these three types of pre-eclampsia have been identified by studies, including differences in the rate of detection and the ability to prevent them with treatment.

Fetal growth restriction (FGR) is the failure of the fetus to grow to its full potential due to placental insufficiency. This occurs due to poor placental implantation and insufficient angiogenesis in the first trimester. The fetus diverts blood flow away from the peripheries and toward the heart and brain. This can result in fetuses, which may have a normal length and head circumference but a smaller abdominal circumference and less subcutaneous fat [2]. FGR is significantly associated with perinatal mortality and morbidity. It is associated with pre-eclampsia, preterm delivery, cesarean section, intrauterine death, neonatal death and long-term health complications for preterm children [8]. Early identification and intervention has the most potential to alter the disease progression later on in the pregnancy.

Chorionic villus sampling (CVS) has been traditionally known to cause miscarriage in 1% of cases, and there have been questions as to whether CVS may increase the risk of pre-eclampsia. When studying the UtA-PI, in women who undergo CVS in the first or second trimester, it was discovered that the procedure did not affect the UtA-PI, thus showing that CVS does not interfere with long-term placentation [9]. Recent studies and meta-analyses have suggested that the procedure-related miscarriage risk is much lower than 1% [10].

19.2 Relationship Between the Uteroplacental Circulation and the Maternal Systemic Circulation

During pregnancy, the maternal cardiovascular system undergoes a variety of physiological adaptations to support the developing fetus and placenta. The cardiac output increases, and there is peripheral vasodilation [11].

In a normal pregnancy, the mean arterial pressure (MAP) initially decreases with gestational age until around 22–24 weeks. This is most likely due to progesterone causing vasodilation, which results in a decreased systemic vascular resistance. After 22–24 weeks, the MAP increases with gestational age. This is likely due to the normal physiological increase in the maternal cardiac output, increased blood volume and reduced vascular resistance [3]. In FGR pregnancies, the MAP is low-to-normal, but, in pre-eclampsia pregnancies, the MAP is high [11].

There is increasing evidence that maternal cardiac dysfunction may be associated with poor placentation and poor pregnancy outcome [12]. An abnormal uteroplacental Doppler flow has been reported in women with known congenital cardiac disease both before and during pregnancy [12]. Conversely, women with no known congenital cardiac disease, but with abnormal uterine artery resistance and complications of pregnancy, have cardiac dysfunction up to 1 year postpartum [12]. This may be a sign of subclinical cardiac disease that may occur later in life [12].

There is limited regulation of uteroplacental flow in the placenta; the flow is directly dependent on the maternal cardiac output [12]. When the cardiac output is impaired, the suboptimal blood flow may lead to placental hypoperfusion and high uterine artery resistance [12]. This shows that the physiology of trophoblastic inva-

sion of the spiral arteries may in some way be affected by placental hypoperfusion.

In the first trimester, the cardiac output is found to be elevated in pregnancies that will develop pre-eclampsia and low in pregnancies that will develop FGR [11]. By the third trimester, pregnancies complicated by FGR and pre-eclampsia have a low cardiac output [11]. Women who develop pre-eclampsia have reduced left ventricle contractility and impaired diastolic function, unlike in FGR, where women tend to have normal results [11].

Arterial stiffness is associated with pre-eclampsia and may represent generalized endothelial dysfunction and a low-grade chronic inflammatory response [11].

19.3 First-Trimester Doppler Velocimetry of the Uteroplacental Circulation for the Prediction of Fetal Growth Restriction and Pre-eclampsia

The early identification of women at a risk of pre-eclampsia allows preventative measures to be carried out, such as early low-dose aspirin treatment [13].

The Doppler UtA-PI is one such test that helps identify women at risk; it is the measurement of the mean pulsatility index of the right and left uterine arteries. This primarily assesses the maternal uteroplacental blood flow resistance. Screening for pre-eclampsia can be achieved by Doppler assessment of the UtA-PI between 11 and 13 + 6 weeks of gestation. The measurement of the UtA-PI can be easily carried out as part of the 11–13-week scan by sonographers, but they require training [7]. It is currently not routinely performed; this additional test adds an extra 2–3 min to the current 20–30-min, first-trimester ultrasound scan, which would cost around an extra £18–25 [14, 15]. It is also not readily available in general antenatal clinics [14].

A meta-analysis concluded that the first-trimester uterine artery Doppler in low-risk women is a useful tool to predict early-onset pre-eclampsia and other adverse pregnancy outcomes, thus justifying aspirin prophylaxis in positive tests [16].

The UtA-PI alone or in combination with notching is the most predictive Doppler index for pre-eclampsia [17, 18]. The UtA-PI is a better predictor of pre-eclampsia than of intrauterine growth restriction [17]. Notching is a characteristic waveform that indicates a decrease in the early diastolic flow of the uterine artery when compared to the later diastolic flow [17]. Impedance to flow in the uterine arteries is increased in pre-eclampsia and/or growth restriction [19].

19.4 Protocol for Recording the Uterine Artery Doppler in the First Trimester

1. First, obtain a sagittal section of the uterus and cervical canal by transabdominal ultrasound. Then, zoom into the area of interest [20]. This is shown in Fig. 19.1.
2. Second, to identify the uterine arteries, first identify the internal cervical os and gently tilt

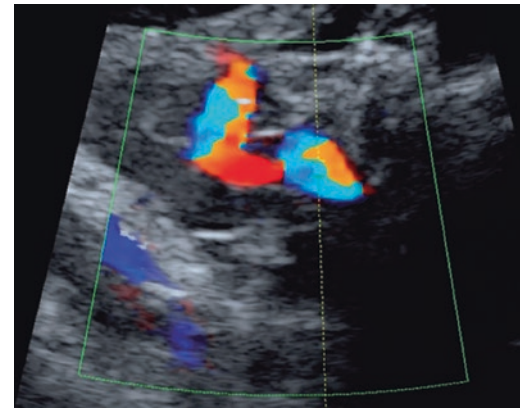

Fig. 19.1 Sagittal section of the uterus and cervix. The color flow mapping is used to identify the uterine arteries along the side of the cervix and uterus [20]

the transducer from side to side using color flow mapping to find the arteries. When you apply color Doppler, narrow the color box and adjust the velocity scale and the filter [20]. This is shown in Fig. 19.2.

3. Third, apply pulsed wave Doppler with the sampling gate set at 2 mm to cover the whole vessel. Ensure that the angle of insonation is <30° [20].
4. Finally, record at least three consecutive uniform waveforms [20]. This is seen in Fig. 19.3.
5. The UtA-PI should be measured for both the left and right uterine arteries and the mean calculated. The pulsatility index of each artery is calculated as the difference between the peak systolic velocity (S) and the end-diastolic velocity (D). This is then divided by the mean velocity (V_m); PI = $(S - D)/V_m$.

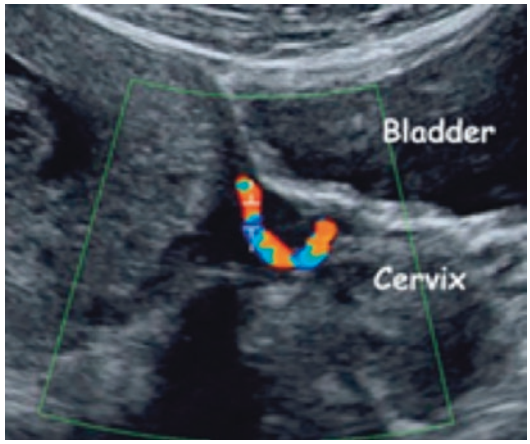

Fig. 19.2 The ascending branch of the uterine artery at its paracervical section and at the point closest to the internal os. Pulsed wave Doppler has been used to obtain the flow velocity waveforms [20]

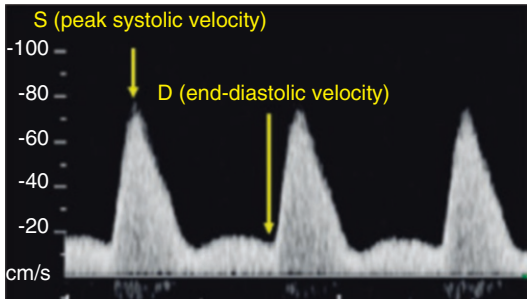

Fig. 19.3 Schematic of three similar consecutive waveforms. The pulsatility index should be measured and the mean taken from the left and right uterine arteries [20]

19.5 First-Trimester-Combined Screening Algorithms for Fetal Growth Restriction and Pre-eclampsia

A variety of screening tools are used in the first trimester to predict the likelihood of complications later on in pregnancy. The combination of different assessments has the most successful prediction of complications. These assessments can include Doppler velocimetry, maternal risk factors, biophysical profile and serum biomarkers.

19.5.1 Maternal Risk Factors

A simple and traditional screening of pregnant mothers is the assessment of predisposing factors for developing pre-eclampsia [2]. The National Institute of Health and Care Excellence (NICE) guidelines recommend that pre-eclampsia screening be carried out by ascertaining the maternal risk factors.

The NICE guidelines have a list of "high-risk" and "moderate-risk" maternal risk factors for pre-eclampsia [21]. The NICE states that if a woman has two or more "moderate-risk" maternal risk factors, then she is classified as "high-risk" for pre-eclampsia [21]. Figure 19.4 shows these moderate- and high-risk maternal risk factors [21].

Other known maternal risk factors for pre-eclampsia include thrombophilia, connective tissue diseases, hydatidiform mole, hydrops fetalis and triploidy [2].

The NICE guidelines suggest treatment based on the presence of the above-mentioned "moderate-risk" and "high-risk" maternal risk factors [21]. The treatment plan they suggest is shown in Fig. 19.5.

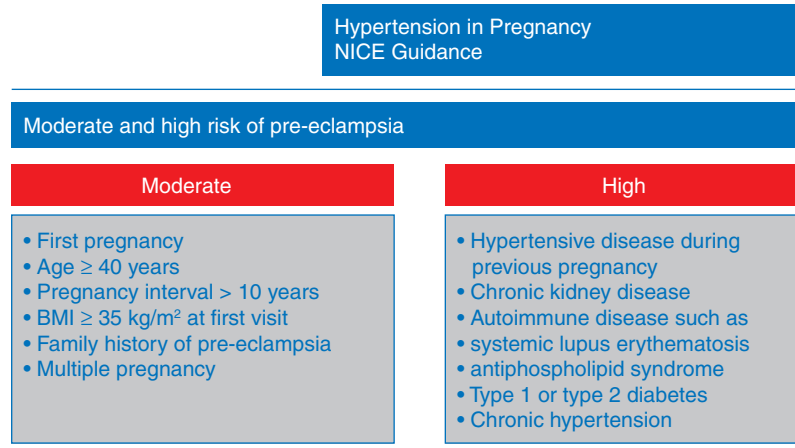

Fig. 19.4 "Moderate-risk" and "high-risk" maternal risk factors as laid out by the NICE guidelines. Any woman with two or more moderate-risk maternal risk factors is classified as "high-risk" [21]

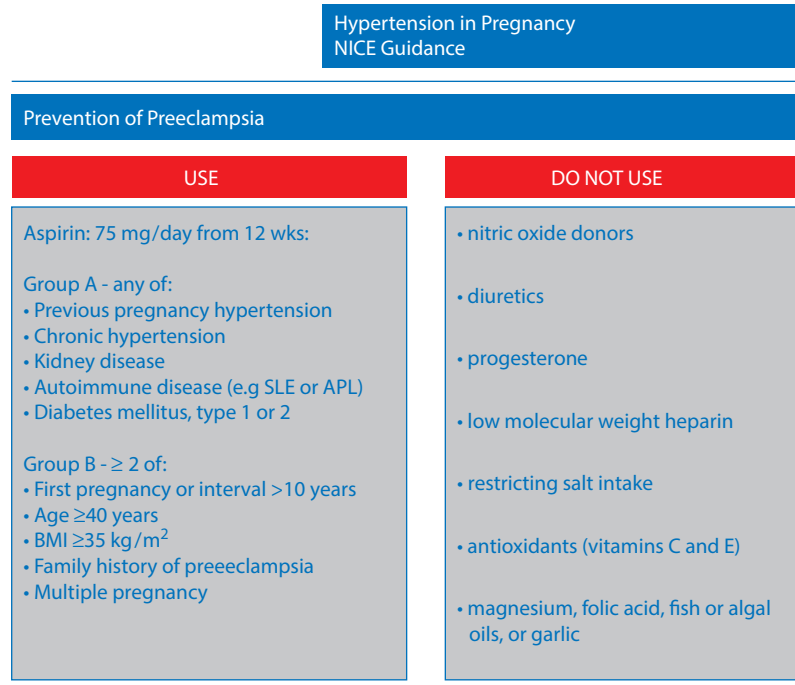

Fig. 19.5 The NICE guidelines suggest the prescription of aspirin for prophylaxis; the drugs that do not work in pre-eclampsia prophylaxis are also displayed here [21]

19.5.2 Serum Biomarkers

Measurement of placental growth factor (PlGF) from maternal blood samples has been suggested as a test for pre-eclampsia. Low PlGF results improve the predictive accuracy for preterm pre-eclampsia [22]. This test could easily be added to the blood tests carried out as part of the screening test for Down's syndrome, but there would be an additional cost [7].

Studies have found that maternal serum beta-human chorionic gonadotropin (beta-hCG) is not a useful biomarker for pre-eclampsia prediction [23].

The first-trimester low levels of serum placental protein 13 (PP13), PlGF and pregnancy-associated plasma protein-A (PAPP-A), plus an increased level of inhibin A, are significantly associated with the risk of term pre-eclampsia [23]. These need to be tested for in combination,

as they have limited potential as single serum biomarkers [23].

19.5.3 The Uterine Artery Pulsatility Index in Combination with Other Tests

A combined screening is by far more superior than the more traditional screening, which is based on maternal risk factors alone [7, 14]. The NICE guidelines recommend screening of maternal risk factors alone, but it has been found that as few as 41% of early, 39% of preterm and 34% of term pre-eclampsia are detected by this screening approach [24]. Many research studies have identified that first-trimester screening for term pre-eclampsia yields poor results [7, 25].

A variety of different combination tests have been investigated by various studies. The following paragraphs illustrate some of these potentially useful combinations.

The UtA-PI can be carried out in combination with maternal history, blood pressure (BP), plasma protein-A and PlGF. For a 5% false-positive rate, it is estimated that 90% of pre-eclampsia cases requiring preterm delivery can be predicted and 45% of term pre-eclampsia cases can be predicted [20].

The UtA-PI can be carried out in combination with serum PP13 and pulse wave analysis. In women at a high risk of pre-eclampsia, for a 10% false-positive rate, it is estimated that it can achieve a 92.9% detection rate of preterm pre-eclampsia and an 85.7% detection rate of all pre-eclampsia cases [26]. These estimates were reported in a cohort of high-risk women for pre-eclampsia.

The combination of the UtA-PI, MAP, maternal risk factors and PlGF can predict 90% of early pre-eclampsia, 75% of preterm pre-eclampsia and 41% of term pre-eclampsia [7]. An identical research study found that 100% of early pre-eclampsia cases were identified [24]. With this combination of screening, it has been found that prediction is more successful in Afro-Caribbean women than in Caucasian women.

- The detection rate of early pre-eclampsia is 88% in Caucasian women and 100% in Afro-Caribbean women [7].
- The detection rate of + preterm pre-eclampsia is 69% in Caucasian women and 92% in Afro-Caribbean women [7].
- The detection rate of term pre-eclampsia is 40% in Caucasian women and 75% in Afro-Caribbean women [7].

PlGF has been found to be the best individual biomarker out of UtA-PI, MAP and maternal risk factors. The UtA-PI and MAP are both the next best as individual biomarkers [7].

19.6 Second-Trimester Doppler Velocimetry of the Uteroplacental Circulation for the Prediction of Fetal Growth Restriction and Pre-eclampsia

Second-trimester Doppler examination of the uterine artery offers the opportunity to identify those pregnancies at a high risk of stillbirth due to placental dysfunction [27].

It has been shown that an abnormal UtA-PI has a 3–4-factor increase in the likelihood of stillbirth in the general population [15]. The measurement of the UtA-PI alone has been shown to predict around 24–35% of stillbirths occurring both preterm and at term [27]. The UtA-PI is still relatively easy to measure during the second trimester [15]. It could be done at the time of the 20-week anomaly scan, thus saving money and time [15].

An increased UtA-PI with notching best predicts overall pre-eclampsia in high- and low-risk patients [17]. An increased UtA-PI or bilateral notching best predicts severe pre-eclampsia [17]. For FGR, an increased UtA-PI alone or with notching is the best predictor in low-risk patients [17]. For FGR in high-risk patients, the best predictor is an increased resistance index [17].

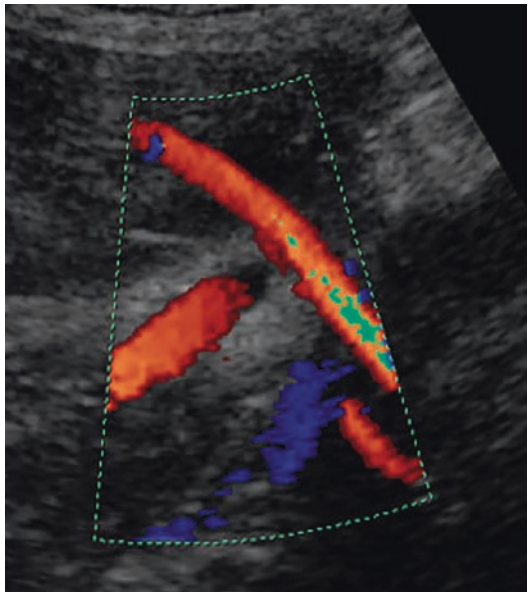

Fig. 19.6 Color Doppler image of the uterine artery at the level at which it crosses the external iliac artery [19]

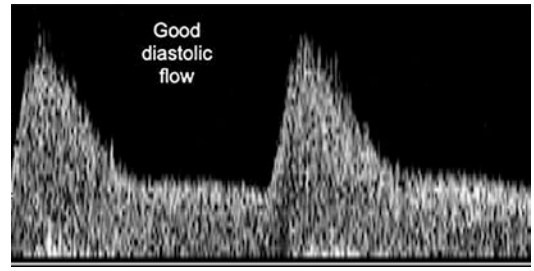

Fig. 19.7 Waveform of the UtA-PI showing a good diastolic flow in the second trimester

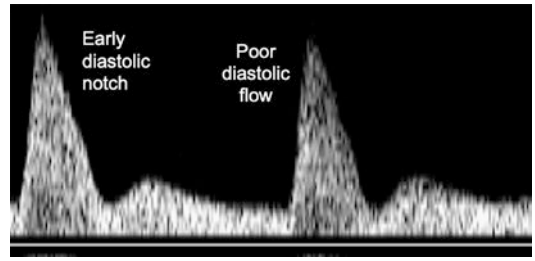

Fig. 19.8 Waveform showing early diastolic notching, which indicates a decrease in the early diastolic flow of the uterine artery in the second trimester

19.7 Protocol for Recording the Uterine Artery Doppler in the Second Trimester

1. Using a color Doppler, first, obtain a view of the left and right uterine arteries at the level at which they cross over to the external iliac artery. A Doppler of this image can be seen in Fig. 19.6.
2. Second, use pulsed wave Doppler to measure the UtA-PI at an angle of insonation <30°.
3. Finally, record at least three consecutive uniform waveforms.
4. The UtA-PI should be measured for both the left and right uterine arteries and the mean calculated. The pulsatility index of each artery is calculated as the difference between the peak systolic velocity and the end-diastolic velocity. This is then divided by the mean velocity.

As gestation progresses, the mean UtA-PI shows a steady decrease [28]. The prevalence of bilateral notching decreases as the gestational age increases, and it continues to do so until 34 weeks' gestation [28]. This could be explained by the trophoblastic invasion proceeding slowly through the late second and third trimesters or by the increase in maternal cardiac output and reduction in peripheral resistance and blood viscosity [28]. As was mentioned earlier, the UtA can also increase due to a hormonal effect on the arterial wall's elasticity [1]. An abnormal result of the UtA-PI in the uterine artery is defined as either a pulsatility index higher than the 95 percentile or the presence of an early diastolic notch [19]. Figure 19.7 shows a good diastolic flow waveform in the second trimester, and Fig. 19.8 shows a poor diastolic flow waveform in the second trimester.

19.8 Second-Trimester-Combined Screening Algorithms for Fetal Growth Restriction and Pre-eclampsia

In the UK, there is currently no routine screening for detecting pregnancies at a high risk of stillbirth [15].

Studies have shown that second-trimester screening can identify the majority of high-risk pregnancies for small-for-gestational-age babies as well as for detecting lower-birthweight babies and earlier gestational ages at birth [29]. This can be done by screening for maternal factors, UtA-PI and fetal biometry in combination [29].

It has been shown that combining the Doppler characteristics of the UtA-PI or the uterine artery resistance index (UtA-RI) and bilateral notching with maternal characteristic screening can improve the identification of pre-eclampsia in nulliparous women [30].

Screening for early pre-eclampsia in the second trimester may not require as many biomarkers, given that uterine artery Doppler alone is substantially more accurate in the second trimester [5]. A study found uterine artery Doppler, MAP and maternal history to be simple, inexpensive and sufficient for second-trimester screening [5].

19.9 Third-Trimester-Combined Screening Algorithms for Fetal Growth Restriction and Pre-eclampsia

Low PlGF results have heightened the predictive accuracy for preterm pre-eclampsia in the third trimester, particularly for cases requiring preterm delivery [22].

Research shows that third-trimester screening is most beneficial to women who develop term pre-eclampsia. Screening of these women in the first trimester by the UtA-PI has a low detection rate for term pre-eclampsia. Furthermore, prophylactic aspirin is also not effective in reducing the risk of term pre-eclampsia. However, first-trimester screening by a combination of serum biomarkers could potentially be more successful for the identification of term pre-eclampsia than third-trimester screening [7]. The biomarkers identified as having the ability to screen for term pre-eclampsia are a combination of maternal factors, MAP, PlGF and serum soluble fms-like tyrosine kinase-1 (sFlT) [7]. This combination has a detection rate of 70% at a screen positive rate of 10%; it would identify women who require close monitoring and potentially early delivery [7].

19.10 Longitudinal Screening for Changes in Doppler Velocimetry of the Uteroplacental Circulation for the Prediction of Fetal Growth Restriction and Pre-eclampsia

Longitudinal screening for changes in Doppler velocimetry of the uteroplacental circulation has the ability to predict particular disease outcomes. An increase in the mean UtA-PI throughout a pregnancy has been associated with the risk of developing hypertensive disorders of pregnancy [3, 31]. As gestational age increases, the difference in the UtA-PI also increases between normal pregnancies and pre-eclampsia pregnancies. Interestingly, the increase in the UtA-PI has been seen in the first trimester in preterm pre-eclampsia, whereas some studies have found that the changes in term pre-eclampsia become apparent only during the third trimester [3]. This is believed to be due to preterm pre-eclampsia being associated with insufficient trophoblastic invasion of the spiral arteries, whereas term pre-eclampsia could be associated with vasoconstriction of the spiral arteries in later stages of the pregnancy [3]. The measurement of the UtA-PI could therefore be considered as a screening tool for preterm pre-eclampsia.

19.11 Limitations of Doppler Velocimetry of the Uteroplacental Circulation

Doppler signals can be affected by maternal body mass index (BMI), size of the placenta, placental location, red blood cell density and site of vascular measurement within the placenta [32]. This is also dependent on the ability and training of the practitioner.

19.12 Effect of Low-Dose Aspirin on the Uteroplacental Circulation during Pregnancy in Women at a Risk of Developing Pre-eclampsia

It has been shown that the administration of aspirin to women in the first trimester with high-risk pregnancies for pre-eclampsia results in a significant reduction in the incidence of severe pre-eclampsia, fetal growth restriction and preterm birth [6, 33, 34]. Women who are classified as "high-risk" by uterine artery Doppler alone and started on aspirin showed a significant reduction in pre-eclampsia [35].

There is an increase in thromboxane A2 vasoconstrictor levels in pre-eclampsia. Low-dose aspirin suppresses platelet activity, which produce and release thromboxane [2]. Aspirin has also been shown to modify the release of cytokines, reduce apoptosis and improve the function of trophoblasts in early pre-eclampsia cases [32]. The beneficial effect is an improvement of the uterine spiral arteries' transformation stage [33].

"Low-dose" aspirin varies among studies from 50 to 150 mg per day [33]. It seems that higher doses of aspirin are more efficient than are lower doses in improving placental parameters before 11 weeks [6]. Low-dose aspirin is safe, inexpensive and widely available [6].

Administering aspirin before 16 weeks' gestation has been shown to reduce the risk of perinatal death, pre-eclampsia, fetal growth restriction and preterm birth more so than aspirin administered after 16 weeks [33]. Aspirin before 16 weeks can reduce the relative risk of pre-eclampsia and IUGR by almost half [13]. Figure 19.9 shows the benefit of administering aspirin before 16 weeks on certain pathologies compared to its administration after 16 weeks.

Some studies only show significant effects in the group that takes aspirin before 16 weeks and not in the group that takes aspirin after 16 weeks [35]. This is due to placental implantation and spiral artery transformation being mostly com-

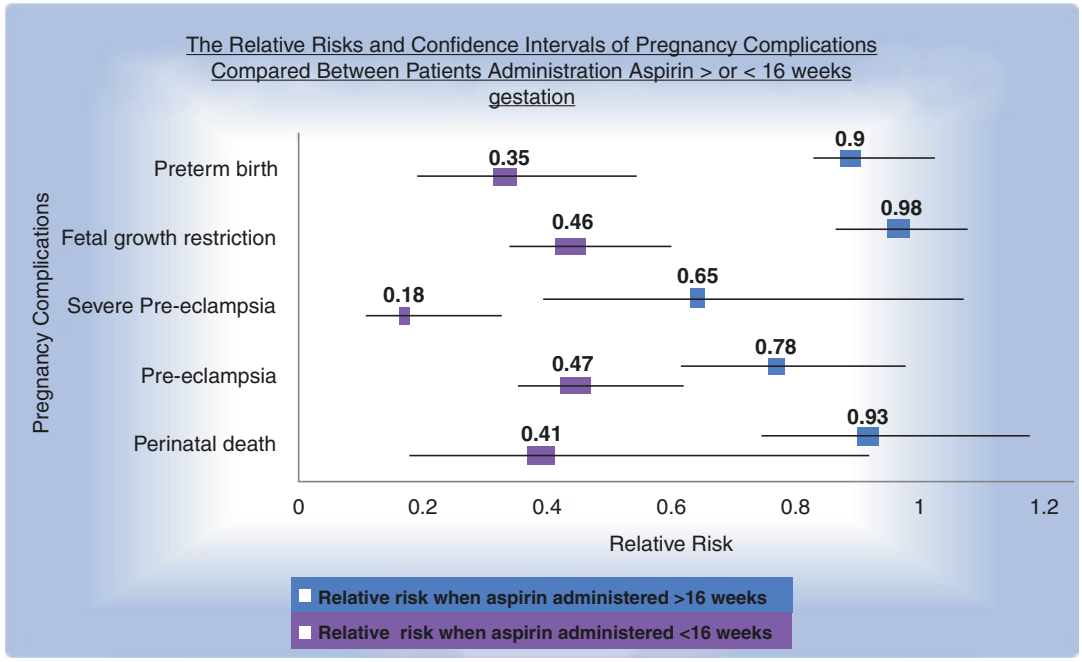

Fig. 19.9 Relative risk and 95% confidence intervals of complications during pregnancy when administration of aspirin occurs at <16 weeks or >16 weeks in women at a high risk of pre-eclampsia [33]

plete by weeks 16–20 [33]. Aspirin has an effect on the function of trophoblast cells during placental implantation [33].

The Aspirin for Evidence-Based Preeclampsia Prevention (ASPRE) trial has demonstrated the benefits of aspirin to be dependent on compliance. The higher the compliance, the more substantial is the effect of aspirin [36]. Factors that are associated with reduced compliance are smoking, belonging to the Afro-Caribbean or South Asian race, maternal age less than 25 years and multiparity with a history of pre-eclampsia [36]. In women with compliance >90%, their preterm pre-eclampsia incidence was reduced by 75% [36]. In women with compliance <90%, their preterm pre-eclampsia incidence was reduced by only 40% [36].

It must be noted that 30% of pregnant women are resistant to the effects of aspirin [37]. Higher doses may be required for these women [37]. In one such study, it seems that aspirin does not improve the perfusion of the uteroplacental circulation nor does it improve placental volume if the aspirin dose is not high enough [32].

The risk of early pre-eclampsia may be reduced by as much as 90% by low-dose aspirin prophylaxis. Preterm pre-eclampsia risk is reduced by as much as 60% by low-dose aspirin prophylaxis [25], whereas term pre-eclampsia is not only difficult to screen for during the first trimester but also it has been shown that the use of low-dose aspirin is not effective in reducing its incidence [7, 25].

19.12.1 Pharmacology in Pre-eclampsia

Maternal sildenafil was investigated as a potential treatment to prolong the pregnancy or improve pregnancy outcomes in cases of severe early-onset fetal growth restriction. However, it did not prove successful [38].

Alpha-methyldopa is an antihypertensive widely used in obstetrics. The benefits must always outweigh the risks when prescribing this drug, and informed consent from the mother is required [21]. Alpha-methyldopa was also investigated for its effect on the UtA-PI. It was discovered that there was no significant effect on uterine artery blood flow resistance. This suggests that there are no adverse effects on the uteroplacental circulation but that there is also no beneficial effect on it either [39]. This shows that although antihypertensives are beneficial for maternal outcomes, there is no beneficial effect on reducing the risk of fetal demise [39]. When using alpha-methyldopa, it should be stopped 2 days before delivery [21].

Nifedipine is widely used in obstetrics, but it is advised that nifedipine be contraindicated before 20 weeks and not be administered throughout the entire pregnancy without informed consent and with the benefits outweighing the risks [21].

The atenolol antihypertensive has possible risks in the first and second trimesters, and, so, its benefits and risks must be weighed [21]. Informed consent is required from the mother.

Labetalol is an antihypertensive used in pregnancy. The NICE states that it should only be used during the first trimester of pregnancy; after that, the benefits and risks must be weighed and informed consent gained [21].

Angiotensin-converting enzyme (ACE) inhibitors or angiotensin 2 receptor blockers (ARBs) reduce blood pressure but cannot be taken during pregnancy due to their risk of increased congenital abnormalities [21]. Women with chronic hypertension need to therefore be changed to another antihypertensive treatment if they are planning a pregnancy [21].

Chlorothiazide is an antihypertensive medication used in chronic hypertension; there is limited evidence showing no increased risk of congenital abnormalities [21]. There may, however, still be an increased risk of congenital abnormalities. The risks and benefits must be weighed, and other hypertensive treatments could be discussed if the woman is planning a pregnancy [21].

Dietary sodium should be reduced in women with chronic hypertension who are planning a pregnancy [21]. This can reduce BP but not prevent pre-eclampsia [21].

19.13 Conclusions

It is clear that a combined screening for pre-eclampsia is superior than the traditional screening approach recommended by the NICE guidelines [24]. The main objective of the first- and second-trimester screening for pre-eclampsia is to identify women at a high risk of early and preterm pre-eclampsia [7]. It is these women who are more easily identified and who will benefit most from prophylactic aspirin [7]. By far the most promising combination screening is the use of uterine artery Doppler, maternal characteristics and multiple serum markers, such as PlGF [23].

Although uterine artery Doppler studies are more accurate in the second trimester, it is important to identify high-risk pregnancies and start the aspirin prior to 16 weeks of gestation to gain the benefit [33]. Although early and preterm pre-eclampsia are less frequent than term pre-eclampsia, they are the main contributors to maternal and perinatal morbidity and mortality [8]. This makes it just as important to be screened for as term pre-eclampsia in the third trimester. A large meta-analysis has justified the prophylactic use of aspirin in low-risk women who have a positive uterine artery Doppler test for pre-eclampsia due to its sufficiently high performance [16].

Term pre-eclampsia is more difficult to screen for in the first and second trimesters. Research supports the concept that early or preterm and term pre-eclampsia are different disease entities [4, 5]. Third-trimester screening would be more successful for term pre-eclampsia. It would identify who requires further monitoring and potentially early delivery [7].

Currently, the best method of screening would be a whole-population approach rather than specifically focusing on women with a significant "high-risk" medical history [7]. This would avoid missing women at a risk of pre-eclampsia who have no significant medical history. This type of screening would have an effect on cost and resources, but, until criteria are laid out that minimizes the number of missed pre-eclampsia cases, this may be the best strategy. An alternative approach could be to screen all women with the most successful biomarker, and, then, carry out the combined screening tests on those deemed "high-risk" [7]. It has also been recommended that women with a pre-eclampsia risk of at least 6–10%, such as women with a past history of pre-eclampsia, can be recommended aspirin without additional assessment; in these cases, the simple screening of maternal factors currently in use is effective [14, 34]. This is justified by aspirin being effective, safe and inexpensive [34].

With regard to aspirin dosing, it is difficult knowing who may be more resistant to aspirin and require a higher dose in order to have the same prophylactic benefit [37]. Until research has looked into this, all women will need to be screened for in the first trimester and given the standard dose of aspirin.

Further research is required to see how feasible a combined screening is for nation-wide antenatal clinics. Would the benefits of treating more pre-eclampsia cases outweigh the extra cost and time?

Combined screening programs have proven more successful than the traditional route of maternal risk screening by the NICE guidelines, but maternal risk screening is still important [24].

A study has demonstrated that the use of aspirin in low-risk women has no significant effect on the UtA-PI, placental Doppler indices or placental volume [32]. However, a universal screening program of all women is the best approach until further research is carried out [7].

References

1. Maulik D, Zalud I. Doppler ultrasound in obstetrics and gynecology, 2nd ed. Springer; 2005.
2. Magowan B, Owen P, Drife J. Clinical obstetrics & gynaecology, 3rd ed. Saunders Elsevier; 2009.
3. Khalil A, Garcia-Mandujano R, Maiz N, Elkhaouli M, Nicolaides KH. Longitudinal changes in uterine artery Doppler and blood pressure and risk of pre-eclampsia. Ultrasound Obstet Gynecol. 2014;43:541–7.
4. Nelson DB, Ziadie MS, McIntire DD, Rogers BB, Leveno KJ. Placental pathology suggesting that pre-eclampsia is more than one disease. Am J Obstet Gynecol. 2014;210(1):66.e1–7.

5. Pedrosa AC, Matias A. Screening for pre-eclampsia: a systematic review of tests combining uterine artery Doppler with other markers. J Perinat Med. 2011;39(6):619–35.
6. Zvanca ME, Bot M, Radu D, Radu N, Petca A. Impact of early supplementation with low-dose aspirin on functional first trimester parameters in low-risk pregnancies. J Matern Fetal Neonatal Med. 2019;32(4):604–9.
7. Tan MY, Syngelaki A, Poon LC, Rolnik DL, O'Gorman N, Delgado JL, et al. Screening for pre-eclampsia by maternal factors and biomarkers at 11-13 weeks' gestation. Ultrasound Obstet Gynecol. 2018;52(2):186–95.
8. Rosemary T, Khalil A. First trimester combined screening algorithms for fetal growth restriction. In: Lees C, Visser GHA, Hecher K, editors. Placental–fetal growth restriction. Cambridge: Cambridge University Press; 2018. p. 95–104.
9. Khalil A, Akolekar R, Syngelaki A, Perez Penco JM, Nicolaides KH. Effect of chorionic villus sampling on uterine artery Doppler. Fetal Diagn Ther. 2010;28:9–13.
10. Salomon LJ, Sotiriadis A, Wulff C, Odibo A, Akolekar R. Risk of miscarriage following amniocentesis or chorionic villus sampling: systematic review of the literature and updated meta-analysis. Ultrasound Obstet Gynecol. 2019;54(4):442–51. https://doi.org/10.1002/uog.20353.
11. Townsend R, Khalil A. Maternal cardiovascular function and fetal growth restriction. In: Lees C, Visser GHA, Hecher K, editors. Placental-fetal growth restriction. Cambridge: Cambridge University Press; 2018. p. 65–73.
12. Kampman MA, Bilardo CM, Mulder BJ, Aarnoudse JG, Ris-Stalpers C, van Veldhuisen DJ, et al. Maternal cardiac function, uteroplacental Doppler flow parameters and pregnancy outcome: a systematic review. Ultrasound Obstet Gynecol. 2015;46(1):21–8.
13. Bujold E, Roberge S, Lacasse Y, Bureau M, Audibert F, Marcoux S, et al. Prevention of preeclampsia and intrauterine growth restriction with aspirin started in early pregnancy: a meta-analysis. Obstet Gynecol Surv. 2010;116(2):402–14.
14. Al-Rubaie Z, Askie LM, Ray JG, Hudson HM, Lord SJ. The performance of risk prediction models for pre-eclampsia using routinely collected maternal characteristics and comparison with models that include specialised tests and with clinical guideline decision rules: a systematic review. BJOG. 2016;123(9):1441–52.
15. Allen RE, Morlando M, Thilaganathan B, Zamora J, Khan KS, Thangaratinam S, et al. Predictive accuracy of second-trimester uterine artery Doppler indices for stillbirth: a systematic review and meta-analysis. Ultrasound Obstet Gynecol. 2016;47(1):22–7.
16. Velauthar L, Plana MN, Kalidindi M, Zamora J, Thilaganathan B, Illanes SE, et al. First-trimester uterine artery Doppler and adverse pregnancy outcome: a meta-analysis involving 55,974 women. Ultrasound Obstet Gynecol. 2014;43(5):500–7.
17. Cnossen JS, Morris RK, ter Riet G, Mol BW, van der Post JA, Coomarasamy A, et al. Use of uterine artery Doppler ultrasonography to predict pre-eclampsia and intrauterine growth restriction: a systematic review and bivariable meta-analysis. CMAJ. 2008;178(6):701–11.
18. Townsend R, Khalil A, Premakumar Y, Allotey J, Snell KIE, Chan C, et al. Prediction of pre-eclampsia: review of reviews. Ultrasound Obstet Gynecol. 2019;54:16–27.
19. Nicolaides K, Rizzo G, Hecher K, Ximenes R. Doppler in obstetrics. The Fetal Medicine Foundation; 2002.
20. Khalil A, Nicolaides KH. How to record uterine artery Doppler in the first trimester. Ultrasound Obstet Gynecol. 2013;42:478–9.
21. National Institute for Health and Care Excellence. Hypertension in pregnancy: diagnosis and management. 2019.
22. Navaratnam K, Abreu P, Clarke H, Jorgensen A, Alfirevic A, Alfirevic Z. Evaluation of agreement of placental growth factor (PlGF) tests and the soluble FMS-like tyrosine kinase 1 (sFlt-1)/PlGF ratio, comparison of predictive accuracy for pre-eclampsia, and relation to uterine artery Doppler and response to aspirin. J Matern Fetal Neonatal Med. 2019;32(2):179–87.
23. Kuc S, Wortelboer EJ, van Rijn BB, Franx A, Visser GH, Schielen PC. Evaluation of 7 serum biomarkers and uterine artery Doppler ultrasound for first-trimester prediction of preeclampsia: a systematic review. Obstet Gynecol Surv. 2011;66(4):225–39.
24. O'Gorman N, Wright D, Poon LC, Rolnik DL, Syngelaki A, de Alvarado M, et al. Multicenter screening for pre-eclampsia by maternal factors and biomarkers at 11-13 weeks' gestation: comparison with NICE guidelines and ACOG recommendations. Ultrasound Obstet Gynecol. 2017;49(6):756–60.
25. Rolnik DL, Wright D, Poon LC, O'Gorman N, Syngelaki A, de Paco Matallana C, et al. Aspirin versus placebo in pregnancies at high risk for preterm preeclampsia. N Engl J Med. 2017;377(7):613–22.
26. Khalil A, Cowans NJ, Spencer K, Goichman S, Meiri H, Harrington K. First-trimester markers for the prediction of pre-eclampsia in women with a-priori high risk. Ultrasound Obstet Gynecol. 2010;35:671–9.
27. Familiari A, Scala C, Morlando M, Bhide A, Khalil A, Thilaganathan B. Mid-pregnancy fetal growth, uteroplacental Doppler indices and maternal demographic characteristics: role in prediction of stillbirth. Acta Obstet Gynecol Scand. 2016;95:1313–8.
28. Gómez O, Figueras F, Fernández S, Bennasar M, Martínez JM, Puerto B, et al. Reference ranges for uterine artery mean pulsatility index at 11-41 weeks of gestation. Ultrasound Obstet Gynecol. 2008;32(2):128–32.
29. Familiari A, Bhide A, Morlando M, Scala C, Khalil A, Thilaganathan B. Mid-pregnancy fetal biometry, uterine artery Doppler indices and maternal demographic

characteristics: role in prediction of small-for-gestational-age birth. Acta Obstet Gynecol Scand. 2015;95:238–44.
30. Kleinrouweler CE, Bossuyt PM, Thilaganathan B, Vollebregt KC, Arenas Ramírez J, Ohkuchi A, et al. Value of adding second-trimester uterine artery Doppler to patient characteristics in identification of nulliparous women at increased risk for pre-eclampsia: an individual patient data meta-analysis. Ultrasound Obstet Gynecol. 2013;42(3):257–67.
31. Binder J, Monaghan C, Thilaganthan B, Carta S, Khalil A. De-novo abnormal uteroplacental circulation in third trimester: pregnancy outcome and pathological implications. Ultrasound Obstet Gynecol. 2018;52:60–5.
32. Mulcahy C, Mone F, McParland P, Breathnach F, Cody F, Morrison JJ, et al. The impact of aspirin on ultrasound markers of uteroplacental flow in low-risk pregnancy: secondary analysis of a multicenter RCT. Am J Perinatol. 2019;36(8):855–63.
33. Roberge S, Nicolaides KH, Demers S, Villa P, Bujold E. Prevention of perinatal death and adverse perinatal outcome using low-dose aspirin: a meta-analysis. Ultrasound Obstet Gynecol. 2013;41(5):491–9.
34. Bartsch E, Park AL, Kingdom JC, Ray JG. Risk threshold for starting low dose aspirin in pregnancy to prevent preeclampsia: an opportunity at a low cost. PLoS One. 2015;10(3):e0116296.
35. Bujold E, Morency AM, Roberge S, Lacasse Y, Forest JC, Giguère Y. Acetylsalicylic acid for the prevention of preeclampsia and intra-uterine growth restriction in women with abnormal uterine artery Doppler: a systematic review and meta-analysis. J Obstet Gynaecol Can. 2009;31(9):818–26.
36. Wright D, Poon LC, Rolnik DL, Syngelaki A, Delgado JL, Vojtassakova D, et al. Aspirin for evidence-based preeclampsia prevention trial: influence of compliance on beneficial effect of aspirin in prevention of preterm preeclampsia. Am J Obstet Gynecol. 2017;217(6):685.
37. Dumont A, Flahault A, Beaufils M, Verdy E, Uzan S. Effect of aspirin in pregnant women is dependent on increase in bleeding time. Am J Obstet Gynecol. 1999;180(1):135–40.
38. Sharp A, Cornforth C, Jackson R, Harrold J, Turner MA, Kenny LC, et al. Maternal sildenafil for severe fetal growth restriction (STRIDER): a multicentre, randomised, placebo-controlled, double-blind trial. Lancet Child Adolesc Health. 2018;2:93–102.
39. Khalil A, Harrington K, Muttukrishna S, Jauniaux E. Effect of antihypertensive therapy withα-methyldopa on uterine artery Doppler in pregnancies with hypertensive disorders. Ultrasound Obstet Gynecol. 2010;35:688–94.

Uterine Doppler Velocimetry and Hypertensive Disease

20

Tiziana Frusca, Andrea Dall'Asta, and Elvira Di Pasquo

20.1 Introduction

The uterine arteries are paired vessels that supply nutrients to the feto-placental unit during pregnancy [1]. Sufficient uteroplacental blood flow is essential for a normal pregnancy outcome and is usually granted by the "remodeling" process, which, under normal circumstances, leads to a deep invasion of the spiral arteries up to the myometrial radial arteries [2]. This process, starting from the first weeks of pregnancy, is usually completed by 24 weeks and is responsible for the increased flow in diastole and the steep decrease in uterine artery impedance [3].

Early studies demonstrated a relationship between the placental histological findings and the presence of pregnancy complications named as "placental syndromes," which include pre-eclampsia (PE) and intrauterine growth restriction (IUGR). In particular, these studies noted the absence of physiological changes in the myometrial segments of the uterine arteries in women presenting "placental syndromes" and a shallower placentation due to the fact that the remodeling process was limited to the decidual segments alone. This anomaly led to an increased resistance of the uteroplacental circulation and ultimately to impaired placental function [4]. The structural changes of the spiral arteries related to the remodeling process are reflected by quantitative (e.g., decrease in the pulsatility index (PI) and resistance index (RI)) and qualitative (e.g., disappearance of the protodiastolic notching) waveform modifications at Doppler assessment [5, 6]. In early studies, the clinical conditions associated with defective deep placentation included chronic hypertension, pre-eclampsia, and pre-eclampsia with intrauterine growth restriction.

It should be noted that histological studies have shown a strong association between impaired remodeling process and PE and IUGR arising at early gestation [4]. Conversely, a clear relationship between defective placentation and late-onset PE or IUGR has not been demonstrated [7–9].

The increasing use of color Doppler ultrasound has allowed a better understanding of the pathophysiological changes of the uterine circulation since the first weeks of gestation and has led to increasing attention on the potential use of Doppler velocimetry of the uterine arteries as part of the antenatal screening strategy [10]. Moreover, the clinical importance of uterine artery (UtA) Doppler as a screening test for PE and other hypertensive disorders in pregnancy (HDP) is not only related to the positive and negative predictive values of the test but also is dependent on the possibility of performing a prophylactic strategy and a targeted follow-up on the population identified to be at high risk [7, 8].

T. Frusca (✉) · A. Dall'Asta · E. Di Pasquo
Department of Medicine and Surgery, Obstetrics and Gynecology Unit, University of Parma, Parma, Italy
e-mail: tiziana.frusca@unipr.it

D. Maulik, C. C. Lees (eds.), *Doppler Ultrasound in Obstetrics and Gynecology*,
https://doi.org/10.1007/978-3-031-06189-9_20

20.2 Technical Considerations

Different techniques for the assessment of UtA Doppler have been described for each trimester of pregnancy [11]. The uterine arteries can be visualized either transabdominally or transvaginally, and different ranges have been published for each approach [12, 13].

The transvaginal assessment requires an empty bladder and a dorsal lithotomic position. After having identified the midsagittal plane of the cervix and the uterus, the probe moves into the lateral fornix and the uterine arteries are usually identified by means of color Doppler paracervically at the level of the internal cervical os.

For the transabdominal assessment, a midsagittal section of the uterus and the cervix has to be obtained as well, and, then, the probe is moved sideways so that the uterine arteries could be identified by the use of color Doppler paracervically during the first trimester and at the region of apparent crossover to the external iliac arteries during the second trimester. The pulsed wave Doppler set at about 2 mm should have an insonation angle <30°, and the obtained peak of systolic velocity should be >60 cm/s; finally, three similar consecutive waveforms should be considered to calculate the UtA pulsatility index (PI) and resistance index (RI) [11] (Fig. 20.1).

A considerable amount of evidence indicates the superiority of the mean UtA-PI as the preferred Doppler index for the screening of PE in the first and second trimesters. For this reason, the pulsatility index (PI) rather than the resistance index (RI) should be used in the clinical context [14]. Although the presence of bilateral notches is known to be associated with maternal endothelial dysfunction, caution should be exercised, as in the first trimester these may also occur in uncomplicated pregnancies, thus reducing the specificity of the test. On the other hand, the assessment of UtA Doppler in the second trimester has similar sensitivity to that of an increased PI but for a higher screen-positive rate [14].

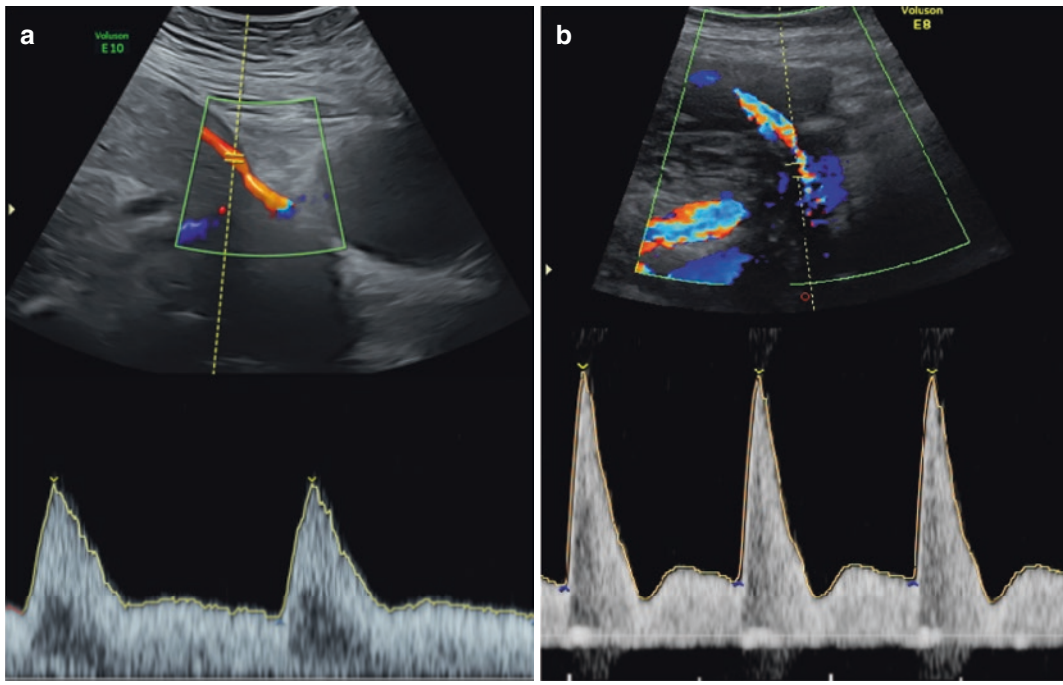

Fig. 20.1 Second-trimester uterine artery Doppler waveform: (**a**) left, normal waveform: no notch and good diastolic flow and (**b**) right, early diastolic notch with restricted diastolic flow

20.3 Role of Uterine Artery Velocimetry in the Prediction of Hypertensive Disorders of Pregnancy

Since the 1990s, various studies have demonstrated an association between high uterine resistances and an increased risk of perinatal complications; however, the positive predictive value of the test was found to be extremely low [15, 16]. Lees et al. [17] first tested the predictive value of the UtA-PI performed at 23 weeks for severe adverse pregnancy outcomes including fetal death, pre-eclampsia before 34 weeks, small for gestational age (SGA) <10th percentile and placental abruption. Analyzing more than 5000 women, they described a quadratic relationship between the increasing mean UtA-PI and the likelihood of subsequent severe perinatal complications not affected by other maternal characteristics (age, ethnicity, or parity), except for smoking: using the 95th percentile of the mean UtA-PI as the cut-off value, the likelihood ratio (LR) for severe adverse pregnancy outcomes was about five-fold higher.

In 2008, a meta-analysis [18] including 74 studies on pre-eclampsia prediction (n = 79,547) and 61 studies on IUGR prediction found that the predictive value of uterine Doppler indices varies according to the *patient risk profile* and *outcome severity*. The second-trimester rather than the first-trimester UtA-PI, alone or in combination with notching, is the best predictive parameter with a positive likelihood ratio (LR+) of the PI associated with notching for pre-eclampsia, which is different among high- (LR+ = 21.0) and low-risk patients (LR+ = 7.5).

Although this study had some important biases affecting the definition of "low-risk" and "high-risk" women, these findings suggested a possible different performance of uterine Doppler evaluation depending on the following characteristics:

- "A priori" risk of the patient (i.e., low- vs. high-risk)
- Severity of the evaluated outcome (i.e., early- vs. late-onset disease)
- Gestational age at the screening test (i.e., first trimester vs second trimester)

20.4 Role of Uterine Artery Velocimetry in the Prediction of Hypertensive Disorders of Pregnancy in Low- and High-Risk Women

Traditional methods to stratify the risk of pre-eclampsia and IUGR are based on the evaluation of the personal risk profile (including age, ethnicity, parity, smoking, medical and obstetric history, and conception method) and the metabolic risk profile (including body mass index (BMI) and history of diabetes).

Based on the maternal personal and metabolic risk profiles, different studies tested the value of UtA Doppler in predicting HDP in low-risk women and found contrasting results. In 2005, Yu et al. [19] performed a prospective screening study for pre-eclampsia using the UtA-PI in 32,157 consecutive low-risk women defined on the basis of maternal characteristics, smoking and alcohol intake, medical and obstetric history, and family history of pre-eclampsia. They found that ultrasound was better at predicting pre-eclampsia than maternal characteristics, but the combination of both methods provided the best estimate. Interestingly, by splitting the analysis to evaluate the predictive value of both maternal and ultrasound characteristics for early- and late-onset disease, they found that the predictive value of ultrasound alone was not improved by adding maternal predictors (area under the curve (AUC) 0.92 vs 0.94, respectively; p = 0.27) for early-onset PE. Conversely, late-onset PE was better predicted by the combined model rather than by ultrasound or maternal characteristics alone.

Myatt et al. [20] evaluated uterine artery velocimetry in a cohort of 2188 low-risk nulliparous women. They reported a poor sensitivity of second-trimester Doppler ultrasound measurements for prediction of pre-eclampsia with a sensitivity of 43% and a specificity of 67% for prediction of pre-eclampsia overall.

More consistent results were obtained from studies on the predictive value of UtA Doppler in women at a high risk of HDP. Early studies [21, 22] tested the RI and/or the presence of uterine notching to evaluate the predictive value for

hypertensive disorders of pregnancy and other adverse pregnancy outcomes. Their results consistently demonstrated that UtA Doppler assessment in the second trimester of gestation is a useful method to predict adverse outcomes, with high negative predictive values.

Further studies [23–25] on high-risk categories of women, including those with chronic hypertension, previous history of pre-eclampsia and antiphospholipid antibodies, were all concordant with the evidence that UtA Doppler velocimetry identifies a subgroup of women with a high frequency of HDP or pregnancy complications. However, in 2009, Herraiz et al. [26] performed a longitudinal study including 152 high-risk pregnancies (at least one among previous pre-eclampsia, hypertension, pre-gestational diabetes, renal disease, obesity, thrombophilia, autoimmune disorders, hyperlipidemia, recurrent pregnancy loss) to test a first-trimester predictive model for pre-eclampsia based on UtA Doppler and maternal history. They demonstrated that such a model had a 25% detection rate for late-onset PE and a 50–60% detection rate for early-onset disease, highly similar to that observed in the low-risk women.

20.5 Role of Doppler Velocimetry of the Uterine Arteries in the Prediction of Early-Onset vs Late-Onset Pre-eclampsia

In an unselected population of women, Papageorghiou et al. [27] demonstrated that the mid-gestation mean UtA-PI >95th percentile had a poor sensitivity in detecting all cases of pre-eclampsia (41%), but this sensitivity value rose to 93% considering those cases of pre-eclampsia requiring delivery before 32 weeks of gestation. Similarly, Onwudiwe et al. [28] found that a combination of maternal variables, UtA Doppler and mean arterial pressure (MAP) in a population of more than 3500 women was able to detect 100% of early pre-eclampsia and 56.4% of late pre-eclampsia at a false-positive rate of 10%.

Further studies involving both high- and low-risk women were consistent in demonstrating that the predictive value of UtA Doppler is higher in the prediction of early-onset disease compared to that of late-onset disease. Such a finding was also confirmed by studies conducted during the first trimester. Martin et al. [29] reported that the mean UtA-PI >95th percentile performed between 11 and 13 weeks of gestation was able to detect 60% of pre-eclampsia and 27.8% of IUGR requiring delivery before 32 weeks, while the sensitivity for the overall incidence of these complications was extremely low (27% and 11.7%, respectively).

In conclusion, there is conflicting evidence on the predictive value for pre-eclampsia of UtA Doppler in low-risk women; more favorable results have been demonstrated in high-risk women. In both cases, UtA Doppler best identifies the severe early-onset complications of impaired placentation.

20.6 Role of Doppler Velocimetry of the Uterine Arteries in the First and Second Trimesters

Given the evidence that preventive strategies for reducing the risk of PE are effective if started at <16 weeks, a considerable amount of studies have investigated the performance of UtA Doppler in the first trimester. Most studies were consistent in demonstrating that the sensitivity in predicting overall pre-eclampsia was not extremely high, ranging between 7 and 41%; this value was slightly higher considering early-onset disease (24–81%) [29–33].

The meta-analysis by Cnossen et al. [18] concluded that UtA provided a more accurate prediction when performed in the second trimester than in the first trimester, but preventive strategies have proved to be effective only if started before 16 weeks of gestation. Based on the fact that the predictive value of UtA Doppler varies based on the "a priori" patient risk, alternative approaches to estimate the risk of pre-eclampsia have been developed. The most used one is the algorithm for pre-eclampsia risk at 11–13 weeks developed by the Fetal Medicine Foundation

(FMF). Such an algorithm uses a combination of maternal factors with biophysical markers (mean arterial pressure (MAP) and mean UtA-PI) and biochemical markers (pregnancy-associated plasma protein-A (PAPP-A) and placental growth factor (PlGF)). When all markers are used, 90% of pre-eclampsia cases require delivery before 32 weeks, 75% of pre-eclampsia cases require delivery before 37 weeks and 55% were identified in the first trimester [34, 35].

Evidence indicates that the performance of the FMF algorithm is superior to the methods recommended by the National Institute of Health and Clinical Excellence and the American College of Obstetricians and Gynecologists [36]. However, the utility of this test in the context of first-trimester screening is still debatable. A recent cohort study has concluded that adding first-trimester MAP, PAPP-A, and PlGF did not improve the prediction value compared to the model based on a simple risk score including maternal history [37].

20.7 Longitudinal Changes in Uterine Artery Doppler Indices

Longitudinal changes in uterine artery Doppler indices have gained much interest in the prediction of pre-eclampsia [38, 39]. A longitudinal study on 870 women reported that an increased PI recorded between 11 and 14 weeks then normalized in the second trimester (between 19 and 22 weeks of gestation) in 73% of cases. Cases with a mean UtA-PI >95th percentile, which were persistently abnormal in the second trimester (37%), were at the highest risk of HDP and IUGR [39]. Another study on 104 women with an increased uterine artery PI at 20–22 weeks reported that abnormal findings persisted at 26–28 weeks in 59.6% of cases; in this latter group, the risk of PE was much higher (16% vs 1%) than in those women showing a normal mean UtA-PI in the third trimester [40].

Finally, a recent multi-center study [41] has investigated the potential value of repeat measurements of the UtA-PI, mean arterial pressure (MAP), and serum placental growth factor (PlGF) at 12, 22, and 32 weeks' gestation in the prediction of pre-eclampsia (PE) developing after 32 weeks. This study demonstrated that screening at 30–34 weeks by the UtA-PI, MAP, and PlGF detected, at a 10% false-positive rate, 79%, 86%, and 92% of preterm PE and 42%, 50%, and 56% of term PE, respectively. The addition of biomarker values at 11–13 and/or 19–24 weeks was not associated with any improvement in the detection rate of preterm pre-eclampsia.

20.8 Role of Uterine Artery Doppler in the Management of Hypertensive Disorders of Pregnancy

The outcome of pregnancies complicated by HDP is dependent upon factors including the gestational age at onset and the severity of the disease as well as on pre-existing maternal complications such as diabetes mellitus, systemic lupus erythematosus, and chronic kidney disease. According to the latest recommendations proposed by the International Society for the Study of Hypertension in Pregnancy, HDP encompass conditions characterized either by hypertension known before pregnancy or present in the first 20 weeks of gestation, including chronic hypertension, white coat hypertension, and masked hypertension, or by hypertension arising de novo at or beyond 20 weeks, as it happens in the case of gestational hypertension (GH), pre-eclampsia (PE), and PE superimposed on chronic hypertension [42].

Doppler velocimetry of the uterine arteries has been investigated in relation to the risk of maternal and neonatal complications in women with GH. Frusca et al. demonstrated a lower mean gestational age at delivery and a lower mean birthweight in women with GH and abnormal UtA Doppler, which was also associated with a nine-fold higher incidence of preterm delivery <34 weeks and a 15-fold higher rate of IUGR. In the same study, the comparison of the perinatal outcomes between women with GH and abnormal UtA Doppler with all cases of PE

yielded no difference between the two groups. Overall, abnormal UtA Doppler was associated with more than a 13-fold higher risk of IUGR or delivery <34 weeks compared to cases with normal UtA Doppler [43]. Consistently, two studies focusing on women with chronic hypertension demonstrated a strong association between Doppler abnormalities of the UtA and superimposed PE, IUGR, early delivery and maternal and perinatal complications [25, 44]. More specifically, the higher the gestational age at identification of the abnormal UtA Doppler findings, the higher is the likelihood of superimposed PE [25, 44]. On the other hand, a normal UtA Doppler beyond 25 weeks of gestation was associated with an overall risk of developing superimposed PE as low as 8% [44].

Other research groups have investigated the prognostic role of UtA Doppler in women with HDP. Meler et al. first demonstrated the predictive role of UtA Doppler in the occurrence of adverse perinatal outcomes in women with early- and late-onset PE [45]. On the grounds of this, another study from the same research group, evaluating 120 women with severe early-onset PE, showed that abnormal UtA Doppler represents a risk factor for adverse outcomes in terms of low gestational age at diagnosis and at delivery, low birthweight and increased rate of maternal and perinatal complications [46]. Similar findings were observed in another observational study including women diagnosed with pre-eclampsia beyond 34 weeks and showing lower gestational age at diagnosis and lower mean birthweight in cases with abnormal mean UtA Doppler, among whom the neonatal admission occurred in more than 30% of cases and was over three-fold higher compared to women with normal UtA Doppler [47]. Additionally, the incidence of maternal complications was shown to be higher in women with late-onset PE and abnormal UtA Doppler compared to those with normal flow across the uterine arteries.

Therefore, available evidence has shown that abnormal UtA Doppler represents a risk factor for the progression and occurrence of complications related to HDP independently from the gestational age at the onset of disease. On this basis, it has been hypothesized that UtA Doppler may be included as a primary surveillance test in women with PE [45]. It is important to note, however, that abnormal UtA Doppler has been demonstrated to occur only in approximately one out of three women with PE [48] and is far more common in early-onset compared to late-onset disease [45].

20.9 Insights into the Dual Etiology of Pre-eclampsia: Role of the Assessment of Uterine Artery Doppler

Placental perfusion and function are known to be involved in the pathogenesis of the so-called "placental syndromes," among which are PE and IUGR. A former echocardiographic study including a selected cohort of normotensive and asymptomatic nulliparous women submitted to UtA Doppler and echocardiographic assessment at 24 weeks of gestation demonstrated the existence of two different hemodynamic patterns in the context of PE: the former, most commonly referred to as "early-onset" PE and characterized by reduced cardiac output (CO), increased systemic vascular resistance (SVR), and fetal smallness, and the latter, known as "late-onset" PE, showing the opposite hemodynamic pattern and associated with appropriate or large-for-gestational-age (LGA) fetuses [49]. As expected, this study showed a strong association between the gestational age at the onset of disease and the finding of bilateral notching at UtA Doppler assessment. In detail, 60% women eventually diagnosed with early-onset PE showed abnormal UtA Doppler waveform at 24 weeks, which was significantly higher compared to the rate recorded in the late-onset PE group (15.6%).

In this context, a study including more than 26,000 pregnancies—among which 1167 cases were women with late-onset PE—showed a higher incidence of IUGR in women with late-onset PE and abnormal UtA Doppler assessment at mid-trimester, and, conversely, a higher rate of large-for-gestational-age (LGA) neonates compared to healthy controls in cases of late-onset PE

was associated with low impedance of the uterine arteries in the second trimester [50]. Such a finding supports the role of UtA Doppler in discriminating the conditions of PE associated with fetal smallness—i.e., in the case of an increased mean UtA-PI—from those with normal fetal growth—i.e., in the case of UtA Doppler velocimetry characterized by normal or low resistance.

Very recently, an observational study by Tay et al. has confirmed the relationship between abnormal UtA Doppler and fetal smallness in patients diagnosed with PE independently from the GA of onset as well as the association between UtA Doppler and maternal cardiovascular function in PE with and without associated IUGR [51].

On this basis, a retrospective study conducted by Ferrazzi et al. on 441 women with HDP further supported the hypothesis that the evaluation of UtA Doppler may help in the discrimination of conditions of HDP characterized by fetal smallness from those associated with normal fetal growth or overgrowth [52]. In detail, the relationship between fetal smallness, as defined by abdominal circumference <5th percentile of local standards, and abnormal UtA Doppler in terms of the mean UtA pulsatility index >95th percentile was confirmed in almost 75% of the included cases. Furthermore, the coexistence of normal AC and UtA Doppler within the context of HDP identified a cohort of normally grown fetuses with no difference in terms of birthweight percentile between cases of GH and PE [52]. Such findings again support the concept that fetal size and UtA Doppler may better discriminate between the two different phenotypes of PE compared to the gestational age at the onset of disease.

References

1. Pijnenborg R, Vercruysse L, Hanssens M. The uterine spiral arteries in human pregnancy: facts and controversies. Placenta. 2006;27(9–10):939–58.
2. James JL, Saghian R, Perwick R, Clark AR. Trophoblast plugs: impact on utero-placental haemodynamics and spiral artery remodelling. Hum Reprod. 2018;33(8):1430–41.
3. Clark AR, James JL, Stevenson GN, Collins SL. Understanding abnormal uterine artery Doppler waveforms: a novel computational model to explore potential causes within the utero-placental vasculature. Placenta. 2018;66:74–81.
4. Khong Y, Brosens I. Defective deep placentation. Best Pract Res Clin Obstet Gynaecol. 2011;25(3):301–11.
5. Jurkovic D, Jauniaux E, Kurjak A, Hustin J, Campbell S, Nicolaides KH. Transvaginal color Doppler assessment of the uteroplacental circulation in early pregnancy. Obstet Gynecol. 1991;77:365–9.
6. Jauniaux E, Jurkovic D, Campbell S, Hustin J. Doppler ultrasonographic features of the developing placental circulation; correlation with anatomic findings. Am J Obstet Gynecol. 1992;166:585–7.
7. Redman CWG, Staff AC. Preeclampsia, biomarkers, syncytiothrophoblast stress and placenta capacity. Am J Obstet Gynaecol. 2015;13:1–4.
8. Staff AC, Redman CWG. IFPA award in placentology lecture: making sense of preeclampsia. Placenta. 2014;35:20–5.
9. Fisher SJ. Why is placentation abnormal in preeclampsia? Am J Obstet Gynecol. 2015;213(4 Suppl):S115–22.
10. Steel SA, Pearce JM, McParland P, Chamberlain GV. Early Doppler ultrasound screening in prediction of hypertensive disorders of pregnancy. Lancet. 1990;335(8705):1548–51.
11. Sotiriadis A, Hernandez-Andrade E, da Silva Costa F, et al. ISUOG practice guidelines: role of ultrasound in screening for and follow-up of pre-eclampsia. Ultrasound Obstet Gynecol. 2019;53(1):7–22.
12. Gòmez O, Figueras F, Fernàndez S, Bennasar M, Martìnez JM, Puerto B, Gratacòs E. Reference ranges for uterine artery mean pulsatility index at 11–41 weeks of gestation. Ultrasound Obstet Gynecol. 2008;32:128–32.
13. Bower S, Vyas S, Campbell S, Nicolaides KH. Color Doppler imaging of the uterine artery in pregnancy: normal ranges of impedance to blood flow, mean velocity and volume of flow. Ultrasound Obstet Gynecol. 1992;2(4):261–5.
14. Campbell S, Diaz-Recasens J, Griffin DR, et al. New doppler technique for assessing uteroplacental blood flow. Lancet. 1983;1(8326 Pt 1):675–7.
15. Zimmermann P, Eiriö V, Koskinen J, Kujansuu E, Ranta T. Doppler assessment of the uterine and uteroplacental circulation in the second trimester in pregnancies at high risk for pre-eclampsia and/or intrauterine growth retardation: comparison and correlation between different Doppler parameters. Ultrasound Obstet Gynecol. 1997;9(5):330–8.
16. Kurdi W, Campbell S, Aquilina J, England P, Harrington K. The role of color Doppler imaging of the uterine arteries at 20 weeks' gestation in stratifying antenatal care. Ultrasound Obstet Gynecol. 1998;12(5):339–45.
17. Lees C, Parra M, Missfelder-Lobos H, Morgans A, Fletcher O, Nicolaides KH. Individualized risk assessment for adverse pregnancy outcome by uter-

ine artery Doppler at 23 weeks. Obstet Gynecol. 2001;98(3):369–73.
18. Cnossen JS, Morris RK, ter Riet G, Mol BW, van der Post JA, Coomarasamy A, Zwinderman AH, Robson SC, Bindels PJ, Kleijnen J, Khan KS. Use of uterine artery Doppler ultrasonography to predict pre-eclampsia and intrauterine growth restriction: a systematic review and bivariable meta-analysis. CMAJ. 2008;178(6):701–11.
19. Yu CK, Smith GC, Papageorghiou AT, Cacho AM, Nicolaides KH, Fetal Medicine Foundation Second Trimester Screening Group. An integrated model for the prediction of preeclampsia using maternal factors and uterine artery Doppler velocimetry in unselected low-risk women. Am J Obstet Gynecol. 2005;193(2):429–36.
20. Myatt L, Clifton RG, Roberts JM, et al. The utility of uterine artery Doppler velocimetry in prediction of preeclampsia in a low-risk population. Obstet Gynecol. 2012;120(4):815–22.
21. Axt-Fliedner R, Schwarze A, Nelles I, et al. The value of uterine artery Doppler ultrasound in the prediction of severe complications in a risk population. Arch Gynecol Obstet. 2005;271(1):53–8.
22. Coleman MA, McCowan LM, North RA. Mid-trimester uterine artery Doppler screening as a predictor of adverse pregnancy outcome in high-risk women. Ultrasound Obstet Gynecol. 2000;15(1):7–12.
23. Fratelli N, Rampello S, Guala M, Platto C, Frusca T. Transabdominal uterine artery Doppler between 11 and 14 weeks of gestation for the prediction of outcome in high-risk pregnancies. J Matern Fetal Neonatal Med. 2008;21(6):403–6.
24. Pagani G, Reggia R, Andreoli L, et al. The role of second trimester uterine artery Doppler in pregnancies with systemic lupus erythematosus. Prenat Diagn. 2015;35(5):447–52.
25. Frusca T, Soregaroli M, Zanelli S, Danti L, Guandalini F, Valcamonico A. Role of uterine artery Doppler investigation in pregnant women with chronic hypertension. Eur J Obstet Gynecol Reprod Biol. 1998;79(1):47–50.
26. Herraiz I, Arbués J, Camaño I, Gómez-Montes E, Grañeras A, Galindo A. Application of a first-trimester prediction model for pre-eclampsia based on uterine arteries and maternal history in high-risk pregnancies. Prenat Diagn. 2009;29(12):1123–9.
27. Papageorghiou AT, Yu CK, Bindra R, Pandis G, Nicolaides KH, Fetal Medicine Foundation Second Trimester Screening Group. Multicenter screening for pre-eclampsia and fetal growth restriction by transvaginal uterine artery Doppler at 23 weeks of gestation. Ultrasound Obstet Gynecol. 2001;18(5):441–9.
28. Onwudiwe N, Yu CK, Poon LC, Spiliopoulos I, Nicolaides KH. Prediction of pre-eclampsia by a combination of maternal history, uterine artery Doppler and mean arterial pressure. Ultrasound Obstet Gynecol. 2008;32(7):877–83.
29. Martin AM, Bindra R, Curcio P, Cicero S, Nicolaides KH. Screening for pre-eclampsia and fetal growth restriction by uterine artery Doppler at 11-14 weeks of gestation. Ultrasound Obstet Gynecol. 2001;18(6):583–6.
30. Melchiorre K, Wormald B, Leslie K, Bhide A, Thilaganathan B. First-trimester uterine artery Doppler indices in term and preterm pre-eclampsia. Ultrasound Obstet Gynecol. 2008;32(2):133–7.
31. Gómez O, Martínez JM, Figueras F, et al. Uterine artery Doppler at 11-14 weeks of gestation to screen for hypertensive disorders and associated complications in an unselected population. Ultrasound Obstet Gynecol. 2005;26(5):490–4.
32. Plasencia W, Maiz N, Bonino S, Kaihura C, Nicolaides KH. Uterine artery Doppler at 11 + 0 to 13 + 6 weeks in the prediction of pre-eclampsia. Ultrasound Obstet Gynecol. 2007;30(5):742–9.
33. Pilalis A, Souka AP, Antsaklis P, et al. Screening for pre-eclampsia and small for gestational age fetuses at the 11-14 weeks scan by uterine artery Dopplers. Acta Obstet Gynecol Scand. 2007;86(5):530–4.
34. Tan MY, Syngelaki A, Poon LC, et al. Screening for pre-eclampsia by maternal factors and biomarkers at 11-13 weeks' gestation. Ultrasound Obstet Gynecol. 2018;52(2):186–95.
35. O'Gorman N, Wright D, Poon LC, et al. Accuracy of competing-risks model in screening for pre-eclampsia by maternal factors and biomarkers at 11–13 weeks' gestation [published correction appears in Ultrasound Obstet Gynecol. 2017 Dec;50(6):807]. Ultrasound Obstet Gynecol. 2017;49(6):751–5.
36. O'Gorman N, Wright D, Poon LC, et al. Multicenter screening for pre-eclampsia by maternal factors and biomarkers at 11-13 weeks' gestation: comparison with NICE guidelines and ACOG recommendations [published correction appears in Ultrasound Obstet Gynecol. 2017 Dec;50(6):807]. Ultrasound Obstet Gynecol. 2017;49(6):756–60.
37. Sovio U, Smith G. Evaluation of a simple risk score to predict preterm pre-eclampsia using maternal characteristics: a prospective cohort study. BJOG. 2019;126(8):963–70.
38. Plasencia W, Maiz N, Poon L, Yu C, Nicolaides KH. Uterine artery Doppler at 11 + 0 to 13 + 6 weeks and 21 + 0 to 24 + 6 weeks in the prediction of pre-eclampsia. Ultrasound Obstet Gynecol. 2008;32(2):138–46.
39. Gómez O, Figueras F, Martínez JM, et al. Sequential changes in uterine artery blood flow pattern between the first and second trimesters of gestation in relation to pregnancy outcome. Ultrasound Obstet Gynecol. 2006;28(6):802–8.
40. Ghi T, Contro E, Youssef A, Giorgetta F, Farina A, Pilu G, Pelusi G. Persistence of increased uterine artery resistance in the third trimester and pregnancy outcome. Ultrasound Obstet Gynecol. 2010;36:577–81.
41. Andrietti S, Carlucci S, Wright A, Wright D, Nicolaides KH. Repeat measurements of uterine artery pulsatility index, mean arterial pressure and serum placental growth factor at 12, 22 and 32 weeks

in prediction of pre-eclampsia. Ultrasound Obstet Gynecol. 2017;50(2):221–7.
42. Brown MA, Magee LA, Kenny LC, et al. Hypertensive disorders of pregnancy: ISSHP classification, diagnosis, and management recommendations for international practice. Hypertension. 2018;72(1):24–43.
43. Frusca T, Soregaroli M, Platto C, Enterri L, Lojacono A, Valcamonico A. Uterine artery velocimetry in patients with gestational hypertension. Obstet Gynecol. 2003;102(1):136–40.
44. Roncaglia N, Crippa I, Locatelli A, et al. Prediction of superimposed preeclampsia using uterine artery Doppler velocimetry in women with chronic hypertension. Prenat Diagn. 2008;28(8):710–4.
45. Meler E, Figueras F, Mula R, et al. Prognostic role of uterine artery Doppler in patients with preeclampsia. Fetal Diagn Ther. 2010;27(1):8–13.
46. Meler E, Figueras F, Bennasar M, Gomez O, Crispi F, Gratacos E. The prognostic role of uterine artery Doppler investigation in patients with severe early-onset preeclampsia. Am J Obstet Gynecol. 2010;202(6):559.e1–4.
47. Ghi T, Youssef A, Piva M, et al. The prognostic role of uterine artery Doppler studies in patients with late-onset preeclampsia. Am J Obstet Gynecol. 2009;201(1):36.e1–5. https://doi.org/10.1016/j.ajog.2009.02.024.
48. Li H, Gudnason H, Olofsson P, Dubiel M, Gudmundsson S. Increased uterine artery vascular impedance is related to adverse outcome of pregnancy but is present in only one-third of late third-trimester pre-eclamptic women. Ultrasound Obstet Gynecol. 2005;25(5):459–63. https://doi.org/10.1002/uog.1895.
49. Valensise H, Vasapollo B, Gagliardi G, Novelli GP. Early and late preeclampsia: two different maternal hemodynamic states in the latent phase of the disease. Hypertension. 2008;52(5):873–80.
50. Verlohren S, Melchiorre K, Khalil A, Thilaganathan B. Uterine artery Doppler, birth weight and timing of onset of pre-eclampsia: providing insights into the dual etiology of late-onset pre-eclampsia. Ultrasound Obstet Gynecol. 2014;44(3):293–8.
51. Tay J, Masini G, McEniery CM, et al. Uterine and fetal placental Doppler indices are associated with maternal cardiovascular function. Am J Obstet Gynecol. 2019;220(1):96.e1–8.
52. Ferrazzi E, Zullino S, Stampalija T, et al. Bedside diagnosis of two major clinical phenotypes of hypertensive disorders of pregnancy. Ultrasound Obstet Gynecol. 2016;48(2):224–31.

21 Fetal Doppler Velocimetry in Monochorionic Pregnancy: Twin Reversed Arterial Perfusion, Twin-to-Twin Transfusion Syndrome, and Twin Anemia Polycythemia Sequence

Lee Na Tan, Fionnuala Mone, and Mark D. Kilby

21.1 Twin Pregnancies

Since the advent of assisted reproductive therapies, the incidence of multiple pregnancies has increased significantly. Multiple pregnancies are associated with increased risks of fetal complications such as preterm birth, stillbirth, and neonatal complications [1, 2]. Monochorionicity occurs in 20% of all twin pregnancies and is the result of the cleavage of a single zygote (monozygotic), resulting in fetuses sharing a placenta [3, 4]. Complications specific to monochorionic pregnancies result from the presence of vascular placental anastomoses between the shared placenta, thus connecting the circulation of the twins with consequent disequilibrium of blood flow, which is described later. The majority of monochorionic (MC) pregnancies are monochorionic diamniotic (MCDA) but can also occur in rarer monochorionic-monoamniotic twins (MCMA) (~1%), in addition to higher-order multiples. Detailed ultrasound imaging techniques with pulsed waved and color Doppler are invaluable to the assessment of complicated MC pregnancies and for monitoring following fetal therapy. This chapter aims to discuss the use of several Doppler techniques in the assessment of complicated MC pregnancies.

21.1.1 Diagnosis of Dichorionic Versus Monochorionic Pregnancies

The distinction between dichorionic and monochorionic pregnancies is important to identify monochorionic pregnancies, which require closer monitoring for sequelae of vascular anastomotic complications, whereas uncomplicated dichorionic pregnancies are followed up less frequently. Different methods have been used to determine chorionicity including the number of placentae, the presence of lambda or T signs, membrane thickness, the number of membrane layers, and concordant/discordant fetal sex (from the second trimester onwards) [5].

L. N. Tan
West Midlands Fetal Medicine Centre, Birmingham Women's and Children's NHS Foundation Trust, Birmingham, UK

F. Mone (✉)
Centre for Public Health, Queen's University Belfast, Belfast, UK
e-mail: f.mone@qub.ac.uk

M. D. Kilby
West Midlands Fetal Medicine Centre, Birmingham Women's and Children's NHS Foundation Trust, Birmingham, UK

Institute of Metabolism and Systems Research, College of Medical and Dental Sciences, University of Birmingham, Birmingham, UK

D. Maulik, C. C. Lees (eds.), *Doppler Ultrasound in Obstetrics and Gynecology*,
https://doi.org/10.1007/978-3-031-06189-9_21

The first-trimester assessment conducted at 10–14 weeks using a combination of lambda and T signs and the number of placental masses has been shown to have the highest sensitivity and specificity in differentiating chorionicity [6]. Prenatal ultrasonography was found to correctly diagnose chorionicity in 99.3% of pregnancies, with the most reliable findings for dichorionicity being the combination of lambda signs and two separate placental masses, with a sensitivity of 97.4% and a specificity of 100%, whereas the identification of T signs was 100% sensitive and 98.2% specific for the diagnosis of monochorionicity [6]. The presence of lambda signs, therefore, indicates dichorionic placentation, but, in its absence, dichorionicity cannot be completely ruled out. A systematic review and meta-analysis conducted in 2016 showed that the presence of lambda signs before 14 weeks' pregnancy was 99% sensitive and 95% specific for the prediction of dichorionicity, whereas its absence was 96% sensitive and 99% specific for monochorionicity [7].

The measurement of inter-twin membrane thickness with a cut-off of 1.5 mm has a sensitivity and specificity for monochorionicity of 92.6% [6]. The ultrasonographic findings of two separate placental masses may be seen in almost 3% of monochorionic placentas and therefore may still have inter-twin placental vascular anastomoses [8]. A combination of all ultrasonographic findings, therefore, increases the detection of chorionicity rather than when used in isolation [6].

21.1.2 Vascular Anastomoses

Monochorionic pregnancies are at a significantly greater risk of adverse outcomes than are those that are dichorionic, primarily due to unequal sharing of placental territory and the presence of placental vascular anastomoses. Vascular anastomoses are present in up to 95% of MC pregnancies [9, 10] and subtypes, including (1) arterio-arterial (AA), (2) venovenous (VV), and (3) arteriovenous (AV). AA and VV anastomoses are superficial with bidirectional flow, whereas AV anastomoses are associated with unidirectional blood flow [9, 10]. It is the unidirectional nature of AV anastomoses that predisposes to the net imbalance of blood flow from one fetus to another, resulting in twin-to-twin transfusion syndrome (TTTS) and twin anemia polycythemia sequence (TAPS). It is postulated that the presence of superficial bidirectional AA and VV anastomoses confers some protection against the aforementioned pathological entities [11].

21.2 Adverse Outcomes in Monochorionic Pregnancies

21.2.1 Growth Discordance

Several methods have been described to detect selective fetal growth restriction (sFGR), which include >25% discrepancy in estimated fetal weight (EFW), EFW <10th percentile for gestational age or fetal abdominal circumference discordance ≥20% or 25% [12]. Selective fetal growth restriction is believed to be a consequence of unequal placental territorial sharing and occurs in 25% of MC pregnancies [13, 14]. Such ultrasound findings are associated with not only an increased incidence of intrauterine death (25–30%) and neurological injury (30%), typically in the smaller fetus, but also in the normally grown twin due to the increased risk of acute feto-fetal transfusion following the demise of the co-twin [9, 10, 15–20]. Selective fetal growth restriction is classified based on the appearances of the umbilical artery (UA) Doppler waveform in the growth-restricted twin (Fig. 21.1).

Type I—positive end-diastolic flow (EDF)
Type II—persistently absent or reversed EDF (AREDF) and
Type III—intermittently absent/reversed EDF (iAREDF)

Type I sFGR is associated with more favorable outcomes with a risk of intrauterine loss of 2–4% and neurological injury in 0–4% [22]. There is a relatively small number of AA anastomoses, which allows for relative hemodynamic stability [23]. Such pregnancies can be managed expectantly with close (weekly) ultrasonographic

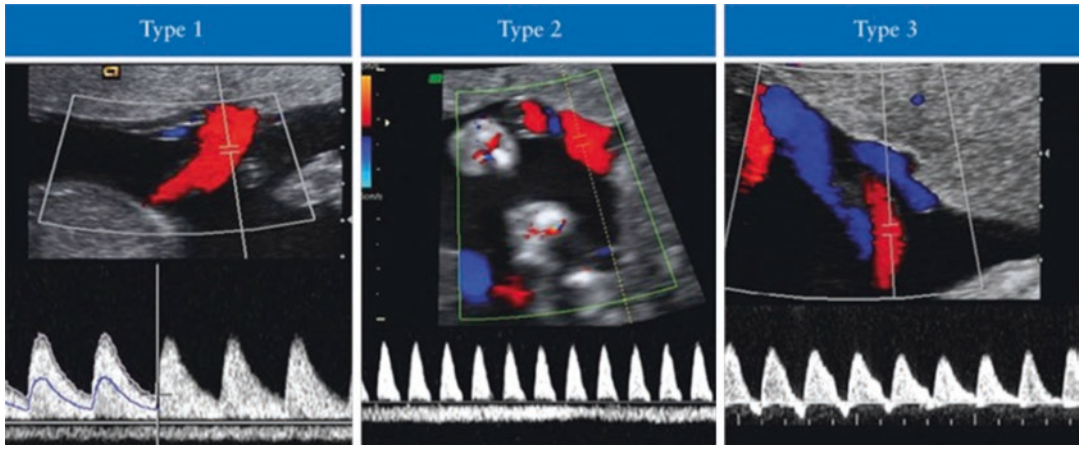

Fig. 21.1 Classification of selective fetal growth restriction in MCDA twin pregnancy using umbilical artery Doppler. Type I—positive end-diastolic flow; type II—absent or reversed end-diastolic flow (AREDF) and type III—cyclical/intermittent pattern of AREDF [21]. (Reproduced with permission from RightsLink® 2019)

surveillance until delivery at 34–35 weeks, depending on the course [23].

Type II sFGR is at a greater risk of deterioration, with 90% having abnormal arterial and venous Dopplers or biophysical profile and neurological damage in 14–15%, and the rates of demise in the growth-restricted and appropriately grown fetuses are 30–40% and 22%, respectively [15, 24]. A systematic review has shown that fetuses with type II sFGR are at a higher risk of perinatal morbidity and mortality than are those with type I sFGR [23].

Although these adverse outcomes are not significantly different in types II and III, type III sFGR usually has an unpredictable clinical course [23]. Type III sFGR is unique to MC pregnancies, which have much larger AA anastomoses compared to those of types I and II sFGR, and these allow continuous blood transfer between the two fetuses [23, 25]. These fetuses are at a higher risk of unexpected fetal demise despite stable Doppler findings, and, therefore, the optimal management of these pregnancies remains controversial. Prenatal fetal surgery, such as cord occlusion or fetoscopic laser ablation (FLA) of placental anastomoses, are treatment options before viable gestation, but these are technically more difficult to perform and with higher rates of complications [23–26].

It is a challenge to estimate the placental share ratio antenatally, with the umbilical cord insertion site or cord mapping a commonly used entity. The cord insertions may include a combination of central/peripheral (peripheral includes marginal and velamentous insertions) or peripheral/peripheral cord insertion sites, which, if present, are likely to correlate with unequal placental sharing and thus the risk of weight discordance [9, 27]. However, the risk of growth discordance in the presence of placental territory discordance is reduced with protective features of increasing diameter of AA anastomoses, net AV transfusion, and total anastomotic diameter [11]. Therefore, inappropriate use of FLA of vascular anastomoses to treat severe discordant growth may lead to the demise of the twin with the smaller placenta, which is reliant upon the anastomoses to obtain sufficient circulation [11].

The management of sFGR in MC pregnancies remains challenging because the natural history of the clinical course is not fully understood and there is a lack of randomized controlled trials to conclude the optimal management pathway [23]. Individualized care should be catered to each pregnancy, taking into account the gestational age at diagnosis, the severity of weight discordance, and Doppler abnormalities [23].

21.2.2 Twin-to-Twin Transfusion Syndrome

TTTS complicates up to 10–15% of MC pregnancies and has a fetal mortality rate of 90–100% if untreated [28, 29]. The earlier TTTS Quintero staging system is based on ultrasonographic findings (Table 21.1), but weight discordance, fetal echocardiography, and the presence or absence of superficial anastomoses are not part of the diagnostic criteria although these may have crucial prognostic values [30, 31]. This staging system is simple and most commonly used, but its prognostic and chronological values are still debatable. The Children's Hospital of Philadelphia (CHOP) cardiovascular score was developed to represent the cardiovascular status of the twins, and a prospective cohort study to evaluate its usefulness to prognosticate MC pregnancies showed that the preoperative cardiac function system was not predictive of twin survival or perinatal prognosis [32].

More recently, a prognostic score has been proposed for post-operative perinatal survival based on fetal, obstetric, and intraoperative factors, which include gestational age at diagnosis, weight discordance, umbilical artery and ductus venosus abnormalities in the donor and recipient, cervical length, selectivity of surgery, and transplacental approach [33]. Dual twin survival is associated with smaller weight discordance and cervical length of more than 15 mm, whereas single twin survival is associated with transplacental approach, UA Doppler abnormalities in either twin and type III sFGR [33]. Further studies are required to validate these findings and their use in a clinical setting.

TTTS may occur at any gestation, and its course is unpredictable; for example, most stage I TTTS remain stable or resolve, but, when progression occurs (30% of stage I progress), it may quickly progress to severe TTTS, or bladder for donor twins may be visible in "atypical" stage III or IV TTTS, or TTTS may sometimes regress/improve spontaneously [32]. In the case of single twin demise, the survivor twin has a 10% risk of demise and 10–30% risk of neurological injury [34]. Clinical guidance recommends that MC pregnancies have surveillance ultrasonography for TTTS fortnightly from 16 weeks, including assessment of liquor volume, bladder visualization, and UA Doppler by an appropriately trained professional [35]. Concomitant sFGR may complicate the diagnosis of TTTS, as abnormal UA Doppler waveforms are seen in both pathologies. MC fetuses with abnormal UA Doppler should have more frequent monitoring should the coexistence of either pathology be suspected [35].

Discrepancies in crown rump length, elevated nuchal translucency and/or abnormal ductus venous waveforms in the first trimester serve as predictors of TTTS, and more frequent surveillance should be conducted in these instances [35]. Although fetal cardiac function is not formally required for diagnosis of TTTS, functional cardiac abnormalities may be used to identify cases in early TTTS who may benefit from early selective FLA as well as assessment treatment response [35]. Normalization in cardiac function can be seen by 4 weeks of selective

Table 21.1 Staging of twin-to-twin transfusion syndrome (Quintero staging)

Stage	Criteria
I	Discordance in amniotic fluid volumes Oligohydramnios with MPD <2 cm sac Polyhydramnios with MPD > 8 cm (<20 weeks gestation) or >10 cm (>20 weeks gestation)
II	Bladder of donor twin not visible for at least 1 h of scanning
III	Persistent critically abnormal arterial or venous Doppler studies in either or both Umbilical artery Doppler AREDF Ductus venosus Doppler AREDF in A-wave Umbilical vein pulsatile flow
IV	Ascites, skin edema, pericardial effusion, pleural effusion, or hydrops in one or both fetuses
V	Death of one or both fetuses

MPD maximum pool depth, *AREDF* absent or reversed end-diastolic flow

FLA; however, the donor fetus may develop transient abnormalities in DV flow and tricuspid regurgitation, which usually regress within 4 weeks [36].

Selective FLA of vascular anastomoses has been shown to improve the survival of fetuses with TTTS, with a single twin survival of 91% and a dual twin survival of 67%, and is superior to other treatment options including serial amniodrainage, septostomy, or selective reduction [37]. Single twin survival does not differ across stages, although dual twin survival is reduced in stage III disease, secondary to decreased donor twin survival (sFGR is also seen more frequently in donor twins in this group) [37]. The neurological outcomes of fetuses with TTTS have been shown to improve following selective FLA compared to serial amniodrainage [38]. Post-FLA assessment should include liquor and Doppler studies to exclude persistence/recurrence of TTTS or TAPS. The use of the Solomon technique (ablation of the vascular equator to "di-chorionise" the placenta) during FLA has reduced the occurrence of recurrent TTTS and TAPS from 7% to 1% and 16% to 3%, respectively [39].

21.2.3 Twin Anemia Polycythemia Sequence

TAPS may occur spontaneously or following FLA, with an incidence of 1–5% and 1–16%, respectively [40]. This occurs when there are small AV anastomoses, leading to slow, unidirectional transfusion of blood from the donor to the recipient, in the absence of compensation from AA anastomoses [41]. TAPS is diagnosed prenatally through assessment of the peak systolic velocity (PSV) of the middle cerebral artery (MCA) Doppler and postnatally by hemoglobin discordances between the fetuses in MC pregnancies (Table 21.2). Additional ultrasound features include differences in thickness and echogenicity of the shared placenta [42]. Spontaneous TAPS typically occurs after 26 weeks' gestation, whereas TAPS post FLA occurs up to 5 weeks following FLA, with the former "recipient" in TTTS becoming the "donor" in TAPS and vice versa [41]. There is a paucity of perinatal outcome data for TAPS, with neonatal outcomes also spanning from isolated inter-twin hemoglobin differences to severe morbidity, with the need for donor blood transfusion and an increased incidence of renal damage and cerebral injury [42]. Recipient neonates may require partial exchange transfusions and are at an increased risk of "hyperviscosity syndrome," leading to skin necrosis, limb ischemia, and severe cerebral injury [42].

The optimal management of TAPS is unclear, although there are therapies for the same including FLA, intrauterine blood transfusion (donor) with partial exchange transfusion (recipient), selective feticide, expectant management, or earlier delivery [42, 43]. Post-FLA TAPS has been attributed to the presence of residual AA anastomoses (usually near the placental margin); hence, use of the Solomon technique can reduce the incidence of TAPS from 16% to 3% without adversely affecting morbidity/mortality, serious adverse events, and neurodevelopmental outcomes of the fetuses [39, 44].

Table 21.2 Prenatal staging of twin anemia polycythemia sequence

Stage	Criteria	Postnatal hemoglobin discrepancy (g/L)
I	MCA PSV >1.5 MoM (donor) and <1.0 MoM (recipient)	>80
II	MCA PSV >1.7 MoM (donor) and <0.8 MoM (recipient)	>110
III	Critically abnormal Doppler • Umbilical artery Doppler AREDF • Ductus venosus Doppler AREDF of A-wave • Umbilical vein pulsatile flow	>140
IV	Hydrops of one or both fetuses	>170
V	Death of one or both fetuses	>200

MCA middle cerebral artery, *PSV* peak systolic velocity, *MoM* multiples of the median, *AREDF* absent or reversed end-diastolic flow

21.2.4 Twin Reversed Arterial Perfusion Sequence

The TRAP sequence is a rare complication of MC pregnancies, occurring in 2.6%, with an overall incidence of 1 in 10,000 pregnancies [45]. The TRAP sequence consists of an apparently normal "pump" twin, which perfuses an abnormal "acardiac" fetus via unidirectional AA and VV anastomoses. Color Doppler assessment of the UA typically shows reversed arterial flow for the acardiac fetus [46].

Formation of acardiac twins has been postulated to be due to irregular splitting of the embryoblasts, and this hypothesis was supported by model simulations [47]. Before the "acardiac" onset, the placenta of the smaller twin is highly likely to be growing normally [48]. However, the smaller (future "acardiac") twin has a smaller-than-normal pressure gradient of body perfusion to the future "pump" twin, so it is forced to share the perfusion of its placenta with the larger twin [48]. This results in chronic hypoperfusion of the smaller twin, allowing the larger twin to increase its blood volume and pressures with larger-than-normal placental access [48]. There is limited access to oxygenated blood for the acardiac twin as the smaller placenta of the acardiac twin is subsequently perfused completely by the pump twin only, and acardiac circulation is by substantially less oxygenated blood from the pump twin via AA anastomoses [48].

The onset of acardiac twins, therefore, requires both the presence of AA and VV anastomoses and cessation of cardiac function of the smaller twin [48]. Chronic hypoxia and underperfusion lead to impaired development of organs in the acardiac twin with severe and often bizarre malformations, with a continuously decreasing acardiac flow resistance, which triggers cardiovascular complications in pump twins [48]. Lower limbs are usually better developed in the acardiac fetus than in the upper body as blood enters the iliac arteries, but some fetuses have good development of the upper part of the body including the heart, and hence the name "pseudo"-acardiac [47, 48].

Without treatment, the overall perinatal mortality of pump twins is 55% as a result of high-output cardiac failure and prematurity, occurring frequently as a consequence of polyhydramnios [49]. Prognosis is strongly related to the weight ratio of the acardiac pump twin, with an incidence of preterm delivery of 90%, polyhydramnios of 40%, and pump twin congestive heart failure of 30% with a weight ratio >70% [49]. Recent studies via model simulations for acardiac twin pregnancies have disputed this, suggesting that the acardiac fetus blood volumetric size may not affect the pump twin very much if any at all [48, 49]. An initial study reported that uncomplicated TRAP pregnancies show relatively larger umbilical vein (UV) diameter ratios with gestation, whereas TRAP twins that developed complications had decreasing ratios [50]. A model simulation study performed based on this proposal agreed with this concurred finding that the UV diameter ratio may predict the outcomes of pump twins by measuring their excess cardiac output fraction [49]. The UV measurement is preferred in this instance because each fetus has one UV, which makes acquisition easier [50]. The size of AA anastomoses (reflecting resistance) is the main factor that determines the pump twin's excess cardiac output [48, 49]. Larger AA anastomoses with lower resistance lead to a larger acardiac perfusion flow and a larger acardiac fetus [49]. Subsequent pump twin venous hypertension is a probable cause of fetal hydrops in pump fetuses [49].

The TRAP sequence is increasingly diagnosed in the first trimester due to first-trimester screening, and the use of color Doppler where suspected is paramount [46, 50]. Therapies for the TRAP sequence include bipolar cord coagulation, fetoscopic laser coagulation, intra-fetal laser coagulation, cord ligation, radiofrequency ablation and high-intensity focused ultrasound with selection depending on operator preference, amnionicity, and gestation [45]. Conservative management is also optional in the absence of pump twin compromise. The treatment of choice depends on the operator experience as well as the gestation and amnionicity of the pregnancies. Treatment may be delayed until there is evidence of pump twin compromise, or prophylactically at 16–19 weeks, after obliteration of the celomic

cavity to reduce the risk of miscarriage and talipes, or prophylactically at 12–14 weeks to avoid the risk of pump twin death before 16 weeks [46]. The technical difficulty with intervening only when there is evidence of pump twin compromise is achieving a complete arrest of flow in the larger, often hydropic acardiac mass later on in the pregnancy, in which case the outcome for the pump twin may be worse when there is the presence of cardiac strain prior to treatment [46]. Patients with TRAP treated prophylactically between 16 and 18 weeks have been associated with 90% survival with an average delivery at 37–38 weeks' gestation [46]. However, up to half of the pump twins in cases diagnosed in the first trimester had spontaneous demise by 18 weeks in the absence of treatment, with survivors at an increased risk of neurological injury (85%) [46]. Studies assessing early intervention using intrafetal coagulation with a small diameter equipment have shown promising results with a loss rate of 25% [45]. A multi-center randomized controlled trial named the TRAPIST study (TRAP Intervention STudy) is currently ongoing to compare the outcomes of early with those of late intervention [51].

21.2.5 Other Complications

The risk of perinatal loss is significantly increased (10–40%) in monochorionic monoamniotic twins, due to the proposed additional risk of cord accidents, an increased incidence of congenital anomalies including conjoined twins and discordant anomalies, spontaneous miscarriage, and TRAP [52–58]. Cord transection following selective fetal reduction, even after spontaneous cessation of perfusion to a monoamniotic TRAP twin, may reduce the complications of fetal demise resulting from cord strangulation of the co-twin [59, 60]. Higher-order multiple pregnancies are associated with higher perinatal morbidity and mortality associated with early miscarriage, preterm delivery, and the aforementioned complications attributed to monochorionicity, for which technical complexities of treatment are increased [61].

21.3 Imaging Modalities Used in the Assessment of Monochorionic Pregnancies

21.3.1 Doppler Velocimetry

21.3.1.1 Umbilical Artery Doppler

UA Doppler is the key Doppler waveform used in the assessment of complications in MC twins as it correlates with adverse fetal outcomes. UA Doppler can be measured at three different sites, namely, the fetal end, the free loop, and the placental end of the umbilical cord [62]. The impedance is the highest at the fetal end of the umbilical cord insertion, and, therefore, this is where the absent/reverse end-diastolic flow is first seen [62]. Identification of the UA of each fetus is more reliable when acquisition is attempted at fixed sites, i.e., the fetal end, placental end or intra-abdominal portion. Measurements from fixed sites are also less variable and are therefore more accurate in fetuses with IUGR compared to readings taken from the long and free loop of the cord [63]. The site where the measurement is taken should be recorded clearly and reference ranges for the corresponding anatomical sites compared, with the same site used for serial measurements [62–64]. In comparison to singleton and dichorionic pregnancies, the UA pulsatility index (PI) and resistance index (RI) are shifted slightly higher for all centiles, and, therefore, reference ranges specific to MC pregnancies should be used (Fig. 21.2) [65]. AREDF is classified as one of the critical Doppler abnormalities in stage III TTTS, sGR, and TAPS [57]. AREDF, in UA Doppler when seen in the presence of sFGR, reflects increased placental blood flow resistance and identifies a fetus at a risk of fetal deterioration [66]. The use of DV Doppler (discussed more in the section for DV Doppler) and computerized cardiotocography (cCTG) in these fetuses helps guide the timing of delivery [66].

At 48 h post FLA for TTTS, UA PI values in the donor twin are already reduced while there is little change in UA Doppler in the recipient, although reversal of AREDF occurring preoperatively in both fetuses may be seen [67].

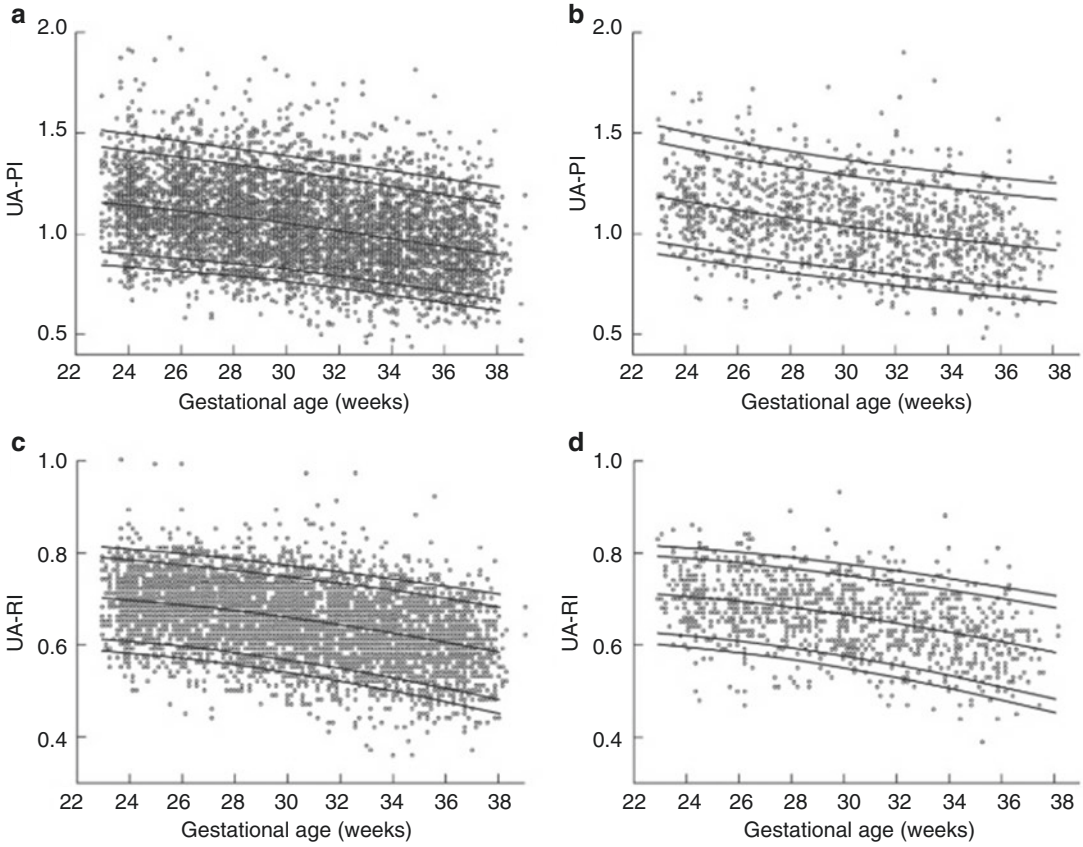

Fig. 21.2 Reference ranges for the UA PI and RI in DCDA (**a**, **c**) vs. MCDA (**b**, **d**) twin pregnancy [65]. (Reproduced with permission from RightsLink® 2019)

It has been reported that intermittent AREDF may be characteristic of MC pregnancies (5% in uncomplicated MC twins) due to the presence of large AA anastomoses, representing an extreme manifestation of the bidirectional flow in these vessels [68]. There is, however, a greater prevalence in pregnancies complicated by sFGR and less so with TTTS (45% and 2%, respectively) and increased perinatal mortality in pregnancies with sFGR (19.4%) [68]. Such findings correlate with postnatal placental examination, revealing large AA anastomoses in all cases with intermittent AREDF and in 3.6% of cases without [68].

21.3.1.2 Middle Cerebral Artery Doppler

An MCA PSV of >1.5 MoM correlates with fetal anemia, and, as with UA Doppler, reference ranges specific to MC pregnancies tend to be higher than those in singleton and dichorionic pregnancies, notably between 15 and 18 weeks (Fig. 21.3) [69]. Fetal anemia in MC pregnancies can include causes such as TAPS, acute feto-fetal transfusion (peri-mortem/intra-partum), fetal infections, red cell alloimmunization, and hemoglobinopathies [69]. A low MCA PSV (<1.0 MoM) suggests polycythemia, although the acceptable level to indicate polycythemia is still debatable (<1.0 MoM or <0.8 MoM) [70]. Some argue that it is the inter-twin MCA PSV (delta MCA PSV) discordance, which is more representative of TAPS, as over a third of MC fetuses with a postnatal diagnosis of polycythemia can have a normal MCA PSV in utero [70]. Hence, it has been proposed that delta MCA PSV >0.5 MoM is superior in predicting postnatal TAPS compared to the fixed MCA PSV values, with a sensitivity of 83% vs. 46%, a

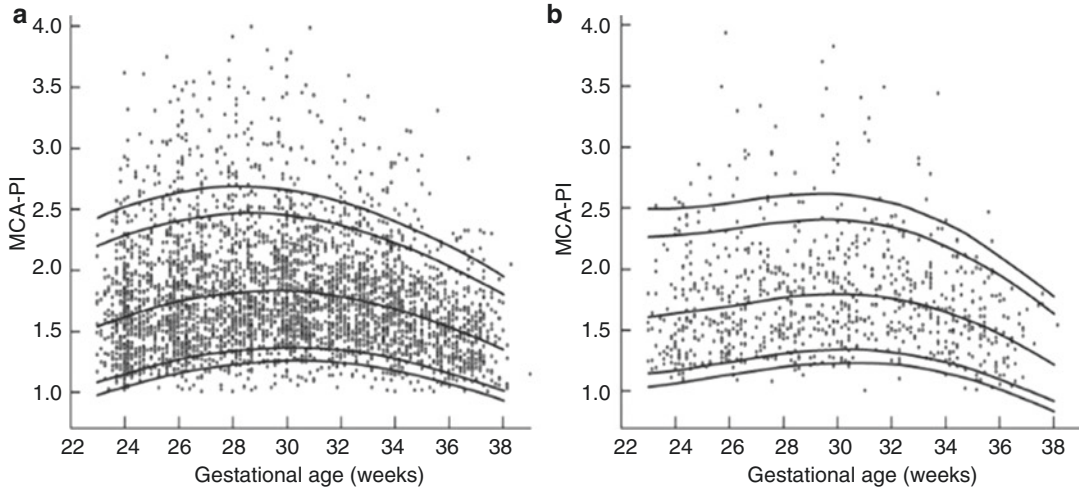

Fig. 21.3 Reference ranges for the MCA PI in DCDA (**a**) vs. MCDA (**b**) [5] twin pregnancy [65]. (Reproduced with permission from RightsLink® 2019)

specificity of 100% vs. 100%, a positive predictive value of 100% vs. 100%, and a negative predictive value of 88% vs. 70%, respectively [64]. An adverse outcome has been reported with a delta MCA PSV of >0.9 MoM, and fetuses in this group may be equivalent to fetuses with stage II TAPS and may therefore benefit from antenatal treatment, although larger studies are needed to validate these results [66].

The cerebroplacental ratio (CPR) is calculated using the equation (MCA PI)/(UA PI) and is proposed to reflect cerebral redistribution in compromised singleton fetuses [71]. Its role in multiple predictive outcomes of complicated MC pregnancies is not well-established, although specific reference ranges for the CPR in MC twins are available [65].

21.3.1.3 Ductus Venosus Doppler

The presence of DV Doppler abnormalities in MC twins in first-trimester ultrasonography is associated with an increased likelihood of developing TTTS, probably reflecting hemodynamic imbalances between the donor and the recipient [72]. From the second trimester, abnormalities in DV Doppler in either fetus are part of critical Doppler changes in stage III TTTS and TAPS [72]. The reason for DV abnormalities in donor fetuses with TTTS is due to underlying growth restriction, whereas, in TAPS, it is attributed to fetal anemia [72]. DV abnormalities are more common in the recipient fetus and reflect hypervolemia and high-output cardiac failure with impending hydrops [72, 73]. Abnormal venous flow (AREDF in DV Doppler and pulsatile/reversal of flow in the umbilical vein) is associated with high perinatal mortality in the presence of hydrops [72].

In singleton fetuses with early-onset growth restriction (<34 weeks) and an abnormal UA Doppler (indicating placental insufficiency), DV Doppler is typically used to aid decisions regarding the optimal timing of delivery [72]. In this context, an abnormal DV Doppler may reflect the massive increase in placental afterload, decreased myocardial performance and compliance as a result of myocardial hypoxia, or as an autoregulatory increase in DV diameter to allow an increase in shunting [72]. When there is an absence or reversal of a wave in the DV waveform, fetal survival beyond 1 week is predicted to be less likely [72, 73]. However, in cases of singleton late-onset growth restriction (>34 weeks), an abnormal DV waveform may not be observed as the underlying pathology is that of impaired diffusion across the placenta, resulting in hypoxemia rather than an increase in afterload [72]. There is a paucity of evidence to suggest that the

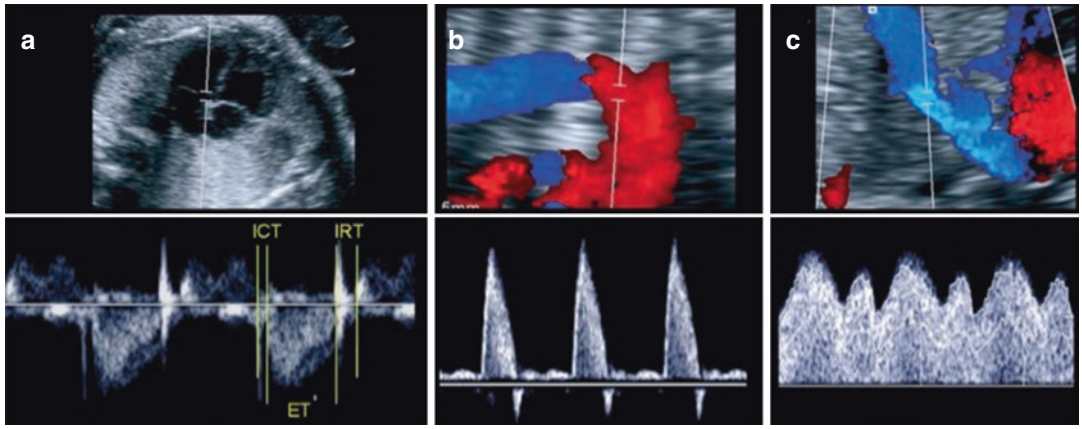

Fig. 21.4 Doppler ultrasound images with spectral waveforms illustrating measurement of the myocardial performance index (**a**), aortic isthmus flow (**b**) and ductus venosus flow (**c**). *ET* ejection time, *ICT* isovolumic contraction time, *IRT* isovolumic relaxation time [74]. (Reproduced with permission from RightsLink® 2019)

same phenomenon occurs in MC twin pregnancy, and, therefore, a normal DV Doppler in this context may not be predictive of fetal well-being or the risk of stillbirth [72]. Figure 21.4 demonstrates a typical ductus venosus waveform.

After treatment for TTTS, DV Doppler may be used to monitor the response to therapy, with significant and immediate improvement in the DV pulsatility index for veins (PIV) seen following FLA in the recipient [67, 72]. As with UA Doppler, resolution of AREDF during atrial contraction in the DV for either fetus may be seen as early as 48 hours post FLA [67]. Transient abnormalities in the DV Doppler (increase in the DV PIV) or hydropic changes may be observed in the donor fetuses following FLA due to relative transient hypervolemia and volume redistribution [67, 72]. Recipient fetuses are also at risk of developing pulmonary valve stenosis due to chronic right-sided volume overload and myocardial hypertrophy while donor fetuses may have tricuspid regurgitation, and such changes usually resolve within 4 weeks of treatment regardless of the severity at the time of diagnosis [72].

As mentioned previously, DV Doppler waveforms are already altered in early and pre-TTTS and therefore may be predictive of evolving into TTTS [73]. Additional DV measurements that can be performed include (1) DV time intervals during systole (S1, S2), diastolic filling time (FT), early diastolic filling time (eT), and late diastolic filling time (aT) and (2) velocity–time integrals (VTI) during systole (VT1, VT2) and diastole (VT3, VT4) [73]. Inter-twin differences can then be calculated and compared [73]. In TTTS, there is typically prolongation of the late systolic phase as represented by higher values of S2 and VT2, due to increased ventricular end-systolic pressure and impaired ventricular relaxation [73]. On the other hand, the diastolic phase is reduced as seen in lower values of eT, FT, VT3, and VT4 [73]. This means that the differences in DV measurements can distinguish uncomplicated MCDA from cases with TTTS [73]. While abnormal absolute velocity ratios are only seen in advanced TTTS, early signs of evolving congestive heart failure are apparent in the recipients' DV flow even in early and pre-TTTS, with the optimal parameter being eT [73].

21.3.1.4 Umbilical Vein Doppler

Pulsatile umbilical venous flow (PUVF) is one of the critical Doppler abnormalities to diagnose stage III TTTS and TAPS. Pulsatile umbilical venous flow is associated with adverse outcomes and congestive cardiac failure, which may be due to hypoxia, increased afterload, increased venous pressure, or augmented atrial contractions [75]. Various diagnostic criteria for PUVF have been proposed, but a typical PUVF waveform is one that is undulating and coincides with the systolic phase of the UA [75]. The suggested cut-off PUVF

RI value is >15%, which represents the minimum deflection of the UV waveform characteristic of the subjective definition of PUVF, and more detailed assessments for the degree of hemodynamic compromise in fetuses at risk of heart failure should be conducted [75]. In growth restricted fetuses, PUVF is associated with up to a five-fold increase in perinatal mortality and worse cord blood gases postnatally compared to fetuses without PUVF [75]. However, PUVF may be a false-positive finding throughout gestation, particularly in earlier gestation <15 weeks [75]. This may be due to transmission of umbilical arterial pulses through the walls of the umbilical cord or lack of standardization of the definition of PUVF [75].

Umbilical vein flow (UVF) has been used to monitor treatment response for fetuses affected by TTTS [76]. Absolute UVF is calculated by multiplying the umbilical vein's cross-sectional area by the average blood velocity [76]. The vein area is calculated by the formula: Area = $\pi(D/2)$ [2], where D is the internal diameter of a transverse section of a straight portion of the intra-abdominal umbilical vein [75]. The average blood velocity is also measured in the straight portion of the intra-abdominal umbilical vein, ensuring that the angle of insonation is kept to the minimum and that assessment is conducted during fetal quiescence [76]. UVF changes with gestational age, and, therefore, the R/D-UVF ratio may be more reliable as it is independent of gestational age [76]. The ratio between recipient (R) and donor (D) UVF is calculated using the formula: ratio (UVF) = R/D, which can be corrected for weight (R/D-UVF/kg) [76]. Prior to FLA, recipients have been shown to have higher UVF measurements than donors, and this level may decrease with advancing disease severity, indicating increasingly impaired cardiac function to accommodate venous return [77]. Post FLA, UVF parameters in these fetuses have been shown to decrease or may be unaffected. [67, 76] For donor fetuses, there is an improvement in weight-corrected blood flow, reflected by a significant increase (>50%) in absolute and weight-corrected UVF 48 hours after FLA. [67] A favorable outcome post FLA is predicted by a significant decrease in R/D-UVF, which serves as an early marker of a successful therapy [76]. Bladder filling (a clinical sign of successful correction of volume in donor fetuses) at 48 h is associated with higher post-operative UVF/kg values compared to donors without bladder filling [67].

21.3.1.5 The Umbilical Arterial-Venous Index

Recipient umbilical artery elongation has been found to occur in half of the recipients in association with abnormal Doppler and signs of cardiac dysfunction, and this finding may represent the chronicity (arterial stretching) and severity of hypertension in recipient fetuses [78]. Three-dimensional (3D) color Doppler volume images of the umbilical cord are obtained prior to software processing based on the hypothesis that any increase in umbilical artery (UA) length would create elongation in this vessel, resulting in increased tortuosity around the umbilical vein (UV) and, therefore, an increased AV angle (angle between UA and UV) [78]. The recipient and donor cords are imaged 5 cm from the placental insertion, keeping the angle of insonation <45° [78]. The AV index is calculated by the formula = UA length/UV length; the length is obtained by manual tracing of the vessels in a 2.5 cm length of the cord [78]. Measurements of the AV angle are done by placing one caliper on the lower edge of one of the arteries and another along the lower edge of the corresponding vein, and the angle of inclination is determined by the intersection of the lines calculated by the software [78].

21.3.2 Placental Anastomosis Mapping

21.3.2.1 Two-Dimensional (2D) Ultrasound Mapping

Arteriovenous Anastomoses

The presence of AV anastomoses increases the risk of TTTS in MC pregnancies. Studies evaluating the feasibility of 2D ultrasound detection of deep, unidirectional AV anastomoses suggest that detection is possible if the placenta is anterior but is challenging otherwise [77–80]. Placental mapping

is done followed by identification of cord insertions at the placental sites for both fetuses using gray scale and color Doppler [79]. The area between cord insertions is meticulously scanned using gray scale and color Doppler to identify the unaccompanied and unpaired vessels on the fetal surface of the placenta [78, 79]. Spectral Doppler is then used by placing the cursor gate within the vascular structure at several sites along its course [79]. AV anastomoses can then be identified through pulsatile arterial flow in the donor segment and through the non-pulsatile venous flow further downstream toward the recipient's cord insertion site [79]. The flow direction for both vascular segments should be the same (unidirectional) [79]. This technique can detect AV anastomoses in 24% of cases and AA anastomoses in 48% [79]. Antenatal mapping and detection of AV anastomoses may aid in detecting pregnancies at a risk of developing TTTS and for surgical planning prior to FLA [78, 79]. However, it is time-consuming and technically challenging in posteriorly located placentas and obese mothers. Its value in prognostication is unknown as well as the earliest gestational age from which it may be applied [79].

Arterio-Arterial Anastomoses

AA anastomoses may offer some protection against TTTS (a nine-fold reduction) and fetal demise in sFGR if there is adequate compensation in the blood flow [81]. Early TTTS (stage I) may even regress spontaneously [82]. AA anastomoses are associated with an increased incidence of TAPS and acute transfusional injuries in cases of single twin demise [82]. The sonographic detection of AA anastomoses can aid in the confirmation of monochorionicity [82]. Using the same scanning method described in the previous section, AA anastomoses are identified by a bidirectional pattern on pulsed wave Doppler and a speckled pattern on color Doppler, representing blood being shunted back and forth [82]. The sensitivity, specificity and positive and negative predictive values of sonographic AA anastomoses detection are 75%–85%, 97%–100%, 100%, and 43%, respectively [81–83]. The detection rate increases with gestational age, related to the increasing diameter of the vessels [82].

Venovenous Anastomoses

VV anastomoses are present in 27% of MC placentas, and their presence is associated with an increased risk of TTTS and perinatal mortality [84]. A total of 20% of MC pregnancies with VV anastomoses develop TTTS compared to 10% of MC pregnancies and is associated with an overall perinatal mortality of 16% and 10%, respectively [84]. However, the presence of VV anastomoses is not an independent risk factor for perinatal mortality in MC pregnancies [84].

21.3.2.2 3D Mapping

Acquisition of 3D ultrasound images enables high-quality vascular anatomical imaging [85]. This is performed by combining fully freehand power Doppler image acquisition with offline image segmentation and reconstruction techniques [85]. The anatomy of AA and AV anastomoses can be visualized in detail from the 3D reconstruction, but it is unlikely that the whole placenta can be screened due to the limitations from the width of the transducer [85]. This method is cheaper and more easily accessible than magnetic resonance imaging (MRI) but requires experience, training, and further studies to validate its utility in a clinical setting.

21.3.2.3 MRI Mapping

Virtual fetoscopy is a non-invasive technique utilizing MRI to enable visualization of fetuses, placental cord insertions, and the placental equator, with a high resolution [86]. MRI is less easily accessible and more costly but is safe in pregnancy. This may be of value in challenging cases such as obese mothers and may help with FLA planning; however, it is currently reserved as a research tool.

21.3.3 Intra-cardiac Doppler

21.3.3.1 Fetal Cardiovascular Hemodynamics in TTTS

TTTS results from an imbalance of blood flow through placental anastomoses with a net transfer of blood and vasoactive mediators from one fetus to another [77]. In recipient fetuses, natriuretic

peptides are released from the cardiomyocytes in response to cardiac stretch, which increases the glomerular filtration rate and decreases tubular reabsorption, leading to polyuria and polyhydramnios [77]. For donors, there is hypoperfusion to the fetal kidneys, causing oliguria and oligo/anhydramnios, which leads to an upregulation of renin secretion and activation of the renin–angiotensin–aldosterone system (RAAS) [77]. The release of angiotensin II increases peripheral vascular resistance as it is a potent vasoconstrictor and causes secretion of aldosterone from the adrenal cortex to retain water, which may regulate against hypovolaemia and maintain the blood pressure in the donor fetus [77]. Renin mRNA is upregulated in the donor kidneys and downregulated in the recipient kidneys, but equally elevated cord blood renin levels have been documented in both donors and recipients, suggesting the transfer of these vasoactive mediators from the donor to the recipient via placental anastomoses [77]. There is a chronic volume shift from the donor to the recipient, which results in continuous activation of the RAAS in the donor to aggravate renal hypoperfusion and more transfer of vasoactive agents to the recipient, and this vicious cycle continues until treatment is instituted [77].

21.3.3.2 The Recipient

Functional Pulmonary Atresia/Stenosis

Volume overload and increased peripheral resistance resulting from the transfer of vasoactive mediators from the donor twin leads to anatomical or functional cardiac compromise in 70% of the recipients [77]. Up to 8% of the recipients develop pulmonary stenosis/atresia secondary to severe right cardiac dysfunction, which resolves 24 hours after FLA in most cases [77]. This resolution differentiates functional from true anatomical pulmonary stenosis/atresia [77]. Vasoactive mediators cause myocardial hypertrophy and fetal hypertension, reflected by tricuspid regurgitant velocities [77]. AREDF in the UA is less commonly seen in recipients and may reflect (1) severe systolic dysfunction in cases with heart failure and/or (2) placental compression from polyhydramnios [77]. Preload effects are reflected by changes in the UVF, whereas afterload effects from ventricular end-diastolic pressure and atrial filling pressure are represented in the DV Doppler [77]. In early TTTS, impaired filling in the recipient heart is suspected when there is relative prolongation of systolic flow and shortening of diastolic filling time in the DV [77]. An increased afterload results in an abnormal DV PIV, which may progress to AREDF during atrial contraction and subsequent pulsation in the umbilical vein [77]. Diastolic dysfunction is usually more pronounced and precedes the systolic dysfunction in recipient fetuses [77].

Myocardial Performance (Tei) Index (MPI)

Doppler imaging (color, conventional spectral, tissue, spectral tissue, color tissue), M mode, speckle tracking techniques, and spatio-temporal image correlation (STIC) have been used to assess fetal cardiac function [87]. Conventional spectral Doppler imaging on the arterio-ventricular valves enables measurement of the E-wave (passive ventricular filling) and A-wave (active ventricular filling associated with atrial contraction) peak velocities, and the E/A ratio can be obtained to serve as the AA measure of diastolic myocardial function [87]. The fetal E/A ratio is typically <1 and increases with gestation (as ventricular compliance decreases and the relative contribution of passive filling to diastole increases, which is reflected with increased E velocity and therefore an increased E/A ratio), approaching 1 at term [87]. Under normal conditions, the right ventricular E/A ratio is slightly lower than the left [87]. Monophasic ventricular filling seen as a fusion of the E- and A-waves is seen in 20–30% of recipient fetuses, often with a measurable shortening of ventricular filling time from increased ventricular pressure [86]. The result is significant arterio-ventricular valve regurgitation, often extending to more than half of the cardiac cycle along with prolongation of isovolumic relaxation time (IRT) and an increase in the myocardial performance (Tei) index (MPI) [77].

The MPI is a measure of global cardiac function and reflects early cardiac adaptation to different disease states [87]. The MPI is calculated

by MPI = (isovolumic contraction time (ICT) + isovolumic relaxation time (IRT))/ejection time (ET) (Fig. 21.4) [77, 87]. It is prolonged in ventricular dysfunction but cannot differentiate between systolic and diastolic dysfunction. The main parameters that are affected in complicated MC pregnancies are the IRT, whereas MPI and MPI values have been shown to vary only slightly during gestation with a mean MPI value of 0.36 (range 0.28–0.44) [87].

Assessment of Myocardial Deformation

Speckle Tracking

Myocardial deformation is a better reflection of myocardial function [77]. Cardiac muscles lengthen in diastole and shorten in systole [87]. Strain is the extent of deformation, whereas strain rate measures the velocity of deformation [87]. Strain is calculated by the final length (L) of the myocardial segment minus the initial length (L_0) of the segment, divided by the initial length (L_0) of the segment [87]. The strain rate is calculated by strain divided by the time interval between frames [87]. A positive strain rate indicates lengthening of the tissue, whereas shortening is represented by a negative strain rate [87]. Myocardial deformation is measured using Speckle tracking, which is a non-Doppler technique, which measures myocardial strain, strain rate, and displacement using offline analysis of 2D stored clips and tracking algorithms [87, 88]. A bright myocardial speckle pattern, generated by the reflection of the ultrasound beam is tracked frame by frame and referenced back to the reference position in the previous frame to provide velocity and displacement data [87]. Tracking lines are drawn along the inner borders of the ventricles from the four-chamber or short-axis view of the fetal heart [87]. The software then tracks the ventricular border in subsequent frames, and a calculation of myocardial deformation is obtained [87]. Although ventricular strain is decreased in both right and left ventricles in advanced stages of TTTS, ventricular strain in the left ventricle is decreased more so in early TTTS, representing early changes in afterload [77].

Spectral Tissue Doppler Imaging

Spectral tissue Doppler imaging (S-TDI) is a Doppler myocardial imaging technique used to assess the long-axis function of the ventricles [87, 89]. S-TDI is performed by placing a pulsed wave Doppler sample volume within the myocardium at the lateral aspect of the arterio-ventricular valve annulus, with the ultrasound beam aligned parallel to the myocardial wall studied [87]. E′ represents early diastolic annular relaxation velocity, and S′ represents annular velocity during ventricular systole [87]. Measurements of other parameters (A′, ICT′, IRT′, MPI′) can also be taken as described for conventional spectral Doppler imaging, but of interest here are changes in the annular velocity ratio (E/E′) and shortening velocity (S′), which have been found to be predictive of ventricular filling pressure and systolic function, respectively [87]. There is an increase in left ventricular filling pressures in recipient fetuses in early-stage TTTS (stages I and II), with preservation of systolic function, whereas an increase in right ventricular pressures is seen in later stages [89]. In advanced stages of TTTS, systolic function in the left heart is reduced, whereas no changes in the systolic function of the right heart is seen. This reflects the early increase in afterload from vasoactive mediators and volume loading in the recipient heart, with changes in the left ventricular function being affected before abnormalities in the right heart become apparent [89].

Aortic Fractional Area Change (AFAC)

A promising non-invasive technique is the assessment of aortic dispensability as a proxy measure of inter-twin blood pressure differences and is useful in monitoring treatment response [89]. Aortic fractional area change (AFAC) is measured using the Speckle tracking method mentioned previously [89]. A cardiac four-chamber clip, which includes a cross section of the mid-thoracic aorta, is recorded for offline processing [89]. The endovascular border of the aorta is traced manually during cardiac systole, and software then tracks the endovascular border in subsequent frames for the entire cardiac cycle [89]. The AFAC has been shown to be significantly

higher in recipients, representing their higher pulse pressure [89]. Further studies to evaluate the role of this examination in treatment response are awaited [89].

The Aortic Isthmus Systolic Index (ISI)

Evaluation of the aortic isthmic systolic index (ISI) can serve as a pre-treatment prognostic marker for the recipient, with a lower ISI corresponding to post-operative demise [90]. This is assessed by obtaining real-time images of the aortic arch in the sagittal view and positioning the Doppler sample volume in the aortic isthmus (AoI) just beyond the left subclavian artery and before the point of connection of the ductus arteriosus with the thoracic aorta (Fig. 21.4) [90]. Measurements of end-systolic velocity (systolic nadir) and peak systolic velocity of the AoI Doppler waveforms (AoIDw) are measured, and calculation of the ISI is done using the formula = systolic nadir/AoIDw [90]. The ISI may be a marker of the severity of circulatory volume overload in recipient fetuses and hence may have a role in predicting their outcome [90].

21.3.3.3 The Donor

Most donor fetuses have a normal echocardiogram at diagnosis, with 3–10% having abnormal Doppler waveforms or UV pulsations [77]. AREDF in the UA may be due to (1) placental insufficiency, (2) unequal placental sharing, or (3) hypovolemia [77]. The DV inlet may dilate to allow more shunting of blood, leading to an increased transmission of the DV pulsed wave into the UV [77].

In selective fetal growth restriction, reduced E- and A-wave velocities reflect decreased cardiac preload [87]. The Tei index is also prolonged, indicating decreased global cardiac function, which can be seen before the onset of AREDF in UA Doppler, thus serving as an early marker of fetal compromise [87].

21.3.3.4 Assessment of Post-laser Ablation

Rapid improvements in cardiovascular function in the recipient with normalization of systolic and diastolic functions have been observed after treatment with FLA, with a significant decrease in the DV PIV and normalization of time intervals [77]. Cardiac remodeling in the recipient fetuses following FLA improves outcomes and reduces postnatal interventions compared to that in non-FLA fetuses [77]. There is also significant improvement in the Tei index and an increase in the shortening fraction in both fetuses [77]. In the donor, normalization of UA Dopplers is consistent with an increase in blood volume and blood pressure, with improvements seen in weight-corrected UVF within 48 h of FLA in more than 50% of donor fetuses and improvements in renal perfusion evidenced by bladder filling [77]. However, this initial rapid correction of the hemodynamic imbalance causes relative hypervolemia in the chronically hypovolemic donor, which may result in transient abnormalities in the DV Doppler and potential hydropic features [77]. Medium-term follow-up of survivors of TTTS treated with amnioreduction or FLA showed no cases of hypertension during the pre-pubertal period, while functional cardiac assessment in the medium term has not shown any significant differences between ex-donor and ex-recipient after treatment with FLA. [77] Further studies are required to assess the long-term outcomes for the survivors of TTTS following FLA.

References

1. Goldenberg RL, Culhane JF, Iams JD, Romero R. Epidemiology and causes of preterm birth. Lancet. 2008;371(9606):75–84.
2. Cheong-See F, Schuit E, Arroyo-Manzano D, et al. Prospective risk of stillbirth and neonatal complications in twin pregnancies: systematic review and meta-analysis. BMJ. 2016;354:i4353.
3. Glinianaia SV, Obeysekera MA, Sturgiss S, et al. Stillbirth and neonatal mortality in monochorionic and dichorionic twins: a population-based study. Hum Reprod. 2011;26:2549–57.
4. Sepulveda W, Sebire NJ, Hughes K, Odibo A, Nicolaides KH. The lambda sign at 10-14 weeks of gestation as a predictor of chorionicity in twin pregnancies. Ultrasound Obstet Gynecol. 1996;7:421–3.
5. National Institute for Health and Clinical Excellence. Multiple pregnancy: antenatal care for twin and triplet pregnancies. Clinical guideline (CG129); 2011.
6. Carroll SGM, Soothill PW, Abdel-Fattah SA, Porter H, Montague I, Kyle PM. Prediction of chorionicity in

twin pregnancies at 10-14 weeks of gestation. BJOG. 2002;109:182–6.
7. Maruotti GM, Saccone G, Morlando M, Martinelli P. First-trimester ultrasound determination of chorionicity in twin gestations using the lambda sign: a systematic review and meta-analysis. Eur J Obstet Gynecol Reprod Biol. 2016;202:66–70.
8. Lopriore E, Sueters M, Middeldorp JM, Klumper F, Oepkes D, Vandenbussche FPHA. Twin pregnancies with two separate placental masses can still be monochorionic and have vascular anastomoses. Am J Obstet Gynecol. 2006;194:804–8.
9. Lewi L, Cannie M, Blickstein I, et al. Placental sharing, birthweight discordance, and vascular anastomoses in monochorionic diamniotic twin placentas. Am J Obstet Gynecol. 2007;197(6):587.e1–8.
10. Denbow ML, Cox P, Taylor M, Hammal DM, Fisk NM. Placental Angioarchitecture in monochorionic twin pregnancies: relationship to fetal growth, fetofetal transfusion syndrome, and pregnancy outcome. Am J Obstet Gynecol. 2000;182(2):417–26.
11. Lewi L, Deprest J, Hecher K. The vascular anastomoses in monochorionic twin pregnancies and their clinical consequences. Am J Obstet Gynecol. 2013;208(1):19–30.
12. Bennasar M, Eixarch E, Martinex JM, Gratacos E. Selective intrauterine growth restriction in monochorionic diamniotic twin pregnancies. Semin Fetal Neonatal Medicine. 2017;22(6):376–82.
13. O'Brien WF, Knuppel RA, Scerbo JC, Rattan PK. Birth weight in twins: an analysis of discordancy and growth retardation. Obstet Gynecol. 1986;67:483–6.
14. Erkkola R, Ala-Mello S, Piiroinen O, Kero P, Sillanpää M. Growth discordancy in twin pregnancies: a risk factor not detected by measurements of biparietal diameter. Obstet Gynecol. 1985;66:203–6.
15. Bejar R, Vigliocco G, Gramajo H, et al. Antenatal origin of neurologic damage in newborn infants. II. Multiple gestations. Am J Obstet Gynecol. 1990;162:1230–6.
16. Ishii K, Murakoshi T, Takahashi Y, et al. Perinatal outcome of monochorionic twins with selective intrauterine growth restriction and different types of umbilical artery Doppler under expectant management. Fetal Diagn Ther. 2009;26:157–61.
17. Gratacós E, Carreras E, Becker J, et al. Prevalence of neurological damage in monochorionic twins with selective intrauterine growth restriction and intermittent absent or reversed end-diastolic umbilical artery flow. Ultrasound Obstet Gynecol. 2004;24:159–63.
18. Adegbite AL, Castille S, Ward S, Bajoria R. Neuromorbidity in preterm twins in relation to chorionicity and discordant birth weight. Am J Obstet Gynecol. 2004;190:156–63.
19. Lopriore E, Slaghekke F, Vandenbussche FP, et al. Cerebral injury in monochorionic twins with selective intrauterine growth restriction and/or birthweight discordance. Am J Obstet Gynecol. 2008;199:628–5.
20. Lopriore E, Sluimers C, Pasman SA, et al. Neonatal morbidity in growth-discordant monochorionic twins: comparison between the larger and the smaller twin. Twin Res Hum Genet. 2012;15:541–6.
21. Khalil A, Rodgers M, Baschat A, et al. ISUOG practice guidelines: role of ultrasound in twin pregnancy. Ultrasound Obstet Gynecol. 2016;47(2):247–63.
22. Valsky DV, Eixarch E, Martinez JM, Crispi F, Gratacos E. Selective intrauterine growth restriction in monochorionic twins: pathophysiology, diagnostic approach and management dilemmas. Semin Fetal Neonatal Med. 2010;15:342–8.
23. Buca D, Pagani G, Rizzo G, et al. Outcome of monochorionic twin pregnancy with selective intrauterine growth restriction according to umbilical artery Doppler flow pattern of smaller twin: systematic review and meta-analysis. Ultrasound Obstet Gynecol. 2017;50:559–68.
24. Quintero RA, Bornick PW, Morales WJ, Allen MH. Selective photocoagulation of communicating vessels in the treatment of monochorionic twins with selective growth retardation. Am J Obstet Gynecol. 2001;185:689–96.
25. Gratacos E, Antolin E, Lwei L, et al. Monochorionic twins with selective intrauterine growth restriction and intermittent absent or reversed end-diastolic flow (type III): feasibility and perinatal outcome of fetoscopic placental laser coagulation. Ultrasound Obstet Gynecol. 2008;31:669–75.
26. Rossi AC, D'Addario V. Umbilical cord occlusion for selective feticide in complicated monochorionic twin fetuses. Ultrasound Obstet Gynecol. 2005;26:44–9.
27. Fick AL, Feldstein VA, Norton ME, Fyr CW, Caughey AB, Machin GA. Unequal placental sharing and birth weight discordance in monochorionic diamniotic twins. Am J Obstet Gynecol. 2006;195:178–83.
28. Berghella V, Kaufmann M. Natural history of twin-twin transfusion syndrome. J Reprod Med. 2001;46(5):480–4.
29. Kontopoulos EV, Quintero RA. Treatment of twin-twin transfusion syndrome: an evidence-based analysis. In: Quintero RA, editor. Twin-twin transfusion syndrome. London: Informa; 2007. p. 127–37.
30. Kontopoulos E, Chmait RH, Quintero RA. Twin-to-twin transfusion syndrome: definition, staging, and ultrasound assessment. Twin Res Hum Genet. 2016;19(3):175–83.
31. Chalouhi GE, Essaoui M, Strinemann J, et al. Laser therapy for twin-twin transfusion syndrome (TTTS). Prenat Diagn. 2011;31:637–46.
32. Stirnemann JJ, Nasr B, Proulx F, Essaoui M, Ville Y. Evaluation of the CHOP cardiovascular score as a prognostic predictor of outcome in twin-twin transfusion syndrome after laser coagulation of placental vessels in a prospective cohort. Ultrasound Obstet Gynecol. 2010;36:52–7.
33. Djaafri F, Stirnemann J, Mediouni I, Colmant C, Ville Y. Twin-twin transfusion syndrome—what have we learned from clinical trials. Semin Fetal Neonatal Med. 2017;22(6):367–75.

34. Quintero RA, Morales WJ, Allen MH, Bornick PW, Johnson PK, Kruger M. Staging of twin-twin transfusion syndrome. J Perinatol. 1999;19:550–5.
35. Society for Maternal-Fetal Medicine (SMFM), Simpson LL. Twin-twin transfusion syndrome. Am J Obstet Gynecol. 2013;208(1):3–18.
36. Van Mieghem T, Klaritsch P, Done E, et al. Assessment of fetal cardiac function before and after therapy for twin-to-twin transfusion syndrome. Am J Obstet Gynecol. 2009;200(4):400.e1–7.
37. Chmait RH, Kontopoulos EV, Korst LM, Llanes A, Petisco I, Quintero RA. Stage-based outcomes of 682 consecutive cases of twin-twin transfusion syndrome treated with laser surgery: the US fetus experience. Am J Obstet Gynecol. 2011;204:393.e1–6.
38. Salomon LJ, Ortqvist L, Aegerter P, et al. Long-term developmental follow-up of infants who participated in a randomized clinical trial of amniocentesis vs laser photocoagulation for the treatment of twin-to-twin transfusion syndrome. Am J Obstet Gynecol. 2010;203:444.e1–7.
39. Slaghekke F, Lopriore E, Lewi L, et al. Fetoscopic laser coagulation of the vascular equator versus selective coagulation for twin-to-twin transfusion syndrome: an open-label randomised controlled trial. Lancet. 2014;383(9935):2144–51.
40. Slaghekke F, Favre R, Peeters SHP, et al. Laser surgery as a management option for twin anemia-polycythemia sequence. Ultrasound Obstet Gynecol. 2014;44:304–10.
41. Baschat AA, Oepkes D. Twin anemia-polycythemia sequence in monochorionic twins: implications for diagnosis and treatment. Am J Perinatol. 2014;31:S25–30.
42. Tollenaar LSA, Slaghekke F, Middeldorp JM, et al. Twin anemia polycythemia sequence: current views on pathogenesis, diagnostic criteria, perinatal management, and outcome. Twin Res Hum Genet. 2016;19(3):222–33.
43. Slaghekke F, van den Wijngaard JPHM, Akkermans J, et al. Intrauterine transfusion combined with partial exchange transfusion for twin anemia polycythemia sequence: modeling a novel technique. Placenta. 2015;36(5):599–602.
44. van Klink JM, Slaghekke F, Balestriero MA, et al. Neurodevelopmental outcome at 2 years in twin-twin transfusion syndrome survivors randomized for the Solomon trial. Am J Obstet Gynecol. 2016;214(1):113.e1–7.
45. Van Gemert MJC, Van Den Wijngaard JPHM, Vandenbussche FPHA. Twin reversed arterial perfusion sequence is more common than generally accepted. Birth Defects Res A Clin Mol Teratol. 2015;103(7):641–3.
46. Lewi L, Valencia C, Gonzalez E, Deprest J, Nicolaides KH. The outcome of twin reversed arterial perfusion sequence diagnosed in the first trimester. Am J Obstet Gynecol. 2010;203(213):e1–4.
47. Benirschke K. Monozygotic twinning. Surg Pathol Clin. 2013;6(1):27–32.
48. van Gemert MJC, van den Wijngaard JPHM, Paarlberg KM, Gardiner HM, Nikkels PGJ. Acardiac twin pregnancies part IV: acardiac onset from unequal embryonic splitting simulated by a fetoplacental resistance model. Birth Defects Res. 2017;109(3):211–23.
49. van Gemert MJC, Ross MG, Nikkels PGJ, van den Wijngaard JPHM. Acardiac twin pregnancies part III: model simulations. Birth Defects Res A Clin Mol Teratol. 2016;106(12):1008–15.
50. van Gemert MJC, Pistorius LR, Benirschke K, et al. Hypothesis acardiac twin pregnancies: pathophysiology-based hypothesis suggest risk prediction by pump/acardiac umbilical venous diameter ratios. Birth Defects Res A Clin Mol Teratol. 2016;106(2):114–21.
51. U.S. National Library of Medicine. TRAP Intervention STudy: early versus late intervention for Twin Reversed Arterial Perfusion Sequence (TRAPIST). ClinicalTrials.gov Identifier: NCT02621645.
52. Roqué H, Gillen-Goldstein J, Funai E, Young BK, Lockwood CJ. Perinatal outcomes in monoamniotic gestations. J Matern Fetal Neonatal Med. 2003;13:414–21.
53. Hack KE, Derks JB, Schaap AH, et al. Perinatal outcome of monoamniotic twin pregnancies. Obstet Gynecol. 2009;113:353–60.
54. Heyborne KD, Porreco RP, Garite TJ, Phair K, Abril D, Obstetrix/Pediatrix Research Study Group. Improved perinatal survival of monoamniotic twins with intensive inpatient monitoring. Am J Obstet Gynecol. 2005;192:96–101.
55. Ezra Y, Shveiky D, Ophir E, et al. Intensive management and early delivery reduce antenatal mortality in monoamniotic twin pregnancies. Acta Obstet Gynecol Scand. 2005;84:432–5.
56. Dias T, Contro E, Thilaganathan B, et al. Pregnancy outcome of monochorionic twins: does amnionicity matter? Twin Res Hum Genet. 2011;14:586–92.
57. Lewi L. Cord entanglement in monoamniotic twins: does it really matter? Ultrasound Obstet Gynecol. 2010;35:139–41.
58. Rossi AC, Prefumo F. Impact of cord entanglement on perinatal outcome of monoamniotic twins: a systematic review of the literature. Ultrasound Obstet Gynecol. 2013;41:131–5.
59. Berg C, Koninger A, Gembruch U, Geipel A. Twin Reversed Arterial Perfusion (TRAP) sequence—does monoamniocity preclude early intervention? Ultrasound Obstet Gynecol. 2014;44:241–3.
60. Valsky DV, Martinez-Serrano MJ, Sanz M, et al. Cord occlusion followed by laser cord transection in monochorionic monoamniotic discordant twins. Ultrasound Obstet Gynecol. 2011;37:684–8.
61. De Catte L, Camus M, Foulon W. Monochorionic high-order multiple pregnancies and multifetal pregnancy reduction.
62. Bhide A, Acharya G, Bilardo CM, et al. ISUOG practice guidelines: use of Doppler ultrasonography in obstetrics. Ultrasound Obstet Gynecol. 2013;41(2):233–9.

63. Acharya G, Wilsgaard T, Berntsen GKR, Maltau JM, Kiserud T. Reference ranges for serial measurements of blood velocity and pulsatility index at the intra-abdominal portion, and fetal and placental ends of the umbilical artery. Ultrasound Obstet Gynecol. 2005;26:162–9.
64. Acharya G, Wilsgaard T, Rosvold Berntsen GKR, Maltau JM, Kiserud T. Reference ranges for serial measurements of umbilical artery Doppler indices in the second half of pregnancy. Am J Obstet Gynecol. 2005;192:937–44.
65. Mulcahy C, McAuliffe FM, Breathnach F, et al. Umbilical and fetal middle cerebral artery Doppler reference ranges in a twin population followed longitudinally from 24 to 38 weeks' gestation. Ultrasound Obstet Gynecol. 2014;44:461–7.
66. Tollenaar LSA, Lopriore E, Middeldorp JM, et al. Improved antenatal prediction of twin anaemia-polycythemia sequence by Delta middle cerebral artery peak systolic velocity: a new antenatal classification system. Ultrasound Obstet Gynecol. 2019;53(6):788–93. https://doi.org/10.1002/uog.20096.
67. Baschat AA, Gungor S, Glosemeyer P, Huber A, Hecher K. Changes in umbilical venous volume flow after fetoscopic laser occlusion of placental vascular anastomoses in twin-to-twin transfusion syndrome. Am J Obstet Gynecol. 2010;203(5):479.e1–6.
68. Gratacos E, Lewi L, Carreras E, et al. Incidence and characteristics of umbilical artery intermittent absent and/or reversed end-diastolic flow in complicated and uncomplicated monochorionic twin pregnancies. Ultrasound Obstet Gynecol. 2004;23:456–60.
69. Klaritsch P, Deprest J, Van Mieghem T, et al. Reference ranges for middle cerebral artery peak systolic velocity in monochorionic diamniotic twins: a longitudinal study. Ultrasound Obstet Gynecol. 2009;34:149–54.
70. Fishel-Bartal M, Weisz B, Mazaki-Tovi S, et al. Can middle cerebral artery peak systolic velocity predict polycythemia in monochorionic-diamniotic twins? Evidence from a prospective cohort study. Ultrasound Obstet Gynecol. 2016;48:470–5.
71. Dunn L, Sherrell H, Kumar S. Review: systematic review of the utility of the fetal cerebroplacental ratio measured at term for the prediction of adverse perinatal outcome. Placenta. 2017;54:68–75.
72. Seravalli V, Miller JL, Block-Abraham D, Baschat AA. Ductus venosus Doppler in the assessment of fetal cardiovascular health: an updated practical approach. Acta Obstet Gynecol Scand. 2016;95:635–44.
73. Wohlmuth C, Osei FA, Moise KJ Jr, et al. Changes in ductus venosus flow profile in twin-twin transfusion syndrome: role in risk stratification. Ultrasound Obstet Gynecol. 2016;48:744–51.
74. Cruz-Martinez R, Figueras F, Benavides-Serralde A, Crispi F, Hernandez-Andrade E, Gratacos E. Sequence of changes in myocardial performance index in relation to aortic isthmus and ductus venosus Doppler in fetuses with early-onset intrauterine growth restriction. Ultrasound Obstet Gynecol. 2011;38(2):179–84.
75. Russell Z, Quintero RA, Kontopoulos EV. What is the definition of pulsatile umbilical venous flow in twin-twin transfusion syndrome? Am J Obstet Gynecol. 2008;199(6):634.e1–4.
76. Yamamoto M, Nasr B, Ortqvist L, Bernard JP, Takahashi Y, Ville Y. Intertwin discordance in umbilical venous volume flow: a reflection of blood volume imbalance in twin-to-twin transfusion syndrome. Ultrasound Obstet Gynecol. 2007;29:317–20.
77. Wohlmuth C, Gardiner HM, Diehl W, Kecher K. Fetal cardiovascular hemodynamics in twin-twin transfusion syndrome. Acta Obstet Gynecol Scand. 2016;95:664–71.
78. Sau A, Weber M, Shennan AH, Maxwell D. Antenatal detection of arteriovenous anastomoses in monochorionic twin pregnancy. Int J Gynecol Obstet. 2008;100:56–9.
79. Machin GA, Feldstein VA, Van Gemert MJC, Keith LG, Hecher K. Doppler sonographic demonstration of arterio-venous anastomosis in monochorionic twin gestation. Ultrasound Obstet Gynecol. 2000;16:214–7.
80. Taylor MJO, Farquharson D, Cox PM, Fisk NM. Identification of arterio-venous anastomoses *in vivo* in monochorionic twin pregnancies: preliminary report. Ultrasound Obstet Gynecol. 2000;16:218–22.
81. Taylor MJ, Denbow ML, Tanawattanacharoen S, Gannon C, Cox PM, Fisk NM. Doppler detection of arterio-arterial anastomoses in monochorionic twins: feasibility and clinical application. Hum Reprod. 2000;15:1632–6.
82. Fichera A, Mor E, Soregaroli M, Frusca T. Antenatal detection of arterio-arterial anastomoses by Doppler placental assessment in monochorionic twin pregnancies. Fetal Diagn Ther. 2005;20:519–23.
83. Denbow ML, Cox P, Talbert D, Fisk NM. Colour Doppler energy insonation of placental vasculature in monochorionic twins: absent arterio-arterial anastomoses in association with twin-to-twin transfusion syndrome. Br J Obstet Gynaecol. 1998;105:760–4.
84. de Villiers SF, Zhao DP, Cohen D, et al. Correlation between veno-venous anastomoses, TTTS and perinatal mortality in monochorionic twin pregnancies. Placenta. 2015;36(5):603–6.
85. Welsh AW, Taylor MJO, Cosgrove D, Fisk NM. Freehand three-dimensional Doppler demonstration of monochorionic vascular anastomoses *in vivo*: a preliminary report. Ultrasound Obstet Gynecol. 2001;18:317–24.
86. Werner H, Dos Santos JL, Sa RA, et al. Visualisation of the vascular equator in twin-to-twin syndrome by virtual fetoscopy. Arch Gynecol Obstet. 2015;292(6):1183–4.

87. Abuhamad A, Chaoui R. A practical guide to fetal echocardiography: normal and abnormal hearts. 3rd ed. Alphen aan den Rijn: Wolters Kluwer; 2016.
88. Taylor-Clarke MC, Matsui H, Roughton M, Wimalasundera RC, Gardiner HM. Ventricular strain changes in monochorionic twins with and without twin-to-twin transfusion syndrome. Am J Obstet Gynecol. 2013;208(462.e6):462.e1–6.
89. Wohlmuth C, Osei FA, Moise KJ, et al. Aortic distensibility as a surrogate for intertwin pulse pressure differences in monochorionic pregnancies with and without twin-twin transfusion syndrome. Ultrasound Obstet Gynecol. 2016;48(2):193–9.
90. Leduc F, Delabaere A, Gendron R, et al. Aortic isthmus flow recording predicts the outcome of the recipient twin after laser coagulation in twin-twin transfusion syndrome. Fetal Diagn Ther. 2018;44(2):135–41.

22 Doppler Sonography in Pregnancies Complicated by Pre-gestational Diabetes Mellitus

Gustavo Vilchez and Dev Maulik

22.1 Introduction

Diabetes mellitus represents, for the obstetrician, one of the most challenging complications during pregnancy [1]. The global number of people affected by diabetes is expected to increase from 642 million in 2015 to 829 million by 2040 [2]. In the United States, the prevalence of diabetes is projected to increase from 14% in 2010 to 21% by 2050 [3]. Therefore, it is predicted that the prevalence of diabetes in women of childbearing age will continue increasing over the subsequent years, with a resulting impact on the global burden of disease, thus impairing the health of mothers and their newborns [4].

The successful management of a pre-gestational diabetic mother requires timely and appropriate antepartum fetal surveillance, which permits the pregnancy to progress while identifying the fetus that may be compromised and may benefit from delivery. Doppler velocimetry enables the investigation of fetal circulatory decompensation and thus provides a non-invasive monitoring tool for assessing fetal well-being. There is considerable evidence affirming the efficacy of umbilical arterial Doppler sonography in predicting and improving adverse perinatal outcomes in pregnancies with fetal growth restriction (FGR) and pre-eclampsia; however, the utility of Doppler fetal surveillance in managing uncomplicated pregnancies with pre-gestational diabetes remains controversial.

This chapter presents a historical review of the role of Doppler sonography in assessing the fetus of a pre-gestational diabetic mother and recommends a management plan based on the current evidence.

22.2 Maternal Glycemic State and Fetal Hemodynamics

The fetal circulatory response to an altered maternal glycemic state appears to be complex. The pathophysiology of hyperglycemia-induced cardiac dysfunction and structural defects is still not entirely understood [5]. High cellular glucose is believed to trigger generation of reactive oxygen species in addition to depletion of cellular antioxidant capacity in the developing cells, resulting, due to several mechanisms, in diabetic embryopathy [5]. This section briefly addresses the pathophysiology pertaining to both hyper- and hypoglycemia.

G. Vilchez (✉) · D. Maulik
Department of Obstetrics and Gynecology, UMKC School of Medicine/Truman Medical Center, UMKC School of Medicine, Kansas City, MO, USA
e-mail: vilchezg@umkc.edu

D. Maulik, C. C. Lees (eds.), *Doppler Ultrasound in Obstetrics and Gynecology*,
https://doi.org/10.1007/978-3-031-06189-9_22

22.2.1 Hyperglycemia and Fetal Hemodynamics

Several researchers have studied the effects of hyperglycemia in the fetal cardiovascular hemodynamics. In an experimental model involving late gestation ewes, induction of acute maternal hyperglycemia produced a 27–29% reduction in the placental share of the cardiac output, which was redistributed to the fetal heart and renal, adrenal, and splanchnic circulations [6]. Concordant with the changes in perfusion, the fetuses also developed systemic hypoxemia and mixed acidemia during induced maternal hyperglycemia without any alterations in fetal cardiac, brain, and renal oxygenation. The response to the hyperglycemic challenge, however, was different in the fetuses of ewes rendered diabetic by streptozocin administration [7]. The umbilical–placental blood flow did not change significantly in these fetuses but declined significantly in the controls, whereas fetal brain and renal perfusion was significantly higher in the former at all times than in the controls. Fetuses of the diabetic mothers were also more hypoxemic than those of the controls.

In another experiment using dam embryos, streptozotocin-induced hyperglycemia increased the pulsatility indices of the umbilical artery, descending aorta and ductus venosus, demonstrating a significant hemodynamic compromise in the circulatory system of the hyperglycemic rat embryo [8]. In a similar study, maternal streptozotocin-induced hyperglycemia was associated with an increased cardiac size, a lower heart rate, a higher frequency of atrioventricular valve regurgitation, and a decreased outflow mean velocity, suggesting diminished cardiac output [9]. Similarly, in hyperglycemia-induced chicken embryos, the blood flow velocity through the outflow tracts was significantly decreased, including flow reversal in 30% of the cardiac cycle [10]. Hyperglycemia was also noted to cause dilation of the fetal cardiac ventricular chambers and reduction of the total ventricular myocardial area in another model of streptozocin-induced diabetic dams [11]. Similarly, in the human fetus, Turan et al. studied the effect of hyperglycemia from pre-gestational diabetes on fetal cardiac performance (Fig. 22.1). The authors found that fetuses of diabetic mothers presented more

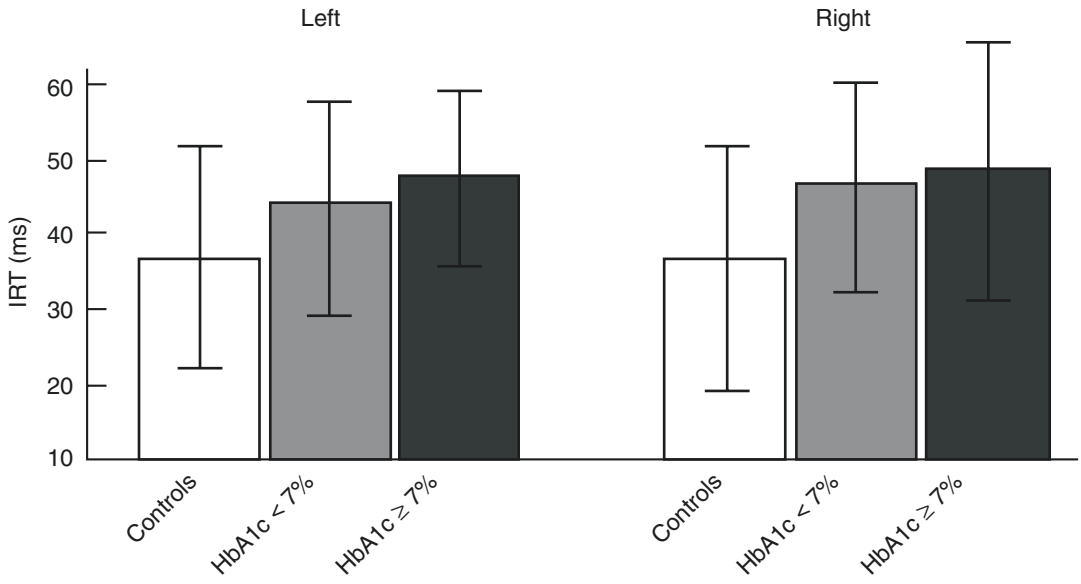

Fig. 22.1 Isovolumic relaxation times of the heart according to the pre-gestational diabetes status. Isovolumic relaxation time of the left and right sides of the heart in controls and in diabetic patients with glycosylated hemoglobin either <7% or ≥7%. (Courtesy of Turan et al. [12])

impaired diastolic myocardial function compared with those of non-diabetic controls [12].

Fetal hypoxemia induced by maternal hyperglycemia could be explained by the earlier observation that chronic fetal hyperglycemia is associated with accelerated fetal oxidative metabolism. In the latter study, chronic fetal hyperglycemia produced by fetal glucose infusion via chronic in utero catheterization led to an increase in calculated fetal O_2 consumption by approximately 30% ($p < 0.01$) [13]. The intensity of fetal hyperglycemia, and not the degree of fetal hyperinsulinemia, was the prime determinant of the magnitude of fetal O_2 consumption, which was associated with a significant increase in fetal O_2 extraction with no alterations in either fetal O_2 delivery or fetal blood O_2 affinity.

The effect of hyperglycemia in the uterine arteries was characterized in streptozotocin-induced hyperglycemic dams [14]. Increased wall distensibility and decreased wall stiffness was noted in diabetic uterine radial arteries [14]. The authors concluded that experimental diabetes in rat pregnancy altered the passive mechanical properties of the uterine radial arteries [14]. The relationship between fetal hypoxemia and acidemia, and fetal and uterine hemodynamics, was investigated in a cross-sectional study involving women with well-controlled diabetes mellitus [15]. Of the 65 patients who had Doppler investigations performed, 41 had cordocentesis. The changes in the umbilical arterial Doppler indices correlated well with the changes in fetal pH (correlation coefficient −0.402; $p < 0.01$) and in pO_2 (correlation coefficient −0.544; $p < 0.001$); however, this correlation was limited to the cases with FGR or pre-eclampsia as the Doppler findings were abnormal only in the presence of these complications. This finding is consistent with the known association between umbilical arterial abnormality and fetal growth restriction and pre-eclampsia. As the mothers' glycemic state was well-controlled, this study did not address the issue of human fetal hemodynamic response to in utero hyperglycemia.

22.2.2 Hypoglycemia and Fetal Hemodynamics

The effects of maternal hypoglycemia on the fetal cardiovascular system have been investigated in animal models and also in humans. Maternal hypoglycemia induced by infusion of insulin in an ewe model led to increased fetal plasma catecholamine and free fatty acid levels ($p < 0.01$) [16]; however, no significant effects were noted on the fetal heart rate, blood pressure, or arterial blood gases. Moreover, fetal insulin and glucagon levels were also unaffected. The studies in pregnant diabetic mothers were experimental in design and involved the use of the insulin clamp method for inducing hypoglycemia. Moderate maternal hypoglycemia induced by the insulin clamp technique in 10 insulin-dependent diabetic women in the third trimester was associated with no consistent changes in the umbilical arterial Doppler waveform. No significant alterations were observed in fetal breathing movements or the heart rate, although maternal epinephrine and growth hormone levels were significantly ($p < 0.001$) increased [17]. In a similar study, the effect of hypoglycemia induced by a hyperinsulinemic hypoglycemic clamp on the fetal heart rate and the umbilical artery flow velocity waveforms was investigated in a prospective experimental study in 10 women with insulin-dependent diabetes mellitus in the third trimester of pregnancy. Maternal hypoglycemia led to increases in the frequency and amplitude of fetal heart rate accelerations and maternal catecholamine levels but only a slight decline in the pulsatility index (PI) of the umbilical artery [18].

In summary, the above experimental and clinical studies enhance our understanding of maternal diabetes-induced modifications in fetal circulatory homeostasis. The fetal response to the hyperglycemic challenge is modulated by the chronic glycemic state and the intensity of the glycemic challenge. In the presence of maternal diabetes, the fetus increases its oxidative metabolism, becoming more hypoxemic. Perfusion of the brain and kidneys increases without any significant changes in the feto-placental perfusion,

and the Doppler velocimetry of the umbilical arteries remains unchanged unless FGR is also present. Cordocentesis data confirm that significant hypoxemia and acidemia in maternal diabetes mellitus may not be associated with Doppler-recognizable changes in fetal flow impedance, unless the pregnancy is complicated by FGR or pre-eclampsia. Human and animal studies indicate that the fetal response to moderate maternal hypoglycemia is unremarkable and inconsistent.

22.3 Umbilical Artery Doppler Sonography in Diabetic Pregnancies

This section reviews the role of Doppler ultrasound investigation of the umbilical artery in relation to both adverse perinatal outcomes and the maternal glycemic state.

22.3.1 Umbilical Artery Doppler and Perinatal Outcomes

The efficacy of the umbilical arterial Doppler indices for predicting adverse perinatal outcomes in high-risk pregnancies has been affirmed by numerous studies. Abnormally elevated umbilical arterial Doppler indices have been associated with a low Apgar score, fetal distress (late and severe variable decelerations), absent variability, low fetal scalp and umbilical cord arterial pH, the presence of a thick meconium and admission to the neonatal intensive care unit [19]. As presented in the Chap. 25, an absent or reversed end-diastolic velocity in the umbilical arterial Doppler waveform is particularly ominous and is associated with markedly adverse perinatal outcomes including a high perinatal mortality rate.

It remains somewhat controversial whether such diagnostic efficacy of Doppler sonography also encompasses pregnancies with diabetes. Studies in this area differ in several respects including sample size, the Doppler parameter used and its threshold value, the measures of perinatal outcomes, and the prevalence of complications such as vasculopathy. Although there is no complete unanimity in the conclusions regarding efficacy, critical appraisal of these studies reveal that the controversy is mostly apparent. The relevant studies regarding adverse perinatal outcomes are summarized in Table 22.1 and are selectively discussed below.

Bracero and associates [20] observed a significant correlation between elevated umbilical arterial systolic-to-diastolic ratio (S/D) and adverse perinatal outcomes including increased stillbirths and neonatal morbidity such as hypoglycemia and hyperbilirubinemia in a mixed population of class A and insulin-dependent diabetic mothers. In a more recent report, the same investigators have noted that the umbilical arterial S/D ratio was superior to the biophysical profile or nonstress test (NST) in predicting preterm labor (<37 weeks), FGR, hypoglycemia, hyperbilirubinemia, respiratory distress, and cesarean for fetal distress (relative risk 2.6, 1.7, and 1.7, respectively; $p < 0.001$).

Landon and colleagues [21] performed multiple umbilical arterial S/D measurements in 35 insulin-dependent diabetic women and observed significantly elevated mean second- and third-trimester S/D values in women with vasculopa-

Table 22.1 Diagnostic efficacy of umbilical arterial Doppler in diabetic pregnancy (from Maulik et al. [23])

Reference	Outcome	Prevalence	Sensitivity	Specificity	PPV	NPV	LR+	LR–	Accuracy
[20]	Stillbirth	0.04	1	0.83	0.22	1	7.6	0	0.85
[21]	FGR, FD	0.09	1	0.89	0.51	1	9.7	0	0.90
[22]	FD	0.05	0.42	0.95	0.33	0.96	8.6	0.6	0.92
[24]	C/S for FD	0.30	0.93	0.93	0.75	0.75	6.0	0.7	0.75
[25]	Composite	0.23	0.32	0.92	0.57	0.81	4.2	0.7	0.78
[26]	C/S for FD	0.27	0.61	0.75	0.48	0.84	2.5	0.5	0.71

PPV positive predictive value, *NPV* negative predictive value, *LR+* positive likelihood ratio, *LR−* negative likelihood ratio, *FGR* fetal growth restriction, *FD* fetal distress, *C/S* cesarean section

thy compared with women without the complication (4.34 ± 0.7 and 3.2 ± 0.65 vs 3.72 ± 0.42 and 2.55 ± 0.32, respectively; $p < 0.03$). The elevated ratio preceded the development of pre-eclampsia and fetal growth restriction.

Johnstone and associates [22] prospectively investigated the efficacy of the umbilical arterial resistance index in 128 pregnancies with uncomplicated diabetes mellitus. An abnormally elevated umbilical arterial resistance index (RI) significantly predicted non-assuring antepartum fetal heart rate tracing and/or a low biophysical profile score requiring an immediate cesarean delivery; however, the RI was not predictive in four of seven pregnancies with fetal compromise, which led the authors to caution against undue dependence on the umbilical arterial RI in uncomplicated diabetic pregnancies.

In a patient population of 56 diabetic mothers including 14 with vasculopathy, Reece and associates [27] observed higher mean umbilical arterial indices in those with vasculopathy than in those without vasculopathy or diabetes. Elevated Doppler indices were significantly associated with FGR and neonatal metabolic complications. This relationship between the abnormal umbilical arterial Doppler indices and the presence of maternal vasculopathic complications and various adverse perinatal outcomes has been corroborated by other investigators [24–26, 28].

More recently, Higgins et al. have studied the association between umbilical artery Dopplers and delayed villous maturation (a marker of perinatal mortality) in pre-gestational diabetic mothers. The authors found that the umbilical artery pulsatility index was significantly lower in cases with delayed villous maturation at 30 weeks of gestation only and not at 33 or 36 weeks of gestation [29].

The predictive ability of umbilical artery Dopplers for fetal macrosomia has also been studied. Maruotti et al. found a significant relationship between the umbilical artery pulsatility index and neonatal weight ($r = 0.512$; $p < 0.01$) in 102 pregnant women with type I diabetes. The umbilical artery pulsatility indices were significantly lower in the macrosomic compared to those in the non-macrosomic group (PI (95% confidence interval (CI)) = 0.78 (0.73–0.84) vs. 1.00 (0.97–1.04), $p < 0.001$ [30]). Similarly, Sirico et al. showed in 106 pregnant women with gestational diabetes that the mean umbilical artery pulsatility index was significantly lower in newborns with birthweight > 4000 g than in controls (PI (95% CI) = 0.69 (0.64–0.74) vs. 0.87 (0.84–0.90), $p < 000.1$).

22.3.2 Umbilical Arterial Doppler Sonography and Maternal Glycemic Control

In contrast to adverse outcomes, the relationship between abnormal umbilical arterial Doppler indices and the quality of glycemic control remains highly controversial. Bracero and associates [20] first noted a significant positive correlation between umbilical arterial S/D and the mean serum glucose values ($r = 0.52$, $p < 0.001$). Pietryga et al. also found a significant correlation between the umbilical artery pulsatility index and hemoglobin A1c (HbA1c) levels [31]. A more recent study has also found that the umbilical artery resistance index was significantly lower in diabetic pregnancies with glycated hemoglobin levels ≥6.5% than in those with HbA1c levels <6.5% [32].

These findings, however, were refuted by Landon and associates [21] who found no significant correlation between mean third-trimester umbilical arterial S/D and glycosylated hemoglobin ($r = 0.25$) or mean blood glucose levels ($r = 0.15$). This lack of correlation was corroborated by other investigators. These studies are summarized in Table 22.2.

In summary, most studies suggest significant diagnostic efficacy in diabetic pregnancies complicated by the presence of FGR or hypertension. It is noteworthy that these studies were heterogeneous regarding the outcome measures and the population size and that the Doppler method demonstrated varying degrees of diagnostic efficacy. Moreover, the presence of normal Doppler may not always rule out fetal compromise. The

Table 22.2 Umbilical arterial Doppler and maternal glycemic control (from Maulik et al. [23])

Reference	Doppler index	HbA1c	Δ HbA1c	Mean blood glucose
[20]	S/D			$r = 0.52$, $p < 0.001$
[21]	S/D	$r = 0.25$, NS		$r = 0.15$, NS
[22]	RI	$r = 0.02$–0.17, NS		
[28]	S/D	$r = 0.28$, NS		0.19
[27]	S/D	NS		NS
[24]	PI	NS		
[15]	Δ PI		0.011, NS	
[32]	Resistance index	Higher (≥6.5%), $p < 0.001$		
[31]	Pulsatility index	$r = 0.27$, $p < 0.001$		

S/D systolic-to-diastolic ratio, *RI* resistance index, *Δ* the change, *r* correlation coefficient, *NS* not statistically significant

ability of the umbilical artery Doppler indices to reflect maternal glycemic control remains controversial.

22.4 Doppler Sonography of Other Fetal and Uterine Circulations in Pre-Gestational Diabetic Pregnancies

22.4.1 Fetal Middle Cerebral Artery Doppler

In neonates, Van Bel and associates found unaffected cerebral hemodynamics in macrosomic infants of insulin-dependent diabetic mothers during the first 4 days of life even in the presence of ventricular septal hypertrophy with reduced cardiac output and stroke volume [33]. Salvesen and co-workers found no significant changes in the fetal circulation in a longitudinal Doppler study of 48 relatively well-controlled diabetic pregnancies, except when complicated by pre-eclampsia or FGR [15]. The study included Doppler velocimetry of the middle cerebral artery. In a separate report, the authors found normal Doppler results in the uterine and fetal circulations including the middle cerebral artery of most patients (five of six) with diabetic nephropathy, despite the cordocentesis evidence of fetal acidemia within 24 h before delivery [34]. Ishimatsu and colleagues observed that the Doppler waveforms of the middle cerebral artery in 43 pregnant women with diabetes mellitus between 24 and 38 weeks of gestation were unaffected by maternal glycemic control [35].

In the setting of gestational diabetes, however, recent data have demonstrated a potential utility of middle cerebral artery Doppler interrogation. A study showed lower middle cerebral artery peak systolic velocities in fetuses of gestational diabetic mothers compared to controls, although there was no correlation of the same marker with either hemoglobin A1c or serum glucose levels [36]. However, another study showed that a cerebroplacental ratio of less than the tenth percentile was associated with adverse perinatal outcomes [37]. Furthermore, another study showed that the middle cerebral artery pulsatility index was a good predictor of low Apgar scores in the first minute, cord blood pH, and a composite of adverse perinatal outcomes [38] (Fig. 22.2).

In summary, the utility of middle cerebral artery Doppler studies in pre-gestational diabetes remains controversial and is under investigation. Current evidence shows contradicting results, with more recent data showing a significant predictive ability in the setting of gestational diabetes.

22.4.2 Doppler Analysis of the Fetal Venous System

Researchers have studied the difference in the fetal venous system's Doppler parameters in pre-gestational diabetes and controls. Marcantonio

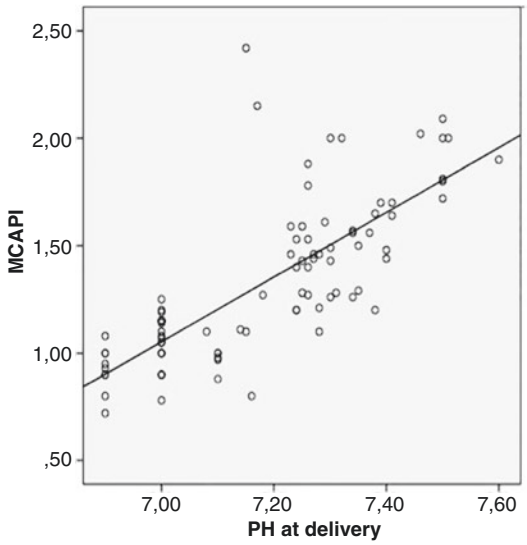

Fig. 22.2 Correlation between the neonatal acid–base status and the prenatal middle cerebral umbilical artery pulsatility index. Linear regression analysis of middle cerebral artery pulsatility index and neonatal pH showing a statistically significant association ($p < 0.02$). (Courtesy of Familiari et al. [38])

et al. showed that the ductus venosus pulsatility index was significantly higher in fetuses of diabetic mothers [39]. Lund et al. found that the umbilical vein flow and ductus venosus flow were significantly different in pre-gestational diabetes compared to those in healthy controls [40]. Lund et al. also later demonstrated that the umbilical venous flow to the liver, the total venous liver flow, and the left portal vein blood velocity were significantly higher in pre-gestational diabetes, likely contributing toward increased perinatal risks and altered liver function with long-term metabolic consequences [41].

Recent data have demonstrated a potential value for the Doppler assessment of the fetal venosus system in predicting adverse pregnancy outcomes in patients with pre-gestational diabetes. Wong et al. studied the ability of the ductus venosus peak velocity index for veins to predict adverse perinatal outcomes in pre-gestational diabetes [42] The authors found a 32% frequency of adverse outcomes in cases with abnormal Doppler studies, compared to a 12.3% frequency of the same outcomes when Doppler studies were normal (sensitivity and specificity were 53.3% and 74.6%, respectively). The authors concluded that the ductus venosus peak velocity index for veins may be useful in antenatal screening of pregnancies complicated by pre-gestational diabetes [42]. In a similar study, Miller et al. studied the utility of ductus venosus Doppler studies for the detection of fetal anomalies in pre-gestational diabetes, finding no significant difference [43].

22.4.3 Fetal Cardiac Doppler

Rizzo and colleagues studied the fetal cardiac function in 37 mothers with type I diabetes [44, 45]. The ratio between the peak velocities during early passive ventricular filling and active atrial filling (the E/A ratio) was measured at the level of the mitral and tricuspid valves. The investigators demonstrated that the E/A ratios were significantly lower in the fetuses of diabetic mothers than in control fetuses and were significantly and independently affected by the interventricular wall thickness, heart rate, and hematocrit values. No significant alterations were observed in aortic and pulmonary peak velocities or in time-to-peak velocity values. The investigators also noted interventricular septal hypertrophy, despite adequate glycemic control. This was corroborated by Miyake who observed significantly smaller E/A ratios of the left and right ventricles in later gestation in the fetuses of diabetic mothers than in those of the controls [46]. More recently, other authors have corroborated the findings of a thicker interventricular septum as well as a lower peak velocity of the tricuspid E-wave and the E/A ratio in pre-gestational diabetes [39, 47, 48]. Using tissue Doppler imaging techniques, Dervisoglu et al. found that the Ea value and the Ea/Aa ratio were lower in the diabetic group [49].

Rizzo and associates also investigated the venous blood flow patterns in insulin-dependent diabetic mothers in early gestation and observed higher values of percentage reverse flow in the inferior vena cava and a significantly higher frequency of umbilical venous pulsations at 12 weeks, which lasted until 16 weeks [50]. These abnormalities were more pronounced in pregnan-

cies with poorer glycemic control. In fetuses of well-controlled insulin-dependent diabetic mothers, Gandhi and co-workers demonstrated that the ratio of the right ventricular shortening fraction/left ventricular shortening fraction was significantly higher than that in the control group, indicating increased right ventricular hypercontractility in late diabetic pregnancy [51].

Recent advances in fetal cardiac Doppler analysis techniques have allowed a more comprehensive evaluation of the fetal heart function, with promising results. Moodley et al. found that the fetal aortic valve velocity time integral was higher in fetuses of diabetic mothers [32] The left ventricular myocardial performance index was also lower in the study group [32]. Figueroa et al. also demonstrated that a modified myocardial performance index was significantly higher in diabetes [52]. Similarly, Sanhal et al. also showed that the fetal left ventricular myocardial performance index was significantly higher in pre-gestational diabetes, whereas the E/A ratio was lower. A receiver operating characteristic analysis (Fig. 22.1) revealed >0.39 as the optimal cut-off level for the myocardial performance index in perinatal adverse outcome prediction (sensitivity: 90.9%, specificity: 47.7%, area under the curve: 0.690, 95% confidence interval: 0.598–0.782, $p < 0.001$) [53].

Researchers have also compared different fetal cardiac Doppler techniques for the assessment of cardiac function in pre-gestational diabetes. The reproducibility, agreement, and sensitivity of pulsed wave Doppler tissue imaging and spectral Doppler assessment of the right ventricular myocardial performance index were studied by Bui et al. The authors found that in the fetuses of mothers with diabetes, the two methods produced different measurements. Doppler tissue imaging had a lower intra-observer/inter-observer bias and was more sensitive to and precise in demonstrating subtle abnormalities in the fetal cardiac function [54].

Studies have also showed shown that cardiac Doppler changes can be detected early in pregnancy, shedding a light on the pathogenesis of cardiac disease. Russell et al. provided evidence of a lower left early/atrial ratio, a longer isovolumetric isovolumic relaxation time, and a higher left myocardial performance index (all markers of cardiac dysfunction) in pre-gestational diabetes [47]. These findings provide sonographic evidence of an altered cardiac function before evidence of structural changes, suggesting that an altered cardiac function may precede a structural disease [47].

The cardiac dysfunction continues in the neonatal period as shown by Kozak-Barany et al. who investigated the left ventricular systolic and diastolic functions in term neonates of mothers with well-controlled pre-gestational and gestational diabetes between 2 and 5 days after birth [55]. A prolonged deceleration time of early left ventricular diastolic filling was observed. The authors speculated that this probably reflected an impaired left ventricular relaxation related to maternal hyperglycemia, leading to subsequent fetal hyperinsulinemia and cardiac hypertrophy. Similarly, Al-Biltagi et al. found significant deterioration of both systolic and diastolic functions measured by conventional echocardiography and tissue Doppler imaging in infants of diabetic mothers [47]. In the same study, two-dimensional speckle tracking imaging showed that the cardiac torsion and the global strain were also significantly impaired [47] (Fig. 22.3).

22.4.4 Uterine Artery Doppler

The efficacy of uterine artery Doppler for managing pregnancies with pre-gestational diabetes remains unproven despite initial enthusiasm.

Bracero and associates noted abnormal uterine artery velocity waveforms in 15.4% of 52 diabetic pregnancies compared with 2% in a non-diabetic population ($p < 0.001$) [56]. Those with abnormal uterine Doppler had a higher occurrence of suboptimal glycemic control, chronic hypertension, polyhydramnios, vasculopathy, pre-eclampsia, cesarean delivery for fetal distress and neonates with respiratory distress syndrome. In 37 pregnant patients with pre-gestational and gestational diabetes, uterine Doppler demonstrated a sensitivity of 44.5%, a specificity of 100%, a positive predictive value of 100%, and a negative predictive value of 84.3%

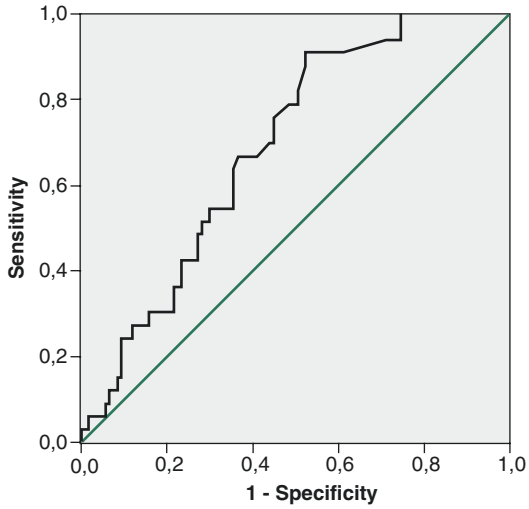

Fig. 22.3 Receiver operating characteristic curve for the myocardial performance index in predicting adverse perinatal outcomes in pregnancies complicated by pre-gestational diabetes. Receiver operating characteristic analysis revealed >0.39 as the optimal cut-off level for the myocardial performance index in perinatal adverse outcome prediction (sensitivity: 90.9%, specificity: 47.7%, area under the curve: 0.690, 95% confidence interval: 0.598–0.782, $p < 0.001$). (Courtesy of Sanhal et al. [53])

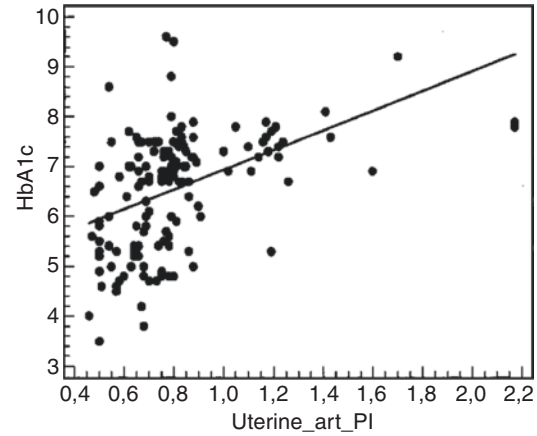

Fig. 22.4 Hemoglobin A1c and the uterine artery in pre-gestational diabetes. Scatterplot of red blood cell HbA1c in relation to the mean uterine artery pulsatility index (a marker of vascular impedance). An increase of the mean pulsatility index was significantly related to an increase of glycosylated hemoglobin ($r = 0.54$, $p < 0.001$; courtesy of Pietryga et al. [31])

in predicting the later development of vascular complications [57].

Bracero and associates studied the association between uterine artery Doppler velocimetry discordance and perinatal outcome in 265 women with singleton pregnancies complicated by diabetes who underwent Doppler examinations within 1 week before delivery [58]. An adverse outcome was defined as stillbirth, intrauterine growth restriction, delivery before 37 weeks' gestation or cesarean delivery for fetal risk. A considerable overlap in discordance was present between the good and adverse outcome groups. The discordance between the right and left uterine artery systolic–diastolic ratios was significantly higher in pregnancies with an adverse outcome ($p = 0.018$). The uterine artery S/D ratio difference of 0.60 or greater was predictive of cesarean delivery for fetal risk. In diabetic women with chronic hypertension, the discordance was not predictive of an adverse outcome.

Grunewald and associates noted the absence of the normal third-trimester decline in the uteroplacental pulsatility indices in 24 well-controlled insulin-dependent pre-gestational diabetics [24]. The pulsatility index was not influenced by glycemic control. Barth and co-workers investigated the uterine arcuate artery Doppler and decidual microvascular pathology in 47 gravidas with type I diabetes mellitus [59]. A significant correlation was noted between the abnormal Doppler indices from the uterine arcuate arteries and decidual microvascular pathology including fibrinoid necrosis, atherosis, and thrombosis ($p < 0.05$).

Pietrygra et al. also studied the relation between maternal uterine artery Dopplers and pre-gestational diabetes. The authors found that abnormal uterine artery Doppler was related to pre-gestational vasculopathy and adverse obstetric outcomes [31]. There was also a correlation between the levels of HbA1c and increased vascular impedance in the uterine artery pulsatility index (Fig. 22.4). These findings suggest that the uterine arteries are affected in women displaying clinical signs of diabetic vasculopathy, which may influence placental perfusion and fetal well-being [31].

In contrast to the above findings, other studies failed to confirm any predictive utility of uterine

Doppler velocimetry in pregnancies complicated by diabetes. Kofinas and associates observed that in gravidas with gestational ($n = 31$) and insulin-dependent ($n = 34$) diabetes mellitus, the umbilical and uterine artery flow velocity waveforms could not differentiate between good and poor glycemic control, although it discriminated patients with pre-eclampsia from those without pre-eclampsia [60]. The investigators concluded that the clinical utility of Doppler waveform analysis in diabetic pregnancies might be limited to only those with pre-eclampsia.

In a cross-sectional study of 65 well-controlled diabetic pregnancies, Salvesen and co-investigators found that the Doppler indices of the placental and fetal circulations were essentially normal, except when complicated by pre-eclampsia or FGR [15]. In a study involving 43 pregnancies with insulin-dependent diabetes mellitus, Zimmermann and colleagues reported that long- and short-term glycemic controls were unrelated to vascular resistance in the uterine artery, although the latter was higher in the presence of vasculopathy; however, more than half of the diabetics without vasculopathic complications showed a persistent notch in the uterine artery Doppler waveforms. Furthermore, uterine artery Doppler velocimetry did not demonstrate efficacy in predicting diabetes-related adverse fetal outcomes [61].

In summary, the Doppler sonographic investigations of fetal central and cerebral circulations and the maternal uterine circulation have yielded information of varying degrees of importance on maternal and fetal hemodynamic changes in pregnancies complicated by pre-gestational diabetes; however, there is no evidence that they are clinically useful in managing these pregnancies.

22.4.5 Doppler Analysis of Placental Vascularization

The utility of Doppler assessment of the placental blood flow in pre-gestational diabetes has also shown apparent promising results in the prediction of perinatal complications in diabetic mothers. Jones et al. studied the utility of stereological three-dimensional power Doppler in the placental fractional volume of power Doppler in women with and without pre-gestational diabetes. The authors found that the fractional volume of power Doppler was smaller in the diabetic group [62]. Moran et al. also studied the utility of three-dimensional power Doppler analysis in pre-gestational diabetes. The authors found that the placental flow index was significantly lower and the vascularization flow index was significantly higher [63]. The placental flow index was also significantly lower in cases with an HbA1c level $\geq 6.5\%$ [63]. Gonzalez et al. also found that three-dimensional power Doppler placental vascular indices were significantly lower in women with pre-gestational diabetes [64].

More recently, Kozinszky et al. have studied three-dimensional placental power Doppler indices in pre-gestational diabetes and healthy controls. The authors found that pre-gestational diabetes expressed lower placental vascularization indices. These indices also had a significant correlation with HbA1C, and optimal glycemic control was associated with lower placental perfusion (Fig. 22.5). Interestingly, adverse neonatal

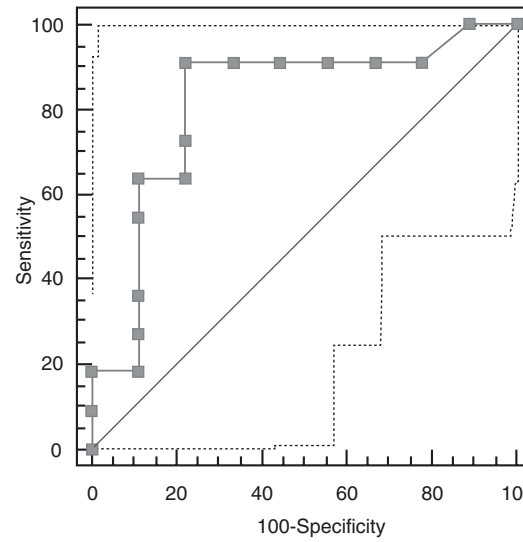

Fig. 22.5 Receiver operating characteristic curve of the placental vascular index for the prediction of poor glycemic control in pre-gestational diabetes. Receiver operating characteristic curve for predicting poor glycemic control using the placental vascular index. Area under the curve = 0.81, specificity = 77.8%, and sensitivity = 90.9%

outcomes were predicted by lower placental power Doppler indices [65].

22.5 Clinical Effectiveness and Guidelines

The clinical effectiveness of umbilical Doppler velocimetry has been demonstrated in high-risk pregnancies by randomized clinical trials. The non-stress test and the biophysical profile score are also tests of fetal surveillance that are usually initiated at 32 weeks of gestation. Daily fetal movement count is also used as an adjunct screening test. There are no randomized trials dealing exclusively with the clinical effectiveness of Doppler fetal surveillance in pregnancies complicated by pre-gestational diabetes mellitus; however, in a randomized trial reported by Williams and colleagues, umbilical artery Doppler was compared with NST as a test for fetal well-being in a population of 1360 high-risk gravidas, 11% of whom had diabetes mellitus [66]. The Doppler group had a significantly lower cesarean delivery rate for fetal distress than did the NST group (4.6% vs 8.7%, respectively; $p < 0.006$). The greatest effect was observed in pregnancies with hypertension and suspected FGR, suggesting that diabetic pregnancies with these complications may benefit from the use of Doppler velocimetry of the umbilical artery.

Wong et al. also studied the utility of umbilical artery Doppler velocimetry for the monitoring of diabetic pregnancies. The authors found that only 52% of all abnormal Dopplers had adverse perinatal outcomes, with a sensitivity and specificity of 30% and 83%, respectively. The authors concluded that umbilical artery Doppler velocimetry is not a good predictor of adverse perinatal outcomes in diabetic pregnancies [67].

In utilizing the Doppler results, the clinical practice guidelines derived from the available evidence are also applicable to managing selected pregnant patients with pre-gestational diabetes. These guidelines are summarized here. It is emphasized that the overall obstetric management in pre-gestational diabetes in pregnancy depends on multiple factors, which include the severity of diabetes, adequacy of glycemic control, presence of vasculopathic complications, gestational age, assurance of fetal well-being, and obstetric history.

In diabetic pregnancies with FGR or pre-eclampsia, umbilical artery Doppler sonography could be added to the current standards of practice for fetal surveillance that only include non-stress tests or biophysical profiles. If the Doppler index remains within the normal limits or is not progressively rising, then weekly Doppler tests should continue. A high or increasing S/D ratio warrants more intense fetal surveillance consisting of umbilical Doppler ultrasound twice a week or more along with NST and BPP. If absent end-diastolic flow velocity (AEDV) develops, then the likelihood of a poor perinatal outcome is high and urgent clinical response is indicated. At or near term, the development of AEDV should prompt an immediate consideration for delivery. A cesarean delivery may be preferable in the presence of reversed end-diastolic velocity or other ominous fetal monitoring findings (non-reactive NST, FHR with minimal variability, persistent late decelerations, oligohydramnios, and BPP score < 4). In preterm pregnancies, further assurance of fetal well-being is sought by daily surveillance with umbilical Doppler, NST, and BPP. Determination of fetal lung maturity may also assist in timing the delivery in this circumstance. In preterm pregnancies, considerations should also be given to steroid administration along with the modification of glycemic management as needed. Delivery is indicated when a single test or a combination of the fetal tests indicate imminent fetal danger irrespective of lung maturity or when a fetal risk from a hostile intrauterine environment is judged to be greater than that from pulmonary immaturity in a given neonatal service.

22.6 Conclusions

Antepartum fetal surveillance constitutes an essential component of the standards of care in managing pregnancies complicated by pre-gestational diabetes mellitus. Fetal hyperglyce-

mia is associated with increased oxidative metabolism, hypoxemia, and increased brain and renal perfusion without any significant changes in feto-placental perfusion. Moreover, the relationship between abnormal umbilical arterial Doppler indices and the quality of glycemic control remains unproven; however, observational studies suggest significant diagnostic efficacy of the umbilical arterial Doppler method in diabetic pregnancies complicated by FGR or hypertension. Although there are no randomized trials specifically addressing this issue, existing evidence suggests that Doppler velocimetry of the umbilical artery may be beneficial for antepartum fetal surveillance in diabetic pregnancies in the presence of these complications. Such utilization should be integrated with the existing standards of practice.

References

1. ACOG practice bulletin no. 201: pregestational diabetes mellitus. Obstet Gynecol. 2018;132(6):e228–e248.
2. Ogurtsova K, da Rocha Fernandes JD, Huang Y, Linnenkamp U, Guariguata L, Cho NH, et al. IDF diabetes atlas: global estimates for the prevalence of diabetes for 2015 and 2040. Diabetes Res Clin Pract. 2017;128:40–50.
3. Boyle JP, Thompson TJ, Gregg EW, Barker LE, Williamson DF. Projection of the year 2050 burden of diabetes in the US adult population: dynamic modeling of incidence, mortality, and prediabetes prevalence. Popul Health Metrics. 2010;8:29.
4. Resnik R, Lockwood CJ, Moore TR, Greene MF, Copel JA, Silver RM, et al. Creasy and Resnik's maternal-fetal medicine: principles and practice. 8th ed. Philadephia: Elsevier; 2019. 1 online resource (xviii, 1388 pages) p.
5. Asoglu MR, Gabbay-Benziv R, Turan OM, Turan S. Exposure of the developing heart to diabetic environment and early cardiac assessment: a review. Echocardiography. 2018;35(2):244–57.
6. Crandell SS, Fisher DJ, Morriss FH Jr. Effects of ovine maternal hyperglycemia on fetal regional blood flows and metabolism. Am J Phys. 1985;249(5 Pt 1):E454–60.
7. Dickinson JE, Meyer BA, Palmer SM. Fetal vascular responses to maternal glucose administration in streptozocin-induced ovine diabetes mellitus. J Obstet Gynaecol Res. 1998;24(5):325–33.
8. Lehtoranta L, Vuolteenaho O, Laine J, Polari L, Ekholm E, Rasanen J. Placental structural abnormalities have detrimental hemodynamic consequences in a rat model of maternal hyperglycemia. Placenta. 2016;44:54–60.
9. Lehtoranta L, Vuolteenaho O, Laine VJ, Koskinen A, Soukka H, Kyto V, et al. Maternal hyperglycemia leads to fetal cardiac hyperplasia and dysfunction in a rat model. Am J Physiol Endocrinol Metab. 2013;305(5):E611–9.
10. Lawson TB, Scott-Drechsel DE, Chivukula VK, Rugonyi S, Thornburg KL, Hinds MT. Hyperglycemia alters the structure and hemodynamics of the developing embryonic heart. J Cardiovasc Dev Dis. 2018;5(1):13.
11. Gutierrez JC, Hrubec TC, Prater MR, Smith BJ, Freeman LE, Holladay SD. Aortic and ventricular dilation and myocardial reduction in gestation day 17 ICR mouse fetuses of diabetic mothers. Birth Defects Res A Clin Mol Teratol. 2007;79(6):459–64.
12. Turan S, Turan OM, Miller J, Harman C, Reece EA, Baschat AA. Decreased fetal cardiac performance in the first trimester correlates with hyperglycemia in pregestational maternal diabetes. Ultrasound Obstet Gynecol. 2011;38(3):325–31.
13. Philipps AF, Porte PJ, Stabinsky S, Rosenkrantz TS, Raye JR. Effects of chronic fetal hyperglycemia upon oxygen consumption in the ovine uterus and conceptus. J Clin Invest. 1984;74(1):279–86.
14. Phillips JK, Vance AM, Raj RS, Mandala M, Linder EA, Gokina NI. Impact of experimental diabetes on the maternal uterine vascular remodeling during rat pregnancy. Reprod Sci. 2012;19(3):322–31.
15. Salvesen DR, Higueras MT, Mansur CA, Freeman J, Brudenell JM, Nicolaides KH. Placental and fetal Doppler velocimetry in pregnancies complicated by maternal diabetes mellitus. Am J Obstet Gynecol. 1993;168(2):645–52.
16. Harwell CM, Padbury JF, Anand RS, Martinez AM, Ipp E, Thio SL, et al. Fetal catecholamine responses to maternal hypoglycemia. Am J Phys. 1990;259(6 Pt 2):R1126–30.
17. Reece EA, Hagay Z, Roberts AB, DeGennaro N, Homko CJ, Connolly-Diamond M, et al. Fetal Doppler and behavioral responses during hypoglycemia induced with the insulin clamp technique in pregnant diabetic women. Am J Obstet Gynecol. 1995;172(1 Pt 1):151–5.
18. Bjorklund AO, Adamson UK, Almstrom NH, Enocksson EA, Gennser GM, Lins PE, et al. Effects of hypoglycaemia on fetal heart activity and umbilical artery Doppler velocity waveforms in pregnant women with insulin-dependent diabetes mellitus. Br J Obstet Gynaecol. 1996;103(5):413–20.
19. Maulik D, Yarlagadda P, Youngblood JP, Ciston P. The diagnostic efficacy of the umbilical arterial systolic/diastolic ratio as a screening tool: a prospective blinded study. Am J Obstet Gynecol. 1990;162(6):1518–23; discussion 23–5.
20. Bracero L, Schulman H, Fleischer A, Farmakides G, Rochelson B. Umbilical artery velocimetry in diabetes and pregnancy. Obstet Gynecol. 1986;68(5):654–8.

21. Landon MB, Gabbe SG, Bruner JP, Ludmir J. Doppler umbilical artery velocimetry in pregnancy complicated by insulin-dependent diabetes mellitus. Obstet Gynecol. 1989;73(6):961–5.
22. Johnstone FD, Steel JM, Haddad NG, Hoskins PR, Greer IA, Chambers S. Doppler umbilical artery flow velocity waveforms in diabetic pregnancy. Br J Obstet Gynaecol. 1992;99(2):135–40.
23. Maulik D, Lysikiewicz A, Sicuranza G. Umbilical arterial Doppler sonography for fetal surveillance in pregnancies complicated by pregestational diabetes mellitus. J Matern Fetal Neonatal Med. 2002;12(6):417–22.
24. Grunewald C, Divon M, Lunell NO. Doppler velocimetry in last trimester pregnancy complicated by insulin-dependent diabetes mellitus. Acta Obstet Gynecol Scand. 1996;75(9):804–8.
25. Bracero LA, Figueroa R, Byrne DW, Han HJ. Comparison of umbilical Doppler velocimetry, nonstress testing, and biophysical profile in pregnancies complicated by diabetes. J Ultrasound Med. 1996;15(4):301–8.
26. Fadda GM, D'Antona D, Ambrosini G, Cherchi PL, Nardelli GB, Capobianco G, et al. Placental and fetal pulsatility indices in gestational diabetes mellitus. J Reprod Med. 2001;46(4):365–70.
27. Reece EA, Hagay Z, Assimakopoulos E, Moroder W, Gabrielli S, DeGennaro N, et al. Diabetes mellitus in pregnancy and the assessment of umbilical artery waveforms using pulsed Doppler ultrasonography. J Ultrasound Med. 1994;13(2):73–80.
28. Dicker D, Goldman JA, Yeshaya A, Peleg D. Umbilical artery velocimetry in insulin dependent diabetes mellitus (IDDM) pregnancies. J Perinat Med. 1990;18(5):391–5.
29. Higgins MF, Russell NM, Mooney EE, McAuliffe FM. Clinical and ultrasound features of placental maturation in pre-gestational diabetic pregnancy. Early Hum Dev. 2012;88(10):817–21.
30. Maruotti GM, Rizzo G, Sirico A, Sarno L, Cirigliano L, Arduini D, et al. Are there any relationships between umbilical artery pulsatility index and macrosomia in fetuses of type I diabetic mothers? J Matern Fetal Neonatal Med. 2014;27(17):1776–81.
31. Pietryga M, Brazert J, Wender-Ozegowska E, Biczysko R, Dubiel M, Gudmundsson S. Abnormal uterine Doppler is related to vasculopathy in pregestational diabetes mellitus. Circulation. 2005;112(16):2496–500.
32. Moodley S, Arunamata A, Stauffer KJ, Nourse SE, Chen A, Quirin A, et al. Maternal arterial stiffness and fetal cardiovascular physiology in diabetic pregnancy. Ultrasound Obstet Gynecol. 2018;52(5):654–61.
33. Van Bel F, Van de Bor M, Walther FJ. Cerebral blood flow velocity and cardiac output in infants of insulin-dependent diabetic mothers. Acta Paediatr Scand. 1991;80(10):905–10.
34. Salvesen DR, Higueras MT, Brudenell JM, Drury PL, Nicolaides KH. Doppler velocimetry and fetal heart rate studies in nephropathic diabetics. Am J Obstet Gynecol. 1992;167(5):1297–303.
35. Ishimatsu J, Matsuzaki T, Yakushiji M, Hamada T. Blood flow velocity waveforms of the fetal middle cerebral artery in pregnancies complicated by diabetes mellitus. Kurume Med J. 1995;42(3):161–6.
36. Dantas AMA, Palmieri ABS, Vieira MR, Souza MLR, Silva JC. Doppler ultrasonographic assessment of fetal middle cerebral artery peak systolic velocity in gestational diabetes mellitus. Int J Gynaecol Obstet. 2019;144(2):174–9.
37. Gibbons A, Flatley C, Kumar S. The fetal cerebroplacental ratio in diabetic pregnancies is influenced more by the umbilical artery rather than middle cerebral artery pulsatility index. Eur J Obstet Gynecol Reprod Biol. 2017;211:56–61.
38. Familiari A, Neri C, Vassallo C, Di Marco G, Garofalo S, Martino C, et al. Fetal Doppler parameters at term in pregnancies affected by gestational diabetes: role in the prediction of perinatal outcomes. Ultraschall Med. 2020;41(6):675–80.
39. Zielinsky P, Marcantonio S, Nicoloso LH, Luchese S, Hatem D, Scheid M, et al. Ductus venosus flow and myocardial hypertrophy in fetuses of diabetic mothers. Arq Bras Cardiol. 2004;83(1):51–6; 45–50.
40. Lund A, Ebbing C, Rasmussen S, Kiserud T, Kessler J. Maternal diabetes alters the development of ductus venosus shunting in the fetus. Acta Obstet Gynecol Scand. 2018;97(8):1032–40.
41. Lund A, Ebbing C, Rasmussen S, Kiserud T, Hanson M, Kessler J. Altered development of fetal liver perfusion in pregnancies with pregestational diabetes. PLoS One. 2019;14(3):e0211788.
42. Wong SF, Petersen SG, Idris N, Thomae M, McIntyre HD. Ductus venosus velocimetry in monitoring pregnancy in women with pregestational diabetes mellitus. Ultrasound Obstet Gynecol. 2010;36(3):350–4.
43. Miller JL, de Veciana M, Turan S, Kush M, Manogura A, Harman CR, et al. First-trimester detection of fetal anomalies in pregestational diabetes using nuchal translucency, ductus venosus Doppler, and maternal glycosylated hemoglobin. Am J Obstet Gynecol. 2013;208(5):385.e1–8.
44. Rizzo G, Arduini D, Romanini C. Cardiac function in fetuses of type I diabetic mothers. Am J Obstet Gynecol. 1991;164(3):837–43.
45. Rizzo G, Pietropolli A, Capponi A, Cacciatore C, Arduini D, Romanini C. Analysis of factors influencing ventricular filling patterns in fetuses of type I diabetic mothers. J Perinat Med. 1994;22(2):149–57.
46. Miyake T. Doppler echocardiographic studies of diastolic cardiac function in the human fetal heart. Kurume Med J. 2001;48(1):59–64.
47. Al-Biltagi M, Tolba OA, Rowisha MA, Mahfouz Ael S, Elewa MA. Speckle tracking and myocardial tissue imaging in infant of diabetic mother with gestational and pregestational diabetes. Pediatr Cardiol. 2015;36(2):445–53.
48. Fouda UM, Abou ElKassem MM, Hefny SM, Fouda RM, Hashem AT. Role of fetal echocardiography in

the evaluation of structure and function of fetal heart in diabetic pregnancies. J Matern Fetal Neonatal Med. 2013;26(6):571–5.
49. Dervisoglu P, Kosecik M, Kumbasar S. Effects of gestational and pregestational diabetes mellitus on the foetal heart: a cross-sectional study. J Obstet Gynaecol. 2018;38(3):408–12.
50. Rizzo G, Arduini D, Capponi A, Romanini C. Cardiac and venous blood flow in fetuses of insulin-dependent diabetic mothers: evidence of abnormal hemodynamics in early gestation. Am J Obstet Gynecol. 1995;173(6):1775–81.
51. Gandhi JA, Zhang XY, Maidman JE. Fetal cardiac hypertrophy and cardiac function in diabetic pregnancies. Am J Obstet Gynecol. 1995;173(4):1132–6.
52. Figueroa H, Silva MC, Kottmann C, Viguera S, Valenzuela I, Hernandez-Andrade E, et al. Fetal evaluation of the modified-myocardial performance index in pregnancies complicated by diabetes. Prenat Diagn. 2012;32(10):943–8.
53. Sanhal CY, Daglar HK, Kara O, Uygur D, Yucel A. Assessment of fetal myocardial performance index in women with pregestational and gestational diabetes mellitus. J Obstet Gynaecol Res. 2017;43(1):65–72.
54. Bui YK, Kipps AK, Brook MM, Moon-Grady AJ. Tissue Doppler is more sensitive and reproducible than spectral pulsed-wave Doppler for fetal right ventricle myocardial performance index determination in normal and diabetic pregnancies. J Am Soc Echocardiogr. 2013;26(5):507–14.
55. Kozak-Barany A, Jokinen E, Kero P, Tuominen J, Ronnemaa T, Valimaki I. Impaired left ventricular diastolic function in newborn infants of mothers with pregestational or gestational diabetes with good glycemic control. Early Hum Dev. 2004;77(1–2):13–22.
56. Bracero LA, Schulman H. Doppler studies of the uteroplacental circulation in pregnancies complicated by diabetes. Ultrasound Obstet Gynecol. 1991;1(6):391–4.
57. Haddad B, Uzan M, Tchobroutsky C, Uzan S, Papiernik-Berkhauer E. Predictive value of uterine Doppler waveform during pregnancies complicated by diabetes. Fetal Diagn Ther. 1993;8(2):119–25.
58. Bracero LA, Evanco J, Byrne DW. Doppler velocimetry discordancy of the uterine arteries in pregnancies complicated by diabetes. J Ultrasound Med. 1997;16(6):387–93.
59. Barth WH Jr, Genest DR, Riley LE, Frigoletto FD Jr, Benacerraf BR, Greene MF. Uterine arcuate artery Doppler and decidual microvascular pathology in pregnancies complicated by type I diabetes mellitus. Ultrasound Obstet Gynecol. 1996;8(2):98–103.
60. Kofinas AD, Penry M, Swain M. Uteroplacental Doppler flow velocity waveform analysis correlates poorly with glycemic control in diabetic pregnant women. Am J Perinatol. 1991;8(4):273–7.
61. Zimmermann P, Kujansuu E, Tuimala R. Doppler flow velocimetry of the uterine and uteroplacental circulation in pregnancies complicated by insulin-dependent diabetes mellitus. J Perinat Med. 1994;22(2):137–47.
62. Jones NW, Deshpande R, Mousa HA, Mansell P, Raine-Fenning N, Bugg G. Fractional volume of placental vessels in women with diabetes using a novel stereological 3D power Doppler technique. Placenta. 2013;34(11):1002–8.
63. Moran M, Mulcahy C, Daly L, Zombori G, Downey P, McAuliffe FM. Novel placental ultrasound assessment: potential role in pre-gestational diabetic pregnancy. Placenta. 2014;35(8):639–44.
64. Gonzalez Gonzalez NL, Gonzalez Davila E, Castro A, Padron E, Plasencia W. Effect of pregestational diabetes mellitus on first trimester placental characteristics: three-dimensional placental volume and power Doppler indices. Placenta. 2014;35(3):147–51.
65. Kozinszky Z, Altorjay A, Molnar A, Nyari T, Vari SG, Nemeth G, et al. Ultrasonographic evaluation of glycemic control effect on placental vascularization in pregnancy with type 1 diabetes mellitus. Exp Clin Endocrinol Diabetes. 2020;128(12):788–95.
66. Williams KP, Farquharson DF, Bebbington M, Dansereau J, Galerneau F, Wilson RD, et al. Screening for fetal well-being in a high-risk pregnant population comparing the nonstress test with umbilical artery Doppler velocimetry: a randomized controlled clinical trial. Am J Obstet Gynecol. 2003;188(5):1366–71.
67. Wong SF, Chan FY, Cincotta RB, McIntyre DH, Stone M. Use of umbilical artery Doppler velocimetry in the monitoring of pregnancy in women with pre-existing diabetes. Aust N Z J Obstet Gynaecol. 2003;43(4):302–6.

Doppler Velocimetry in Prolonged Pregnancy

23

Richard Bronsteen, Ali Alhousseini, and Ray Bahado-Singh

23.1 Introduction

Pregnancies progressing past 42 weeks/294 days are associated with an increase in perinatal morbidity and mortality [1, 2]. The terminologies used to identify these situations include "postdate," "post-term," and "prolonged pregnancy," which are terms sometimes used interchangeably and at other times overlap with differing gestational-age starting points (40, 41, or 42 weeks). A single specific etiology for an increased adverse outcome has not been established with certainty, and multiple factors may be involved. As fetal growth continues, it is possible that the fetal size exceeds the placental ability to provide adequate nutritional and respiratory support.

The prevalence of postdate pregnancy is variable worldwide. European data from 15 different areas drawn predominantly from 2000 found that 0.4–8.1% of deliveries occurred at or beyond 294 [3]. Birth certificate data for the United States from the National Center for Health Statistics covering the years 2010–2017 (just under four million births annually) show pregnancies beyond 294 days occurring for 0.33–0.46% of deliveries [4]. This sub-1% rate is considerably lower than the earlier reported rates of 5–6%. In 2014, the National Center for Health Statistics changed how they calculated gestational age from birth certificate data, switching from the last menstrual period to obstetric estimate [5, 6]. Recent statistics for the United States have shown late preterm delivery (41–0/7 weeks–41-6/7 weeks) rates of just over 6% [4].

The standard testing for fetal evaluation includes non-stress tests (NSTs) and biophysical profiles as markers of fetal health. In postdate pregnancies, amniotic fluid volume is also measured. For over three decades, Doppler velocimetry has been used as an additional tool for fetal evaluation. Doppler provides us with the capability to evaluate hemodynamic changes in both the placenta and fetus. Uterine and umbilical artery Doppler, as a measure of placental resistance, can provide insights into placental perfusion from the maternal and fetal circulations. As compromises in fetal health develop, hemodynamic changes that can occur include hypovolemia and redistribution of fetal blood flow, which are changes potentially detectable through Doppler testing. In this chapter, we will review the information available on Doppler velocimetry in postdate pregnancies. The most common fetal vessels that have been studied and the ones most commonly used for clinical purposes are the umbilical and middle cerebral arteries. Many of the studies include Doppler testing in both vessels. For these reasons,

R. Bronsteen (✉) · R. Bahado-Singh
Beaumont Health System, Ob/Gyn,
Royal Oak, MI, USA
e-mail: Richard.Bronsteen@beaumont.org

A. Alhousseini
Michigan State University, Lansing, MI, USA

D. Maulik, C. C. Lees (eds.), *Doppler Ultrasound in Obstetrics and Gynecology*,
https://doi.org/10.1007/978-3-031-06189-9_23

studies on these vessels will be covered together in the second section of this chapter. The first section reviews the data on "other vessels," aorta, pulmonary artery, renal artery, and uterine artery. Studies that performed multi-vessel analysis appear in more than one section.

23.2 Other Vessels

23.2.1 Aortic Blood Flow Doppler

Doppler parameters that have been evaluated in the fetal aorta include velocity (either mean or peak) and blood flow volume. Several of the studies reviewed show a positive association between aortic Doppler results and adverse pregnancy outcomes.

-Battaglia et al. studied 82 pregnancies with Doppler evaluation beginning at 41 weeks. Based on unpublished preliminary data, a mean velocity of 25 cm/s in the thoracic aorta was chosen as the cut-off to separate normal from decreased mean velocity. Pregnancies with low mean thoracic aortic velocities were associated with cesarean delivery for fetal distress, oligohydramnios, meconium-stained amniotic fluid, and abnormal non-stress tests in individual analyses [7].

-Anteby et al. studied 78 pregnancies starting at 41 weeks' gestation. Patients who had fetal distress, defined by the presence of the meconium, abnormal fetal heart rate pattern, or intervention for abnormal fetal heart rate pattern, had a significantly lower mean thoracic aortic velocity [8].

-Olofsson et al. followed 44 patients who delivered after 43 weeks with serial descending aortic testing, which included mean velocity, flow volume, and a pulsatility index (PI) ratio. These three indices were then compared in patients grouped according to four different measures of adverse outcomes: oligohydramnios (maximum amniotic fluid vertical pocket (MVP) ≤2 cm), meconium, asphyxia (low Apgar scores or acidosis), or fetal distress (delivery for abnormal fetal heart tones). Of these 12 analyses, the only significant difference was between aortic flow volume and fetal distress. Interestingly, patients delivering with fetal distress had a higher flow volume than did those without [9].

-Weiner et al. published two studies in 1996, which evaluated fetal aortic Doppler in postdate pregnancies [10, 11]. Serial Doppler testing was begun at 41 weeks with measurements of the peak aortic systolic velocity and aortic flow volume. These Doppler indices were compared with pregnancy outcomes of amniotic fluid volume and fetal heart rate testing. The two studies overlap in the periods when patient data were collected; it is not clear whether some patients were included in both studies. In one study of 45 patients, the percentage changes for both aortic Doppler velocity and flow volume were analyzed with the percentage change in amniotic fluid (linear regression) and with fetal heart rate patterns (non-parametric median testing) [10]. A significant decline in both aortic Doppler parameters were noted in association with decreases in amniotic flow volume, while only the aortic flow volume but not the peak velocity correlated with non-reassuring fetal heart rate abnormalities. In the second study, the same 4 parameters (aortic peak velocity, aortic flow volume, amniotic fluid volume, and fetal heart rate pattern) were evaluated in 120 patients. The analysis here used absolute Doppler values instead of percentage change, amniotic fluid index (AFI) ≤ 5 instead of percentage change of amniotic fluid, and low fetal heart rate variability on computerized fetal monitoring was used to define an abnormal fetal heart rate pattern.11 Both measures of aortic Doppler were significantly lower in patients with oligohydramnios and decreased fetal heart rate variability. Of the eight statistical analyses in these two studies, seven showed a significant association with lower aortic indices seen with adverse outcomes.

Other studies did not find a positive association between aortic Doppler and clinical outcome in postdate pregnancies.

-Rightmire and Campbell evaluated 35 pregnancies beginning at 42 weeks. The mean Doppler velocity in the thoracic aorta was observed to decrease with gestational age. Although the mean thoracic velocities from fetuses with a compromised outcome were lower than those obtained from fetuses with a normal outcome, this difference was not statistically significant [12].

-Malcus et al. followed 102 pregnancies with testing beginning at or after 42 weeks. Doppler evaluation included the mean velocity and PI for the descending thoracic aorta. Neither of these Doppler measurements were associated with abnormal outcomes of a non-reactive non-stress test or asphyxia, with the latter defined by an umbilical artery pH less than 7.10 or low Apgar scores [13].

-Kauppinen et al. followed 160 pregnancies beginning at 41 weeks. Aortic measurements included the PI ratio, peak systolic velocity, and volume flow. No differences were noted in any of these Doppler parameters between pregnancies with (n = 135) and without (n = 25) a favorable outcome [14].

23.2.2 Pulmonary Artery Doppler

Three of the above studies on aortic Doppler including both studies by Weiner et al. also evaluated the pulmonary artery [10, 11, 14].

-In the first study by Weiner et al., looking at the percentage change for pulmonary artery parameters of peak systolic velocity and flow volume, neither Doppler parameter was associated with the percentage change in amniotic fluid volume. The percentage change in the flow volume was associated with decreased fetal heart rate variability, whereas the percentage change in peak velocity was not [10].

-In the second larger study, neither Doppler parameter was associated with oligohydramnios, but both were associated with decreased fetal heart rate variability [11].

Combining the data from both studies by Weiner et al., none of the four analyses showed an association between pulmonary Doppler testing and amniotic fluid volume, whereas three of the four showed an association with abnormal fetal heart rate.

-Kauppinen et al. did not find a significant difference in pulmonary artery Doppler testing with PI ratio, peak systolic velocity, or volume flow between patients with and without a favorable outcome [14].

23.2.3 Renal Artery Doppler

Amniotic fluid volume begins to decrease in the mid-third trimester, a trend that continues in postdate pregnancies. Several studies have evaluated renal artery hemodynamics in the late term and in postdate pregnancies in conjunction with amniotic fluid volumes, looking for a potential explanation for the declining fluid volumes.

-Arduini and Rizzo followed 97 pregnancies beginning at 42 weeks. The renal artery PI values obtained from these pregnancies were not statistically different from those from a term reference group. When study patients were classified by amniotic fluid volumes (normal, decreased, oligohydramnios), no significant differences in the renal artery PI values were noted between the groups [15].

--Battaglia et al. evaluated 82 pregnancies beginning at 41 weeks with multi-vessel Doppler testing. Statistical Doppler comparisons were made for patients grouped according to normal or decreased mean thoracic aortic velocity. This outcome parameter was chosen for their analyses because in their data it was associated with cesarean delivery for fetal distress, oligohydramnios, meconium-stained amniotic fluid, and abnormal non-stress tests in individual analyses. No differences in the renal artery PI values were noted between pregnancies with normal vs. decreased mean thoracic aortic velocity [7].

-Bar-Hava et al. began serial renal artery Doppler testing at 41 weeks, studying 57 patients. The renal artery resistance index (RI) for pregnancies with oligohydramnios (AFI < 5 cm) was not significantly different from values obtained in patients with normal fluid [16].

In opposition to these negative studies, others did not find a significant difference in renal artery Doppler velocimetry in association with amniotic fluid volume.

-Veille et al. evaluated 50 pregnancies, with Doppler testing beginning at 40 weeks. A significant negative correlation was obtained between oligohydramnios (AFI ≤5 cm, n = 17) and an increased renal artery systolic-to-diastolic ratio (S/D) [17].

-Oz et al. began Doppler testing at 41 weeks, evaluating 147 pregnancies. The renal artery RI was significantly higher in 21 pregnancies with oligohydramnios, defined as an AFI < 5 cm. A low renal artery end-diastolic velocity also increased the risk of oligohydramnios, although on regression analysis only the renal artery RI was associated with oligohydramnios [18].

-The study by Selam evaluated 38 pregnancies beginning at 41 weeks, 10 of which had oligohydramnios (AFI < 5 cm). The renal artery PI was significantly elevated in these patients in comparison to those with normal fluid volume [19].

23.2.4 Uterine Artery Doppler

The placenta is a vital organ for maintaining ongoing fetal health, providing respiratory, nutritive, and excretory functions to the developing fetus. Placental hemodynamic changes, as a potential marker of placental dysfunction, can be evaluated through Doppler of both the maternal (uterine artery) and fetal (umbilical artery) circulations. Studies on uterine artery Doppler have been uniform in their not finding a significant association with complications in postdate pregnancies.

-Battaglia et al. compared the mean Doppler values in 82 pregnancies, with patients grouped according to the mean thoracic aortic velocity. No differences in the uterine artery RI ratios were noted between these two groups [7].

-Olofsson et al. did not find any difference in the uterine artery PIs in 44 patients delivering after 43 weeks in individual statistical analyses for patients with and without the meconium, asphyxia, oligohydramnios, and fetal distress [9].

-Malcus et al. evaluated 102 pregnancies beginning at 42 weeks. A significant association was not found between the uterine artery PI ratio and asphyxia, which was defined by the parameters of umbilical artery pH, Apgar scores, and operative delivery for fetal distress [13].

-Fischer et al. evaluated 75 pregnancies beginning at 41 weeks, grouping pregnancy outcomes as either normal or abnormal based on a composite of multiple clinical parameters. Uterine artery Doppler testing, with waveform analysis by either the RI or S/D, was not significantly different between the normal and abnormal outcome groups [20].

-Zimmerman et al. followed 153 pregnancies beginning at 41 weeks. Clinical outcomes that were evaluated included Apgar scores, umbilical artery pH, neonatal intensive care unit (NICU) admission with asphyxial encephalopathy, postmaturity syndrome, thick meconium, and operative delivery. No differences in the uterine artery RI were noted between pregnancies with and without abnormal outcomes [21].

-Kauppinen et al. performed uterine artery Doppler testing in patients just prior to scheduled delivery after 41 weeks. No difference in the uterine artery PI was noted between the pregnancies with a normal outcome and those with an abnormal outcome defined by umbilical artery pH, Apgar scores, C-section for fetal distress, and NICU admission [14].

-Brar et al. evaluated uterine artery Doppler testing in 26 pregnancies beginning at 41 weeks. These pregnancies were grouped into those with either reassuring or non-reassuring antenatal testing based on NSTs and fluid volume. No significant difference in the mean uterine artery S/D ratios was noted between these groups [22].

-Weiner et al. followed 142 pregnancies beginning at 41 weeks. No significant difference was noted in the uterine artery RI between the normal and abnormal pregnancy outcome groups, with the abnormal group defined by a composite of multiple clinical parameters [23].

-Forouzan and Cohen followed 30 patients with arcuate artery S/D ratios. Adverse outcomes were defined as abnormal intrapartum fetal heart rate patterns requiring cesarean delivery, umbilical artery acidosis or neonatal diagnosis of intrapartum hypoxia requiring NICU care and were seen in 20% of the study group. The mean arcuate artery S/D ratios were not significantly different between the two groups [24].

-Farmakides et al. obtained uterine S/D ratios in 149 pregnancies beginning at 41 weeks. Abnormal pregnancy outcomes were defined by a composite of morbidities, and statistical analysis was performed separately for Doppler testing conducted at 41, 42, and 43 weeks. The mean S/D ratios for the normal and abnormal outcome

groups were not significantly different at any of those gestational ages [25].

The vessels reviewed in the section above have been studied for their potential role in the pathophysiology of postdate pregnancies. Decreased fetal cardiac output can be a measure of hypovolemia or a response to a compromised environment. Positive results could provide insights into why adverse outcomes occur and could potentially be useful for ongoing clinical antenatal surveillance.

Are Doppler abnormalities of the aorta and pulmonary artery involved in the adverse outcomes seen in postdate pregnancies? The studies reviewed above do not show a consistent association with postdate pregnancy pathology. The positive results obtained may be suggestive, but, overall, the data neither exclude nor confirm significant Doppler changes in these vessels, which are detectable in postdate pregnancies with adverse outcomes. It would not be unexpected that renal artery hemodynamic alterations would be involved with the decrease in fluid volume noted in postdate pregnancies. In three of the five studies reviewed above, in which renal Doppler was compared between pregnancies grouped according to fluid volume, a positive association was noted. As with the aortic and pulmonary Doppler studies, these results are not conclusive, and it is not clear whether significant Doppler changes are associated with decreased fluid in postdate pregnancies. Uterine artery Doppler studies are more consistent in their findings; placental hemodynamics, as measured from the maternal circulation, are not associated with adverse postdate pregnancy outcomes.

23.3 Umbilical and Middle Cerebral Artery Doppler

Most of the data available on Doppler in postdate pregnancy involve testing in the umbilical and middle cerebral arteries. Umbilical artery Doppler evaluates placental hemodynamics from the fetal perspective, with increased indices indicative of increased resistance and potentially decreased function. Middle cerebral artery Doppler testing showing decreases in resistance is suggestive of a fetal response to a compromised environment, the so-called brain-sparing effect. Taking advantage of these divergent trends, Doppler velocimetry from both vessels can be paired together as the cerebroplacental ratio or CPR (the middle cerebral artery Doppler index/umbilical artery Doppler index). As Doppler evaluations of these two vessels are often used clinically, and are often evaluated together, the data available on their association with adverse outcomes in postdate pregnancy will be covered together.

When evaluating the appropriateness of any test for clinical use, here, Doppler velocimetry, the issues that need to be addressed include:

1. Are Doppler results consistent from study to study, with an accepted cut-off level separating normal from abnormal?
2. Is there an association between abnormal Doppler testing and adverse pregnancy outcomes?
3. Is Doppler testing a good discriminator (sensitivity and specificity) between normal and abnormal pregnancy outcomes, and how does it compare to the antenatal tests currently in use?
4. Does the use of Doppler testing improve outcomes in postdate pregnancies?

These questions will be addressed below.

1. Are Doppler results consistent from study to study, with accepted cut cut-off levels separating normal from abnormal?
   Physiologically, Doppler indices change throughout pregnancy. All of the standard indices used in waveform analysis (PI, RI, S/D) decrease at the end of pregnancy, beginning prior to or at the midpoint of the third trimester [26, 27]. Although week-to-week changes in Doppler indices are small, normalized Doppler results for specific gestational ages are preferable. Multiple nomograms are available to provide normative Doppler data throughout pregnancy. Two recent review articles with similar authorship have highlighted the problems with the normative Doppler data available [27, 28]. For studies that were spe-

cifically conducted to establish normative Doppler data (38 published studies), a high degree of variability in both methodological quality and reported gestational age-specific 5th and 95th percentile values was noted. Even when the comparisons were limited to those studies with the highest methodological quality, significant variation in the Doppler results remained [28]. When the most frequently referenced nomograms were applied to a cohort of 617 intrauterine growth restriction (IUGR) fetuses, wide ranges in the percentage of abnormal tests were obtained: for the umbilical artery, the range of Doppler values above the 95th percentile in the different studies ranged from 2.1 to 24.5%, whereas the range of Doppler values below the 5th percentile was 0.9–23.1% for the middle cerebral artery and 5.5–33.1% for the CPR [27].

Most normative Doppler data available do not cover late-term or postdate pregnancies. Published normative data in late pregnancies are limited, but similar concerns on consistency have been raised. D'Antonio et al. noted that prior studies had used a wide range of CPR cut-off values in postdate pregnancy evaluation (CPR 0.81–1.3) [29]. Palacio noted a similar wide range in published gestational age-specific Doppler cut-offs for the umbilical and middle cerebral arteries after 40 weeks. Including their own data, the 95th percentiles for the umbilical artery PI ranged from 1.0 to 1.5 at 41 weeks and 0.9 to 1.5 at 42 weeks, whereas the 5th percentile cut-offs for the MCA-PI ranged from 0.70 to 1.98 at 41 weeks and 0.65 to 1.94 at 42 weeks [30]. A large recent study from the Fetal Medicine Foundation, testing nearly 2400 patients at 41 weeks, has found the 95th percentile for the umbilical artery PI to be 1.05 and the 5th percentiles for the MCA-PI and CPR to be 0.89 and 1.0.25, respectively.

2. Is there an association between abnormal Doppler testing and adverse pregnancy outcomes?

Many of the studies that sought to address this question utilized a similar methodology. Doppler testing, usually on a serial basis, was initiated at a specific gestational age, typically at 41 or 42 weeks. For statistical analysis, the pregnancies were divided into normal and abnormal outcome groups as defined by a preselected list of adverse outcomes that typically included non-reassuring fetal testing, delivery for fetal distress, low Apgar scores, abnormal umbilical blood gas values, NICU admission, and meconium. Most studies compared the mean Doppler values between the normal and abnormal pregnancy outcome groups, whereas some studies compared the percentage abnormal Doppler values between the two outcome groups. Patients with underlying risk factors were usually excluded. These studies are summarized below and are listed in Table 23.1. In many of the studies, no significant difference was noted between the adverse and normal outcome groups.

- Gupta et al. followed 31 pregnancies with biweekly umbilical and middle cerebral artery Doppler testing beginning at 40 weeks. Umbilical artery waveforms were evaluated by S/D ratios, whereas middle cerebral artery waveforms were evaluated by PI ratios. A CPR was also calculated (apparently from the MCA-PI and umbilical artery S/D). Adverse outcomes were noted in 16% of the study population. No significant differences were noted in any of the mean Doppler indices between the abnormal and normal groups [31].
- Guidetti et al. followed 46 pregnancies with umbilical artery S/D ratios starting at 42 weeks. Abnormal outcomes were noted in 42%. No statistically significant difference was noted in the mean umbilical artery S/D ratios between the outcome groups [32].
- Stokes et al. followed 70 pregnancies with umbilical S/D ratios starting at 41 weeks. Abnormal clinical outcomes were seen in 31%. No significant difference in the mean

Table 23.1 Studies comparing the mean Doppler results between pregnancies with normal and adverse outcomes, where an adverse outcome was defined by a composite of outcome measures (unless stated, statistical). Comparisons were made between the mean Doppler values

First author	N GA % abn	Umbilical artery	Middle cerebral artery	CPR
Gupta [31]	31 40 16%	No association S/D	No association PI	No association CPR-PI
Guidetti [32]	46 42W 43%	No association S/D		
Olofsson [9]	44 43W 36%	+ Association PI *PI lower in abn group		
Stokes [33]	70 41W 31%	No association S/D		
Malcus [13]	101 42W 26%	No association PI		
Lebovitz [34]	120 40W 17.5%	No association RI, S/D or PI	No association RI or PI	No association PI
Forouzan [24]	30 41W 20%	No association S/D		
Farmakides [25]	149 41W	No association S/D		
Weiner	142 41W 8.5%	No association RI		
Kauppinen [14]	160 41W 16%	No association PI	No association PI	No association CPR
Rightmire [12]	32 42W 25%	+ Association RI		
Fischer [20]	75 41W 28%	+ Association SD and RI		
Devine [35]	49 41W 20%	No association S/D	Association S/D	+ Association S/D
Maged [36]	100 40W 44%	+ Association PI	Association PI	+ Association PI
Brar [22]	45/ 41W 42%	No association mean S/D and % abnormal S/D	Association S/D	+ Association both mean S/D and % S/D <1 (CPR = internal carotid S/D/ UmbA S/D)
D'Antonio [29]	328 41+W 18%	No association PI	No association PI	No association mean PI, % PI <0.98 or % PI <0.90

Column 2: *N*: number of patients, GA: gestational age at start of Doppler testing, Abn: % of patients with adverse clinical outcomes
Boxes in the table are blank if those Doppler parameters were not evaluated
RI Resistance index, *PI* pulsatility index, *CPR* Cerebroplacental ratio

S/D ratios was detected between the normal and adverse outcome groups [33].

- Malcus et al. followed 101 pregnancies beginning at 42 weeks. Serial umbilical artery waveforms were evaluated by PI ratios, with abnormal outcomes noted in 26%. No difference in the mean PI ratio was noted between the outcome groups [13].
- Lebovitz et al. followed120 pregnancies with an abnormal outcome rate of 17.5%. Both PI and RI ratios were obtained from the umbilical and middle cerebral arteries, with testing beginning at 40 weeks. There were no differences in any of the Doppler parameters studied between the normal and abnormal outcome groups [34].
- Weiner et al. followed 142 pregnancies with serial umbilical artery RI testing beginning at 41 weeks. In 8.5%, an abnormal outcome was obtained. In addition to calculating the mean RI ratios for the normal and abnormal outcome groups, the percentage of cases with an RI ratio above the 95th percentile was also calculated. No significant differences were noted between the groups for either method of Doppler evaluation [23].
- Kauppinen et al. followed 160 women with an abnormal outcome rate of 16%. Doppler testing was limited to a single measurement of umbilical and middle cerebral artery PI ratios that was obtained just prior to elective induction after 41 weeks. No differences were noted between the normal and abnormal groups for either mean PI values for umbilical or middle cerebral arteries or in the calculated CPR [14].
- -Farmakides et al. obtained umbilical S/D ratios in 149 pregnancies beginning at 41 weeks. Abnormal pregnancy outcomes were defined by a composite of morbidities, and abnormal statistical analysis was performed separately for testing conducted at 41, 42, and 43 weeks. The mean S/D ratios for the normal and abnormal outcome groups were evaluated separately for Doppler testing conducted at 41, 42, and 43 weeks, and none of the analyses showed a significant difference [25].

Although all the above studies failed to detect a significant difference in Doppler testing between the normal and abnormal pregnancy outcome groups, several studies utilizing the same format did find significant differences.

-Rightmire and Campbell followed 32 patients with serial umbilical artery Doppler testing beginning at 42 weeks. A "less-than-acceptable outcome" was noted in 25%. The mean umbilical artery RI was higher in the adverse outcome group when compared to that seen in the normal outcome group [12].

-Fischer et al. followed 75 pregnancies with twice-a-week umbilical artery Doppler testing. Both S/D and RI ratios were obtained beginning at 41 weeks. Abnormal outcomes were noted in 28. The differences in the mean Doppler indices between the two groups were small but statistically significant with higher indices in the abnormal group [20].

-Devine et al. followed 49 women with serial S/D ratios of the umbilical and middle cerebral arteries beginning at 41 weeks. An abnormal pregnancy outcome was noted in 20%. Although the umbilical artery S/D ratio was not different between the two groups, the MCA S/D ratio and the CPR were significantly lower in the adverse outcome group. It should be noted that this study was unusual, in that patients with underlying high risk factors were not excluded and made up one-third of the overall study group. A higher prevalence of chronic hypertension was present in the adverse outcome group [35].

-Maged et al. followed 100 pregnancies with serial umbilical and middle cerebral artery PI ratios beginning at 40 weeks. A total of 44% of the group had an abnormal outcome. Significant differences were noted in both umbilical and middle cerebral artery PI ratios and the calculated CPR between the normal and abnormal groups. Of the three parameters, the CPR was the best to discriminate between the normal and abnormal groups [36].

-Olofsson et al. began serial Doppler testing at 42 weeks with umbilical artery PI levels. Analyses

were conducted on 44 patients who delivered after 43 weeks. Adverse outcomes were noted in 16 of the patients. Although a significant difference in the Doppler testing was noted between patients with and without adverse outcomes, it was the adverse outcome group that had lower umbilical artery PIs. In separate analyses for individual adverse outcomes, significant differences were noted between patients delivering with and without the meconium and fetal distress but not oligohydramnios or asphyxia. Again, lower umbilical artery PIs were noted in association with adverse outcomes. The reason for the finding of lower umbilical artery PIs in association with adverse outcomes was unknown, and the authors hypothesized the possibility of placental vasodilation in response to fetal hypoxia [9].

A similar methodology of comparing the Doppler values between normal and abnormal pregnancy outcomes, but with a more limited list of abnormal outcomes, was utilized in the following studies:

-Brar et al. followed 45 patients beginning at 41 weeks, with the criteria for abnormal pregnancy outcomes limited to non-reassuring fetal heart rate testing and low amniotic fluid volume. These abnormalities were noted in 42% of the study population. Along with umbilical artery testing, the internal carotid artery was also evaluated as a measure of lowered intracranial resistance/brain-sparing effect. Both the mean and percentage abnormal Doppler values were evaluated, with abnormal S/D cut-offs being set at 3.0 for the umbilical artery and at 1.0 for the CPR calculated from the internal carotid artery–umbilical artery ratios. No differences in either the mean or percentage abnormal umbilical artery Doppler indices were noted between the normal and abnormal outcome groups. Distinct from the negative umbilical artery results, both internal carotid artery S/D ratios and the calculated CPR were significantly different, with mean values for both being significantly lower in the abnormal outcome group. In addition, using a CPR cut-off <1.0, the percentage of the abnormal CPR ratios was significantly higher in the adverse outcome group [22].

-D'Antonio et al. followed 320 women with serial testing beginning at 41 weeks. Adverse outcomes included only abnormal umbilical artery blood gas at delivery or operative intervention for non-reassuring ST segment analysis in labor. One or both abnormal outcomes were seen in 18% of the study population. Doppler calculations included umbilical and middle cerebral artery PI ratios and a calculated CPR. No significant difference between the outcome groups was noted. The percentage of abnormal CPR ratios was also calculated for each outcome group. Two different cut-off values were used for this calculation: 0.9, which was the 5th percentile from a published nomogram K, and 0.98, which was the 5th percentile for this study. The percentage of abnormal cases was not statistically significant between the two study groups. A power analysis showed that this study was significantly underpowered to determine whether the detected differences were significant [29].

-Forouzan and Cohen followed 30 patients with umbilical artery S/D ratios beginning at 41 weeks. Adverse outcomes were defined as abnormal intrapartum fetal heart rate patterns requiring cesarean delivery, umbilical artery acidosis, or neonatal diagnosis of intrapartum hypoxia requiring NICU care and were seen in 20% of the study group. The mean umbilical artery S/D ratios were not significantly different between the two groups [24].

The above studies compared Doppler testing between pregnancies classified as normal or abnormal based on a composite of clinical findings. Different approaches were used in other studies to evaluate the association between Doppler testing and adverse pregnancy outcomes in postdate pregnancies. These studies are summarized below and are listed in Table 23.2.

-Zimmerman et al. followed 153 pregnancies with serial middle cerebral and umbilical artery RI testing beginning at 41 weeks. Pregnancy outcomes were divided into asphyxial and non-asphyxial complications, which were noted in 25 and 20%, respectively. Statistical analysis involved comparing the range of RI ratios obtained from both abnormal groups with the range of values obtained from pregnancies with normal outcomes. Two normal outcome groups were used: the normal outcome group from this

Table 23.2 Studies evaluating Doppler velocimetry in postdate pregnancies by methods other than comparison of Doppler values within normal and adverse pregnancy outcome groups, where an adverse outcome was defined by a composite of morbidities

First author	N GA	Clinical outcomes (% adverse outcomes)	Umbilical artery	Middle cerebral artery	CPR
Lam [37]	118 40w	Evaluation of individual outcomes of a thick meconium (22%), SGA (8.3%) and AFI < 3 Doppler testing categorized as <10th, >10th–<90th and >90th	+ Association PI >0.97 (90%) – SGA No association PI >0.97 (90%) – Low AFI – Thick meconium	+ Association PI <0.84 (10%) – Thick meconium No association PI <0.84 (10%) – SGA – Low AFI	+ Association PI < 1.09 (10%) – SGA No association PI < 1.09 (10%) – Low AFI – Thick meconium
Selam [19]	38 41w	AFI < 5 cm (26%)	No association mean PI	+ Association mean PI	+ Association mean PI
Bar-Hava [16]	57 41w	AFI < 5 (26%)	No association mean RI	No association mean RI	No association mean RI
Veille [17]	50 40w	AFI < 5 (34%)	No association mean S/D		
Battaglia [7]	82 41w	Patients grouped by normal or decreased peak fetal thoracic aorta velocities (28%)	No association mean RI	No association mean RI	
Anteby [8]	78 41w	Evaluation of individual outcomes of moderate-to-thick meconium (21%), moderate/severe persistent intrapartum heart rate abnormalities (42%), and operative delivery for fetal heart rate abnormalities (19%)	+ Association S/D – Operative delivery No association PI – Operative delivery – Meconium – FHR abnormalities No association S/D – Meconium – FHR abnormalities	+ Association PI – FHR abnormalities No association S/D – FHR abnormalities – Meconium – Operative delivery No association PI – Meconium – Operative delivery	+ Association (not specified if S/D or PI) – Operative delivery No association (not specified if S/D or PI) – Meconium – FHR abnormalities
Pearce [38]	534 42w	Cohen kappa statistic for absent/reverse end-diastolic flow in the umbilical artery and fetal distress in the first stage of labor (2.1%)	+ Association		

Zimmerman [21]	153 41w	Asphyxial (25%) and non-asphyxial (20%) complications	No association RI All Doppler ratios from both abnormal outcome groups within the 5th–95th percentiles from the normal group	No association RI All Doppler ratios from both abnormal outcome groups within the 5th–95th percentiles from the normal group	
Olofsson [9]	34 42w	Evaluation of individual outcomes of oligohydramnios, fetal distress, asphyxia, and meconium (overall 36% with adverse clinical outcomes)	No association PI – Oligohydramnios – Asphyxia + Association PI – Meconium – Fetal distress (PI lower with these abnormal outcomes)		
Figueras [39]	56 41w	Stepwise linear regression with Doppler indices and umbilical artery blood gas values at birth	No association PI – Umbilical artery blood gas results	+ Association PI – Proximal MCA with umbilical artery pO_2 – Distal umbilical artery PI with umbilical artery pH	No association PI – Umbilical artery blood gas results
Ropacka-Lesiak [40]	148/ 40w	Patients grouped by normal/abnormal Doppler results evaluated for clinical outcomes of emergency cesarean section (15.5%), abnormal fetal heart rate patterns (39%), and adverse neonatal outcomes (27%)	Abnormal cut-off values and statistical significance for RI and PI not specified Likelihood ratios for adverse neonatal outcomes and abnormal fetal heart rate patterns, 2.3–3.1	Abnormal cut-off values and statistical significance for RI and PI not specified Likelihood ratios for abnormal fetal heart rate patterns and adverse neonatal outcomes, 1.3–2.6	+ Association – CPR-RI < 1.1 associated with a variety wide variety of adverse outcomes, emergency cesarean section, abnormal fetal heart rate pattern, IUGR, umbilical cord blood gas analysis, and adverse neonatal outcomes

Column 2: *N*: study size, GA: gestational age at start of Doppler testing. Blank spaces indicate that the Doppler parameters were not evaluated
PI pulsatility index, *RI* resistance index, *CPR* cerebroplacental ratio

study and a separate term reference group. All of the Doppler RI values from both the asphyxial and non-asphyxial complications fell within the 5th–95th percentiles for both normal outcome groups [21].

-Battaglia et al. chose fetal thoracic aortic velocities for their outcome measure instead of specific clinical morbidities. This parameter was chosen as it was the only ultrasound parameter that was associated with clinical outcome, with abnormal velocities being seen in 29% of the study group. Serial Doppler testing was conducted in 82 patients with umbilical artery RI and middle cerebral artery PI values beginning at 41 weeks. No significant difference was noted for either umbilical or middle cerebral artery Doppler indices between the normal and abnormal thoracic aortic velocity groups [7].

-Anteby et al. analyzed Doppler results for individual outcome parameters rather than a composite abnormal outcome group. Serial umbilical and middle cerebral artery Doppler testing was conducted on 78 pregnancies starting at 41 weeks, with statistical evaluation performed on 3 outcome measures: moderate-to-thick meconium (21%), moderate-to-severe persistent intrapartum heart rate abnormalities (42%) and heart rate abnormalities requiring operative delivery (9%). The mean Doppler indices (umbilical artery S/D and PI, middle cerebral artery S/D and PI, CPR S/D and PI) and the mean S/D and PI ratios for both the umbilical and middle cerebral arteries were compared with the presence or absence of each of the three outcome measures individually. Of these 12 analyses, the only statistically significant differences found were for the mean umbilical artery S/D ratios for the presence or absence of intervention for abnormal fetal heart rates and for the mean MCA-PI for the presence or absence of abnormal fetal heart rate patterns. Separate from the statistical analysis involving the individual fetal heart rate, the mean CPR was associated with the intervention for fetal heart rate abnormalities. Not stated in the study, but presumed by its absence, is that the CPR was not associated with the other two outcome measures. It was also not stated whether this significant association was for the CPR-S/D, CPR-PI, or both [8].

-Lam et al. analyzed individual outcome measures with umbilical and middle cerebral artery Doppler testing that were classified as ≤10th, 10th–90th, and > 90th. The pregnancy outcomes evaluated included the presence or absence of a thick meconium (22%), AFI ≤ 3 cm and small for gestational age (SGA) (8.3%). Pregnancies with an umbilical artery PI above the 90th percentile were associated with the presence of a thick meconium and SGA fetus. Pregnancies with the middle cerebral artery PI below the 10th percentile were associated only with a thick meconium, whereas the CPR ratio below the 10th percentile was associated only with SGA [37].

-In a large study, Pearce and McParland evaluated umbilical artery Doppler testing with fetal distress in labor. Serial testing was conducted in 534 pregnancies beginning at 42 weeks. A Cohen kappa statistic was calculated from sensitivity and predictive values. Absent end-diastolic umbilical artery flow was associated with fetal distress in the first stage of labor, with a value of 0.91 (values above 0.8 are consistent with a strong correlation). Although specific data were not provided, the addition of umbilical artery Doppler results where end-diastolic flow was present did not improve the evaluation. It should be noted that both absent end-diastolic flow and fetal distress in the first stage of labor were infrequent at 2.1% each [38].

- Figueras et al. performed stepwise linear regression for Doppler indices with umbilical artery blood gas testing at birth. The Doppler indices evaluated included separate PI ratios for the proximal and distal segments of the middle cerebral artery, the umbilical artery PI, and a calculated CPR. Doppler testing began at 41 weeks, and 56 patients that were delivered within 48 hours of their final Doppler evaluation were analyzed. Significant correlations were only noted for the proximal MCA and umbilical artery pO_2 and a weak correlation for the distal MCA and umbilical artery pH [39].

-Ropacka-Lesiak et al. analyzed pregnancy outcomes in patients grouped by Doppler results

rather than by pregnancy outcomes. A total of 144 women had umbilical and middle cerebral artery Doppler PI and RI testing conducted between 40 and 42 weeks. Although listed as a low-risk group, 47% of the pregnancy showed a brain-sparing effect, defined as a CPR-RI <1.1. The brain-sparing group showed a significantly worse outcome in a wide variety of clinical parameters including abnormal fetal heart rate patterns (62.3% versus 19.0%), emergency cesarean sections (24.6% versus 7.6%), lower birth weight and Apgar scores and worse umbilical artery blood gas testing. The clinical outcome for pregnancies grouped by the individual umbilical and middle cerebral artery values rather than the CPR was not provided [40].

-Studies by Selam, Veille et al., and Bar-Hava et al. limited their statistical evaluation to a single outcome: amniotic fluid volume [16, 17, 19]. Oligohydramnios (AFI < 5) was found in 26%, 34%, and 26% of the pregnancies studied, respectively. In each study, the frequency of low fluid volume was 26%. The mean umbilical artery indices between normal and oligohydramnios pregnancies were not significantly different in any of the three studies. In the study by Selam, the MCA Doppler indices and calculated CPR were significantly lower in the oligohydramnios group, a finding that was not found by Bar-Hava et al. and not studied by Veille et al.

3. Is Doppler testing a good discriminator between normal and abnormal pregnancy outcomes (sensitivity/specificity), and how does it compare to the antenatal tests currently in use? Most of the studies reviewed above compare the results of Doppler testing between pregnancies with normal and abnormal outcomes. Although useful in evaluating the association between Doppler testing and clinical outcome, this type of analysis does not provide information on the ability of Doppler testing to discriminate between normal and abnormal outcomes. Sensitivity and specificity calculations are provided in some of the studies and, when available, are summarized in Table 23.3. Included in this table is information from the study by El-Sokkary et al. [41] Umbilical and middle cerebral artery Doppler testing was conducted in 100 hospitalized patients, finding a significant difference between all Doppler indices that did and did not need NICU admission. This study was not reviewed in the above sections as half of the pregnancies were evaluated prior to 40 weeks and a separate analysis was not provided for the 50 patients tested at 41 weeks. Sensitivity and specificity calculations were provided for the patients tested at 41 weeks and are included in Table 23.3.

The studies summarized in Table 23.3 show significant variability in their sensitivities and specificities for adverse outcomes. Combining the studies, Doppler evaluations for the umbilical and middle cerebral arteries and the calculated CPR all have similar averaged specificities of approximately 75%. Averaged sensitivities for the umbilical and middle cerebral arteries are just under 50%, whereas the sensitivity for the CPR is higher at approximately 75%. Although it has been suggested that the calculated CPR may be the best Doppler index for risk assessment, comparative evaluations should be made cautiously. These studies utilize varying methodologies in terms of the various aspects of Doppler testing and evaluation and differ in terms of which pregnancy outcomes were evaluated. Most of the studies in this table found a positive association between Doppler testing and adverse pregnancy outcomes. Studies in which no such association was found are less likely to provide sensitivity and specificity information, and thus they are underrepresented in this table. The low likelihood ratios in most of the studies suggest that the predicted increase in abnormal outcomes with abnormal Doppler testing is at best a modest one.

In six of the studies, listed in bold type at the bottom of Table 23.3, sensitivity and specificity calculations were also provided for currently used clinical antenatal tests (BPP, NST, fluid volume). In two of these studies, information for CPR is provided, showing a higher likelihood ratio than both other Doppler indi-

Table 23.3 Predictive ability of Doppler and standard antenatal testing (BPP, fluid volume, and NST in bold) for evaluating adverse pregnancy outcomes

Study	Test	Cut-off	Outcome measure	Sensitivity (%)	Specificity (%)	Likelihood ratio
Anteby [8]	UA-S/D 	2.5 2.4 2.3	Intervention for fetal distress	60 80 93	71 55 48	2.1 1.8 1.8
Lam [37]	MCA	10th percentile	Thick meconium	34	94	5.7
Ropaka-Lesiak [40]	CPR-RI MCA-RI MCA-PI UA-RI UA-PI	1.1 Not stated Not stated Not stated Not stated	Abnormal FHR in labor	74.1 12.0 56.9 32.8 27.6	71.1 91.1 77.8 87.8 91.1	2.6 1.3 2.6 2.7 3.1
Ropaka-Lesiak [40]	CPR-(RI) MCA-RI MCA-PI UA-RI UA-PI	1.1 Not stated Not stated Not stated Not stated	Adverse neonatal outcome	87.8 17.5 65.0 40.0 27.5	68.5 92.6 75.0 87.0 88.0	2.8 2.3 2.6 3.1 2.3
El-Sokkary [41]	UA-S/D UA-RI UA-PI MCA-S/D MCA-RI MCA-PI CPR-RI	2.57 0.62 0.93 2.45 0.67 0.94 0.85	NICU admission	56 50 40 48 40 50 80	45 92 16 60 39 40 72	1.0 6.3 0.5 1.2 0.7 0.8 2.9
Gupta [31]	CPR	1.1 1.3	Multiple clinical parameters	40 80	77 54	1.7 1.7
Forouzan [24]	UA-S/D	3.12	Multiple clinical parameters	83.3	87.5	6.7
Fischer [20]	UA-S/D **NST/AFV**	2.4 **MVP <2 cm**	Multiple clinical parameters	57 **19**	78 **85**	2.6 **1.3**
Pearce [38]	UA **NST** **AFV**	AEDF **MVP<3 cm**	Fetal distress in the first stage of labor	91 **55** **82**	100 **98** **99**	– **27.5** **82.0**

Weiner [23]	UA-RI **AFV** **NST**	0.68 **Not stated non-reactive, recurrent FHR decelerations**	Multiple clinical parameters	17 **25** **8**	96 **94** **95**	4.3 **6.3** **1.6**
Zimmerman [21]	UA-RI UA-RI **AFV** **NST/CST**	0.62 0.58 **MVP < 2**	Asphyxial complications	37 53 **16** **8**	75 55 **95** **96**	1.5 1.2 **3.2** **2.0**
Devine [35]	CPR-S/D **AFV** **BPP** **NST**	1.059**AFI < 5 cm** **<6** **Non-reactive**	Multiple clinical parameters	80 **20** **30** **40**	95 **97** **92** **90**	16.0 **6.7** **3.0** **4.0**
Maged [36]	UA-PI MCA-PI CPR-PI **AFV** **BPP**	0.82 1 1.05 **MVP < 2 cm** **≤4**	Multiple clinical parameters	68.2 77.3 75.0 **77.7** **63.6**	76.8 87.5 98.2 **91.1** **89.3**	2.9 6.2 41.7 **8.7** **5.9**

ces and standard antenatal tests [35, 36]. It should be noted that the CPR likelihood ratios in these two studies are higher than those obtained by other studies listed in this table, and, given the limited number of studies evaluated, caution is advised when making comparative evaluations.

4. Does the use of Doppler testing improve outcomes in postdate pregnancies?
   No studies were identified that directly evaluate whether Doppler testing when used clinically in postdate pregnancies improves the clinical outcomes.

23.4 Conclusions

In this chapter, we have reviewed the data on Doppler testing in postdate pregnancies. The one remaining issue to be discussed is should Doppler testing be recommended for clinical evaluation of these pregnancies? Doppler testing is an attractive option for a variety of reasons. In postdate pregnancies, the risk of fetal and neonatal morbidity and mortality is increased. Doppler velocimetry can evaluate two separate aspects of pregnancy health: hemodynamic changes within the placenta as a measure of placental function and fetal hemodynamic alterations as a measure of fetal response to its environment and possible compromised health. The negative consequences of a false-positive test, likely the induction of labor, are limited. Neonatal sequelae of prematurity are obviously not an issue at this gestational age. A 2018 Cochrane Database Review analyzed 30 randomized trials (12,479 pregnancies) that compared routine induction of labor with expectant management for pregnancies at or beyond term. Induction of labor was associated with a decrease in perinatal deaths (relative risk (RR) 0.33), stillbirths (RR 0.33), cesarean section rate (RR 0.92), NICU admission (RR 0.88), and 5-min Apgar less than 7 (RR 0.7). Operative vaginal delivery was increased (RR 1.07) with elective induction [42].

Concerns with the use of Doppler for evaluating postdate pregnancies span a wide range of issues involved with this testing. Starting with the normative Doppler data, prior studies have not provided consistent results, with significant differences noted between studies on normal values. Uniformly accepted cut-off levels are not available. Using the different cut-off levels that are currently available results in a wide range of the percentage of pregnancies that are classified as abnormal. It is also not clear whether there is an association between Doppler testing and adverse pregnancy outcomes. The studies available and the literature utilize a wide range of methodologies, with differences in the initiation and frequency of Doppler testing, which Doppler indices are evaluated, what cut-off values were used for identifying abnormal results, and which pregnancy morbidities were evaluated. As noted in Tables 23.1 and 23.2, an association between Doppler testing and adverse pregnancy outcomes has not been consistently shown; most of the studies did not find a positive association. Finally, studies showing that the use of Doppler on a clinical basis in postdate pregnancies improves outcomes have not been conducted. For these reasons, we cannot recommend the use of Doppler testing in the evaluation of postdate pregnancies. Although there certainly is room for an adequately powered well-designed randomized study to evaluate this issue directly, the prospects of successfully completing such a study is uncertain given evidence suggesting consideration for induction instead of expectant management [42, 43].

References

1. Clausson B, Cnattingius S, Axelsson. Outcomes of post-term births: the role of fetal growth restriction. Obstet Gynecol. 1999;94:758–62.
2. Linder N, Hiersch L, Fridman E, Klinger G, Lubin D, Kouadio F, Melamed N. Post–term pregnancy is an independent risk factor for neonatal morbidity even in low risk singleton pregnancies. Arch Dis Child Fetal Neonatal Ed. 2017;102:F286–90.
3. Zeitlin J, Blondel B, Alexander S, Breart G, the PERISTAT. Group variation in rates of post-term births in Europe: reality our artefact? BJOG. 2007;114:1097–103.
4. Martin JA, Hamilton BE, Osterman MJK, Driscoll AK, Drake P. Births: final data for 2017. Natl Vital Stat Rep. 2017;67(8):1–50.

5. Martin JA, Hamilton BE, Osterman MJK, Curtin SC, Mathews TJ. Births: final data for 2013. Natl Vital Stat Rep. 2015;64(1):1–68.
6. Hamilton BE, Martin JA, Osterman MJK, Curtin SC, Mathews TJ. Births: final data for 2014. Natl Vital Stat Rep. 2015;64(12):1–64.
7. Battaglia C, Larocca E, Lanzani A, Coukos G, Genazzani AR. Doppler velocimetry in prolonged pregnancy. Obstet Gynecol. 1991;77:213–6.
8. Anteby EY, Tadmor O, Revel A, Yagel S. Post-term pregnancies with normal cardiotocographs and amniotic fluid columns: the role of Doppler evaluation in predicting perinatal outcome. Eur J Obstet Gynecol Reprod Biol. 1994;54:93–8.
9. Olofsson P, Saldeen P, Maršál K. Association between a low umbilical artery pulsatility index and fetal distress in very prolonged pregnancies. Eur J Obstet Gynecol Reprod Biol. 1997;73:23–9.
10. Weiner Z, Farmakides G, Barnhard Y, Bar-Hava I, Divon MY. Doppler study of fetal cardiac function in prolonged pregnancies. Obstet Gynecol. 1996;88:200–2.
11. Weiner Z, Farmakides G, Schulman H, Casale A, Itsko-vitz-Eldor J. Central and peripheral haemodynamic changes in post-term fetuses: correlation with oligohydramnios and abnormal fetal heart rate pattern. Br J Obstet Gynecol. 1996;103:541–6.
12. Rightmire DA, Campbell S. Fetal and maternal Doppler blood flow parameters in post-term pregnancies. Obstet Gynecol. 1987;69:891–4.
13. Malcus P, Maršál K, Persson PH. Fetal and uteroplacental blood flow in prolonged pregnancies. A clinical study. Ultrasound Obstet Gynecol. 1991;1:40–5.
14. Kauppinen T, Kantomaa T, Tekay A, Makikallio K. Placental and fetal hemodynamics in prolonged pregnancies. Prenat Diagn. 2016;36:622–7.
15. Arduini D, Rizzo G. Fetal renal artery velocity wavelength and amniotic fluid volume in growth-retarded and post-term fetuses. Obstet Gynecol. 1991;77:370–3.
16. Bar-Hava I, Divon MY, Sardo M, Barnhard Y. Is oligohydramnios in postterm pregnancy associated with redistribution of fetal blood flow? Am J Obstet Gynecol. 1995;173:519–22.
17. Veille JC, Penry M, Mueller-Heubach E. Fetal renal pulsed Doppler waveform in prolonged pregnancies. Am J Obstet Gynecol. 1993;169:882–4.
18. Oz AV, Holub B, Mendilcioglu I, Mari G, Bahado-Singh RO. Renal artery Doppler investigation of the etiology of oligohydramnios in post-term pregnancy. Obstet Gynecol. 2002;100:715–8.
19. Selam B, Koksal R, Ozcan T. Fetal arterial and venous Doppler parameters in the interpretation of oligohydramnios in postterm pregnancies. Ultrasound Obstet Gynecol. 2000;15:403–6.
20. Fischer RL, Kuhlman KA, Depp R, Wapner RJ. Doppler evaluation of umbilical and uterine–arcuate arteries in the postdates pregnancy. Obstet Gynecol. 1991;78:363–8.
21. Zimmerman P, Alback T, Kiskinen J, Vaalamo R, Tuimala R, Ranta T. Doppler flow velocimetry of the umbilical artery, uteroplacental arteries and fetal middle cerebral artery in prolonged pregnancy. Ultrasound Obstet Gynecol. 1995;5:189–97.
22. Brar HS, Horenstein J, Medearis AL, Platt LD, Phelan JP, Paul RH. Cerebral, umbilical, and uterine resistance using Doppler velocimetry in post-term pregnancy. J Ultrasound Med. 1989;8:187–91.
23. Weiner Z, Reichler A, Zlozover M, Mendelson A, Thaler I. The value of Doppler ultrasonography in prolonged pregnancies. Eur J Obstet Gynecol. 1993;48:93–7.
24. Forouzan I, Cohen AW. Can umbilical and arcuate artery Doppler velocimetry predict fetal distress among prolonged pregnancies? J Ultrasound Med. 1991;10:15–7.
25. Farmakides G, Schulman H, Ducey J, Guzman E, Saladana L, Penny B, Winter D. Uterine and umbilical artery Doppler velocometry in postterm pregnancy. J Reprod Med. 1988;33:259–61.
26. Ciobanu A, Wright A, Syngelaki A, Wright D, Akolekar R, Nicolaides KH. Fetal Medicine Foundation reference ranges for umbilical artery and middle cerebral artery pulsatility index and cerebroplacental ratio. Ultrasound Obstet Gynecol. 2019;53:465–72.
27. Ruiz-Martinez S, Papageorghiou AT, Staines-Urias E, Villar J, de Aguero RG, Oros D. Clinical impact of Doppler referenced charts to manage fetal growth restriction: need for standardization. Ultrasound Obstet Gynecol. 2020;56(2):166–72.
28. Oros D, Ruiz-Martinez S, Staines-Urias E, Conde-Agudelo A, Villar J, Fabre E, Papageorghiou AT. Reference ranges for Doppler indices of umbilical and fetal middle cerebral arteries and cerebroplacental ratio: systematic review. Ultrasound Obstet Gynecol. 2019;53:454–64.
29. D'Antonio F, Patel D, Chandrasekharan N, Thilaganathan B, Bhide A. Role of cerebroplacental ratio for fetal assessment in prolonged pregnancy. Ultrasound Obstet Gynecol. 2013;42:196–200.
30. Palacio M, Figueras F, Zamora L, Jimenez JM, Puerto B, Coll O, Cararach V, Vanrell JA. Reference ranges for umbilical and middle cerebral artery pulsatility index and cerebroplacental ratio in prolonged pregnancies. Ultrasound Obstet Gynecol. 2004;24:647–53.
31. Gupta U, Chandra S, Narula MK. Value of middle cerebral artery to umbilical artery ratio by Doppler velocimetry in pregnancies beyond term. J Obstet Gynecol India. 2006;56:37–40.
32. Guidetti DA, Divon MY, Cavalieri RL, Langer O, Merkatz IR. Fetal umbilical artery flow velocimetry in postdate pregnancies. Am J Obstet Gynecol. 1987;57:1521–3.
33. Stokes HJ, Roberts RV, Newnham JP. Doppler flow velocity waveform analysis in postdate pregnancies. Aust N Z J Obstet Gynecol. 1991;31:27–30.
34. Lebovitz O, Barzilay E, Mazaki-Tovi S, Gat I, Achiron R, Gilboa Y. The clinical value of maternal

and fetal Doppler parameters in low risk postdates pregnancies—a prospective study. J Matern Fetal Neonatal Med. 2018;31:2893–7.
35. Devine PA, Bracero LA, Lysikiewicz A, Evans R, Womack S, Byrne DW. Middle cerebral to umbilical artery Doppler ratio in postdate pregnancies. Obstet Gynecol. 1994;84:856–60.
36. Maged AM, Abdelhafez A, Al Mostafa W, Elsherbiny W. Fetal middle cerebral and umbilical artery Doppler after 40 weeks gestational age. J Matern Fetal Neonatal Med. 2014;27:1880–5.
37. Lam H, Leung C, Lee CP, Lao TT. The use of fetal Doppler cerebroplacental blood flow and amniotic fluid volume measurement in the surveillance of postdated pregnancies. Acta Obstet Gynecol Scand. 2005;84:844–8.
38. Pearce JM, McParland PI. A comparison of Doppler flow velocity waveforms, amniotic fluid columns, and non-stress test as a means of monitoring postdates pregnancies. Obstet Gynecol. 1991;77:204–8.
39. Figueras F, Lanna M, Palacio M, Zamora L, Puerto B, Coll O, Cararach V, Vanrell JA. Middle cerebral artery Doppler indices at different sites: prediction of umbilical cord gases in prolonged pregnancies. Ultrasound Obstet Gynecol. 2004;24:529–33.
40. Ropacka-Lesiak M, Korbelak T, Swider-Musielak J, Breborowicz G. Cerebroplacental ratio in prediction of adverse perinatal outcome and fetal heart rate disturbances in uncomplicated pregnancy at 40 weeks and beyond. Arch Med Sci. 2015;11:142–8.
41. El-Sokkary M, Omran M, Ahmed H. Ratio of middle cerebral artery/umbilical artery velocimetry and status of newborn in postterm pregnancy. J Am Sci. 2011;7:542–9.
42. Middleton P, Shepherd E, Crowther CA. Induction of labor for improving birth outcomes for women at or beyond term (review). Cochrane Database Syst Rev. 2018;5(5):CD004945.
43. ACOG Practice Bulletin No. 146. Management of late–term and postterm pregnancies. Obstet Gynecol 2014;124:390–396.

Umbilical Artery Doppler for Fetal Surveillance: Diagnostic Efficacy

24

Dev Maulik and Tara Daming

24.1 Introduction

The primary objective of fetal surveillance is to detect and manage fetal compromise arising from defective placentation. A variety of obstetric complications, especially fetal growth restriction (FGR), may expose the fetus to such risks. Although the precise mechanisms of chronic nutritional and respiratory deficiencies in the fetus are not fully known, there is evidence that a growth-restricted fetus, suffering from chronic hypoxia and acidosis, mobilizes a spectrum of compensatory responses, including preferential preservation of fetal growth over placental growth, changes in the fetal movement pattern and eventual deceleration of the fetal growth rate. In the face of deepening deprivation, compensation gives way to decompensation. A central component of the fetal homeostatic response involves flow redistribution, which favors the vital organs (i.e., the brain, heart, adrenals), whereas flow to the muscles, viscera, skin, and other less-critical tissues and organs declines [1]. Underlying this phenomenon are the diverse changes in impedance in these vascular systems. The increased impedance in the feto-placental circulation is evident in the decreasing end-diastolic flow in the umbilical artery (UA) and rising Doppler indices, especially noticeable in early-onset fetal growth restriction. With progressive fetal decompensation, the end-diastolic flow becomes absent or even reversed.

The introduction of Doppler velocimetry has enabled us to investigate this phenomenon in the human fetus for detecting fetal compromise. Extensive information exists on the diagnostic efficacy of UA Doppler for identifying the fetus with adverse outcomes. This chapter provides an updated review of the efficacy of elevated UA Doppler indices for predicting adverse perinatal outcomes in high- and low-risk pregnancies. The sequence of changes in antepartum tests with progressive fetal compromise is discussed in Chap. 25, which focuses on the absent or reversed end-diastolic velocity (AREDV) because of its severe clinical and prognostic significance. The efficacy of the method in relation to specific pregnancy disorders is considered in other dedicated chapters in this book.

24.2 Diagnostic Efficacy in High-Risk Pregnancies

The efficacy of UA Doppler sonography for predicting adverse perinatal outcomes in complicated pregnancies has been widely investigated. A selection of these studies is summarized in

D. Maulik (✉) · T. Daming
Department of Obstetrics and Gynecology, UMKC School of Medicine/Truman Medical Center, UMKC School of Medicine, Kansas City, MO, USA
e-mail: dmaulik2014@gmail.com

D. Maulik, C. C. Lees (eds.), *Doppler Ultrasound in Obstetrics and Gynecology*,
https://doi.org/10.1007/978-3-031-06189-9_24

Table 24.1, some of which are also discussed later.

Most studies indicated that UA Doppler was efficacious for identifying the fetus at risk in complicated pregnancies. There are, however, wide variations in the performance of the technique, with the sensitivity ranging from 21% to more than 90% and the specificity from 63 to 97%. This range may not be surprising, as the studies were heterogeneous in several aspects, including the population selection criteria, the method of using Doppler surveillance (e.g., the frequency of examination), and the diagnostic threshold value of the test result. The studies were not uniform in their selection criteria of an adverse perinatal outcome, which included fetal smallness for gestational age (SGA), operative delivery for fetal distress, Apgar score, the need for admission to the neonatal intensive care unit (NICU), and various other conditions.

In addition, many investigations were deficient in their experimental approach. For example, many studies were not blinded, which might have compromised their validity because of bias [2, 4]. In one of the first studies reported on the diagnostic efficacy of Doppler velocimetry, the investigators did not state whether the clinicians were blind to the Doppler results. Moreover, in one of the largest studies on Doppler efficacy, which also included a nonstress test (NST) and biophysical profile (BPP), the clinicians had ready access to the Doppler and other fetal monitoring results, which obviously compromised the reliability of the conclusions drawn from this investigation.

There was also heterogeneity in the selection of the Doppler indices and in their diagnostic thresholds. While some studies used a specific cut-off value derived from receiver operating characteristic (ROC) analysis, others employed statistical variability thresholds such as the standard deviation or percentile values.

Despite such limitations, most investigators have confirmed that fetal Doppler velocimetry is an effective method for identifying fetal jeopardy in high-risk pregnancies, especially those complicated by FGR.

This affirmative conclusion remains valid irrespective of whether the study utilized the Bayesian or signal analytical approach or both. The Bayesian approach determines the probabilistic measures of efficacy, such as sensitivity, specificity or predictive values, at a given test value. The signal analysis method, the receiver operating characteristic (ROC) method [5], measures the overall discriminatory performance of a test from its true- and false-positive rates for all available values and assists in determining its optimal threshold for a particular application. In addition to these two techniques, the kappa index has been used, which measures the degree of concordance between the test result and the diagnosis beyond chance; the value of this index has been utilized to assess the magnitude of the test's efficacy [6, 7].

These analytical techniques were utilized by Maulik et al. [3] to evaluate the diagnostic efficacy of the UA-systolic/diastolic (S/D) ratio for predicting adverse perinatal outcomes. As indicated, the study was blinded so that those responsible for clinical management of the patient did not have access to the Doppler results. A free-standing continuous wave Doppler device with a 4-MHz transducer was used. The criteria for an abnormal perinatal outcome included (1) an SGA at birth (<10th percentile); (2) a 5-min Apgar score <7; (3) an umbilical cord arterial pH below 7.2; (4) fetal distress during labor (late and severe variable deceleration, subnormal short-term variability, and fetal scalp pH <7.20); (5) the presence of a thick meconium; and (6) NICU admission. The ROC curve assisted in determining the optimal cut-off value of the S/D ratio (demonstrated in Fig. 24.1). The ROC analysis indicated that this test had an impressive but less-than-perfect capability of discriminating between an adverse and a normal outcome. Ratios of 2.9 and 3.0 exhibited the maximum inherent discriminatory

Table 24.1 Diagnostic efficacy of umbilical Doppler velocimetry for high-risk pregnancies

Study, first author	No. of patients	Risk	Outcome	Prev (%)	Design	DI	Sens (%)	Spec (%)	PPV (%)	NPV (%)	KI
Trudinger [2]	170	GHR	SGA <10th C, $AS_5 < 7$	31	?	S/D ≥ 3	60	85	64	83	
Laurin[a]	159	SGA	IUGR <2SD ODFD	47 19	Blind	BFC II–III	50 83	97 90	93 66	69 96	0.48 0.66
Dempster[b]	205	GHR	Late deceleration	16	Blind	S/D ≥ 97th C	70	89	54	94	
Berkowitz[c]	172	Risk of IUGR	ODFD, AF, Mec, AS, PND, RDS, SGA	21	Blind	S/D ≥ 3	47	84	57	86	
	43	SGA	Complications	43			67	63	57	71	
Chambers[d]	145	SGA, HTN	CSFD	17	Blind	RI ≥ 2SD	100[e]	77	46	100	
Maulik [3]	350	GHR	SGA <10th C, IPFD, AS_5 <7, UApH <7.2, NICU admission	28	Blind	S/D ≥ 3	79	93	83	91	0.73
Devoe [4]	1000	GHR	PND, IPFD, AS_5 <7, UApH <7.2	19	Not blind	S/D ≥ 90th C, AEDV	21	95	49	85	
Pattinson[f]	369	GHR	Abnormal NST CSFD	8 3	Blind	RI ≥95th C	93 92	78 89	8 22	100 100	

Risk risk characteristics of the study population, *GHR* general high risk, *SGA* small for gestational age, *HTN* hypertension, *IUGR* intrauterine growth restriction, *C* percentile, AS_5 Apgar score at 5 min, *SD* standard deviation, *ODFD* operative delivery for fetal distress, *AF* amniotic fluid, *Mec* meconium, *PND* perinatal death, *RDS* respiratory distress syndrome, *CSFD* cesarean section for fetal distress, *IPFD* intrapartum fetal distress, *UApH* umbilical arterial pH, *NICU* neonatal intensive care unit, *NST* non-stress test, *Prev* prevalence, *DI* Doppler index, *Sens* sensitivity, *Spec* specificity, *PPV* positive predictive value, *NPV* negative predictive value, *KI* kappa index

[a] *Br J Obstet Gynecol* 69:895, 1987

[b] *Eur J Obstet Gynecol Reprod Biol* 29:21, 1988

[c] *Obstet Gynecol* 71:742, 1988

[d] *Br J Obstet Gynaecol* 96:803, 1989

[e] Analysis was performed with the sensitivity kept fixed at 100% (i.e., no cases of adverse outcome would be missed)

[f] *Obstet Gynecol* 78:353, 1991

power: the former of the two values exhibited greater sensitivity, and, the latter, which is the more prevalent standard, showed greater specificity and a higher kappa index (Table 24.2). Furthermore, when the fetal SGA status was excluded from the outcome, the S/D ratio had the best diagnostic efficacy; in contrast, when small fetal size was the only outcome criterion, the test demonstrated the worst efficacy. These results further confirmed that the UA arterial Doppler indices are more capable of identifying fetal compromise than small fetal size.

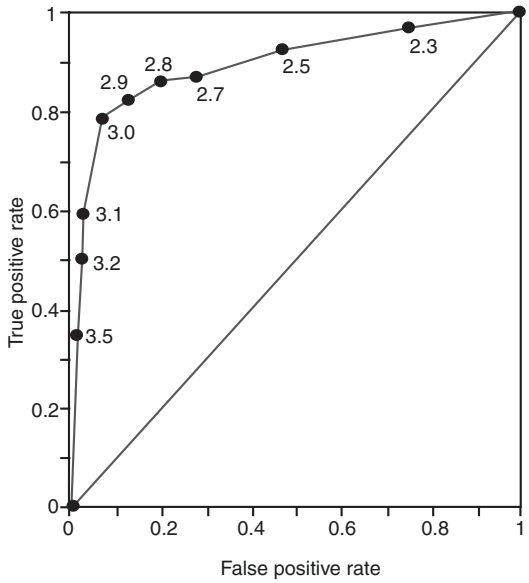

Fig. 24.1 Receiver operating characteristic curve of the umbilical arterial systolic/diastolic (S/D) ratio. Note that the S/D ratio cut-off point (2.9) closest to the upper left corner of the graph has the best ability to discriminate between the normal and abnormal outcome groups (reprinted from Maulik et al. [3] with permission)

24.3 Umbilical Artery Doppler, Non-Stress Test, and Biophysical Profile: Comparative Efficacy

When appraising the diagnostic efficacy of fetal Doppler, an important consideration is to compare it with that of the currently utilized fetal surveillance procedures. This section presents the comparative effectiveness of these modalities in relation to the prediction of adverse perinatal outcomes.

The effectiveness of the UA-A/B (systolic/diastolic) ratio for predicting adverse outcomes was investigated by Trudinger et al. [2] in 170 high-risk patients. The parameters of fetal compromise included birth weight below the 10th percentile or an Apgar score of less than 7 at 5 min. The fetal heart rate was assessed in terms of reactivity and a modified Fischer score. In this study, the UA-S/D ratio appeared to be more sensitive but less specific than electronic fetal heart rate monitoring. Farmakides et al. [8] investigated the diagnostic efficacy of the NST and the UA-S/D ratio in 140 pregnancies. The measures of outcome included FGR, fetal distress, cesarean section for fetal distress, and admission to the NICU. Fetuses with a normal NST but abnormal S/D ratio had an outcome worse than those with an abnormal NST and a normal S/D ratio; those for whom both tests were abnormal experienced the worst outcome.

Further corroboration came from Arduini et al. [9], who noted in a cross-sectional study involving 1000 unselected pregnancies at 36–40 weeks' gestation that UA Doppler was more effective than the NST for identifying fetuses at risk of adverse outcomes (cesarean section for fetal distress, lower birth weight, 5-min

Table 24.2 Test performance values for various systolic/diastolic ratio cut-off points (from Maulik et al. [3] with permission)

Cut-off point	Sensitivity	Specificity	PPV	NPV	KI
2.5	0.93	0.53	0.47	0.94	0.36
2.9	0.83	0.87	0.74	0.92	0.68
3.0	0.79	0.93	0.83	0.91	0.73
3.5	0.35	0.99	0.93	0.77	0.41

PPV positive predictive value, *NPV* negative predictive value, *KI* kappa index

Apgar score <7, admission to the NICU). The relative strengths of the individual and the combined use of the various tests were investigated by Hastie et al. [10] in 50 pregnant patients. These investigators observed that the repeat nonreactive NST was highly sensitive (92%) and the S/D ratio was highly specific (83%); they therefore suggested the effectiveness of combining the two tests for predicting adverse perinatal outcomes. The suggestion of a combined approach also came from Nordstrom et al. [11], who determined the UA-S/D ratio and BPP in 69 high-risk pregnancies within 10 days preceding the delivery. Intrapartum fetal distress and SGA occurred in 43% of the infants. The S/D ratio demonstrated a higher sensitivity (37%), specificity (92%), a positive predictive value (PPV) (79%), and a negative predictive value (NPV) (66%) than the BPP (27%, 82%, 53%, and 59%, respectively).

More recently, Crimmins and colleagues [12] have compared the changes in fetal Dopplers and BPP, leading to stillbirths in 987 singleton pregnancies with fetal growth restriction (FGR) in a retrospective study and observed gestational age-based patterns in the efficacy of the tests for predicting the stillbirths. Prior to 34 weeks of gestation, worsening of the UA and ductus venosus Dopplers occurred before that of the BPP, whereas only middle cerebral artery (MCA) Dopplers deteriorated in pregnancies after 34 completed weeks of gestation. Significantly, the BPP failed to predict most stillbirths in the latter group. This topic is further discussed in Chaps. 25 and 26.

24.4 Fetal Asphyxia and Umbilical Doppler Indices

A number of clinical studies have been reported on the efficacy of UA Doppler measurements for detecting fetal hypoxia and asphyxia. The studies employed two distinct approaches for assessing fetal asphyxia. In four studies, umbilical cord blood sampling was performed at the time of elective cesarean section. Blood gases measured in this manner, however, may not reflect the antepartum acid–base status of the fetus. In the remaining five studies, blood gases in fetal blood samples were determined by cordocentesis. All studies measured pH, most determined the $p0_2$, and some also measured pCO_2 and lactate. There was also considerable variability in the patient populations, ranging from those with sonographic diagnosis of fetal growth compromise to those without recognized risks. Most investigators found a significant association between fetal acid–base compromise and Doppler indices from the umbilical circulation. As expected, the higher the risk category of the pregnancy, the greater is the association of the Doppler results with fetal asphyxia. The association between fetal hypoxia and the UA Doppler index was less impressive. These studies are discussed below according to whether the investigations were restricted to the Doppler method or included other methods of fetal surveillance.

Nicolaides et al. investigated the efficacy of UA Doppler for indirectly reflecting fetal blood gas status [13]. Umbilical venous blood gases were determined by cordocentesis in 59 fetuses, with abdominal circumferences below the 5th percentile for gestational age, who also suffered from the absence of umbilical artery end-diastolic flow. In 88% of the cases, the blood gases were abnormal, 42% were hypoxic, 37% were asphyxiated, and 9% were acidotic. Furthermore, there was a poor correlation between the degree of fetal smallness and the acidosis or severity of hypoxia. Ferrazzi et al. [14] used cord blood sampling at cesarean section on 14 high-risk pregnant patients, 10 of whom also underwent cordocentesis. A significant relation was found between the umbilical artery pulsatility index (PI) and the fetal blood pH, pCO_2, and lactate concentrations. Umbilical venous oxygen content failed to show this association. A noteworthy observation was the sharp rise in umbilical venous lactate concentration when the umbilical arterial PI exceeded 1.5.

The fetal cerebral and umbilical circulatory responses to hypoxia, hypercapnia, and acidosis were investigated by Chiba and Murakami [15] in 17 SGA fetuses. Cordocentesis was performed to determine umbilical venous blood gases and pH. The MCA demonstrated decreased imped-

ance in the presence of hypoxia and acidosis. In contrast, the UA impedance increased with acidosis but was insensitive to hypoxia and hypercapnia. These observations were corroborated by Akalin-Sel et al. [16].

These findings have significant clinical implications for managing high-risk pregnancies. Significant progress has been made in integrating the current modes of fetal surveillance, such as computerized cardiotocography or BPP scoring, with the UA, MCA, and ductus venosus Doppler offering opportunities for improving the clinical outcome. This topic is further discussed in Chaps. 25 and 26 and elsewhere in this book.

The diagnostic efficacy of UA Doppler in reflecting fetal asphyxia has been compared with that of other modalities of antepartum fetal surveillance. Pardi and colleagues [17] studied SGA fetuses (abdominal circumference <5th percentile) regarding the UA-PI and used cardiotocography to detect cordocentesis-derived fetal blood gas abnormalities. Fetuses with normal cardiotocography and a normal PI did not demonstrate hypoxia or acidemia. In contrast, when both tests were abnormal, two-thirds of the fetuses had lactic acidosis, low blood oxygen content, and low pH values. In contrast, Vintzileos and coinvestigators [18] found no association between the Doppler results and cord arterial and venous pH. The authors concluded that the UA-S/D ratio, as determined by continuous wave Doppler velocimetry, is inferior to the BPP and NST, and it has no value for antepartum surveillance for fetal acidosis.

These findings, however, were contradicted by Yoon et al., who used both approaches of cord blood sampling: collection from the cord vessels at cesarean section or from the umbilical vein by antepartum cordocentesis. In the first study [19], the BPP and Doppler velocimetry showed comparable effectiveness in detecting fetal acidosis. Patients with abnormal Doppler results showed a significantly higher prevalence of fetal acidosis, and all the fetuses with abnormal Doppler results were either acidotic or growth-restricted. Upon recognizing the limited validity of cord blood gases sampled at cesarean section for reflecting the antepartum fetal acid–base status, the investigators conducted a second study [20], which used cordocentesis to assess fetal blood gases. The prevalence of fetal acidemia (pH at 2 standard deviation (SD) below the mean for gestational age) was 41.7%. A statistically significant relation was noted between the change in the UA-PI and fetal acidemia ($p < 0.001$) and hypercarbia ($p < 0.001$) but not hypoxemia ($p > 0.1$). Similarly, a significant relation was noted between the BPP score and fetal acidemia ($p < 0.001$) and hypercarbia ($p < 0.005$) but not hypoxemia ($p > 0.1$). Stepwise multiple logistic regression and ROC analyses demonstrated that UA Doppler was a better predictor of acidemia and hypercarbia than the BPP score.

24.5 Fetal Doppler Sonography and Neurodevelopmental Outcome

As indicated above, the currently utilized immediate measures of outcome may not effectively prognosticate the long-term effects of in utero fetal compromise on subsequent neurological development. This point is particularly relevant when assessing the efficacy of antepartum surveillance, which is a relatively difficult area of investigation. This topic has been reviewed in Chap. 12.

24.6 Efficacy of Doppler Sonography for Screening Low-Risk and Unselected Pregnancies

Although the diagnostic efficacy of the Doppler technique in a high-risk population is encouraging, its performance in a low-risk population is disappointing, as indicated by several studies summarized below.

In a prospective study involving 2097 singleton pregnancies, Beattie and Dornan [21] evaluated the capability of the UA Doppler pulsatility index (PI), S/D ratio, and resistance index (RI) to detect FGR and perinatal compromise. It was noted that the indices did not adequately predict

any of the parameters of adverse perinatal outcomes. It is noteworthy, however, that elevated Doppler indices were the only abnormal findings in three cases of unexplained fetal death in this population. Moreover, although the investigators did not find the indices to be useful for timing the death, there were no indications that these fetuses underwent adequate surveillance after the abnormal Doppler findings, as up to 6 weeks transpired between the abnormal findings and the fetal death. There is an important methodological issue related to the Doppler examination technique. The high-pass filter, which screens out low-frequency components of the Doppler signal, was set at 200 Hz, thereby increasing the odds of a false-positive diagnosis of an absent end-diastolic velocity. Regrettably, such an inappropriately high setting of the high-pass filter has been used by many other investigators, which may have compromised the validity of their results. Despite these limitations, the main finding that Doppler insonation of the umbilical arteries may not be efficacious in a low-risk population has been corroborated by others. A selection of such studies is briefly discussed below.

Hanretty and co-workers [22] investigated the association between the uteroplacental and umbilical arteries and the obstetric outcomes in unselected pregnant mothers. Only the results of the UA Doppler studies are discussed here. Their study utilized a prospective blind design and the populations of 326 women at 26–30 weeks' gestation and 356 women at 34–36 weeks' gestation. There was a significant ($p < 0.05$–0.002) decrease in the birth weight of fetuses with an abnormal UA-S/D ratio at either gestation. There were no statistically significant differences between the groups in relation to other obstetric outcomes, including antepartum admission, pre-eclampsia, preterm delivery, antepartum and intrapartum cesarean section, Apgar score, and NICU admission.

Newnham and associates [23] evaluated the UA-S/D ratio as a screening tool in a prospective double-blind study of 535 pregnancies at medium risk of fetal compromise. Ultrasound biometry and Doppler measurements were performed at 18, 24, 28, and 34 weeks' gestation. The UA-S/D ratios at 24, 28, and 34 weeks' gestation were found to be predictive of intrauterine growth restriction (IUGR). This predictive capability was enhanced in the growth-restricted fetuses in whom hypoxia developed but was weak when the UA-S/D ratios were evaluated as primary screening tests for fetal hypoxia. The results confirm the role of Doppler-determined S/D ratios in the evaluation of high-risk pregnancies but do not support their role as primary screening tests in low-risk obstetric populations.

Sijmons and colleagues [24] conducted a prospective blind assessment of the efficacy of the UA-PI screening for predicting infants with SGA (birth weight <2.3rd and 10th percentile) and a low ponderal index (<3rd and 10th percentile). The population consisted of 400 women at 28 and 34 weeks' gestation attending a university tertiary medical center. The prevalence of the outcome varied between 3.3 and 22.1%. For the different outcome parameters, the test sensitivity ranged from 6.9 to 41.7%, the specificity from 91.5 to 99.7%, the PPV from 10.0 to 52.9% and the NPV from 79.1 to 97.8%.

The lack of clinical utility of fetal Doppler in low-risk pregnancies was further evident in the Cochrane Systematic Review, which analyzed five trials comprised of 14,185 women [25]. Routine fetal and UA Doppler in low-risk or unselected populations did not significantly reduce perinatal mortality (average risk ratio (RR) 0.80, 95% confidence interval (CI) 0.35–1.83; 4 studies, 11,183 participants) or neonatal morbidity (average risk ratio (RR) 0.80, 95% confidence interval (CI) 0.35–1.83; 4 studies, 11,183 participants). The authors did not find any available evidence supporting the routine use of Doppler in low-risk and unselected pregnancies.

A more recent study, however, has suggested the benefits of UA Doppler screening for low-risk pregnancies in a developing country. In a prospective observational study, Nkosi and colleagues [26] managed a cohort of 2868 low-risk pregnancies at gestational ages 28–30 weeks utilizing the UA-RI measured with a hand-held continuous wave Doppler device. The pregnancies were categorized as high-risk if the UA-RI

was greater than the 75th centile. The control group comprised of 12,168 women without Doppler screening. Absent end-diastolic velocity (AEDV) was found in 1.5% of the Doppler screened pregnancies. The perinatal mortality rate was significantly lower in the Doppler screened group than in the control group, i.e., 11.4 per 1000 births vs. 21.3 per 1000 births, respectively (risk ratio 0.58, 95% confidence interval 0.42–0.81). It should be noted that the prevalence of AEDV in these apparently low-risk pregnancies was several times higher than that reported in the literature (see Chap. 25). This strongly suggests an inherently higher risk for this obstetric population. Importantly, these results offer the potential of using continuous wave Doppler of the UA as a relatively low-technology screening tool for reducing stillbirth rates in under-resourced communities.

References

1. Cohn H, Sachs E, Heymann M, Rudolph A. Cardiovascular responses to hypoxemia and acidemia in fetal lambs. Am J Obstet Gynecol. 1974;120:817–23.
2. Trudinger BJ, Cook CM, Jones L, Giles WB. A comparison of fetal heart rate monitoring and umbilical artery waveforms in the recognition of fetal compromise. Br J Obstet Gynaecol. 1986;93:171–5.
3. Maulik D, Yarlagadda P, Youngblood JP, Ciston P. The diagnostic efficacy of the umbilical arterial systolic/diastolic ratio as a screening tool: a prospective blinded study. Am J Obstet Gynecol. 1990;162:1518–23.
4. Devoe LD, Gardner P, Dear C, Castillo RA. The diagnostic values of concurrent nonstress testing, amniotic fluid measurement, and Doppler velocimetry in screening a general high-risk population. Am J Obstet Gynecol. 1990;163:1040–7.
5. Swets JA, Pickett RM. Evaluation of diagnostic systems: methods from signal detection theory. Orlando: Academic; 1982.
6. Cohen J. A coefficient of agreement for nominal scales. Educ Psychol Meas. 1960;20:37–44.
7. Landis JR, Koch GG. The measurement of observer agreement for categorical data. Biometrics. 1977;33:159–60.
8. Farmakides G, Schulman H, Winter D, et al. Prenatal surveillance using non-stress testing and Doppler velocimetry. Obstet Gynecol. 1988;71:184–9.
9. Arduini D, Rizzo G, Soliani A, Romanini C. Doppler velocimetry versus nonstress test in the antepartum monitoring of low-risk pregnancies. J Ultrasound Med. 1991;10:331–5.
10. Hastie SJ, Brown MF, Whittle MJ. Predictive values of umbilical artery waveforms and repeat cardiotocography in pregnancies complicated by nonreactive cardiotocography. Eur J Obstet Gynecol Reprod Biol. 1990;34:67–72.
11. Nordstrom UL, Patel NB, Taylor DJ. Umbilical artery waveform analysis and biophysical profile: a comparison of two methods to identify compromised fetuses. Eur J Obstet Gynecol Reprod Biol. 1989;30:245–51.
12. Crimmins S, Desai A, Block-Abraham D, Berg C, et al. A comparison of Doppler and biophysical findings between liveborn and stillborn growth-restricted fetuses. Am J Obstet Gynecol. 2014;211:669.e1–669.e10.
13. Nicolaides KH, Bilardo CM, Soothill PW, Campbell S. Absence of end diastolic frequencies in umbilical artery: a sign of fetal hypoxia and acidosis. BMJ. 1988;297:1026–127.
14. Ferrazzi E, Pardi G, Bauscaglia M. The correlation of biochemical monitoring versus umbilical flow velocity measurements of the human fetus. Am J Obstet Gynecol. 1988;159:1081–7.
15. Chiba Y, Murakami M. Cerebral blood flow dynamics in fetus. No To Hattatsu. 1992;24:136–42.
16. Akalin-Sel T, Nicolaides KH, Peacock J, Campbell S. Doppler dynamics and their complex interrelation with fetal oxygen pressure, carbon dioxide pressure, and pH in growth-retarded fetuses. Obstet Gynecol. 1994;84:439–46.
17. Pardi G, Cetin I, Marconi AM, et al. Diagnostic value of blood sampling in fetuses with growth retardation. N Engl J Med. 1993;328:692–6.
18. Vintzileos AM, Campbell W, Rodis J, et al. The relationship between fetal biophysical assessment, umbilical artery velocimetry, and fetal acidosis. Obstet Gynecol. 1991;77:622–7.
19. Yoon BH, Syn HC, Kim SW. The efficacy of Doppler umbilical velocimetry in identifying fetal acidosis: a comparison with fetal biophysical profile. J Ultrasound Med. 1992;11:1–6.
20. Yoon BH, Romero R, Roh CR, et al. Relationship between the fetal biophysical profile score, umbilical artery Doppler velocimetry, and fetal blood acid-base status determined by cordocentesis. Am J Obstet Gynecol. 1993;169:1586–94.
21. Beattie RB, Dornan JC. Antenatal screening for intrauterine growth retardation with umbilical artery Doppler ultrasonography. BMJ. 1989;298:631–5.
22. Hanretty KP, Primrose MH, Neilson JP, Whittle MJ. Pregnancy screening by Doppler uteroplacental and umbilical waveforms. Br J Obstet Gynaecol. 1989;96:1163–67.
23. Newnham JP, Patterson LL, James IR, Diepeveen DA, Reid SE. An evaluation of the efficacy of Doppler flow velocity waveform analysis as a screening test in pregnancy. Am J Obstet Gynecol. 1990;162:403–10.

24. Sjmons EA, Reuwer PJ, van Beek E, Bruinse HW. The validity of screening for small-for-gestational-age and low-weight-for-length infants by Doppler ultrasound. Br J Obstet Gynaecol. 1989;96:557–61.
25. Zarko, Alfirevic Tamara, Stampalija Nancy, Medley Fetal and umbilical Doppler ultrasound in normal pregnancy. Cochrane Database Syst Rev. https://doi.org/10.1002/14651858.CD001450.pub4.
26. Nkosi S, Makin J, Hlongwane T, Pattinson RC. Screening and managing a low-risk pregnant population using continuouswave Doppler ultrasound in a low-income population: A cohort analytical study. SAMJ: South African Medical Journal. 2019;109:347–52.

25 Absent End-Diastolic Velocity in the Umbilical Artery and Its Clinical Significance

Dev Maulik and Tabitha Schrufer-Poland

25.1 Introduction

Of the various characteristics of an umbilical artery (UA) Doppler waveform, end-diastolic velocity is of primary hemodynamic and clinical significance. As discussed in Chap. 14, the end-diastolic velocity continuously increases throughout gestation, which is attributable to an ever-increasing decline of the feto-placental flow impedance. This phenomenon results in a concomitant decrease in the pulsatility of the UA Doppler waveform, which is reflected in a progressive decline in the Doppler indices, such as the systolic/diastolic (S/D) ratio, the pulsatility index (PI), and the resistance index (RI), with the advancing gestation. These changes are prognostically reassuring. In contrast, any decline in the end-diastolic velocity with a consequent elevation of the Doppler indices indicates rising impedance in the feto-placental vascular bed and signifies a worsening prognosis. With further increase of impedance, the end-diastolic flow eventually becomes absent and may even be reversed. Such a development, though rare, is ominous and leads to profoundly adverse perinatal outcomes [1–26]. Absent end-diastolic velocity (AEDV) and reverse end-diastolic velocity are demonstrated in Figs. 25.1 and 25.2, respectively. An updated review of the UA's absent and reverse end-diastolic velocity is presented in this chapter.

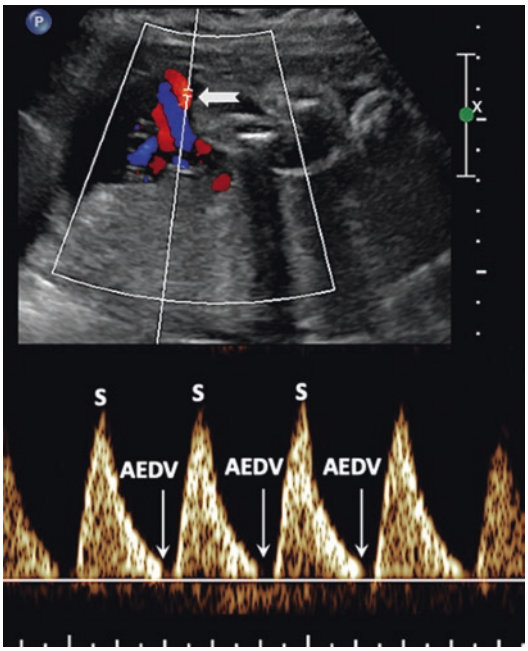

Fig. 25.1 An example of absent end-diastolic velocity in the umbilical artery. Top: Color Doppler-directed pulsed Doppler interrogation of the umbilical vessels. The white arrow points at the Doppler sampling location. Bottom: umbilical arterial Doppler waveforms. *S* peak systolic velocity, *AEDV* absent end-diastolic velocity

D. Maulik (✉) · T. Schrufer-Poland
Department of Obstetrics and Gynecology, UMKC School of Medicine/Truman Medical Center, UMKC School of Medicine, Kansas City, MO, USA
e-mail: Dev.Maulik@uhkc.org; dmaulik2014@gmail.com

D. Maulik, C. C. Lees (eds.), *Doppler Ultrasound in Obstetrics and Gynecology*,
https://doi.org/10.1007/978-3-031-06189-9_25

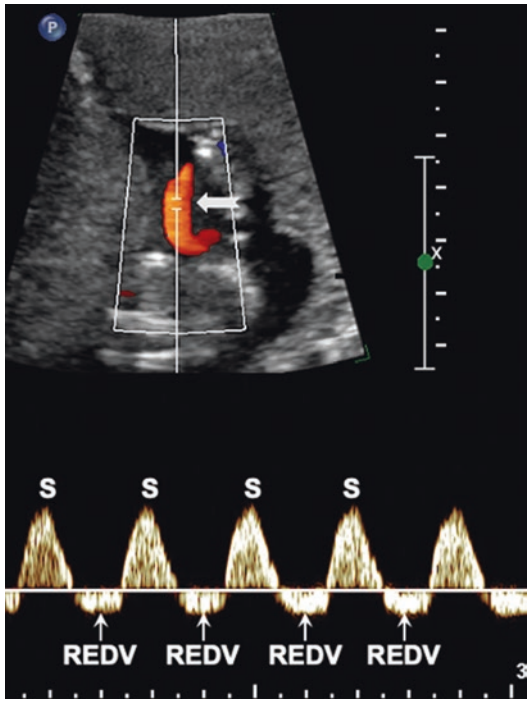

Fig. 25.2 An example of reverse end-diastolic velocity in the umbilical artery. Top: Color Doppler-directed pulsed Doppler interrogation of the umbilical vessels. The white arrow points at the Doppler sampling location. Bottom: umbilical arterial Doppler waveforms. *S* peak systolic velocity, *REDV* reverse end-diastolic velocity

25.2 Incidence

The frequency of absent or reverse end-diastolic velocity (AREDV) in the UA varies according to the risk category of the obstetric population, the time of gestation at which the observation is made and the Doppler examination technique. For high-risk pregnancies, the incidence varies from 2.1 to 56.0% (Table 25.1). Such a wide range may be explained by the differing definitions of a high-risk pregnancy used by the investigators and by the level of the high-pass filter used. For example, the basis for a high-risk categorization of a pregnancy may range from clearly defined clinical criteria, such as hypertension, to ill-defined groupings of various clinical conditions.

In probably the largest reported series on AREDV, Karsdorp et al. [24] used well-defined criteria for selecting the population for a multicenter study. Only patients with hypertension or fetal growth restriction (or both) were included. Hypertension was defined as a diastolic pressure of 110 mmHg by a single measurement or 90 mmHg by two or more measurements. Also included were patients with hypertension plus proteinuria; the latter was defined as urinary pro-

Table 25.1 Incidence of absent and reverse end-diastolic velocity in high- and low-risk populations

First author, year, [Reference]	Number of patients	Risk category	Doppler	AREDV	
				No.	%
Johnstone, 1988 [7]	380	High	PW, CW	24	6.30
Beattie, 1989 [27]	2097	Low	CW	6	0.29
Huneke, 1991 [14]	226	High	CW	18	8.00
Malcolm, 1991 [15]	1000	High	PW	25	2.50
Wenstrom, 1991 [17]	450	High	PW	22	4.90
Weiss, 1992 [19]	2400	Unselected	PW	51	2.10
Battaglia, 1993 [23]	46	Very high	PW	26	56.20
Pattinson, 1993 [22]	342	Very high	PW, CW	120	34.50
Karsdorp, 1994 [24]	459	Very high	?PW	245	53.40
Rizzo, 1994 [25]	6134	High	PW	192	3.10
Unterscheider, 2013 [63]	1116	FGR	PW	78	7
Nkosi, 2019 [28]	2539	Low	CW	38	1.5

CW continuous wave, *PW* pulsed wave, *AEDV* absent end-diastolic velocity, *NA* not available

[a] Fetuses with congenital anomalies and dyskaryosis were clearly excluded. The other studies either included these fetuses or were unclear

tein loss of more than 300 mg in 24 h. Intrauterine growth restriction (IUGR) was defined as the abdominal circumference measuring less than the fifth percentile for gestational age based on local population-specific nomograms. The lowest possible high-pass filter threshold was used. Of the 459 patients selected in this manner, 245 developed AREDV, for an incidence of 53.4%. In contrast, Beattie and Dornan [27] found that only 6 of 2097 singleton low-risk pregnancies developed AREDV for an incidence of 0.29%. The actual rate might even be lower if one considers that the high-pass filter setting was 200 Hz, which is relatively high for umbilical arterial Doppler. In contrast, Nkosi et al. have recently reported a 1.5% prevalence of UA AREDV in a low-risk under-resourced pregnant population between 28 and 32 weeks' gestation who were screened utilizing a continuous wave Doppler device [28].

25.3 Technical Considerations

As discussed in Chap. 14, the procedure used for Doppler measurement may affect the measured magnitude of the end-diastolic frequency shift. There are two technical sources of this problem: (1) the threshold setting of the high-pass filter and (2) the angle of insonation between the Doppler beam and the flow axis. The high-pass filter (Chap. 3) eliminates the low-frequency/high-amplitude frequency component from the Doppler signal and is used to remove signals generated by movement of the vascular wall or other adjacent tissues. This filter, however, also removes low-frequency components generated from the slow-moving blood flow as encountered during the end-diastolic phase of the cardiac cycle. Thus, end-diastolic frequencies are removed from the umbilical Doppler waveform. A relatively high setting of the filter may therefore lead to a false impression of AEDV. It is strongly recommended that the high-pass filter should be at the lowest possible setting, which should not exceed 100 Hz. The second consideration is the angle of insonation, which is inversely related to the magnitude of the estimated Doppler shift due to the cosine function of the angle in the Doppler equation (Chap. 2). A larger angle therefore leads to a lower frequency measurement, which leads to disappearance of the end-diastolic frequency, even in the presence of end-diastolic flow.

25.4 Absent End-Diastolic Velocity and Its Adverse Consequences

Absent or reverse end-diastolic flow in the UA is associated with serious adverse consequences. These include significantly increased perinatal mortalities and morbidities (Table 25.2) as well as various pregnancy complications. These are further discussed below.

Table 25.2 Absent and reverse end-diastolic velocity in the umbilical artery and adverse perinatal outcomes

Perinatal outcome	Mean	Range
Death (%)	45	17–100
Gestational age (weeks)	31.6	29–33
Birth weight (g)	1056	910–1481
Small for gestational age (%)	68	53–100
Cesarean section for fetal distress (%)	73	24–100
Apgar score <7 at 5 min (%)	26	7–69
Admission to neonatal intensive care unit (%)	84	77–97
Congenital anomalies (%)	10	0–24
Aneuploidy (%)	6.4	0–18

25.5 Perinatal Mortality

Perinatal mortality is increased in pregnancies affected by AREDV and reverse end-diastolic velocity (REDV). From a total of 1126 cases of AREDV collated from studies cited in this chapter, 193 were stillborn and 312 died during the neonatal period. These data translate into uncorrected stillbirth and neonatal mortality rates of 170/1000 and 280/1000, respectively. Most deaths are attributable to obstetric complications, including preterm births, fetal growth restriction, fetal anomalies and aneuploidy encountered in these infants, as well as prematurity. When the end-diastolic flow in the UA is reversed, the outcome is worse. The European Multicenter Study observed that 98% of such infants required neonatal intensive care unit (NICU) admission, and the odds ratio for perinatal mortality was 10.6 when compared to those with positive end-diastolic velocity. The reverse flow therefore indicates severe fetal decompensation and, if unattended, eventually leads to fetal death. An example of such a case is presented in Fig. 25.3.

Caradeux et al. have provided more comprehensive information on the risk of stillbirths in early-onset FGR in a recent systematic review [29]. The analysis included 31 publications comprised of 3 randomized trials and 28 cohorts, with a total of 5909 Doppler assessments and 336 stillbirths. There were 863 cases of AEDV and 376 cases of reverse end-diastolic velocity (REDV), with 6.8% and 19% pooled risks of stillbirths, respectively. The corresponding odds ratios are presented in forest plots in Figs. 25.4 and 25.5.

25.6 Perinatal Morbidity

Not only is there a high rate of perinatal loss but also the surviving fetuses and infants demonstrate signs of profound compromise, with a marked increase in the incidence of various measures of morbidity (Table 25.2). There is a higher incidence of iatrogenic preterm births, attributable to fetal or maternal complications, mandating early intervention. Perinatal morbidity is increased in preterm infants complicated by fetal growth restriction. In addition to prematurity, there is a much higher frequency of fetal acidosis, cardiotocographic abnormalities contributing to a three- to four-fold increase in the number of cesarean deliveries, low Apgar scores, and the need for NICU admission. Furthermore, the

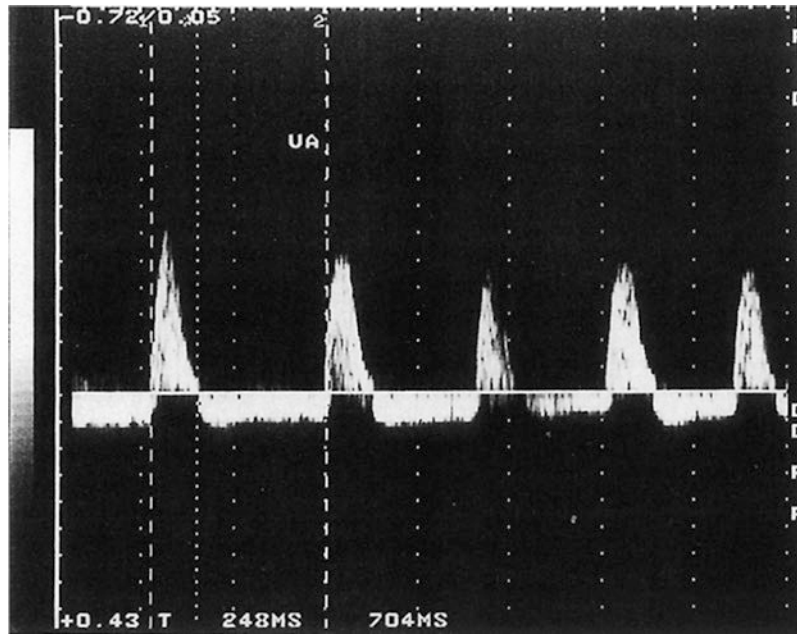

Fig. 25.3 Umbilical arterial Doppler velocimetry showing an agonal pattern. Note that reverse end-diastolic velocity was present for most of the cardiac cycle (60–70%). This pattern signifies that feto-placental perfusion, which is normally present for the duration of the cardiac cycle, was seen in this case for only a fraction of that time

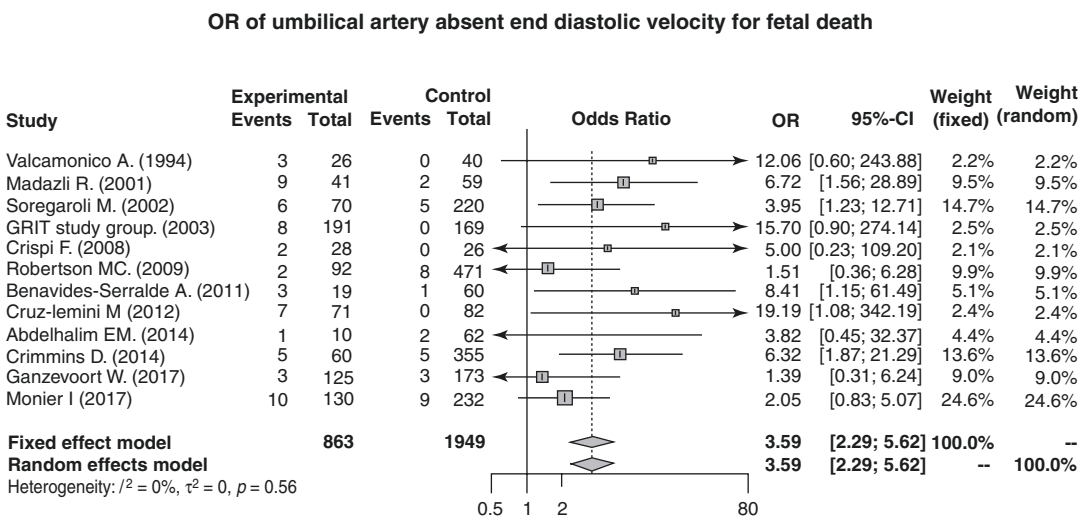

Forest plot of the odds ratio of umbilical artery absent end diastolic velocity for fetal death (weighted by the inverse of the variance under fixed and random effects model). CI, confidence interval; OR odds ratio.
Caradeux. Doppler changes and risk of fetal death. Am J Obstet Gynecol 2018.

Fig. 25.4 OR of umbilical artery absent end-diastolic velocity for fetal death. Forest plot of the odds ratio of umbilical artery absent end-diastolic velocity for fetal death (weighted by the inverse of the variance under a fixed and random effects model). *CI* confidence interval, *OR* odds ratio (with permission from Caradeux et al. Doppler changes and risk of fetal death. *Am J Obstet Gynecol* 2018) [29]

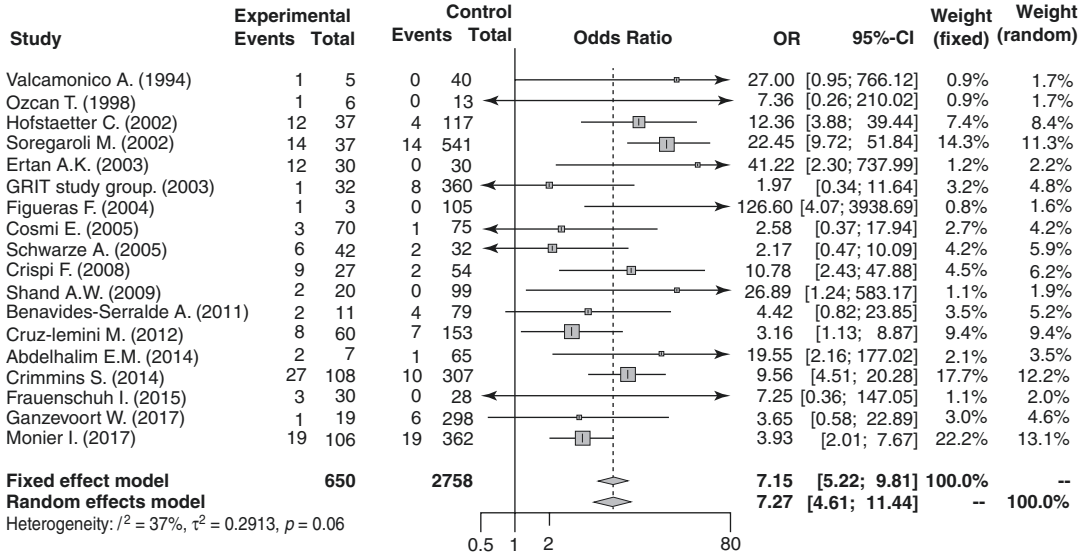

Fig. 25.5 OR of umbilical artery absent end-diastolic velocity for fetal death. Forest plot of the odds ratio of umbilical artery absent end-diastolic velocity for fetal death (weighted by the inverse of the variance under a fixed and random effects model). *CI* confidence interval, *OR* odds ratio (with permission from Caradeux et al. *Am J Obstet Gynecol* 2018) [29]

combination of fetal asphyxia and prematurity exposes the fetus to the additional danger of end-organ damage, such as necrotizing enterocolitis and cerebral hemorrhage. This is confounded by a higher incidence of aneuploidy and congenital malformations associated with Doppler abnormalities.

25.7 Congenital Malformations and Chromosomal Abnormalities

There is a preponderance of congenital malformations and abnormal chromosomes in fetuses afflicted with umbilical arterial AREDV. Cumulative data, as summarized in Table 25.2, demonstrate that as high as 1 in 10 fetuses with AREDV have anatomical maldevelopment. There is heterogeneity, however, in the reported incidence, and studies conflict on incidence, depending on the populations studied.

The anomalies associated with AREDV involve most organ systems (Table 25.3), although the anomalies of the cardiovascular system are encountered most frequently. Isolated and multiple malformations are encountered with equal frequency, and most cases of multiple anomalies are seen with aneuploidy. Hence, most cases with normal chromosomes have isolated malformations, whereas most cases of aneuploidy are associated with multiple malformations.

Table 25.3 Absent end-diastolic velocity and congenital malformations

Cardiovascular system
Ventricular septal defect
Hypoplastic left heart syndrome
Double outlet right ventricle
Ebstein anomaly
Arrhythmia: congenital heart block
Central nervous system
Hydrocephaly
Holoprosencephaly
Agenesis of corpus callosum
Urogenital system
Renal agenesis
Hydronephrosis
Gastrointestinal system/abdominal wall
Oesophageal atresia
Omphalocele
Gastroschisis
Skeletal system
Polydactyly
Dysplasia

The frequency of chromosomal abnormalities is 1 in 16. Autosomal trisomy dominates, with trisomy 18 being the most frequently encountered aneuploidy. The relative distribution of various chromosomal anomalies in AREDV fetuses is shown in Fig. 25.4. Martinez et al. [30] had prospectively recorded the UA pulsatility index (PI) in 1785 pregnancies before undergoing chorionic villus sampling or genetic amniocentesis. They observed that fetuses with trisomy 18 had an elevated PI. The PI was measured transvaginally for pregnancies from 10 to 13 weeks and transabdominally for pregnancies from 14 to 18 weeks. In all, 7 of the 10 fetuses with trisomy 18 had an elevated PI above the 95th percentile; 9 fetuses had an elevated PI above the 90th percentile. The PI as a marker for trisomy 18 had good sensitivity (70–90%), specificity (>90%), and a negative predictive value (99%) but a poor positive predictive value (5–7%). Reversed end-diastolic flow was detected in two cases, both of which had trisomy 18. Borrell et al. [31] screened 2970 pregnancies at 10–14 weeks' gestation and observed 11 cases of reversed end-diastolic flow for an incidence of 0.4%. Autosomal trisomy complicated seven cases, a congenital heart defect was found in two cases and the remaining had no findings.

The appearance of AREDV early in gestation, in combination with fetal malformations and the absence of comorbidities (hypertension, pre-eclampsia, etc.), greatly increases the likelihood of a chromosomal abnormality. Although these fetuses are severely growth-restricted, there is no difference in the pattern of growth compromise between those with abnormal chromosomes and those without. Snijders et al. [32] studied a population of 458 growth-restricted fetuses and observed that fetuses with chromosomal abnormalities had a higher mean head circumference/abdominal circumference ratio than did fetuses

with a normal karyotype. Rizzo et al. [25], in their investigation of fetuses with AEDV, found no significant difference in head/abdomen circumference between those with an abnormal karyotype and those with a normal karyotype.

Many of these infants also tend to develop abnormal fetal heart rate patterns during labor, which may lead to a cesarean delivery if intervention is desired. The mechanism of increased feto-placental impedance is not fully understood. The work of Rochelson et al. [33], however, may shed light on this phenomenon. A quantitative morphometric analysis of the placentas complicated by trisomy revealed a significant reduction in the small muscular artery count and the small muscular artery/villus ratio. Abnormal Doppler waveforms correlated closely with reduced small muscular artery counts. These findings suggest that aneuploidy may adversely affect feto-placental vascularization, which results in increased feto-placental circulatory impedance, and may contribute to fetal growth restriction.

25.8 Fetal Growth Restriction

The strength of the association between AREDV and fetal growth compromise depends on the stringency of the definition of growth restriction. A small-for-gestational-age (SGA) fetus may not necessarily be growth-restricted, just constitutionally small. It is also probable that a fetus that fails to realize its full growth potential may not necessarily be SGA. Being SGA does not necessarily indicate a compromised outcome. Despite these ambiguities, fetuses experiencing a significant growth deficit often suffer from in utero asphyxia and its adverse consequences. These fetuses also demonstrate Doppler evidence of increasing feto-placental arterial impedance. Thus, 50% or more of the fetuses with AREDV demonstrate suboptimal growth (Table 25.2). A similar proportion of fetuses with sonographic evidence of serious growth restriction develop AREDV. Thus, Battaglia et al. [23] noted that 57% of the fetuses that identified as being growth-restricted by serial ultrasound measurements developed AEDV. Similarly, Pattinson et al. [22] observed that 48% of the fetuses suspected of severe growth restriction in their series developed umbilical arterial AREDV. It is noteworthy that pregnancies complicated by both growth restriction and hypertension demonstrate a greater propensity for developing AREDV than do those with either growth restriction or hypertension [24].

25.9 Fetal Asphyxia and Hypoxemia

The significant association between elevated umbilical arterial Doppler indices and fetal hypoxemia and acidosis is discussed in Chap. 24. The morbid sequelae of AREDV can be largely attributed to fetal exposure to chronic acidemic and asphyxial insults. It is apparent that the umbilical hemodynamics are more affected by asphyxia or acidemia and less by hypoxemia. Nicolaides et al. [34] measured umbilical venous blood gases by cordocentesis in 59 growth-restricted fetuses with AEDV. In 88% of the cases, the blood gases were abnormal: 42% of the fetuses demonstrated hypoxemia (oxygen saturation < 2.5 standard deviations from normal), 9% were acidemic (venous pH <7.25) and 37% were both hypoxemic and acidemic (asphyxiated). There was a poor correlation between the degree of fetal growth restriction and the presence of acidemia or the severity of hypoxemia noted. Other investigators [35] have also observed this relationship between AEDV and fetal acidemia. The AEDV identified acidosis with a sensitivity of 90%, a specificity 92%, a positive predictive value of 53% and a negative predictive value of 100%.

As noted above, not all fetuses with AREDV are hypoxemic or acidemic. Normal fetal blood gas values, however, do not ensure fetal well-being. Several investigators have noted progressive fetal deterioration and adverse perinatal outcomes in fetuses with AREDV, despite a normal fetal acid–base status as determined by cordocentesis [9, 36]. It appears that a progressive fetal hemodynamic decline, as manifested by AREDV, is not necessarily related to fetal

asphyxia and presents a serious threat to the fetus, independent of fetal hypoxemia or acidemia.

25.10 Cerebral Hemorrhage

One of the major concerns regarding chronic intrauterine asphyxia is its potential effect on the fetal brain. Although the risk of neurological injury due to prematurity and birth asphyxia has been well-investigated, the roles that chronic antepartum hypoxemia and asphyxia play require further elucidation.

Although cerebral hemorrhage has been associated with AREDV, it is unclear whether this phenomenon is independent of prematurity and fetal growth restriction. Studies have inconsistently identified AREDV as an independent risk factor. Weiss et al. [19] conducted a case–control study, comparing 47 fetuses with AREDV to 47 control fetuses matched for gestational age and with forward end-diastolic velocity in the UA. Fetuses with AREDV showed an increased incidence of cerebral hemorrhage, but it was not statistically significant. Pattinson et al. [21] also performed a case–control study that showed no difference in cerebral hemorrhage between the 16 matched pairs of fetuses with the presence or absence of UA end-diastolic velocity. Both of the above findings were refuted by much larger studies.

In the largest study of its kind, the European Community Multicenter Study, Karsdorp et al. [24] demonstrated a significantly increased incidence of severe cerebral hemorrhage in fetuses with AREDV, which persisted despite controlling for prematurity with multiple logistic regression. The odds ratios for the association of cerebral hemorrhage were 2.6 and 4.8 in cases with absent and reverse end-diastolic velocity (EDV), respectively.

In contrast, in their case–control studies, Weiss et al. in 1992 [19] and Pattinson et al. [21] demonstrated a non-significant increase in intraventricular hemorrhage in the case groups. Adiotomre et al. [37] and, later, Spinillo et al. [38] found that AREDV was poorly predictive of the presence of intraventricular hemorrhage after controlling for prematurity and fetal growth restriction. However, in all of these studies, the incidence of intraventricular hemorrhage was higher in the case group compared to that of the control group, suggesting that they may have been underpowered for this outcome.

Although not entirely understood, the pathophysiology of brain injury in fetuses with AREDV is believed to be related to altered cerebroplacental hemodynamics. AREDV is associated with increased right ventricular afterload and, subsequently, greater left ventricular cardiac output. In addition to greater volume associated with increased cardiac output, cerebral vasodilation increases both blood flow and volume to the cerebral circulation. An increased mechanical force on these vessels is expected to cause vascular wall strain, which may contribute to the pathophysiology of hemorrhage [39]. Furthermore, AREDV has been associated with thrombocytopenia, which may contribute to both hemorrhagic placental vasculitis and infarction as well as cerebral hemorrhage [40–43]. Reperfusion in the areas of hypoxemic injury is likely to play a causative role.

25.11 Necrotizing Enterocolitis

Several investigators have reported an increased risk of necrotizing enterocolitis in neonates who had suffered from AREDV of the UA or the aorta. This serious complication is typically seen in premature neonates who experienced perinatal asphyxia, often secondary to the respiratory distress syndrome caused by pulmonic immaturity.

Prematurity is believed to play a significant role, and, in the studies reviewed herein, the average gestational age at delivery was less than 32 weeks (Table 25.2). Therefore, it is likely that these infants have a predisposition to develop these complications independent of the existence of AREDV. Hackett et al. [4] investigated 82 consecutive cases of fetal growth restriction and identified 29 fetuses with an absence of end-diastolic frequencies in the fetal aorta. These

fetuses were more likely to be affected by growth restriction and deliver earlier ($p < 0.001$). Following delivery, there was a higher incidence of necrotizing enterocolitis ($p < 0.01$) or hemorrhage ($p < 0.05$). Additionally, the incidence of perinatal mortality was higher in these cases. Malcolm et al. [15] studied 25 high-risk pregnancies with AREDV in the UA and observed a significantly increased risk of necrotizing enterocolitis in the morphologically normal fetuses (53%), compared with the controls (6%) who had forward UA end-diastolic flow in utero. This increased risk appeared to be independent of the degree of growth restriction, prematurity, or perinatal asphyxia. These findings were supported by those of McDonnell et al., [44] who noted that infants who had AREDV were more likely to start enteral feeds later, receive parenteral nutrition and develop necrotizing enterocolitis more frequently than were a gestational age-matched control group.

There is conflicting evidence on whether AREDV is an independent risk factor for necrotizing enterocolitis. In the European Community Multicenter Study, although proportionately more infants with AREDV developed necrotizing enterocolitis, the difference was not statistically significant ($p = 0.20$) [24]. Other studies have also failed to find AREDV as an independent risk factor [4, 15, 45–47].

In summary, these studies suggest that while AREDV may predispose infants to necrotizing enterocolitis, it is likely not the primary nor sole etiology.

25.12 Hematological Changes

Neonates with AREDV during fetal life are prone to develop hematological anomalies, including anemia and thrombocytopenia. In the European Community Multicenter Study, neonates with absent and reverse EDV had odds ratios of 3.0 and 6.1, respectively, for developing anemia compared to a control group of infants who were growth-restricted but had forward UA end-diastolic flow [24]. The reason for developing anemia independent of prematurity and other known complications remains to be determined.

Neonates with AREDV are at an increased risk of having a low platelet count at birth and are more likely to become significantly thrombocytopenic during the first week of life than are those without Doppler abnormalities. In a study comparing 67 fetuses with an elevated pulsatility index to 48 fetuses with AREDV, Baschat et al. demonstrated that 22 (46%) the 48 fetuses with AREDV had thrombocytopenia compared to 3 (4%) of the 67 fetuses in the control group. Neonates with AREDV had a relative risk of 10.3 in the incidence of thrombocytopenia when compared to that of the control group [48].

Furthermore, neonates with AREDV have been noted to have a higher nucleated red blood cell (nRBC) count than that of the control group. Axt-Fliedner et al. [49] reported an increased number of nucleated red blood cells in the UA at birth in growth-restricted neonates with AREDV compared to those with only an elevated pulsatility index. Moreover, the nucleated red blood cells persisted in the neonatal circulation for a longer period of time in the neonates with AREDV. Other studies have also corroborated these findings [42, 50–52]. While nRBCs may be seen in variable numbers in the newborn circulation, high numbers of nucleated red blood cells in the umbilical cord have been associated with hypoxemia during intrauterine life, hemorrhagic placental vasculitis and infarction and cerebral hemorrhage [41–44], contributing to subsequent neurological impairment. The etiology of erythroblastosis has been attributed to increased erythropoiesis in the fetal liver as a result of chronic hypoxemia. Despite greater RBC production, studies have demonstrated that neonates with a higher number of nRBCs have lower hematocrits, hemoglobin levels, and platelet counts than those with a normal amount [48, 49].

25.13 Hypoglycemia

Infants with AREDV are more likely to become hypoglycemic than are their counterparts without Doppler abnormalities. This finding cannot be fully attributed to prematurity or growth restriction. Infants with AREDV have an odds

ratio of 5.0 for developing hypoglycemia when compared to fetuses with growth restriction but forward end-diastolic velocity in the UA [24]. The etiology of hypoglycemia in neonates with a history of fetal growth restriction is multifactorial. Decreased adipose tissue mass is associated with decreased substrate and, subsequently, the ability to perform oxidative functions for gluconeogenesis. Additionally, these infants have decreased glycogen stores in the muscle and liver. Hormonal dysregulation also likely plays a role, with decreased counter-regulatory hormones, such as glucagon and epinephrine, as well as demonstrated increased insulin sensitivity. Finally, prematurity and sequelae of coexisting morbid conditions, including hypothermia, anemia or polycythemia, and hypoxemia, exacerbate the underlying pathophysiology. The specific etiology for the greater incidence of hypoglycemia in infants with previous AREDV compared to those without UA Doppler abnormalities is yet to be elucidated.

25.14 Neurodevelopmental Sequelae

Any assessment of efficacy of the umbilical arterial Doppler velocimetry for fetal prognostication must encompass immediate and long-term neurological performance and should include moderate-to-severe neurological deficits and also more subtle compromises in cognitive and motor performance. These and other related issues are reviewed in Chap. 12.

25.15 Maternal Hypertension and Absent End-Diastolic Velocity

The most frequent maternal complication seen in conjunction with AREDV is hypertension, predominantly pre-eclampsia. The association of perinatal complications, including pre-eclampsia, with AREDV is reviewed in detail in Chap. 20.

The frequency with which hypertension is associated with AREDV varies from 40 to 70%, and the proportion of hypertensive mothers who develop UA AREDV may be as high as 36% [22]. It is noteworthy that when a pregnancy is complicated by hypertension alone, the risk of developing AREDV is significantly lower than when fetal growth restriction complicates hypertension. This risk was quantified by Karsdorp et al. [24], who noted that in comparison with hypertension, the odds ratio for developing AREDV was 3.1 with growth restriction alone and 7.4 when hypertension was complicated by growth restriction.

Other vasculopathies are also associated with the development of AREDV, including systemic lupus erythematosus and vascular or long-standing diabetes mellitus. As anticipated, these disease processes are also frequently complicated by fetal growth restriction and maternal hypertension.

25.16 Reappearance of End-Diastolic Velocity

Once AREDV develops in the UA, it is usually regarded as a non-reversible phenomenon during the course of progressive fetal decompensation. Several investigators, however, have reported apparent improvement of the hemodynamic situation, as indicated by the reappearance of forward flow during the UA end-diastolic phase. Hanretty et al. [53] were among the first to report the reappearance in a case report in which a mother was treated for hypertension. Subsequently, Brar and Platt [10] reported improvement of the end-diastolic velocity in 5 of 31 cases of AREDV followed closely during hospitalization. The improved fetuses had better perinatal outcomes than did those with continuing AREDV. This observation received support from others. Other studies also reported better perinatal outcomes in pregnancies with improved UA Doppler assessments managed conservatively at bedrest [16, 20]. In these studies, the reappearance of end-diastolic velocity occurred in 19.0–51.5% cases of AREDV and resulted in an increase in the diagnosis-delivery interval by 11–37 days, gestational age by 2–4 weeks and birth weight by 400–1400 g. These results, particularly the frequency of the reappearance and

impressive improvements in the perinatal outcome noted in one of the studies [20], are remarkable, are not encountered in common experience and require corroboration.

In a prospective interventional study, Karsdorp et al. treated a study group of 7 patients with daily volume expansion. The control and study groups were both managed with bedrest and antihypertensives. The Doppler waveform improved in the volume-expansion group, which demonstrated statistically significant improved survival (5/7 in the study and 1/7 in the control group, $p < 0.05$). There were no significant differences between the groups with regard to birth weight or gestational age. Although the results are encouraging, this investigation should be regarded as preliminary because of the lack of randomization and the small sample size. As the authors suggested, randomized trials should be conducted to confirm their observations.

The appearance of AREDV does not necessarily lead to immediate fetal demise. Days to weeks may pass before the emergence of other ominous signs of fetal jeopardy necessitating delivery. In some cases, as noted above, the end-diastolic velocity returns and the fetal risk may be diminished. It is not known how frequently this pattern of improvement occurs. On rare occasions, Doppler abnormalities may appear suddenly and may not follow an expected progression. As demonstrated in Fig. 25.5, an apparently normal waveform rapidly changed to absent, then reversal of end-diastolic flow occurred, returning quickly to baseline in a discordant, presumed donor twin. Although the hemodynamic mechanism of this phenomenon remains to be elucidated, the fetus eventually developed persistent AREDV. Variable end-diastolic velocity in the UA of a donor fetus with twin-to-twin transfusion syndrome has been documented [54]. The UA end-diastolic velocity in the donor fluctuated between positive, absent, and reversed. Eventually, the fetus was delivered at 28 weeks due to fetal distress of the donor. A velamentous cord insertion, suspected during ultrasound evaluation, was confirmed.

In summary, a variable absence of the UA end-diastolic velocity should prompt close monitoring as its prognostic assurance is uncertain.

25.17 Sequence of Changes in Fetal Surveillance Parameters with Progressive Antepartum Fetal Compromise

The homeostatic significance of absent end-diastolic velocity in relation to alterations in other components of the fetal circulation and other parameters of fetal well-being needs clarification. The diagnostic efficacy of abnormal fetal Doppler indices has been reviewed in Chap. 24. Although some degree of overlap is inevitable, the focus of this chapter is specifically on the umbilical arterial AREDV. Reports provide considerable insights into this area. Teyssier et al. [55] observed in an animal model a hierarchical sequence in the decline of the end-diastolic flow when feto-placental vascular resistance increased; flow in the aortic isthmus was first affected, followed by flow in the descending aorta and the UA. Subsequent studies in human pregnancies were mostly confirmatory of this sequence [56].

Bekedam et al. [13] performed longitudinal measurements of the umbilical arterial PI in 29 growth-restricted fetuses with antepartum late heart rate decelerations. In 17 of these fetuses (59%), AEDV preceded the occurrence of decelerations, with a median interval of 12 days.

Arduini et al. [57] evaluated 37 fetuses without structural and chromosomal abnormalities regarding the various maternal and fetal factors that affect the time interval between the occurrence of AEDV in the UA and either the development of abnormal fetal heart rate patterns or delivery. The interval between the first occurrence of umbilical arterial AEDV and delivery ranged from 1 to 26 days. Multivariate analysis revealed that gestational age, the presence of hypertension and the appearance of umbilical venous pulsation are the principal determinants of this time interval.

Weiner et al. [58] studied hemodynamic changes in the middle cerebral artery and the aortic and pulmonic outflow tracts, correlating these changes with the computerized fetal heart rate pattern in fetuses with AREDV in the UA. They observed that when the middle cerebral artery

began to lose its compensatory vasodilatation, other ominous fetal cardiovascular signs emerged, including decreases in the left cardiac output ($p < 0.05$) and the fetal heart rate's long-term variability (<30 ms) and the occurrence of repetitive fetal heart rate decelerations. These observations contribute to elucidation of the evolving cardiovascular responses to progressive fetal decompensation and should lead to the development of more effective fetal surveillance and clinical intervention.

James et al. [59] evaluated the chronology of the abnormalities of: (1) UA Doppler results, (2) fetal growth as indicated by ultrasound measurement of the fetal abdominal circumference and (3) biophysical profile score. The retrospective study of 103 fetuses at a risk of chronic fetal asphyxia revealed that the UA Doppler results deteriorated first, followed by the abdominal circumference and then the biophysical profile score. Whereas an abnormality of one of these parameters in isolation did not result in any adverse consequences, an abnormality of all three ultrasonographic features led to the worst outcome.

A prospective longitudinal study was conducted by Hecher et al. [60], in which 110 singleton pregnancies with growth-restricted fetuses after 24 weeks' gestation were included. The first variables to become abnormal were the amniotic fluid index and the UA-PI. Abnormalities of the middle cerebral artery, aorta, fetal heart rate's short-term variation, ductus venosus, and inferior vena cava then followed. The decrease in the PI of the middle cerebral artery followed the abnormalities in the umbilical PI and became progressively abnormal until delivery in the pregnancies delivered before 32 weeks. In the pregnancies delivered after 32 weeks, the authors found a normalization of the middle cerebral artery PI before abnormalities in the fetal heart rate.

Baschat et al. [61] longitudinally examined 44 growth-restricted fetuses with an elevated UA-PI (>2 standard deviations above mean) and birth weight below the tenth percentile who required delivery for abnormal scores in the biophysical profile. First, there was a change in the Doppler variables. In 42 (95.5%) fetuses, one or more of the Doppler variables were abnormal. The UA and ductus venosus PI abnormalities progressed rapidly at a median of 4 days before the biophysical profile worsened. Fetal breathing movement began to decline 2–3 days before delivery, followed by a decrease in the amniotic fluid volume. Loss of fetal movement and tone was observed on the day of the delivery. Additionally, in 31 fetuses, deterioration in the Doppler parameters was completed 23 h before a worsening of the biophysical profile, whereas in 11 fetuses, deterioration of the Doppler parameters and the biophysical profile occurred simultaneously.

Ferrazzi et al. [62] prospectively investigated the temporal sequence of Doppler changes in the fetal circulation in 26 women with early-onset FGR and abnormal umbilical and uterine arteries and observed sequential Doppler changes in the various components of the fetal circulation. In 50% of patients, UA and MCA Doppler showed abnormality 15–16 days prior to delivery. Reverse end-diastolic flow in the UA and abnormalities in the ductus venosus and aortic and pulmonary outflows were noted in 50% of the mothers 4–5 days before the delivery. The latter findings were associated with significantly increased perinatal mortality.

In summary, these reports suggest a sequence of Doppler deterioration from the UA, the MCA and then to the DV, reflecting progression from an increasing impedance in the feto-placental circulation followed by compensatory flow redistribution with cerebral vasodilation culminating in right heart dysfunction.

This sequence, however, was refuted by Unterscheider et al., who conducted a multicenter prospective observational study involving more than 1100 singleton pregnant patients with FGR (estimated fetal weight < tenth centile) and failed to confirm a dominant pattern of sequential Doppler compromise [63]. The authors also noted that Doppler assessment of the UA and MCA identified 88% of all adverse outcomes (Figs. 25.6 and 25.7).

More recently, these findings have been contradicted by Morales-Roselló et al., who retrospectively investigated the progression of hemodynamic deterioration in the UA, middle

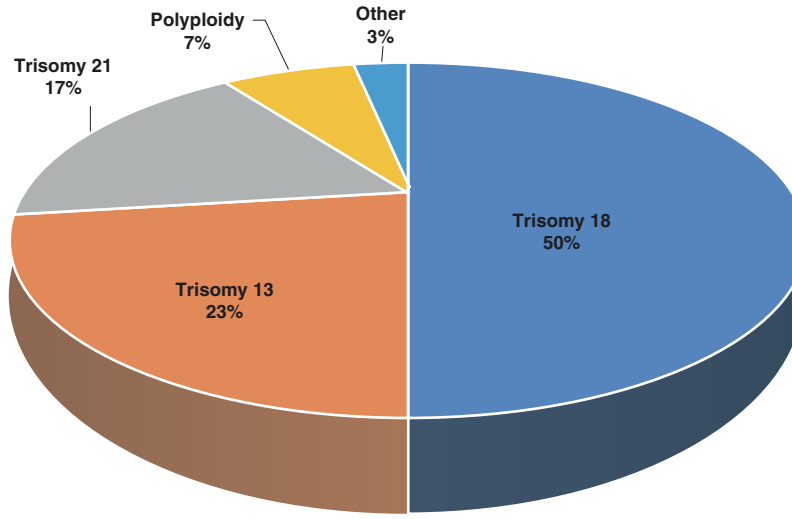

Fig. 25.6 Relative frequency of the various chromosomal abnormalities associated with umbilical arterial absent end-diastolic velocity

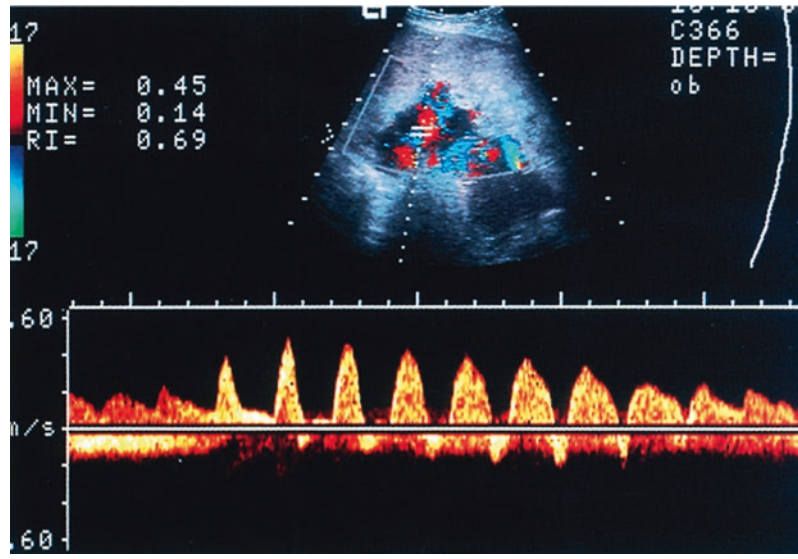

Fig. 25.7 Doppler sonogram of the umbilical artery showing transient absence and reversal of end-diastolic velocity followed by prompt recovery of a discordant twin

cerebral artery and ductus venosus utilizing Doppler ultrasound between 24 and 33 weeks' gestation in more than 400 fetuses with early-onset growth restriction [64]. In more than 70% of the cases, the Doppler evidence of fetal hemodynamic deterioration progressed from the UA, the middle cerebral artery, and then to the ductus venosus (Fig. 25.8).

The sequential fetal hemodynamic changes as discussed above may not be applicable to term and near-term FGR. Several investigators have recently reported that middle cerebral artery Doppler and the cerebroplacental ratio (CPR) are superior to UA Doppler in predicting adverse perinatal outcomes [65–67]. The Royal College of *Obstetricians and Gynecologists actually recommends* that MCA Doppler should guide the timing of the delivery in term small-for-gestational-age fetuses [68]. This approach, however, is not supported by the American College *Obstetricians and Gynecologists* [65]. Despite the positive observational studies, so far, there have been no randomized trials of the effectiveness of cerebral Doppler in improving

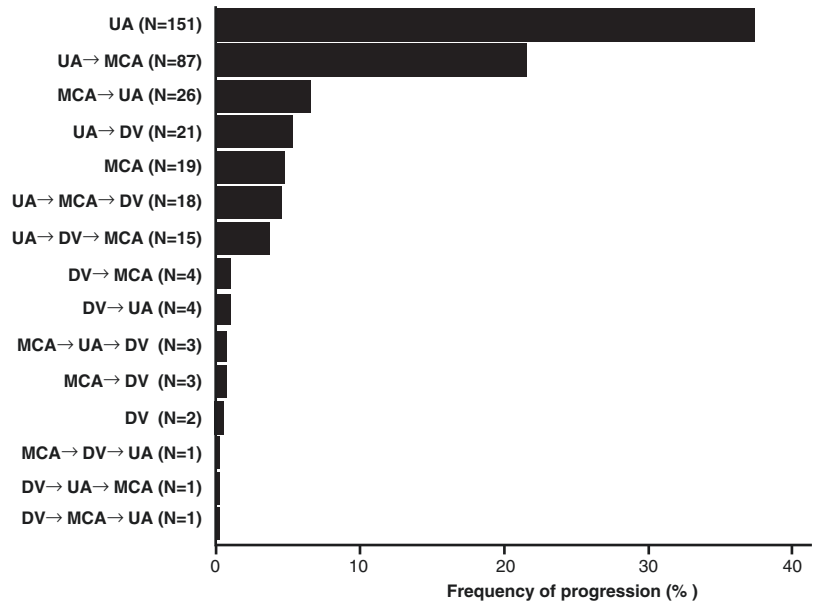

Fig. 25.8 Sequence of progression for Doppler anomalies observed in the studied group of small-for-gestational-age fetuses. A total of 71% of cases coincided with the progressive sequence of abnormal values in the UA-PI, MCA-PI, and DV-PIV. Exceptions to this scenario occur mostly in the last stages of the hemodynamic progression (with permission from Morales-Roselló et al. *J Maternal-Fetal Neonatal Med.* 2018.18;31:1000–8) [64]

perinatal outcomes. There is also a dearth of trials on the effectiveness of MCA Doppler. To our knowledge, there is only one randomized trial of the CPR (MCA to UA systolic/diastolic ratio) involving 665 high-risk pregnancies, which demonstrated no improvement in perinatal outcomes when the CPR was added to the biophysical profile (BPP) [66]. However, in those at risk of uteroplacental insufficiency such as hypertensive diseases, addition of the CPR significantly reduced cesarean sections. Although pioneering, the study was underpowered to be conclusive.

As evident in this chapter, UA AREDV is associated with adverse perinatal mortalities and morbidities. Most fetuses with AREDV require neonatal intensive care. Absent end-diastolic flow may transiently improve. In early-onset FGR, fetal Doppler reflects progressive sequential hemodynamic deterioration, although the existence of a dominant pattern is controversial.

References

1. Rochelson B, Schulman H, Framakides G, et al. The significance of absent end-diastolic velocity in umbilical artery velocity waveforms. Am J Obstet Gynecol. 1987;156:1213–8.
2. Woo JS, Liang ST, Lo RL. Significance of an absent or reversed end diastolic flow in Doppler umbilical artery waveforms. J Ultrasound Med. 1987;6:291–7.
3. Reuwer PJ, Sijmons EA, Rietman GW, van Tiel MW, Bruines HW. Intrauterine growth retardation: prediction of perinatal distress by Doppler ultrasound. Lancet. 1987;2:415–8.
4. Hackett GA, Campbell S, Gamsu H, Cohen-Overbeek T, Pearce JM. Doppler studies in the growth retarded fetus and prediction of neonatal necrotising enterocolitis, haemorrhage, and neonatal morbidity. BMJ. 1987;294:13–6.
5. Arabin B, Siebert M, Jimenez E, Saling E. Obstetrical characteristics of a loss of end-diastolic velocities in the fetal aorta and/or umbilical artery using Doppler ultrasound. Gynecol Obstet Invest. 1988;25:173–80.
6. Hsieh FJ, Chang FM, Ko TM, Chen HY, Chen YP. Umbilical artery flow velocity waveforms in fetuses dying with congenital anomalies. Br J Obstet Gynaecol. 1988;95:478–82.
7. Johstone FD, Haddad NG, Hoskins P, et al. Umbilical artery Doppler flow velocity waveform: the outcome of pregnancies with absent end diastolic flow. Eur J Obstet Gynecol Reprod Biol. 1988;28:171–8.
8. Brar HS, Platt LD. Reverse end-diastolic flow velocity on umbilical artery velocimetry in high-risk pregnancies: an ominous finding with adverse pregnancy outcome. Am J Obstet Gynecol. 1988;159:559–61.
9. Tyrrell S, Obaid AH, Lilford RJ. Umbilical artery Doppler velocimetry as a predictor of fetal hypoxia and acidosis at birth. Obstet Gynecol. 1989;74:332–7.
10. Brar HS, Platt LD. Antepartum improvement of abnormal umbilical artery velocimetry: does it occur? Am J Obstet Gynecol. 1989;160:36–9.

11. Divon MY, Girz BA, Lieblich R, Langer O. Clinical management of the fetus with markedly diminished umbilical artery end-diastolic flow. Am J Obstet Gynecol. 1989;161:1523–7.
12. McParland P, Steel S, Pearce JM. The clinical implications of absent or reversed end-diastolic frequencies in umbilical artery flow velocity waveforms. Eur J Obstet Gynecol Reprod Biol. 1990;37:15–23.
13. Bekedam DJ, Visser GH, van der Zee AG, Snijders RJ, Poelmann-Weesjes G. Abnormal velocity waveforms of the umbilical artery in growth retarded fetuses: relationship to antepartum late heart rate decelerations and outcome. Early Hum Dev. 1990;24:79–89.
14. Huneke B, Carstensen MH, Schroder HJ, Gunther M. Perinatal outcome in fetuses with loss of end-diastolic blood flow velocities in the descending aorta and/or umbilical arteries. Gynecol Obstet Invest. 1991;32:167–72.
15. Malcolm G, Ellwood D, Devonald K, Beilby R, Hender-son-Smart D. Absent or reversed end diastolic flow velocity in the umbilical artery and necrotising enterocolitis. Arch Dis Child. 1991;66:805–7.
16. Sengupta S, Harrigan JT, Rosenberg JC, Davis SE, Knuppel RA. Perinatal outcome following improvement of abnormal umbilical artery velocimetry. Obstet Gynecol. 1991;78:1062–6.
17. Wenstrom KD, Weiner CP, Williamson RA. Diverse maternal and fetal pathology associated with absent diastolic flow in the umbilical artery of high-risk fetuses. Obstet Gynecol. 1991;77:374–8.
18. Schmidt W, Ruhle W, Ertan AK, Boos R, Gnirs J. Doppler ultrasonography—perinatal data in cases with end-diastolic block and reverse flow. Geburtshilfe Frauenheilk. 1991;51:288–92.
19. Weiss E, Ulrich S, Berle P. Condition at birth of infants with previously absent or reverse umbilical artery end-diastolic flow velocities. Arch Gynecol Obstet. 1992;252:37–43.
20. Bell JG, Ludomirsky A, Bottalico J, Weiner S. The effect of improvement of umbilical artery absent end-diastolic velocity on perinatal outcome. Am J Obstet Gynecol. 1992;167:1015–20.
21. Pattinson RC, Hope P, Imhoff R, et al. Obstetric and neonatal outcome in fetuses with absent end-diastolic velocities of the umbilical artery: a case-con-trolled study. Am J Perinatol. 1993;10:135–8.
22. Pattinson RC, Odendaal HJ, Kirsten G. The relationship between absent end-diastolic velocities of the umbilical artery and perinatal mortality and morbidity. Early Hum Dev. 1993;33:61–9.
23. Battaglia C, Artini PG, Galli PA, et al. Absent or reversed end-diastolic flow in umbilical artery and severe intrauterine growth retardation: an ominous association. Acta Obstet Gynecol Scand. 1993;72:167–71.
24. Karsdorp VH, van Vugt JM, van Geijn HP, et al. Clinical significance of absent or reversed end diastolic velocity waveforms in umbilical artery. Lancet. 1994;344:1664–8.
25. Rizzo G, Pietropolli A, Capponi A, Arduini D, Romanini CC. Chromosomal abnormalities in fetuses with absent end-diastolic velocity in umbilical artery: analysis of risk factors for an abnormal karyotype. Am J Obstet Gynecol. 1994;171:827–31.
26. Poulain P, Palaric JC, Milon J, et al. Absent end diastolic flow of umbilical artery Doppler: pregnancy outcome in 62 cases. Eur J Obstet Gynecol Reprod Biol. 1994;53:115–9.
27. Beattie RB, Dornan JC. Antenatal screening for intrauterine growth retardation with umbilical artery Doppler ultrasonography. BMJ. 1989;298:631–5.
28. Nkosi S, Makin J, Hlongwane T, Pattinson RC. Screening and managing a low-risk pregnant population using continuous-wave Doppler ultrasound in a low-income population: a cohort analytical study. SAMJ. 2019;109:347–52.
29. Caradeux J, Martinez-Portilla RJ, Basuki TR, et al. Risk of fetal death in growth-restricted fetuses with umbilical and/or ductus venosus absent or reversed end-diastolic velocities before 34 weeks of gestation: a systematic review and meta-analysis. Am J Obstet Gynecol. 2018;218(2S):S774–S782.e21.
30. Martinez JM, Antolin E, Borrell A, Puerto B, Casals E, Ojuel J, Fortuny A. Umbilical Doppler velocimetry in fetuses with trisomy 18 at 10–18 weeks' gestation. Prenat Diagn. 1997;17:319–22.
31. Borrell A, Martinez JM, Farre MT, Azulay M, Cararach V, Fortuny A. Reversed end-diastolic flow in first-trimester umbilical artery: an ominous new sign for fetal outcome. Am J Obstet Gynecol. 2001;185:204–7.
32. Snijders RJ, Sherrod C, Gosden CM, Nicolaides KH. Fetal growth retardation: associated malformations and chromosomal abnormalities. Am J Obstet Gynecol. 1993;168:547–55.
33. Rochelson B, Kaplan C, Guzman E, et al. A quantitative analysis of placental vasculature in the third-trimester fetus with autosomal trisomy. Obstet Gynecol. 1990;75:59–63.
34. Nicolaides KH, Bilardo CM, Soothill PW, Campbell S. Absence of end-diastolic frequencies in umbilical artery: a sign of fetal hypoxia and acidosis. BMJ. 1988;297:1026–7.
35. Ashmead GG, Lazebnik N, Ashmead JW, Stepanchak W, Mann LI. Normal blood gases in fetuses with absence of end-diastolic umbilical artery velocity. Am J Perinatol. 1993;10:67–70.
36. Warren W, Ronkin S, Chayen B, Needleman L, Wapne RJ. Absence of end-diastolic umbilical artery blood flow predicts poor fetal outcome despite normal blood gases. Am J Obstet Gynecol. 1989;160:197.
37. Adiotomre PN, Johnstone FD, Laing IA. Effect of absent end diastolic flow velocity in the fetal umbilical artery on subsequent outcome. Arch Dis Child Fetal Neonatal Ed. 1997;76:35–8.
38. Spinillo A, Montanari L, Bergante C, Gaia G, Chiara A, Fazzi E. Prognostic value of umbilical artery Doppler studies in unselected preterm deliveries. Obstet Gynecol. 2005;105:613–20.
39. Al-Ghazali W, Chita SK, Chapman MG, Allan LD. Evidence of redistribution of cardiac output in asymmetrical growth retardation. Br J Obstet Gynaecol. 1989;96:697–704.

40. Wilcox GR, Trudinger BJ. Fetal platelet consumption: a feature of placental insufficiency. Obstet Gynecol. 1991;77:616–21.
41. Steiner H, Staudach A, Spitzer D, Schaffer KH, Gregg A, Weiner CP. Growth deficient fetuses with absent or reversed umbilical artery end-diastolic flow are metabolically compromised. Early Hum Dev. 1995;41:1–9.
42. Phelan JP, Korst LM, Ahn MO, Martin GI. Neonatal nucleated red blood cell and lymphocyte counts in fetal brain injury. Obstet Gynecol. 1998;91:485–9.
43. Viscardi RM, Sun CC. Placental lesion multiplicity: risk factor for IUGR and neonatal cranial ultrasound abnormalities. Early Hum Dev. 2001;62:1–10.
44. McDonnell M, Serra-Serra V, Gaffney G, Redman CW, Hope PL. Neonatal outcome after pregnancy complicated by abnormal velocity waveforms in the umbilical artery. Arch Dis Child. 1994;70:F84–9.
45. Kirsten GF, van Zyl N, Smith M, Odendaal H. Necrotizing enterocolitis in infants born to women with severe early preeclampsia and absent end-diastolic umbilical artery Doppler flow velocity waveforms. Am J Perinatol. 1999;16:309–14.
46. Gonzalez JM, Stamilio DM, Ural S, Macones GA, Odibo AO. Relationship between abnormal fetal testing and adverse perinatal outcomes in intrauterine growth restriction. Am J Obstet Gynecol. 2007;196(5):e48–51.
47. Manogura AC, Turan O, Kush ML, et al. Predictors of necrotizing enterocolitis in preterm growth-restricted neonates. Am J Obstet Gynecol. 2008;198:638.e1–5.
48. Baschat AA, Gembruch U, Reiss I, Gornter L, Weiner CP, Harman CR. Absent umbilical artery end-diastolic velocity in growth-restricted fetuses: a risk factor for neonatal thrombocytopenia. Obstet Gynecol. 2000;96:162–6.
49. Axt-Fliedner R, Hendrik HJ, Schmidt W. Nucleated red blood cell counts in growth-restricted neonates with absent or reversed-end-diastolic umbilical artery velocity. Clin Exp Obstet Gynecol. 2002;29:242–6.
50. Alawani SS, Prakash R, Kumar GM, Rudrappa S, Krishnamurthy B. Predictive ability of venous blood nucleated red blood cells counts in term infants with perinatal asphyxia: a diagnostic study. J Clin Neonatol. 2018;7:250–3.
51. Mirunalini S. Nucleated RBCs in cord blood as a predictor of fetal asphyxia. IAIM. 2018;5(9):48–53.
52. Boskabadi H, Maamouri G, Sadeghian MH, Ghayour-Mobarhan M, Heidarzade M, Shakeri MT, Ferns G. Early diagnosis of perinatal asphyxia by nucleated red blood cell count: a case-control study. Arch Iran Med. 2010;13(4):275–81. https://doi.org/010134/AIM.005.
53. Hanretty KP, Whittle MJ, Rubin PC. Reappearance of end-diastolic velocity in a pregnancy complicated by severe pregnancy-induced hypertension. Am J Obstet Gynecol. 1988;158:1123–4.
54. Kush ML, Jenkins CB, Baschat AA. Variable umbilical artery end-diastolic velocity: a possible sign of velamentous cord insertion in monochorionic gestation. Ultrasound Obstet Gynecol. 2003;21:95–6.
55. Teyssier G, Fouron JC, Maroto D, Sonesson SE, Bonnin P. Blood flow velocity in the fetal aortic isthmus: a sensitive indicator of changes in systemic peripheral resistance. I. Experimental studies. J Matern Fetal Invest. 1993;3:213–8.
56. Fouron JC, Teyssier G, Bonnin P, et al. Blood flow velocity in the fetal aortic isthmus: a sensitive indicator of changes in systemic peripheral resistances. II. Preliminary observations. J Matern Fetal Invest. 1993;3:219–24.
57. Arduini D, Rizzo G, Romanini C. The development of abnormal heart rate patterns after absent end-diastolic velocity in umbilical artery: analysis of risk factors. Am J Obstet Gynecol. 1993;168:43–50.
58. Weiner Z, Farmakides G, Schulman H, Penny B. Central and peripheral hemodynamic changes in fetuses with absent end-diastolic velocity in umbilical artery; correlation with computerized fetal heart rate pattern. Am J Obstet Gynecol. 1994;170:509–15.
59. James DK, Parker MJ, Smoleniec JS. Comprehensive fetal assessment with three ultrasonographic characteristics. Am J Obstet Gynecol. 1992;166:1486–95.
60. Hecher K, Bilardo CM, Stigter RH, et al. Monitoring of fetuses with intrauterine growth restriction: a longitudinal study. Ultrasound Obstet Gynecol. 2001;18:564–70.
61. Baschat AA, Gembruch U, Harman CR. The sequence of changes in Doppler and biophysical parameters as severe fetal growth restriction worsens. Ultrasound Obstet Gynecol. 2001;18:571–7.
62. Ferrazzi E, Bozzo M, Rigano S, Bellotti M, Morabito A, Pardi G, Battaglia FC, Galan HL. Temporal sequence of abnormal Doppler changes in the peripheral and central circulatory systems of the severely growth-restricted fetus. Ultrasound Obstet Gynecol. 2002;19:140–6.
63. Unterscheider J, Daly S, Geary MP, et al. Predictable progressive Doppler deterioration in IUGR: does it really exist? Am J Obstet Gynecol. 2013;209:539.e1–7.
64. Morales-Roselló J, Khalil A, Fornés-Ferrer V, Alberola-Rubio J, Hervas-Marín D, Peralta Llorens N, Perales-Marín A. Progression of Doppler changes in early-onset small for gestational age fetuses. How frequent are the different progression sequences? J Matern Fetal Neonatal Med. 2018;18(31):1000–8.
65. American College of Obstetricians and Gynecologists. ACOG practice bulletin no. 204. Fetal growth restriction. Obstet Gynecol. 2019;133:e97–e109.
66. Ott WJ, Mora G, Arias F, Sunderji S, Sheldon G. Comparison of the modified biophysical profile to a "new" biophysical profile incorporating the middle cerebral artery to umbilical artery velocity flow systolic/diastolic ratio. Am J Obstet Gynecol. 1998;178:1346–53.

67. Karsdorp VH, van Vugt JM, Dekker GA, van Geijn HP. Reappearance of end-diastolic velocities in the umbilical artery following maternal volume expansion: a preliminary study. Obstet Gynecol. 1992;80:679–83.

68. Royal College of Obstetricians and Gynecologists. Small-for-gestational-age fetus, investigation and management (green-top guideline no. 31); 2013.

26 Fetal Doppler Velocimetry in High-Risk Pregnancies: Randomized Clinical Trials

Christoph C. Lees and T. Stampalija

26.1 Introduction

Doppler technology has spread progressively with advances in ultrasound machines' performance, operators' training, and better understanding of the physiopathology of the feto-placental circulation in pathologies such as fetal growth restriction, hypertensive disorders in pregnancy, and twin pregnancies among others. For example, the cascade of Doppler changes in early fetal growth restriction, caused by uteroplacental insufficiency, and its association with an adverse perinatal outcome is now well-known [1–3]. The identification of hypoxia and acidemia constitutes the rationale for using Doppler ultrasound as one of the main tools for fetal well-being assessment and management in fetal growth restriction [4, 5]. Similarly, the management of monochorionic twin pregnancy [6] or fetal anemia [7] is unthinkable without Doppler ultrasound assessment of specific vascular domains. Although not universally adopted, Doppler of the uterine arteries, first applied in the mid-trimester [8, 9], represents one of the main components of first-trimester screening of preterm pre-eclampsia and fetal growth restriction [10, 11]. Hence, the application of Doppler ultrasound in high-risk pregnancies has become a standard clinical practice worldwide.

On the other hand, multiple Doppler interrogations of vascular districts may also cause false-positive findings, consequent unnecessary interventions, and potential adverse outcomes such as prematurity and patient and physician anxiety. Last but not least, for some widespread Doppler ultrasound applications, such as the assessment of the middle cerebral artery in fetal growth restriction, there is no high-quality evidence for its value, leading to variable clinical practice and management.

In this chapter, we will summarize the evidence from randomized clinical trials on Doppler velocimetry in high-risk pregnancies with a particular focus on fetal growth restriction and the effect of its application on maternal and fetal outcomes.

C. C. Lees (✉)
Department of Metabolism, Digestion and Reproduction, Imperial College Hospitals NHS Trust, London, UK

Centre for Fetal Care, Queen Charlotte's and Chelsea Hospital, Imperial College Hospitals NHS Trust, London, UK
e-mail: christoph.lees@nhs.net

T. Stampalija
Unit of Fetal Medicine and Prenatal Diagnosis, Institute for Maternal and Child Health, IRCCS Burlo Garofolo, Trieste, Italy

Department of Medicine, Surgery and Health Sciences, University of Trieste, Trieste, Italy
e-mail: tamara.stampalija@burlo.trieste.it

D. Maulik, C. C. Lees (eds.), *Doppler Ultrasound in Obstetrics and Gynecology*,
https://doi.org/10.1007/978-3-031-06189-9_26

26.2 Trials of Umbilical Artery Doppler in High-Risk Pregnancies

26.2.1 Evidence from Randomized Studies

The Cochrane Systematic Review and meta-analysis on randomized and quasi-randomized controlled trials on fetal and umbilical Doppler ultrasound in high-risk pregnancies [12] reported 18 studies that compared the use of umbilical artery Doppler with no-Doppler (or Doppler not revealed to clinicians). In 14 studies, umbilical artery Doppler was used in addition to the standard fetal monitoring strategy [13–26], whereas in 4 studies, umbilical artery Doppler was evaluated compared to cardiotocography [27–30]. Table 26.1 shows the characteristics of the included studies in this meta-analysis. It should be noted that two of the included studies evaluated the Doppler of the umbilical and uteroplacental arteries [19, 26]: one evaluated the Doppler of the umbilical artery and aorta [21] and the other evaluated the middle cerebral to umbilical artery velocity flow systolic/diastolic ratio [23].

The pooled data of the use of umbilical artery Doppler ultrasound in high-risk pregnancies showed fewer perinatal deaths (risk ratio (RR) 0.71, 95% confidence interval (CI) 0.52–0.98, 16 studies, 10,225 babies, 1.2% versus 1.7% number needed to treat (NNT) 203, 95% CI 103–4352, evidence graded as moderate) [12]. The findings for stillbirths and neonatal deaths were similar, showing fewer adverse outcomes in the Doppler group, although these did not reach statistical significance (stillbirth: RR 0.65, 95% CI 0.41–1.04, 15 studies, 9560 babies, evidence graded as low; neonatal deaths: RR 0.81, 95% CI 0.53–1.24, 8167 babies, 13 studies) [12]. Only three studies reported relevant neonatal morbidity data [19, 22, 26]. However, the heterogeneity was high and the quality of evidence extremely low, making the analysis uncertain [12].

Moreover, the use of umbilical artery Doppler was associated with fewer inductions of labor and fewer cesarean sections (induction of labor: RR 0.89, 95% CI 0.80–0.99, 10 studies, 5633 women, evidence graded as moderate; cesarean section: RR 0.90, 95% CI 0.84–0.97, 14 studies, 7918 women, evidence graded as moderate) [12]. Data for serious neonatal morbidity could not be pooled due to high heterogeneity between the studies. Finally, although not a pre-specified outcome, there were fewer antenatal admissions in the Doppler group (RR 0.72, 95% CI 0.60–0.88, 839 women, 2 studies) [12].

Four trials [27–30] compared the umbilical artery Doppler assessment with cardiotocography assessment. However, for this comparison, there was insufficient evidence to detect a significant difference in perinatal mortality.

In summary, as presented in Table 26.2, these data suggest that the use of umbilical artery Doppler ultrasound, with or without cardiotocography, in high-risk pregnancies reduces the risk of perinatal deaths and reduces obstetric interventions compared to no-Doppler [12].

However, it has to be acknowledged that this meta-analysis included all pregnancies defined to be at a higher risk of fetal compromise, such as fetal growth restriction, post-term pregnancies, multiple pregnancies, previous pregnancy loss, women with hypertension, women with diabetes or other maternal pathologies. When a subgroup analysis was performed (i.e., only singleton or multiple or only small for gestational age or fetal growth restriction), there was no evidence of the treatment effect. There are five randomized controlled trials that assessed Doppler in the umbilical artery versus no-Doppler ultrasound in women with suspected small-for-gestational-age/growth-restricted fetuses [18, 20, 24, 27, 28]; only one study assessed the role of Doppler ultrasound in the umbilical artery versus no-Doppler ultrasound in pregnancies complicated by hypertension or pre-eclampsia [24] and only one study assessed the role of Doppler ultrasound in the umbilical artery versus no-Doppler ultrasound in women with previous pregnancy loss [22]. There were no significant differences in terms of perinatal mortality in the treatment group versus that in the no-treatment group (small-for-gestational-age/fetal growth restriction group: RR 0.72, 95% CI 0.38–1.35, 1292 women, 5 studies; hypertensive disorders in pregnancy group: RR 3.57, 95%

Table 26.1 Characteristics of the included studies in the cochrane meta-analysis (adapted from Alfirevic et al. 2017) [12]

Study	Participants	Number of participants	Intervention	Comparison	Outcomes	Notes
Almstrom, 1992 [27]	Singleton pregnancies with suspected FGR at 31 completed gestational weeks	427	Doppler of the umbilical artery only	CTG only	Primary: GA at delivery, frequency of CS, vacuum, forceps, operative delivery for fetal distress, length of stay at the NICU Secondary: number of fetal monitoring occasions, duration of antenatal hospital stay, frequency of labor induction, birth weight, frequency of small-for-date infants, Apgar score at 1 min and 5 min, need for respiratory support	
Biljan, 1992 [13]	High-risk singleton pregnancies	674	Doppler of the umbilical artery	No-Doppler	Elective births; GA at birth; birth weight; Apgar scores, admissions to the NICU, length of time in the NICU, number of babies ventilated, length of ventilation, perinatal mortality	Poster presentation
Burke, 1992 [14]	High-risk pregnancies (suspected FGR, HDP, previous birth weight <2.5 kg, antepartum hemorrhage, previous perinatal death, diminished fetal movements, post-maturity, diabetes, and others)	476	Doppler of the umbilical artery, fetal biometry, and BPP scoring	Fetal biometry and BPP scoring	Induction of labor, elective and emergency CS, preterm delivery, and perinatal loss	
De Rochambeau, 1992 [15]	Singleton post-term pregnancies	107	Doppler of the umbilical artery	No-Doppler	CS, RDS, and post-maturity	

(continued)

Table 26.1 (continued)

Study	Participants	Number of participants	Intervention	Comparison	Outcomes	Notes
Giles, 2003 [16]	Twin pregnancies (monochorionic and dichorionic) at 25 weeks	539	Doppler of the umbilical artery and biometry at 25, 30, and 35 weeks; advised to undertake interventions if there was an abnormal umbilical artery Doppler (>95th centile S/D ratio) or abnormal biometry, indicating discordant growth. The suggested intervention was intensive surveillance by obstetric caregivers; if other indicators of fetal well-being (lack of serial growth, decreased amniotic fluid or abnormal fetal monitoring) were abnormal, then early delivery was advised >25 weeks; an abnormality of Doppler waveforms themselves was not considered an indication for immediate delivery unless there was an absence of diastolic flow velocity at >32 weeks	Biometry at 25, 30, and 35 weeks	Maternal: antenatal admission, presence of hypertension, gestation at delivery, indication for delivery, and mode of delivery Fetal: biometry measurements, umbilical artery Doppler systolic diastolic ratios and the occurrence of fetal death and causative factors Neonatal: birth weight, Apgar scores, admission to NICU, admission to special care nursery, requirements for ventilation, and occurrence of neonatal death (up to 28 days of life)	
Haley, 1997 [28]	Singleton pregnancies at risk of FGR >26 weeks	150	Only Doppler of the umbilical artery	Only CTG	Duration of hospital antenatal admission, induction of labor rate; number of investigations (CTG or Doppler), number of outpatient visits to hospital, emergency CS rate, length of stay in the NICU, birth weight and 1 min and 5 min Apgar score; women views on their care	
Hofmeyr, 1991 [29]	Women of a high-risk obstetric unit	867	Doppler of the umbilical artery	cCTG	Number and duration of tests; perinatal outcomes	

Johnstone, 1993 [17]	Pregnancies identified clinically as being at increased risk	2289	Doppler of the umbilical artery and standard monitoring (CTG/BPP)	Standard monitoring (CTG/BPP)	Fetal mortality and morbidity; obstetric interventions; use of other tests of fetal monitoring; impact on obstetric decision-making; health and personal costs; women's satisfaction	
Neals, 1994 [18]	Singleton pregnancy with FGR >24 weeks	467	Doppler of the umbilical artery revealed	Doppler of the umbilical artery concealed	Obstetric management: gestation at birth, time from enrolment to birth, mode of birth/onset of labor, fetal distress in labor Neonatal outcome: perinatal mortality, birth weight, admission to the NICU, neonatal outcome	Personal communication
Newnham, 1991 [19]	High-risk pregnancies, singleton and twins, stratified for twins	505	Doppler of the umbilical and uteroplacental (within the placental bed) arteries	No-Doppler	Primary: duration of neonatal stay in hospital Secondary: number and type of fetal heart monitoring studies, obstetric interventions, frequency of fetal distress, birth weight, Apgar score, and need for a NICU	
Nienhuis, 1997 [20]	Singleton pregnancies at risk of FGR	161	Doppler of the umbilical artery revealed	Doppler of the umbilical artery concealed	Effect on costs in terms of hospitalization, perinatal outcome, neurological development and postnatal catch-up growth, onset and mode of birth, birth weight and GA at birth	
Nimrod, 1992 [21]	Women post-term (>40 weeks)		Doppler of the umbilical artery and fetal aorta revealed, BPP and CTG	Doppler of the umbilical artery and fetal aorta concealed, BPP and CTG	CS; gestation at birth; meconium in amniotic fluid; need for phototherapy	Conference abstract
Norman, 1992 [22]	High-risk pregnancies with recurrent pregnancy loss (two or more mid-trimester or early third-trimester losses, which resulted in IUFD, stillbirth or neonatal death) >24 weeks	564	Doppler of the umbilical artery revealed	Doppler of the umbilical artery concealed	Maternal intervention, hospital stay, induction of labor, CS, perinatal mortality and morbidity	Conference abstract

(continued)

Table 26.1 (continued)

Study	Participants	Number of participants	Intervention	Comparison	Outcomes	Notes
Ott, 1998 [23]	High-risk pregnancies (risk of uteroplacental insufficiency, fetal risk, post-dates, maternal diabetes, PROM/PTL and fluid abnormalities)	715	Fetal and umbilical artery Doppler, modified BPP	Modified BPP	Primary outcome: neonatal morbidity rate (admission to the NICU, length of stay in the NICU, significant neonatal morbidity) Secondary outcome: GA at delivery, neonatal weight, CS for fetal distress	
Pattison, 1994 [24]	Singleton pregnancies with HDP and/or SGA >28 weeks	212	Doppler of the umbilical artery revealed and standard care	Doppler of the umbilical artery concealed and standard care	Perinatal mortality and morbidity, antenatal hospitalization, maternal intervention, admission to the NICU, and hospitalization until discharge from the neonatal wards	
Trudinger, 1987 [25]	Singleton high-risk pregnancy >28 weeks	300	Doppler of the umbilical artery revealed and standard care	Doppler of the umbilical artery concealed and standard care	Perinatal mortality, CS, induction of labor	
Tyrell, 1990 [26]	Singleton pregnancies at risk of FGR or stillbirth	500	Doppler of the umbilical and uteroplacental arteries, BPP and other tests	Doppler of the umbilical and uteroplacental arteries and BPP revealed only on special request (n = 12 women), only other tests	Total number of days of antenatal admission, rate of induction of labor (by any method), mode of birth (elective and emergency CS), 1 and 5 min Apgar, birth weight, admission to the NICU	
Williams, 2003 [30]	Singleton high-risk pregnancies: FGR 7%, HDP 10%, diabetes 11%, prolonged pregnancy 43%, decreased fetal movements 22%, >32 weeks	1360	Doppler of the umbilical artery: if Doppler is normal, then women seen twice a week; if equivocal, then amniotic fluid index done; if abnormal, then proceeded to induction/delivery within 24 h	Electronic FHR with NST: twice a week; Kulbi score (five components). If equivocal (identified Kulbi = 6), then assessment of amniotic fluid volume; if abnormal (identified Kulbi = 4), then induction/delivery within 24 h	Primary outcome: incidence of CS for fetal distress in labor (non-reassuring FHR) Secondary outcome: total CS, Apgar score 1 and 5 min, the incidence of stillbirth, the presence of meconium and the incidence of transfer to the NICU with severe neonatal morbidity	

FGR fetal growth restriction, *CTG* cardiotocography, *GA* gestational age, *CS* cesarean section, *NICU* neonatal intensive care unit, *HDP* hypertensive disorders in pregnancy, *BPP* biophysical profile, *IUFD* intrauterine fetal demise, *PROM* preterm rupture of membranes, *PTL* preterm labor, *SGA* small for gestational age, *FHR* fetal heart rate, *NST* non-stress test

Table 26.2 Summary of the findings from a systematic review and meta-analysis of randomized controlled trials on the Doppler of the umbilical artery versus no-Doppler in high-risk pregnancies (adapted from Alfirevic et al. 2017) [12]

Outcome	Relative effect (95% CI)	Number of participants	Number of studies	Quality of evidence (GRADE)	Comments
Any perinatal death after randomization	RR 0.71 (0.52–0.98)	10,225	16	Moderate +++	
Serious neonatal morbidity		1098	3		Not possible to pool the data due to high heterogeneity
Stillbirth	RR 0.65 (0.41–1.04)	9560	15	Low ++	
Apgar <7 at 5 min	RR 0.92 (0.69–1.24)	6321	7	Low ++	
Cesarean section (elective and emergency)	RR 0.90 (0.84–0.97)	7918	14	Moderate +++	
Induction of labor	RR 0.89 (0.80–0.99)	5633	10	Moderate +++	

CI confidence interval, *RR* risk ratio

CI 0.42–30.73, 89 women, 1 study; previous pregnancy loss group: RR 0.26, 95% CI 0.03–2.17, 53 women, 1 study).

The lack of evidence in subgroup analysis might be due to several factors such as a small number of included cases, publication bias, and heterogeneity of the included studies. It is noteworthy that all studies were published more than 20 years ago, the reason being the fact that at present not performing umbilical artery Doppler in high-risk pregnancies would now be considered as unethical. Finally, the fact that the majority of the studies were performed in the 1990s, before the international agreement on how to report clinical trials [31], makes quality assessment of the older studies imprecise, and very few studies are graded as high-quality by today's standards.

The next question might be whether there is a specific group of high-risk pregnancies that benefits most from umbilical artery Doppler assessment. In order to answer this question, Westergaard et al. [32] performed a meta-analysis dividing the studies into "well-defined studies," i.e., studies that included pregnancies complicated by fetal growth restriction and/or hypertensive disorders in pregnancy, and "general risk studies," i.e., studies that included a variety of high-risk pregnancies. There were no statistically significant differences for perinatal mortality in both groups (well-defined studies: odds ratio (OR) 0.66, 95% CI 0.36–1.22; general risk studies: OR 0.68, 95% CI 0.43–1.08). However, an international experts' audit on perinatal deaths concluded that the use of Doppler in "well-defined studies" potentially might have prevented some. In the same group, there was a significant reduction in antenatal admissions, induction of labor, elective deliveries (induction and cesarean sections), and overall cesarean sections (OR 0.56, 95% CI 0.43–0.72; OR 0.78, 95% CI 0.63–0.96; OR 0.73, 95% CI 0.61–0.88 and OR 0.78, 95% CI 0.65–0.94, respectively). In conclusion, this meta-analysis suggests that pregnancies complicated by fetal growth restriction and/or hypertensive disorders in pregnancy would benefit most from umbilical artery Doppler assessment [32].

There are no randomized controlled trials on the umbilical artery in high-risk pregnancies, which evaluated long-term infant outcomes.

26.2.2 Implication for Practice

The findings from the first systematic review and meta-analysis of randomized controlled trials on fetal and umbilical artery Doppler in high-risk

pregnancies [33, 34], and subsequent updates [12, 35, 36], showed an improvement in perinatal outcomes and a reduction in operative deliveries. This led to the introduction of umbilical artery Doppler assessment in the management of high-risk pregnancies like fetal growth restriction [37]. The data from the meta-analysis of randomized trials suggest that the availability of umbilical artery Doppler in high-risk pregnancies allows for better timing of delivery to reduce the perinatal mortality and emergency cesarean sections, indicating a better identification of compromised babies before or during labor. This seems particularly true for cases with underlying placental insufficiency, such as fetal growth restriction and hypertensive disorders in pregnancy [32].

As a diagnostic test, umbilical artery Doppler is of importance for the diagnosis of fetal growth restriction and the distinction from small-for-gestational-age fetuses [38, 39], especially at the earlier gestational age epochs. However, it is still not completely clear which intervention, and when, should follow an abnormal umbilical artery Doppler finding in fetal growth restriction, with this being a crucial point in influencing the outcome. In fact, there are no randomized controlled clinical trials on delivery timing in fetal growth restriction based on umbilical artery Doppler. The same applies to the findings of absent or reverse end-diastolic flow in the umbilical artery. The latter findings reflect a more severe placental compromise [40] and are associated with higher perinatal morbidity and mortality [41]. However, there are no randomized controlled trials to support the optimum management protocol in these cases.

26.3 Trials of Ductus Venosus Doppler in High-Risk Pregnancies

26.3.1 Evidence from Randomized Studies

Abnormalities of the ductus venosus waveform are reported to be a good predictor of a perinatal outcome in early fetal growth restriction [1, 2, 42]. The alterations in ductus venosus flow, especially absent or reversed A-wave, represent late changes in the biophysical cascade of events in early fetal growth restriction, together with alterations of short-term variation and biophysical profile, preceding fetal acidemia, and intrauterine fetal demise [1–3]. It is believed that these changes in the ductal waveform are caused by progressive dilatation of the isthmus in an attempt to increase the blood flow toward the heart and to compensate for hypoxia [43, 44]. Thus, from the beginning, it has been clear that the assessment of the ductus venosus in early fetal growth restriction plays a crucial role. However, balancing delivery timing with prematurity is also of critical importance for perinatal and long-term outcomes [45–47]. This raises the question regarding the best biophysical tool and delivery timing in these fetuses.

The only randomized controlled trial that compared different biophysical tools in delivery decision-making in early fetal growth restriction is the TRUFFLE (TRial of Umbilical Fetal FLow in Europe) study [48, 49]. This trial involved 20 European centers and compared 3 interventional arms, early and late ductus venosus changes and short-term variation at computerized cardiotocography, as a trigger for delivery in singleton pregnancies with fetal growth restriction between 26 and 32 weeks of gestation in 503 women [49]. Fetal growth restriction was defined as an abdominal circumference below the tenth centile and an umbilical artery pulsatility index above the 95th centile. The three randomization interventional arms were as follows:

1. Early changes in the ductus venosus, defined as a pulsatility index above the 95th centile
2. Late changes in the ductus venosus, defined as absent or reverse A-wave
3. Reduced short-term variation, below 3.5 ms between 26^{+0} and 28^{+6} weeks of gestation and below 4 ms between 29^{+0} and 31^{+6} gestational weeks

There was a cardiotocography “safety net” for all three arms representing an absolute indication for delivery represented by:

- Spontaneous, repeated, persistent unprovoked decelerations in all three arms
- Short-term variation below 2.6 ms at 26^{+0}–28^{+6} weeks and below 3 ms at 29^{+0}–31^{+6} weeks in ductus venosus arms

The short-term variation "safety net" was deliberately set at a level below that of the cardiotocography arm (arm 3); hence, changes needed to be more extreme in the two ductus venosus groups. In addition, maternal conditions represented an indication for delivery in any group and at any gestational week. Figure 26.1 is the schematic representation of TRUFFLE randomization interventional arms and safety net.

The primary outcome of the TRUFFLE study was a 2-year survival without neurological impairment. The proportion among survivors without neurodevelopmental impairment at 2 years was 85% in the short-term variation group and 91% and 95% in early and late ductus venosus groups, respectively. A significant proportion of babies delivered in the late changes ductus venosus group was due to the short-term variation safety net criteria. Moreover, in the same group, there was a statistically non-significant increase in perinatal and infant mortality rate.

Overall, the results from the TRUFFLE study provided evidence that the timing of delivery based on ductus venosus Doppler measurement in conjunction with short-term variation "safety net" improves long-term (2-year neurodevelopmental) infant outcome in survivors [49]. Despite the fact that data from the TRUFFLE study showed better than assumed results in terms of survival without neurological impairment (overall, 82% of children), the gestational age at study entry and delivery and birth weight were strongly related to an adverse outcome as shown in Fig. 26.2.

26.3.2 Implication for Practice

Besides providing evidence for the best delivery trigger and timing in early fetal growth restriction

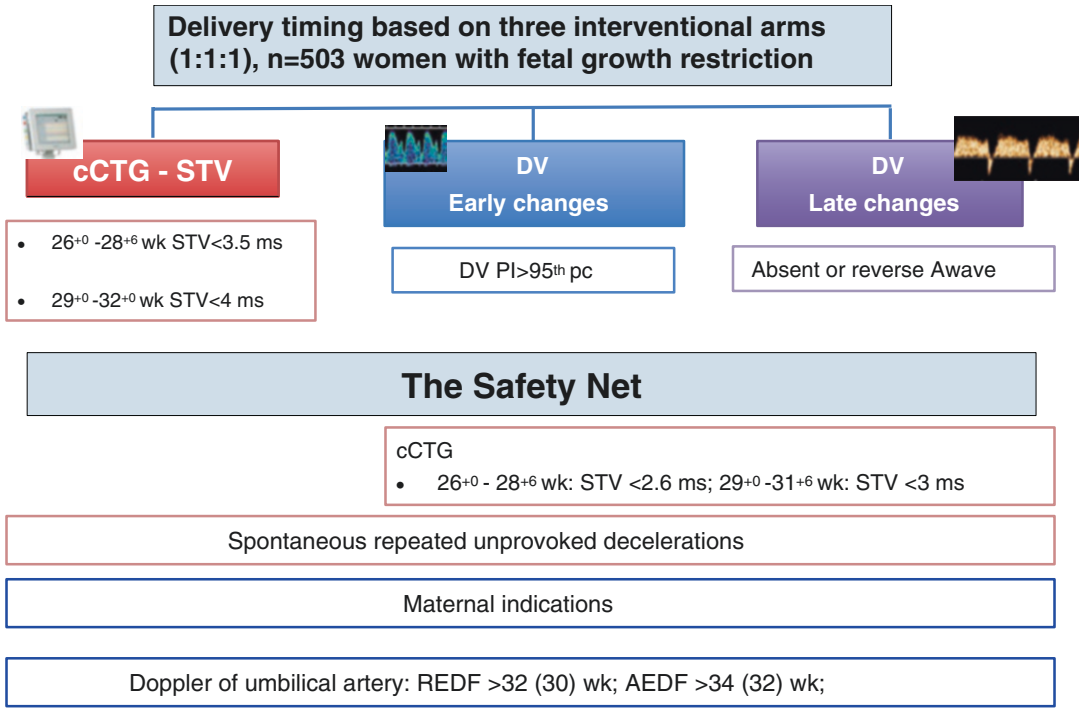

Fig. 26.1 Schematic representation of the TRUFFLE randomization interventional arms and safety net (adopted from Lees et al.) [48, 49]

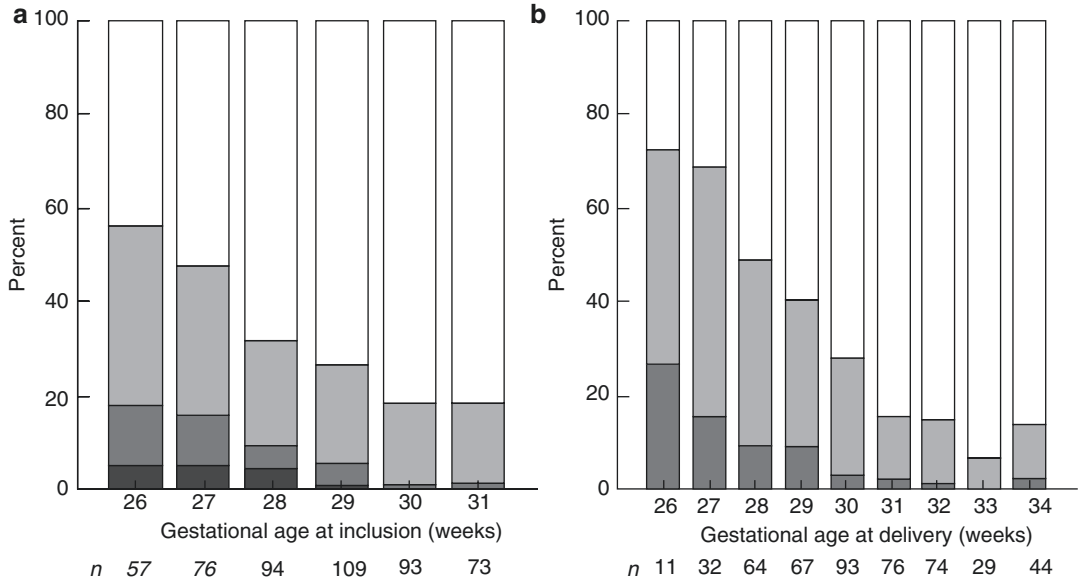

Fig. 26.2 Proportion of neonates without severe morbidity (white bars), with severe morbidity (light gray bars), neonatal death (dark gray bars), and fetal death (black bars) according to a) gestational age at inclusion and b) gestational age at delivery. Severe morbidity was defined as bronchopulmonary dysplasia, severe germinal matrix cerebral hemorrhage grade III or IV, cystic periventricular leukomalacia of more than grade I, proven neonatal sepsis or necrotizing enterocolitis (from Lees et al. [49] and Bilardo et al. [50])

between 26 and 32 weeks of gestation, as shown in the flowchart of the recommended protocol (Fig. 26.3) [50], the TRUFFLE study provided other important information with implications for practice. The study clearly demonstrated that when a specific protocol is uniformly applied and pregnancies are managed by expert multidisciplinary obstetric and neonatal teams, then the outcomes are better than might be expected from contemporary data. Nearly three-quarters of women developed hypertensive disorders in pregnancy, implying the need for strict blood pressure monitoring in these women. The onset of maternal hypertension had an impact on the interval from inclusion to delivery, much shorter in women who had pre-eclampsia at inclusion (median 4 days, interquartile range (IQR) 2–10) than in those that did not (median 12 days, IQR 5–20) [48]. Finally, data presented in Fig. 26.2 might be helpful in counseling parents regarding morbidity, mortality, and adverse long-term outcomes at diagnosis and at delivery according to gestational age.

It is important to highlight that outcomes similar to that of the TRUFFLE trial can be replicated only in fetal growth restriction from 26 to 32 weeks, using the monitoring strategy and delivery decision-making based on ductus venosus Doppler in conjunction with the assessment of short-term variation obtained by computerized cardiotocography.

26.4 Trials of Middle Cerebral Artery Doppler or its Ratio to the Umbilical Artery in High-Risk Pregnancies

26.4.1 Evidence from Randomized Studies

The fetal response to hypoxemia is the redistribution of the blood flow to vital organs such as the brain, heart, and adrenal glands [5]. Thus, the so-called brain-sparing effect, or cerebral redistribution, represents a fetal adaptation to reduced

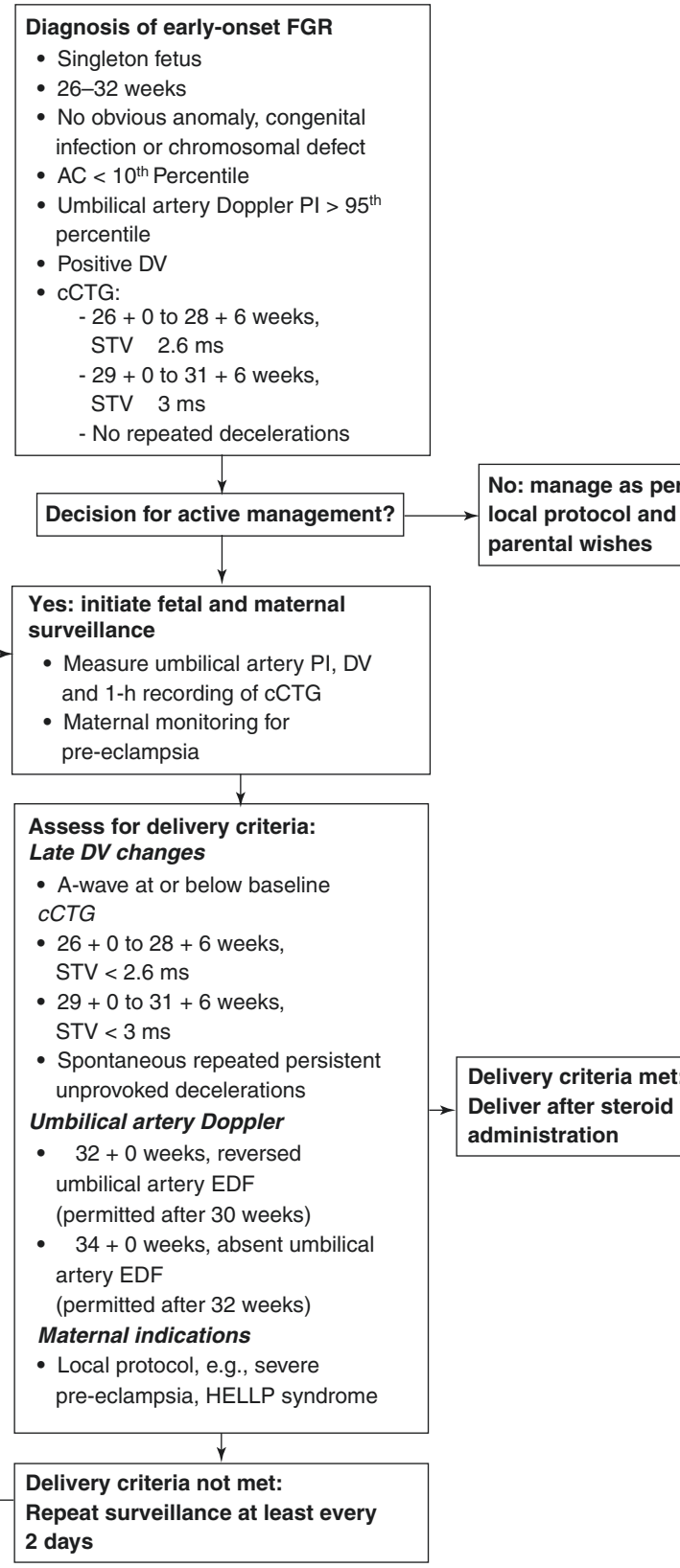

Fig. 26.3 Flowchart of the TRUFFLE protocol (from Bilardo et al. [50])

oxygen availability. This observation might be relevant especially in late fetal growth restriction where alterations of the umbilical artery and ductus venosus districts are rare and fail to identify the majority of late fetal growth-restricted fetuses [51].

Several studies have found an association between cerebral redistribution with a poorer perinatal outcome, including stillbirth [52], a higher risk of cesarean delivery [53–55], and an increased risk of abnormal neurodevelopment at birth [56] and at 2 years of age [57]. These data are also supported by systematic reviews [58–60] and meta-analyses [61, 62].

To our knowledge, the only randomized study that evaluated the impact of cerebral redistribution on a perinatal outcome in patients at high risk was the study by Ott et al [23] In this study, the addition of the middle cerebral to umbilical artery systolic/diastolic velocity waveform ratio to the modified biophysical profile was evaluated. The study included a heterogeneous group of pregnancies considered to be at a higher risk (risk of uteroplacental insufficiency, post-dates, maternal diabetes, fluid abnormalities, and others). Overall, there were no statistically significant differences in the perinatal outcome. However, when only a subgroup of fetuses at a risk of uteroplacental insufficiency was considered, a significant difference in the cesarean section rate for fetal distress was observed, with fewer cesarean sections in the intervention group (1/63, 1.6%) than in the control group (6/56, 10.7%, $p = 0.04$) [23].

There are no randomized controlled trials on the application of middle cerebral artery Doppler and its impact on long-term outcomes in high-risk pregnancies, including fetal growth restriction. This makes the quality of the evidence, on which the application of middle cerebral artery Doppler is based, extremely low, mainly based on retrospective or prospective observational data or secondary analysis of primary studies. Thus, the application of middle cerebral artery Doppler and its ratio in high-risk pregnancies, particularly in fetal growth restriction, based on high-quality studies and strong evidence is still missing, leaving it as an unresolved question. The difficulty in interpreting these studies pertains to whether abnormal cerebral Doppler is in itself injurious to fetal outcome and neurodevelopment or whether it is simply a marker of hypoxia and it is hypoxia itself that is damaging or alternatively that these Doppler changes lead to iatrogenic delivery and prematurity.

26.4.2 Implication for Practice

There is no international consensus as to the timing of delivery in late fetal growth restriction (somewhat arbitrarily defined as after 32 weeks) due to the lack of interventional management randomized trials based on Doppler indices or other biophysical tools. In fact, the national guidelines for the management of late fetal growth restriction are highly variable [63], and, hence, management is mainly based on expert opinion [64, 65].

The secondary analysis of the TRUFFLE study showed a weak association between the low middle cerebral artery pulsatility index and adverse short-term neonatal outcome and between the low middle cerebral artery pulsatility index and high umbilical-cerebral (but not cerebral-placental) ratio with 2-year adverse neurodevelopmental outcome [66]. However, the gestational age at delivery and birth weight had the most pronounced impact on these outcomes (Fig. 26.4). These data suggest that middle cerebral artery Doppler might be used to guide monitoring before 32 weeks of gestation, but there is no evidence that it should be used to determine delivery timing [67].

A recent secondary analysis of the PORTO study (Perinatal Ireland Multicenter Observational Prospective Observational Trial to Optimize Pediatric Health in Fetal Growth Restriction) has shown that fetuses with growth restriction across all gestational age epochs and with an abnormal cerebro-placental ratio (<1) had a significantly poorer neurological outcome at 3 years [68]. The authors conclude that the study "further substantiates the benefit of routine assessment of cerebroplacental ratio in fetal growth restricted pregnancies and for counseling parents regarding the long-term outcome of affected infants." When

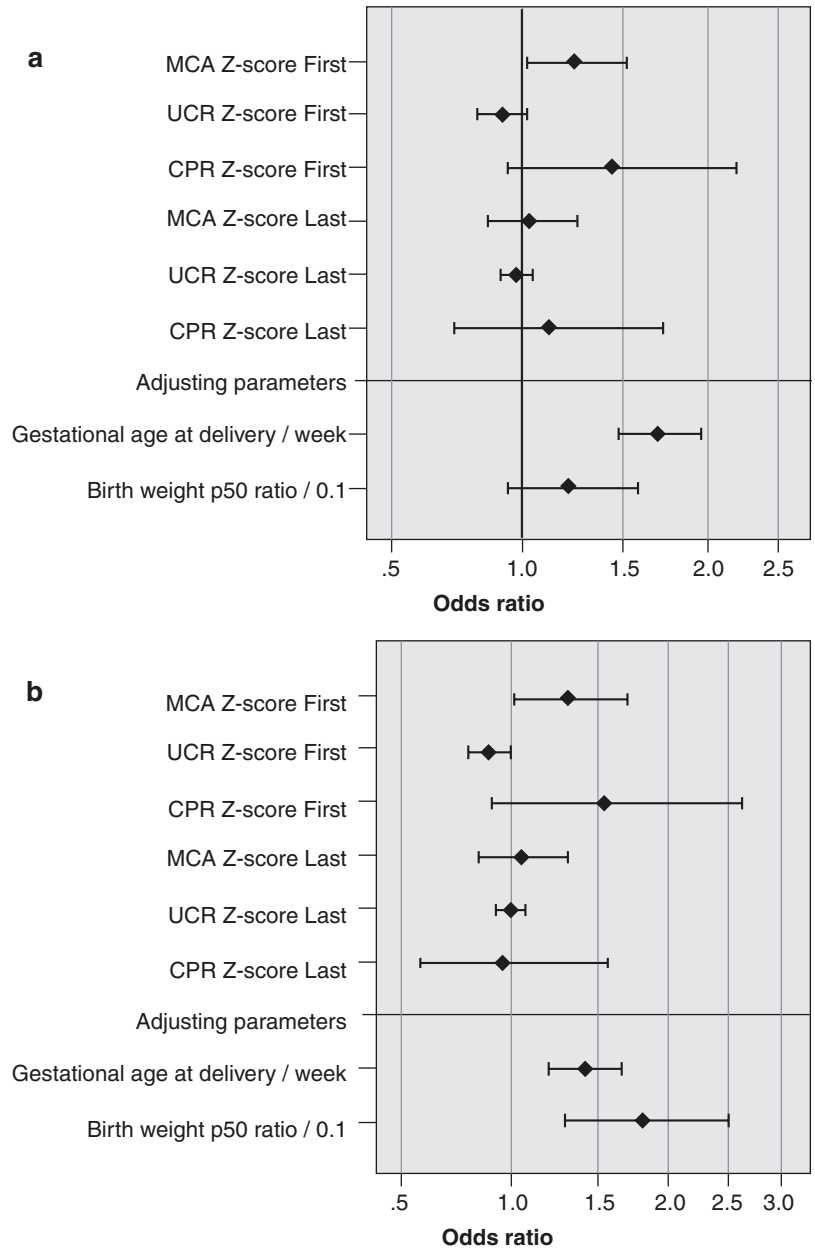

Fig. 26.4 Secondary analysis of the TRUFFLE study: odds ratios with 95% confidence intervals for neonatal and 2-year infant outcome (from Stampalija et al. [66]). The upper panel (**a**) represents the odds ratios for neonatal outcome (survival until the first discharge home without severe morbidity), and the lower panel (**b**) represents the odds ratios for the 2-year infant outcome (survival without neurological impairment at 2 years) of the *z*-scores of the middle cerebral artery (MCA) pulsatility index, umbilical-cerebral ratio (UCR), and cerebroplacental ratio (CPR) at inclusion (first) and within 1 week before delivery (last), adjusted for birth weight, p50 ratio, and gestational age. The odds ratios of the adjusting parameters are shown below the horizontal line. DV p95: early changes in the ductus venosus (DV-PI>95th percentile); DV no A: late changes in the ductus venosus (no or reverse A-wave flow)

assessing an adverse short- or long-term outcome, both the severity of growth restriction and gestational age at delivery should be taken into account while representing an independent risk factor for the adverse outcome. It still remains to be elucidated whether cerebral redistribution is an independent risk factor for an adverse outcome or it "only" reflects the severity of growth restriction.

The TRUFFLE-2 feasibility study explored the association between cerebral redistribution and outcome in late preterm (32^{+0}–36^{+6} weeks of gestation) pregnancies at a risk of fetal growth restriction [69]. In this large multi-center (33 European centers) prospective cohort study of 862 women, infants with composite adverse outcome were delivered at a lower gestational age (36 versus 38 weeks) with a lower birth weight (1900 g ver-

sus 2540 g). However, the first observation of cerebral redistribution after inclusion, defined as the middle cerebral artery pulsatility index below the fifth centile and specific umbilicoplacental ratio *z*-score thresholds (1.5 at 32–33 weeks and 1.0 at 34–36 weeks, respectively), had the highest relative risk of a composite adverse outcome (RR 2.1; 95% CI 1.5–3.2 and RR 2.1; 95% CI 1.4–3.1, respectively). This effect was independent of gestational age below 36 weeks of gestation, as shown in Tables 26.3 and 26.4. These data would support an association between cerebral redistribution and adverse outcome, but like other un-blinded observational studies, the weakness is that there might be a treatment paradox. Finally, the association does not imply causality. Thus, a randomized trial is required to answer the uncertainties regarding delivery timing in late fetal growth restriction in relation to cerebral blood flow redistribution.

26.5 Implications for Research

The type and frequency of monitoring after the identification of abnormal umbilical artery Doppler in fetal growth restriction is still not clear, or, at least, it has not been tested by randomized controlled trials. There is no doubt that umbilical artery assessment is of crucial importance to identify fetal growth restriction, especially early-onset, due to placental insufficiency. However, the best delivery timing and impact on short- and long-term outcomes, in the presence of absent or reverse end-diastolic flow or increased pulsatility index in the umbilical artery, from 32 weeks, has not been appropriately evaluated in randomized controlled trials.

Despite emerging awareness that there might be an association between cerebral blood flow redistribution and adverse perinatal outcome, in the absence of randomized controlled trials, it is still not clear whether the assessment and delivery decision based on Doppler evaluation of cerebral blood flow redistribution is beneficial in terms of short- and long-term neurodevelopmental outcomes and which is the optimal gestational age to deliver (beside the optimal Doppler parameter and threshold).

Key Messages

The available evidence from randomized controlled trials suggests:

- Umbilical artery assessment improves perinatal outcome in high-risk pregnancies, particularly in pregnancies at risk of placental insufficiency.
- In early fetal growth restriction (26–32 weeks), the best outcome at 2 years is obtained by timing the decision for delivery on combined monitoring by the ductus venosus and short-term variation obtained by computerized cardiotocography.
- In late fetal growth restriction (after 32 weeks), there is little or no evidence to inform the frequency of Doppler evaluation and the timing of delivery based on umbilical artery and/or middle cerebral artery assessment.

Table 26.3 Composite adverse outcome and gestational age at delivery for fetuses with signs of cerebral blood flow redistribution compared to those that always had a normal fetal Doppler, specified for gestational age at the ultrasound Doppler examination. Women who had an abnormal ultrasound were only counted once at the gestational age epoch when the first abnormal Doppler was registered. Women with normal Doppler could have ultrasound at more than one gestational age epoch after inclusion. Totals are therefore higher than the total number of included women. Middle cerebral artery pulsatility index cut-off at the fifth percentile

	Below cut-off at least once		Always above cut-off		RR (95% CI) for composite adverse outcome	
Gestational epoch at Doppler	Composite adverse outcome	Gestational age at delivery	Composite adverse outcome	Gestational age at delivery		*p*
32–33 weeks	24/63 = 38%[a]	36 (34–38)[a]	26/283 = 9%	38 (37–39)	4.1 (2.6–6.7)	<0.01
34–35 weeks	14/94 = 15%[a]	37 (36–38)[a]	37/513 = 7%	38 (37–40)	2.1 (1.2–3.4)	0.01
36 weeks	6/63 = 10%	38 (37–38)[a]	27/568 = 5%	39 (38–40)	2.0 (0.8–4.7)	0.1

[a] Statistically significant difference from fetuses that always had a middle cerebral artery pulsatility index below cut-off (a chi-square test or the Mann–Whitney test)

Table 26.4 Composite adverse outcome and gestational age at delivery for fetuses with signs of cerebral blood flow redistribution compared to those that always had a normal fetal Doppler, specified for gestational age at the ultrasound Doppler examination. Women who had an abnormal ultrasound were only counted once at the gestational age epoch when the first abnormal Doppler was registered. Women with normal Doppler could have ultrasound at more than one gestational age epoch after inclusion. Totals are therefore higher than the total number of included women. Umbilicocerebral ratio gestational age-specific cut-off at a *z*-score of 1.5 at 32–33 weeks and 1.0 at 34–36 weeks

	Above cut-off at least once		Always below cut-off		RR (95% CI) for composite adverse outcome	
Gestational epoch at Doppler	Composite adverse outcome	Gestational age at delivery	Composite adverse outcome	Gestational age at delivery		*p*
32–33 weeks	12/31 = 39%[a]	34 (3–36)[a]	33/291 = 11%	38 (37–39)	3.4 (2.0–5.9)	<0.01
34–35 weeks	15/86 = 17%[a]	36 (35–37)[a]	46/563 = 8%	38 (37–40)	2.1 (1.2–3.7)	0.01
36 weeks	3/45 = 8%	37 (37–38)[a]	34/626 = 5%	39 (38–40)	1.2 (0.4–3.8)	0.7

[a] Statistically significant difference from fetuses that always had an umbilicocerebral ratio below cut-off (a chi-square test or the Mann–Whitney test)

References

1. Ferrazzi E, Bozzo M, Rigano S, Bellotti M, Morabito A, Pardi G, Battaglia FC, Galan HL. Temporal sequence of abnormal Doppler changes in the peripheral and central circulatory systems of the severely growth-restricted fetus. Ultrasound Obstet Gynecol. 2002;19:140–6.
2. Baschat AA, Gembruch U, Harman CR. The sequence of changes in Doppler and biophysical parameters as severe fetal growth restriction worsens. Ultrasound Obstet Gynecol. 2001;18:571–7.
3. Hecher K, Bilardo CM, Stigter RH, Ville Y, Hackeloer BJ, Kok HJ, Senat MV, Visser GH. Monitoring of fetuses with intrauterine growth restriction: a longitudinal study. Ultrasound Obstet Gynecol. 2001;18:564–70.
4. Hecher K, Snijders R, Campbell S, Nicolaides K. Fetal venous, intracardiac, and arterial blood flow measurements in intrauterine growth retardation: relationship with fetal blood gases. Am J Obstet Gynecol. 1995;173:10–5.
5. Richardson BS, Bocking AD. Metabolic and circulatory adaptations to chronic hypoxia in the fetus. Comp Biochem Physiol A Mol Integr Physiol. 1998;119:717–23.
6. Khalil A, Rodgers M, Baschat A, Bhide A, Gratacos E, Hecher K, Kilby MD, Lewi L, Nicolaides KH, Oepkes D, Raine-Fenning N, Reed K, Salomon LJ, Sotiriadis A, Thilaganathan B, Ville Y. ISUOG practice guidelines: role of ultrasound in twin pregnancy. Ultrasound Obstet Gynecol. 2016;47:247–63.
7. Mari G, Norton ME, Stone J, Berghella V, Sciscione A, Tate D, Schenone MH. Society for Maternal-Fetal Medicine (SMFM) clinical guideline #8: the fetus at risk for anemia: diagnosis and management. Am J Obstet Gynecol. 2015;212:697–710.
8. Albaiges G, Missfelder-Lobos H, Lees C, Parra M, Nicolaides KH. One-stage screening for pregnancy complications by color Doppler assessment of the uterine arteries at 23 weeks' gestation. Obstet Gynecol. 2000;96:559–64.
9. Papageorghiou AT, Yu CK, Bindra R, Pandis G, Nicolaides KH, Fetal Medicine Foundation Second Trimester Screening Group. Multicenter screening for pre-eclampsia and fetal growth restriction by transvaginal uterine artery Doppler at 23 weeks of gestation. Ultrasound Obstet Gynecol. 2001;18:441–9.
10. Sotiriadis A, Hernandez-Andrade E, da Silva CF, Ghi T, Glanc P, Khalil A, Martins WP, Odibo AO, Papageorghiou AT, Salomon LJ, Thilaganathan B, ISUOG CSC Pre-eclampsia Task Force. ISUOG practice guidelines 2019: role of ultrasound in screening and follow-up of pre-eclampsia. UOG. 2019;53:7–22.
11. Tan MY, Wright D, Syngelaki A, Akolekar R, Cicero S, Janga D, Singh M, Greco E, Wright A, Maclagan K, Poon LC, Nicolaides KH. Comparison of diagnostic accuracy of early screening for pre-eclampsia by NICE guidelines and a method combining maternal factors and biomarkers: results of SPREE. Ultrasound Obstet Gynecol. 2018;51:743–50.
12. Alfirevic Z, Stampalija T, Dowswell T. Fetal and umbilical Doppler ultrasound in high-risk pregnancies. Cochrane Database Syst Rev. 2017;6:CD007529.
13. Biljan M, Haddad N, McVey K, Williams J. Efficiency of continuous-wave Doppler in screening high risk pregnancies in a district general hospital (a prospective randomized study on 674 singleton pregnancies). Proceedings of 26th British Congress of Obstetrics and Gynaecology; 1992 July7–10; Manchester, UK.
14. Burke G, Stuart B, Crowley P, Ni Scanaill S, Drumm J. Does Doppler ultrasound alter the management of high-risk pregnancy? Care concern and cure in perinatal medicine. 13th European Congress of Perinatal Medicine; 1992 May; Amsterdam, The Netherlands. Parthenon; 1992. pp. 597–604.
15. De Rochambeau B, Jabbour N, Mellier G. Umbilical Doppler velocimetry in prolonged pregnancies [La velocimetrie Doppler ombilicale dans les grossesses prolongees]. Revue Francaise de Gynecologie et d Obstetrique. 1992;87(5):289–94.
16. Giles W, Bisits A, O'Callaghan S, Gill A, DAMP Study Group. The Doppler assessment in multiple pregnancy randomised controlled trial of ultrasound biometry versus umbilical artery Doppler ultrasound and biometry in twin pregnancy. BJOG. 2003;110(6):593–7.
17. Johnstone FD, Prescott R, Hoskins P, Greer IA, McGlew T, Compton M. The effect of introduction of umbilical Doppler recordings to obstetric practice. Br J Obstet Gynaecol. 1993;100:733–41.
18. Neales K. (St. Mary's Hospital, Manchester, UK). [personal communication]. Letter to: Z Alfirevic (Department of Women's and Children's Health, The University of Liverpool, Liverpool, UK) 24 January 1994; Vol. Located at: Cochrane Office, Department of Women's and Children's Health, The University of Liverpool, Liverpool, UK.
19. Newnham JP, O'Dea MRA, Reid KP, Diepeveen DA. Doppler flow velocity waveform analysis in high risk pregnancies: a randomized controlled trial. Br J Obstet Gynaecol. 1991;98:956–63.
20. Nienhuis SJ, Vles JS, Gerver WJ, Hoogland HJ. Doppler ultrasonography in suspected intrauterine growth retardation: a randomized clinical trial. Ultrasound Obstet Gynecol. 1997;9(1):6–13.
21. Nimrod C, Yee J, Hopkins C, Pierce P, Lange I, Fick G, et al. The utility of pulsed Doppler studies in the evaluation of postdate pregnancies. J Matern Fetal Invest. 1992;1:127.
22. Norman K, Pattinson RC, Carstens E. Doppler velocimetry in recurrent pregnancy loss: is there a role? Proceedings of 11th Conference on Priorities in Perinatal Care in South Africa; 1992 March; Caledon, South Africa; 1992. pp. 71–74.
23. Ott WJ, Mora G, Arias F, Sunderji S, Sheldon G. Comparison of the modified biophysical profile to a new biophysical profile incorporating the

middle cerebral artery to umbilical artery velocity flow systolic/diastolic ratio. Am J Obstet Gynecol. 1998;178(6):1346–53.
24. Pattinson RC, Norman K, Odendaal HJ. The role of Doppler velocimetry in the management of high risk pregnancies. Br J Obstet Gynaecol. 1994;101:114–20.
25. Trudinger BJ, Cook CM, Giles WB, Connelly AJ, Thompson RS. Umbilical artery flow velocity waveforms in high-risk pregnancy: randomised controlled trial. Lancet. 1987;1:188–90.
26. Tyrrell SN, Lilford RJ, MacDonald HN, Nelson EJ, Porter J, Gupta JK. Randomized comparison of routine vs highly selective use of Doppler ultrasound and biophysical scoring to investigate high risk pregnancies. Br J Obstet Gynaecol. 1990;97:909–16.
27. Almstrom H, Axelsson O, Cnattingius S, Ekman G, Maesel A, Ulmsten U, Armstrom K, Marsal K. Comparison of umbilical artery velocimetry and cardiotocography for surveillance of small-for-gestational-age fetuses. Lancet. 1992;340:936–40.
28. Haley J, Tuffnell DJ, Johnson N. Randomised controlled trial of cardiotocography versus umbilical artery Doppler in the management of small for gestational age fetuses. Br J Obstet Gynaecol. 1997;104(4):431–5.
29. Hofmeyr GJ, Pattinson R, Buckley D, Jennings J, Redman CWG. Umbilical artery resistance index as a screening test for fetal well-being. II. Randomized feasibility study. Obstet Gynecol. 1991;78:359–62.
30. Williams KP, Farquharson DF, Bebbington M, Dansereau J, Galerneau F, Wilson RD, Shaw D, Kent N. Screening for fetal wellbeing in a high-risk pregnant population comparing the non-stress test with umbilical artery Doppler velocimetry: a randomized controlled clinical trial. Am J Obstet Gynecol. 2003;188(5):1366–71.
31. Moher D, Schulz KF, Altman DG. The CONSORT statement: revised recommendations for improving the quality of reports of parallel-group randomised trials. Lancet. 2001;357(9263):1191–4.
32. Westergaard HB, Langhoff-Roos J, Lingman G, Marsal K, Kreiner S. A critical appraisal of the use of umbilical artery Doppler ultrasound in high-risk pregnancies: use of meta-analyses in evidence-based obstetrics. Ultrasound Obstet Gynecol. 2001;17:466–76.
33. Alfirevic Z, Neilson JP. Doppler ultrasonography in high risk pregnancies: systematic review with meta-analysis. Am J Obstet Gynecol. 1995;172:379–87.
34. Neilson JP, Alfirevic Z. Doppler ultrasound for fetal assessment in high risk pregnancies. Cochrane Database Syst Rev. 1995;(1). https://doi.org/10.1002/14651858.CD000073.
35. Alfirevic Z, Stampalija T, Gyte GML. Fetal and umbilical Doppler ultrasound in high-risk pregnancies. Cochrane Database Syst Rev. 2010;(1). https://doi.org/10.1002/14651858.CD007529.pub2.
36. Alfirevic Z, Stampalija T, Gyte GML. Fetal and umbilical Doppler ultrasound in high-risk pregnancies. Cochrane Database Syst Rev. 2013;(11). https://doi.org/10.1002/14651858.CD007529.pub3.
37. Royal College of Obstetrics & Gynecologists (RCOG). Green-top guideline no.31. The investigation and management of the small-for-gestational-age fetus. 2013.
38. Gordijn SJ, Beune IM, Thilaganathan B, Papageorghiou A, Baschat AA, Baker PN, Silver RM, Wynia K, Ganzevoort W. Consensus definition for placental fetal growth restriction: a Delphi procedure. Ultrasound Obstet Gynecol. 2016;48(3):333–9.
39. Unterscheider J, Daly S, Geary MP, Kennelly MM, McAuliffe FM, O'Donoghue K, Hunter A, Morrison JJ, Burke G, Dicker P, Tully EC, Malone FD. Optimizing the definition of intrauterine growth restriction: the multicenter prospective PORTO study. Am J Obstet Gynecol. 2013;208(4):290–2.
40. Burton GJ, Woods AW, Jauniaux E, Kingdom JC. Rheological and physiological consequences of conversion of the maternal spiral arteries for uteroplacental blood flow during human pregnancy. Placenta. 2009;30(6):473–82.
41. Kurkinen-Räty M, Kivelä A, Jouppila P. The clinical significance of an absent end-diastolic velocity in the umbilical artery detected before the 34th week of pregnancy. Acta Obstet Gynecol Scand. 1997;76(5):398–404.
42. Bilardo CM, Wolf H, Stigter RH, Ville Y, Baez E, Visser GHA, Hecher K. Relationship between monitoring parameters and outcome in severe, early intrauterine growth restriction. Ultrasound Obstet Gynecol. 2004;23:119–25.
43. Kiserud T, Kessler J, Ebbing C, Rasmussen S. Ductus venosus shunting in growth-restricted fetuses and the effect of umbilical circulatory compromise. Ultrasound Obstet Gynecol. 2006;28(2):143–9.
44. Ferrazzi E, Lees C, Acharya G. The controversial role of the ductus venosus in hypoxic human fetuses. Acta Obstet Gynecol Scand. 2019;98(7):823–9.
45. Raju TN, Mercer BM, Burchfield DJ, Joseph GFJ. Periviable birth: executive summary of a joint workshop by the Eunice Kennedy Shriver National Institute of Child Health and Human Development, Society for Maternal-Fetal Medicine, American Academy of Pediatrics, and American College of Obstetricians and Gynecologists. Obstet Gynecol. 2014;123(5):1083–96.
46. EXPRESS Group. Incidence of and risk factors for neonatal morbidity after active perinatal care: extremely preterm infants study in Sweden (EXPRESS). Acta Paediatr. 2010;99(7):978–92.
47. Baschat AA, Cosmi E, Bilardo CM, Wolf H, Berg C, Rigano S, Germer U, Moyano D, Turan S, Hartung J, Bhide A, Müller T, Bower S, Nicolaides KH, Thilaganathan B, Gembruch U, Ferrazzi E, Hecher K, Galan HL, Harman CR. Predictors of neonatal outcome in early-onset placental dysfunction. Obstet Gynecol. 2007;109(2 Pt 1):253–61.
48. Lees C, Marlow N, Arabin B, Bilardo CM, Brezinka C, Derks JB, Duvekot J, Frusca T, Diemert A, Ferrazzi

E, Ganzevoort W, Hecher K, Martinelli P, Ostermayer E, Papageorghiou AT, Schlembach D, Schneider KT, Thilaganathan B, Todros T, van Wassenaer-Leemhuis A, Valcamonico A, Visser GH, Wolf H, TRUFFLE Group. Perinatal morbidity and mortality in early-onset fetal growth restriction: cohort outcomes of the trial of randomized umbilical and fetal flow in Europe (TRUFFLE). Ultrasound Obstet Gynecol. 2013;42(4):400–8.

49. Lees CC, Marlow N, van Wassenaer-Leemhuis A, Arabin B, Bilardo CM, Brezinka C, Calvert S, Derks JB, Diemert A, Duvekot JJ, Ferrazzi E, Frusca T, Ganzevoort W, Hecher K, Martinelli P, Ostermayer E, Papageorghiou AT, Schlembach D, Schneider KT, Thilaganathan B, Todros T, Valcamonico A, Visser GH, Wolf H, TRUFFLE Study Group. 2 year neurodevelopmental and intermediate perinatal outcomes in infants with very preterm fetal growth restriction (TRUFFLE): a randomised trial. Lancet. 2015;385(9983):2162–72.
50. Bilardo CM, Hecher K, GHA V, Papageorghiou AT, Marlow N, Thilaganathan B, Van Wassenaer-Leemhuis A, Todros T, Marsal K, Frusca T, Arabin B, Brezinka C, Derks JB, Diemert A, Duvekot JJ, Ferrazzi E, Ganzevoort W, Martinelli P, Ostermayer E, Schlembach D, Valensise H, Thornton J, Wolf H, Lees C, TRUFFLE Group. Severe fetal growth restriction at 26-32 weeks: key messages from the TRUFFLE study. Ultrasound Obstet Gynecol. 2017;50(3):285–90.
51. Savchev S, Figueras F, Sanz-Cortes M, Cruz-Lemini M, Triunfo S, Botet F, Gratacos E. Evaluation of an optimal gestational age cut-off for the definition of early- and late-onset fetal growth restriction. Fetal Diagn Ther. 2014;36(2):99–105.
52. Crimmins S, Desai A, Block-Abraham D, Berg C, Gembruch U, Baschat AA. A comparison of Doppler and biophysical findings between liveborn and stillborn growth-restricted fetuses. Am J Obstet Gynecol. 2014;211(6):669.e1–669.e10.
53. Cruz-Martínez R, Figueras F, Hernandez-Andrade E, Oros D, Gratacos E. Fetal brain Doppler to predict cesarean delivery for nonreassuring fetal status in term small-for-gestational-age fetuses. Obstet Gynecol. 2011;117(3):618–26.
54. Severi FM, Bocchi C, Visentin A, Falco P, Cobellis L, Florio P, Zagonari S, Pilu G. Uterine and fetal cerebral Doppler predict the outcome of third-trimester small-for-gestational age fetuses with normal umbilical artery Doppler. Ultrasound Obstet Gynecol. 2002;19(3):225–8.
55. Hershkovitz R, Kingdom JC, Geary M, Rodeck CH. Fetal cerebral blood flow redistribution in late gestation: identification of compromise in small fetuses with normal umbilical artery Doppler. Ultrasound Obstet Gynecol. 2000;15(3):209–12.
56. Oros D, Figueras F, Cruz-Martinez R, Padilla N, Meler E, Hernandez-Andrade E, Gratacos E. Middle versus anterior cerebral artery Doppler for the prediction of perinatal outcome and neonatal neurobehavior in term small-for-gestational-age fetuses with normal umbilical artery Doppler. Ultrasound Obstet Gynecol. 2010;35(4):456–61.
57. Eixarch E, Meler E, Iraola A, Illa M, Crispi F, Hernandez-Andrade E, Gratacos E, Figueras F. Neurodevelopmental outcome in 2-year-old infants who were small-for-gestational age term fetuses with cerebral blood flow redistribution. Ultrasound Obstet Gynecol. 2008;32(7):894–9.
58. Meher S, Hernandez-Andrade E, Basheer SN, Lees C. Impact of cerebral redistribution on neurodevelopmental outcome in small-for-gestational-age or growth-restricted babies: a systematic review. Ultrasound Obstet Gynecol. 2015;46(4):398–404.
59. Hernandez-Andrade E, Stampalija T, Figueras F. Cerebral blood flow studies in the diagnosis and management of intrauterine growth restriction. Curr Opin Obstet Gynecol. 2013;25(2):138–44.
60. DeVore GR. The importance of the cerebroplacental ratio in the evaluation of fetal well-being in SGA and AGA fetuses. Am J Obstet Gynecol. 2015;213(1):5–15.
61. Vollgraff Heidweiller-Schreurs CA, De Boer MA, Heymans MW, Schoonmade LJ, Bossuyt PMM, Mol BWJ, De Groot CJM, Bax CJ. Prognostic accuracy of cerebroplacental ratio and middle cerebral artery Doppler for adverse perinatal outcome: systematic review and meta-analysis. Ultrasound Obstet Gynecol. 2018;51(3):313–22.
62. Conde-Agudelo A, Villar J, Kennedy SH, Papageorghiou AT. Predictive accuracy of cerebroplacental ratio for adverse perinatal and neurodevelopmental outcomes in suspected fetal growth restriction: systematic review and meta-analysis. Ultrasound Obstet Gynecol. 2018;52(4):430–41.
63. McCowan LM, Figueras F, Anderson NH. Evidence-based national guidelines for the management of suspected fetal growth restriction: comparison, consensus, and controversy. Am J Obstet Gynecol. 2018;218(2S):S855–68.
64. Figueras F, Gratacos E. An integrated approach to fetal growth restriction. Best Pract Res Clin Obstet Gynaecol. 2017;38:48–58.
65. Baschat AA. Planning management and delivery of the growth-restricted fetus. Best Pract Res Clin Obstet Gynaecol. 2018;49:53–65.
66. Stampalija T, Arabin B, Wolf H, Bilardo CM, Lees C, TRUFFLE Investigators. Is middle cerebral artery Doppler related to neonatal and 2-year infant outcome in early fetal growth restriction? Am J Obstet Gynecol. 2017;216(5):521.e1–521.e13.
67. Stampalija T, Arabin B, Wolf H, Bilardo CM, Lees C. An abnormal cerebroplacental ratio (CPR) is predictive of early childhood delayed neurodevelopment in the setting of fetal growth restriction. Am J Obstet Gynecol. 2019;221(3):273.e1–9. Epub ahead of print.
68. Monteith C, Flood K, Pinnamaneni R, Levine TA, Alderdice FA, Unterscheider J, McAuliffe FM, Dicker P, Tully EC, Malone FD, Foran A. An abnormal cerebroplacental ratio (CPR) is predictive of

early childhood delayed neurodevelopment in the setting of fetal growth restriction. Am J Obstet Gynecol. 2019;221(3):273.e1–9.
69. Stampalija T, Thorton J, Marlow N, Napolitano R, Bhide A, et al.; TRUFFLE-2 Group. Fetal cerebral Doppler changes and outcome in late preterm growth restriction: a prospective cohort study. Ultrasound Obstet Gynecol. 2020;56(2):173–181.

27 Doppler Interrogation of the Umbilical Venous Flow

Enrico Ferrazzi, Daniela Di Martino, and Tamara Stampalija

In recent years and with the advent of newer ultrasound equipment, measurement of umbilical venous flow (UBVF) has become feasible. The intra-observer coefficients of variation for the vein diameter, mean velocity, and absolute umbilical venous blood are around 3%, 9%, and 11%, respectively. Systematic errors are inherent to different methodologies and can either be overcome by a shared consensus or each center should consistently use the same methodology. Although there are many possible systematic differences, flow volume data obtained by different groups in late gestation vary within a narrow range, from 104 mL/min kg^{-1} to 126.0 ± 23.4 mL/min kg^{1}, not much different from data obtained in 1982 by Eik-Nes et al. (115 mL/min).

In fetal lambs, the volume flow in each of the two umbilical veins of these fetuses was significantly correlated with the number and weight of cotyledons that supplied the flow of each vein. The relationship between pO_2 and umbilical vein flow volume reduction was independently proved in fetal lambs by Kiserud and Padoan.

A similar important, although indirect, correlation was reported in severe FGR human fetuses. Umbilical blood flow increases throughout pregnancy in a normal human fetus from 63 mL/min at 20 weeks to 373 mL/min at 38 weeks. The "normalization" of the absolute flow per unit fetal weight or per biometric direct measurement such as the abdominal or head circumference might help avoid additional errors (estimated fetal weight) and/or better understand fetal pathophysiology.

In severe early fetal growth restriction, UBVF is significantly reduced, but in those fetuses with an abnormal heart rate, just before elective delivery (mean gestational age 29 ± 3 weeks; mean weight 962 ± 334 g), the UBVF was 63.0 ± 22.1 vs 124.0 ± 30.3 mL/min kg^{-1} in matched normal fetuses ($p < 0.001$). A similar value was replicated by Boito and co-workers (59.6 vs 104.7 mL/min kg^{-1}; $p < 0.001$). Interestingly, the physiological dimension mostly affected in these cases is blood flow velocity, i.e., a proxy of blood vein pressure, and not the diameter of the vein (when normalized for fetal growth parameters).

It is of major interest that UVBF might be in late FGR in which the Doppler indices of placental vascular damage might be frequently normal. According to M. Parra-Saavedra et al., small-for-gestational-age (SGA) fetuses at term with an

E. Ferrazzi (✉) · D. Di Martino
Department of Clinical Sciences and Community Health, Iniversita' Delgi Studi, Obstetrics Unit, Fondazione IRCCS Ca' Granda Ospedale Maggiore Policlinico, University of Milan, Milan, Italy
e-mail: enrico.ferrazzi@unimi.it

T. Stampalija
Unit of Fetal Medicine and Prenatal Diagnosis, Institute for Maternal and Child Health, IRCCS Burlo Garofolo, Trieste, Italy

Department of Medicine, Surgery and Health Sciences, University of Trieste, Trieste, Italy

D. Maulik, C. C. Lees (eds.), *Doppler Ultrasound in Obstetrics and Gynecology*,
https://doi.org/10.1007/978-3-031-06189-9_27

UBVF below 68 mL/min kg^{-1} had twice the risk of non-reassuring fetal status in induced labor. This value is very much close to the UVBF measured in 1987 by Laurin et al. 2 days before delivery in late FGR fetuses (68 mL/min kg^{-1}) and close to the one we observed in early FGR with an abnormal heart rate in utero (63 mL/min/kg) as reported above.

In conclusion, UBVF is an easy and reproducible measurement, an additional index of early severe fetal conditions. In late gestation, it might help diagnose severe conditions in late FGR and also identify, among "constitutionally" small fetuses, those that are indeed suffering from impaired intrauterine growth due to limited nutritional support by the placenta.

27.1 Introduction

The first reports about measurements of fetal umbilical venous blood flow in human fetuses go back to the early 1980s. Eik-Nes et al. [1] in 1980, Gill et al. [2] in 1981, and Eik-Nes et al. [3] in 1982 reported measurements obtained from the "intrahepatic" umbilical vein. This pioneering approach came to an end when Erskine and Ritchie [4] and then Giles et al. [5] concluded that "The results obtained are in keeping with previous studies, but indicate that, although the method is relatively simple, determination of absolute blood flow in these vessels has little clinical potential because of inherent measurement inaccuracies." Since then, these negative claims on quantitative "measurement inaccuracies" and on "poor clinical potential" in the diagnosis of fetal growth restriction were challenged, among others by Gerson et al. [6], Reed et al. [7], Sutton et al. [8], Schmidt et al. [9], and Challis et al. [10].

In the past 30 years, the potential role of the measurement of flow in the umbilical vein, ductus venosus and cardiac outflow tract was perceived as a possible direct insight into the core of cardiovascular pathophysiology, not just how it looks from the velocimetric waveforms but also how it supplies fetal metabolism and growth. However, for many years, the real limitation was set by expensive research ultrasound machines and by the expertise of research sonologists, until high-technology digital instruments have become the standard of quality in commercial ultrasound units nowadays.

27.2 Fetal Flow Volume Measurements in the Era of Digital Computing and Imaging

27.2.1 Sources of Inaccuracies

Umbilical venous fetal flow is a simple computed measure:

UV flow(mL/min) = crosscross − sectional area of the vein × mean velocity × 60where the flow is expressed in mL/min, the cross-sectional area is expressed in mm^2 and is calculated as $\pi \times \text{radius}^2$ and the mean velocity is computed in mm/s.

This formula underlines that the measure of the diameter is critical since its possible error will be squared by the calculation. Similar, but more complex, care should be taken for the error in the angle of interrogation of the Doppler beam, which can be corrected on the plane of the image itself but not within the thickness of the sonographic "slice" of the vessel. This is why the angle between the Doppler beam and the visible longitudinal axis of the vessel on the sonographic plane should always be less than 30°. The third source of error is determined by the attempt to calculate the true mean velocity of the venous flow. Most sonographic software are designed to extract the mean velocity out of the instantaneous Doppler shift analysis as an intensity-weighted mean velocity; however, when interrogated peak velocities are relatively slow (14–18 cm/s from 20 to 38 weeks of gestation), the amount of blood flow "cut" by high-pass filters might become relevant, and, in addition to this, each software operates on an analog-to-digital conversion of the Doppler shift and on the signal-to-noise ratio, which is largely dependent on the gain and on the software itself. The ideal flow model is a perfect parabolic flow evenly distributed in the vessel in

which the mean velocity is half that of the peak velocity (mean velocity = time-averaged peak velocity × 0.5). Therefore, the mean instantaneous velocity could be calculated by this simple coefficient, which takes into account the ideal shape of the flow in the cross-sectional area. These methodological problems are solved in a similar manner when the umbilical flow is measured in the intra-abdominal portion of the umbilical vein prior to its branching. Unfortunately, the conditions of a perfect parabolic flow are not always met in this vein. According to Pennati et al., [11] one should consider the fact that close to the placenta the flow profile is similar to a flat profile in which the mean velocity and peak velocity differ by a coefficient of 0.74, whereas all along the free loops, this coefficient is 0.61. This is higher than 0.5, and the normative data derived from the formula reported above underestimate true flow by 18%. However, in spite of this evidence, the general convention is to correct the time-averaged maximum velocity as if it were a perfect parabolic flow.

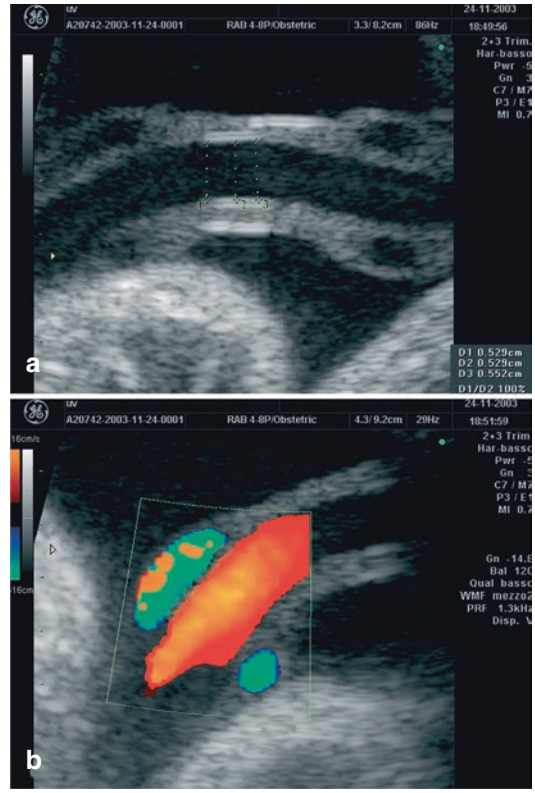

Fig. 27.1 (**a**) Magnified image of a straight section of the umbilical vein. (**b**) Magnified image of color imaging of the umbilical vein. Note how the peak velocities are skewed toward the external wall of the curved vein

27.2.2 Source of Accuracy

Imaging quality, color imaging quality, and pulsed Doppler velocimetry quality of today's technology have all overcome most of these limitations (Fig. 27.1).

In 1999, [12] we checked the intra- and inter-observer coefficients of variation of the umbilical vein diameter, mean velocity, and absolute flow. The diameter was calculated as the mean of three measurements on a magnified section of the cord. The brightest spot at a low amplification was assumed as the best marker of true diameter. The brightest ultrasound echoes are in fact those reflected back by orthogonal surfaces, which can be the case only when the ultrasound plane intersects the vessel at its true maximum diameter (Fig. 27.1). The ultrasound probe was tilted by 90°, and the Doppler beam was spotted on the same section of the vessel where the diameter was measured. We considered that it was more reproducible, simpler, and probably more accurate to assume for the given viscosity of blood, the diameter of the vessel and its length that an ideal parabolic flow truly occurs in those tracts of the umbilical vein where the lumen is linear for at least an approximate length of three times its diameter. The intra-observer coefficients of variation for the vein diameter, mean velocity, and absolute umbilical venous blood were 3.3%, 9.7%, and 10.9%, respectively. The inter-observer variabilities for the same parameters were 2.9%, 7.9%, and 12.7%, respectively. The same results were obtained by Lees et al. [13] and proved to be a little better for the intra-observer mean diameter calculated from four measurements of the UV (0.22 mm, respectively). Similar positive findings in reproducibility were reported by Boito et al. [14]. The coefficient of variation for the umbilical vein's cross-sectional area was 6.6%, and, for the time-averaged velocity, it was 10.5%, resulting in a coefficient of variation of 11.9% for

volume flow. The mean time required to obtain a complete set of measurements in our study was 3 min. These findings obtained in three different centers provide enough evidence to support the hypothesis that as far as reproducibility and clinical feasibility are concerned, today's technology is able to achieve accurate measurements of the umbilical vein flow in the human fetus.

27.2.3 Volume Flow Values and Problems of Standardization

The specific umbilical vein flow we calculated from our findings [12] was 129 mL/min kg^{-1} at 20 weeks of gestation and 104 mL/min kg^{-1} at 38 weeks of gestation. Boito et al. reported similar but lower values, i.e., 117.5 ± 33.6 mL/min kg^{-1} to 78.3 ± 12.4 mL/min kg^{-1}, for the same gestational age span [14].

di Naro et al., with a similar methodology, reported values of 126.0 ± 23.4 mL/kg per min at term [15]. Lees et al. [13] reported values as high as 176 mL/min kg^{-1}, which are closer to the mean arterial values measured by Kunzel et al. in 1992 (143 mm/kg min^{-1}) [16]. Actually, Lees et al. [13] was measuring an average of arterial and venous volume flow, and Kunzel et al. [16] was measuring the mean arterial flow. Accurate hemodynamic modeling of a pulsatile flow is quite complex, mostly because of problems in assessing the time-averaged mean velocity [17]. If we compare our present (108 mL/min kg^{-1} at 32–41 weeks of gestation), we appreciate the fact that these mean values are at the same level of umbilical volume flow measured by Eik-Nes et al. back in 1982 [3] (115 mL/min kg^{-1}). The only difference with these "historical" reports is the time required to obtain these measurements and their reproducibility. Other methodologies had been tested for the same purpose by Kiserud [18] and Chantraine et al. [19]. In this brief analysis, we have met many methodologies that differ from our simple diameter–peak velocity interrogation: offline measurement of the cross-sectional area, software-dependent measurements of time-averaged mean velocity, mean values of venous and arterial flow measurements, and non-Doppler flow measurements. It is quite evident from published methodologies and results that the variability in measurements between centers is not stochastic; rather it is systematic, depending on the different methodologies adopted. So far, the simpler the better should be the preferred choice.

27.2.4 Comparison Between Non-invasive Doppler Volume Flow Values and Experimental Research

The simple "diameter–peak velocity × 0.5" methodology was applied to the two veins of fetal lambs versus historical measurements of flow obtained with an invasive technique [12]. Gestational age and fetal weights were not different between the animals studied by the Doppler technique (129.6 ± 2.8 days and 2.75 ± 0.26 kg, respectively) and steady-state data (131.6 ± 4.1 days and 2.94 ± 0.68, respectively). Variability between the groups was similar (*f*-test; $p = 0.138$). No significant differences were detected between the Doppler and diffusion technique groups for umbilical venous flow (210.8 ± 18.8 and 205.7 ± 38.5 mL/min kg^{-1}; $p = 0.881$).

A second study was then performed on the same set of seven animals [20]. Ultrasound Doppler and the steady-state diffusion technique yielded virtually identical results (207 ± 9 vs 208 ± 7 mL/min kg^{-1}). A serendipitous result of that study was that the venous flow in each one of the two veins of the lamb was strictly correlated with the weight of the cotyledons serving each vein. The accuracy of volume flow measurements was tested by di Naro et al. [15] on human fetuses with different characteristics of the umbilical cord, normal coiled cord, and non-coiled lean cord, assuming and proving that the latter is a less favorable hemodynamic condition for umbilical circulation.

The next step, which is relatively independent from systematic differences caused by various methodologies, is to observe what is happening under varied intrauterine conditions of the fetus

and the placenta. According to Kiserud et al., maternal hypoxemia in 12 pregnant sheep caused significantly reduced maximum and weighted mean blood velocity [21]. According to Padoan et al. at the University of Colorado Health Sciences Center, weight-specific umbilical venous flow is significantly reduced in fetal lambs affected by health stress chronic growth restriction compared with normal fetuses of comparable gestational age (129.4 ± 14.8 vs 176.4 ± 13.3 mL/min kg^{-1}; $p < 0.05$) and is correlated with pO_2 (10.9 ± 1.2 vs 19.1 ± 0.7; $p < 0.001$) [22].

27.3 The Relationship of Umbilical Vein Blood Flow with Growth in the Human Fetus

Umbilical blood flow increases throughout pregnancy from 63 mL/min at 20 weeks to 373 mL/min at 38 weeks [12]. This is related to fetoplacental growth, and normalization of the absolute volume flow per fetal growth is obviously necessary. However, in general, the estimation of fetal weight has a possible error of approximately ±10% in 68% of cases. This error can even be larger in growth-restricted or macrosomic fetuses in which there is a change in the volumetric proportion between the head and abdomen. As a result, expressing blood flow per kilogram estimated fetal weight introduces unnecessary random errors and may obscure the underlying pathophysiology. In contrast, the abdominal circumference as measured by ultrasound has been shown in many studies to serve as an early and sensitive biometric indicator of fetal growth restriction. In severe FGR, the head circumference growth might be partially spared by redistribution of flow to the central nervous system, and, as such, in these cases, normalization of absolute blood flow according to the head circumference might help correlate poor growth with umbilical vein flow. The chapter on the ductus venosus will help clarify the shunting mechanism that allows the umbilical vein flow to be diverted from the liver to the head. Therefore, reporting data both as weight-specific or abdominal or head circumference-specific values might serve different research aims. The latter two could help compare "real measurements," and it could better serve the purpose of using flow volume in clinical practice.

27.4 Clinical Value of Umbilical Vein Blood Flow in Severe Fetal Growth Restriction

When comparing normal fetuses to early severe FGR, it is important that the flow be related to some index of tissue mass and not to gestational age. In our experience [23], umbilical volume flow in growth-restricted fetuses is reduced both as an absolute value and on a weight basis (Fig. 27.2).

If we consider only those growth-restricted fetuses delivered without ominous heart rate signs (mean gestational age 32 ± 4 weeks; mean weight 1265 ± 424 g) weight-specific umbilical flow (mL/min kg^{-1}) was significantly lower than that in controls of comparable gestational age (98.4 ± 19.1 vs 117.1 ± 29.9; $p < 0.001$). A much larger difference was observed when flow measurements were obtained on growth-restricted fetuses with an abnormal heart rate, just before elective delivery (mean gestational age

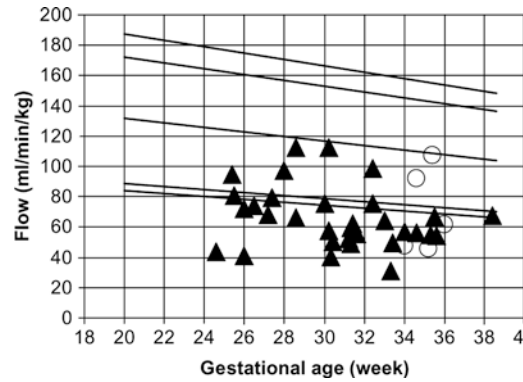

Fig. 27.2 Umbilical venous flow per unit weight (ml/min kg^{-1}). Growth-restricted fetuses with an abnormal umbilical arterial pulsatility index (triangles). Growth-restricted fetuses with a normal umbilical arterial pulsatility index (circles). The 2nd, 5th, 50th, 95th, and 98th percentiles of normal reference values

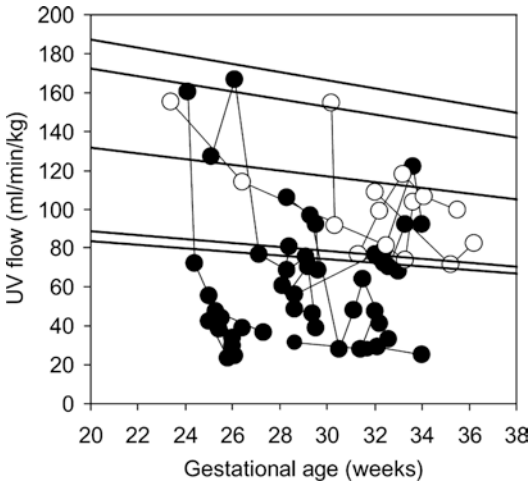

Fig. 27.3 Longitudinal assessment of umbilical venous flow per unit weight (mL/min kg^{-1}). Growth-restricted fetuses with an abnormal umbilical arterial pulsatility index (full circles). Growth-restricted fetuses with a normal umbilical arterial pulsatility index (empty circles). The 2nd, 5th, 50th, 95th, and 98th percentiles of normal reference values

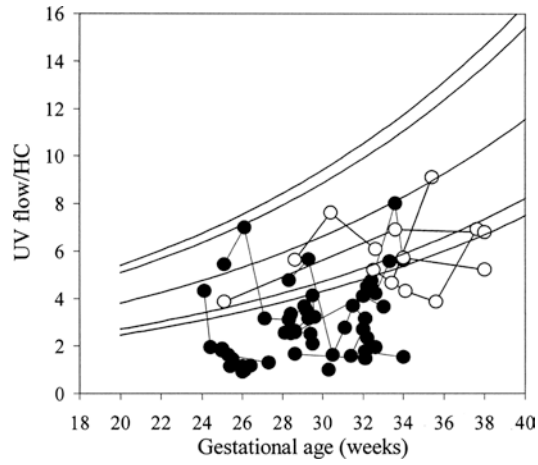

Fig. 27.4 Longitudinal assessment of umbilical venous flow per head circumference (mL/min mm^{-1}). Growth-restricted fetuses with an abnormal umbilical arterial pulsatility index (full circles). Growth-restricted fetuses with a normal umbilical arterial pulsatility index (empty circles). The 2nd, 5th, 50th, 95th, and 98th percentiles of normal reference values. HC, head circumference

29 ± 3 weeks; mean weight 962 ± 334 g; 63.0 ± 22.1 vs 124.0 ± 30.3 mL/min kg^{-1}; $p < 0.001$). Boito et al. reported umbilical volume flows per kilogram fetal weight below the normal range in 21 of 33 growth-restricted fetuses [14]. These findings were replicated by the same group on a second series [24] of 23 growth-restricted fetuses who showed a significant lower weight-specific flow compared with that of controls (59.6 vs 104.7 mL/min kg^{-1}; $p < 0.001$).

A better understanding of fetal physiology under a condition of growth restriction due to poor placental development can be derived by umbilical flow volume measurements when cross-sectional measurements obtained at a late stage of growth restriction, i.e., just before elective premature delivery, are proceeded by longitudinal observation from the early stage of the disease. Rigano et al. [25] showed that UV weight-specific flow (mL/min kg^{-1}) was reduced at the time of patient enrolment in 15 of 21 FGR fetuses. By the time of delivery, 16 of these FGR fetuses had UV weight-specific flow less than the tenth percentile. Figure 27.3 shows longitudinal umbilical flow volumes in growth-restricted fetuses per unit fetal weight both with an abnormal and a normal umbilical pulsatility index (PI). These observations suggest that flow reduction is present weeks before heart rate abnormalities. These data were replicated by di Naro et al. [26]. Despite the different methodologies and slightly different absolute values, the same message of early reduction was confirmed.

Figure 27.4 shows the same volume flow measurements as Fig. 27.3. In this analysis, absolute flow values are normalized by the head circumference (mL/min mm^{-1}). The advantage of this normalization stems from the fact that the fetal head is an area of preferential distribution of flow and growth in fetuses with restricted delivery of nutrients, energy, and oxygen [27]; therefore, this index of fetal body mass improves the sensitivity of flow assessment in asymmetrical growth-restricted fetuses.

The increase in flow volume throughout gestation in normal fetuses is accounted for mainly by growth of the diameter of the vein. This increased from 4.1 to 8.3 mm, which would lead to a four-fold increase in the cross-sectional area, whereas the velocity increased by only 20% from 0.08 m/s at 20 weeks to 0.10 m/s at 38 weeks [12]. When blood velocity and diameter are normalized for

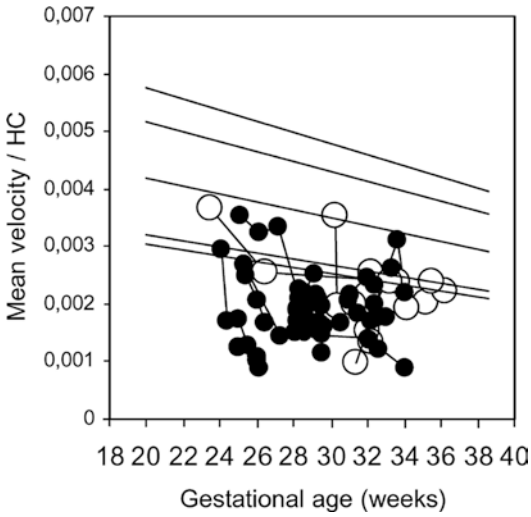

Fig. 27.5 Umbilical venous mean velocity per unit head circumference (mL/min mm^{-1}). Growth-restricted fetuses with an abnormal umbilical arterial pulsatility index (full circles). Growth-restricted fetuses with a normal umbilical arterial pulsatility index (empty circles). The 2nd, 5th, 50th, 95th, and 98th percentiles of normal reference values. HC, head circumference

fetal mass, an interesting result that can be observed in growth-restricted fetuses is that the diameter in small fetuses is not narrower than that of normal fetuses of comparable mass, whereas the main variable to decrease is blood velocity (Fig. 27.5). According to these data, velocity itself could be used as a simple diagnostic test in growth-restricted fetuses. According to fetal sheep experiments, [28] pressures and flow velocities are inversely related in the venous inflow tract from the umbilical vein into the ductus venosus and inferior vena cava. This finding brings in both vessels, the umbilical vein and ductus venosus, a diagnostic potential and a pathophysiological variable of interest.

In the work by Boito et al. [24], a complex set of ultrasound volumetric measurements was performed on the head and on the abdomen of restricted and normal fetuses and a significant ($p < 0.001$) inverse relationship was observed between the fetal weight-related umbilical venous volume flow and the fetal brain/liver volume ratio. The same diagnostic-oriented usage of umbilical venous flow was adopted by Tchirikov and coworkers [29]. In their reported experience, the ratio between the weight-specific umbilical vein blood volume (mL/min kg^{-1}) and the umbilical artery PI was a better predictor of poor fetal outcome than the umbilical arterial PI alone.

The importance of umbilical vein flow volume is such that its measurement is included in the 6 years' multi-center study EVVEREST focused on early severe FGR prior to 26 weeks of gestation [29] and even in randomized studies designed to prevent FGR by low-molecular-weight heparin [30].

27.5 Diagnostic Usage of Umbilical Vein Blood Flow in Late Growth Restriction and in "Constitutionally Small Fetuses"

Late growth restriction is becoming a topic of major interest both because it covers a much larger clinical field and because the criteria for diagnosis and timing of delivery are still under extensive clinical research, probably due to the heterogeneity of conditions apparently sharing the same poor "biometric sonographic" growth [31]. With regard to the prediction of outcomes, two parallel papers agree on the fact that umbilical vein flow yielded better predictive gains than did other biophysical diagnostic tools in late growth-restricted fetuses [32, 33].

According to M. Parra-Saavedra et al. [33], fetuses with an UBVF below 68 mL/min/kg had twice the risk of non-reassuring fetal status in induced labor. If we go back to 1987, the UVBF measured 2 days before delivery in late FGR fetuses delivered at 35 weeks of gestation with an average weight of 1635 g was 68 mL/min/kg [34]. This value is very close to the one that we observed in early FGR with an abnormal heart rate in utero (63 mL/min/kg) [23]. Based on these similarities observed by diverse centers with different equipment and different cohorts of fetuses, it is not a speculation that fetal metabolism should be close to its biological limits when this value of flow is reached.

Rizzo et al. [32] observed in a prospective study on 243 pregnancies complicated by late

FGR that "UVBF/AC showed a significantly better although moderate accuracy in predicting adverse outcome at the time of their diagnosis," as such performing as a better predictor than the cerebroplacental ratio. Unfortunately, UVBF is reported as a *z*-value and never as the real observed measure.

The timing of examination seems to be of critical importance. For near term, on the occasion of the diagnosis, it is no surprise the UBVF is a better predictor of poor nutrition as a source of growth restriction. Whereas, the cerebroplacental ratio might better represent a critical sign of flow redistribution at term to preserve the central nervous tissue for its energy dependence.

Our personal experience is in agreement with works that show the superiority of umbilical vein flow volume measurement over the simple umbilical artery waveform and its impedance indices in late FGR with normal uterine and umbilical Doppler velocimetry and an AC not below the third centile. Figure 27.6 shows how the vast majority of a cohort of naturally screened fetuses, at the Burlo Garofolo Research Institute, Trieste, Italy, after 34 weeks of gestation, with an abdominal circumference below the tenth percentile or a late flattening of two quartiles with a normal umbilical artery PI had indeed significantly low values of flow volume both as absolute and as normalized per kilogram weight.

Special attention ought to be focused on those fetuses with low absolute flow volume, poor growth, and "normal" flow per kilogram of weight. In our view, these fetuses adapted to a poor environment, thus reducing their growth and metabolism. These fetuses, who otherwise fall under the category of "constitutionally small fetuses," could be defined as affected by growth impairment, or stunted growth, much similar to the concept of stunted child growth occurring in undernourished children who adapt to a poor environment and grow along the lower childhood centiles and are healthy under normal environmental conditions but are more fragile and prone to succumb to infections and/or trauma.

We have observed a similar adaptive phenomenon when measuring the flow volume of the uterine arteries [35]. Uterine artery blood flow volume was strikingly reduced per unit of fetal weight at mid-gestation, when the estimated fetal weight was still within normal values, in fetuses then showing early growth restriction, 142 mL/min/kg vs. 538 mL/min/kg in uneventful normal pregnancies matched for gestational age, between

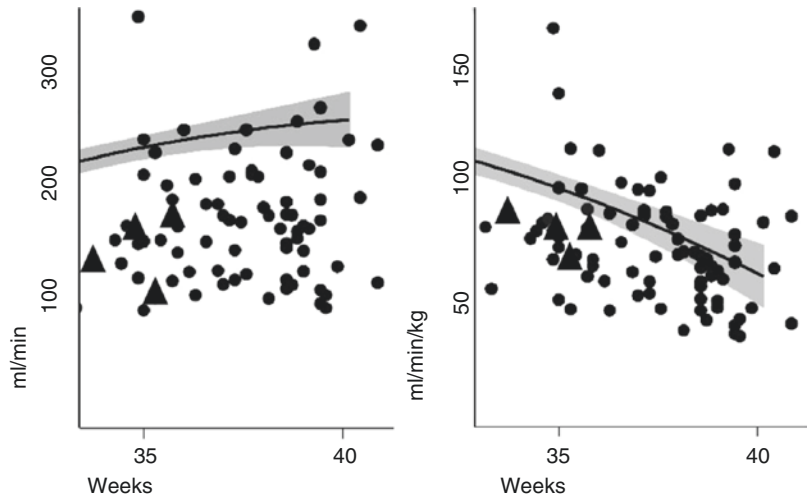

Fig. 27.6 Blood flow at the last detection by the UVBF in fetuses with growth appropriate for gestational age (solid line: quadratic regression; dashed lines: 95% confidence intervals of the regression) and fetuses with CA <10° or late growth impairment of more than two quartiles (orange points: umbilical artery PI abnormal, $n = 4$; green points: normal umbilical artery PI, $n = 72$). Panel (**a**) absolute blood flow. Panel (**b**) blood flow normalized for fetal weight; SGA fetuses with a normal umbilical PI vs controls, $p = 0.03$)

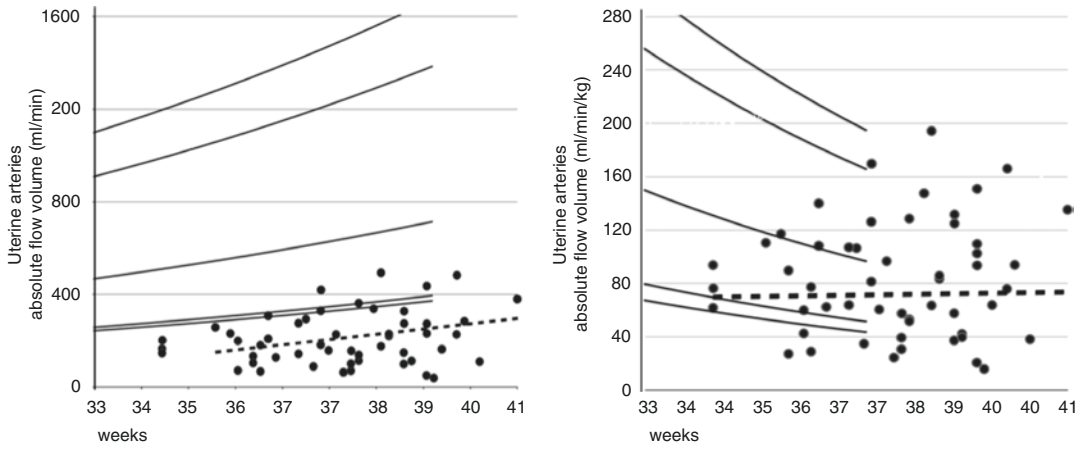

Fig. 27.7 Black lines: reference values for uterine blood flow volume, 3rd, 5th, 50th, 95th, and 97 centiles. Black dots: 54 "constitutionally small fetuses." Panel (**a**) absolute uterine blood flow volume. Panel (**b**) uterine blood flow volume per unit fetal weight

20 and 25 weeks of gestation ($p < 0.0001$). To further investigate this relation between uterine blood flow volume and late "constitutionally" small-for-gestational-age fetuses, in a recent, unpublished pilot study, we have measured the uterine blood flow in 54 SGA fetuses with normal uterine and umbilical Doppler velocimetry, not meeting the definition of late FGR according to the Delphi consensus [36] prior to any sign of fetal distress at fetal heart rate examination or middle cerebral artery interrogation.

Figure 27.7 shows how absolute uterine blood flow in these "constitutionally" small fetuses was significantly below the normal range [37]. Yet, when normalized for unit weight, many of these showed an "appropriate" uterine blood flow supply. This could be interpreted as a result of an adaptive mechanism, resulting in a reduced thrifty growth to match a poor nutritional environment.

References

1. Eik-Nes SH, Brubak AO, Ulstein M. Measurement of human fetal blood flow. Br Med J. 1980;280:283–4.
2. Gill RW, Trudinger BJ, Garrett WJ, Kossoff G, Warren PS. Fetal umbilical venous flow measured in utero by pulsed Doppler and B-mode ultrasound. I. Normal pregnancies. Am J Obstet Gynecol. 1981;139:720–5.
3. Eik-Nes SH, Maršál K, Brubak AO, Kristofferson K, Ulstein M. Ultrasonic measurement of human fetal blood flow. J Biomed Eng. 1982;4:28–36.
4. Erskine RL, Ritchie JW. Quantitative measurement of fetal blood flow using Doppler ultrasound. Br J Obstet Gynaecol. 1985;92:600–4.
5. Giles WB, Lingman G, Maršál K, Trudinger BJ. Fetal volume blood flow and umbilical artery flow velocity waveform analysis: a comparison. Br J Obstet Gynaecol. 1986;93:461–5.
6. Gerson AG, Wallace DM, Stiller RJ, Paul D, Weiner S, Bolognese RJ. Doppler evaluation of umbilical venous and arterial blood flow in the second and third trimesters of normal pregnancy. Obstet Gynecol. 1987;70:622–6.
7. Reed KL, Meijboom EJ, Sahn DJ, Scagnelli SA, Valdes-Cruz LM, Shenker L. Cardiac Doppler flow velocities in human fetuses. Circulation. 1986;73:41–6.
8. Sutton MS, Theard MA, Bhatia SJ, Plappert T, Saltzman DH, Doubilet P. Changes in placental blood flow in the normal human fetus with gestational age. Pediatr Res. 1990;28:383–7.
9. Schmidt KG, di Tommaso M, Silverman NH, Rudolph AM. Doppler echocardiographic assessment of fetal descending aortic and umbilical blood flows. Validation studies in fetal lambs. Circulation. 1991;83:1731–7.
10. Challis DE, Warren PS, Gill RW. The significance of high umbilical venous blood flow measurements in a high-risk population. J Ultrasound Med. 1995;14:907–12.
11. Pennati G, Bellotti M, Ferrazzi E, Rigano S, Garberi A. Hemodynamic changes across the human ductus venosus: a comparison between clinical findings and mathematical calculations. Ultrasound Obstet Gynecol. 1997;9:383–91.
12. Barbera A, Galan HL, Ferrazzi E, Rigano S, Jzwik M, Battaglia FC, Pardi G. Relationship of umbilical vein blood flow to growth parameters in the human fetus. Am J Obstet Gynecol. 1999;181:174–9.

13. Lees C, Albaiges G, Deane C, Parra M, Nicolaides KH. Assessment of umbilical arterial and venous flow using color Doppler. Ultrasound Obstet Gynecol. 1999;14:250–5.
14. Boito S, Struijk PC, Ursem NT, Stijnen T, Wladimiroff JW. Umbilical venous volume flow in the normally developing and growth-restricted human fetus. Ultrasound Obstet Gynecol. 2002;19:344–9.
15. di Naro E, Ghezzi F, Raio L, Franchi M, D'Addario V, Lanzillotti G, Schneider H. Umbilical vein blood flow in fetuses with normal and lean umbilical cord. Ultrasound Obstet Gynecol. 2001;17:224–8.
16. Kunzel W, Jovanovic V, Grussner S, Colling T. Blood flow velocity in the fetal abdominal aorta and in the umbilical artery in uncomplicated pregnancies. Eur J Obstet Gynecol Reprod Biol. 1992;23:31–40.
17. Kiserud T, Rasmussen S. How repeat measurements affect the mean diameter of the umbilical vein and the ductus venosus. Ultrasound Obstet Gynecol. 1998;11:419–25.
18. Kiserud T. Umbilical venous blood flow and reference ranges. Acta Obstet Gynecol Scand. 2003;82:1061.
19. Chantraine F, Reihs T, Henrich W, Tutschek B. Measurement of volume flow by "colour velocity imaging (CVI)": technique of measurement in the intrahepatic fetal umbilical vein. Zentralbl Gynäkol. 2003;125:179–82.
20. Galan HL, Jozwik M, Rigano S, Regnault TR, Hobbins JC, Battaglia FC, Ferrazzi E. Umbilical vein blood flow determination in the ovine fetus: comparison of Doppler ultrasonographic and steady-state diffusion techniques. Am J Obstet Gynecol. 1999;181:1149–53.
21. Kiserud T, Jauniaux E, West D, Ozturk O, Hanson MA. Circulatory responses to maternal hyperoxaemia and hypoxaemia assessed non-invasively in fetal sheep at 0.3–0.5 gestation in acute experiments. BJOG. 2001;108:359–64.
22. Padoan A, Regnault TRH, Limesand SW, Russell AV, Enrico Ferrazzi A, Wilkening RB, Galan HL. Endothelial nitric oxide synthase in uteroplacental vasculature in an ovine model of FGR. Am J Obstet Gynecol Suppl. 2004.
23. Ferrazzi E, Rigano S, Bozzo M, Bellotti M, Giovannini N, Galan H, Battaglia FC. Umbilical vein blood flow in growth-restricted fetuses. Ultrasound Obstet Gynecol. 2000;16:432–8.
24. Boito S, Struijk PC, Ursem NT, Fedele L, Wladimiroff JW. Ultrasound fetal brain/liver volume ratio and umbilical volume flow parameters relative to normal and abnormal human development. Ultrasound Obstet Gynecol. 2003;21:256–61.
25. Rigano S, Bozzo M, Ferrazzi E, Bellotti M, Battaglia FC, Galan HL. Early and persistent reduction in umbilical vein blood flow in the growth-restricted fetus: a longitudinal study. Am J Obstet Gynecol. 2001;85:834.
26. di Naro E, Raio L, Ghezzi F, Franchi M, Romano F, Addario VD. Longitudinal umbilical vein blood flow changes in normal and growth-retarded fetuses. Acta Obstet Gynecol Scand. 2002;81:527–33.
27. Lngman G, Maršál K. Noninvasive assessment of cranial blood circulation in the fetus. Biol Neonate. 1989;56:129–35.
28. Schroder HJ, Tchirikov M, Rybakowski C. Pressure pulses and flow velocities in central veins of the anesthetized sheep fetus. Am J Physiol Heart Circ Physiol. 2003;284:H1205–11.
29. Spencer R, Ambler G, Brodszki J, Diemert A, Figuera F, Gratacós E, Hansson SR, Hecher K, Huertas-Ceballos A, Marlow N, Marsál K, Morsing E, Peebles D, Rossi C, Sebire NJ, Timms JF, David AL, EVERREST Consortium. EVERREST prospective study: a 6-year prospective study to define the clinical and biological characteristics of pregnancies affected by severe early onset fetal growth restriction. BMC Pregnancy Childbirth. 2017;17:43–50.
30. Mazarico E, Peguero A, Camprubí M, Carlota Rovira C, Roig MDG, Oros D, Ibáñez-Burillo P, Schoorlemmer J, Masoller N, Tàssies MD, Figuera F. Study protocol for a randomised control trial: treatment of early fetal growth restriction with low molecular weight heparin (TRACIP). BMJ Open. 2018;8:e020501.
31. Bernardes TP, Broekhuijsen K, Koopmans CM, Boers KE, van Wyk L, Tajik P, van Pampus MG, Scherjon SA, Mol BW, Franssen MT. Caesarean section rates and adverse neonatal outcomes after induction of labour versus expectant management in women with an unripe cervix: a secondary analysis of the HYPITAT and DIGITAT trials. BJOG. 2016;123:1501–8.
32. Rizzo G, Mappa I, Bitsadze V, Słodki M, Khizroeva J, Alexander Makatsarya A, D'Antonio F. Role of Doppler ultrasound in predicting perinatal outcome in pregnancies complicated by late-onset fetal growth restriction at the time of diagnosis: a prospective cohort study. Ultrasound Obstet Gynecol. 2019;55:793–8. Epub ahead of print.
33. Parra-Saavedra M, Crovetto F, Triunf S, Savchev S, Parra G, Sanz M, Gratacos E, Figueras F. Added value of umbilical vein flow as a predictor of perinatal outcome in term small-for-gestational-age fetuses. Ultrasound Obstet Gynecol. 2013;42:189–95.
34. Laurin J, Lingamn G, Marsal K, Persson P. Fetal blood flow in pregnancies complicated by intrauterine growth retardation. Obstet Gynecol. 1987;69:895–902.
35. Ferrazzi F, Rigano S, Padoan A, Boito S, Pennati G, Galan HL. Uterine artery blood flow volume in pregnant women with an abnormal pulsatility index of the uterine arteries delivering normal or intrauterine growth restricted newborns. Placenta. 2011;32:487–92.

36. Gordijn SJ, Beune IM, Thilaganathan B, Papageorghiou A, Baschat A, Baker PN, Silver RM, Wynia K, Ganzevoort K. Consensus definition of fetal growth restriction: a Delphi procedure. Ultrasound Obstet Gynecol. 2016;48:333–9.

37. Rigano S, Ferrazzi E, Boito S, Pennati G, Padoan A, Galan HL. Blood flow volume of uterine arteries in human pregnancies determined using 3D and bi-dimensional imaging, angio-Doppler, and fluid-dynamic modeling. Placenta. 2010;31:37–43.

The Ductus Venosus

28

Torvid Kiserud and Jörg Kessler

28.1 Historical Background

The ductus venosus (ductus Arantii, venous duct) is one of the three physiological shunts responsible for the circulatory adaptation to intrauterine life. It is attributed to Giulio Cesare Aranzi (1530–1589), but the first written account dates back to his contemporary Andreas Vesalius, the Flemish Andries van Wesel, in 1561 [1]. Its function has long been recognized [2–5], but was of hardly any clinical importance until ultrasound techniques were introduced [6–10]. It is now widely used as part of the hemodynamic assessment of the fetus [11–14].

28.2 Functional Anatomy

During the early days of gestation, the ductus venosus is formed as a confluence of hepatic sinuses that develops into a separate channel [15–18]. Ultrasound visualization [19–24] and volume flow calculations [25–27] indicate that the ductus venosus has a prominent role from early pregnancy when its flow is relatively high compared with the last trimester. During the second and third trimesters, the ductus venosus is a thin, slightly trumpet-shaped vessel connecting the intra-abdominal umbilical vein with the inferior vena cava (IVC) (Figs. 28.1 and 28.2). Its inlet, the isthmus, grows from an average of 0.7 mm at 18 weeks to 1.7 mm at 40 weeks of gestation; its outlet grows correspondingly from 2 to 3 mm and its length from 5 to 15 mm [25, 29, 30]. It leaves the umbilical vein (the portal sinus) in a cranial and dorsal direction and reaches the IVC at the level of the hepatic venous confluence shortly below the atria. This section of the IVC is shaped as a funnel [31] but expands predominantly to the left side to receive blood from the ductus venosus and the left and middle hepatic veins [28, 32]. Although variations in direction have been reported, the ductus venosus approaches the IVC at a fairly steep angle (on average, 48°) [32]. In early pregnancy, the ductus venosus tends to be a straight continuation of the umbilical vein. In late pregnancy, a curvature after the isthmus is common but at varying degrees (Fig. 28.3). The relation to the left and middle hepatic veins is close, and, sometimes, their junction with the IVC cannot be distinguished from that of the ductus venosus [33].

Supplementary Information The online version contains supplementary material available at [https://doi.org/10.1007/978-3-031-06189-9_28].

T. Kiserud (✉) · J. Kessler
Department of Obstetrics and Gynecology, Haukeland University Hospital, Bergen, Norway

Department of Clinical Science, Medical Faculty, University of Bergen, Bergen, Norway
e-mail: torvid.kiserud@uib.no

D. Maulik, C. C. Lees (eds.), *Doppler Ultrasound in Obstetrics and Gynecology*,
https://doi.org/10.1007/978-3-031-06189-9_28

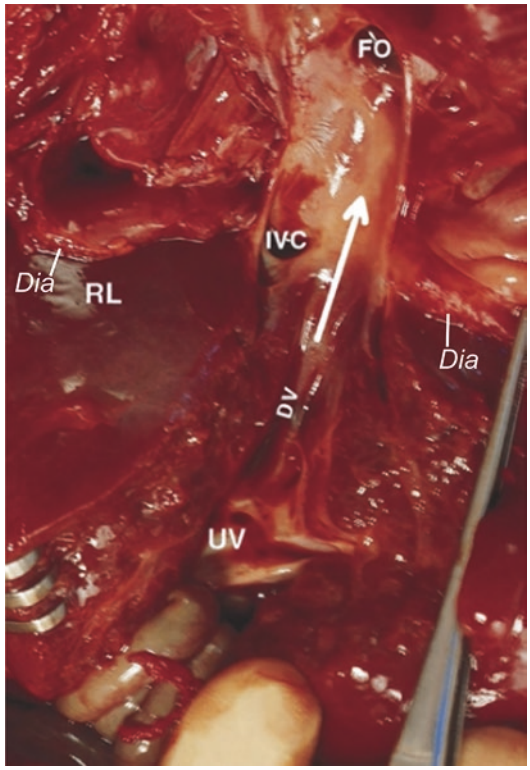

Fig. 28.1 Anterior anatomical view of the fetal liver divided to expose the trumpet-shaped ductus venosus (DV) at 39 weeks of gestation. The DV leaves the abdominal portion of the umbilical vein (UV) in the direction of the foramen ovale (FO). When the abdominal inferior vena cava (IVC) reaches the liver, it expands into a funnel to receive the flow from the hepatic veins and DV. The funnel widens predominantly to the left where it guides the DV flow (arrow) toward the FO. Dia, diaphragm; RL, right lobe of the liver (modified from Kiserud [28])

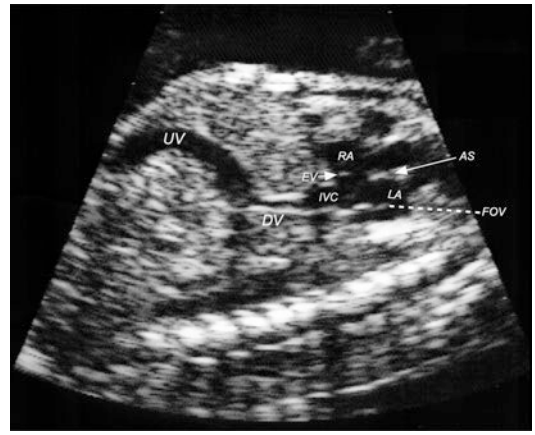

Fig. 28.2 Ultrasound image of the fetal shunt ductus venosus (DV) at 30 weeks of gestation, connecting the intra-abdominal umbilical vein (UV) directly to the inferior vena cava (IVC) just before the latter penetrates the diaphragm to enter the heart. Note that in this sagittal section, the abdominal IVC is not visualized as it is slightly to the right in the fetus. Envisage that the blood from the DV flowing through the IVC is directed essentially behind the atrial septum (AS) to enter the left atrium (LA). Note also that the foramen ovale valve (FOV) and the shorter Eustachian valve (EV) operate as an extension of the IVC, fencing the ascending blood column from the LA and right atrium (RA) until it hits the edge of the AS, called the crista dividens, and is either distributed to the LA via the channel between the AS and FOV or to the RA. A corresponding sagittal section to the right would have exposed the abdominal IVC in a more anterior direction connecting to the RA

A sphincter has been suggested to operate at the inlet, the isthmus [15, 34–37], but the scarcity of muscular and neuronal elements in the human ductus venosus has raised doubts as to whether such a sphincter exists [38–41]. Adrenergic nerves have been traced in the inlet area [42]. An α-adrenergic constriction and a β-adrenergic relaxation have been reported [41, 43, 44]. Both the prostaglandin and a peroxidase P-450 mechanisms have been suggested to function in the ductus venosus in the same manner as described for the ductus arteriosus [45–48]. The mechanisms could be responsible for the patency during fetal life and its closure in postnatal life; however, in contrast to the ductus arteriosus, oxygen does not seem to trigger the obliteration of the ductus venosus [49]. Other studies indicate that it is the entire length of the ductus venosus that is active during regulation [41, 50, 51], which makes sense since resistance increases in proportion to the length of the tube (see Chap. 5). Additionally, this regulatory mechanism is less sensitive to adrenergic stimuli than the portal venous branches in the liver tissue [41].

Topographically and functionally, the ductus venosus appears to be connected to the foramen ovale in the primate [52], fetal lamb [53, 54], and human fetus [3, 7, 55, 56]. In the fetal sheep, there is a valvular membrane that directs blood from the ductus venosus into the fairly long tho-

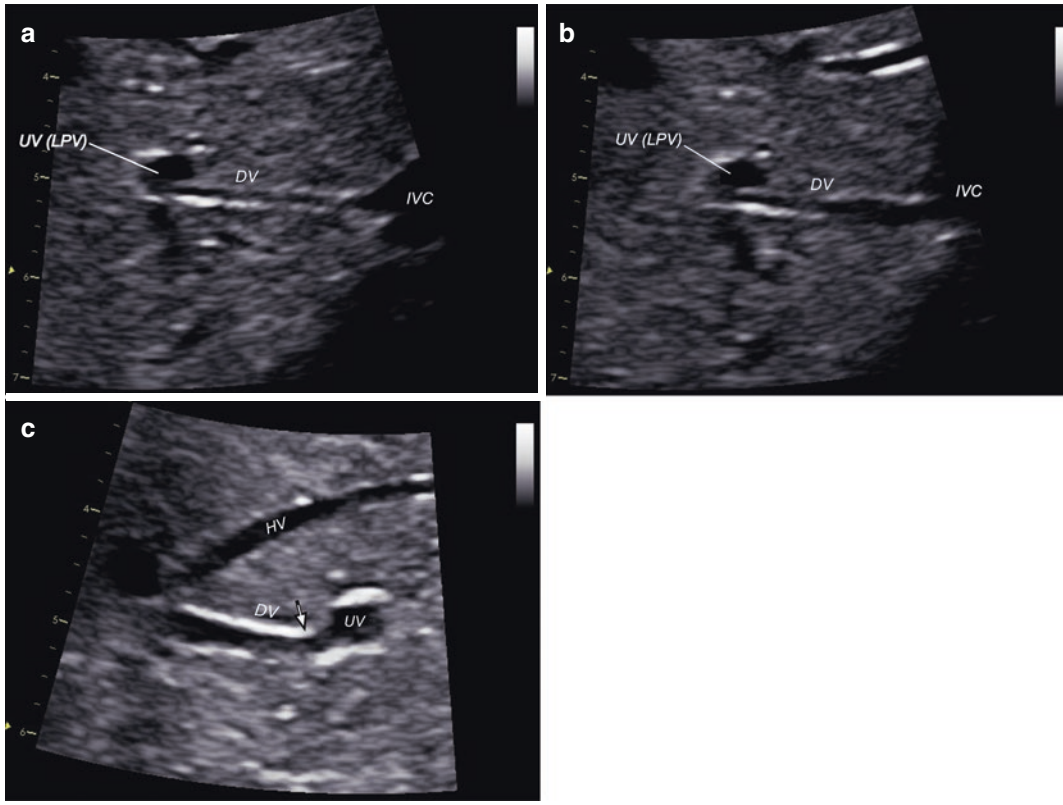

Fig. 28.3 At its inlet, the ductus venosus (DV) has an isthmus that tends to be straight for a few millimeters and stays slim, at an average one-fourth of the diameter of the umbilical vein (UV) during the second and third trimesters. However, variation occurs commonly with a corresponding contribution to flow resistance. In panel (**a**), the DV remains slim throughout its length (31 weeks' gestation). In panel (**b**), moments later, the same DV had widened toward its outlet, reducing vascular resistance. While the inlet isthmus tends to remain straight, the body of the DV frequently bends or angulates (arrow) as pregnancy progresses (panel **c**). *HV* hepatic vein, *IVC* inferior vena cava, *LPV* left portal vein

racic IVC to reach the foramen ovale streaming with minimal blending with the low-oxygenated abdominal IVC blood [4]. Although this pattern is the common method of presenting the topographical relation in anatomical illustrations of the human anatomy, it is quite different from the true human anatomy. The thoracic IVC is short or non-existent in the human fetus in which the heart with its atria is positioned on top of the liver only separated by a thin diaphragm (Figs. 28.1 and 28.4). Furthermore, there is no valve developed at the ductus venosus outlet. Thus, the ductus venosus is directed toward the foramen ovale from a short distance and avoids extensive blending with low-oxygenated blood from the abdominal IVC [32].

28.3 Hemodynamic Background

Since the placenta, not the lungs, is the site for gas exchange during fetal development, the circulation is organized correspondingly differently (see Chap. 8). The ductus venosus plays an important role in this, directing oxygenated blood from the umbilical vein to the left atrium as part of the via sinistra (Fig. 28.4). Simultaneously, the ductus is involved in tuning liver perfusion.

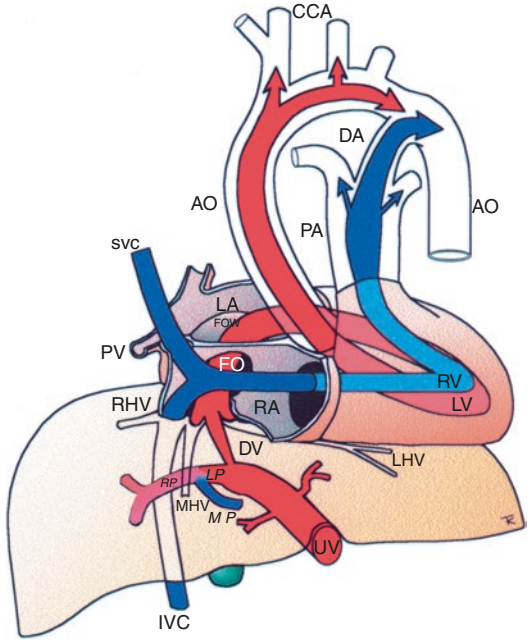

Fig. 28.4 Fetal circulatory pathways showing the three shunts, ductus arteriosus (DA), ductus venosus (DV), and the foramen ovale (FO). The via sinistra (red) directs blood from the umbilical vein (UV) through the DV and FO to reach the left atrium (LA), left ventricle (LV), and ascending aorta (AO), thus supplying the coronary and cerebral circuit with well-oxygenated blood before joining with the via dextra (blue) in the descending AO. The via dextra receives deoxygenated blood from the abdominal inferior vena cava (IVC) and the superior vena cava (SVC) directed toward the right atrium (RA), right ventricle (RV), and pulmonary trunk (PA), bypassing the pulmonary circuit through the DA. Splanchnic blood from the main portal stem (MP) is provided to the right liver lobe after blending with umbilical blood that reaches the right portal branch (RP) through the left branch (LP). *CCA* common carotid artery, *FOV* foramen ovale valve, *LHV* left hepatic vein, *MHV* medial hepatic vein, *PV* pulmonary vein, *RHV* right hepatic vein (modified from Kiserud et al. [25])

28.3.1 Via Sinistra and Via Dextra

The classical concepts of the two central pathways, via sinistra and via dextra, are still valid. While the via dextra transports deoxygenated blood, the via sinistra carries well-oxygenated blood, and the ductus venosus is an important part of the that (Fig. 28.4). As a direct connection between the umbilical vein and the central venous system, it has the capacity to shunt well-oxygenated blood directly into the central circulation and feed the left atrium through the foramen ovale, thus ensuring oxygenated blood to the coronary and cerebral circuit. During the second half of a normal pregnancy, the ductus flow steadily increases, but, relative to fetal weight, it actually decreases (Fig. 28.5) [25, 27].

Animal studies have shown that around 50% of the umbilical blood enters the ductus venosus [52, 53, 57, 58]. However, in human fetuses, it is around 30% at 20 weeks and reaches a nadir of roughly 20% in the third trimester when measured by Doppler ultrasound techniques (Fig. 28.6) [25–27, 59]. Thus, shunting through the ductus venosus seems more prominent at mid-gestation than at term, but variation is substantial. During experimental hypoxemia and hypovolemia, the ductus venosus flow is maintained [52, 57, 60–63]; however, since the flow to the liver is reduced, the fraction of umbilical blood directed through the ductus venosus increases to 70% [52, 57, 59–63]. A similar effect seems to be present in growth-restricted human fetuses (Fig. 28.7) [59, 64–66].

28.3.2 The Distributional Unit Ductus Venosus–Foramen Ovale

As mentioned above (Sect. 28.2), the human anatomy is different from those of experimental animals such as sheep and pigs. Since this distinction is not well-known, but has implications for understanding how blood actually flows in the human fetus, some words are warranted. In the same vein, it is also worth noting that fetal anatomy at times is different from postnatal anatomy. In the human fetus, the ductus venosus ascends toward the IVC in a steep dorsal direction (48°) to enter the IVC shortly before it penetrates the diaphragm. At this level, the IVC expands and the ductus joins its left part and points at the foramen ovale (Figs. 28.1 and 28.2). The distance is short compared with those in fetal lambs, and the position to the left in the IVC reduces the possibility of blending with low-oxygenated abdominal IVC blood (Fig. 28.8 and Video 28.1). Additionally, the umbilical blood entering the ductus venosus

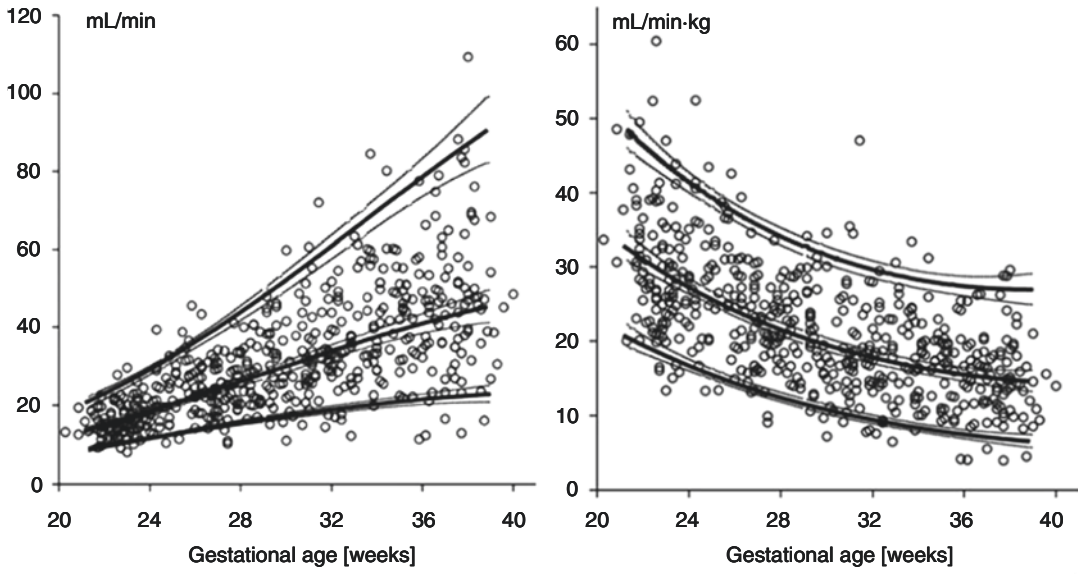

Fig. 28.5 Ductus venosus blood flow (mL/min) is increasing as observed longitudinally during the second half of low-risk pregnancies (left panel). However, the flow normalized for fetal weight is correspondingly decreasing (right panel) (from Kessler et al. [27])

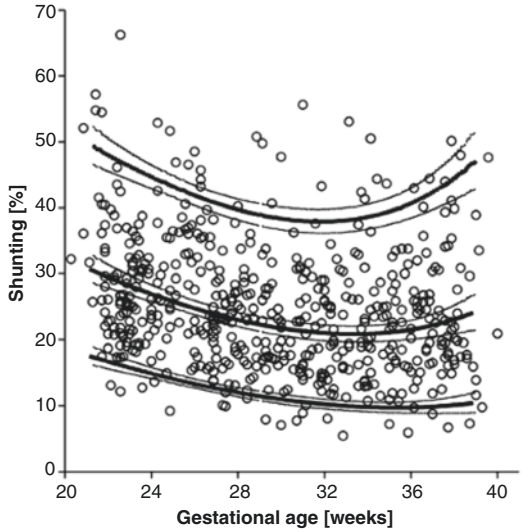

Fig. 28.6 Longitudinal observations of ductus venosus shunting during the second half of normal pregnancies. At mid-gestation, roughly one-third of the umbilical blood bypasses the fetal liver, but this fraction declines to one-fifth in the third trimester (from Kessler et al. [27])

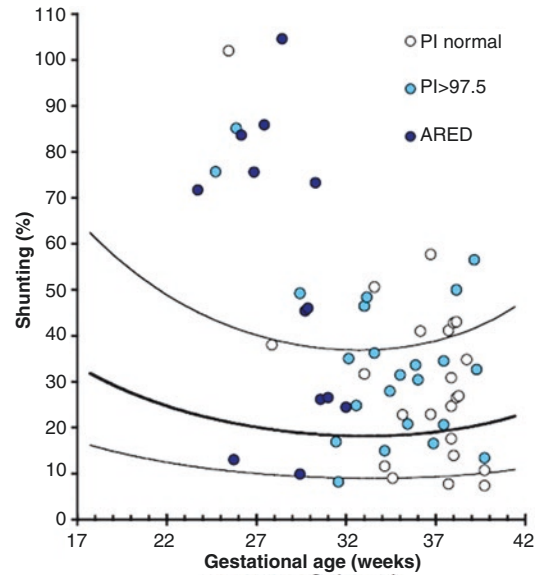

Fig. 28.7 Ductus venosus shunting (% of umbilical venous flow) in 60 severely growth-restricted fetuses (≤2.5 percentile) compared with reference ranges. Their degree of placental hemodynamic compromise is represented by the degree of umbilical artery pulsatility. Empty circles, normal pulsatility index; blue circles, pulsatility index ≥97.5 percentile; dark blue circles, absent or reversed end-diastolic velocity (from Kiserud et al. [64])

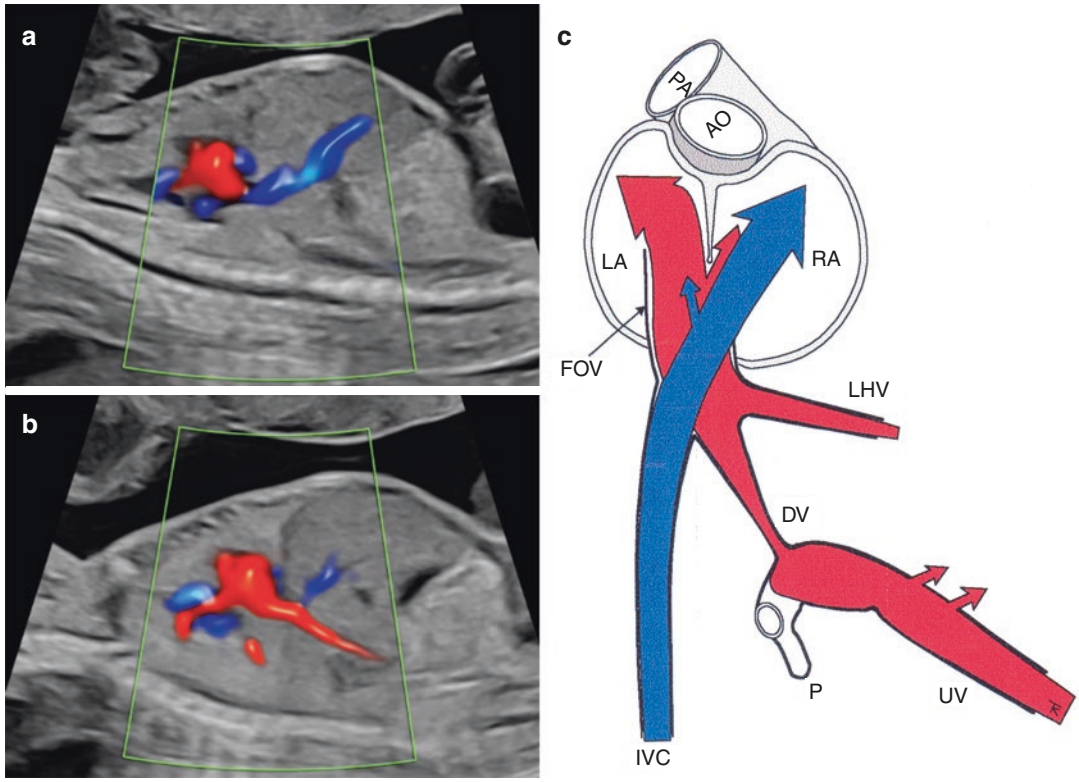

Fig. 28.8 Panel (**a**): Color Doppler imaging at 19 weeks of gestation showing the umbilical flow entering the ductus venosus (DV) streaming in a steep dorsal direction to cross the inferior vena cava (IVC) and hit the left atrium (LA) directly. Apart from the upper-most left compartment, the IVC is not visualized in this plane. Note that the LA is the most posterior atrium since the heart is rotated toward the left. Panel (**b**): In a parallel plane, a fraction to the right of the previous insonation, the entire IVC is observed directing abdominal blood in a steep slightly anterior direction to enter the right atrium (RA). Panel (**c**): Graphical presentation of the two pathways operating in two neighboring planes and crossing in the distended upper section of the IVC, the oxygenated umbilical blood in the left compartment and the low-oxygenated abdominal blood in the right compartment of this distended IVC section. The foramen ovale valve (FOV) and the shorter Eustachian valve (EV) form an extension of the IVC, separating the blood column from the two atria. The longer FOV additionally forms a channel (windsock) with the atrial septum, guiding the blood into the LA, but also represents a restricting factor. During fetal life, the atrial septum is positioned slightly more to the right, thus making the IVC ambiguously dedicated to both the atria. *AO* aorta, *LHV* left hepatic vein, *P* portal stem, *PA* pulmonary artery (panels **a** and **b**: courtesy Prof. Rabih Chaoui, Berlin; panel **c** from Kiserud [28])

is accelerated 2–4 times, loading the oxygenated blood with a high kinetic energy sufficient to bridge the gap, forcing the foramen ovale open by distending the foramen ovale valve and delivering the blood to the left atrium [7, 28, 32].

On the receiver side, the interatrial septum with the foramen ovale is somehow shifted toward the right atrium, tilting the foramen ovale to face the column of blood coming from the IVC (Fig. 28.9). The delicate foramen ovale valve and the shorter Eustachian valve (inferior vena cava valve) form an extension of the IVC between the atria. The ascending blood column with the ductus venosus blood in the left compartment pointing dorsally, and the abdominal IVC blood in the right compartment pointing slightly forward, hits the edge of the foramen ovale (crista dividens) that cleaves the flow in a left and right stream [2, 32, 55, 67].

Since oxygen extraction in the left liver lobe is modest, i.e., 15% [68–70], the left and middle hepatic veins joining the ductus venosus in the

left compartment of the upper IVC are an additional source of oxygen presented to the foramen ovale. In total, it is an abundant volume of oxygenated blood that predominantly fills the foramen ovale and additionally spills over to the right side. The result is a notably small difference in oxygen saturation between the left and right ventricles, which is 10% under experimental conditions and increases to 12% during hypoxemic insults [4, 71].

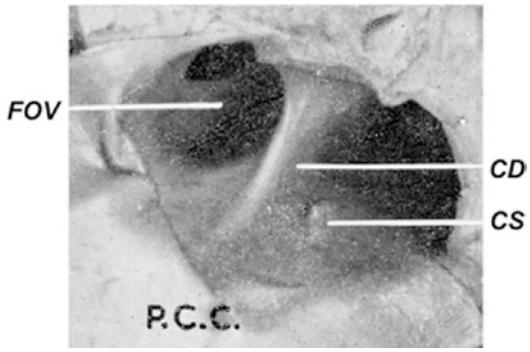

Fig. 28.9 Photographic view of the lower caval entry into the heart after the inferior vena cava (IVC) has been removed in a horse fetus. Note the interatrial septum with its edge, crista dividens (CD), residing over the caval inlet, demonstrating that the IVC is ambiguously dedicated to both atria in fetal life. The foramen ovale valve (FOV) is seen to the left of the crista, and, on the right side, the coronary sinus (CS) has its outlet. P.C.C. denotes posterior caval channel in this classical work (from Barcroft [2])

28.3.3 Distribution to the Ductus Venosus or Liver Perfusion

Another aspect of the ductus venosus function is its role in the fetal liver circulation. Since 20–30% of the umbilical blood is shunted through the ductus, 70–80% of the umbilical blood is distributed to the liver as the first organ in the fetus [25]. The pattern indicates the importance of the fetal liver during intrauterine development: the umbilical blood flow through the fetal liver induces liver hepatocyte proliferation and hepatic growth factor production, leading to differential fetal organ growth (Fig. 28.10) [72, 73]. Degrees of maternal adiposity and dietary habits modulate the flow [74], and, on the other hand, variation in fetal venous flow is traced in postnatal health development [75, 76].

However, the fetal liver and the ductus venosus are competing for the same resource, the nutritious umbilical venous blood. During placental compromise, hypoxia and hypovolemia, the ductus distends to maintain or increase the flow and fraction of shunting at the expense of the liver.

This redistribution to the ductus venosus is further facilitated when the umbilical venous pressure declines and when the hematocrit increases. Then, the viscous resistance increases in the low-velocity perfusion of the large capillary bed of the liver, whereas the ductus venosus is less affected, i.e., still flowing at sufficient velocity to keep the viscos resistance low (see Chap. 5) [53, 77, 78].

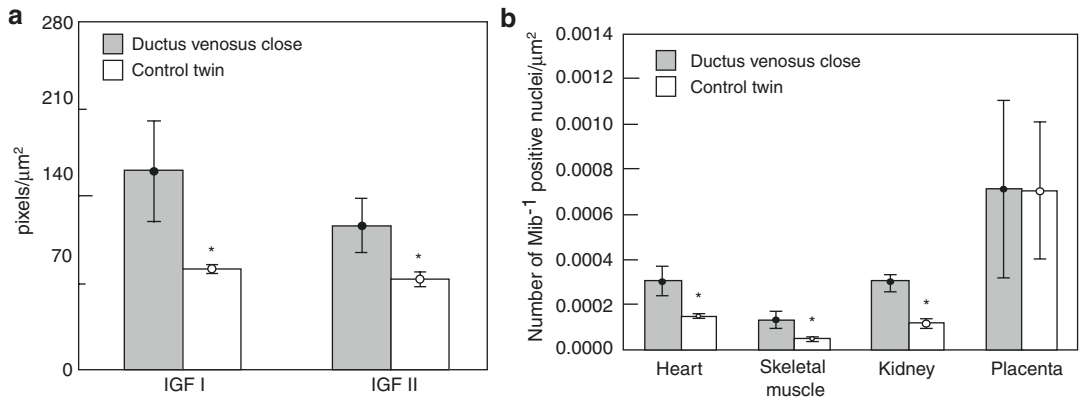

Fig. 28.10 Experimentally occluded ductus venosus in fetal lambs forces the entire umbilical flow through the fetal liver, which induces increased production of IGF-1 and IGF-2 in the liver (^{35}S-labeled) (Panel **a**). There is a correspondingly increased proliferative activity in various organs (Panel **b**). Mib^{-1} antibodies were used to identify nuclear proliferation of antigen pKi-67 (from Tchirikov et al. [72])

In addition to these passive regulatory mechanisms comes active endocrine regulation [41, 79, 80]. The portal venules of the liver are markedly more sensitive to endocrine stimulation than those of the ductus venosus [41], thus augmenting the redirection of blood.

In acute challenges, these mechanisms are efficient in sparing the via sinistra and feed the heart and brain with well-oxygenated blood. If the challenge persists, then the fetus adapts by downregulating growth as signaled by the liver's low flow and reduced growth factor production [81, 82].

In diabetic pregnancies, however, the competing distribution between the ductus venosus and the liver turns out differently. A lasting hyperglycemic load sets the fetal liver to low vascular resistance and high umbilical perfusion at the expense of the ductus venosus, which, in spite of distension, develops a low-fraction shunting during the third trimester, not a favorable setting when faced with a hypoxic challenge (Fig. 28.11) [83, 84].

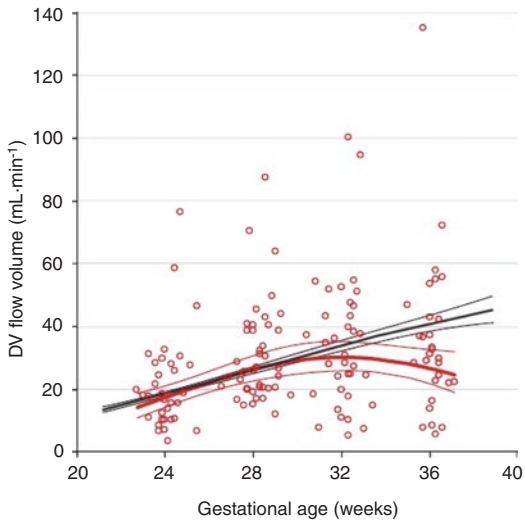

Fig. 28.11 Serial measurements in 49 fetuses (red) exposed to maternal diabetes mellitus, showing a distorted regulation of umbilical venous blood distribution. Compared with their peers (black), their livers are increasingly prioritized during the third trimester at the expense of the ductus venosus. Although the ductus is distended, relative flow reduces, which is not a favorable starting point when facing hypoxic challenges. Thick rules, mean; thin rules, 95% confidence limits of the mean (from Lund et al. [83])

28.3.4 The Umbilicocaval (Portosystemic) Pressure Gradient

The pressure in the intra-abdominal umbilical vein, or rather the umbilicocaval pressure gradient, is critical for transporting the blood either through the liver circuit or the ductus venosus to reach the heart. Postnatally, this gradient is known as the portosystemic pressure gradient. Since the ductus venosus is a connection between the umbilical vein (i.e., the portal sinus) and the IVC, the pressure gradient is loaded on the blood as kinetic energy, and the correspondingly accelerated velocity reflects the magnitude of the pressure gradient as explained in detail in Chap. 5 [30, 85, 86]. The pressure gradient (Δp; in mmHg) can be calculated using the simplified Bernoulli's equation when velocities are measured in m/s:

$$\Delta p = 4\left(V_{DV}^2 - V_{UV}^2\right)$$

where V_{DV} is the ductus venosus blood velocity measured in m/s, and, correspondingly, V_{UV} is the velocity in the umbilical vein. Since the velocity in the umbilical vein is relatively low and therefore has little impact on pressure calculation, it is commonly neglected, making the calculation even simpler:

$$\Delta p = 4V_{DV}^2$$

With the fetus at rest, Δp varies between 0.3 and 3.5 mmHg depending on the phase of the cardiac cycle and gestational age (20–40 weeks) [30, 87]. It would be even simpler to visually assess and use an absolute systolic or time-averaged maximum velocity above the normal ranges as the representation of the increased Δp, and vice versa, and a reduced Δp if these velocities are below the reference ranges. Such an assessment, however, depends on a Doppler recording accurately aligned with the flow direction and preferably not angle-corrected.

An increased V_{DV} (typically >>90 cm/s) can be seen in fetal liver diseases such as lymphoproliferative infiltration, virus infections, and mitochondrial diseases and also when the hematocrit

is abnormally high (e.g., the recipient twin in a twin-to-twin transfusion syndrome).

A reduced V_{DV} could be found in, e.g., a case of an abnormal shunt (e.g., an intrahepatic portosystemic shunt). Such a shunt would drain the umbilical blood away and reduce the Δp, thus reducing liver perfusion with a risk of fetal liver failure (Fig. 28.12) [88].

28.3.5 Abdominal–Thoracic Pressure Difference

The pressure gradient between the ductus venosus and the atria, which is reflected in the velocity of the ductus venosus blood flow, is also a reflection of the abdominal–thoracic pressure across the diaphragm. The ductus is embedded in the fetal liver that is glued to the diaphragm. Second, as opposed to the adult, in the fetus, all organs of the chest are packed with fluid with no air space to buffer pressure variation. The abdominal–thoracic pressure difference varies during fetal breathing movements, and pressure differences of ≥20 mmHg are calculated based on recorded ductus venosus blood velocities of ≥2.25 m/s (Fig. 28.13) [30]. High values occur during fetal breathing with closed vocal cords. The phenomenon is equally well-observed in the inferior vena cava with similar velocity and pressure values [89] and offers a possibility to study fetal breathing force, which is physiologically interesting and clinically potentially useful.

28.3.6 Ultrasound Gray-Scale Imaging

A sagittal anterior insonation offers the best gray-scale visualization of the ductus venosus (Fig. 28.2) [7, 29]. To assess its course and diameters, the perpendicular insonation through the fetal liver suits best, but a dorsal interrogation is also commendable. However, be that the perpendicular visualization provides optimal identification of the vessel walls and dimensions, it is not the optimal position for the pulsed Doppler measurement. An oblique transverse section of the

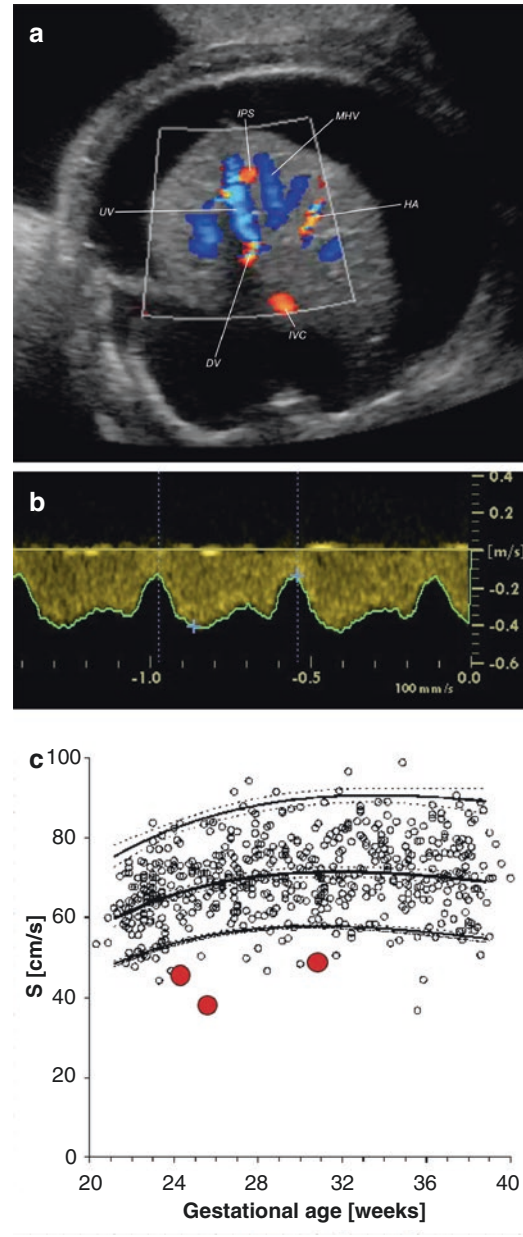

Fig. 28.12 Color Doppler imaging in a case of fetal hydrops in the late second trimester (panel **a**). Pulsed Doppler recording of the ductus venosus (DV) (panel **b**) revealed a normal waveform, but the absolute velocity was extremely low (panel **c**; modified from [ ]) as demonstrated by the repeated observations (red circles) of the systolic peak velocity (S), reflecting the low umbilicocaval pressure gradient. Thus, the liver is hypo-perfused, leading to liver failure with, e.g., reduced albumin production, causing hydrops. The cause is an intrahepatic portosystemic shunt (IPS) draining blood from the umbilical vein (UV) to the medial hepatic vein (MHV), thus reducing the pressure. An augmented hepatic arterial flow (HA) is a compensatory response that confirms the severity of the condition

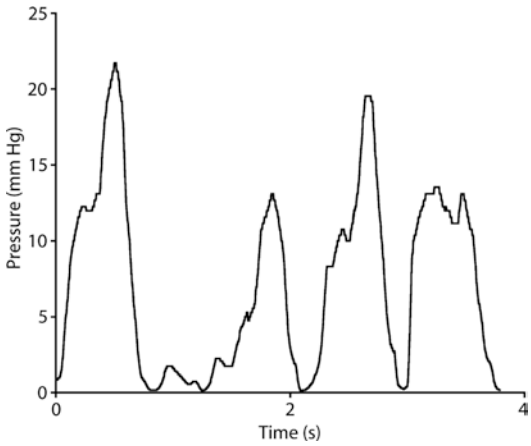

Fig. 28.13 Pressure difference between the chest and abdomen during fetal respiratory activity at 39 weeks of gestation with irregular intensity but, at times, forceful and exceeding 20 mmHg. It is based on the assumption that the close proximity to the diaphragm makes the ductus venosus blood velocity an indicator of the difference in pressure above and below the liver. The pressure is calculated from the velocities using the simplified Bernoulli's equation (from Kiserud et al. [30])

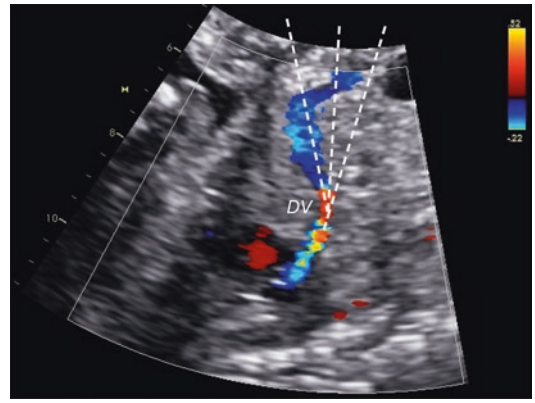

Fig. 28.14 Anterior sagittal color Doppler imaging through the lower abdomen to optimize the pulsed Doppler recording. The isthmic inlet of the ductus venosus (DV*)* is recognized with its high velocity coding. This approach is advantageous as no ribs or pelvic bone blocks the visualization, unless small parts are positioned in front of the abdomen. The preferred interrogation for Doppler recording (interrupted lines) aims at full alignment with the flow direction and should need no angle correction. A liberal sample volume ensures that the maximum velocity along the curvature is included in the recording

fetal abdomen may be more convenient in some fetal positions but may not always capture the entire length of the vessel to confirm the identity, i.e., connecting the umbilical vein (the portal sinus) to the inferior vena cava.

The perpendicular insonation of the isthmus of the ductus is particularly important when the diameter is measured for volume flow calculation (see Chap. 5 for details).

28.3.7 Color Doppler Imaging

Once gray-scale imaging visualizes the ductus venosus, color Doppler is a valuable addition confirming the typical high velocity (Fig. 28.14). Setting the scale slightly below the expected peak velocities permits aliasing to spot the isthmus where velocities are regularly the highest and the area where pulsed Doppler recording is recommended. A scale set too low will result in aliasing all over and will obscure the identification. Adjusting the low-velocity filter (high-pass filter) will reduce the interference of unwanted signals from a highly vascularized area and tissue movements. Including variance coding may also be a useful tool for visualizing the ductus.

28.3.8 Pulsed Wave Doppler Recording

In contrast to two-dimensional (2D) imaging, pulsed Doppler measurement depends on aligning the Doppler beam with blood velocity. Once the sagittal anterior imaging has identified the isthmus of the ductus venosus in gray-scale and color Doppler, the transducer needs to be moved and rotated to insonate through the lower fetal abdomen, directing the Doppler beam upwards along the ductus to position the sample volume at the isthmus (Fig. 28.14). The advantage of this access is avoiding the ribs and spine, but small parts anterior to the fetus may sometimes narrow down the insonation window substantially. An excellent alternative is the posterior parasagittal insonation between the spine and the scapula, directing the Doppler beam from the level of the heart or higher to align the pulsed Doppler beam with the ductus venosus inlet or the following

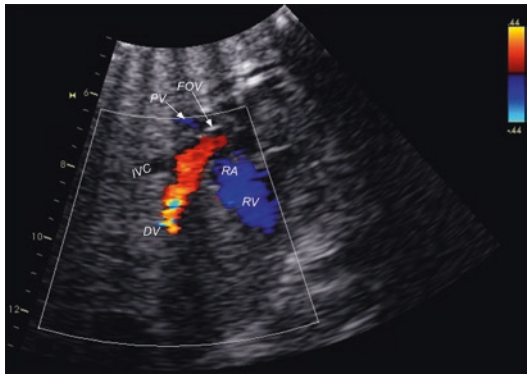

Fig. 28.15 Posterior sagittal color Doppler imaging between the spine and the scapula provides excellent interrogation of the ductus venosus (DV) for a pulsed Doppler recording. For this technique, a well-tuned sector transducer tends to be more successful than a broad linear or curved transducer, particularly when it comes to a perfect alignment of the pulsed Doppler beam. *FOV* foramen ovale valve, *IVC* inferior vena cava, *PV* pulmonary vein, *RA* right atrium, *RV* right ventricle

curvature of the body of the ductus (Fig. 28.15). Obviously, these accesses may compromise the 2D visualization, but they prioritize the magnitude and quality of the velocity signal recorded. Compared with a curved or linear transducer, a well-tuned sector transducer better suits this type of recording.

A transverse or oblique scan of the fetal abdomen will commonly identify the ductus, particularly when aided by color Doppler. The disadvantage is less control of the alignment and the frequent need for an uncertain angle correction. Carrying out Doppler recording through this access will regularly achieve a ductus blood velocity wave. Although this scanning plane does not control for the ductus direction in the axial direction of the fetus, the recording will benefit from the transducer being moved such that the Doppler beam direction aligns as closely as possible with the mid-sagittal plane of the fetus where the ductus venosus and umbilical vein are running. Generally, this recording will suffice when the waveform is the aim of the interrogation. When there is a clinical need for gauging the pressure gradient across the liver and ductus venosus, then a correct alignment in a sagittal insonation provides a reliable recording of the absolute velocity required as a basis for the pressure assessment.

It is a good strategy to start out with a liberal sample volume to ensure that the maximum velocity is recorded at any time. If velocities during the atrial contraction phase come down to nearly zero, then an adjustment of the sample volume (gate) may be needed. This is particularly true in early pregnancy when the vasculature is minute, the velocities are generally lower than those in late pregnancy and the distinction between a reverted or orthograde velocity is of diagnostic importance [19, 23, 24, 90–92].

Both angle of insonation and angle correction need particular attention. Transducers commonly used by obstetricians are broad with a flat or curved surface. Compared with sector scanners, these transducers make it harder to achieve an accurate alignment along the ductus venosus without a need for angle-correcting the Doppler recording. If the recording of absolute velocities has any diagnostic consequence, then there is much to gain from a sector scanner. Rather than angle-correcting, it is worth redoing the recording a couple of times at the best achievable insonation and choose the best recording with the highest velocities achieved under standard conditions. The reason for this strategy is that an angle correction easily overcorrects a true velocity. Color Doppler has a poor resolution and may not visualize small curvatures or bends. When the ductus has an obvious bend, repeating the recording tangentially to the curvature should ensure an appropriate measurement without correcting for the angle.

Once the optimal interrogation position is visually determined, the pulsed Doppler recording starts with a frozen image on the screen, and it is an audible Doppler shift that continues to inform the operator whether the sample volume is still in position or not, a crucial detail to achieve high-quality recordings.

Adjustments of the low-velocity filter (high-pass filter) are required if wall motion or velocities from neighboring structures interfere with the signal of interest, with the usual problem being the nadir during the A-wave.

28.3.9 Normal Ductus Venosus Blood Velocity

Typically, the ductus venosus blood flow has a high velocity during the entire cardiac cycle compared with those of the neighboring veins at the corresponding gestational age (Fig. 28.16) [7, 8, 29, 93–98]. Starting in early pregnancy (e.g., 10 weeks of gestation), the velocity increases until it reaches a plateau after 28 weeks of gestation. For the rest of the pregnancy, the peak velocity ranges between 55 and 90 cm/s (Fig. 28.17). Some variation in reference ranges is seen, depending on the study design and recording techniques.

The velocity reflects two aspects of circulation: (1) the pressure difference between the umbilical vein and the heart represented by the magnitude of the velocity and (2) the atrial pressure variation during the cardiac cycle represented by the waveform superimposed on the velocity. This waveform has a peak during ventricular systole, another during passive diastolic ventricular filling and a nadir during active diastolic filling (atrial contraction; Fig. 28.17). Typically, the nadir during atrial contraction does not reach the zero line during the second half of the pregnancy, in contrast to other precordial veins. However, below 15 weeks of gestation, an increasing number of zero or below-zero velocities are observed in normal fetuses [28]. Reference ranges have been established for all the components of the velocity wave as well as for the time-averaged maximum velocity during the entire cardiac cycle. Those recommended for general use follow advocated principles, i.e., they are based on longitudinal data from low-risk pregnancies recruited specifically for the normative study in statistically justified numbers, e.g., Fig. 28.17 [96]. During the second half of the pregnancy, the time-averaged intensity-weighted mean velocity is typically 0.7 of the maximum velocity. The relation is established by mathematical modeling, and experimental and clinical observations, and is a quite useful information when calculating volume flow (see Chap. 5) [86, 99–102]. In early pregnancy, mathematical modeling predicts the relation to be 0.53, which is close to the parabolic flow [103, 104].

It is important to acknowledge the wide normal variation of the waveform. In 11% of normal recordings, no second antegrade velocity peak *D* (diastolic passive ventricular filling) will be iden-

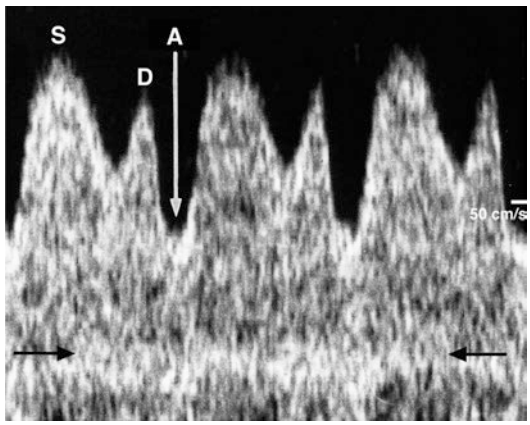

Fig. 28.16 Doppler recording of the blood velocity at the isthmus of the ductus venosus at 33 weeks of gestation. Typically, there is high velocity during the entire cardiac cycle with a peak during ventricular systole (*S*), another peak during passive diastolic filling (*D*), and a deflection (white arrow) during atrial contraction (*A*). The velocity of the interfering umbilical vein is faintly seen between the black arrows, as the sample volume has covered both the isthmus and a portion of the connected umbilical vein

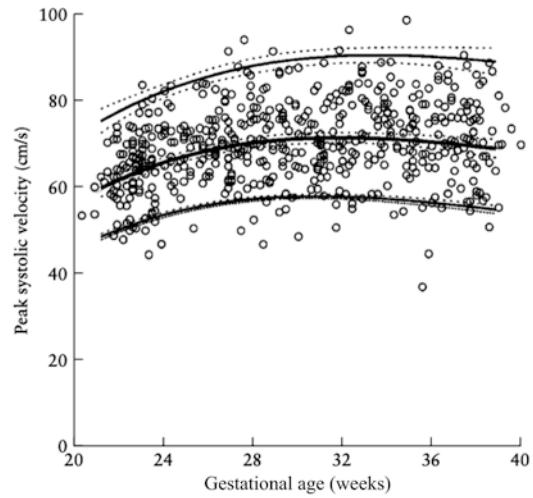

Fig. 28.17 Longitudinal reference ranges for peak systolic blood velocity in the ductus venosus with the 5th, 50th, and 95th percentiles and their 95% CI (from Kessler et al. [96])

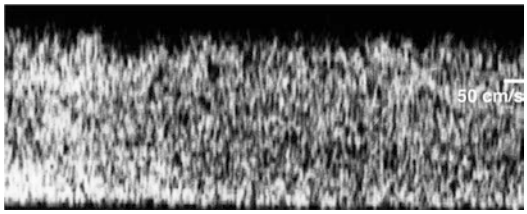

Fig. 28.18 Doppler recording of the blood velocity at the isthmus of the ductus venosus at 32 weeks of gestation shows no discernible pulsation. The phenomenon occurs in 3% of all recordings in low-risk pregnancies (see Chap. 5 for the hemodynamic explanation)

tified during the passive diastolic filling, and in 3%, there will be no well-defined nadir visible (Fig. 28.18) [29]. These patterns reflect the wide range of normal heart functions and the range of geometrical variations of the precordial veins that healthy fetuses can afford. Squeezing of the ductus venosus outlet or the IVC at the level of the liver or diaphragm will cause an increased wave reflection and correspondingly less pulse waves (or no pulse) transmitted to the ductus venosus isthmus (see Chap. 5) [28, 105].

28.3.10 Waveform Analysis

To make an angle-independent evaluation, ratios of various components of the waveform during the heart cycle have been suggested, some of which are also used for other fetal veins or arterial blood velocity waves [8, 93, 106]. The indices that include the entire heart cycle are more robust, and the pulsatility index for veins (PIV) [93] has become the prevailing index:

$$\mathrm{PIV} = \frac{V_S - V_A}{V_{\mathrm{TAMax}}}$$

where V_S is the systolic peak velocity, V_A is the nadir of the velocity deflection during atrial contraction (A-wave) and V_{TAMax} is the time-averaged maximum velocity during the entire cardiac cycle. The PIV declines during the second half of the pregnancy (Table 28.1) [96].

Essentially, the waveform reflects cardiac events, i.e., the intra-cardiac pressure variation, which is emitted into the precordial venous system. As mentioned above, using the waveform as the only analysis of the velocity means disregarding the portocaval pressure gradient represented by the absolute velocity.

28.3.11 Interpretation of the Waveform: A-Wave

The atrial contraction wave (A-wave) is the single most important part of the waveform from a diagnostic point of view. The augmented atrial contraction wave signifies an increased end-diastolic filling pressure in the heart. A distension of the atria leads to an augmented contraction (the Frank–Starling effect) commonly seen in cases with increased preload or congestive heart failure [7, 9, 107–113]. An increased afterload and an increased inotropic drive also augment the A-wave (Fig. 28.19) [10, 114–117]. Experimentally imposed hypoxia causes an increased A-wave not only in late pregnancy [102, 118, 119] but also at mid-gestation and early pregnancy [120]. In the latter case, the effect is believed to primarily be a direct hypoxic effect on the myocardium. In late pregnancy, the effect is predominantly orchestrated via immediate neural responses and secondary endocrine effects on the cardiac rhythm and contractility as well as on peripheral vascular impedance [58, 121, 122].

Heart rate is an important determinant of the precordial venous waveforms [111]. A slowing of the heart rate permits an extended venous filling, distension of the atrium, and a correspondingly augmented atrial contraction. The effect is seen in fetal bradycardic conditions.

A faltering ventricular contractility leads to congestion and a distended atrium causing an increased atrial contraction according to the Frank–Starling mechanism. Increased adrenergic drive and possibly aggravation by atrioventricular regurgitation may further increase the atrial pressure and augment the A-wave. Typically, this occurs in the twin-to-twin transfusion syndrome with one of the fetuses being overloaded [123]. Arteriovenous malformations in the placenta,

Table 28.1 Reference ranges for the pulsatility index for veins (PIV) in the ductus venosus [96]

	Percentile								
Gestation (weeks)	2.5	5	10	25	50	75	90	95	97.5
21	0.27	0.32	0.38	0.47	0.57	0.68	0.77	0.83	0.88
22	0.28	0.32	0.38	0.47	0.57	0.68	0.77	0.83	0.88
23	0.28	0.32	0.38	0.47	0.57	0.68	0.77	0.83	0.88
24	0.27	0.32	0.38	0.47	0.57	0.68	0.77	0.83	0.88
25	0.27	0.32	0.37	0.47	0.57	0.67	0.77	0.83	0.88
26	0.27	0.31	0.37	0.46	0.57	0.67	0.77	0.82	0.87
27	0.26	0.31	0.36	0.46	0.56	0.67	0.76	0.82	0.87
28	0.26	0.31	0.36	0.45	0.56	0.66	0.76	0.81	0.86
29	0.25	0.30	0.35	0.45	0.55	0.65	0.75	0.81	0.86
30	0.25	0.29	0.35	0.44	0.54	0.65	0.74	0.80	0.85
31	0.24	0.28	0.34	0.43	0.53	0.64	0.73	0.79	0.84
32	0.23	0.28	0.33	0.42	0.53	0.63	0.73	0.78	0.83
33	0.22	0.27	0.32	0.41	0.52	0.62	0.72	0.77	0.82
34	0.21	0.26	0.31	0.40	0.51	0.61	0.71	0.76	0.81
35	0.20	0.25	0.30	0.39	0.50	0.60	0.70	0.75	0.80
36	0.19	0.24	0.29	0.38	0.49	0.59	0.69	0.74	0.79
37	0.18	0.23	0.28	0.37	0.48	0.58	0.67	0.73	0.78
38	0.17	0.22	0.27	0.36	0.46	0.57	0.66	0.72	0.77
39	0.16	0.21	0.26	0.35	0.45	0.56	0.65	0.71	0.76

fetal liver, and fetal brain or increased load due to cystic adenomatoid lung malformations are other examples of conditions causing an increased atrial pressure.

Hyperkinetic circulation, such as in fetal anemia, regularly increases the preload and the A-wave [124]. With deterioration of the cardiac function, i.e., congestive heart failure, the sign of the augmented A-wave becomes more marked, with the velocity nadir reaching the zero line or below, even in late pregnancy.

In general, the compliance of the heart is reflected in the A-wave. The reduced distensibility of the myocardium in cardiomyopathies, myocarditis (e.g., parvovirus B19 infection), hypoxemia and acidosis is commonly associated with a deepened A-wave. The compliance can also be influenced by extracardiac restrictions in the chest.

The timing of the atrial contraction is also an important determinant of the magnitude of the A-wave. The various patterns found in arrhythmias are particularly instructive [125, 126]. An atrial contraction following the compensatory postictal pause has been given the extra time and load of volume to cause an augmented A-wave. An even more amplified version of the A-wave is seen in cases of atrioventricular block. When the atrial contraction coincides with the ventricular systole, the result is a stronger pulse wave directed into the precordial veins, including the ductus venosus. During tachycardia, the timing of the atrial contraction, the size of the atria, whether the atrioventricular valves are open, the momentary degree of filling, the functional condition of the myocardium itself and probably details of where the contraction starts and how it propagates all determine the details of the A-wave [127].

For some years, the A-wave has been the focus of research on methods of monitoring patients with placental compromise. Short-time variation of the computerized cardiotocography (CTG) and the ductus venosus A-wave (or pulsatility) show late changes compared with umbilical artery pulsatility and changes in the middle cerebral artery (Fig. 28.20) [128–130]. Although this sequence of events is common, recent data have

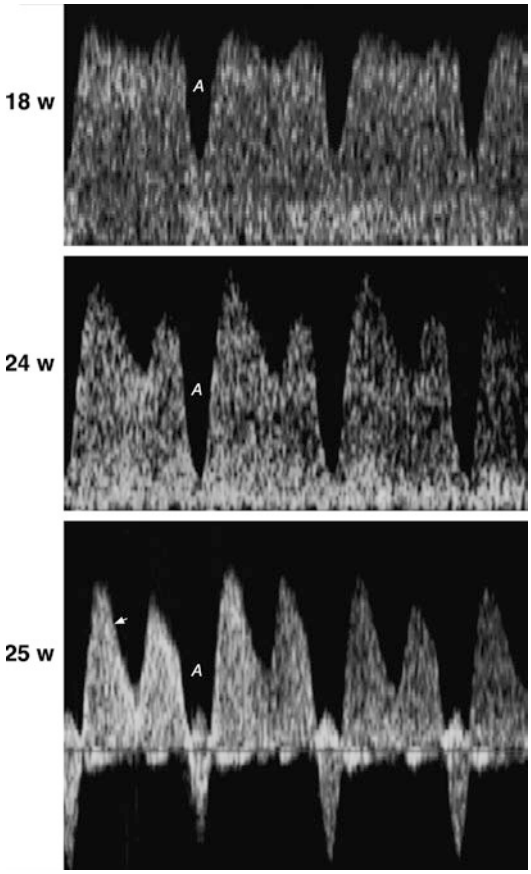

Fig. 28.19 A case of progressive placental compromise and fetal growth restriction shows normal ductus venosus blood velocities at 18 weeks with a normal A-wave (*A*) (upper panel). At 24 weeks, the augmented A-wave was apparent (middle panel). At 25 weeks, a further deterioration was seen with a reversed A-wave and an increasing dichotomy between the systolic and diastolic peaks (lower panel). The quick downstroke of the systolic peak (arrow) signifies a quick increase in atrial pressure, which could be due to reduced atrial distensibility, increased blood volume in the atrium due to congestion or tricuspid regurgitation, reduced ventricular contractility or a combination of all these factors

suggested that other event profiles are also possible [131]. Including the ductus venosus wave analysis in monitoring in early fetal growth restriction improves the prediction of perinatal events and postnatal morbidity [14]. Since the ductus venosus velocity pattern is an instantaneous reflection of the cardiac function, these changes are probably useful signs in other conditions where the fetus is at risk as well.

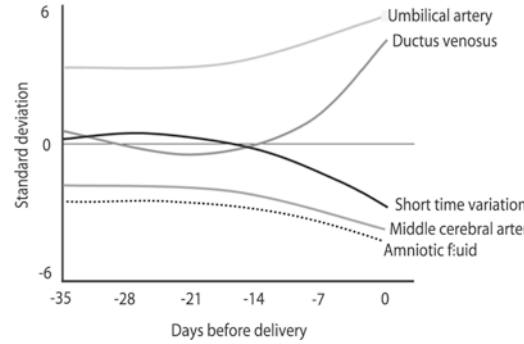

Fig. 28.20 Serial observations of cases with severe fetal growth restriction delivered ≤32 weeks of gestation. Changes in the pulsatility index of the umbilical and middle cerebral arteries and oligohydramnios are common findings 3–5 weeks before delivery. Alterations in the ductus venosus waveform and short-time variation are notable during the last 2 weeks before delivery, indicating that these two parameters are candidates for determining the time of delivery (modified from Hecher et al. [128])

28.3.12 A-Wave in Early Pregnancy

Ductus venosus Doppler velocimetry has also been introduced in early pregnancy testing and has proved useful in identifying cardiac malformations and fetuses at risk of chromosomal abnormalities [19, 23, 24, 90, 92, 132, 133]. An A-wave crossing the zero line has been the sign (Fig. 28.21). As for later in pregnancy, an increased preload augments the atrial contraction and the A-wave. Additionally, the overall velocity in the ductus is lower than that later in pregnancy, causing a shift of the wave, including the atrial contraction wave, toward the zero line or beyond. During the short A-wave, the almost parabolic velocity profile breaks down with partially inverted areas, i.e., antegrade and retrograde velocities in the same cross section (Fig. 28.22) [103, 104]. At times, this may pose a challenge to assessing the A-wave nadir, be it visual or by automatic velocity tracing.

28.3.13 Interpretation of the Systolic Wave

Conventionally, the systolic peak during ventricular contraction is smooth and rounded

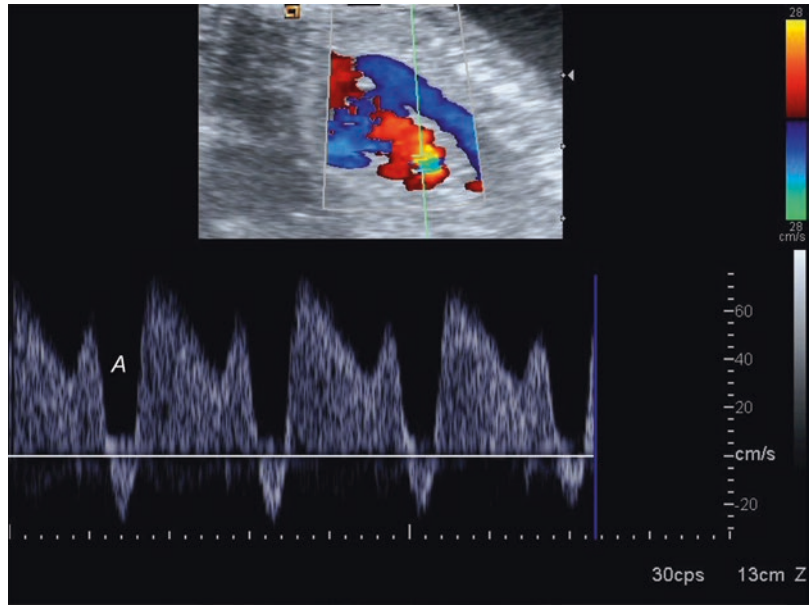

Fig. 28.21 Doppler recording of the ductus venosus blood velocity at gestational week 12 + 6, showing an augmented atrial contraction wave (A), with the nadir reaching negative velocities being a sign of increased risk of cardiac disease and chromosomal abnormality (courtesy of Antoni Borrell MD PhD, BCNatal, Hospital Clinic Barcelona)

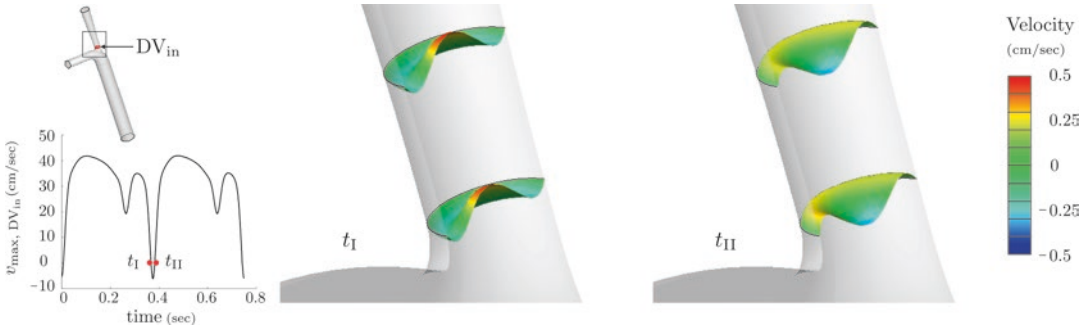

Fig. 28.22 Mathematical simulation of the spatial distribution of velocity in the ductus venosus inlet (DV_{in}) in early pregnancy. During an augmented A-wave, when the velocity deflection reaches time t_I, the peripheral velocities of the cross section have turned negative, whereas the axial velocities are still positive. After the nadir has been passed (t_{II}), the peripheral velocities have turned positive, whereas the axial velocities are now negative (from Leinan et al. [104])

(Fig. 28.23), but that changes when the cardiac function is driven to extremes. For example, with growing congestive heart failure, tricuspid regurgitation commonly occurs. This retrograde flow adds to the atrial filling and the pressure quickly increases correspondingly, the result of which is a falling blood velocity of the systolic peak in the ductus venosus since the flow velocity depends on the umbilical atrial pressure gradient (Fig. 28.23). In addition, changes in the function of the myocardium itself are reflected in this part of the cardiac cycle. Under conditions of reduced compliance and contractility, the downstroke of the velocity becomes more acute. This is particularly apparent during the deterioration seen in placental compromise [11, 134] when hypoxemia and acidosis drive the myocardial function toward less compliance and less relaxation and contractility dynamics [135–137]. The visible result is the acute up- and downstroke of the systolic peak (Fig. 28.23). A steep upstroke indicates that the ventricles contract behind the closed AV valves and suck blood into the atria, but within a short period of time, the systolic velocity peak is reached and a steep downstroke follows, indicating a restrictive ventricular contractility and atrial

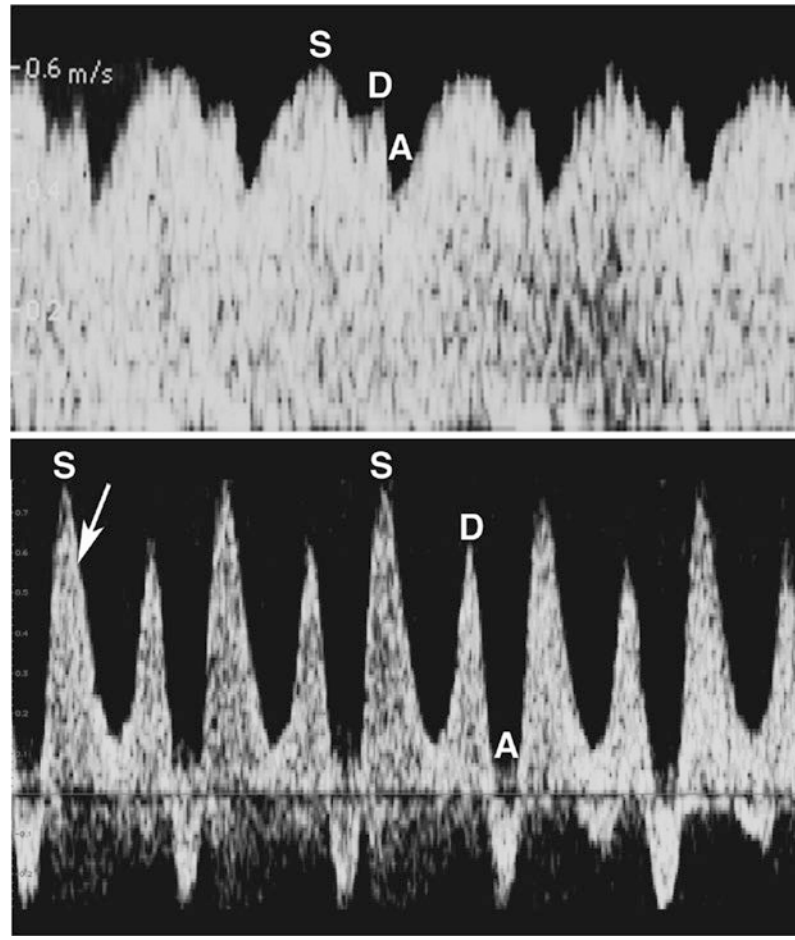

Fig. 28.23 Conventionally, the systolic peak (*S*) is smooth and rounded, signifying good ventricular contraction dynamics and atrial compliance (upper panel). Increased stiffness of the myocardium due to hypoxia and acidosis, such as in advanced placental compromise, results in a pointed peak with a rapid downstroke (arrow) of the *S* (lower panel). Typically, the waveform is transformed into acute velocity changes and a dissociation between *S* and diastolic peak (*D*). The velocity of the *D*-wave increases sharply when the atrioventricular valves open but develops similar to *S* due to the same mechanisms. The augmented A-wave (*A*) reaching below zero is a common part of the pattern

distensibility. This quick deflection of the systolic wave leads to a dichotomy between the systolic and diastolic peaks commonly seen at a terminal stage (Fig. 28.23).

28.4 Pitfalls

For a beginner, sampling the velocity in a neighboring vein, or including interference from the IVC or other vessels, may falsely give the impression of an abnormal ductus venosus recording. The velocity in the hepatic veins tends to be more acute waveforms, and, particularly during the second trimester, these veins have a zero or reversed velocity during atrial contraction. Before jumping to conclusions, it is prudent to reproduce the recording in a renewed insonation. It is also helpful to know that the augmented pulsatility in the ductus venosus commonly has a corresponding pulsatile flow in the umbilical vein. If the insonation makes the identification of the ductus venosus less certain, then the pulsatility and A-wave should be checked in more accessible precordial veins such as the IVC or hepatic veins.

The pulsatile flow in the left portal vein (when it occurs) is the mirror image of the ductus venosus waveform [138]. One of the consequences is that the A-wave occurs not as a nadir but as a peak (see Chap. 5). The simultaneous sampling of the ductus venosus inlet and the left portal vein could then cause a masking of the true nadir in the ductus venosus. Masking may also be the case during simultaneous sampling at the isthmus of the ductus venosus and the umbilical vein

where the pulsatility is usually less-pronounced. This is a common problem in early pregnancy.

Local changes of no pathological significance may influence the waveform. The fetal position may be such a factor. A fetus bending forward, particularly in extreme situations of oligohydramnios, may squeeze the IVC, the outlet or the entire length of the ductus venosus to the extent that most of the wave is reflected and not propagated to be picked up at the inlet of the ductus (see Chap. 5). This benign phenomenon disappears as soon as the fetus changes its body position.

A normal ductus venosus flow velocity does not exclude abnormal physiology. Compensating factors may mask the functional shortcomings, e.g., increased size of the heart and altered myocardial thickness. Adding other corroborating findings ensures the quality of a diagnosis.

Increased vascular resistance in the fetal liver tissue may cause portal hypertension and ascites. Exclusively examining the waveform of the ductus venosus using indices may not reveal any abnormality since the waveform predominantly reflects the cardiac function. It is a common error not to observe the absolute velocities, which may exceed 1 m/s and signify portal hypertension and an affected liver [139, 140].

28.5 Reproducibility

In experienced hands, a recording of ductus venosus blood velocimetry is achieved in almost all women both in early and late pregnancies, even with substandard equipment. The limits of agreement for intra-observer variation are [−13; 12 cm/s] for the systolic peak and [−15; 12 cm/s] during the A-wave [29]. The reproducibility is better for the indices than for the absolute velocity recordings [94]. This is due to the additional challenge it poses to record the absolute velocities at a zero or low angle of insonation, a less important detail when using the waveform analysis.

Doppler assessment of the ductus venosus during early pregnancy seems to have a reduced reproducibility, particularly for the peak systolic velocity and the nadir in the A-wave during transabdominal scanning at 10–14 weeks of gestation. The coefficient of variation for systolic and end-diastolic velocity was 19% and 29%, respectively [141]. The coefficient for the PIV was better, i.e., 9%. These results were reproduced in another study but with somewhat better numbers [142]. High reproducibility requires instructions and experience. Instructed sonographers require an average of 80 scans to achieve 95% successful ductus venosus recordings in early pregnancy [143].

The reference ranges for absolute velocities in the pioneering studies have been confirmed and reproduced [7, 29, 93, 94], now in line with modern requirements of design and with reliable extreme values (Fig. 28.17 and Table 28.1) [96]. When recording Doppler signals without the control of color Doppler, the velocities appeared to be slightly less, possibly due to less control of the correct insonation angle. For the pulsatility indices, there is little variation from study to study.

The volume of blood flow through the ductus venosus is physiologically interesting, but it is a step up in skill demands to achieve reproducible results, particularly since the isthmus of the ductus is slim (0.5–2 mm during the second half of the pregnancy [25, 29, 30], requiring consistency in equipment setting and insonation techniques and repeated measurements to reduce random errors [144, 145]. Acceptable agreement has been achieved between studies when such methods were used consistently including repeated diameter measurements [25, 27, 74, 75, 83, 146, 147]. For individual patient assessment, however, the result has to be used with great caution as the error of flow calculation may easily exceed 20–50% [144, 145].

28.6 Agenesis of the Ductus Venosus

An increasing number of case reports link agenesis of the ductus venosus to fetal demise, hydrops fetalis, asphyxia, vascular and cardiac anomalies, and chromosomal aberrations [148–157]. This has led to the recommendation of an

extended scan if the ductus venosus is not identified. It is likely that agenesis occurs more commonly in connection with chromosomal aberrations and anomalies, but, so far, there are no statistics to prove it. Some have taken the presence of ductus venosus agenesis in hydrops and intrauterine demise as an indication that a patent ductus venosus is vital for intrauterine development; however, it can be argued that ductus venosus agenesis was discovered in these fetuses after a primary finding had made an extended ultrasound scan necessary or during post-mortem examination. In a study of 203 normal pregnancies, 1 fetus had an isolated agenesis with normal outcome including birth weight at the 39th percentile [25]. Experienced clinicians at times observe a premature occlusion, particularly during the third trimester, without any clinical consequences. In a population of 65,840 pregnant women screened for aneuploidies at 11–13 weeks of gestation, the prevalence of ductus venosus agenesis was 1/1532 [158]. Of those with ductus venosus agenesis, one-third had no abnormalities; their nuchal translucency was below the 95th centile and the outcome was good.

Experimental occlusion of the ductus venosus in fetal sheep leads to increased umbilical vein pressure and hepatic venous flow but otherwise has no impact on regional blood distribution [159]; however, such an occlusion has a considerable impact on liver cell proliferation and insulin-like growth factor (IGF)-1 and IGF-2 production and thus on growth [72, 73].

There is an interesting study of fetuses with agenesis of the ductus venosus but with an extrahepatic portosystemic shunt, draining umbilical venous blood directly to the central veins or heart [156]. These fetuses do not seem to be in the position of being able to regulate shunting in the same manner as a normal ductus venosus, although the shunt may be situated near to where the ductus venosus should have been. Correspondingly, these fetuses tend to permit more umbilical blood bypass the liver, which increases the preload and develop hyperkinetic circulation, with hydrops being common. If the shunting also reduces the umbilicocaval pressure gradient, and accordingly the fetal liver perfusion, then a liver failure may aggravate the condition.

A normally developing fetus with agenesis of the ductus venosus is not a contradiction to the concept that ductus venosus is important. At the moment, the story unfolds with the ductus venosus having at least two functions. In the long run, regulation of the umbilical liver perfusion is crucial for fetal development and growth; however, during acute or chronic challenges of hypoxemia or hypovolemia, the priority of the liver is reduced to permit life-saving maneuvres of providing oxygenated blood to the heart and brain or as some physiologists have put it: "The fetal dilemma: spare the brain and spoil the liver" [160].

28.7 Immediate Postnatal Development

After birth, the ductus venosus is obliterated within 1–3 weeks (Fig. 28.24) [161, 162]. Interestingly, the high blood velocity seen prenatally seems to be maintained during that period [161], reflecting the fact that the portal perfusion pressure for the liver circulation is maintained but now essentially by the portal vein. Observations of prematurely born neonates show that the ductus remains patent longer than in infants born at

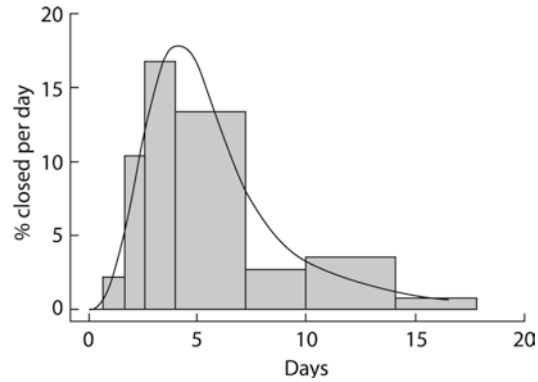

Fig. 28.24 Time of obliteration of the ductus venosus in healthy neonates. The bars represent the percentage closure per day, and the curve represents the fitted log-logistic distribution (from [161])

term [163, 164]. The hypothesis that a patent ductus venosus represents a bypass of the liver in the first weeks of postnatal life to the extent that it influences the clearance rate has been addressed by assessing the galactose concentration in prematurely born neonates [165]. No effect of the patent ductus was found, but the degree of shunting in the ductus venosus was not quantified. The ductus venosus also stays open longer in infants with congenital heart defects or persistent pulmonary hypertension [166].

References

1. Franklin KJ. Ductus venosus (Arantii) and ductus arteriosus (Botalli). Bull Hist Med. 1941;9:580–4.
2. Barcroft J. Researches on pre-natal life. Oxford: Blackwell Scientific Publications; 1946. 287 p.
3. Rudolph AM, Heymann MA, Teramo K, Barrett C, Räihä N. Studies on the circulation of the previable human fetus. Pediatr Res. 1971;5:452–65.
4. Rudolph AM. Distribution and regulation of blood flow in the fetal and neonatal lamb. Circ Res. 1985;57:811–21.
5. Dawes GS. Foetal and neonatal physiology. Chicago: Year Book Medical Publishers; 1968. 247 p.
6. Chinn DH, Filly RA, Callen PW. Ultrasonographic evaluation of fetal umbilical and hepatic vascular anatomy. Radiology. 1982;144:153–7.
7. Kiserud T, Eik-Nes SH, Blaas HG, Hellevik LR. Ultrasonographic velocimetry of the fetal ductus venosus. Lancet. 1991;338(8780):1412–4.
8. Huisman TWA, Stewart PA, Wladimiroff JW. Ductus venosus blood flow velocity waveforms in the human fetus—a Doppler study. Ultrasound Med Biol. 1992;18:33–7.
9. Kiserud T, Eik-Nes SH, Hellevik LR, Blaas H-G. Ductus venosus blood velocity changes in fetal cardiac diseases. J Matern Fetal Invest. 1993;3:15–20.
10. Kiserud T, Eik-Nes SH, Blaas H-G, Hellevik LR, Simensen B. Ductus venosus blood velocity and the umbilical circulation in the seriously growth retarded fetus. Ultrasound Obstet Gynecol. 1994;4:109–14.
11. Kiserud T. The ductus venosus. Seminars Perinat. 2001;25(1):11–20.
12. Baschat AA, Cosmi E, Bilardo CM, Wolf H, Berg C, Rigano S, et al. Predictors of neonatal outcome in early-onset placental dysfunction. Obstet Gynecol. 2007;109(2 Pt 1):253–61.
13. Baschat AA. Arterial and venous Doppler in the diagnosis and management of early onset fetal growth restriction. Early Hum Dev. 2005;81(11):877–87.
14. Lees CC, Marlow N, van Wassenaer-Leemhuis A, Arabin B, Bilardo CM, Brezinka C, et al. 2 year neurodevelopmental and intermediate perinatal outcomes in infants with very preterm fetal growth restriction (TRUFFLE): a randomised trial. Lancet. 2015;385(9983):2162–72.
15. Chako AW, Reynolds SRM. Embryonic development in the human of the sphincter of the ductus venosus. Anat Rec. 1953;115:151–73.
16. Dickson AD. The development of the ductus venosus in man and the goat. J Anat. 1957;91:358–68.
17. Severn CB. A morphological study of the development of the human liver. Am J Anat. 1972;133:85–108.
18. Lassau JP, Bastian D. Organogenesis of the venous structures of the human liver: a hemodynamic theory. Anat Clin. 1983;5:97–102.
19. Borrell A, Antolin E, Costa D, Farre MT, Martinez JM, Fortuny A. Abnormal ductus venosus blood flow in trisomy 21 fetuses during early pregnancy. Am J Obstet Gynecol. 1998;179:1612–7.
20. Huisman TW, Stewart PA, Wladimiroff JW, Stijnen T. Flow velocity waveforms in the ductus venosus, umbilical vein and inferior vena cava in normal human fetuses at 12-15 weeks of gestation. Ultrasound Med Biol. 1993;19(6):441–5.
21. Brezinka C, Hagenaars AM, Wladimiroff JW, Los FJ. Fetal ductus venosus flow velocity waveforms and maternal serum AFP before and after first-trimester transabdominal chorionic villus sampling. Prenat Diagn. 1995;15(8):699–703.
22. van Splunder IP, Stijnen T, Wladimiroff JW. Fetal pressure gradient estimations across the ductus venosus in early pregnancy using Doppler ultrasonography. Ultrasound Obstet Gynecol. 1995;6(5):334–9.
23. Montenegro N, Matias A, Areias JC, Barros H. Ductus venosus revisited: a Doppler blood flow evaluation in the first trimester of pregnancy. Ultrasound Med Biol. 1997;23(2):171–6.
24. Matias A, Gomes C, Flack N, Montenegro N, Nikolaides KH. Screening for chromosomal defects at 11-14 weeks: the role of ductus venosus blood flow. Ultrasound Obstet Gynecol. 1998;12:380–4.
25. Kiserud T, Rasmussen S, Skulstad SM. Blood flow and degree of shunting through the ductus venosus in the human fetus. Am J Obstet Gynecol. 2000;182:147–53.
26. Bellotti M, Pennati G, De Gasperi C, Battaglia FC, Ferrazzi E. Role of ductus venosus in distribution of umbilical blood flow in human fetuses during second half of pregnancy. Am J Physiol Heart Circ Physiol. 2000;279(3):H1256–63.
27. Kessler J, Rasmussen S, Godfrey K, Hanson M, Kiserud T. Longitudinal study of umbilical and portal venous blood flow to the fetal liver: low pregnancy weight gain is associated with preferential supply to the fetal left liver lobe. Pediatr Res. 2008;63(3):315–20.
28. Kiserud T. Hemodynamics of the ductus venosus. Eur J Obstet Gynecol Reprod Biol. 1999;84(2):139–47.
29. Kiserud T, Eik-Nes SH, Hellevik LR, Blaas H-G. Ductus venosus—a longitudinal doppler velo-

cimetric study of the human fetus. J Matern Fetal Invest. 1992;2:5–11.
30. Kiserud T, Hellevik LR, Eik-Nes SH, Angelsen BA, Blaas HG. Estimation of the pressure gradient across the fetal ductus venosus based on Doppler velocimetry. Ultrasound Med Biol. 1994;20(3):225–32.
31. Huisman TWA, Gittenberger-de Groot AC, Wladimiroff JW. Recognition of a fetal subdiaphragmatic venous vestibulum essential for fetal venous doppler assessment. Pediatr Res. 1992;32:338–41.
32. Kiserud T, Eik-Nes SH, Blaas H-G, Hellevik LR. Foramen ovale: an ultrasonographic study of its relation to the inferior vena cava, ductus venosus and hepatic veins. Ultrasound Obstet Gynecol. 1992;2:389–96.
33. Champetier J, Yver R, Tomasella T. Functional anatomy of the liver of the human fetus: application to ultrasonography. Surg Radiol Anat. 1989;11:53–62.
34. Barron DH. The "sphincter" of the ductus venosus. Anat Rec. 1942;82:389.
35. Gennser G, Owman CH, Sjöberg N-O. Histochemical evidence of an aminergic sphincter mechanism in the ductus venosus of the human fetus. In: Horsky J, Stembera ZK, editors. Intrauterine dangers to the foetus. Amsterdam: Exterpa Medica Foundation; 1967.
36. Pearson AA, Sauter RW. The innervation of the umbilical vein in human embryos and fetuses. Am J Anat. 1969;125:345–52.
37. Pearson AA, Sauter RW. Observations on the phrenic nerves and the ductus venosus in human embryos and fetuses. Am J Obstet Gynecol. 1971;110:560–5.
38. Mavrides E, Moscoso G, Carvalho JS, Campbell S, Thilaganathan B. The human ductus venosus between 13 and 17 weeks of gestation: histological and morphometric studies. Ultrasound Obstet Gynecol. 2002;19:39–46.
39. Meyer WW, Lind J. Über die struktur und den verschlussmechanismus des ductus venosus. Zeitsch Zellforschung. 1965;67:390–405.
40. Meyer WW, Lind J. The ductus venosus and the mechanism of its closure. Arch Dis Child. 1966;41:597–605.
41. Tchirikov M, Kertschanska S, Schroder HJ. Differential effects of catecholamines on vascular rings from ductus venosus and intrahepatic veins of fetal sheep. J Physiol. 2003;548(Pt 2):519–26.
42. Ehinger B, Gennser G, Owman C, Persson H, Sjöberg N-O. Histochemical and pharmacological studies on amine mechanisms in the umbilical cord, umbilical vein and ductus venosus of the human fetus. Acta Physiol Scand. 1968;72:15–24.
43. Coceani F, Adeagbo ASO, Cutz E, Olley PM. Autonomic mechanisms in the ductus venosus of the lamb. Am J Phys. 1984;247:H17–24.
44. Coceani F. The control of the ductus venosus: an update. Eur J Pediatr. 1993;152:976–7.
45. Adeagbo ASO, Coceani F, Olley PM. The response of the lamb ductus venosus to prostaglandins and inhibitors of prostaglandin and thromboxane synthesis. Circ Res. 1982;51:580–6.
46. Adeagbo ASO, Breen CA, Cutz E, Lees JG, Olley PM, Coceani F. Lamb ductus venosus: evidence of a cytochrome P-450 mechanism in its contractile tension. J Pharmacol Exp Ther. 1989;252:875–9.
47. Adeagbo ASO, Bishai I, Lees J, Olley PM, Coceani F. Evidence for a role of prostaglandine I2 and thromboxane A2 in the ductus venosus of the lamb. Can J Physiol Pharmacol. 1984;63:1101–5.
48. Morin FCI. Prostaglandin E1 opens the ductus venosus in the newborn lamb. Pediatr Res. 1987;21:225–8.
49. Coceani F, Olley PM. The control of cardiovascular shunts in the fetal and perinatal period. Can J Pharmacol. 1988;66:1129–34.
50. Momma K, Ito T, Ando M. In situ morphology of the ductus venosus and related vessels in the fetal and neonatal rat. Pediatr Res. 1992;32:386–9.
51. Kiserud T, Ozaki T, Nishina H, Rodeck C, Hanson MA. Effect of NO, phenylephrine, and hypoxemia on ductus venosus diameter in fetal sheep. Am J Physiol Heart Circ Physiol. 2000;279(3):H1166–71.
52. Behrman RE, Lees MH, Peterson EN, de Lannoy CW, Seeds AE. Distribution of the circulation in the normal and asphyxiated fetal primate. Am J Obstet Gynecol. 1970;108:956–69.
53. Edelstone DI, Rudolph AM, Heymann MA. Liver and ductus venosus blood flows in fetal lambs in utero. Circ Res. 1978;42:426–33.
54. Edelstone DI, Rudolph AM. Preferential streaming of ductus venosus blood to the brain and heart in fetal lambs. Am J Phys. 1979;237:H724–9.
55. Lind J, Wegelius C. Angiocardiographic studies on the human foetal circulation. Pediatrics. 1949;4:391–400.
56. Mavrides E, Moscoso G, Carvalho JS, Campbell S, Thilaganathan B. The anatomy of the umbilical, portal and hepatic venous system in the human fetus at 14-19 weeks of gestation. Ultrasound Obstet Gynecol. 2001;18:598–604.
57. Itskovitz J, LaGamma EF, Rudolph AM. The effect of reducing umbilical blood flow on fetal oxygenation. Am J Obstet Gynecol. 1983;145:813–8.
58. Jensen A, Berger R, editors. Regional distribution of cardiac output. Cambridge: Cambridge University Press; 1993.
59. Tchirikov M, Rybakowski C, Hünecke B, Schröder HJ. Blood flow through the ductus venosus in singleton and multifetal pregnancies and in fetuses with intrauterine growth retardation. Am J Obstet Gynecol. 1998;178:943–9.
60. Edelstone DI, Rudolph AM, Heymann MA. Effect of hypoxemia and decreasing umbilical flow on liver and ductus venosus blood flows in fetal lambs. Am J Phys. 1980;238:H656–63.
61. Itskovitz J, LaGamma EF, Rudolph AM. Effects of cord compression on fetal blood flow distribution and O2 delivery. Am J Phys. 1987;252:H100–9.

62. Meyers RL, Paukick RP, Rudolph CD, Rudolph AM. Cardiovascular responses to acute, severe haemorrhage in fetal sheep. J Dev Physiol. 1991;15:189–97.
63. Jensen A, Roman C, Rudolph AM. Effect of reduced uterine flow on fetal blood flow distribution and oxygen delivery. J Dev Physiol. 1991;15:309–23.
64. Kiserud T, Kessler J, Ebbing C, Rasmussen S. Ductus venosus shunting in growth-restricted fetuses and the effect of umbilical circulatory compromise. Ultrasound Obstet Gynecol. 2006;28(2):143–9.
65. Kessler J, Rasmussen S, Godfrey K, Hanson M, Kiserud T. Fetal growth restriction is associated with prioritization of umbilical blood flow to the left hepatic lobe at the expense of the right lobe. Pediatr Res. 2009;66(1):113–7.
66. Bellotti M, Pennati G, De Gasperi C, Bozzo M, Battaglia FC, Ferrazzi E. Simultaneous measurements of umbilical venous, fetal hepatic, and ductus venosus blood flow in growth-restricted human fetuses. Am J Obstet Gynecol. 2004;190(5):1347–58.
67. Lind J, Wegelius C, editors. Human fetal circulation: changes in the cardiovascular system at birth and disturbances in the post-natal closure of the foramen ovale and ductus arteriosus. 1954.
68. Bristow J, Rudolph AM, Itskovitz J. A preparation for studying liver blood flow, oxygen consumption, and metabolism in the fetal lamb in utero. J Dev Physiol. 1981;3:255–66.
69. Bristow J, Rudolph AM, Itskovitz J, Barnes R. Hepatic oxygen and glucose metabolism in the fetal lamb. J Clin Invest. 1982;71:1047–61.
70. Townsend SF, Rudolph CD, Rudolph AM. Changes in ovine hepatic circulation and oxygen consumption at birth. Pediatr Res. 1989;25:300–4.
71. Dawes GS, Mott JC. Changes in O2 distribution and consumption in foetal lambs with variations in umbilical blood flow. J Physiol Lond. 1964;170:524–40.
72. Tchirikov M, Kertschanska S, Schroder HJ. Obstruction of ductus venosus stimulates cell proliferation in organs of fetal sheep. Placenta. 2001;22(1):24–31.
73. Tchirikov M, Kertschanska S, Sturenberg HJ, Schroder HJ. Liver blood perfusion as a possible instrument for fetal growth regulation. Placenta. 2002;23(Suppl A):S153–8.
74. Haugen G, Hanson M, Kiserud T, Crozier S, Inskip H, Godfrey KM. Fetal liver-sparing cardiovascular adaptations linked to mother's slimness and diet. Circ Res. 2005;96(1):12–4.
75. Godfrey KM, Haugen G, Kiserud T, Inskip HM, Cooper C, Harvey NC, et al. Fetal liver blood flow distribution: role in human developmental strategy to prioritize fat deposition versus brain development. PLoS One. 2012;7(8):e41759.
76. Ikenoue S, Waffarn F, Ohashi M, Sumiyoshi K, Ikenoue C, Buss C, et al. Prospective association of fetal liver blood flow at 30 weeks gestation with newborn adiposity. Am J Obstet Gynecol. 2017;217(2):204.e1–8.
77. Edelstone DI. Regulation of blood flow through the ductus venosus. J Dev Physiol. 1980;2:219–38.
78. Kiserud T, Stratford L, Hanson MA. Umbilical flow distribution to the liver and the ductus venosus: an in vitro investigation of the fluid dynamic mechanisms in the fetal sheep. Am J Obstet Gynecol. 1997;177(1):86–90.
79. Paulick RP, Meyers RL, Rudolph CD, Rudolph AM. Venous and hepatic vascular responses to indomethacin and prostaglandin E1 in the fetal lamb. Am J Obstet Gynecol. 1990;163:1357–63.
80. Paulick RP, Meyers RL, Rudolph CD, Rudolph AM. Umbilical and hepatic venous responses to circulating vasoconstrictive hormones in fetal lamb. Am J Phys. 1991;260:H1205–13.
81. Bocking AD, Gagnon R, White SE, Homan J, Milne KM, Richardson B. Circulatory responses to prolonged hypoxemia in fetal sheep. Am J Obstet Gynecol. 1988;159:1418–24.
82. Bocking AD, editor. Effect of chronic hypoxaemia on circulation control. Cambridge: Cambridge University Press; 1993.
83. Lund A, Ebbing C, Rasmussen S, Kiserud T, Kessler J. Maternal diabetes alters the development of ductus venosus shunting in the fetus. Acta Obstet Gynecol Scand. 2018;97:1032–40.
84. Lund A, Ebbing C, Rasmussen S, Kiserud T, Hanson M, Kessler J. Altered development of fetal liver perfusion in pregnancies with pregestational diabetes. PLoS One. 2019;14(3):e0211788.
85. Hellevik LR, Kiserud T, Irgens F, Ytrehus T, Eik-Nes SH. Simulation of pressure drop and energy dissipation for blood flow in a human fetal bifurcation. ASME J Biomech Eng. 1998;120:455–62.
86. Pennati G, Redaelli A, Bellotti M, Ferrazzi E. Computational analysis of the ductus venosus fluid dynamics based on Doppler measurements. Ultrasound Med Biol. 1996;22(6):1017–29.
87. Schröder HJ, Tchirikov M, Rybakowski C. Pressure pulses and flow velocities in central veins of the anesthetized sheep fetus. Am J Physiol Heart Circ Physiol. 2003;284(4):H1205–11.
88. Jerabek-Klestil S, Brantner C, Nehoda R, D'Costa E, Campei S, Scheier M. Prenatal sonographic diagnosis of intrahepatic portosystemic shunts. J Ultrasound Med. 2014;33(3):543–6.
89. Nyberg MK, Johnsen SL, Rasmussen S, Kiserud T. Hemodynamics of fetal breathing movements: the inferior vena cava. Ultrasound Obstet Gynecol. 2011;38(6):658–64.
90. Matias A, Huggon I, Areias JC, Montenegro N, Nicolaides KH. Cardiac defects in chromosomally normal fetuses with abnormal ductus venosus blood flow at 10-14 weeks. Ultrasound Obstet Gynecol. 1999;14(5):307–10.
91. Matias A, Montenegro N, Areias JC, Leite LP. Haemodynamic evaluation of the first trimester fetus with special emphasis on venous return. Hum Reprod Update. 2000;6(2):177–89.

92. Borrell A, Martinez JM, Serés A, Borobio V, Cararach V, Fortuny A. Ductus venosus assessment at the time of nuchal translucency measurement in the detection of fetal aneuploidy. Prenat Diagn. 2003;23(11):921–6.
93. Hecher K, Campbell S, Snijders R, Nicolaides K. Reference ranges for fetal venous and atrioventricular blood flow parameters. Ultrasound Obstet Gynecol. 1994;4:381–90.
94. Bahlmann F, Wellek S, Reinhardt I, Merz E, Welter C. Reference values of ductus venosus flow velocities and calculated waveform indices. Prenat Diagn. 2000;20:623–34.
95. Prefumo F, Risso D, Venturini PL, De Biasio P. Reference values for ductus venosus Doppler flow measurements at 10-14 weeks of gestation. Ultrasound Obstet Gynecol. 2002;20:42–6.
96. Kessler J, Rasmussen S, Hanson M, Kiserud T. Longitudinal reference ranges for ductus venosus flow velocities and waveform indices. Ultrasound Obstet Gynecol. 2006;28(7):890–8.
97. Axt-Fliedner R, Diler S, Georg T, Friedrich M, Diedrich K. Reference values of ductus venosus blood flow velocities and waveform indices from 10 to 20 weeks of gestation. Arch Gynecol Obstet. 2004;269(3):199–204.
98. Axt-Fliedner R, Wiegank U, Fetsch C, Friedrich M, Krapp M, Georg T, et al. Reference values of fetal ductus venosus, inferior vena cava and hepatic vein blood flow velocities and waveform indices during the second and third trimester of pregnancy. Arch Gynecol Obstet. 2004;270(1):46–55.
99. Pennati G, Bellotti M, Ferrazzi E, Rigano S, Garberi A. Hemodynamic changes across the human ductus venosus: a comparison between clinical findings and mathematical calculations. Ultrasound Obstet Gynecol. 1997;9(6):383–91.
100. Pennati G, Bellotti M, Ferrazzi E, Bozzo M, Pardi G, Fumero R. Blood flow through the ductus venosus in human fetus: calculation using Doppler velocimetry and computational findings. Ultrasound Med Biol. 1998;24(4):477–87.
101. Kiserud T, Hellevik LR, Hanson MA. Blood velocity profile in the ductus venosus inlet expressed by the mean/maximum velocity ratio. Ultrasound Med Biol. 1998;24(9):1301–6.
102. Tchirikov M, Eisermann K, Rybakowski C, Schröder HJ. Doppler ultrasound evaluation of ductus venosus blood flow during acute hypoxia in fetal lambs. Ultrasound Obstet Gynecol. 1998;11:426–31.
103. Leinan PR, Degroote J, Kiserud T, Skallerud B, Vierendeels J, Hellevik LR. Velocity profiles in the human ductus venosus: a numerical fluid structure interaction study. Biomech Model Mechanobiol. 2013;12(5):1019–35.
104. Leinan PR, Kiserud T, Hellevik LR. Human ductus venosus velocity profiles in the first trimester. Cardiovasc Eng Technol. 2013;4(3):257–66.
105. Kiserud T. Fetal venous circulation—an update on hemodynamics. J Perinat Med. 2000;28:90–6.
106. DeVore GR, Horenstein J. Ductus venosus index: a method for evaluating right ventricular preload in the second-trimester fetus. Ultrasound Obstet Gynecol. 1993;3(5):338–42.
107. Reed KL, Appleton CP, Anderson CF, Shenker L, Sahn DJ. Doppler studies of vena cava flows in human fetuses; insights into normal and abnormal cardiac physiology. Circulation. 1990;81:498–505.
108. Reed KL, Chaffin DG, Anderson CF, Newman AT. Umbilical venous velocity pulsations are related to atrial contraction pressure waveforms in fetal lambs. Obstet Gynecol. 1997;89(6):953–6.
109. Kanzaki T, Chiba Y. Evaluation of the preload condition of the fetus by inferior vena caval blood flow pattern. Fetal Diagn Ther. 1990;5:168–74.
110. Gudmundsson S, Huhta JC, Wood DC, Tulzer G, Cohen AW, Weiner S. Venous Doppler ultrasonography in the fetus with nonimmune hydrops. Am J Obstet Gynecol. 1991;164:33–7.
111. Gudmundsson S, Gunnarsson G, Hökegård K-H, Ingmarsson J, Kjellmer I. Venous Doppler velocimetry in relationship to central venous pressure and heart rate during hypoxia in ovine fetus. J Perinat Med. 1999;27:81–90.
112. Tulzer G, Gudmundsson S, Rotondo KM, Wood DC, Cohen AW, Huhta J. Doppler in the evaluation and prognosis of fetuses with tricuspid regurgitation. J Matern Fetal Invest. 1991;1:15–8.
113. Tulzer G, Gudmundsson S, Wood DC, Cohen AW, Weiner S, Huhta JC. Doppler in non-immune hydrops fetalis. Ultrasound Obstet Gynecol. 1994;4:279–83.
114. Hecher K, Campbell S, Doyle P, Harrington K, Nicolaides K. Assessment of fetal compromise by Doppler ultrasound investigation of the fetal circulation. Arterial, intracardiac, and venous blood flow velocity studies. Circulation. 1995;91(1):129–38.
115. Hecher K, Snijders R, Campbell S, Nicolaides K. Fetal venous, intracardiac, and arterial blood flow measurements in intrauterine growth retardation: relationship with fetal blood gases. Am J Obstet Gynecol. 1995;173:10–5.
116. Rizzo G, Capponi A, Rinaldo D, Arduini D, Romanini C. Ventricular ejection force in growth-retarded fetuses. Ultrasound Obstet Gynecol. 1995;5:247–55.
117. Rizzo G, Capponi A, Talone P, Arduini D, Romanini C. Doppler indices from inferior vena cava and ductus venosus in predicting pH and oxygen tension in umbilical blood at cordocentesis in growth-retarded fetuses. Ultrasound Obstet Gynecol. 1996;7:401–10.
118. Reuss ML, Rudolph AM, Dae MW. Phasic blood flow patterns in the superior and inferior venae cavae and umbilical vein of fetal sheep. Am J Obstet Gynecol. 1983;145:70–6.
119. Hasaart TH, de Haan J. Phasic blood flow patterns in the common umbilical vein of fetal sheep during umbilical cord occlusion and the influence of autonomic nervous system blockade. J Perinat Med. 1986;14:19–26.

120. Kiserud T, Jauniaux E, West D, Ozturk O, Hanson MA. Circulatory responses to acute maternal hyperoxaemia and hypoxaemia assessed non-invasively by ultrasound in fetal sheep at 0.3-0.5 gestation. Br J Obstet Gynaecol. 2001;108:359–64.
121. Giussani DA, Spencer JAD, Moor PD, Bennet L, Hanson MA. Afferent and efferent components of the cardiovascular response to acute hypoxia in term fetal sheep. J Physiol. 1993;461:431–49.
122. Giussani DA, Riquelme RA, Moraga FA, McGarrigle HHG, Gaete CR, Sanhueza EM, et al. Chemoreflex and endocrine components of cardiovascular responses to acute hypoxemia in the llama fetus. Am J Phys. 1996;271:R73–83.
123. Ville Y, Hyett J, Hecher K, Nicolaides K. Preliminary experience with endoscopic laser surgery for severe twin-twin transfusion syndrome. N Engl J Med. 1995;332(4):224–7.
124. Hecher K, Snijders R, Campbell S, Nicolaides K. Fetal venous, arterial, and intracardiac blood flows in red blood cell isoimmunization. Obstet Gynecol. 1995;85(1):122–8.
125. Gembruch U, Krapp M, Baumann P. Changes of venous blood flow velocity waveforms in fetuses with supraventricular tachycardia. Ultrasound Obstet Gynecol. 1995;5(6):394–9.
126. Gembruch U, Krapp M, Germer U, Baumann P. Venous Doppler in the sonographic surveillance of fetuses with supraventricular tachycardia. Eur J Obstet Gynecol Reprod Biol. 1999;84(2):187–92.
127. Fouron JC, Fournier A, Proulx F, Lamarche J, Bigras JL, Boutin C, et al. Management of fetal tachyarrhythmia based on superior vena cava/aorta Doppler flow recordings. Heart. 2003;89(10):1211–6.
128. Hecher K, Bilardo CM, Stigter RH, Ville Y, Hackelöer BJ, Kok HJ. Monitoring of fetuses with intrauterine growth restriction: a longitudinal study. Ultrasound Obstet Gynecol. 2001;18:564–70.
129. Baschat AA, Gembruch U, Harman CR. The sequence of changes in Doppler and biophysical parameters as severe fetal growth restriction worsen. Ultrasound Obstet Gynecol. 2001;18:571–7.
130. Ferrazzi E, Bozzo M, Rigano S, Bellotti M, Morabito A, Pardi G, et al. Temporal sequence of abnormal Doppler changes in peripheral and central circulatory systems of the severely growth-restricted fetus. Ultrasound Obstet Gynecol. 2002;19:140–6.
131. Unterscheider J, Daly S, Geary MP, Kennelly MM, McAuliffe FM, O'Donoghue K, et al. Predictable progressive Doppler deterioration in IUGR: does it really exist? Am J Obstet Gynecol. 2013;209(6):539.e1–7.
132. Montenegro N, Matias A, Areias S, Castedo S, Barros H. Increased fetal nuchal translucency: possible involvement of early cardiac failure. Ultrasound Obstet Gynecol. 1997;10:265–8.
133. Matias A, Montenegro N, Areias JC. Anomalous venous return associated with major chromosomopathies in the late first trimester of pregnancy. Ultrasound Obstet Gynecol. 1998;11:209–13.
134. Kiserud T. The fetal venous circulation. Fetal Matern Med Rev. 2003;14(1):57–95.
135. Bhide A, Vuolteenaho O, Haapsamo M, Erkinaro T, Rasanen J, Acharya G. Effect of hypoxemia with or without increased placental vascular resistance on fetal left and right ventricular myocardial performance index in chronically instrumented sheep. Ultrasound Med Biol. 2016;42(11):2589–98.
136. Bhide A, Rasanen J, Huhta H, Junno J, Erkinaro T, Ohtonen P, et al. Effect of hypoxemia on fetal ventricular deformation in a chronically instrumented sheep model. Ultrasound Med Biol. 2017;43(5):967–73.
137. Acharya G, Räsänen J, Mäkikallio K, Erkinaro T, Kavasmaa T, Haapsamo M, et al. Metabolic acidosis decreases fetal myocardial isovolumic velocities in a chronic sheep model of increased placental vascular resistance. Am J Physiol Heart Circ Physiol. 2008;294(1):H498–504.
138. Kiserud T, Kilavuz Ö, Hellevik LR. Venous pulsation in the left portal branch—the effect of pulse and flow direction. Ultrasound Obstet Gynecol. 2003;21:359–64.
139. Smrcek JM, Baschat AA, Germer U, Gloeckner-Hofmann K, Gembruch U. Fetal hydrops and hepatosplenomegaly in the second half of pregnancy: a sign of myeloproliferative disorder in fetuses with trisomy 21. Ultrasound Obstet Gynecol. 2001;17:403–9.
140. Kiserud T. Ductus venosus blood velocity in myeloproliferative disorders. Ultrasound Obstet Gynecol. 2001;18(2):184–5.
141. Mavrides E, Holden D, Bland JM, Tekay A, Thilaganathan B. Intraobserver and interobserver variability of transabdominal Doppler velocimetry measurements of the fetal ductus venosus between 10 and 14 weeks of gestation. Ultrasound Obstet Gynecol. 2001;17:306–10.
142. Prefumo F, De Biasio P, Venturini PL. Reproducibility of ductus venosus Doppler flow measurements at 11-14 weeks of gestation. Ultrasound Obstet Gynecol. 2001;17:3001–305.
143. Maiz N, Kagan K, Milovanovic Z, Celik E, Nicolaides K. Learning curve for Doppler assessment of ductus venosus flow at 11 + 0 to 13 + 6 weeks' gestation. Ultrasound Obstet Gynecol. 2008;31(5):503–6.
144. Kiserud T, Rasmussen S. How repeat measurements affect the mean diameter of the umbilical vein and the ductus venosus. Ultrasound Obstet Gynecol. 1998;11(6):419–25.
145. Kiserud T, Saito T, Ozaki T, Rasmussen S, Hanson MA. Validation of diameter measurements by ultrasound: intraobserver and interobserver variations assessed in vitro and in fetal sheep. Ultrasound Obstet Gynecol. 1999;13(1):52–7.
146. Haugen G, Kiserud T, Godfrey K, Crozier S, Hanson M. Portal and umbilical venous blood supply to the liver in the human fetus near term. Ultrasound Obstet Gynecol. 2004;24(6):599–605.

147. Kessler J, Rasmussen S, Godfrey K, Hanson M, Kiserud T. Venous liver blood flow and regulation of human fetal growth: evidence from macrosomic fetuses. Am J Obstet Gynecol. 2011;204(5):429.e1–7.
148. Jørgensen C, Andolf E. Four cases of absent ductus venosus: three in combination with severe hydrops fetalis. Fetal Ther. 1994;9:395–7.
149. Sivén M, Ley D, Hägerstrand I, Svenningsen N. Agenesis of the ductus venosus and its correlation to hydrops fetalis and the fetal hepatic circulation. Pediatr Pathol Lab Med. 1995;15:39–50.
150. Gembruch U, Baschat AA, Gortner L. Prenatal diagnosis of ductus venosus agenesis: a report of two cases and review of the literature. Ultrasound Obstet Gynecol. 1998;11:185–9.
151. Hofstaetter C, Plath H, Hansmann M. Prenatal diagnosis of abnormalities of the fetal venous system. Ultrasound Obstet Gynecol. 2000;15:231–41.
152. Achiron R, Hegesh J, Yagel S, Lipitz S, Cohen SB, Rotstein Z. Abnormalities of the fetal central veins and umbilico-portal system: prenatal ultrasonographic diagnosis and proposed classification. Ultrasound Obstet Gynecol. 2000;16:539–48.
153. Avni EF, Ghysels M, Donner C, Damis E. In utero diagnosis of congenital absence of the ductus venosus. J Clin Ultrasound. 1997;25:456–8.
154. Contratti G, Banzi C, Ghi T, Perolo A, Pilu G, Visenti A. Absence of the ductus venosus: report of 10 new cases and review of the literature. Ultrasound Obstet Gynecol. 2001;18:605–9.
155. Brozot ML, Schultz R, Patroni LT, Lopes LM, Armbruster Moraes E, Zugaib M. Trisomy 10: ultrasound features and natural history after first trimester diagnosis. Prenat Diagn. 2001;21:672–5.
156. Jaeggi ET, Fouron JC, Hornberger LK, Proulx F, Oberhänsli I, Yoo SJ, et al. Agenesis of the ductus venosus that is associated with extrahepatic umbilical vein drainage: prenatal features and clinical outcome. Am J Obstet Gynecol. 2002;187(4):1031–7.
157. Pacheco D, Brandão O, Montenegro N, Matias A. Ductus venosus agenesis and fetal malformations: what can we expect?—a systematic review of the literature. J Perinat Med. 2018;47(1):1–11.
158. Staboulidou I, Pereira S, JeJ C, Syngelaki A, Nicolaides KH. Prevalence and outcome of absence of ductus venosus at 11(+0) to 13(+6) weeks. Fetal Diagn Ther. 2011;30(1):35–40.
159. Rudolph CD, Meyers RL, Paulick RP, Rudolph AM. Effects of ductus venosus obstruction on liver and regional blood flows in the fetal lamb. Pediatr Res. 1991;29:347–52.
160. Nathanielsz PW, Hanson MA. The fetal dilemma: spare the brain and spoil the liver. J Physiol. 2003;548(Pt 2):333.
161. Fugelseth D, Lindemann R, Liestøl K, Kiserud T, Langslet A. Ultrasonographic study of ductus venosus in healthy neonates. Arch Dis Child. 1997;77:F131–4.
162. Loberant N, Barak M, Gaitini D, Herkovits M, Ben-Elisha M, Roguin N. Closure of the ductus venosus in neonates: findings on real-time gray-scale, color-flow Doppler, and duplex Doppler sonography. AJR. 1992;159:1083–5.
163. Fugelseth D, Lindemann R, Liestol K, Kiserud T, Langslet A. Postnatal closure of ductus venosus in preterm infants or = 32 weeks. An ultrasonographic study. Early Hum Dev. 1998;53(2):163–9.
164. Loberant N, Herkovits M, Ben-Elisha M, Herschkowitz S, Sela S, Roguin N. Closure of the ductus venosus in premature infants: findings on real-time gray-scale, color-flow Doppler, and duplex Doppler sonography. Am J Roentgenol. 1999;172:227–9.
165. Fugelseth D, Guthenberg C, Hagenfeldt L, Liestøl K, Hallerud M, Lindemann R. Patent ductus venosus does not lead to alimentary galactosaemia in preterm infants. Acta Paediatr. 2001;90(2):192–5.
166. Fugelseth D, Kiserud T, Liestol K, Langslet A, Lindemann R. Ductus venosus blood velocity in persistent pulmonary hypertension of the newborn. Arch Dis Child Fetal Neonatal Ed. 1999;81(1):F35–9.

Doppler Examination of the Fetal Pulmonary Venous Circulation

29

Jay D. Pruetz, Jodie K. Votava-Smith, and Shuo Wang

29.1 Introduction

Evaluation of pulmonary venous anatomy and physiology is one of the more challenging components of the fetal heart examination. As a result, the prenatal detection rate of congenital pulmonary venous anomalies in the current era is extremely low at ~10% [1–3]. Existing fetal echo guidelines recommend 2D and color Doppler visualization of the pulmonary venous connections. However, in most guidelines the confirmation of just 2 pulmonary vein connections by 2D or color Doppler, when technically feasible, is considered acceptable [4]. It is not clearly stated the number of veins to evaluate, which ones should be seen (left, right, or both) and how best to demonstrate normal pulmonary venous anatomy and physiology. Furthermore, pulsed wave (PW) Doppler of the pulmonary veins is not mandated by any current guidelines [4–6]. Advancements in spectral Doppler ultrasound technology, such as HDPD and Eflow Doppler techniques, have made a complete pulmonary venous evaluation more feasible [7]. Recent publications have focused attention on key anatomic vdefects of the pulmonary veins [8–11]. Diagnoses, such as TAPVR, are important to be detected prenatally such that care can be delivered promptly after birth (Shi et al. 2017, Khan et al. 2015) [1, 12, 13]. Furthermore, the assessment of pulmonary vein Doppler flow patterns has revealed important insights into the progression of heart disease in utero and aids in the diagnosis of fetal arrhythmia [1, 14–16]. The use of pulmonary vein Doppler is an active area of study for understanding fetal cardiopulmonary physiology and maternofetal interactions. This chapter will review the approach to fetal pulmonary venous circulation evaluation, highlighting both normal and abnormal findings as well as targeted use of Doppler echocardiography in specific clinical scenarios.

J. D. Pruetz (✉)
Division of Cardiology, Children's Hospital Los Angeles, Heart Institute, Los Angeles, CA, USA

Department of Pediatrics, Keck School of Medicine, University of Southern California, Los Angeles, CA, USA

Department of Obstetrics and Gynecology, Keck School of Medicine, University of Southern California, Los Angeles, CA, USA
e-mail: JPruetz@chla.usc.edu; jvotavasmith@chla.usc.edu

J. K. Votava-Smith
Division of Cardiology, Children's Hospital Los Angeles, Heart Institute, Los Angeles, CA, USA

Department of Pediatrics, Keck School of Medicine, University of Southern California, Los Angeles, CA, USA

S. Wang
Division of Cardiology, Children's Hospital Los Angeles, Heart Institute, Los Angeles, CA, USA

D. Maulik, C. C. Lees (eds.), *Doppler Ultrasound in Obstetrics and Gynecology*,
https://doi.org/10.1007/978-3-031-06189-9_29

29.1.1 Pulmonary Venous Anatomy and Embryology

The pulmonary veins form during the fifth week of gestation from the primordial lung buds and splanchnic plexus (vascular plexus of the foregut) [17]. This plexus forms into a common pulmonary vein (CPV) confluence that connects to the back wall of the sinoatrial portion of the heart [18]. Initially, the CPV is connected to the systemic venous system, but gradually this venous plexus involutes as the CPV incorporates into the left atrium (LA) [19]. The connection to the systemic venous circulation is lost and the individual pulmonary veins form direct connections to the LA with 4 distinct pulmonary venous ostia (Fig. 29.1). Invagination of CPV into the LA results in the majority of the LA being smooth-walled and the rough-walled primitive atrium is solely the LA appendage (auricle). A complete or partial failure of this connection to the LA results in anomalous pulmonary venous return or cor triatriatum usually with a retained communication to the systemic venous circulation (Fig. 29.2). In partial or total anomalous pulmonary venous return (PAPVR or TAPVR, respectively) there will be drainage of the pulmonary venous system to the right atrium either directly or via the systemic veins from above or below the diaphragm [20]. The various types of anomalous pulmonary venous return will be reviewed under the congenital anomalies section.

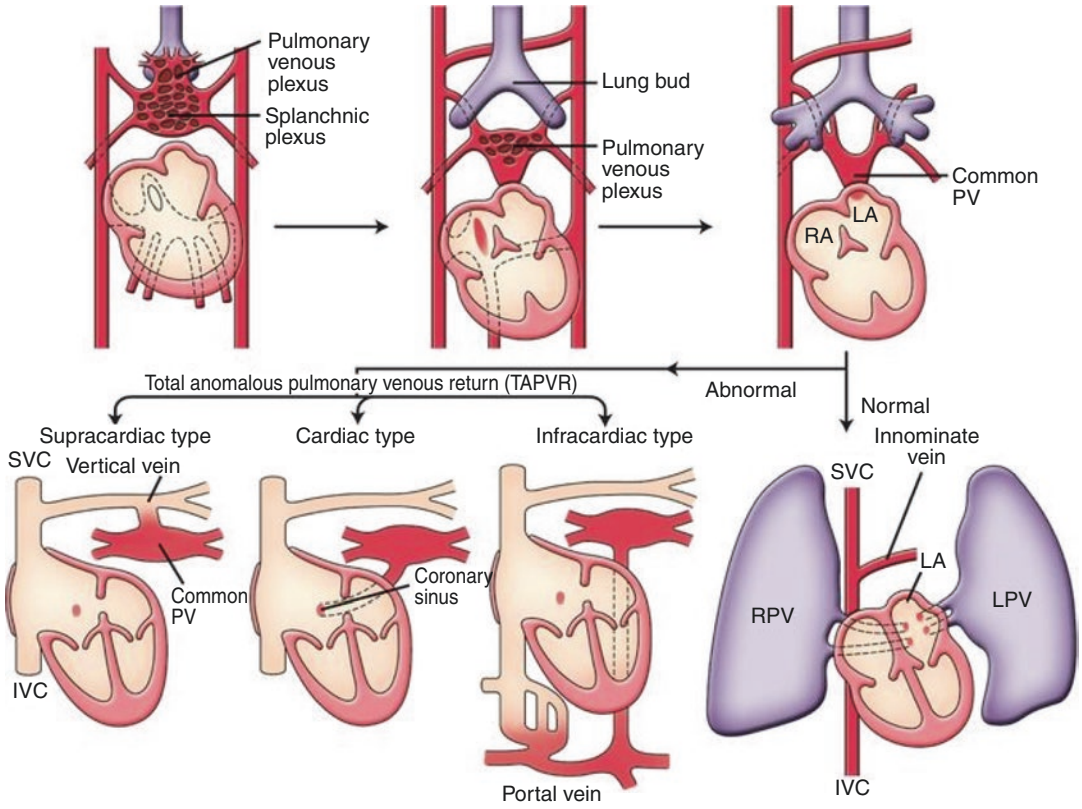

Fig. 29.1 Embryology of pulmonary vein development showing normal incorporation of the common pulmonary vein (PV) confluence to the back wall of the left atrium (LA). The connection to the systemic venous circulation is lost and the individual pulmonary veins form 4 distinct connections to the LA. Also shown is what occurs when there is failure of the common PV connection to the LA resulting in the various forms of TAVPR depending on which venous communication is retained. Inferior Vena Cava (IVC), left pulmonary veins (LPV), right pulmonary veins (RPV), Superior Vena Cava (SVC). From Reprinted by permission from Springer Nature: Embryology by Hiroyuk Yamagishi, Chihiro Yamagashi, Springer eBook 2014

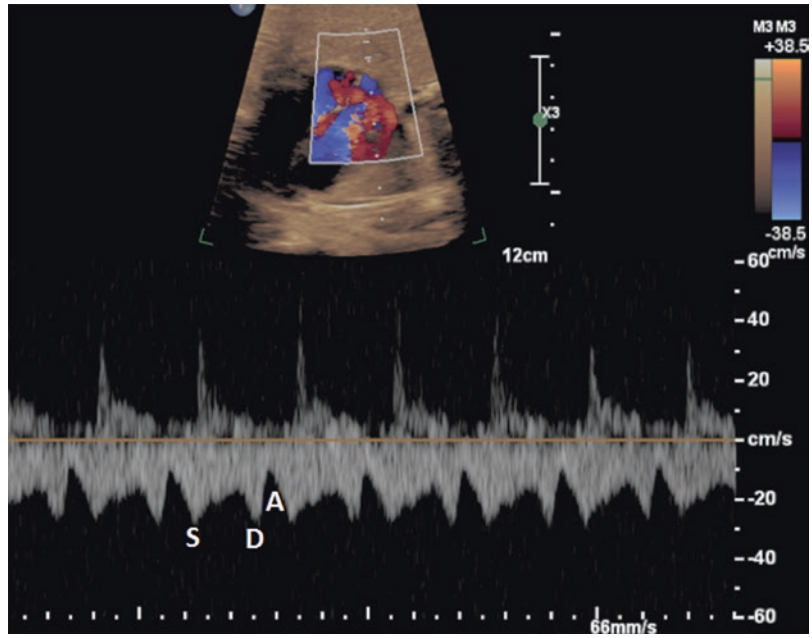

Fig. 29.2 Normal Pulmonary vein PW Doppler waveforms highlighting the S, D, and A waves. Using a Philips Epiq machine with a C5–1 MHz curvilinear probe

29.1.2 Fetal Pulmonary Vein Physiology

The pulmonary veins are small structures in fetal life measuring only 1–2 mm in diameter at the time of second trimester fetal heart screening. The flow in the pulmonary venous system is much less in the fetus accounting for just ~10–15% of combined cardiac output (CCO) [21, 22]. This low pulmonary venous flow is a result of the high pulmonary vascular resistance maintained in the fetus and the ability for pulmonary artery blood flow to cross the ductus arteriosus connection back to the fetal systemic circulation which has low resistance [21]. The pulmonary blood flow will gradually increase over gestation, reaching 20–25% for CCO in the third trimester, making visualization of flow in the pulmonary veins easier later in gestation. Alterations in pulmonary blood flow volume due to cardiac or extracardiac disease can directly impact the volume of flow in the pulmonary veins and thus make it easier or more difficult to evaluate them. Premature ductus arteriosus constriction/closure, aortopulmonary collaterals, and large vascular arteriovenous malformations can increase pulmonary venous flow making visualization easier. However, in cases of pulmonary atresia, pulmonary hypoplasia, and large chest masses, such as congenital cystic pulmonary malformation or congenital diaphragmatic hernia, there can be decreased flow in the some or all of the pulmonary veins making accurate visualization more difficult.

In the healthy fetus, pulmonary venous Doppler flow velocities have a triphasic pattern and are primarily influenced by changes in left atrial (LA) and left ventricular (LV) contraction and compliance [23, 24]. The waveform components include a ventricular systolic (S) and diastolic (D) peak forward flow velocity during LA filling and a brief flattened or reversed atrial (A) flow velocity during LA contraction (Fig. 29.3). During ventricular systole (S) the forward flow in the pulmonary veins occurs due to reduced LA pressure and the downward movement of the mitral valve. In diastole (D) forward flow continues as rapid emptying of the LA occurs during LV relaxation. During atrial contraction (A) there is diminished flow or negative flow in the pulmonary veins due to the acute rise in LA pressure [25–28].

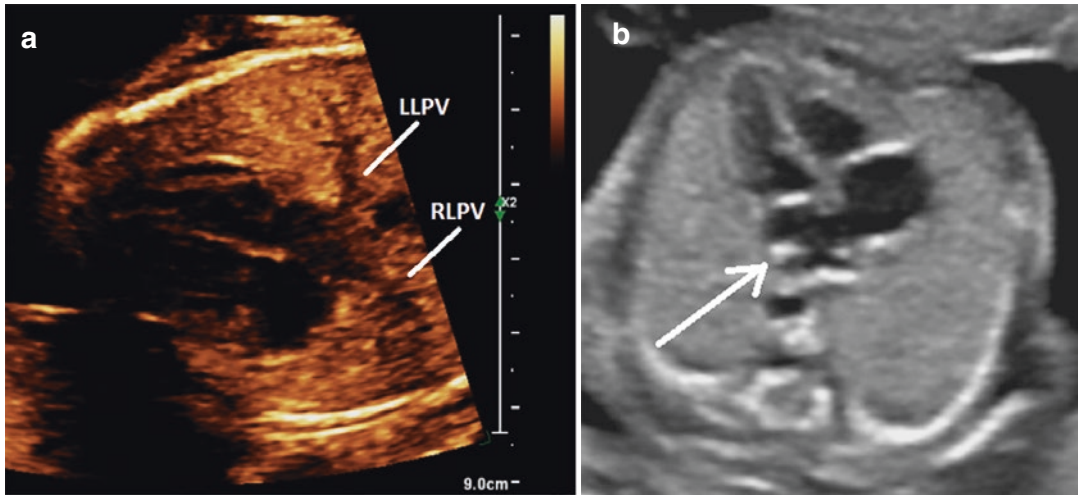

Fig. 29.3 (**a**) Left Lateral 2D view of pulmonary vein connections highlighting the right (RLPV) and left lower pulmonary veins (LLPV). Using a Philips Epiq machine with a C5–1 MHz curvilinear probe. (**b**) A four-chamber 2D view showing lower pulmonary veins and highlighting the coumadin ridge. Using a Philips Epiq machine with a C5–1 MHz curvilinear probe

29.2 Approach to Imaging of the Pulmonary Veins

29.2.1 2D Assessment

Imaging of the pulmonary veins begins with a thorough two-dimensional (2D) assessment of the pulmonary venous circulation using key landmarks for identifying and confirming the pulmonary vein connections to the left atrium. It is important to note that visualization of all four pulmonary veins in the same plane is difficult to achieve because they enter the LA separately and have their own ostia. The right and left upper pulmonary veins course from a superior to inferior plane and anterior to posterior trajectory which makes them more difficult to see from straight AP interrogation (lateral view is better) (Fig. 29.4a). In contrast, the right and left lower pulmonary veins course from an inferior to superior plane taking a posterior to anterior course which makes them more readily/easily identified in the straight AP projection, such as the 4-chamber view (Fig. 29.4b). A clue to finding the entrance of the left upper pulmonary veins to the LA is the so-called "coumadin ridge" which represents an infolding between the smooth-walled LA (incorporated CPV) and LA appendage (primitive atria) (Fig. 29.4b) [29]. This serves as a useful landmark for the connections of the left upper and lower pulmonary veins to the LA. The right lower pulmonary vein can be identified along the plane of the atrial septum extending behind the heart into the right lung which is best seen on a 4-chamber view with the fetus positioned right side up (Fig. 29.5). Additional 2D findings that suggest pulmonary venous anomalies are right heart disproportion, left axis cardiac deviation, and dilated systemic veins

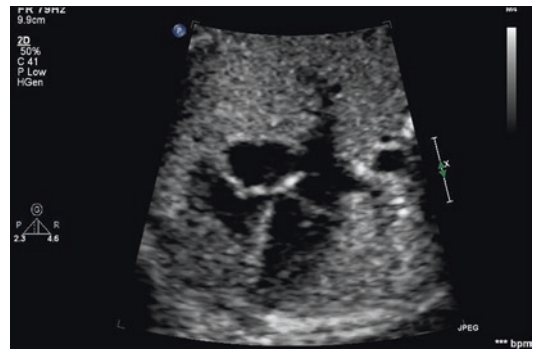

Fig. 29.4 Right lateral view of lower pulmonary vein 2D view. Using a Philips Epiq machine with a C5–1 MHz curvilinear probe

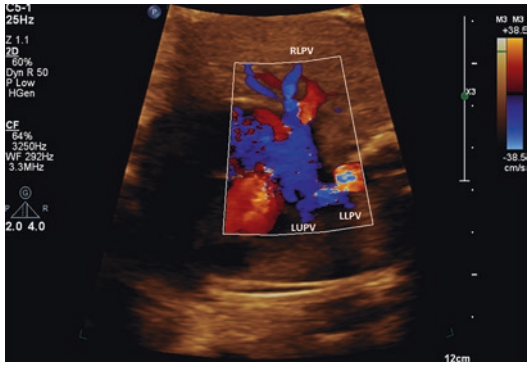

Fig. 29.5 Color Doppler evaluation of the normal pulmonary venous connections (left). PW Doppler interrogation is the best when the line of acquisition is parallel to the vessel of interest, the left lower pulmonary vein in this case (right). Using a Philips Epiq machine with a C5–1 MHz curvilinear probe

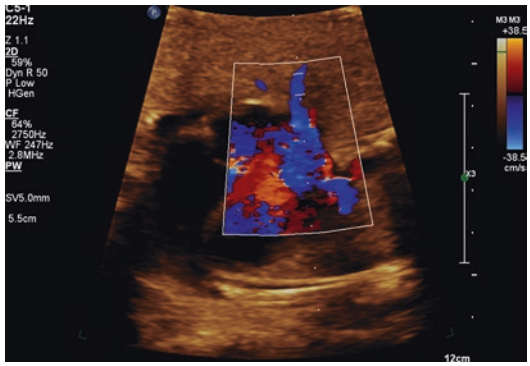

Fig. 29.6 Proper placement of the PW Doppler sample volume in the pulmonary vein just before the entrance into the left atrium at an angle of insonation that is parallel to the pulmonary vein. Using a Philips Epiq machine with a C5–1 MHz curvilinear probe

with additional venous channels [8, 10]. This is reviewed in great detail under the section on congenital anomalies of the pulmonary venous system (Fig. 29.6).

29.2.2 Color Doppler Assessment

Color Doppler evaluation is critically important to pulmonary venous system evaluation and is particularly useful in cases of difficult fetal position or maternal obesity. Color Doppler should be used at lower gain, Nyquist limit of 15–25 cm/s, to detect the low velocity flow in the pulmonary veins [10, 30]. First the 2D landmarks are identified and then a color Doppler box is placed over the left atrium and lung fields of interest. This can be done separately over the right and left pulmonary veins for improved tissue differentiation and resolution or over the entire LA region (Fig. 29.7). Using color Doppler to best identify the course of the pulmonary veins is also very helpful for properly positioning the PW Doppler acquisition line parallel to the vessel of interest. Abnormal color flow patterns can often suggest pulmonary vein anomalies that might not otherwise be appreciated [9]. In TAPVR, the pulmonary venous flow will initially course back toward the heart and meet at a confluence behind the LA, but often a separate color Doppler flow signal will be seen going away from the heart which highlights the anomalous drainage pathway heading either above or below the diaphragm (Fig. 29.8). Reversal of flow in the pulmonary veins on color Doppler can also suggest elevated LA pressure (LV cardiomyopathy) or downstream obstruction (mitral atresia).

29.2.3 Pulsed Wave (PW) Doppler Assessment

Once the pulmonary vein anatomy has been defined by 2D and color Doppler, then PW Doppler can be applied to evaluate pulmonary vein flow patterns. In order to accurately measure the peak velocities in the pulmonary veins it is crucial that the angle of insonation be as parallel to the vessel as possible (Fig. 29.7). Normal pulmonary vein Doppler waveforms include ventricular systolic and diastolic forward flow called the S and D waves as the left atrium fills during systole and diastole with a brief pause or reversal of flow during atrial contraction called the A wave. The A wave is usually very short (<10 ms) and not very deep (Fig. 29.3). It is important to assess all three components of the pulmonary vein triphasic pattern. The volume of pulmonary blood flow in the fetus increases over gestation and reaches a peak level in the third trimester. Correspondingly,

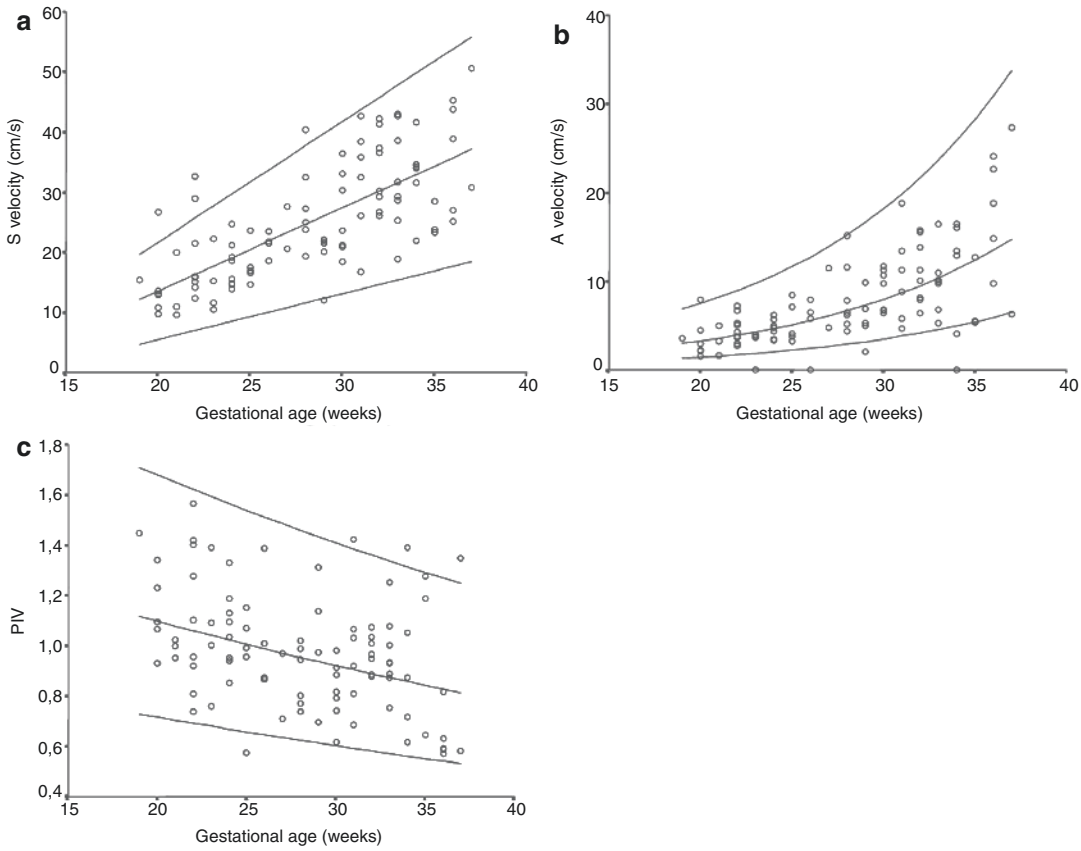

Fig. 29.7 Graphs of pulmonary vein S (**a**) and A wave (**b**) velocities and pulsatility index (**c**) of the pulmonary veins (PIV) over gestation. Reference ranges displayed as individual values, mean reference line, and 95% data intervals for pulmonary vein velocities and PIV plotted against gestational age. (From [27] with permission)

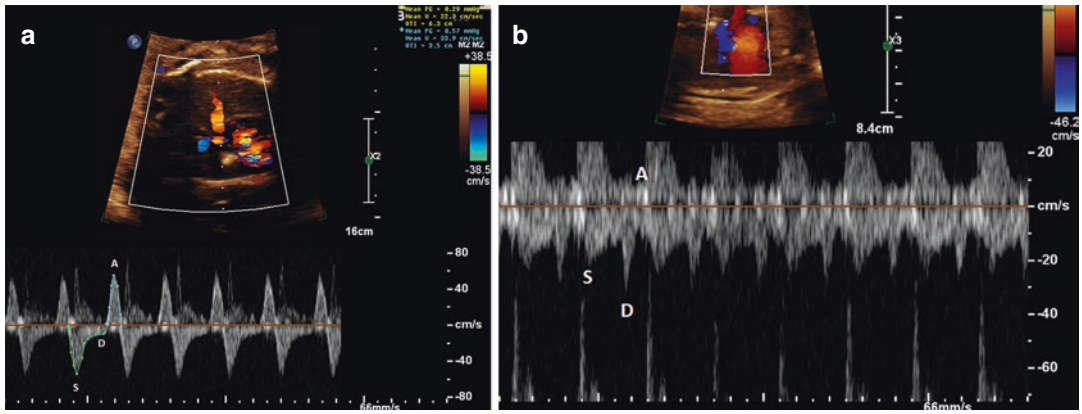

Fig. 29.8 (**a**) Pulmonary vein PW Doppler in the setting of HLHS with RAS showing decreased forward flow in the pulmonary vein during the systole (S wave) and early diastole (D wave) as well as increased flow during atrial systole (A wave) and prominent A wave reversal. Using a Philips Epiq machine with a C5–1 MHz curvilinear probe. (**b**) Pulmonary vein PW Doppler showing decreased S and D wave velocities in the setting of fetal cardiomyopathy. Also it is noted the short, peeked D wave suggesting decreased LV compliance (elevated LV end diastolic pressure). Obtained with a Philips Epiq machine with a C5–1 MHz Curvilinear probe

the peak systolic and diastolic flow velocities as well as the velocity time integral (VTI) also increase significantly during late gestation (Fig. 29.9) [26]. However, the pulsatility index decreases which corresponds to increasing LA and LV relaxation/compliance over gestation [26]. The normal fetus has elevated filling pressures early in gestation and as the baby develops, the ventricles and atria undergo maturation in diastolic relaxation properties, which evolves from dominant systolic emptying to dominant diastolic emptying of the pulmonary veins. This continues even after birth over the first several months of life and has been well documented by PW Doppler E/A ratio changes and TDI changes that show improved LV diastolic compliance over the first year of life [31–33].

In the fetus pulmonary vein Doppler waveforms are influenced by (1) volume of pulmonary blood flow; (2) foramen ovale size and flow; (3) LA compliance (LA EDP); (4) LV compliance and function (LVEDP); and (5) mitral valve size and function [34]. Increase in pulmonary blood flow may result in elevated S and D velocities (such as arteriovenous malformations, HLHS), whereas a decrease in pulmonary circulation may result in decreased velocities (such as pulmonary atresia, hypoplastic lungs). In addition, elevated LA pressure or left-sided obstructive lesions can lead to pulmonary vein dilation and increased flow reversal during atrial systole (A wave reversal) [35, 36]. This has been well documented in cases of HLHS with restrictive or intact atrial septum (Fig. 29.10a) [37]. Downstream filling abnormalities of the left ventricle (elevated LVEDP or decreased function) seen in cardiomyopathies and diseases of the mitral valve, such as mitral stenosis or regurgitation, can also influence flow dynamics in the pulmonary venous circulation leading to diminished S and D velocities or increased A wave reversal (Fig. 29.10b). Some of these Doppler findings are helpful in the assessment of fetal CHD and will be highlighted in a later section.

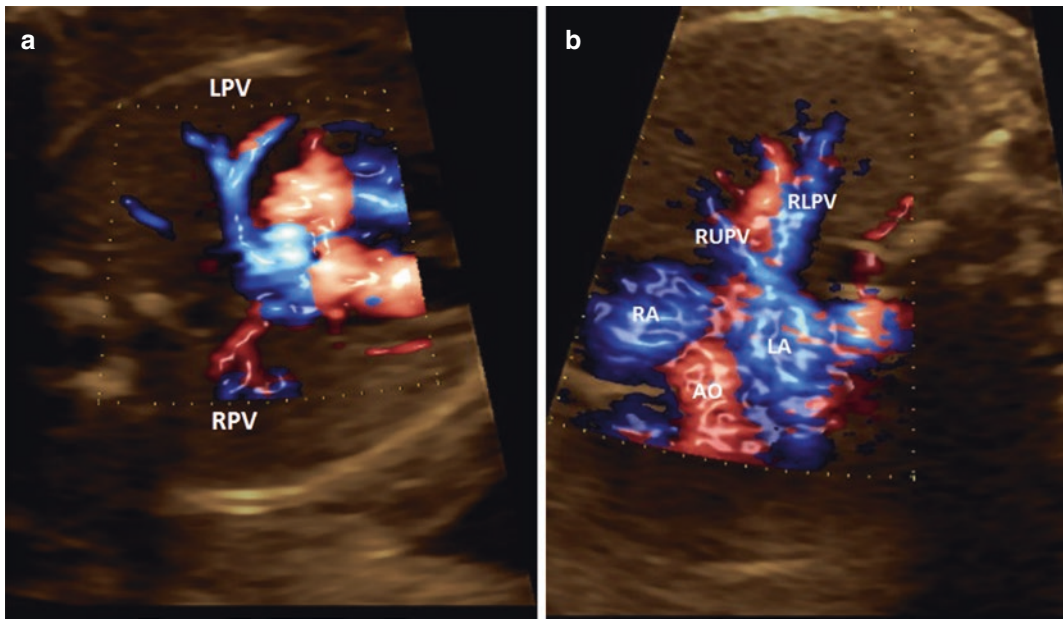

Fig. 29.9 (**a**, **b**) Demonstration of enhanced flow (e-flow) color Doppler technique in normal pulmonary venous return using a Hitachi machine with a C6–1 MHz curvilinear probe. The right lower (RLPV), right upper (RUPV), and left lower pulmonary vein (LLPV) are visualized from the lung parenchyma entering the left atrium (LA)

29.2.4 Power Doppler and Microflow Imaging Modalities

Power Doppler imaging is a very useful tool for detecting pulmonary vein flow and can also help determine the precise location for pulsed Doppler interrogation. Visualization of the pulmonary venous flow can be improved with e-flow imaging or Power Doppler imaging modalities because it provides high spatial and temporal resolution [7]. By using a composite pulse emission technique with shorter pulse length it is able to better visualize low blood flow velocity, such as seen in the pulmonary veins [7]. It is also very good at distinguishing the blood flow from surrounding tissue and displaying blood flow continuity even at the level of the capillary bed [38]. By displaying all flow velocities simultaneously overlaid on the 2D image it can dramatically increase the visualization of blood vessel flow, particularly for low velocity flows (Fig. 29.11). These techniques are ideal for highlighting low velocity flows in very small vessels in as early as 12 weeks EGA which may allow for even earlier diagnosis of pulmonary venous anomalies [7].

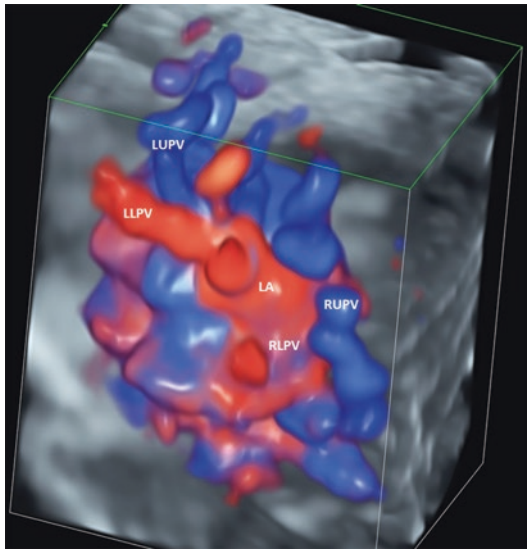

Fig. 29.10 3D volume showing normal pulmonary venous return using a GE Voluson E10 with 3D probe

29.2.5 3D and 4D Fetal Pulmonary Vein Imaging with STIC, TUI, and B-Flow

The advantages of 3D and 4D sonography are the ability to display multiple imaging planes simul-

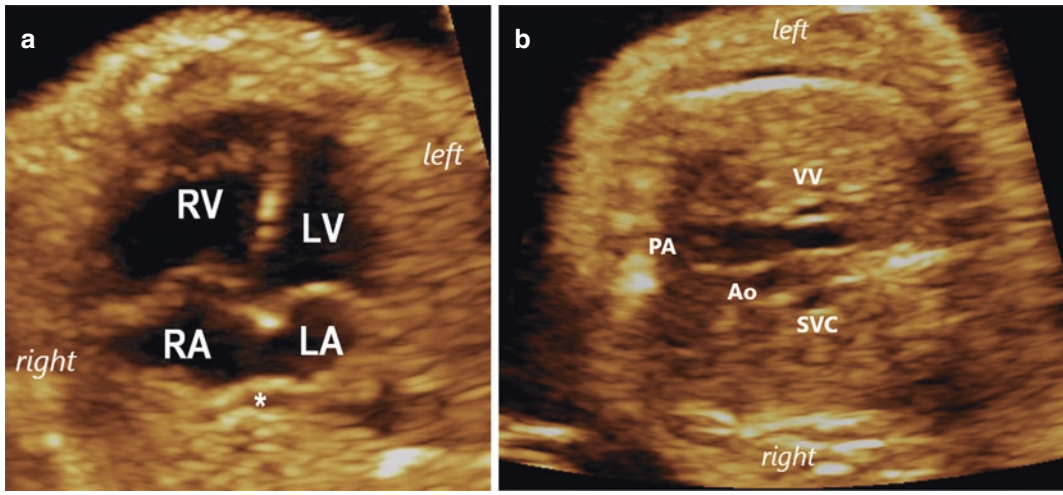

Fig. 29.11 (**a**) Fetal echocardiogram at 28 2/7 weeks gestation demonstrates the "twig sign" with pulmonary veins seen draining into a confluence (*) behind the left atrium (LA) without a direct connection to the LA. There is mild right atrial (RA) and right ventricular (RV) dilation. (**b**) Sweeping cranially, 4 vessels are identified on the "3-vessel view" with the additional vessel representing the left-sided vertical vein (VV) which was noted to drain into the left innominate vein. There was dilation of the innominate vein and the right-sided superior vena cava (SVC). Using a Philips Epiq machine with a C5–1 MHz curvilinear probe

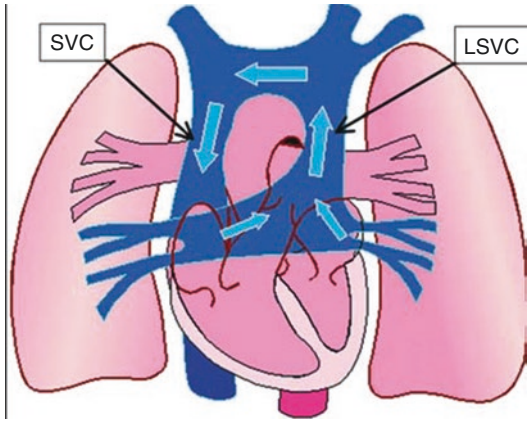

Fig. 29.12 Supracardiac TAPVR. Pulmonary veins from the right and left lungs join to a confluence behind the left atrium then draining via a persistent left vertical vein to the innominate vein to right SVC then back to the right atrium. It is noted that pulmonary venous blood flow drains away from the heart, toward the head superiorly (with permissions, Courtesy of Philippe Jeanty from www.Thefetus.net)

taneously which are typically inaccessible by 2D sonography, the ability to manipulate imaging planes through 180° along the three rotation axes, and the ability to use post-processing of 3D volume sets to preferentially render images to highlight specific anatomy within a volume. Four-dimensional (4D) sonography and spatiotemporal image correlation (STIC) allow acquisition of cardiac volume data sets that are displayed and analyzed in multiple rendering modes to aid in detailed prenatal diagnosis of CHD [39]. The addition of three-dimensional (3D) fetal echo with STIC in combination with color Doppler or high definition power flow Doppler has the ability to image cardiac structures and flows in 3 dimensions which can aid in the diagnosis of pulmonary vein anomalies [40] (Fig. 29.12). Using a STIC rendering mode with color or power Doppler has been shown to enable clearer visualization of all four pulmonary vein connections to the confluence and the drainage pathway to aid in classification of the TAPVR type [41–43]. This is because with STIC one can adjust and rotate the cardiac volume data set for better visualization of the pulmonary vein connections as well as display the entire route of anomalous pulmonary venous return, which is not possible with traditional 2D fetal sonography (Fig. 29.13).

29.3 Congenital Anomalies of the Pulmonary Venous System

29.3.1 Total Anomalous Pulmonary Venous Return (TAPVR)

TAPVR accounts for only 0.5–2% of CHD, but continues to have one of the lowest rates of prenatal diagnosis and highest risks for mortality [3, 44]. In TAPVR, there is a failure of pulmonary venous blood to return normally to the left atrium; instead, it returns to the right atrium either directly or via anomalous venous channels. There are four anatomical subtypes of TAPVR: (1) supracardiac (47%), (2) intracardiac (16%), (3) infradiaphragmatic (13–23%), and (4) mixed type (7–10%) [45] (Fig. 29.14: diagram of different drainage patterns). Drainage is usually via a vertical vein, which is an embryologic venous remnant of the cardinal veins or sinus venosus. TAPVR can occur in isolation or in association with CHD, particularly right atrial isomerism or asplenia syndrome [46].

Obstruction to pulmonary venous return can occur at multiple locations, including at areas of extrinsic compression, at the vertical vein due to its length, at insertion sites of the draining vertical vein to the systemic venous system, such as the portal or hepatic veins, and rarely at the level of the atrial communication. Obstructed TAPVR occurs in approximately 34% of cases [46], and has important clinical consequences, including acute postnatal severe congestion and pulmonary hypertension as well as the chronic pathological effects on lung development in utero [47]. Thus, prenatal diagnosis is critical and given the small size of the pulmonary veins and low flow in the fetus as mentioned previously, color and spectral Doppler are important in achieving an accurate diagnosis [40].

Echocardiographic clues that raise suspicion for TAPVR include the inability to demonstrate a

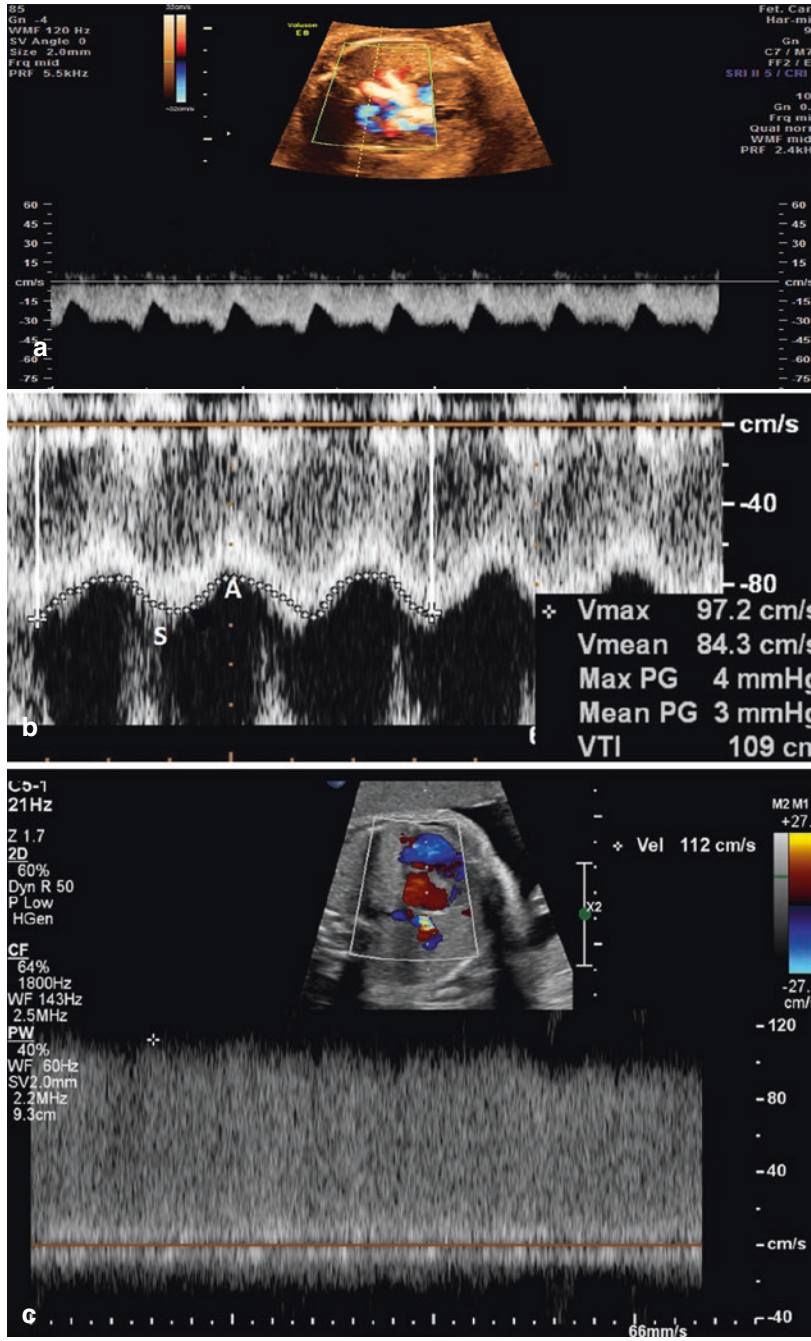

Fig. 29.13 Vertical vein PW Doppler findings in TAPVR. (**a**) Triphasic pulsed wave Doppler pattern with low peak systolic velocity in unobstructed supracardiac TAPVR at 26 weeks EGA using a Philips Epiq C5–1 probe. (**b**) PW Doppler of the vertical vein in a case of infracardiac TAPVR at 34 weeks EGA. It is noted the biphasic PV Doppler pattern with elevated peak systolic velocity and increased pressure gradient in borderline obstructed infracardiac TAPVR. Using a Phillips IE-33 machine with a C5–1 MHz curvilinear probe. (**c**) PW Doppler of the vertical vein in a case of obstructed supracardiac TAPVR at 31 weeks EGA. It is noted the monophasic Doppler pattern with significantly increased peak systolic velocity of 1.1 m/s, minimal atrial systolic velocity, and elevated pressure gradient. Using a Phillips IE-33 machine with a C5–1 MHz curvilinear probe

direct pulmonary venous (PV) connection to the left atrium (LA), smooth posterior LA wall, separation between the posterior wall of the LA and the descending aorta quantified as a "post-LA space index" [11], and the presence of a PV confluence posterior to the LA termed the "twig" sign (Fig. 29.15) [8]. Additionally, right heart disproportion with the right heart being enlarged from increased preload can be seen, though this is an inconsistent finding and may not occur until later in gestation in half of cases presumably due to the increase in pulmonary blood flow in later gestation [8, 48]. Additional echocardiographic findings specific to the type of TAPVR are addressed below and summarized in Table 29.1.

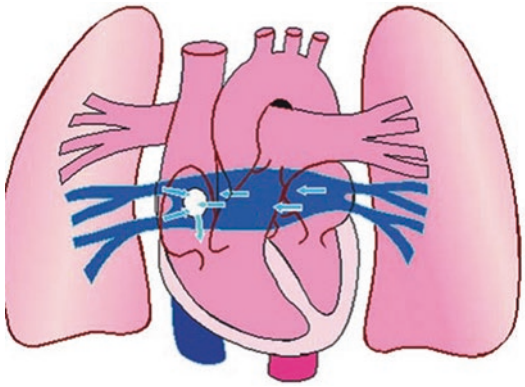

Fig. 29.14 Intracardiac TAPVR. All pulmonary veins come to a confluence behind the heart and then connect back directly to the right atrium (with permissions, Courtesy of Philippe Jeanty from www.Thefetus.net)

29.3.1.1 Supracardiac TAPVR

The supracardiac type is the most common type, in which pulmonary veins usually come to a confluence posterior to the left atrium (LA) and connect via a left-sided vertical vein to the innominate vein which then drains into the superior vena cava (SVC). However, drainage may also occur via a right-sided vertical vein, into the azygous vein, or directly into the SVC. A left-sided vertical vein manifests as a fourth vessel in the three-vessel view (Fig. 29.16). It is important to distinguish this from a persistent left SVC to CS, which can be done with color imaging to demonstrate direction of flow in the vertical vein away from the heart rather than toward the heart in the sagittal plane. Additionally, the innominate vein and RSVC may appear dilated on both axial and sagittal views as a result of increased flow from the pulmonary venous return.

Obstruction may occur in the supracardiac type of TAPVR, particularly if the left vertical vein passes between the left pulmonary artery (LPA) and left bronchus rather than anterior to

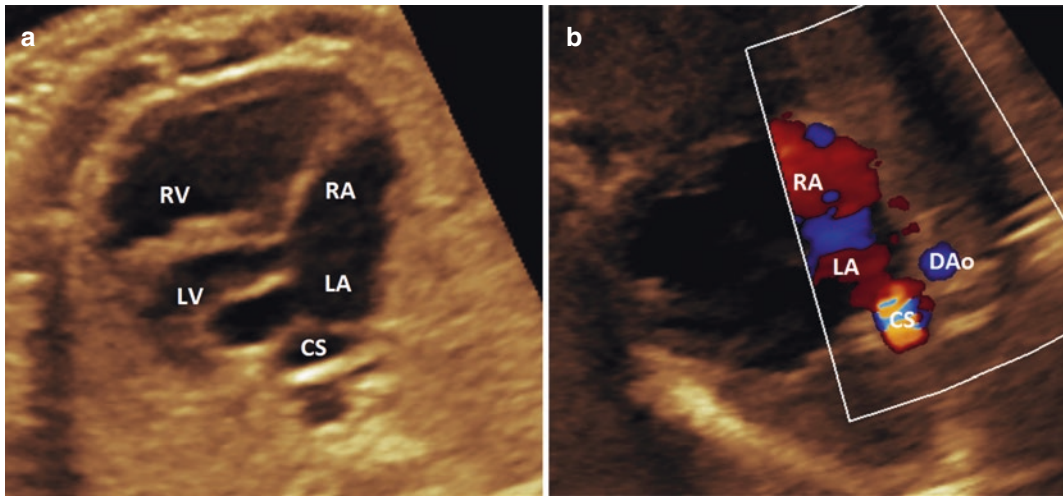

Fig. 29.15 (**a**, **b**) Intracardiac TAPVR with connection to the coronary sinus (CS). Fetal echocardiogram at 35 0/7 weeks gestation shows right heart dilation with a dilated coronary sinus (CS), left. With color Doppler, there is flow acceleration noted into the CS from the pulmonary veins related to increased flow, right. Postnatally, this patient was confirmed to have unobstructed TAPVR to the CS. Philips Epiq C5–1 probe

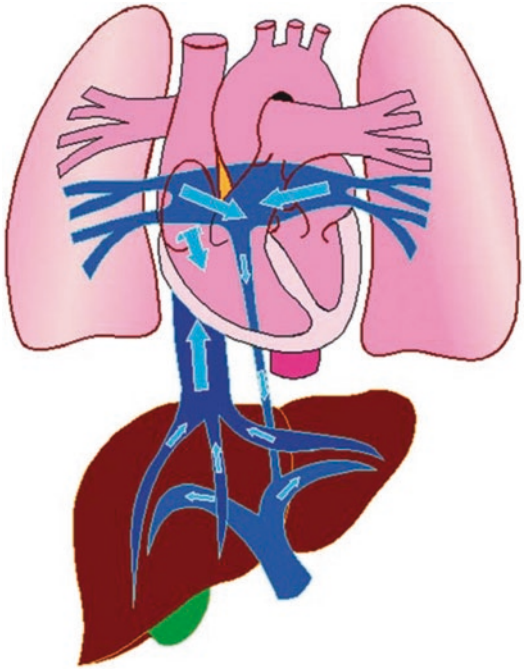

Fig. 29.16 Infracardiac TAPVR. All the pulmonary veins come to a confluence behind the heart then drain via a vertical vein inferiorly, across the diaphragm to connect into the portohepatic system (with permissions, Courtesy of Philippe Jeanty from www.Thefetus.net)

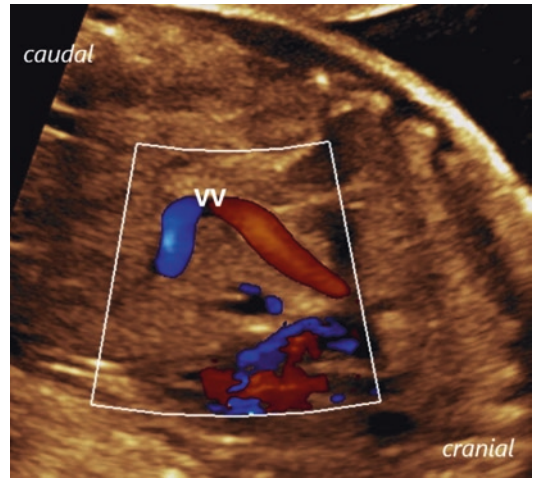

Fig. 29.17 Infracardiac TAPVR with vertical vein (VV) draining below the diaphragm with color Doppler confirming the direction of flow away from the heart. Fetal echo at 31 4/7 weeks gestation obtained on Philips Epiq with C5–1 probe

the LPA. This results in risk for external compression of the vertical vein, termed a "hemodynamic vice." There is also potential for obstruction at the insertion site of the vertical vein into the innominate vein. It is important to evaluate for flow turbulence on color Doppler in the vertical vein at these sites. Instead of the normal triphasic pulmonary venous flow pattern, PW Doppler demonstrates high velocity continuous flow at the area of obstruction and low velocity monophasic continuous flow pattern upstream from the area of obstruction [8, 49]. Vertical vein Doppler peak velocity > 0.74 m/s has been used to predict postnatal pulmonary venous obstruction [1].

29.3.1.2 Intracardiac TAPVR

Intracardiac TAPVR involves drainage of a pulmonary venous confluence into the coronary sinus in the region of the left atrioventricular groove. While intracardiac TAPVR tends not to be obstructed, there is the rare potential for obstruction at the coronary sinus, such as by the Thebesian valve. A dilated coronary sinus may be a diagnostic clue, though a persistent LSVC to CS should be excluded [10]. Rarely, the pulmonary veins may insert directly into the right atrium, usually in the case of right atrial isomerism and this can be visualized on 2D and color imaging (Fig. 29.17).

29.3.1.3 Infracardiac TAPVR

Infracardiac TAPVR involves connection to the umbilicovitelline system via a descending vertical vein that tracks anterior to the esophagus as it courses below the diaphragm. Most commonly, it drains into the portal venous system, but may also drain to the ductus venosus, hepatic vein, or inferior vena cava. Due to multiple reasons, including the long course that the pulmonary venous flow takes, the interposition of hepatic sinusoids, and postnatal closure of the ductus venosus, there is a high incidence of obstruction [46].

An additional venous channel between the aorta and the IVC representing the descending

vertical vein may be visualized on axial and parasagittal views below the diaphragm and this vein should be followed to identify the site of insertion. Color and spectral Doppler shows the direction of flow in this vein to be away from the heart, which distinguishes it from the IVC (Fig. 29.18). PW Doppler should be performed at the site of insertion, as obstruction manifests as high velocity monophasic flow [8].

29.3.1.4 Mixed TAPVR

The rarest among the four, mixed type TAPVR, is defined as involvement of two or more of the above drainage sites. This can be very challenging to diagnose prenatally as there may be no pulmonary vein confluence visualized posterior to the LA and normal-appearing systemic veins as the volume of flow from a few pulmonary venous is not significant enough to cause dilation/enlargement.

Summary of TAPVR findings on fetal ECHO	2D	Color Doppler	Pulsed wave Doppler
General findings	RHD (dilated RA and RV) Left Axis deviation Small-appearing LA Smooth-walled LA Lack of a coumadin ridge Lack of PV connection to the LA	Venous color Doppler flow away from the heart	Increased flow velocity across the pulmonary valve and DA
Supracardiac	Twig sign (CPV confluence behind LA) Increased post-LA space index Fourth vessel (on 3VV) Dilated innominate vein Dilated SVC	Flow away from heart Starfish sign on 3D B-flow [42]	High velocity continuous flow at site of obstruction Low velocity continuous flow upstream
Intracardiac	Dilated CS PV confluence behind the RA	Abnormal color flow in the heart Left to right shunt visualized at atrial septum	
Infracardiac	Additional venous vessel coursing between the IVC and aorta	Flow away from heart	High velocity continuous flow at site of obstruction

29.3.2 Partial Anomalous Pulmonary Venous Return (PAPVR)

PAPVR is defined as the abnormal drainage of one or more, but not all, of the pulmonary veins to the right atrium (RA) and similarly, it can be difficult to detect in utero.

29.3.2.1 PAPVR with Sinus Venosus Atrial Septal Defect

In association with a superior sinus venosus atrial septal defect, the right pulmonary veins, usually the upper and middle veins, enter the SVC, while the right lower pulmonary vein enters the LA (Gustafson). Less commonly, the right middle and lower veins may enter the IVC in association with an inferior sinus venosus atrial septal defect [50].

29.3.2.2 PAPVR in Scimitar Syndrome

In Scimitar syndrome, the right pulmonary veins, all or only middle and lower veins, drain into the IVC above or below the diaphragm. The right pulmonary vein, as it curves downward in the right chest, creates a characteristic chest X-ray appearance of a scimitar sword. Scimitar syndrome is frequently associated with right lung hypoplasia, right pulmonary artery hypoplasia, and aortopulmonary connections from the aorta to the right lung [51]. Unlike pulmonary sequestration, there is connection to the tracheobronchial tree in Scimitar syndrome.

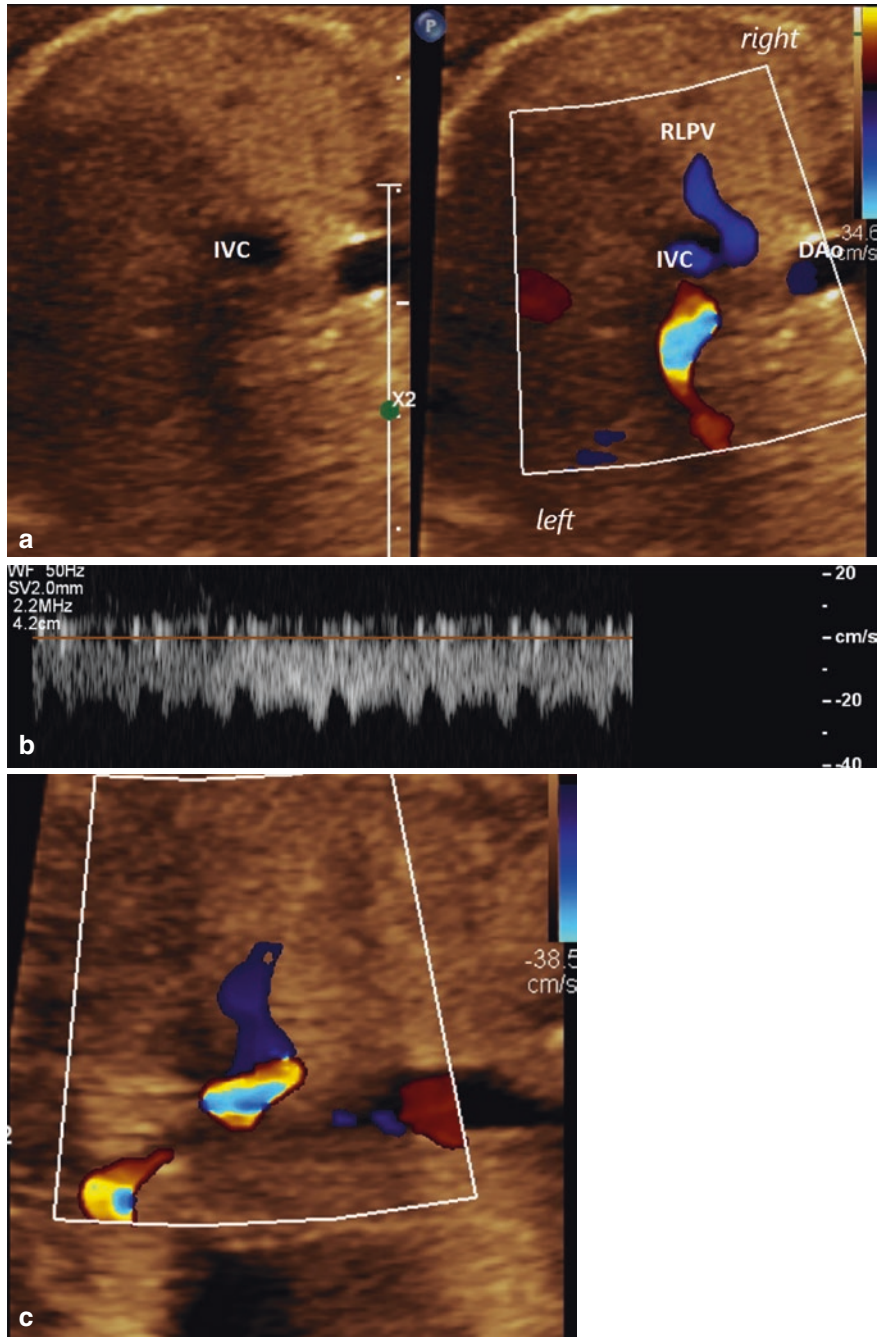

Fig. 29.18 Fetal echocardiogram at 30 4/7 weeks demonstrating PAPVR in Scimitar syndrome using the Philips Epiq C5–1 probe. (**a**) The right lower pulmonary vein (RLPV) draining into the inferior vena cava (IVC) at the junction with the right atrial (RA) on axial view. The remaining right pulmonary veins were seen draining normally into the LA. (**b**) PW Doppler interrogation confirms unobstructed pulmonary venous flow pattern with normal S, D, and A waves. (**c**) On parasagittal view Color imaging, the RLPV is seen draining into the IVC right below the RA junction

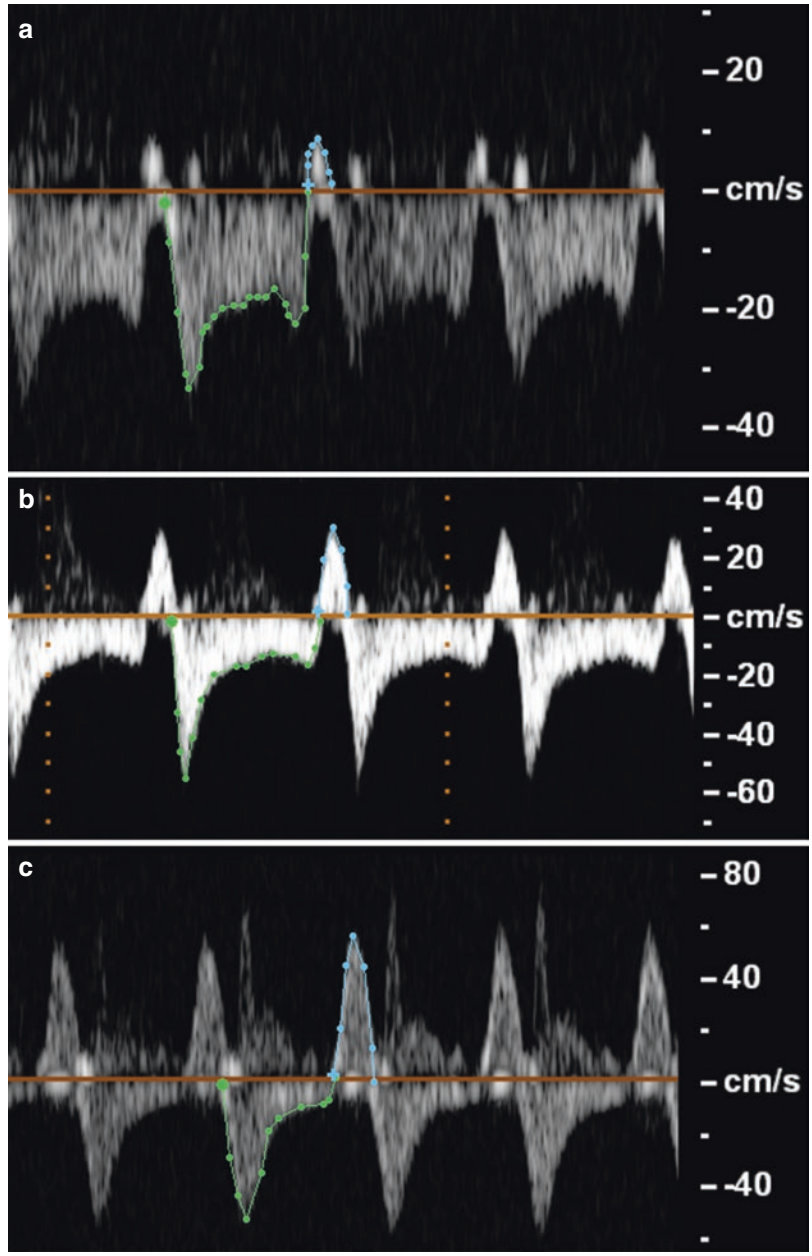

Fig. 29.19 PW Doppler patterns of pulmonary veins in fetuses with hypoplastic left heart syndrome with varying degrees of atrial septal restriction. Pulmonary venous forward flow is outlined in green and atrial systolic reversal is outlined in blue, with VTIs calculated from area under the curve of these tracings. (**a**) Minimal atrial systolic reversal, VTI forward/reverse ratio was 50, suggesting very low risk for postnatal atrial septal restriction (over 5). (**b**) Moderate atrial systolic reversal, VTI forward/reverse ratio was 4.7, which places this fetus at intermediate risk for postnatal atrial septal restriction (range 3–5). (**c**) Severe atrial systolic reversal, VTI forward/reverse ratio was 1.8, which places the fetus at very high risk for needing immediate postnatal intervention to open the atrial septum (under 3)

Echocardiographic clues include dextroposition of the fetal heart in the absence of thoracic pathology which results from right lung hypoplasia [49, 52]. Detection of the anomalous right pulmonary venous drainage requires a careful transverse sweep with color Doppler from the four-chamber view down to the upper abdomen in the area of the IVC–RA junction (Fig. 29.19). Doppler should also be used to identify systemic arterial supply to the right lung, though it is often difficult to detect due to that the fact that the lung is hypoplastic with high vascular resistance limiting the amount of blood flow (Bhide, Michailidis) [52, 53].

29.3.2.3 PAPVR of the Left Pulmonary Veins

Left pulmonary veins, either all or just the left upper pulmonary vein, may drain to the left innominate vein via a vertical vein. This is often associated with other cardiac defects and syndromes, such as Turner syndrome [54]. Similar to cases of supracardiac TAPVR, the 3-vessel view is useful for diagnosis in that it shows the presence of a fourth venous vessel [55]. The sagittal view demonstrates the flow of blood away from the heart.

29.3.3 Other Rare Pulmonary Venous Anomalies

29.3.3.1 Cor Triatriatum Sinister

Cor triatriatum sinister is a rare anomaly in which there is abnormal incorporation of the common pulmonary vein into the LA resulting in formation of two separate chambers with the posterior chamber receiving the pulmonary veins and the anterior chamber communicating with the mitral valve. While the pulmonary veins connect in the correct position, there is potential for the physiology of obstructed pulmonary venous flow. It is thought that the embryologic origin of cor triatriatum is similar to that of TAPVR [56]. Cor triatriatum sinister has also been reported in association with other left-sided cardiac lesions, including HLHS [57–59]. While the diagnosis is made by visualization of a membrane in the LA, interrogation of pulmonary venous flow pattern on the fetal echo is important for the diagnosis, particularly when the waveform suggests significant obstruction out of proportion to the appearance of the degree of atrial septal restriction [59].

29.4 Utility of Pulmonary Venous Doppler in Setting of Cardiac Disease

Assessment of pulmonary venous flow patterns can assist with diagnosis and risk stratification of fetal heart disease. HLHS is a disease involving severe stenosis or atresia of the mitral valve which impedes the natural LA egress. This anatomy results in reversal of foramen ovale flow as obligate shunt for LA exit. The foramen ovale may become decreased in size or closed in this state, known as restrictive atrial septum (RAS) or intact atrial septum (IAS). HLHS with RAS or IAS is associated with prenatal development of pulmonary venous vasculopathy, including "arterialization" of the pulmonary veins and marked dilation of lymphatics on histopathology, and results in postnatal hemodynamic instability and high rate of mortality [60, 61]. Due to LA hypertension and inability to empty with LA contraction, pulmonary venous Doppler is affected by this condition, which can be demonstrated as reversal of atrial systolic flow and elevation of systolic velocity, with loss of the diastolic waveform and elevation of the S/D ratio [37]. Degree of restriction can be graded by the prominence of the atrial systolic reversal, and specifically, measurement of forward-to-reverse VTI has been found to be a sensitive predictor of critically restrictive foramen ovale, which can be utilized to risk stratify the degree of atrial septal restriction prenatally [14, 62] (Fig. 29.20). VTI forward-to-reverse ratio of greater than 5 is classified as low risk, between 3 and 5 as intermediate risk, and less than 3 as the highest risk for needing urgent postnatal intervention [62]. Pulmonary venous assessment is therefore a crucial aspect of the fetal assessment of HLHS, including qualitative 2D findings of pulmonary venous dilation and color Doppler assessment of bidirectional flow, as well as the quantitative pulsed Doppler assessment with calculation of forward-to-reverse VTI ratio. Identification of RAS or IAS in HLHS subjects prenatally is critically important for parental counseling of prognosis, to allow delivery planning to facilitate immediate postnatal intervention, as well as identification of patients who may qualify for fetal cardiac intervention to create an atrial communication by balloon septostomy or interatrial stenting of the fetal atrial septum [63, 64].

D-transposition of the great arteries (TGA) is another type of CHD which may result in extreme hemodynamic instability postnatally. Neonates with d-TGA rely on intracardiac mixing at the level of the atrial septum to allow oxygenated blood to reach the systemic circulation; however,

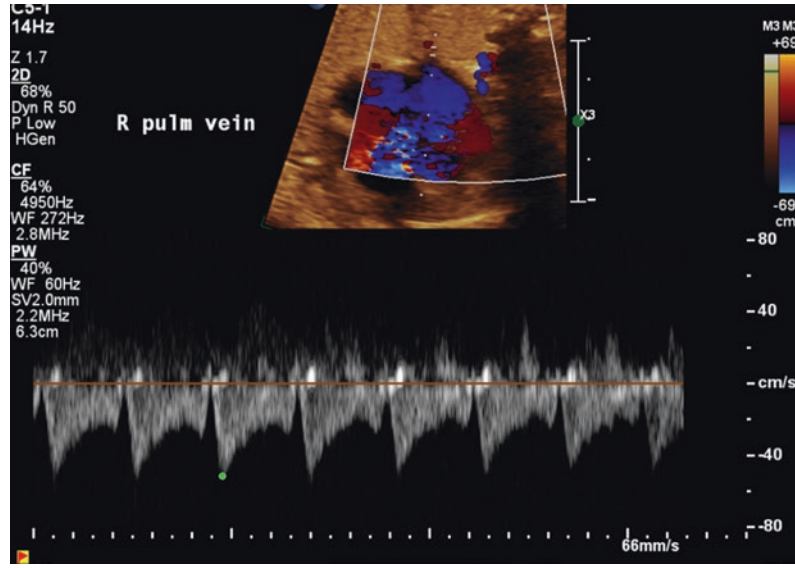

Fig. 29.20 PW Doppler of pulmonary venous flow in fetus with d-transposition of the great arteries. In this case the peak of the "S" wave (green dot) was greater than 0.41 cm/sec which predicts postnatal restriction of the atrial septum [16]

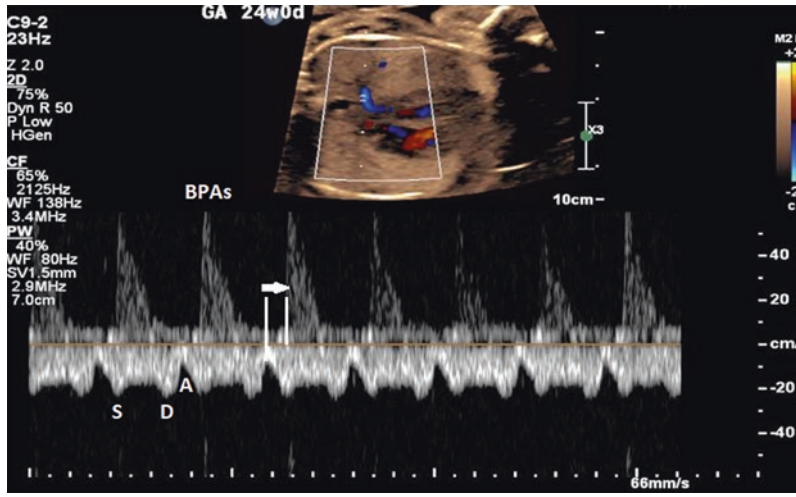

Fig. 29.21 Simultaneous PW Doppler of pulmonary artery and pulmonary vein to assess fetal heart rhythm. The atrial systolic contraction (A) is indicated by an indentation in the pulmonary venous Doppler (below the baseline) and the onset of ventricular systole is the upstroke in the branch pulmonary artery (BPA) Doppler. The distance between these two points is the mechanical PR interval (arrow) which measures 100 ms

determination of which fetuses with d-TGA will have postnatally RAS can be challenging. In addition to assessment of atrial septal movement and excursion, and flow reversal in the ductus arteriosus [65, 66], pulmonary venous Doppler assessment has recently been introduced as a parameter to assist risk stratification of d-TGA fetuses [15]. Slodki and colleagues found that increased pulmonary venous flow as assessed by the maximum velocity on pulmonary venous pulsed Doppler was significantly higher in d-TGA fetuses who postnatally required emergency balloon atrial septostomy, and that a cut-off value of 0.41 m/s provided 100% specificity and 100% positive predictive value with 82% sensitivity and 86% negative predictive value [15] (Fig. 29.21).

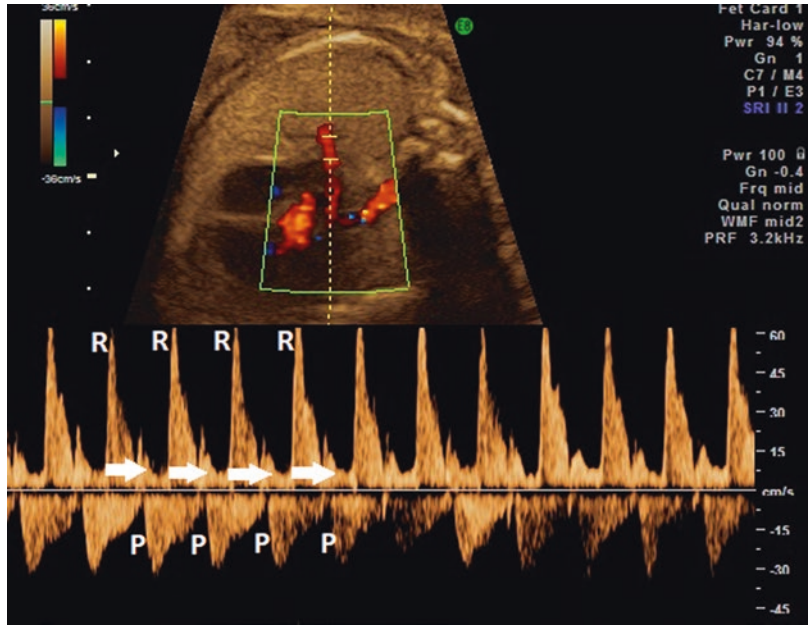

Fig. 29.22 Simultaneous PW Doppler of a pulmonary artery and pulmonary vein in a fetal tachycardia, in which identification of a long RP interval [time from onset of systolic contraction as measured by the pulmonary artery upstroke (R), to the next atrial contraction (P) noted by the onset of atrial systolic reversal], guides the choice of transplacental therapy

29.5 Role for PV Doppler in Diagnosis of Fetal Arrhythmia

Evaluation of the fetal heart rhythm by ultrasound requires using mechanical sequela to evaluate the electrical activity leading to atrial and ventricular contractions, generally performed by obtaining an M-mode through the atria and ventricle, or pulsed Doppler at the junction of the mitral inflow and aortic outflow of the left ventricle. Given the close relationship of the pulmonary vein and pulmonary artery as they cross the lung parenchyma, PW Doppler assessment in the peripheral pulmonary vein simultaneous with the pulmonary artery allows for evaluation of relationships between atrial and ventricular contraction. This technique was first described by Devore and Horenstein in 1993 [2]. The onset of the pulmonary arterial Doppler systolic waveforms signifies onset of ventricular systole, and the indentation of the atrial systolic waveform in the pulmonary venous tracing indicates the onset of atrial systole (Fig. 29.22). The technique can be done relatively independent of fetal position, and also offers an advantage of rhythm assessment in cases of complex CHD where there may not be availability of LV inflow/outflow Doppler assessment. Carvalho and colleagues described using this technique for diagnosis of a variety of fetal arrhythmias where they found it to be accurate and superior to M-mode, including diagnosis of supraventricular tachycardias, including atrial flutter with both 1 to 1 and 2 to 1 atrial to ventricular conduction, ventricular tachycardia, atrial and ventricular premature contractions, sinus bradycardia, and heart block [16]. The simultaneous pulmonary artery and pulmonary vein pulsed Doppler technique can provide superior ability to define atrial to ventricular and ventricular to atrial conduction intervals, which can be more precisely measured than via M-mode, and assist with determination on mechanism of tachycardia which can guide treatment and management [67]. Demonstrates a fetal tachyarrhythmia diagnosed with a long RP mechanism of tachycardia using the simultaneous pulmonary artery and pulmonary vein pulsed Doppler technique, which guided choices for transplacental antiarrhythmic therapy.

29.6 Role for Prenatal Diagnosis Improving Perinatal Management

Due to the nature of fetal circulation and the relatively small amount of pulmonary blood flow, TAPVR and other congenital heart lesions are generally well tolerated in utero. However, transition to neonatal circulation may be poorly tolerated, particularly in cases of obstructed TAPVR, D-TGA with RAS, and HLHS with restrictive or intact atrial septum. Accurate pulmonary venous interrogation by fetal echocardiography is crucial to identifying and risk stratifying these cases for highly coordinated delivery and postnatal intervention [68].

In cases of obstructed TAPVR there is complete mixing of pulmonary and systemic blood in the right heart as well as a lack of egress for pulmonary venous return resulting in severe pulmonary congestion and pulmonary hypertension after birth. When we identify abnormal findings consistent with obstruction on fetal echocardiography or when the type of TAPVR is associated with high risk of obstruction (infradiaphragmatic), a highly coordinated delivery plan should be in place to facilitate immediate stabilization. Specifically, scheduled C-section should be considered with the presence of neonatology team ready for placement of venous access and intubation. The neonate may develop pulmonary edema and respiratory distress requiring intubation for respiratory support. The team should expect preductal oxygen saturations in the range of 75%–85% and to adjust supplemental oxygen accordingly. The team should also expect the possibility for pulmonary hypertension and inhaled nitric oxide should be readily available. Prostaglandin E (PGE) has been thought to be unhelpful in TAPVR in the past, however, recent literature suggests potential benefit in select cases for two reasons: (1) to maintain patency of the ductus venosus in the case of infradiaphragmatic TAPVR as this is often the site of obstruction and (2) to maintain patency of the ductus arteriosus in the setting of pulmonary hypertension to maintain systemic blood flow [69, 70]. Arrangements should be made in advance for rapid transfer for emergent surgical TAPVR repair with surgical team and cardiac operating room on standby.

In HLHS with RAS or IAS, pulmonary venous interrogation is crucial in identifying patients that (1) would be a candidate for a fetal intervention, such as atrial stent placement, and (2) would need emergent intervention at birth with either balloon atrial septostomy (BAS), atrial stent placement or surgical atrial septectomy. Typically, fetuses with HLHS with unrestrictive atrial septum tolerate transition to neonatal circulation without significant hemodynamic compromise; however, this is not the case when atrial septal restriction is detected. Then the latter is identified, a highly coordinated delivery is recommended, with scheduled C-section and neonatology presence at delivery for intubation for respiratory distress and/or hypoxemia and placement of venous access for initiation of PGE. Both cardiac interventional and surgical teams should be on standby with immediate transfer of the patient to either the cardiac catheterization lab or operating room to open the atrial septum.

Finally, D-TGA with RAS is another cardiac lesion that may manifest with hemodynamic instability at birth. When fetal echo findings suggest a RAS, a scheduled C-section with neonatology presence at delivery is important. If there is inadequate mixing of the parallel circulations in D-TGA, the neonate may be cyanotic with saturations below the target range of 75%–85%, requiring intubation. In rare circumstances, there can be associated pulmonary hypertension necessitating inhaled nitric oxide therapy. Venous access should be obtained for initiation of PGE to maintain ductal patency to increase pulmonary blood flow and thus left to right atrial shunting. While these interventions may improve the neonate's oxygenation temporarily, the patient should be transferred immediately to a center with interventional cardiology to perform a BAS either in the catheterization lab under fluoroscopy or at the bedside with echocardiographic guidance. This definitively augments intracardiac mixing and improvement in hemodynamic stability prior to surgical arterial switch operation.

29.7 Summary

The evaluation of pulmonary venous circulation continues to be critically important to the assessment of CHD and fetal physiology. Through the use of newer US technologies, such as power Doppler, eflow, and 3D/4D STIC-TUI, the visualization of pulmonary venous anatomy and pathology has become much more feasible. Application of pulmonary vein Doppler in conjunction with standard fetal echocardiography can provide greater insight into fetal physiology and help anticipate hemodynamic changes at birth. Particularly in cases of critical CHD, such as TAPVR, HLHS with IAS, and DTGA with RAS in which pulmonary venous interrogation is crucial to identifying and risk stratifying those at the greatest risk for postnatal hemodynamic compromise. The resulting delivery coordination and perinatal management can be optimized such that emergent postnatal intervention can be successfully accomplished.

References

1. Domadia S, Kumar SR, Votava-Smith JK, Pruetz JD. Neonatal outcomes in total anomalous pulmonary venous return: the role of prenatal diagnosis and pulmonary venous obstruction. Pediatr Cardiol. 2018;39(7):1346–54. https://doi.org/10.1007/s00246-018-1901-0.
2. DeVore GR, Horenstein J. Simultaneous Doppler recording of the pulmonary artery and vein: a new technique for the evaluation of a fetal arrhythmia. J Ultrasound Med. 1993;12(11):669–71. https://doi.org/10.7863/jum.1993.12.11.669.
3. Seale AN, Carvalho JS, Gardiner HM, Mellander M, Roughton M, Simpson J, Tometzki A, Uzun O, Webber SA, Daubeney PE. Total anomalous pulmonary venous connection: impact of prenatal diagnosis. Ultrasound Obstet Gynecol. 2012;40(3):310–8. https://doi.org/10.1002/uog.11093.
4. International Society of Ultrasound in O, Gynecology CJS, Allan LD, Chaoui R, Copel JA, DeVore GR, Hecher K, Lee W, Munoz H, Paladini D, Tutschek B, Yagel S. ISUOG practice guidelines (updated): sonographic screening examination of the fetal heart. Ultrasound Obstet Gynecol. 2013;41(3):348–59. https://doi.org/10.1002/uog.12403.
5. AIUM practice guideline for the performance of fetal echocardiography. J Ultrasound Med. 2013;32(6):1067–82. https://doi.org/10.7863/ultra.32.6.1067.
6. Donofrio MT, Moon-Grady AJ, Hornberger LK, Copel JA, Sklansky MS, Abuhamad A, Cuneo BF, Huhta JC, Jonas RA, Krishnan A, Lacey S, Lee W, Michelfelder EC Sr, Rempel GR, Silverman NH, Spray TL, Strasburger JF, Tworetzky W, Rychik J. Diagnosis and treatment of fetal cardiac disease: a scientific statement from the American Heart Association. Circulation. 2014;129(21):2183–242. https://doi.org/10.1161/01.cir.0000437597.44550.5d.
7. Dong FQ, Zhang YH, Li ZA, Hou ZZ, He XJ, Guo YZ. Evaluation of normal fetal pulmonary veins from the early second trimester by enhanced-flow (e-flow) echocardiography. Ultrasound Obstet Gynecol. 2011;38(6):652–7. https://doi.org/10.1002/uog.8965.
8. Ganesan S, Brook MM, Silverman NH, Moon-Grady AJ. Prenatal findings in total anomalous pulmonary venous return: a diagnostic road map starts with obstetric screening views. J Ultrasound Med. 2014;33(7):1193–207. https://doi.org/10.7863/ultra.33.7.1193.
9. Olsen R, Doyle Z, Levy D, Anton T, Molkara D, Tarsa M, Sklansky M, Pretorius DH. Anomalous pulmonary venous return: insights into prenatal detection. J Ultrasound Med. 2016;35(6):1193–206. https://doi.org/10.7863/ultra.15.04041.
10. Tongsong T, Luewan S, Jatavan P, Tongprasert F, Sukpan K. A simple rule for prenatal diagnosis of total anomalous pulmonary venous return. J Ultrasound Med. 2016;35(7):1601–7. https://doi.org/10.7863/ultra.15.08016.
11. Kawazu Y, Inamura N, Shiono N, Kanagawa N, Narita J, Hamamichi Y, Kayatani F. 'Post-LA space index' as a potential novel marker for the prenatal diagnosis of isolated total anomalous pulmonary venous connection. Ultrasound Obstet Gynecol. 2014;44(6):682–7. https://doi.org/10.1002/uog.13357.
12. Khan MS, Bryant R 3rd, Kim SH, Hill KD, Jacobs JP, Jacobs ML, Pasquali SK, Morales DL. Contemporary outcomes of surgical repair of total anomalous pulmonary venous connection in patients with heterotaxy syndrome. Ann Thorac Surg. 2015;99(6):2134–9; discussion 2139-2140. https://doi.org/10.1016/j.athoracsur.2015.02.035.
13. Shi G, Zhu Z, Chen J, Ou Y, Hong H, Nie Z, Zhang H, Liu X, Zheng J, Sun Q, Liu J, Chen H, Zhuang J. Total anomalous pulmonary venous connection: the current management strategies in a pediatric cohort of 768 patients. Circulation. 2017;135(1):48–58. https://doi.org/10.1161/CIRCULATIONAHA.116.023889.
14. Michelfelder E, Gomez C, Border W, Gottliebson W, Franklin C. Predictive value of fetal pulmonary venous flow patterns in identifying the need for atrial septoplasty in the newborn with hypoplastic left ventricle. Circulation. 2005;112(19):2974–9. https://doi.org/10.1161/CIRCULATIONAHA.105.534180.
15. Slodki M, Axt-Fliedner R, Zych-Krekora K, Wolter A, Kawecki A, Enzensberger C, Gulczynska E,

Respondek-Liberska M. New method to predict need for Rashkind procedure in fetuses with dextro-transposition of the great arteries. Ultrasound Obstet Gynecol. 2018;51(4):531–6. https://doi.org/10.1002/uog.17469.
16. Carvalho JS, Prefumo F, Ciardelli V, Sairam S, Bhide A, Shinebourne EA. Evaluation of fetal arrhythmias from simultaneous pulsed wave Doppler in pulmonary artery and vein. Heart. 2007;93(11):1448–53. https://doi.org/10.1136/hrt.2006.101659.
17. Fasouliotis SJ, Achiron R, Kivilevitch Z, Yagel S. The human fetal venous system: normal embryologic, anatomic, and physiologic characteristics and developmental abnormalities. J Ultrasound Med. 2002;21(10):1145–58. https://doi.org/10.7863/jum.2002.21.10.1145.
18. Hofstaetter C, Plath H, Hansmann M. Prenatal diagnosis of abnormalities of the fetal venous system. Ultrasound Obstet Gynecol. 2000;15(3):231–41. https://doi.org/10.1046/j.1469-0705.2000.00066.x.
19. DeRuiter MC, Gittenberger-De Groot AC, Wenink AC, Poelmann RE, Mentink MM. In normal development pulmonary veins are connected to the sinus venosus segment in the left atrium. Anat Rec. 1995;243(1):84–92. https://doi.org/10.1002/ar.1092430110.
20. Achiron R, Hegesh J, Yagel S, Lipitz S, Cohen SB, Rotstein Z. Abnormalities of the fetal central veins and umbilico-portal system: prenatal ultrasonographic diagnosis and proposed classification. Ultrasound Obstet Gynecol. 2000;16(6):539–48. https://doi.org/10.1046/j.1469-0705.2000.00220.x.
21. Rudolph AM, Heymann MA. Circulatory changes during growth in the fetal lamb. Circ Res. 1970;26(3):289–99. https://doi.org/10.1161/01.res.26.3.289.
22. Rasanen J, Wood DC, Weiner S, Ludomirski A, Huhta JC. Role of the pulmonary circulation in the distribution of human fetal cardiac output during the second half of pregnancy. Circulation. 1996;94(5):1068–73. https://doi.org/10.1161/01.cir.94.5.1068.
23. Keren G, Sherez J, Megidish R, Levitt B, Laniado S. Pulmonary venous flow pattern—its relationship to cardiac dynamics. A pulsed Doppler echocardiographic study. Circulation. 1985;71(6):1105–12. https://doi.org/10.1161/01.cir.71.6.1105.
24. Akamatsu S, Terazawa E, Kagawa K, Arakawa M, Dohi S. Transesophageal Doppler echocardiographic assessment of pulmonary venous flow pattern in subjects without cardiovascular disease. Int J Card Imaging. 1993;9(3):195–200. https://doi.org/10.1007/bf01145321.
25. Laudy JA, Huisman TW, de Ridder MA, Wladimiroff JW. Normal fetal pulmonary venous blood flow velocity. Ultrasound Obstet Gynecol. 1995;6(4):277–81. https://doi.org/10.1046/j.1469-0705.1995.06040277.x.
26. Lenz F, Chaoui R. Reference ranges for Doppler-assessed pulmonary venous blood flow velocities and pulsatility indices in normal human fetuses. Prenat Diagn. 2002;22(9):786–91. https://doi.org/10.1002/pd.410.
27. Better DJ, Kaufman S, Allan LD. The normal pattern of pulmonary venous flow on pulsed Doppler examination of the human fetus. J Am Soc Echocardiogr. 1996;9(3):281–5. https://doi.org/10.1016/s0894-7317(96)90141-8.
28. Paladini D, Palmieri S, Celentano E, Guida F, Salviati M, Morra T, Martinelli P. Pulmonary venous blood flow in the human fetus. Ultrasound Obstet Gynecol. 1997;10(1):27–31. https://doi.org/10.1046/j.1469-0705.1997.10010027.x.
29. McKay T, Thomas L. 'Coumadin ridge' in the left atrium demonstrated on three dimensional transthoracic echocardiography. Eur J Echocardiogr. 2008;9(2):298–300. https://doi.org/10.1016/j.euje.2006.10.002.
30. Chaoui R, Lenz F, Heling K-S. Doppler examination of the fetal pulmonary venous circulation. Doppler Ultrasound in Obstetrics and Gynecology. Berlin, Heidelberg: Springer; 2005.
31. O'Leary PW, Durongpisitkul K, Cordes TM, Bailey KR, Hagler DJ, Tajik J, Seward JB. Diastolic ventricular function in children: a Doppler echocardiographic study establishing normal values and predictors of increased ventricular end-diastolic pressure. Mayo Clin Proc. 1998;73(7):616–28. https://doi.org/10.4065/73.7.616.
32. Harada K, Suzuki T, Tamura M, Ito T, Shimada K, Takada G. Effect of aging from infancy to childhood on flow velocity patterns of pulmonary vein by Doppler echocardiography. Am J Cardiol. 1996;77(2):221–4. https://doi.org/10.1016/s0002-9149(96)90607-4.
33. Eidem BW, McMahon CJ, Cohen RR, Wu J, Finkelshteyn I, Kovalchin JP, Ayres NA, Bezold LI, O'Brian Smith E, Pignatelli RH. Impact of cardiac growth on Doppler tissue imaging velocities: a study in healthy children. J Am Soc Echocardiogr. 2004;17(3):212–21. https://doi.org/10.1016/j.echo.2003.12.005.
34. Kiserud T. Fetal venous circulation--an update on hemodynamics. J Perinat Med. 2000;28(2):90–6. https://doi.org/10.1515/JPM.2000.011.
35. Appleton CP. Hemodynamic determinants of Doppler pulmonary venous flow velocity components: new insights from studies in lightly sedated normal dogs. J Am Coll Cardiol. 1997;30(6):1562–74. https://doi.org/10.1016/s0735-1097(97)00354-9.
36. Kirkpatrick EC, Steltzer J, Simpson P, Pan A, Dragulescu A, Falkensammer CB, Gelehrter S, Lai WW, Levine J, Miller S, Miller TA, Pruetz J, Sachdeva R, Thacker D, Frommelt P. Pulmonary vein Doppler patterns in infants with single right ventricle anomalies after initial staged palliations. Pediatr Cardiol. 2017;38(6):1288–95. https://doi.org/10.1007/s00246-017-1660-3.
37. Better DJ, Apfel HD, Zidere V, Allan LD. Pattern of pulmonary venous blood flow in the hypoplastic left

heart syndrome in the fetus. Heart. 1999;81(6):646–9. https://doi.org/10.1136/hrt.81.6.646.
38. Zhu WYX, Wang XY. Evaluation of hemodynamic changes of finger tip capillary vessels in patients with primary hypertension using E-flow imaging technology. Chin J Ultrasonograph Image. 2008;17:504–7.
39. Yagel S, Cohen SM, Rosenak D, Messing B, Lipschuetz M, Shen O, Valsky DV. Added value of three−/four-dimensional ultrasound in offline analysis and diagnosis of congenital heart disease. Ultrasound Obstet Gynecol. 2011;37(4):432–7. https://doi.org/10.1002/uog.8867.
40. Zhang Y, Shao Q, Sun L, Ge S, He Y. Prenatal diagnosis of total anomalous pulmonary venous connection by 2D and 3D fetal echocardiography. Echocardiography. 2017;34(12):1852–7. https://doi.org/10.1111/echo.13698.
41. Volpe P, Campobasso G, De Robertis V, Di Paolo S, Caruso G, Stanziano A, Volpe N, Gentile M. Two- and four-dimensional echocardiography with B-flow imaging and spatiotemporal image correlation in prenatal diagnosis of isolated total anomalous pulmonary venous connection. Ultrasound Obstet Gynecol. 2007;30(6):830–7. https://doi.org/10.1002/uog.5145.
42. Lee W, Espinoza J, Cutler N, Bronsteen RA, Yeo L, Romero R. The 'starfish' sign: a novel sonographic finding with B-flow imaging and spatiotemporal image correlation in a fetus with total anomalous pulmonary venous return. Ultrasound Obstet Gynecol. 2010;35(1):124–5. https://doi.org/10.1002/uog.7503.
43. Peng R, Xie HN, Du L, Shi HJ, Zheng J, Zhu YX. Four-dimensional sonography with spatiotemporal image correlation and tomographic ultrasound imaging in the prenatal diagnosis of anomalous pulmonary venous connections. J Ultrasound Med. 2012;31(10):1651–8. https://doi.org/10.7863/jum.2012.31.10.1651.
44. Quartermain MD, Pasquali SK, Hill KD, Goldberg DJ, Huhta JC, Jacobs JP, Jacobs ML, Kim S, Ungerleider RM. Variation in prenatal diagnosis of congenital heart disease in infants. Pediatrics. 2015;136(2):e378–85. https://doi.org/10.1542/peds.2014-3783.
45. Burroughs JT, Edwards JE. Total anomalous pulmonary venous connection. Am Heart J. 1960;59:913–31. https://doi.org/10.1016/0002-8703(60)90414-2.
46. Paladini D, Pistorio A, Wu LH, Meccariello G, Lei T, Tuo G, Donarini G, Marasini M, Xie HN. Prenatal diagnosis of total and partial anomalous pulmonary venous connection: multicenter cohort study and meta-analysis. Ultrasound Obstet Gynecol. 2018;52(1):24–34. https://doi.org/10.1002/uog.18907.
47. Haworth SG. Total anomalous pulmonary venous return. Prenatal damage to pulmonary vascular bed and extrapulmonary veins. Br Heart J. 1982;48(6):513–24. https://doi.org/10.1136/hrt.48.6.513.
48. Allan LD, Sharland GK. The echocardiographic diagnosis of totally anomalous pulmonary venous connection in the fetus. Heart. 2001;85(4):433–7. https://doi.org/10.1136/heart.85.4.433.
49. Valsangiacomo ER, Hornberger LK, Barrea C, Smallhorn JF, Yoo SJ. Partial and total anomalous pulmonary venous connection in the fetus: two-dimensional and Doppler echocardiographic findings. Ultrasound Obstet Gynecol. 2003;22(3):257–63. https://doi.org/10.1002/uog.214.
50. Plymale J, Kolinski K, Frommelt P, Bartz P, Tweddell J, Earing MG. Inferior sinus venosus defects: anatomic features and echocardiographic correlates. Pediatr Cardiol. 2013;34(2):322–6. https://doi.org/10.1007/s00246-012-0449-7.
51. Neill CA, Ferencz C, Sabiston DC, Sheldon H. The familial occurrence of hypoplastic right lung with systemic arterial supply and venous drainage "scimitar syndrome". Bull Johns Hopkins Hosp. 1960;107:1–21.
52. Michailidis GD, Simpson JM, Tulloh RM, Economides DL. Retrospective prenatal diagnosis of scimitar syndrome aided by three-dimensional power Doppler imaging. Ultrasound Obstet Gynecol. 2001;17(5):449–52. https://doi.org/10.1046/j.1469-0705.2001.00375.x.
53. Bhide A, Murphy D, Thilaganathan B, Carvalho JS. Prenatal findings and differential diagnosis of scimitar syndrome and pulmonary sequestration. Ultrasound Obstet Gynecol. 2010;35(4):398–404. https://doi.org/10.1002/uog.7555.
54. Gutmark-Little I, Hor KN, Cnota J, Gottliebson WM, Backeljauw PF. Partial anomalous pulmonary venous return is common in turner syndrome. J Pediatr Endocrinol Metab. 2012;25(5–6):435–40. https://doi.org/10.1515/jpem-2012-0046.
55. Sun X, Lei W, Wang Y, Amber Siddiqui F, Zhang Y. Two- and four-dimensional echocardiography with high-definition flow imaging and spatiotemporal image correlation in the diagnosis of fetal isolated partial anomalous pulmonary venous connection. Echocardiography. 2018;35(4):566–70. https://doi.org/10.1111/echo.13849.
56. Gaio G, Santoro G, Iacono C, Palladino MT, Russo MG, Calabro R. Left cor triatriatum: a rare potential cause of total anomalous pulmonary vein connection obstruction. Int J Cardiol. 2008;129(2):e41–2. https://doi.org/10.1016/j.ijcard.2007.06.113.
57. Eidem BW, Cetta F. Unusual finding of cor triatriatum in a newborn with hypoplastic left heart syndrome. J Am Soc Echocardiogr. 2001;14(8):850–2. https://doi.org/10.1067/mje.2001.112025.
58. Yang PK, Chang CI, Lee CC, Lin MW, Shih JC. Cor triatriatum sinister presenting in the fetus: beware of association with total anomalous pulmonary venous connection. Ultrasound Obstet Gynecol. 2015;45(5):622–4. https://doi.org/10.1002/uog.14710.
59. Pruetz J, Detterich J, Trento L, Sklansky M. Prenatal diagnosis of cor triatriatum sinister in association with hypoplastic left heart syndrome. Pediatr Cardiol. 2011;32(6):818–21. https://doi.org/10.1007/s00246-011-9941-8.
60. Rychik J, Rome JJ, Collins MH, DeCampli WM, Spray TL. The hypoplastic left heart syndrome with intact atrial septum: atrial morphology, pulmonary

vascular histopathology and outcome. J Am Coll Cardiol. 1999;34(2):554–60.
61. Atz AM, Feinstein JA, Jonas RA, Perry SB, Wessel DL. Preoperative management of pulmonary venous hypertension in hypoplastic left heart syndrome with restrictive atrial septal defect. Am J Cardiol. 1999;83(8):1224–8.
62. Divanovic A, Hor K, Cnota J, Hirsch R, Kinsel-Ziter M, Michelfelder E. Prediction and perinatal management of severely restrictive atrial septum in fetuses with critical left heart obstruction: clinical experience using pulmonary venous Doppler analysis. J Thorac Cardiovasc Surg. 2011;141(4):988–94. https://doi.org/10.1016/j.jtcvs.2010.09.043.
63. Marshall AC, van der Velde ME, Tworetzky W, Gomez CA, Wilkins-Haug L, Benson CB, Jennings RW, Lock JE. Creation of an atrial septal defect in utero for fetuses with hypoplastic left heart syndrome and intact or highly restrictive atrial septum. Circulation. 2004;110(3):253–8. https://doi.org/10.1161/01.CIR.0000135471.17922.17.
64. Slodki M, Respondek-Liberska M, Pruetz JD, Donofrio MT. Fetal cardiology: changing the definition of critical heart disease in the newborn. J Perinatol. 2016;36(8):575–80. https://doi.org/10.1038/jp.2016.20.
65. Jouannic JM, Gavard L, Fermont L, Le Bidois J, Parat S, Vouhe PR, Dumez Y, Sidi D, Bonnet D. Sensitivity and specificity of prenatal features of physiological shunts to predict neonatal clinical status in transposition of the great arteries. Circulation. 2004;110(13):1743–6. https://doi.org/10.1161/01.CIR.0000144141.18560.CF.
66. Punn R, Silverman NH. Fetal predictors of urgent balloon atrial septostomy in neonates with complete transposition. J Am Soc Echocardiogr. 2011;24(4):425–30. https://doi.org/10.1016/j.echo.2010.12.020.
67. Fouron JC, Fournier A, Proulx F, Lamarche J, Bigras JL, Boutin C, Brassard M, Gamache S. Management of fetal tachyarrhythmia based on superior vena cava/aorta Doppler flow recordings. Heart. 2003;89(10):1211–6. https://doi.org/10.1136/heart.89.10.1211.
68. Pruetz JD, Wang SS, Noori S. Delivery room emergencies in critical congenital heart diseases. Semin Fetal Neonatal Med. 2019;24(6):101034. https://doi.org/10.1016/j.siny.2019.101034.
69. Adeagbo AS, Kelsey L, Coceani F. Endothelin-induced constriction of the ductus venosus in fetal sheep: developmental aspects and possible interaction with vasodilatory prostaglandin. Br J Pharmacol. 2004;142(4):727–36. https://doi.org/10.1038/sj.bjp.0705849.
70. Cirstoveanu C, Cinteza E, Marcu V, Bizubac M, Balomir A, Barascu I, Coman M, Balgradean M. Prostaglandin e1 on infradiaphragmatic type of total anomalous pulmonary venous connection - a case report. Maedica. 2012;7(2):167–72.

Introduction to Fetal Doppler Echocardiography

30

Dev Maulik and Sarah Hostetter

30.1 Introduction

Evaluation of the fetal heart constitutes one of the critical areas of prenatal diagnosis. Advances in diagnostic medical ultrasound continue to be of central importance in this progress. Of the various ultrasound modes, two-dimensional (2D) real-time high-resolution imaging forms the technical foundation for echocardiographic assessment of the anatomic integrity of the fetal heart. The diagnostic capabilities of the procedure are substantially extended by the incorporation of other echocardiographic modalities, such as the M-mode, the color Doppler ultrasound, the reconstructed three-dimensional (3D) echocardiography using spatiotemporal image correlation, live 3D echocardiography using 2D matrix technology, and tissue Doppler mode [1–10]. Table 30.1 summarizes these developments. A brief review of tissue Doppler is included in this chapter, whereas 3D echocardiography is reviewed in Chap. 32.

An essential component of this progress is the development of Doppler echocardiography in clinical practice. Maulik et al. were the first to describe the use of the duplex Doppler method for characterizing normal and abnormal flow patterns in the fetal cardiac chambers and outflow tracts, and demonstrated its potential for morphological and functional assessment [6, 10]. Subsequent work has established the utility of these techniques in clinical practice for both physiologic and diagnostic evaluation [6, 11–

Table 30.1 Pioneering publications on fetal echocardiography

Fetal echo mode	First author	Reference
M-mode	Winsberg	[1]
Two-dimensional echo	Allan et al.	[3]
	Kleinman et al.	[4]
Duplex M-mode	DeVore et al.	[5]
Duplex pulse-wave Doppler	Maulik et al.	[6]
Tissue Doppler	Harada et al.	[21]
Color flow Doppler	Maulik et al.	[10]
Three-dimensional fetal echocardiography–two-dimensional image integration	Sklansky et al.	[8]
Reconstructed three-dimensional fetal echocardiography utilizing spatiotemporal image correlation	DeVore et al.	[9]
Live 3D (real-time three-dimensional fetal echocardiography) utilizing two-dimensional matrix transducer	Maulik et al.	[10]

D. Maulik (✉) · S. Hostetter
Department of Obstetrics and Gynecology, UMKC School of Medicine/Truman Medical Center, UMKC School of Medicine, Kansas City, MO, USA
e-mail: dmaulik2014@gmail.com

D. Maulik, C. C. Lees (eds.), *Doppler Ultrasound in Obstetrics and Gynecology*,
https://doi.org/10.1007/978-3-031-06189-9_30

15]. The color and spectral pulsed-wave Doppler modalities allow assessment of normal and abnormal cardiac flow patterns, and extend the diagnostic information generated by the 2D and M-mode echocardiographic methods. Spectral pulsed Doppler offers range resolution, allows evaluation of flow velocities in specific target locations, and when used as a duplex system, the method allows assessment of circulatory dynamics in specific intracardiac locations and outflow tracts of the fetal heart. The technique of Doppler color flow mapping significantly enhances our ability to investigate cardiac hemodynamics by depicting color-coded 2D flow velocity distribution in cardiac chambers and great vessels.

In this chapter we review the basic principles of Doppler echocardiography as applied to the hemodynamic assessment of the fetal heart.

30.2 General Considerations

The diagnostic utility of fetal echocardiographic imaging depends on the capabilities of the ultrasound device for producing high-resolution images, the experience and skill of the sonographer, and patient characteristics pertaining to the quality and ease of imaging (Fig. 30.1). The imageability is determined by fetal position, fetal movements (breathing, movement, hiccup), gestational age, maternal movement, and maternal body habitus. An advanced ultrasound machine may mitigate against many of these challenges on the quality and diagnostic utility of the echocardiographic information, but the utility of a device depends on the skill of the operator in generating the diagnostic information and the skill of the diagnostician in interpreting that information. For reliable and confident fetal echocardiographic assessment, it is crucial to ensure not only the adequacy of the instrumentation but also the sufficiency of training and skill of the provider.

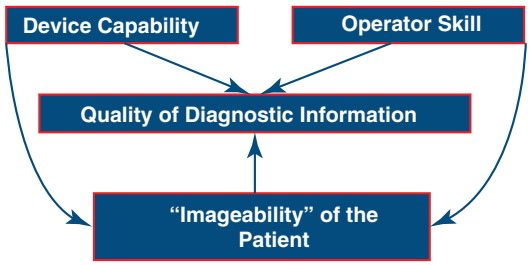

Fig. 30.1 Factors affecting the quality of diagnostic information derived from fetal cardiac imaging

30.3 Choice of Equipment for Doppler Echocardiography

The basic principles of duplex pulsed-wave Doppler and color flow Doppler instrumentation have been described in Chaps. 3 and 6. Here the relevant issues specifically related to fetal echocardiographic application are briefly discussed. The desirable configuration of an ultrasound device for fetal echocardiographic examination consists of a multiplex system. Several ultrasound modalities comprise such a system, including high-quality 2D imaging, M-mode, color and spectral Doppler modes, and other advanced features, such as 3D/4D capabilities. As with any other field of medical ultrasound imaging, an effective and user-friendly archival system is selected so images and reports can be reliably saved and accessed.

Integration of 2D imaging with Doppler sonography offers some unique challenges, and the various approaches to their solution are reflected in the device's features. For example, high-resolution imaging requires a high-frequency transducer; in contrast, Doppler signals are weaker than the pulse echocardiographic specular reflections of imaging and require a low-frequency transducer for optimal sensitivity. The introduction of multifrequency transducers offers an innovative solution, as higher imaging resolution can be achieved at higher frequency, whereas Doppler sensitivity is improved using a lower frequency. Because of the angle dependence of Doppler signals, the optimal imaging plane is often not consistent with the optimal Doppler plane. Beam steering capability of the array

transducers may assist in these circumstances. Careful consideration of these factors helps the operator select the appropriate device for fetal echocardiographic application.

The choice of transducer frequencies appropriate for fetal echocardiographic examination should be individualized to achieve the best possible resolution for a given depth of the scanning target. The higher the frequency of the incident beam, the greater the spatial (axial) resolution and the lower the depth of penetration. Depending on the maternal habitus, gestational age, and fetal position, the fetal heart often lies deep from the maternal abdominal surface. Although a 5-MHz transducer produces a higher-resolution image of the fetal heart, it may not be able to reach such depth. In this circumstance, a 3-MHz transducer may be necessary. As mentioned previously, multifrequency transducers offer a convenient solution. Advances in ultrasound technology, such as extended depth penetration with high resolution, have effectively addressed many of these issues.

Consideration should also be given to the type of transducer array appropriate for fetal cardiac evaluation (discussed in detail in Chaps. 3 and 6). It is generally recognized that electronic array design offers significant advantages. Both convex sequential array and phased array transducers may be used for fetal echocardiographic applications. For most obstetric applications, including fetal cardiac evaluation, convex sequential transducers are often preferred, as they provide uniform high resolution in the image plane. However, phased array devices may be helpful when fetal orientation limits acoustic access to the fetal heart.

Finally, continuing advances in the ultrasound technology have not only addressed many of the challenges discussed above but also expanded its capabilities.

30.4 Doppler Modalities for Fetal Echocardiography

This section presents the various Doppler ultrasound modalities for fetal cardiac assessment.

30.4.1 Fetal Cardiac Color Doppler

The introduction of color Doppler echocardiographic technique represents one of the major advances in non-invasive cardiac diagnosis [16, 17]. Whereas 2D imaging provides information on the structural integrity of the fetal heart, the addition of Doppler ultrasonography provides information on the cardiac circulatory state, which may reflect the presence of fetal cardiac disease. Thus, color Doppler ultrasonography is of diagnostic value and is an integral component of fetal cardiac assessment.

Fetal cardiac hemodynamics have been imaged using the color mapping technique [18]. Its capabilities have been further expanded with continuing innovations, such as real-time 3D color Doppler imaging, postprocessing, and visualization techniques. These are further discussed in other chapters and a few examples are given below.

The depiction of Doppler mean frequency shifts by 2D flow mapping requires a balance between spatial resolution, Doppler accuracy, and temporal resolution. The normal range of the fetal cardiac cycle in 0.375–0.545 seconds (corresponding to a heart rate of 120–160 bpm). This degree of rapidity of fetal cardiac events necessitates an adequate processing speed to maintain temporal resolution. The small size and deep location of the fetal heart and the inability to ensure its favorable orientation impose further restrictions on obtaining adequate signals.

With Doppler color flow mapping for a given sector size, the more numerous the scan lines, the better the spatial resolution of the color (see Chap. 6). Furthermore, the more numerous the samples per scan line, the more accurate the mean velocity estimation. However, increasing the scan lines and sample points leads to a greater processing time, which in turn leads to a slower frame rate and therefore a consequent loss of temporal resolution, especially in a hyperdynamic situation with a shorter cardiac cycle as is encountered in the fetus. The small size of the fetal heart compensates for this problem to some extent by allowing an adequate anatomic exposure with a relatively

smaller scan area. Limiting the scanned area of interrogation can substantially improve both color sensitivity and temporal resolution. Another important consideration is the device's ability to distinguish between the various types of motion detected by the Doppler mode within the interrogated area. Doppler shift signals are generated not only by blood flow but also by tissue motions, such as fetal cardiac wall movements or during fetal breathing, which result in color artifacts. Although these artifacts can be eliminated by a high-pass filter, the latter also eliminates low-velocity flow information. Many devices now minimize this problem by utilizing advanced filtering technology that processes multiple parameters including velocity and amplitude. These issues are discussed in detail in Chap. 6.

Appropriate 2D views of the fetal heart are first obtained by 2D echocardiography. The mode of operation is then changed to color Doppler sonography, which results in the depiction of 2D color-coded flow patterns superimposed on real-time gray-scale images of the heart (Fig. 30.2). Manipulation of the transducer allows interrogation of various cardiac chambers, orifices, and outflow tracts. The presence of the color flow patterns facilitates identification of cardiac anatomy,

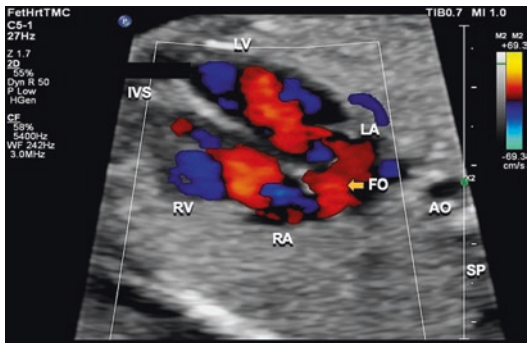

Fig. 30.2 Color Doppler echocardiogram showing color Doppler flow in a four-chamber view of the fetal heart. Atrioventricular flow through the tricuspid and mitral orifices, and interatrial flow from the right to left atrium through foramen ovale (horizontal arrow) are depicted here. *LA* left atrium, *LV* left ventricle, *RA* right atrium, *RV* right ventricle, *IVS* interventricular septum, *AO* aorta, *FO* foramen ovale, *SP* spine

particularly of those components that often are not amenable to ready recognition by 2D echocardiographic imaging. This method, however, has limitations for fetal application, some of which have been briefly discussed above. An additional problem may arise from the relatively high-velocity fetal cardiac wall movement, which results in color artifacts of "ghosting." This problem can be eliminated by increasing the high-pass filter, but this step also eliminates low-velocity flow components. The problem is compounded if the fetal position is such that the fetal heart is oriented perpendicular to the beam axis. In this situation, because of the high angle, Doppler frequency shifts are significantly attenuated. In contrast, the ventricular wall movement is in the beam axis, thus enhancing ghosting. Finally, color flow depiction in high-velocity flow areas, such as the ductus arteriosus, aortic root, or pulmonary root, frequently demonstrates velocity ambiguity or the Nyquist effect, so color directionality of the flow is depicted as reversed.

30.4.2 Fetal Cardiac Spectral Doppler

Spectral Doppler sonographic interrogation of the fetal heart can be performed only with a pulsed-wave duplex Doppler technique in which imaging provides guidance for the Doppler sample volume placement. Continuous-wave Doppler ultrasonography has limited use for assessing fetal cardiac flow because it lacks range discrimination.

Once a detailed anatomic examination of the heart has been performed, the Doppler cursor is moved across the plane of the 2D cardiac image, and the Doppler sample volume is then placed at the desired intracardiac or outflow locations. The ultrasound mode is then changed to pulsed-wave spectral Doppler sonography and the frequency shift signals are obtained (Fig. 30.3). Because of fetal movement and consequent unpredictable changes in the fetal position, repeated verification of the location of the Doppler sample volume is essential.

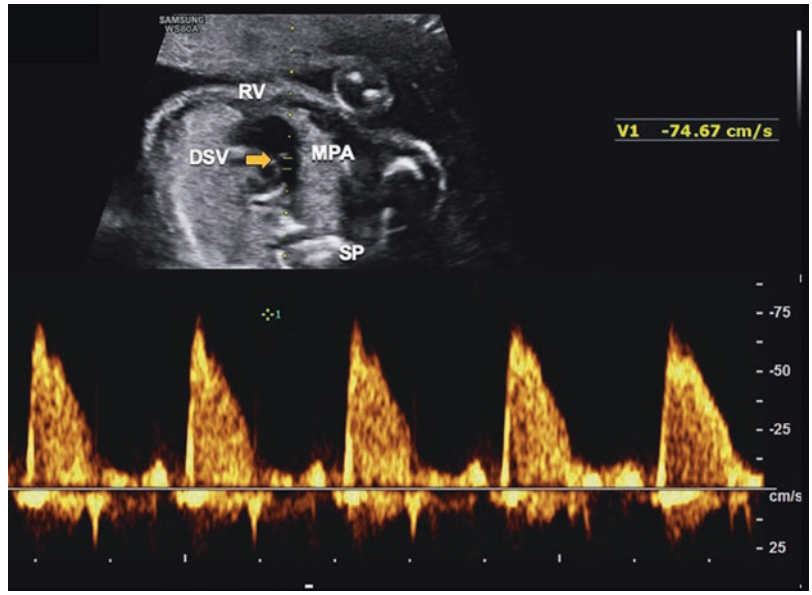

Fig. 30.3 Spectral Doppler interrogation of the pulmonary outflow. Upper panel: Pulmonary outflow. The Doppler path is indicated by the cursor line. The Doppler sample volume (horizontal lines) is placed in the outflow tract (horizontal arrow). Lower panel: Spectral Doppler waveforms from the pulmonary artery. *RV* right ventricle, *MPA* main pulmonary artery, *DSV* Doppler sample volume, *SP* fetal spine

30.4.3 Fetal Cardiac M-Mode

The designation M-mode represents motion mode, or time-motion mode, as it displays unidimensional moving images of tissues and organs. A single line of ultrasound is transmitted, and the echoes returning from the tissue reflectors along the line of transmission are displayed in the intensity modulation mode. If the display is now swept across, the motion changes in the image are displayed or recorded as a function of time. It is customary to display and record M-mode images with the vertical axis representing the tissue depth from the transducer and the horizontal axis representing the time. Usually the former is marked at 1-cm intervals and the latter at 0.5 second intervals. Color Doppler sonography can be used in conjunction with M-mode sonography. For fetal applications it is obvious that duplex mode sonography must be used so the M-mode cursor can be precisely aligned with the target. Such a combined approach can offer substantial benefit when identifying abnormal hemodynamics with high temporal accuracy as demonstrated in the example of fetal tricuspid regurgitation presented in Fig. 30.4. With the Doppler color M-mode technique, multigated Doppler sampling is performed on a single scan line, which is sampled 1000 times a second, and the unidimensional tissue and color flow images are scrolled (usually from right to left on the video screen) and therefore displayed as a function of time. Because of the high sampling rate from a single line, the color M-mode technique provides a high Doppler sonographic sensitivity and temporal resolution and allows reliable timing of the flow with the events of the cardiac cycle. For these reasons, color M-mode sonographic technique is useful for fetal echocardiographic examination.

30.4.4 Fetal Cardiac Tissue Doppler

Tissue Doppler sonography comprises processing and analyzing Doppler frequency shift generated by tissue movement. The physical and technical principles of tissue Doppler imaging of the heart are similar to those of Doppler sonography of blood flow with the exception of the approach to filtering. Doppler insonation of the heart generates signals from cardiac blood flow and myocardial movement. However, the Doppler signals generated by blood flow are of substantially lower amplitude and higher frequency than

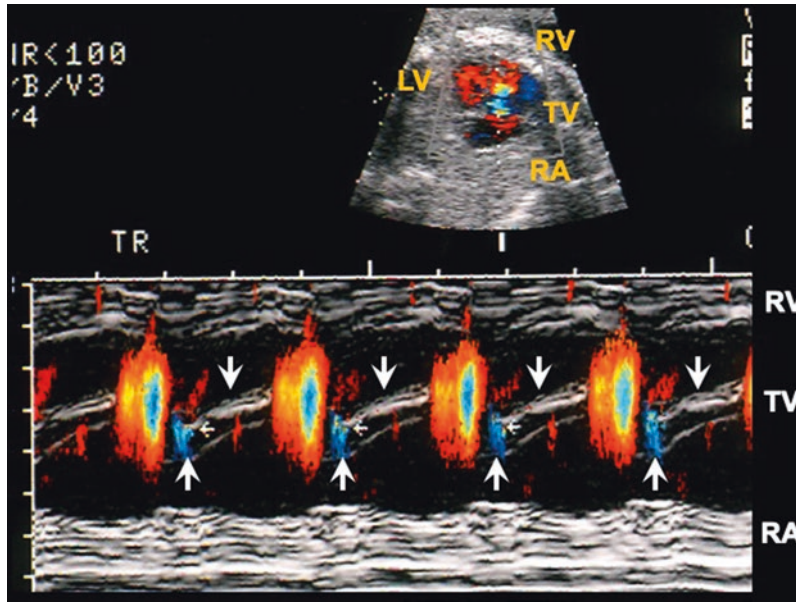

Fig. 30.4 Color M-mode echocardiogram of the fetal heart showing fetal tricuspid regurgitation. Top: Color Doppler image of the apical four-chamber view with the M-line cursor passing through the right ventricle (RV) and right atrium (RA). LV left ventricle, RV right ventricle. Bottom: color M-mode tracing. The atrioventricular flow across the tricuspid orifice is depicted in red. The mosaic color in blue and white indicates aliasing from high velocity turbulent flow. It is noted the motion of the tricuspid valve. The down arrows show the valve leaflets prior to their opening at the beginning of the ventricular diastole. The up arrow indicates tricuspid regurgitation

those from myocardial movement. In depicting flow, the high-pass filter system eliminates the high-amplitude and low-frequency myocardial Doppler signals so that only flow signals are displayed. In contrast, tissue Doppler echocardiography utilizes filtering that eliminates the low-amplitude high-frequency flow signals permitting tissue Doppler signals being displayed. There are two types of tissue Doppler: pulse-wave tissue Doppler mode and color tissue Doppler M-mode, which superimposes color-coded tissue velocities over 2D and M-mode images. An example of pulse tissue Doppler depiction of atrioventricular displacement is shown in Fig. 30.5. The technique can be used for measuring cardiac strain (Fig. 30.6).

In the adult, tissue Doppler echocardiography has been used for assessing cardiac systolic and diastolic functions [19–21]. Such assessments can be performed by measuring myocardial velocity, myocardial velocity gradient, myocardial strain, and strain rate. Myocardial strain is its deformation during systole and diastole. Strain implies differential velocities in the cardiac wall and does not reflect overall movement of the heart, including its translational motion within the thorax in relation to the other structures. Detailed reviews of these concepts may be found elsewhere [22].

Relatively recently, the application of tissue Doppler sonography for fetal cardiac assessment has been reported. Harada and associates measured motion velocities of the left ventricular posterior wall, right ventricular anterior wall, and interventricular septum along the longitudinal axis in normal fetuses aged 19–38 weeks' gestation and observed gestational age-specific increases in the peak myocardial velocities during early diastole and atrial contraction in the left and the right ventricular walls [23]. The authors speculated that such changes in tissue Doppler velocities may indicate maturational changes in the diastolic function. Tutschek et al. performed fetal tissue Doppler echocardiography with a high-resolution ultrasound system by changing the Doppler settings optimized for low-velocity motion assess-

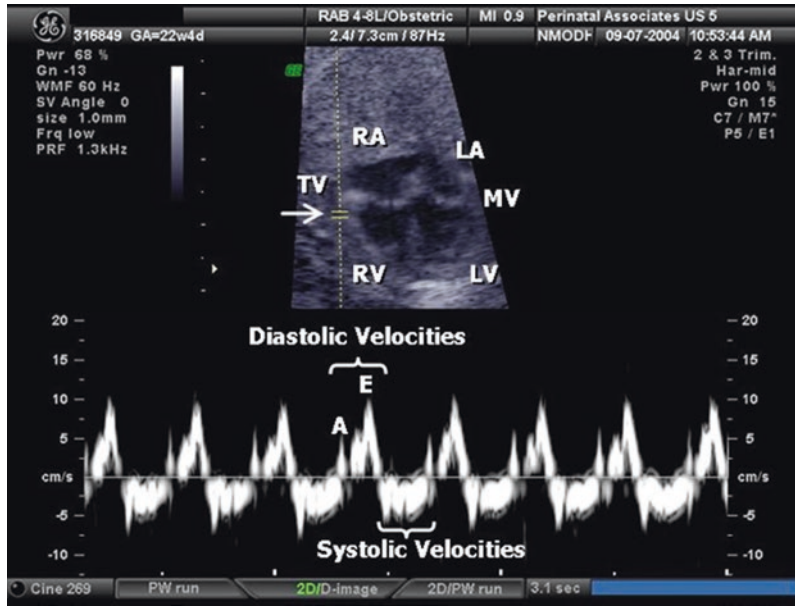

Fig. 30.5 Pulse-wave tissue Doppler imaging depicting tissue velocity waveforms from the atrioventricular annular displacement. The sampling site is indicated by the horizontal arrow pointing to the Doppler sample volume (two horizontal lines). The diastolic and systolic velocity waveforms are indicated on the lower panel. A indicates arterial systole and E indicates end-diastole. *RA* right atrium, *LA* left atrium, *MV* mitral valve, *TV* tricuspid valve, *RV* right ventricle, *LV* left ventricle

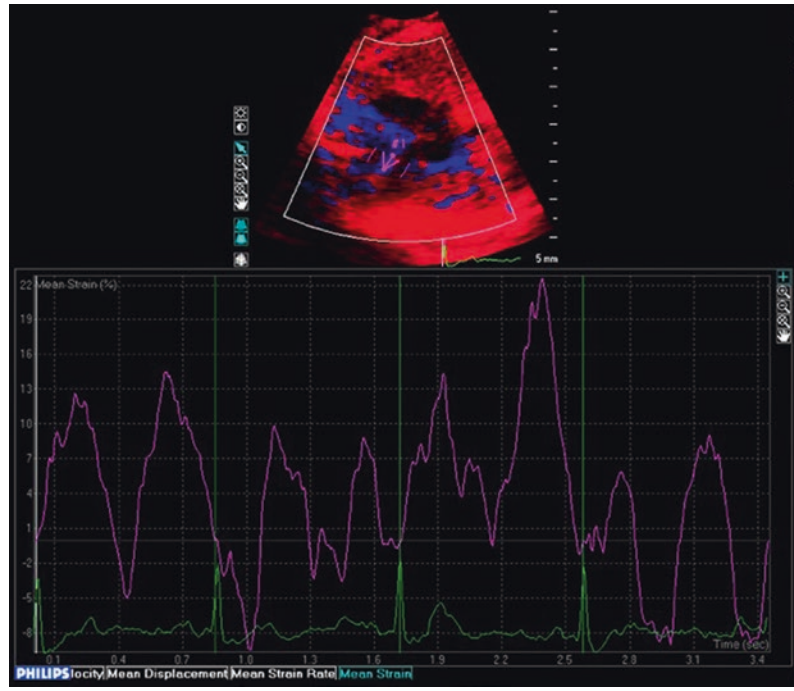

Fig. 30.6 Color tissue Doppler imaging of fetal cardiac strain measurement. The upper panel shows color tissue Doppler imaging of the fetal heart. The lower panel shows the mean strain measured at the interventricular septum

ment and observed increasing longitudinal contraction velocities of the fetal heart with the progression of gestation [24]. This finding was corroborated by Paladini et al. [25] in a study of 89 fetuses. Right and left systolic and diastolic velocities increased with increasing gestational age and were acceptably reproducible. The limitations of the technique include angle dependency which may compromise the accuracy of measuring myocardial motion. Moreover, translational movements of the heart within the thorax will also generate Doppler shift. However, this effect can be reduced by restricting the velocity measurements within the cardiac wall rather than in relation to the transducer. Such assessments include determination of myocardial velocity gradient and myocardial strain rate imaging as briefly noted above.

30.5 Indications for Fetal Echocardiography

There are numerous indications for fetal echocardiography ranging from a family history of congenital heart disease to pregestational diabetes. Table 30.2 presents common indications. A comprehensive review of the indications is the beyond the scope of this chapter. There are, however, screening and referral guidelines published by various professional organizations that include American Institute of Ultrasound in Medicine, International Society of Ultrasound in Obstetrics and Gynecology, and American Heart Association [26–28].

Table 30.2 Indications for fetal echocardiography

Maternal indications
Pregestational diabetes
Diabetes detected in the first trimester
Phenylketonuria
Auto-antibodies: Anti-Ro (SSA)/anti-La (SSB) positivity
Infection: Rubella, cytomegalovirus, parvovirus
First degree relatives with congenital heart disease: Mother, sibling, father
Familial inherited disorders: Marfan syndrome
In vitro fertilization pregnancy
Teratogenic medication exposure: Retinoic acid, valproic acid, paroxetine, lithium, others
Fetal indications
Non-reassuring screening cardiac ultrasound
Extracardiac congenital malformations
Cardiac arrhythmia
Aneuploidy
Abnormal first trimester screening
Hydrops fetalis
Idiopathic severe polyhydramnios
Monochorionic twin gestation

30.6 Method of Fetal Doppler Echocardiography

A preliminary ultrasound examination is initially performed to determine fetal orientation and situs, followed by systematic echocardiographic imaging utilizing all the modalities. A segmental approach is used employing the standard echocardiographic planes (Table 30.3), systematically evaluating the atria and the precordial veins, the ventricles, and the outflow tracts. Fetal cardiac flow dynamics is imaged using 2D/3D color flow Doppler and spectral Doppler. M-mode echocardiography may be used combined with color flow Doppler mode.

30.7 Doppler Assessment of Fetal Cardiac Hemodynamics

Color flow mapping and directed pulsed-wave spectral Doppler characterization of normal and abnormal fetal cardiac circulation assist in the

Table 30.3 Echocardiographic planes

Four-chamber views
Apical
Basal
Lateral
Outflow tract long-axis views
Aortic outflow
Pulmonic outflow
Cross-over
Ventricular short-axis views
Ventricular chambers
Mitral–tricuspid plane
Three vessel view
Outflow tract long-axis arch views
Aortic arch
Pulmonic–ductal arch

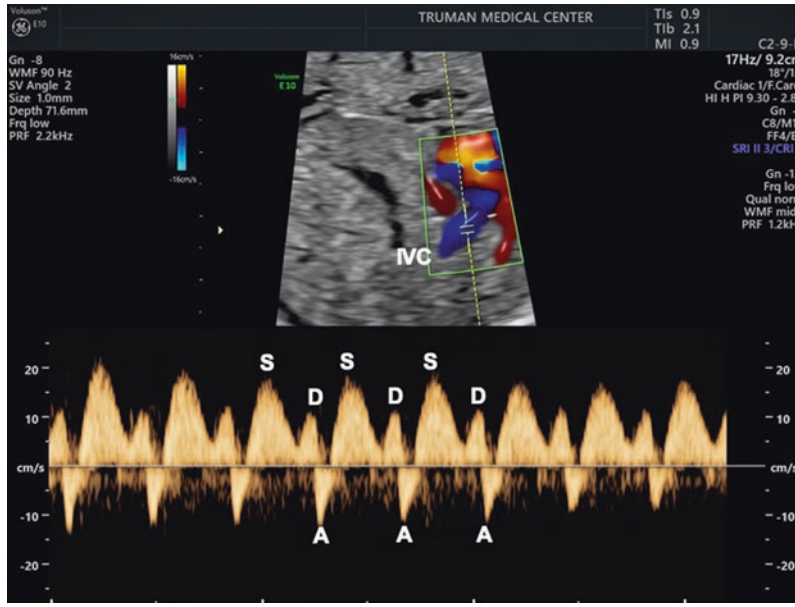

Fig. 30.7 Color and spectral Doppler of the inferior vena cava (IVC). Spectral Doppler interrogation of the inferior vena caval flow. Right: Color flow imaging of the inferior vena cava and placement of the Doppler sample volume. Left: Inferior vena caval Doppler waveforms. It is noted the triphasic waveform, two positive peaks and a negative peak, reflecting the events of the cardiac cycle. The first positive peak (S) coincides with ventricular systole and the second positive peak (V) with ventricular diastole. The negative peak is associated with atrial systole (A)

morphological assessment of fetal cardiac malformations supplementing the B-mode echocardiography, and allow for the assessment of the fetal cardiac function. The technique and Doppler flow characteristics of fetal cardiac hemodynamics are described below.

30.7.1 Atrial Flow

The right and left atrial inflows can be assessed using color and spectral Doppler. Spectral Doppler waveforms from inferior vena cava exhibit a triphasic flow pattern (Fig. 30.7). Doppler investigation of vena caval hemodynamics is presented in Chap. 29. The superior vena caval flow entering the right atrium can be visualized separately from the inferior vena caval return. These two inflows become confluent in the right atrial chamber. The pulmonary veins can be investigated using color and spectral Doppler systems. The left pulmonary veins are more readily accessible. Doppler waveforms from the pulmonary veins reflect atrial and ventricular cycles (Fig. 30.8).

Spectral Doppler investigation of fetal atrial hemodynamics may be conducted in apical and lateral four-chamber and other views. Such interrogation demonstrates complex flow patterns (Fig. 30.9) consistent with multiple inflows in the atria, two outflows of the right atrium, and a single outflow of the left atrium. A higher Doppler frequency shift is observed in the right atrium than in the left atrium. This description of the Doppler flow characteristics of the atria further elucidates the previously reported observations in previable human fetuses using acute radio angiographic studies [29] and in fetal sheep [30].

The foramen ovale valve movement is associated with changes in the Doppler frequency shift in the left atrium; a higher frequency shift is observed when the valve is open than when it is closed [6]. Flow across the foramen ovale is optimally investigated with the lateral four-chamber view or a short-axis view, which allows angle-appropriate alignment of the Doppler cursor with flow direction across the foramen. Spectral Doppler investigation of the flow across the foramen shows a biphasic flow velocity pattern

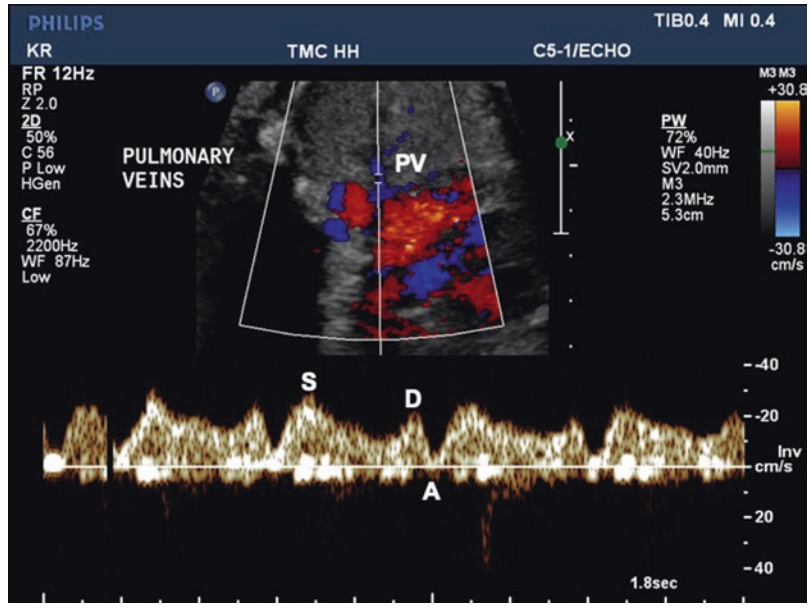

Fig. 30.8 Doppler imaging of pulmonary venous return. Top: Lateral four-chamber view of the fetal heart, with the Doppler sample volume placed at the upper left pulmonary vein (PV). Bottom: Pulmonary venous Doppler waveforms. The first peak coincides with ventricular systole (S), the second peak with ventricular diastole (D), and the trough coincides with atrial systole (A)

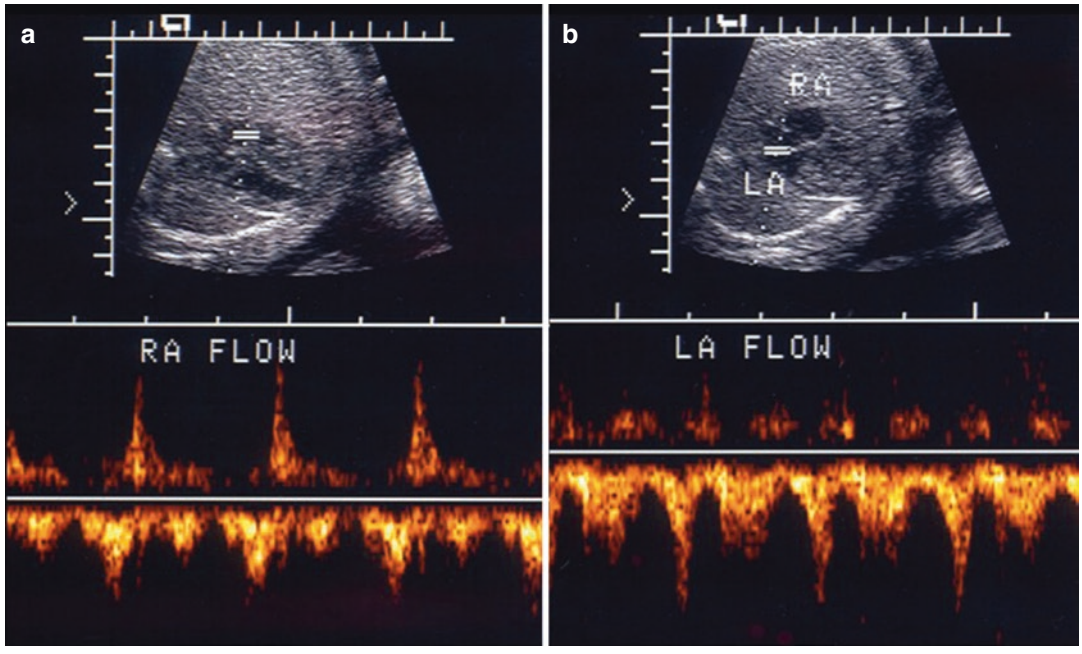

Fig. 30.9 Doppler waveforms from the atria. (**a**) Top panel shows interrogation of the right atrium. Bottom panel shows the complex pattern of the right atrial Doppler waves. (**b**) Top panel shows the complex interrogation of the left atrium. Bottom panel shows the complex pattern of the left atrial Doppler waves. *RA* right atrium, *LA* left atrium

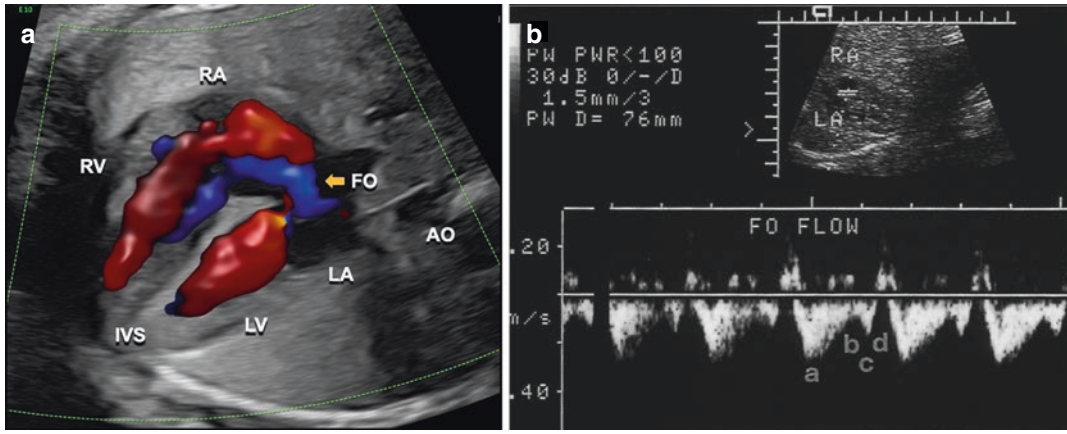

Fig. 30.10 Doppler insonation of the foramen ovale flow. (**a**) Color Doppler radiant flow imaging of the atrioventricular and foramen ovale circulations. Fetal heart is depicted in basal four-chamber view. *LA* left atrium, *LV* left ventricle, *RA* right atrium, *RV* right ventricle, *IVS* interventricular septum, *SP* spine, *R* right side of the fetus, *L* left side of the fetus. (**b**) Duplex spectral Doppler interrogation of the foramen ovale flow. Top: Placement of the Doppler sample volume at the foramen ovale. *RA* right atrium, *LA* left atrium. Bottom: Interatrial Doppler waves. *FO* foramen ovale, *a* ventricular peak systole, *b* ventricular end-systole, *c* atrial passive filling, *d* atrial systole

(Fig. 30.10a, b). Ventricular systole is associated with a sharp rise in the frequency shift, reaching a peak coinciding with peak systole, following which the shift decelerates to a nadir at end-systole. With passive atrial filling the shift rises again, reaching a second peak that is lower than the first peak. This phase is followed by a rapid decline that coincides with atrial systole. These changes are influenced by the fetal behavioral state. The ventricular end-systolic and atrial passive filling phases demonstrate a significantly higher-frequency shift when the fetus actively sleeps (state 2F) than when it sleeps quietly (state 1F). It is reflective of flow redistribution and increased right-to-left shunt during active sleep.

30.7.2 Atrioventricular: Tricuspid and Mitral Flow

The color Doppler flow technique vividly portrays the flow patterns across the atrioventricular flow channels (Fig. 30.11). Color imaging may facilitate acquisition of the Doppler signals from the various areas of the atrioventricular flow jets.

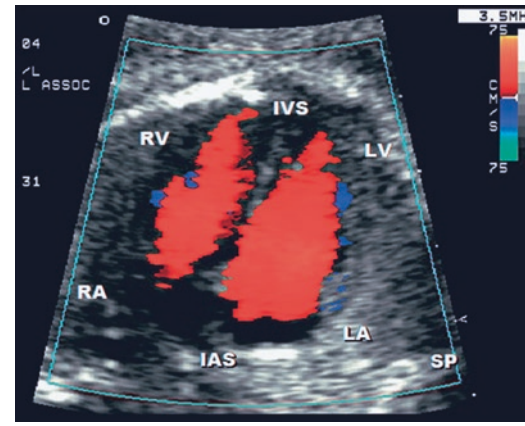

Fig. 30.11 Color Doppler echocardiogram of the mitral and tricuspid flow. The fetal heart is viewed in the apical four-chamber plane. *RA* right ventricle, *LV* left ventricle, *IVS* interventricular septum, *RA* right atrium, *LA* left atrium, *IAS* interatrial septum, *SP* fetal spine

Spectral Doppler insonation demonstrates a biphasic flow pattern across the tricuspid and mitral orifices, reflecting the contributions of ventricular relaxation and atrial contractions to the atrioventricular flow. The peak flow velocity due to contraction of the atrium (A wave) is significantly greater than the peak flow velocity

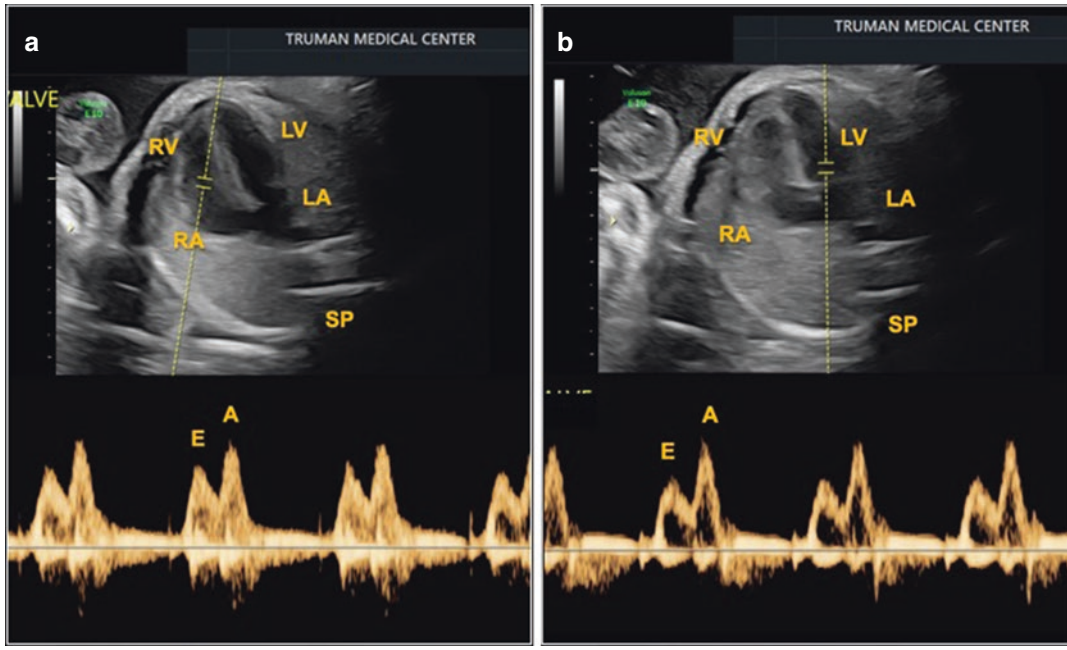

Fig. 30.12 (**a**, **b**) Doppler interrogation of the tricuspid and mitral flow. The right panel presents the Doppler interrogation of the tricuspid flow. It is noted the location of the Doppler sample volume in the right ventricular chamber just distal to the tricuspid orifice. Bottom panel presents the biphasic tricuspid Doppler waveforms. E peak velocity related to forward flow during the ventricular diastole, A peak velocity related to forward flow during the atrial systole. The left panel shows the Doppler interrogation of the mitral flow. Top panel shows the Doppler echogram of the fetal heart in the apical four-chamber plane. It is noted the location of the Doppler sample volume in the left ventricular chamber just distal to the mitral orifice. Bottom panel presents the biphasic mitral Doppler waveforms. E peak velocity related to forward flow during the ventricular diastole, A peak velocity related to forward flow during atrial systole

caused by ventricular diastole (E wave) (Fig. 30.12). However, in the left heart, the A wave is less than, equal to, or only marginally greater than the E wave. These findings suggest a physiologically lower compliance of the right ventricle than of the left ventricle and are similar to the pulsed-wave Doppler echocardiographic observations in neonates and infants.

Takahashi et al. [13] investigated mitral and tricuspid flows using pulsed-wave Doppler sonography in 23 fetuses of 31–38 weeks gestational age. They noted that the peak velocity across the mitral orifice was 52.1 ± 9.9 cm/s (mean ± SD) and that across the tricuspid orifice was 56.1 ± 8.7 cm/s. They also reported that the velocity patterns of the right ventricle and left ventricle inflow demonstrated two peaks consistent with the rapid filling phase and the atrial contraction phase, and the peak velocity of the atrial contraction phase was slightly greater than that of the rapid filling phase. Kenny et al. [31] investigated E and A waves comprehensively in 80 normal human fetuses at 19–40 weeks' gestation. They identified clearly defined E and A waves from the tricuspid orifice in 48% of the fetuses and from the mitral orifice in 60%. The ratio for both atrioventricular orifices increased during gestation.

These gestational age-related changes in the atrioventricular flow velocities were confirmed by Reed et al. [14] and Rizzo et al. [32]. The latter group prospectively studied 125 normally grown fetuses and 35 small-for-gestational-age (SGA) fetuses longitudinally at 27–42 weeks' gestation. In normal fetuses the ratio between the E velocity (early passive ventricular filling) and the A velocity (active ventricular filling during atrial contraction) increased progressively and significantly ($p < 0.01$) during pregnancy in both transmitral

and transtricuspid waveforms, approaching 1.0 at term. These changes suggest progressive structural and functional maturation of the ventricles resulting in age-related increases in myocardial compliance. Romero et al. [33] studied the pressure–volume relation in fetal, neonatal, and adult hearts and demonstrated low compliance of the fetal heart. These changes may also be related to the known fetal hemodynamic changes with the progression of gestation, including the significant fall in fetoplacental vascular impedance.

30.7.3 Ventricular Outflows: Pulmonary Artery and Aorta

The right and left ventricular outflow can be imaged in the ventricular long-axis plane (Fig. 30.13). This plane allows clear assessment of the aortic-pulmonary crossover relation (Fig. 30.14a). This relationship can be also be observed in other planes. Color flow imaging facilitates recognition of this important normal characteristic of the outflow tracts. Real-time 3D Doppler with a matrix probe, especially in the transparency mode, can be useful in this visualization (Fig. 30.14b).

The main pulmonary arterial flow can be conveniently seen in the parasternal short-axis plane at the base of the heart, which demonstrates the aortic cross section surrounded by the right atrium, right ventricle and pulmonary trunk, and right pulmonary artery. The orientation of the main pulmonary artery in this plane often facilitates alignment of the Doppler beam along the pulmonary blood flow axis, ensuring an optimal angle of insonation. Aortic and pulmonary arterial hemodynamics can also be readily investigated in the aortic arch (Fig. 30.15) and ductal arch (Fig. 30.16) planes, respectively. Doppler frequency shift waveforms from the main pulmonary artery are characterized by rapidly accelerating and decelerating slopes, with sharp peaks during right ventricular systole (Fig. 30.17a, b). In comparison with the maximal aortic velocity wave, however, the immediate postpeak deceleration slope is less acute in the pulmonary waveform. The peak velocity values from the

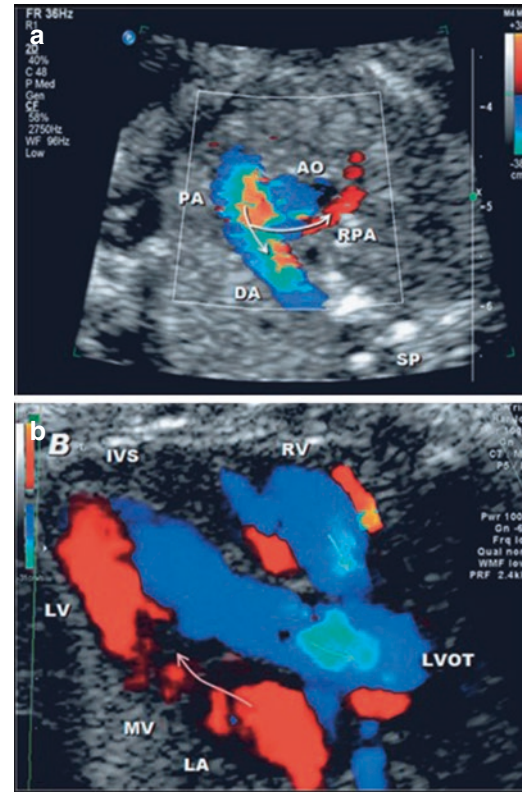

Fig. 30.13 (**a**, **b**) Color Doppler echocardiogram of the ventricular outflow tracts. The upper panel: Right ventricular outflow tract is shown in the aortic short-axis plane of the fetal heart. It is noted aliasing in the outflow tracts. The lower panel: Left ventricular outflow is shown in the oblique long-axis view of the fetal heart. The lighter color at the beginning of the aorta is indicative of higher velocity. The arrows depict flow direction AO aorta, IVS interventricular septum, *DA* ductus arteriosus, *LV* left ventricle, *RV* right ventricle, *LVOT* left ventricular outflow tract, *MV* mitral valve, *PA* pulmonary artery, *RPA* right pulmonary artery, *SP* fetal spine

pulmonary artery and the aorta, measured longitudinally in 27 normal pregnancies from 18 weeks to term, are presented in Table 30.4 (Maulik and Ciston, unpublished data).

In a longitudinal study, Rizzo et al. [34] showed significant increases in the pulmonic peak velocity ($p \leq 0.001$) and in the aortic peak velocity ($p \leq 0.05$) during early pregnancy between the end of the first trimester (11–13 weeks) and midgestation (20 weeks). Hata et al. [35] performed a cross-sectional investigation of 54 normal fetuses at 16–40 weeks of pregnancy and noted increases in transpulmonic peak

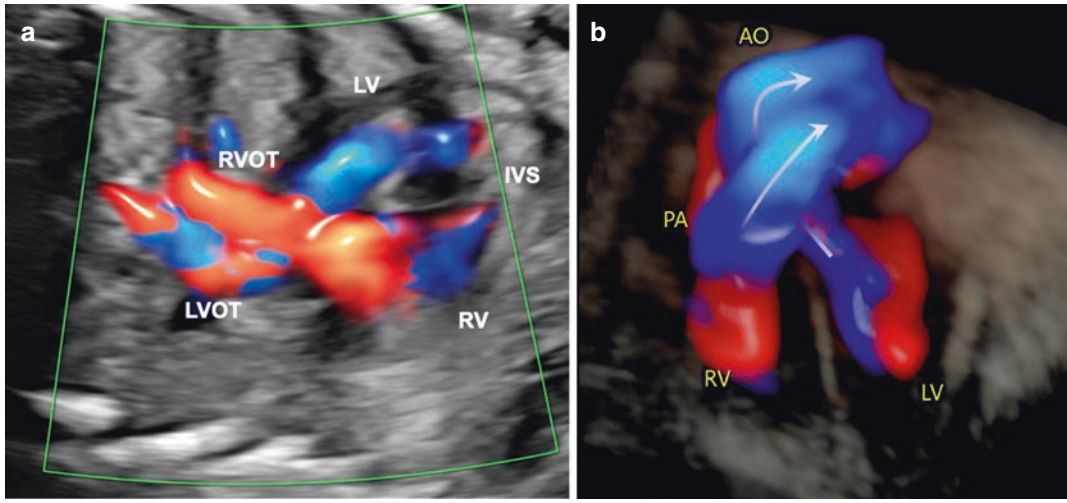

Fig. 30.14 Color Doppler imaging of the cross-over relation between the origins of the great arteries. (**a**) Two dimensional color mapping. *SP* fetal spine, *LV* left ventricle, *RV* right ventricle, *IVS* interventricular septum, *RVOT* right ventricular outflow, *LVOT* left ventricular outflow. (**b**) Real-time matrix 3D color Doppler. The four-dimensional matrix array image depicts the cross-over in the transparency mode. *AO* aorta, *LV* left ventricle, *RV* right ventricle, *PA* pulmonary artery. The arrows depict the flow directions in the great vessels

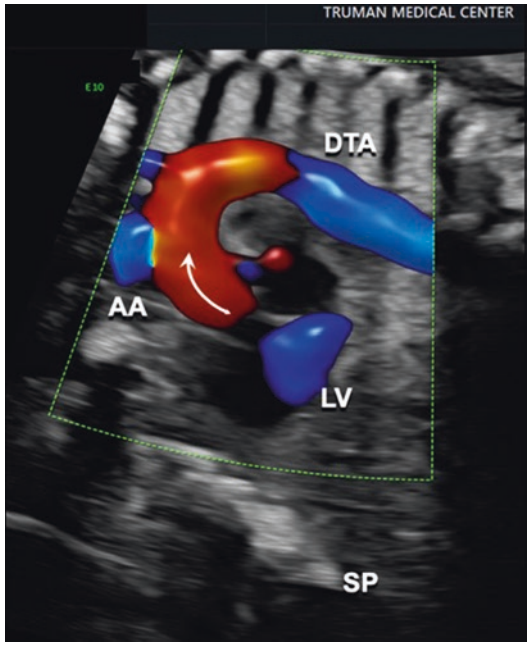

Fig. 30.15 Color Doppler echocardiogram of the aortic arch in "radiant flow" display. It is noted the tighter curve of the arch and the change in the color depiction of flow, reflecting the changes in the flow direction in relation to the transducer. The curved arrow indicates flow direction at the root of the aorta. Vertical arrow indicates root of aorta. *AA* aortic arch, *LV* left ventricle, *DTA* descending thoracic aorta

velocity ($r = 0.39$, $p < 0.05$) and transaortic peak velocity ($r = 0.61$, $p < 0.001$) throughout the gestation. The transpulmonary peak velocity/transaortic peak velocity ratio was 1:1 in 45% of the instances. In contrast, Reed et al. [36], in a cross-sectional study of 87 fetuses at 17–41 weeks' gestation, did not note any changes in the peak aortic velocity with advancing gestational age ($p < 0.001$). Moreover, peak Doppler flow velocities were greater in the aorta than in the pulmonary artery ($p < 0.001$).

30.7.4 Doppler Determination of Myocardial Performance Index

Myocardial performance index (MPI), also known as the Tei index, assesses global ventricular function. Originally developed by Tei et al. for evaluating left ventricular systolic and diastolic performance in dilated cardiomyopathy in adults [37], this spectral Doppler index is derived from the isovolumetric contraction time (ICT), isovolumetric relaxation time (IRT), and ejection time (ET), and reflects global ventricu-

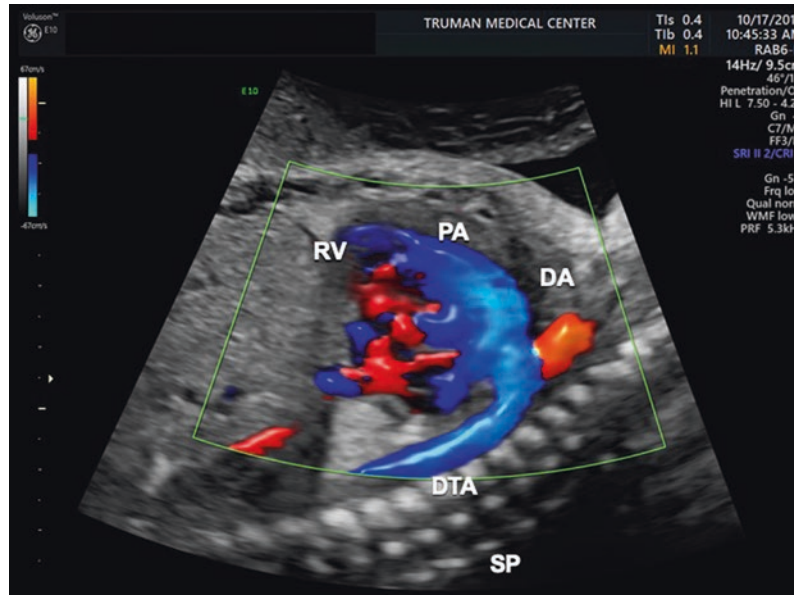

Fig. 30.16 Color Doppler echocardiogram of the ductal arch in "Radiantflow™." It is noted the wider curve of the arch and color aliasing at the ductal level. *DA* ductal arch, *PA* pulmonary artery, *RV* right ventricle, *DTA* descending thoracic aorta, *S* fetal spine

lar function. Tsutsumi and others applied the Tei index for evaluating fetal myocardial performance by obtaining separate atrioventricular and outflow tract waveforms, and observed slight linear decline with the progression of gestation and significant increases with fetal growth restriction and diabetes [38]. Friedman and coworkers improved the technique by obtaining both mitral and aortic outflow Doppler waveforms from the same cardiac cycle and observed a gradual decline in MPI with advancing gestation [39]. An example of the Doppler echocardiographic is presented in Fig. 30.18. Further modification was introduced by Hernandez-Andrade who used movements of the mitral and aortic valves and observed significant improvements in intra- and inter-observer variability [40]. More recently, however, MacDonald and others noted poorer reproducibility of the modified MPI early pregnancy [41]. MPI measurement utilizing tissue Doppler echocardiography has been shown to be more sensitive and reproducible [42]. MPI has been shown to be abnormal in various complications, including fetal growth restriction, diabetes, and recipient twin in twin transfusion syndrome. The technique, despite its limitations, provides a useful tool for fetal functional echocardiography.

30.7.5 Doppler Determination of Fetal Cardiac Output

The theoretic basis, technical implementation, and limitations of Doppler sonographic flow quantification are discussed in Chap. 4. The methodology for fetal cardiac output measurement was first described by Maulik et al. [6]. Briefly, the stroke volume is determined by integrating the temporal average velocity (also known as the time–velocity integral) across the valvular orifice or vascular lumen with the cross-sectional area of the vascular tract. The cardiac output is obtained by multiplying the stroke volume by the fetal heart rate. The combined cardiac output is the sum of the right and left cardiac outputs. The various measures of the fetal cardiac output are presented in Table 30.5. In the fetus the right and the left sides of the heart work in parallel. Therefore, fetal cardiac output must be determined separately for each side. The measurements may be performed either at the root of the great or across the atrioventricular orifices [6, 43–45]. The right ventricular output may be measured either across the tricuspid orifice or at the root of the main pulmonary artery just distal to the pulmonary semilunar valves [6]. Similarly, the left ventricular output may be measured

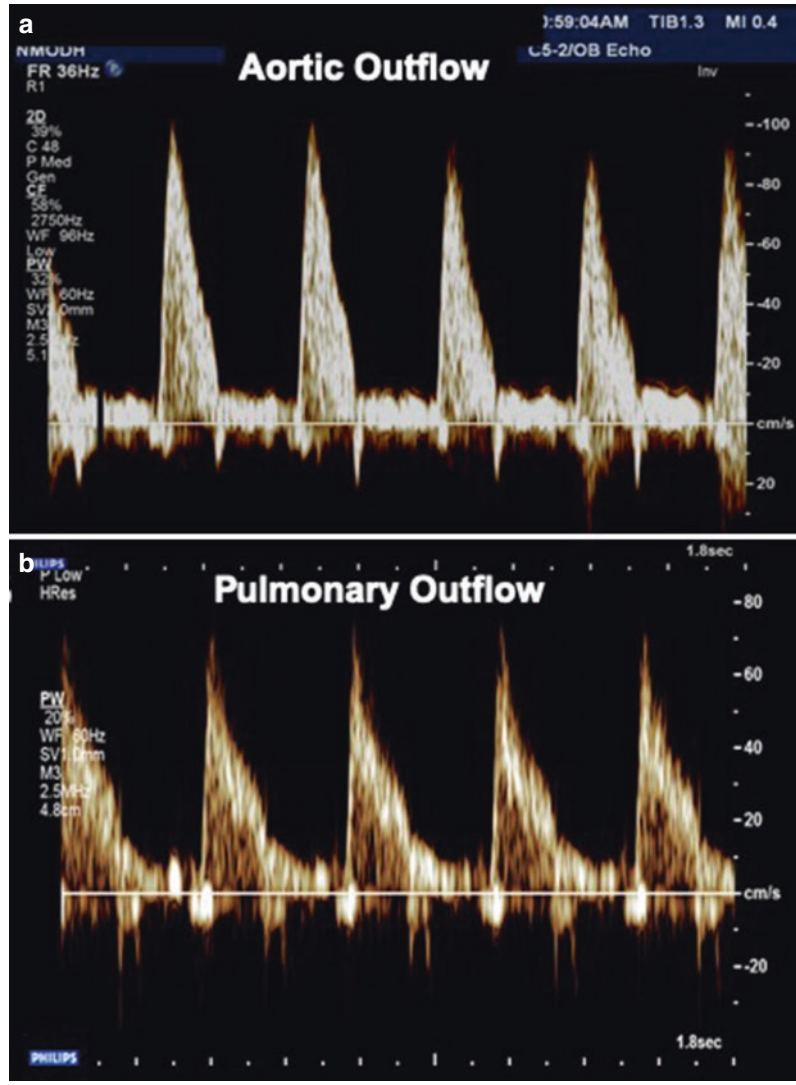

Fig. 30.17 Spectral Doppler waveforms from the pulmonary artery (panel **a**) and aorta (panel **b**). Both waves show rapid accelerations. The deceleration slope of the pulmonary artery, however, is slightly less step than that of the aorta

Table 30.4 Peak velocity in fetal pulmonary artery and aorta

Site	Peak velocity (cm/s) at three gestational ages (mean ± SD)		
	18–23 weeks	24–31 weeks	32–40 weeks
Pulmonary artery	51 ± 7	59 ± 9	61 ± 11
Aorta	55 ± 10	63 ± 12	73 ± 11

across the mitral orifice or at the root of the aorta immediately distal to the aortic semilunar valves (Fig. 30.19). The precision of the technique in terms of reproducibility depends on the site of measurement, the parameters measured, the imageability of the patient in a given instance, and operator skill. In our experience, the roots of the great vessels provide a more reliable measure than the atrioventricular channels. Groenenberg et al. [46] investigated this question and noted high reproducibility of peak systolic velocity and average velocity measured in the ductus arteriosus, pulmonary artery, and ascending aorta. The coefficients of variation between tests within individual patients were less than or equal to 7%. In a study by Reed et al. [45], there was less than 6% mean variation between measures of peak

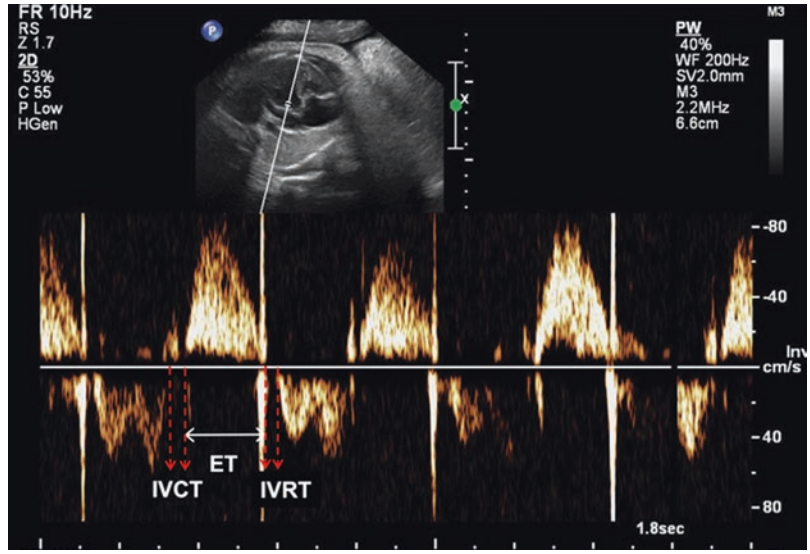

Fig. 30.18 Myocardial performance index of fetal left ventricle. Upper panel shows placement of the Doppler sample in distal to the mitral valve in proximity to aortic outflow. Lower panel shows aortic outflow (directed upward) and mitral (directed downward) Doppler waveforms. Dotted red arrows indicate caliper placement. *IVCT* isovolumetric contraction time, *IVRT* isovolumetric relaxation time, *ET* ejection time

Table 30.5 Measures of fetal cardiac output

Stroke volume (mL) = temporal mean velocity (cm/s) × cross-sectional area (cm^2)
Cardiac or ventricular output (mL/min) = stroke volume (mL) × fetal heart rate (bpm)
Left cardiac output = cardiac output measured at the aortic or mitral orifice
Right cardiac output = cardiac output measured at the pulmonic or tricuspid orifice
Combined cardiac output (mL/min) = sum of the right and left cardiac outputs

systolic velocity through the mitral, tricuspid, and atrioventricular valves within the same fetus during gestation. Similarly, Al-Ghazali et al. [47] measured the average and peak systolic velocity through the pulmonary and aortic valves and noted a mean variation between measurements of 7.6%. Brezinka et al. [48] noted similar reproducibility of the ductus arteriosus.

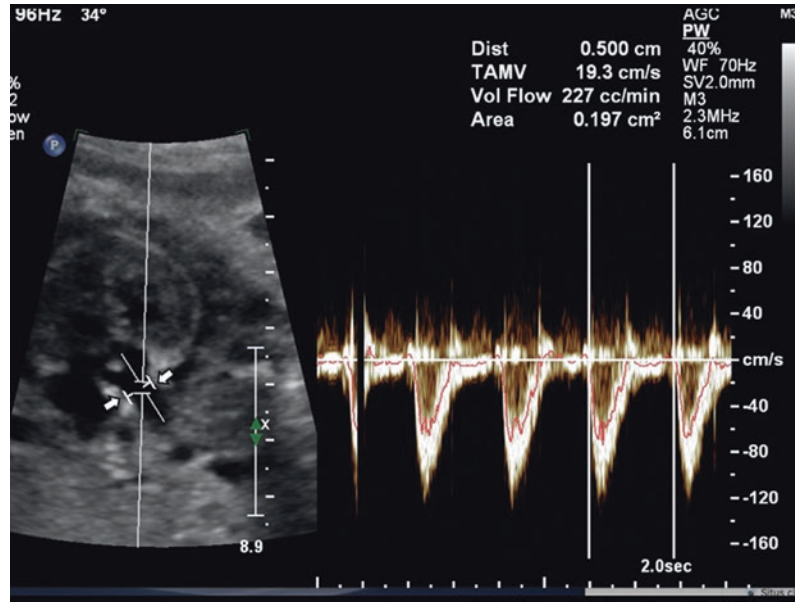

Fig. 30.19 An example of duplex Doppler determination of fetal left cardiac output. The left panel shows placement of the Doppler sample volume at the left ventricular outflow tract at the root of the aorta. The cross-sectional area was estimated from the measurement of vascular diameter as shown in the image by white arrows. The right panel shows Doppler velocity waveforms. The measurements are shown in the right upper corner

30.7.6 Cardiac Output: Normative Data

Maulik et al. [6], in a preliminary report, noted a right ventricular output range of 148 mL/min in a 28-week fetus to 451 mL/min in a near-term fetus. Reed et al. [45] observed a tricuspid flow rate of 307 ± 30 $mL \cdot kg^{-1} \cdot min^{-1}$ and a mitral flow rate of 232 ± 25 $mL \cdot kg^{-1} \cdot min^{-1}$ in fetuses of 26–30 weeks gestational age. In a comprehensive longitudinal study, De Smedt et al. [49] performed echocardiographic examinations on 28 normal fetuses at 4-week intervals from 15–18 weeks to term. The fetal cardiac output was measured from the tricuspid and mitral orifices. They observed that with advancing gestation the mean temporal blood flow velocities increased linearly, whereas the area of blood flow and calculated right and left ventricular output increased exponentially. The combined ventricular output at term was noted to be 1735 mL/min and 553 ± 153 $mL \cdot kg^{-1} \cdot min^{-1}$ when corrected for sonographically estimated fetal weight. Mielke and Benda [50] prospectively measured right and ventricular outputs in 222 normal fetuses from 13 to 41 weeks to establish reference ranges. The 50th centile for the biventricular output rose from about 40 mL/min at 15 weeks to 1470 mL/min at 40 weeks. The authors reported that the median biventricular output per 1 kg fetal weight was 425 mL per min per kg, which was independent of the gestational age. The calculated right and left ventricular outputs per minutes as the function of the gestational age are shown in Fig. 30.20.

30.7.7 Right Heart Versus Left Heart Dominance

It has been shown in the ovine fetal model that right ventricular output is twice that of the left [51]. Maulik et al. [6] noted evidence of human fetal right ventricular dominance in a preliminary report. In a comprehensive, longitudinal study of 28 fetuses, De Smedt et al. [49] demonstrated that the right ventricular output was significantly higher than that of the left ventricle, and the right/left ventricular output ratio decreased from 1.34 ± 0.28 (standard deviation) at 15 weeks to 1.08 ± 0.28 at 40 weeks. In contrast, Allan et al. [52], in a much larger study of 120 fetuses, 36 of which had measurements of all 4 valves, reported that right ventricular output was higher than that of the left throughout gestation and was noted to maintain a constant right/left ventricular output ratio of 1.3. Similarly, Mielke and Brenda [50] reported a ratio of 1.5, which was constant over gestation in a study of 87 fetuses.

30.7.8 Limitations of Cardiac Output Measurement

As discussed in Chap. 4, the Doppler approach for volume flow measurement is based on a few assumptions, such as the velocity profile of the flow and the uniformity of insonation, which may compromise the reliability of the measurement. Furthermore, the results are subject to significant error also because of the inherent imprecision when measuring vascular diameter and the angle of insonation. Of these measurements, the former is the more significant source of imprecision in the cardiac output measurement. Of the two sites for such measurements, the atrioventricular (mitral and tricuspid) orifices may be more difficult to measure in a consistent manner. Nevertheless, some investigators prefer these sites instead of the roots of the great vessels. The problems contributing to imprecision are compounded because of the deep location, small size, and unfavorable orientation of the fetal heart. For these reasons absolute volumetric flow determination in the fetal heart has been of little practical value for clinical application, although it has been a valuable research tool for extending our knowledge of the physiology and pathology of fetal cardiac function.

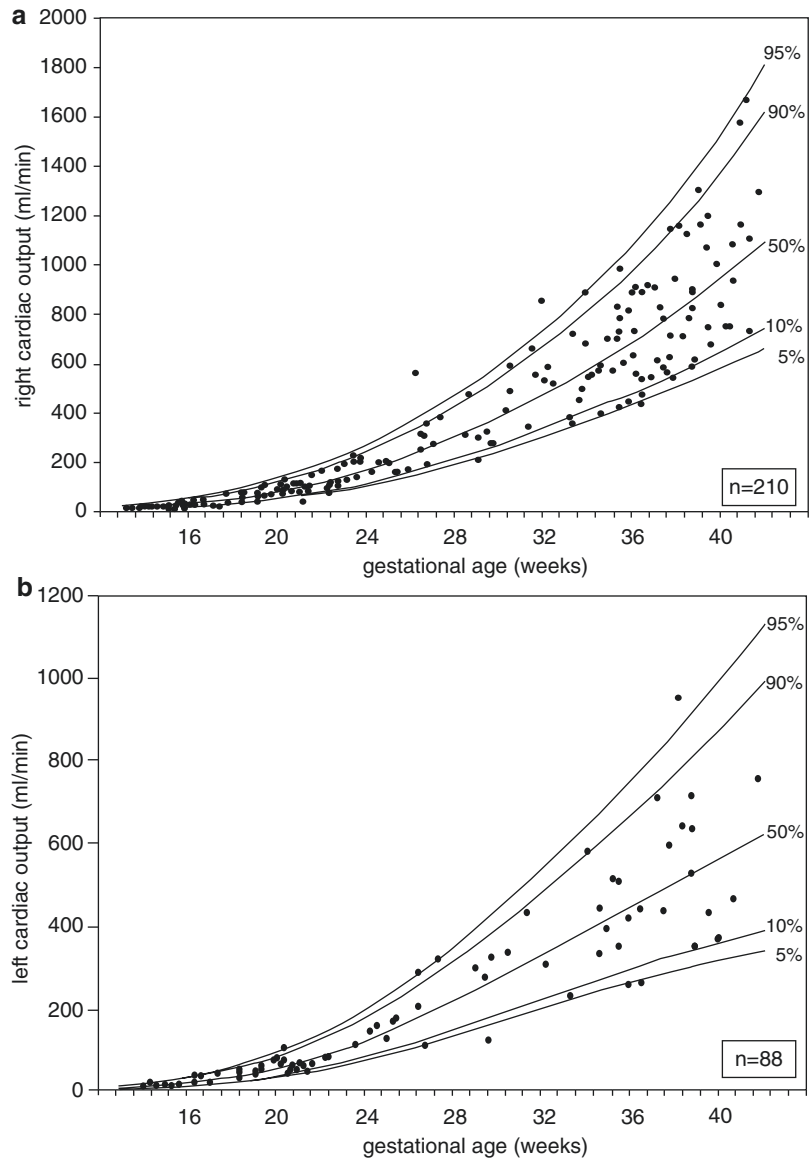

Fig. 30.20 (**a**) Individual values and calculated fifth, 10th, 50th, 90th, and 95th centiles of right ventricular output per minute. (From [49], with permission). (**b**) Individual values and calculated fifth, 10th, 50th, 90th, and 95th centiles of left ventricular output per minute. (From [49], with permission)

30.8 Doppler Echocardiography During Early Pregnancy

Although it has been customary to initiate fetal echocardiography at 18–22 weeks' gestation, advances in imaging resolution, color Doppler sonography, and transvaginal sonography have made it possible to assess embryonic or fetal heart in early pregnancy [53]. These developments have led to the early diagnosis of congenital heart disease and the use of Doppler echocardiography, specifically Doppler evaluation of the tricuspid and ductus venosus flow, for first trimester genetic screening. Any inter-

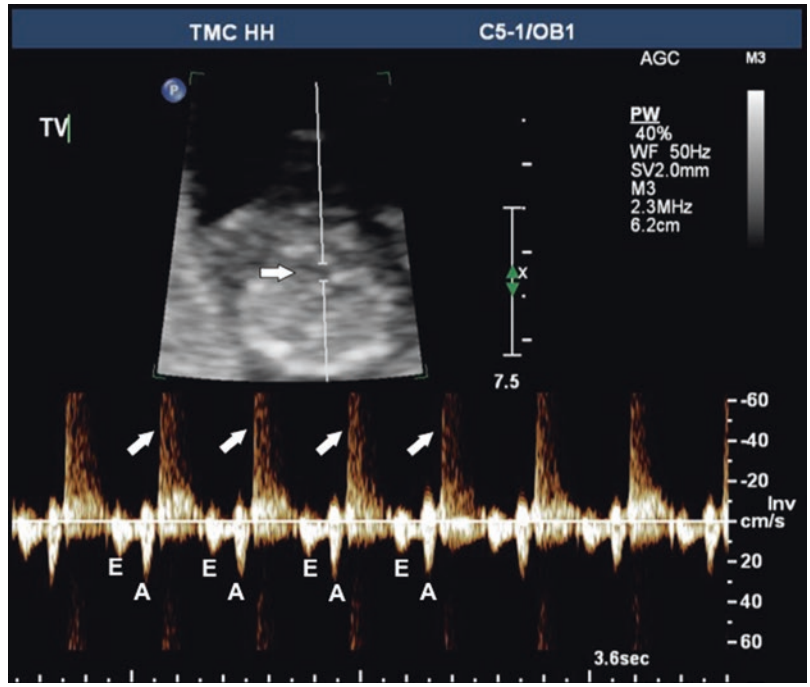

Fig. 30.21 The sonogram illustrates tricuspid regurgitation in a first trimester fetus. The upper panel shows placement of the Doppler sample volume. E = peak flow velocity during ventricular diastole. A = peak flow velocity during the atrial systole. The upward oblique arrows indicate the high velocity regurgitant flow jets from the right ventricle to the right atrium. It is noted aliasing of the flow jets due to their high velocity. (From [38], with permission)

pretation of fetal cardiac flow pattern should take into consideration gestational changes that reflect fetal cardiac structural and functional maturation.

Doppler sonography in early pregnancy has been reviewed recently [54]. Figure 30.21 shows tricuspid regurgitation in a case of trisomy 21. As noted earlier in this chapter, atrioventricular flow is unidirectional with blood moving from the atria to the ventricles in a biphasic pattern, although tricuspid regurgitation may be observed in normal fetuses, first reported in a case by Maulik [6] and others and confirmed extensively by others [55]. Presence of tricuspid regurgitation in the first trimester, however, substantially increases the risk of aneuploidy. Using Doppler imaging in 1557 fetuses, Falcon and others reported regurgitation in only 4.4% of the euploid fetuses but in 67.5% and 33.3% of the fetuses with trisomy 21 and trisomy 18, respectively [56].

The accuracy of first trimester Doppler echo has shown promising rates of detection for major cardiac defects when compared to subsequent second trimester echocardiography findings. In a prospective echocardiographic study involving 202 fetuses with gestational ages from 6 + 1 to 13 + 6 weeks who also had follow-up echocardiograms at 18 weeks or later, Hutchinson et al. [57] noted significant improvement in identifying cardiac anatomy at all gestational ages with the use of color Doppler mode. Thus, at 10 weeks, color Doppler imaging increased identification of the aortic and ductal arches to 58% from only 29% using 2D imaging. The authors also noted the limitation of both the ultrasound modes in visualizing pulmonary veins before 11 weeks.

While studies show increasing utility of the first trimester Doppler echo, it is not currently considered the routine standard of care. Echocardiograms performed in the first trimester, even if complete and normal appearing, should have a second trimester follow-up echo performed.

References

1. Winsberg F. Echocardiography of the fetal and newborn heart. Investig Radiol. 1972;7:152–8.
2. Ianniruberto A, Iccarino M, Deluca I et al. Analisi delle strutture cardiache fetali mediante ecografia:

nota tecnica. In: Proceedings of the 3rd Congress of SI-SUM; 1977. pp. 285–286.
3. Allan LD, Tynan M, Campbell S, et al. Echocardiographic and anatomical correlates in the fetus. Br Heart J. 1980;44:444–51.
4. Kleinman CS, Donnerstein RL, Jaffe CC, et al. Echocardiographic studies of the human fetus: prenatal diagnosis of congenital heart disease and cardiac dysrhythmias. Pediatrics. 1980;65:1059–66.
5. DeVore GR, Donnerstein RL, Kleinman CS, Hobbins JC. Real-time-directed M-mode echocardiography: a new technique for accurate and rapid quantitation of the fetal preejection period and ventricular ejection time of the right and left ventricles. Am J Obstet Gynecol. 1981;141:470–1.
6. Maulik D, Nanda NC, Saini VD. Fetal Doppler echocardiography: methods and characterization of normal and abnormal hemodynamics. Am J Cardiol. 1984;53:572–8.
7. Sklansky MS, Nelson T, Strachan M, Pretorius D. Real-time three-dimensional fetal echocardiography: initial feasibility study. J Ultrasound Med. 1999;18:745–52.
8. DeVore GR, Falkensammer P, Sklansky MS, Platt LD. Spatio-temporal image correlation (STIC): new technology for evaluation of the fetal heart. Ultrasound Obstet Gynecol. 2003;22:380–7.
9. Maulik D, Nanda NC, Singh V, Dod H, Vengala S, Sinha A, Sidhu MS, Khanna D, Lysikiewicz A, Sicuranza G, Modh N. Live three-dimensional echocardiography of the human fetus. Echocardiography. 2003;20:715–21.
10. Maulik D, Nanda NC, Moodley S, Saini VD, Thiede HA. Application of Doppler echocardiography in the assessment of fetal cardiac disease. Am J Obstet Gynecol. 1985;151:951–7.
11. Huhta JC, Smallhorn JF, Macartney FJ. Two dimensional echocardiographic diagnosis of situs. Br Heart J. 1982;48:97–102.
12. Kleinman CS, Donnerstein RL, DeVore GR, et al. Fetal echocardiography for evaluation of in utero congestive heart failure: a technique for study of nonimmune fetal hydrops. N Engl J Med. 1982;306:568–75.
13. Takahashi M, Shimada H, Yanagisawa H, Katagiri S, Kobayashi H. Fetal hemodynamics evaluated by pulsed Doppler echocardiography. J Cardiogr. 1985;15:535–42.
14. Reed KL, Sahn DJ, Scagnelli S, Anderson CF, Shenker L. Doppler echocardiographic studies of diastolic function in the human fetal heart: changes during gestation. J Am Coll Cardiol. 1986;8:391–5.
15. Arduini D, Rizzo G, Pennestri F, Romanini C. Modulation of echocardiographic parameters by fetal behavior. Prenat Diagn. 1987;7:179–84.
16. Omoto R, Yokote Y, Takamoto S, et al. The development of real time two dimensional Doppler echocardiography and its clinical significance in acquired valvular disease. Jpn Heart J. 1984;25:325–40.
17. Switzer DF, Nanda NC. Doppler color flow mapping. Ultrasound Med Biol. 1985;11:403–6.
18. Maulik D, Nanda NC, Shiung MC, Youngblood JP. Doppler color flow mapping of the fetal heart. Angiology. 1986;37:628–32.
19. Isaaz K, Thompson A, Ethevenot G, et al. Doppler echocardiographic measurement of low velocity motion of the left ventricular posterior wall. Am J Cardiol. 1989;64:66–75.
20. McDicken WN, Sutherland GR, Moran CM, Gordon LN. Colour Doppler velocity imaging of the myocardium. Ultrasound Med Biol. 1992;18:651–4.
21. Price DJA, Wallbridge DR, Stewart MJ. Tissue Doppler imaging: current and potential clinical applications. Heart. 2000;84(Suppl 2):ii11–8.
22. Smiseth OA, Stoylen A, Ihlen H. Tissue Doppler imaging for the diagnosis of coronary artery disease. Curr Opin Cardiol. 2004;19:421–9.
23. Harada K, Tsuda A, Orino T, Tanaka T, Takada G. Tissue Doppler imaging in the normal fetus. Int J Cardiol. 1999;71:227–34.
24. Tutschek B, Zimmermann T, Buck T, Bender HG. Fetal tissue Doppler echocardiography: detection rates of cardiac structures and quantitative assessment of the fetal heart. Ultrasound Obstet Gynecol. 2003;21:26–32.
25. Paladini D, Lamberti A, Teodoro A, et al. Tissue Doppler imaging of the fetal heart. Ultrasound Obstet Gynecol. 2000;2000(16):530–5.
26. American Institute of Ultrasound in Medicine. AIUM practice guideline for the performance of fetal echocardiography. J Ultrasound Med. 2013;32(6):1067–82.
27. Lee W, Allan L, Carvalho JS, Chaoui R, Copel J, Devore G, Hecher K, Munoz H, Nelson T, Paladini D, Yagel S. ISUOG fetal echocardiography task force. ISUOG consensus statement: what constitutes a fetal echocardiogram? Ultrasound Obstet Gynecol. 2008;32:239–42.
28. Donofrio MT, Moon-Grady AJ, Hornberger LK, et al. Diagnosis and treatment of fetal cardiac disease: a scientific statement from the American Heart Association. Circulation. 2014;129(21):2183–242.
29. Rudolph AM, Heymann MA, Teramo KAW, Barett CT, Raiha NCR. Studies on the circulation of the previable human fetus. Pediatr Res. 1971;5:452–63.
30. Walsh SZ, Lind J. The fetal circulation and its alteration at birth. In: Stave U, editor. Perinatal physiology. New York: Plenum; 1978. p. 128–43.
31. Kenny JF, Plappert T, Doubilet P, et al. Changes in intracardiac blood flow velocities and right and left ventricular stroke volumes with gestational age in the normal human fetus: a prospective Doppler echocardiographic study. Circulation. 1986;74:1208–16.
32. Rizzo G, Arduini D, Romanini C, Mancuso S. Doppler echocardiographic assessment of atrioventricular velocity waveforms in normal and small-for-gestational-age fetuses. Br J Obstet Gynaecol. 1988;95:65–9.
33. Romero T, Covell J, Friedman WF. A comparison of pressure-volume relations of the fetal, newborn and adult heart. Am J Phys. 1972;222:1285–90.

34. Rizzo G, Arduini D, Romanini C. Fetal cardiac and extra cardiac circulation in early gestation. J Matern Fetal Invest. 1991;1:173–9.
35. Hata T, Aoki S, Hata K, Kitao M. Intracardiac blood flow velocity waveforms in normal fetuses in utero. Am J Cardiol. 1987;59:464–8.
36. Reed KL, Anderson CF, Shenker L. Fetal pulmonary artery and aorta: two-dimensional Doppler echocardiography. Obstet Gynecol. 1987;69:175–8.
37. Tei C, Ling LH, Hodge DO, Bailey KR, Oh JK, Rodeheffer RJ, Tajik AJ, Seward JB. New index of combined systolic and diastolic myocardial performance: a simple and reproducible measure of cardiac function—A study in normals and dilated cardiomyopathy. J Cardiol. 1995;26:357–66.
38. Tsutsumi T, Ishii M, Eto G, Hota M, Kato H. Serial evaluation for myocardial performance in fetuses and neonates using a new Doppler index. Pediatr Int. 1999;4:722–7.
39. Friedman D, Buyon J, Kim M, Glickstein JS. Fetal cardiac function assessed by Doppler myocardial performance index (Tei index). Ultrasound Obstet Gynecol. 2003;21:33–6.
40. Hernandez-Andrade E, Lopez-Tenorio J, Figueroa-Diesel H, Sanin-Blair J, Carreras E, Cabero L, Gratacos E. A modified myocardial performance (Tei) index based on the use of valve clicks improves reproducibility of fetal left cardiac function assessment. Ultrasound Obstet Gynecol. 2005;26:227–32.
41. MacDonald TM, Robinson AJ, Walker SP, Hui L. Prospective longitudinal assessment of the fetal left modified myocardial performance index. J Matern Fetal Neonatal Med. 2019;32:760–7.
42. Bui YK, Kipps AK, Brook MM, Moon-Grady AJ. Tissue Doppler is more sensitive and reproducible than spectral pulsed-wave Doppler for fetal right ventricle myocardial performance index determination in normal and diabetic pregnancies. J Am Soc Echocardiogr. 2013;26:507–14.
43. Maulik D, Nanda NC. Doppler echocardiography. Part VI Fetal Doppler echocardiography. Echocardiography. 1985;2:377–91.
44. Rizzo G, Arduini D. Fetal cardiac function in intrauterine growth retardation. Am J Obstet Gynecol. 1991;165:876–82.
45. Reed KL, Meijboom EJ, Sahn DJ, et al. Cardiac Doppler flow velocities in human fetuses. Circulation. 1986;73:41–6.
46. Groenenberg IA, Hop WC, Wladimiroff JW. Doppler flow velocity waveforms in the fetal cardiac outflow tract: reproducibility of waveform recording and analysis. Ultrasound Med Biol. 1991;17:583–7.
47. Al-Ghazali W, Chita S, Chapman M, et al. Evidence of redistribution of cardiac output in asymmetrical growth retardation. Br J Obstet Gynecol. 1989;96(6):697–704.
48. Brezinka C, Stijnen T, Wladimiroff JW. Doppler flow velocity waveforms in the fetal ductus arteriosus during the first half of pregnancy: a reproducibility study. Ultrasound Obstet Gynecol. 1994;4:121–3.
49. De Smedt MC, Visser GH, Meijboom EJ. Fetal cardiac output estimated by Doppler echocardiography during mid- and late gestation. Am J Cardiol. 1987;60:338–42.
50. Mielke G, Benda N. Cardiac output and central distribution of blood flow in the human fetus. Circulation. 2001;103:1662–8.
51. Rudolph AM, Heyman MA. Circulatory changes during growth in the fetal lamb. Circ Res. 1970;26:289–308.
52. Allan LD, Chita SK, Al-Ghazali W, et al. Doppler echocardiographic evaluation of the normal human fetal heart. Br Heart J. 1987;57:528–33.
53. McBrien A, Hornberger LK. Early fetal echocardiography. Birth Defects Res. 2019;111(8):370–9.
54. Maulik D., Bennett T.L., Porter B., Babbar S., Maulik D. (2016) Doppler sonography in early pregnancy. In: Abramowicz J. (eds) First-trimester ultrasound. Springer, Cham 30(8):763–772.
55. Gembruch U, Smrcek JM. The prevalence and clinical significance of tricuspid valve regurgitation in normally grown fetuses and those with intrauterine growth retardation. Ultrasound Obstet Gynecol. 1997;9:374–82.
56. Falcon O, Faiola S, Huggon I, Allan L, Nicolaides KH. Fetal tricuspid regurgitation at the 11 + 0 to 13 + 6-week scan: association with chromosomal defects and reproducibility of the method. Ultrasound Obstet Gynecol. 2006;27:609–12.
57. Hutchinson D, McBrien A, Howley L, Yamamoto Y, Sekar P, Motan T, Jain V, Savard W, Hornberger LK. First-trimester fetal echocardiography: identification of cardiac structures for screening from 6 to 13 weeks' gestational age. J Am Soc Echocardiogr. 2017;30(8):763–72.

31 Fetal Echocardiography to Plan Postnatal Management in Fetuses with Congenital Heart Disease

Shivani M. Bhatt and Mary T. Donofrio

31.1 Introduction

Congenital heart disease (CHD) is the most common birth defect, affecting nearly 1% of all births in the United States per year [1]. Prenatal detection of fetuses with CHD has significantly increased due to advances in prenatal diagnosis with fetal echocardiography with detection rates reported as high as 95% in tertiary perinatal centers [2, 3]. There are data that suggest antenatal detection may improve postnatal preoperative risk factors and outcomes in neonates with CHD [4–6].

In the current era, fetal echocardiography is critical in the perinatal management of CHD. It allows for detailed examination of the cardiac anatomy and specific diagnosis of the congenital heart defect. Beyond providing information to guide parental counseling, fetal echocardiography enables monitoring of fetal hemodynamic changes throughout the course of gestation, risk stratification to plan for perinatal management, as well as identifying potential candidates for fetal cardiac intervention or neonates who may require immediate cardiac intervention after birth [7].

In addition to 2D cardiac imaging which is important in the anatomical evaluation of fetal CHD, Doppler echocardiography, including color flow imaging and pulsed wave Doppler, plays a crucial role in understanding the associated complex hemodynamic abnormalities. Doppler assessment during fetal echocardiographic evaluation provides information that enables risk stratification of neonates with CHD which enables providers the ability to better determine perinatal management of the fetus with CHD. In this chapter, we will focus on the use of Doppler echocardiography in risk stratification and classification of CHD in the fetus and determining postnatal management.

31.2 Fetal Circulation/Doppler Assessment Under Normal Conditions and in the Presence of CHD

During fetal life, the circulation is characterized by a parallel circuit of the left and right heart with a system of three shunts, including the ductus venosus, the foramen ovale (FO), and the ductus arteriosus (DA). The placenta serves as the site for gas exchange and oxygenated blood returns to the fetus via the umbilical vein (UV). The most highly oxygenated blood is preferentially shunted through the FO by the ductus venosus into the left heart, supplying the cerebral circulation via the ascending aorta. Deoxygenated blood returning from the fetal body combines with the

S. M. Bhatt (✉) · M. T. Donofrio (✉)
Fetal Heart Program, Division of Cardiology, Children's National Hospital, Washington, DC, USA
e-mail: smbhatt@childrensnational.org; mdonofri@childrensnational.org

D. Maulik, C. C. Lees (eds.), *Doppler Ultrasound in Obstetrics and Gynecology*,
https://doi.org/10.1007/978-3-031-06189-9_31

remainder of the umbilical venous return and is pumped by the right ventricle into the pulmonary artery. The majority of blood flow, approximately 80%, from the pulmonary artery reaches the DA and joins the descending aorta, supplying the lower body [8, 9].

After birth, there is transition to a circulation in series with separation of the right and left heart. At delivery, pulmonary vascular resistance significantly decreases with respiration as well as an increase in systemic vascular resistance after separation from the low-resistance placenta. Pulmonary venous return to the left atrium increases with subsequent increase of left atrial pressure and closure of the FO. Within the 12–72 hours of birth, the DA spontaneously closes [10, 11].

The presence of CHD may alter the fetal circulation and affect systemic oxygenation depending on the underlying lesion. A majority of congenital heart defects are well tolerated in utero due to the presence of fetal shunts that allow for redistribution of blood flow in the setting of inflow or outflow obstruction. The key determinants of postnatal hemodynamic stability in CHD include the type of CHD and whether the circulation is dependent on the patency of fetal shunts, such as the DA and/or FO, for systemic or pulmonary blood flow.

Fetal echocardiography can be used to identify those at higher risk for postnatal compromise and also plan delivery management, such as initiation of prostaglandin or need for immediate cardiac interventions. Routine Doppler examination in fetal echocardiography includes evaluation of the fetal circulatory shunts: the ductus venosus, FO, DA, as well as other fetal cardiac structures, including atrioventricular and semilunar valves, aortic arch, and pulmonary veins [12].

In the normal fetal circulation, color Doppler imaging of the FO demonstrates flow from the right atrium into the left atrium, which is always the normal direction of shunting [13]. The DA acts as a conduit for right ventricular ejection via the main pulmonary artery to the descending aorta. Color Doppler of the DA in the normal fetus demonstrates antegrade direction of flow from the main pulmonary artery to the descending aorta. Doppler flow pattern is characterized by a dominant systolic waveform with small degree of persistent forward flow in diastole (Fig. 31.1) [14]. The systolic velocity in the DA increases with gestational age [15]. A bridging connection between the UV and the

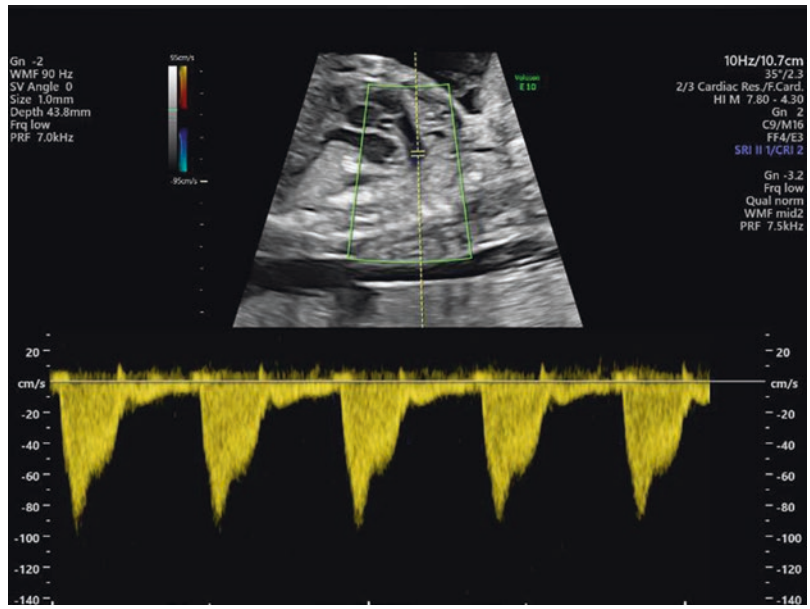

Fig. 31.1 Doppler flow pattern in DA

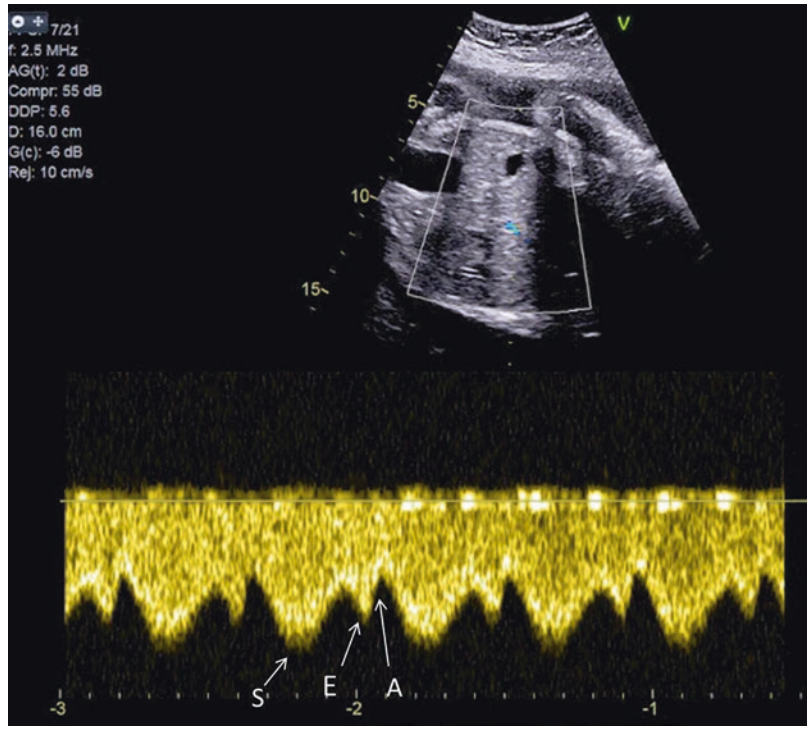

Fig. 31.2 Doppler flow pattern in normal ductus venosus

right atrium, the ductus venosus is identifiable by color flow imaging by aliasing and increased flow velocity within the body of the liver as the vessel caliber narrows at this site. Normal spectral Doppler flow pattern in the ductus venosus demonstrates all forward flow with triphasic waveform and components related to ventricular systole (S), early diastole (E), and a decrease in flow with atrial contraction (A) (Fig. 31.2) [16–19].

Doppler assessment of the atrioventricular valves provides information on the functional properties of the ventricular inflows as well as the ventricular relaxation during diastole. Color imaging assess for the presence of valvar regurgitation. Pulsed wave Doppler is performed beneath the level of the atrioventricular valve annulus. Normal waveform demonstrates two peaks, the first (E wave) represents early filling phase of diastole and the second (A wave) represents active filling which corresponds with atrial contraction. In the normal fetus, the A wave, representing atrial contraction, is dominant due to the less compliant and stiffer nature of the fetal myocardium (Fig. 31.3) [20, 21]. Doppler assessment of semilunar valves can evaluate for outflow obstruction as well as valvar insufficiency. Pulsed wave Doppler interrogation is performed at the level of the valve annulus. Color Doppler interrogation is used to evaluate forward flow through the aortic arch into the descending aorta [12].

Color flow imaging is used to identify the pulmonary veins which carry venous return from the lungs to the left atrium. Normal pulsed wave Doppler interrogation of the pulmonary veins demonstrates a triphasic waveform that corresponds with systole (S wave), early diastole (D wave), and atrial contraction (A wave). There is normally forward flow of the S wave and D wave into the left atrium, with dominance of the S wave. The A wave flow may be reversed during early gestation, but progressively becomes more antegrade as pulmonary blood flow increased during gestation (Fig. 31.4) [22].

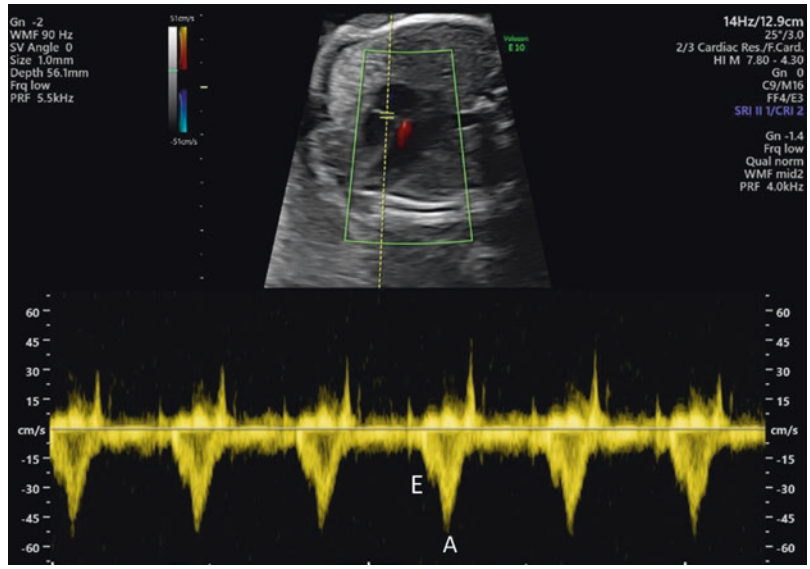

Fig. 31.3 Doppler tracing of flow across the tricuspid valve with normal double-peak inflow pattern. Early diastolic (E wave) and atrial contraction diastolic flow (A wave)

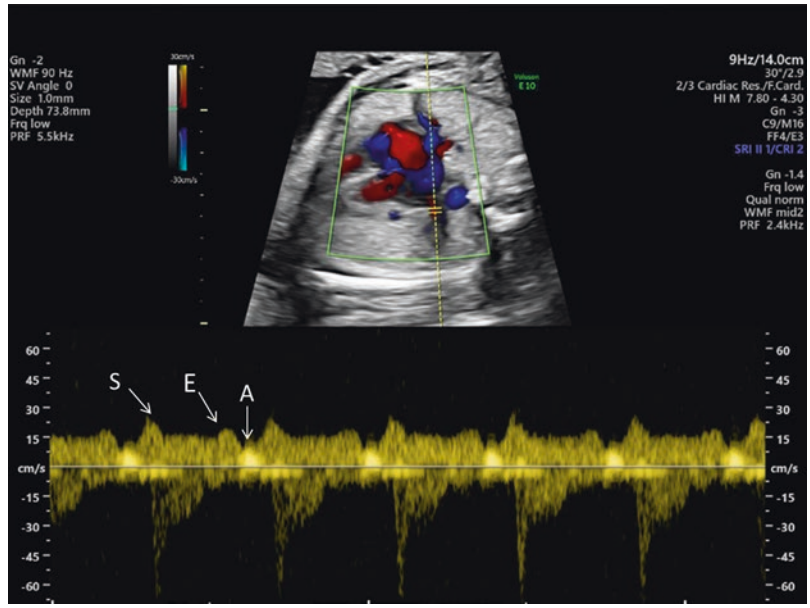

Fig. 31.4 Pulmonary vein Doppler flow tracing with triphasic pattern consisting of a systolic (S), early diastolic (E), and atrial contraction (A) waves

31.3 Doppler in Fetal Echocardiography to Risk Stratify and Plan Postnatal Management

The American Heart Association statement on the Diagnosis and Treatment of Fetal Cardiac Disease has presented a protocol on the use of fetal echocardiography to allow risk stratification of fetuses with a prenatal diagnosis of CHD in the perinatal period and delivery room. Classification is based on the degree of severity and level of postnatal care required with four categories ranging from minimal risk of hemodynamic compromise at birth to high risk requiring immediate specialized care and possible intervention [7].

31.4 Low-Risk CHD

Low-risk congenital heart defects include are expected to be hemodynamically stable at birth and can generally require cardiology consultation with confirmation of the diagnosis with outpatient follow-up. Examples include ventricular or atrial septal defects, atrioventricular septal defects and mild valve abnormalities with preserved ventricular function.

31.4.1 Shunt Lesions

Doppler echocardiography is important in the assessment of shunt lesions, such as atrial septal defects (ASDs) and ventricular septal defects (VSDs). VSDs are among the most common of congenital heart defects. 2D as well as color Doppler imaging of the ventricular septum in different planes is an essential component in identifying the presence of VSDs. The ventricular septum should be assessed in the four-chamber view at the level of the atrioventricular valves, at the level of the outflows as well as in the short-axis views. In order to confirm diagnosis of VSD, it should be visualized in two different orthogonal views. Color Doppler imaging may demonstrate flow in the region of the defect with bidirectional flow. However, given that the pressures in both ventricles are equal in the fetal circulation, Color Doppler imaging will usually not demonstrate a high velocity shunt, so it may be necessary to reduce the PRF or color scale to better visualize flow. Color Doppler echocardiography can be useful in the diagnosis of small VSDs that are not appreciable on 2D imaging. Small defects detectable only by Color Doppler imaging have been shown to have a high rate of spontaneous closure during gestation or in the postnatal period (Fig. 31.5) [23].

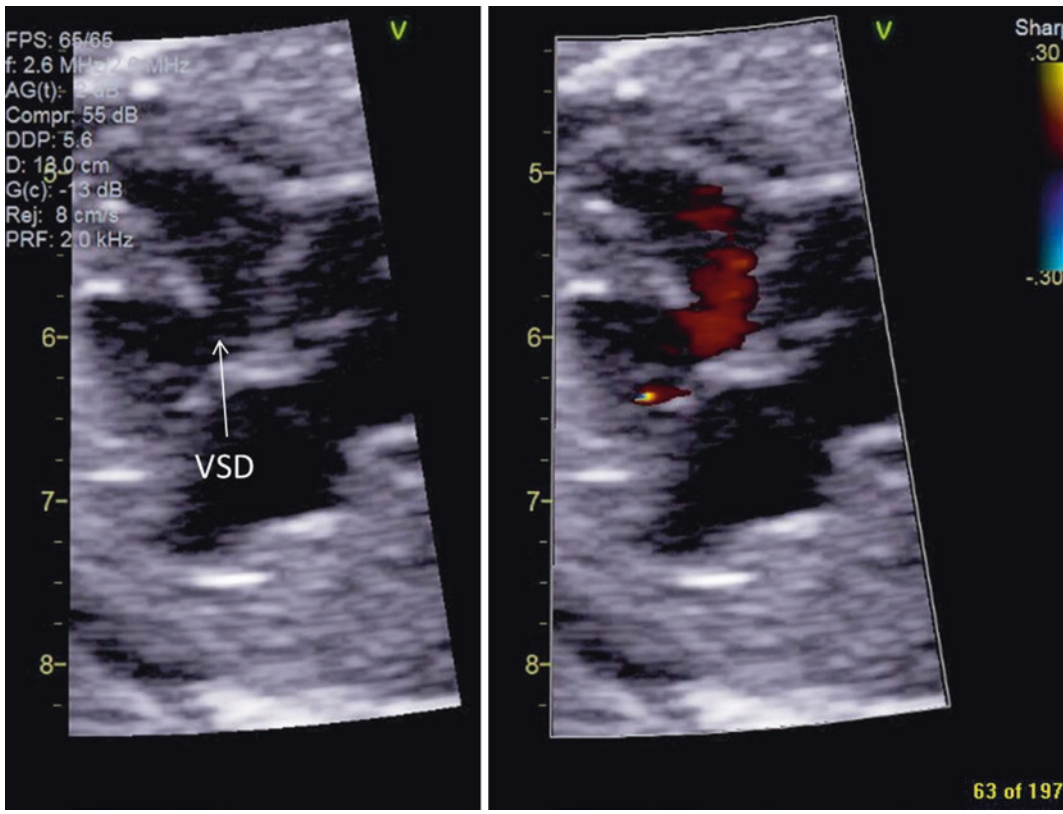

Fig. 31.5 2D and color Doppler four-chamber view demonstrating VSD with shunting across the ventricular septum

Atrial septal defects can be challenging to diagnose in the fetus due to the presence of the normal FO shunt across the atrial septum. In the absence of other associated fetal cardiac defects, an isolated ASD typically does not have a significant hemodynamic impact on fetal physiology. 2D imaging of the atrial septum is important to assess for larger deficiency of the atrial septum than normal or in a region other than that of the typically location of the FO. Color Doppler imaging will demonstrate right to left shunting across the defect in the normal fetus. Given the difficult nature of reliably identifying size and location of ASDs prenatally, postnatal echocardiography is recommended if there is a prenatal suspicion.

Common atrioventricular canal defects (CAVCs) represent a spectrum of more complex shunt lesions that generally consist of atrial and ventricular septal deficiency resulting from abnormal embryological development of structures from the endocardial cushions. There is a common inlet or AV valve into both ventricles and defect in the atrioventricular septum that can result in an ASD and VSD, an isolated ASD, or an exclusive VSD. In addition to 2D evaluation of the atrioventricular septum, Color Doppler imaging is used to identify the location and degree of shunting, which is generally right to left at the atrial level and bidirectional at the ventricular level. In addition, it is important to assess the degree of regurgitation of the common atrioventricular valve which is by definition an abnormal valve.

31.4.2 Valve Abnormalities

Mild abnormalities of the atrioventricular or semilunar valves are another form of low-risk CHD that can be identified using Doppler echocardiography. Color Doppler assessment of the valves is important to evaluate for regurgitation. Doppler interrogation is performed at the level of the semilunar valve to assess flow pattern across the outflow and evaluate for turbulent non-laminar flow and/or increased flow velocity that may indicate stenosis. In cases of atrioventricular valve stenosis, in addition to small 2D measurement of the valve, Color Doppler imaging may demonstrate a narrow swath of color entering the ventricular cavity and Doppler interrogation may demonstrate a single peak inflow pattern. Mild valvar stenosis or regurgitation can progress throughout the course of gestation; therefore, serial echocardiographic monitoring is indicated if mild abnormalities are identified.

31.5 Minimal-Risk CHD

Minimal-risk congenital heart defects include those that require patency of the DA to maintain systemic or pulmonary output after birth, such as structural defects with severe systemic or pulmonary outflow tract obstruction or atresia. For these defects, initiation of prostaglandin E1 (PGE) is required after birth to ensure ductal patency. Delivery room care includes establishment of intravenous access, administration of PGE, and transport to a cardiac center often under the supervision of a neonatologist. Fetal echocardiography using color Doppler can predict the presence of postnatal ductal-dependent CHD enabling the initiation of PGE infusion at delivery and lowering the risk of compromise after birth [24].

31.5.1 Pulmonary Obstruction

Doppler echocardiography plays a critical role in determining the presence of ductal-dependent pulmonary circulation in various types of CHD, such as pulmonary stenosis or atresia, tetralogy of Fallot, and tricuspid valve stenosis or atresia with or without a VSD [25]. Reversed flow in the DA with aortic to pulmonary shunting on Doppler echocardiography is a predictive feature of ductal-dependent pulmonary circulation after delivery [26, 27].

In tetralogy of Fallot, the most common cyanotic CHD, delivery plan is based on pre-

diction of significant cyanosis after ductal closure in order to determine if PGE will be required to main ductal patency to ensure adequate pulmonary blood flow after birth. Color and pulse Doppler echocardiography to determine the presence of retrograde flow in the DA (aorta to pulmonary) have been shown to predict the need for PGE and neonatal surgical intervention in fetuses with tetralogy of Fallot with high sensitivity and specificity (Fig. 31.6) [24, 28].

31.5.1.1 Systemic Outflow Obstruction

Serial assessment on fetal echocardiography can also help determine postnatal ductal-dependent systemic circulation in CHD with systemic outflow obstruction, including mitral stenosis, aortic stenosis, coarctation of the aorta, or hypoplastic left heart syndrome (HLHS) [25].

The prenatal diagnosis of coarctation of the aorta can be challenging. In the fetal circulation, the aortic isthmus is a relatively small structure in comparison to a large DA as only approximately 10% of fetal cardiac output traverses the aortic isthmus [29]. Severe forms of coarctation are ductal-dependent systemic flow lesions and require the initiation of PGE after birth. 2D fetal echocardiographic parameters for prenatal diagnosis of coarctation include assessment for the presence of left ventricular/right ventricular size discrepancy using mitral to aortic and aortic to pulmonary valve ratios of less than 0.6 [30]. The relative size of the aortic isthmus and DA in the 3-vessel view with isthmal to ductal ratio of less than 0.75 and aortic isthmus Z score of less than

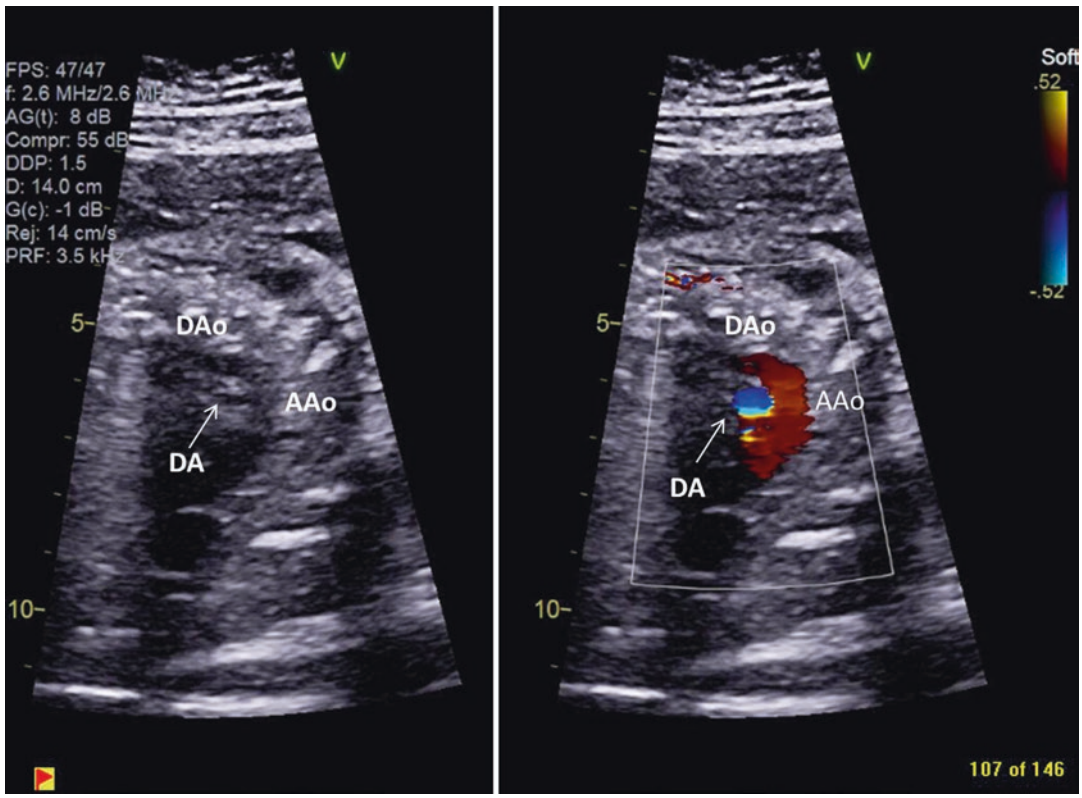

Fig. 31.6 2D and color Doppler imaging of sagittal view of aortic and ductal arch in a fetus with tetralogy of Fallot. Color Doppler demonstrates reversed flow in the DA (blue). *DA* Ductus arteriosus, *AAo* ascending aorta, *DAo* descending aorta

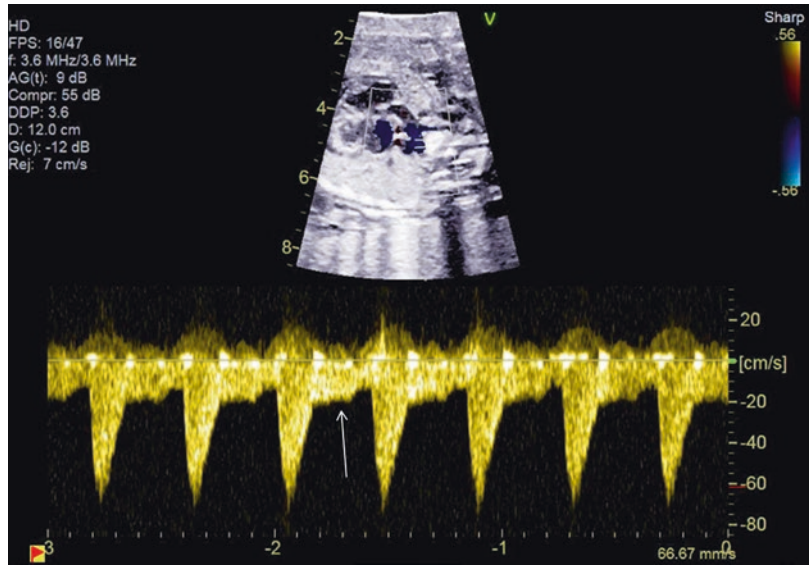

Fig. 31.7 Abnormal Pulse wave Doppler flow pattern of the aortic isthmus in coarctation of the aorta showing continuous forward flow in diastole (arrow)

−2 have also been shown to be sensitive indicators of fetal coarctation [31, 32]. In the setting of fetal coarctation, Color Doppler imaging may demonstrate turbulent flow in the region of a posterior shelf or hypoplastic aortic isthmus. Pulsed wave Doppler interrogation of flow in the aortic isthmus will often demonstrate an abnormal Doppler flow pattern characterized by persistence of forward flow in diastole (Fig. 31.7) [24, 33].

Hypoplastic left heart syndrome is characterized by hypoplasia of the left-sided heart structures resulting in a left ventricle that is inadequate to provide systemic output. For this reason, an adequate interatrial communication (FO) and DA is required to maintain the systemic circulation. Doppler echocardiography is important in distinguishing between hypoplastic left ventricle that is inadequate to support systemic output, such as in HLHS, versus borderline small but adequate left ventricle. Color Doppler imaging in HLHS demonstrates reversal of blood flow across the FO with left to right shunting across from left atrium to right atrium [34, 35]. In addition, there will be retrograde systolic flow in the aortic isthmus and most often distal transverse arch due to perfusion of the aortic arch via the DA (Fig. 31.8) [34, 35]. For these defects, a PGE infusion is needed to keep the DA open after delivery.

31.6 High-Risk CHD

High-risk CHD includes those CHD that require immediate intervention in the delivery room for stabilization, with most requiring urgent cardiac interventions soon after birth. Interventions include cardiac catheterization procedures, such as balloon atrial septostomy (BAS), urgent cardiac surgery, or initiation of extracorporeal membrane oxygenation (ECMO). Therefore, in these cases it is recommended that a delivery is planned at a tertiary hospital with immediate access to neonatology and cardiology services or immediate planned transfer to a pediatric center with cardiology services after initial stabilization. Delivery planning in high-risk CHD often involves multidisciplinary care team, including obstetrics, maternal fetal medicine, neonatology, cardiology, and cardiac surgery, due to possibility of cardiac intervention required in the immediate postnatal period.

31.6.1 CHD Dependent on FO Patency

A restrictive or intact atrial septum can result in obstruction to pulmonary venous egress in HLHS and lead to hemodynamic compromise after birth.

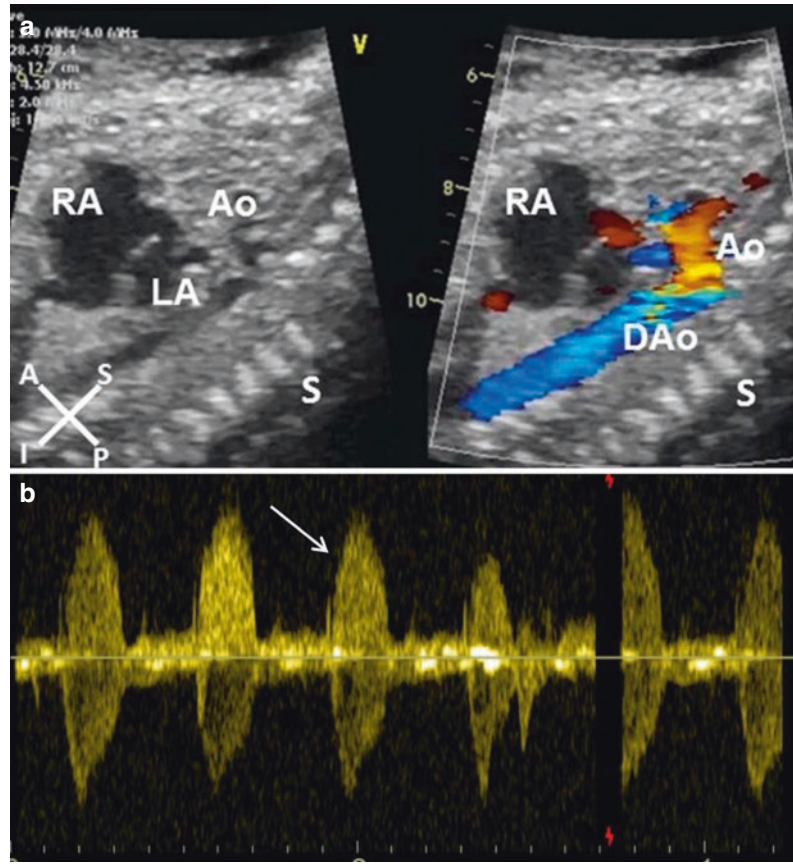

Fig. 31.8 (**a**) 2D and color Doppler imaging of sagittal view of the aortic arch in a fetus with HLHS. Color Doppler demonstrates reversed flow in the transverse aortic arch (red). *TAo* transverse aortic arch, *DAo* descending aorta. (**b**) Spectral Doppler demonstrating reversed flow in the TAo (arrow)

Urgent BAS to open the atrial septum and allow for left atrial egress of pulmonary venous flow is required in newborns with HLHS and an inadequate atrial communication [36]. Assessment of pulmonary vein flow using Doppler is used to predict need for immediate cardiac intervention after birth in these patients. In the setting of HLHS with restrictive or intact atrial septum, a pulmonary venous Doppler flow pattern characterized by greater reversal of flow with atrial contraction relative to forward flow as compared to HLHS with an unrestrictive atrial septum. The ratio of the forward to reversed velocity time integral of flow on pulsed wave Doppler interrogation of the pulmonary veins that is less than 3 has been shown to be a marker of severe obstruction to pulmonary venous egress and is predictive of increased risk of need for immediate intervention after birth (Fig. 31.9) [24, 37, 38].

Maternal hyperoxygenation testing can be used during the third trimester to elicit an increase in fetal pulmonary blood flow and allows for assessment of pulmonary vasoreactivity [39–41]. Lack of pulmonary vasoreactivity is determined by pulsed wave Doppler assessment of the proximal pulmonary arteries prior to and after the administration of maternal oxygen and has been associated with need for atrial septoplasty for a restrictive atrial septum in HLHS [39]. Increased diastolic flow in the pulmonary arteries compared to baseline administration of maternal oxygen is a marker of pulmonary vasoreactivity. Pulmonary vasoreactivity is measured using the pulsatility index (PI) [(peak systolic velocity-end-diastolic velocity)/mean velocity] of the pulmonary artery and an adequate response is considered a greater than 10% decrease in the PI with maternal hyperoxygenation (Fig. 31.10) [39, 40].

Newborns with D-transposition of the great arteries (D-TGA) and restrictive FO and/or restrictive DA are also at risk for postnatal compromise due to severe hypoxemia and acidosis

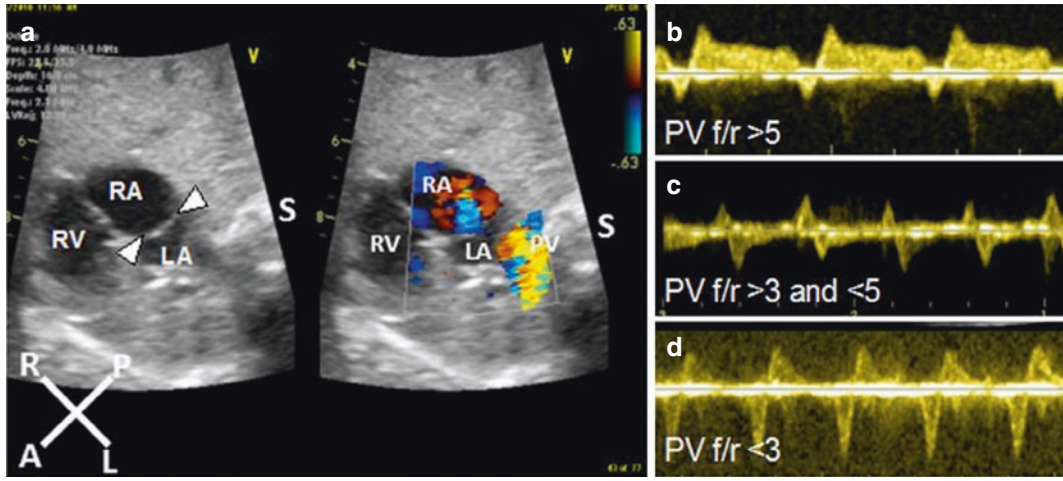

Fig. 31.9 Four-chamber view in a fetus with HLHS demonstrating restrictive atrial septum by 2D imaging. (**a**) Pulse wave Doppler interrogation of pulmonary vein (PV) flow in a fetus with HLHS. PV flow with f/r ratio > 5. (**b**) PV flow with f/r ratio > 3 and < 5. (**c**) PV flow with f/r ratio < 3 suggesting atrial level restriction. *PV* pulmonary vein, *f/r ratio* ratio of velocity-time integral forward/reversed flow of the pulmonary vein, *f* forward, *r* reversed

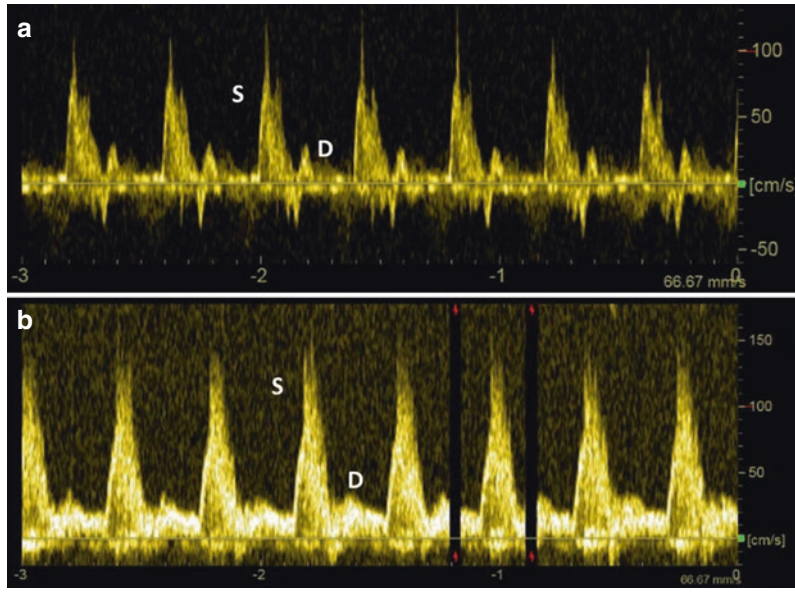

Fig. 31.10 Maternal hyperoxygenation testing in a fetus with HLHS in the third trimester. (**a**) Pulse wave Doppler of the proximal branch pulmonary artery at baseline while the mother breathes room air. (**b**) Pulse wave Doppler of the same proximal branch pulmonary artery during maternal hyperoxygenation via administration of oxygen via non-breather face mask. As compared to baseline, diastolic flow in the pulmonary artery is increased with maternal hyperoxygenation. *D* diastole, *s* systole

from limited mixing between parallel circulations [42]. Immediate cardiac intervention with BAS after birth is required in the setting of inadequate atrial communication in D-TGA. Serial evaluation of the atrial septum throughout gestation with fetal echocardiography can aid in predicting the need for urgent BAS although the predictive value is overall low [24]. Abnormal

anatomy of the atrial septum, such as hypermobile or tethered septum primum, can be observed on 2D imaging of the atrial septum. There may also be a bowing appearance or entirely intact atrial septum [43, 44]. Color Doppler imaging can be used to further assess the size of the atrial communication. An abnormal DA may also be observed in conjunction with inadequate atrial communication. The DA may be small, or in rare cases absent. Color and pulse Doppler evaluation of the DA may demonstrate bidirectional or reversal of flow (Fig. 31.11) [43, 45, 46]. Currently, prediction of need for BAS is limited by fetal echocardiography and close to half of neonates with D-TGA will require a BAS in the immediate postnatal period [24, 47, 48]. Therefore, neonates with D-TGA are considered to be high risk as immediate cardiac interventions will likely be required [7].

31.6.2 CHD Resulting in Diminished Systemic Perfusion

Ebstein's anomaly of the tricuspid valve and tricuspid valve dysplasia (EA/TVD) consist of a spectrum of abnormal tricuspid valve architecture often with grossly malformed or rudimentary leaflets. Tricuspid valve function is abnormal and can result in severe tricuspid valve regurgitation, visualized using color Doppler, which leads to massive cardiomegaly, hydrops, diminished ventricular function, arrhythmia, and even in utero demise in the fetus [49]. In cases of severe EA/TVD, perinatal mortality is very high, reported as up to 45% and the five-year survival is less than a 50% [50, 51]. In addition to early gestational age at diagnosis (<32 weeks), fetal echocardiographic predictors of increased risk of perinatal mortality in EA/TVD have been identi-

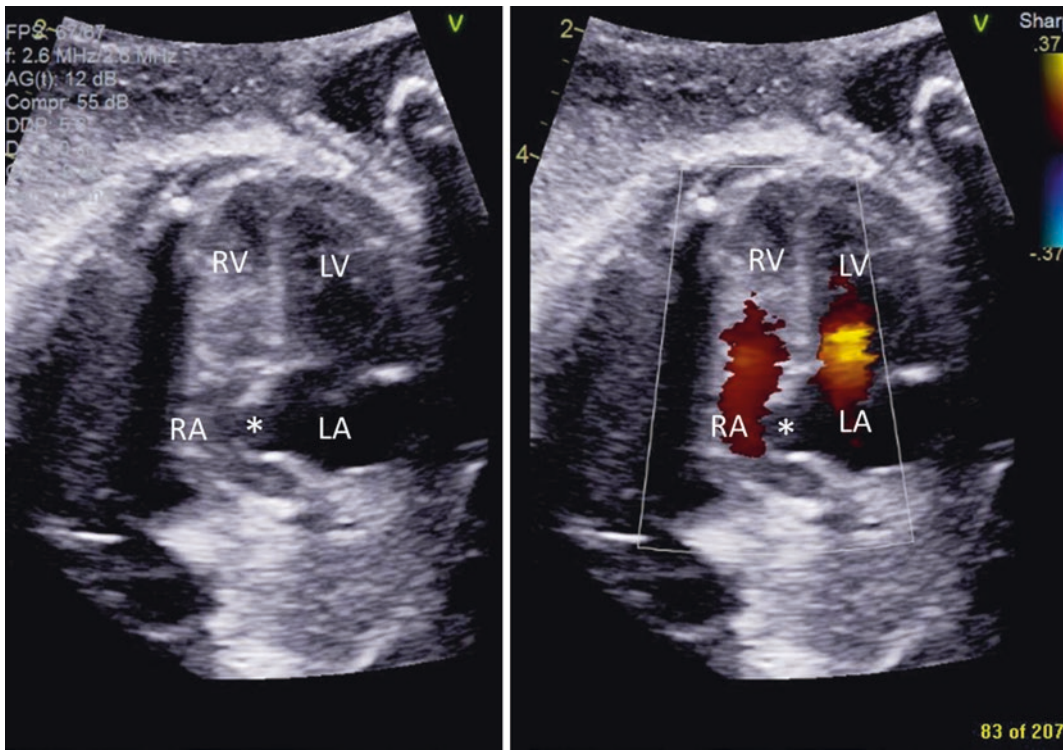

Fig. 31.11 2D and color Doppler imaging of four-chamber view of a fetus with D-transposition of the great arteries and restrictive atrial septum. The atrial septum (asterisk) has a bowing appearance and there is no evidence of shunting across on color Doppler imaging

fied in a large multicenter study of over 200 fetuses [50]. The identified markers on 2D imaging include a dilated tricuspid valve annulus, cardiomegaly as measured by a larger cardiothoracic area ratio, pericardial effusion, and diminished left ventricular function [50]. Predictors identified on Color Doppler imaging include the presence of pulmonary valve regurgitation, lack of antegrade flow across the pulmonary valve (functional pulmonary atresia), and low tricuspid regurgitation jet velocity (Fig. 31.12) [50]. Serial echocardiographic evaluation is required to monitor for progression and assess risk of in utero compromise due to hydrops, ventricular dysfunction, or arrhythmia as well as poor perinatal outcome.

Tetralogy of Fallot with Absent Pulmonary Valve (TOF/APV) is characterized by the lack of a functional pulmonary valve with rudimentary leaflets that results in pulmonary insufficiency and stenosis. This results in severe dilation of the pulmonary arteries and right-sided volume overload and failure. The risk of in utero demise is close to 50% due to heart failure and fetal hydrops [52, 53]. Abnormal dilation of the pulmonary arteries is associated with compression of the airways and lung abnormalities. Therefore, there is also high perinatal morbidity and mortality due to severe hypoxia [54]. The DA is typically absent in fetuses with TOF/APV [55].

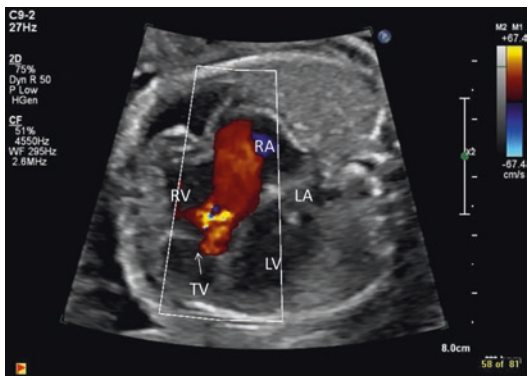

Fig. 31.12 Four-chamber view with color Doppler of tricuspid valve in Ebstein's anomaly of the tricuspid valve. There is apical displacement of the tricuspid valve (arrow) with severe tricuspid regurgitation (red). *RA* right atrium, *RV* right ventricle, *TV* tricuspid valve, *LA* left atrium, *LV* left ventricle

Fetal echocardiography has largely been unsuccessful in identifying prenatal predictors of outcomes in fetuses with TOF/APV. There are mixed results in the literature regarding the ability of fetal echocardiographic parameters, such as pulmonary valve annulus, pulmonary artery size, as well as aortic to pulmonary valve annulus to accurately predict postnatal clinical outcomes [54, 56]. There has been some evidence that Fetal MRI may add important prognostic information in these patients. Lung abnormalities on fetal MRI in fetuses with TOF/APV have been associated with worse postnatal outcomes and therefore can be used in conjunction with fetal echocardiography in risk stratification and delivery planning [57, 58].

Given the high risk of in utero demise as well as perinatal compromise close serial monitoring is warranted for development of cardiac failure and hydrops. Delivery at a center with multidisciplinary team, including neonatologist, cardiologist, and cardiothoracic surgery, is often necessary due to potential need for cardiopulmonary support and stabilization [7]. After birth, respiratory distress may necessitate mechanical ventilation and prone positioning may help improve respiratory status. Given the lack of a DA in this disease, prostaglandin infusion is typically not beneficial. Measures to decrease pulmonary vascular resistance, such as inhaled nitric oxide and supplemental 100% oxygen, may be employed to promote antegrade pulmonary blood flow. In severe cases, ECMO may be implemented for cardiopulmonary support.

Total anomalous pulmonary venous return (TAPVR) with obstruction is a rare and high risk type of CHD that can lead to pulmonary venous congestion and severe hypoxemia in the postnatal period. Prenatal diagnosis and detection of obstruction in TAPVR are important for delivery planning as immediate intervention for stabilization and early cardiac surgery is often required. TAPVR can be challenging to diagnose in the fetus. Lack of identification of at least 2 pulmonary veins connecting normally to the left atrium by 2D and Color Doppler imaging and the presence of a posterior venous confluence or abnormal 3-vessel view with an enlarged SVC or vertical vein suggest possible TAPVR. Doppler echocar-

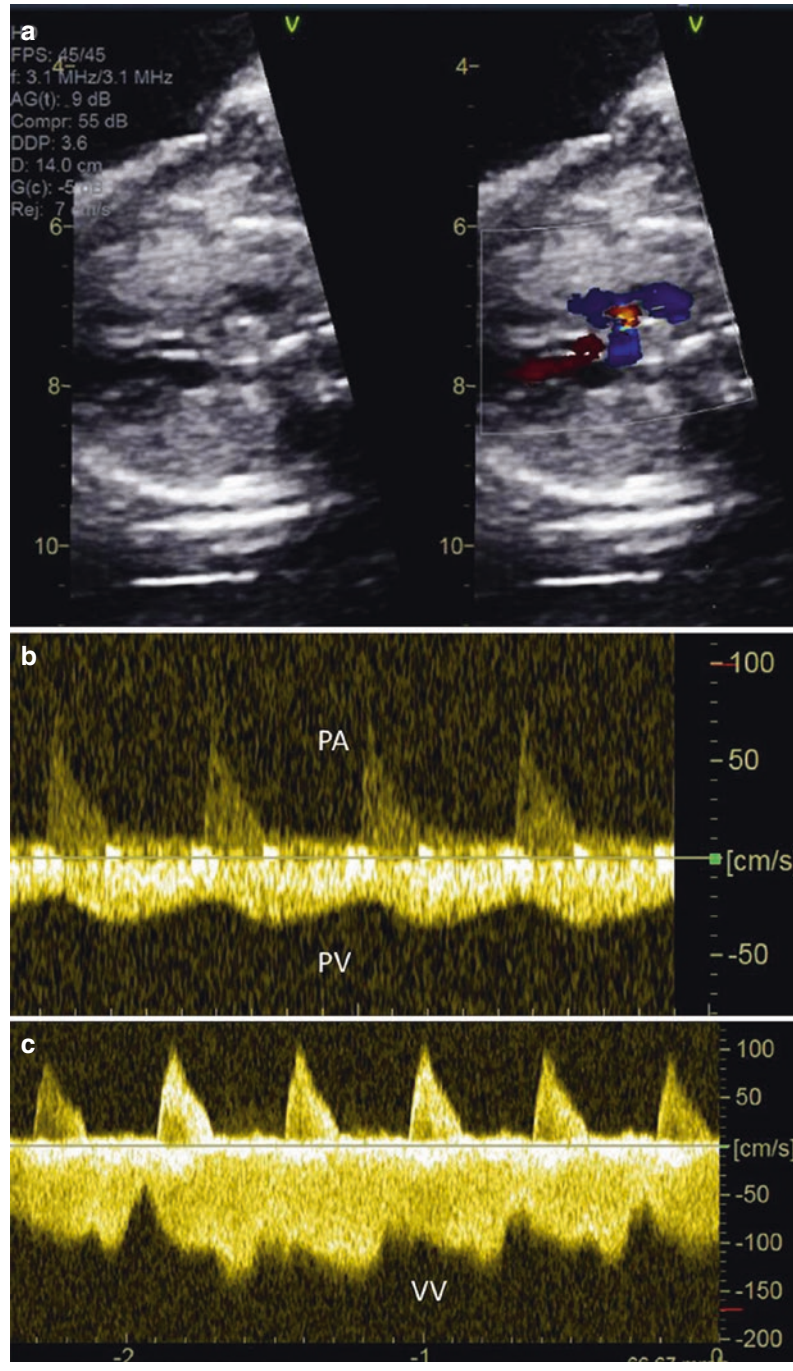

Fig. 31.13 (**a**) 2D and color Doppler of a fetus with total anomalous pulmonary venous return (TAPVR), supracardiac type. The pulmonary veins drain to a vertical vein (VV) that drains to the superior vena cava (SVC). Color Doppler imaging demonstrates aliasing in the VV. (**b**) Spectral Doppler waveform of pulmonary venous flow in a fetus with supracardiac TAPVR. (**c**) Spectral Doppler waveform of the vertical vein draining into the SVC shows high velocity continuous flow suggesting obstruction

diography is used to evaluate the flow pattern in the pulmonary veins and assess for obstruction. In cases of TAPVR with obstruction, pulmonary vein Doppler waveform will be abnormal with loss of phasic pattern and non-pulsatile, high-velocity, mono-phasic flow (Fig. 31.13) [59]. If TAPVR with obstruction is identified, delivery at a cardiac center or in close proximity with plan for urgent intervention, such as cardiac surgery or catheter-based procedure, is recommended.

References

1. Hoffman JI, Kaplan S. The incidence of congenital heart disease. J Am Coll Cardiol. 2002;39(12):1890–900. https://doi.org/10.1016/s0735-1097(02)01886-7.
2. Yagel S, Weissman A, Rotstein Z, Manor M, Hegesh J, Anteby E, Lipitz S, Achiron R. Congenital heart defects: natural course and in utero development. Circulation. 1997;96(2):550–5. https://doi.org/10.1161/01.cir.96.2.550.
3. Stumpflen I, Stumpflen A, Wimmer M, Bernaschek G. Effect of detailed fetal echocardiography as part of routine prenatal ultrasonographic screening on detection of congenital heart disease. Lancet. 1996;348(9031):854–7. https://doi.org/10.1016/S0140-6736(96)04069-X.
4. Bonnet D, Coltri A, Butera G, Fermont L, Le Bidois J, Kachaner J, Sidi D. Detection of transposition of the great arteries in fetuses reduces neonatal morbidity and mortality. Circulation. 1999;99(7):916–8. https://doi.org/10.1161/01.cir.99.7.916.
5. Franklin O, Burch M, Manning N, Sleeman K, Gould S, Archer N. Prenatal diagnosis of coarctation of the aorta improves survival and reduces morbidity. Heart. 2002;87(1):67–9. https://doi.org/10.1136/heart.87.1.67.
6. Levey A, Glickstein JS, Kleinman CS, Levasseur SM, Chen J, Gersony WM, Williams IA. The impact of prenatal diagnosis of complex congenital heart disease on neonatal outcomes. Pediatr Cardiol. 2010;31(5):587–97. https://doi.org/10.1007/s00246-010-9648-2.
7. Donofrio MT, Moon-Grady AJ, Hornberger LK, Copel JA, Sklansky MS, Abuhamad A, Cuneo BF, Huhta JC, Jonas RA, Krishnan A, Lacey S, Lee W, Michelfelder EC Sr, Rempel GR, Silverman NH, Spray TL, Strasburger JF, Tworetzky W, Rychik J, American Heart Association Adults With Congenital Heart Disease Joint Committee of the Council on Cardiovascular Disease in the Y, Council on Clinical Cardiology CoCS, Anesthesia, Council on C, Stroke N. Diagnosis and treatment of fetal cardiac disease: a scientific statement from the American Heart Association. Circulation. 2014;129(21):2183–242. https://doi.org/10.1161/01.cir.0000437597.44550.5d.
8. Kiserud T. Physiology of the fetal circulation. Semin Fetal Neonatal Med. 2005;10(6):493–503. https://doi.org/10.1016/j.siny.2005.08.007.
9. Rudolph AM. Congenital diseases of the heart: clinical-physiological considerations. 3rd ed. Wiley-Blackwell: Chichester/Hoboken, NJ; 2009.
10. Rudolph AM. Fetal and neonatal pulmonary circulation. Annu Rev Physiol. 1979;41:383–95. https://doi.org/10.1146/annurev.ph.41.030179.002123.
11. Gentile R, Stevenson G, Dooley T, Franklin D, Kawabori I, Pearlman A. Pulsed Doppler echocardiographic determination of time of ductal closure in normal newborn infants. J Pediatr. 1981;98(3):443–8. https://doi.org/10.1016/s0022-3476(81)80719-6.
12. Rychik J, Ayres N, Cuneo B, Gotteiner N, Hornberger L, Spevak PJ, Van Der Veld M. American Society of Echocardiography guidelines and standards for performance of the fetal echocardiogram. J Am Soc Echocardiogr. 2004;17(7):803–10. https://doi.org/10.1016/j.echo.2004.04.011.
13. Atkins DL, Clark EB, Marvin WJ Jr. Foramen ovale/atrial septum area ratio: a marker of transatrial blood flow. Circulation. 1982;66(2):281–3. https://doi.org/10.1161/01.cir.66.2.281.
14. Mielke G, Benda N. Blood flow velocity waveforms of the fetal pulmonary artery and the ductus arteriosus: reference ranges from 13 weeks to term. Ultrasound Obstet Gynecol. 2000;15(3):213–8. https://doi.org/10.1046/j.1469-0705.2000.00082.x.
15. Huhta JC, Moise KJ, Fisher DJ, Sharif DS, Wasserstrum N, Martin C. Detection and quantitation of constriction of the fetal ductus arteriosus by Doppler echocardiography. Circulation. 1987;75(2):406–12. https://doi.org/10.1161/01.cir.75.2.406.
16. Kiserud T. The ductus venosus. Semin Perinatol. 2001;25(1):11–20.
17. Kiserud T, Eik-Nes SH, Blaas HG, Hellevik LR. Ultrasonographic velocimetry of the fetal ductus venosus. Lancet. 1991;338(8780):1412–4. https://doi.org/10.1016/0140-6736(91)92720-m.
18. Kessler J, Rasmussen S, Hanson M, Kiserud T. Longitudinal reference ranges for ductus venosus flow velocities and waveform indices. Ultrasound Obstet Gynecol. 2006;28(7):890–8. https://doi.org/10.1002/uog.3857.
19. Huisman TW, Stewart PA, Wladimiroff JW. Ductus venosus blood flow velocity waveforms in the human fetus—a Doppler study. Ultrasound Med Biol. 1992;18(1):33–7.
20. Reed KL, Meijboom EJ, Sahn DJ, Scagnelli SA, Valdes-Cruz LM, Shenker L. Cardiac Doppler flow velocities in human fetuses. Circulation. 1986;73(1):41–6. https://doi.org/10.1161/01.cir.73.1.41.
21. Szwast A, Rychik J. Current concepts in fetal cardiovascular disease. Clin Perinatol. 2005;32(4):857-875:viii. https://doi.org/10.1016/j.clp.2005.09.012.
22. Lenz F, Chaoui R. Reference ranges for Doppler-assessed pulmonary venous blood flow velocities and pulsatility indices in normal human fetuses. Prenat Diagn. 2002;22(9):786–91. https://doi.org/10.1002/pd.410.
23. Axt-Fliedner R, Schwarze A, Smrcek J, Germer U, Krapp M, Gembruch U. Isolated ventricular septal defects detected by color Doppler imaging: evolution during fetal and first year of postnatal life. Ultrasound Obstet Gynecol. 2006;27(3):266–73. https://doi.org/10.1002/uog.2716.
24. Donofrio MT, Skurow-Todd K, Berger JT, McCarter R, Fulgium A, Krishnan A, Sable CA. Risk-stratified postnatal care of newborns with congenital heart disease determined by fetal echocardiography. J Am

Soc Echocardiogr. 2015;28(11):1339–49. https://doi.org/10.1016/j.echo.2015.07.005.
25. Sanapo L, Pruetz JD, Slodki M, Goens MB, Moon-Grady AJ, Donofrio MT. Fetal echocardiography for planning perinatal and delivery room care of neonates with congenital heart disease. Echocardiography. 2017;34(12):1804–21. https://doi.org/10.1111/echo.13672.
26. Quartermain MD, Glatz AC, Goldberg DJ, Cohen MS, Elias MD, Tian Z, Rychik J. Pulmonary outflow tract obstruction in fetuses with complex congenital heart disease: predicting the need for neonatal intervention. Ultrasound Obstet Gynecol. 2013;41(1):47–53. https://doi.org/10.1002/uog.11196.
27. Hornberger LK, Sanders SP, Sahn DJ, Rice MJ, Spevak PJ, Benacerraf BR, McDonald RW, Colan SD. In utero pulmonary artery and aortic growth and potential for progression of pulmonary outflow tract obstruction in tetralogy of Fallot. J Am Coll Cardiol. 1995;25(3):739–45. https://doi.org/10.1016/0735-1097(94)00422-M.
28. Arya B, Levasseur SM, Woldu K, Glickstein JS, Andrews HF, Williams IA. Fetal echocardiographic measurements and the need for neonatal surgical intervention in Tetralogy of Fallot. Pediatr Cardiol. 2014;35(5):810–6. https://doi.org/10.1007/s00246-013-0857-3.
29. Rudolph AM. Congenital cardiovascular malformations and the fetal circulation. Arch Dis Child Fetal Neonatal Ed. 2010;95(2):F132–6. https://doi.org/10.1136/adc.2007.128777.
30. Quartermain MD, Cohen MS, Dominguez TE, Tian Z, Donaghue DD, Rychik J. Left ventricle to right ventricle size discrepancy in the fetus: the presence of critical congenital heart disease can be reliably predicted. J Am Soc Echocardiogr. 2009;22(11):1296–301. https://doi.org/10.1016/j.echo.2009.08.008.
31. Matsui H, Mellander M, Roughton M, Jicinska H, Gardiner HM. Morphological and physiological predictors of fetal aortic coarctation. Circulation. 2008;118(18):1793–801. https://doi.org/10.1161/CIRCULATIONAHA.108.787598.
32. Pasquini L, Mellander M, Seale A, Matsui H, Roughton M, Ho SY, Gardiner HM. Z-scores of the fetal aortic isthmus and duct: an aid to assessing arch hypoplasia. Ultrasound Obstet Gynecol. 2007;29(6):628–33. https://doi.org/10.1002/uog.4021.
33. Beattie M, Peyvandi S, Ganesan S, Moon-Grady A. Toward improving the fetal diagnosis of coarctation of the aorta. Pediatr Cardiol. 2017;38(2):344–52. https://doi.org/10.1007/s00246-016-1520-6.
34. Makikallio K, McElhinney DB, Levine JC, Marx GR, Colan SD, Marshall AC, Lock JE, Marcus EN, Tworetzky W. Fetal aortic valve stenosis and the evolution of hypoplastic left heart syndrome: patient selection for fetal intervention. Circulation. 2006;113(11):1401–5. https://doi.org/10.1161/CIRCULATIONAHA.105.588194.
35. Berning RA, Silverman NH, Villegas M, Sahn DJ, Martin GR, Rice MJ. Reversed shunting across the ductus arteriosus or atrial septum in utero heralds severe congenital heart disease. J Am Coll Cardiol. 1996;27(2):481–6. https://doi.org/10.1016/0735-1097(95)00446-7.
36. Sathanandam SK, Philip R, Gamboa D, Van Bergen A, Ilbawi MN, Knott-Craig C, Waller BR, Javois AJ, Cuneo BF. Management of hypoplastic left heart syndrome with intact atrial septum: a two-centre experience. Cardiol Young. 2016;26(6):1072–81. https://doi.org/10.1017/S1047951115001791.
37. Divanovic A, Hor K, Cnota J, Hirsch R, Kinsel-Ziter M, Michelfelder E. Prediction and perinatal management of severely restrictive atrial septum in fetuses with critical left heart obstruction: clinical experience using pulmonary venous Doppler analysis. J Thorac Cardiovasc Surg. 2011;141(4):988–94. https://doi.org/10.1016/j.jtcvs.2010.09.043.
38. Michelfelder E, Gomez C, Border W, Gottliebson W, Franklin C. Predictive value of fetal pulmonary venous flow patterns in identifying the need for atrial septoplasty in the newborn with hypoplastic left ventricle. Circulation. 2005;112(19):2974–9. https://doi.org/10.1161/CIRCULATIONAHA.105.534180.
39. Szwast A, Tian Z, McCann M, Donaghue D, Rychik J. Vasoreactive response to maternal hyperoxygenation in the fetus with hypoplastic left heart syndrome. Circ Cardiovasc Imaging. 2010;3(2):172–8. https://doi.org/10.1161/CIRCIMAGING.109.848432.
40. Rasanen J, Wood DC, Debbs RH, Cohen J, Weiner S, Huhta JC. Reactivity of the human fetal pulmonary circulation to maternal hyperoxygenation increases during the second half of pregnancy: a randomized study. Circulation. 1998;97(3):257–62. https://doi.org/10.1161/01.cir.97.3.257.
41. Broth RE, Wood DC, Rasanen J, Sabogal JC, Komwilaisak R, Weiner S, Berghella V. Prenatal prediction of lethal pulmonary hypoplasia: the hyperoxygenation test for pulmonary artery reactivity. Am J Obstet Gynecol. 2002;187(4):940–5. https://doi.org/10.1067/mob.2002.127130.
42. Rudolph AM. Aortopulmonary transposition in the fetus: speculation on pathophysiology and therapy. Pediatr Res. 2007;61(3):375–80. https://doi.org/10.1203/pdr.0b013e318030d5b9.
43. Punn R, Silverman NH. Fetal predictors of urgent balloon atrial septostomy in neonates with complete transposition. J Am Soc Echocardiogr. 2011;24(4):425–30. https://doi.org/10.1016/j.echo.2010.12.020.
44. Jouannic JM, Gavard L, Fermont L, Le Bidois J, Parat S, Vouhe PR, Dumez Y, Sidi D, Bonnet D. Sensitivity and specificity of prenatal features of physiological shunts to predict neonatal clinical status in transposition of the great arteries. Circulation. 2004;110(13):1743–6. https://doi.org/10.1161/01.CIR.0000144141.18560.CF.
45. Talemal L, Donofrio MT. Hemodynamic consequences of a restrictive ductus arteriosus and foramen ovale in fetal transposition of the great arteries. J Neonatal Perinatal Med. 2016;9(3):317–20. https://doi.org/10.3233/NPM-16915122.

46. Maeno YV, Kamenir SA, Sinclair B, van der Velde ME, Smallhorn JF, Hornberger LK. Prenatal features of ductus arteriosus constriction and restrictive foramen ovale in d-transposition of the great arteries. Circulation. 1999;99(9):1209–14. https://doi.org/10.1161/01.cir.99.9.1209.
47. Sarris GE, Chatzis AC, Giannopoulos NM, Kirvassilis G, Berggren H, Hazekamp M, Carrel T, Comas JV, Di Carlo D, Daenen W, Ebels T, Fragata J, Hraska V, Ilyin V, Lindberg HL, Metras D, Pozzi M, Rubay J, Sairanen H, Stellin G, Urban A, Van Doorn C, Ziemer G, European Congenital Heart Surgeons A. The arterial switch operation in Europe for transposition of the great arteries: a multi-institutional study from the European congenital heart Surgeons association. J Thorac Cardiovasc Surg. 2006;132(3):633–9. https://doi.org/10.1016/j.jtcvs.2006.01.065.
48. Garne E, Loane MA, Nelen V, Bakker MK, Gener B, Abramsky L, Addor MC, Queisser-Luft A. Survival and health in liveborn infants with transposition of great arteries—A population-based study. Congenit Heart Dis. 2007;2(3):165–9. https://doi.org/10.1111/j.1747-0803.2007.00093.x.
49. McElhinney DB, Salvin JW, Colan SD, Thiagarajan R, Crawford EC, Marcus EN, del Nido PJ, Tworetzky W. Improving outcomes in fetuses and neonates with congenital displacement (Ebstein's malformation) or dysplasia of the tricuspid valve. Am J Cardiol. 2005;96(4):582–6. https://doi.org/10.1016/j.amjcard.2005.04.024.
50. Freud LR, Escobar-Diaz MC, Kalish BT, Komarlu R, Puchalski MD, Jaeggi ET, Szwast AL, Freire G, Levasseur SM, Kavanaugh-McHugh A, Michelfelder EC, Moon-Grady AJ, Donofrio MT, Howley LW, Tierney ES, Cuneo BF, Morris SA, Pruetz JD, van der Velde ME, Kovalchin JP, Ikemba CM, Vernon MM, Samai C, Satou GM, Gotteiner NL, Phoon CK, Silverman NH, McElhinney DB, Tworetzky W. Outcomes and predictors of perinatal mortality in fetuses with Ebstein anomaly or tricuspid valve dysplasia in the current era: a multicenter study. Circulation. 2015;132(6):481–9. https://doi.org/10.1161/CIRCULATIONAHA.115.015839.
51. Yetman AT, Freedom RM, McCrindle BW. Outcome in cyanotic neonates with Ebstein's anomaly. Am J Cardiol. 1998;81(6):749–54. https://doi.org/10.1016/s0002-9149(97)01009-6.
52. Wertaschnigg D, Jaeggi M, Chitayat D, Shannon P, Ryan G, Thompson M, Yoo SJ, Jaeggi E. Prenatal diagnosis and outcome of absent pulmonary valve syndrome: contemporary single-center experience and review of the literature. Ultrasound Obstet Gynecol. 2013;41(2):162–7. https://doi.org/10.1002/uog.11193.
53. Donofrio MT, Jacobs ML, Rychik J. Tetralogy of Fallot with absent pulmonary valve: echocardiographic morphometric features of the right-sided structures and their relationship to presentation and outcome. J Am Soc Echocardiogr. 1997;10(5):556–61. https://doi.org/10.1016/s0894-7317(97)70010-5.
54. Moon-Grady AJ, Tacy TA, Brook MM, Hanley FL, Silverman NH. Value of clinical and echocardiographic features in predicting outcome in the fetus, infant, and child with tetralogy of Fallot with absent pulmonary valve complex. Am J Cardiol. 2002;89(11):1280–5. https://doi.org/10.1016/s0002-9149(02)02326-3.
55. Emmanoulides GC, Thanopoulos B, Siassi B, Fishbein M. "Agenesis" of ductus arteriosus associated with the syndrome of tetralogy of Fallot and absent pulmonary valve. Am J Cardiol. 1976;37(3):403–9. https://doi.org/10.1016/0002-9149(76)90290-3.
56. Szwast A, Tian Z, McCann M, Soffer D, Combs J, Donaghue D, Rychik J. Anatomic variability and outcome in prenatally diagnosed absent pulmonary valve syndrome. Ann Thorac Surg. 2014;98(1):152–8. https://doi.org/10.1016/j.athoracsur.2014.03.002.
57. Chelliah A, Berger JT, Blask A, Donofrio MT. Clinical utility of fetal magnetic resonance imaging in tetralogy of Fallot with absent pulmonary valve. Circulation. 2013;127(6):757–9. https://doi.org/10.1161/CIRCULATIONAHA.112.139758.
58. Sun HY, Boe J, Rubesova E, Barth RA, Tacy TA. Fetal MRI correlates with postnatal CT angiogram assessment of pulmonary anatomy in tetralogy of Fallot with absent pulmonary valve. Congenit Heart Dis. 2014;9(4):E105–9. https://doi.org/10.1111/chd.12091.
59. Ganesan S, Brook MM, Silverman NH, Moon-Grady AJ. Prenatal findings in total anomalous pulmonary venous return: a diagnostic road map starts with obstetric screening views. J Ultrasound Med. 2014;33(7):1193–207. https://doi.org/10.7863/ultra.33.7.1193.

Doppler Echocardiography of Fetal Cardiac Arrhythmias

32

Varsha Thakur and Edgar Jaeggi

32.1 Introduction

The main role of the heart is to pump blood throughout the body to allow adequate supply of oxygen and nutrients to the tissues while removing toxic wastes. In the normal fetus, the heart rate is regular and typically ranges from 140 to 160 bpm in the second trimester and from 120 to 140 bpm before birth [1]. Heartbeats result from rhythmic electrical impulse generation within the sinoatrial (SA) node followed by electrical impulse propagation across the atriums, the atrioventricular (AV) node, the His-Purkinje system, and the ventricular myocardium. Following depolarization, the myocardium resets or repolarizes to its resting state in preparation for the next signal to occur. The coordinated sequence of myocardial depolarization and repolarization leads to synchronized contraction and relaxation of the atrial and ventricular myocardium with each heartbeat.

Cardiac arrhythmias represent deviations from the normal cadence of electro-mechanical activity and will either manifest as an irregularity of the rhythm, a slow or fast heart rate, or a combination of abnormal rhythm and rate. Fetal rhythm disturbances are detectable in at least 2% of pregnancies during routine ultrasound scanning and are common reasons for referral to the fetal cardiologist [2, 3]. In more than 90% of cases, however, cardiac arrhythmias are brief and self-resolving events of little clinical relevance [2]. Of more concern are arrhythmias that display with prolonged or persistently abnormal heart rates [3]. This includes forms of supraventricular tachycardia (SVT) and complete heart block (CHB) as major arrhythmia mechanisms. Accurate differentiation of a major arrhythmia from benign rhythm disorders (e.g., irreversible CHB versus reversible blocked atrial bigeminy) is extremely important for parental counseling about the prognosis of the arrhythmia and potential management decisions [4–10]. The primary objective of a newly detected fetal arrhythmia should be (1) to understand the underlying arrhythmia mechanism; (2) to clarify the clinical significance; and (3) to determine the need for treatment. Real-time 2-dimensional echocardiography provides the first visible impression about the fetal heart rate (slow, normal, or fast), arrhythmia pattern (regular or irregular; intermittent or persistent), the hemodynamic consequences of the arrhythmia (effusion; cardiomegaly; polyhydramnios; fetal movements), and determines if an underlying anomaly, such as cardiac tumors or structural heart disease are underlying the arrhythmia [11]. M-Mode and Doppler ultra-

V. Thakur · E. Jaeggi (✉)
Labatt Family Heart Centre, Hospital for Sick Children, University of Toronto, Toronto, ON, Canada
e-mail: varsha.thakur@sickkids.ca; edgar.jaeggi@sickkids.ca

D. Maulik, C. C. Lees (eds.), *Doppler Ultrasound in Obstetrics and Gynecology*,
https://doi.org/10.1007/978-3-031-06189-9_32

sound techniques are then used to examine the mechanism of the fetal arrhythmia [2, 12–17].

32.2 Methods and Techniques of Fetal Cardiac Activity Assessment

After birth, electrocardiography (ECG) is commonly used to record the sequence of cardiac electrical activation (Fig. 32.1). There are three main components of a normal ECG: P wave, QRS complex, and T wave. The electric signal created by the SA node causes atrial myocytes to depolarize which is seen as a P wave and results in atrial contraction. Depolarization of the ventricular myocardium, represented by the QRS complex, then causes the ventricles to contract and to eject blood into the great arteries. The PR interval reflects the electrical conduction through the AV node. T wave represents repolarization of the ventricular myocardium back to its electrical resting state, in anticipation of a next electrical signal from the SA node. It is also possible to indirectly record electrical cardiac events in the fetus by means of transabdominal magnetocardiography (MCG), but currently available MCG systems are still costly and thus not widely available. Fetal echocardiography has therefore been used as a surrogate modality to study the beat-to-beat chronology of atrial and ventricular electrical events by their respective mechanical consequences. Echocardiography does not inform on the morphology, duration, and amplitude of electrical events, such as QRS waves and ventricular repolarization.

The principle of echocardiographic fetal rhythm assessment is based on the simultaneous recording of events that occur during atrial (A) and ventricular (V) systolic contraction. During atrial systole, the atrial myocardium shortens, which leads (a) to increased inflow across the AV valves (A wave) and (b) brief flow reversal in the precordial systemic and pulmonary veins (a waves). During ventricular systolic contraction, the myocardium shortens to eject blood into the aorta (V wave) and pulmonary artery, respectively. M-mode is an imaging technique used to examine atrial and ventricular wall motions, while pulse wave Doppler allows interrogation of venous, AV valvar, and arterial blood flows during the cardiac cycle. If the M-mode beam is aligned across atrial and ventricular myocardium, it is possible to record the chronology of atrial and ventricular wall movements on the same tracing. An example of a normal M-mode tracing is shown in Fig. 32.2. Using a similar approach with Doppler flow imaging [18], it is possible to show the relationship of atrial and ventricular systolic flow events to each other, which requires placement of the Doppler sample volume across structures that simultaneously inform about atrial and ventricular systolic flows, respectively. This is obtained from concurrent Doppler flow record-

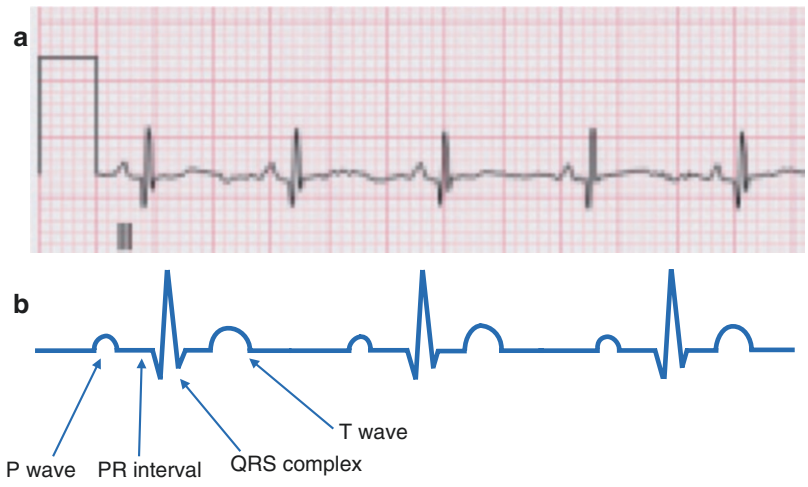

Fig. 32.1 (**a**) Normal rhythm strip from an ECG performed in a neonate (**b**). Schematic showing the various components of the cardiac cycle. The "p" wave represents atrial contraction, the PR interval represents the time for the electric signal to be processed in the AV node, the "QRS" complex represents ventricular contraction, and the T wave represents ventricular repolarization

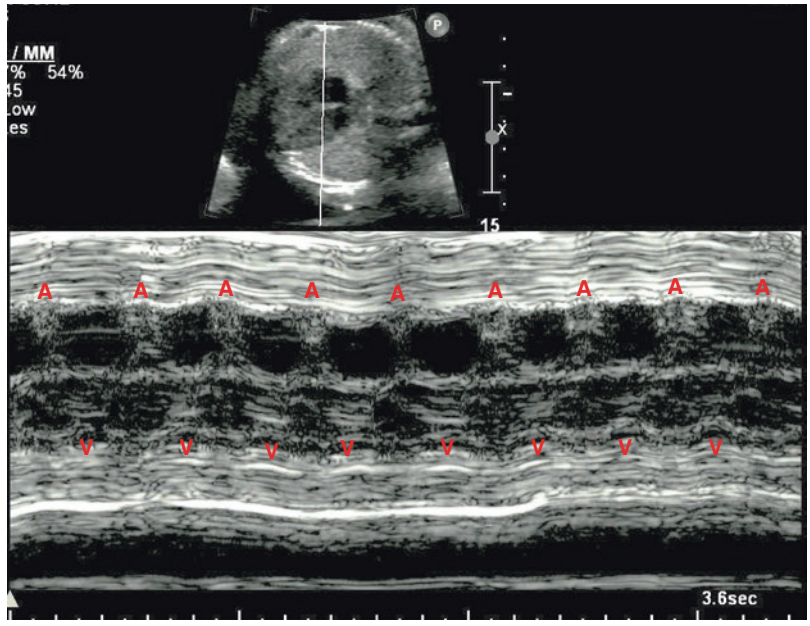

Fig. 32.2 M-Mode tracing in normal rhythm. The ultrasound beam is placed across the posterior wall of the right atrium and the anterior wall of the left ventricle to simultaneously show atrial and ventricular contraction. The tracing can show the rate of atrial and ventricular contraction simultaneously. Using M-mode, the rates of contraction of the atria and the ventricles and the relationship of atrial to ventricular contraction can be assessed in the evaluation of fetal rhythm

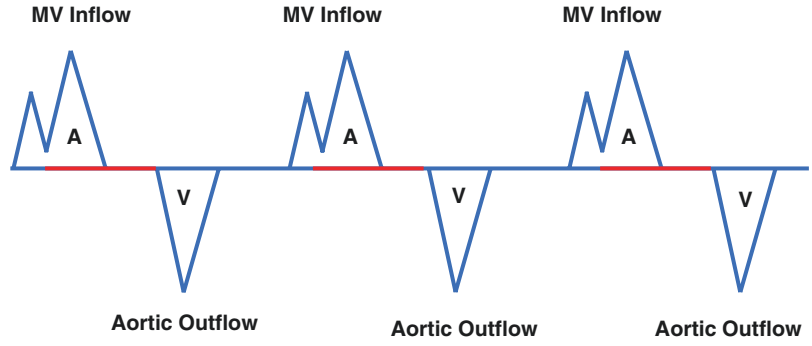

Fig. 32.3 Schematic showing the mitral valve inflow and aortic outflow. The red line shows the AV time

ings of (a) the mitral valve and the ascending aorta (inflow/outflow Doppler; (Figs. 32.3 and 32.4), (b) the superior vena cava and the ascending aorta (SVC/aorta Doppler; (Figs. 32.5 and 32.6), or (c) the pulmonary vein and the pulmonary artery (PV/PA Doppler), respectively. The sample volume gate should be wide enough to assess flow in the structures being assessed. Gain setting should be adjusted to show the Doppler signals appropriately. Finally, the horizontal sweep speed should be adjusted to show the relationship between atrial and ventricular flows and to allow precise measurement of the relationship between atrial and ventricular events (usually 50–100 cm/s, faster for tachycardia).

The different imaging modalities are briefly reviewed:

- *Inflow/outflow Doppler* is best achieved by obtaining a 4-chamber view of the heart and tilting anteriorly until the aortic outflow is seen with the mitral inflow. The sample vol-

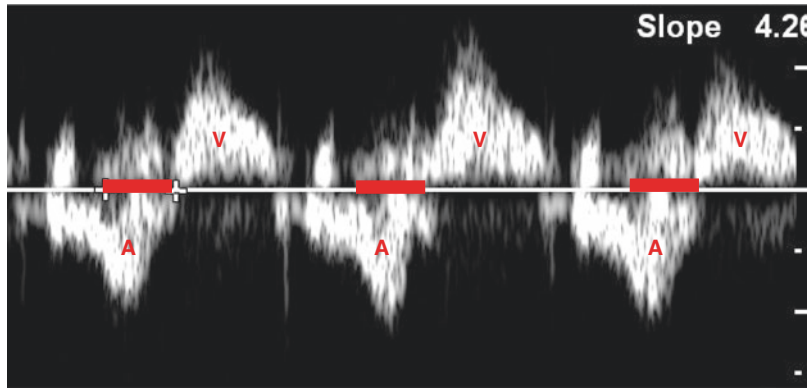

Fig. 32.4 Pulse Doppler of the mitral valve inflow with simultaneous aortic outflow Doppler. The "A" wave of the mitral valve inflow represents ventricular filling during atrial contraction and corresponds to the "P" wave on ECG. The aortic outflow Doppler represents ventricular contraction ("V") and corresponds to the "QRS" complex on the ECG. The red line represents the time from the atrial contraction to the ventricular contraction (AV interval) which represents the PR interval on ECG

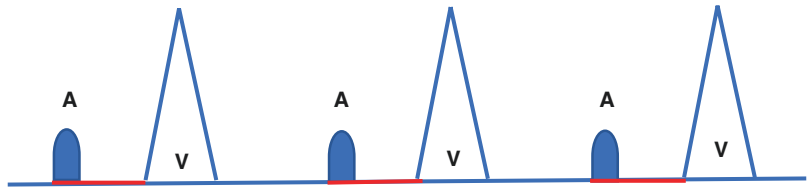

Fig. 32.5 Schematic showing simultaneous Doppler tracing of the SVC and aortic outflow. "A" wave reversal is seen on the SVC tracing representing atrial contraction. Doppler of the aortic outflow is consistent with ventricular contraction, "V"

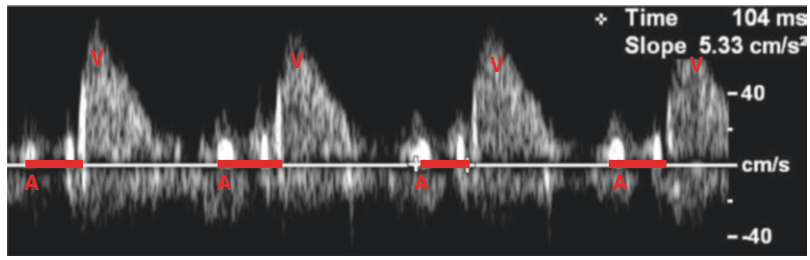

Fig. 32.6 Pulse Doppler of SVC and aorta simultaneously. The "A" wave is seen representing atrial contraction followed by ventricular contraction (V). The red line represents the AV interval

ume should be placed below the aortic valve where the signal for mitral valve inflow and the aortic outflow can be acquired simultaneously. Color Doppler can be helpful in visualizing the inflow and the outflow, so the pulse Doppler sample volume is appropriately placed. A normal Doppler inflow of a ventricle is biphasic (E and A waves): the second wave form (A wave) represents active ventricular filling in response to atrial systole (Figs. 32.3 and 32.4) [19, 20]. Inflow/outflow Doppler is most useful in measuring AV intervals during a normal cardiac rhythm as an indirect measure of electrical impulse conduction (PR

interval on the ECG) through the AV node. The AV interval is measured from the beginning of the mitral inflow A wave to the beginning of the ascending aortic flow (Fig. 32.4). Normal conduction is seen when each inflow is followed by a timely normal outflow wave for gestational age, confirming normal 1:1 AV conduction. It is important to note that AV time intervals physiologically prolong with increasing heart size to birth. Significant AV prolongation may suggest an abnormality in conduction [18, 21]. On the other hand, Inflow/outflow Doppler is of little use to examine arrhythmias when it becomes difficult to distinguish between mitral E and A waves.

- *SVC/aorta Doppler* [22] is used to simultaneously record the flow within these two neighboring blood vessels (Figs. 32.5 and 32.6). The venous A wave and the aortic flow wave signals are useful to assess the cardiac rhythm/rate, including AV intervals. Importantly SVC/aorta Doppler is also very useful to examine cardiac arrhythmias. The ideal plane to image both vessels is in the sagittal view with the sample volume being placed just above the aortic valve and in the SVC–right atrial junction.
- *PV/PA Doppler* [23] applies the same concept as SVC/aorta Doppler and is best obtained in the cardiac 4-chamber view.
- *M-mode* [24] is an ultrasound technique that can be used to assess fetal arrhythmias. To evaluate rhythm, the beam is placed through the atria and ventricle at the same time. Contraction of the atrial wall and ventricular wall are seen simultaneously and can be used to assess the relationship between atrial and ventricular contraction. M-mode is best achieved in the 4-chamber view with the heart perpendicular to the ultrasound probe. The ultrasound beam can then be placed in the posterior wall of the left atrium and the anterior wall of the right ventricle to obtain an M-mode tracing (Fig. 32.2). M-mode and pulse Doppler techniques should be used in combination to evaluate arrhythmias.

32.3 Fetal Arrhythmias

Fetal arrhythmias either manifest as an irregularity of the heart rhythm, a slow or fast heart rate, or a combination of abnormal rhythm and rate. The underlying mechanisms of these arrhythmia patterns are reviewed.

(a) **Irregular Rhythm**

Intermittent irregularities of the heart rhythm account for up to 80–85% of arrhythmias seen before birth [2]. Mechanisms in order of frequency include (1) premature atrial beats; (2) premature ventricular beats; and (3) incomplete heart block.

- **Premature atrial beats (PACs)** are the most common cause of an irregular heartbeat [2]. They result from a premature atrial electrical impulse outside of the SA node. If a PAC occurs very early after a ventricular impulse, the atrial impulse is typically not propagated to the ventricles as the AV node is still refractory. The result is a "blocked PAC" that manifests as a "dropped" ventricular contraction. If the PAC occurs later and is conducted across the AV node, the ventricular beat will also appear prematurely. In both situations, the PAC leads to an irregular beat (Figs. 32.7, 32.8, and 32.9). Isolated PACs may occur in a more regular pattern, e.g., in bigeminy (every second beat is a PAC; Figs. 32.10 and 32.11) or trigeminy (every third beat is a PAC) (Fig. 32.12). In persistent bigeminy with non-conducted/blocked PACs, the heart rhythm will be regular but the ventricular rate significantly slower from normal, usually between 70 and 90 bpm. PACs are usually found in structurally normal hearts and may then be triggered by an aneurysmal or redundant atrial septum that intermittently touches the atrial free wall [25]. Rarely PACs are associated with cardiac tumors [26]. Isolated fetal PACs are benign and spontaneously resolve either in utero or early after birth [27]. However, frequent PACs

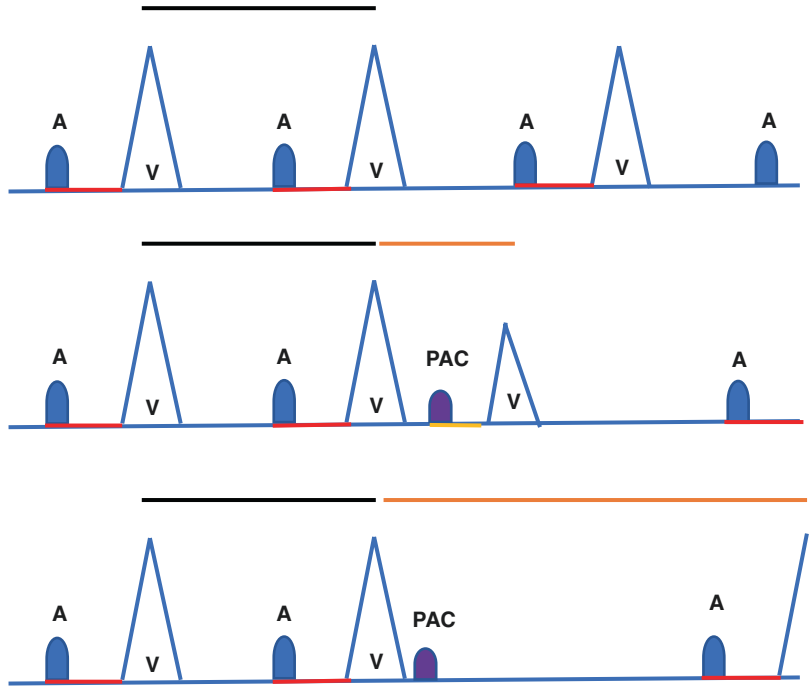

Fig. 32.7 A schematic showing the difference between a normal rhythm (top strip), a conducted premature atrial contraction (PAC) (middle strip), and a non-conducted PAC (lower strip). "A" represents atrial contraction while "V" represents the ventricular contraction. The black line indicates the time interval between ventricular contractions (between heart beats) while the red line represents the AV interval with normal beats. The yellow line represents the AV interval for the PAC. The orange line represents the time between ventricular contraction when a conducted PAC (middle) or blocked PAC (lower)

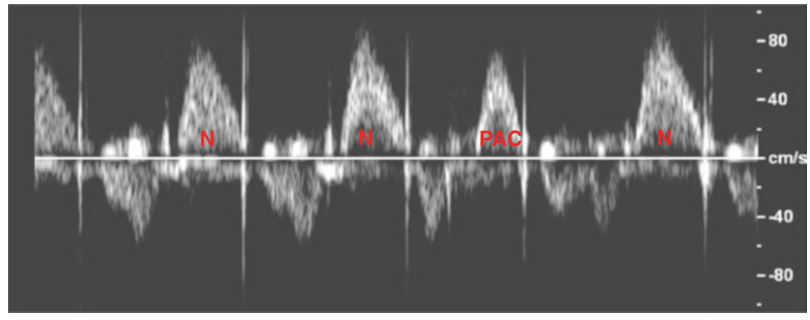

Fig. 32.8 Pulse Doppler tracing of the mitral valve inflow and aortic outflow showing a conducted PAC

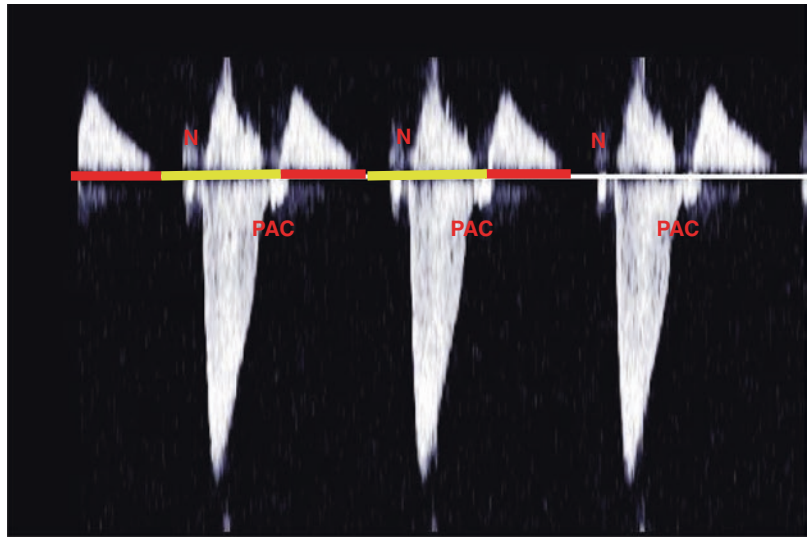

Fig. 32.9 Pulse Doppler of the SVC and aortic outflow showing non-conducted PACs

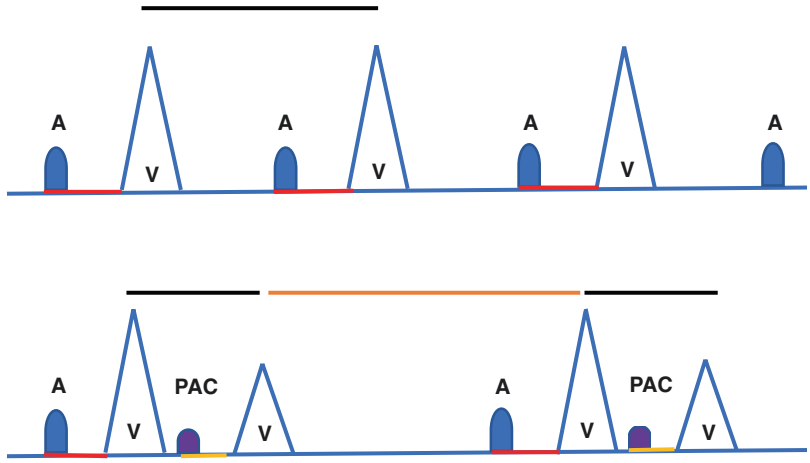

Fig. 32.10 Schematic showing PACs conducted in bigeminy in comparison to a normal heart rate and rhythm. Top strip shows normal conduction while the bottom strip shows PACs in bigeminy. "A" represents atrial contraction while "V" represents the ventricular contraction. The black line indicates the time interval between ventricular contractions (between heart beats) while the red line represents the AV interval with normal beats. The yellow line represents the AV interval for the PAC. The orange line represents the time between ventricular contraction when a conducted PAC (middle) or blocked PAC (lower)

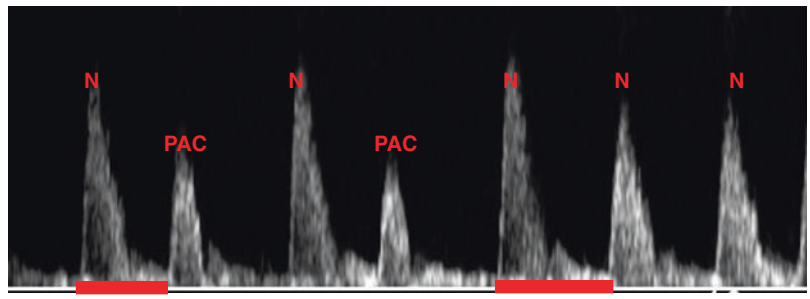

Fig. 32.11 Pulse Doppler of the aortic outflow showing PACs in bigeminy. A normal beat alternates with a premature beat

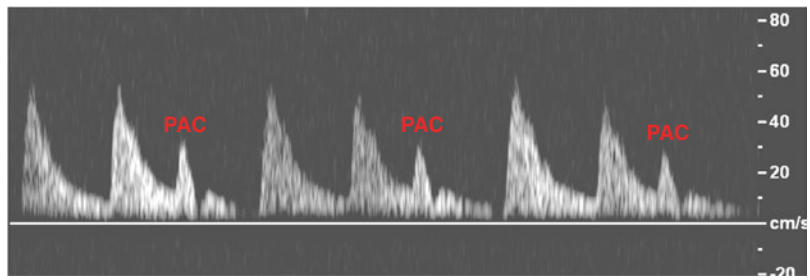

Fig. 32.12 Pulse Doppler of the aortic outflow showing PACs in trigeminy. A PAC occurs every third beat

carry a 1% risk of progression to fetal SVT and follow-up assessment are therefore warranted, usually until resolution of the arrhythmia [28].

- **Premature ventricular contractions (PVCs)** are rare observations in the fetal heart (Figs. 32.13, 32.14, and 32.15). It results from spontaneous electrical impulse generation within a ventricle. This leads to premature ventricular contraction, while the normal electrical impulse from the SA node fails to reach the ventricle. On the Doppler tracing, the atrial rate remains regular, while the ventricular rate is irregular. PVCs may occur in isolation or in a

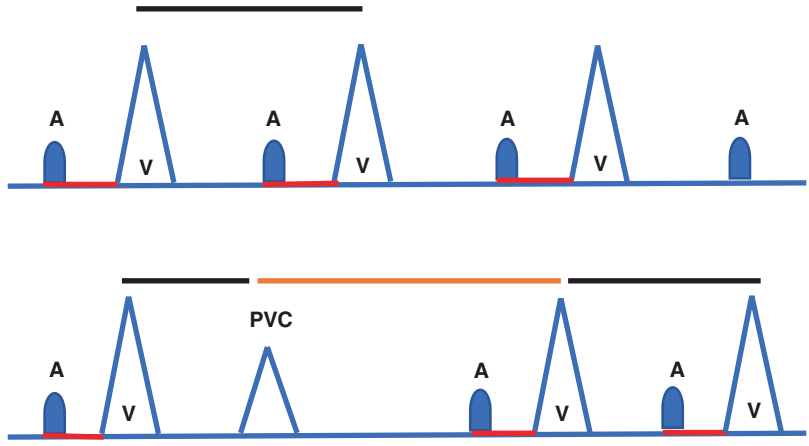

Fig. 32.13 Schematic showing normal conduction versus PVC. Top strip shows normal conduction while the bottom strip shows a PVC compared to normal beats. "A" represents atrial contraction while "V" represents the ventricular contraction. The black line indicates the time interval between ventricular contractions (between heart beats) while the red line represents the AV interval with normal beats. The orange line represents the time between ventricular contraction when a conducted PAC (middle) or blocked PAC (lower)

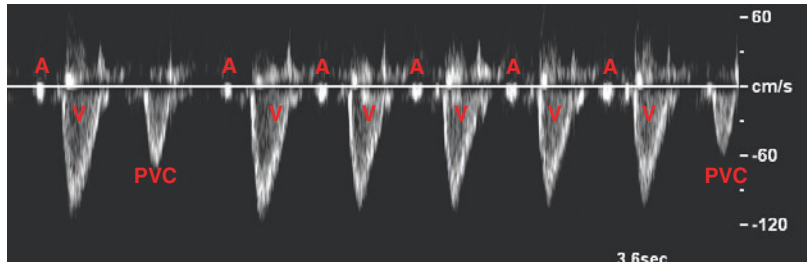

Fig. 32.14 SVC–Ao Doppler showing normal beats and PVC. M-mode showing normal ventricular contraction and PVCs. Normal ventricular contraction is preceded by atrial contraction, while there is no atrial contraction preceding the PVC

repeated pattern (e.g., bigeminy). PVCs in a structurally normal heart are benign and usually self-resolving with not need of treatment [27]. Rarely, PVCs can be associated with cardiac tumors or cardiac inflammation.

- **Second degree heart block** is another mechanism that can manifest with skipped ventricular beats. In second degree AV block type I, the atrial rate is regular but the AV conduction progressively prolongs with each beat until the AV node fails conduction to the ventricle which leads to a dropped heartbeat. In second degree AV block type II, the dropped ventricular beat occurs suddenly and is not preceded by progressive prolongation of the AV interval (Figs. 32.16 and 32.17). Both types may be seen in association with cardiac inflammation, e.g., secondary to maternal anti-Ro antibodies and with some forms of structural heart disease (cc-TGA, left isomerism) and then progress to complete heart block.

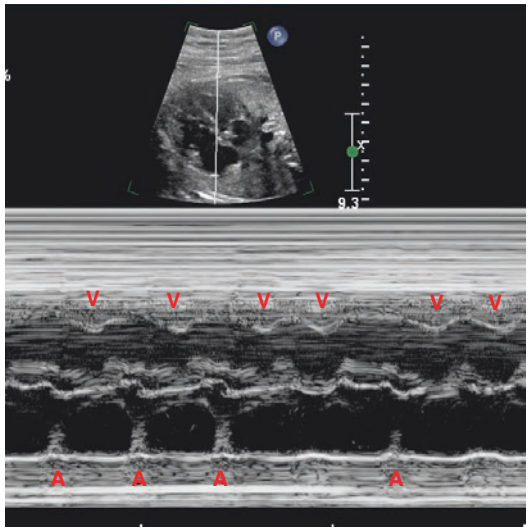

Fig. 32.15 M-Mode tracing showing normal beats and a PVC. Each normal ventricular contraction is preceded by an atrial contraction. The PVC is an early ventricular contraction and is not preceded by an atrial contraction

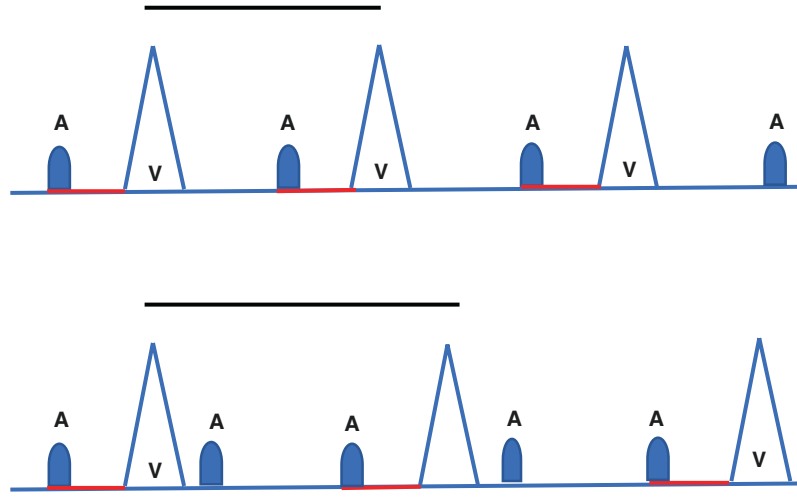

Fig. 32.16 A schematic showing 2:1 Heart block versus normal rate and rhythm. Every other "A" is conducted. Top strip shows normal heart rate while the bottom strip shows 2:1 heart block. "A" represents atrial contraction while "V" represents the ventricular contraction. The black line indicates the time interval between ventricular contractions (between heart beats) while the red line represents the AV interval with normal beats

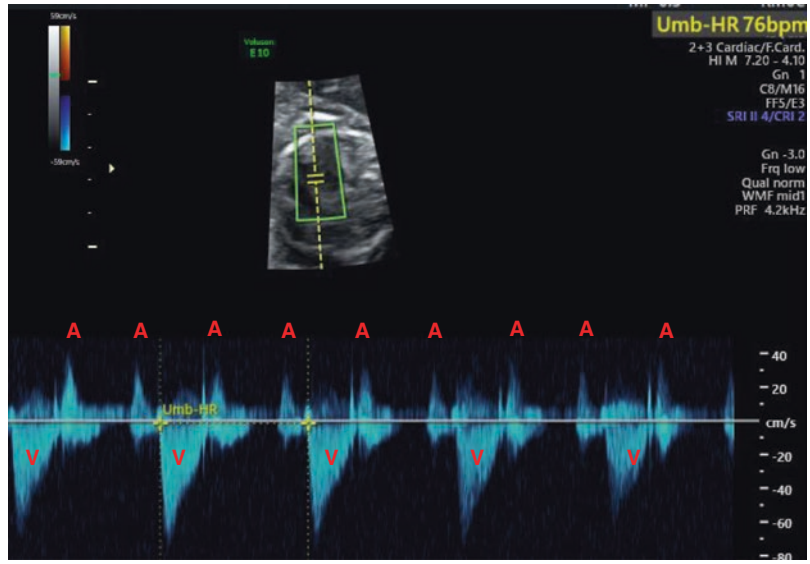

Fig. 32.17 SVC–aortic Doppler showing 2:1 heart block. The ventricular rate is 76 bpm

32.4 Bradyarrhythmia

Persistent bradycardia may have different etiologies including (1) sinus bradycardia, (2) atrial bigeminy with blocked PACs, (3) 2:1 AV block, or (4) complete heart block.

- **Sinus bradycardia** (Figs. 32.18 and 32.19) can be defined as an atrial rate below the third percentile for gestational age [29]. Using this definition, an average fetal heart below 120 bpm becomes abnormal for any gestational age other than term. Brief slowing of the heart rate is a common observation during first trimester ultrasound exams and of no clinical relevance. It is caused by pressure from the ultrasound probe and ease of pressure will immediately restore a normal fetal heart rate. Sustained sinus bradycardia may be secondary to fetal hypoxia/acidosis [30], fetal long QT syndrome (e.g., KCNQ1 mutation), [29, 31] or maternal anti-Ro antibody-mediated damage of the AV node. The AV conduction may also be affected. The prenatal evaluation of a fetus with persistent bradycardia should entail an urgent assessment for signs of fetal compromise, and, once excluded, a fetal echocardiogram for possible congenital heart disease, testing for maternal anti-Ro antibodies, and potentially a work-up for fetal long QT syndrome (family history, parental ECGs, genetic testing). The perinatal management of sinus bradycardia depends on the underlying etiology and may include no treatment, anti-inflammatory medication for myocarditis (anti-Ro antibodies), premature delivery (fetal distress), and postnatal therapy with beta-blocker ± pacing (LQTS).
- **Atrial bigeminy with blocked PACs** has been discussed under PACs. Non-conducted atrial bigeminy is a common cause of fetal bradycardia and may sometimes persist for days to weeks. Key findings for the diagnosis (Fig. 32.9) include alternating length of atrial beats (sinus beat: normal A and V followed by PAC: premature A, no V). This is a benign and self-resolving arrhythmia.
- **2:1 AV block** (Fig. 32.17) may be related to QT prolongation should not be confused with atrial bigeminy and vice versa. Unlike with atrial bigeminy, the atrial rhythm in 2:1 AV block is regular. In addition, 1:1 AV conduction may recur at slower atrial rates. Similar to other possible manifestations of long LQT syndrome, such as unexplained sinus bradycardia and ventricular tachycardia (VT), patients with 2:1 AV block and their families should undergo a work-up for the possibility of genetic ion chan-

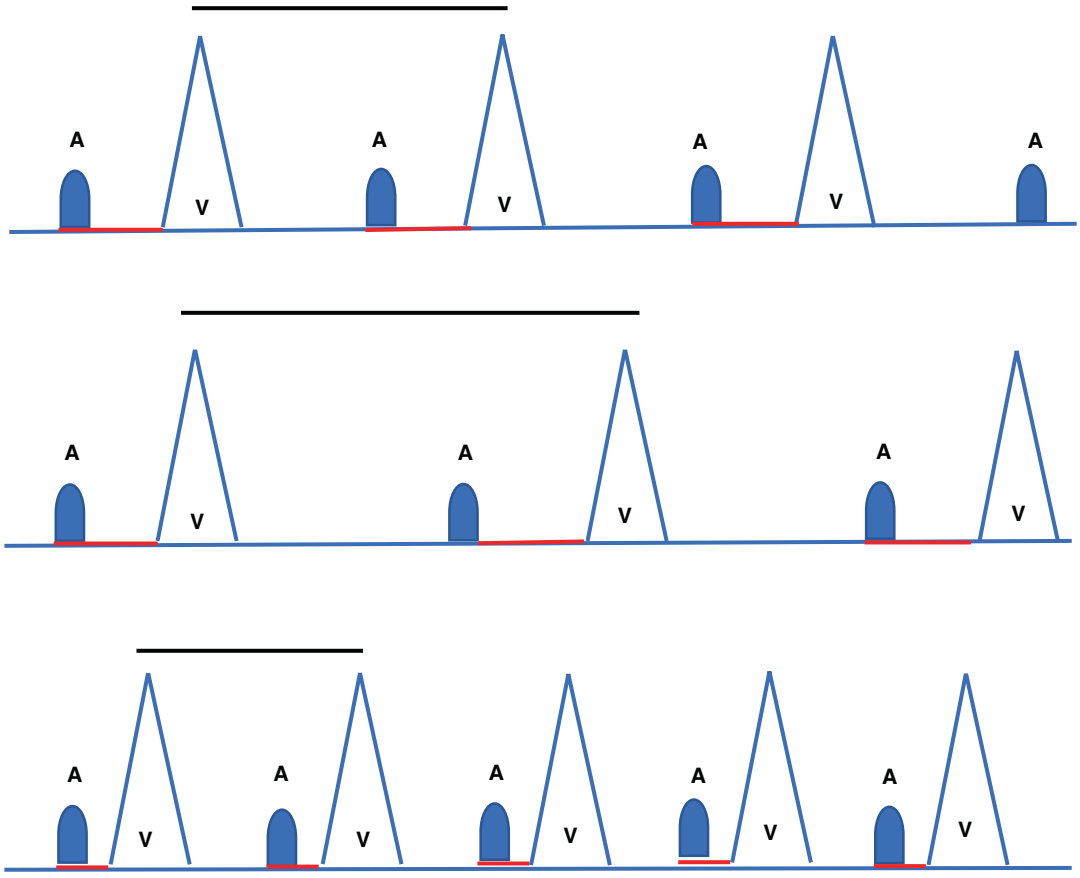

Fig. 32.18 Schematic showing the difference between sinus rhythm, sinus bradycardia, and Sinus tachycardia. Top strip sinus rhythm, middle strip sinus bradycardia, bottom strip sinus tachycardia. "A" represents atrial contraction while "V" represents the ventricular contraction. The black line indicates the time interval between ventricular contractions (between heart beats) while the red line represents the AV interval with normal beats

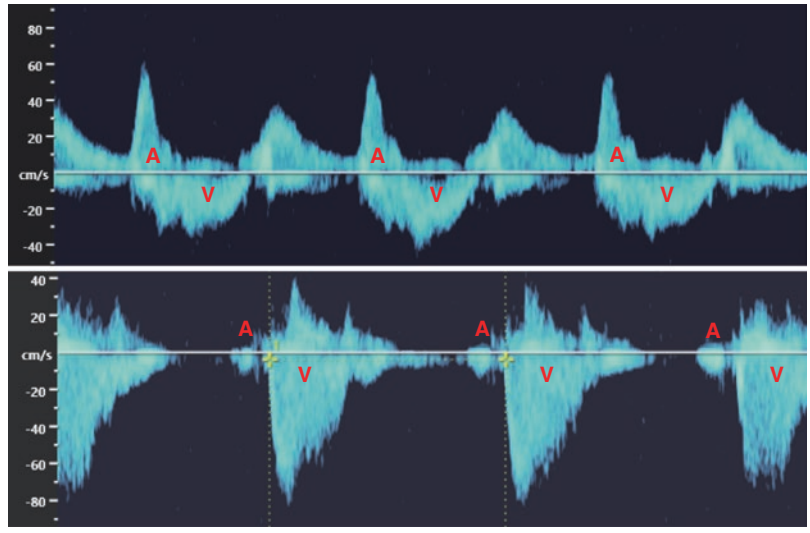

Fig. 32.19 MV–aortic Doppler and SVC–aortic Doppler showing sinus bradycardia. Each "A" is followed by a "V"; however, the rate is 96 bpm, lower than usual in the fetus

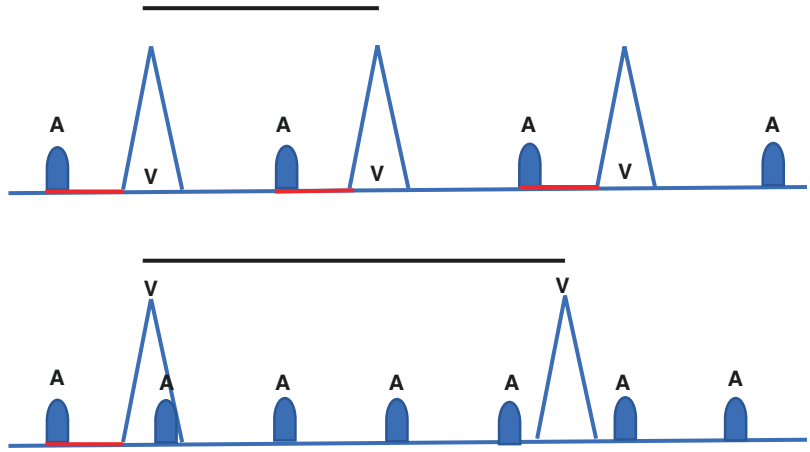

Fig. 32.20 Schematic showing normal rate and rhythm versus complete heart block. In complete heart block, atrial contraction and ventricular contraction are not synchronized. Atrial contractions are independent of ventricular contractions. Top strip normal heart rate. The bottom strip shows complete heart block. "A" represents atrial contraction while "V" represents the ventricular contraction. The black line indicates the time interval between ventricular contractions (between heart beats) while the red line represents the AV interval with normal beats

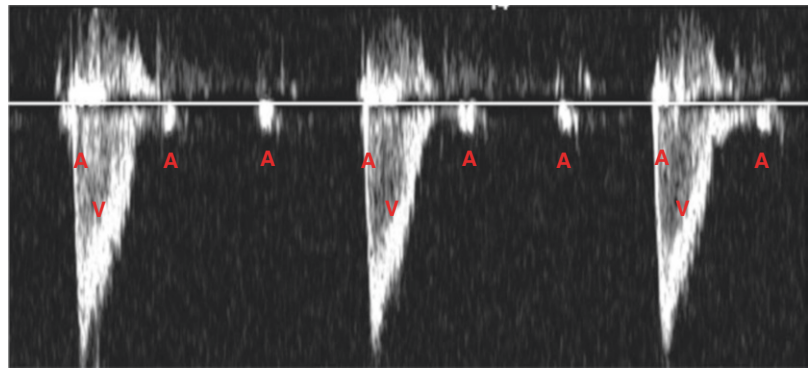

Fig. 32.21 SVC–aorta Doppler showing complete heart block. Ventricular rate is 55 bpm. There are more atrial beats than ventricular. In addition, there is no relationship between the atrial beats and the ventricular beats in complete heart block

nel disorders. Due to the predisposition of LQTS patients for VT-related cardiac arrests and sudden death, postnatal treatment with a long-acting β-blocker ± pacemaker or implantable cardioverter-defibrillator is usually required.

- **Complete or third degree heart block** occurs when the AV node does not transmit any signals generated by the SA node. The typical fetal echocardiogram of CHB (Figs. 32.20, 32.21, and 32.22) is that of a regular normal atrial rhythm, while the ventricles beat independently at a much slower rate of between 40–80 bpm. The echocardiographic differentiation between non-conduction across a functionally refractory AV node (as in atrial bigeminy with blocked PACs and 2:1 AV block) and CHB is clinically important as the latter is irreversible and represents advanced AV nodal damage. In about half of fetal cases with CHB, this is associated with major structural heart disease, most importantly left atrial isomerism [32, 33, 34–36], or congenitally corrected transposition of the great arteries (CCTGA) [33–36]. Left atrial isomerism complicated by CHB carries a very high risk of in

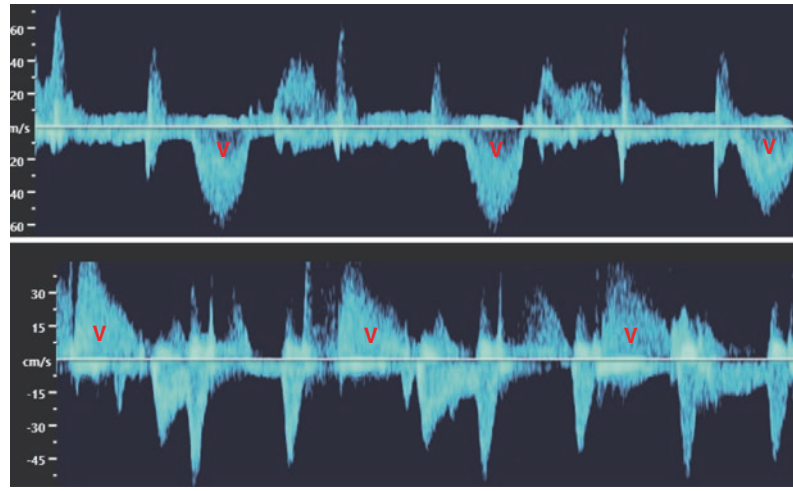

Fig. 32.22 Mitral valve inflow Doppler with simultaneous aortic Doppler. Atrial and ventricular contraction is not in synchrony as seen in complete heart block

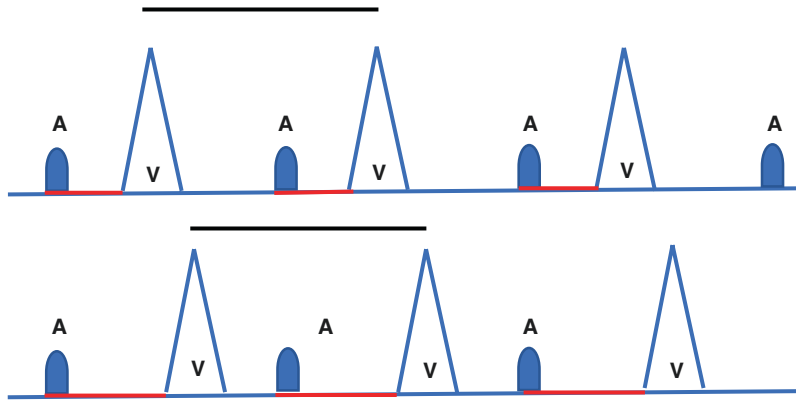

Fig. 32.23 Schematic diagram showing first degree AV block compared to normal. In first degree AV block, the time for the electric signal to propagate from the atria to the ventricles is increased; however, the rate is unchanged. Top strip shows normal AV conduction while the bottom strip shows 1st degree block win increased AV time interval. "A" represents atrial contraction while "V" represents the ventricular contraction. The black line indicates the time interval between ventricular contractions (between heart beats) while the red line represents the AV interval with normal beats

utero demise. In the absence of structural heart disease, congenital CHB is strongly linked to maternal anti-Ro/SSA antibody-mediated damage of the fetal AV node, which are detected in about 2% of pregnant women [33, 35, 36]. Fetuses affected by antibody-mediated heart block may be treated with steroids and/or IVIG to temper the cardiac inflammation and salbutamol to increase the fetal heart rate. Delivery in a tertiary care center is recommended [7, 37] with postnatally insertion of a permanent pacemaker if indicated [38]. Unlike second and third degree heart block, first degree heart block does not cause bradycardia: the AV conduction is 1:1 but the duration is prolonged (Figs. 32.23 and 32.24). First degree heart block is a rare diagnosis in the fetus exposed to anti-Ro antibodies but can also be seen if there is an intrinsic problem with the AV node.

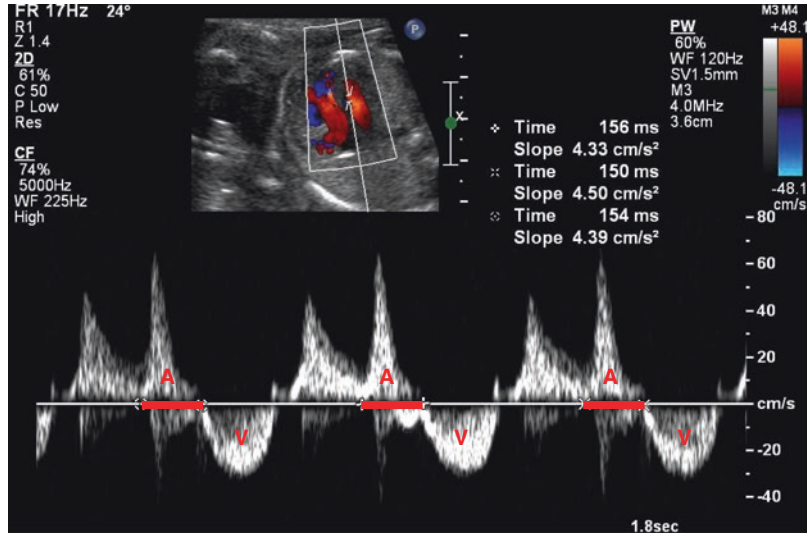

Fig. 32.24 Pulse Doppler of the mitral valve inflow and the aortic valve outflow showing prolonged AV interval in keeping with first degree AV block

32.5 Tachyarrhythmias

Fetal tachycardia can be defined as heart rate that exceeds 180 bpm. Possible mechanisms of sustained tachycardia include in order of frequency: (1) forms of SVT, (2) atrial flutter (AF), (3) sinus tachycardia (ST), and (4) VT and junctional ectopic tachycardia (JET). Irrespective of the mechanism, fetal tachycardia represents a medical emergency as it carries a risk of hemodynamic compromise and mortality and may require acute treatment.

- **Sinus tachycardia** (Figs. 32.18 and 32.25) originates from a SA node that discharges at a faster rate than usual. The Doppler echocardiogram will show a long VA tachycardia with 1:1 AV conduction similar to AET and PJRT. Nonetheless, the atrial rate during ST is usually slower (<200 bpm) compared with AET/PJRT and also displays some heart rate variability. Brief ST is benign and is often related to increased fetal activity. Persistent fetal ST may be secondary to thyrotoxicosis, anemia, infection, and/or hypoxia/acidosis of the fetus [39–41]. Urgent evaluation and treatment of underlying condition is warranted.
- **AV re-entry tachycardia (AVRT),** the most common of the fetal SVT mechanism (Figs. 32.26, 32.27, and 32.28), manifests as an intermittent or persistent 1:1 tachycardia between 190 and 300 bpm. It results from an electrical re-entrant circuit that involves the AV node for anterograde conduction (AV) and a fast retrograde (VA) conducting accessory pathway. The accessory re-pathway can be located anywhere along the AV groove in the otherwise structurally normal fetal heart. A key finding of AVRT is its sudden onset with a PAC and termination of the arrhythmia with an AV block. Moreover, as the retrograde accessory pathway conducts faster to the atriums than the anterograde AV node to the ventricles, the atrial contraction occurs close to the preceding ventricular contraction (short VA interval, longer AV interval) (Fig. 32.11). **Atrial ectopic tachycardia (AET)** and **permanent junctional reciprocating tachycardia (PJRT)** are less common form of SVT and better tolerated by the fetus than AVRT. Key features of AET (Figs. 32.29 and 32.30) and PJRT (Figs. 32.29 and 32.31) include a 1:1 tachycardia at around 190–220 bpm with a longer VA than AV interval. Irrespective of the SVT form, prenatal (and postnatal) treatment with antiarrhythmics may be required to terminate and suppress the tachyarrhythmia from recurring [8, 9] in par-

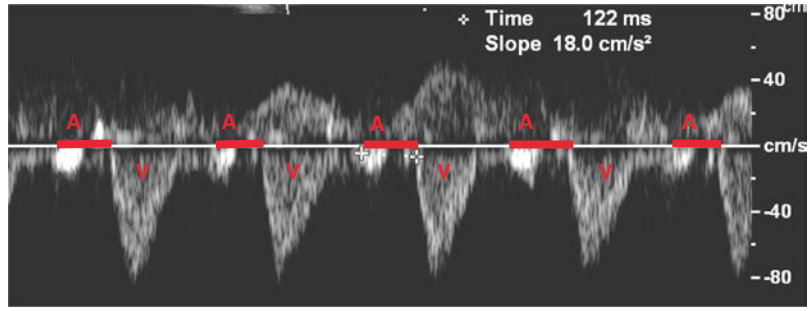

Fig. 32.25 SVC–aorta Doppler showing 1:1 A:V conduction; however, rate is 185 bpm, faster than usual for developing fetus, in keeping with a ST

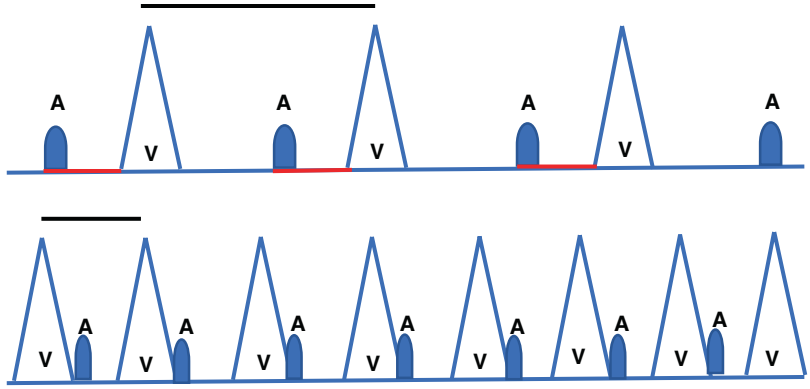

Fig. 32.26 Schematic of normal rhythm versus SVT. Top strip shows normal heart rate and conduction while the bottom strip shows SVT. "A" represents atrial contraction while "V" represents the ventricular contraction. The black line indicates the time interval between ventricular contractions (between heart beats) while the red line represents the AV interval with normal beats

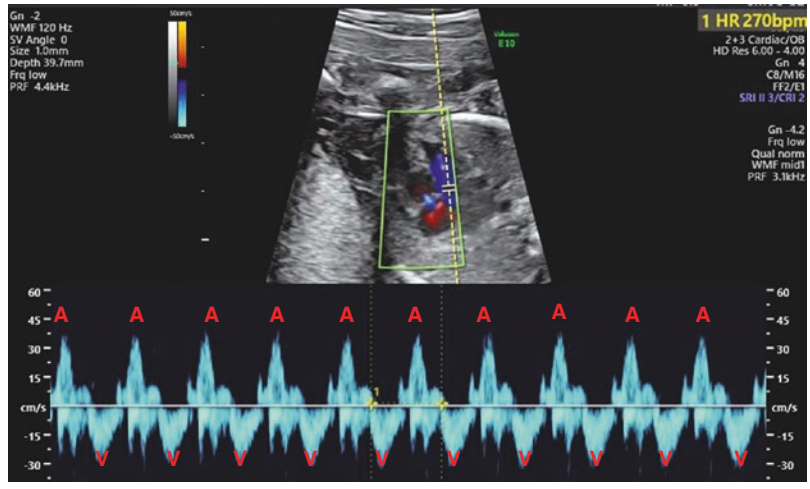

Fig. 32.27 MV inflow–aorta Doppler tracing of SVT with a rate of 270 bpm

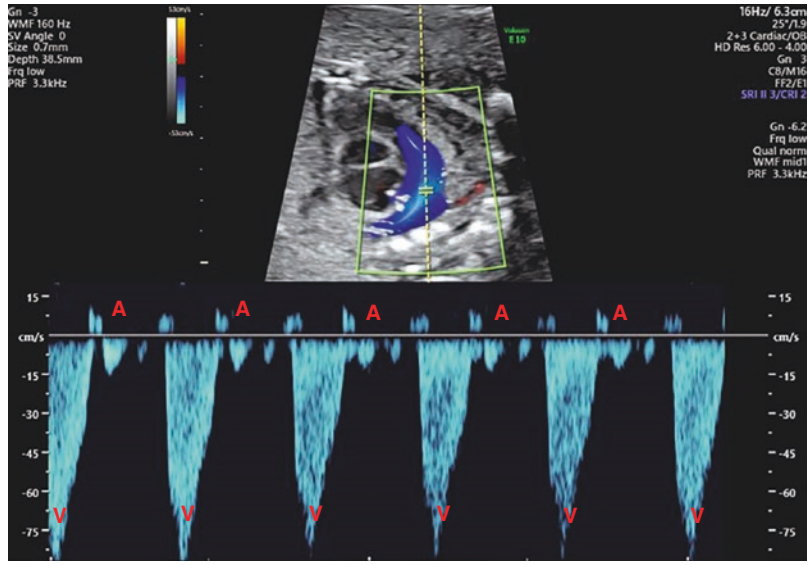

Fig. 32.28 SVC–aorta Doppler of SVT from the same patient

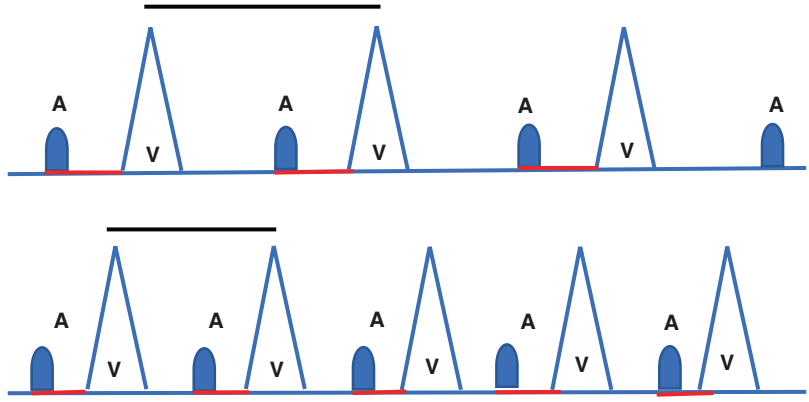

Fig. 32.29 Schematic showing the difference between normal rate and rhythm versus an AET or PJRT. Conduction is 1:1 in all cases; however, the heart rate is faster in AET or PJRT compared to the normal heart rate. Top strip shows normal conduction while bottom strip shows AET or PJRT. "A" represents atrial contraction while "V" represents the ventricular contraction. The black line indicates the time interval between ventricular contractions (between heart beats) while the red line represents the AV interval with normal beats

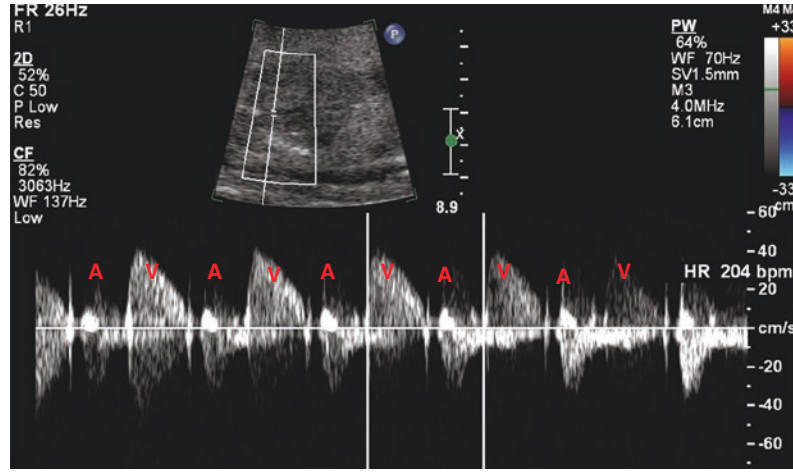

Fig. 32.30 SVC–aorta Doppler showing AET in the fetus with a rate of 204 bpm

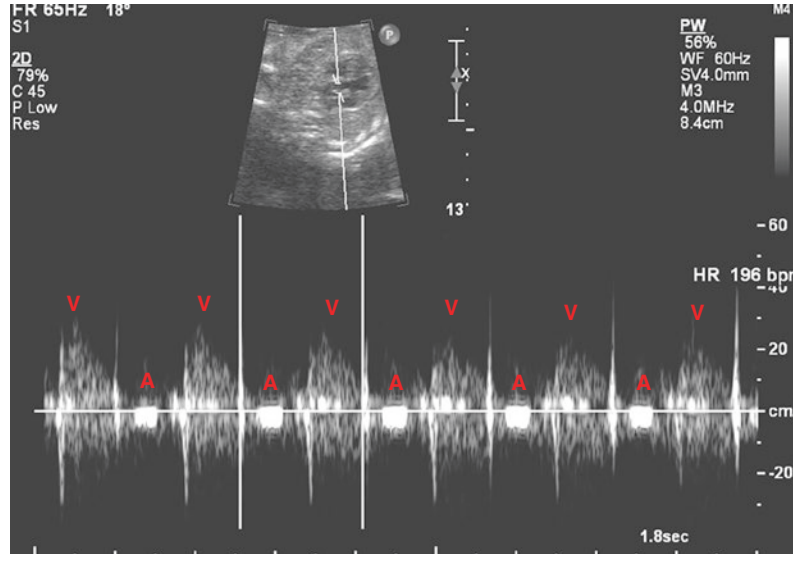

Fig. 32.31 SVC–aorta Doppler showing PJRT in the fetus at a rate of 196 bpm. PFRT can be difficult to distinguish from AET or a normal rate and rhythm

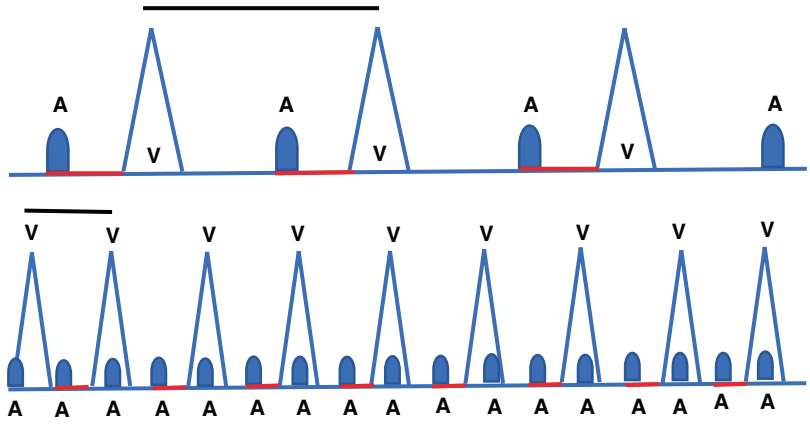

Fig. 32.32 Schematic of AF. There are more atrial contractions versus ventricular and the ventricular rate is greater than 200 bpm. The atrial rate is at 400 bpm; there are two atrial contractions for every ventricular contraction. The top strip shows normal heart rate and rhythm while the bottom strip shows atrial flutter. "A" represents atrial contraction while "V" represents the ventricular contraction. The black line indicates the time interval between ventricular contractions (between heart beats) while the red line represents the AV interval with normal beats

ticular, if the arrhythmia is fast, more enduring occurs earlier in pregnancy and is not well tolerated.

- **Atrial flutter** (Figs. 32.32, 32.33, and 32.34) results from a fast re-entrant circuit (300–600 bpm) that is located within the atriums. The AV node is not part of the re-entry but allows conduction of every second or third atrial re-entrant wave to the ventricles. AF at a rate of 440 bpm (the most frequent atrial rate) and the usual 2:1 AV conduction will therefore result in VT of 220 bpm, while the ventricular rate becomes normal with 3:1 AV conduction. AF is most commonly found in a structurally normal heart. M-mode is imaging modality of choice to evaluate AF. Referral to a fetal cardiologist and treatment with antiarrhythmics to birth is usually warranted [8–10] due to the risk of fetal compromise. AF, once converted to a normal rhythm, does not recur after birth.
- **Ventricular Tachycardia** and **Junctional Ectopic Tachycardia** are rare fetal tachyarrhythmia diagnoses. This type of tachycardia occurs when an impulse is generated within the ventricular myocardium (VT) or the AV node–His bundle (JET). The echocardiographic diagnosis of VT is based on a ventricular rate that is higher than the atrial rate and there is no clear relation between ventricular and atrial events (AV dissociation) (Figs. 32.35 and 32.36). VT most is most often seen in association with a normal heart. Other possible association include a cardiac tumors [26], long QT syndrome [31, 42], and cardiac inflammation. Urgent referral to a cardiologist for diagnostic work-up and perinatal management is warranted.

In summary, although fetal arrhythmia are not uncommon, major life-threatening conditions are fortunately rare. A stepwise diagnostic approach is useful to distinguish the different arrhythmias based on the regularity, rates, chronology, and conduction ratio of atrial and ventricular events. This approach will reduce the risk of irrational drug treatment or premature delivery of fetuses with relatively benign findings, while it may facilitate the management and improve the outcome of those with major rhythm disturbances, such as SVT and CHB.

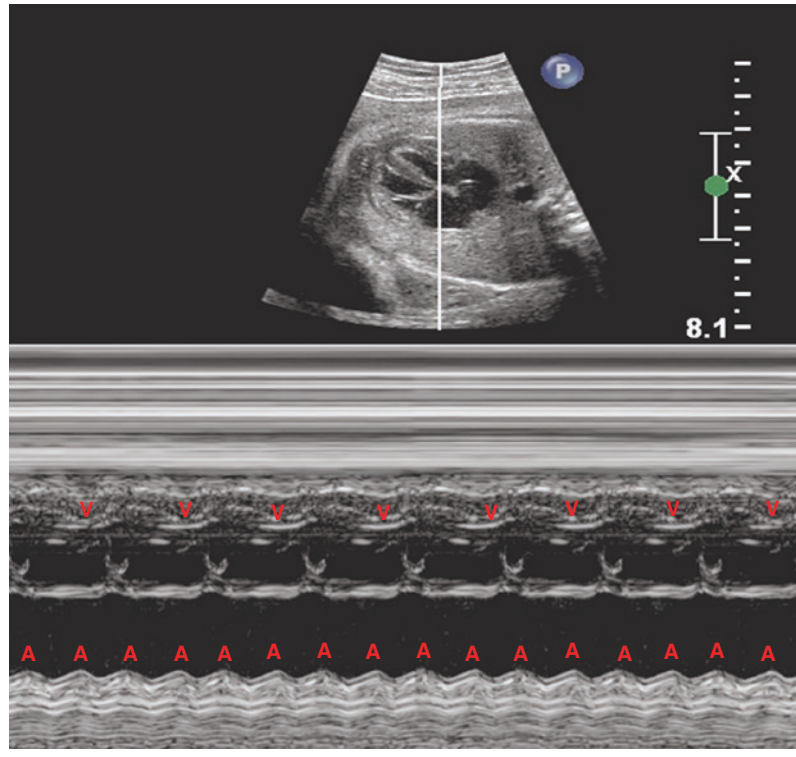

Fig. 32.33 M-mode showing AF. The ventricular rate is 220 bpm. The atrial rate is 440 bpm. There is 2:1 block

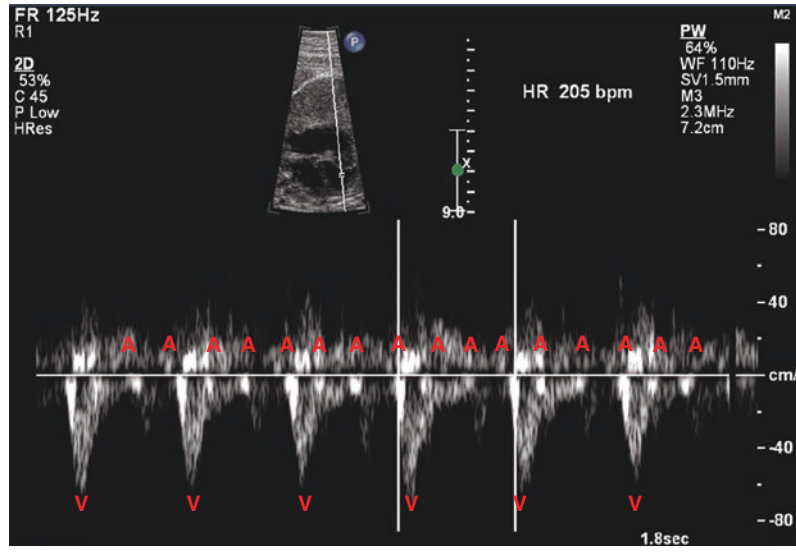

Fig. 32.34 SVC–Ao Doppler showing AF. The ventricular rate is 205 bpm

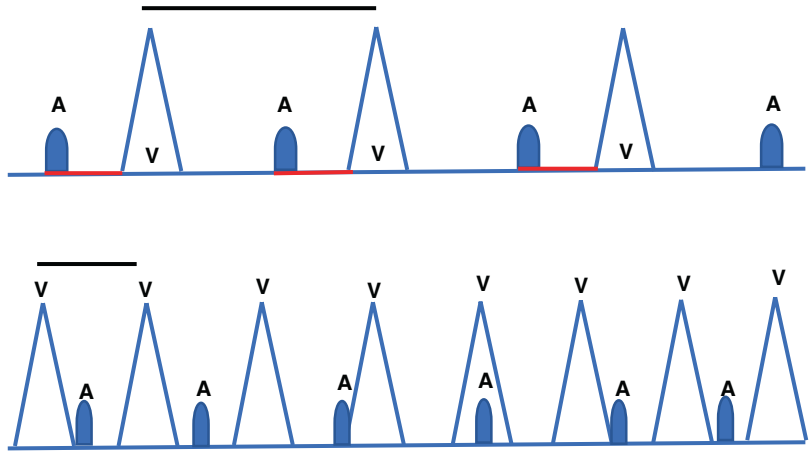

Fig. 32.35 Schematic showing normal versus VT in the fetus. There are more ventricular contractions seen versus atrial contractions. Top strip shows normal conduction while the bottom strip shows VT. "A" represents atrial contraction while "V" represents the ventricular contraction. The black line indicates the time interval between ventricular contractions (between heart beats) while the red line represents the AV interval with normal beats

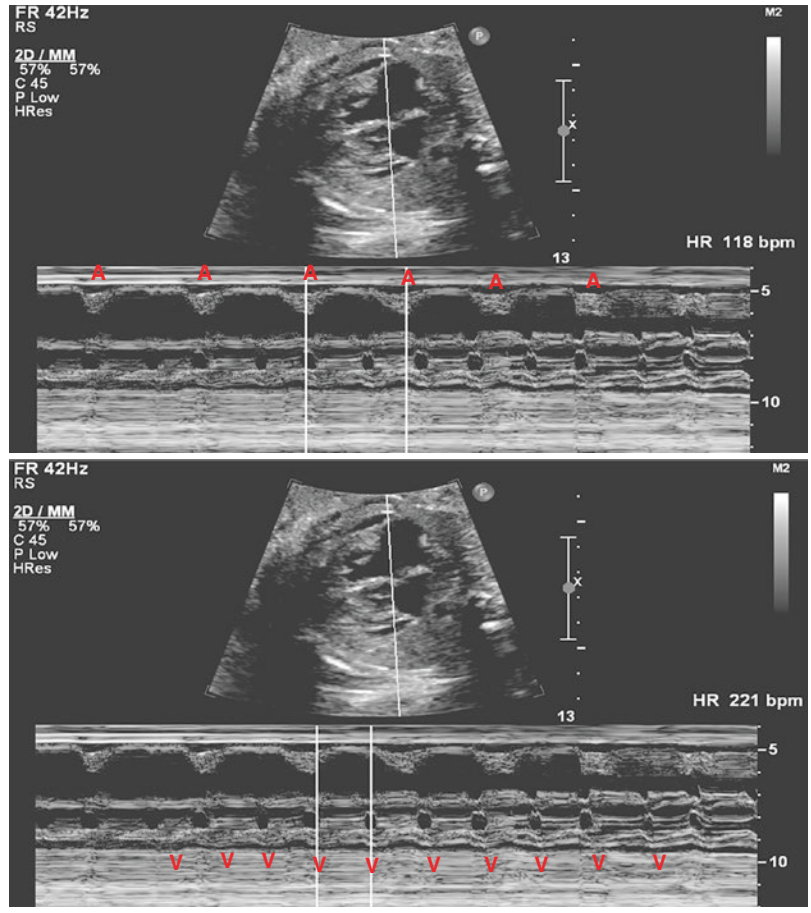

Fig. 32.36 M-mode showing VT. The ventricular rate is greater than 200 bpm. There are more ventricular contractions in comparison to atrial contraction. The atrial contractions are dissociated from the ventricular contractions and occur at a lower rate as seen in VT

References

1. Pildner von Steinburg S, Boulesteix AL, Lederer C, Grunow S, Schiermeier S, Hatzmann W, et al. What is the "normal" fetal heart rate? PeerJ. 2013;1:e82.
2. Copel JA, Kleinman CS. The impact of fetal echocardiography on perinatal outcome. Ultrasound Med Biol. 1986;12(4):327–35.
3. CMR MC, Kathryn L. Fetal arrythmias. In: Copel JAR, Kathryn L, editors. Doppler ultrasound in obsterics and gynecology. New York: Raven Press; 1995. p. 253–70.
4. Donofrio MT, Moon-Grady AJ, Hornberger LK, Copel JA, Sklansky MS, Abuhamad A, et al. Diagnosis and treatment of fetal cardiac disease: a scientific statement from the American Heart Association. Circulation. 2014;129(21):2183–242.
5. Kleinman CS, Copel JA. Electrophysiological principles and fetal antiarrhythmic therapy. Ultrasound Obstet Gynecol. 1991;1(4):286–97.
6. Kleinman CS, Copel JA. Direct fetal therapy for cardiac arrhythmias: who, what, when, where, why and how? Ultrasound Obstet Gynecol. 1991;1(3):158–60.
7. Jaeggi ET, Fouron JC, Silverman ED, Ryan G, Smallhorn J, Hornberger LK. Transplacental fetal treatment improves the outcome of prenatally diagnosed complete atrioventricular block without structural heart disease. Circulation. 2004;110(12):1542–8.
8. Jaeggi ET, Carvalho JS, De Groot E, Api O, Clur SA, Rammeloo L, et al. Comparison of transplacental treatment of fetal supraventricular tachyarrhythmias with digoxin, flecainide, and sotalol: results of a nonrandomized multicenter study. Circulation. 2011;124(16):1747–54.
9. Simpson JM, Sharland GK. Fetal tachycardias: management and outcome of 127 consecutive cases. Heart. 1998;79(6):576–81.
10. Jaeggi E, Fouron JC, Drblik SP. Fetal atrial flutter: diagnosis, clinical features, treatment, and outcome. J Pediatr. 1998;132(2):335–9.
11. Kleinman CS, Donnerstein RL, Jaffe CC, DeVore GR, Weinstein EM, Lynch DC, et al. Fetal echocardiography. A tool for evaluation of in utero cardiac arrhythmias and monitoring of in utero therapy: analysis of 71 patients. Am J Cardiol. 1983;51(2):237–43.
12. Fouron JC. Fetal arrhythmias: the Saint-Justine hospital experience. Prenat Diagn. 2004;24(13):1068–80.
13. Raboisson MJ, Fouron JC, Sonesson SE, Nyman M, Proulx F, Gamache S. Fetal Doppler echocardiographic diagnosis and successful steroid therapy of Luciani-Wenckebach phenomenon and endocardial fibroelastosis related to maternal anti-Ro and anti-La antibodies. J Am Soc Echocardiogr. 2005;18(4):375–80.
14. Dancea A, Fouron JC, Miro J, Skoll A, Lessard M. Correlation between electrocardiographic and ultrasonographic time-interval measurements in fetal lamb heart. Pediatr Res. 2000;47(3):324–8.
15. Strasburger JF, Huhta JC, Carpenter RJ Jr, Garson A Jr, McNamara DG. Doppler echocardiography in the diagnosis and management of persistent fetal arrhythmias. J Am Coll Cardiol. 1986;7(6):1386–91.
16. Reed KL, Sahn DJ, Marx GR, Anderson CF, Shenker L. Cardiac Doppler flows during fetal arrhythmias: physiologic consequences. Obstet Gynecol. 1987;70(1):1–6.
17. Tutschek B, Schmidt KG. Pulsed-wave tissue Doppler echocardiography for the analysis of fetal cardiac arrhythmias. Ultrasound Obstet Gynecol. 2011;38(4):406–12.
18. Wojakowski A, Izbizky G, Carcano ME, Aiello H, Marantz P, Otano L. Fetal Doppler mechanical PR interval: correlation with fetal heart rate, gestational age and fetal sex. Ultrasound Obstet Gynecol. 2009;34(5):538–42.
19. Gagnon C, Bigras JL, Fouron JC, Dallaire F. Reference Values and Z Scores for Pulsed-Wave Doppler and M-Mode Measurements in Fetal Echocardiography. J Am Soc Echocardiogr. 2016;29(5):448–60 e9.
20. Kurihara Y, Tachibana D, Yanai S, Kitada K, Sano M, Wada N, et al. Characteristic differences and reference ranges for mitral, tricuspid, aortic, and pulmonary Doppler velocity waveforms during fetal life. Prenat Diagn. 2015;35(3):236–43.
21. Bolnick AD, Borgida AF, Egan JF, Zelop CM. Influence of gestational age and fetal heart rate on the fetal mechanical PR interval. J Matern Fetal Neonatal Med. 2004;15(5):303–5.
22. Fouron JC, Proulx F, Miro J, Gosselin J. Doppler and M-mode ultrasonography to time fetal atrial and ventricular contractions. Obstet Gynecol. 2000;96(5 Pt 1):732–6.
23. Carvalho JS, Prefumo F, Ciardelli V, Sairam S, Bhide A, Shinebourne EA. Evaluation of fetal arrhythmias from simultaneous pulsed wave Doppler in pulmonary artery and vein. Heart. 2007;93(11):1448–53.
24. Allan LD, Joseph MC, Boyd EG, Campbell S, Tynan M. M-mode echocardiography in the developing human fetus. Br Heart J. 1982;47(6):573–83.
25. Stewart PA, Wladimiroff JW. Fetal atrial arrhythmias associated with redundancy/aneurysm of the foramen ovale. J Clin Ultrasound. 1988;16(9):643–50.
26. Wacker-Gussmann A, Strasburger JF, Cuneo BF, Wiggins DL, Gotteiner NL, Wakai RT. Fetal arrhythmias associated with cardiac rhabdomyomas. Heart Rhythm. 2014;11(4):677–83.
27. Jaeggi E, Ohman A. Fetal and Neonatal Arrhythmias. Clin Perinatol. 2016;43(1):99–112.
28. Kleinman CS, Copel JA, Weinstein EM, Santulli TV Jr, Hobbins JC. In utero diagnosis and treatment of fetal supraventricular tachycardia. Semin Perinatol. 1985;9(2):113–29.
29. Mitchell JL, Cuneo BF, Etheridge SP, Horigome H, Weng HY, Benson DW. Fetal heart rate predictors of long QT syndrome. Circulation. 2012;126(23):2688–95.

30. Young BK, Katz M, Klein SA, Silverman F. Fetal blood and tissue pH with moderate bradycardia. Am J Obstet Gynecol. 1979;135(1):45–7.
31. Horigome H, Nagashima M, Sumitomo N, Yoshinaga M, Ushinohama H, Iwamoto M, et al. Clinical characteristics and genetic background of congenital long-QT syndrome diagnosed in fetal, neonatal, and infantile life: a nationwide questionnaire survey in Japan. Circ Arrhythm Electrophysiol. 2010;3(1):10–7.
32. Lin JH, Chang CI, Wang JK, Wu MH, Shyu MK, Lee CN, et al. Intrauterine diagnosis of heterotaxy syndrome. Am Heart J. 2002;143(6):1002–8.
33. Berg C, Geipel A, Kohl T, Breuer J, Germer U, Krapp M, et al. Atrioventricular block detected in fetal life: associated anomalies and potential prognostic markers. Ultrasound Obstet Gynecol. 2005;26(1):4–15.
34. Jaeggi ET, Hornberger LK, Smallhorn JF, Fouron JC. Prenatal diagnosis of complete atrioventricular block associated with structural heart disease: combined experience of two tertiary care centers and review of the literature. Ultrasound Obstet Gynecol. 2005;26(1):16–21.
35. Lopes LM, Tavares GM, Damiano AP, Lopes MA, Aiello VD, Schultz R, et al. Perinatal outcome of fetal atrioventricular block: one-hundred-sixteen cases from a single institution. Circulation. 2008;118(12):1268–75.
36. Schmidt KG, Ulmer HE, Silverman NH, Kleinman CS, Copel JA. Perinatal outcome of fetal complete atrioventricular block: a multicenter experience. J Am Coll Cardiol. 1991;17(6):1360–6.
37. Hutter D, Silverman ED, Jaeggi ET. The benefits of transplacental treatment of isolated congenital complete heart block associated with maternal anti-Ro/SSA antibodies: a review. Scand J Immunol. 2010;72(3):235–41.
38. Epstein AE, DiMarco JP, Ellenbogen KA, Estes NA 3rd, Freedman RA, Gettes LS, et al. ACC/AHA/HRS 2008 guidelines for device-based therapy of cardiac rhythm abnormalities: a report of the American College of Cardiology/American Heart Association Task Force on Practice guidelines (Writing Committee to Revise the ACC/AHA/NASPE 2002 Guideline Update for Implantation of Cardiac Pacemakers and Antiarrhythmia Devices) developed in collaboration with the American Association for Thoracic Surgery and Society of Thoracic Surgeons. J Am Coll Cardiol. 2008;51(21):e1–62.
39. Odendaal HJ, Crawford JW. Fetal tachycardia and maternal pyrexia during labour. S Afr Med J. 1975;49(45):1873–5.
40. Cohn HE, Piasecki GJ, Jackson BT. The effect of beta-adrenergic stimulation on fetal cardiovascular function during hypoxemia. Am J Obstet Gynecol. 1982;144(7):810–6.
41. Cohn HE, Sacks EJ, Heymann MA, Rudolph AM. Cardiovascular responses to hypoxemia and acidemia in fetal lambs. Am J Obstet Gynecol. 1974;120(6):817–24.
42. Cuneo BF, Strasburger JF, Yu S, Horigome H, Hosono T, Kandori A, et al. In utero diagnosis of long QT syndrome by magnetocardiography. Circulation. 2013;128(20):2183–91.

4D Fetal Doppler Echocardiography

33

Greggory R. DeVore

33.1 Introduction

In the late 1980s color Doppler ultrasound was introduced to examine cardiovascular flow characteristics in fetuses with congenital heart defects [1–14]. With the introduction of 3D and 4D ultrasound probes in 2003 by General Electric and Philips Ultrasound, a new era of fetal cardiovascular imaging was introduced as research concepts evolved into clinical tools [15–20]. The 3D and 4D probes used a mechanical sweep technique called Spatiotemporal Image Correlation (STIC) in which multiple 2-dimensional images were stacked one behind the other to create a volume dataset [15, 16]. The STIC was placed on endovaginal and transabdominal probes from which three-dimensional voxels were created that had X, Y, and Z components, resulting in three simultaneously displayed images referred to as the A, B, and C planes which were displayed in a cine loop (Fig. 33.1). Since the first publication by DeVore in 2003, over 150 scientific papers have been cited in PubMed describing the use of STIC technology [15]. In addition to the mechanical STIC probe, Philips ultrasound offered an xMATRIX array probe that was designed for applications in adult and pediatric cardiology. However, this probe did not gain wide utilization in the obstetrical community as supported by the paucity of publications describing its use in fetal cardiology [20–26].

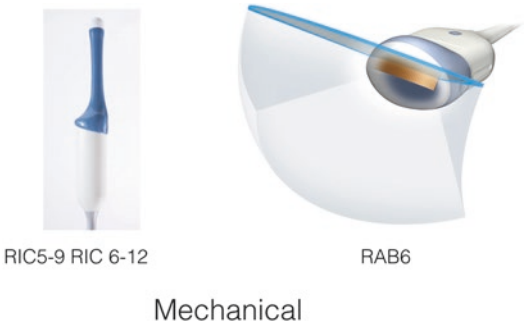

Fig. 33.1 Two mechanical STIC probes used for evaluating the fetal heart during the first, second, and third trimesters of pregnancy. The RIC5–9 and RIC 6–12 are used for first trimester imaging and the RAB6 used for first, second, and third trimester evaluations. For each probe the 2-dimensional ultrasound beam is mechanically swept over a distance from which images are acquired and then combined to create the 3D and 4D volumes

In 2014 GE ultrasound introduced a 4D matrix probe in which the voxels comprising the 3-dimensional volume were simultaneously recorded as sub-volumes, and then stitched together to comprise a single 4D volume (Fig. 33.2). Unlike the xMATRIX probe, the GE matrix probe could be used for a number of different fetal applications, other than just imaging the fetal cardiovascular system. The benefits of the GE matrix probe were

G. R. DeVore (✉)
Division of Maternal-Fetal Medicine, Department of Obstetrics and Gynecology, David Geffen School of Medicine at UCLA, Pasadena, CA, USA

Fetal Diagnostic Centers, Pasadena, Tarzana, and Lancaster, Pasadena, CA, USA
e-mail: grdevore@gmail.com

D. Maulik, C. C. Lees (eds.), *Doppler Ultrasound in Obstetrics and Gynecology*,
https://doi.org/10.1007/978-3-031-06189-9_33

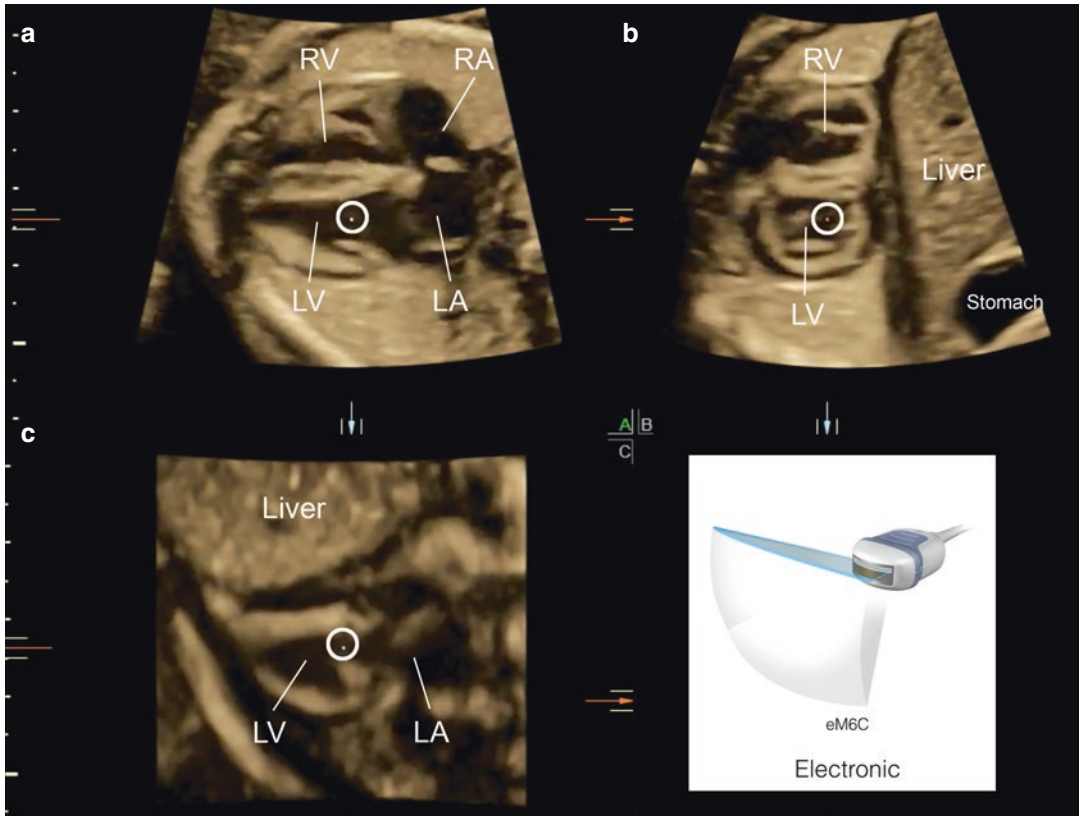

Fig. 33.2 This represents an eSTIC image acquisition in which a matrix probe beam is directed through the area of interest. The matrix sweep allows for non-artifact acquisition of voxels so that the image is artifact free. Depending upon the size of the sweep, either a single volume is used or multiple volumes are stitched together to display the cardiac structures in three planes that are perpendicular to each other. The (**a**) plane represents the 4-chamber view, the (**b**) plane a short axis of the 4-chamber view, and the (**c**) plane the 2-chamber view of the left ventricle (LV). The reference dot (white circle) indicates the point in each plane that corresponds to the images in the other 2 planes. *RV* right ventricle, *RA* right atrium, *LA* left atrium

the following: (1) the size of the acquired volume sweep was no longer related to the resolution, as it was with the mechanical STIC probe; (2) each sub-volume was artifact free in the X,Y, and Z planes; (3) depending upon the size of the fetus, two or fewer sub-volumes could be used to image the fetal cardiovascular system during the first and second trimesters of pregnancy, and (4) 40 volumes comprised a single cardiac cycle providing improved image resolution.

This review will focus on the use of STIC technology to evaluate the use of 4D color and power Doppler to evaluate fetal cardiovascular anatomy to identify normal as well as abnormal cardiovascular anatomy from 11 to 40 weeks of gestation.

33.2 Historical Perspective of Spatiotemporal Imaging Technology (STIC) and the Incorporation of Color and Power Doppler Imaging Modalities

In 2004 Chaoui reported using Color Doppler STIC technology in 35 normal fetuses and 27 fetuses with congenital heart defects examined between 18 and 35 weeks of gestation [27]. The image display reported by Chaoui was similar to that first reported by DeVore in 2003, except they incorporated a color Doppler overlay superimposed on the 2-dimensional grayscale image (Fig. 33.3) [15]. Adequate color Doppler STIC

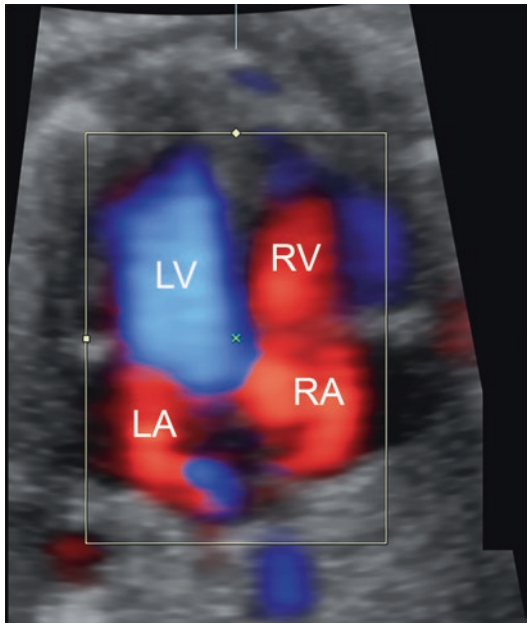

Fig. 33.3 The color Doppler superimposed on the gray-scale image of the 4-chmaber view obtained from a mechanical STIC acquisition. Because of the low volume frame rate, the systolic flow (blue image in the LV) is superimposed on the image in which diastolic flow is indicted (red). *LV* left ventricle, *RV* right ventricle, *LA* left atrium, *RA* right atrium

imaging was feasible in 24 of 27 fetuses with congenital heart defects. The STIC color technology accurately identified fetuses with a hypoplastic right ventricle with tricuspid regurgitation, hypoplastic left ventricle, tetralogy of Fallot, D-transposition of the great arteries, and an atrioventricular canal defect [27].

In 2005, DeVore reported the use of STIC to display color Doppler flow in the heart and great arteries using Tomographic Ultrasound Imaging (TUI) in which a volume dataset was sliced in equidistant transverse planes to demonstrate the 4-chamber, 5-chamber, 3-vessel, and tracheal views (Fig. 33.4) [14, 28–30]. In 2006, Goncalves examined 168 fetuses using STIC color Doppler and the TUI display [31]. They reported visualization of the 4-chamber view in 98.5%, 5-chamber view in 97%, and the 3-vessel view and tracheal view in 83.6%. In 16 fetuses with congenital heart effects. They reported that TUI color Doppler imaging added additional diagnostic information in 31.5% of fetuses with heart malfomations [31]. In these studies the mechanical STIC probe was used which often resulted in diastolic and systolic flows superimposed upon each other (Fig. 33.3).

In 2009 Gindes examined 128 fetuses with CHD between 13 and 38 weeks of gestation using STIC technology in which they combined 3 imaging modalities; 2-dimensional grayscale, B-flow, and color Doppler ultrasound [32]. They reported that integration of all 3 modalities were necessary to optimally identify the pathological conditions identified in their study [32].

In 2009 Turan examined 107 low-risk patients for fetal CHD evaluated between 11 and 13 weeks 6 days of gestation with STIC color Doppler ultrasound using the TUI imaging display [33]. Each fetus was evaluated for adequacy of imaging the cardiac axis, four-chamber view, 5-chamber view, 3-vessel view, and tracheal views. The body mass index of the pregnant women ranged between 17.2 and 50.2 kg/m^2 [33]. More than 3 volumes were required in 20% of patients and the time to acquire the volumes ranged between 1 and 4 min, with an average of 1 min 40 s [33]. Visualization of all structures occurred in 85%, with the highest visualization occurring for the 4-chamber view (100%%) [33]. The transabdominal probe successfully identified the anatomy in 91.6%, with 8.4% requiring an endovaginal probe to complete the examination [33].

Following the feasibility study by Turan, Votino in 2013 reported their results examining fetuses between 11 and 14 weeks in 139 fetuses, of which 27 had congenital heart defects [34]. They reported that STIC color Doppler imaging improved the identification of the outflow tracts compared to 2D imaging (Fig. 33.5) with an accuracy of 94.2% for detection of cardiac malformations [34]. The major abnormalities that were correctly identified included fetuses with ventricular disproportion (hypoplastic left ventricle, coarctation of the aorta, and tricuspid atresia), transposition of the greater arteries, and atrioventricular canal defects [34].

In 2013 Tudorache evaluated the intra- and interobserver agreement for first trimester fetal cardiac examinations in which they evaluated 11

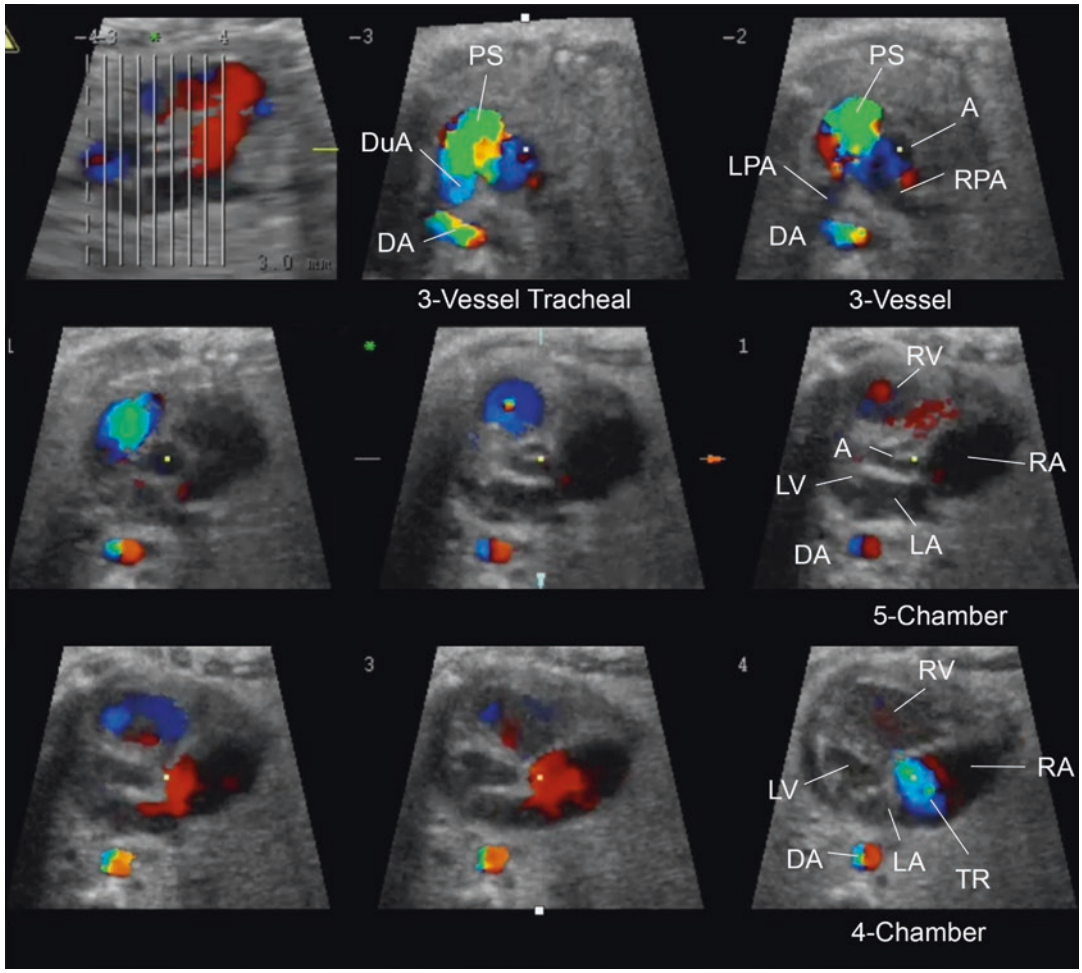

Fig. 33.4 The TUI image acquisition using a mechanical STIC acquisition in which the 4-chamber, 5-chamber, 3-vessel, and tracheal views are displayed. The image demonstrates tricuspid regurgitation in the 4-chamber view and pulmonary stenosis as represented by aliasing of blood flow at the level of the pulmonary outflow tract in both the 3-vessel and tracheal views. *A* aorta, *RV* right ventricle, *LV* left ventricle, *RA* right atrium, *LA* left atrium, *DA* descending aorta, *TR* tricuspid regurgitation, *RPA* right pulmonary artery, *LPA* left pulmonary artery, *DuA* ductus arteriosus, *PS* pulmonary stenosis

anatomical relationships comparing the 2-dimensional freehand sweep with 4D STIC TUI acquisition to assess the advantages of the STIC technique in 100 randomly selected fetuses from a database of 632 fetuses who had confirmed normal neonatal cardiovascular examinations [35]. The fetuses presented between 12 and 13 weeks 6 days. The intraobserver and interobserver variability between the two methods demonstrated good agreement (kappa >0.6). They also reported that color Doppler added valuable information for evaluating cardiac structures compared to grayscale imaging, irrespective of the acquisition method used (2D vs STIC) [35].

In 2013 Lima prospectively examined 54 fetuses between 12 and 14 weeks using STIC B-mode and color Doppler to evaluate the efficiency of these two modalities for identifying the 4-chamber, right and left ventricular outflow tracts, and the aortic arch views using the TUI image display with either an abdominal or and endovaginal probe [36]. When comparing B-mode with color Doppler, the addition of color Doppler increased the accurate identification of

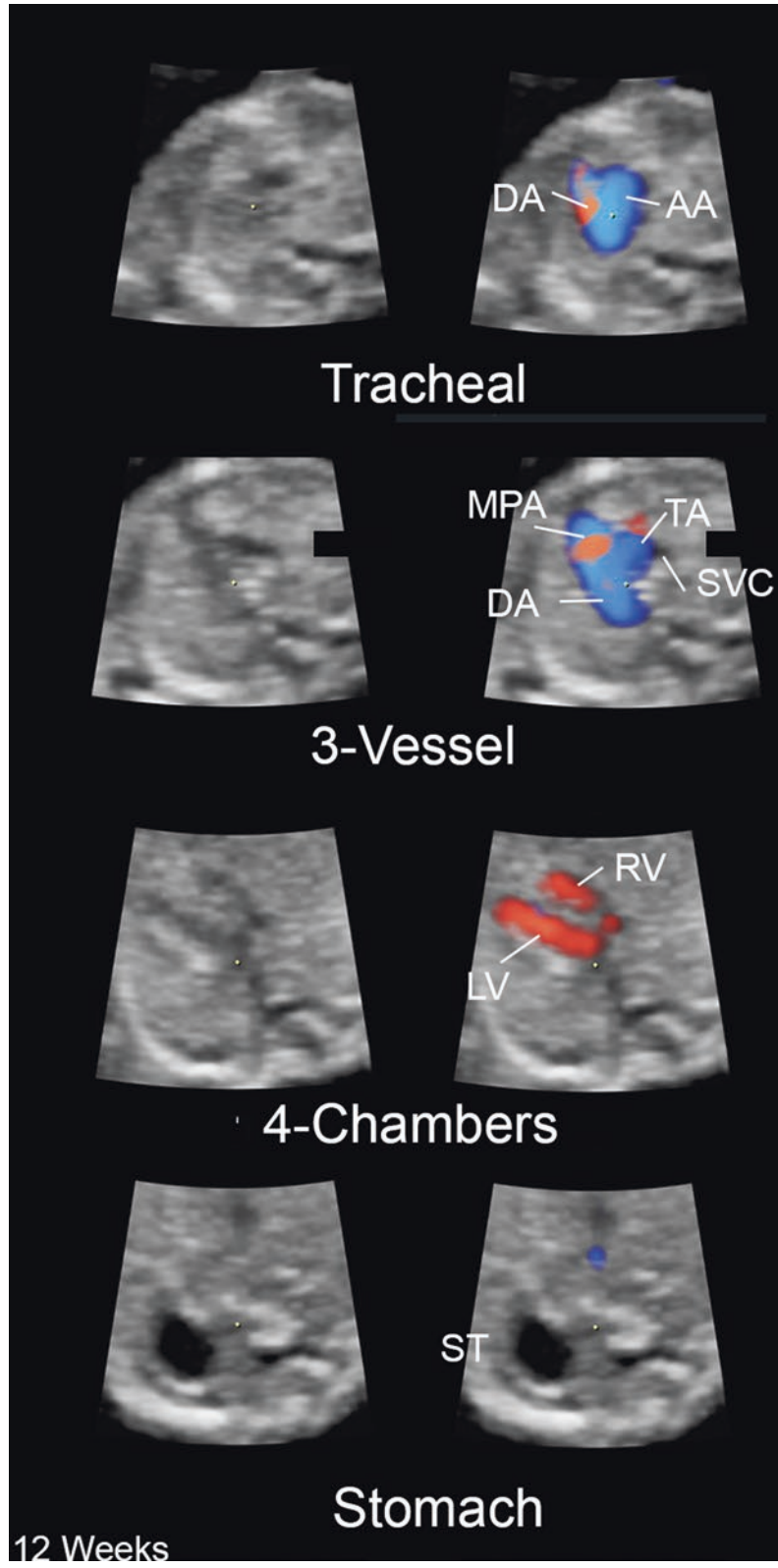

Fig. 33.5 Transverse images from a 12-week fetus comparing grayscale with the power Doppler imaging. The power Doppler clearly identifies the main pulmonary artery (MPA), transverse aorta (TA), and the ductus arteriosus (DA) in the 3-vessel view as well as the DA and aortic arch (AA) in the tracheal view when compared to the corresponding grayscale image. *RV* right ventricle, *LV* left ventricle, *ST* stomach

cardiac anatomy from 30.2 to 75.5% for the abdominal approach, and from 30.2 to 66% with the endovaginal approach [36]. When the abdominal and endovaginal image acquisitions were combined, the identification of the cardiac structures using B-mode was 52.8%, which was increased to 90.6% with the incorporation of color Doppler ultrasound [36].

In 2017 Yeo reported a new application of STIC color Doppler imaging technology using automation derived from an artificial intelligence algorithm to identify the following: (1) stomach within the abdominal cavity, (2) 4-chamber view, (3) 5-chamber view, (4) left outflow tract, (5) short axis of the great vessels, (6) right outflow tract, (7) 3-vessel and tracheal views, (8) ductal arch, (9) aortic arch, and (10) the superior and inferior vena cava [37]. They applied this technique to 60 fetuses in which color Doppler (N = 27) or power Doppler (N = 33) was used (Fig. 33.6) [37]. They noted that this technique consistently identified the first 9 views listed

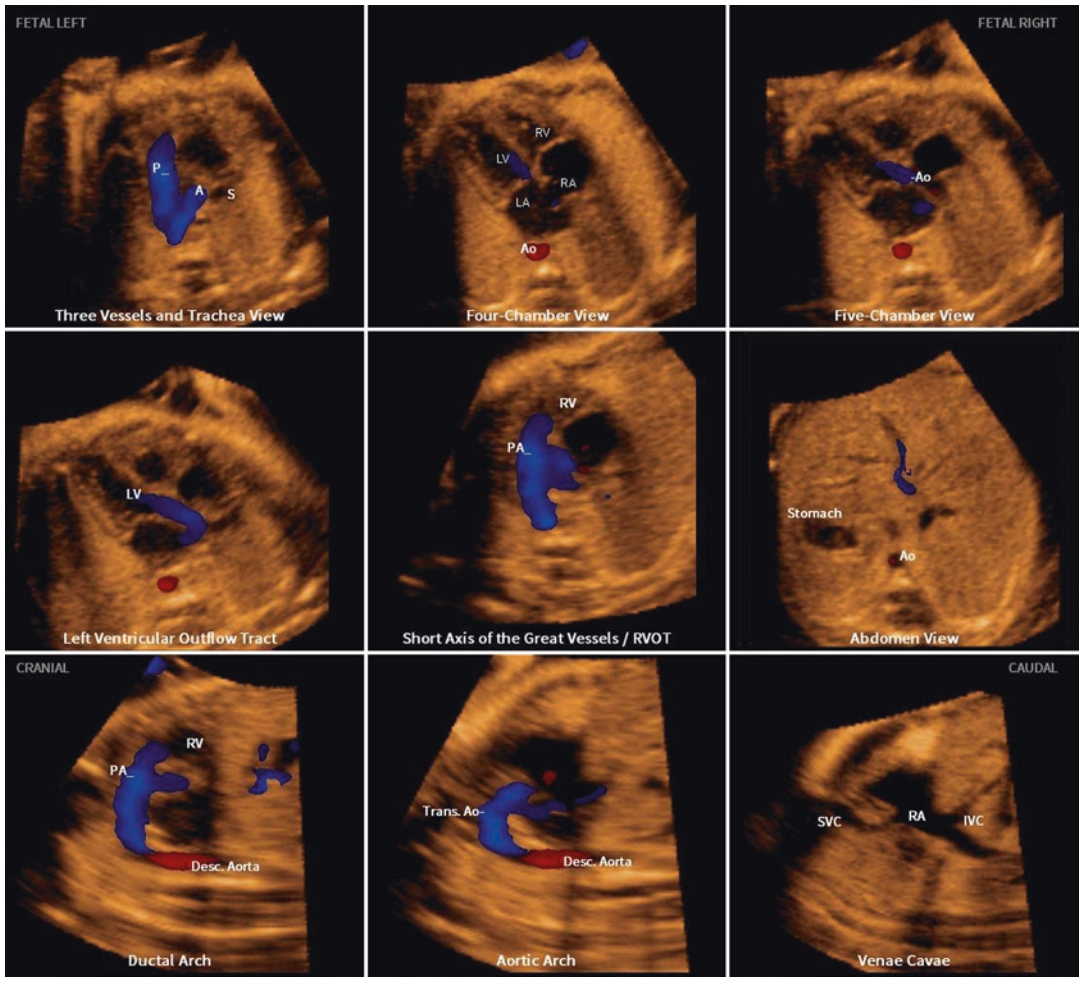

Fig. 33.6 Color Doppler spatiotemporal image correlation volume dataset of a normal fetal heart, showing nine cardiac diagnostic planes displayed automatically in a single template through color Doppler Fetal Intelligent Navigation Echocardiography (FINE) or 5D Heart Color. The color Doppler signals are displayed in systole. The unique feature of automatic labeling (through intelligent navigation) of each plane, anatomical structures, fetal left and right sides, and cranial and caudal ends is shown. *A* transverse aortic arch; *Ao* aorta; *Desc* descending; *IVC* inferior vena cava; *LA* left atrium; *LV* left ventricle; *P* pulmonary artery; *PA* pulmonary artery; *RA* right atrium; *RV* right ventricle; *RVOT* right ventricular outflow tract; *S* superior vena cava; *SVC* superior vena cava; *Trans* transverse [37]

above during the second and third trimesters of pregnancy, with the lowest detection rate for the superior and inferior vena cava [37].

33.3 Newer Applications of Color and Power Doppler STIC Technology

33.3.1 First Trimester Rendered Images of the Cardiovascular System

In 2018 DeVore reported the use of a new imaging technology called Radiant flow in which the rendered color and power Doppler image display displayed appeared to have a 3-dimensional perspective (Fig. 33.7) [38]. Using the new Radiant flow imaging technology, rendered STIC volumes were obtained using the vaginal probe displaying the fetal cardiovascular system using color and power Doppler ultrasound (Figs. 33.8, 33.9, and 33.10). From the STIC acquisition the image could be displayed in real time, as a still image, or as a still image rotated around a 360 degree axis. This technique was especially useful when the fetal body was not perpendicular to the ultrasound beam from which the cardiac structures are viewed in the transverse plane. Therefore, using this technique, hypoplastic ventricular chambers, D-transposition, and arch and other vessel anomalies can be excluded (Fig. 33.11).

33.3.2 Second and Third Trimester Identification of Complicated Arch Anomalies and Pulmonary Veins

Rendering of STIC and eSTIC volumes using color and power Doppler allows the examiner to create 3-dimensional models of arch anomalies, as well as identify the 4 pulmonary veins as well as other vascular structures, such as the mammary arteries (Figs. 33.12, 33.13, 33.14, and 33.15).

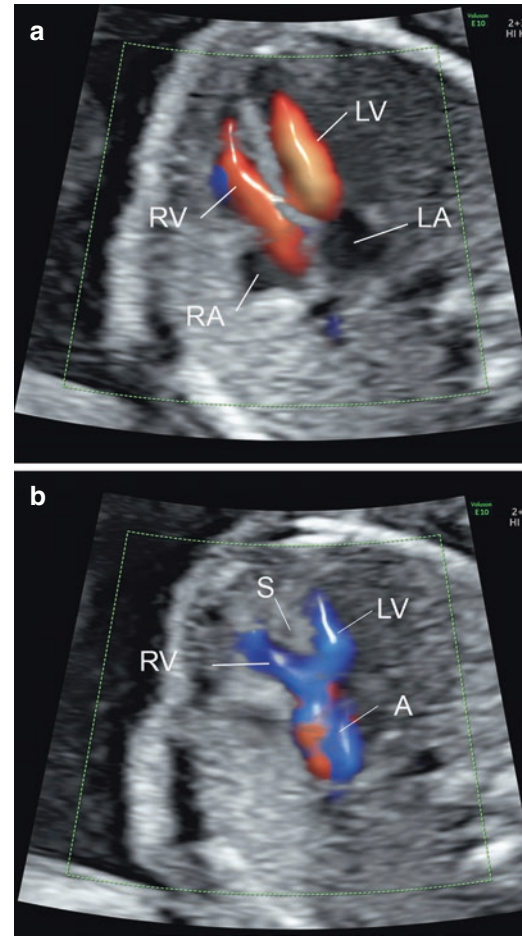

Fig. 33.7 Radiant flow from a 2-dimensional image from a fetus with tetralogy of Fallot. The color rendering has a 3-dimensional appearance. (**a**) Inflow of blood into the right and left ventricles. (**b**) Blood flow along the right and left interventricular septum during systole entering the ascending aorta. This flow pattern is commonly seen with tetralogy of Fallot. *RV* right ventricle, *LV* left ventricle, *RA* right atrium, *LA* left atrium, *S* interventricular septum, *A* ascending aorta

33.3.3 Second and Third Trimester Identification of the Location of Ventricular Septal Defects

Using STIC color and power Doppler technology the examiner can image the heart in 3D and render blood flow patterns to illustrate cardiac pathology (Figs. 33.16 and 33.17).

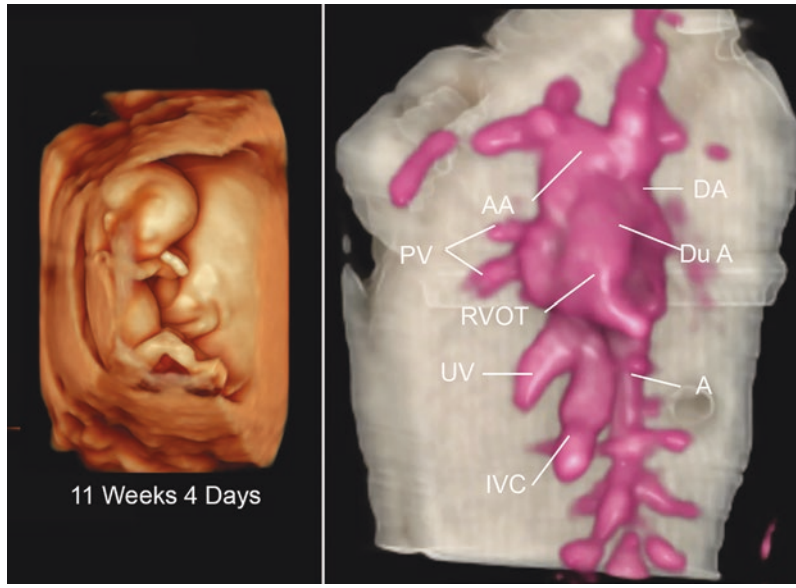

Fig. 33.8 This STIC acquisition using an endovaginal probe from a fetus of 11 weeks and 4 days. Because the fetus was in a position that a transverse sweep through the chest was not possible, 4D acquisition using monochromatic Power Doppler illustrates cardiovascular anatomy. From this image D-transposition can be excluded as the ductus arteriosus (DuA) can be observed under the aortic arch. In addition, pulmonary veins can be observed (PV). *IVC* inferior vena cava, *UV* umbilical vein, *RVOT* right ventricular outflow tract, *AA* ascending aorta, *A* aorta

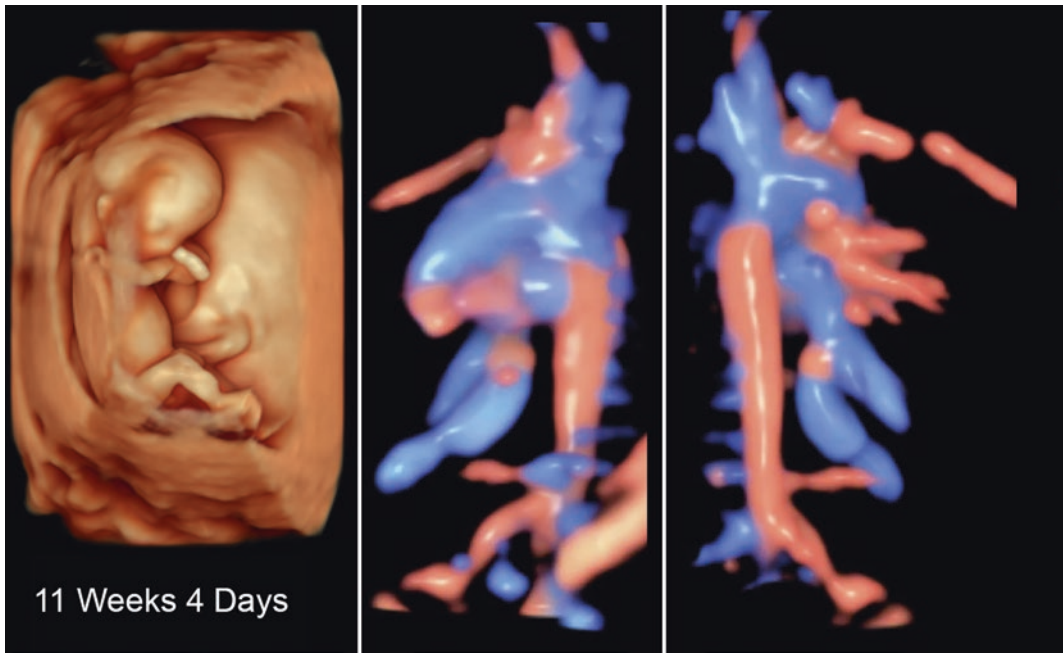

Fig. 33.9 STIC acquisition using an endovaginal probe from a fetus at 11 weeks 4 days. The rendered volume using radiant flow imaging demonstrates detailed anatomy of the aorta and venous vessels as well as the ventricles and atrial chambers. These images were obtained by rotating the 4D rendered volume to identify the vascular structures

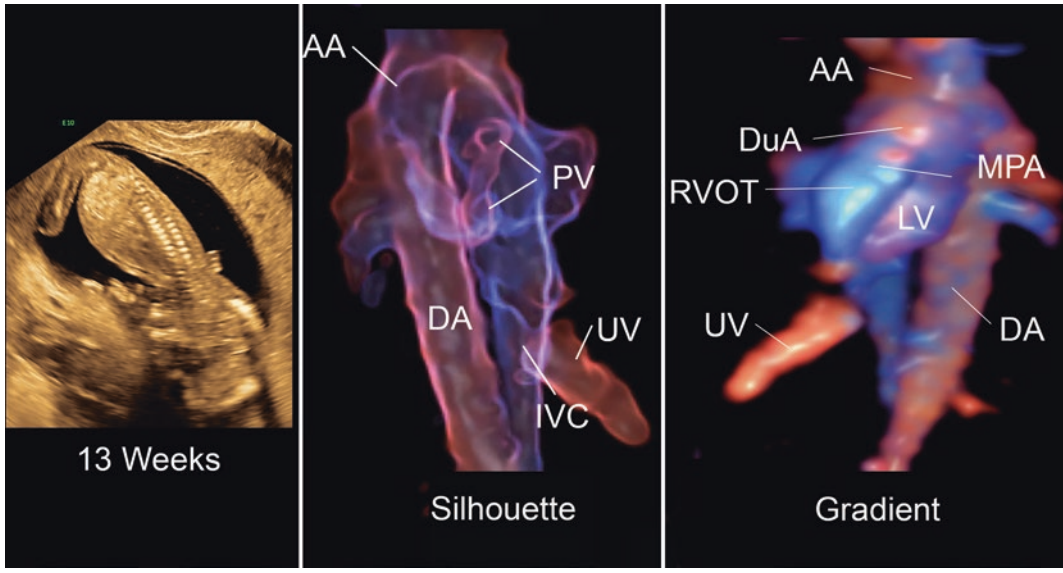

Fig. 33.10 A 13-week fetus in which a Silhouette algorithm is used to highlight the walls of the vessels. In this image the pulmonary veins (PV) are clearly identified. The gradient flow image demonstrates the ductus arteriosus (DuA) entering below the aortic arch, as well as the right ventricular outflow tract (RVOT). *AA* ascending aorta, *DA* descending aorta, *IVC* inferior vena cava, *UV* umbilical vein, *RVOT* right ventricular outflow tract, *MPA* main pulmonary artery

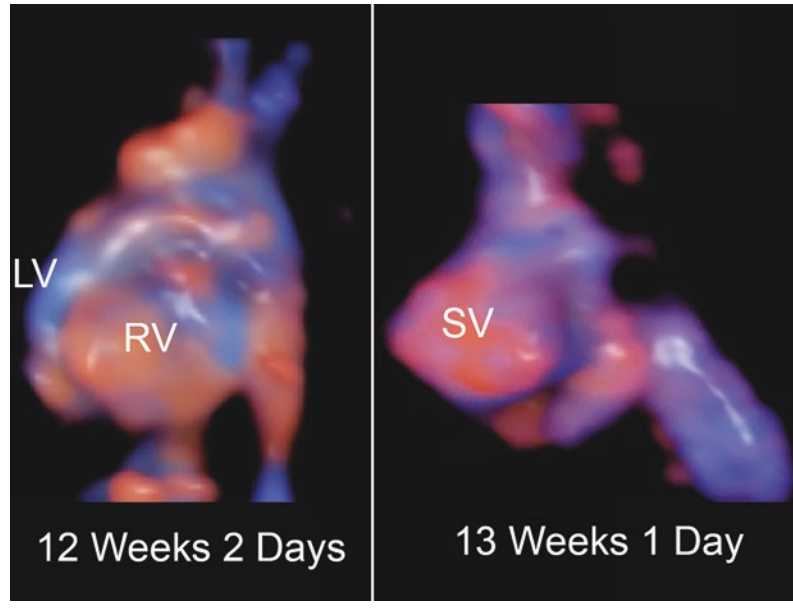

Fig. 33.11 Rendering of two first trimester hearts. (**a**) Normal fetal heart at 12 weeks and 2 days. (**b**) Abnormal fetal heart with a single ventricle (SV) at 13 weeks and 1 day. *LV* left ventricle, *RV* right ventricle

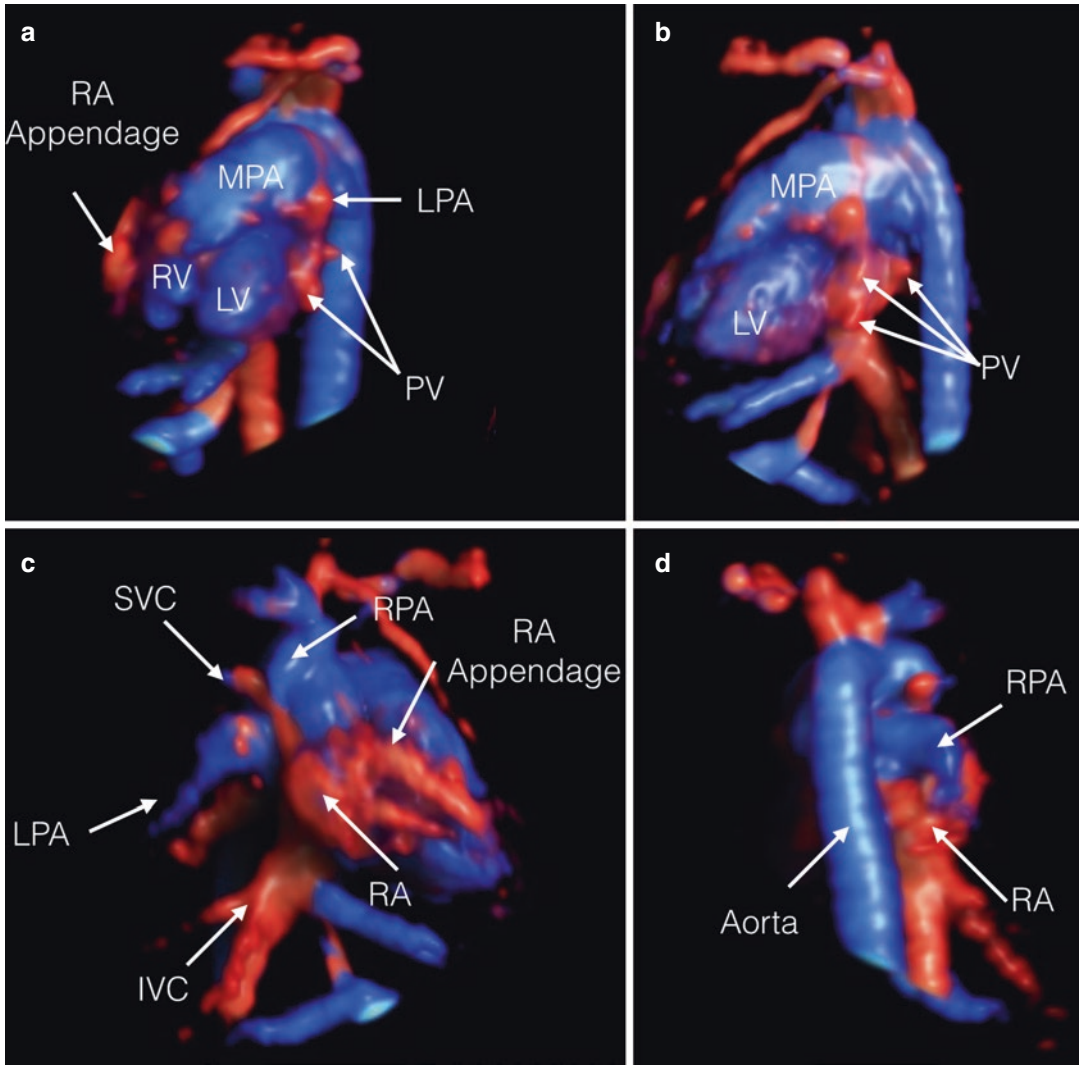

Fig. 33.12 Rendered fetal heart at 25 weeks demonstrating cardiac and vascular structures as the rendered volume is rotated to examine the front (**a**), side (**b**), and back (**c**, **d**) of the heart and vessels. *RA* right atrium, *MPA* main pulmonary artery, *LPA* left pulmonary artery, *PV* pulmonary veins, *RV* right ventricle, *LV* left ventricle, *IVC* inferior vena cava, *RA* right atrium, *RPA* right pulmonary artery, *RA* right atrium

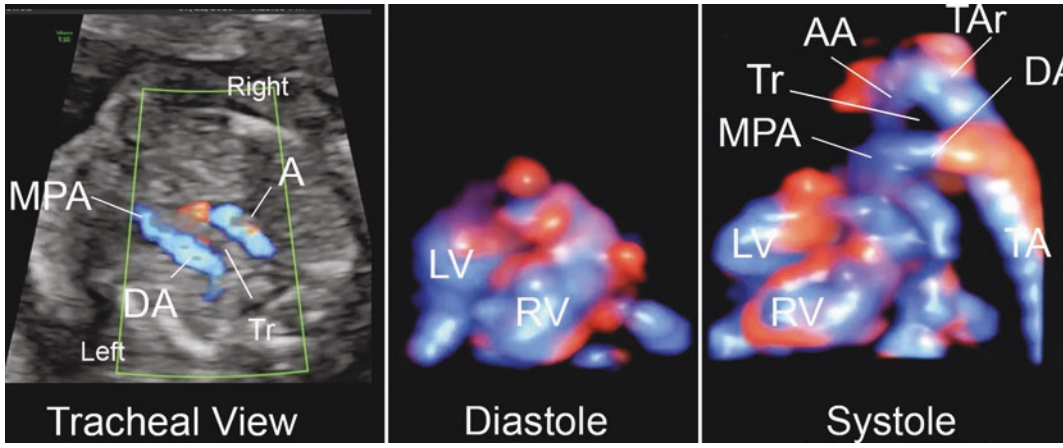

Fig. 33.13 Right-sided aortic arch in a 20-week fetus. The 2-dimensional tracheal view demonstrates separation of the ductus arteriosus (DA) from the transverse aortic arch. The rendered STIC images are illustrated in diastole and systole. The systolic image demonstrates the right-sided aortic arch (AA). The fetus has DiGeorge syndrome. *Tr* trachea, *MPA* main pulmonary artery, *MPA* main pulmonary artery, *Tar* transverse aortic arch, *TA* thoracic aorta, *LV* left ventricle, *RV* right ventricle

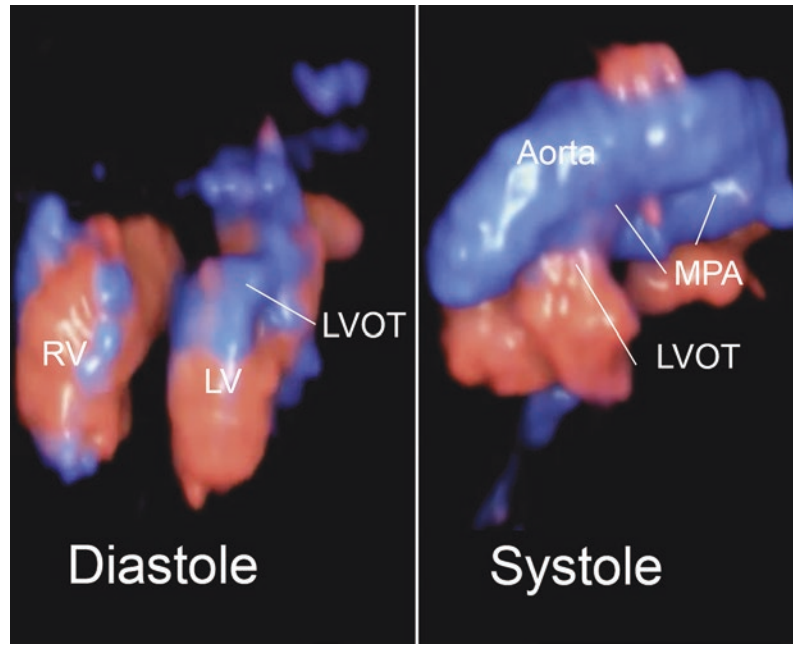

Fig. 33.14 D-transposition of the great arteries in a 21-week fetus. The diastolic image demonstrates filling of the right (RV) and left (LV) ventricles and the position of the left outflow tract (LVOT). The systolic image demonstrates the LVOT which becomes the MPA. The larger vessel originates from the RV and becomes the aorta with vessels originating from the cephalad portion of the vessel

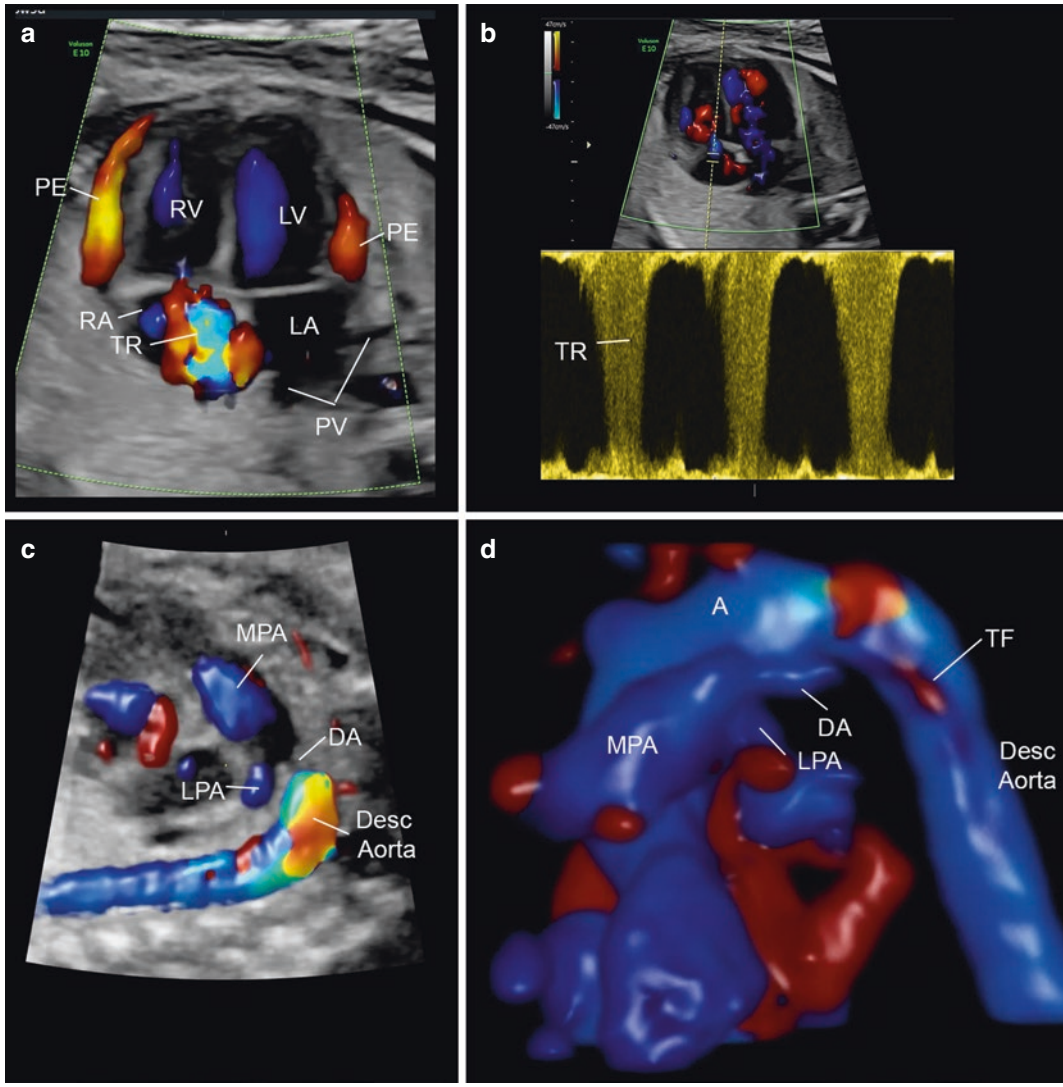

Fig. 33.15 28-week constricted ductus arteriosus. (**a**) Color Doppler image demonstrating abnormalities that include bilateral pericardial effusions (PE) along the right and left ventricles and tricuspid regurgitation (TR). (**b**) Pulsed Doppler from the right atrial chamber demonstrates holosystolic tricuspid regurgitation. (**c**) Short-axis view of the ductal arch demonstrating the narrow ductus arteriosus (DA) and the aliasing distal to the severe narrowing. (**d**) 4D color rendering of the heart demonstrates the narrowed DA and the turbulent flow (TR) in the descending aorta (Desc Aorta). *PV* pulmonary veins, *LA* left atrium, *RA* right atrium, *LPA* left pulmonary artery, *MPA* main pulmonary artery

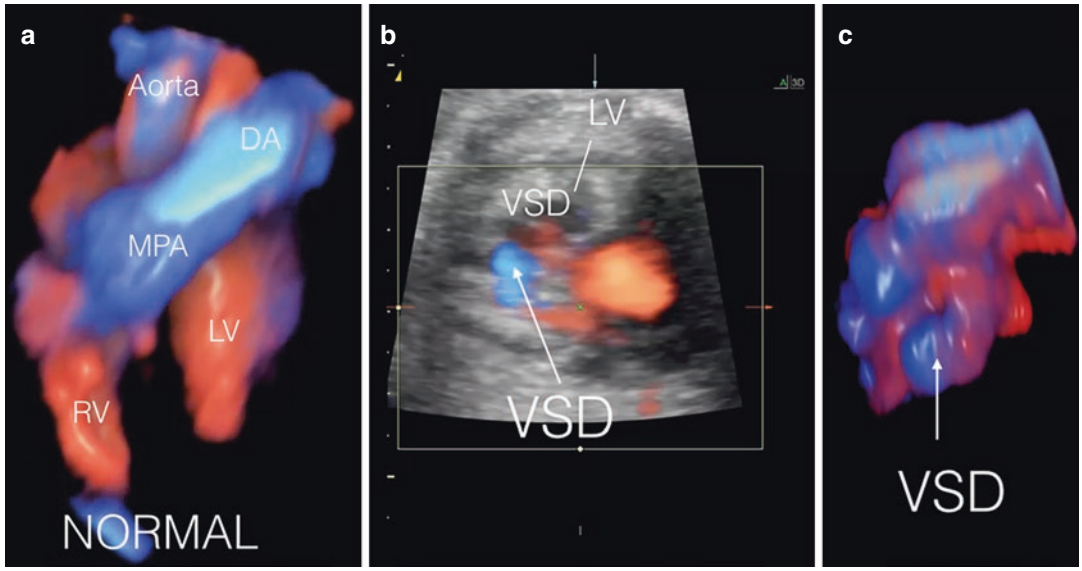

Fig. 33.16 (**a**) Rendered image of the ventricles and outflow tracts. It is noted the separation between the RV and LV, representing the interventricular septum. (**b**) A 2D color Doppler image obtained from the STIC volume demonstrating a ventricular septal defect. (**c**) The VSD in the rendered image obtained in the same plane as (**a**). *LV* left ventricle, *VSD* ventricular septal defect, *MPA* main pulmonary artery, *DA* ductus arteriosus

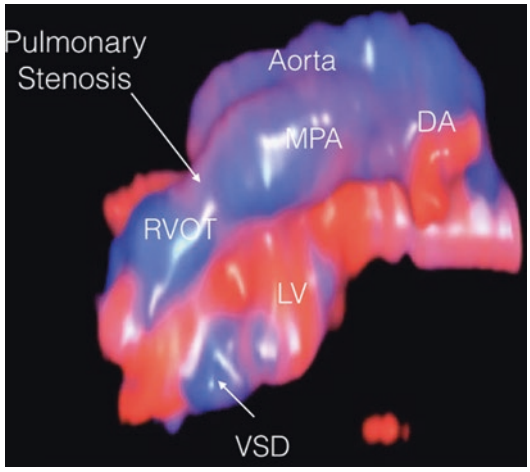

Fig. 33.17 A rendered volume from a second trimester fetus demonstrating a ventricular septal defect (VSD) and pulmonary stenosis. *RVOT* right ventricular outflow tract, *LV* left ventricle, *MPA* main pulmonary artery, *DA* ductus arteriosus

33.4 Benefits of STIC Color and Power Image Acquisition

Although the initial application of STIC was to simultaneous display three perpendicular planes obtained from a volume acquisition through the fetal chest, the addition of color and power Doppler to the volume acquisition has the following benefits: (1) For first trimester imaging of the fetal heart the rendered cardiovascular system displayed with radiant flow provides a virtual 3-dimensional model of the cardiovascular system and can be used to screen for major malformations that alter ventricular chamber size and alter the orientation of the outflow tracts; (2) whether the examiner uses the A, B, and C planes to display the 2-dimensional color/power Doppler images or the TUI, the addition of blood flow

enhances the detection of congenital heart defects in both the first and second trimesters of pregnancy; and (3) the examiner can view 2-dimensional grayscale cardiac anatomy from a STIC volume, with or without the color/power Doppler display, thus allowing for more precise evaluation of blood flow patterns integrated with cardiac anatomical structures.

References

1. Maulik D, Nanda NC, Hsiung MC, Youngblood JP. Doppler color flow mapping of the fetal heart. Angiology. 1986;37(9):628–32.
2. De Vore GR, Brar HS, Platt LD. Doppler ultrasound in the fetus: a review of current applications. J Clin Ultrasound. 1987;15(9):687–703.
3. DeVore GR, Horenstein J, Siassi B, Platt LD. Fetal echocardiography. VII. Doppler color flow mapping: a new technique for the diagnosis of congenital heart disease. Am J Obstet Gynecol. 1987;156(5):1054–64.
4. Sharland GK, Chita SK, Allan LD. The use of colour Doppler in fetal echocardiography. Int J Cardiol. 1990;28(2):229–36.
5. DeVore GR, Horenstein J. Simultaneous Doppler recording of the pulmonary artery and vein: a new technique for the evaluation of a fetal arrhythmia. J Ultrasound Med. 1993;12(11):669–71.
6. DeVore GR, Horenstein J. Ductus venosus index: a method for evaluating right ventricular preload in the second-trimester fetus. Ultrasound Obstet Gynecol. 1993;3(5):338–42.
7. DeVore GR. Color Doppler examination of the outflow tracts of the fetal heart: a technique for identification of cardiovascular malformations. Ultrasound Obstet Gynecol. 1994;4(6):463–71.
8. DeVore GR, Alfi O. The use of color Doppler ultrasound to identify fetuses at increased risk for trisomy 21: an alternative for high-risk patients who decline genetic amniocentesis. Obstet Gynecol. 1995;85(3):378–86.
9. DeVore GR. Second trimester ultrasonography may identify 77 to 97% of fetuses with trisomy 18. J Ultrasound Med. 2000;19(8):565–76.
10. DeVore GR. Trisomy 21: 91% detection rate using second-trimester ultrasound markers. Ultrasound Obstet Gynecol. 2000;16(2):133–41.
11. DeVore GR. The genetic sonogram: its use in the detection of chromosomal abnormalities in fetuses of women of advanced maternal age. Prenat Diagn. 2001;21(1):40–5.
12. DeVore GR. The role of fetal echocardiography in genetic sonography. Semin Perinatol. 2003;27(2):160–72.
13. Huggon IC, DeFigueiredo DB, Allan LD. Tricuspid regurgitation in the diagnosis of chromosomal anomalies in the fetus at 11-14 weeks of gestation. Heart. 2003;89(9):1071–3.
14. International Society of Ultrasound in O, Gynecology, Carvalho JS, et al. ISUOG Practice Guidelines (updated): sonographic screening examination of the fetal heart. Ultrasound Obstet Gynecol. 2013;41(3):348–59.
15. DeVore GR, Falkensammer P, Sklansky MS, Platt LD. Spatio-temporal image correlation (STIC): new technology for evaluation of the fetal heart. Ultrasound Obstet Gynecol. 2003;22(4):380–7.
16. Goncalves LF, Lee W, Chaiworapongsa T, et al. Four-dimensional ultrasonography of the fetal heart with spatiotemporal image correlation. Am J Obstet Gynecol. 2003;189(6):1792–802.
17. Maulik D, Nanda NC, Singh V, et al. Live three-dimensional echocardiography of the human fetus. Echocardiography (Mount Kisco, NY). 2003;20(8):715–21.
18. Vinals F, Poblete P, Giuliano A. Spatio-temporal image correlation (STIC): a new tool for the prenatal screening of congenital heart defects. Ultrasound Obstet Gynecol. 2003;22(4):388–94.
19. Bhat AH, Corbett VN, Liu R, et al. Validation of volume and mass assessments for human fetal heart imaging by 4-dimensional spatiotemporal image correlation echocardiography: in vitro balloon model experiments. J Ultrasound Med. 2004;23(9):1151–9.
20. Sklansky MS, DeVore GR, Wong PC. Real-time 3-dimensional fetal echocardiography with an instantaneous volume-rendered display: early description and pictorial essay. J Ultrasound Med. 2004;23(2):283–9.
21. Goncalves LF, Espinoza J, Kusanovic JP, et al. Applications of 2-dimensional matrix array for 3- and 4-dimensional examination of the fetus: a pictorial essay. J Ultrasound Med. 2006;25(6):745–55.
22. Yuan Y, Leung KY, Ouyang YS, et al. Simultaneous real-time imaging of four-chamber and left ventricular outflow tract views using xPlane imaging capability of a matrix array probe. Ultrasound Obstet Gynecol. 2011;37(3):302–9.
23. Black D, Vettukattil J. Advanced echocardiographic imaging of the congenitally malformed heart. Curr Cardiol Rev. 2013;9(3):241–52.
24. Zheng M, Schaal M, Chen Y, et al. Real-time 3-dimensional echocardiographic assessment of ventricular volume, mass, and function in human fetuses. PLoS One. 2013;8(3):e58494.
25. Acar P, Battle L, Dulac Y, et al. Real-time three-dimensional foetal echocardiography using a new transabdominal xMATRIX array transducer. Arch Cardiovasc Dis. 2014;107(1):4–9.
26. La Torre R, Bevilacqua E, D'Ambrosio V, et al. Matrix array transducer for the examination of fetal heart. Clin Exp Obstet Gynecol. 2014;41(5):581–2.
27. Chaoui R, Hoffmann J, Heling KS. Three-dimensional (3D) and 4D color Doppler fetal echocardiography using spatio-temporal image correlation (STIC). Ultrasound Obstet Gynecol. 2004;23(6):535–45.

28. Donofrio MT, Moon-Grady AJ, Hornberger LK, et al. Diagnosis and treatment of fetal cardiac disease: a scientific statement from the American Heart Association. Circulation. 2014;129(21):2183–242.
29. Lee W. Performance of the basic fetal cardiac ultrasound examination. J Ultrasound Med. 1998;17(9):601–7.
30. Devore GR, Polanko B. Tomographic ultrasound imaging of the fetal heart: a new technique for identifying normal and abnormal cardiac anatomy. J Ultrasound Med. 2005;24(12):1685–96.
31. Goncalves LF, Espinoza J, Romero R, et al. Four-dimensional ultrasonography of the fetal heart using a novel Tomographic Ultrasound Imaging display. J Perinat Med. 2006;34(1):39–55.
32. Gindes L, Hegesh J, Weisz B, Gilboa Y, Achiron R. Three and four dimensional ultrasound: a novel method for evaluating fetal cardiac anomalies. Prenat Diagn. 2009;29(7):645–53.
33. Turan S, Turan OM, Ty-Torredes K, Harman CR, Baschat AA. Standardization of the first-trimester fetal cardiac examination using spatiotemporal image correlation with tomographic ultrasound and color Doppler imaging. Ultrasound Obstet Gynecol. 2009;33(6):652–6.
34. Votino C, Cos T, Abu-Rustum R, et al. Use of spatio-temporal image correlation at 11-14 weeks' gestation. Ultrasound Obstet Gynecol. 2013;42(6):669–78.
35. Tudorache S, Cara M, Iliescu DG, Novac L, Cernea N. First trimester two- and four-dimensional cardiac scan: intra- and interobserver agreement, comparison between methods and benefits of color Doppler technique. Ultrasound Obstet Gynecol. 2013;42(6):659–68.
36. Lima AI, Araujo Junior E, Martins WP, Nardozza LM, Moron AF, Pares DB. Assessment of the fetal heart at 12-14 weeks of pregnancy using B-mode, color Doppler, and spatiotemporal image correlation via abdominal and vaginal ultrasonography. Pediatr Cardiol. 2013;34(7):1577–82.
37. Yeo L, Romero R. Color and power Doppler combined with Fetal Intelligent Navigation Echocardiography (FINE) to evaluate the fetal heart. Ultrasound Obstet Gynecol. 2017;50(4):476–91.
38. DeVore GR, Satou G, Sklansky M. 4D fetal echocardiography-An update. Echocardiography (Mount Kisco, NY). 2017;34(12):1788–98.

Cardiac Function in Fetal Growth Restriction

34

Giuseppe Rizzo, Ilenia Mappa, Victoria Bitsadze, Jamilya Khizroeva, Alexander Makatsarya, and Domenico Arduini

34.1 Introduction

Fetal Growth Restriction (FGR) is defined as the inability of the fetus to reach its growth potential and there is ample evidence showing that it is a major risk factor for the poor neonatal condition at birth and impaired neurodevelopment and diseases, such as hypertension, metabolic syndrome, and obesity in the adulthood [1–6].

FGR is currently subclassified according to a Delphi consensus into two groups, namely early FGR and late FGR, which differ in terms of clinical manifestations, association with hypertension, Doppler features, and patterns of deterioration and severity of placental dysfunction [7–11] other than for gestational age at diagnosis, which is conventionally set at or below 32 weeks for early FGR and beyond 32 weeks for late-onset FGR. As a general rule, early FGR is defined by fetal smallness and abnormal UA PI and shows a 60–70% association with a hypertensive disorder or the pregnancy; on the other hand, UA PI is normal in most cases of late FGR and its association with gestational hypertension and preeclampsia is weak [7, 9].

Chronic placental insufficiency and hypoxia affect cardiac fetal cardiac function both early and late with different adaptive mechanisms.

The objective of this chapter is to describe the cardiac hemodynamic changes occurring in these two conditions of FGR.

34.2 Early FGR

Early FGR is a progressive process of adaptation of the growing fetus to the restricted metabolic supply of the placenta. Monitoring fetal adaptation is based on the Doppler of Umbilical Artery (UA) Pulsatility Index (PI), Middle Cerebral Artery (MCA) PI, and their ratio (Placental cerebral ratio PCR, PI MCA/PI UA). Placental insufficiency results in increased resistance of the fetoplacental unit and in compensatory hemodynamic changes which include blood flow redistribution toward essential fetal organs (brain, heart, and adrenal

G. Rizzo (✉) · V. Bitsadze · J. Khizroeva
Department of Obstetrics and Gynecology
Fondazione Policlinico Tor Vergata, Università di Roma Tor Vergata, Rome, Italy

Department of Obstetrics and Gynecology, The First I.M. Sechenov Moscow State Medical University, Moscow, Russia
e-mail: giuseppe.rizzo@uniroma2.it

I. Mappa
Department of Obstetrics and Gynecology
Fondazione Policlinico Tor Vergata, Università di Roma Tor Vergata, Rome, Italy

A. Makatsarya
Department of Obstetrics and Gynecology, The First I.M. Sechenov Moscow State Medical University, Moscow, Russia

D. Arduini
Department of Developmental Medicine and Prevention, Università di Roma Tor Vergata, Rome, Italy

D. Maulik, C. C. Lees (eds.), *Doppler Ultrasound in Obstetrics and Gynecology*,
https://doi.org/10.1007/978-3-031-06189-9_34

glands) at the expense of other organ systems [12–17].

The hemodynamic changes secondary to uteroplacental insufficiency are characterized by selective changes of peripheral vascular resistance (i.e., the so-called brain sparing effect) Indeed there is an increase in the blood supply to the brain, myocardium, and the adrenal glands and a reduction in the perfusion of the kidneys, gastrointestinal tract and the lower extremities.

Although knowledge of factors causing the circulatory readjustments and their mechanism of action is still incomplete, it appears that partial pressures of oxygen and carbon dioxide play a role, presumably through their action on chemoreceptors. This mechanism allows preferential delivery of nutrients and oxygen to vital organs, thereby compensating for diminished placental resources. However, compensation through cerebral vasodilatation is limited and a plateau corresponding to a nadir of pulsatility index in cerebral vessels is reached at least 2 weeks before the development of fetal jeopardize. Similar findings may be found in the other arterial vessels. As a consequence, arterial vessels are unsuitable for longitudinal monitoring of growth-restricted fetuses.

Indeed we [18] examined FGR fetuses longitudinally and described a curvilinear relationship between impedance in cerebral vessels and the state of fetal oxygenation; the progressive fall in impedance reached a nadir 2 weeks before the onset of late fetal heart rate decelerations. This suggests that the maximum degree of vascular adaptation to hypoxemia precedes the critical degree of impairment of fetal oxygenation.

Secondary to the brain sparing condition selective modifications occur in cardiac afterload with a decreased left ventricle afterload due to the cerebral vasodilatation and an increased right ventricle afterload due to the systemic and pulmonary vasoconstriction [14, 19]. Furthermore, hypoxemia might impair myocardial contractility while the polycythemia usually present might alter blood viscosity and therefore preload [14].

As a consequence, early FGR fetuses show impaired ventricular filling properties with a lower early/atrial peak velocity ratio (E/A) at the level of atrioventricular valves [20] (Fig. 34.1), lower Peak Velocity (PV) PV in the aorta and pulmonary arteries [21] (Fig. 34.2), increased aortic and decreased pulmonary time to peak velocity (TPV) [22] and a relative increase of Left Cardiac Output (LCO) associated with decreased Right Cardiac Output (RCO) [22, 23]. These hemodynamic intracardiac changes are compatible with a preferential shift of cardiac output in favor of the left ventricle leading to improved perfusion to the brain. Thus, in the first stages of the disease, the supply of substrates and oxygen can be maintained at near-normal levels despite any absolute reduction of placental transfer.

The E/A ratio is one of the parameters suggested for the evaluation of the cardiac diastolic function in the fetus. It is defined by the ratio between the E (early or passive) velocity, which is measured during the early passive ventricular filling and is related to the process of myocardial relaxation and negative pressure applied by the ventricles, and the A (atrial, active, or late) velocity, which represents the active ventricular filling during atrial contraction.

The E/A ratio can be measured by evaluating the trans-mitral or the trans-tricuspid waveforms obtained with pulsed-wave Doppler and continuous wave Doppler. Recordings are obtained at the level of the four-chamber view of the fetal heart, in which the Doppler sample gate is located just below either atrioventricular valve, where a biphasic waveform is usually displayed in the normal fetus (Fig. 34.1) There are some mild differences between both sides of the heart which are constantly observed in all normal pregnancies: the right E/A waveforms have higher velocities and the ratio is slightly lower than that of the left side [20]. Uncomplicated pregnancies show a progressive increase in the E/A ratio across gestation [20]. On the other hand, in SGA fetuses the E/A ratio does not increase and its values are significantly lower than in normal fetuses. A reduced E/A ratio indicates that the process of ventricular filling depends more on the atrial contraction than on the negative pressure during relaxation. The two main conditions affecting the ratios, chronic hypoxia, and cardiac overload, might affect the relaxation process, thus reducing the E/A ratios. On a small cohort of FGR fetuses,

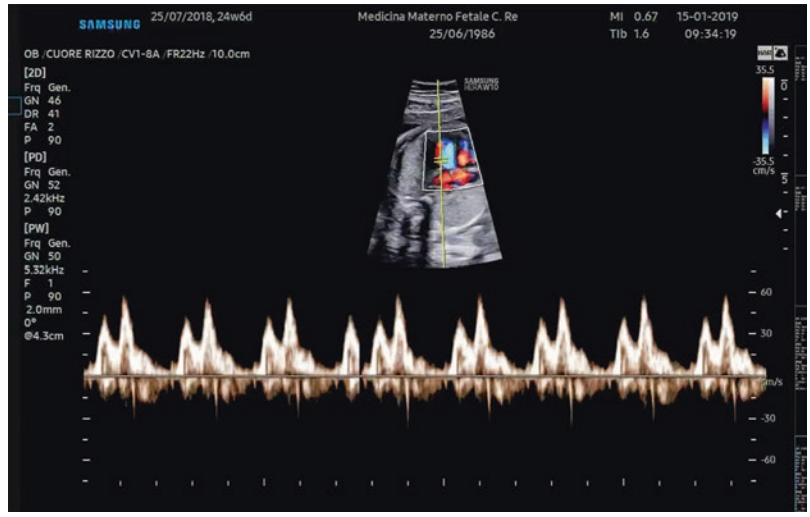

Fig. 34.1 Cardiac velocity waveforms from mitral valve showing the early (E) and atrial (A) components of ventricular inflow

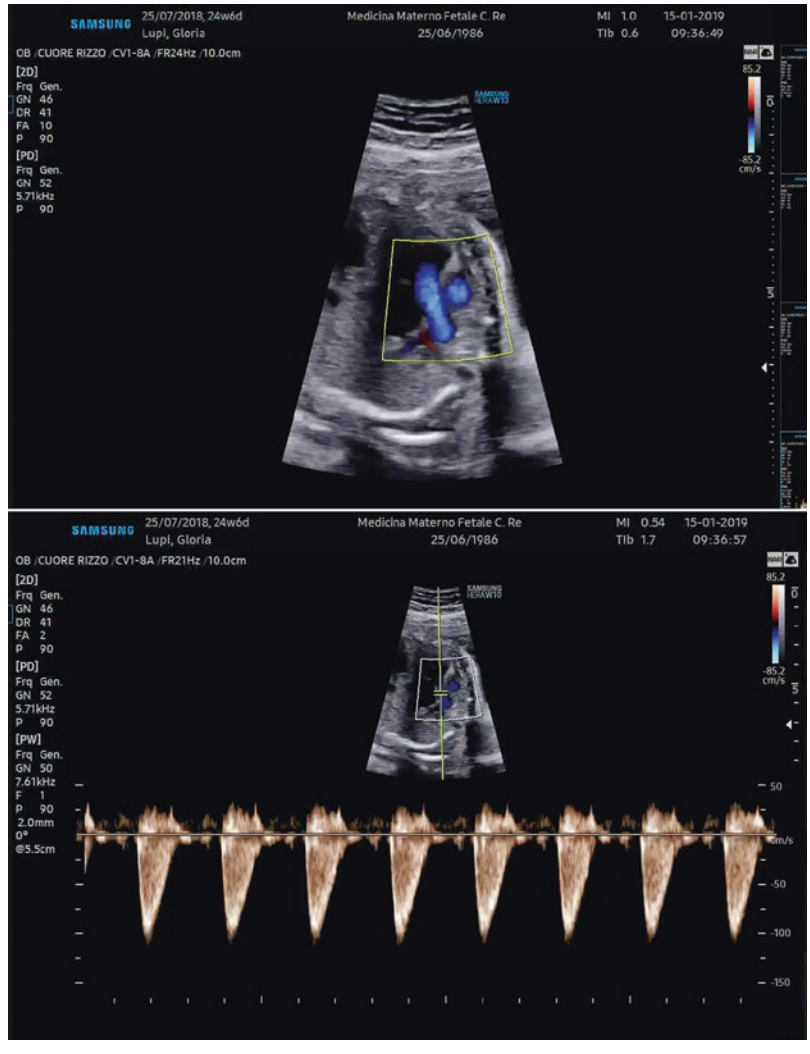

Fig. 34.2 Left ventricle outflow tract (upper panel) and blood flow velocity waveforms from ascending aorta (lower panel)

Figueras et al. reported lower E/A ratios in both atrioventricular valves compared to normally grown fetuses with early deterioration of the right E/A ratio [24]. More recent data suggested that there is a "continuum" in the deterioration of the E/A ratio, with monophasic diastolic waves associated with abnormalities in all prenatal cardiac parameters in fetuses with severe FGR who eventually died or developed neurological damage [25]. However, this observation was not confirmed in prospective studies, hence to date, there is no clinical role for the E/A ratio in the diagnosis and management of FGR fetuses.

Longitudinal studies of progressively deteriorating IUGR fetuses have allowed elucidating the natural history of these hemodynamic modifications during uteroplacental insufficiency [26–28]. Such studies have shown that both TPV in the aorta and pulmonary arteries and the ratios between right and left ventricle outputs remain stable during serial recordings. These findings are consistent with the absence of other significant changes in outflow resistances (a parameter inversely related to TPV values) and with cardiac output redistribution after the establishment of the brain sparing mechanism [26]. However, in deteriorating IUGR fetuses PV and cardiac output gradually decline to suggest a progressive deterioration of cardiac function [26] (Fig. 34.2). As a consequence, also cardiac filling is impaired. Studies in the fetal venous circulation [27, 28] have demonstrated that an increase of Inferior Vena Cava (IVC) reverse flow during atrial contraction occurs with progressive fetal deterioration suggesting a higher pressure gradient in the right atrium. The next step of the disease is the extension of the abnormal reversal of blood velocities in the IVC to the ductus venous inducing an increase of the PI mainly due to a reduction of the A component of the velocity waveforms [29–31]. Finally, the high venous pressure induces a reduction of velocity at end-diastole in the umbilical vein causing typical end-diastolic pulsations [31, 32]. The development of these pulsations is close to the onset of fetal heart rate anomalies and is frequently associated with academia and fetal endocrine changes [32]. At this stage reduced or reverse end-diastolic velocity may be also present in pulmonary veins and coronary blood flow may be visualized with higher velocity than in normally grown third-trimester fetuses if fetuses were not delivered intrauterine death may occur after a median of 3.5 days [33].

Studies of Ventricular Ejections Fraction (VEF) in early FGR have demonstrated that it is significantly and symmetrically decreased at the level of both ventricles [34]. The presence of a symmetrical decrease of VEF from both ventricles, despite the dramatically different hemodynamic conditions present in the vascular district of ejection of the two ventricles (i.e., reduced cerebral resistances for the left ventricle and increased splanchnic and placental resistances for the right ventricle), supports a pivotal role of the intrinsic myocardial function in the compensatory mechanism of the early FGR fetus following the establishment of the brain sparing effect. Indeed, it was demonstrated in fetuses followed longitudinally until either intrauterine death or the onset of abnormal fetal heart rate patterns requiring early delivery, VEF dramatically decreases in a short time interval (i.e., 1-week) showing an impairment of ventricular force close to fetal distress [34]. Furthermore, a significant relationship between the severity of fetal acidosis at cordocentesis and VEF values [34] validates the association between the pivotal role of the fetal heart in the progressive fetal compromise.

It can be speculated that the fall in cardiac output and VEF terminally may reflect a decompensation of a normal protective mechanism responsible for the brain sparing effect. According to this model fetal heart adapts to placental insufficiency in an order to maximize brain substrates and oxygen supply. With the progressive deterioration of fetal conditions, this protective mechanism is overwhelmed by the fall of cardiac output and fetal distress occurs.

Earlier predictors would be desirable and preliminary results suggest that the evaluation of Aortic Isthmus (AoI) may be useful in the early identification of fetuses at the verge of compromise [35, 36].

The AoI is the segment of the aorta located between the origin of the left subclavian artery

and the connection of the ductus arteriosus to the descending aorta. The AoI is the only arterial connection between the right ventricle, which supplies mainly the systemic and placental circulations, and the left ventricle, which supplies essentially the cerebral vascular network [35], therefore its blood flow patterns reflect the balance between ventricular outputs and the relative difference in vascular impedance in either vascular system. The rationale for the Doppler assessment of the AoI is represented by the fact that during diastole, when the aortic and pulmonary valves are closed, the direction of blood flow in the AoI solely reflects the differences between the downstream impedances of the right (mainly placental vascular resistance) and left (mainly cerebral vascular resistance) ventricles [35].

The AoI can be visualized using grayscale (B-mode) ultrasound either on the longitudinal view of the aortic arch or on the cross-sectional view of the upper thorax at the level of the three-vessel/trachea views [36, 37] (Fig. 34.3) (Antenatal Doppler study of the AoI includes the quantitative assessment of the peak systolic (PSV), end-diastolic (EDV) and time-averaged maximum (TAMXV) velocities through the AoI itself, the semiquantitative evaluation of the PI and/or of the isthmic flow index (IFI), which was devised in order to include the amount and direction of blood flow and is computed as (PSV + EDV)/PSV [38, 39], and the qualitative description of antegrade or retrograde flow [37]. Under normal conditions, AoI velocity waveforms show antegrade flow during systole and diastole because the placental resistances are lower than those present in the fetal upper body.

There is evidence showing a relationship between the Doppler indices through the AoI and UA and DV Doppler features as a consequence of the changes in peripheral and cerebral resistances, controversial results have emerged from the studies evaluating such correlations [37]. Regarding postnatal assessment, available data suggest an association between adverse perinatal outcomes and neurodevelopmental deficits and abnormal Doppler recordings in the AoI in terms of predominant reversed diastolic blood flow and IFI <0.70 with net reversed diastolic flow through the AoI (85), even though this relationship has shown a low sensitivity [40].

Cardiac function in FGR has been evaluated using the myocardial performance index (MPI)–also named as Tei index–is a parameter that reflects both systolic and diastolic function as the sum of the Isovolumetric Contraction Time (ICT) and Isovolumetric Relaxation Time (IRT) divided by the ejection time (EJT) (ICT + IRT) EJT [41].

The isovolumetric contraction time (ICT, ms) represents the time from the closure of the mitral valve to the opening of the aortic valve; the iso-

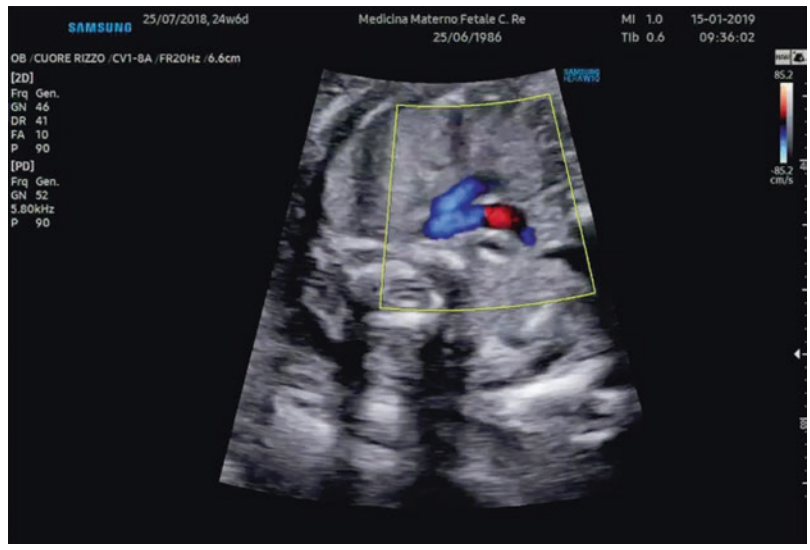

Fig. 34.3 Three vessels view showing aortic isthmus

volumetric relaxation time (IRT, ms) represents the time from the closure of the aortic valve to the opening of the mitral valve; the Ejection Time (ET, ms) or systolic time interval represents the time from the opening of the aortic valve to its closure. Using the Tissue Doppler technique, the MPI can be measured by placing a 2–3 mm pulsed-wave gate in the basal part of the left and right ventricular free walls (at the level of the mitral and tricuspid valve annulus, respectively). Peak annular velocities need to be measured during early diastole (E), atrial contraction (A), and systole and provide the same waveform landmarks used with PW Doppler. Using either technique, measurements of all the components needed to calculate the MPI need to be obtained from the same cardiac cycle.

A significantly higher MPI in FGR compared to appropriately grown fetuses was demonstrated by Hassan et al. [25]. Raised MPI is seen in the early stages of cardiac adaptation to FGR, presumably secondary to hypoxia, and remains elevated throughout the different stages of deterioration in FGR deterioration, similar to the AoI and DV PI. Available evidence from longitudinal studies has demonstrated that an abnormal increase of the MPI can be detected prior to the umbilical artery Doppler becoming abnormal [42] and showing absent or reversed end-diastolic blood flow [43].

The finding of increased MPI has been suggested as a potential discriminator between FGR and SGA in fetuses showing reduced biometry but normal Doppler [43, 44]. Hernandez-Andrade et al. suggested that the combination of these parameters might be useful for defining the monitoring strategy and the optimal time of delivery [45], however, there is no evidence-based strategy including the MPI among the parameters for the monitoring of FGR fetuses.

Concerning the monitoring strategy of early FGR, the only randomized controlled study available is the Trial Randomizing Umbilical and Fetal Flow in Europe (TRUFFLE) evaluated and demonstrated the effectiveness of standardized monitoring and delivery protocol for early FGR fetuses [10].

Based on the assumption that cCTG and DV represent those parameters that safely allow delayed delivery before the fetal compromise, the TRUFFLE protocol has demonstrated that the perinatal outcome of surviving early FGR fetuses is significantly better among those delivered based on late DV changes [46, 47], even though no differences were noted among the three randomization arms of the TRUFFLE as regard the primary outcome—i.e., survival without neurodevelopmental impairment. DV has been demonstrated to be the most important Doppler parameter in the prediction of the short-term risk of intrauterine death in early-onset FGR [46]. Absent or reversed DV A-wave have been associated with an increased risk of intrauterine fetal death (40–70%) and late-stage acidemia independently from gestational age at delivery and shortly precedes spontaneous decelerations at CTG monitoring. DV PI above the 95th centile also confers a high risk of adverse outcomes, although at a lesser extent than that of reversed or absent A-wave [47]. Similarly, STV becomes abnormal in the case of advanced fetal deterioration [46], providing information similar to those of late DV changes for the short-term prediction of fetal death. Although the optimal cut-off value of the STV for delivery has yet to be clarified, it is important to point out that, between 26 and 32 weeks, expectant management is accepted as long as either the DV or the STV is abnormal but not if both are abnormal [10, 47].

34.3 Late Fetal Growth Restriction

Late FGR is defined as the inability of the fetus to reach its growth potential and is diagnosed after 32 weeks of gestation [7]. Although the burden of perinatal complications is lower compared to early-onset disease, late FGR is associated with an increased risk of adverse short-and long-term outcomes, including hypoxemic events and mild neurodevelopmental delay, compared to normally grown fetuses [48–51].

Identification of fetuses at higher risk of perinatal compromise is crucial in order to maximize

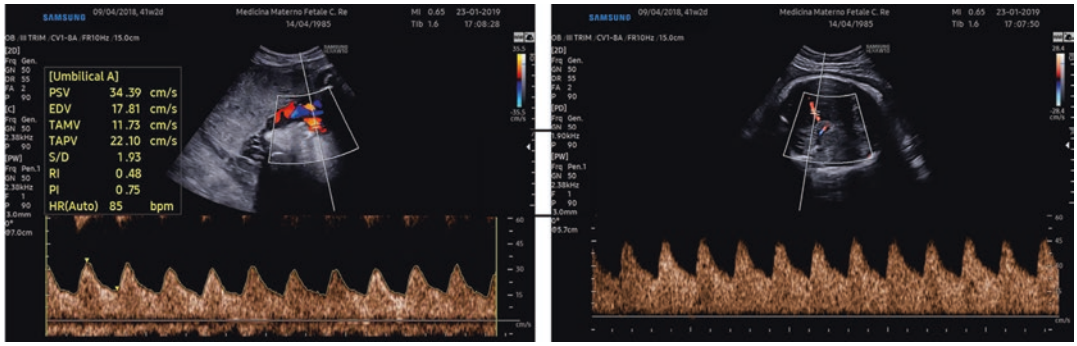

Fig. 34.4 Doppler velocity waveforms in a late FGR. Umbilical artery PI is normal (left panel) while middle cerebral artery PI is reduced (right panel)

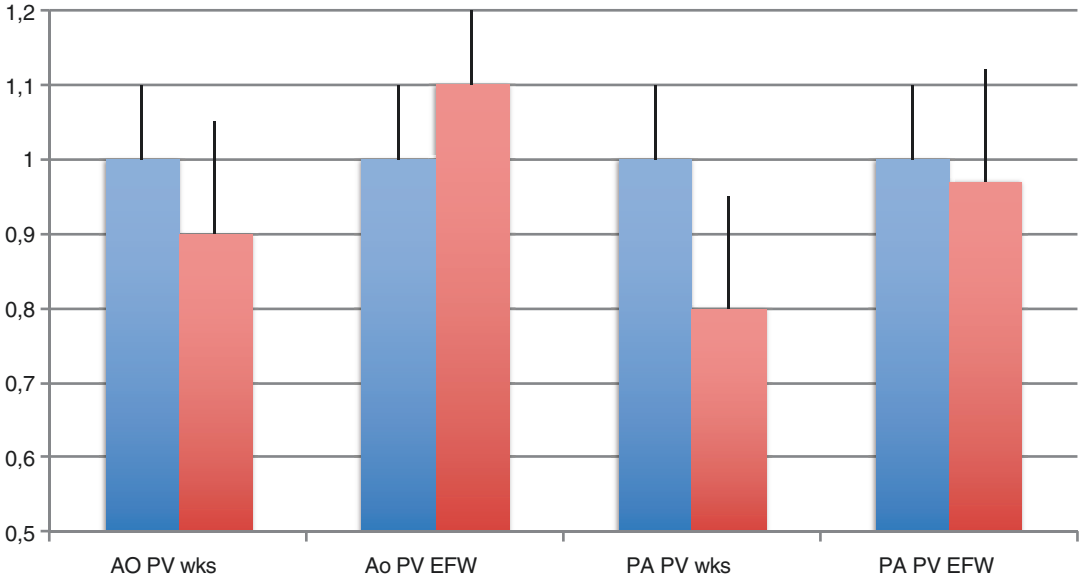

Fig. 34.5 PV from the aorta and pulmonary artery in late FGR (red bars) and control fetuses (blue) as absolute value and corrected for fetal weight

the outcome of pregnancies affected by late-onset FGR [52] Blood flow in the umbilical artery (UA), which represents the clinical standard for the identification and management of pregnancies affected by early FGR, is frequently normal in fetuses with late-onset disease. Reduced impedance to flow in the cerebral circulation, expressed as low pulsatility index (PI) in the middle cerebral artery (MCA) or cerebroplacental ratio (CPR), has been shown in late FGR to be associated with abnormal acid-base status and admission to neonatal intensive care at birth [52] (Fig. 34.4).

This condition affects cardiac hemodynamics differently from early-onset FGR. Indeed, PV from the outflow tract (Fig. 34.5) is not different from normal fetuses corroborating the hypothesis that cardiac afterload is not significantly affected (Fig. 34.6). Similarly, RCO, LCO, and their ratio are not significantly different when corrected for fetal weight [53].

However in such fetuses to maintain ventricular output the myocardium develops a variety of changes in cardiac macro and microstructure and function, which is defined as cardiac remodeling Indeed the heart develops a more spherical shape

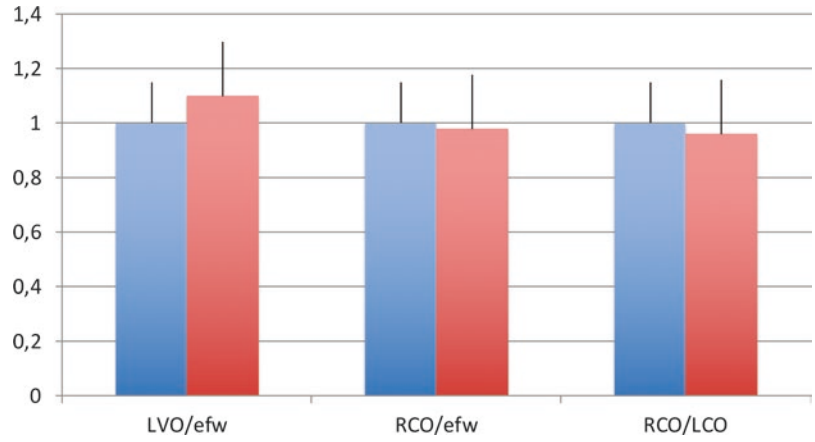

Fig. 34.6 RCO LCO and RCO/LCO in late FGR (red bars) and control fetuses (blue) corrected for fetal weight

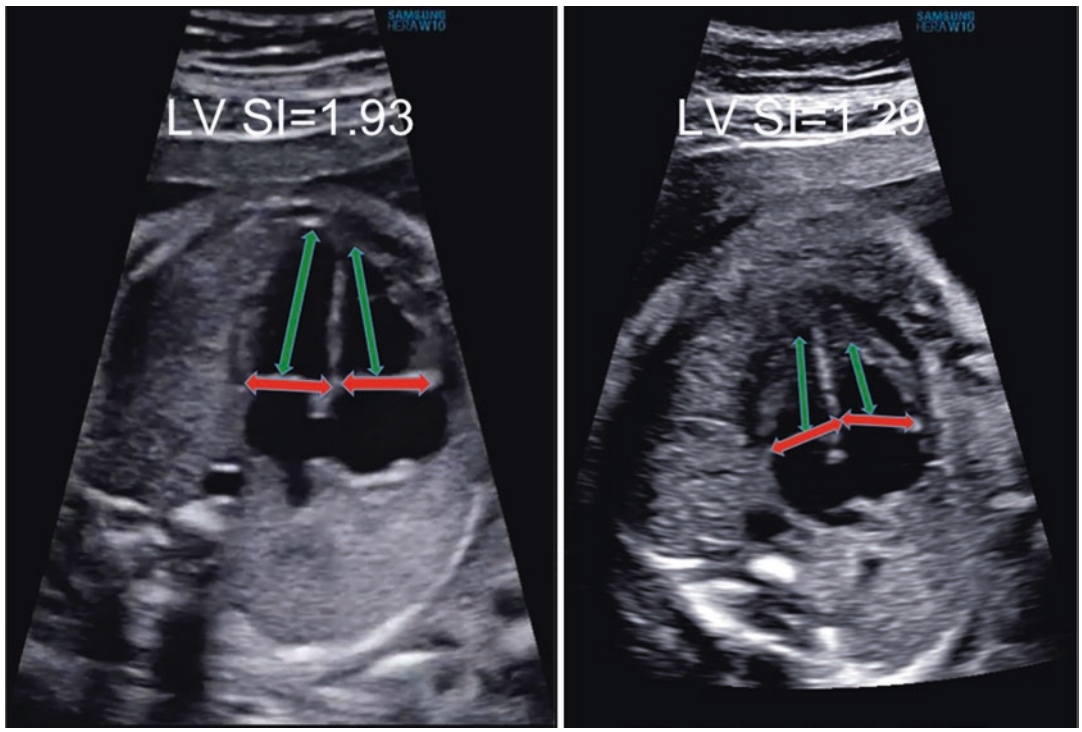

Fig. 34.7 Echocardiographic images of two late FGR fetuses with (left panel) and abnormal (right panel) sphericity index (SI) values. For the computation of SI, the end-diastolic mid-basal–apical length (green arrows) are divided by basal transverse length (red arrows) Modified from [56]

that allows maintaining stroke volume with less contraction force, while also reducing wall stress to better tolerate pressure overload [54]. The Sphericity Index (SI), calculated as the ratio between the end-diastolic mid-basal–apical and transverse lengths is usually used to quantify this cardiac remodeling [55] (Fig. 34.7).

We demonstrated that fetal cardiac remodeling occurs in approximately one-half of the pregnancies complicated by late-onset FGR. The fetuses with cardiac remodeling did not show differences in baseline clinical characteristics and Doppler indices from maternal and fetal artery Doppler velocity waveforms but developed a

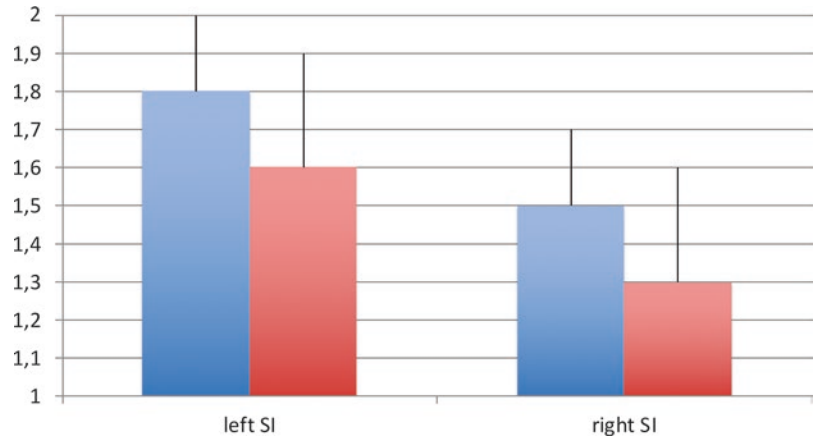

Fig. 34.8 Sphericity Index (SI) values in late FGR with normal (blue bar) l and abnormal outcome (red bar) [56]

poorer short-term perinatal outcome [56] (Fig. 34.8) Moreover a reduced left and right ventricle SI was associated with lower Umbilical Vein Blood Flow (UVBF) As a consequence, a reduced umbilical vein blood flow is associated with the cardiac remodeling in late FGR independently from fetal size and fetal peripheral arterial Doppler hemodynamic. The identification of such fetuses may improve the identification of FGR fetuses with a higher risk of perinatal complications and long-term cardiovascular risks.

The potential role of Umbilical Vein (UV) flow in identifying fetuses at higher risk of perinatal compromise deserves further investigation. UV blood flow may be difficult to sample; furthermore, the reproducibility of such inter-and intra-observer variability when measuring this vessel have not been consistently reported yet in the published literature. Small errors in the UVBF components may result in larger errors in the absolute flow calculation and this is particularly evident for UV diameter whose values are halved and squared in the calculation of the vessel area [57]. To overcome these limitations, in this study we evaluated UV flow in its intra-abdominal portion using a semi-automated method of measurements of the UV diameter that allows obtaining a higher reproducibility than the manual modality and may allow an easier application in clinical practice [58] (Figs. 34.9 and 34.10).

Identification of fetuses affected by late-FGR at higher risk of adverse perinatal outcome is

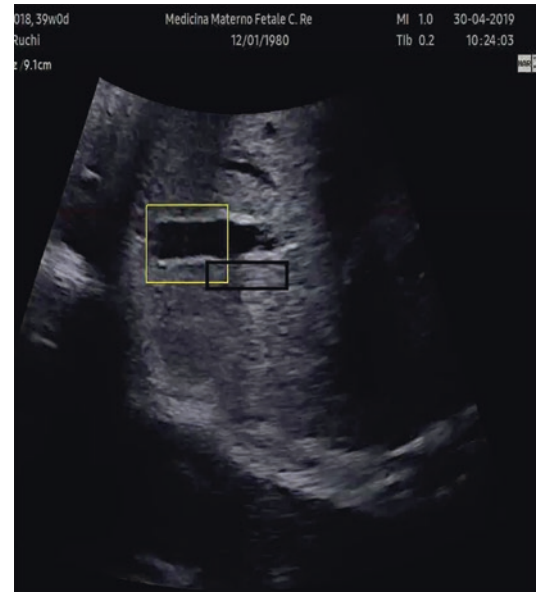

Fig. 34.9 Example of semiautomatic measurement of umbilical vein in the third trimester

challenging, Adverse perinatal outcome occurs in approximately one-third of pregnancies complicated by late-onset FGR. When recently explored the role of different Doppler parameters and evidenced that mean uterine artery PI was higher, while UVBF, MCA PI, and CPR were lower in pregnancies who experienced compared to those who did not experience composite adverse outcomes, while there was no difference in the mean values of UA PI between the study groups [59]. On multivariable logistic regression analysis, mean uterine artery PI, CPR, and UVBF/AC

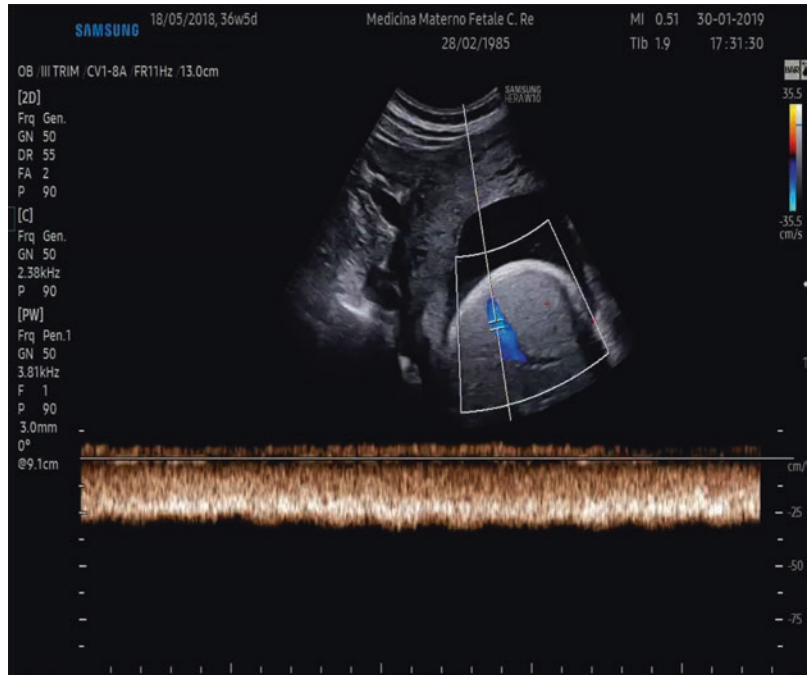

Fig. 34.10 Blood flow velocity waveforms recorded from the umbilical vein

were all independently associated with composite adverse perinatal outcomes. However, when exploring the diagnostic performance of Doppler in predicting the outcome, only UVBF/AC showed a moderate accuracy in predicting adverse outcomes, while the diagnostic performance of both CPR and uterine arteries was low.

A randomized study is needed in order to overcome such uncertainty as regards the optimal monitoring strategy and timing of delivery of late FGR. The ongoing trial by the TRUFFLE group and the planned TRUFFLE 2 randomized controlled study are likely to provide further insights into the actual role of the cerebral Doppler–on its own or paired with UA within the CPR–in the management of late-onset FGR and particularly to clarify whether anticipating delivery based on the abnormal CPR is beneficial for the short-and long-term health of the late FGR fetus [60].

References

1. Mcintire DD, Bloom SL, Casey BM, Leveno KJ. Birth weight in relation to morbildity and mortality among newborn infants. N Engl J Med. 1999;340:1234–8.
2. Garite TJ, Combs CA, Maurel K, Das A, Huls K, Porreco R, et al. A multicenter prospective study of neonatal outcomes at less than 32 weeks associated with indications for maternal admission and delivery. Am J Obstet Gynecol. 2017;217:72.e1–9.
3. Society for Maternal-Fetal Medicine Publications Committee, Berkley E, Chauhan SP, Abuhamad A. Doppler assessment of the fetus with intrauterine growth restriction. Am J Obstet Gynecol. 2012;206:300–8.
4. Yanney M, Marlow N. Paediatric consequences of fetal growth restriction. Semin Fetal Neonatal Med. 2004;9:411–8.
5. Marlow N, Wolke D, Bracewell MA, Samara M. The Epicure Study Group. Neurologic and developmental disability at six years of age after extremely preterm birth. N Engl J Med. 2005;352:9–19.
6. Low J, Handley M, Burke S, Peters RD, Pater EA, Killen HL, et al. Association of intrauterine growth retardation and learning deficits at age 9 to it years. Am J Obstet Gynecol. 1992;162:1499–505.
7. Gordijn SJ, Beune IM, Thilaganathan B, Papageorghiou A, Baschat AA, Baker PN, et al. Consensus definition of fetal growth restriction: a Delphi procedure. Ultrasound Obstet Gynecol. 2016;48:333–9.
8. Figueras F, Gardosi J. Intrauterine growth restriction: new concepts in antenatal surveillance, diagnosis, and management. Am J Obstet Gynecol. 2011;204:288–300.
9. Kennelly MM, Farah N, Turner MJ, Stuart B. Aortic isthmus Doppler velocimetry: role in assessment

of preterm fetal growth restriction. Prenat Diagn. 2010;30:395–401.
10. Lees C, Marlow N, Arabin B, Bilardo CM, Brezinka C, Derks JB, et al. Perinatal morbidity and mortality in early-onset fetal growth restriction: cohort outcomes of the trial of randomized umbilical and fetal flow in Europe (TRUFFLE). Ultrasound Obstet Gynecol. 2013;42:400–8.
11. Gardosi J, Chang A, Kalyan B, Sahota D, Symonds EM. Customised antenatal growth charts. Lancet. 1992;339:283–7.
12. Gardosi J, Giddings S, Buller S, Southam M, Williams M. Preventing stillbirths through improved antenatal recognition of pregnancies at risk due to fetal growth restriction. Public Health. 2014;128:698–702.
13. Van den Wijngaard JA, Groenenberg IA, Wladimiroff JW, Hop WC. Cerebral Doppler ultrasound of the human fetus. Br J Obstet Gynaecol. 1989;96:845–9.
14. Rizzo G, Arduini D, Romanini C. Doppler echocardiographic assessment of fetal cardiac function. Ultrasound Obstet Gynecol. 1992;2:434–45.
15. Stampalija T, Casati D, Monasta L, Sassi R, Rivolta MW, Muggiasca ML, et al. Brain sparing effect in growth-restricted fetuses is associated with decreased cardiac acceleration and deceleration capacities: a case-control study. BJOG. 2016;123:1947–54.
16. Turan OM, Turan S, Gungor S, Berg C, Moyano D, Gembruch U, et al. Progression of Doppler abnormalities in intrauterine growth restriction. Ultrasound Obstet Gynecol. 2008;32:160–7.
17. Baschat AA, Güclü S, Kush ML, Gembruch U, Weiner CP, Harman CR. Venous Doppler in the prediction of acid-base status of growth-restricted fetuses with elevated placental blood flow resistance. Am J Obstet Gynecol. 2004;191:277–84.
18. Arduini D, Rizzo G, Romanini C. Changes of Pulsatility Index preceding the onset of late decelerations in growth retarded fetuses. Obstet Gynecol. 1992;79:605–10.
19. Rizzo G, Capponi A, Chaoui R, Taddei F, Arduini D, Romanini C. Blood flow velocity waveforms from peripheral pulmonary arteries in normally grown and growth-retarded fetuses. Ultrasound Obstet Gynecol. 1996;8:87–92.
20. Rizzo G, Arduini D, Romanini C, Mancuso S. Doppler echocardiographic assessment of atrioventricular velocity waveforms in normal and small for gestational age fetuses. Br J Obstet Gynaecol. 1988;95:65–9.
21. Rizzo G, Arduini D, Romanini C, Mancuso S. Doppler echocardiographic evaluation of time to peak velocity in the aorta and pulmonary artery of small for gestational age fetuses. Br J Obstet Gynaecol. 1990;97:603–7.
22. Rizzo G, Arduini D. Fetal cardiac function in intrauterine growth retardation. Am J Obstet Gynecol. 1991;165:876–82.
23. Rizzo G, Capponi A, Cavicchioni O, Vendola M. Arduini, D Low cardiac output to the placenta: an early hemodynamic adaptive mechanism in intrauterine growth restriction. Ultrasound Obstet Gynecol. 2008;32:155–9.
24. Figueras F, Puerto B, Martinez JM, Cararach V, Vanrell JA. Cardiac function monitoring of fetuses with growth restriction. Eur J Obstet Gynecol Reprod Biol. 2003;110:159–63.
25. Hassan WA, Brockelsby J, Alberry M, Fanelli T, Wladimiroff J, Lees CC. Cardiac function in early onset small for gestational age and growth restricted fetuses. Eur J Obstet Gynecol Reprod Biol. 2013;171:262–5.
26. Rizzo G, Arduini D, Romanini C. Inferior vena cava flow velocity waveforms in appropriate and small for gestational age fetuses. Am J Obstet Gynecol. 1992;166:1271–80.
27. Hecker K, Hackeloer BJ. Cardiotocogram compared to Doppler investigation of the fetal circulation in the premature growth-retarded fetus: longitudinal observations. Ultrasound Obstet Gynecol. 1997;9:152–61.
28. Rizzo G, Capponi A, Soregaroli M, Arduini D, Romanini C. Umbilical vein pulsations and acid base status at cordocentesis in growth retarded fetuses with absent end diastolic velocity in umbilical artery. Biol Neonate. 1995;68:163–8.
29. Rizzo G, Capponi A, Talone PE, Arduini D, Romanini C. Doppler indices from inferior vena cava and ductus venosus in predicting pH and oxygen tension in umbilical blood at cordocentesis in growth retarded fetuses. Ultrasound Obstet Gynecol. 1996;7:401–10.
30. Kiserud T, Kessler J, Ebbing C, Rasmussen S. Ductus venosus shunting in growth-restricted foetuses and the effect of umbilical circulatory compromise. Ultrasound Obstet Gynecol. 2006;28:143–9.
31. Rizzo G, Capponi A, Arduini D, Romanini C. The value of fetal arterial, cardiac and venous flows in predicting pH and blood gases measured in umbilical blood at cordocentesis in growth retarded fetuses. Br J Obstet Gyanecol. 1995;102:963–9.
32. Arduini D, Rizzo G, Romanini C. The development of abnormal heart rate pattern after absent end diastolic velocity in umbilical artery: analysis of risk factors. Am J Obstet Gynecol. 1993;168:43–50.
33. Rizzo G, Capponi A, Pietrolucci ME, Boccia C, Arduini D. The significance of visualizing coronary blood flow in early onset severe growth restricted fetuses with reverse flow in the ductus venosus. J Matern Fetal Neonatal Med. 2009;22:547–51.
34. Rizzo G, Capponi A, Rinaldo D, Arduini D, Romanini C. Ventricular ejection force in growth retarded fetuses. Ultrasound Obstet Gynecol. 1995;5:247–52.
35. Del Río M, Martínez JM, Figueras F, Bennasar M, Olivella A, Palacio M, et al. Doppler assessment of the aortic isthmus and perinatal outcome in preterm fetuses with severe intrauterine growth restriction. Ultrasound Obstet Gynecol. 2008;31:41–7.
36. Del Río M, Martinez JM, Figueras F, Bennasar M, Palacio M, Gomez O, et al. Doppler assessment of fetal aortic isthmus blood flow in two different sono-

graphic planes during the second half of gestation. Ultrasound Obstet Gynecol. 2005;26:170–4.
37. Rizzo G, Capponi A, Vendola M, Pietrolucci ME, Arduini D. Relationship between aortic isthmus and ductus venosus velocity waveforms in severe growth restricted fetuses. Prenat Diagn. 2008;28:1042–7.
38. Acharya G. Technical aspects of aortic isthmus Doppler velocimetry in human fetuses. Ultrasound Obstet Gynecol. 2009;33:628–33.
39. Ruskamp J, Fouron JC, Gosselin J, Raboisson MJ, Infante-Rivard C, Proulx F. Reference values for an index of fetal aortic isthmus blood flow during the second half of pregnancy. Ultrasound Obstet Gynecol. 2003;21:441–4.
40. Fouron JC, Gosseli J, Raboisson MJ, Lamoureux J, Tison CA, Fouron C, et al. The relationship between an aortic isthmus blood flow velocity and the postnatal neurodevelopmental status of fetuses with placental circulatory insufficiency. Am J Obstet Gynecol. 2005;192:497–503.
41. Tei C, Ling LH, Hodge DO, Bailey KR, Oh JK, Rodeheffer RJ, et al. New index of combined systolic and diastolic myocardial performance: a simple and reproducible measure of cardiac function a study in normal and dilated cardiomyopathy. J Cardiol. 1995;26:357–66.
42. Benavides-Serralde A, Scheier M, Cruz-Martinez R, Crispi F, Figueras F, Gratacos E, et al. Changes in central and peripheral circulation in intrauterine growth-restricted fetuses at different stages of umbilical artery flow deterioration: new fetal cardiac and brain parameters. Gynecol Obstet Investig. 2011;71:274–80.
43. Pérez-Cruz M, Cruz-Lemini M, Fernández MT, Parra JA, Bartrons J, Gómez-Roig MD, et al. Fetal cardiac function in late-onset intrauterine growth restriction vs small-for-gestational age, as defined by estimated fetal weight, cerebroplacental ratio and uterine artery Doppler. Ultrasound Obstet Gynecol. 2015;46:465–71.
44. Cruz-Martinez R, Figueras F, Hernandez-Andrade E, Oros D, Gratacos E. Changes in myocardial performance index and aortic isthmus and ductus venosus Doppler in term, small-for-gestational age fetuses with normal umbilical artery pulsatility index. Ultrasound Obstet Gynecol. 2011;38:400–5.
45. Hernandez-Andrade E, Crispi F, Benavides-Serralde JA, Plasencia W, Diesel HF, Eixarch E, et al. Contribution of the myocardial performance index and aortic isthmus blood flow index to predicting mortality in preterm growth-restricted fetuses. Ultrasound Obstet Gynecol. 2009;34:430–6.
46. Lees CC, Marlow N, van Wassenaer-Leemhuis A, Arabin B, Bilardo CM, Brezinka C, et al. 2 year neurodevelopmental and intermediate perinatal outcomes in infants with very preterm fetal growth restriction (TRUFFLE): a randomised trial. Lancet. 2015;385:2162–72.
47. Bilardo CM, Hecher K, Visser GH, Papageorghiou AT, Marlow N, Thilaganathan B, et al. Severe fetal growth restriction at 26-32 weeks: key messages from the TRUFFLE study. Ultrasound Obstet Gynecol. 2017;50:285–90.
48. Figueras F, Caradeux J, Crispi F, Eixarch E, Peguero A, Gratacos E. Diagnosis and surveillance of late-onset fetal growth restriction. Am J Obstet Gynecol. 2018;218:S790–802.e1.
49. Doctor BA, O'Riordan MA, Kirchner HL, Shah D, Hack M. Perinatal correlates and neonatal outcomes of small for gestational age infants born at term gestation. Am J Obstet Gynecol. 2001;185:652–9.
50. Chauhan SP, Rice MM, Grobman WA, et al. Neonatal morbidity of small- and large-for-gestational-age neonates born at term in uncomplicated pregnancies. Obstet Gynecol. 2017;130:511–9.
51. Arcangeli T, Thilaganathan B, Hooper R, Khan KS, Bhide A. Neurodevelopmental delay in small babies at term: a systematic review. Ultrasound Obstet Gynecol. 2012;40:267–75.
52. Souka AP, Papastefanou I, Pilalis A, Michalitsi V, Panagopoulos P, Kassanos D. Performance of the ultrasound examination in the early and late third trimester for the prediction of birth weight deviations. Prenat Diagn. 2013;33:915–20.
53. Mappa I, Maqina P, Bitsadze V, Khizroeva J, Makatsarya A, Arduini D, Rizzo G. Cardiac function in fetal growth restriction. Minerva Obstet Gynecol. 2021;73(4):423–34. https://doi.org/10.23736/S2724-606X.21.04787.
54. Crispi F, Miranda J, Gratacós E. Long-term cardiovascular consequences of fetal growth restriction: biology, clinical implications, and opportunities for prevention of adult disease. Am J Obstet Gynecol. 2018;218:S869–79.
55. DeVore GR, Klas B, Satou G, Sklansky M. 24-segment sphericity index: a new technique to evaluate fetal cardiac diastolic shape. Ultrasound Obstet Gynecol. 2018;51:650–8.
56. Rizzo G, Mattioli CA, Mappa I, Bitsadze V, Khizroeva J, Słodki M, Makatsarya A, D'Antonio F. Hemodynamic factors associated with fetal cardiac remodeling in late fetal growth restriction: a prospective study. J Perinat Med. 2019;47(7):683–8. https://doi.org/10.1515/jpm-2019-0217.
57. Rizzo G, Rizzo L, Aiello E, Allegra E, Arduini D. Modelling umbilical vein blood flow normograms at 14-40 weeks of gestation by quantile regression analysis. J Matern Fetal Neonatal Med. 2016;29:701–6.
58. Rizzo G, Capponi A, Aiello E, Arduini D. First-trimester assessment of umbilical vein diameter using the semiautomated system for nuchal translucency measurement. Ultrasound Obstet Gynecol. 2011;37:741–2.
59. Rizzo G, Mappa I, Bitsadze V, Słodki M, Khizroeva J, Makatsarya A, D'Antonio F. Role of Doppler ultrasound in predicting perinatal outcome in pregnancies complicated by late-onset fetal growth restriction at the time of diagnosis: a prospective cohort study. Ultrasound Obstet Gynecol. 2019;55:793–8. https://doi.org/10.1002/uog.20406.
60. http://www.truffle-study.org/research/.

Role of Ultrasonography in Placenta Accreta Spectrum

35

Marcus J. Rijken, Rozi Aditya Aryananda, and Sally Collins

35.1 Introduction, Epidemiology and Risk Factors

Placenta Accreta Spectrum (PAS) also known as abnormally invasive placenta (AIP), describes the clinical situation when after delivery of the fetus the placenta does not detach spontaneously from the uterus and if forcibly removed can cause potentially catastrophic maternal hemorrhage [1–3]. This "spectrum disorder" ranges from abnormally adherent to deeply invasive placental tissue, traditionally categorized as placenta accreta, when villi are directly attached to the myometrium without interposing decidua (abnormally adherent); placenta increta, when the villi penetrate the myometrium up to the uterine serosa (abnormally invasive); and placenta percreta, when the villi penetrate through the uterine serosa to invade neighboring tissues and organs, such as the bladder (abnormally invasive); but all grades can co-exist within the same placenta [4, 5]. The incidence of PAS has increased worldwide, most likely associated with the rising rates of cesarean delivery [1]. Cesarean section is the greatest risk factor, and therefore PAS could be seen as an iatrogenic disease [6]. Other surgical risk factors include uterine procedures (such as curettage, myomectomy, endometrial ablation, manual removal of the placenta, or adhesiolysis for Asherman syndrome). Advanced maternal age, increasing parity and In vitro Fertilization (IVF) are additional risk factors. Even though PAS is still rare (0.83.1 per 1000 births after a prior cesarean), PAS is the most common reason for peripartum hysterectomy and contributes to the current failure to reduce maternal death rate in high-income countries.

Antenatal recognition of PAS is vital to initiate multidisciplinary planning for a safe delivery in a center of expertise which has been shown to reduce maternal mortality and morbidity. However, the available evidence is complicated by methodologically flawed study designs and variations in the definitions and diagnostic criteria used. In an attempt to address these problems international groups, including the International Federation of Gynecology and Obstetrics (FIGO) and the International Society for AIP (IS-AIP), have published proposals for standardized diagnostic criteria [7] and clinical classification [8].

M. J. Rijken (✉)
University Medical Centre Utrecht, Utrecht, The Netherlands
e-mail: m.j.rijken@umcutrecht.nl

R. A. Aryananda
Dr. Soetomo Academic General Hospital, Universitas Airlangga, Surabaya, Indonesia

S. Collins
Oxford University Hospitals NHS Foundation Trust, Oxford, United Kingdom and Associate Professor of Obstetrics, University of Oxford, Oxford, UK
e-mail: sally.collins@wrh.ox.ac.uk

D. Maulik, C. C. Lees (eds.), *Doppler Ultrasound in Obstetrics and Gynecology*,
https://doi.org/10.1007/978-3-031-06189-9_35

35.2 Clinical Implications

Optimal management requires accurate antenatal diagnosis, multidisciplinary teamwork, and a robust perinatal management strategy. During routine care, the mid-pregnancy fetal anomaly scan should include placental localization thereby identifying women at risk of persisting low-lying placenta or who have a placenta previa. Women with significant clinical risk factors for PAS (most notably placenta previa and previous cesarean section) should undergo further diagnostic evaluation by an experienced sonographer [9]. MRI is reported to be of adjunctive value for posterior placenta previa, to assess potential bladder invasion and could be a useful tool for multidisciplinary planning for surgery [10–12]. Patients with suspected PAS should be referred to a center of excellence. FIGO recommends the use of a clinical grading system for diagnosis at delivery [9] (Table 35.1).

Table 35.1 FIGO clinical classification for the diagnosis of Placenta accreta spectrum (PAS) at delivery [8]

Grade		
1	Abnormally adherent placenta (PLACENTA ADHERENTA OR CRETA)	
	Clinical criteria	At vaginal delivery – No separation with synthetic oxytocin and gentle controlled cord traction – Attempts at manual removal of the placenta results in heavy bleeding from the placental implantation site requiring mechanical or surgical procedures If laparotomy is required: the same as above
	Histologic criteria	– Macroscopically, the uterus shows no obvious distension over the placental bed (placental "bulge"), no placental tissue is seen invading through the surface of the uterus, and there are no or minimal superficial vascular changes – Microscopic examination of the placental bed samples from the hysterectomy specimen shows extended areas of absent decidua between villous tissue and myometrium with placental villi attached directly to the superficial myometrium – The diagnosis cannot be made on just delivered placental tissue nor on random biopsies of the placental bed
2	Abnormally invasive placentation (PLACENTA INCRETA)	
	Clinical criteria	At laparotomy – Abnormal macroscopic findings over the placental bed: bluish/purple coloring, distension (placental "bulge") – Increased vascularity around the placental bed (dense tangled bed of vessels or multiple vessels running parallel cranio-caudally in the uterine serosa – No placental tissue was seen to be invading through the surface of the uterus – Gentle cord traction results in the uterus being pulled inwards without separation of the placenta (the "dimple" sign)
	Histologic criteria	Hysterectomy specimen or partial myometrial resection of the increta area shows placental villi within the muscular fibers and sometimes in the lumen of the deep uterine vasculature
3	GRADE 3 Abnormally invasive placentation (PLACENTA PERCRETA)	
3A	Limited to the uterine serosa	
	Clinical criteria	At laparotomy – Abnormal macroscopic findings on the uterine surface (as above) and placental tissue seen to be invading through the surface of the uterus (serosa) – No invasion into any other organ, including the posterior wall of the bladder (a clear surgical plane can be identified between the bladder and uterus)
	Histologic criteria	Hysterectomy specimen showing villous tissue within or breaching the uterine serosa
3B	With urinary bladder invasion	
	Clinical criteria	At laparotomy – The same as 3A – Placental villi are seen to be invading into the bladder but no other organs – Clear surgical plane cannot be identified between the bladder and the uterus
	Histologic criteria	Hysterectomy specimen showing villous tissue breaching the uterine serosa and invading the bladder wall tissue or urothelium

Table 35.1 (continued)

Grade		
3C	With the invasion of other pelvic tissues/organs	
	Clinical criteria	At laparotomy – The same as 3A – Placental villi are seen to be invading into the broad ligament, vaginal wall, pelvic sidewall or any other pelvic organ (+/− invasion of the bladder)
	Histologic criteria	Hysterectomy specimen showing villous tissue breaching the uterine serosa and invading pelvic tissues/organs

Although the sensitivity of ultrasound diagnosis of PAS is crucial, there is a price of a false-positive diagnosis. A midline laparotomy proceeding straight to post-cesarean hysterectomy is frequently used when a PAS is anticipated. Further risks for complications include the frequently used prophylactic balloons in the pelvic vasculature or planned preterm delivery, resulting in possible iatrogenic maternal and neonatal morbidity [13]. Therefore, the positive predictive value (PPV) and negative predictive value (NPV) of the ultrasound signs are as important as the sensitivity and specificity. Practically, the PPV indicates the confidence with which clinicians can proceed straight to post-cesarean hysterectomy without removing the placenta. In contrast, the NPV characterizes the confidence with which obstetricians can remove a placenta previa without concerns of severe bleeding [14].

Clinical outcomes of women affected by PAS are related to the depth and location of placental invasions, such as bladder involvement or parametrium invasion, although variability in surgical outcome in women presenting with the same degree of placental invasion has been described. A recent approach to prenatal ultrasound staging of PAS showed a good correlation with surgical outcomes, depth of invasion, and the FIGO clinical grading system [15]. Although prenatal diagnosis by ultrasound is an extremely valuable tool, the absence of ultrasound signs does not preclude the diagnosis of focal PAS especially at the abnormally adherent, accreta end of the spectrum and clinical factors as described above remain important in identifying women at high risk.

35.3 Ultrasound Findings

Antenatal ultrasound is the primary tool to identify the location of the placenta and its relation to the uterine scar. The detecting PAS, however, still relies on subjective interpretation of typical sonographic signs of the uterine wall and placenta with two-dimensional (2D) grayscale and color Doppler imaging. Its accuracy depends not only on the experience of the operator, which is limited in many settings by the rarity of the condition but also on technical aspects. Several signs have been reported with varying results in diagnostic accuracy, mainly due to differences in definitions of the ultrasound signs (e.g., how abnormal lacunae are defined), as well as the final clinical diagnosis. To improve consistency and allow for comparison of the ultrasound markers, the IS-AIP proposed a uniform description of ultrasound signs used for the prenatal diagnosis of PAS and an adhoc International Expert Group produced a proforma protocol for the ultrasound assessment (Tables 35.2 and 35.3) [16, 17].

Recent systematic reviews and meta-analysis of ultrasound studies in pregnancies at risk of PAS (women with a prior cesarean delivery, presenting with the anterior low placenta or placenta previa) found that the overall performance of ultrasound, when performed by skilled operators, was very good with a sensitivity and specificity of >95% [18–20]. Myometrial thinning, bladder

Table 35.2 Grayscale 2D ultrasound signs of PAS and definitions

Descriptors	Definition
Loss of "clear zone"	Loss, or irregularity, of the hypoechoic plane in myometrium underneath placental bed ("clear zone")
Abnormal placental lacunae	Presence of numerous lacunae including some that are large and irregular (Finberg Grade 3), often containing turbulent flow visible on grayscale imaging
Bladder wall interruption	Loss or interruption of the bright bladder wall (hyperechoic band or "line" between uterine serosa and bladder lumen)
Myometrial thinning	Thinning of myometrium overlying placenta to <1 mm or undetectable
Placental bulge	Deviation of uterine serosa away from the expected plane, caused by an abnormal bulge of placental tissue into neighboring organ, typically bladder; uterine serosa appears intact but outline shape is distorted
Focal exophytic mass	Placental tissue is seen breaking through uterine serosa and extending beyond it; most often seen inside a filled urinary bladder

Table 35.3 Color Doppler ultrasound signs of PAS and definitions [16, 17]

2D color Doppler	
Uterovesical hypervascularity (Fig. 35.1)	Striking amount of color Doppler signal seen between myometrium and posterior wall of the bladder; this sign probably indicates numerous, closely packed, tortuous vessels in that region (demonstrating multidirectional flow and aliasing artifact)
Subplacental hypervascularity (Fig. 35.2)	Striking amount of color Doppler signal seen in placental bed; this sign probably indicates numerous, closely packed, tortuous vessels in that region (demonstrating multidirectional flow and aliasing artifact)
Bridging vessels (Fig. 35.3)	Vessels appearing to extend from placenta, across the myometrium and beyond serosa into the bladder or other organs; often running perpendicular to the myometrium
Placental lacunae feeder vessels (Fig. 35.4)	Vessels with high-velocity blood flow leading from myometrium into placental lacunae, causing turbulence upon entry
3D ultrasound +/− power Doppler	
Intraplacental hypervascularity (Figs. 35.5 and 35.6)	Complex, irregular arrangement of numerous placental vessels, exhibiting tortuous courses and varying calibers

wall interruption, and uterovesical hypervascularity were associated with the most severe types of PAS (percreta) [21]. Placental lacunae and the increased vascularity of the placental bed with large feeder vessels entering the lacunae were the most common ultrasound signs associated with PAS [8]. The highest level of inter-observer agreement for ultrasound signs was found for loss of clear zone, myometrial thinning, the presence of lacunar feeding vessels on 2D color Doppler and crossing vessels and lacunae on 3D color Doppler [4]. Abnormal implantation of the placenta is not always homogeneous, but usually combines areas of abnormal adherence and invasion in the same placenta. This may explain why yet no single sign or combination of markers has been found to be specific for the depth of PAS on histology.

35.4 Color Doppler Ultrasound

The introduction of color Doppler ultrasound has enabled better visualization of the uteroplacental circulation: PAS is often associated with hypervascularization patterns within the placenta and between the placental basal plate and underlying tissues (myometrium, bladder wall). However, despite attempts to standardize these signs, the exact interpretation of color Doppler ultrasound findings remains subjective [22].

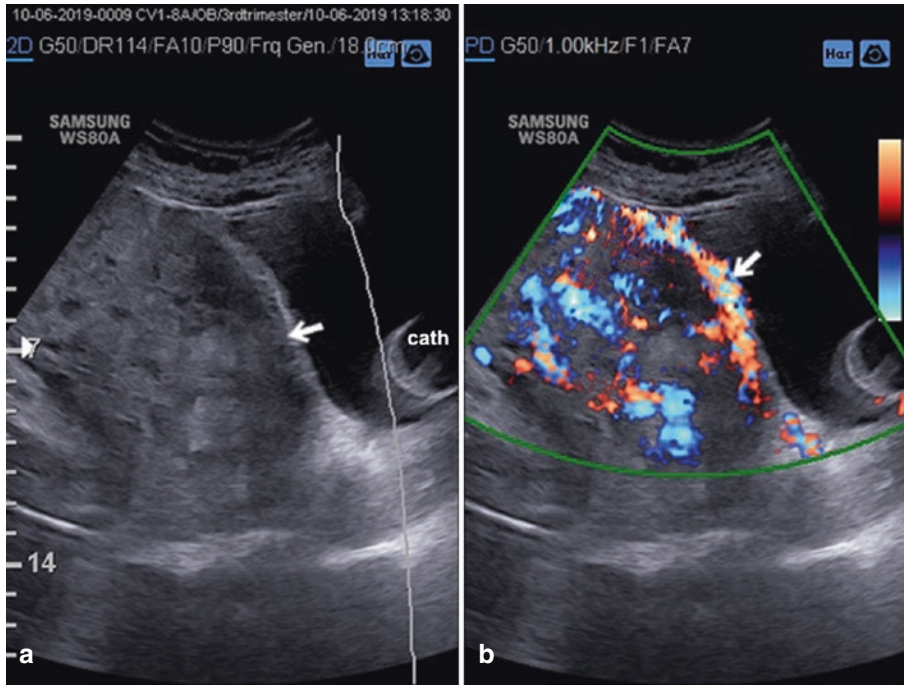

Fig. 35.1 (**a**) Transabdominal 2D Ultrasound. Loss of "clear zone" (arrow) and (**b**) Uterovesical hypervascularity in 2D Doppler ultrasound (arrow) in 30 weeks of gestational age

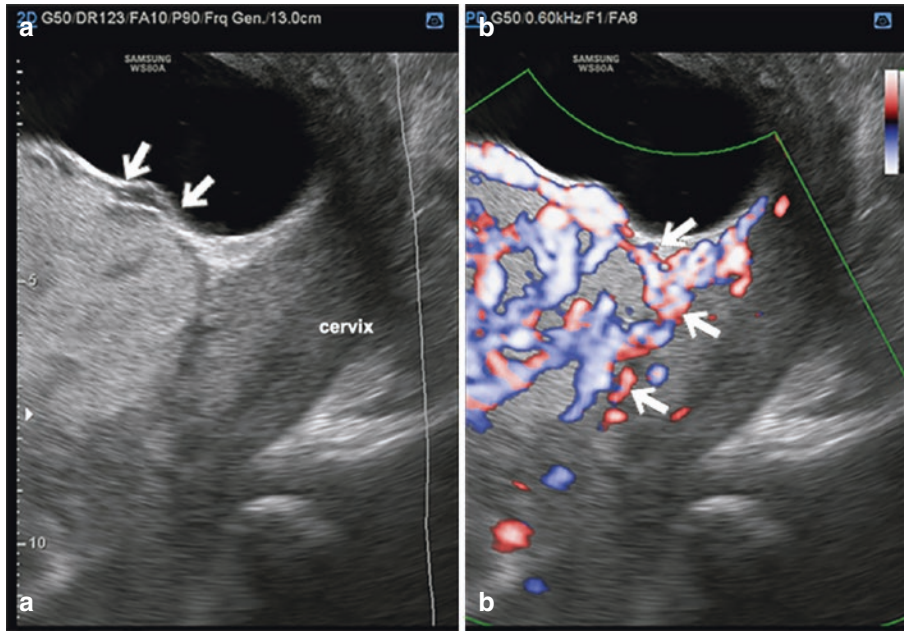

Fig. 35.2 (**a**) Transvaginal 2D. Bladder wall interruption (arrow) in lower bladder and (**b**) Subplacental hypervascularity (arrow) in 27 weeks of gestational age

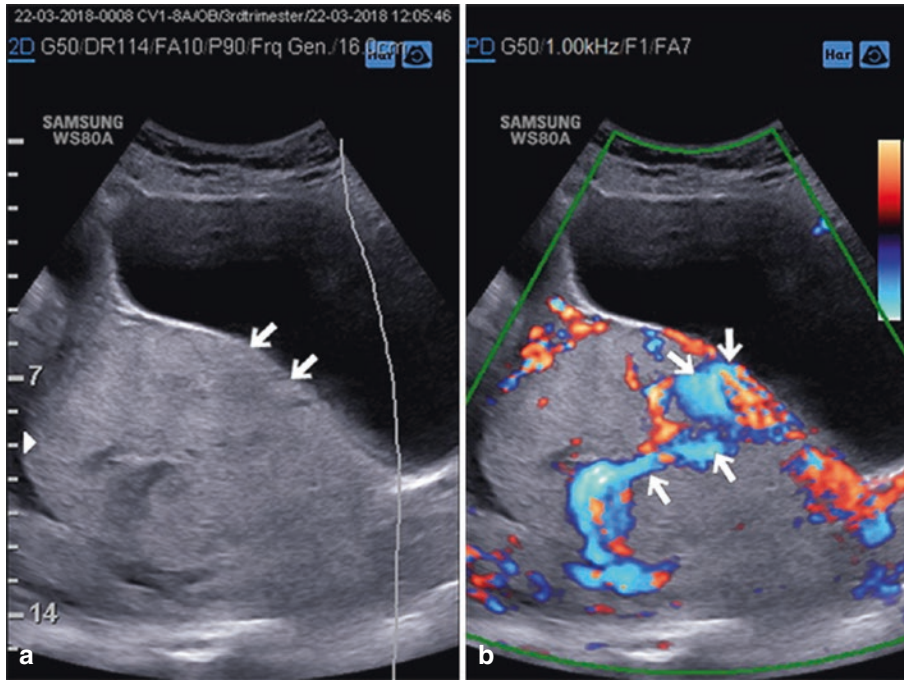

Fig. 35.3 (**a**) Undetectable of myometrial wall (arrow) in Transabdominal 2D ultrasound and (**b**) bridging vessel which is appearing to extend from placenta into bladder (arrow) in 33 weeks of gestational age

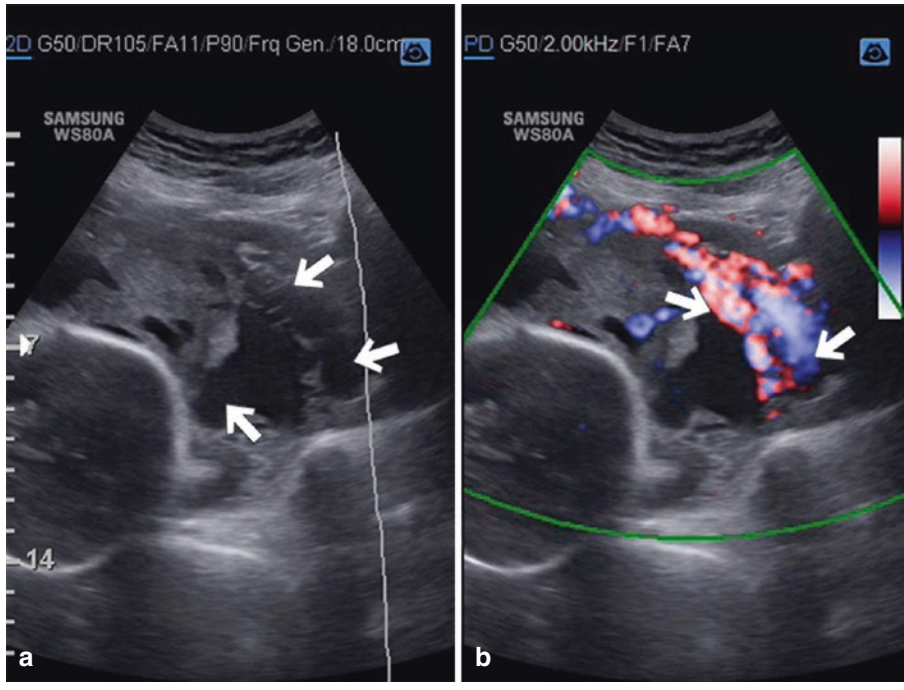

Fig. 35.4 (**a**) Large and irregular Abnormal placental lacunae (arrow) in Transabdominal 2D ultrasound with (**b**) Placental lacunae feeder vessels (arrow) in 2D Doppler ultrasound (arrow) in 33 weeks of gestational age

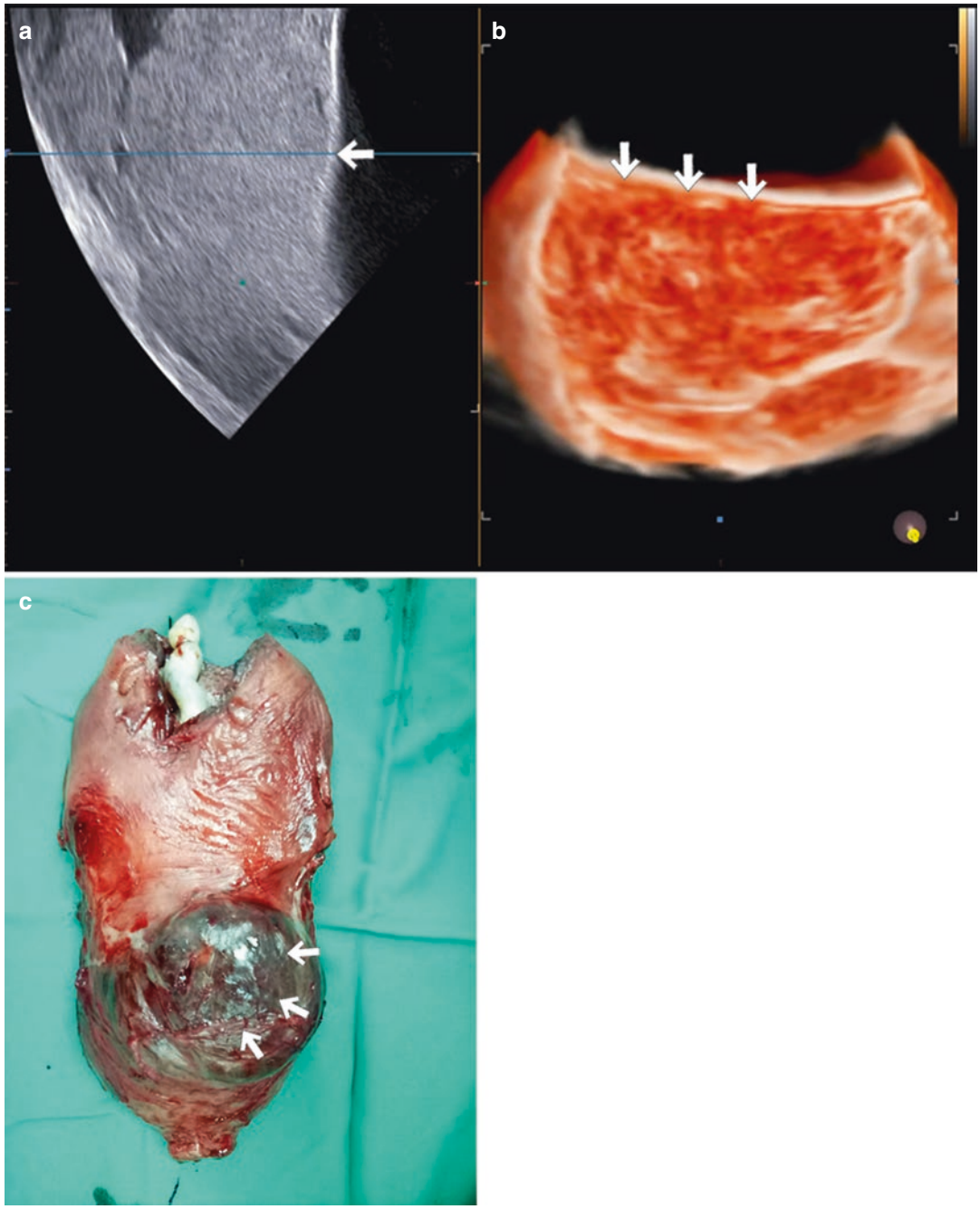

Fig. 35.5 (**a**) Loss of "clear zone" and undetected myometrial wall (arrow), which is seen in (**b**) 3D volume rendering ultrasound (axial plane), which is predominantly a uterine wall defect in the left lower uterine segment (arrow) in 33 weeks of gestational age and (**c**) proven during surgery (arrow) at 34 weeks of gestational age

The combination of grayscale and color Doppler imaging ultrasound markers is reported to have increased the sensitivity of ultrasound imaging with NPV ranging between 95% and 98%. In a recent study, ultrasound staging had a high correlation with surgical outcome, depth of invasion, and the FIGO classification system [15].

35.5 3D and Power Doppler Imaging

The 3D color Doppler technique has been increasingly used: the placental borders can be manually traced and placental volume can be assessed and measured [22]. In studies to diagnose PAS with three-dimensional (3D) power Doppler, the placenta was assessed in various ways: subjective for abnormal vascularity; intraplacental hypervascularity, inseparable cotyledonal (fetal) and intervillous (maternal) circulations or tortuous confluent vessels across the placental width [14, 23]. In order to quantify hypervascularity, new measurements have been suggested, such as 3D Volume Rendering for placental–bladder interface, the area of confluence or the vascular index [13, 22, 24]. In prospective studies, these measurements differentiated between the presence and absence of PAS and were more predictive of severe cases of PAS than were the 2D ultrasound signs [13]. Although these findings are promising, they need to be confirmed in multicenter trials before appropriate clinical applications can be determined (Figs. 35.6 and 35.6).

35.6 Technical Aspects [16]

35.6.1 Bladder Volume [25]

PAS is most commonly associated with an anterior low-lying placenta or placenta previa. To visualize the anterior lower segment of the uterus, an ultrasound examination must be carried out with a full bladder (around 250–300 mL). Without a full bladder, signs such as bladder wall interruption, placental bulge, and uterovesical hypervascularity cannot be appropriately assessed. On the other hand, if the bladder is overfilled (>500 mL), compression of the placental bed may obscure the vascular architecture and change the appearance of the interface.

35.6.2 Angle of Insonation

The best angle of insonation of the area of interest, the border between the placenta and the myo-

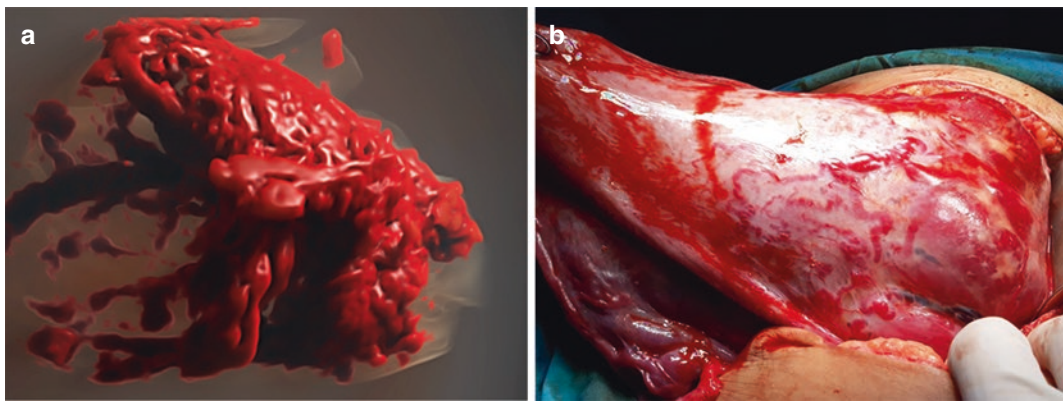

Fig. 35.6 (**a**) 3D power Doppler in diffuse placenta percreta with intraplacental hypervascularity, inseparable cotyledons and intervillous circulation, irregular branches of intraplacental vascularity which is found in (**b**) placenta percreta during surgery

metrium, is 90°; this angle is not easily achieved by either transabdominal or transvaginal scanning. If the angle is close to 0°, artifacts can make the correct analysis of the placental-myometrial interface difficult and result in false-positives in particular regarding "myometrial thinning."

35.6.3 Transabdominal and Transvaginal Probe Pressure

The required pressure used by the operator on the probe depends on the woman's body habitus and distribution of adipose tissue. Pressing too hard may result in artifacts such as "loss of the clear zone" and myometrial thinning.

35.6.4 Color Doppler and (3D) Power Doppler

Attention must be paid to using the appropriate blood flow velocity settings (pulse repetition frequency, PRF, usually 1.3 kHz for color Doppler and 0.9 kHz for power Doppler). If the PRF is too low there will be increased aliasing potentially leading to the suggestion of hypervascularization. To select the appropriate Doppler setting the gain should be increased until the image is saturated with color and then slowly reduce the gain until the apparent artifacts disappear (called the Sub-Noise Gain (SNG) setting). Using the SNG ensures that the difference in Doppler signal attenuation caused by differences in the amount and type of tissue being insonated is appropriately corrected for.

35.7 Clinical Examples

35.7.1 Clinical Cases-Imaging-Related to Clinical Findings During Surgery

Case 1 Mrs. A, 36-year-old, Gravida 4, Parity 3, 35 weeks of gestational age with three previous cesarean sections (Fig. 35.7).

Case 2 Mrs. L, 30-year-old, Gravida 2, Parity 1, 33 weeks gestational age with one previous cesarean section (Fig. 35.8).

All examinations were carried out using a transabdominal probe from 4.0 to 6.0 MHz or transvaginal 5.0–7.0 MHz (GE Voluson® 730, General Electric, and Samsung WS80A Elite, Samsung); when using color Doppler ultrasound, the pulse repetition frequency (PRF) or scale was set at 1.3 KHz, but this was adapted to identify the presence of placental lacunar flow.

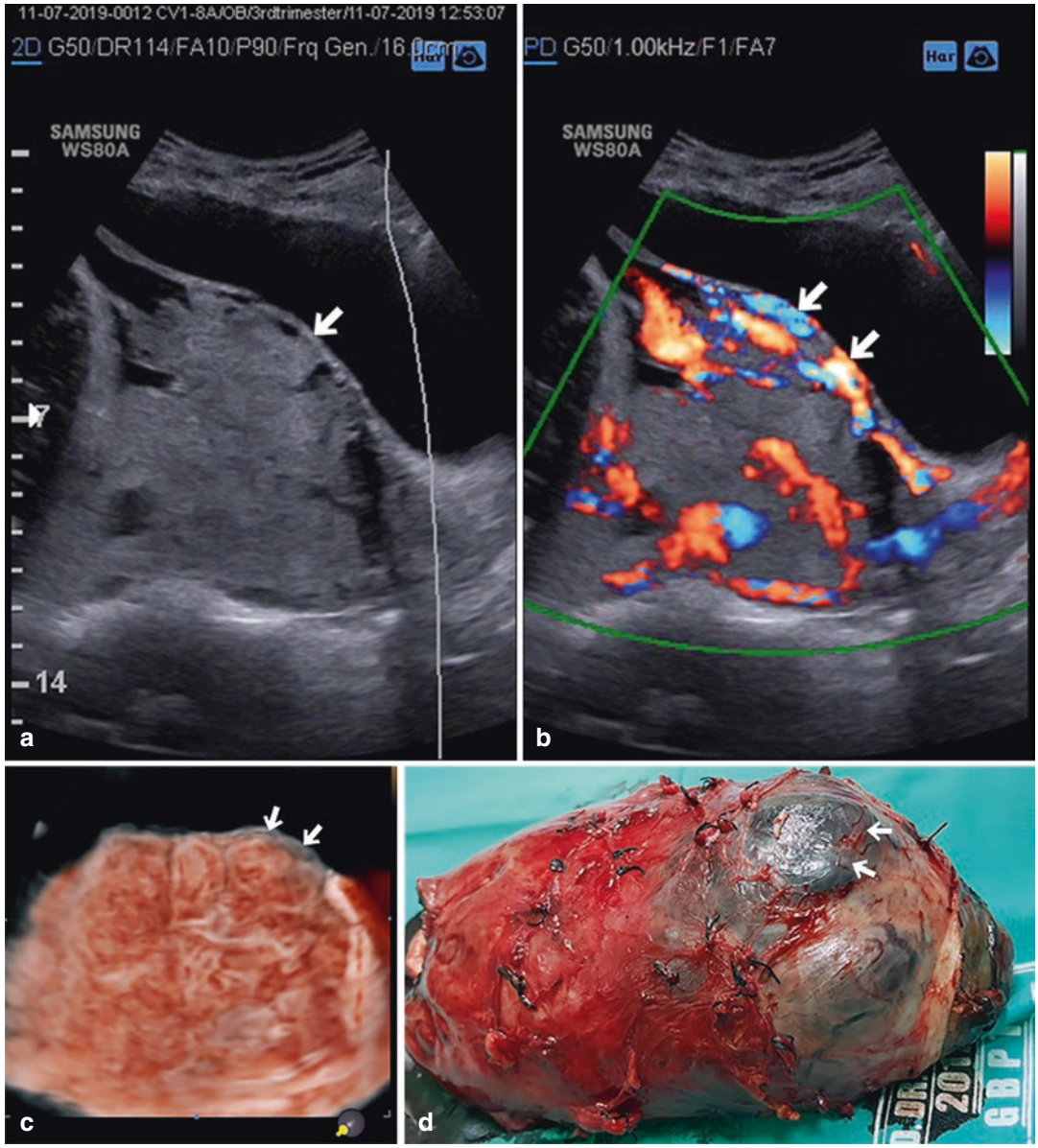

Fig. 35.7 (**a**) Placental Bulge (arrow) in Transabdominal 2D Ultrasound with (**b**) uterovesical hypervascularity (arrow) that analyze using 3D volume rendering ultrasound (**c**) in the same ultrasound probe plane shows highly suspicious of placenta percreta invasion (arrow) that proven (**d**) during surgery (arrow)

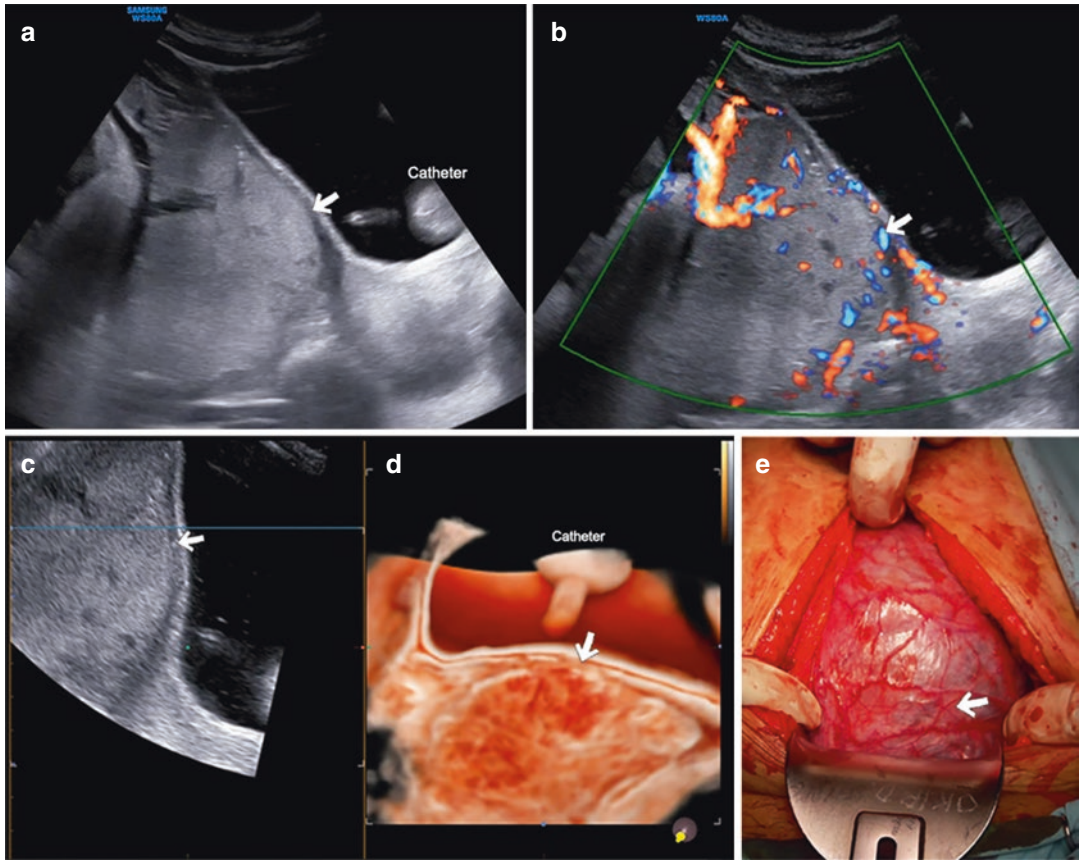

Fig. 35.8 (**a**) Loss of "clear zone" (arrow), (**b**) no evidence of subplacental hypervascularity and uterovesical hypervascularity. (**c**) Slightly placental bulge in 2D ultrasound with (**d**) small area of placental invasion in 3D volume rendering ultrasound that proven as placenta accreta during surgery (**e**)

References

1. Silver RM, Landon MB, Rouse DJ, et al. Maternal morbidity associated with multiple repeat cesarean deliveries. Obstet Gynecol. 2006;107(6):1226–32.
2. Hasegawa J, Tanaka H, Katsuragi S, Sekizawa A, Ishiwata I, Ikeda T. Maternal deaths in Japan due to abnormally invasive placenta. Int J Gynaecol Obstet. 2018;140(3):375–6.
3. Palacios-Jaraquemada JM, D'Antonio F, Buca D, Fiorillo A, Larraza P. Systematic review on near miss cases of placenta accreta spectrum disorders: correlation with invasion topography, prenatal imaging, and surgical outcome. J Matern Fetal Neonatal Med. 2019:1–8.
4. Zosmer N, Jauniaux E, Bunce C, Panaiotova J, Shaikh H, Nicholaides KH. Interobserver agreement on standardized ultrasound and histopathologic signs for the prenatal diagnosis of placenta accreta spectrum disorders. Int J Gynaecol Obstet. 2018;140(3):326–31.
5. Bhide A, Sebire N, Abuhamad A, Acharya G, Silver R. Morbidly adherent placenta: the need for standardization. Ultrasound Obstet Gynecol. 2017;49(5):559–63.
6. Jauniaux E, Jurkovic D. Placenta accreta: pathogenesis of a 20th century iatrogenic uterine disease. Placenta. 2012;33(4):244–51.
7. Collins SL, Alemdar B, van Beekhuizen HJ, et al. Evidence-based guidelines for the management of abnormally invasive placenta: recommendations from the International Society for Abnormally Invasive Placenta. Am J Obstet Gynecol. 2019;220(6):511–26.
8. Jauniaux E, Hussein AM, Fox KA, Collins SL. New evidence-based diagnostic and management strategies for placenta accreta spectrum disorders. Best Pract Res Clin Obstet Gynaecol. 2019;61:75–88.
9. Jauniaux E, Bhide A, Kennedy A, et al. FIGO consensus guidelines on placenta accreta spectrum disorders: prenatal diagnosis and screening. Int J Gynaecol Obstet. 2018;140(3):274–80.
10. Palacios-Jaraquemada JM, Karoshi M, Keith LG. Uterovaginal blood supply: the S1 and S2 seg-

mental concepts and their clinical relevance. 2nd ed. London: Sapiens Publishing; 2012.
11. Palacios Jaraquemada JM, Bruno CH. Magnetic resonance imaging in 300 cases of placenta accreta: surgical correlation of new findings. Acta Obstet Gynecol Scand. 2005;84(8):716–24.
12. Palacios Jaraquemada JM, Bruno CH, Martin E. MRI in the diagnosis and surgical management of abnormal placentation. Acta Obstet Gynecol Scand. 2013;92(4):392–7.
13. Collins SL, Stevenson GN, Al-Khan A, et al. Three-dimensional power doppler ultrasonography for diagnosing abnormally invasive placenta and quantifying the risk. Obstet Gynecol. 2015;126(3):645–53.
14. Shih JC, Palacios Jaraquemada JM, Su YN, et al. Role of three-dimensional power Doppler in the antenatal diagnosis of placenta accreta: comparison with gray-scale and color Doppler techniques. Ultrasound Obstet Gynecol. 2009;33(2):193–203.
15. Cali G, Forlani F, Lees C, et al. Prenatal ultrasound staging system for placenta accreta spectrum disorders. Ultrasound Obstet Gynecol. 2019;53(6):752–60.
16. Collins SL, Ashcroft A, Braun T, et al. Proposal for standardized ultrasound descriptors of abnormally invasive placenta (AIP). Ultrasound Obstet Gynecol. 2016;47(3):271–5.
17. Alfirevic Z, Tang AW, Collins SL, Robson SC, Palacios-Jaraquemada J. Group obotA-hIAE. Pro forma for ultrasound reporting in suspected abnormally invasive placenta (AIP): an international consensus. Ultrasound Obstet Gynecol. 2016;47(3):276–8.
18. D'Antonio F, Iacovella C, Bhide A. Prenatal identification of invasive placentation using ultrasound: systematic review and meta-analysis. Ultrasound Obstet Gynecol. 2013;42(5):509–17.
19. Jauniaux E, Bhide A. Prenatal ultrasound diagnosis and outcome of placenta previa accreta after cesarean delivery: a systematic review and meta-analysis. Am J Obstet Gynecol. 2017;217(1):27–36.
20. Jauniaux E, Alfirevic Z, Bhide A, et al. Placenta praevia and placenta accreta: diagnosis and management. Int J Obstet Gynecol. 2019;126(1):e1–e48.
21. Pagani G, Cali G, Acharya G, et al. Diagnostic accuracy of ultrasound in detecting the severity of abnormally invasive placentation: a systematic review and meta-analysis. Acta Obstet Gynecol Scand. 2018;97(1):25–37.
22. Haidar ZA, Papanna R, Sibai BM, et al. Can 3-dimensional power Doppler indices improve the prenatal diagnosis of a potentially morbidly adherent placenta in patients with placenta previa? Am J Obstet Gynecol. 2017;217(2):202.e201–13.
23. Cali G, Giambanco L, Puccio G, Forlani F. Morbidly adherent placenta: evaluation of ultrasound diagnostic criteria and differentiation of placenta accreta from percreta. Ultrasound Obstet Gynecol. 2013;41(4):406–12.
24. Aryananda RA, Akbar A, Wardhana MP, et al. New three-dimensional/four-dimensional volume rendering imaging software for detecting the abnormally invasive placenta. J Clin Ultrasound. 2019;47(1):9–13.
25. Maynard H, Zamudio S, Jauniaux E, Collins SL. The importance of bladder volume in the ultrasound diagnosis of placenta accreta spectrum disorders. Int J Gynaecol Obstet. 2018;140(3):332–7.

Three-Dimensional Doppler Ultrasound in Gynecology

36

Mark Hiraoka and Ivica Zalud

Three-dimensional (3D) reconstruction of ultrasound images was first demonstrated over 25 years ago and has since become incorporated into routine clinical practice. Methods for 3D reconstruction of Computed Tomography (CT) and Magnetic Resonance Imaging (MRI) predate ultrasound, and 3D imaging with these modalities has been more widely applied in clinical practice. Three-dimensional applications in ultrasound have lagged behind CT and MRI, because ultrasound data is much more difficult to render in 3D, for a variety of technical reasons, than either CT or MRI data. However, the computing power of ultrasound equipment has reached a level adequate for the complex signal processing tasks needed to render ultrasound data in three dimensions and new 3D ultrasound techniques and applications continue to appear [1]. Especially within obstetrics and gynecology several papers on that topic have described promising results. Gynecologic diagnostics relying on morphologic signs and accurate distance and volume measurements is one of the areas that has benefited from 3D ultrasound.

Why do we need 3D ultrasound in gynecology? Great strides have been made in gynecology secondary to the development of high-performance transvaginal ultrasound (TVS) instruments; however, even this advanced technology can provide only two-dimensional (2D) views of three-dimensional (3D) structures. Although an experienced examiner can easily piece together sequential 2D planes for creating a mental 3D image, individual sectional planes cannot be achieved in a 2D image because of various difficulties. Presently, 3D TVS can portray not only individual image planes, but it can also store complex tissue volumes which can be digitally manipulated to display a multiplanar view, allowing a systematic tomographic survey of any particular field of interest. The same technology can also display surface rendering and transparency views to provide a more realistic 3D portrayal of various structures and anomalies.

36.1 Technique

Since the end of the 1980s, 3D ultrasound has become a major field of research in gynecology. The technique of acquiring 3D data involves making a set of consecutive 2D ultrasound slices by moving the transducer and continuously storing the images. These ultrasound data must be converted into a regular cubic representation before presentation in different 3D visualization modes. The creation of new ultrasound sections from the 3D block, and the surface shading of a structure of interest, promise improvement in the

M. Hiraoka · I. Zalud (✉)
Department of OB/GYN and Women's Health, John A Burns School of Medicine, University of Hawaii, Honolulu, HI, USA
e-mail: Ivica@hawaii.edu

D. Maulik, C. C. Lees (eds.), *Doppler Ultrasound in Obstetrics and Gynecology*,
https://doi.org/10.1007/978-3-031-06189-9_36

diagnosis of congenital uterine anomalies and pelvic masses. In addition, the possibility of volume calculation by 3D ultrasound has to be considered a clear innovation. At present, most of the diagnoses illustrated by 3D ultrasound can be made by 2D ultrasound, and this will continue to be so in the foreseeable future. Recently, computer-assisted treatment of sonographic images has permitted 3D reconstruction in gynecology. This is achieved by scanning a given volume containing the organ of interest. Two practical options exist. Some ultrasound probes are equipped with an automatic scanning device while others use manual scanning, electronically normalized or not. Both approaches make use of an electronic matrix, i.e., a pile of 2D sonographic images. Secondary cuts are possible through the electronic matrix, including plans not normally accessible to ultrasound scanning because of anatomical limitations. One of the secondary cuts most clinically useful is the frontal plane of the uterus. This enables one to visualize the organ lying flat as it is commonly drawn on medical sketches. Studying the frontal plane of the uterus acquired electronically from a 3D matrix improves the visualization of possible interactions between structures such as uterine fibroids and the endometrium. The frontal plane of the uterus also offers marked improvements for studying uterine malformations.

Three-dimensional ultrasound offers several options extending conventional 2D scanning. Various imaging modes are available. Three perpendicular planes displayed simultaneously can be rotated and translated in order to obtain accurate sections and suitable views needed for diagnosis and geometric measurements. Three-dimensional ultrasound tomography combines the advantages of ultrasound, e.g., safety, simplicity of application, and inexpensiveness, with the advantages of sequentially depictable sections in numerous rotatable and translatable sections. Surface rendering gives detailed plastic images if there are surrounding layers of different echogenicity allowing for the definition of a certain threshold. Transparent modes provide imaging of structures with a higher echogenicity in the interior of the object. A combination of the two modes sequentially definable by the sonographer allows for the optimal viewing of structures. These imaging modes are innovative features that have to be evaluated for clinical applicability and usefulness (Fig. 36.1). Digital documentation of whole volumes enables full evaluation without loss of information at a later point. The 3D technology provides an enormous number of technical options that have to be evaluated for their diagnostic significance and limitations in obstetrics and gynecology.

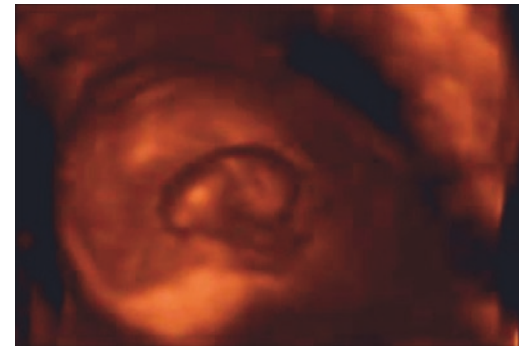

Fig. 36.1 Three-dimensional ultrasound surface rendering of ectopic pregnancy

36.2 3D Doppler Measurements

Doppler methods are routinely used to study the vascular system. Flow and tissue motion information can be obtained by frequency and time-domain processing. Instruments range in complexity from simple continuous-wave devices without imaging capability to advanced real-time 2D color-flow scanners and intravascular devices. A 3D display is now available. Contrast agents can be used to increase the detectability of blood flow signals. The properties of the tissue impose an envelope on achievable ultrasonic imaging. Doppler studies can provide information about flow velocity profile, vessel compliance, wall shear rate, pressure gradient, perfusion, tumor blood flow, and the presence of emboli. These capabilities can be integrated into a holistic picture of ultrasonic vascular studies [2, 3].

Three-dimensional Doppler ultrasound has the potential to study pelvic blood flow and the

process of neovascularization. The 3D Doppler superimposed to 3D grayscale can detect early vasculogenesis within the uterine or adnexal mass. Traditionally, we defined blood flow information as (a) quantitative, i.e., volume flow measurements (cc/min), and (b) semiquantitative, i.e., pulsed Doppler waveform analysis (RI, PI, S/D index).

Three-dimensional power Doppler introduces a new way to look at blood flow detection and analysis. Using the computer-generated VOCAL imaging program (*v*irtual *o*rgan *c*omputer-aided *a*nal*y*sis), different patterns of blood flow can be described:

1. Vascularization Index (VI)
2. Flow Index (FI)
3. Vascularization Flow Index (VFI)

Vascularization index gives information (in percentage) about the amount of color values (vessels) in the observed organ or area (e.g., uterus, ovary, or mass). Flow index is a dimensionless index (0–100) with information about the intensity of blood flow. It is calculated as a ratio of weighted color values (amplitudes) to the number of color values. Vascularization flow index (VFI) is combined information of vascularization and mean blood flow intensity. It is also a dimensionless index (1–100) that is calculated by dividing weighted color values (amplitudes) by the total voxels minus background voxels. Three-dimensional Doppler was used to acquire volumes (Fig. 36.2). VOCAL was then used to delineate the 3D areas of interest (Fig. 36.3) and the "histogram facility" was employed to generate three indices of vascularity: the VI; the FI; and the VFI (Fig. 36.4). The ultrasonographer should be aware that 3D Doppler is prone to the same artifacts and pitfalls as 2D Doppler. This information should be taken into account when any assessment of pelvic or tumor blood flow is made.

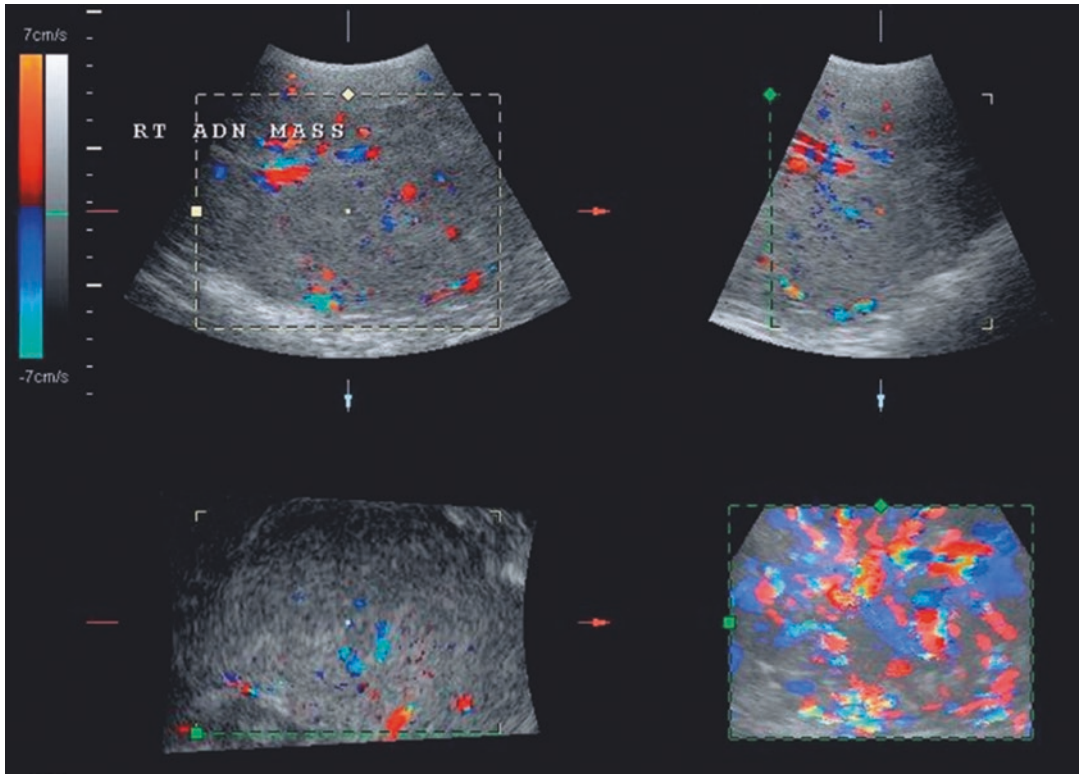

Fig. 36.2 Three-dimensional Doppler was used to acquire volumes

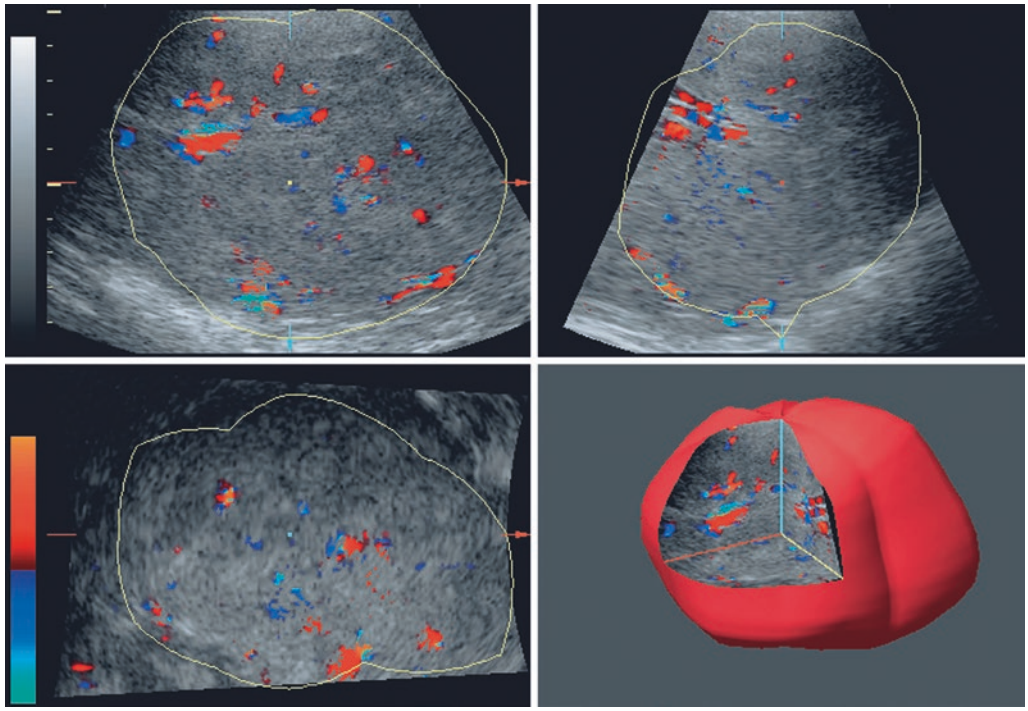

Fig. 36.3 Virtual organ computer-aided analysis was then used to delineate the 3D areas of interest

Fig. 36.4 The "histogram facility" was employed to generate three indices of vascularity: the vascular index; the flow index; and the vascularization flow index

36.3 3D Doppler in Human Reproduction

Three-dimensional Doppler ultrasound is a new modality finding its way into clinical practice. We discuss recent publications related to 3D Doppler applications in human reproduction, gynecologic oncology, and the field of benign gynecology. Pan et al. aimed to test the hypothesis that the decreased ovarian sensitivity to gonadotropins observed in women embarking on an In-vitro Fertilization (IVF) treatment may be due to changes in ovarian stromal blood flow [4]. They used 3D power Doppler ultrasonographic indexes to quantify ovarian stromal blood flow and vascularization in poor responders. Forty patients undergoing an IVF cycle were collected and divided into two groups, a poor responder group (n = 17; estradiol <600 pg/mL or ≤3 oocytes retrieved) and a normal responder group (n = 23), based on their response to a standard down-regulation protocol for controlled ovarian stimulation. During ovarian stimulation, on the day of administration of Human Chorionic Gonadotropin (HCG), patients underwent hormonal (serum E2), ultrasonographic (follicular number and diameter), and 3D power Doppler (ovarian stromal blood flow) evaluation. Compared with poor responders, the serum estradiol levels on the day of administration of HCG, the number of follicles >14 mm, the number of oocytes retrieved, the number of embryos transferred, and the pregnancy rate were significantly higher in normal responders. The vascularization index, flow index, and vascularization flow index were significantly lower in the poor responders compared with the women with a normal response. They concluded that the 3D power Doppler indexes of ovarian stromal blood flow in poor responders were significantly lower than those of normal responders. This may help to explain the poor response during HCG administration in controlled ovarian stimulation.

The British group used 3D power Doppler to examine the periodic changes in endometrial and subendometrial vascularity during the normal menstrual cycle in 27 women without obvious menstrual dysfunction or subfertility [5]. Doppler exam was performed on alternate days from day 3 of the cycle until ovulation and then every 4 days until menses. Virtual organ computer-aided analysis and shell imaging were used to define and quantify the power Doppler signal within the endometrial and subendometrial regions producing indices of their relative vascularity. Both the endometrial and subendometrial VI and VFI increased during the proliferative phase, peaking approximately 3 days prior to ovulation before decreasing to a nadir 5 days post-ovulation; thereafter, both vascular indices gradually increased during the transition from early to mid-secretory phase. The FI showed a similar pattern but with a longer nadir post-ovulation. Smoking was associated with a significantly lower VI and VFI. The FI was significantly lower in women aged ≥31 years and significantly higher in parous patients. The authors concluded that endometrial vascularity, as assessed by 3D Doppler, varies significantly during the menstrual cycle and is characterized by a pre-ovulatory peak and post-ovulatory nadir during the peri-implantation window.

Three-dimensional power Doppler has been largely used for the subjective assessment of vascular patterns, but semiquantification of the power Doppler signal is now possible. Raine-Fenning et al. addressed the intraobserver and interobserver error of the semiquantification of pelvic blood flow using 3D Doppler, VOCAL, and shell imaging [6]. The 3D Doppler was used to acquire 20 ovarian and 20 endometrial volumes from 40 different patients at various stages of in vitro fertilization treatment. The VOCAL was then used to delineate the 3D areas of interest and the "histogram facility" was employed to generate three indices of vascularity: the VI; the FI; and the VFI. Intraobserver and interobserver reliability was assessed by two-way, mixed, Intra-class Correlation Coefficients (ICCs) and general linear modeling was used to examine for differences in the mean values between each observer. The intraobserver reliability for both observers were extremely high and there were no differences in reliability between the observers for measurements of both volume and vascularity within the ovary or endometrium and its shells.

With the exception of the outside subendometrial shell volumes, there were no significant differences between the two observers in the mean values obtained for either endometrial or ovarian volume and vascularity measurements. The interobserver reliability of measurements was equally high throughout with all measurements obtaining a mean ICC of above 0.985. They concluded that 3D Doppler and shell imaging offer a reliable, practical, and noninvasive method for the assessment of ovarian, endometrial, and subendometrial blood flow. Future work should concentrate on confirming the reliability of data acquisition and the validity of the technique before its predictive value can be truly tested in prospective clinical studies.

Vlaisavljevic et al. wanted to study whether they might predict the outcome of unstimulated in vitro fertilization/intracytoplasmic sperm injection (IVF/ICSI) cycles with quantitative indices of perifollicular blood flow assessed with the 3D reconstruction of power Doppler images [7]. This prospective study included an analysis of 52 unstimulated cycles. Color and power Doppler ultrasound examinations of a single dominant preovulatory follicle were performed on the day of oocyte pick-up. With 3D reconstruction and processing, quantitative indices were obtained, i.e., the percentage of volume showing a flow signal (VFS) inside a 5-mm capsule of perifollicular tissue and the percentage of VFS of each of the three largest vessels in this capsule. These indices as well as pulsed Doppler indices were compared between the groups of cycles with different outcomes using a one-way analysis of variance test. In nine cycles no oocyte was retrieved (group A), in seven cycles no fertilization occurred (group B), and in 30 cycles no implantation occurred (group C). Six cycles resulted in pregnancy (group D). There were no statistically significant differences in pulsed and power Doppler indices between these groups; however, the percentage of VFS in the capsule was higher than average in cycles with implantation and the percentage of VFS in the main vessel exhibited lower than average values in cycles with implantation, but only reached borderline statistical significance. It can be hypothesized that the follicles containing oocytes able to produce a pregnancy have a distinctive and more uniform perifollicular vascular network.

Other authors also looked at 3D Doppler of the ovary and its relationship with hormonal status in IVF patients. Wu et al. investigated, in a retrospective study, whether the quantification of ovarian stromal blood flow and/or leptin concentration is predictive of IVF outcomes in women after laparoscopic ovarian cystectomy for large endometriomas [8]. Twenty-two women undergoing IVF after laparoscopic surgery for ovarian endometriomas (>6 cm) comprised the study group. Twenty-six women with tubal factor infertility constituted the control group. Ovarian stromal blood flow was evaluated by 3D power Doppler ultrasound imaging using VOCAL. Serum and follicular fluid (FF) leptin concentrations were quantified using an enzyme-linked immunosorbent assay kit. There were significantly decreased ovarian stromal blood flow parameters (including VI, FI, and VFI) in the endometriosis group without an evident difference in total ovarian volume on the day of human chorionic gonadotropin. The value of FF leptin demonstrated a negative correlation with ovarian stromal FI in the control group, but there was a loss of this effect in the endometriosis group. It appeared that the quantification of ovarian stromal blood flow by 3D power Doppler ultrasound in women with endometriosis may provide an important prognostic indicator in those undergoing IVF.

Kupesic and Kurjak designed the study to evaluate whether ovarian antral follicle number, ovarian volume, stromal area, and ovarian stromal blood flow are predictive of ovarian response and IVF outcome [9]. A total of 56 women with normal basal serum FSH concentrations who had no history of ovarian surgery and no ovarian and/or uterine pathology were non-smokers and undergoing their first IVF cycle using a standard long GnRH-agonist protocol were examined. Total ovarian antral follicle number, total ovarian volume, total stromal area, and mean FI of the ovarian stromal blood flow were determined by 3D

and power Doppler ultrasound after pituitary suppression. Pretreatment 3D ultrasound ovarian measurements were compared with subsequent ovulation induction parameters [peak estradiol (E2) on HCG administration day and number of oocytes] and cycle outcome (fertilization and pregnancy rates). The total antral follicle number achieved the best predictive value for favorable IVF outcome, followed by ovarian stromal FI, peak E2 on HCG administration day, total ovarian volume, total ovarian stromal area, and age. Using these six parameters, they were able to predict a favorable IVF outcome in 50% (11 of 22) of patients and a poor outcome in 85% (29 of 34) of patients. Three-dimensional ultrasound facilitates the determination of the antral follicle number, ovarian volume calculation, evaluation of the ovarian stroma, and analysis of the intensity of ovarian stromal blood flow in a short time without increasing the patient's discomfort.

Schild et al. investigated the role of 3D power Doppler sonography of the subendometrial area on the first day of ovarian stimulation in predicting the outcome of an IVF program [10]. Among the 75 cycles analyzed, the overall pregnancy rate was 20% (15 of 75) per cycle and 23.8% (15 of 63) per embryo transfer. Intraobserver variability of the color histogram was checked in 14 patients with the results demonstrating a high level of agreement. Neither endometrial measurements nor uterine blood flow was correlated with the pregnancy rate. In contrast, all 3D indices were significantly lower in conception compared with non-conception cycles. Logistic regression analysis found the subendometrial flow index to be the strongest predictive factor of IVF success among the tested sonographic parameters. More recent studies have been mixed. A study by Jarvela et al. did not demonstrate using 3D power Doppler sonography to evaluate the subendometrial vascularity is useful in predicting IVF success [11]. While in a study by Ng et al., IVF patients who had a live birth demonstrated significantly higher endometrial VI and VFI and subendometrial VI, FI, and VFI, when compared with those who suffered a pregnancy loss [12]. Thus, the utility of 3D power Doppler in the quantitative assessment of spiral artery blood flow in the endometrium and subendometrium may be of use in predicting IVF outcome, however, it remains controversial. More data is required before routine use is recommended.

36.4 3D Doppler in Gynecologic Oncology

The differentiation of benign from the malignant pelvic mass is still a considerable clinical challenge using traditional 2D real-time and Doppler ultrasound. One could hope that 3D Doppler would add to a more accurate diagnosis or at least shorten usually a long differential diagnosis list. Recent publications are certainly directed in this direction; however, when a new diagnostic modality is introduced into clinical practice, the pendulum usually swings from a very high optimism to the other side. Ultimately, it will get settled somewhere in the middle once many prospective studies are done and papers are published. One can still remember a similar story in the early 1990s when transvaginal color Doppler was optimistically introduced into programs for the early detection of ovarian cancer. We present the most recent publications dealing with 3D Doppler power Doppler and assessment of adnexal mass based on ultrasound criteria.

In their study, Kurjak et al. aimed to determine the diagnostic accuracy of 3D sonography and 3D power Doppler imaging, used together with standard 2D transvaginal grayscale and color/power Doppler modalities, for preoperative sonographic assessment of suspected ovarian lesions [13]. Five-year retrospective analysis was performed by their experts on ultrasonography and surgery on the reports from 43 referred patients with suspected stage-I ovarian cancer. All patients were evaluated during the week prior to surgery at our department. Preoperative sonographic assessment included careful examination of ovarian volume, morphology, and vascularity by four complementary sonographic methods. Scoring systems combining morphologic and Doppler parameters were adopted for 2D and 3D sono-

graphic examinations. The final diagnosis was confirmed by a histopathologist. Of the 43 stage-I ovarian cancers, 42 cases were successfully detected preoperatively by four complementary sonographic methods. Only 30 (69.8%) and 37 (86.1%) cases of stage-I ovarian cancers were detected by 2D grayscale and combined 2D grayscale and color Doppler sonography, respectively. Morphologic analysis obtained by 3D sonography alone detected 32 of 43 ovarian malignancies, reaching a diagnostic rate of 74.4%. Qualitative analysis of tumor vascularity architecture by 3D power Doppler significantly improved the sonographic management process and successfully detected 41 cases of stage-I ovarian cancer (95.4%). When morphologic features obtained by 3D sonography were added to 3D power Doppler findings, we achieved an even higher diagnostic accuracy of 97.7%. The Zagreb group found a statistically significant difference in diagnostic rates of 3D power Doppler, and especially the combined use of 3D sonography and 3D power Doppler in comparison with those obtained with transvaginal 2D grayscale or 3D sonography. They concluded that in comparison with transvaginal 2D grayscale or 3D sonography, 3D power Doppler and especially the combined use of 3D sonography and power Doppler imaging significantly improve diagnostic accuracy in the preoperative sonographic assessment of suspected ovarian lesions.

It appears that 3D sonography is a novel diagnostic method proposed to be an additional noninvasive tool in the assessment of ovarian tumors. Czekierdowski et al. also studied the diagnostic potential of 3D sonography and power Doppler in the preoperative differentiation of adnexal masses [14]. One hundred and twenty-eight women with tumors thought to be of adnexal origin were examined preoperatively. Following morphologic (papillae, septa, tumor size, and volume) and color Doppler (PI, RI, V_{max}, and TAMX) assessment, 3D Doppler ultrasound of adnexal tumors was performed. Various scanners were used and included: ATL 5000 HDI (Phillips, Bothell, Mass.) and Combison 530 and Voluson 730 (Kretztechnik, Austria) machines. The following variables were studied: inner wall structure; presence of papillae; thickening >3 mm of septa as well as vascular branching pattern; number and localization of small blood vessels; and the presence of vascular anastomoses. Twenty-one tumors were malignant (3 FIGO stage I) and 101 masses were benign. Power Doppler combined with 3D sonography predicted malignancy with a sensitivity of 92.6% (25 of 27 patients). Commonly used morphologic and Doppler criteria produced lower sensitivity, the values being in the range of 45–87.5%. Negative predictive value of 97.2% was the highest for 3D sonography. The authors concluded that the selective use of 3D ultrasound and power Doppler could be used to better characterize adnexal tumors. Detailed 3D sonography can help in identifying women who can have less invasive surgical procedures, if needed, such as laparoscopy, or be referred to a gynecologic oncologist.

Cohen and co-authors wanted to determine if 3D power Doppler ultrasound improves the specificity for ovarian cancer detection as compared with 2D ultrasound [15]. Seventy-one women with a known complex pelvic mass were referred for a preoperative ultrasound evaluation with both 2D and 3D grayscale ultrasonography. The 3D studies were performed with the Kretz Voluson 530D using a mechanized transvaginal probe. Surface rendering and power Doppler imaging were performed by the same gynecologic so-nologist and reassigned to one of four echo patterns: cystic; multicystic; complex; or solid. Sonographic criteria used for diagnosing ovarian cancer were based on a system that included morphologic characteristics, histologic prediction, and power Doppler imaging. Seventy-one women underwent surgical exploration: 14 (19.7%) had ovarian cancer (2 FIGO stage I, 2 stage II, 7 stage III, and 3 metastatic colon) and 2 had uterine cancer. Two-dimensional grayscale ultrasound identified 40 masses as suspicious for cancer, including all 14 malignancies, yielding a sensitivity, specificity, and positive predictive value of 100%, 54%, and 35%, respectively; however, evaluation with 3D power Doppler identified only 28 cases as suspicious (including all 14 cancers), resulting in a sensitivity, specificity, and positive predictive value of 100%, 75%,

and 50%, respectively. It was an obvious conclusion from this study that 3D power Doppler imaging better defines the morphologic and vascular characteristics of ovarian lesions. Both 2D and 3D imaging correctly identified all malignancies; however, the specificity significantly improved with the addition of 3D power Doppler. This improved diagnostic accuracy may promote improved patient care by separating complex benign masses from ovarian cancer, thereby facilitating appropriate physician referral.

In another study, the Zagreb group tried to determine whether 3D and 3D power Doppler can improve the ability to differentiate benign from malignant ovarian lesions [16]. Transvaginal ultrasound, transvaginal color Doppler, 3D US, and 3D power Doppler were performed on 90 patients with ovarian lesions during the week prior to surgery. Four independent sonographers were blinded to the results of other ultrasound studies. Color Doppler studies added to the transvaginal grayscale characterization of ovarian lesions resulted in a sensitivity of 88.89 and specificity of 97.53% in diagnosing ovarian malignancy. Qualitative analysis of tumor vascularity by 3D power Doppler added to morphologic features obtained by 3D ultrasound was clinically pertinent and reached sensitivity and specificity of 100% and 98.76%, respectively. They concluded that 3D ultrasound and power Doppler can enhance and facilitate the morphologic and functional evaluation of both benign and malignant ovarian lesions. The introduction of the 3D quantitative technique for measurements of blood flow and vascularization may increase the clinical relevance of these studies.

The same authors investigated the potential usefulness of contrast-enhanced 3D power Doppler sonography in the differentiation of benign and malignant adnexal lesions [17]. Thirty-one patients with complex adnexal lesions of uncertain malignancy at transvaginal B-mode and/or color Doppler sonography were prospectively evaluated with 3D power Doppler sonography before and after injection of a contrast agent. Presence of a penetrating pattern and a mixed penetrating and/or peripheral pattern suggested adnexal malignancy. The results were compared with histopathologic findings. There were 10 cases of ovarian malignancy and 21 benign adnexal lesions. Of 10 ovarian cancers, 6 showed vascular distribution suggestive of malignancy at non-enhanced 3D power Doppler sonography. After injection of contrast agent, a penetrating vascular pattern and/or mixed penetrating and peripheral pattern was detected in all cases of ovarian malignancy as well as in two benign lesions (fibroma and cystadenofibroma), which were misdiagnosed as malignant. The use of a contrast agent with 3D power Doppler sonography showed diagnostic efficiency of 96.7%, superior to that of non-enhanced 3D power Doppler sonography (93.5%). The study conclusion was that contrast-enhanced 3D power Doppler sonography provides better visualization of tumor vascularity in complex adnexal masses. If used together with 3D morphologic ultrasound assessment, enhanced 3D power Doppler imaging may precisely discriminate benign from malignant adnexal lesions.

Not all studies have demonstrated the significant benefit of 3D power Doppler over traditional 2D sonographic techniques. Sladkevicius et al. evaluated 104 women who were scheduled for removal of known adnexal masses with both 2D grayscale transvaginal and 3D power Doppler sonography [18]. There were 77 benign, 6 borderline, and 21 invasive tumors. 2D sonographic features correctly identified all 27 borderline or invasive tumors and 69 of 77 (90%) benign tumors. Add 3D power Doppler assessment of the vascular tree morphology added little to the tumors that were classified as clearly malignant or benign tumors via 2D sonography. However, there may be a small benefit in tumors difficult to classify via 2D sonographic features. The same group performed a similar study utilizing 3D power Doppler and generated various indices of vascularity (VI, FI, and VFI) using the VOCAL software [19]. Although various indices were elevated in malignant tumors, the authors came to a similar conclusion that the use of 3D power Doppler did not contribute much to traditional 2D power Doppler sonography.

The International Ovarian Tumor Analysis (IOTA) group has published the IOTA Simple

Rules tool to help distinguish benign from malignant adnexal tumors [20]. Silvetre et al. evaluated whether the addition of 3D power Doppler findings could reduce the IOTA Simple Rules false positive rate [21]. 75 women who were scheduled for operative removal of adnexal masses were included in the study. The IOTA Simple Rules classified 26 as benign, 9 as inconclusive, and 40 as malignant. They found eight false positives and no false negatives when surgical histology was compared to the IOTA data. Using VI, FI, and VFI from data derived from 3D power Doppler to the inconclusive and malignant tumors resulted in 14 false positives. 3D power Doppler as a secondary diagnostic method did not help to decrease the IOTA Simple Rules false positive rate. Thus, further data should be gathered prior to the routine use of 3D power Doppler to differentiate benign from malignant adnexal masses.

More recently, the utility of 3D power Doppler as part of the management of cervical cancer has been evaluated. It is well known that angiogenesis is a fundamental event in the growth of tumors as well as in physiologic conditions. In a prospective study by Belitsos et al. VI, FI and VFI were all significantly higher in the cervical cancer group compared to the precancerous group [22]. In addition, VI was noted to be significantly elevated in advanced stage cervical cancer when compared to patients with less advanced disease. Qin et al. demonstrated that in 61 patients with advanced cervical cancer undergoing neoadjuvant chemotherapy, 3D power Doppler-derived VI, FI. and VFI were all significantly higher in clinical responders compared to non-responders [23]. FI was the only index significantly higher in histologic responders (41.36) compared to non-responders (33.99). Since tissue hypoxia in solid tumors has been associated with decreased response to standard therapies, the lower FI value may represent a lower erythrocyte density and a lower oxygen concentration. This may account for the association with nonresponse to chemotherapy regimens. Although promising, the utility of 3D power Doppler in advanced cervical cancer therapy is still experimental.

36.5 3D Doppler in Benign Gynecology

Recent developments in ultrasound have presented new opportunities for assessing tissue vascularity and blood flow with ultrasound. These new methods include 3D imaging, power Doppler sonography, and a variety of harmonic imaging techniques, ultrasound contrast agents, electronic compounding, and pulse-sequencing methods that improve the signal-to-noise relationship as well as structural conspicuity. By using these technologic advances, it is now possible to assess macroscopic blood flow in organs and tumors and to assess changes in flow and vascularity that occur in response to therapeutic efforts.

It is obvious that technologic advances in ultrasonographic imaging have revolutionized the management of women's health care. Following the course, we also started to evaluate the clinical applications of 3D ultrasonography. Our study prospectively evaluated 161 obstetric and gynecologic patients [24]. Both 2D and 3D imaging data were acquired from real-time ultrasonography. Three orthogonal planes were displayed on a monitor and were used to create the rendered 3D images. Two hundred one 3D ultrasonographic study was performed, 165 transabdominally and 36 transvaginally. Transabdominally, an average of eight acquisitions per patient were obtained. Of the clinically suspected abnormalities, 29 of 32 (91%) were confirmed by 3D imaging. Three of 32 (9%) improved the diagnostic capabilities or changed the diagnosis. Of the 36 transvaginal studies, an average of four acquisitions per patient were done. Thirty (83%) of these patients had suspected abnormalities and all were confirmed. We concluded that 3D ultrasonographic imaging appears to be highly promising in the clinical setting.

Recent advances in ultrasound technology have enabled the diagnosis of overall tissue vascularization by 3D power Doppler (Fig. 36.5). The published case report describes 3D power Doppler characteristics of unilateral ovarian torsion 2 weeks after an embryo transfer in a pregnant patient with bilateral hyperstimulated

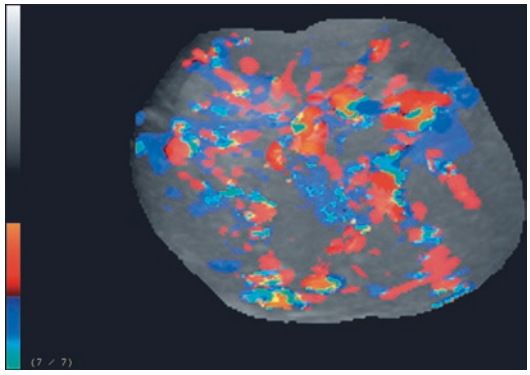

Fig. 36.5 Overall tissue vascularization of the enlarged ovary as assessed by 3D power Doppler

ovaries [25]. Before laparoscopic treatment, the twisted right ovary showed the following 3D power Doppler indices: mean grayness index, 15.66; vascularization index, 0.24; flow index, 21.99; and vascularization flow index, 0.05. One hour after laparoscopic treatment, 3D power Doppler indices of the untwisted ovary were as follows: mean grayness index, 25.61; vascularization index, 3.81; flow index, 42.80; and vascularization flow index, 1.63. The resistance index of the ovarian vessels before and after laparoscopy showed no significant difference (5.1 vs. 5.2). The diagnosis of ovarian torsion can be better made with 3D power Doppler sonography than with 2D Doppler sonography.

Sladkevicius et al. performed the study to evaluate the feasibility of 3D Doppler in the assessment of the patency of the Fallopian tubes during hysterosalpingo-contrast sonography (HyCoSy) [26]. Women attending the fertility clinic were offered a Fallopian tubal patency test as part of the initial investigation. Hysterosalpingo-contrast sonography using contrast medium Echovist was performed on 67 women. Findings on 2D grayscale scanning and 3D power Doppler imaging were compared. The first technique visualizes positive contrast in the Fallopian tube; the second demonstrates the flow of medium through the tube. Contrast medium Echovist produced prominent signals on the 3D Doppler image. Free spill from the fimbrial end of the Fallopian tubes was demonstrated in 114 (91%) tubes using the 3D Doppler technique and in 58 (46%) tubes using conventional HyCoSy. The mean duration of the imaging procedure was less with 3D Doppler, but the operator time that included post-procedure analysis of the stored information was similar. A significantly lower volume of contrast medium (5.9 ± 0.6 mL) was used for 3D Doppler in comparison with that (11.2 ± 1.9 mL) used for conventional 2D HyCoSy. The authors concluded that 3D Doppler with surface rendering allowed visualization of the flow of contrast through the entire tubal length and free spill of contrast was clearly identified in the majority of cases. The 3D Doppler method appeared to have advantages over the conventional HyCoSy technique, especially in terms of visualization of spill from the distal end of the tube, which was achieved twice as often with the 3D technique. Although the design of the investigation did not allow the side effects of the two techniques to be compared, the shorter duration of the imaging and lower volume of the contrast medium used suggested that the 3D Doppler technique might have a better side-effect profile. This technique allowed better storage of the information for reanalysis and archiving than conventional HyCoSy.

Whether salpingectomy affects ovarian function is controversial. In Chan's et al. study, an ovarian function was assessed by antral follicle count, ovarian volume, and ovarian stromal blood flow measured by 3D power Doppler ultrasonography [27]. The objectives of the study were to compare the ovarian function of the surgically treated side with the non-surgically treated side after unilateral salpingectomy performed through laparoscopy or laparotomy for ectopic pregnancy. Thirty-two patients with unilateral salpingectomy performed for ectopic pregnancy were recruited: 18 through laparoscopy and 14 through laparotomy. Ultrasound scans were performed in the early follicular phase. Ovarian volume, antral follicle count, and 3D power Doppler indices were comparable between the surgically treated and the nonsurgically treated side in the whole group and the laparotomy group. The antral follicle count and 3D power Doppler indices were significantly reduced on the surgically treated

side in the laparoscopy group. Based on this study, the ovarian function seems to be impaired after laparoscopic unilateral salpingectomy at short-term assessment.

More recent work has looked at using 3D power Doppler in the management of uterine fibroids. A prospective study by Nieuwenhuis, et al. evaluated whether vascularity visualized by 3D power Doppler helped predict fibroid growth [28]. All premenopausal women with a maximum of two fibroids and with a maximum size of 8 cm were included in the study. 3D ultrasounds including power Doppler were performed at 3, 6, and 12 months. Volume and vascular parameters were calculated using the VOCAL software. 66 women completed the 12-month studies without treatment. A 1% increase in VI was associated with a 7 cm^3 increase in fibroid volume. VI was also associated with a fibroid growth rate per year. Czuczwar et al. studied the effects of uterine artery embolization and ulipristal acetate therapy focusing on vascularity evaluated by 3D power Doppler and the VOCAL software [29]. They demonstrated a significant decrease in VI, FI, and VFI after both therapies, although percentage reduction appeared greater with ulipristal acetate therapy. Although additional research is required before 3D power Doppler is used in routine clinical management of fibroids, preliminary findings are promising.

Three-dimensional ultrasound, as an ultrasound image, is not immune from artifacts. Nelson and coauthors wanted to increase awareness of clinicians and sonographers with respect to common 3D ultrasound artifacts and to use this increased awareness to avoid or reduce the occurrence of misdiagnosis in clinical practice [30]. Patient 3D ultrasound data were acquired using several different scanners and reviewed interactively on the scanner and graphics workstations. Artifacts were cataloged according to artifact origin. Two-dimensional ultrasound (2D US) artifacts were classified whether they were of a B-mode or color/power Doppler origin and their presentation in the original scan planes and the resulting volume re-sliced planes and rendered images were identified. Artifacts unique to the 3D US were observed, noted, and cataloged on the basis of whether they arose during acquisition, rendering, or volume-editing operations. Acoustic artifacts identified included drop-out, shadowing, etc., the presentation of which depended on the relationship between slice and imaging plane orientation. Color/power Doppler artifacts were related to gain, aliasing, and flash which could add apparent structure or confusion to the volume images. Rendered images also demonstrated artifacts due to shadowing and motion of adjacent structures, cardiac motion, or pulsatility of the cardiac septum, or vessel walls. Editing artifacts potentially removed important structures. Three-dimensional ultrasound is prone to the same types of artifacts encountered in 2D US imaging plus others unique to volume acquisition and visualization. The consequences of these diagnostically significant artifacts include mimicking abnormal development, masses, or missing structures thus requiring careful study before reaching a diagnosis.

The 3D reconstruction of ultrasound images has become a widespread option in ultrasound equipment. Specific software have become available and 3D reconstruction feasible since the early 1990s, particularly since 1994. Several clinical applications are feasible in some parenchymatous organs (such as uterus or ovaries), hollow pelvic masses (e.g., ovarian cysts), peripheral vessels (uterine artery and branches), and newformed vessels (e.g., tumor neovascularization) or ectopic pregnancy. Moreover, tumoral vessels in pelvic organs can be reconstructed (Fig. 36.6). The introduction of echo contrast agents and second harmonic imaging has permitted the study of normal and abnormal peripheral, central, and parenchymatous vessels, with patterns similar to

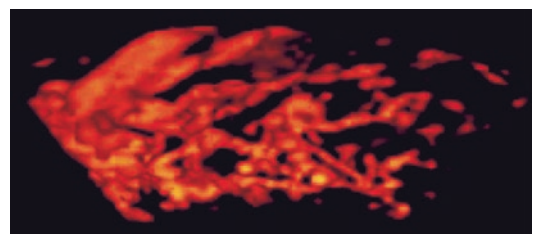

Fig. 36.6 Tumoral vessels network in ovarian mass reconstructed by 3D Doppler

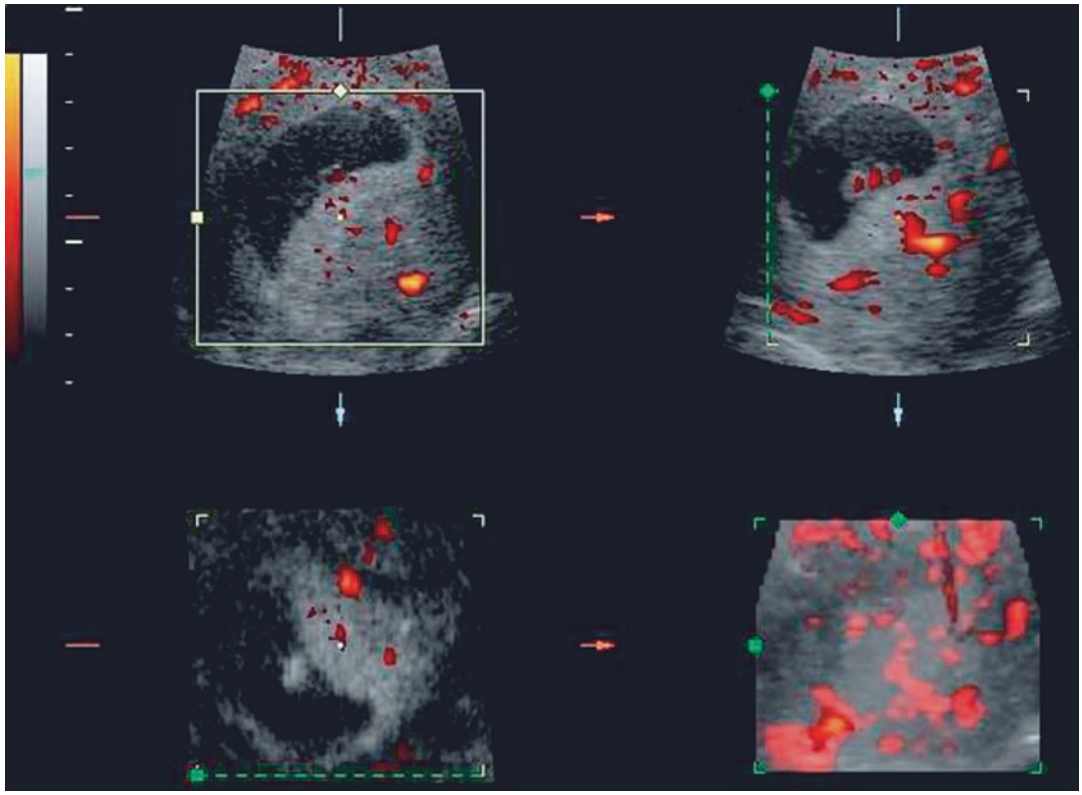

Fig. 36.7 The spatial relationships between the vascular structures of ectopic pregnancy and Fallopian tubes as studied by 3D Doppler ultrasound

those obtained with digital angiography. The spatial relationships between the vascular structures of the uterus, ovaries, and Fallopian tubes were studied with 3D Doppler ultrasound (Fig. 36.7). The applications of this new technique include the analysis of vascular anatomy and the potential assessment of organ perfusion. The latest application is an intravascular study. Some catheters with an ultrasound transducer in the tip have been tested for intra-vascular studies. Just like conventional transducers, they provide 2D images which are then post-processed into longitudinal 3D or volume reconstructions. The former resembles angiographic images and can be viewed in 3D rotating the image along its longitudinal axis. Volume images, which are more complex and slower to obtain, can be rotated on any spatial plane and provide rich detailing of the internal vascular lumen. The clinical importance of intravascular ultrasound with 3D volume reconstructions lies in the diagnosis of vascular conditions and the assessment and monitoring of intravascular interventional procedures, e.g., to detect inaccurate deployment of intravascular stents and endoluminal grafts during the maneuver. Three-dimensional reconstructions involve geometric data assembly and volumetric interpolation of a spatially related sequence of tomographic cross-sections generated by an ultrasound catheter withdrawn at a constant rate through a vascular segment of interest, resulting in the display of a straight segment; therefore, particular care is needed and there are some useful hints to avoid mistakes.

Three-dimensional reconstructions of B-mode and Doppler images are no longer a work in progress and their clinical importance and possible applications are both established and ever-increasing. On the other hand, independent of the different types of energy used, also computed

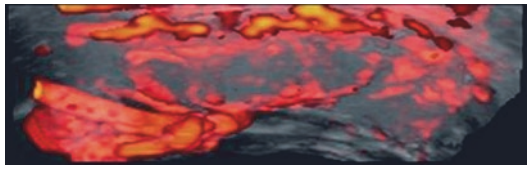

Fig. 36.8 Ovarian artery and vein and intraovarian vascular network as seen by 3D Doppler

tomography and magnetic resonance 3D reconstructions are very useful from a clinical viewpoint and they have become an established routine technique for both these methods. It is very likely that 3D volume reconstructions in ultrasound will find numerous applications in the near future (Fig. 36.8). They may help to increase the diagnostic confidence and to facilitate diagnosis, intraprocedure monitoring in interventional radiology, and follow-up and to reduce the number of invasive examinations with iodinated contrast agents.

36.6 Conclusion

At this point in time, the clinical application of 3D Doppler ultrasound is likely to advance rapidly, as improved 3D rendering technology becomes more widely available. In the past 20 years, gynecological ultrasonography has proliferated rapidly, and is by some gynecologists considered an integral part of the gynecological exam. Abnormalities are detected in asymptomatic women at a high rate, resulting in a number of surgical interventions due to suspected malignancy. Present evidence is insufficient to determine the medical and economical value, if any, of surgical removal. Such intervention may in fact be as detrimental as leaving an abnormality in place. Gynecologic ultrasonography should therefore be performed on strict medical indications. Proper training of operators is also vital. In the past decade, research investigators and commercial companies have further advanced ultrasound imaging with the development of 3D ultrasound. This new imaging approach is rapidly achieving widespread use with numerous applications in human reproduction, gynecologic oncology, and benign gynecology. The major reason for the increase in the use of 3D ultrasound is related to the limitations of 2D viewing of 3D anatomy, using conventional ultrasound. This occurs because:

1. Conventional ultrasound images are 2D, yet the anatomy is 3D; hence, the diagnostician must integrate multiple images in his mind. This practice is inefficient and may lead to variability and incorrect diagnoses.
2. The 2D ultrasound image represents a thin plane at some arbitrary angle in the body. It is difficult to localize the image plane and reproduce it at a later time for follow-up studies.

Three-dimensional Doppler ultrasound is a new modality finding its way into clinical practice. Most of the major ultrasound vendors are now developing 3D ultrasound capabilities. We expect that, although 3D ultrasound will not replace 2D ultrasound, many additional benefits will be identified and its use will continue to grow, especially when 3D Doppler is used. The ability to evaluate pelvic anatomy, pathology, and blood flow with multiplanar and surface-rendered images provides physicians with additional valuable clinical information. Volume data allows for a specific point in space to be evaluated from many different orientations by rotating, slicing, and referencing the slice to other orthogonal slices. It also allows for new volume-rendering displays that show depth, curvature, and surface images not available with conventional methods. The current limitations of image resolution, intuitive interfaces for obtaining and displaying optimal images, and technologic limitations for data storage and manipulation (including real-time 3D ultrasound) will surely be overcome in the near future. As 3D Doppler ultrasound continues to develop, the presence of real-time 3D (or 4D) imaging equipment in the clinical setting will expand and stimulate new areas of investigation and identify new frontiers where 3D ultrasound can further enhance clinical care.

References

1. Campani R, Bottinelli O, Calliada F, Coscia D. The latest in ultrasound: three-dimensional imaging. Part II. Eur J Radiol. 1998;27(Suppl 2):S183–7.
2. Fleischer AC. New developments in the sonographic assessment of ovarian, uterine, and breast vascularity. Semin Ultrasound CTMR. 2001;22:42–9.
3. Wells PN. Doppler studies of the vascular system. Eur J Ultrasound. 1998;7:3–8.
4. Pan HA, Wu MH, Cheng YC, Wu LH, Chang FM. Quantification of ovarian stromal Doppler signals in poor responders undergoing in vitro fertilization with three-dimensional power Doppler ultrasonography. Am J Obstet Gynecol. 2004;190:338–44.
5. Raine-Fenning NJ, Campbell BK, Kendall NR, Clewes JS, Johnson IR. Quantifying the changes in endometrial vascularity throughout the normal menstrual cycle with three-dimensional power Doppler angiography. Hum Reprod. 2004;19:330–8.
6. Raine-Fenning NJ, Campbell BK, Clewes JS, Kendall NR, Johnson IR. The reliability of virtual organ computer-aided analysis (VOCAL) for the semiquantification of ovarian, endometrial and subendometrial perfusion. Ultrasound Obstet Gynecol. 2003;22:633–9.
7. Vlaisavljevic V, Reljic M, Gavric Lovrec V, Zazula D, Sergent N. Measurement of perifollicular blood flow of the dominant preovulatory follicle using three-dimensional power Doppler. Ultrasound Obstet Gynecol. 2003;22:520–6.
8. Wu MH, Tsai SJ, Pan HA, Hsiao KY, Chang FM. Three-dimensional power Doppler imaging of ovarian stromal blood flow in women with endometriosis undergoing in vitro fertilization. Ultrasound Obstet Gynecol. 2003;21:480–5.
9. Kupesic S, Kurjak A. Predictors of IVF outcome by three-dimensional ultrasound. Hum Reprod. 2002;17:950–5.
10. Schild RL, Holthaus S, d'Alquen J, Fimmers R, Dorn C, van der Ven H, Hansmann M. Quantitative assessment of subendometrial blood flow by three-dimensional-ultrasound is an important predictive factor of implantation in an in-vitro fertilization program. Hum Reprod. 2000;15:89–94.
11. Jarvela IY, Sladkevicius P, Kelly S, Ojha K, Campbell S, Nargund G. Evaluation of endometrial receptivity during in-vitro fertilization using three-dimensional power Doppler ultrasound. Ultrasound Obstet Gynecol. 2005;26:765–9.
12. Ng EH, Chan CC, Tang OS, Yeung WS, Ho PC. Endometrial and subendometrial vascularity is higher in pregnant patients with livebirth following ART than in those who suffer a miscarriage. Hum Reprod. 2007;22:1134–41.
13. Kurjak A, Kupesic S, Sparac V, Prka M, Bekavac I. The detection of stage I ovarian cancer by three-dimensional sonography and power Doppler. Gynecol Oncol. 2003;90:258–64.
14. Czekierdowski A, Smolen A, Bednarek W, Kotarski J. Three dimensional sonography and 3D power angiography in differentiation of adnexal tumors. Ginekol Pol. 2002;73:1061–70.
15. Cohen LS, Escobar PF, Scharm C, Glimco B, Fishman DA. Three-dimensional power Doppler ultrasound improves the diagnostic accuracy for ovarian cancer prediction. Gynecol Oncol. 2001;82:40–8.
16. Kurjak A, Kupesic S, Sparac V, Kosuta D. Three-dimensional ultrasonographic and power Doppler characterization of ovarian lesions. Ultrasound Obstet Gynecol. 2000;16:365–71.
17. Sparac V, Kupesic S, Kurjak A. What do contrast media add to three-dimensional power Doppler evaluation of adnexal masses? Croat Med J. 2000;41:257–61.
18. Sladkevicius P, Jokubkiene L, Valentin L. Contribution of morphological assessment of the vessel tree by three-dimensional ultrasound to a correct diagnosis of malignancy in ovarian masses. Ultrasound Obstet Gynecol. 2007;30:874–82.
19. Jokubkiene L, Sladkevicius P, Valentin L. Does three-dimensional power Doppler ultrasound help in discrimination between benign and malignant ovarian masses? Ultrasound Obstet Gynecol. 2007;29:215–25.
20. Timmerman D, Ameye L, Fischerova D, Epstein E, Melis GB, Guerriero S, et al. Simple ultrasound rules to distinguish between benign and malignant adnexal masses before surgery prospective validation by IOTA group. BMJ. 2010;341:c6839.
21. Silvestre L, Martins WP, Candido-Dos-Reis FJ. Limitations of three-dimensional power Doppler angiography in preoperative evaluation of ovarian tumors. J Ovarian Res. 2015;29(8):47–52.
22. Belitsos P, Papoutsis D, Rodolakis A, Mesogitis S, Antsaklis A. Three-dimensional power Doppler ultrasound for the study of cervical cancer and precancerous lesions. Ultrasound Obstet Gynecol. 2012;40:576–81.
23. Qin J, Cheng X, Chen X, Zhang X, Lu W, Xie X. Value of three-dimensional power Doppler to predict clinical and histological response to neoadjuvant chemotherapy in locally advanced cervical carcinoma. Ultrasound Obstet Gynecol. 2012;39:226–34.
24. Platt LD, Santulli T Jr, Carlson DE, Greene N, Walla CA. Three-dimensional ultrasonography in obstetrics and gynecology: preliminary experience. Am J Obstet Gynecol. 1998;178:1199–206.
25. Yaman C, Ebner T, Jesacher K. Three-dimensional power Doppler in the diagnosis of ovarian torsion. Ultrasound Obstet Gynecol. 2002;20:513–5.
26. Sladkevicius P, Ojha K, Campbell S, Nargund G. Three-dimensional power Doppler imaging in the assessment of Fallopian tube patency. Ultrasound Obstet Gynecol. 2000;16:644–7.

27. Chan CC, Ng EH, Li CF, Ho PC. Impaired ovarian blood flow and reduced antral follicle count following laparoscopic salpingectomy for ectopic pregnancy. Hum Reprod. 2003;18:2175–80.
28. Nieuwenhuis LL, Keizer AL, Stoelinga B, Twisk J, Hehenkamp W, Brolmann H, Huirnea J. Fibroid vascularisation assessed with three-dimensional power Doppler ultrasound is a predictor for uterine fibroid growth: a prospective cohort study. BJOG. 2018;125:577–58.
29. Czuczwar P, Wozniak S, Szkodziak P, Milart P, Wozniakowska E, Wrona W, Paszkowski T. Influence of ulipristal acetate therapy compared with uterine artery embolization on fibroid volume and vascularity indices assessed by three-dimensional ultrasound: prospective observational study. Ultrasound Obstet Gynecol. 2015;45:744–50.
30. Nelson TR, Pretorius DH, Hull A, Riccabona M, Sklansky MS, James G. Sources and impact of artifacts on clinical three-dimensional ultrasound imaging. Ultrasound Obstet Gynecol. 2000;16:374–83.

37 Doppler Ultrasound in Early Pregnancy Including Miscarriage, Ectopic Pregnancy, and Implantation

Mercedes Espada Vaquero, Mathew Leonardi, and George Condous

37.1 Introduction

37.1.1 Types of Doppler and Their Application in Early Pregnancy

Doppler ultrasound in early pregnancy is used to evaluate and estimate blood flow in both the major and the minor vessels of the internal genital tract. The Doppler mode uses a phenomenon called "Doppler shift," which is a change in frequency from the sent to the returning sound wave. These "shifts" are generated by sound waves reaching moving particles. The change of the frequency (or "shifts") correlate with the direction and velocity of particle motion (Fig. 37.1). The velocity of particle motion can be measured by the so-called Pulsatility Index (PI) and Resistance Index (RI) by using Pulsed-Wave Spectral Doppler (PWSD).

There are six different types of Doppler modes: Continuous-Wave Doppler (CWD), Color-Doppler (CD), Pulsed-Doppler (PD), Spectral Doppler (SD), PWSD (pulsed-wave spectral Doppler) and 3D power Doppler [1].

M. E. Vaquero · M. Leonardi · G. Condous (✉)
Acute Gynaecology, Early Pregnancy, and Advanced Endoscopy Surgery Unit, Sydney Medical School Nepean, Nepean Hospital, University of Sydney, Sydney, NSW, Australia
e-mail: george.condous@omnigynaecare.com.au

CWD utilizes continuous transmission and reception of ultrasound waves. This is accomplished by two dedicated transducer elements: one that only sends Doppler signals and another one that only receives (Fig. 37.2). As no pulses are emitted, CWD does not allow us to determine where exactly the wave is reflected. We only know that the velocity curve emerges somewhere along the path of the ultrasound transmitted wave, which is called the CWD line.

CD is able to show blood flow or tissue motion in a selected two-dimensional area. Direction and velocity are color-coded and superimposed in the B-mode (2D ultrasound) (Fig. 37.3).

PD does not examine flow velocity or the direction of the flow. Instead, it reflects the amplitude of the returning wave and it is able to detect very low flows (Fig. 37.4). This subtype of Doppler mode is very useful when assessing gynecological vascular emergencies such as ovarian torsion and ectopic pregnancies.

SD is a continuous and pulsed-wave form allowing for the conversion of Doppler shift signals into audible frequencies over a loudspeaker (no image is produced). This technique is often utilized at the bedside to demonstrate fetal tones during advanced pregnancy.

PWSD shows the "spectrum" of the returned Doppler wave in a two-dimensional shape. Arterial waves are more triangle-shaped whereas venous waves display a more continuous band-like shape.

D. Maulik, C. C. Lees (eds.), *Doppler Ultrasound in Obstetrics and Gynecology*,
https://doi.org/10.1007/978-3-031-06189-9_37

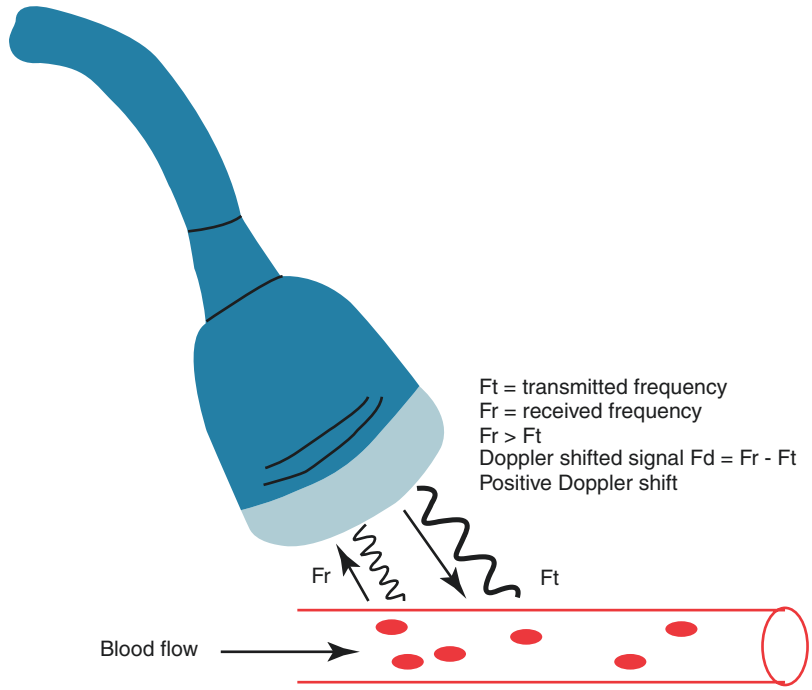

Fig. 37.1
Representation of the "Doppler Shift"

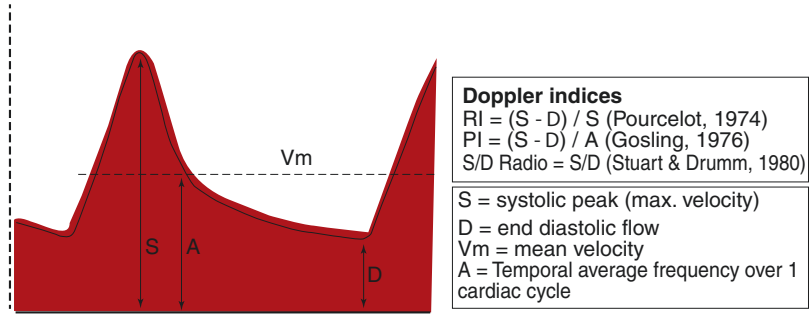

Fig. 37.2
Representation of the Doppler indices

Calculation of the **three 3D power Doppler** ultrasound vascular indices, the Vascularization Index (VI), Flow Index (FI), and Vascularization Flow Index (VFI) is based on and related to the total and relative amounts of power Doppler information within a volume of interest. VI denotes the ratio of color-coded voxels to all voxels within the volume and is expressed as a percentage, FI represents the mean power Doppler signal intensity from all color-coded voxels and VFI is the simple mathematical relationship derived from multiplying VI by FI and dividing the result by 100. Both FI and VFI are unitless and are expressed as numerical values ranging from 0 to 100. The indices are thought to reflect the number of vessels within the Volume of Interest (VI), the intensity of flow at the time of the 3D sweep (FI), and both blood flow and vascularization (VFI) [1].

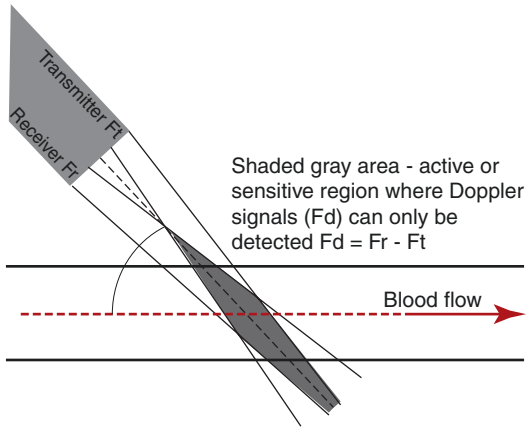

Fig. 37.3 Ultrasound transducer transmitting a Doppler signal with a Continuous wave. These two elements are set at an angle to each other so that the transmit and reception beams overlap one another. The crossover region is known as the active or sensitive area and is where Doppler signals can only be detected. *Fd* Doppler shift signals; *Fr* Doppler received signals; *Ft* Doppler transmitted signal

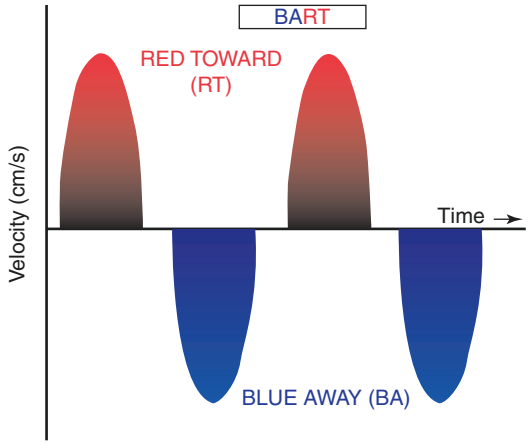

Fig. 37.4 Representation of the PD mode

37.1.2 Normal Pelvic Blood Flow During the Ovulation, Luteal Phase, Implantation, and Early Pregnancy: General Concepts

Transvaginal Doppler Sonography (TVDS) is a valuable tool in the assessment of the luteal phase, implantation, and early pregnancy [1].

Normal menstruating women are preferably scanned on days 3–10 of the menstrual cycle to exclude changes in the pelvic blood flow associated with ovulation, especially in the ovarian vessels. There are physiologic flow patterns important to recognize when assessing the female pelvis by using the Doppler mode in the iliac, uterine, and ovarian arteries in pregnant and non-gravid women.

The common and external iliac arteries (which are part of the aorto-femoral segment) show a triphasic flow, with an early diastolic flow reversal, a diastolic forward flow, and a systolic flow.

The internal artery, in contrast, shows a high-velocity biphasic flow.

The ovarian artery is a high-impedance system with low Doppler shifts with low velocity. The waveform shape varies with the state of activity of the ovary [2]. Throughout the menstrual cycle, the dominant-follicle containing ovary will usually show decreased impedance thus increasing the blood flow to that ovary in order to promote ovulation and maintain the corpus luteum at the same time (the corpus luteum will therefore act as a low-impedance ovarian shunt). Conversely, the non-ovulating ovary will show low-end diastolic flow.

Intra-ovarian circulation however is very different from ovarian artery circulation. Near the ovarian hilum, the penetrating vessels are coiled and tortuous, demonstrating high-impedance blood flow [2]. The intra-ovarian vascular network is dynamic throughout the menstrual cycle, increasing the number of numerous arteriovenous shunts during the luteal phase. These changes in the intra-ovarian blood flow may involve angiogenesis and the production of hormonal factors before the ovulation during the proliferative phase, while vascular accommodation and low impedance are important in the luteal phase in order to maintain the corpus luteum throughout the second half of the menstrual cycle and the first 12 weeks in pregnancy.

The uterine arteries are direct branches from the internal iliac or hypogastric arteries and typically show a high-resistance/low-diastolic-flow velocity waveform with a characteristic notch during early diastole in the first trimester and non-gravid uterus. CD analysis allows the identification of the small vessels within the myome-

trium (e.g., arcuate arteries and their branches). Schulman and colleagues described the typical shape of the uterine waveform on PW, which has a rapid rise and fall in the flow velocity during systole and a "notch" in the descending waveform in early diastole [3]. The type of velocity waveform obtained depends on the phase of the menstrual cycle, pregnancy state, age of the patient, and pathologic conditions.

Successful intra-uterine implantation is the result of a complex process involving the interaction between different molecules with the genital tract (especially with the endometrium), and ultrasonography can give important information on many of these. The endometrium thickens and undergoes morphologic changes under the influence of increasing estradiol levels from the developing ovarian follicles. This process is also associated with increased vascularity from the basal arteries with the growth of vessels developing along with the glandular crypts of the functional layer during the luteal phase [3].

Ultrasound monitoring of the endometrium in a natural or stimulated transfer cycle usually involves measuring the Endometrial Thickness (ET) and studying changes in morphology up to the time of ovulation. ET is measured in the mid-sagittal plane of the uterus as the maximum distance between the two interfaces of the endometrial–myometrial junction, as per IETA recommendations [4, 5].

Subendometrial vascularity is usually assessed by visually assessing images of endometrial vascularity before the ovulation trigger injection in ART (artificial reproductive techniques). Vascular penetration of the endometrium is usually graded as grade 1 (no subendometrial blood flow detected); grade 2 (subendometrial blood flow detected); and grade 3 (both endometrial and subendometrial blood flow detected). Most studies show that grade 3 flow is associated with significantly higher clinical pregnancy rates [6].

Measurement of uterine vascular supply on PWSD gives valuable information about uterine perfusion. The increased impedance of uterine artery blood flow presenting as reverse blood flow and elevated UAPI and UARI have been associated with low implantation rates in IVF cycles and increased risk of miscarriage. Additionally, UAPI during the first trimester (11–13 gestational weeks) has been demonstrated to be a useful tool to predict up to 75% of preterm pre-eclampsia and 47% of term preeclampsia in combination with other factors [7]. However, mean UAPI measured at <11 weeks' gestation does not appear to be a useful marker for the prediction of placental-related adverse pregnancy outcomes [8].

37.2 Early Pregnancy States: Definitions

During the first trimester (before the 12th gestational week), we can define different early pregnancy states, including [9]:

- *Intra-uterine Pregnancy of Uncertain Viability*
- Intrauterine mean gestational sac <25 mm in diameter or containing a fetal pole with crown-rump length <7 mm with no fetal cardiac activity visualized.
- *Viable Intrauterine Pregnancy (IUP)*
- Intrauterine gestational sac containing embryo (s) with visible cardiac activity.
- *Non-viable IUP*
- Intra-uterine gestational sac containing the presence of embryo with crown-rump length ≥7 mm without demonstrable cardiac activity on the first scan; OR presence of an embryo with crown-rump length ≤7 mm with no demonstrable cardiac activity at the first scan and then at the second scan 7 days later with still no fetal cardiac activity; OR absence of an embryo in a gestational sac with a mean diameter of >25 mm or a mean gestational sac diameter <25 mm with no growth at ultrasound follow-up.
- *Ectopic Pregnancy (EP)*
- Presence of an adnexal mass separate to the ipsilateral ovary in form of inhomogeneous mass ("blob" sign), gestational sac ("bagel" sign), or gestational sac containing an embryonic pole with or without cardiac activity [10].
- *Pregnancy of Unknown Location (PUL)*

- Defined as a positive pregnancy test with no signs of intra- or extra-uterine pregnancy on transvaginal ultrasonography and an absence of products of conception. PUL is a descriptive term and not a final diagnosis. Women classified with PUL require follow-up visits to determine the final diagnosis: failed PUL (FPUL) (accounting for 44—69% of the PUL group), intrauterine pregnancy (IUP) (30–47% of the PUL), ectopic pregnancy (EP)(814% of the PUL) or persistent PUL (PPUL) (1–3% of the PUL) [9]. As far as we know, Doppler ultrasound examination has not been demonstrated to add useful information to serial Human Chorionic Gonadotrophin (hCG) and progesterone determination in predicting PUL outcome.
- *Persistent PUL (PPUL)*
- Ongoing PUL state classification on TVS over time with serial serum hCG level monitoring without evidence of spontaneous resolution; in our unit, PPUL is classified at D7 if the hCG was plateauing by D7 (initial hCG ratio between 0.80 and 0.99 followed by an increase in hCG on D7) or increasing on D7 with no visible pregnancy on repeat TVS [9].
- Doppler ultrasound may add useful information to conventional 2D pelvic ultrasound examination to confirm viable intrauterine and ectopic pregnancies.

37.3 Role of Doppler Ultrasound in the Diagnosis of Intrauterine Viable Pregnancies

Although the myocardium begins to contract rhythmically by 3 weeks after conception it is first visible on sonography around 6 weeks of gestation. The Fetal Heart Rate (FHR) is then usually around 100–120 beats per minute (bpm) [11].

FHR then increases progressively over the subsequent 2–3 weeks to (mean) 110 bpm by 5–6 weeks and 170 bpm by 9–10 weeks.

A slow FHR is termed fetal bradycardia and is usually defined as FHR <100 bpm before 6.3 weeks gestation, or FHR <120 bpm between 6.3 and 7.0 weeks [12]. A rapid FHR is termed a fetal tachycardia and is usually defined as FHR >160–180 bpm. FHR around 170 bpm may be classified as borderline fetal tachycardia. A rapid and irregular fetal heart rate is usually termed a fetal tachyarrhythmia [13, 14].

Embryonic heart rate below 100 bpm at 6–7 gestational weeks is an ominous finding. The survival rate is zero at heart rates (hr) below 70 bpm at 6–8 weeks of gestation. Embryos having an abnormally slow heart rate between 6 and 7 weeks of gestation that subsequently increases to a normal hr at 8 weeks of gestation remain at increased risk for loss [12, 15].

37.4 Role of Doppler Ultrasound in the Diagnosis of Intra-cavitary Retained Products of Conception (RPOC)

Pelvic ultrasound is the first-line imaging modality in the evaluation of RPOC. The diagnosis should be made promptly because RPOC may act as a source of prolonged bleeding or as a nidus for infection. Evacuation of RPOC often requires dilation and curettage; however, this procedure should be used carefully because there is a risk of uterine perforation and intra-cavitary adhesions (Ashermann's syndrome) after dilation and curettage, especially in the presence of concomitant endometritis.

The assessment of RPOC on PD is subjective and based on the PD Color Scoring (PDCS) system which was adopted from the IOTA group's color scoring system for adnexal masses [16]. While the IOTA group used this scoring system to describe the amount of blood flow within the solid components of ovarian masses, the same principle can be applied to the RPOC within the endometrial cavity. A PDCS of 1 was given when no blood flow was found within the RPOC, a PDCS of 2 when only minimal blood flow was detected, a PDCS of 3 when rather strong blood flow was detected, and a PDCS of 4 when very strong blood flow was detected. Previous studies in a miscarriage population have demonstrated that the presence of any vascularity in the endo-

metrium is associated with a high likelihood of underlying RPOC, with a PPV of 96%. When moderate-high vascularity intra-cavitary patterns were considered separately, all had positive findings for RPOC [16]. The absence of blood flow in residual trophoblastic tissue on PD is associated with a significant improvement in successful expectant management of incomplete miscarriage according to a recent publication [17]. In conclusion, because blood clots and debris can mimic RPOC on grayscale imaging, detection of intrinsic vascularity is helpful in distinguishing simple clots and decidua from RPOC and maybe a helpful tool for the management of patients with incomplete miscarriage.

37.5 Role of Doppler Ultrasound in the Diagnosis of Ectopic Pregnancies

The most common site for ectopic pregnancies is the Fallopian tube. The diagnosis of ectopic pregnancy remains challenging for the clinician despite advances in ultrasound technology. CD and PD imaging have been added to TVS in an attempt to improve the diagnosis on ultrasound. A "ring of fire" characterizes the appearance of flow around an ectopic pregnancy; importantly the ectopic pregnancy mass is separate to and moves separately to the ipsilateral ovary when pressure is applied using the transvaginal probe. The process of placentation is similar whether it occurs within the uterine cavity or out of it. Therefore, not surprisingly a similar high velocity, low-impedance flow pattern of placental perfusion characterizes ectopic pregnancies [18]. When this pattern is seen outside the uterus while the uterine cavity has no Doppler signal, the diagnosis should be considered. However, it is also important to be aware that luteal flow can be confused with the flow from an ectopic pregnancy. The cut-off value for the RI of the corpus luteum blood flow has been described to be 0.4 and the RI of peritrophoblastic blood flow is below 0.4 [19]. CD is most helpful when an extra ovarian mass has not yet been found, because the use of Doppler may allow for the detection of an ectopic surrounded by loops of bowel. Luteal flow can be helpful in identifying an ectopic because about 90% of ectopic pregnancies occur on the same side as the corpus luteum [18, 19]. Other variations of ectopic pregnancies include interstitial/cornual pregnancy, cervical pregnancy, and ovarian pregnancy, sharing similar Doppler characteristics with tubal ectopic pregnancies.

37.6 Role of Doppler Ultrasound in the Diagnosis of Gestational Trophoblastic Disease

Transvaginal US is the accepted standard imaging technique in the evaluation of early pregnancy and suspected complications, including Gestational Trophoblastic Disease (GTD). There is some support for a role for Doppler US in the initial diagnosis and post evacuation follow-up of patients with GTD [19, 20]. A lower Uterine Artery Resistance Index (UARI) before molar evacuation is associated with the development of trophoblastic tumors, a potentially useful means to prospectively recognize patients who are at high risk for progression and, therefore, the need for closer follow-up [21, 22]. In a prospective analysis of 246 women with complete mole, Doppler PI showed potential as a predictor of subsequent development of Gestational Trophoblastic Neoplasm (GTN) [23]. Doppler US can also confirm the absence of vascular flow within a mass, a useful technique in patients with GTD where clots or blood products may simulate solid tissue [20].

37.7 Safety of Ultrasound During Early Pregnancy

The safety of ultrasound examinations during early pregnancy has been subject to debate. Ultrasound has the potential to induce tissue changes through different effects including thermal (heating), cavitation, and microstreaming. The safety of ultrasound use has been correlated

to the increase in temperature that it can produce. Studies have shown that temperature rises to 1 °C are considered to be safe for the developing embryo [24]. The Thermal Index (TI) is a concept that has been introduced to give a guide of the possible increase in temperature by ultrasound, and it depends on the organ being scanned. A TI of 1.0 means that the temperature might increase by 1 °C under worst-case conditions. Additionally, the Mechanical Index (MI) is the complementary index for the mechanical effects of ultrasound. As in the case of TI, MI value of less than 1.0 is considered to be safe for the embryo. The ultrasound examiner, however, should always adhere to the "as-low-as-reasonable achievable (ALARA)" rule, by using the lowest output settings in order to obtain the desired information, and should aim at not prolonging the examination time if it's not necessary. The British Medical Ultrasound Society has also issued recommendations about the duration of ultrasound examinations at different TI and MI [25].

According to World Federation of Ultrasound in Medicine and Biology, Doppler ultrasound should not be used in early pregnancy assessment, unless there is an indication for its use [26–28], in which case TI should be less or equal to 1.0, and the exposure time should be kept as short as possible. All of these concerns justify using only M-mode ultrasound, if possible, to document and measure the fetal heart rate in routine early pregnancy assessment.

37.8 Conclusions

Doppler ultrasound is a promising diagnostic tool that complements grayscale 2D and 3D ultrasound during early pregnancy and holds the promise of being as helpful for the investigation of infertility and early pregnancy loss as Doppler analysis of uterine and umbilical blood flow has demonstrated to be during the first and second trimesters of pregnancy.

References

1. Bourne TH, et al. Transvaginal colour Doppler. The scientific basis and practical application of Doppler in gynaecology. Springer; 2012. ISBN 978-3-642-79264-9.
2. Zalud I. Doppler evaluation of the ovary: clinical applications and challenges. Contemp Obstet Gynecol. 2002;47:37–59.
3. Schulman H, Fleischer A, Farmakides G, Bracero L, Grunfeld L. Development of uterine artery compliance in pregnancy as detected by Doppler ultrasound. Am J Obstet Gynecol. 1986;155:1031–6. Kinkel K, Ascher SM, Reinhold C. Benign Disease of the Uterus. 2018 Mar 21.
4. Leone FPG, Timmerman D, Bourne T, Valentin L, Epstein E, Goldstein SR, Marret H, Parsons AK, Gull B, Istre O, Sepulveda W, Ferrazzi E, Van den Bosch T. Terms, definitions and measurements to describe the sonographic features of the endometrium and intrauterine lesions: a consensus opinion from the International Endometrial Tumor Analysis (IETA) group. Ultrasound Obstet Gynecol. 2010;35(1):103–12.
5. Campbell S. Ultrasound evaluation in female infertility: Part 2, The uterus and implantation of the embryo. Obstet Gynecol Clin N Am. 2019;46(4):697–713. https://doi.org/10.1016/j.ogc.2019.08.002.
6. Zaidi J, Campbell S, Pittrof R, Tan SL. Endometrial thickness, morphology,vascular penetration and velocimetry in predicting implantation in an in vitrofertilization program. Ultrasound Obstet Gynecol. 1995;6(3):191–8.
7. O'Gorman N, Wright D, Syngelaki A, Akolekar R, Wright A, Poon LC, NicolaidesKH. Competing risks model in screening for preeclampsia by maternal factors and biomarkers at 11-13 weeks gestation. Am J Obstet Gynecol. 2016;214(1):103.e1–103.e12. https://doi.org/10.1016/j.ajog.2015.08.034.
8. Taylor TJ, Quinton AE, de Vries BS, Hyett JA. Uterine artery pulsatility index assessment at <11 weeks' gestation: a prospectve study. Fetal Diagn Ther. 2019;5:1–9. https://doi.org/10.1159/000500776. [Epub ahead of print].
9. Nadim B, Leonardi M, Infante F, Lattouf I, Reid S, Condous G. Rationalizing the management of pregnancies of unknown location: diagnostic accuracy of human chorionic gonadotropin ratio-based decision tree compared with the riskprediction model M4. Acta Obstet Gynecol Scand. 2019;99(3):381–90. https://doi.org/10.1111/aogs.13752.
10. Nadim B, Infante F, Lu C, Sathasivam N, Condous G. The morpho-logical ultrasound types known as "blob" and "bagel" signs should be reclassified from probable to definite ectopic pregnancy. Ultrasound Obstet Gynecol. 2018;51:543–9.

11. Doubilet PM, Benson CB. Embryonic heart rate in the early first trimester: what rate is normal? J Ultrasound Med. 1995;14(6):431–4.
12. Benson CB, Doubilet PM. Slow embryonic heart rate in early first trimester: indicator of poor pregnancy outcome. Radiology. 1994;192(2):343–4.
13. Oudijk MA, Visser GH, Meijboom EJ. Fetal tachyarrhythmia—part I: Diagnosis. Indian Pacing Electrophysiol J. 2004;4(3):104–13.
14. Hornberger LK, Sahn DJ. Rhythm abnormalities of the fetus. Heart Heart. 2007;93(10):1294–300. Review.
15. Doubilet PM, Benson CB. Outcome of first-trimester pregnancies with slow embryonic heart rate at 6-7 weeks gestation and normal heart rate by 8 weeks at US. Radiology. 2005;236(2):643–6. https://doi.org/10.1148/radiol.2362040880.
16. Timmerman D, Valentin L, Bourne TH, Collins WP, Ver-relst H, Vergote I, International Ovarian Tumor Analysis(IOTA) Group. Terms, definitions and measurements to describethe sonographic features of adnexal tumors: a consensus opin-ion from the International Ovarian Tumor Analysis (IOTA) Group. Ultrasound Obstet Gynecol. 2000;16:500–5.
17. Casikar I, Lu C, Oates J, Bignardi T, Alhamdan D, Condous G. The use of power Doppler colour scoring to predict successful expectant management in women with an incomplete miscarriage. Hum Reprod. 2012;27(3):669–75.
18. Taylor KJ, Meyer WR. New techniques in the diagnosis of ectopic pregnancy. Obstet Gynecol Clin N Am. 1991;18:39–54.
19. Knez J, Day A, Jurkovic D. Ultrasound imaging in the management of bleeding and pain in early pregnancy. Best Pract Res Clin Obstet Gynaecol. 2014;28(5):621–36. https://doi.org/10.1016/j.bpobgyn.2014.04.003. Epub 2014 Apr 24.
20. Expert Panel on Women's Imaging Panel, Dudiak KM, Maturen KE, Akin EA, Bell M, Bhosale PR, Kang SK, Kilcoyne A, Lakhman Y, Nicola R, Pandharipande PV, Paspulati R, Reinhold C, Ricci S, Shinagare AB, Vargas HA, Whitcomb BP, Glanc P. ACR Appropriateness Criteria® Gestational Trophoblastic Disease. J Am Coll Radiol. 2019;16(11S):S348–63.
21. Garavaglia E, Gentile C, Cavoretto P, Spagnolo D, Valsecchi L, Mangili G. Ultrasound imaging after evacuation as an adjunct to beta-hCG monitoring in posthydatidiform molar gestational trophoblastic neoplasia. Am J Obstet Gynecol. 2009;200:417.e1-5.
22. Lin LH, Bernardes LS, Hase EA, Fushida K, Francisco RP. Is Doppler ultrasound useful for evaluating gestational trophoblastic disease? Clinics (Sao Paulo). 2015;70:810–5.
23. Asmar FTC, Braga-Neto AR, de Rezende-Filho J, Villas-Boas JMS, Charry RC, Maesta I. Uterine artery Doppler flow velocimetry parameters for predicting gestational trophoblastic neoplasia after complete hydatidiform mole, a prospective cohort study. Clinics (Sao Paulo). 2017;72:284–8.
24. National Council on radiation protection and measurements (NCRP). Exposure criteria for medical diagnostic ultrasound: I. Criteria based on thermal mechanisms. (Report No. 113). National Council on Radiation Protection and Measurements, Bethesda, MD; 1992.
25. Safety Group of the British Medical Ultrasound Society. Guidelines for the safe use of diagnostic ultrasound equipment. Ultrasound. 2010;18:52–9.
26. Ang ESB Jr, Gluncic V, Duque A, et al. Prenatal exposure to ultrasound waves impacts neuronal migration in mice. Proc Natl Acad Sci U S A. 2006;103:12903–10.
27. WFUMB Safe use of Doppler ultrasound during 11 to 14 weeks scans (or earlier in pregnancy). Ultrasound Med Biol. 2013;39:373.
28. Salvesen K, Lees C, Abramowicz J, Brezinka C, Ter Haar G, Maršál K, Board of International Society of Ultrasound in Obstetrics and Gynecology (ISUOG). ISUOG statement on the safe use of Doppler in the 11 to 13 +6-week fetal ultrasound examination. Ultrasound Obstet Gynecol. 2011;37(6):628.

38 Doppler in Benign and Malignant Conditions of the Ovary

Andrea Day and Davor Jurkovic

38.1 Introduction

Ovarian abnormalities are common and some of them, such as endometriosis and ovarian cancer, are major global health issues. Standard two-dimensional B-mode imaging is a key part of ultrasound examination in gynecology and, in a large proportion of cases, it provides examiners with all the information that is required to characterize ovarian abnormalities and plan appropriate management. However, in some cases, B-mode findings alone are not sufficient to determine the nature of ovarian lesions with confidence. In these situations, Doppler examination can help to differentiate between benign and malignant adnexal abnormalities. The advent of color Doppler in the late 1980s was a key development that has greatly improved the quality of blood flow studies in gynecology by facilitating the visual mapping of pelvic circulation and enabling more accurate pulsed Doppler flow velocity waveform studies [1]. In this chapter, we describe the effects of ovulation, pregnancy, and other physiological events on ovarian circulation and explore the role of Doppler ultrasound in the assessment of women with suspected ovarian pathology.

38.2 The Normal Ovary and Its Circulation

The ovary is usually located lateral to the uterus within the ovarian fossa, in close proximity to the internal iliac vessels and the ureter. It is covered by a capsule that consists of a simple layer of germinal epithelium and fibrous tissue. On the inside, ovarian stroma is made up of a superficial cortex that contains the ovarian follicles and an inner medulla that forms the hilum through which the blood vessels enter the ovary.

Blood supply to the ovary comes from two sources: the ovarian artery and branches of the uterine artery. The ovarian artery originates directly from the abdominal aorta and enters the ovary laterally through the infundibulopelvic ligament. Uterine vessels, on the other hand, originate from the internal iliac artery and reach the ovary medially, anastomozing with the ovarian counterpart through an arcade of vessels at the mesovarian border of the ovary [2] (Fig. 38.1). Coiled vessels enter the ovary through the hilum and subsequently form a plexus at the corticomedullary junction from

A. Day
Chelsea and Westminster Hospital NHS Foundation Trust, West Middlesex University Hospital, London, UK
e-mail: Andrea.Day1@nhs.net

D. Jurkovic (✉)
University College London Hospitals NHS Foundation Trust, University College Hospital, London, UK
e-mail: Davor.Jurkovic@nhs.net

D. Maulik, C. C. Lees (eds.), *Doppler Ultrasound in Obstetrics and Gynecology*,
https://doi.org/10.1007/978-3-031-06189-9_38

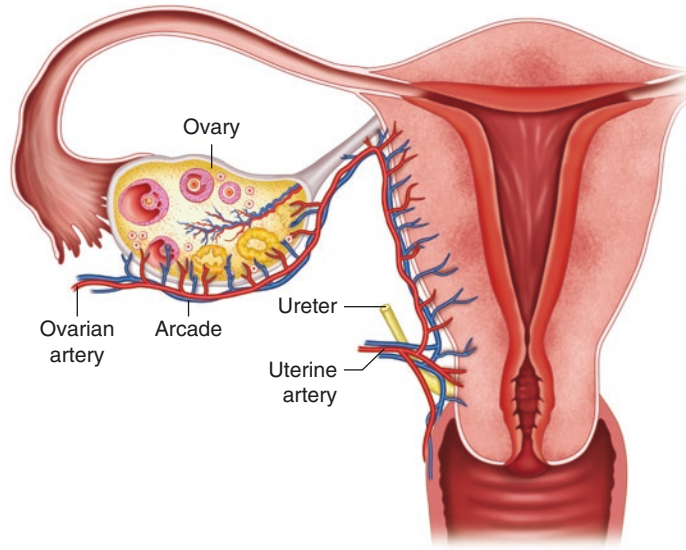

Fig. 38.1 Blood supply to the ovary. (Illustrated by M. Lluch)

which smaller, straight cortical arterioles arise. These interconnect to form arcades that produce capillaries which then run within the external and internal thecal layer to supply the ovarian follicles (Fig. 38.2). Venules and veins parallel the route of the arteries. They form a plexus in the broad ligament known as the pampiniform plexus that drains into a single vein, ending in the inferior vena cava on the right and the left renal vein on the left [3].

Physiological angiogenesis takes place in response to primordial follicle recruitment, dominant follicle selection, and ovulation. A dense perifollicular wreath-like network of concentric vessels forms and capillaries invade the granulosa layer of cells to reach the ovarian follicle [4]. Once ovulation occurs, the granulosa cells transform into large luteal cells and vessels become more prominent to form the corpus luteum [5]. These changes become even more manifest if conception occurs. However, they regress rapidly toward the end of the luteal phase in non-conception cycles (Fig. 38.2).

Angiogenesis happens in response to the increased requirement for oxygen and nutrients necessary to support folliculogenesis, implantation, and embryogenesis [6]. These newly formed blood vessels are composed of three layers: the innermost tunica intima which consists of a single layer of endothelial cells and a basement membrane; the middle smooth muscle layer which provides support and regulates blood flow and the outermost layer that contains connective tissue which attaches vessels to the surrounding. New vessel networks are usually well defined and organized, regularly distributed through the tissue and exhibit normal diameters and blood flow [7].

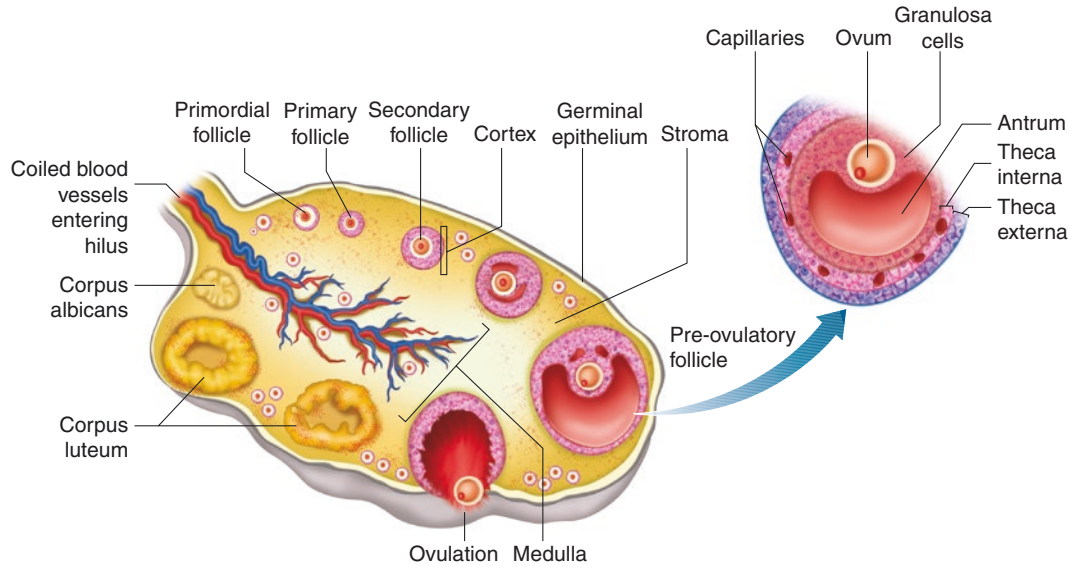

Fig. 38.2 Anatomy of the ovary and schematic representation of folliculogenesis. (Illustrated by M. Lluch)

38.3 Effect of Pathology on the Ovarian Circulation

The ovary is a complex organ made up of several cell types, all with the potential to develop intrinsic tumors or support growth of metastatic lesions from other organs. This is achieved by activating neoangiogenesis to accommodate the increased oxygen demand required for tumor growth. The ovary is also an active organ susceptible to diverse benign pathology that can trigger a decrease or increase of ovarian blood flow to provide an environment for the development of endometriosis and implantation of ectopic trophoblastic tissue. Its mobility makes it prone to twisting around its own attachments resulting in ovarian torsion with partial or complete obstruction of blood supply. Furthermore, its close relation to the Fallopian tubes makes it susceptible to inflammation, which can also trigger angiogenesis to increase perfusion.

Small simple physiological cysts which are often caused by anovulatory cycles can displace existing blood vessels. However, with the resolution of the cyst, the vascular architecture returns to normal. On the other hand, with persistent pathological ovarian tumors which grow beyond 1–2 mm^3 in volume, vascular remodeling will occur [8].

Malignant tumors grow rapidly and in an irregular fashion which results in the formation of abnormal vessels that lack smooth muscle and create multiple arteriovenous shunts. Vessels appear tortuous and irregular, displaying abnormal branching patterns [9]. Leaky vessels and lack of lymphatic drainage cause increased interstitial pressure and as a result, the vessels become occluded contributing to the formation of abnormal new vascular networks [10]. This chaotic process results in dilated, unevenly distributed vessels that exhibit low resistance and high-velocity flow.

38.4 Role of Ultrasound and Doppler in the Assessment of Ovarian Tumors

Ultrasound is used to complement the medical history and physical examination and is part of the diagnostic bundle when pelvic pathology is suspected. Grayscale assessment is simple, non-invasive, and allows clinicians to examine ovarian morphology, monitor physiological changes, and detect pathology. However, in some cases, it can be challenging to assign a diagnosis or to distinguish benign from malignant lesions. Evaluating the vascular anatomy can increase the diagnostic accuracy [11–13] (Fig. 38.3), particularly when an ovarian mass is complex in appearance [14]. Likewise, in an acute setting, Doppler assessment can help identify complications, such as ovarian torsion, ectopic pregnancy or cyst rupture.

38.4.1 Pulsed Doppler

Pulsed Doppler assessment of the ovarian vasculature was first reported in 1989 by Kurjak and colleagues, who analyzed the waveforms to quantify the velocity, resistance, and impedance of ovarian vessels [1]. In their publication, they reported that ovarian malignancy exhibited lower impedance than benign pelvic conditions or normal ovaries. Similar findings were reported by Bourne et al. who used pulsatility index (PI) to discriminate between benign and malignant lesions [15]. Fleischer et al. however, showed that there was an overlap of PI values recorded in

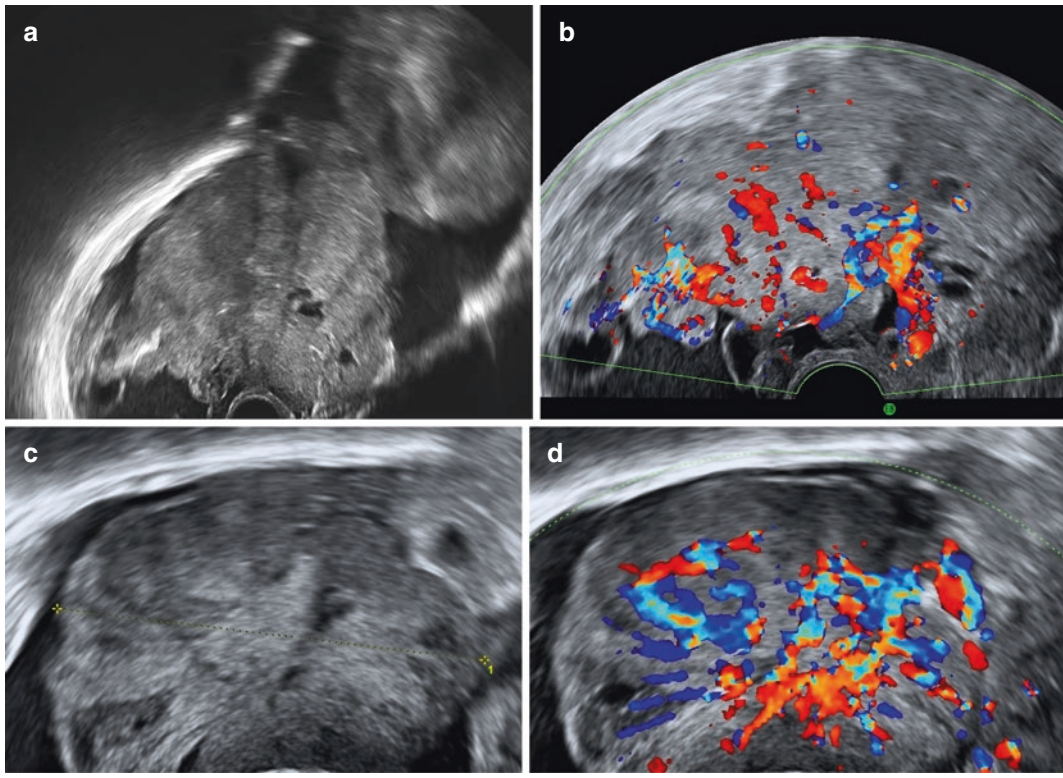

Fig. 38.3 Color Doppler assessment of ovarian tumors. (**a**) Grayscale evaluation of a primary ovarian malignancy presenting as a solid mass with irregular outline and ascites. (**b**) On color Doppler the lesion shows high vascularity. (**c**) Gray scale appearance of a metastatic ovarian tumor (Krukenberg tumor). (**d**) Color Doppler examination of the same lesion showed high vascularity and a tree-shaped pattern with large vessels

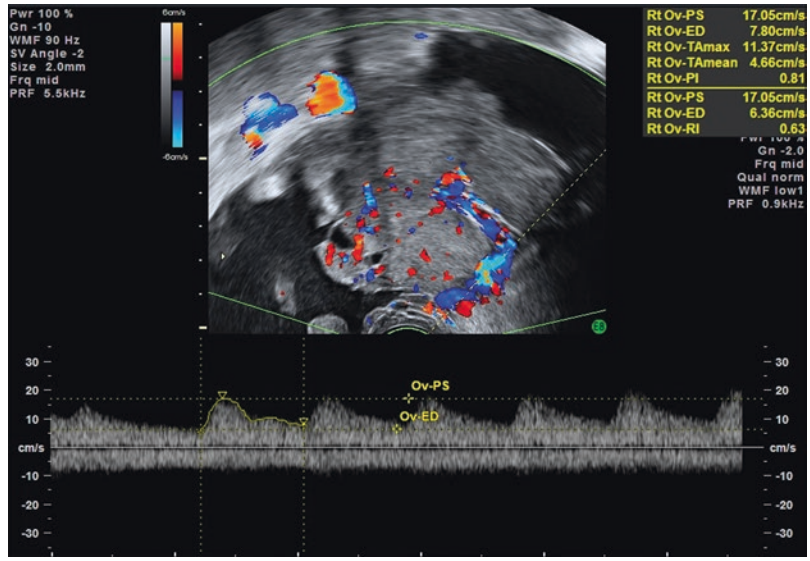

Fig. 38.4 An example of pulsed Doppler flow velocity waveform analysis in a case of ovarian malignancy showing low impedance to flow

benign and malignant conditions resulting in a high false-positive rate with one in four lesions displaying a low PI (≤1.0) with the potential of misclassifying as malignant when in fact they were benign [16] (Fig. 38.4).

Subsequently, Kurjak et al. advocated that resistance index (RI) was superior to PI in diagnosing ovarian cancer and suggested a cut-off of less than 0.40 [17, 18]. Further work, however, showed that this test is neither sensitive nor specific [19–21] and the search for a more accurate parameter continued. Absence of a diastolic notch in the waveform was thought to be characteristic of malignant tumors [22–24], but again, found to be an infrequent occurrence with no significant difference in some studies [25]. In 1996, Tailor et al. showed that Time-Averaged Maximum Velocity (TAMXV) was superior to the indices of impedance and they suggested using a cut-off value of ≥12 cm/s to indicate malignancy with a sensitivity and specificity of 88.9% and 81.0%, respectively [26]. In view of the heterogenicity of the evidence and the lack of consensus on the cut-off values that could be used to predict malignancy, a large prospective study was completed in 2005 involving nine European ultrasound centers and 1066 women with a pelvic mass judged to be of adnexal origin. No significant difference was found in the indices of impedance between benign and malignant lesions and the authors concluded that pulsed Doppler waveform analysis is of limited use in determining the nature of adnexal lesions. As a result, the impedance indices and velocity measurements are rarely used nowadays in clinical practice and research.

38.4.2 Color Doppler

Color Doppler displays ovarian blood flow in two dimensions and can be used to map vascular trees and carry out semi-quantitative blood flow studies. Color score categorizes blood flow into four groups: a score of 1 means that no color Doppler signals are detected in the tumor; a score of 2 indicates that a minimal amount of flow is detected; a score of 3 represents a moderate amount and a score of 4 suggests abundant vascularity [27] (Fig. 38.5). This system is considered by many experts to be the most useful Doppler parameter for differential diagnosis of adnexal tumors [14, 25]. An important limitation, however, is its inability to distinguish borderline from invasive tumors or to discriminate between epithelial and non-epithelial malignant tumors [28].

To obtain an accurate vascular score, it is essential to consider the physical and technical aspects which affect the Doppler signal. Velocity,

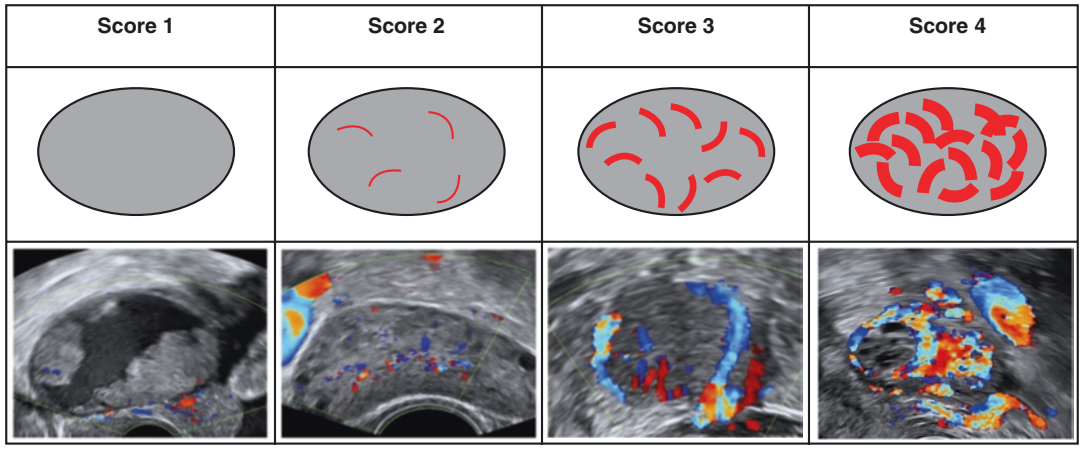

Fig. 38.5 An illustration of semiquantitative color Doppler score system to assess vascularity of ovarian lesions. (**a**) Score 1 demonstrating no color Doppler signals. (**b**) Score 2 demonstrating minimal amount of blood flow. (**c**) Score 3 demonstrating moderate amount of blood flow. (**d**) Score 4 demonstrating abundant vascularity

Pulse Repetition Frequency (PRF) and gain should be adjusted to maximize sensitivity. A PRF between 0.3 and 0.6 kHZ and a velocity scale 3–6 cm/s are recommended. Thereafter, gradual adjustment of gain just below artifact level should be carried out to concentrate analysis on the highest velocity signals. When assessing large or deep pelvic masses, the signal could be weaker which can affect the interpretation of the test. Transabdominal approach may help to overcome this problem, although the image resolution would be impaired. Timing of the examination in premenopausal women is also important to avoid false-positive findings caused by physiological angiogenesis of the corpus luteum.

Mapping blood flow can also be useful to support B-mode findings when assessing a pelvic mass. Pericystic or peripherally increased vascularity is suggestive of a benign tumor while central vessels may indicate malignancy [24]. A clear example of pericystic vascularity is that of a corpus luteum, which demonstrates a peripheral dense halo of confluent vessels formed during the physiological angiogenesis following ovulation (Fig. 38.6). Endometriomas can also demonstrate pericystic vascularity at the level of the ovarian hilum [29] and dermoids, although mostly avascular, can exhibit some blood flow signals commonly seen at the cyst capsule [30]. It is important to highlight, that if vessels follow the outline of a solid tumor, a pedunculated fibroid should be considered in the differential diagnosis.

Malignant adnexal tumors, on the other hand, undergo neovascularization that can appear on Doppler assessment centrally, at the base of papillary projections, within the septa or in solid areas. Color Doppler mapping is therefore particularly useful when assessing multiloculated cysts with solid components [14]. Similarly, if a "lead vessel" is present in the central part of the ovary displaying tree-shaped morphology, a metastatic lesion needs to be considered [31] (Fig. 38.7). Consequently, color Doppler should not be interpreted in isolation and should be used together with B-mode morphological assessment to help clinicians to characterize adnexal pathology.

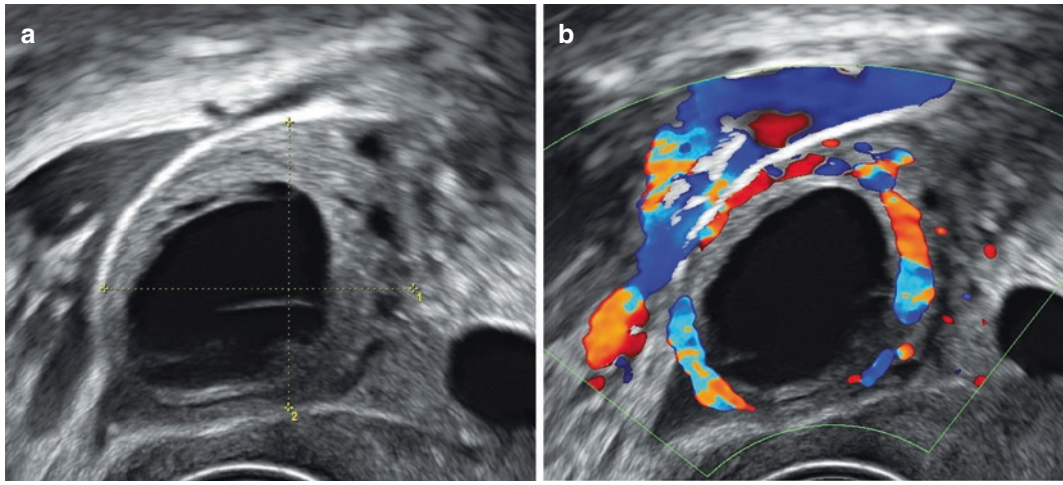

Fig. 38.6 Assessment of corpus luteum. (**a**) A grayscale image of a cystic corpus luteum which is surrounded by normal ovarian tissue. (**b**) Color Doppler showed typical "ring of fire" distribution of blood vessels

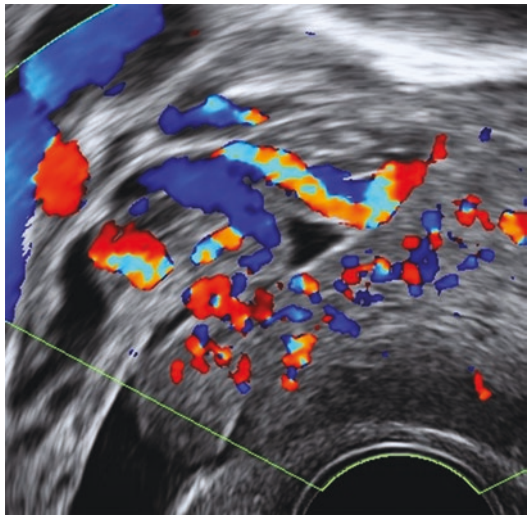

Fig. 38.7 Color Doppler signals displaying a "lead vessel" which is sometimes observed in metastatic tumors

38.4.3 Other Methods

Two-dimensional grayscale assessment of ovarian tumors by an experienced examiner ("pattern recognition") is considered to be the best method to discriminate between benign and malignant adnexal masses and has been repeatedly shown to have high sensitivity and specificity [32–34]. Most benign masses have pathognomonic features that have been described in the literature [27]. Dermoids, endometriomas, hemorrhagic corpus luteum, ovarian fibroma, and thecomas are the most recognizable lesions. On the other hand, ovarian malignancy is suspected if cysts are large (>10 cm in postmenopausal women) with irregular borders, septations, papillary projections, or solid components [27]. Nevertheless, a small proportion of adnexal masses remain difficult to classify (cystadenofibromas, Brenner, granulosa cell) because they have overlapping characteristics and benign can mimic malignant [28, 35]. Therefore, if there is any doubt, or the assessment is being carried out by a less experienced clinician, further tests are needed.

Several quantitative scoring systems and mathematical algorithms have been created in an attempt to calculate pre-operative risk of malignancy with the aim to optimize surgical management and final outcomes. Some of them have utilized various Doppler parameters to improve diagnostic performance. Brown et al. [36] included the location of blood flow in their scoring system together with grayscale features. Following that, Alcazar et al. [37] developed a scoring system based on data collection from 705

adnexal masses using grayscale morphological and two Doppler parameters reported as independent predictors of malignancy: location of blood flow (central) and high velocity (PSV ≥10 cm/s) with low resistance flow (RI ≤ 0.45). The main limitation with color Doppler variables in mathematical models is that they require optimal machine settings, high-quality equipment, and experienced examiners to make them work.

The International Ovarian Tumor Analysis (IOTA) group have created Logistic Regression Models (LR) which use the presence of blood flow within the papillary projections (yes – 1, no = 0) as one of their 12 variables in LR1 and one of six variables in LR2 [38, 39]. Their simple rules also incorporate color content as one of the five diagnostic criteria [40], where the absence of detectable blood flow (color score of 1) is classed as a benign criterion and very strong blood flow (color score 4) as malignant. However, ADNEX (Assessment of Different NEoplasias in the adnexa), their most recent model, which is recommended when an adnexal mass is not classifiable using Simple Rules, does not include any Doppler variables.

An alternative to conventional color Doppler imaging is power Doppler which works with amplitude instead of Doppler signal frequency shift thus eliminating aliasing and angle dependence. Consequently, power Doppler facilitates the examination of vascular features throughout the course of the vessel and distinguishes better true flow from background noise making it easier to assess low-velocity blood flow (Fig. 38.8). Various papers have been published reporting power Doppler to be superior in displaying tumor vascular distribution and microvessels but then again, it does not give any information on speed or direction of flow which makes it hard to distinguish arteries from veins [41]. Other developments include High-Definition Flow (HDF), three-dimensional (3D), four-dimensional (4D) technology, and the use of contrast in the form of microbubbles some of which will be discussed in other chapters.

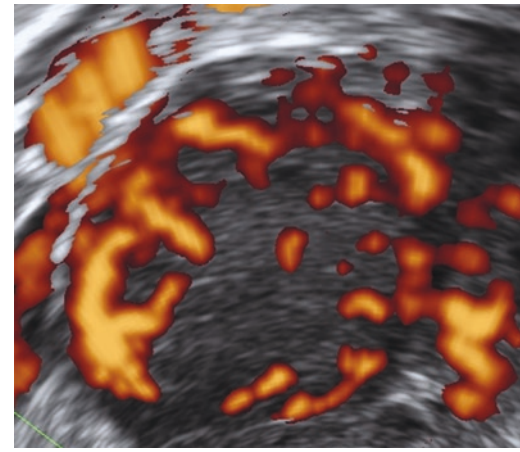

Fig. 38.8 Power Doppler demonstrating abundant vascularity in a solid malignant ovarian tumor

38.5 Role of Ovarian Doppler in Early Pregnancy

38.5.1 The Corpus Luteum

Corpus luteum is a highly vascular structure that develops following the rupture of the dominant follicle. It can have a variable appearance on transvaginal ultrasound, but the most characteristic feature is the "ring of fire" seen on color Doppler (Fig. 38.6b). The location of the corpus luteum is helpful when searching for a tubal ectopic pregnancy as 80% are found in the ipsilateral adnexa [42]. The number of corpora lutea is important as it alerts the examiner to the possibility of multiple pregnancies some of which could be heterotopic.

38.5.2 Ovarian Ectopic Pregnancy

Ovarian pregnancy occurs when the fertilized ovum implants on the surface or within the ovary itself; it accounts for approximately 3% of all ectopic pregnancies [43]. Ultrasound criteria are not generally agreed, but usually include findings of a heterogenous swelling or a cystic struc-

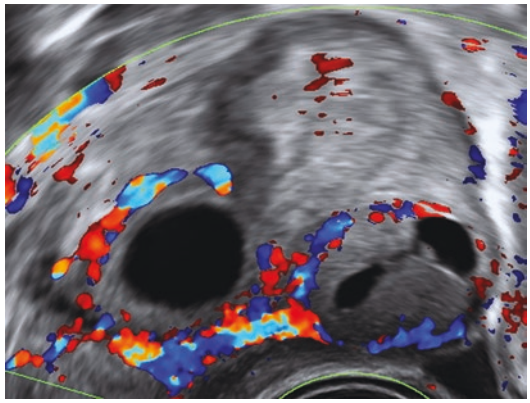

Fig. 38.9 Color Doppler facilitating the differentiation between the corpus luteum and an ovarian ectopic

ture with an echogenic rim that cannot be separated from the ovary when gentle pressure is applied with the probe ("negative sliding organ sign"). The presence of a yolk sac or an embryo helps to make the correct diagnosis. Ovarian pregnancies, however, often present with rupture and hemoperitoneum which makes it difficult to differentiate between ovarian and ruptured tubal pregnancy [44].

Trophoblastic tissue generally exhibits increased vascularity on color Doppler assessment and can be identified separately from the corpus luteum which is usually ipsilateral to the ovarian ectopic (Fig. 38.9). Unfortunately, the indices of impedance from corpus luteum and ovarian pregnancy blood flow overlap and for that reason, pulsed Doppler cannot be used to differentiate between the two.

38.5.3 Decidualized Endometrioma

Endometriomas are typically seen on ultrasound as unilocular cysts containing homogenous low-level internal echoes ("ground glass" echogenicity) with scarce color Doppler signals [45]. However, in pregnancy, the hormonal changes that promote deciduosis in the endometrium with the aim to support implantation and early pregnancy development, trigger similar glandular cell differentiation and vascular remodeling in the adnexal endometriotic foci. This decidualization can cause changes in the appearance of the endometriomas in about 12% of women which could mimic borderline or malignant tumors [46]. This diagnostic uncertainty causes significant anxiety and can lead to unnecessary surgery; therefore, it is essential to understand this process and consider this transformation when reviewing an ovarian cyst in pregnancy.

The rise in progesterone causes a morphological change in the endometrial stromal cells which triggers the formation of wall irregularities and papillary projections within endometriomas (Fig. 38.10a). Vascular changes also occur, which are seen on color Doppler as areas of high vascularity within the papillations (Fig. 38.10b). Considering that vascular papillary projections are often found in borderline tumors and malignancy, and rarely in endometriomas in non-pregnant women [45], a careful review of the history, symptoms, family history, and concomitant ultrasound features of deep endometriosis should be explored prior to suggesting a diagnosis.

Ovarian endometriomas are rarely found in isolation and the presence of adhesions, endometriotic nodules, pouch of Douglas obliteration, or an endometrioma in the contralateral ovary can support the diagnosis. Holland et al. report that 96% of women with an endometrioma had endometriotic lesions in other locations and therefore careful mapping of the pelvis should be carried out, including examination of the bowel and urinary tract [47] (Fig. 38.10c). To evaluate the mobility of the ovary, gentle pressure with the vaginal probe while palpating abdominally with the examiner's free hand should be carried out. In a similar way, the pouch of Douglas should be assessed and endometriotic nodules in the uterosacral ligaments, adnexa, rectovaginal space, and urinary bladder should be sought.

Decsidualized endometriomas are dynamic and tend to shrink as the pregnancy progresses and the cyst content becomes more solid as the pregnancy advances (Fig. 38.10d). On the other

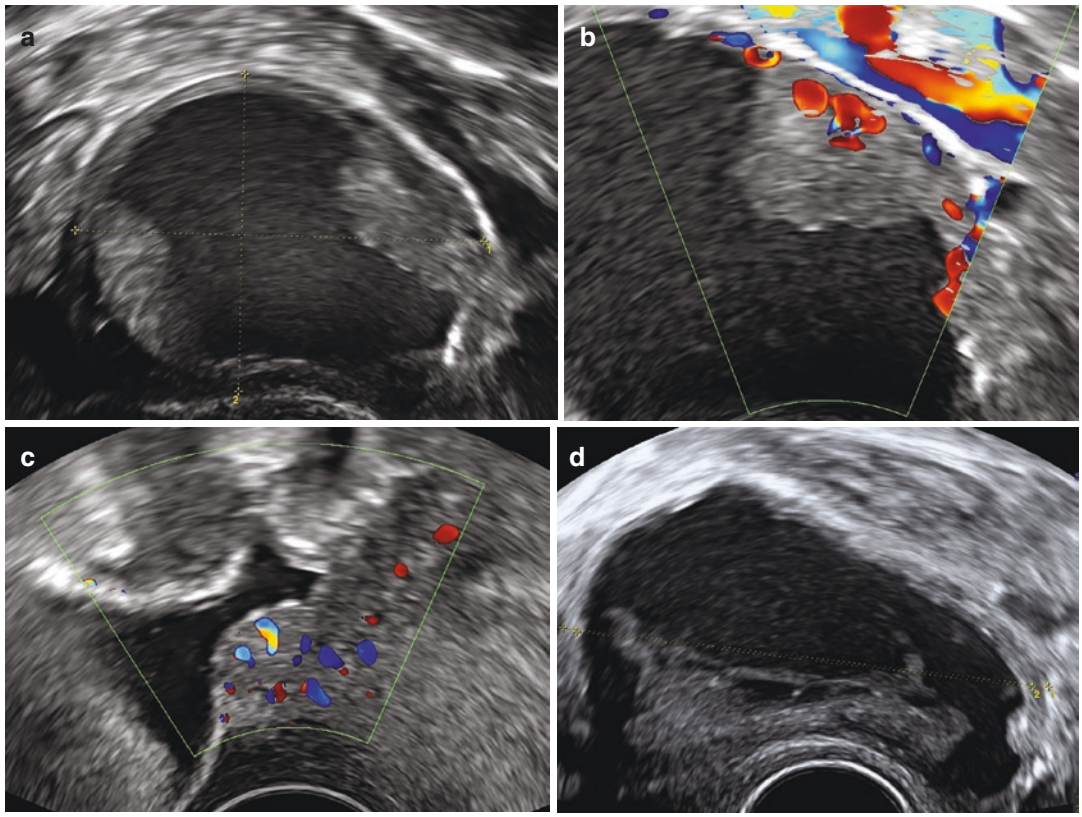

Fig. 38.10 Natural history of a decidualized endometrioma in pregnancy. (**a**) Grayscale assessment displaying cyst wall irregularities and papillary projections mimicking an ovarian malignancy. (**b**) Vascularity present on color Doppler evaluation. (**c**) Concomitant endometriotic nodule (in the pouch of Douglas). (**d**) Dynamic changes as pregnancy progresses (smaller size and a more solid content)

hand, borderline or malignant tumors exhibit an opposite tendency and therefore regular follow-up visits are required. Expert advice from a specialist center should be considered if there is any uncertainty.

38.6 Other Conditions Affecting the Ovary

38.6.1 Ovarian Torsion

Ovarian torsion occurs when the ovary twists and the supporting ligaments holding the neurovascular bundle gets sealed off with various degrees of vascular and lymphatic obstruction. This leads to ovarian congestion, edema, and subsequent infarction [48]. Ovarian torsion presents clinically with the sudden onset of severe lower abdominal pain which is often associated with vomiting. On ultrasound scan, the torted ovary is frequently located in the midline and anterior to the uterus. It typically appears enlarged and edematous with ill-defined borders and peripherally arranged follicles (a string of pearls) [49] (Fig. 38.11a).

The presence, size, and characteristics of an adnexal mass can also support the diagnosis of ovarian torsion as it makes the ovary heavier and more predisposed to rotate (Fig. 38.11b). The risk is highest when the lesion measures 8–12 cm [50] and dermoid cysts, in particular, are thought to be most susceptible to torsion. On the contrary, invading tumors such as endometriomas or

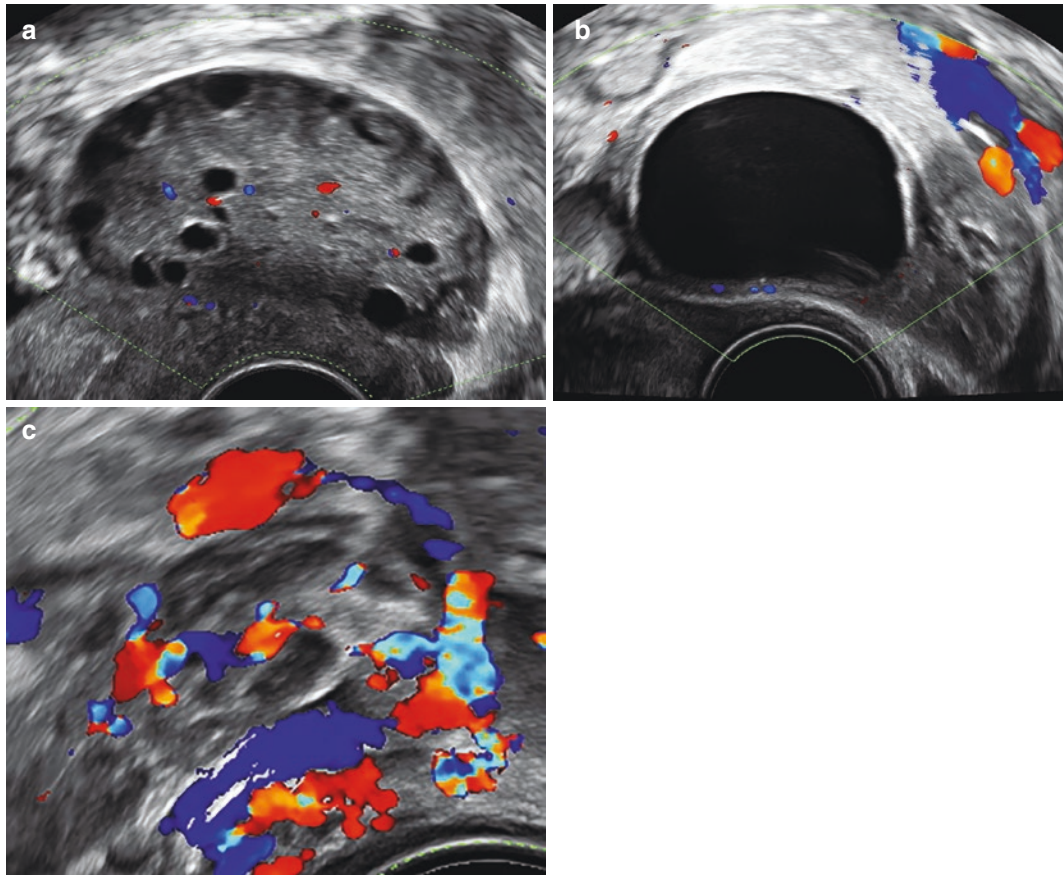

Fig. 38.11 Ultrasound findings in ovarian torsion. (**a**) String of pearls demonstrated by the presence of small cysts mostly at the periphery of the ovary. (**b**) Ovarian torsion in the presence of an ovarian cyst. (**c**) The "whirlpool sign" indicating a twisted ovarian pedicle

malignancy is less likely to undergo torsion due to the reduced mobility secondary to adhesions and invasion.

Doppler findings in ovarian torsion are variable and depend on the degree of vascular compromise. The most frequent finding is decreased or absent venous flow. The arterial blood supply is usually maintained, and the presence of arterial blood flow should not be used to rule out torsion. The twisted pedicle may be seen as a spiral-like structure on grayscale with coiled vessels on color Doppler assessment. These features are described in the literature as a positive "whirlpool" sign, which is almost pathognomonic of ovarian torsion [51] (Fig. 38.11c). The tube may also twist, become thickened, and contain hemorrhagic fluid. Comparison with the contralateral side can be very helpful. Clinical findings should always prevail and any patient complaining of acute onset of unilateral abdominal pain associated with nausea and vomiting and unilaterally enlarged or abnormal ovary should be treated as potentially having ovarian torsion.

38.6.2 Pelvic Inflammatory Disease

Patients with pelvic inflammatory disease can display a variety of ultrasound features in response to adnexal edema, vasodilatation, necrosis, and fibrosis triggered by ascending infection. Ultrasound findings can be subtle and non-spe-

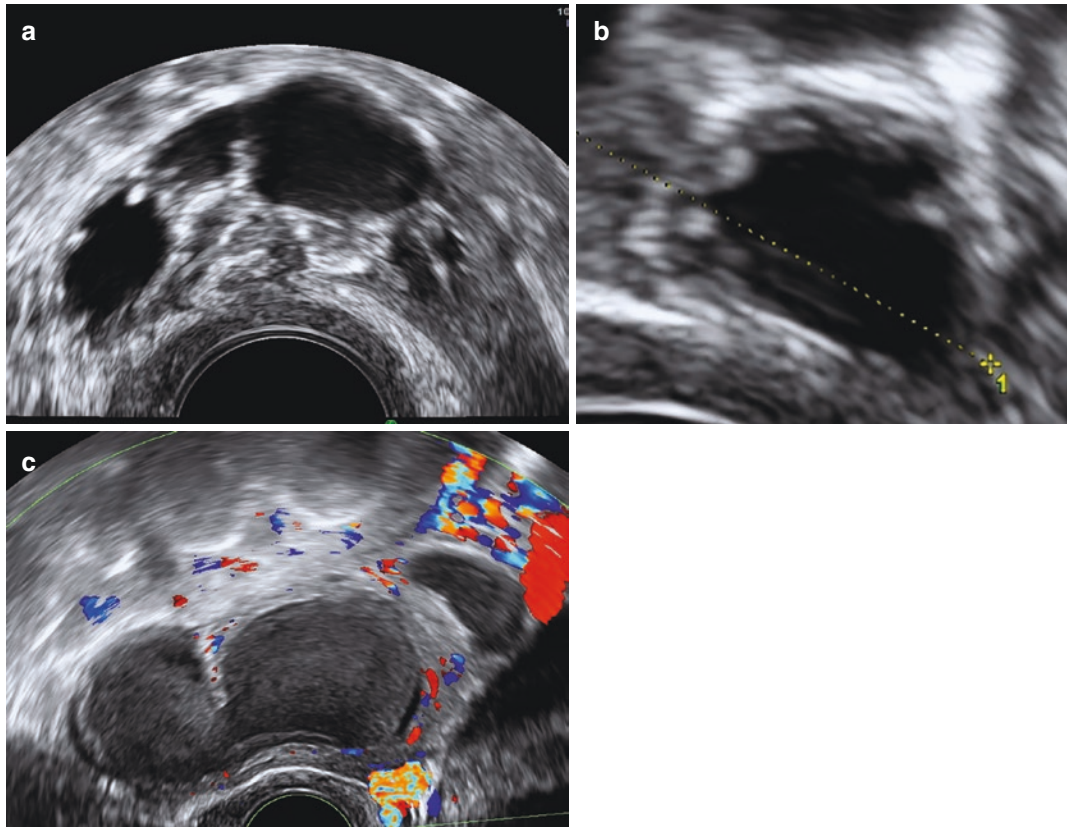

Fig. 38.12 Ultrasound findings in pelvic inflammatory disease. (**a**) An illustration of the "cogwheel sign" created by swollen mucosal folds protruding in the lumen of dilated tube. (**b**) "Beads on a string" sign which is sometimes seen in chronic salpingitis. (**c**) A case of tubo-ovarian abscess with increased vascularity on color Doppler evaluation

cific, such as free fluid or tubal thickening; or distinct and complex, such as pyosalpinx or a tubo-ovarian abscess (TOA) [52]. In addition, echogenicity of pus can resemble the "ground glass" appearance of endometriomas, and vascularity of inflamed structures can mimic a malignant tumor. Therefore, it is essential that ultrasound findings should always be interpreted in the context of the full clinical picture to avoid errors.

The inflamed tube can be visible on ultrasound as a solid homogenous ill-defined mass near the ovary or a fluid-filled "sausage shaped" structure with incomplete septations. The swollen mucosal folds protruding in the fluid-filled lumen can resemble a cogwheel and are characteristic of salpingitis (Fig. 38.12a). If the tube is mildly swollen, the mucosal folds form a "beads on a string" appearance (Fig. 38.12b). The ovary can demonstrate reactive edema and it could become adherent to the uterus or other pelvic structures. This tubo-ovarian complex is usually situated near the pouch of Douglas and it can contain one or more cavities filled with pus (Fig. 38.12c). On ultrasound, a tubo-ovarian abscess usually appears multilocular with thick walls. It is usually filled with homogenous echogenic fluid that can contain a fluid level and gas which gives rise to shadowing.

Doppler assessment can help distinguish dilated blood vessels from hydro/pyosalpinx as well as demonstrate increased vascularity in the acute phase. Large number of vessels with low impedance (hyperemia) and abundant blood flow

localized in the thickened walls and septa of pyosalpinx and TOA are often found [53]. These findings should be correlated with clinical and laboratory results to help start early and appropriate treatment in patients with suspected pelvic infection.

38.7 Non-ovarian Pathology

Various uterine and non-gynecological lesions can be found in the adnexal region and they could be mistaken for an ovary. A pedunculated fibroid, loop of bowel, appendix tumor, peritoneal pseudocysts, or a pelvic kidney should always be considered, especially if the ultrasound findings are atypical or unexpected. A systematic and thorough ultrasound examination of the pelvis is key to recognize the ovary separate from a non-ovarian mass as well as identifying other relevant structures that may facilitate a correct diagnosis. Doppler assessment can be used in these cases to exclude pelvic varicosities mimicking a cystic tumor.

38.7.1 Pedunculated Fibroid

Fibroids are generally seen as well-defined rounded hypoechoic lesions of myometrial origin and they typically display acoustic shadowing due to the presence of connective tissue and calcifications within. However, sometimes, they can be pedunculated, display different echogenicity and contain cystic areas of necrosis, which can make differentiation with an ovary difficult. A meticulous assessment of the uterus should be carried out to identify concomitant myomas as they rarely are solitary. Examining the whole mass and its surroundings is crucial, both to locate the ipsilateral ovary and also to identify the vascular pedicle carrying the blood supply from the uterus to the pedunculated fibroid (Fig. 38.13). Color Doppler is therefore very helpful in these cases.

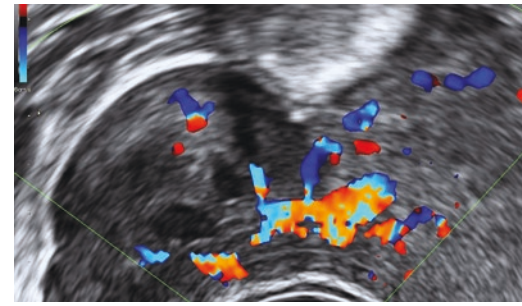

Fig. 38.13 An ultrasound image of a pedunculated fibroid with a vascular pedicle demonstrated on Doppler assessment

38.7.2 Peritoneal Pseudocysts

Fluids produced during an inflammatory process or ovulation can become entrapped within dense pelvic adhesions and form peritoneal pseudocysts. These fluid-filled spaces can cause diagnostic challenges as they are irregularly shaped and can contain septations (Fig. 38.14a) or blood clots mimicking solid components. Often an ovary could be found within a cystic lesion and can also be mistaken for a solid focus within the cystic tumor (Fig. 38.14b). Color Doppler helps to differentiate blood clots that have no detectable blood flow, from solid components which can exhibit color Doppler signals. It can also help identify the "ring of fire" of a corpus luteum and assess septations that may exist.

38.7.3 Pelvic Kidney

Pelvic kidney can also be seen when performing a pelvic transvaginal ultrasound and it may be mistaken for an adnexal tumor (Fig. 38.15a). On Doppler examination pelvic kidney appears very vascular which can alarm an inexperienced examiner. However, a more detailed examination should reveal a highly organized blood supply typical of an organ as opposed to the chaotic vascularity of a malignant adnexal tumor (Fig. 38.15b).

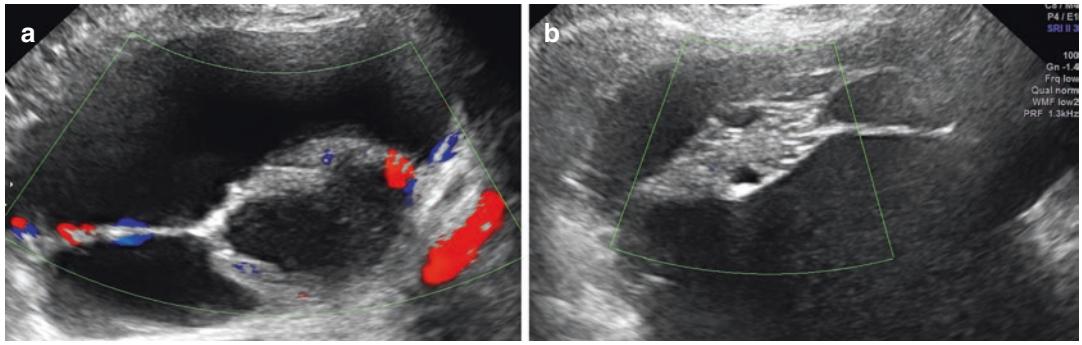

Fig. 38.14 Ultrasound images of peritoneal pseudocysts. (**a**) A gray-scale image showing thick, irregular septations which are poorly vascularized on color Doppler. (**b**) An image of normal ovary suspended within the pseudocyst

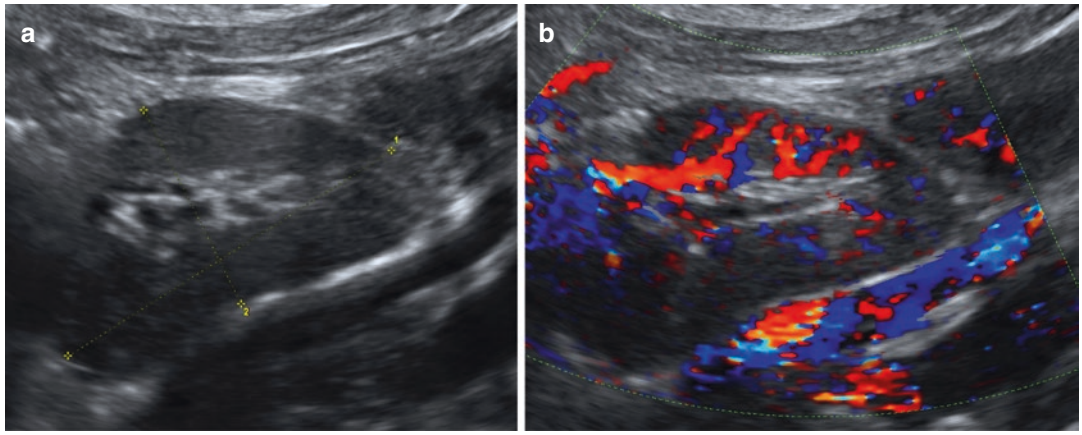

Fig. 38.15 Non-ovarian pathology. (**a**) A gray-scale image of a pelvic kidney mimicking an adnexal mass. (**b**) Highly organized distribution of vascular supply to the kidney is shown on color Doppler evaluation

38.8 Conclusion

Ovarian blood supply is affected by both physiological activity and various ovarian abnormalities. In view of that, color Doppler blood flow studies are often carried out to facilitate better characterization of morphological changes observed on B-mode grayscale imaging. Doppler studies are particularly helpful to characterize ovarian tumors, but they should always be used as a second-line investigation. They are most useful when interpreted in the context of other available clinical and morphological information.

References

1. Kurjak A, Žalud I, Jurković D, Alfirević Ž, Miljan M. Transvaginal color Doppler for the assessment of pelvic circulation. Acta Obstet Gynecol Scand. 1989;68(2):131–5.
2. Blaustein A. Anatomy and histology of the human ovary BT. In: Blaustein A, editor. Pathology of the female genital tract. New York, NY: Springer; 1977. p. 365–86. https://doi.org/10.1007/978-1-4757-6143-6_19.
3. Arulkumaran S, Regan L, Papageorghiou A, Monga A, Farquharson D. Oxford desk reference: obstetrics and gynaecology. OUP Oxford; 2011. p. 472. (Oxford Desk Reference Series). https://books.google.co.uk/books?id=IiqQDwAAQBAJ.
4. Reynolds LP, Grazul-Bilska AT, Redmer DA. Angiogenesis in the corpus luteum. Endocrine.

2000;12(1):1–9. https://doi.org/10.1385/ENDO:12:1:1.
5. Suzuki T, Sasano H, Takaya R, Fukaya T, Yajima A, Nagura H. Cyclic changes of vasculature and vascular phenotypes in normal human ovaries. Hum Reprod. 1998;13(4):953–9.
6. Reynolds LP, Killilea SD, Redmer DA. Angiogenesis in the female reproductive system. FASEB J. 1992;6(3):886–92. https://doi.org/10.1096/fasebj.6.3.1371260.
7. Lugano R, Ramachandran M, Dimberg A. Tumor angiogenesis: causes, consequences, challenges and opportunities. Cell Mol Life Sci. 2019;77:1745–70. https://doi.org/10.1007/s00018-019-03351-7.
8. Gimbrone MA, Leapman SB, Cotran RS, Folkman J. Tumor dormancy in vivo by prevention of neovascularization. J Exp Med. 1972;136(2):261–76.
9. Sladkevicius P, Jokubkiene L, Valentin L. Contribution of morphological assessment of the vessel tree by three-dimensional ultrasound to a correct diagnosis of malignancy in ovarian masses. Ultrasound Obstet Gynecol. 2007;30(6):874–82.
10. Jain RK. Determinants of tumor blood flow: a review. Cancer Res. 1988;48(10):2641–58.
11. Kinkel K, Hricak H, Lu Y, Tsuda K, Filly RA. US characterization of ovarian masses: a meta-analysis. Radiology. 2000;217(3):803–11.
12. Valentin L. Pattern recognition of pelvic masses by gray-scale ultrasound imaging: the contribution of Doppler ultrasound. Ultrasound Obstet Gynecol. 1999;14(5):338–47.
13. Fleischer AC, Rogers WH, Rao BK, Kepple DM, Jones HW. Transvaginal color Doppler sonography of ovarian masses with pathological correlation. Ultrasound Obstet Gynecol. 1991;1(4):275–8.
14. Valentin L. Gray scale sonography, subjective evaluation of the color Doppler image and measurement of blood flow velocity for distinguishing benign and malignant tumors of suspected adnexal origin. Eur J Obstet Gynecol Reprod Biol. 1997;72(1):63–72. https://doi.org/10.1016/S0301-2115(96)02661-9.
15. Bourne T, Campbell S, Steer C, Whitehead MI, Collins WP. Transvaginal colour flow imaging: a possible new screening technique for ovarian cancer. BMJ. 1989;299(6712):1367–70.
16. Fleischer AC, Rodgers WH, Rao BK, Kepple DM, Worrell JA, Williams L, et al. Assessment of ovarian tumor vascularity with transvaginal color Doppler sonography. J Ultrasound Med. 1991;10(10):563–8.
17. Kurjak A, Zalud I, Alfirevic Z. Evaluation of adnexal masses with transvaginal color ultrasound. J Ultrasound Med. 1991;10(6):295–7.
18. Kurjak A, Schulman H, Sosic A, Zalud I, Shalan H. Transvaginal ultrasound, color flow, and Doppler waveform of the postmenopausal adnexal mass. Obstet Gynecol. 1992;80(6):917–21.
19. Brown DL, Frates MC, Laing FC, DiSalvo DN, Doubilet PM, Benson CB, et al. Ovarian masses: can benign and malignant lesions be differentiated with color and pulsed Doppler US? Radiology. 1994;190(2):333–6.
20. Hamper UM, Sheth S, Abbas FM, Rosenshein NB, Aronson D, Kurman RJ. Transvaginal color Doppler sonography of adnexal masses: differences in blood flow impedance in benign and malignant lesions. Am J Roentgenol. 1993;160(6):1225–8. https://doi.org/10.2214/ajr.160.6.8498222.
21. Prömpeler HJ, Madjar H, Sauerbrei W, Lattermann U, Pfleiderer A. Quantitative flow measurements for classification of ovarian tumors by transvaginal color Doppler sonography in postmenopausal patients. Ultrasound Obstet Gynecol. 1994;4(5):406–13. https://doi.org/10.1046/j.1469-0705.1994.04050406.x.
22. Fleischer AC, Rodgers WH, Kepple DM, Williams LL, Jones HW 3rd, Gross PR. Color Doppler sonography of benign and malignant ovarian masses. Radiographics. 1992;12(5):879–85.
23. Maly Z, Riss P, Deutinger J. Localization of blood vessels and qualitative assessment of blood flow in ovarian tumors. Obstet Gynecol. 1995;85(1):33–6.
24. Fleischer AC, Rodgers WH, Kepple DM, Williams LL, Jones HW 3rd. Color Doppler sonography of ovarian masses: a multiparameter analysis. J Ultrasound Med. 1993;12(1):41–8. https://doi.org/10.7863/jum.1993.12.1.41.
25. Twickler DM. The ovarian tumor index predicts risk for malignancy [1]. Cancer. 2002;94(10):2793.
26. Tailor A, Jurkovic D, Bourne TH, Natucci M, Collins WP, Campbell S. A comparison of intratumoural indices of blood flow velocity and impedance for the diagnosis of ovarian cancer. Ultrasound Med Biol. 1996;22(7):837–43.
27. Timmerman D, Valentin L, Bourne TH, Collins WP, Verrelst H, Vergote I. Terms, definitions and measurements to describe the sonographic features of adnexal tumors: a consensus opinion from the International Ovarian Tumor Analysis (IOTA) group. Ultrasound Obstet Gynecol. 2000;16(5):500–5.
28. Valentin L, Ameye L, Jurkovic D, Metzger U, Lécuru F, Van Huffel S, et al. Which extrauterine pelvic masses are difficult to correctly classify as benign or malignant on the basis of ultrasound findings and is there a way of making a correct diagnosis? Ultrasound Obstet Gynecol. 2006;27(4):438–44.
29. Kurjak A, Kupesic S. Scoring system for prediction of ovarian endometriosis based on transvaginal color and pulsed Doppler sonography. Fertil Steril. 1994;62(1):81–8. http://www.sciencedirect.com/science/article/pii/S0015028216568204.
30. Zalel Y, Caspi B, Tepper R. Doppler flow characteristics of dermoid cysts: unique appearance of struma ovarii. J Ultrasound Med. 1997;16(5):355–8. https://doi.org/10.7863/jum.1997.16.5.355.
31. Testa AC, Mancari R, Di Legge A, Mascilini F, Salutari V, Scambia G, et al. The 'lead vessel': a vascular ultrasound feature of metastasis in the ovaries. Ultrasound Obstet Gynecol. 2008;31(2):218–21. https://doi.org/10.1002/uog.5251.

32. Valentin L. Prospective cross-validation of Doppler ultrasound examination and gray-scale ultrasound imaging for discrimination of benign and malignant pelvic masses. Ultrasound Obstet Gynecol. 1999;14(4):273–83.
33. Sokalska A, Timmerman D, Testa AC, Van Holsbeke C, Lissoni AA, Leone FPG, et al. Diagnostic accuracy of transvaginal ultrasound examination for assigning a specific diagnosis to adnexal masses. Ultrasound Obstet Gynecol. 2009;34(4):462–70.
34. Meys EMJ, Kaijser J, Kruitwagen RFPM, Slangen BFM, Van Calster B, Aertgeerts B, et al. Subjective assessment versus ultrasound models to diagnose ovarian cancer: a systematic review and meta-analysis. Eur J Cancer. 2016;58:17–29. https://doi.org/10.1016/j.ejca.2016.01.007.
35. Yazbek J, Ameye L, Testa AC, Valentin L, Timmerman D, Holland TK, et al. Confidence of expert ultrasound operators in making a diagnosis of adnexal tumor: effect on diagnostic accuracy and interobserver agreement. Ultrasound Obstet Gynecol. 2010;35(1):89–93. https://doi.org/10.1002/uog.7335.
36. Brown DL, Doubilet PM, Miller FH, Frates MC, Laing FC, DiSalvo DN, et al. Benign and malignant ovarian masses: selection of the most discriminating gray-scale and doppler sonographic features. Radiology. 1998;208(1):103–10.
37. Alcázar JL, Mercé LT, Laparte C, Jurado M, López-García G. A new scoring system to differentiate benign from malignant adnexal masses. Am J Obstet Gynecol. 2003;188(3):685–92. https://doi.org/10.1067/mob.2003.176.
38. Nunes N, Ambler G, Hoo W-L, Naftalin J, Foo X, Widschwendter M, et al. A prospective validation of the IOTA logistic regression models (LR1 and LR2) in comparison to subjective pattern recognition for the diagnosis of ovarian cancer. Int J Gynecol Cancer. 2013;23(9):1583–9. http://ijgc.bmj.com/content/23/9/1583.abstract
39. Timmerman D, Testa AC, Bourne T, Ferrazzi E, Ameye L, Konstantinovic ML, et al. Logistic regression model to distinguish between the benign and malignant adnexal mass before surgery: a multicenter study by the International Ovarian Tumor Analysis Group. J Clin Oncol. 2005;23(34):8794–801.
40. Timmerman D, Testa AC, Bourne T, Ameye L, Jurkovic D, Van Holsbeke C, et al. Simple ultrasound-based rules for the diagnosis of ovarian cancer. Ultrasound Obstet Gynecol. 2008;31(6):681–90.
41. Kilsun P, Bihn C, Hjin W, Jb S, Sh K, Taek K, et al. Intratumoral vascularity of experimentally induced VX2 carcinoma: comparison of color Doppler sonography, power Doppler sonography, and microangiography. Investig Radiol. 1998;33(1):39–44. https://journals.lww.com/investigativeradiology/Fulltext/1998/01000/Intratumoral_Vascularity_of_Experimentally_Induced.6.aspx.
42. Jurkovic D, Bourne TH, Jauniaux E, Campbell S, Collins WP. Transvaginal color Doppler study of blood flow in ectopic pregnancies. Fertil Steril. 1992;57(1):68–73.
43. Bouyer J, Coste J, Fernandez H, Pouly JL, Job-Spira N. Sites of ectopic pregnancy: a 10 year population-based study of 1800 cases. Hum Reprod. 2002;17(12):3224–30. https://doi.org/10.1093/humrep/17.12.3224.
44. Dooley WM, Chaggar P, De Braud LV, Bottomley C, Jauniaux E, Jurkovic D. Effect of morphological type of extrauterine ectopic pregnancy on accuracy of preoperative ultrasound diagnosis. Ultrasound Obstet Gynecol. 2019;54(4):538–44. https://doi.org/10.1002/uog.20274.
45. Van Holsbeke C, Van Calster B, Guerriero S, Savelli L, Paladini D, Lissoni AA, et al. Endometriomas: their ultrasound characteristics. Ultrasound Obstet Gynecol. 2010;35(6):730–40.
46. Pateman K, Moro F, Mavrelos D, Foo X, Hoo W-L, Jurkovic D. Natural history of ovarian endometrioma in pregnancy. BMC Womens Health. 2014;14(1):128.
47. Holland TK, Yazbek J, Cutner A, Saridogan E, Hoo WL, Jurkovic D. Value of transvaginal ultrasound in assessing severity of pelvic endometriosis. Ultrasound Obstet Gynecol. 2010;36(2):241–8. https://doi.org/10.1002/uog.7689.
48. Chang HC, Bhatt S, Dogra VS. Pearls and pitfalls in diagnosis of ovarian torsion.1. Radiographics. 2008;28(5):1355–68.
49. Graif M, Shalev J, Strauss S, Engelberg S, Mashiach S, Itzchak Y. Torsion of the ovary: sonographic features. Am J Roentgenol. 1984;143(6):1331–4. https://doi.org/10.2214/ajr.143.6.1331.
50. McWilliams GDE, Hill MJ, Dietrich CS III. Gynecologic emergencies. Surg Clin North Am. 2008;88(2):265–83.
51. Vijayaraghavan SB. Sonographic whirlpool sign in ovarian torsion. J Ultrasound Med. 2004;23(12):1643–9.
52. Timor-Tritsch IE, Lerner JP, Monteagudo A, Murphy KE, Heller DS. Transvaginal sonographic markers of tubal inflammatory disease. Ultrasound Obstet Gynecol. 1998;12(1):56–66.
53. Molander P, Sjöberg J, Paavonen J, Cacciatore B. Transvaginal power Doppler findings in laparoscopically proven acute pelvic inflammatory disease. Ultrasound Obstet Gynecol. 2001;17(3):233–8. https://doi.org/10.1046/j.1469-0705.2001.00353.x.

Doppler in Benign and Malignant Conditions of the Uterus

39

Thierry Van den Bosch

39.1 Introduction

Color/power Doppler imaging should be part of every sonographic examination of the uterus and is mainly based on the vascular pattern recognition.

This chapter gives an overview of the vascular features of the most common benign and malignant conditions of the uterus involving myometrium, endometrium, and uterine cavity.

To obtain a good color image quality, it is important, to apply an optimal image magnification or the region of interest and to use optimal color settings. The gain is first increased till color artifacts appear and subsequently slowly turned down till all artifacts have disappeared. To visualize low flow vessels (e.g., in an endometrial polyp) power Doppler is preferred and the pulse repetition frequency (PRF) should be set low (e.g., 0.3 kHz). In high flow lesions (e.g., retained products on conception with enhanced myometrial vascularity) a low PRF will result in a "color splash," precluding further analysis of the vascular branching. Increasing the PRF will select the imaging of blood flow above the selected threshold. Turning the Wall Motion Filter (WMF) cut-off frequencies up will enable further analysis of the branching pattern by filtering out the lower frequency waves caused by soft tissue (e.g., vessel wall) vibrations.

If the Peak Systolic Velocity (PSV) is to be measured in a highly vascularized lesion, the vessel(s) with the highest velocity is selected by increasing the PRF till only a few vessels remain visible. The velocity is measured using an angle approaching 0° between the Doppler beam and the direction of the blood flow [1].

The blood flow within the uterus is highly affected by myometrial contractions. A contraction may cause a transient interruption of the blood flow. Sometimes the patient may tell the examiner she is feeling some lower abdominal cramping, while other myometrial contractions remain asymptomatic. It is therefore mandatory for the examination to last long enough or to repeat the examination at a later time, especially in the absence of detectable flow.

Finally, the intensity of the signal depends on the focal depth. Therefore, the part of the uterus most remoted from the ultrasound probe often appears less vascularized. Scar tissue (e.g., after cesarean section) or calcifications (e.g., a calcified fibroid) may also decrease the Doppler signal. The volume and the position of the uterus as well as possible hampering lesions should therefore be reported to enable a proper interpretation of the Doppler findings.

The advantages of the recognition of vascular patterns in the diagnosis of endometrial and myometrial lesions are well established while the use

T. Van den Bosch (✉)
Department of Obstetrics & Gynecology, University Hospitals Leuven, Leuven, Belgium
e-mail: thierry.vandenbosch@uzleuven.be

D. Maulik, C. C. Lees (eds.), *Doppler Ultrasound in Obstetrics and Gynecology*,
https://doi.org/10.1007/978-3-031-06189-9_39

of more objective Doppler measurements and indices has not been implemented in general practice yet [2]. Objective Doppler flow measurements include flow velocity (e.g., peak systolic velocity or PSV) and flow indices (e.g., pulsatility index or PI) using real-time 2-Dimensional ultrasonography, and vascularization indices (vascularization index or VI, Flow index or FI, vascularization flow index or VFI) using 3-Dimensional power Doppler and Virtual Organ Computer-aided Analysis (VOCAL) [3, 4].

39.2 Myometrium and Myometrial Lesions

The 2015 Morphological Uterus Sonographic Assessment (MUSA) terms and definitions consensus paper [5] reports on how to describe the myometrium and myometrial lesions. The color score of a myometrial lesion reflects the color content of the lesion and varies from 1 to 4. A color score of 1 indicates the absence of color while color scores of 2, 3, and 4 indicate minimal, moderate, and abundant color, respectively.

The myometrium or a myometrial lesion may exhibit different vascular patterns. The myometrial vascularity may be uniform or non-uniform. A nonuniform vascularity means that part of the myometrium shows an enhanced vessel pattern as compared to other parts. A nonuniform vascular pattern of the myometrium should be differentiated from normal variations in color intensities due to differences in focal depth or secondary to transient myometrial contractions.

The vascularity of a myometrial lesion may be circumferential and/or intralesional. If the vessels seem to cross the lesion without noticeable deviation, it is reported as translesional vascularity.

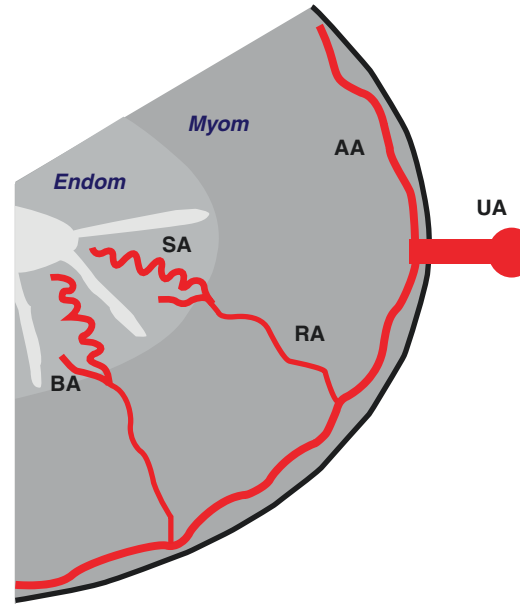

Fig. 39.1 Schematic representation of the uterine vascularity. *Endom* endometrium; *Myom* myometrium; *UA* uterine artery; *AA* arcuate artery; *RA* radial artery; *BA* basal artery; *SA* spiral artery

39.2.1 Normal Myometrium

The uterine arteries entering the uterus at the level of the isthmus, branch cranially into the arcuate arteries. The arcuate vessels run parallel with the serosa of the corpus uteri. From the arcuate arteries, numerous radial arteries branch perpendicularly and cross the myometrium toward the junctional zone, basal, and spiral arteries supplying the endometrium [5] (Fig. 39.1).

On color Doppler imaging both the arcuate and radial vessels are often visible (Fig. 39.2). The arcuate vessels may be prominent (Fig. 39.3) or hardly visible. The radial vessels of the myometrium nearest to the probe are more easily visible.

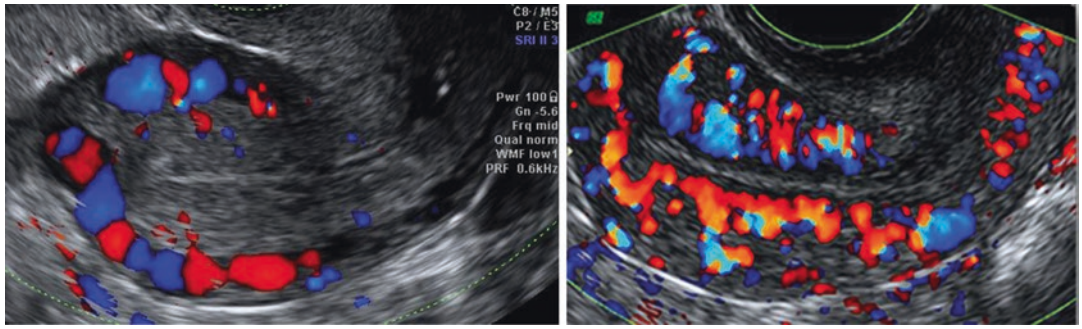

Fig. 39.2 Color Doppler of the normal uterine vascularity (sagittal section): left, the arcuate vessels are more prominent, whereas, right, the radial arteries are visible

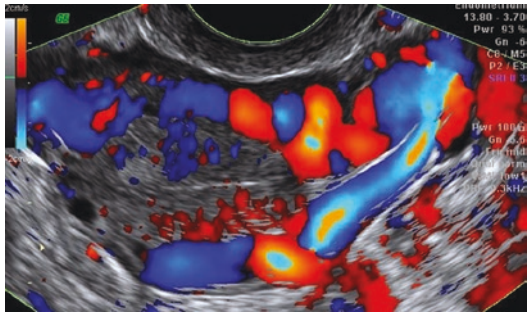

Fig. 39.3 Color Doppler image of a transverse section of the uterus: the parametrial as well as the arcuate vessels are prominent. Some of the radial arteries are also detectable (the arterial blood in the anterior uterine wall, near the probe, flows away from the probe, and appears bleu, whereas the direction of the arterial flow in the posterior wall is toward the probe and appears red)

39.2.2 Benign Lesions

39.2.2.1 Fibroids

A fibroid or leiomyoma is a well-defined round myometrial lesion. Typically, fibroids show circumferential vascularization surrounding the lesion [6] (Fig. 39.4). This vascular shape has been compared with a "wire salad basket" (J.M. Levaillant, personal communication). The internal vascularization of fibroids is highly variable, ranging from undetectable to prominent. Especially in calcified lesions, there is often an absence of any color signal.

The amount of (internal) vascularization has been related to the growth potential of the fibroid: a highly vascularized being more likely to be fast growing [7].

In Pedunculated Subserosal (FIGO 7) fibroids [8], color Doppler imaging may indicate the lesion stalk (Fig. 39.5). This is important for management, a pedunculated fibroid being a contraindication for selective embolization.

Detection of circumferential vascularization helps to identify fibroids and to differentiate them from other myometrial lesions such as adenomyosis or leiomyosarcomas.

39.2.2.2 Adenomyosis

Adenomyosis is defined as the presence of endometrial tissue within the myometrium [6, 9]. This creates ill-defined myometrial lesions, that may be focal or diffuse.

On color Doppler imaging the radial vessels seem to follow their habitual course through the myometrium as though there was no lesion: this

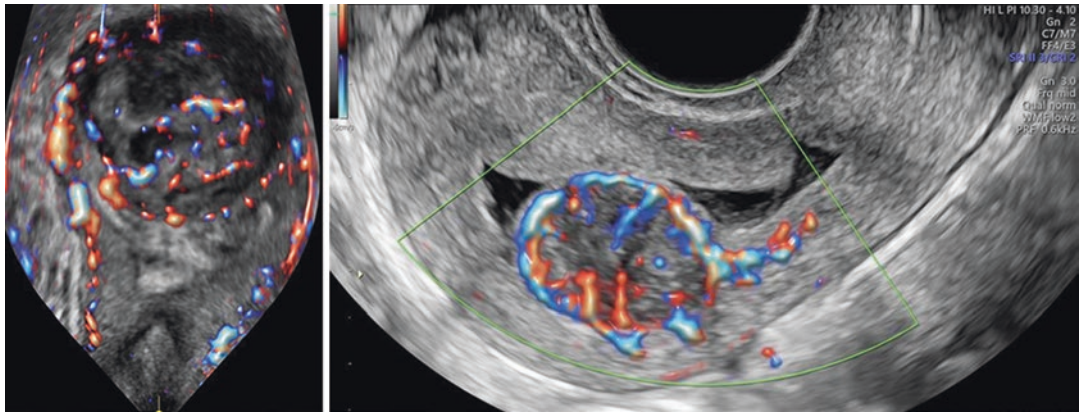

Fig. 39.4 Color Doppler images of two patients presenting with a fibroid: on the left case (reconstructed 3D-polyline frontal section), the intramural fibroid in the fundus of the uterus shows subtle circumferential flow as well as moderate internal vascularity; on the right case a FIGO 1 fibroid shows marked circumferential vessels as well as moderate internal vascularization

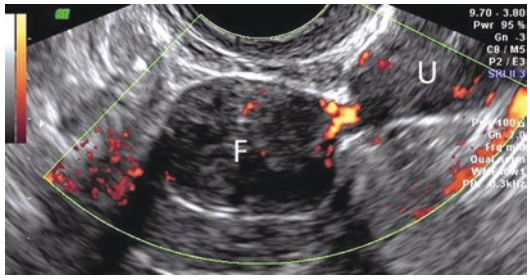

Fig. 39.5 Pedunculated subserosal fibroid (FIGO 7) with distinct vascularization of the stalk: *U* uterus; *F* fibroid

is called translesional vascularity [6, 10] (Fig. 39.6). The color intensity may be unremarkable or slightly increased.

39.2.3 Malignant Lesions

Uterine sarcomas (including leiomyosarcoma, endometrial stromal sarcoma, and undifferentiated endometrial sarcoma) are rare but highly malignant myometrial lesions. Typically, sarcomas have been reported to show irregular but high internal vascularization [6, 11] (Fig. 39.7). However, in a recent series [12] of 195 uterine sarcomas, most sarcomas were moderately or highly vascularized, although up to one-third were not. Especially endometrial stromal sarcomas are reportedly less vascularized.

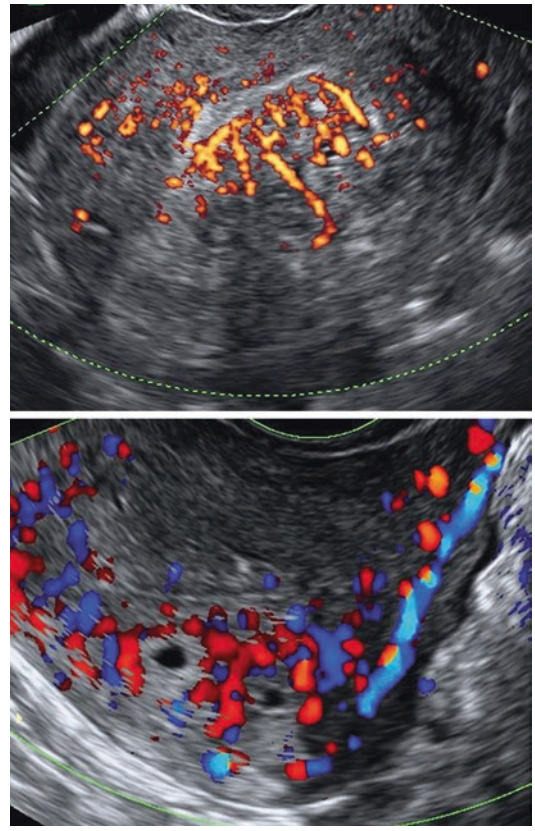

Fig. 39.6 Two cases of adenomyosis of the posterior myometrial wall (top) and of the anterior myometrial wall (bottom): note the translesional vascularity

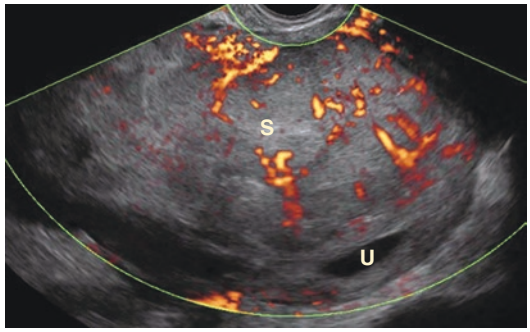

Fig. 39.7 Power Doppler image of a sarcoma in the anterior wall of the uterus with irregular internal vascularization: *U* uterus; *S* sarcoma

39.3 Endometrium and Intracavitary Lesions

The 2010 international Endometrial Tumor Analysis (IETA) consensus paper describes the sonographic terms and definitions to be used in reporting the endometrium and intracavitary lesions [13]. The color score reflects the color content in the endometrium and varies from 1 to 4. A color score of 1 indicates the absence of color while color scores of 2, 3, and 4 indicate minimal, moderate, and abundant color, respectively.

Different vascular patterns have been defined [13]: a single dominant vessel with or without branching, multiple vessels with focal origin (i.e., sharing a common stem) or multifocal origin (at the myometrial–endometrial junction) (Fig. 39.8), scattered vessels (without identifiable origin at the myometrialendometrial junction) and circular flow.

39.3.1 Physiological Changes

In the first part of a normal menstrual cycle, endometrial vessels are usually not detectable within the endometrium, while at the end of the secretory phase multiple peripheral vessels are visible crossing the myometrial–endometrial junction into the endometrium.

After menopause, the atrophic endometrium has no detectable internal vessels (Fig. 39.9).

39.3.2 Benign Lesions

39.3.2.1 Endometrial Polyps

Typically, a polyp has a dominant feeding vessel. In unenhanced ultrasonography, the presence of a single dominant vessel from the junctional zone extending beyond the expected endometrial midline is highly suggestive of an endometrial polyp [13–15] (Fig. 39.10). At hydrosonography the polyp outline is well-visible: the feeding vessel enters the polyp in the polyp stalk of pedunculated lesions or relatively centrally in sessile polyps and is often visible till the beyond the center of the lesion (Fig. 39.10). The polyp vessels are usually tiny and of low velocity. Therefore, the PRF is to be lowered to allow the visualization of low-velocity flow (e.g., PRF as low as 0.3 or even 0.1). Traditionally, the vascular pedicle of a polyp has been described as a single dominant vessel without branching.

However, using new high-end ultrasound machines, and with proper settings (adequate zooming, low PFR, and optimal color gain and WMF) subtle branching may be detectable in most polyps.

It is important to ascertain the myometrium is not contracting during imaging as this may lead to the transient disappearance of the polyp vascularization. The examination should therefore last long enough or be repeated. Direct pressure by the ultrasound probe on the uterus should be avoided, as should be excessive intrauterine pressure during hydrosonography. However, gel instillation sonography does not seem to interfere with the color signal [16].

39.3.2.2 Intracavitary Fibroids

Typically, fibroids show circumferential vascularization. In the case of small intracavitary lesions, the visualization of—often tiny—vessels parallel with the lesion circumference is suggestive of type 0 fibroids, whereas a single central

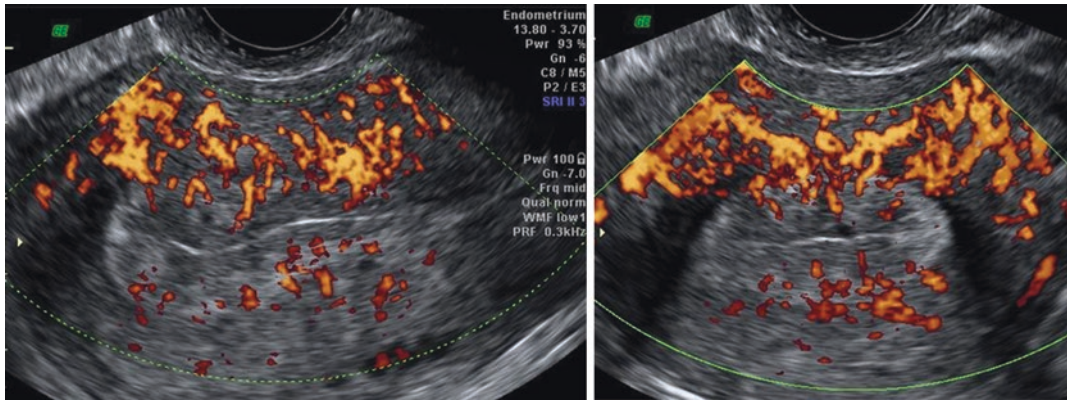

Fig. 39.8 Power Doppler image of the uterus in sagittal (left) and transverse (left) section: note the multiple vessels of multifocal origin. The histological examination showed proliferative endometrial changes with focal endometrial hyperplasia without atypia

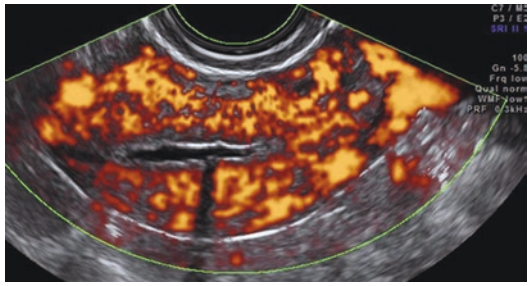

Fig. 39.9 Power Doppler image of the uterus: prominent myometrial color signals but absence of detectable endometrial vessels (this is a normal finding in an atrophic or a postmenstrual endometrium)

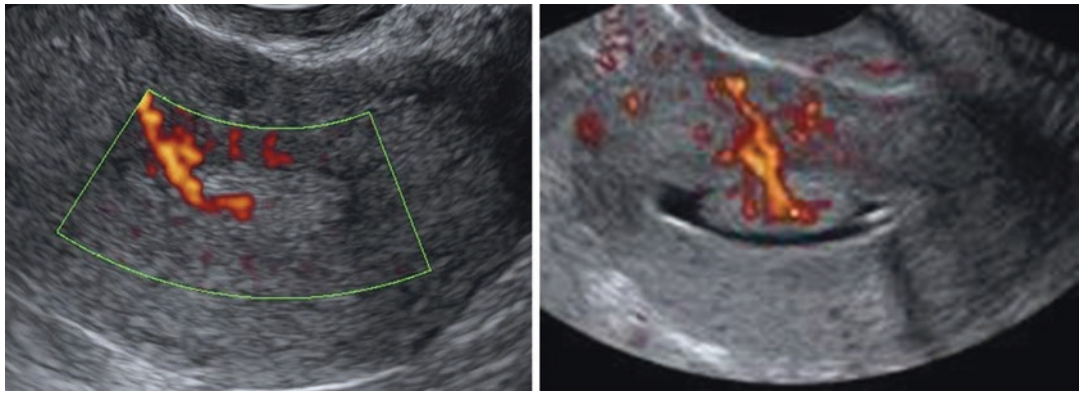

Fig. 39.10 Power Doppler image of an endometrial polyp with a distinct dominant vessel at unenhanced ultrasonography (left) and at hydrosonography (right)

vessel is more indicative of a polyp. An adequate setting should be used to allow the detection of small, low flow velocity vessels (low PRF, high color gain). However, in tiny intracavitary fibroids, and especially in calcified lesions, there is often an absence of any color signal. The internal vascularization is highly variable ranging from absent to prominent.

39.3.2.3 Retained Products of Conception (RPOC)

In retained product of conception (RPOC), the underlying myometrial vascularity is often prominent: enhanced myometrial vascularity (EMV) [17, 18] (Fig. 39.11). The presence of focal EMV is highly suggestive for the presence of RPOC and has been linked to subinvolution of the placental bed [19, 20]. EMV may be highly prominent, with numerous vessels with high velocity (Fig. 39.11). This has originally been reported as arterio-venous malformations (AVM) [21]. Although congenital AVM is extremely rare, acquired AVM or EMV are common in the presence of RPOC. AVM has also been reported after uterine surgery. Incomplete removal or persistence of retained trophoblast associated with high-velocity EMV may lead to heavy and potentially life-threatening bleeding [22]. Spontaneous expulsion or complete surgical removal of the RPOC leads to immediate disappearance of the EMV and hence of the bleeding (risk) [17, 23]. Ultrasound examination with color Doppler imaging is therefore of utmost importance to obtain a detailed and exact preoperative mapping of the EMV and hence of the location of the overlying retained tissue in the uterine cavity. Although tissue removal under direct hysteroscopic view is the method of choice for retained products, (heavy) bleeding may hinder visualization. In those cases, the exact preoperative knowledge of the RPOC location, as well as peroperative ultrasound scanning, enables the surgeon to achieve a quick and complete removal of the retained tissue.

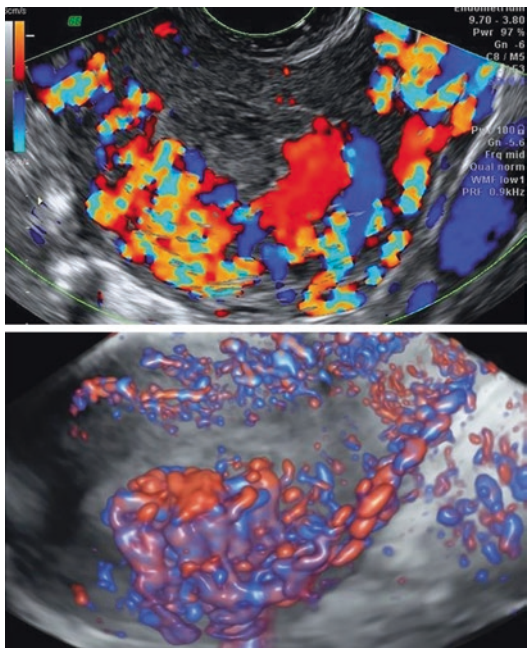

Fig. 39.11 Two cases of retained products of conception (RPOC) with enhanced vascular vascularity (EMV): 2D image (top) and 3D rendering (bottom)

The color image of EMV depends on vessel number, size, and flow velocity. In typical high-velocity EMV, the amount of color is striking at standard-setting, and does not allow the visualization of individual vessels. Due to the brightness of the color, it is initially impossible to discern the retained tissue. The latter is similar to an "overexposed photo." Therefore, to obtain a better image of the myometrial vascular tree underlying the retained trophoblastic tissue, the PRF should be increased. The vessels are tortuous and of different sizes. To measure the highest flow velocity (peak systolic velocity or PSV) the PRF should be turned up even more till only a few vessels remain visible: these are the vessels with the highest flow velocity. Although heavy bleeding occurs in EMV and has been related to the PSV, complete and swift surgical removal of the retained tissue overlying the EMV—even in case of high PSV—is mostly associated with low or moderate blood loss.

39.3.3 Malignant Lesions

39.3.3.1 Endometrial Cancer

Endometrial cancer is typically associated with high internal vascularity including multiple ves-

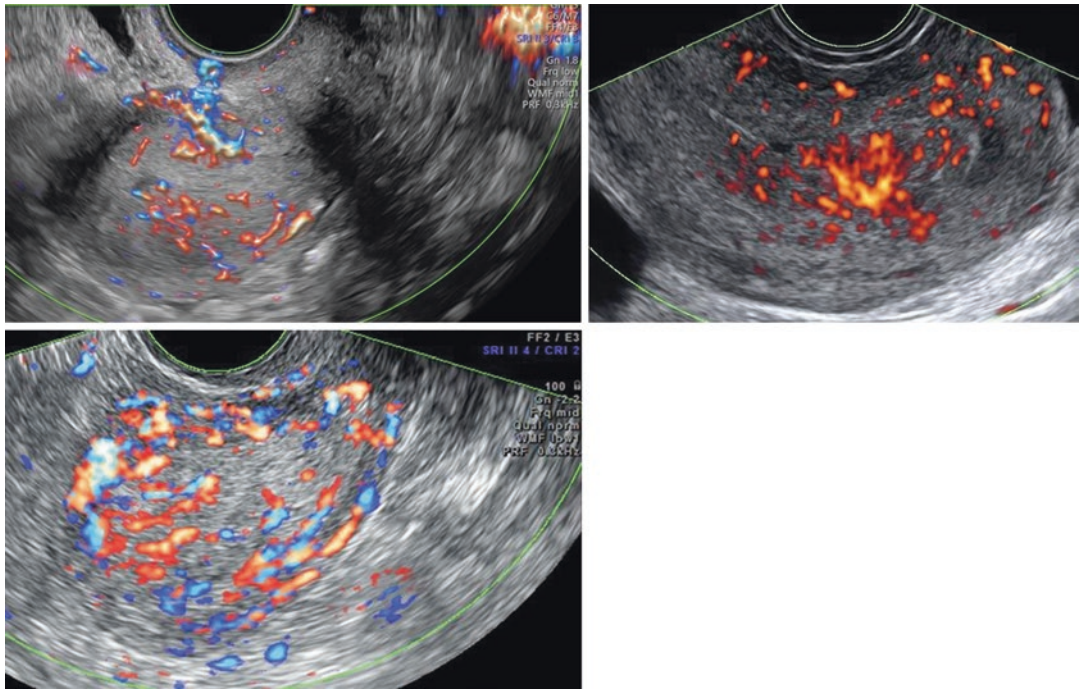

Fig. 39.12 Three cases of endometrial cancer: note the multiple vessels from multifocal origin. However, in the middle case, the main part of the tumor is perfused by multiple high-flow vessels from focal origin on the anterior wall of the uterus

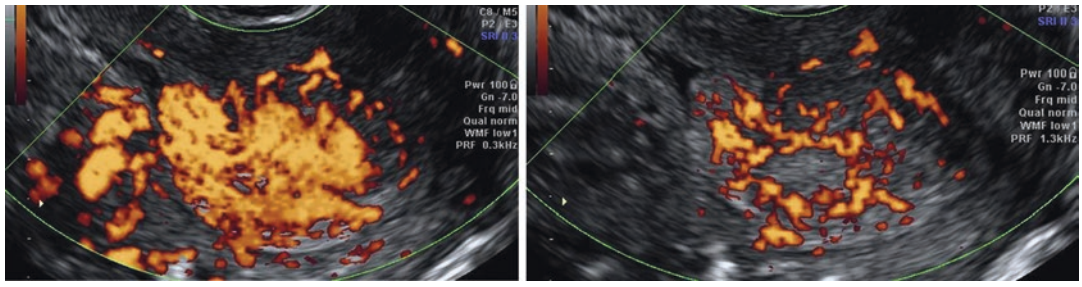

Fig. 39.13 Power Doppler images of a patient with endometrial cancer: note on the left image the presence of striking and intense signals, called "color splashes," while, on the right image, multiple vessels can be identified. Both images have been taken at the same section, with the same magnification, but on the left image the pulse repetition frequency (PFR) was set at 0.3 kHZ while on the right image the PRF has been increase to 1.3 kHz

sels of multifocal origin with irregular branching [24–27] (Fig. 39.12). The color intensity is often high (color score of 3 or 4 according to the IETA terminology). Some reported "color splashes" as highly suspicious for cancer (Fig. 39.13). The latter is due to the shape of the vascular tree and the high flow velocity at standard Doppler settings. Increasing the PRF and the WMF cut-off frequency allows to distinguish an irregular vascular tree.

However, some endometrial tumors do not have prominent vessels. Moreover, in case of necrosis or hemorrhage, (part of) the tumor may become avascular.

Compared with low-risk endometrial cancer, high-risk tumors are more likely to have a multifocal vessel pattern and a higher color score [28, 29].

39.4 Miscellaneous

Color Doppler imaging during ultrasound scanning of the uterus proved useful for other indications. It may be helpful in differentiating vessels from cystic lesions (e.g., myometrial cysts versus vessels; hematometra versus soft tissue tumor) (Fig. 39.14) or in the detection of other malignancies of the uterus characterized by prominent vascularization (e.g., cervical cancer) [30] (Fig. 39.15). Although in cervical cancer higher color scores have been reported with deep stromal invasion, the same group did not find any association between lymph node metastases and vascularity indices.

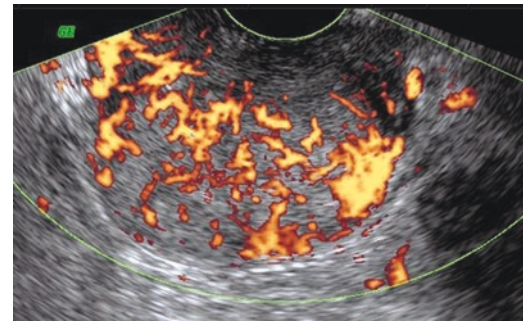

Fig. 39.15 Power Doppler of a transverse section though the cervix: the grossly enlarged cervix is diffusely and prominently vascularized. The histology was a squamous cell carcinoma of the cervix

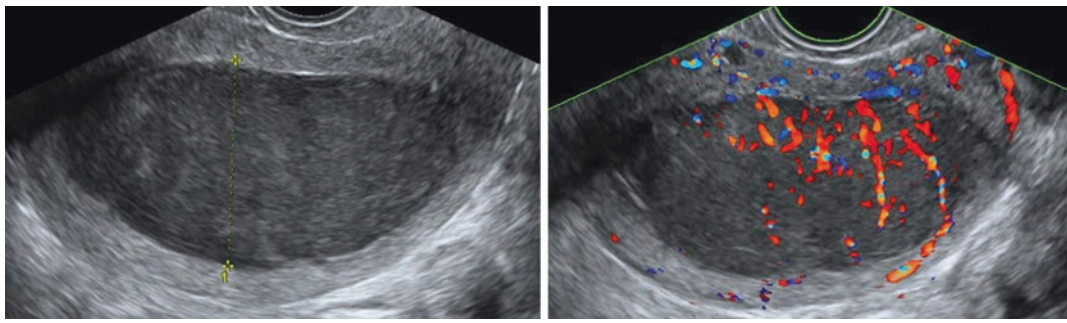

Fig. 39.14 Sagittal section of the uterus on gray-scale (left) and with color Doppler (right): while, on gray-scale, the hypoechogenic area could be misinterpreted as a hematometron, the presence of color signals at color Doppler clearly indicated vascularized tissue. The pathologist reported a B-cell non-Hodgkin lymphoma

References

1. Kaelin Agten A, Ringel N, Ramos J, Timor-Tritsch IE, Agten CA, Monteagudo A. Standardization of peak systolic velocity measurement in enhanced myometrial vascularity. Am J Obstet Gynecol. 2016;215:802–3.
2. De Smet F, De Brabanter J, Van den Bosch T, Pochet N, Amant F, Van Holbeke C, Moerman P, De Moor B, Vergote I, Timmerman D. New model to predict depth of infiltration in endometrial carcinoma based of transvaginal sonography. Ultrasound Obstet Gynecol. 2006;27:664–71.
3. Nieuwenhuis LL, Bij de Vaate MA, Hehenkamp WJ, Heymans MW, van Baal MW, Brölmann HA, Huirne JA. Reproducibility of three-dimensional gel installation sonohysterography in the assessment and classification of intrauterine abnormalities. Eur J Obstet Gynecol Reprod Biol. 2014;179:141–6.
4. Nieuwenhuis LL, Hehenkamp WJK, Brölmann HAM, Huirne JAF. 3D power Doppler in uterine fibroids; influence of gain, cardiac cycle and off-line measurement techniques. J Obstet Gynaecol. 2018;38:103–9.
5. Fleischer AC. Color Doppler sonography of uterine disorders. Ultrasound Q. 2003;19:179–89.
6. Van den Bosch T, Dueholm M, Leone FP, Valentin L, Rasmussen CK, Votino A, Van Schoubroeck D, Landolfo C, Installé AJ, Guerriero S, Exacoustos C, Gordts S, Benacerraf B, D'Hooghe T, De Moor B, Brölmann H, Goldstein S, Epstein E, Bourne T, Timmerman D. Terms, definitions and measurements to describe sonographic features of myometrium and uterine masses: a consensus opinion from the Morphological Uterus Sonographic Assessment (MUSA) group. Ultrasound Obstet Gynecol. 2015;46:284–98.
7. Nieuwenhuis LL, Keizer AL, Stoelinga B, Twisk J, Hehenkamp W, Brölmann H, Huirne J. Fibroid vascularisation assessed with three-dimensional power Doppler ultrasound is a predictor for uterine fibroid growth: a prospective cohort study. BJOG. 2018;125:577–84.
8. Munro MG, Critchley HOD, Fraser IS. FIGO Menstrual Disorders Committee. The two FIGO systems for normal and abnormal uterine bleeding symptoms and classification of causes of abnormal uterine bleeding in the reproductive years: 2018 revisions. Int J Gynaecol Obstet. 2018 Dec;143(3):393–408.
9. Vandermeulen L, Cornelis A, Kjaergaard Rasmussen C, Timmerman D, Van den Bosch T. Guiding histological assessment of uterine lesions using 3D in vitro ultrasonography and stereotaxis. Facts Views Vis Obgyn. 2017;9:77–84.
10. Van den Bosch T, de Bruijn AM, de Leeuw RA, Dueholm M, Exacoustos C, Valentin L, Bourne T, Timmerman D, Huirne JAF. Sonographic classification and reporting system for diagnosing adenomyosis. Ultrasound Obstet Gynecol. 2019;53:576–82.
11. Brölmann H, Tanos V, Grimbizis G, Ind T, Philips K, Van den Bosch T, Sawalhe S, van den Haak L, Jansen FW, Pijnenborg J, Taran FA, Brucker S, Wattiez A, Campo R, O'Donovan P, de Wilde RL. European Society of Gynaecological Endoscopy (ESGE) steering committee on fibroid morcellation. Options on fibroid morcellation: a literature review. Gynecol Surg. 2015;12:3–15.
12. Ludovisi M, Moro F, Pasciuto T, Di Noi S, Giunchi S, Savelli L, Pascual MA, Sladkevicius P, Alcazar JL, Franchi D, Mancari R, Moruzzi MC, Jurkovic D, Chiappa V, Guerriero S, Exacoustos C, Epstein E, Frühauf F, Fischerova D, Fruscio R, Ciccarone F, Zannoni GF, Scambia G, Valentin L, Testa AC. Imaging of gynecological disease: clinical and ultrasound characteristics of uterine sarcomas. Ultrasound Obstet Gynecol. 2019;54:676–87. https://doi.org/10.1002/uog.20270.
13. Leone F, Timmerman D, Bourne T, Valentin L, Epstein E, Goldstein SR, Marret H, Parsons AK, Gull B, Istre O, Sepulveda W, Ferrazzi E, Van den Bosch T. Terms, definitions and measurements to describe the sonographic features of the endometrium and intrauterine lesions: a consensus opinion from the International Endometrial Tumor Analysis (IETA) group. Ultrasound Obstet Gynecol. 2010;35:103–12.
14. Timmerman D, Verguts J, Konstantinovic ML, Moerman P, Van Schoubroeck D, Deprest J, Van Huffel S. The pedicle artery sign based on sonography with color Doppler imaging can replace second-stage tests in women with abnormal vaginal bleeding. Ultrasound Obstet Gynecol. 2003;22:166–71.
15. Van den Bosch T, Ameye L, Van Schoubroeck D, Bourne T, Timmerman D. Intra-cavitary uterine pathology in women with abnormal uterine bleeding: a prospective study of 1220 women. Facts Views Vis Obgyn. 2015;7:17–24.
16. Van den Bosch T, Van Schoubroeck D, Luts J, Bignardi T, Condous G, Epstein E, Leone FP, Testa AC, Valentin L, Van Huffel S, Bourne T, Timmerman D. Effect of gel-instillation sonography on Doppler ultrasound findings in endometrial polyps. Ultrasound Obstet Gynecol. 2011;38:355–9.
17. Van den Bosch T, Van Schoubroeck D, Timmerman D. The maximum peak systolic velocity and the management of highly vascularized retained products of conception. J Ultrasound Med. 2015;34:1577–82.
18. Timor-Tritsch IE, Haynes MC, Monteagudo A, Khatib N, Kovács S. Ultrasound diagnosis and management of acquired uterine enhanced myometrial vascularity/arteriovenous malformations. Am J Obstet Gynecol. 2016;214:731.e1–731.e10.
19. Van den Bosch T, Van Schoubroeck D, Chuan L, De Brabanter J, Van Huffel S, Timmerman D. Color Doppler and gray-scale ultrasound evaluation of the postpartum uterus. Ultrasound Obstet Gynecol. 2002;20:586–91.
20. Van Schoubroeck D, Van den Bosch T, Scharpe K, Lu C, Van Huffel S, Timmerman D. Prospective evalu-

ation of blood flow in the myometrium and in the uterine arteries in the puerperium. Ultrasound Obstet Gynecol. 2004;23:378–81.
21. Timmerman D, Van den Bosch T, Peeraer K, Debrouwere E, Van Schoubroeck D, Stockx L, Spitz B. Vascular malformations of the uterus: ultrasonographic diagnosis and conservative management. Eur J Obstet Gynecol. 2000;92:172–8.
22. Timmerman D, Wauters J, Van Calenberg S, Van Schoubroeck D, Maleux G, Van den Bosch T, Spitz B. Color Doppler imaging is a valuable tool for the diagnosis and management of uterine vascular malformations. Ultrasound Obstet Gynecol. 2003;21:570–7.
23. Van den Bosch T, Daemen A, Van Schoubroeck D, Pochet N, De Moor B, Timmerman D. Occurrence and outcome of residual trophoblastic tissue: a prospective study. J Ultrasound Med. 2008;27:357–61.
24. Alcázar JL, Castillo G, Mínguez JA, Galán MJ. Endometrial blood flow mapping using transvaginal power Doppler sonography in women with postmenopausal bleeding and thickened endometrium. Ultrasound Obstet Gynecol. 2003;21:583–8.
25. Alcazar JL, Galvan R. Three-dimensional power Doppler ultrasound scanning for the prediction of endometrial cancer in women with postmenopausal bleeding and thickened endometrium. Am J Obstet Gynecol. 2009;200(44):e1–6.
26. Epstein E, Skoog L, Isberg PE, De Smet F, De Moor B, Olofsson PA, Gudmundsson S, Valentin L. An algorithm including results of gray-scale and power Doppler ultrasound examination to predict endometrial malignancy in women with postmenopausal bleeding. Ultrasound Obstet Gynecol. 2002;20:370–6.
27. Epstein E, Valentin L. Gray-scale ultrasound morphology in the presence or absence of intrauterine fluid and vascularity as assessed by color Doppler for discrimination between benign and malignant endometrium in women with postmenopausal bleeding. Ultrasound Obstet Gynecol. 2006;28:89–95.
28. Epstein E, Van Holsbeke C, Mascilini F, Måsbäck A, Kannisto P, Ameye L, Fischerova D, Zannoni G, Vellone V, Timmerman D, Testa AC. Gray-scale and color Doppler ultrasound characteristics of endometrial cancer in relation to stage, grade and tumor size. Ultrasound Obstet Gynecol. 2011;38:586–93.
29. Epstein E, Fischerova D, Valentin L, Testa AC, Franchi D, Sladkevicius P, Frühauf F, Lindqvist PG, Mascilini F, Fruscio R, Haak LA, Opolskiene G, Pascual MA, Alcazar JL, Chiappa V, Guerriero S, Carlson JW, Van Holsbeke C, Leone FPG, De Moor B, Bourne T, van Calster B, Installe A, Timmerman D, Verbakel JY, Van den Bosch T. Ultrasound characteristics of endometrial cancer as defined by International Endometrial Tumor Analysis (IETA) consensus nomenclature: prospective multicenter study. Ultrasound Obstet Gynecol. 2018;51:818–28.
30. Pálsdóttir K, Fischerova D, Franchi D, Testa A, Di Legge A, Epstein E. Preoperative prediction of lymph node metastasis and deep stromal invasion in women with invasive cervical cancer: prospective multicenter study using 2D and 3D ultrasound. Ultrasound Obstet Gynecol. 2015;45:470–5.